AMINO ACIDS IN PLANTS: REGULATION AND FUNCTIONS IN DEVELOPMENT AND STRESS DEFENSE

EDITED BY: Maurizio Trovato, Dietmar Funck, Giuseppe Forlani, Sakiko Okumoto and Rachel Amir

PUBLISHED IN: Frontiers in Plant Science

frontiers Research Topics

Frontiers eBook Copyright Statement

The copyright in the text of individual articles in this eBook is the property of their respective authors or their respective institutions or funders. The copyright in graphics and images within each article may be subject to copyright of other parties. In both cases this is subject to a license granted to Frontiers.

The compilation of articles constituting this eBook is the property of Frontiers.

Each article within this eBook, and the eBook itself, are published under the most recent version of the Creative Commons CC-BY licence. The version current at the date of publication of this eBook is CC-BY 4.0. If the CC-BY licence is updated, the licence granted by Frontiers is automatically updated to the new version.

When exercising any right under the CC-BY licence, Frontiers must be attributed as the original publisher of the article or eBook, as applicable.

Authors have the responsibility of ensuring that any graphics or other materials which are the property of others may be included in the CC-BY licence, but this should be checked before relying on the CC-BY licence to reproduce those materials. Any copyright notices relating to those materials must be complied with.

Copyright and source acknowledgement notices may not be removed and must be displayed in any copy, derivative work or partial copy which includes the elements in question.

All copyright, and all rights therein, are protected by national and international copyright laws. The above represents a summary only. For further information please read Frontiers' Conditions for Website Use and Copyright Statement, and the applicable CC-BY licence.

ISSN 1664-8714
ISBN 978-2-88971-842-9
DOI 10.3389/978-2-88971-842-9

About Frontiers

Frontiers is more than just an open-access publisher of scholarly articles: it is a pioneering approach to the world of academia, radically improving the way scholarly research is managed. The grand vision of Frontiers is a world where all people have an equal opportunity to seek, share and generate knowledge. Frontiers provides immediate and permanent online open access to all its publications, but this alone is not enough to realize our grand goals.

Frontiers Journal Series

The Frontiers Journal Series is a multi-tier and interdisciplinary set of open-access, online journals, promising a paradigm shift from the current review, selection and dissemination processes in academic publishing. All Frontiers journals are driven by researchers for researchers; therefore, they constitute a service to the scholarly community. At the same time, the Frontiers Journal Series operates on a revolutionary invention, the tiered publishing system, initially addressing specific communities of scholars, and gradually climbing up to broader public understanding, thus serving the interests of the lay society, too.

Dedication to Quality

Each Frontiers article is a landmark of the highest quality, thanks to genuinely collaborative interactions between authors and review editors, who include some of the world's best academicians. Research must be certified by peers before entering a stream of knowledge that may eventually reach the public - and shape society; therefore, Frontiers only applies the most rigorous and unbiased reviews.
Frontiers revolutionizes research publishing by freely delivering the most outstanding research, evaluated with no bias from both the academic and social point of view. By applying the most advanced information technologies, Frontiers is catapulting scholarly publishing into a new generation.

What are Frontiers Research Topics?

Frontiers Research Topics are very popular trademarks of the Frontiers Journals Series: they are collections of at least ten articles, all centered on a particular subject. With their unique mix of varied contributions from Original Research to Review Articles, Frontiers Research Topics unify the most influential researchers, the latest key findings and historical advances in a hot research area! Find out more on how to host your own Frontiers Research Topic or contribute to one as an author by contacting the Frontiers Editorial Office: frontiersin.org/about/contact

AMINO ACIDS IN PLANTS: REGULATION AND FUNCTIONS IN DEVELOPMENT AND STRESS DEFENSE

Topic Editors:
Maurizio Trovato, Sapienza University of Rome, Italy
Dietmar Funck, University of Konstanz, Germany
Giuseppe Forlani, University of Ferrara, Italy
Sakiko Okumoto, Texas A&M University, United States
Rachel Amir, Migal - Galilee Research Institute, Israel

Citation: Trovato, M., Funck, D., Forlani, G., Okumoto, S., Amir, R., eds. (2021). Amino Acids in Plants: Regulation and Functions in Development and Stress Defense. Lausanne: Frontiers Media SA. doi: 10.3389/978-2-88971-842-9

Table of Contents

06 ***Editorial: Amino Acids in Plants: Regulation and Functions in Development and Stress Defense***
Maurizio Trovato, Dietmar Funck, Giuseppe Forlani, Sakiko Okumoto and Rachel Amir

12 ***Increased Glyphosate-Induced Gene Expression in the Shikimate Pathway Is Abolished in the Presence of Aromatic Amino Acids and Mimicked by Shikimate***
Ainhoa Zulet-González, Maria Barco-Antoñanzas, Miriam Gil-Monreal, Mercedes Royuela and Ana Zabalza

22 ***Functional Relevance of Citrulline in the Vegetative Tissues of Watermelon During Abiotic Stresses***
Qiushuo Song, Madhumita Joshi, James DiPiazza and Vijay Joshi

35 ***Lysine Catabolism Through the Saccharopine Pathway: Enzymes and Intermediates Involved in Plant Responses to Abiotic and Biotic Stress***
Paulo Arruda and Pedro Barreto

45 ***Visualizing Genotypic and Developmental Differences of Free Amino Acids in Maize Roots With Mass Spectrometry Imaging***
Kelly C. O'Neill and Young Jin Lee

57 ***Structural Studies of Glutamate Dehydrogenase (Isoform 1) From* Arabidopsis thaliana*, an Important Enzyme at the Branch-Point Between Carbon and Nitrogen Metabolism***
Marta Grzechowiak, Joanna Sliwiak, Mariusz Jaskolski and Milosz Ruszkowski

74 ***Structural and Functional Characteristics of Two Molecular Variants of the Nitrogen Sensor PII in Maritime Pine***
María Teresa Llebrés, María Belén Pascual, Carolina Valle, Fernando N. de la Torre, José Miguel Valderrama-Martin, Luis Gómez, Concepción Avila and Francisco M. Cánovas

88 ***In* Arabidopsis thaliana *Substrate Recognition and Tissue- as Well as Plastid Type-Specific Expression Define the Roles of Distinct Small Subunits of Isopropylmalate Isomerase***
Kurt Lächler, Karen Clauss, Janet Imhof, Christoph Crocoll, Alexander Schulz, Barbara Ann Halkier and Stefan Binder

106 ***Connections Between Amino Acid Metabolisms in Plants: Lysine as an Example***
Qingqing Yang, Dongsheng Zhao and Qiaoquan Liu

114 ***Shaping Durum Wheat for the Future: Gene Expression Analyses and Metabolites Profiling Support the Contribution of BCAT Genes to Drought Stress Response***
Valentina Buffagni, Filippo Vurro, Michela Janni, Mariolina Gullì, Arturo A. Keller and Nelson Marmiroli

130 ***The Neighboring Subunit Is Engaged to Stabilize the Substrate in the Active Site of Plant Arginases***
Bartosz Sekula

142 ***Cysteine and Methionine Biosynthetic Enzymes Have Distinct Effects on Seed Nutritional Quality and on Molecular Phenotypes Associated With Accumulation of a Methionine-Rich Seed Storage Protein in Rice***
Sarah J. Whitcomb, Apidet Rakpenthai, Franziska Brückner, Axel Fischer, Saroj Parmar, Alexander Erban, Joachim Kopka, Malcolm J. Hawkesford and Rainer Hoefgen

161 ***How Does Proline Treatment Promote Salt Stress Tolerance During Crop Plant Development?***
Ahmed El Moukhtari, Cécile Cabassa-Hourton, Mohamed Farissi and Arnould Savouré

177 ***The Level of Methionine Residues in Storage Proteins Is the Main Limiting Factor of Protein-Bound-Methionine Accumulation in Arabidopsis Seeds***
Aiswarya Girija, David Shotan, Yael Hacham and Rachel Amir

192 ***Challenges and Prospects of New Plant Breeding Techniques for GABA Improvement in Crops: Tomato as an Example***
Pietro Gramazio, Mariko Takayama and Hiroshi Ezura

208 ***Differential Contribution of P5CS Isoforms to Stress Tolerance in Arabidopsis***
Dietmar Funck, Lukas Baumgarten, Marc Stift, Nicolaus von Wirén and Luise Schönemann

223 ***A Specific and Sensitive Enzymatic Assay for the Quantitation of L-Proline***
Giuseppe Forlani and Dietmar Funck

235 ***Proline Accumulation in Pollen Grains as Potential Target for Improved Yield Stability Under Salt Stress***
Roberto Mattioli, Noemi Palombi, Dietmar Funck and Maurizio Trovato

243 ***Lysine, Lysine-Rich, Serine, and Serine-Rich Proteins: Link Between Metabolism, Development, and Abiotic Stress Tolerance and the Role of ncRNAs in Their Regulation***
P. B. Kavi Kishor, Renuka Suravajhala, Guddimalli Rajasheker, Nagaraju Marka, Kondle Kavya Shridhar, Divya Dhulala, Korubothula Prakash Scinthia, Kummari Divya, Madhavi Doma, Sujatha Edupuganti, Prashanth Suravajhala and Rathnagiri Polavarapu

258 ***Appropriate Activity Assays Are Crucial for the Specific Determination of Proline Dehydrogenase and Pyrroline-5-Carboxylate Reductase Activities***
Sandrine Lebreton, Cécile Cabassa-Hourton, Arnould Savouré, Dietmar Funck and Giuseppe Forlani

267 ***Physiological, Nutritional and Metabolomic Responses of Tomato Plants After the Foliar Application of Amino Acids Aspartic Acid, Glutamic Acid and Alanine***
Marina Alfosea-Simón, Silvia Simón-Grao, Ernesto Alejandro Zavala-Gonzalez, Jose Maria Cámara-Zapata, Inmaculada Simón, Juan José Martínez-Nicolás, Vicente Lidón and Francisco García-Sánchez

283 ***Enhanced Production of Aromatic Amino Acids in Tobacco Plants Leads to Increased Phenylpropanoid Metabolites and Tolerance to Stresses***
Moran Oliva, Aviv Guy, Gad Galili, Evgenia Dor, Ron Schweitzer, Rachel Amir and Yael Hacham

300 ***Increased Expression of UMAMIT Amino Acid Transporters Results in Activation of Salicylic Acid Dependent Stress Response***
Julien Besnard, Unnati Sonawala, Bal Maharjan, Eva Collakova, Scott A. Finlayson, Guillaume Pilot, John McDowell and Sakiko Okumoto

310 ***A Wild Allele of* Pyrroline-5-Carboxylate Synthase1 *Leads to Proline Accumulation in Spikes and Leaves of Barley Contributing to Improved Performance Under Reduced Water Availability***
Felix Frimpong, Carel W. Windt, Dagmar van Dusschoten, Ali A. Naz, Michael Frei and Fabio Fiorani

326 ***Metabolism and Regulatory Functions of* O*-Acetylserine,* S*-Adenosylmethionine, Homocysteine, and Serine in Plant Development and Environmental Responses***
Mutsumi Watanabe, Yukako Chiba and Masami Yokota Hirai

347 ***BZR1 Regulates Brassinosteroid-Mediated Activation of* AMT1;2 *in Rice***
Shuo Yang, Depeng Yuan, Yang Zhang, Qian Sun and Yuan Hu Xuan

358 ***Enzymology and Regulation of δ^1-Pyrroline-5-Carboxylate Synthetase 2 From Rice***
Giuseppe Sabbioni, Dietmar Funck and Giuseppe Forlani

frontiers in Plant Science

EDITORIAL
published: 18 October 2021
doi: 10.3389/fpls.2021.772810

Editorial: Amino Acids in Plants: Regulation and Functions in Development and Stress Defense

Maurizio Trovato[1]*, *Dietmar Funck*[2]*, *Giuseppe Forlani*[3]*, *Sakiko Okumoto*[4]* and *Rachel Amir*[5,6]*

[1] Department of Biology and Biotechnology, Sapienza University of Rome, Rome, Italy, [2] Laboratory of Plant Physiology and Biochemistry, Department of Biology, University of Konstanz, Konstanz, Germany, [3] Laboratory of Plant Physiology and Biochemistry, Department of Life Science and Biotechnology, University of Ferrara, Ferrara, Italy, [4] Department of Plant Pathology, Physiology and Weed Science, Virginia Tech, Blacksburg, VA, United States, [5] Department of Plant Sciences, MIGAL - Galilee Research Institute, Kiryat Shmona, Israel, [6] Tel-Hai College, Upper Galilee, Israel

Keywords: amino acid metabolism, amino acid transport, stress responses, nitrogen sensing, signaling and assimilation, nitrogen use efficiency, crop enhancement

OPEN ACCESS

Edited and reviewed by:
Xiao Qiu,
University of Saskatchewan, Canada

***Correspondence:**
Maurizio Trovato
maurizio.trovato@uniroma1.it
Dietmar Funck
dietmar.funck@uni-konstanz.de
Giuseppe Forlani
flg@unife.it
Sakiko Okumoto
sokumoto@tamu.edu
Rachel Amir
rachel@migal.org.il

Specialty section:
This article was submitted to Plant Metabolism and Chemodiversity, a section of the journal Frontiers in Plant Science

Received: *08 September 2021*
Accepted: *21 September 2021*
Published: *18 October 2021*

Citation:
Trovato M, Funck D, Forlani G, Okumoto S and Amir R (2021) Editorial: Amino Acids in Plants: Regulation and Functions in Development and Stress Defense. Front. Plant Sci. 12:772810. doi: 10.3389/fpls.2021.772810

Editorial on the Research Topic

Amino Acids in Plants: Regulation and Functions in Development and Stress Defense

In the last decades, the importance of amino acids in plant development and stress defense has become increasingly evident, attracting growing interest in basic and applied plant science. Here we present novel findings on amino acid research and propose a picture, as up-to-date as possible, of the current knowledge on this fascinating aspect of plant physiology. Besides being building blocks for protein synthesis, many amino acids, including some not involved in protein synthesis, turned out to have active roles in plant development and participate in the plant's response to environmental stresses. In addition, amino acids serve as precursors for many primary and secondary metabolites and have pivotal roles in human nutrition, either as a source of nutraceutical compounds or as essential dietary components. Indeed, nine out of twenty-one proteinogenic amino acids cannot be synthesized in animals, including human beings, and three or more others are not synthesized in sufficient quantities to satisfy the metabolic needs (**Figure 1**). These nutritionally essential amino acids must be taken up from the diet and by far the greatest share is derived from plants (Galili et al., 2016, Hou and Wu, 2018). In contrast to humans and animals, plants synthesize all twenty-one proteinogenic amino acids themselves (**Figure 1**).

Lysine, as one of those essential amino acids is often present at low levels in plants and thus limits their nutritional value. The review of Yang et al. focuses on lysine catabolism and describes the connections between the degradation intermediates of this amino acid and other metabolic pathways, such as tryptophan metabolism, tricarboxylic acid cycle, abiotic and biotic stress responses, starch metabolism, and the unfolded protein response. A closer look at the relationships between lysine and serine is provided by Kavi Kishor et al., who summarize the current knowledge on the biosynthetic pathways, regulatory mechanisms, and biological effects of both amino acids, focusing on the complexity of their interactions. The authors report the complex mechanisms of transcriptional and post-transcriptional regulation and highlight the importance of proteins rich in lysine and serine for plant development and stress tolerance. Furthermore, the role of non-coding RNAs in the regulation of lysine- and serine-rich proteins and the possibility of using genome-wide strategies to identify novel interactions are discussed. While the interest in lysine biosynthesis largely aims at improving the nutritional value of crops, the research on the catabolism of this amino acid focuses more on tolerance to biotic and abiotic stresses. Arruda and Barreto surveyed

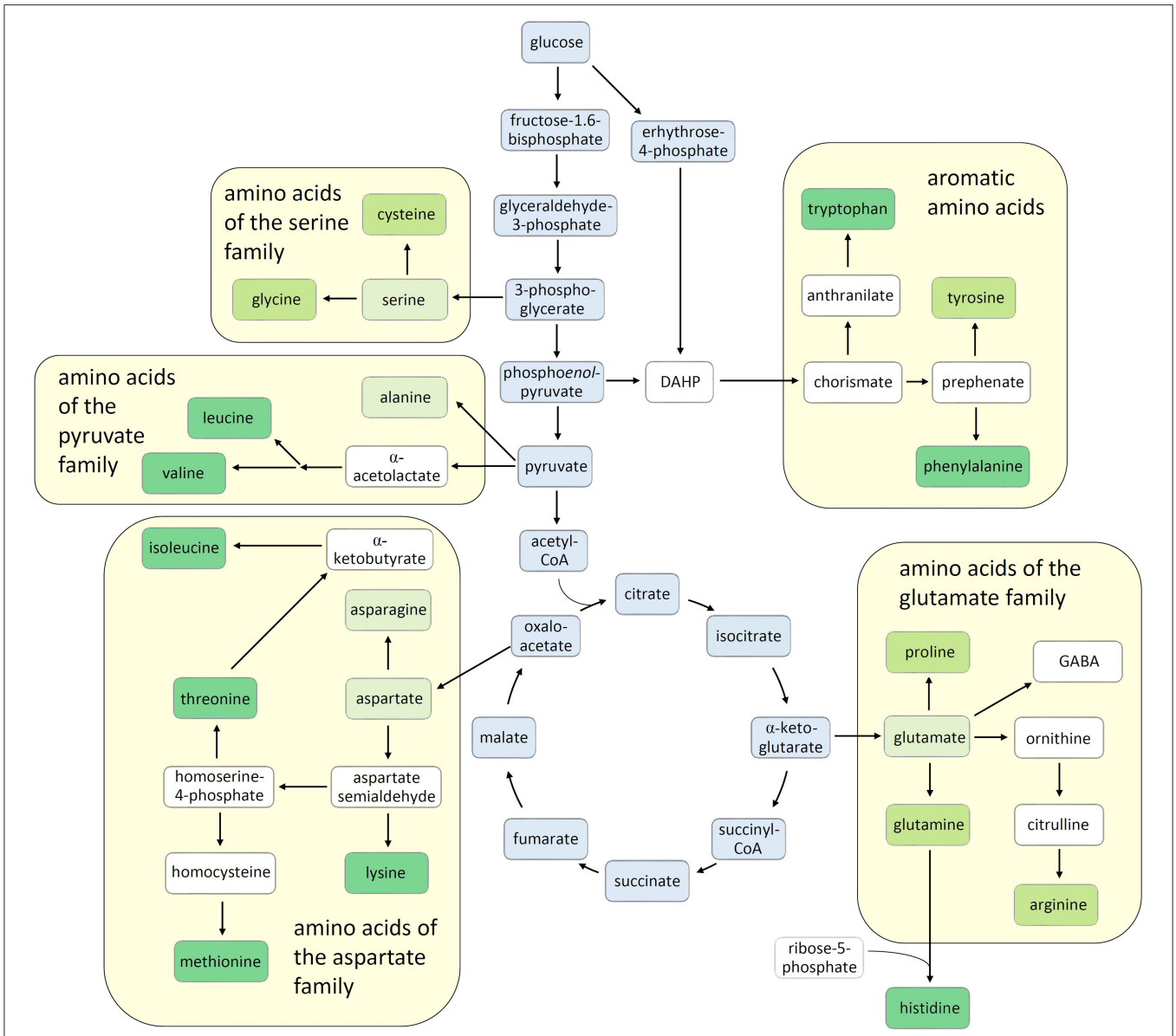

FIGURE 1 | Amino acid biosynthesis in plants. The carbon skeletons of amino acids are derived from different intermediates of the central carbon metabolism (boxed in blue). According to their respective precursors, the amino acids are grouped into five families derived from glutamate, serine, pyruvate, aspartate, or chorismate. The nine amino acids that cannot be synthesized in animals are shown in dark-green boxes, while those that can be synthesized but additionally need to be taken up with the diet are in brighter boxes. Proteinogenic amino acids that can be sufficiently synthesized in animals are in pale green boxes and non-proteinogenic amino acids and other important intermediates are boxed in white. DAHP, 3-deoxy-D-*arabino*heptulosonate-7-phosphate.

the known pathways of lysine degradation, with special attention to the saccharopine pathway. As described in the review, the effects of lysine catabolism on stress tolerance are probably due to the production of proline and pipecolate from glutamate and α-aminoadipate-δ-semialdehyde, respectively, mediated by the saccharopine pathway.

Methionine is another essential amino acid intensively studied to increase its content, which is usually very low in crop plants and vegetables. Cysteine can be synthesized from methionine but is still considered nutritionally essential due to the low methionine content in many plant tissues. Whitcomb et al. used a metabolic engineering approach to increase the content of both methionine and cysteine in rice seeds by generating a pair of transgenic lines. Each transgenic line contained a methionine-rich seed storage protein and an exogenous enzyme for either methionine or cysteine biosynthesis. This strategy successfully increased methionine content in seeds by approximately 50% but revealed an unexpected sulfur deficiency-like molecular phenotype and an alteration in seed protein profile, possibly caused by the accumulation of unfolded proteins

in the endoplasmic reticulum. A similar approach was used by Girija et al. to investigate whether the overall capacity to synthesize methionine or the density of methionine residues in seed proteins is the limiting factor for methionine content in seeds. The authors' conclusions suggest that the abundance of methionine residues in storage proteins is likely the main factor limiting methionine accumulation in Arabidopsis seeds. Moreover, they confirmed the association between the increase in methionine content and the accumulation of stress-related metabolites in seeds, although the reasons for this correlation remain unknown. The complexity and importance of sulfur-containing amino acids are also tackled by Watanabe et al. who reviewed the metabolism and regulatory functions of O-acetylserine, S-adenosylmethionine, homocysteine, and serine, as essential precursors of cysteine and methionine synthesis.

Besides being essential components of the animal and human diet, amino acids or their derivatives can provide a rich source of nutraceutical metabolites. An example of a health-promoting functional compound is represented by γ-aminobutyric acid (GABA), a non-proteinogenic amino acid whose remarkable properties have been reviewed by Gramazio et al. Additionally, this review summarizes the newest breeding strategies to increase GABA content in crops focusing on new CRISPR/Cas9-based approaches recently used to successfully improve GABA concentration in ripe tomato fruits with no adverse side effects.

Methionine, as well as other amino acids, are also used for the synthesis of glucosinolates, a large class of sulfur-containing metabolites with recognized antioxidant and anticancer properties. Lächler et al. investigated the function of isopropylmalate isomerase, an enzyme essential for leucine synthesis and possibly involved in methionine chain elongation. The active enzyme is a heterodimer composed of a large subunit and one among three possible small subunits. In Arabidopsis, the large protein is encoded by a single gene, while three different genes encode the small subunit. By studying the substrate specificity and the expression patterns of the subunits, the authors found that the large subunit is involved in both leucine and glucosinolate metabolism, and the small subunits appear specific for each pathway. In particular, the small subunit 1 is involved in leucine biosynthesis and the small subunits 2 and 3 function in methionine-derived glucosinolate synthesis.

Besides their role as nutraceutical molecules, many non-proteinogenic amino acids are involved in the plant responses to environmental stresses, as confirmed by Song et al. for citrulline, an intermediate in the synthesis of arginine from ornithine. By transcriptomic and metabolomic analysis, the authors demonstrated that the rapid accumulation of citrulline and related metabolites in watermelon subjected to water stress is mediated by the synchronized activation of biosynthesis and suppression of catabolism. Additionally, they found that the nitrogen status of the plant regulates citrulline synthesis.

Polyamines in plants are generated either from arginine or ornithine. In the former route, arginine is decarboxylated to agmatine by arginine decarboxylase and then converted into putrescine by agmatine iminohydrolase and N-carbamoylputrescine amidohydrolase. In the latter route, arginine is hydrolyzed to ornithine by arginase and then decarboxylated by ornithine decarboxylase to putrescine. It was recently shown, however, that arginases from Arabidopsis and soybean can act also as agmatinases, providing a third route for putrescine synthesis (Patel et al., 2017). To shed light on the mechanism of this reaction, Sekula analyzed, by X-ray and small-angle X-ray scattering, the crystal structures of two arginases from *Arabidopsis thaliana* and *Medicago truncatula* and proposed a model to explain the dual binding properties of plant arginases.

Among the amino acids involved in stress defense, proline is especially important because it accumulates in most plant species in response to different stresses and is believed to contribute to stress tolerance. Proline accumulation largely depends on the transcriptional activation of δ^1-pyrroline-5-carboxylate synthetase (P5CS), the enzyme catalyzing the rate-limiting step of proline biosynthesis, which in most plants species is encoded by two paralogous genes. As reported by Sabbioni et al., the activity of P5CS2 in rice is additionally regulated by post-translational mechanisms to regulate proline synthesis in accordance with the redox and nitrogen status of the plant cell. In Arabidopsis, different expression patterns of the two P5CS isoforms indicate functions of P5CS1 in stress-induced proline accumulation and stress tolerance and of P5CS2 in proline synthesis for growth and development. Additionally, variable localization of the two isoforms in both the cytosol and plastids was reported (Székely et al., 2008). Funck et al., however, partly challenged these notions, finding that both P5CS1- and P5CS2-GFP fusion proteins were only present in the cytosol and that the contribution of both isoforms to stress tolerance was very low. Surprisingly, these authors found that p5cs2 mutants were more salt-tolerant than either p5cs1 mutants or wildtypes, despite a lower proline content. These results suggest a new function for P5CS2 in salt tolerance and reinforce the hypothesis that proline metabolism rather than proline itself is responsible for stress tolerance. A novel assay for the quantitation of L-proline was reported by Forlani and Funck. This assay is more specific than the widely used ninhydrin method (Bates et al., 1973). According to the authors, ninhydrin-based methods erroneously detect related molecules, such as ornithine, hydroxyproline, and D-proline, and lose linearity in the presence of high amino acid concentrations, resulting in overestimations of proline content. The method proposed by Forlani and Funck, based on the reverse reaction of P5C reductase (P5CR) at unphysiological pH of 10.5, can overcome the specificity limits of the conventional colorimetric methods while maintaining similar sensitivity.

Regardless of whether proline metabolism or proline accumulation confers stress tolerance, circumstantial evidence points to the importance of this amino acid in the reproductive stage and suggests that its accumulation may maintain productivity under stress conditions, as reported in Arabidopsis by Mattioli et al. and in barley by Frimpong et al. Based on previous work (Mattioli et al., 2018), Mattioli et al. confirmed the importance of proline accumulation in pollen grains to maintain seed production under salt stress, although the possibility to further improve grain yield by forcing proline synthesis in pollen grains remains unproven. With a completely different approach, Frimpong et al. analyzed five spring barley genotypes with

contrasting responses to drought, including two lines harboring a P5CS1 allele introgressed from a wild barley accession. They found a correlation between proline accumulation and water stress tolerance, particularly in spikes. The lines bearing the wild P5CS1 allele turned out to be the more drought-tolerant at the reproductive stage leading to improved grain yield under water stress. Intriguingly, the beneficial effects of proline under stress may also occur when proline is provided from the outside, as reviewed by El Moukhtari et al., who updated the current knowledge on this topic and proposed possible mechanisms of action. Although we still do not know how exogenous proline can improve salt stress tolerance in crops, this procedure is recognized as an effective method of improving stress tolerance in crops and regarded as of utmost biotechnological interest. A similar approach is reported by Alfosea-Simón et al., who investigated the use of external formulations made up of or enriched in different amino acids to improve plants' resilience to climate changes. By morphological, physiological, and metabolomic analyses, the authors studied the effects of exogenous applications of glutamate, aspartate, and alanine on tomato growth, and found a synergistic and positive effect of aspartic and glutamic acid and a negative effect of alanine.

Proline accumulation during stress relies on both stimulation of proline synthesis and inhibition of proline degradation. The former process is catalyzed in the cytosol by the sequential action of P5CS and P5CR, while the latter is catalyzed in mitochondria by the sequential action of proline dehydrogenase (ProDH) and pyrroline-5-carboxylate dehydrogenase (P5CDH). Because P5CS and ProDH catalyze the rate-limiting steps of proline synthesis and oxidation from and to glutamate, respectively, a careful determination of their activity levels is often used as a marker of proline accumulation. A common mistake in ProDH activity determination was disclosed by Lebreton et al., who showed that, at pH 10, ProDH does not catalyze the proline-dependent reduction of NAD^+. On the contrary, this activity was attributed to P5CR, which at high, non-physiological pH, is also able to work in the reverse direction.

In addition to proline, various other amino acids have been involved in stress tolerance, among which the branched-chain amino acids (BCAAs) have been recently proposed. Buffagni et al. investigated the role of BCAAs in two durum wheat cultivars with contrasting sensitivity to drought, performing a comparative bioinformatic and expression analysis of the genes coding for BCAA transferases (BCAAT), and investigating, through NMR analysis, the metabolic profile of the BCAAs. Overall, they showed that BCAAT genes are induced transcriptionally in early phases of the stress response, and the accumulation of BCAAs reflects the cultivars' drought tolerance, supporting the involvement of BCAAs in the drought defense response.

In plants, the aromatic amino acids (AAAs) are synthesized from chorismate, the final product of the shikimate pathway, and are precursors of a wide range of secondary metabolites. To investigate a possible role of AAAs in the resistance to biotic and abiotic stress, Oliva et al. generated transgenic tobacco plants overexpressing a feedback-insensitive version of AroG, a 3-deoxy-D-*arabino*-heptulosonate 7-phosphate synthase gene, encoding the first enzyme of the shikimate pathway. A metabolomic analysis confirmed that the leaves of the transgenic plants contained higher levels of phenylalanine, tyrosine, and tryptophan, as well as related metabolites compared to control plants. The transgenic plants gained some resistance to salt stress but not to oxidative or drought stress and strong resistance to infections with the plant parasite *Phelipanche aegyptica*, suggesting that increasing AAA levels in plants can be an effective strategy to combat plant parasites. The shikimate pathway, and thus the synthesis of AAAs, is the target of glyphosate, a herbicide used world-wide. In particular, glyphosate is a competitive inhibitor of the enzyme 5-*enol* pyruvyl-shikimate-3-phosphate synthase (EPSPS). Zulet-González et al. analyzed the fast-growing weed *Amaranthus palmeri*, some populations of which are glyphosate-tolerant because they overexpress EPSPS, to investigate the role of AAAs in the regulation of the shikimate pathway and glyphosate resistance. They found a complex interaction of glyphosate and AAAs in feedback-regulation of the shikimate pathway, which was altered by EPSPS overexpression. The mechanisms underlying this effect, however, remain unknown.

Regardless of the multiple functions of amino acids in plant development and stress defense, amino acids need nitrogen for their biosynthesis, and understanding how nitrogen is taken up, stored, and transported in plants is of utmost interest in amino acid biology. O'Neill and Lee describe a method to determine both the abundance and localization of free amino acids in plant tissues, which can be of great help to address these topics. The authors successfully used matrix-assisted laser desorption ionization (MALDI)- mass spectrometry imaging (MSI), coupled with coniferyl aldehyde derivatization, to study the uptake and distribution of amino acids in the maize root, proposing the use of MALDI-MSI as a valid method to study nitrogen assimilation, storage, and transportation in plants.

Because arginine has a high nitrogen-to-carbon ratio, plants tend to store nitrogen as arginine when nitrogen is abundant. Arginine accumulation is achieved by relieving feedback inhibition of the arginine biosynthesis gene N-acetylglutamate kinase (NAGK). This mechanism depends on the regulatory protein PII, which is able to sense the nitrogen and carbon status of the cell to optimize arginine biosynthetic activity. In a study from Llebrés et al. the structural and functional characteristics of the PII protein from maritime pine are presented, adding new information on the mechanisms of arginine metabolism regulation.

Ammonium is the primary source of inorganic nitrogen used for amino acid synthesis. Ammonium assimilation and recycling require the concerted activity of glutamine synthetase (GS), glutamate synthase (GOGAT), and glutamate dehydrogenase (GDH). While GS and GOGAT are the most important enzymes for the assimilation of organic molecules in plants, GDH participates in glutamate homeostasis and provides the TCA cycle with 2-oxoglutarate (2OG) when carbon availability is limiting. A structural study on GDH1 from *Arabidopsis thaliana*, is presented by Grzechowiak et al. who analyzed the crystal structure of AtGDH1, both in its apo form and when bound to its cofactor NAD^+ and the reaction product 2OG. The research revealed that the enzyme undergoes an open/closed

conformational change, which needs the binding of both NAD^+ and 2OG for its full activation. Most of the soil ammonium is taken up by the plant members of the high-affinity ammonium transporter (AMT) family, especially AMT1;1 and AMT1;2. Recent evidence (Xuan et al., 2016) showed that treatment with brassinosteroids (BRs) enhances the expression of AMT1;1 and AMT1;2 in rice with a mechanism yet to be understood. To investigate the relationships between AMTs and BRs, Yang et al. studied the levels of AMT expression and the AMT-dependent efficiency of ammonium uptake in rice lines with altered expression of BES1 and BZR1, two master regulators of BR signaling in plants. The authors' conclusions suggest that BR regulation of $NH4^+$ uptake in rice involves transcriptional regulation of ammonium transporters and that BR-dependent ammonium uptake is partially controlled by BZR1.

A class of transporters, namely USUALLY MULTIPLE ACIDS MOVE IN AND OUT TRANSPORTERS (UMAMITs), were recently identified as amino acid transporters (Ladwig et al., 2012). A specific function of amino acids to sense the nitrogen availability of the cell and share this information among different pathways to trigger appropriate metabolic responses was addressed by Besnard et al. They studied the overexpression of some UMAMIT genes in Arabidopsis to investigate possible links between amino acid transport and stress responses and found strong evidence that amino acid export activity is positively correlated with stress phenotypes and pathogen resistance, most likely due to the establishment of a constitutive salicylic acid-mediated stress response. The relationships between amino acids and hormonal pathways found by Besnard et al. and Yang et al. and the connections with key metabolic pathways reported by different authors of this collection, highlight the central role of amino acids in stress and development and pave the way to new and exciting discoveries in basic and applied plant science.

AUTHOR CONTRIBUTIONS

All authors listed have made a substantial, direct and intellectual contribution to the work, and approved it for publication.

FUNDING

MT acknowledges support from Sapienza University (Progetti Ateneo 2020), GF acknowledges support from the University of Ferrara (FAR 2021), SO acknowledges support from National Science Foundation (MCB 1052048, IOS 135336), RA acknowledges support from Tel Hai College and from Israel Science Foundation (1857/20).

ACKNOWLEDGMENTS

The Guest Editors are pleased to acknowledge all the authors who have contributed their articles to this Research Topic. We also express our gratitude to the reviewers, the editors, and the editorial office for their technical and scientific support.

REFERENCES

Bates, L. S., Waldren, R. P., and Teare, I. D. (1973). Rapid determination of free proline for water-stress studies. *Plant Soil* 39, 205–207. doi: 10.1007/BF00018060

Galili, G., Amir, A., and Fernie, A. (2016). The regulation of essential amino acid synthesis and accumulation in plants. *Annu. Rev. Plant Biol.* 67, 53–78. doi: 10.1146/annurev-arplant-043015-112213

Hou, Y., and Wu, G. (2018). Nutritionally essential amino acids. *Adv. Nutr.* 9, 849–851. doi: 10.1093/advances/nmy054

Ladwig, F., Stahl, M., Ludewig, U., Hirner, A. A., Hammes, U. Z., Stadler, R., et al. (2012). *Siliques Are Red1* from arabidopsis acts as a bidirectional amino acid transporter that is crucial for the amino acid homeostasis of siliques. *Plant Physiol.* 158, 1643–1655. doi: 10.1104/pp.111.192583

Mattioli, R., Biancucci, M., El Shall, A., Mosca, L., Costantino, P., Funck, D., et al. (2018). Proline synthesis in developing microspores is required for pollen development and fertility. *BMC Plant Biol.* 18:356. doi: 10.1186/s12870-018-1571-3

Patel, J., Ariyaratne, M., Ahmed, S., Ge, L., Phuntumart, V., Kalinoski, A., et al. (2017). Dual functioning of plant arginases provides a third route for putrescine synthesis. *Plant Sci.* 262, 62–73. doi: 10.1016/j.plantsci.2017.05.011

Székely, G., Ábrahám, E., Cséplo, Á., Rigó, G., and Zsigmond, L., Csiszár, J., et al. (2008), Duplicated P5CS genes of Arabidopsis play distinct roles in stress regulation and developmental control of proline biosynthesis. *Plant J.* 53, 11–28. doi: 10.1111/j.1365-313X.2007.03318.x

Xuan, H. X., Duan, F. Y., Je, B. I., Kim, C. M., Li, T. Y., Liu, J. M., et al. (2016). *Related to ABI3/VP1-like 1* (*RAVL1*) regulates brassinosteroid-mediated activation of AMT1;2 in rice (*Oryza sativa*). *J. Exp. Bot.* 68, 727–737. doi: 10.1093/jxb/erw442

Conflict of Interest: The authors declare that the research was conducted in the absence of any commercial or financial relationships that could be construed as a potential conflict of interest.

Publisher's Note: All claims expressed in this article are solely those of the authors and do not necessarily represent those of their affiliated organizations, or those of the publisher, the editors and the reviewers. Any product that may be evaluated in this article, or claim that may be made by its manufacturer, is not guaranteed or endorsed by the publisher.

Copyright © 2021 Trovato, Funck, Forlani, Okumoto and Amir. This is an open-access article distributed under the terms of the Creative Commons Attribution License (CC BY). The use, distribution or reproduction in other forums is permitted, provided the original author(s) and the copyright owner(s) are credited and that the original publication in this journal is cited, in accordance with accepted academic practice. No use, distribution or reproduction is permitted which does not comply with these terms.

frontiers in Plant Science

ORIGINAL RESEARCH
published: 29 April 2020
doi: 10.3389/fpls.2020.00459

Increased Glyphosate-Induced Gene Expression in the Shikimate Pathway Is Abolished in the Presence of Aromatic Amino Acids and Mimicked by Shikimate

*Ainhoa Zulet-González, Maria Barco-Antoñanzas, Miriam Gil-Monreal, Mercedes Royuela and Ana Zabalza**

Institute for Multidisciplinary Research in Applied Biology (IMAB), Universidad Pública de Navarra, Pamplona, Spain

OPEN ACCESS

Edited by:
Maurizio Trovato, Sapienza University of Rome, Italy

Reviewed by:
S. Caretto, Institute of Sciences of Food Production, Italian National Research Council, Italy
Ricardo Alcántara-de la Cruz, Federal University of São Carlos, Brazil

***Correspondence:**
Ana Zabalza
ana.zabalza@unavarra.es

Specialty section:
This article was submitted to Plant Metabolism and Chemodiversity, a section of the journal Frontiers in Plant Science

Received: *17 January 2020*
Accepted: *27 March 2020*
Published: *29 April 2020*

Citation:
Zulet-González A, Barco-Antoñanzas M, Gil-Monreal M, Royuela M and Zabalza A (2020) Increased Glyphosate-Induced Gene Expression in the Shikimate Pathway Is Abolished in the Presence of Aromatic Amino Acids and Mimicked by Shikimate. Front. Plant Sci. 11:459. doi: 10.3389/fpls.2020.00459

The herbicide glyphosate inhibits the plant enzyme 5-enolpyruvylshikimate-3-phosphate synthase (EPSPS) in the aromatic amino acid (AAA) biosynthetic pathway, also known as the shikimate pathway. *Amaranthus palmeri* is a fast-growing weed, and several populations have evolved resistance to glyphosate through increased *EPSPS* gene copy number. The main objective of this study was to elucidate the regulation of the shikimate pathway and determine whether the regulatory mechanisms of glyphosate-sensitive and glyphosate-resistant plants were different. Leaf disks of sensitive and resistant (due to *EPSPS* gene amplification) *A. palmeri* plants were incubated for 24 h with glyphosate, AAA, glyphosate + AAA, or several intermediates of the pathway: shikimate, quinate, chorismate and anthranilate. In the sensitive population, glyphosate induced shikimate accumulation and induced the gene expression of the shikimate pathway. While AAA alone did not elicit any change, AAA applied with glyphosate abolished the effects of the herbicide on gene expression. It was not possible to fully mimic the effect of glyphosate by incubation with any of the intermediates, but shikimate was the intermediate that induced the highest increase (three-fold) in the expression level of the genes of the shikimate pathway of the sensitive population. These results suggest that, in this population, the lack of end products (AAA) of the shikimate pathway and shikimate accumulation would be the signals inducing gene expression in the AAA pathway after glyphosate application. In general, the effects on gene expression detected after the application of the intermediates were more severe in the sensitive population than in the resistant population. These results suggest that when *EPSPS* is overexpressed, as in the resistant population, the regulatory mechanisms of the AAA pathway are disrupted or buffered. The mechanisms underlying this behavior remain to be elucidated.

Keywords: ***Amaranthus palmeri*, aromatic amino acids, shikimate, quinate, chorismate, anthranilate, glyphosate**

INTRODUCTION

Besides to their function in protein synthesis, aromatic amino acids (AAA) serve as precursors of a wide variety of natural products that play crucial roles in plant signaling, growth and development, including responses to biotic and abiotic stresses (Zeier, 2013; Häusler et al., 2014), such as a wide range of secondary metabolites (Herrmann, 1995; Less et al., 2010). These amino acids are essential

compounds in the diets of humans and monogastric livestock, which are unable to synthesize them (Galili and Hofgen, 2002; Tzin and Galili, 2010).

The AAA biosynthetic pathway, also known as the shikimate pathway, is located in plastids and can be subdivided into two steps: the prechorismate pathway and the postchorismate pathway, which via two different routes can lead from chorismate to the synthesis of Phe and Tyr or Trp (Maeda and Dudareva, 2012; Tohge et al., 2013). The prechorismate pathway consists of seven enzymatic reactions that act sequentially: D-arabino-heptulosonate 7-phosphate synthase (DAHPS), dehydroquinate synthase (DHQS), 3-dehydroquinate dehydratase-shikimate dehydrogenase (DQSD), shikimate kinase (SK), 5-enolpyruvylshikimate-3-phosphate synthase (EPSPS) and chorismate synthase (CS) (Herrmann, 1995; Dev et al., 2012). Chorismate can be used as a substrate at the first step of the postchorismate pathway by two different branches. The synthesis of Trp from chorismate is performed via six enzymatic reactions, and its first step is mediated by the anthranilate synthase (AS). The other branch, leading to Tyr or Phe biosynthesis, is mediated in its first step by the chorismate mutase (CM) for prephenate biosynthesis. After prephenate, the synthesis of Tyr or Phe may occur via two alternative pathways: the arogenate pathway, where the arogenate dehydratase (ADH) is located, and the phenylpyruvate/4-hydroxyphenylpyruvate pathway (Maeda et al., 2010). The shikimate pathway also presents lateral branches synthesizing secondary metabolites, such as quinate (Herrmann, 1995; Boudet, 2012). A scheme of the shikimate pathway is shown in **Supplementary Figure 1**.

As sessile organisms, plants should regulate and adjust their metabolism to dynamic changes. These changes can be at the level of amino acid metabolic networks (Less and Galili, 2009), or at the level of each biosynthetic pathway. The carbon flux through the shikimate pathway is regulated at the transcriptional (Bentley and Haslam, 1990; Maeda and Dudareva, 2012), posttranscriptional and posttranslational levels. In plants, the expression of genes seems to be closely regulated, often by the same transcription factors, such as MYB, ODO1 and EOBII (Takatsuji et al., 1992; Bender and Fink, 1998; Verdonk, 2005; Spitzer-Rimon et al., 2010).

The major factors limiting the production of essential amino acids in plants are the regulatory factors that control their synthesis by feedback inhibition loops and their efficient catabolism (Galili et al., 2016). In plants, how the carbon flux into the shikimate pathway is specifically regulated is ambiguous (Maeda and Dudareva, 2012). The entrance of carbon through this pathway is mediated by the DAHPS enzyme. While it has been described that the expression of the DAHPS is regulated in response to cellular levels of AAA in microbes (Aharoni and Galili, 2011), there is limited information about its regulation in plants. Studies with transgenic plants containing bacterial feedback-insensitive DAHPS show that this enzyme is key in the shikimate pathway and secondary metabolism derived from AAA (Tzin et al., 2012; Oliva et al., 2015). The bifurcation of the pathway toward Trp and Phe/Tyr pathways is controlled by AS and CM enzymes, as both enzymes are feedback-inhibited by the AAA of their corresponding pathways (Romero et al., 1995; Bohlmann et al., 1996). Moreover, Trp also activates CM activity to redirect flux from Trp to Phe/Tyr biosynthesis (Benesova and Bode, 1992; Lopez-Nieves et al., 2017), while Tyr activates arogenate dehydratase to redirect the flux from Tyr to Phe biosynthesis (Siehl and Conn, 1988).

The EPSPS is the target of glyphosate (Steinrücken and Amrhein, 1980), the most commonly used herbicide worldwide, which makes the study of this enzyme and shikimate interesting from an agronomic perspective. EPSPS has been studied extensively in plants, although the significance of EPSPS activity in the synthesis of AAA has still not been sufficiently addressed (Aharoni and Galili, 2011).

The repeated use of glyphosate selects for the corresponding resistance in weed populations, and one of the most problematic weed species resistant to glyphosate is *Amaranthus palmeri* S. Wats (Powles and Yu, 2010). *EPSPS* gene amplification is the main mechanism conferring glyphosate resistance in this species (Gaines et al., 2010; Chandi et al., 2012; Vila-Aiub et al., 2014). When this gene is overexpressed, the EPSPS enzyme accumulates such that the recommended field dose of glyphosate is not sufficient to inhibit EPSPS activity, and consequently, the plants survive. Although glyphosate induce upregulation of the genes of the shikimate pathway in both glyphosate-sensitive and glyphosate-resistant populations (Fernández-Escalada et al., 2017, 2019), it is not clear how glyphosate affects shikimate pathway regulation.

Despite the significance of the AAA and the herbicide glyphosate accounting for the major motivation to clarify the regulation of the shikimate pathway, it has not been completely elucidated to date. The regulatory mechanisms underlying the response of the pathway and the specific role of the intermediates or final products (AAA) have not been thoroughly investigated. Moreover, the use of a *A. palmeri* population with *EPSPS* gene amplification offers the opportunity to study if the regulation of the shikimate pathway is affected by the overexpression of one of its enzymes due to extra *EPSPS* copies.

The aim of this study was to evaluate the role of AAA and its intermediates in the regulation of the shikimate pathway. This evaluation was performed by analyzing whether AAA could revert the effects of glyphosate on the pathway and if the supply of intermediates of the pathway could mimic the glyphosate effects using *A. palmeri* glyphosate-sensitive (GS) and glyphosate-resistant (GR) plants. Finally, the shikimate content, relative gene expression level and protein content of the shikimate pathway were assessed in presence of glyphosate, intermediates and final products of the AAA biosynthetic pathway in leaf disks of GS and GR *A. palmeri* plants.

MATERIALS AND METHODS

Plant Material

Amaranthus palmeri GS and GR biotypes were originally collected from North Carolina (United States) (Chandi et al., 2012; Fernández-Escalada et al., 2016). The resistance mechanism

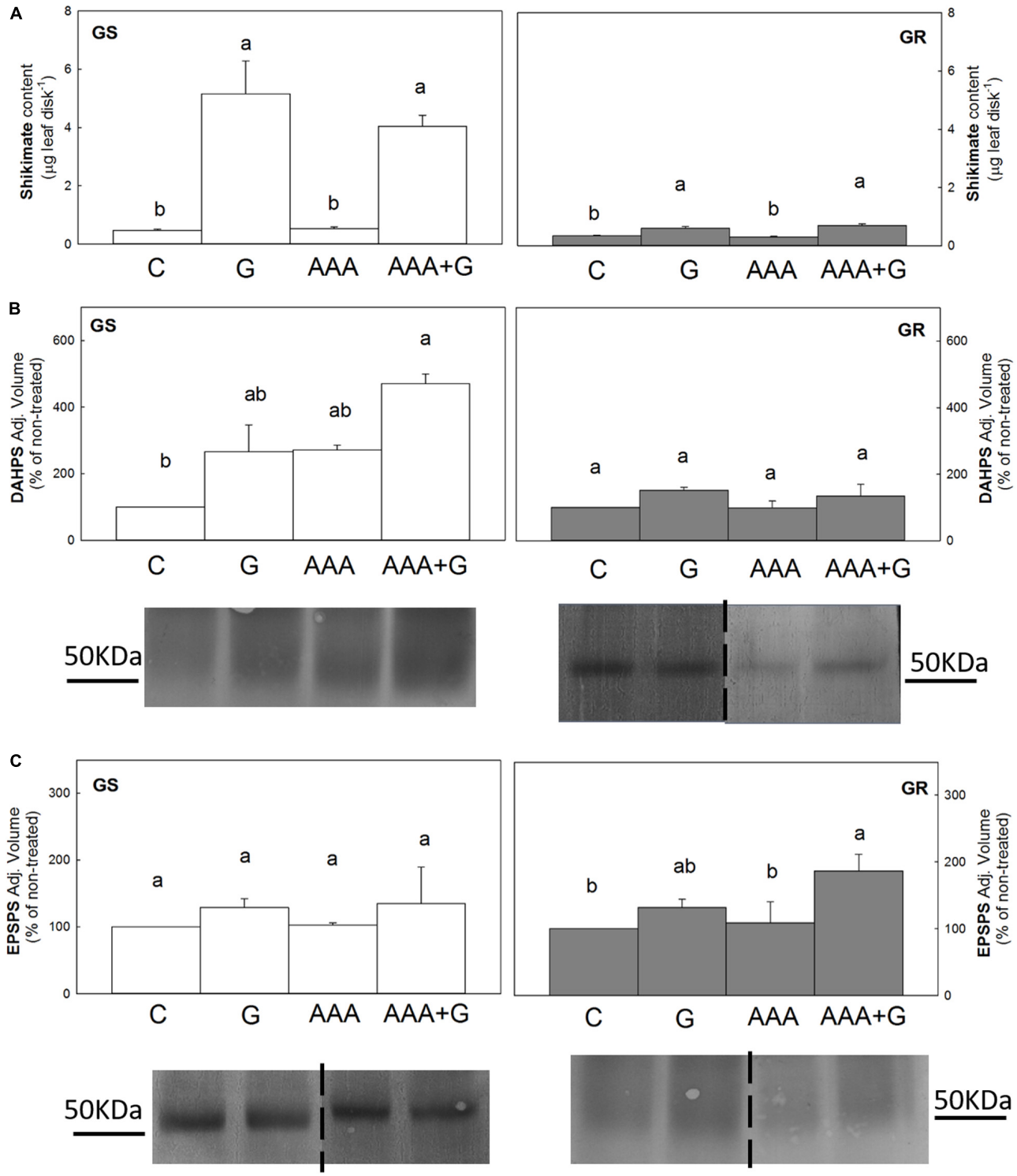

FIGURE 1 | Leaf disks of glyphosate-sensitive (white bars, left; GS) and glyphosate-resistant (gray bars, right; GR) *Amaranthus palmeri* populations were incubated for 24 h with water (C), aromatic amino acids (AAA), glyphosate (G) or the combination of aromatic amino acids and glyphosate (AAA+G) (Mean ± SE). Different letters indicate differences between treatments in each population (p-value $\leq$0.05, Tukey). **(A)** Shikimate content (n = 10). **(B)** and **(C)** 3-deoxy-D-arabino-heptulosonate-7-phosphate-synthase (DAHPS) and 5-enolpyruvylshikimate 3-phosphate synthase (EPSPS) protein contents. Analyses of band intensity on blots are presented in graphs as the relative ratio of the control (n = 3). Control is arbitrarily presented as 100% of the Adjusted volume (Relative density * mm^2). For each protein, one representative blot is shown. Original blots are shown in **Supplementary Figures 3 4**. Lanes contained 40 µg of total soluble proteins for DAHPS immunoblotting and, in the case of EPSPS, 80 µg of total soluble proteins for GS and 15 µg for GR.

of the GR biotype was described to be *EPSPS* gene amplification (Chandi et al., 2012), with 47.5 more gene copies in GR plants than in GS plants (Fernández-Escalada et al., 2016). Seeds were surface-sterilized and germinated. The seeds were then transferred to 2.7-L tanks in a phytotron and grown in aerated hydroponic culture under controlled conditions, as described previously (Fernández-Escalada et al., 2016).

Before performing the incubation, a leaf of each plant of the A. *palmeri* GR population was harvested and immediately frozen in liquid nitrogen to determine the *EPSPS* relative genomic copy number of those individuals. After evaluating the results, 30 out of 48 evaluated plants were selected to obtain a homogeneous population with a similar relative *EPSPS* genomic copy number (between 60 and 100) to perform the experiments.

Leaf Disk Incubation

When the GS and selected GR plants were 21 days old, leaf disks were excised from the leaves using a Harris Uni-Core puncher (4-mm diameter) (Healthcore, Bucks, United States), avoiding the leaf nerves. From each plant, the two youngest fully expanded leaves were used: one leaf to determine the shikimate content and another leaf to determine transcript levels and enzyme content measurements.

The same treatments and doses were applied in both populations (**Table 1**). Leaf disks were incubated for 24 h under continuous light (300 μmol m^{-2} s^{-1} photosynthetic photon flux) at 24°C. Solutions were freshly prepared, and the pH was adjusted to 7.0 with NaOH in all the treatments. Technical glyphosate (glyphosate, isopropylamine salt, 61%; Dr. Ehrenstorfer GmbH, Augsburg, Germany) was used. All other reagents were purchased from Sigma–Aldrich Chemical, Co. (St. Louis, MO, United States).

The incubation system is shown in **Supplementary Figure 2**. For shikimate content determination, individual disks were placed in individual wells of a 96-well microtiter plate containing 100 μL of treatment solutions. To obtain one disk per treatment from the same plant, as many disks as treatments were obtained from the youngest leaf of the plant. For enzyme content and transcript level determinations, 25 or 45 disks were placed, respectively, in the wells of 6-well microplates containing 2.5 mL of each treatment. In each well, disks from different leaves were incubated, but the same proportion of original plants was maintained in all treatments tested. In both incubation options, each well was considered a biological replicate.

After incubation, disks incubated in 96-well plants were washed thoroughly before freezing, and the plates were placed in a freezer (−20°C). Disks incubated in 6-well microplates were removed from the incubating medium, immediately frozen in liquid nitrogen and stored at −80°C. The experiment was repeated twice.

TABLE 1 | Treatments applied to glyphosate-sensitive and glyphosate-resistant *Amaranthus palmeri* leaf disks.

Identification	Treatment	Dose
C	Control	
G	Glyphosate	1.75 g a.e. L^{-1}
S	Shikimate	20 mM
Q	Quinate	50 mM
Ch	Chorismate	1 mM
At	Anthranilate	1 mM
AAA	Aromatic amino acids	10 μM (each AAA)
AAA+G	Aromatic amino acids + Glyphosate	10 μM + 1.75 g a.e. L^{-1}

a.e. = acid equivalents.

Analytical Determinations

Shikimate Determination

The concentration of shikimate in each leaf disk located in each cell was measured according to the procedure described previously (Fernández-Escalada et al., 2016). Briefly, shikimate was extracted from the frozen-thawed leaf disks by adding 25 μL of 1.25 N HCl and incubating the plates at 60°C for 15 min. The concentration of shikimate in each cell was measured spectrophotometrically after the addition of 0.25% periodic acid/0.25% metaperiodate and 0.6 M sodium hydroxide/0.22 M sodium sulfite (Cromartie and Polge, 2000).

EPSPS and DAHPS Immunoblotting

Protein extraction was performed using 0.1 g of ground leaf tissue in 0.2 mL of extraction buffer (100 mM MOPS, 5 mM EDTA, 1% Triton-X 100, 10% glycerin, 50 mM KCl, 1 mM benzamidine, 100 mM iodoacetamide, 5% PVP and 1 mM PMSF). Proteins were separated by 12.5% SDS-PAGE and immunoblots were produced according to standard techniques. The protein amount loaded per well for each antibody used is specified in the figure legends. EPSPS and DAHPS antibody dilutions were 1:2000 and 1:1000, respectively (Fernández-Escalada et al., 2017). Bands were identified using a BCIP/NBT kit which was Amplified alkaline phosphatase immunoblot assay kit (BIORAD 170, BIORAD Laboratories, Inc., Hercules, CA, United States). Immunoblots were scanned using a GS-800 densitometer, and protein bands were quantified using Quantity One software (BIORAD Laboratories, Inc., Hercules, CA, United States).

Quantitative Reverse Transcription-PCR

The relative transcript level was measured for 11 genes of the AAA biosynthesis pathway. RNA extraction and the subsequent cDNA were performed as described in Fernández-Escalada et al. (2017). As *A. palmeri* was not sequenced, primers were designed using a related sequenced species of the Amaranthaceous family and crossed with *Arabidopsis thaliana*. Most primers were used previously (Fernández-Escalada et al., 2017). The primers for the two isoenzymes of CM (plastidics 1–3 and cytosolic 2) and the two isoforms of ADH (ADHα and ADHβ) were designed in this study. The optimal annealing temperature for each primer was determined using gradient PCR. All primers and annealing temperatures are listed in **Supplementary Table 1**. Melting curve analysis was conducted to verify amplification of single PCR products. Gene expression was monitored in

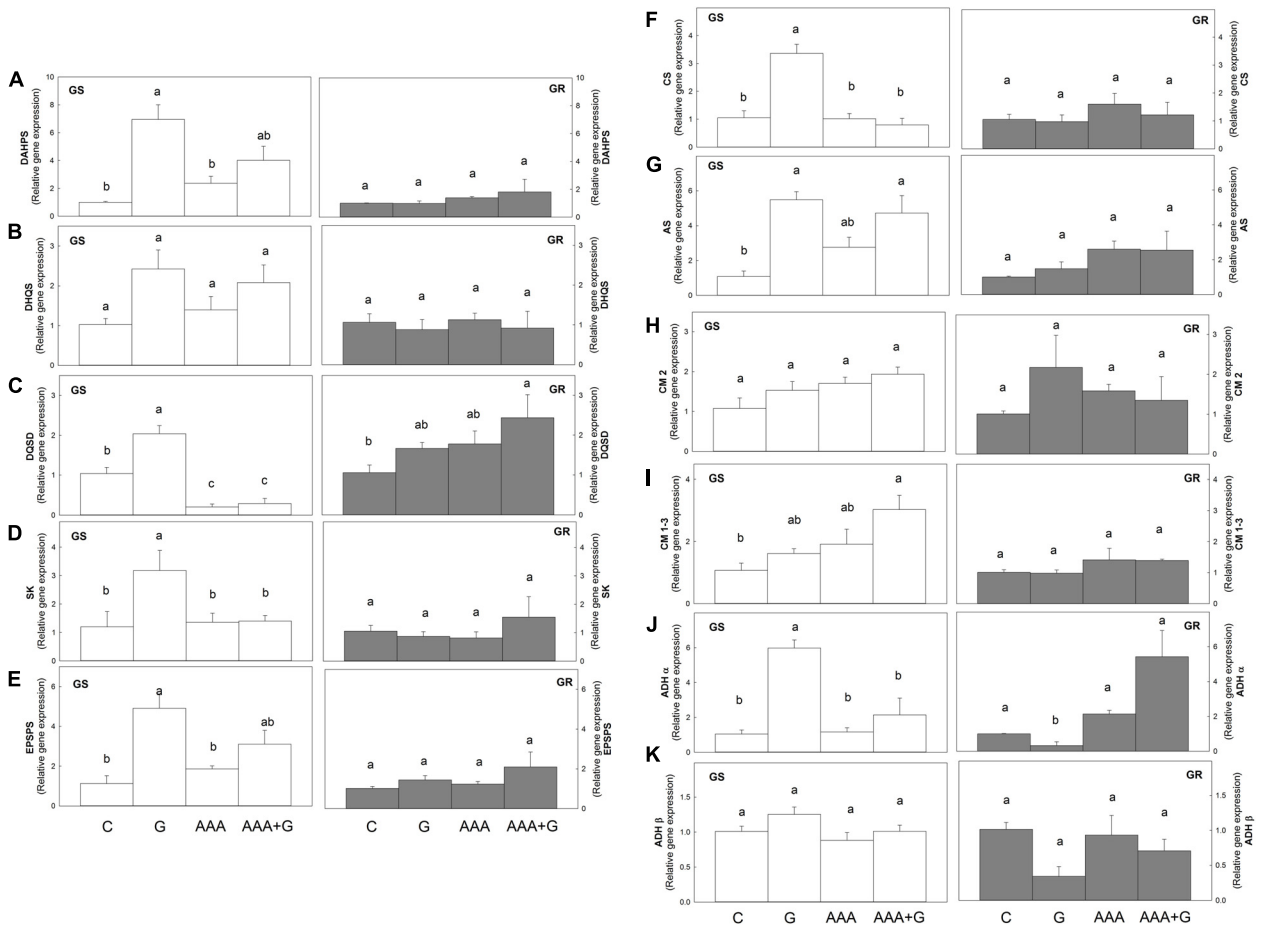

FIGURE 2 | Transcript abundance of genes in the shikimate pathway was measured in *Amaranthus palmeri* leaf disks. Glyphosate-sensitive (white bars, left; GS) and glyphosate-resistant (gray bars, right; GR) populations were incubated for 24 h with water (Control, C), aromatic amino acids (AAA), glyphosate (G) or the combination of aromatic amino acids and glyphosate (AAA+G). Relative transcript abundance was normalized using the normalization gene β tubulin and each population to its own control. **(A)** 3-Deoxy-d-arabino-heptulosonate-7-phosphate synthase (*DAHPS*) **(B)** dehydroquinate synthase (*DHQS*). **(C)** 3-dehydroquinate dehydratase/shikimate dehydrogenase (*DQSD*). **(D)** Shikimate kinase (*SK*). **(E)** 5-enolpyruvylshikimate 3-phosphate synthase (*EPSPS*). **(F)** Chorismate synthase (CS). **(G)** Anthranilate synthase (*AS*). **(H)** Chorismate mutase isoform 2 (*CM2*). **(I)** Chorismate mutase isoforms 1 and 3 (*CM 1-3*). **(J)** Arogenate dehydrogenase isoform α (*ADHα*). **(K)** Arogenate dehydrogenase isoform β (*ADH*β) (Mean ± SE; $n = 4$). Different letters indicate differences between treatments in each population (p-value ≤0.05, Tukey).

four biological replicates. The relative transcript level was calculated using the 2-ΔΔCt method (Livak and Schmittgen, 2001). Relative transcript abundance was normalized using the normalization gene β-tubulin and each population to its own control.

Statistical Analysis

Analysis was performed using 10 biological replicates for shikimate content determination and three or four biological replicates for enzyme content or nucleic acid determination, respectively. Replicates from both experiments were used. In the study of glyphosate and AAAs, differences between treatments for each population were evaluated by one-way ANOVA with a multiple-comparison adjustment (Tukey) at $p \leq 0.05$. In the study using the intermediates, the difference between each parameter of untreated disks and disks of each treatment was evaluated using Student's t-test ($p \leq 0.05$). Statistical analyses were performed using IBM SPSS statistics 24.0 (IBM, Corp., Armonk, NY, United States).

RESULTS AND DISCUSSION

Possible Pathway Regulation by Aromatic Amino Acids. Could AAA Revert the Changes Induced in the Pathway by Glyphosate?

Shikimate content was low and similar (0.4 μg shikimate leaf disk^{-1}) among untreated plants in both populations (**Figure 1A**). After glyphosate treatment, the shikimate content increased 11-fold in the GS population and 1.7-fold in the GR population. AAA applied alone did not modify the shikimate content in any

of the populations, and when they were applied in combination with glyphosate (AAA+G treatment), the shikimate content was similar that accumulated by the herbicide-alone treatment (around 5 or 0.6 μg shikimate leaf disk^{-1} in GS and in GR, respectively).

DAHPS and EPSPS enzymes were determined by immunoblotting of (40 μg of total soluble proteins for DAHPS and, 80 μg or 15 μg for EPSPS for GS GR, respectively) (**Figure 1**). In relation to the untreated control, the content of these enzymes was no altered by glyphosate or AAA treatments applied alone in any of the populations. The incubation with the combination of both compounds provoked different responses depending on the population. In the GS population, the combined treatment provoked a 4.7-fold increase in DAHPS content relative to the untreated plants, but did not modify the content of EPSPS enzyme. In contrast, in the GR population, DAHPS content was not affected by this treatment, but a two-fold increase in EPSPS was observed.

In the GS population, glyphosate produced an increase (of more than two-fold in all cases) in the relative expression level of all the genes of the prechorismate part of the AAA biosynthetic pathway (*DAHPS, DHQS, DQSD, SK, EPSPS*, and *CS*) and only an increase of *ADH*α transcript level in the postchorismate pathway (*AS, CM2, CM1-3, ADH*α, and *ADH*β). In contrast, in the GR population, glyphosate did not induce the relative expression level of these genes in this pathway (**Figure 2**).

The only effect detected after AAA treatment was a five-fold decrease in the *DQSD* relative mRNA level to control plants in GS plants (**Figure 2**), and no effects were observed in the GR population. When AAA was applied in combination with glyphosate (AAA+G), a different response was observed in both populations. On the one hand, the GR population did not show changes in gene expression, with the exception of de *DQSD* gene that presented an increase of 2.3 times compared to the control (**Figure 2**). On the other hand, the presence of AAA in the combined treatment reversed the increase in transcript levels of the shikimate pathway detected after the herbicide alone in the GS population, as in this treatment, the effect of glyphosate on *DQSD, SK, CS*, or *ADH*α expression seemed to be abolished by the presence of AAA (**Figure 2**) and the relative mRNA level was not higher than control plants (**Figure 2**).

With leaf disk incubation, it was possible to reproduce the same physiological effects of glyphosate observed on whole plants. On the one hand, shikimate is a known marker of glyphosate activity (Dyer et al., 1988; Baerson et al., 2002; Zhu et al., 2008; Dillon et al., 2017), and it accumulated more in the GS than in the GR population. On the other hand, glyphosate upregulated the genes participating in the prechorismate pathway in the GS population (**Figure 2**), as previously described in this population (Fernández-Escalada et al., 2017) and in other species (Baerson et al., 2002; Garg et al., 2014). These results validate the incubation system used in this study to approach the regulation of the shikimate pathway by final products and intermediates.

In both populations, the accumulation of shikimate was similar in the two treatments with glyphosate, regardless of the presence of AAA (**Figure 1A**), suggesting that shikimate accumulation would be directly related to EPSPS inhibition and not to other physiological changes caused by the effect of the herbicide, such as a potential transitory modification of AAA content.

An increase in DAHPS or EPSPS enzyme content was not detected after incubation with glyphosate (**Figure 1B,C**), contrary to previous reports (Pinto et al., 1988; Gaines et al., 2010, 2011; Fernández-Escalada et al., 2017), which may be related to the short incubation period or the low dose applied. In previous experiments in which an increase in DAHPS and EPSPS content was observed, the time of treatment was 48 or 72 h (Baerson et al., 2002; Fernández-Escalada et al., 2017).

In microbes, it has been widely described that DAHPS activity is regulated in response to cellular levels of AAA (Herrmann, 1995; Tzin and Galili, 2010). However, most of the studies performed in plants suggest that DAHPS is not regulated by AAA, and only a few reports have described a regulatory effect of AAA levels on this enzyme activity *in vitro* (Graziana and Boudet, 1980; Suzich et al., 1985). Similarly, AAA treatment alone did not modify DAHPS content in this experiment (**Figure 1**). Indeed, the application of AAA and glyphosate together induced an increase in the DAHPS content in the GS population, supporting that in plants, the DAHPS content is not regulated by AAA levels, as it was not downregulated when AAA were externally supplied.

It has been suggested that a reduced level of AAA may act as a signal to induce the expression of the shikimate pathway and restore carbon flux through the pathway in plants (Maeda and Dudareva, 2012). In concordance with this hypothesis, a decrease in the relative expression level after the exogenous supply of AAA could have been expected. Nevertheless, this decrease did not occur, as no changes in the relative expression level were detected in the GS or GR population after AAA supply with the exception of the bifunctional enzyme *DQSD* (**Figure 2**). Similar to the results obtained in this study, the effect of the increase in Phe and Tyr in Arabidopsis transgenic plants on the transcriptome was low (Dubouzet et al., 2007; Tzin et al., 2009; Less et al., 2010).

The reversion of glyphosate effects on growth with exogenous AAA has been previously shown in fungi, bacteria and higher plant cell cultures (Jaworski, 1972; Gresshoff, 1979; Amrhein et al., 1983), while in higher plants, the reversion of the effect on growth effect has been detected in Arabidopsis (Gresshoff, 1979) but not in other plant species (Duke and Hoagland, 1978; Cole et al., 1980; Duke et al., 1980). Nevertheless, reversion of the physiological effects induced by glyphosate, such as anthocyanin (Hollander and Amrhein, 1980) and protein (Tymonko and Foy, 1978) synthesis, has been reported in several plant species. Similarly, in this study, supplemental AAA completely prevented one physiological effect of glyphosate: the upregulation of shikimate pathway genes.

It appears that in the GS population, the increase in gene expression of the enzymes in the shikimate pathway after glyphosate might be mediated by a transitory lack of AAA, as the exogenous supply of AAA can abolish the gene upregulation. This finding might appear contradictory to previous studies in which reduction of AAA was proposed to not elicit the increased expression of AAA pathway genes because the AAA concentrations increase with glyphosate dose (Vivancos et al., 2011; Maroli et al., 2015; Fernández-Escalada et al., 2017). In the

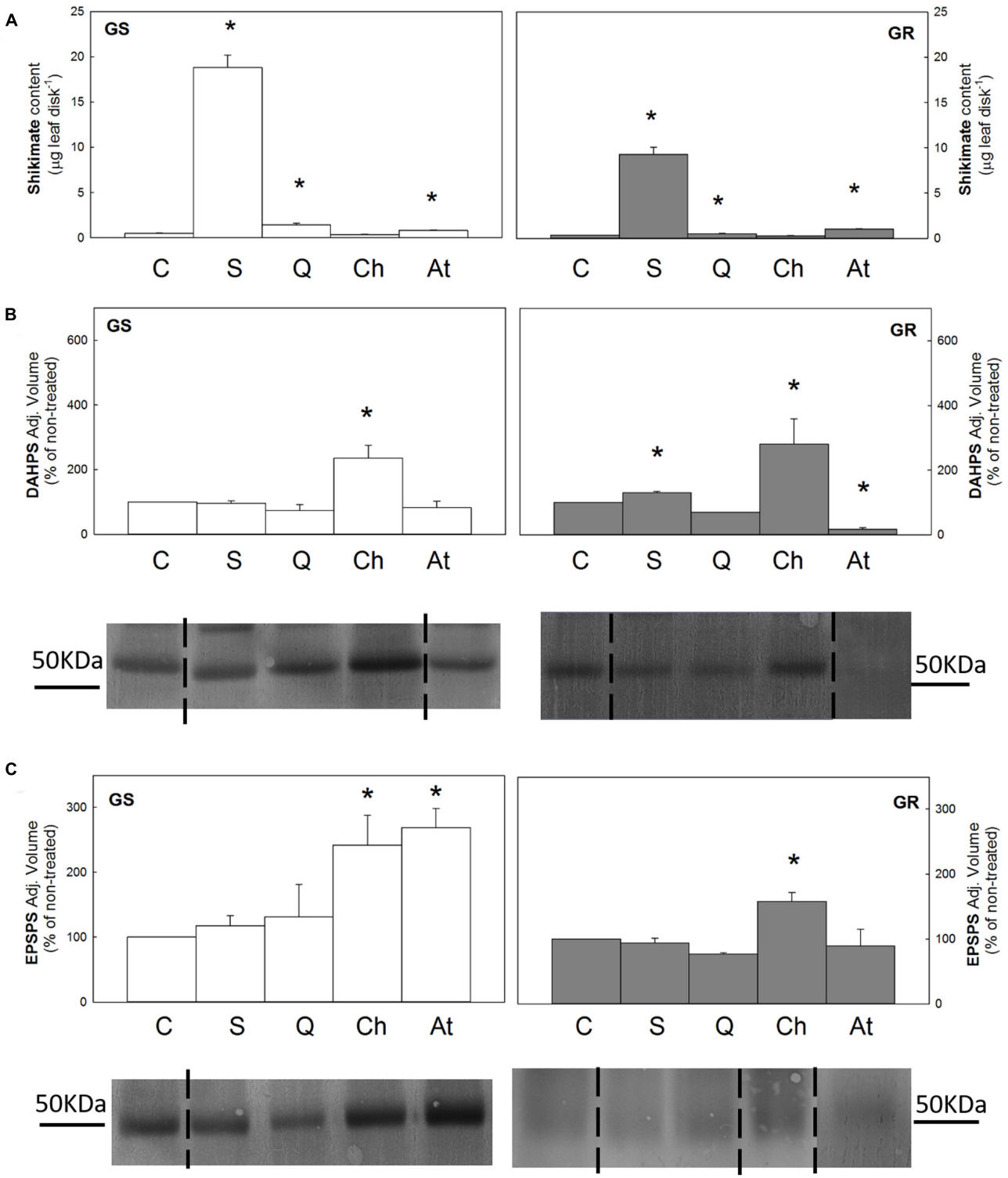

FIGURE 3 | Leaf disks of glyphosate-sensitive (white bars, left; GS) and glyphosate-resistant (gray bar, right; GR) *Amaranthus palmeri* populations were incubated for 24 h with water (C), shikimate (S), quinate (Q), chorismate (Ch) or anthranilate (At) (Mean ± SE). *Symbol indicates differences between control and treatment in each population (p-value $\leq$0.05). **(A)** Shikimate content (n = 10). **(B)** and **(C)** 3-deoxy-D-arabino-heptulosonate-7-phosphate-synthase (DAHPS) and 5-enolpyruvylshikimate 3-phosphate synthase (EPSPS) protein contents. Analyses of band intensity on blots are presented in graphs as the relative ratio of the control (n = 3). Control is arbitrarily presented as 100% of the Adjusted volume (Relative density * mm^2). For each protein, one representative blot is shown. Original blots are shown in **Supplementary Figures 2, 4** Lanes contained 40 µg of total soluble proteins for DAHPS immunoblotting and, in the case of EPSPS, 80 µg of total soluble proteins for GS and 15 µg for GR.

same way, the previously reported DAHPS and EPSPS increases after glyphosate (Pinto et al., 1988; Fernández-Escalada et al., 2016) were not detected. Nevertheless, these results might be explained by the short incubation time used in this study: 24 h compared to 3 days. Indeed, previous studies have shown that in glyphosate-treated pea roots the relative content of AAA was transitorily decreased for 24 h and abolished after 3 days of treatment (Orcaray et al., 2010). The reversion effect of AAA on the upregulation of expression genes of the shikimate pathway enzymes indicated that at least in the 24 h following application of treatment, the effect was mediated by a lack of the end products of the pathway.

Shikimate Pathway Regulation by Intermediates of the Pathway

Shikimate content was determined after incubation with the intermediates, and the pattern observed in both populations was similar (**Figure 3A**). Shikimate content increased in leaf disks after incubation with shikimate (40 times and 27 times in relation to the untreated control in the GS and GR populations, respectively), confirming that the compound was absorbed (**Figure 3A**). Shikimate content also increased after quinate treatment also (3 times in GS and 1.4 times in GR). These results showed that both in shikimate and quinate treatments, the increase observed in GS population was two times the increase observed in the GR population. Interestingly, anthranilate induced an increase in shikimate content in both populations, similar to the increase detected after quinate incubation.

DAHPS and EPSPS contents were determined after disk incubation in both populations (**Figure 3**). The incubation with shikimate and quinate did not induce any changes in the content of these enzymes in relation to the control disks in any population. Incubation with anthranilate elicited different responses, depending on the population and on the specific enzyme: a 2.7-fold increase in EPSPS content in GS and a 5.8-fold decrease in DAHPS expression in the GR population. Interestingly, chorismate was the only intermediate that induced a general increase in both enzymes and in both populations (DAHPS was increased 2.4 and 2.8 times and EPSPS 1.6 and 2.4 times, in GS and GR, respectively).

The incubation with shikimate induced the upregulation of more than half of the genes of the AAA pathway in the GS population (*DHQS, CS, AS, CM2, ADH*α, and *ADH*β), with the post-chorismate part being the more affected. Interestingly, this pattern was not observed in the GR population, where only *DQSD* and the *ADH*α isoform increased their relative mRNA levels after shikimate (**Table 2**).

In the GS population, quinate treatment also increased the relative expression level in five out of the genes, although the level of increase was milder than that detected after shikimate, as the medium relative increase detected after shikimate was 3 times and 2.28 times after quinate (**Table 2**). In the GR population, four genes of the pathway (*DAHPS, DQSD, EPSPS*, and *ADH*α*)* were upregulated after quinate incubation. The incorporation of quinate in the shikimate pathway can occur through two different pathways: through the reversible quinate dehydrogenase to 3-dehydroquinate and through the quinate hydrolyase to shikimate (Ossipov et al., 2000). The 2.6-fold reduction in the relative gene expression in the *DQSD* gene complex in the GS population after quinate would be related to the main incorporation of quinate into the pathway after DQSD, and the increase in the flux only at that point would act as a signal to reduce the relative gene expression of the enzyme to regulate the pathway. The increase in the relative transcript level of one of the isoforms of *CM* (3.6-fold) and *ADH* (1.6-fold) genes in GS and *ADH* (9.4-fold) in GR after quinate would confirm that quinate would direct the flux to the synthesis of Tyr and Phe, as has been described recently (Zulet-González et al., 2019).

The incubation with chorismate did not alter the transcription level of *DAHPS, DQSD, SK, EPSPS, CM2, CM1-3, ADH*α,

TABLE 2 | Transcript abundance of genes in the aromatic amino acid (AAA) biosynthetic pathway.

	Glyphosate-Sensitive (GS)			
	Shikimate	**Quinate**	**Chorismate**	**Anthranilate**
DAHPS	1.13 ± 0.02	1.57 ± 0.40	2.59 ± 0.55	0.63 ± 0.04
DHQS	2.46 ± 0.08*	1.92 ± 0.11*	1.91 ± 0.30*	1.23 ± 0.21
DQSD	1.06 ± 0.20	0.39 ± 0.04*	0.71 ± 0.08	0.87 ± 0.18
SK	1.85 ± 0.48	2.01 ± 0.35	1.49 ± 0.22	1.02 ± 0.18
EPSPS	2.51 ± 0.41	1.26 ± 0.30	0.91 ± 0.10	0.90 ± 0.18
CS	3.43 ± 0.74*	1.58 ± 0.14*	1.34 ± 0.10*	0.94 ± 0.12
AS	5.22 ± 0.11*	2.67 ± 0.22*	4.36 ± 0.79*	1.25 ± 0.16
CM2	2.08 ± 0.39*	3.60 ± 0.52*	1.26 ± 0.14	1.58 ± 0.31
CM1-3	1.62 ± 0.22	0.68 ± 0.10	0.91 ± 0.04	0.70 ± 0.05*
*ADH*α	3.56 ± 0.85*	1.68 ± 0.31	2.03 ± 0.34	0.66 ± 0.06*
*ADH*β	1.31 ± 0.06*	1.63 ± 0.17*	1.04 ± 0.04	0.93 ± 0.28
	Glyphosate-Resistant (GR)			
	Shikimate	**Quinate**	**Chorismate**	**Anthranilate**
DAHPS	1.06 ± 0.36	1.96 ± 0.38*	1.34 ± 0.32	0.57 ± 0.39
DHQS	0.53 ± 0.10	1.29 ± 0.41	0.93 ± 0.14	1.61 ± 0.18
DQSD	2.49 ± 0.29*	3.60 ± 0.75*	2.55 ± 0.59	1.10 ± 0.55
SK	0.88 ± 0.08	1.25 ± 0.32	1.14 ± 0.25	1.75 ± 0.19*
EPSPS	1.33 ± 0.14	2.55 ± 0.33*	1.59 ± 0.15	2.07 ± 0.52
CS	0.70 ± 0.17	1.51 ± 0.43	1.33 ± 0.16	0.58 ± 0.10
AS	0.79 ± 0.14	3.95 ± 1.16	3.82 ± 0.76	2.89 ± 0.53
CM2	1.49 ± 0.20	4.05 ± 1.02	1.51 ± 0.29	0.75 ± 0.24
CM1-3	1.00 ± 0.32	1.29 ± 0.36	0.78 ± 0.06	0.41 ± 0.06
*ADH*α	4.12 ± 0.71*	9.47 ± 1.47*	3.36 ± 0.56	2.08 ± 0.53
*ADH*β	0.93 ± 0.06	1.79 ± 0.36	0.83 ± 0.15	0.95 ± 0.11

*Leaf disks of **glyphosate-sensitive** (GS) and glyphosate-**resistant** populations of Amaranthus palmeri were incubated for 24 h with shikimate, quinate, chorismate or anthranilate. Relative transcript abundance was normalized using the β tubulin gene and in each population to its own control. The measured genes were 3-deoxy-d-arabino-heptulosonate-7-phosphate synthase (DAHPS), dehydroquinate synthase (DHQS), 3-dehydroquinate dehydratase/shikimate dehydrogenase (DQSD), shikimate kinase (SK), 5-enolpyruvylshikimate 3-phosphate synthase (EPSPS), chorismate synthase (CS), anthranilate synthase (AS), chorismate mutase isoform 2 (CM2), chorismate mutase isoforms 1 and 3 (CM1-3), arogenate dehydrogenase isoform α (ADHα) and arogenate dehydrogenase isoform β (ADHβ) (Mean ± SE; n = 4). *Symbol indicates differences between control and treatment in each population (p-value ≤0.05).*

*ADH*β in any population (**Table 2**). In the GR population, no changes in relative gene expression were observed. In GS, only upregulation was observed in *DHQS, CS*, and *AS* genes, with the highest increase being observed for the *AS* gene (4.3-fold), the enzyme that uses chorismate as a substrate. It seems that as happens with glyphosate (Fernández-Escalada et al., 2017), the flux would be redirected toward the Trp biosynthetic pathway when chorismate is added exogenously. In addition, chorismate increased the content of the enzymes DAHPS and EPSPS (**Figure 3**), which does not match the results observed in the relative transcription level of the genes (**Table 2**), in which no changes were detected. It seems that the increase in the content of both enzymes would be due to the posttranscriptional regulation process elicited by the presence of chorismate. Nevertheless, it has to be noted that plants regulate carbon flux toward AAA biosynthesis at the transcriptional and post-transcriptional levels (Maeda and Dudareva, 2012).

Anthranilate was the intermediate that less affected the expression level of the shikimate pathway. In the GR population, only *SK* expression was 1.75-fold upregulated. In the GS population, a different response was observed on the two isoenzymes of *CM*: the plastidics 1 and 3 isoenzymes but not the cytosolic isoform 2 would be downregulated by anthranilate. In the same way, the two isoenzymes of *ADH* also showed different responses, and *ADH*α expression was the only downregulated 1.5-fold by anthranilate. In the same way, differences in the regulation of the isoforms by other metabolites of the pathway has been reported in *Beta vulgaris*, where only the activity of ADHα exhibited relaxed sensitivity to Tyr and ADHβ was strongly inhibited (Lopez-Nieves et al., 2017).

AAA biosynthesis is subjected to complex posttranscriptional and allosteric regulations (Mir et al., 2015). How carbon flow into the shikimate pathway is regulated in plants and the specific role of each intermediate remain ambiguous Siehl (1997) suggested that the inhibition of DAHPS activity by arogenate, a metabolite of the post-chorismate part of the pathway, was the key regulatory process in the shikimate pathway. In the case of glyphosate exposure, this regulatory pathway cannot occur, since chorismate and all its byproducts are not synthesized, resulting in an increase in the flux through this pathway and the accumulation of sikimate-3-phosphate (Gomes et al., 2014) and shikimate. This hypothesis was not confirmed in this study as, contrary to expectations, chorismate incubation increased the content of DAHPS and EPSPS in both populations.

The results showed that in sensitive plants glyphosate affects the shikimate pathway, and no such changes were observed in the *EPSPS* overexpressing population, consistent with its resistance to glyphosate, as has been reported before in susceptible and resistant soybeans (Marchiosi et al., 2009). Beside this, less effect on the pathway was detected on the GR than on the GS population after of the shikimate pathway intermediaries. Indeed, each intermediate induced higher changes in gene expression in the GS population than in the GR population, suggesting that the overexpression of *EPSPS* would have an effect in the regulation of the pathway, buffering or attenuating the transcriptional changes induced by the intermediates.

CONCLUSION

The exogenous supply of AAA did not induce any notable change in the transcriptome of the shikimate pathway. Nevertheless, when applied in combination with glyphosate, the upregulation of gene expression detected after glyphosate was abolished, suggesting that the effect of glyphosate on relative expression level of pre-chorismate genes is mediated by a transitory lack of the final products, as detected in the GS population. Shikimate accumulation was a dose-response direct effect of EPSPS inhibition detected in both populations and cannot be abolished by increased AAA availability.

In conclusion, this study suggests that any perturbation in the shikimate pathway would provoke changes in the relative transcript level of the genes and confirm a complex regulation of this pathway with mechanisms interacting at different levels and behaving differently in each population. No intermediate fully mimicked the effect of the herbicide. Nevertheless, although the toxic effect of the herbicide could be due to a combination of different factors, shikimate incubation, similar to glyphosate, elicited upregulation of most of the shikimate pathway genes.

The effects detected after the application of the final products or the intermediates of the shikimate pathway were more severe in the GS than in the GR population, suggesting that the regulatory mechanisms that operate in the GS population are disrupted or buffered when *EPSPS* is overexpressed.

DATA AVAILABILITY STATEMENT

The datasets generated for this study are available on request to the corresponding author.

AUTHOR CONTRIBUTIONS

MR and AZ conceived and designed the research. AZ-G, MB-A, and MG-M conducted the research. AZ-G and MG-M analyzed the data. AZ-G and AZ wrote the manuscript. All authors have read and approved the manuscript. All authors were involved in the implementation of the experimental design and have read and approved the manuscript.

FUNDING

This work was supported by two grants from the Ministerio Español de Economía y Competitividad (Project number AGL2016-77531-R). AZ-G and MB-A received funding from fellowships through Universidad Pública de Navarra.

SUPPLEMENTARY MATERIAL

The Supplementary Material for this article can be found online at: https://www.frontiersin.org/articles/10.3389/fpls.2020.00459/full#supplementary-material

REFERENCES

Aharoni, A., and Galili, G. (2011). Metabolic engineering of the plant primary-secondary metabolism interface. *Curr. Opin. Biotechnol.* 22, 239–244. doi: 10.1016/j.copbio.2010.11.004

Amrhein, N., Johänning, D., Schab, J., and Schulz, A. (1983). Biochemical basis for glyphosate-tolerance in a bacterium and a plant tissue culture. *FEBS Lett.* 157, 191–196. doi: 10.1016/0014-5793(83)81143-0

Baerson, S. R., Rodriguez, D. J., Biest, N. A., Tran, M., You, J., Kreuger, R. W., et al. (2002). Investigating the mechanism of glyphosate resistance in rigid ryegrass (Lolium rigidum). *Weed Sci.* 50, 721–730.

Bender, J., and Fink, G. R. (1998). A Myb homologue, ATR1, activates tryptophan gene expression in Arabidopsis. *Proc. Natl. Acad. Sci. U.S.A.* 95, 5655–5660. doi: 10.1073/pnas.95.10.5655

Benesova, M., and Bode, R. (1992). Chorismate mutase isoforms from seeds and seedlings of Papaver somniferum. *Phytochemistry* 31, 2983–2987. doi: 10.1016/0031-9422(92)83431-w

Bentley, R., and Haslam, E. (1990). The shikimate pathway - a metabolic tree with many branche. *Crit. Rev. Biochem. Mol. Biol.* 25, 307–384. doi: 10.3109/10409239009090615

Bohlmann, J., Lins, T., Martin, W., and Eilert, U. (1996). Anthranilate synthase from Ruta graveolens. Duplicated AS alpha genes encode tryptophan-sensitive and tryptophan-insensitive isoenzymes specific to amino acid and alkaloid biosynthesis. *Plant Physiol.* 111, 507–514. doi: 10.1104/pp.111.2.507

Boudet, A. M. (2012). "Polyphenols: From plant adaptation to useful chemical resources," in *Recent Advances in Polyphenol Research*, eds V. Cheynier, P. Sarni-Manchado, and S. Quideau (Chichester: Wiley-Backwell), 41–70. doi: 10.1002/9781118299753.ch2

Chandi, A., Milla-Lewis, S. R., Giacomini, D., Westra, P., Preston, C., Jordan, D. L., et al. (2012). Inheritance of evolved glyphosate resistance in a North Carolina palmer amaranth (Amaranthus palmeri) biotype. *Int. J. Agron.* 2012:176108. doi: 10.1155/2012/176108

Cole, D. J., Dodge, A. D., and Caseley, J. C. (1980). Some biochemical effects of glyphosate on plant meristems. *J. Exp. Bot.* 31, 1665–1674. doi: 10.1093/jxb/31.6.1665

Cromartie, T. H., and Polge, N. D. (2000). An improved assay for shikimic acid and its use as monitor for the activity of sulfosate. *Proc. Weed Sci. Soc. Am.* 40:291.

Dev, A., Tapas, S., Pratap, S., and Kumar, P. (2012). Structure and function of enzymes of shikimate pathway. *Curr. Bioinform.* 7, 374–391. doi: 10.2174/157489312803900983

Dillon, A., Varanasi, V. K., Danilova, T. V., Koo, D.-H., Nakka, S., Peterson, D. E., et al. (2017). Physical mapping of amplified copies of the 5-Enolpyruvylshikimate-3-phosphate synthase gene in glyphosate-resistant *Amaranthus tuberculatus*. *Plant Physiol.* 173, 1226–1234. doi: 10.1104/pp.16.01427

Dubouzet, J. G., Ishihara, A., Matsuda, F., Miyagawa, H., Iwata, H., and Wakasa, K. (2007). Integrated metabolomic and transcriptomic analyses of high-tryptophan rice expressing a mutant anthranilate synthase alpha subunit. *J. Exp. Bot.* 58, 3309–3321. doi: 10.1093/jxb/erm179

Duke, S. O., and Hoagland, R. E. (1978). Effects of glyphosate on metabolism of phenolic compounds I. Induction of phenylalanine ammonia-lyase activity in dark-grown maize roots. *Plant Sci. Lett.* 11, 185–190. doi: 10.1016/0304-4211(78)90002-0

Duke, S. O., Hoagland, R. E., and Elmore, C. D. (1980). Effects of glyphosate on metabolism of phenolic compounds: V. l-alpha-aminooxy-beta-phenylpropionic acid and glyphosate effects on phenylalanine ammonia-lyase in soybean seedlings. *Plant Physiol.* 65, 17–21. doi: 10.1104/pp.65.1.17

Dyer, W. E., Weller, S. C., Bressan, R. A., and Herrmann, K. M. (1988). Glyphosate tolerance in tobacco (*Nicotiana tabacum* L.). *Plant Physiol.* 88, 661–666. doi: 10.1104/pp.88.3.661

Fernández-Escalada, M., Gil-Monreal, M., Zabalza, A., and Royuela, M. (2016). Characterization of the *Amaranthus palmeri* physiological response to glyphosate in susceptible and resistant populations. *J. Agric. Food Chem.* 64, 95–106. doi: 10.1021/acs.jafc.5b04916

Fernández-Escalada, M., Zulet-González, A., Gil-Monreal, M., Royuela, M., and Zabalza, A. (2019). Physiological performance of glyphosate and imazamox mixtures on Amaranthus palmeri sensitive and resistant to glyphosate. *Sci. Rep.* 9:18225. doi: 10.1038/s41598-019-54642-9

Fernández-Escalada, M., Zulet-González, A., Gil-Monreal, M., Zabalza, A., Ravet, K., Gaines, T., et al. (2017). Effects of EPSPS copy number variation (CNV) and glyphosate application on the aromatic and branched chain amino acid synthesis pathways in *Amaranthus palmeri*. *Front. Plant Sci.* 8:1970. doi: 10.3389/fpls.2017.01970

Gaines, T. A., Shaner, D. L., Ward, S. M., Leach, J. E., Preston, C., and Westra, P. (2011). Mechanism of resistance of evolved glyphosate-resistant *Palmer amaranth* (*Amaranthus palmeri*). *J. Agric. Food Chem.* 59, 5886–5889. doi: 10.1021/jf104719k

Gaines, T. A., Zhang, W., Wang, D., Bukun, B., Chisholm, S. T., Shaner, D. L., et al. (2010). Gene amplification confers glyphosate resistance in *Amaranthus palmeri*. *Proc. Natl. Acad. Sci. U.S.A.* 107, 1029–1034. doi: 10.1073/pnas.0906649107

Galili, G., Amir, R., and Fernie, A. R. (2016). The regulation of essential amino acid synthesis and accumulation in plants. *Annu. Rev. Plant Biol.* 67, 153–178. doi: 10.1146/annurev-arplant-043015-112213

Galili, G., and Hofgen, R. (2002). Metabolic engineering of amino acids and storage proteins in plants. *Metab. Eng.* 4, 3–11. doi: 10.1006/mben.2001.0203

Garg, B., Vaid, N., and Tuteja, N. (2014). In-silico analysis and expression profiling implicate diverse role of EPSPS family genes in regulating developmental and metabolic processes. *BMC Res. Notes* 7:58. doi: 10.1186/1756-0500-7-58

Gomes, M. P., Smedbol, E., Chalifour, A., Hénault-ethier, L., Labrecque, M., Lepage, L., et al. (2014). Alteration of plant physiology by glyphosate and its by-product aminomethyl-phosphonic acid: an overview. *J. Exp. Bot.* 65, 4691–4703. doi: 10.1093/jxb/eru269

Graziana, A., and Boudet, A. M. (1980). 3-Deoxy-D-arabino heptulosonate 7-phosphate synthase from Zea mays: general properties and regulation by tryptophan. *Plant Cell Physiol.* 21, 793–802. doi: 10.1093/oxfordjournals.pcp.a076054

Gresshoff, P. M. (1979). Growth inhibition by glyphosate and reversal of its action by phenylalanine and tyrosine. *Aust. J. Plant Physiol.* 6, 177–185. doi: 10.1071/PP9790177

Häusler, R. E., Ludewig, F., and Krueger, S. (2014). Amino acids - A life between metabolism and signaling. *Plant Sci.* 229, 225–237. doi: 10.1016/j.plantsci.2014.09.011

Herrmann, K. M. (1995). The shikimate pathway: early steps in the biosynthesis of aromatic compounds. *Plant Cell* 7, 907–919. doi: 10.1105/tpc.7.7.907

Hollander, H., and Amrhein, N. (1980). The site of the inhibition of the shikimate pathway by glyphosate. I. Inhibition by glyphosate of phenylpropanoid synthesis in buckwheat (*Fagopyrum esculentum* Moench). *Plant Physiol.* 66, 823–829. doi: 10.1104/pp.66.5.823

Jaworski, E. G. (1972). Mode of action of N-phosphonomethylglycine. Inhibition of aromatic amino acid biosynthsis. *J. Agric. Food Chem.* 20, 1195–1198. doi: 10.1021/jf60184a057

Less, H., Angelovici, R., Tzin, V., and Galili, G. (2010). Principal transcriptional regulation and genome-wide system interactions of the Asp-family and aromatic amino acid networks of amino acid metabolism in plants. *Amino Acids* 39, 1023–1028. doi: 10.1007/s00726-010-0566-7

Less, H., and Galili, G. (2009). Coordinations between gene modules control the operation of plant amino acid metabolic networks. *BMC Syst. Biol.* 3:14. doi: 10.1186/1752-0509-3-14

Livak, K. J., and Schmittgen, T. D. (2001). Analysis of relative gene expression Data using real-time quantitative PCR and the 2-ΔΔCT method. *Methods* 25, 402–408. doi: 10.1006/meth.2001.1262

Lopez-Nieves, S., Yang, Y., Timoneda, A., Wang, M., Feng, T., Smith, S., et al. (2017). Relaxation of tyrosine pathway regulation underlies the evolution of betalain pigmentation in *Caryophyllales*. *New Phytol.* 217, 896–908. doi: 10.1111/nph.14822

Maeda, H., and Dudareva, N. (2012). The shikimate pathway and aromatic amino acid biosynthesis in plants. *Annu. Rev. Plant Biol.* 63, 73–105. doi: 10.1146/annurev-arplant-042811-105439

Maeda, H., Shasany, A. K., Schnepp, J., Orlova, I., Taguchi, G., Cooper, B. R., et al. (2010). RNAi suppression of Arogenate Dehydratase1 reveals that phenylalanine is synthesized predominantly via the arogenate pathway in petunia petals. *Plant Cell* 22, 832–849. doi: 10.1105/tpc.109.073247

Marchiosi, R., Lucio Ferrarese, M. D. L., Bonini, E. A., Fernandes, N. G., Ferro, A. P., and Ferrarese-Filho, O. (2009). Glyphosate-induced metabolic changes

in susceptible and glyphosate-resistant soybean (Glycine max L.) *roots*. *Pestic. Biochem. Physiol.* 93, 28–33. doi: 10.1016/j.pestbp.2008.09.003

Maroli, A. S., Nandula, V. K., Dayan, F. E., Duke, S. O., Gerard, P., and Tharayil, N. (2015). Metabolic profiling and enzyme analyses indicate a potential role of antioxidant systems in complementing glyphosate resistance in an Amaranthus palmeri biotype. *J. Agric. Food Chem.* 63, 9199–9209. doi: 10.1021/acs.jafc.5b04223

Mir, R., Jallu, S., and Singh, T. P. (2015). The shikimate pathway: review of amino acid sequence, function and three-dimensional structures of the enzymes. *Crit. Rev. Microbiol*. 41, 172–189. doi: 10.3109/1040841X.2013.813901

Oliva, M., Ovadia, R., Perl, A., Bar, E., Lewinsohn, E., Galili, G., et al. (2015). Enhanced formation of aromatic amino acids increases fragrance without affecting flower longevity or pigmentation in Petunia × hybrida. *Plant Biotechnol. J.* 13, 125–136. doi: 10.1111/pbi.12253

Orcaray, L., Igal, M., Marino, D., Zabalza, A., and Royuela, M. (2010). The possible role of quinate in the mode of action of glyphosate and acetolactate synthase inhibitors. *Pest Manag. Sci.* 66, 262–269. doi: 10.1002/ps.1868

Ossipov, V., Bonner, C., Ossipova, S., and Jensen, R. (2000). Broad-specificity quinate (shikimate) dehydrogenasefrom *Pinus taeda needles*. *Plant Physiol. Biochem*. 38, 923–928. doi: 10.1016/s0981-9428(00)01203-1

Pinto, J. E. B. P., Dyer, W. E., Weller, S. C., and Herrmann, K. M. (1988). Glyphosate induces 3-deoxy-D-arabino-heptulosonate 7-phosphate synthase in potato (*Solanum tuberosum* L) cells grown in suspension-culture. *Plant Physiol.* 87, 891–893. doi: 10.1104/pp.87.4.891

Powles, S. B., and Yu, Q. (2010). Evolution in action: plants resistant to herbicides. *Annu. Rev. Plant Biol.* 61, 317–347. doi: 10.1146/annurev-arplant-042809-112119

Romero, R. M., Roberts, M. F., and Phillipson, J. D. (1995). *Chorismate mutase* in microorganisms and plants. *Phytochemistry* 40, 1015–1025. doi: 10.1016/0031-9422(95)00408-y

Siehl, D. L. (1997). "Inhibitors of EPSP sinthase, glutamine synthetase and histidine synthesis," in *Hebicide activity: Toxicology, Biochemistry And Molecular Biology*, eds R. M. Roe, J. D. Burton, and R. J. Kuhr (Amsterdam: IOS press), 37–67.

Siehl, D. L., and Conn, E. E. (1988). Kinetic and regulatory properties of arogenate dehydratase in seedlings of *Sorghum bicolor* (L.) *Moench. Arch. Biochem. Biophys.* 260, 822–829. doi: 10.1016/0003-9861(88)90513-9

Spitzer-Rimon, B., Marhevka, E., Barkai, O., Marton, I., Edelbaum, O., Masci, T., et al. (2010). EOBII, a gene encoding a flower-specific regulator of phenylpropanoid volatiles' biosynthesis in petunia. *Plant Cell* 22, 1961–1976. doi: 10.1105/tpc.109.067280

Steinrücken, H. C., and Amrhein, N. (1980). The herbicide glyphosate is a potent inhibitor of 5-enolpyruvylshikimic acid-3-phosphate synthase. *Biochem. Biophys. Res. Commun.* 94, 1207–1212. doi: 10.1016/0006-291x(80)90547-1

Suzich, J. A., Dean, J. F. D., and Herrmann, K. M. (1985). 3-Deoxy-D-arabino-heptulosonate 7-phosphate synthase from carrot root (*Daucus carota*) is a hysteretic enzyme. *Plant Physiol.* 79, 765–770. doi: 10.1104/pp.79.3.765

Takatsuji, H., Mori, M., Benfey, P. N., Ren, L., and Chua, N. H. (1992). Characterization of a zinc finger DNA-binding protein expressed specifically in Petunia petals and seedlings. *EMBO J.* 11, 241–249. doi: 10.1002/j.1460-2075.1992.tb05047.x

Tohge, T., Watanabe, M., Hoefgen, R., and Fernie, A. R. (2013). Shikimate and phenylalanine biosynthesis in the green lineage. *Front. Plant Sci.* 4:62. doi: 10.3389/fpls.2013.00062

Tymonko, J. M., and Foy, C. L. (1978). Inhibition of protein synthesis by glyphosate. *Plant Physiol.* 61:41.

Tzin, V., and Galili, G. (2010). New Insights into the shikimate and aromatic amino acids biosynthesis pathways in plants. *Mol. Plant* 3, 956–972. doi: 10.1093/mp/ssq048

Tzin, V., Malitsky, S., Aharoni, A., and Galili, G. (2009). Expression of a bacterial bi-functional chorismate mutase/prephenate dehydratase modulates primary and secondary metabolism associated with aromatic amino acids in *Arabidopsis*. *Plant J.* 60, 156–167. doi: 10.1111/j.1365-313x.2009.03945.x

Tzin, V., Malitsky, S., Ben Zvi, M. M., Bedair, M., Sumner, L., Aharoni, A., et al. (2012). Expression of a bacterial feedback-insensitive 3-deoxy-d-arabino-heptulosonate 7-phosphate synthase of the shikimate pathway in *Arabidopsis* elucidates potential metabolic bottlenecks between primary and secondary metabolism. *New Phytol.* 194, 430–439. doi: 10.1111/j.1469-8137.2012.04052.x

Verdonk, J. C. (2005). ODORANT1 regulates fragrance biosynthesis in petunia flowers. *Plant Cell* 17, 1612–1624. doi: 10.1105/tpc.104.028837

Vila-Aiub, M. M., Goh, S. S., Gaines, T. A., Han, H., Busi, R., Yu, Q., et al. (2014). No fitness cost of glyphosate resistance endowed by massive EPSPS gene amplification in Amaranthus palmeri. *Planta* 239, 793–801. doi: 10.1007/s00425-013-2022-x

Vivancos, P. D., Driscoll, S. P., Bulman, C. A., Ying, L., Emami, K., Treumann, A., et al. (2011). Perturbations of amino acid metabolism associated with glyphosate-dependent inhibition of shikimic acid metabolism affect cellular redox homeostasis and alter the abundance of proteins involved in photosynthesis and photorespiration. *Plant Physiol.* 157, 256–268. doi: 10.1104/pp.111.181024

Zeier, J. (2013). New insights into the regulation of plant immunity by amino acid metabolic pathways. *Plant, Cell Environ.* 36, 2085–2103. doi: 10.1111/pce.12122

Zhu, J., Patzoldt, W., and Shealy, R. (2008). Transcriptome response to glyphosate in sensitive and resistant soybean. *J. Agric. Food Chem.* 56, 6355–6363. doi: 10.1021/jf801254e

Zulet-González, A., Fernández-Escalada, M., Zabalza, A., and Royuela, M. (2019). Enhancement of glyphosate efficacy on *Amaranthus palmeri* by exogenous quinate application. *Pestic. Biochem. Physiol.* 158, 1–11. doi: 10.1016/j.pestbp.2019.04.004

Conflict of Interest: The authors declare that the research was conducted in the absence of any commercial or financial relationships that could be construed as a potential conflict of interest.

Copyright © 2020 Zulet-González, Barco-Antoñanzas, Gil-Monreal, Royuela and Zabalza. This is an open-access article distributed under the terms of the Creative Commons Attribution License (CC BY). The use, distribution or reproduction in other forums is permitted, provided the original author(s) and the copyright owner(s) are credited and that the original publication in this journal is cited, in accordance with accepted academic practice. No use, distribution or reproduction is permitted which does not comply with these terms.

frontiers in Plant Science

ORIGINAL RESEARCH
published: 05 May 2020
doi: 10.3389/fpls.2020.00512

Functional Relevance of Citrulline in the Vegetative Tissues of Watermelon During Abiotic Stresses

*Qiushuo Song[1,2], Madhumita Joshi[2], James DiPiazza[2] and Vijay Joshi[1,2]**

[1] Department of Horticultural Sciences, Texas A&M University, College Station, TX, United States, [2] Texas A&M AgriLife Research and Extension Center, Uvalde, TX, United States

A non-protein amino acid, citrulline, is a compatible solute involved in the maintenance of cellular osmolarity during abiotic stresses. Despite its significance, a coherent model indicating the role of citrulline during stress conditions has not yet emerged. We have used watermelon, naturally rich in citrulline, as a model to understand its accumulation during drought stress and nitrogen perturbation using transcriptomic and metabolomic analysis. Experiments were performed in the semi-controlled environment, and open field to study the accumulation of drought-induced citrulline in the vegetative tissues of watermelon by monitoring the stress treatments using physiological measurements. The amino acid profiling of leaves and stems in response to drought stress showed up to a 38 and 16-fold increase in citrulline content, respectively. Correlation between amino acids indicated a concomitant activation of a metabolic pathway that included citrulline, its precursor (ornithine), and catabolic product (arginine). Consistent with its accumulation, the gene expression analysis and RNA-Sequencing confirmed activation of citrulline biosynthesis-related genes – *Ornithine carbamoyl-transferase* (*OTC*), *N-acetylornithine deacetylase* (*AOD*) and *Carbamoyl phosphate synthases* (*CPS*), and down-regulation of catabolic genes; *Arginosuccinate lyase* (*ASL*) and *Arginosuccinate synthases* (*ASS*) in drought-stressed leaf tissues. Based on the relative abundance in the nitrogen-depleted vegetative tissues and down-regulation of genes involved in citrulline biosynthesis, we also demonstrated that the nitrogen status of the plant regulates citrulline. Taken together, these data provide further insights into the metabolic and molecular mechanisms underlying the amino acid metabolism under environmental stress and the significance of non-protein amino acid citrulline in plants.

Keywords: citrulline, drought stress, nitrogen, watermelon, arginine

OPEN ACCESS

Edited by:
Dietmar Funck,
University of Konstanz, Germany

Reviewed by:
Maria Valeria Lara,
National University of Rosario, Argentina
Marco Betti,
University of Seville, Spain

***Correspondence:**
Vijay Joshi
Vijay.Joshi@tamu.edu

Specialty section:
This article was submitted to Plant Metabolism and Chemodiversity, a section of the journal Frontiers in Plant Science

Received: *01 February 2020*
Accepted: *06 April 2020*
Published: *05 May 2020*

Citation:
Song Q, Joshi M, DiPiazza J and Joshi V (2020) Functional Relevance of Citrulline in the Vegetative Tissues of Watermelon During Abiotic Stresses. Front. Plant Sci. 11:512. doi: 10.3389/fpls.2020.00512

INTRODUCTION

Plants accumulate a variety of low molecular weight compatible solutes (osmolytes) in response to abiotic stresses. The most common osmolytes are glycine betaines, organic sugars, polyamines, and amino acids (proline, GABA). These osmolytes provide a range of protective functions such as maintenance of cellular osmotic adjustments and membrane integrity, stabilization of intrinsic proteins, buffering cellular pH, and detoxification of reactive oxygen species (ROS) (Hare et al., 1998; Chen and Murata, 2002; Slama et al., 2015; Ali et al., 2017). Although much research has been

done to show the usefulness of common osmolytes (Lunn et al., 2014; Per et al., 2017; Romero et al., 2018; Annunziata et al., 2019), not all plants are capable of inducing the same set of osmolytes. The onset of these osmolytes varies considerably among plant species, tissue types, longevity, and nature of abiotic stresses.

Citrulline is an intermediate non-protein amino acid in the arginine pathway. In plants, it is synthesized from ornithine and carbamoyl phosphate. Citrulline is a potent scavenger of hydroxyl radicals and protects cellular enzymes from oxidative damage (Akashi et al., 2001, 2004; Yokota et al., 2002). The fruits of watermelon and other members of the *Cucurbitaceae* family accumulates large amounts of free citrulline (Davis et al., 2011; Fish, 2014; Akashi et al., 2017; Joshi et al., 2019). The accumulation of several amino acids during drought stress in different plant species has been reported (Obata and Fernie, 2012; Huang and Jander, 2017). However, limited studies have demonstrated accumulation of citrulline in the vegetative tissues in response to environmental stresses; such as watermelons (Kawasaki et al., 2000; Yokota et al., 2002; Akashi et al., 2008), melons (Mitchell and Madore, 1992; Mitchell et al., 1992; Daşgan et al., 2009; Kusvuran et al., 2013), chickpea (Garg et al., 2016; Khan et al., 2019). Even though the mechanism through which the drought stress leads to citrulline accumulation in plants is not completely understood. Accumulation of amino acids during drought stress has been generally attributed to decreased protein synthesis (Good and Zaplachinski, 1994), increased protein degradation (Huang and Jander, 2017; Hildebrandt, 2018), or changes in a gene network affecting biosynthesis or catabolism of substrate/product availability (Joshi et al., 2010; Hildebrandt et al., 2015). The metanalysis of metabolic and transcriptomic networks has demonstrated that the synthesis of abundant amino acids, such as proline, arginine, asparagine; is upregulated during abiotic stress (Hildebrandt, 2018; Sircar and Parekh, 2019) and these amino acids act as compatible osmolytes, precursors for secondary metabolites, or storage forms of organic nitrogen. In addition to amino acids, ureides such as allantoin, allanotoate, and citrulline are also used as nitrogen transporting molecules. Citrulline has also been suggested to play a role in facilitating nitrogen assimilation, endogenous nitrogen storage, and transport in higher plants (Reuter, 1961; Ludwig, 1993). The central role of citrulline as a molecular modulator for carbon and nitrogen integration into the urea cycle has been demonstrated in photosynthetic marine diatoms (Allen et al., 2011). However, little is known about its role in nitrogen metabolism in agriculturally important monocot or dicot crops. Nonetheless, citrulline has been long back proposed to function as a carrier of organic nitrogen in cucurbits (Kasting and Delwiche, 1958) and occurs at high concentrations in the phloem of cucurbits (Mitchell and Madore, 1992).

Being a naturally rich in citrulline and with the availability of resources such as published genome (Guo et al., 2013, 2015), next-generation sequence (NGS) data (Guo et al., 2015; Nimmakayala et al., 2016), and the databases[1] [International Cucurbit Genomics Initiative (ICuGI)] watermelon would be an ideal model to study the drought-induced accumulation of citrulline in the vegetative tissues. Not much is known about the transcriptional or feedback regulation of citrulline in plants during environmental stresses in plants. The purpose of the proposed experiments is to provide new insights into the induction of citrulline and associated amino acids in vegetative tissues of watermelon and transcriptional regulation of citrulline during drought stress and nitrogen deficit. The outcome of the experiment validated the role of genes associated with the citrulline pathway and the significance of citrulline in drought stress and nitrogen deficit in plants.

MATERIALS AND METHODS

Germination and Seedling Growth Condition

Commercial watermelon cultivars Crimson Sweet and Charleston Gray seeds were sown in 96-well plug trays (25″ length × 15′ width × 2′ depth) in a greenhouse at the Texas A&M AgriLife Research & Extension Center at Uvalde, TX, United States. Additional details regarding the parentage, agronomic performance, and qualities of the two cultivars are available through the Cucurbit Breeding website at NC State[2]. The environmental factors inside the greenhouse were measured and monitored by a centralized control system (Wadsworth, Arvada, CO, United States) with 16 h light followed by 8 h dark. The temperature and humidity were maintained at 30 ± 5°C and 70 ± 5%, respectively.

Drought Stress Experiment

For the drought stress experiment, ∼ 8-weeks old seedlings of the cultivar Crimson Sweet were transplanted to 10 heavy-duty round nursery pots (5 gallons; 28 cm width × 26 cm height) in a semi-controlled high-tunnel greenhouse at the Texas A&M AgriLife Research & Extension Center, Uvalde, TX, United States (**Supplementary Figure S1**). Before transplanting, all pots were filled with the same weight (∼22lb) of soil-less media Absorb-N-Dry (Balcones Minerals Corporation, Flatonia, TX, United States), saturated completely with water and left overnight for drainage. The weights of each pot were recorded to establish initial water content. All pots were applied with standard fertilizer mix to avoid nutritional imbalance (Peters Professional Mix 20:20:20). Decagon 5TE moisture sensors (Decagon Devices, Inc., Pullman, WA, United States) were inserted at a depth of 6 inches and connected to the EM 50 data loggers for recording, monitoring, and downloading the information of the percent volumetric water content (VWC) per pot. The 5TE sensor uses an electromagnetic field to measure the dielectric permittivity of the surrounding medium. The sensor supplies a 70 MHz oscillating wave to the sensor prongs that charges according to the dielectric of the material. The stored charge is proportional to soil VWC. The control (well-watered) pots were frequently watered to maintain 95 ± 5% of relative water content. In contrast, for drought stress treatment, the pots were subjected

[1] http://cucurbitgenomics.org/

[2] http://cucurbitbreeding.com/watermelon-breeding/watermelon-cultivars-ca-cz/

to stress by withholding watering 24 days after transplanting to keep the soil moisture at 35 ± 5% as per VWC data using daily readings recorded from the data loggers. The technique of freezing point depression was used for the determination of cell osmotic potential (ψs) using osmometer (Wescor Vapro osmometers 5520, Logan, UT, United States). Leaf disks (0.25-inch diameter) collected at 8, 24, and 53 days after induction of drought stress [days after initiation of treatment (DAT)] were wrapped in aluminum foils and flash-frozen in liquid nitrogen to measure ψs. When measuring the osmotic potential, leaf disks from control and stress plants were placed into the enclosed measuring chamber. Osmometer readings (mmol·kg^{-1}) were converted to MPa as per the manufacturer's instructions. The differences in the water potentials between the samples were analyzed using Tukey–Kramer HSD (p-value < 0.05). A gas analyzer (LI-6400 XT, LI-COR Bioscience, Lincoln, NE, United States) was used to measure leaf photosynthesis rate (Photo), stomatal conductance (Cond) and transpiration (Trmmol) with parameters (Photosynthetic Active Radiation, PAR,1000 μmol m^{-2} s^{-1}; CO_2 concentration, 400 ppm; leaf temperature, 20°C; VPD, 1 kPa; flow, 500 μmols^{-1}) at 8 and 24 DAT to monitor the progressive changes in the photosynthetic performance due to drought stress. Tissue samples were collected from three to four independent plants for both amino acid analysis and RNA extraction at 8 DAT (Leaf-I and stem) and 24 DAT (Leaf II) and flash-frozen in liquid nitrogen for further analysis. Both Leaf-I and Leaf-II tissues were collected from the middle position of the main vines, while the stem sections were collected from the vine at a point where Leaf-I originated.

Nitrogen (N) Deficit Experiment

Before initiating the N-deficit experiment, soil samples collected at 10 random locations at a depth of 6 inches were analyzed for elemental composition at Texas A&M AgriLife Extension Service Soil, Water and Forage Testing Laboratory[3]. Total Kjeldahl N (TKN) concentrations were estimated by the Kjeldahl method (Easy Chem Plus; Chinchilla Scientific, Oak Brook, IL, United States) with the addition of sulfuric acid for digestion in the presence of Kjeldahl formulated catalyst (Pro-Pac-CT 37; Alfie Packers, Inc., Omaha, NE, United States). Total inorganic nitrogen was calculated by adding the concentrations of soil nitrate, nitrite, and ammonia. Approximately 6-week-old seedlings of the two cultivars – Charleston Gray and Crimson Sweet were transplanted on the raised beds keeping plant to plant distance of 3 ft and rows to row spacing of 12 ft (**Supplementray Figure S2**). The beds were covered with plastic mulch and watered using sub-surface drip irrigation lines when needed depending on the air temperature and soil humidity. Based on the preliminary experiments (data not shown) and indigenous nitrogen levels, two N treatments, high N (HN) and low N (LN), were established to keep the N levels to 168 ± 11 kg/ha N and 44 ± 5 kg/ha, respectively. The nitrogen was applied in the form of Urea (46-0-0, HELENA, TX, United States). Soil samples were collected at a depth of 6-inches every week from the date of transplanting for soil elemental analysis to monitor the soil N content. The nitrate content of the plants was measured 10 weeks after transplanting using the petiole saps with portable Nitrate Pocket Tester (Horiba LAQUA twin NO_3-11 Compact Water Quality Nitrate Ion Meter). The photosynthetic performance was measured 45, 59, and 69 DAT from the leaves located in the middle of the vines (data not shown). SPAD measurements were taken at 39, 45, 52, and 66 DAT. Tissue samples from both the varieties for amino acid analysis and RNA extraction were collected from three independent plants at 45, 59, and 69 days after the initiation of nitrogen stress treatment.

[3]http://soiltesting.tamu.edu

Amino Acid Extraction and Quantification With UPLC-ESI-MS/MS

Approximately 20 mg fresh tissue samples were homogenized into a fine powder in a Harbil model 5G-HD paint shaker (Harbil, Wheeling, IL, United States) using 3 mm Demag stainless steel balls (Abbott Ball Company, West Hartford, CT, United States). Total free amino acids were extracted by suspending the homogenized samples in 10 μL of 100 mM cold HCl per mg of tissues, incubating on ice for around 20 min, and then centrifuging at a speed of 14,609 × g for 20 min at 4°C. The extracts were filtered through a 96-well 0.45-μm-pore filter plate (Pall Life Sciences, United States). The filtrates were used for derivatization using with AccQTag3X Ultra-Fluor kit (Waters Corporation, Milford, MA, United States) as per the manufacturer's protocol. L-Norvaline (TCI AMERICA, United States) was used as an internal control. Amino acid calibrators were obtained from Kairos™ Amino Acid Kit (Waters Corporation, Milford, MA, United States). Lyophilized powder of the mixture of amino acids calibrators was reconstituted in 0.1M HCl before derivatization. Calibration curves were built using TargetLynx™ Application Manager (Waters Corporation, Milford, MA, United States). UPLC-ESI-MS/MS analysis was performed using Water's Acquity H-class UPLC system equipped with Waters Xevo TQ mass spectrometer and electrospray ionization (ESI) probe. The Waters Acquity H-class UPLC system was composed of an autosampler, Waters ACQUITY UPLC Fluorescence (FLR) detector, and a CORTECS™ UPLC C_{18} (1.6 μm, 2.1 mm × 150 mm). The mobile phase was composed of (A) water (0.1% formic acid v/v) and (B) acetonitrile (0.1% formic acid v/v). The column heater was set at 60°C, and the mobile phase flow rate was maintained at 0.5 mL/min. The gradient of non-linear separation was set as follows: 0–1 min (99% A), 3.2 min (87.0% A), 8 min (86.5% A), and 9 min (5% A). Two microliters of the derivatized sample were injected for analysis. Multiple Reaction Monitoring (MRM) transitions and collision energy values and cone voltage were optimized for each amino acid using the Water's IntelliStart software. The ESI source was operated at 150°C, gas desolvation flow rate at 1000 L/h, gas flow cone at 20 L/h, desolvation temperature at 500°C, for detecting all amino acids. MRM was performed in a positive mode. Water's MassLynx software was used for instrument monitoring and data acquisition. The data integration and quantitation were carried out using Waters TargetLynx software.

RNA-Seq Analysis of Drought Stress Leaves

RNA Extraction and Library Preparation for Transcriptome Sequencing

The flash-frozen leaf samples (Leaf-I) collected 8 DAT from three independent plants along with control (well-irrigated) plants were used for RNA-Seq analysis. Total RNA was extracted using a Quick-RNA Miniprep Kit (Zymo Research Corporation, Irvine, CA, United States) as per the manufacturer's protocol and treated with DNase1 (Zymo Research Corporation, Irvine, CA, United States). The purity of the RNA was analyzed using the NanoPhotometer spectrophotometer (IMPLEN, Westlake Village, CA, United States). RNA integrity and quantitation were assessed using the RNA Nano 6000 Assay Kit of the Bioanalyzer 2100 system (Agilent Technologies, Santa Clara, CA, United States). One μg total RNA per sample was used for the RNA library preparations. Sequencing libraries were generated using NEBNext Ultra RNA Library Prep Kit for Illumina (NEB, United States) following the manufacturer's recommendations, and index codes were added to attribute sequences to each sample. Library concentration was first quantified using a Qubit 2.0 fluorometer (Life Technologies), diluted to 1 ng/μl before checking the insert size on an Agilent Bioanalyzer 2100 system and quantified to greater accuracy by quantitative PCR (Q-PCR) (library activity >2 nM).

Data Processing, Analysis, and Mapping to Reference Genome

The clustering of the index-coded samples was performed on a cBot Cluster Generation System using PE Cluster Kit cBot-HS (Illumina) according to the manufacturer's instructions. After cluster generation, the libraries were sequenced on an Illumina Hiseq platform, and 150 bp paired-end reads were generated. Raw reads of fastq format were processed to obtain clean reads by removing the adapter, reads containing ploy N, and low-quality reads from raw data. At the same time, Q20, Q30, and GC content, the clean data were calculated. Watermelon reference genome (cultivar Charleston Gray) and gene model annotation files were downloaded from CuGenDB[1]. Index of the reference genome was built using Bowtie v2.2.3, and paired-end clean reads were aligned to the reference genome using TopHat v2.0.12.

Gene Expression Quantification and DEG Analysis

HTSeq v0.6.1 was used to count the reads mapped to each gene. FPKM (Trapnell et al., 2010) of each gene was calculated based on the length of the gene and reads count mapped to this gene. Differential expression analysis of control and drought-stressed conditions (three biological replicates per tissue per treatment) was performed using the DESeq R package (Anders and Huber, 2010). Genes with p-value < 0.05 found by DESeq were assigned as differentially expressed.

Real-Time Polymerase Chain Reaction

Total RNA was extracted with the Quick-RNA Miniprep Kit (Zymo Research Corporation, Irvine, CA, United States) treated with DNase1 (Zymo Research Corporation, Irvine, CA, United States), and subjected to reverse transcription using iScript RT Supermix (Bio-Rad Laboratories, Inc., Hercules, CA, United States). The quality and quantity of the RNA were analyzed by a Denovix DS-11+ spectrophotometer (Wilmington, DE, United States). Gene expression analysis via reverse transcription-qPCR was performed in the BioRad CFX96 qPCR instrument using SsoAdv Univer SYBR GRN Master Kit (Bio-Rad Laboratories, Inc., Hercules, CA, United States). Relative gene expression levels were determined using a standard curve method, and the value for each target gene was then normalized against the mean of expression values of the watermelon β-actin and α-tubulin5 genes (Kong et al., 2014) as reference genes. The stability of both the reference genes was confirmed using BestKeeper (Pfaffl et al., 2004). The relative expression levels (Cq values) for each gene were normalized to that of reference genes by taking an average of three biological replicates. The relative expression levels were calculated using the $\Delta\Delta$Cq (quantitative cycle) method provided with the Bio-Rad CFX software. Primers for qPCR used in the study and the BestKeeper analysis of expression stability of reference genes are listed in **Supplementary Table S1**.

RESULTS

Validation of Drought Stress Treatment

Soil moisture and leaf osmotic potential: before transplanting seedlings into pots, 5TE probes inserted at a depth of root zones were calibrated by correlating readings (m^3/m^3) from the data loggers with actual water content (%) in the pots. The percent VWC measured by sensors at 8, 24, and 53 DAT is presented in **Figure 1A**. All pots receiving drought stress treatment were maintained at 35 ± 5% water content, implying consistent drought stress. The water content for the control (well-watered) pots was above 95 ± 5%. Osmotic potential (ψs) was measured with a VAPRO 5520 vapor pressure osmometer (Wescor, Logan, UT, United States) (Ball and Oosterhuis, 2005). Ψs is a negative quantity of osmotic pressure, and it decreases during dehydration due to the concentrated solutes in plant cells. The significantly consistent differences in the osmotic pressure (MPa) of leaf samples collected from control (well-watered) and drought-stressed plants were seen at all time points since the initiation of drought stress (**Figure 1B**). The net rates of photosynthesis (Photo), stomatal conductance (Cond), and transpiration rates (Trmmol) in drought-stressed plants were significantly lower than the control plants (**Figure 2**). Decrease of the intercellular CO_2 concentration (Ci) at the beginning of drought stress (8 DAT) indicates that photosynthesis is limited more by the decrease of stomatal conductance.

Drought Stress-Induced Accumulation of Citrulline and Other Amino Acids

Citrulline contents in all the stressed samples after the initiation of the drought stress increased dramatically (**Figure 3A**). At the onset of drought stress treatment, citrulline content in the leaf and stem enhanced rapidly – up to 38 and 16-fold, respectively (**Supplementary Table S2**). The leaf tissue collected during sustained drought stress (24 DAT) also showed threefold

A

	8 DAT	24 DAT	53 DAT
Percent volumetric water content (VWC)			
Control (Well-watered)	99 ± 1%[a]	99 ± 2%[a]	98 ± 2%[a]
Drought	34 ± 2%[b]	30 ± 1%[b]	36 ± 1%[b]

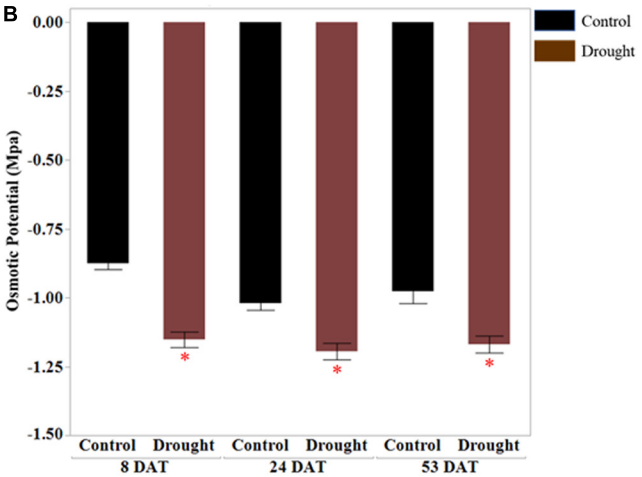

FIGURE 1 | Validation of drought stress treatment. **(A)** Percent volumetric water content (WVC) was measured 8, 24, and 53 days DAT using 5TE sensors. The percent VWC data represent the ratio of actual water volume to maximum water volume (water content in saturated soil pot). The values are means ± SD (n = 3 or 4) and the different letters represents significance between control and drought treatments at $p < 0.05$. **(B)** Osmotic potential (Mpa) of leaf tissues measured at three different time points is shown on vertical axis. The values represent means ± SD (n = 3 or 4) and asterisk (*) represents significant difference between control and drought treatments ($p < 0.05$). DAT, days after initiation of drought treatment.

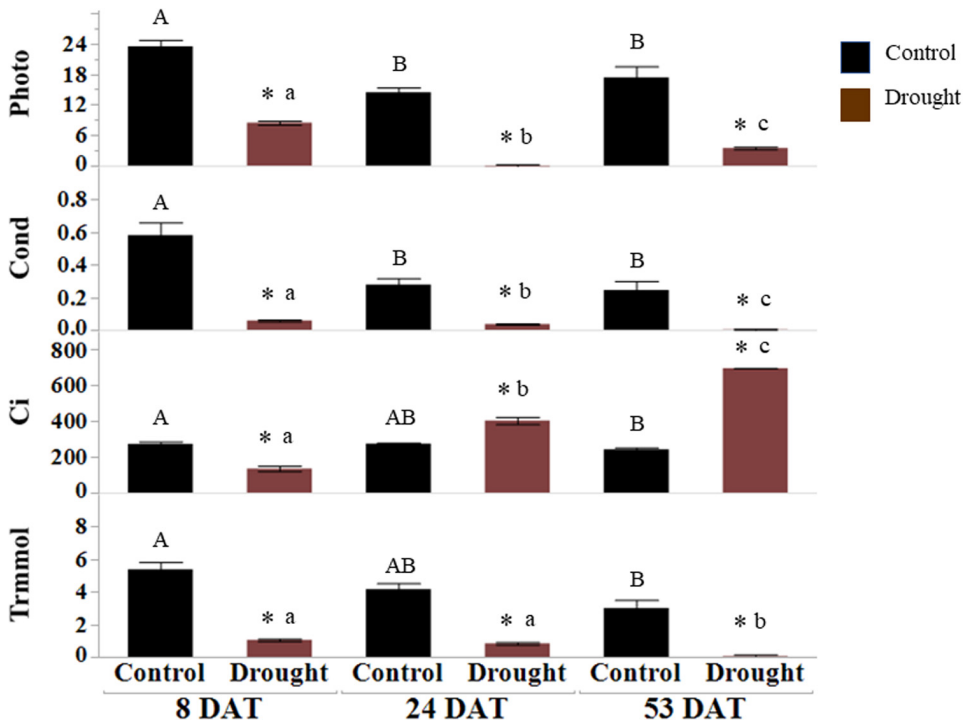

FIGURE 2 | Gas analyzer measurements of drought-stressed leaves. Net photosynthesis (Photo, mol CO_2 m^{-2} s^{-1}), stomatal conductance (Cond, mol H_2O m^{-2} s^{-1}), intercellular CO_2 (C_i, μmol CO_2 mol air^{-1}) and transpiration rate (Trmmol, mol m^{-2} s^{-1}) were measured at 8, 24, and 53 DAT. The values represent means ± SD (n = 3 or 4), asterisk (*) represents significant difference between control and drought treatments, upper case letters between controls and lower-case letters between the drought treatments across DATs ($p < 0.05$). DAT, days after initiation of drought treatment.

increases in citrulline. Although non-significant, the content of both ornithine (precursor of citrulline, p = 0.09) and arginine (catabolic product of citrulline, p = 0.12) (**Figure 3B**) also showed increasing trends at least during early drought stress (8 DAT, Leaf I). Nonetheless, their increases in stem tissue were consistent with the fold changes in citrulline. The correlation analysis of amino acids detected from leaf-I at 8 DAT in drought-stressed plants showed a significant positive correlation between

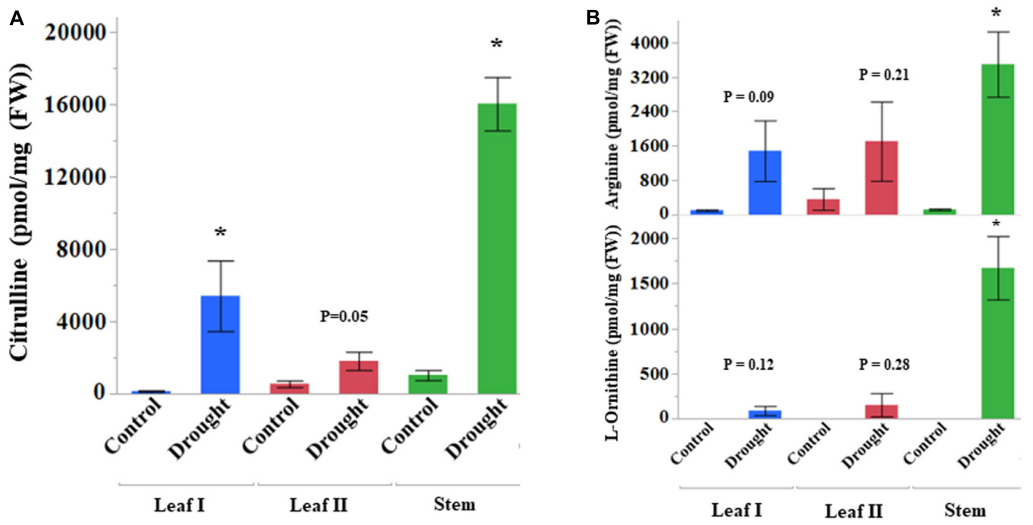

FIGURE 3 | Drought stress induced accumulation of amino acids (pmol/mg FW). Vegetative tissues showing changes in the content of **(A)** Citrulline and **(B)** Ornithine and Arginine. DAT, date after treatment. Leaf I and Stem tissues collected at 8 DAT, Leaf II at 24 DAT, Asterisk (*) indicates significance from control at respective DAT between control and drought treatments at $p < 0.05$ based on Student's *t*-test. Values are mean ± SD (n = 3 or 4) from four independent replications. DAT, days after initiation of drought treatment.

ornithine, citrulline, and arginine (**Supplementary Figure S3**). The content of other amino acids, such as phenylalanine, valine, proline, glycine, serine, glutamine, and glutamic acid was at least twofold higher in drought-stressed leaf tissue at 8 DAT. Most amino acids in stem showed many-fold increases during drought stress than control tissues (**Supplementary Table S2**). In terms of percent distribution, citrulline alone accounted for almost 25 and 21% of total amino acids at 8DAT in the drought-stressed leaf and stem tissues respectively (**Supplementary Figures S4, S5**).

Expression of Genes Involved in Citrulline Metabolism Using RNA-Seq Analysis of Leaf

Transcriptome Sequencing and Assembly of Sequencing Data

To understand the early transcriptomic changes induced due to drought stress, we performed RNA-Sequencing (RNA-Seq) analysis of leaf tissue 8 days after the initiation of drought stress. A total of six libraries from leaf tissue (CT_1, CT_2, CT_3 for control and DT_1, DT_2, DT_3 for drought stress) were sequenced using the Illumina HiSeq platform. On average, 45.53 to 43.47 million raw reads were generated from leaf tissues in both treatments (**Supplementary Table S3**). Across all reads for both treatments, the Q20 and Q30 percentage was more than 98 and 94%, respectively (sequencing error rate was less than 0.02%), and GC content for the libraries was ∼45%. Additional significant characteristics of these libraries are summarized in **Supplementary Table S3**. Among all the libraries, the ratio of total mapped reads was above 97%, of which ∼92% reads uniquely mapped to the reference watermelon genome. The data generated from all libraries provided a foundation for quality analyses. The correlations among biological replicates were assessed using the Pearson correlation coefficient (**Supplementary Figure S6**). The libraries for the same treatment were highly correlated. The weak correlation between treatments suggests a significant impact of drought stress on gene expression profiles.

Analysis of Differentially Expressed Genes (DEGs) Associated With Citrulline Metabolism

The RNA-Seq analysis identified 3971 differentially expressed ($p < 0.05$) genes in the leaf tissue of drought-stressed plants. The volcano map showing a total of 1513 upregulated genes and 2458 downregulated genes is presented in **Figure 4**. The list of genes showing up- and down-regulation of genes due to drought stress are listed in **Supplementary Tables S4, S5**, respectively. The fold-change differences in the expression of a subset of genes associated directly or indirectly with citrulline metabolism are presented in **Table 1**. The transcript quantification confirmed significant increases in the expression of *N-acetylornithine deacetylases* (*AOD*, ClCG09G012030, ClCG09G012020), the large subunit of Carbamoyl *phosphate synthase* (*CPS2*, ClCG09G021680), and *N-acetylornithine aminotransferase* (ClCG09G003180) which all are associated directly with citrulline synthesis. Expression of all three *Arginosuccinate synthases* (*ASS*; ClCG03G003660, ClCG03G003670, and ClCG06G017780) involved in two-step degradation of citrulline was significantly downregulated. Similarly, the expression of *Ornithine decarboxylase* (*ODC*; ClCG08G013990) associated with the alternative pathway of ornithine catabolism was also significantly downregulated.

Ten DEGs associated with citrulline metabolism were used for real-time qRT-PCR analysis to validate the RNA-Seq data.

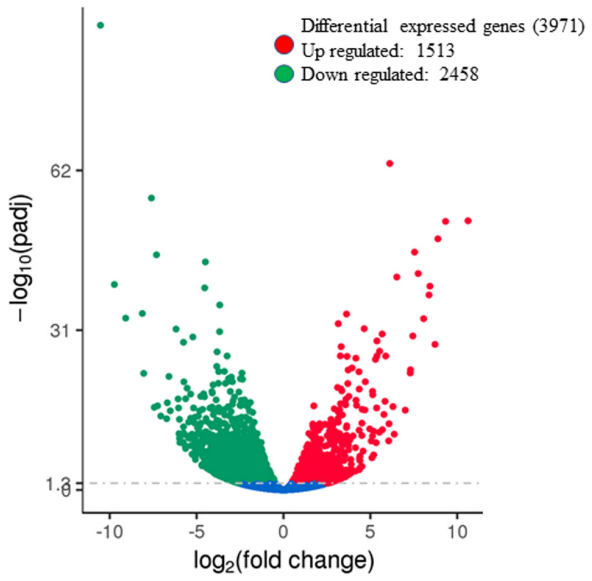

FIGURE 4 | Summary of differentially expressed genes during drought stress. The volcano map showing the number of differentially expressed genes in the leaf tissue (8 DAT) due to drought stress. Red dots represent up-regulated genes and green dots represent down-regulated genes (padj < 0.05). Blue dots indicate no significant difference in genes padj(qvalue) is corrected *p*-value. DAT, days after initiation of drought treatment.

The expression analysis confirmed the induction of *CPS2*, *Ornithine carbamoyltransferase (OTC)*, *AOD2*, *AOD3*, and *N-Acetylornithine aminotransferase* (*AAT*) and trend for down-regulation of *ASS1* (**Figure 5**). The qPCR expression data confirmed the results and reproducibility of the RNA-Seq data for the subset of selected genes (**Supplementary Figure S7**).

Impact of Nitrogen Deficiency on Citrulline Metabolism

Validation of Nitrogen Deficit Treatment

A field experiment was performed to evaluate the impact of nitrogen deficit on citrulline accumulation in the vegetative tissues during development. The nitrogen deficit was validated based on significantly lower total soil inorganic nitrogen (**Supplementary Figure S8A**) and free nitrates (**Supplementary Figure S8B**). Additionally, the estimates of nitrate in the phloem sap (**Supplementary Figure S9**), total nitrogen in leaves (**Supplementary Figure S10**), and chlorophyll content (**Supplementary Figure S11**) further confirmed the compromised nitrogen assimilation in the plants under nitrogen deficit.

Changes in the Citrulline Content and Gene Expression During Nitrogen Deficit

Citrulline content in the leaf tissues was altered significantly, vis-à-vis the availability of nitrogen. The citrulline in leaf tissues collected 45 and 69 days after initiation of nitrogen stress was reduced by 5 to 6-fold in cultivar Charleston Gray and 2 to 6-fold in Crimson Sweet (**Figure 6**). Ornithine content was only detectable in leaves during the early stages of plant development and was reduced by several folds in both the cultivars due to nitrogen stress (**Supplementary Tables S6**, **S7**). While arginine content was down by eightfold due to nitrogen stress in the cultivar Crimson Sweet at 45 days after the initiation of nitrogen stress. Besides, aspartate and glutamine, which reduced significantly due to nitrogen stress, most other amino acids showed a trend for reduced accumulation due to nitrogen stress in leaf tissues. The changes in amino acids were not consistent in the stem of both the cultivars. In terms of relative contribution, percent distribution of citrulline, arginine, or ornithine relative to all amino acids was significantly reduced due to nitrogen stress in the vegetative tissues of both the cultivars (**Supplementary Figures S12**, **S13**). Further, we also evaluated changes in the content of amino acids in the phloem sap due to nitrogen stress. Although differences were insignificant in the case of cultivar Charleston Gray, the amounts of citrulline, arginine, and ornithine were significantly reduced in the cultivar Crimson Sweet subjected to nitrogen stress (**Supplementary Figure S14**). A subset of genes associated with citrulline metabolism was

TABLE 1 | RNA-Seq data showing fold-change differences in the expression of genes associated with citrulline metabolism.

Gene IDs	Gene function	log2 fold-change	*p*-Value
C1CG09G012030	*N*-acetylornithine deacetylase	7.44	0.00
C1CG09G021680	Carbamoyl phosphate synthase, large subunit	1.84	0.00
C1CG09G012020	*N*-acetylornithine deacetylase	1.14	0.00
C1CG04G004210	Pyrroline-5-carboxylate reductase	0.82	0.04
C1CG01G004960	Nitric-oxide synthase, putative	0.81	0.01
C1CG09G003180	*N*-acetylornithine aminotransferase	0.79	0.01
C1CG03G006680	Ornithine-δ-aminotransferase	0.71	0.00
C1CG05G018820	Ornithine carbamoyltransferase	0.67	0.07
C1CG08G011660	Argininosuccinate lyase	0.65	0.09
C1CG11G003830	Arginine decarboxylase	0.63	0.01
C1CG01G014440	P5C dehydrogenase	0.5	0.03
C1CG06G000480	Arginase	0.38	0.32
C1CG01G017650	*N*-acetyl Glu synthase	0.09	0.82
C1CG11G013120	Carbamoyl phosphate synthase, small subunit	−0.22	0.42
C1CG08G012830	*N*-acetylglutamate kinase	−0.24	0.50
C1CG09G004810	P-II	−0.24	0.33
C1CG09G012040	*N*-acetylornithine deacetylase	−0.35	0.72
C1CG10G020940	*N*-acetylornithine-glutamate acetyltransferase	−0.36	0.36
C1CG11G014580	Argininosuccinate lyase	−0.42	0.08
C1CG11G013850	Urease	−0.59	0.12
C1CG11G005180	Proline dehydrogenase	−0.92	0.14
C1CG09G017590	*N*-acetyl-γ-glutamyl-P-reductase	−1.02	0.06
C1CG10G021450	Pyrroline-5-carboxylate synthase	−1.08	0.09
C1CG03G003660	Argininosuccinate synthase	−1.16	0.02
C1CG06G017780	Argininosuccinate synthase	−1.58	0.00
C1CG11G006600	Pyrroline-5-carboxylate synthase	−1.67	0.00
C1CG03G003670	Argininosuccinate synthase	−2.25	0.00
C1CG08G013990	Ornithine decarboxylase	−2.49	0.01

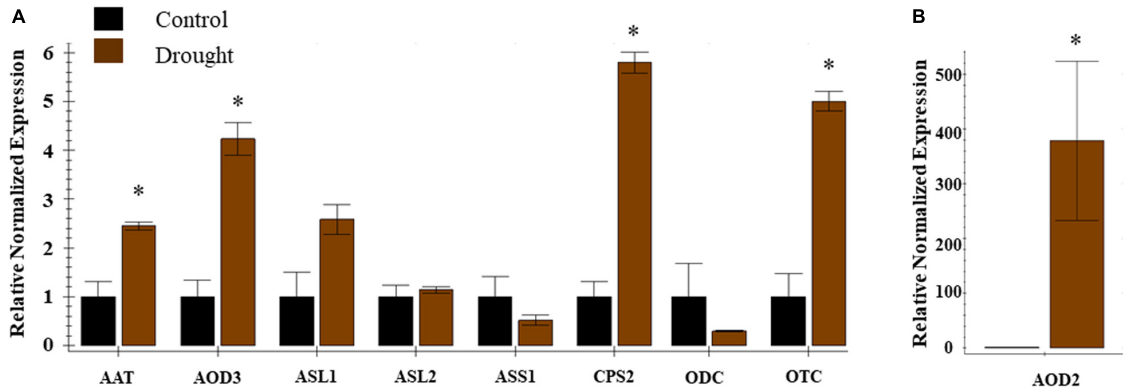

FIGURE 5 | Expression profiles of genes associated with citrulline metabolism during drought stress. Real time expression analysis was carried out in leaf tissue 8 DAT from control and drought stressed plants. The error bars represent the means ± SE (n = 3), asterisk indicates significant differences in the expression of a specific gene compared to control sample (p < 0.1). Relative normalized expression is presented for nine **(A)** genes viz. AAT, *N*-acetylomithine transferase; AOD3, *N-acetylornithine* deacetylase; ASL-1, 2 Arginosuccinate lyase; ASS-1, Arginosuccinate synthase; CPS2, Carbamoyl phosphate synthase -large subunit; OCD, ornithine cyclodeaminase; ODC, Omithine decarboxylase; OTC, Omithine transcarboxylase; DAT, days after initiation of drought treatment and **(B)** AOD2, *N*-acetylornithine deacetylase.

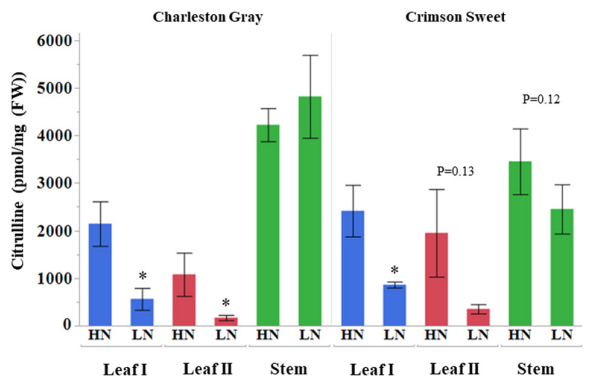

FIGURE 6 | Citrulline accumulation in watermelon tissues during nitrogen deficit (pmol/mg FW). Citrulline content of plant tissues collected during early 45 DAT (Leaf I and stem) and extended 69 DAT (Leaf II) nitrogen deficit treatment is shown on vertical axis. The values represent means ± SD (n = 3 or 4). The asterisk (*) represent significant differences between high (HN) and nitrogen deficit (LN) treatments (p < 0.1, Student's t-test). DAT, days after initiation of nitrogen deficit treatment.

evaluated using the quantitative real-time gene expression analysis of leaf tissue using cv. Crimson Sweet (**Figure 7**). The expression of *AAT* and *CPS2* associated with citrulline biosynthesis were downregulated. Unlike the drought-stressed plants, the expression of other genes associated with citrulline metabolism was mostly unchanged due to nitrogen stress.

DISCUSSION

Induction of Citrulline in the Vegetative Tissues of Watermelon During Drought Stress

Abiotic stresses such as drought stress or sub-optimal nitrogen levels, severely limit the productivity of many crops. Tolerance to abiotic stresses is a complex trait requiring orchestrated regulation of physiological, molecular, and biochemical responses, each making incremental contributions. Exposure to drought stress disrupts the electron transport chains resulting in the accumulation of ROS, which can lead to cellular damage. Amino acids induced in response to abiotic stresses act as powerful ROS-scavengers or antioxidants (Verslues and Juenger, 2011). Being potentially potent hydroxyl radical scavenger than other compatible solutes like mannitol, proline, and glycine betaine (Akashi et al., 2001; Yokota et al., 2002), citrulline contributes to protecting green tissues from the secondary oxidative stress damage during drought stress. Although produced in large amounts in the fruits of cucurbits, not much is known about the physiological or biochemical relevance of citrulline in the vegetative tissues of plants. Citrulline has been proposed to play a broader role in abiotic stress tolerance as an active osmolyte, nitrogen carriers, and possibly a signaling molecule (Joshi and Fernie, 2017). Our results demonstrated a rapid early induction (∼38 fold) of citrulline within 8 days of initiation of drought stress. Citrulline accumulation in leaf tissues further increased during prolonged stress, but its induction relative to control decreased (∼16 fold). The early rapid induction of citrulline implicates its utility as a potential biomarker for drought-induced responses. The fold-change increases in arginine (catabolic product of citrulline) and ornithine (precursor), consistent with the increase in citrulline and their high positive correlations with one another, emphasize the significance of the ornithine-citrulline-arginine pathway in watermelons during drought stress. Nonetheless, the importance of the glutamate-derived arginine pathway in abiotic stress tolerance in higher plants is well-supported, due to the production of stress-induced intermediates such as ornithine, citrulline, nitrous oxide, polyamines and proline (Kalamaki et al., 2009; Winter et al., 2015). Further, in terms of abundance, percent citrulline accumulation due to drought stress varied from 21 to 25% in stem and leaf tissues, respectively.

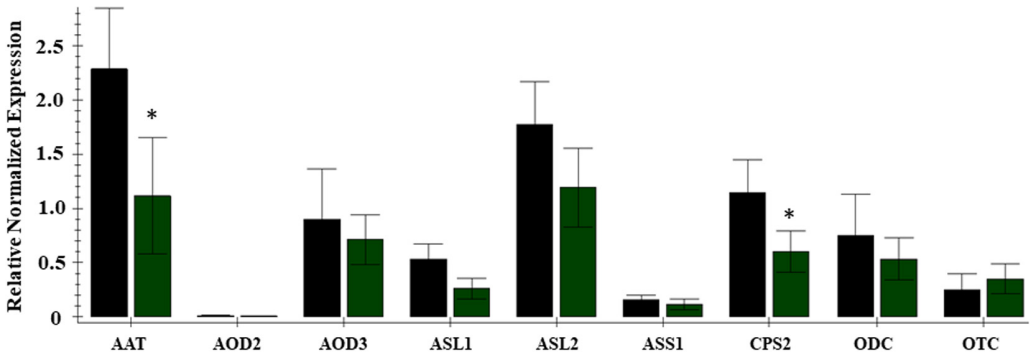

FIGURE 7 | Expression analysis of genes associated with citrulline metabolism during nitrogen deficit in the cultivar Crimson Sweet. Real-time expression analysis was carried out using leaf tissues 45 DAT from plants subjected to nitrogen stress LN (green bars) and control HN (black bars). The error bars represent the means ± SE ($n = 3$); an asterisk indicates significant differences in the expression of a specific gene compared to the control sample ($p < 0.1$) for nine genes viz. *AAT*, *N-acetyrlornithine transferase*; *AOD3*, *N-acetylornithine deacetylase*; *ASL-1*, *2Arginosuccinate lyase*; *ASS-1*, *Arginosuccinate synthase*; *CPS2, Carbamoyl phosphate synthase -large subunit*; *ODC, Omithine decarboxylase*; *OTC, Ornithine transcarboxylase*; *AOD2, N-acetylomithine deacetylase*; DAT, days afterinitiation of drought treatment.

These findings are consistent with a report showing almost 49% accumulation of citrulline during drought stress in the leaves of *Citrullus colocynthis*, a wild relative of watermelon (Kawasaki et al., 2000; Yokota et al., 2002). Transgenic approaches such as overexpression of DOF transcription factor (Massange-Sánchez et al., 2016) and *N*-acetyl-L-glutamate synthase, a first biosynthetic enzyme in the arginine pathway (Kalamaki et al., 2009) in Arabidopsis have demonstrated a positive association between increased citrulline and drought tolerance. Enhanced citrulline accumulation and possibly genes associated with its metabolism in watermelon could provide cues to manipulate citrulline concentrations in plant species that do not accumulate enough citrulline.

Transcriptional Regulation of Citrulline Metabolism

The complex nature of plant responses to drought stress is evident by thousands of differentially expressed genes identified in numerous transcriptomic datasets available in the public domain. However, a coherent picture of a generalized regulation of citrulline metabolism based on gene expression profiles across plant species have not yet emerged. In this study, using the genome sequence of cultivar Charleston Gray, we identified 3971 differentially expressed genes in drought-stressed leaves of watermelon, out of which 132 were novel genes. Our transcriptome data indicated that most genes related to citrulline metabolism were differentially expressed under drought stress (**Table 1**). Notably, the expression of *N-acetylornithine deacetylases*, *Carbamoyl phosphate synthase (large subunit), N-acetylornithine aminotransferase*, and *OTC* directly associated with citrulline synthesis were significantly up-regulated in response to drought stress, which is consistent with the enhanced levels of citrulline and arginine. Moreover, the expression of *Argininosuccinate lyase (ASL2),* and all three *Argininosuccinate synthase* genes associated with citrulline catabolism; and expression of *ODC* involved in ornithine catabolism were significantly downregulated. However, the activation of citrulline biosynthetic genes is consistent with RNAseq profiles of the drought-stressed leaves of *C. colocynthis* plants (Wang et al., 2014).

A model illustrating the possible regulation of citrulline during drought stress by activation of biosynthetic genes (*AAT, AOD, OTC, and CPS2*) and down-regulation of catabolic (*ASS, ASL, ODC*) genes is presented (**Figure 8**). Among the biosynthetic genes, expression of *AAT* which catalyzes the reversible conversion of *N*-acetylglutamate 5-semialdehyde to *N*-acetylornithine in the presence of glutamate, was highly induced in drought-stressed leaves. *N*-acetylornithine aminotransferase in Arabidopsis (Frémont et al., 2013) is highly expressed in leaves and involved in arginine synthesis. Consistent with the induced expression of *N-acetylornithine deacetylases* genes in the drought-stressed leaves of *C. colocynthis* (Wang et al., 2014), both the *AOD2* (ClCG09G012030) and *AOD3* (ClCG09G012020) genes were induced in the leaf tissue in response to drought stress. In Arabidopsis, AOD is involved in ornithine synthesis and regulation of the C: N balance during reproduction via polyamine synthesis (Molesini et al., 2015). It was previously suggested that wild watermelon accumulates high levels of acetylornithine deacetylase (*DRIP1; ArgE*) transcripts (Kawasaki et al., 2000) and *N*-acetylornithine: *N*-acetylglutamate acetyltransferase (*NAOGAcT*) (Takahara et al., 2005) during drought stress. Our RNA-Seq analysis did not show any change in the expression of *NAOGAcT* (ClCG10G020940), which is involved in the non-linear pathway of ornithine/citrulline synthesis (Joshi and Fernie, 2017). Instead, synthesis of citrulline through the linear pathway *via* induction of *AAT* and both *AOD* genes justifies the superfluous energy-intensive regeneration of *N*-acetylglutamate through the non-linear pathway during drought stress. OTC and carbamoyl phosphate synthase (CPS2) catalyzing the first and penultimate steps in citrulline synthesis were both induced due to drought stress aligning with the increased citrulline phenotype in leaf tissues. The indispensable role of these genes in citrulline synthesis is apparent based

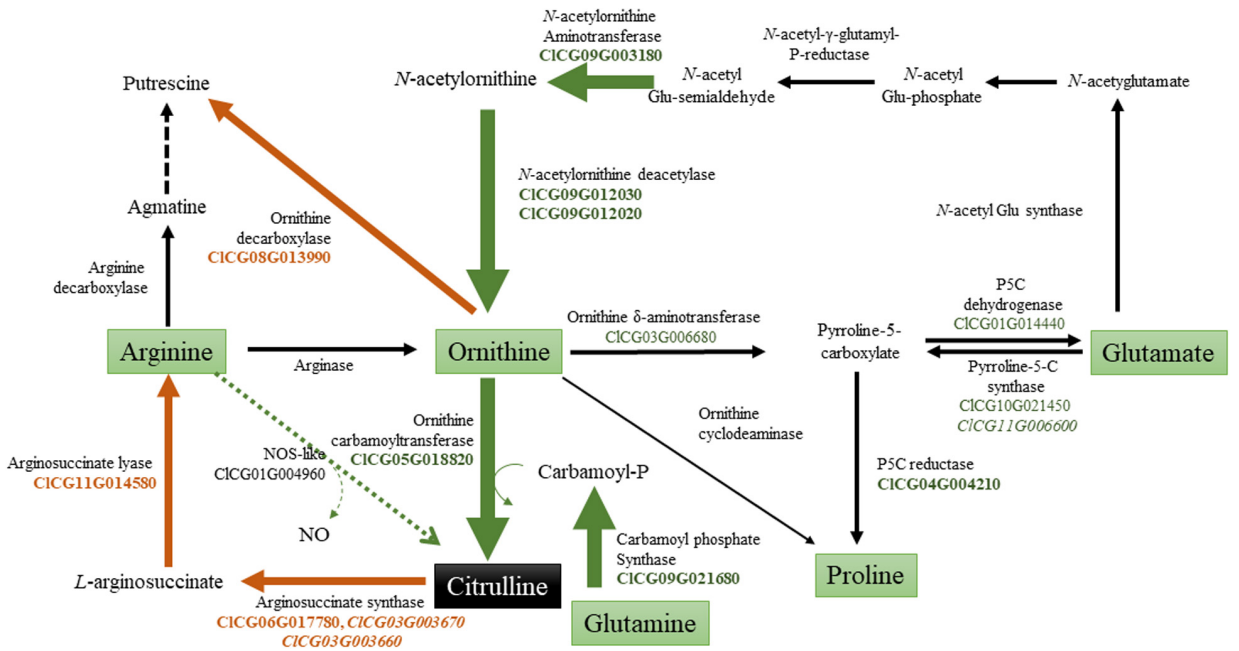

FIGURE 8 | Model showing the regulation ofcitrulline metabolism during drought stress. Based on expression and RNA-Seq analysis, genes involved in citrulline metabolism were grouped in into biosynthetic and catabolic genes. The green arrows indicates induction of genes associated with citrulline synthesis; while brown arrow's down-regulation of genes involved in citrulline/ornithine degradation [Gene EDs from Watermelon genome (cultivar Charleston Gray) [ntemational Cucurbit Genomics Initiative].

on reduced citrulline production in the leaves of ven6 knock-down mutation in the large subunit of Arabidopsis CPS (Mollá-Morales et al., 2011).

The expression of *ASS1* (ClCG06G017780), *ASS2* (ClCG03G003670), *ASS3* (ClCG03G003660), and *ASL2* (ClCG11G014580) genes, involved in citrulline catabolism, were significantly down-regulated corroborating the increased citrulline accumulation in drought-stressed leaves. Although *ASS* and *ASL* genes are critical for the synthesis of arginine and downstream products such as polyamines, not much is known with respect to their functional significance during abiotic stress in plants. Even So, the developmental down-regulation of *ASS* and *ASL* genes has been shown to increase citrulline concentration in maturing watermelon fruits (Guo et al., 2013, 2015; Joshi et al., 2019). The existence of a pathway synthesizing citrulline from arginine via *nitric oxide synthase* (*NOS*) still awaits an experimental confirmation in plants (Moreau et al., 2010; Santolini et al., 2017). Although our data shows the induction of a *NOS*-like (ClCG01G004960) gene, its potential role in citrulline production remains uncertain without its functional validation. Even if ODC is well-studied for its role in polyamine synthesis and abiotic stresses tolerance (Chen et al., 2019), expression of *ODC* gene (ClCG08G013990) was down-regulated in drought-stressed leaf tissue. Given, the ODC and OTC enzymes compete for the common pool of ornithine, down-regulation of *ODC* substantiates the importance of increased citrulline accumulation in drought-stressed tissues in watermelon. Although the downregulation of the ClCG05G008460 gene annotated as *Ornithine cyclodeaminase*[1] justifies the increased citrulline, the enzyme lacks functional validation and shares low homology (42%) with canonical Ornithine cyclodeaminases. Intriguingly, RNA-Seq data also identified the induction of *Ornithine δ-aminotransferase*, *Pyrroline-5-carboxylate synthase* (P5CS), and *Pyrroline-5-carboxylate reductase*, major genes involved in the synthesis of proline. Relative to citrulline, fold-change increase, or percent distribution of proline was minimal. It is plausible to assume that proline and citrulline act synergistically, although proline may play a subordinate role in drought tolerance in watermelon.

Impact of Nitrogen Limitation on Citrulline Metabolism

Although less common than allantoin, it was suggested that nitrogen-rich citrulline could represent a significant portion of the endogenous source of nitrogen storage and transport (Ludwig, 1993). Citrulline has been a mode of transport of nitrogen in legumes (Parsons and Sunley, 2001) xylem saps of trees (Cramer et al., 2002; Frak et al., 2002) and in storage tissues in walnut (Mapelli et al., 2001). Our data demonstrated that citrulline synthesis is regulated by the nitrogen status of the plant. The results (1) significant reduction in citrulline content along with ornithine or arginine in the leaf tissues (2) the percent distribution in the nitrogen depleted leaves and stem (10–18%), comparable to that of nitrogen carrying amino acids – aspartate and glutamate (3) reduction in the phloem sap (cv. Crimson Sweet), during nitrogen stress and

(4) down-regulation of biosynthetic genes *AAT* and *CPS2*, all support the role of citrulline in translocating nitrogen in the vegetative tissues of watermelon. Consistent with our results seedlings of a loss-of-function mutant of Arabidopsis nitrogen regulatory protein P-II, a gene located upstream in the citrulline metabolic pathway (Joshi and Fernie, 2017), grown on nitrogen depleted media accumulated up to 70% less citrulline along with down-regulation of *CPS* expression (Ferrario-Mery et al., 2006), while its over-expression in *Lotus japonicus* resulted in a 10-fold increase in free citrulline in nodules under nitrogen replete conditions (D'apuzzo et al., 2015). The data showing reduced levels of citrulline in the phloem sap further supports the role of citrulline in nitrogen translocation or long-distance transport. Consistent with this observation, citrulline was shown to be a significant component of phloem sap in muskmelon (*Cucumis melo* L) (Mitchell et al., 1992). The drought-induced *N*-acetyl glutamate transferase-like protein – DRIP-1 (Kawasaki et al., 2000) involved in citrulline synthesis was initially identified in the phloem exudates (Yokota et al., 2002). Moreover, the phloem sap transcriptome of watermelon (Guo et al., 2013) indicated a 35-fold higher expression of the *AOD* gene, which also supports the possibility of localized citrulline synthesis in the sieve elements for its long-distance transport. The differences in the amino acid composition of phloem sap among cultivars could be attributed to the genotypic or environmental factors.

CONCLUSION

This study illustrated the significance of citrulline metabolism during abiotic stresses such as drought and nitrogen limitation in watermelon. The drought-induced rapid accumulation of citrulline and related metabolites in the vegetative tissues was demonstrated. Although the metabolic consequences of citrulline accumulation during drought stress are not fully understood, our findings show how the metabolic pathways associated with citrulline synthesis and catabolism are regulated in the vegetative tissues of watermelon during drought stress. The gene expression analysis indicated that citrulline perturbation due to drought stress is regulated simultaneously by activation of its biosynthesis and suppression of its catabolism. The RNA-Sequencing data presented in this study, which characterized the differentially expressed genes during drought stress, would serve as a resource to understand transcriptomic mechanisms induced by drought stress. Our data also demonstrated that the nitrogen status of the plant regulates citrulline synthesis. A detailed analysis of citrulline metabolism in model species using loss-of-function mutants and metabolic flux analysis would allow a better understanding of rate-limiting stages in citrulline synthesis, and its functional relevance in abiotic stresses. The outcome of this study will not only improve the current understanding of citrulline metabolism in agriculturally important crop – watermelon but vertically advance the knowledge about its metabolism in plants that do not accumulate citrulline to facilitate metabolite engineering.

DATA AVAILABILITY STATEMENT

The datasets generated for this study are deposited in NCBI's Gene Expression Omnibus (Edgar et al., 2002) and are accessible through GEO Series accession number GSE144814, https://www.ncbi.nlm.nih.gov/geo/query/acc.cgi?acc=GSE144814.

AUTHOR CONTRIBUTIONS

QS and VJ conceived and designed the work and wrote the manuscript. QS, MJ, and JD performed the experiments. QS, VJ, and MJ analyzed the data. VJ, QS, and MJ revised the manuscript critically.

FUNDING

This work was supported by the USDA National Institute of Food and Agriculture (Hatch Project No. TEX09647/Project Accession No. 1011513).

ACKNOWLEDGMENTS

We appreciate Amit Kumar Mishra and Haramrit Gill for their assistance in sample collection for both metabolic and transcriptomic analysis.

SUPPLEMENTARY MATERIAL

The Supplementary Material for this article can be found online at: https://www.frontiersin.org/articles/10.3389/fpls.2020.00512/full#supplementary-material

REFERENCES

Akashi, K., Mifune, Y., Morita, K., Ishitsuka, S., Tsujimoto, H., and Ishihara, T. (2017). Spatial accumulation pattern of citrulline and other nutrients in immature and mature watermelon fruits. *J. Sci. Food Agric.* 97, 479–487. doi: 10.1002/jsfa.7749

Akashi, K., Miyake, C., and Yokota, A. (2001). Citrulline, a novel compatible solute in drought-tolerant wild watermelon leaves, is an efficient hydroxyl radical scavenger. *FEBS Lett.* 508, 438–442. doi: 10.1016/S0014-5793(01)03123-4

Akashi, K., Nishimura, N., Ishida, Y., and Yokota, A. (2004). Potent hydroxyl radical-scavenging activity of drought-induced type-2 metallothionein in wild watermelon. *Biochem. Biophys. Res. Commun.* 323, 72–78. doi: 10.1016/j.bbrc.2004.08.056

Akashi, K., Yoshimura, K., Nanasato, Y., Takahara, K., Munekage, Y., and Yokota, A. (2008). Wild plant resources for studying molecular mechanisms of drought/strong light stress tolerance. *Plant Biotechnol. J.* 25, 257–263. doi: 10.5511/plantbiotechnology.25.257

Ali, F., Bano, A., and Fazal, A. (2017). Recent methods of drought stress tolerance in plants. *Plant Growth Regul.* 82, 363–375. doi: 10.1007/s10725-017-0267-2

Allen, A. E., Dupont, C. L., Oborník, M., Horák, A., Nunes-Nesi, A., Mccrow, J. P., et al. (2011). Evolution and metabolic significance of the urea cycle in photosynthetic diatoms. *Nature* 473, 203–207. doi: 10.1038/nature10074

Anders, S., and Huber, W. (2010). Differential expression analysis for sequence count data. *Genome Biol.* 11:R106. doi: 10.1038/npre.2010.4282.2

Annunziata, M. G., Ciarmiello, L. F., Woodrow, P., Dell'aversana, E., and Carillo, P. (2019). Spatial and temporal profile of glycine betaine accumulation in plants under abiotic stresses. *Front. Plant Sci.* 10:230. doi: 10.3389/fpls.2019.00230

Ball, R., and Oosterhuis, D. (2005). Measurement of root and leaf osmotic potential using the vapor-pressure osmometer. *Environ. Exp. Bot.* 53, 77–84. doi: 10.1016/j.envexpbot.2004.03.003

Chen, D., Shao, Q., Yin, L., Younis, A., and Zheng, B. (2019). Polyamine function in plants: metabolism, regulation on development, and roles in abiotic stress responses. *Front. Plant Sci.* 9:1945. doi: 10.3389/fpls.2018.01945

Chen, T. H., and Murata, N. (2002). Enhancement of tolerance of abiotic stress by metabolic engineering of betaines and other compatible solutes. *Curr. Opin. Plant Biol.* 5, 250–257. doi: 10.1016/S1369-5266(02)00255-8

Cramer, V. A., Schmidt, S., Stewart, G. R., and Thorburn, P. J. (2002). Can the nitrogenous composition of xylem sap be used to assess salinity stress in *Casuarina glauca*? *Tree Physiol.* 22, 1019–1026. doi: 10.1093/treephys/22.14.1019

D'apuzzo, E., Valkov, V. T., Parlati, A., Omrane, S., Barbulova, A., Sainz, M. M., et al. (2015). PII overexpression in lotus japonicus affects nodule activity in permissive low-nitrogen conditions and increases nodule numbers in high nitrogen treated plants. *Mol. Plant Microb. Interact.* 28, 432–442. doi: 10.1094/MPMI-09-14-0285-R

Daşgan, H. Y., Kuşvuran, S., and Abak, K. (2009). The relationship between citrulline accumulation and salt tolerance during the vegetative growth of melon (*Cucumis melo* L.). *Plant Soil Environ.* 55, 51–57. doi: 10.17221/316-pse

Davis, A., Webber, C., Fish, W., Wehner, T., King, S., and Perkins, P. (2011). L-citrulline levels in watermelon cultigens tested in two environments. *Hort Sci.* 46, 1572–1575. doi: 10.21273/hortsci.46.12.1572

Edgar, R., Domrachev, M., and Lash, A. E. (2002). Gene expression omnibus: NCBI gene expression and hybridization array data repository. *Nucleic Acids Res.* 30, 207–210. doi: 10.1093/nar/30.1.207

Ferrario-Mery, S., Besin, E., Pichon, O., Meyer, C., and Hodges, M. (2006). The regulatory PII protein controls arginine biosynthesis in *Arabidopsis*. *FEBS Lett.* 580, 2015–2020. doi: 10.1016/j.febslet.2006.02.075

Fish, W. W. (2014). The expression of citrulline and other members of the arginine metabolic family in developing watermelon fruit. *Int. J. Agric. Innov. Res.* 2, 665–672.

Frak, E., Millard, P., Le Roux, X., Guillaumie, S., and Wendler, R. (2002). Coupling sap flow velocity and amino acid concentrations as an alternative method to (15)N labeling for quantifying nitrogen remobilization by walnut trees. *Plant Physiol.* 130, 1043–1053. doi: 10.1104/pp.002139

Frémont, N., Riefler, M., Stolz, A., and Schmülling, T. (2013). The Arabidopsis TUMOR PRONE5 gene encodes an acetylornithine aminotransferase required for arginine biosynthesis and root meristem maintenance in blue light. *Plant Physiol.* 161, 1127–1140. doi: 10.1104/pp.112.210583

Garg, R., Shankar, R., Thakkar, B., Kudapa, H., Krishnamurthy, L., Mantri, N., et al. (2016). Transcriptome analyses reveal genotype- and developmental stage-specific molecular responses to drought and salinity stresses in chickpea. *Sci. Rep.* 6, 19228–19228. doi: 10.1038/srep19228

Good, A. G., and Zaplachinski, S. T. (1994). The effects of drought stress on free amino acid accumulation and protein synthesis in *Brassica napus*. *Physiol. Plant.* 90, 9–14. doi: 10.1111/j.1399-3054.1994.tb02185.x

Guo, S., Sun, H., Zhang, H., Liu, J., Ren, Y., Gong, G., et al. (2015). Comparative transcriptome analysis of cultivated and wild watermelon during fruit development. *PLoS One* 10:130267. doi: 10.1371/journal.pone.0130267

Guo, S. G., Zhang, J. G., Sun, H. H., Salse, J., Lucas, W. J., Zhang, H. Y., et al. (2013). The draft genome of watermelon (*Citrullus lanatus*) and resequencing of 20 diverse accessions. *Nat. Genet.* 45, 51–58. doi: 10.1038/ng.2470

Hare, P. D., Cress, W. A., and Van Staden, J. (1998). Dissecting the roles of osmolyte accumulation during stress. *Plant. Cell Environ.* 21, 535–553. doi: 10.1046/j.1365-3040.1998.00309.x

Hildebrandt, T. M. (2018). Synthesis versus degradation: directions of amino acid metabolism during *Arabidopsis* abiotic stress response. *Plant Mol. Biol.* 98, 121–135. doi: 10.1007/s11103-018-0767-0

Hildebrandt, T. M., Nunes, N. A., Araújo, W. L., and Braun, H. P. (2015). Amino acid catabolism in plants. *Mol. Plant* 8, 1563–1579. doi: 10.1016/j.molp.2015.09.005

Huang, T., and Jander, G. (2017). Abscisic acid-regulated protein degradation causes osmotic stress-induced accumulation of branched-chain amino acids in *Arabidopsis thaliana*. *Planta* 246, 737–747. doi: 10.1007/s00425-017-2727-3

Joshi, V., and Fernie, A. R. (2017). Citrulline metabolism in plants. *Amino Acids* 49, 1543–1559. doi: 10.1007/s00726-017-2468-4

Joshi, V., Joshi, M., Silwal, D., Noonan, K., Rodriguez, S., and Penalosa, A. (2019). Systematized biosynthesis and catabolism regulate citrulline accumulation in watermelon. *Phytochemistry* 162, 129–140. doi: 10.1016/j.phytochem.2019.03.003

Joshi, V., Joung, J.-G., Fei, Z., and Jander, G. (2010). Interdependence of threonine, methionine and isoleucine metabolism in plants: accumulation and transcriptional regulation under abiotic stress. *Amino Acids* 39, 933–947. doi: 10.1007/s00726-010-0505-7

Kalamaki, M. S., Alexandrou, D., Lazari, D., Merkouropoulos, G., Fotopoulos, V., Pateraki, I., et al. (2009). Over-expression of a tomato N-acetyl-L-glutamate synthase gene (SlNAGS1) in *Arabidopsis thaliana* results in high ornithine levels and increased tolerance in salt and drought stresses. *J. Exp. Bot.* 60, 1859–1871. doi: 10.1093/jxb/erp072

Kasting, R., and Delwiche, C. C. (1958). Ornithine, citrulline, and arginine metabolism in watermelon seedlings. *Plant Physiol.* 33, 350–354. doi: 10.1104/pp.33.5.350

Kawasaki, S., Miyake, C., Kohchi, T., Fujii, S., Uchida, M., and Yokota, A. (2000). Responses of wild watermelon to drought stress: accumulation of an ArgE homologue and citrulline in leaves during water deficits. *Plant Cell Physiol.* 41, 864–873. doi: 10.1093/pcp/pcd005

Khan, N., Bano, A., Rahman, M. A., Guo, J., Kang, Z., and Babar, M. A. (2019). Comparative physiological and metabolic analysis reveals a complex mechanism involved in drought tolerance in chickpea (*Cicer arietinum* L.) induced by PGPR and PGRs. *Sci. Rep.* 9:2097. doi: 10.1038/s41598-019-38702-8

Kong, Q., Yuan, J., Gao, L., Zhao, S., Jiang, W., Huang, Y., et al. (2014). Identification of suitable reference genes for gene expression normalization in qRT-PCR analysis in watermelon. *PLoS One* 9:e90612. doi: 10.1371/journal.pone.0090612

Kusvuran, S., Dasgan, H. Y., and Abak, K. (2013). Citrulline is an important biochemical indicator in tolerance to saline and drought stresses in melon. *Sci. World J.* 2013, 253414. doi: 10.1155/2013/253414

Ludwig, R. A. (1993). Arabidopsis chloroplasts dissimilate L-arginine and L-citrulline for use as N source. *Plant Physiol.* 101, 429–434. doi: 10.1104/pp.101.2.429

Lunn, J. E., Delorge, I., Figueroa, C. M., Van Dijck, P., and Stitt, M. (2014). Trehalose metabolism in plants. *Plant J.* 79, 544–567. doi: 10.1111/tpj.12509

Mapelli, S., Brambilla, I., and Bertani, A. (2001). Free amino acids in walnut kernels and young seedlings. *Tree Physiol.* 21, 1299–1302. doi: 10.1093/treephys/21.17.1299

Massange-Sánchez, J. A., Palmeros-Suárez, P. A., Espitia-Rangel, E., Rodríguez-Arévalo, I., Sánchez-Segura, L., Martínez-Gallardo, N. A., et al. (2016). Overexpression of grain amaranth (*Amaranthus hypochondriacus*) AhERF or AhDOF transcription factors in *Arabidopsis thaliana* increases water deficit- and salt-stress tolerance, respectively, via contrasting stress-amelioration mechanisms. *PLoS One* 11:164280. doi: 10.1371/journal.pone.0164280

Mitchell, D. E., Gadus, M. V., and Madore, M. A. (1992). Patterns of assimilate production and translocation in muskmelon (*Cucumis melo* L.): I. diurnal patterns. *Plant Physiol.* 99, 959–965. doi: 10.1104/pp.99.3.959

Mitchell, D. E., and Madore, M. A. (1992). Patterns of assimilate production and translocation in muskmelon (*Cucumis melo* L.): II. Low temperature effects. *Plant Physiol.* 99, 966–971. doi: 10.1104/pp.99.3.966

Molesini, B., Mennella, G., Martini, F., Francese, G., and Pandolfini, T. (2015). Involvement of the putative N-acetylornithine deacetylase from *Arabidopsis thaliana* in flowering and fruit development. *Plant Cell Physiol.* 56, 1084–1096. doi: 10.1093/pcp/pcv030

Mollá-Morales, A., Sarmiento-Mañús, R., Robles, P., Quesada, V., Pérez-Pérez, J. M., González-Bayón, R., et al. (2011). Analysis of ven3 and ven6 reticulate mutants reveals the importance of arginine biosynthesis in *Arabidopsis*

leaf development. *Plant J.* 65, 335–345. doi: 10.1111/j.1365-313X.2010.04425.x

Moreau, M., Lindermayr, C., Durner, J., and Klessig, D. F. (2010). NO synthesis and signaling in plants – where do we stand? *Physiol. Plant.* 138, 372–383. doi: 10.1111/j.1399-3054.2009.01308.x

Nimmakayala, P., Tomason, Y. R., Abburi, V. L., Alvarado, A., Saminathan, T., Vajja, V. G., et al. (2016). Genome-wide differentiation of various melon horticultural groups for use in GWAS for fruit firmness and construction of a high resolution genetic map. *Front. Plant Sci.* 7:1437. doi: 10.3389/fpls.2016.01437

Obata, T., and Fernie, A. R. (2012). The use of metabolomics to dissect plant responses to abiotic stresses. *Cell. Mol. Life Sci.* 69, 3225–3243. doi: 10.1007/s00018-012-1091-5

Parsons, R., and Sunley, R. J. (2001). Nitrogen nutrition and the role of root–shoot nitrogen signalling particularly in symbiotic systems. *J. Exp. Bot.* 52, 435–443. doi: 10.1093/jxb/52.suppl_1.435

Per, T. S., Khan, N. A., Reddy, P. S., Masood, A., Hasanuzzaman, M., Khan, M. I. R., et al. (2017). Approaches in modulating proline metabolism in plants for salt and drought stress tolerance: phytohormones, mineral nutrients and transgenics. *Plant Physiol. Biochem.* 115, 126–140. doi: 10.1016/j.plaphy.2017.03.018

Pfaffl, M. W., Tichopad, A., Prgomet, C., and Neuvians, T. P. (2004). Determination of stable housekeeping genes, differentially regulated target genes and sample integrity: bestKeeper-Excel-based tool using pair-wise correlations. *Biotechnol. Lett.* 26, 509–515. doi: 10.1023/b:bile.0000019559.84305.47

Reuter, G. (1961). Biosynthesis of citrulline in plants. *Nature* 190, 447–447. doi: 10.1038/190447a0

Romero, F. M., Maiale, S. J., Rossi, F. R., Marina, M., Ruiz, O. A., and Garriz, A. (2018). Polyamine metabolism responses to biotic and abiotic stress. *Methods Mol. Biol.* 1694, 37–49. doi: 10.1007/978-1-4939-7398-9_3

Santolini, J., Andre, F., Jeandroz, S., and Wendehenne, D. (2017). Nitric oxide synthase in plants: where do we stand? *Nitric Oxide Biol. Chem.* 63, 30–38. doi: 10.1016/j.niox.2016.09.005

Sircar, S., and Parekh, N. (2019). Meta-analysis of drought-tolerant genotypes in *Oryza sativa*: a network-based approach. *PLoS One* 14:e0216068. doi: 10.1371/journal.pone.0216068

Slama, I., Abdelly, C., Bouchereau, A., Flowers, T., and Savouré, A. (2015). Diversity, distribution and roles of osmoprotective compounds accumulated in halophytes under abiotic stress. *Ann. Bot.* 115, 433–447. doi: 10.1093/aob/mcu239

Takahara, K., Akashi, K., and Yokota, A. (2005). Purification and characterization of glutamate N-acetyltransferase involved in citrulline accumulation in wild watermelon. *FEBS J.* 272, 5353–5364. doi: 10.1111/j.1742-4658.2005.04933.x

Trapnell, C., Williams, B. A., Pertea, G., Mortazavi, A., Kwan, G., Van Baren, M. J., et al. (2010). Transcript assembly and quantification by RNA-Seq reveals unannotated transcripts and isoform switching during cell differentiation. *Nat. Biotechnol.* 28, 511–515. doi: 10.1038/nbt.1621

Verslues, P. E., and Juenger, T. E. (2011). Drought, metabolites, and *Arabidopsis* natural variation: a promising combination for understanding adaptation to water-limited environments. *Curr. Opin. Plant Biol.* 14, 240–245. doi: 10.1016/j.pbi.2011.04.006

Wang, Z., Hu, H., Goertzen, L. R., Mcelroy, J. S., and Dane, F. (2014). Analysis of the citrullus colocynthis transcriptome during water deficit stress. *PLoS One* 9:e104657. doi: 10.1371/journal.pone.0104657

Winter, G., Todd, C. D., Trovato, M., Forlani, G., and Funck, D. (2015). Physiological implications of arginine metabolism in plants. *Front. Plant Sci.* 6:534. doi: 10.3389/fpls.2015.00534

Yokota, A., Kawasaki, S., Iwano, M., Nakamura, C., Miyake, C., and Akashi, K. (2002). Citrulline and DRIP-1 protein (ArgE homologue) in drought tolerance of wild watermelon. *Ann. Bot.* 89, 825–832. doi: 10.1093/aob/mcf074

Conflict of Interest: The authors declare that the research was conducted in the absence of any commercial or financial relationships that could be construed as a potential conflict of interest.

Copyright © 2020 Song, Joshi, DiPiazza and Joshi. This is an open-access article distributed under the terms of the Creative Commons Attribution License (CC BY). The use, distribution or reproduction in other forums is permitted, provided the original author(s) and the copyright owner(s) are credited and that the original publication in this journal is cited, in accordance with accepted academic practice. No use, distribution or reproduction is permitted which does not comply with these terms.

frontiers in Plant Science

REVIEW
published: 21 May 2020
doi: 10.3389/fpls.2020.00587

Lysine Catabolism Through the Saccharopine Pathway: Enzymes and Intermediates Involved in Plant Responses to Abiotic and Biotic Stress

Paulo Arruda[1,2,3]* *and Pedro Barreto*[1,2,3]

[1] Centro de Biologia Molecular e Engenharia Genética, Universidade Estadual de Campinas (UNICAMP), Campinas, Brazil, [2] Departamento de Genética, Evolução e Bioagentes, Instituto de Biologia, Universidade Estadual de Campinas (UNICAMP), Campinas, Brazil, [3] Genomics for Climate Change Research Center (GCCRC), Universidade Estadual de Campinas (UNICAMP), Campinas, Brazil

OPEN ACCESS

Edited by:
Maurizio Trovato,
Sapienza University of Rome, Italy

Reviewed by:
Donald Becker,
University of Nebraska-Lincoln,
United States
Qiaoquan Liu,
Yangzhou University, China

***Correspondence:**
Paulo Arruda
parruda@unicamp.br

Specialty section:
This article was submitted to
Plant Metabolism
and Chemodiversity,
a section of the journal
Frontiers in Plant Science

Received: 17 February 2020
Accepted: 20 April 2020
Published: 21 May 2020

Citation:
Arruda P and Barreto P (2020)
Lysine Catabolism Through
the Saccharopine Pathway: Enzymes
and Intermediates Involved in Plant
Responses to Abiotic and Biotic
Stress. Front. Plant Sci. 11:587.
doi: 10.3389/fpls.2020.00587

The saccharopine pathway (SACPATH) involves the conversion of lysine into α-aminoadipate by three enzymatic reactions catalyzed by the bifunctional enzyme lysine-ketoglutarate reductase/saccharopine dehydrogenase (LKR/SDH) and the enzyme α-aminoadipate semialdehyde dehydrogenase (AASADH). The LKR domain condenses lysine and α-ketoglutarate into saccharopine, and the SDH domain hydrolyzes saccharopine to form glutamate and α-aminoadipate semialdehyde, the latter of which is oxidized to α-aminoadipate by AASADH. Glutamate can give rise to proline by the action of the enzymes Δ^1-pyrroline-5-carboxylate synthetase (P5CS) and Δ^1-pyrroline-5-carboxylate reductase (P5CR), while Δ^1-piperideine-6-carboxylate the cyclic form of α-aminoadipate semialdehyde can be used by P5CR to produce pipecolate. The production of proline and pipecolate by the SACPATH can help plants face the damage caused by osmotic, drought, and salt stress. AASADH is a versatile enzyme that converts an array of aldehydes into carboxylates, and thus, its induction within the SACPATH would help alleviate the toxic effects of these compounds produced under stressful conditions. Pipecolate is the priming agent of N-hydroxypipecolate (NHP), the effector of systemic acquired resistance (SAR). In this review, lysine catabolism through the SACPATH is discussed in the context of abiotic stress and its potential role in the induction of the biotic stress response.

Keywords: Saccharopine pathway, lysine catabolism, biotic stress, abiotic stress, drought stress

INTRODUCTION

Plant adaptation to stressful environmental conditions such as drought, salinity, high temperature, and flooding, requires extensive remodeling at the cell, organ, and whole-plant level to sustain structural and metabolic homeostasis. For agriculture, abiotic stress is among the most pressing challenges and, depending on its intensity, frequency, and duration, can cause heavy losses in crop production (Lobell et al., 2011; Ray et al., 2015).

Plants have evolved multiple mechanisms to adapt to biotic and abiotic stress that involve remodeling organelle structure and metabolic pathways associated with protein, nucleic acids, carbohydrates, lipids, amino acids, phytohormones, cations, and small molecule that modulate stress responses (Van Wallendael et al., 2019). Thus, it is expected that not a single component of this integrated network would be capable of modulating cellular and metabolic responses to alleviate the impact of stressful conditions. On the contrary, the performance of plants subjected to biotic and abiotic stress requires a concerted orchestration of the multiple cellular and metabolic remodeling processes. This review focuses on one aspect of amino acid metabolism, lysine catabolism through the saccharopine pathway (SACPATH), which regulates the accumulation of lysine in seeds (Long et al., 2013; and for reviews, see Yu and Tian, 2018; Zhou et al., 2020) and is also involved in abiotic and biotic stress responses (Arruda and Neshich, 2012).

To date, three routes for lysine catabolism have been described in plants: the cadaverine pathway, the SACPATH and the NHP pathway. In the cadaverine pathway, the enzyme lysine decarboxylase converts lysine into the alkaloid cadaverine (Bunsupa et al., 2012). In the SACPATH, that is common to plants, animals, and bacteria, lysine is converted into α-aminoadipate by three enzymatic reactions catalyzed by lysine-ketoglutarate reductase/saccharopine dehydrogenase (LKR/SDH) and α-aminoadipate semialdehyde dehydrogenase (AASADH) (Markovitzs and Chuang, 1987; Papes et al., 1999; Arruda et al., 2000; Azevedo et al., 2003; Struys and Jakobs, 2010; Neshich et al., 2013). In the NHP pathway, lysine is converted into NHP by three reaction steps catalyzed by the enzymes aminotransferase AGD2-like defense response protein (ALD1), which deaminates lysine into dehydropipecolate (DHP), the reductase systemic acquired resistance-deficient 4 (SARD4), which reduces DHP to pipecolate, and flavin-dependent monooxygenase (FMO1), which N-hydroxylates pipecolate to generate NHP (for a review, see Hartmann and Zeier, 2018). NHP is central to plant immunity due to its role in the activation of systemic acquired resistance (SAR) upon pathogen attack (Hartmann and Zeier, 2018). However, the SACPATH has also recently been shown to give rise to pipecolate in a reaction catalyzed by the enzyme Δ^1-pyrroline-5-carboxylate reductase (P5CR), which is critical for proline biosynthesis (Szabados and Savoure, 2009), on Δ^1-piperideine-6-carboxylate, the cyclic form of α-aminoadipate semialdehyde (Struys and Jakobs, 2010, Struys et al., 2014). This review is not intended to provide a comprehensive overview of lysine catabolism in plants. Instead, it focuses on the SACPATH peculiarities that gives support to its role in the abiotic stress response and its potential contribution to the biotic stress response. Many excellent reviews concerning biotic stress response are available in the literature and may help complement the ideas and concepts presented in this review.

ENZYMES OF THE SACPATH

The central enzymes of the SACPATH catalyze a transamination-like reaction involving the enzymes LKR/SDH and AASADH (**Figure 1B**). In this pathway, lysine is condensed with α-ketoglutarate to generate saccharopine using NADPH as a cofactor. Saccharopine is than hydrolyzed to form α-aminoadipate semialdehyde and glutamate using $NAD(P)^+$ as a cofactor. Then, AASADH oxidezes α-aminoadioate semialdehyde to α-aminoadioate using $NAD(P)^+$ as a cofactor. The glutamate generated in the pathway can be metabolized by Δ^1-pyrroline-5-carboxylate synthetase (P5CS) and P5CR to produce proline while the cyclic form of α-aminoadipate semialdehyde, Δ^1-piperideine-6-carboxylate, can be used by P5CR to produce pipecolate (**Figure 2**). The catalytic properties and subcellular localization of each of these enzymes may help in the understanding of their metabolic role in stress response.

LKR/SDH

The enzyme LKR/SDH was first demonstrated to occur in plants in developing maize endosperm (Arruda et al., 1982; Brochetto-Braga et al., 1992). LKR and SDH belong to a single ∼120 kDa bifunctional polypeptide (Gonçalves-Butruille et al., 1996; Gaziola et al., 1997) that localizes in the cytosol (Kemper et al., 1999) in contrasts with the animal LKR/SDH, that localizes in the mitochondria matrix (Markovitzs and Chuang, 1987). Immature endosperms of high-lysine maize mutants, in addition to the bifunctional LKR/SDH polypeptide, also presents a small proportion of an active monofunctional SDH (Pompeu et al., 2006). Monofunctional SDH have also been found in animals (Papes et al., 1999) and in Arabidopsis (Stepansky et al., 2005). A monofunctional SDH have also been detected in Arabidopsis mitochondria (Fuchs et al., 2019). In animals, SDH activity seems to be essential inside mitochondria, as the organelle, in addition to the bifunctional LKR/SDH polypeptide, have significant amounts of a monofunctional SDH (Zhou et al., 2018).

In immature maize and rice endosperm, the enzymatic activity of the LKR domain is activated by Ca^{2+}, Mg^{2+}, high salt, and osmolytes (Kemper et al., 1998; Gaziola et al., 2000). The LKR domain, when separated from the SDH domain by limited proteolysis, retains its Ca^{2+} activation. However, it is inhibited by a protein fraction containing SDH polypeptides, suggesting that the SDH domain appears to negatively regulate the activity of the LKR domain (Kemper et al., 1998). The LKR domain but not the SDH domain is also activated by phosphorylation in a lysine-dependent manner (Arruda et al., 2000; Azevedo and Lea, 2001). In plants, the LKR and SDH domains of the bifunctional polypeptide are separated from each other by an ∼130 amino acid interdomain (Kemper et al., 1999; Anderson et al., 2010). Genome sequencing of genes encoding LKR/SDH revealed that, in most plants, the enzyme is encoded by a single gene, with a lone exception reported for poplar, which has two functional genes. Interestingly, transcripts encoding monofunctional LKR and monofunctional SDH have been identified in several plant species (Anderson et al., 2010).

AASADH

The AASADH enzyme belongs to the superfamily of $NAD(P)^+$-dependent aldehyde dehydrogenases (ALDs) that catalyze the conversion of aliphatic and aromatic aldehydes into their corresponding carboxylates (Singh et al., 2012). AASADH can

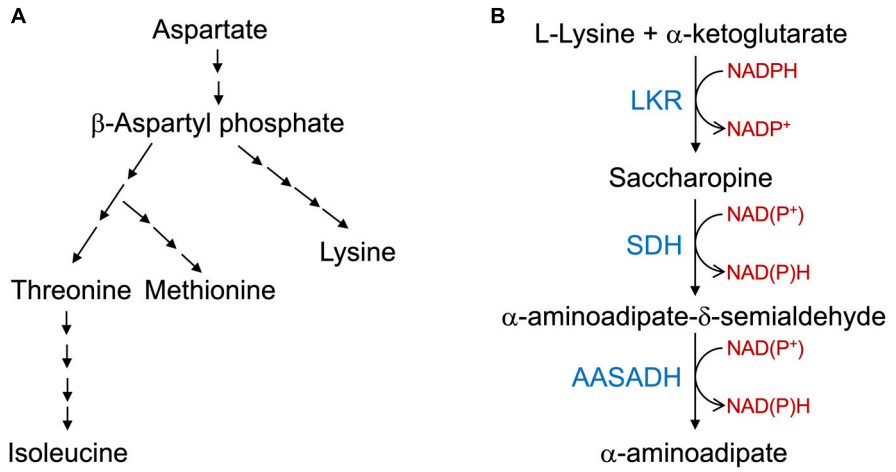

FIGURE 1 | The aspartate pathway for lysine biosynthesis and saccharopine pathway for lysine catabolism. **(A)** Schematic representation of the aspartate pathway. Only the key biosynthetic steps are represented. Aspartate is converted into β-aspartyl phosphate that is used in a serial enzymatic step by steps to produce lysine, threonine, methionine and Isoleucine. The aspartate pathway is localized in the plastids and thus lysine needs to be transported to the cytosol and other organelles. **(B)** The core reactions of the SACPATH involve the conversion of L-lysine into α-aminoadipate. The first two steps of the pathway are catalyzed by the bifunctional enzyme LKR/SDH; the LKR domain condenses L-lysine and α-ketoglutarate into saccharopine using NADPH as a cofactor and the SDH domain hydrolyzes saccharopine into α-aminoadipate semialdehyde and glutamate using $NAD(P)^+$ as cofactors. The α-aminoadipate semialdehyde is then oxidized into α-aminoadipate by the enzyme AASADH using $NAD(P)^+$ as cofactors.

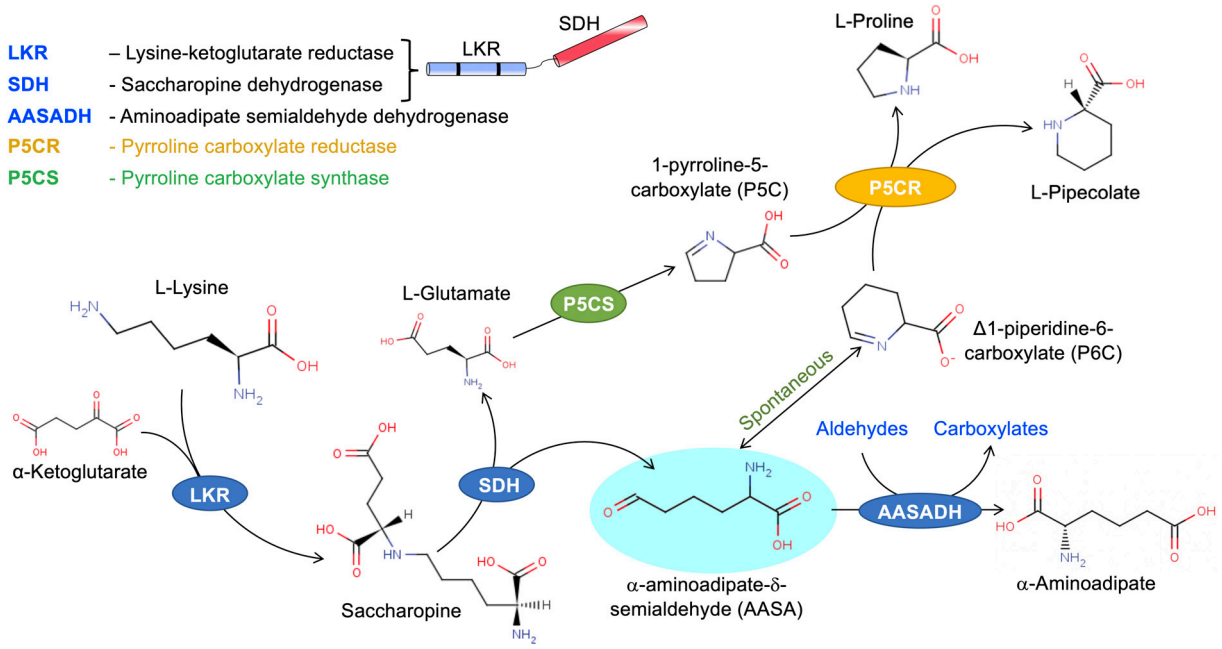

FIGURE 2 | The SACPATH metabolic flux that gives rise to proline and pipecolate. As depicted in **Figure 1**, the hydrolysis of saccharopine gives rise to glutamate and α-aminoadipate semialdehyde. Glutamate can be converted into proline by the action of P5CS and P5CR. P5CS converts glutamate into Δ^1-pyrroline 5-carboxylate that is than transformed into proline by P5CR. The α-aminoadipate semialdehyde spontaneously cyclizes to Δ^1-piperidine 6-carboxylate, which can serve as a substrate for P5CR to produce pipecolate.

use an array of aldehydes as substrates (Brocker et al., 2010; Kyiota et al., 2015) but seems to be the only ALD capable of using α-aminoadipate semialdehyde as a substrate, as null mutations of this enzyme in humans cause the disease pyridoxine-dependent epilepsy (PDE) (Mills et al., 2006). The ability of AASADH to use multiple aldehydes as substrates, such as betaine aldehyde, hexanal, octanal, non-anal, trans-2-non-anal, benzaldehyde and propanal (Brocker et al., 2010; Kyiota et al., 2015), makes it a scavenger of aldehydes generated by lipid peroxidation, carbohydrate metabolism, amino acid catabolism, and oxidative

stress, among others. AASADH has gained attention for its roles in the abiotic stress response and its involvement in human PDE (Mills et al., 2006; Rodrigues et al., 2006; Brocker et al., 2010, 2011; Kyiota et al., 2015; Crowther et al., 2019; Yang et al., 2019).

A detailed characterization of an AASADH enzyme was performed in a study of its role in hyperosmotic protection and cellular homeostasis in mouse (Brocker et al., 2010). AASADH is encoded by a single gene that generates differentially spliced transcripts producing polypeptides targeted to the cytosol and to the mitochondria. The transcript encoding the mitochondrial-targeted AASADH uses an alternative start codon that adds a mitochondrial signal sequence to the amino-terminus of the protein (Brocker et al., 2010).

Interestingly, compared with that for α-aminoadipate semialdehyde, the Km for AASADH from both animals and maize was shown to be 4-20-fold lower for non-anal, hexanal, octanal, benzaldehyde, and propanal (Brocker et al., 2010; Kyiota et al., 2015). The much higher affinity for the aliphatic aldehydes suggests an essential role of AASADH in alleviating the cellular toxicity of aldehydes, especially when plants are subjected to stress.

P5CS

P5CS is a bifunctional polypeptide containing γ-glutamyl kinase (GK) and glutamate-5-semialdehyde dehydrogenase (GPR) domains (Zhang et al., 1995; Perez-Arellano et al., 2010; Verslues and Sharma, 2010). In plants, there are two isoforms, P5CS1 and P5CS2, which are encoded by two closely related genes (Szekely et al., 2008). P5CS1 localizes in chloroplasts, whereas P5CS2 localizes to the cytosol. The P5CS amino acid sequence is highly conserved across species, which suggests its general biological relevance. The GPR catalytic domain converts γ-glutamyl phosphate to glutamate-5-semialdehyde, which then spontaneously cyclizes into Δ^1-pyrroline-5-carboxylate (Verslues and Sharma, 2010) (**Figure 2**). P5CS is a rate-limiting enzyme and thus is critical in increasing proline concentrations when plants are subjected to abiotic stress (Szabados and Savoure, 2009; Verslues and Sharma, 2010; Bhaskara et al., 2015). GK activity, but not GPR activity, is subject to feedback inhibition by proline, implying that the level of free amino acids in cellular medium feedback regulates enzyme activity (Zhang et al., 1995).

P5CR

P5CR has been less studied in plants. The enzyme converts Δ^1-pyrroline-5-carboxylate into proline (**Figure 2**); it is ubiquitous to most plant organs, and its expression is particularly high in soybean root nodules (Szoke et al., 1992). The enzyme is encoded by a single gene and has a 29 kDa monomeric native form. P5CR is mostly localized in the cytosol, although a small proportion of the enzyme also localizes in plastids (Szoke et al., 1992). Despite being encoded by a single gene, two isoforms of the enzymes P5CR-1 and P5CR-2 have been identified in spinach: P5CR-2 is a plastid isoform (Verslues and Sharma, 2010). P5CR is not rate limiting for the synthesis of proline and its expression seems not to be induced by abiotic stress (Verslues and Sharma, 2010), although upregulation of expression of the enzyme has been shown in plants and bacteria subjected to osmotic/salt stress (Neshich et al., 2013; Koenigshofer and Loeppert, 2019).

METABOLIC FLUX THROUGH THE SACPATH

In higher eukaryotes, the metabolic flux from lysine to α-aminoadipate (**Figure 2**) is unidirectional, since there is no evidence of the involvement of the SACPATH in lysine biosynthesis. In certain bacteria, lysine is directly oxidized into α-aminoadipate semialdehyde by the enzyme lysine dehydrogenase (Neshich et al., 2013). However, α-aminoadipate semialdehyde is highly toxic to eukaryotic cells. In humans, for example, its accumulation causes PDE (Mills et al., 2006). Thus, α-aminoadipate semialdehyde must be maintained at low concentrations by AASADH and P5CR to produce α-aminoadipate and pipecolate, respectively (**Figure 2**). Metabolic flux toward α-aminoadipate and pipecolate occurs when plants are exogenously fed lysine (Moulin et al., 2006; Kyiota et al., 2015). The glutamate formed by saccharopine hydrolysis can be used for the synthesis of proline (**Figure 2**). Proline synthesis from lysine was first shown by C^{14}-lysine feeding in the immature endosperm of wheat, maize, and barley (Lawrence and Grant, 1964; Sodek and Wilson, 1970; Brandt, 1975). Although LKR/SDH enzymes were unknown at that time, the SACPATH must have been responsible for the conversion of lysine to proline.

The conversion of Δ^1-piperideine-6-carboxylate to pipecolate (**Figure 2**) was demonstrated in animals in a study designed to investigate whether fibroblasts catabolize lysine through the SACPATH or through the pipecolate pathway, both of which converges to α-aminoadipate semialdehyde (Struys and Jakobs, 2010). A human AASADH-deficient fibroblast cell line fed either L-[α-^{15}N] or L-[ε-^{15}N]lysine catabolized L-[α-^{15}N]lysine into [α-^{15}N]saccharopine, [α-^{15}N]aminoadipic semialdehyde, [α-^{15}N]Δ^1-pyrroline-6-carboxylate, and [α-^{15}N]pipecolate (Struys and Jakobs, 2010). The incubation of recombinant human P5CR with Δ^1-piperideine-6-carboxylate further demonstrated its enzymatic conversion solely into pipecolate (Struys et al., 2014). Previously, studies in an animal model argued that the pipecolate pathway is preferred for lysine catabolism in the brain, while the SACPATH is preferred for the liver and kidney (Sauer et al., 2011; Hallen et al., 2013; Posset et al., 2014). An accurate experimental design to follow the time course of lysine degradation in the mouse liver, kidney, and brain revealed that the catabolic activity peak in response to exogenous lysine fed to the animals occurs 2 h after intraperitoneal injection of lysine (Pena et al., 2016). By the use of this experimental setup, intraperitoneal injection of L-[α-^{15}N] or L-[ε-^{15}N]lysine revealed that lysine catabolism in the mouse liver, kidney, and brain occurs through the SACPATH (Pena et al., 2017). There was no evidence for the synthesis of α-aminoadipate from the pipecolate pathway. In addition, pipecolate derived from L-[α-^{15}N]lysine confirmed its synthesis through the SACPATH in the liver, kidney, and brain (Pena et al., 2017). The prevalence of the SACPATH for lysine catabolism and pipecolate synthesis was also recently observed

for human neuronal progenitor cells and fibroblasts. Isotopic tracing experiments, similar to those carried out in mice, revealed that lysine catabolism occurs exclusively through the SACPATH (Crowther et al., 2019). L-[α-^{15}N] or L-[ε-^{15}N]lysine feeding experiments in bean also indicate preferred incorporation of the α-N group into pipecolate (Schutte and Seeling, 1967 was coted in the text as cited by Hartmann et al., 2017).

INVOLVEMENT OF THE SACPATH IN THE ABIOTIC AND BIOTIC STRESS RESPONSE

Lysine catabolism through the SACPATH is highly responsive to abiotic stress (Moulin et al., 2006; Boex-Fontvieille et al., 2013; Kyiota et al., 2015; Michaletti et al., 2018; Wu et al., 2018; Dudziak et al., 2019; Yadav et al., 2019; You et al., 2019). Nevertheless, to date, there is no direct evidence for the involvement of the SACPATH in the biotic stress response. Instead, the recent discovery of the NHP pathway of lysine catabolism has shown its critical role for the induction of SAR (for a review, see Hartmann and Zeier, 2018).

In the previous sections, we presented the current knowledge of the enzymatic properties that support the synthesis through the SACPATH of two of the most critical osmolytes, proline and pipecolate (Szabados and Savoure, 2009; Bhaskara et al., 2015; Pérez-García et al., 2019). However, the question is how the SACPATH enzymatic activities and derived metabolites contribute to abiotic and biotic stress responses. The response of the SACPATH to osmotic, drought and salt stress is conserved in plants, animals, and bacteria, indicating its evolutionary importance to cope with abiotic stress. Notably, the enzymes LKR/SDH and AASADH are co-upregulated at the transcriptional level by exogenously applied lysine in plants, animals, and bacteria (Papes et al., 1999; Stepansky et al., 2005; Neshich et al., 2013; Kyiota et al., 2015). The induction of LKR activity by phosphorylation in a lysine-dependent manner implies that this enzyme is quickly activated to produce saccharopine once lysine levels start rising. The immediate increase in LKR activity stimulates increases in SDH activity, as the two activities occur within the same polypeptide. The immediate consequence of these two reaction steps is the increase in the concentration of α-aminoadipate semialdehyde, which would require an increase in AASADH and perhaps P5CR activities to maintain α-aminoadipate semialdehyde concentrations below toxic levels.

Metabolic perturbations such as those imposed by osmotic, drought and salt stress, will lead to the recycling of cellular catabolic processes, including proteomic hydrolysis (for a review, see Hildebrandt et al., 2015). Stress-induced protein hydrolysis results in increased free lysine levels. Increased lysine pool could also result from the induction of the aspartate (AK) pathway for lysine biosynthesis (**Figure 1A**) that has also been shown to be induced under abiotic stress (Pratelli and Pilot, 2014). However, the AK pathway for lysine biosynthesis localizes in the chloroplast and the amino acid needs to be transported to the cytosol and other organelles to be effectively metabolized. One of the most well-characterized amino acid transporters that operate in the chloroplast is the LHT1, which transport lysine and histidine (Fischer et al., 1998; Pratelli and Pilot, 2014). LHT1 has also been shown to be induced under abiotic stress and thus connect lysine biosynthesis to its catabolism in an integrated stress response metabolic network (Pratelli and Pilot, 2014). Increased free lysine levels have been observed in plants subjected to abiotic stress, but of relevance is the observation of higher levels of free lysine in sesame and wheat drought-tolerant genotypes compared with susceptible genotypes subjected to drought stress (Yadav et al., 2019; You et al., 2019). These observations suggest that abiotic stress-tolerant genotypes may have selected traits associated with the upregulation of the SACPATH. Indeed, transcriptomic, proteomic and metabolomic profiling of abiotic stress-tolerant sesame and wheat genotypes have revealed an induction of metabolic flux throughout the SACPATH to a greater extent in drought-tolerant genotypes than in drought-susceptible genotypes, which resulted in the accumulation of saccharopine and α-aminoadipate (Michaletti et al., 2018; You et al., 2019).

The role of the SACPATH in the osmotic stress response was first reported in rapeseed leaf disks treated with polyethylene glycol solutions at −1 to −4 MPa (Moulin et al., 2006). It was found that hyperosmotic treatment of rapeseed leaf disks induces an increase in LKR/SDH transcript abundance and enzymatic activity, which correlates with decreased levels of free lysine and increased levels of pipecolate (Moulin et al., 2006). Furthermore, the LKR/SDH activity and pipecolate concentration decrease with the return of the leaf disks to hypoosmotic conditions (Moulin et al., 2006). Exogenous administration of lysine induces LKR/SDH activity and increases pipecolate levels to the same extent as does hyperosmotic treatment, which supports the hypothesis that pipecolate is synthesized via the SACPATH (Moulin et al., 2006). Other abiotic stresses, such as those caused by different illumination conditions, also induce the SACPATH. A metabolic genome-wide association study of 309 Arabidopsis accessions subjected to light and dark treatments revealed a strong stress association between saccharopine accumulation and single-nucleotide polymorphisms (SNPs) at LKR/SDH loci. Saccharopine accumulates under low-light or dark conditions, indicating that the induction of the SACPATH is essential under these stressful conditions (Wu et al., 2018). Moreover, the osmolytes proline and pipecolate accumulate to high levels in halophytes, indicating their role in adaptative metabolism under stressful saline conditions (Slama et al., 2015; Jawahar et al., 2019).

The lysine-to-α-aminoadipate metabolic flux requires the coordinated activities of LKR/SDH and AASADH. Indeed, LKR/SDH, and AASADH are co-upregulated at transcriptional and translational levels in response to exogenous administration of lysine in plants, animals, and bacteria (Neshich et al., 2013; Kyiota et al., 2015; Pena et al., 2016, 2017). The synthesis of pipecolate from Δ^1-piperideine-6-carboxylate by the enzyme P5CR (Struys and Jakobs, 2010; Struys et al., 2014; Pena et al., 2017) suggest that the SACPATH contributes to abiotic stress alleviation by increasing cellular concentrations of both proline and pipecolate (**Figure 2**). However, the accumulation of saccharopine when plants are subjected to abiotic stress

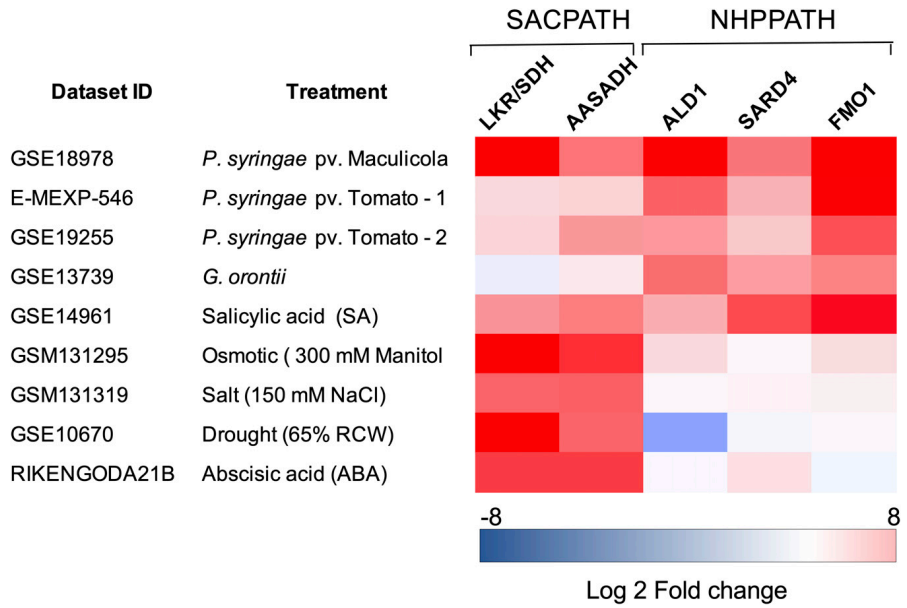

FIGURE 3 | Expression profiling of the core genes of the SACPATH and NHP pathway for lysine catabolism in Arabidopsis subjected to biotic and abiotic stresses. Expression profiling datasets of the genes encoding LKR/SDH and AASADH of the SACPATH and ALD1, SARD4, and FMO1 of the NHP pathway, were retrieved from public databases and analyzed using the Genevestigator platform[1]. Only the data of wild type (Col-0 or Ws-0) subjected to control and stress treatments were used in this analysis. The following datasets were used: **GSE18978**, leaves inoculated or not inoculated with *Pseudomonas syringae* ES4326; **E-MEXP-546**, leaves inoculated or not inoculated with the *P. syringae* pv. tomato avirulent strain DC3000 avrRpm1; **GSE19255**; leaves inoculated or not inoculated with *P. syringae* pv. tomato; **GSE13739**, leaves inoculated or not inoculated with the *G. orontii* MGH isolate; **GSE14961**, seedlings grown for 1 day in 2 mM salicylic acid; **GSM131295**, 16-day-old seedlings grown in 300 mM mannitol (osmotic stress); **GSM131319**, 16-day-old seedlings grown in 150 mM NaCl (salt stress); **GSE10670**, plants subjected to drought stress; and **RIKENGODA21B**, seedlings treated with 10 μM ABA. The values are expressed as log2 of the fold change between treated and untreated plants.

(Michaletti et al., 2018; You et al., 2019) must be further investigated. In animals, the SACPATH is exclusively located in the mitochondria (Blemings et al., 1994), an organelle essential for sustaining cellular energy homeostasis under stress conditions. However, the accumulation of saccharopine is toxic to mitochondria (Zhou et al., 2018). In humans, mutations in the LKR domain of the LKR/SDH enzyme lead to lysinuria, an asymptomatic disease (Sacksteder et al., 2000), but mutations in the SDH domain lead to saccharopinuria, a disease associated with severe brain malfunction and retardation (Houten et al., 2013). Saccharopinuria leads to the accumulation of high levels of saccharopine, which induces mitochondrial malfunction that can be reversed by the expression of a wild-type mitochondrial-targeted SDH (Zhou et al., 2018). In Arabidopsis, a monofunctional SDH probably produced from the same gene encoding the bifunctional enzyme localizes in the mitochondria (Fuchs et al., 2019). Under stress conditions, the targeting of SDH to the mitochondria may help reduce the concentration of saccharopine inside the organelle and maintain its normal function. Another point of significance of the SACPATH when plants are subjected to abiotic stress is the synthesis α-aminoadipate semialdehyde. α-Aminoadipate semialdehyde should be maintained at a low level because it is highly reactive; can bind to proteins, nucleic acids, and small molecules; and can interfere with an array of cellular processes. It is possible that α-aminoadipate semialdehyde acts in the upregulation of AASADH (Brocker et al., 2010, 2011; Kyiota et al., 2015) to help rid cells of aldehydes generated from stress-induced metabolic processes (Singh et al., 2012). Additionally, AASADH can produce other osmolytes such as betaine from betaine aldehyde that would help alleviate stress imposed by salt, osmotic, and drought (Singh et al., 2012) and also sustain cellular energy homeostasis (Yang et al., 2019).

Another relevant question is whether the pipecolate generated by the SACPATH contributes to the stimulation of the plant immune response in addition to pipecolate produced through the NHP pathway (Hartmann et al., 2017, 2018; Chena et al., 2018; Hartmann and Zeier, 2018; Wang C. et al., 2018; Wang Y. et al., 2018). Pipecolate accumulates to high levels upon pathogen attack, stimulating the synthesis of NHP, which subsequently activates SAR at the infected site and in distant leaves (Hartmann and Zeier, 2018). Engineering the NHP pathway by the transient overexpression of ALD1 and FMO1 has been shown to activate the SAR response in tomato plants (Holmes et al., 2019). Is the pipecolate produced by the NHP pathway the only pipecolate source for SAR activation or can the pipecolate produced by the SACPATH contribute, at least in part, to immune response? Perhaps the different intracellular localization of the SACPATH and the NHP pathway may have a role in differentiating the pipecolate source in the activation of the biotic and abiotic

[1]https://genevestigator.com/gv/

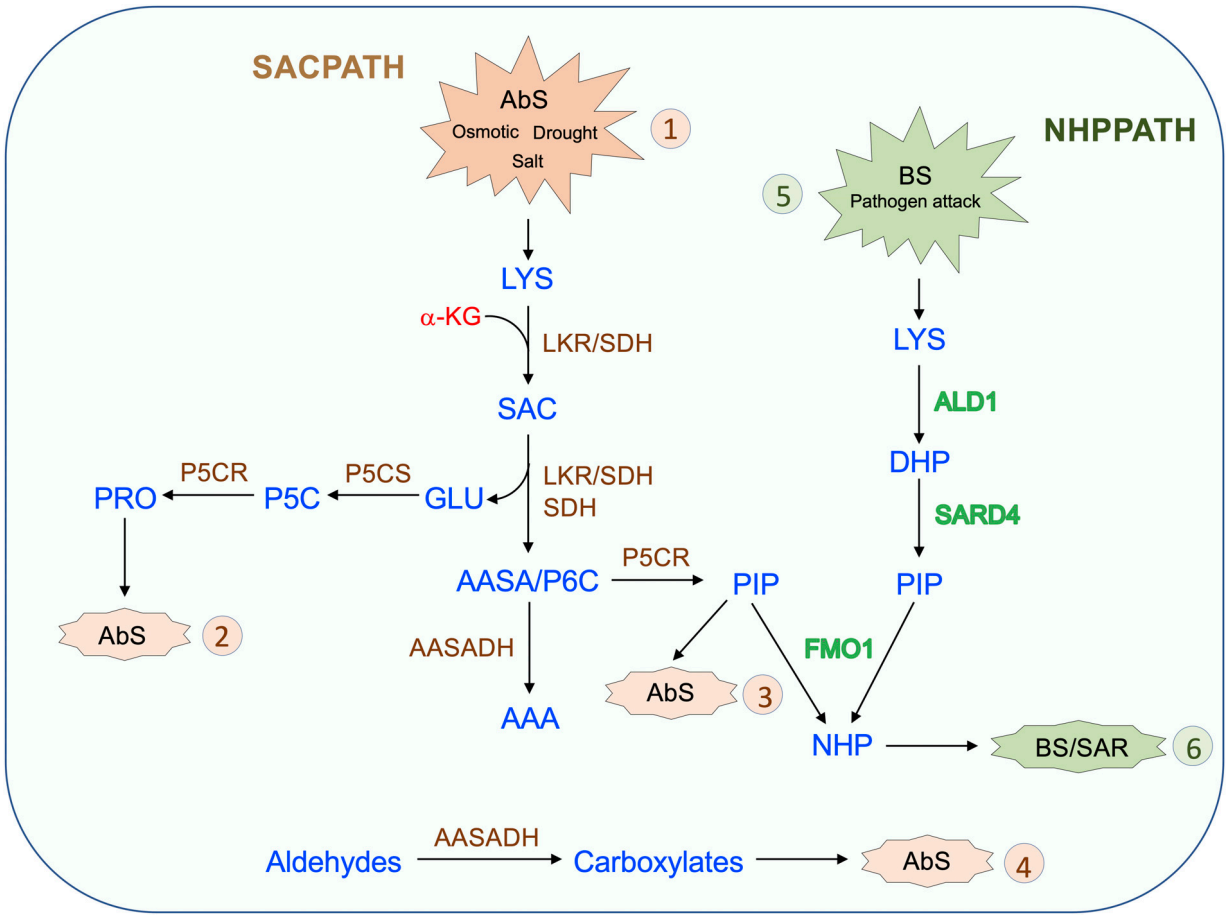

FIGURE 4 | Proposed model for the role of the SACPATH in abiotic and biotic stress responses in plants. Upon abiotic stress (AbS, 1) such as that imposed by osmotic, salt, and drought, the cellular concentration of free lysine increase. As the lysine concentration increases, the transcripts encoding bifunctional LKR/SDH, monofunctional SDH, and AASADH accumulate, increasing the lysine-to-α-aminoadipate metabolic flux. In general, the expression of P5CS and P5CR is also upregulated under abiotic stress, and by the action of these two enzymes, glutamate is converted into proline (AbS, 2), and Δ^1-piperidine 6-carboxylate is converted into pipecolate (AbS, 3). Proline and pipecolate are the two most effective osmolytes and help sustain cellular homeostasis under abiotic stress. The upregulation of AASADH helps metabolize aldehydes generated by stress conditions, including, for example, betaine aldehyde, whose conversion generates betaine, another important osmolyte (AbS, 4). Upon pathogen attack (BS, 5) lysine is also catabolized to pipecolate through the NHP pathway by the enzymes ALD1, which deaminates lysine to Dhp, and SARD4, which reduces Dhp to pipecolate. Dhp is then N-hydroxylated by FMO1 to generate NHP, the effector of SAR (BS, 6). In the proposed model, the pipecolate generated by the SACPATH could also serve as a substrate for FMO1 to produce NHP, therefore contributing to SAR.

stress response. The bifunctional LKR/SDH, at least in immature maize endosperm, is located in the cytosol, but a monofunctional SDH has been found that targets the mitochondria. AASADH is localized both in the cytosol and in the mitochondria but not in the plastids. The intracellular localization of P5CR is not well established, but it has also been found in plastids. The NHP pathway seems to be localized in the chloroplasts of developed leaves. Thus, it is possible that the pipecolate produced from the SACPATH and NHP is differentially compartmentalized so that the NHP pathway, whose enzymes are located in the chloroplast, is directly associated with the biotic stress response and therefore is preferentially associated with pathogen infection. We took advantage of public datasets designed to study the transcriptomic profiling of Arabidopsis to interrogate whether the SACPATH and NHP pathway are differentially expressed under biotic and abiotic stress. A heatmap was constructed to profile the transcriptional response of LKR/SDH, AASADH, ALD1, SARD4, and FMO1 in Arabidopsis subjected to biotic and abiotic stress conditions (**Figure 3**). Although the datasets were retrieved from distinct experiments, we can clearly observe that the expression of the genes encoding the enzymes of the SACPATH and the NHP pathway are co-upregulated under biotic stress imposed by infection with *P. syringae* or treatment with salicylic acid (**Figure 3**). In the case of infection with the fungus *Golovinomyces orontii*, only the NHP pathway is upregulated. In contrast, under abiotic stress imposed by osmotic, salt, or drought stress or when plants were treated with abscisic acid (ABA), the SACPATH was preferentially upregulated (**Figure 3**). This means that the SACPATH may contribute to the synthesis of NHP from the pipecolate produced from Δ^1-pyrroline-6-carboxylate through the enzymatic activity of P5CR (**Figure 3**) but the NHP pathway may not contribute with abiotic stress response.

CONCLUSION

The SACPATH for lysine catabolism is widespread across kingdoms, except for fungi, which use the pathway for lysine synthesis. Upon intracellular increase in lysine concentration, due to metabolism-related organ development programs or responses to abiotic and biotic stress, LKR undergoes posttranscriptional modification mediated by Ca^{2+} and phosphorylation to initiate SACPATH reactions, first by LKR activity to produce saccharopine and then by SDH activity to produce α-aminoadipate semialdehyde and glutamate (**Figure 4**, Abs 1). Increased intracellular free lysine also induces the transcriptional upregulation of the *LKR/SDH* and *AASADH* genes which boost the lysine-to-α-aminoadipate metabolic flux and the use of glutamate to produce proline (**Figure 4**, Abs 2) and the intermediary D^1-piperideine-6-carboxylate to produce pipecolate (**Figure 4**, Abs 3). A monofunctional SDH enzyme is targeted to the mitochondria, perhaps to help maintain saccharopine levels below toxic levels. The upregulation of AASADH in turn would help to maintain α-aminoadipate semialdehyde at low levels and help to reduce the levels of the stress-generated aldehydes, thus contributing to the alleviation of the toxic effects on cellular metabolism (**Figure 4**, Abs 4). The proline and pipecolate generated by the SACPATH must contribute to alleviating the cellular impact of osmotic, salt, and drought stress (**Figure 4**, Abs 1). However, the cellular availability of pipecolate generated by the SACPATH could also contribute to the production of NHP and thus induce SAR, as the enzymes LKR/SDH and AASADH are induced by pathogen attack (**Figure 3**). Perhaps the main difference between the biotic and abiotic stress responses associated with lysine catabolism through the SACPATH and the NHP pathway resides in the mode of action of these two conditions. Pathogen infection is punctual (**Figure 4**, BS 5), and, independent of the plant organ, the infection spots comprise a limited number of cells. At the infection site, lysine catabolism through the NHP pathway must be intense, pipecolate accumulates at high levels, and NHP is produced and spread over long distances to mediate the SAR response (**Figure 4**, BS 6). However, a prerequisite to start the process is the rise of free lysine concentration in the infection site. The rise of free lysine concentrations independent, whether it is due to biotic or abiotic stress, induces the SACPATH (**Figure 3**) that can also mediate the synthesis of NHP. In contrast, osmotic, drought, and salt stress affect whole plant organs simultaneously, leading to the activation of the SACPATH and accumulation of pipecolate. Since abiotic stress must debilitate the plant, making it more prone to pathogen attack, the pipecolate produced by the SACPATH may help to stimulate the immune response in these circumstances.

AUTHOR CONTRIBUTIONS

PA organized and wrote the manuscript. PB contributed with the expression profiling analysis of SACPATH and NHP pathways.

FUNDING

This work was supported by a grant from FAPESP to PA – 2016/23218-0. PB received a FAPESP postdoc fellowship – 14/17634-5.

ACKNOWLEDGMENTS

The authors acknowledge The State University of Campinas (UNICAMP), The Brazilian Agricultural Research Corporation (EMBRAPA) and The São Paulo Research Foundation (FAPESP) for housing and funding the Genomics for Climate Changes Research Center (GCCRC).

REFERENCES

Anderson, O. D., Coleman-Derr, D., Gu, Y. Q., and Heath, S. (2010). Structural and transcriptional analysis of plant genes encoding the bifunctional lysine ketoglutarate reductase saccharopine dehydrogenase enzyme. *BMC Plant Biol.* 10:113. doi: 10.1186/1471-2229-10-113

Arruda, P., Kemper, E. L., Papes, F., and Leite, A. (2000). Regulation of lysine catabolism in higher plants. *Trends Plant Sci.* 5, 324–330. doi: 10.1016/s1360-1385(00)01688-1685

Arruda, P., and Neshich, I. P. (2012). Nutritional-rich and stress-tolerant crops by saccharopine pathway manipulation. *Food Energy Secur.* 1, 141–147. doi: 10.1002/fes3.9

Arruda, P., Sodek, L., and da Silva, W. J. (1982). Lysine-ketoglutarate reductase activity in developing maize endosperm. *Plant Physiol.* 69, 988–989. doi: 10.1104/pp.69.4.988

Azevedo, R. A., Damerval, C., Landry, J., Lea, P. J., Bellato, C. M., Meinhardt, L. W., et al. (2003). Regulation of maize lysine metabolism and endosperm protein synthesis by opaque and floury mutations. *Eur. J. Biochem.* 270, 4898–4908. doi: 10.1111/j.1432-1033.2003.03890.x

Azevedo, R. A., and Lea, P. J. (2001). Lysine metabolism in higher plants. *Amino Acids* 20, 261–279. doi: 10.1007/s007260170043

Bhaskara, G. B., Yang, T.-H., and Verslues, P. E. (2015). Dynamic proline metabolism: importance and regulation in water limited environments. *Front. Plant Sci.* 6:484. doi: 10.3389/fpls.2015.00484

Blemings, K. P., Crenshaw, T. D., Swick, R. W., and Benevenga, N. J. (1994). Lysine-α-ketoglutarate reductase and saccharopine dehydrogenase are located only in the mitochondrial matrix in rat liver. *J. Nutr.* 124, 1215–1221. doi: 10.1093/jn/124.8.1215

Boex-Fontvieille, E. R. A., Gauthier, P. P. G., Gilard, F., Hodges, M., and Tcherkez, G. G. B. (2013). A new anaplerotic respiratory pathway involving lysine biosynthesis in isocitrate dehydrogenase-deficient *Arabidopsis mutants*. *New Phytol.* 199, 673–682. doi: 10.1111/nph.12319

Brandt, A. B. (1975). In vivo incorporation of [14C] lysine into the endosperm proteins of wild type and high-lysine barley. *FEBS Lett.* 52, 288–291. doi: 10.1016/0014-5793(75)80827-1

Brochetto-Braga, M. R., Leite, A., and Arruda, P. (1992). Partial purification and characterization of lysine-ketoglutarate reductase in normal and opaque-2 maize endosperms. *Plant Physiol.* 98, 1139–1147. doi: 10.1104/pp.98.3.1139

Brocker, C., Cantore, M., Failli, P., and Vasiliou, V. (2011). Aldehyde dehydrogenase 7A1 (ALDH7A1) attenuates reactive aldehyde and oxidative stress induced cytotoxicity. *Chem. Biol. Interact* 191, 269–277. doi: 10.1016/j.cbi.2011.02.016

Brocker, C., Lassen, N., Estey, T., Pappa, A., Cantore, M., Orlova, V. V., et al. (2010). Aldehyde dehydrogenase 7A1 (ALDH7A1) Is a novel enzyme involved in cellular defense against hyperosmotic stress. *J. Biol. Chem.* 285, 18452–18463. doi: 10.1074/jbc.M109.077925

Bunsupa, S., Katayama, K., Ikeura, E., Oikawa, A., Toyooka, K., Saito, K., et al. (2012). Lysine decarboxylase catalyzes the first step of quinolizidine alkaloid biosynthesis and coevolved with alkaloid production in leguminosae. *Plant Cell* 24, 1202–1216. doi: 10.1105/tpc.112.095885

Chena, Y. C., Holmes, E. C., Rajniak, J., Kima, J. G., Tang, S., Fischer, C. R., et al. (2018). N-hydroxy-pipecolic acid is a mobile metabolite that induces systemic disease resistance in *Arabidopsis*. *Proc. Natl. Acad. Sci. U.S.A.* 115, e4920–e4929. doi: 10.1073/pnas.1805291115

Crowther, L. M., Mathis, D., Poms, M., and Plecko, B. (2019). New insights into human lysine degradation pathways with relevance to pyridoxine-dependent epilepsy due to antiquitin deficiency. *J. Inherit Metab. Dis.* 42, 620–628. doi: 10.1002/jimd.12076

Dudziak, K., Zapalska, M., Börner, A. M., Szczerba, H., Kowalczyk, K., and Nowak, M. (2019). Analysis of wheat gene expression related to the oxidative stress response and signal transduction under short-term osmotic stress. *Sci. Rep.* 9:2743. doi: 10.1038/s41598-019-39154-w

Fischer, W.-N., Bruno, A., Rentsch, D., Krolkiewicz, S., Tegeder, M., Breitkreuz, K., et al. (1998). Amino acid transport in plants. *Trends Sci.* 3:188. doi: 10.1016/S1360-1385(98)01231-X

Fuchs, P., Rugen, N., Carrie, C., Elsasser, M., Finkemeier, I., Giese, J., et al. (2019). Single organelle function and organization as estimated from *Arabidopsis* mitochondrial proteomics. *Plant J.* 101, 420–441. doi: 10.1111/tpj.14534

Gaziola, S. A., Sodek, L., Arruda, P., Lea, P. J., and Azevedo, R. A. (2000). Degradation of lysine in rice seeds: effect of calcium, ionic strength, S-adenosylmethionine and S-2-aminoethyl-L-cysteine on the lysine 2-oxoglutarate reductase-saccharopine dehydrogenase bifunctional enzyme. *Physiol. Plant.* 110, 164–171. doi: 10.1034/j.1399-3054.2000.110204.x

Gaziola, S. A., Teixeira, C. M. G., Lugli, L., Sodek, L., and Azevedo, R. A. (1997). The enzymology of lysine catabolism in rice seeds Isolation, characterization, and regulatory properties of a lysine 2-oxoglutarate reductase/saccharopine dehydrogenase bifunctional polypeptide. *Eur. J. Biochem.* 247, 364–371. doi: 10.1111/j.1432-1033.1997.00364.x

Gonçalves-Butruille, M., Szajner, P., Torigoi, E., Leite, A., and Arruda, P. (1996). Purification and characterization of the bifunctional enzyme lysine-ketoglutarate reductase-saccharopine dehydrogenase from maize. *Plant Physiol.* 110, 765–771. doi: 10.1104/pp.110.3.765

Hallen, A., Jamie, J. F., and Cooper, A. J. L. (2013). Lysine metabolism in mammalian brain: an update on the importance of recent discoveries. *Amino Acids* 45, 1249–1272. doi: 10.1007/s00726-013-1590-1591

Hartmann, M., Kim, D., Bernsdorff, F., Ajami-Rashidi, Z., Scholten, N., Schreiber, S., et al. (2017). Biochemical principles and functional aspects of pipecolic acid biosynthesis in plant immunity. *Plant Physiol.* 174, 124–153. doi: 10.1104/pp.17.00222

Hartmann, M., and Zeier, J. (2018). L-lysine metabolism to N-hydroxypipecolic acid: an integral immune-activating pathway in plants. *Plant J.* 96, 5–21. doi: 10.1111/tpj.14037

Hartmann, M., Zeier, T., Bernsdorff, F., Reichel-Deland, V., Kim, D., Hohmann, M., et al. (2018). Flavin monooxygenase-generated N-hydroxypipecolic acid is a critical element of plant systemic immunity. *Cell* 173, 456–469. doi: 10.1016/j.cell.2018.02.049

Hildebrandt, T. M., Nunes Nesi, A., Araujo, W. L., and Braun, H. P. (2015). Amino acid catabolism in plants. *Mol. Plant* 8, 1563–1579. doi: 10.1016/j.molp.2015.09.005

Holmes, E. C., Chen, Y.-C., Sattely, E. S., and Mudgett, M. B. (2019). An engineered pathway for N-hydroxy-pipecolic acid synthesis enhances systemic acquired resistance in tomato. *Sci. Signal.* 12:eaay3066. doi: 10.1126/scisignal.aay3066

Houten, S. M., Te Brinke, T., Denis, S., Ruiter, J. P., Knegt, A. C., de Klerk, J. B., et al. (2013). Genetic basis of hyperlysinemia. *Orphanet J. Rare Dis.* 8:57.

Jawahar, G., Rajasheker, G., Maheshwari, P., Punita, D. L., Jalaja, N., Kumari, P. H., et al. (2019). Osmolyte diversity, distribution, and their biosynthetic pathways. *Plant Signal. Mol.* 28, 449–458. doi: 10.1016/B978-0-12-816451-8.00028-29

Kemper, E. L., Cord-Neto, G., Capella, A. N., Gonçalves-Butruile, M., Azevedo, R. A., and Arruda, P. (1998). Structure and regulation of the bifunctional enzyme lysine-oxoglutarate reductase-saccharopine dehydrogenase in maize. *Eur. J. Biochem.* 253, 720–729. doi: 10.1046/j.1432-1327.1998.2530720.x

Kemper, E. L., Cord-Neto, G., Papes, F., Moraes, K. C. M., Leite, A., and Arruda, P. (1999). The role of opaque2 in the control of lysine-degrading activities in developing maize endosperm. *Plant Cell* 11, 1981–1993. doi: 10.1105/tpc.11.10.1981

Koenigshofer, H., and Loeppert, H. G. (2019). The up-regulation of proline synthesis in the meristematic tissues of wheat seedlings upon short-term exposure to osmotic stress. *J. Plant Physiol.* 237, 21–29. doi: 10.1016/j.jplph.2019.03.010

Kyiota, E., Pena, I. A., and Arruda, P. (2015). The saccharopine pathway in seed development and stress response of maize. *Plant Cell Environ.* 38, 2450–2461. doi: 10.1111/pce.12563

Lawrence, J. M., and Grant, D. R. (1964). Incorporation of lysine-C14 into the developing grain of wheat. *Arch. Biochem. Biophys.* 104, 73–78. doi: 10.1016/S0003-9861(64)80036-80039

Lobell, D. B., Schlenker, W., and Costa-Roberts, J. (2011). Climate trends and global crop production since 1980. *Science* 333, 616–620. doi: 10.1126/science.1204531

Long, X., Liu, Q., Chan, M., Wang, Q., and Sun, S. S. M. (2013). Metabolic engineering and profiling of rice with increased lysine. *Plant Biotech. J.* 11:490. doi: 10.1111/pbi.12037

Markovitzs, P. J., and Chuang, D. T. (1987). The bifunctional aminoadipic semialdehyde synthase in lysine degradation. *J. Biol. Chem.* 262, 9353–9358.

Michaletti, A., Naghavi, M. R., Toorchi, M., Zolla, L., and Rinalducci, S. (2018). Metabolomics and proteomics reveal drought-stress responses of leaf tissues from spring-wheat. *Sci. Rep.* 8:5710. doi: 10.1038/s41598-018-24012-y

Mills, P. B., Struys, E., Jakobs, V., Plecko, B., Baxter, P., Baumgartner, M., et al. (2006). Mutations in antiquitin in individuals with pyridoxine-dependent seizures. *Nat. Med.* 12, 307–309. doi: 10.1038/nm1366

Moulin, M., Deleu, C., Larher, F., and Bouchereau, A. (2006). The lysine-ketoglutarate reductase-saccharopine dehydrogenase is involved in the osmo-induced synthesis of pipecolic acid in rapeseed leaf tissues. *Plant Physiol. Biochem.* 44, 474–482. doi: 10.1016/j.plaphy.2006.08.005

Neshich, I. A. P., Kiyota, E., and Arruda, P. (2013). Genome-wide analysis of lysine catabolism in bacteria reveals new connections with osmotic stress resistance. *ISME J.* 7, 2400–2410. doi: 10.1038/ismej.2013.123

Papes, F., Kemper, E. L., Cord-Neto, G., Langone, F., and Arruda, P. (1999). Lysine degradation through the saccharopine pathway in mammals: involvement of both bifunctional and monofunctional lysine-degrading enzymes in mouse. *Biochem. J.* 344, 555–563.

Pena, I. A., Marques, L. A., Laranjeira, A. B. A., Yunes, J. A., Eberlin, M. N., and Arruda, P. (2016). Simultaneous detection of lysine metabolites by a single LC-MS/MS method: monitoring lysine degradation in mouse plasma. *Springerplus* 5:172. doi: 10.1186/s40064-016-1809-1801

Pena, I. A., Marques, L. A., Laranjeira, A. B. A., Yunes, J. A., Eberlin, M. N., MacKenzie, A., et al. (2017). Mouse lysine catabolism to aminoadipate occurs primarily through the saccharopine pathway; implications for pyridoxine dependent epilepsy (PDE). *Biochim. Biophys. Acta Mol. Basis Dis.* 1863, 121–128. doi: 10.1016/j.bbadis.2016.09.006

Perez-Arellano, I., Carmona-Alvarez, F., Martinez, A. I., Rodriguez-Diaz, J., and Cervera, J. (2010). Pyrroline-5-carboxylate synthase and proline biosynthesis: from osmotolerance to rare metabolic disease. *Protein Sci.* 19, 372–382. doi: 10.1002/pro.340

Pérez-García, F., Brito, L. F., and Wendisch, W. F. (2019). Function of L-pipecolic acid as compatible solute in *Corynebacterium glutamicum* as basis for its production under hyperosmolar conditions. *Front. Microbiol.* 10:340. doi: 10.3389/fmicb.2019.00340

Pompeu, G. B., Vendemiatti, A., Gratão, P. L., Gaziola, S. A., Lea, P. J., and Azevedo, R. A. (2006). Saccharopine dehydrogenase activity in the high-lysine opaque and floury maize mutants. *Food Biotechnol.* 20, 55–64. doi: 10.1080/08905430500524101

Posset, R., Opp, S., Struys, E. A., Völkl, A., Mohr, H., Hoffmann, G. F., et al. (2014). Understanding cerebral L-lysine metabolism: the role of L-pipecolate metabolism in Gcdh-deficient mice as a model for glutaric aciduria type I. *J. Inher. Metab. Dis.* 38, 265–272. doi: 10.1007/s10545-014-9762-z

Pratelli, R., and Pilot, G. (2014). Regulation of amino acid metabolic enzymes and transporters in plants. *J. Exp. Bot.* 65, 5535–5556. doi: 10.1093/jxb/eru320

Ray, D. K., Gerber, J. S., MacDonald, G. K., and West, P. C. (2015). Climate variation explains a third of global crop yield variability. *Nat. Commun.* 6:5989. doi: 10.1038/ncomms6989

Rodrigues, S. M., Andrade, M. O., Gomes, A. P. S., Da Matta, F. M., Baracat-Pereira, M. C., and Fontes, E. P. B. (2006). Arabidopsis and tobacco plants ectopically expressing the soybean antiquitin-like ALDH7 gene display enhanced tolerance to drought, salinity, and oxidative stress. *J. Exp. Bot.* 57, 1909–1918. doi: 10.1093/jxb/erj132

Sacksteder, K. A., Biery, B. J., Morrell, J. C., Goodman, B. K., Geisbrecht, B. V., Cox, R. P., et al. (2000). Identification of the α-aminoadipic semialdehyde synthase gene, which is defective in familial hyperlysinemia. *Am. J. Genet.* 66, 1736–1743. doi: 10.1086/302919

Sauer, W. S., Opp, S., Hoffmann, G. F., Koeller, D. M., Okun, J. G., and Kolker, S. (2011). Therapeutic modulation of cerebral L-lysine metabolism in a mouse model for glutaric aciduria type I. *Brain* 134, 157–170. doi: 10.1093/brain/awq269

Singh, S., Brocker, C., Koppaka, V., Chen, Y., Jackson, B. C., Matsumoto, A., et al. (2012). Aldehyde dehydrogenases in cellular responses to oxidative/electrophilic stress. *Free Rad. Biol. Med.* 56, 89–101. doi: 10.1016/j.freeradbiomed.2012.11.010

Slama, I., Abdelly, C., Bouchereau, A., Flowers, T., and Savoure, A. (2015). Diversity, distribution and roles of osmoprotective compounds accumulated in halophytes under abiotic stress. *Ann. Bot.* 115, 433–447. doi: 10.1093/aob/mcu239

Sodek, L., and Wilson, C. M. (1970). Incorporation of leucine-C14 and lysine-C14 into protein in the developing endosperm of normal and opaque-2 corn. *Arch. Biochem. Biophys.* 140, 29–38. doi: 10.1016/0003-9861(70)90006-90008

Stepansky, A., Yao, Y., Tang, G., and Galili, G. (2005). Regulation of lysine catabolism in Arabidopsis through concertedly regulated synthesis of the two distinct gene products of the composite AtLKR/SDH locus. *J. Exp. Bot.* 56, 525–536. doi: 10.1093/jxb/eri031

Struys, E. A., and Jakobs, C. (2010). Metabolism of lysine in alpha-aminoadipic semialdehyde dehydrogenase-deficient fibroblasts: evidence for an alternative pathway of pipecolic acid formation. *FEBS Lett.* 584, 181–186. doi: 10.1016/j.febslet.2009.11.055

Struys, E. A., Jansen, E. E., and Salomons, G. S. (2014). Human pyrroline-5-carboxylate reductase (PYCR1) acts on Δ1-piperideine-6-carboxylate generating L-pipecolic acid. *J. Inherit. Metab. Dis.* 37, 327–332. doi: 10.1007/s10545-013-9673-9674

Szabados, L., and Savoure, A. (2009). Proline: a multifunctional amino acid. *Trends Plant Sci.* 15, 89–97. doi: 10.1016/j.tplants.2009.11.009

Szekely, G., Abraham, E., Cseplo, A., Rigo, G., Zsigmond, L., Csiszar, J., et al. (2008). Duplicated P5CS genes of *Arabidopsis* play distinct roles in stress regulation and developmental control of proline biosynthesis. *Plant J.* 53, 11–28. doi: 10.1111/j.1365-313X.2007.03318.x

Szoke, A., Miao, G.-H., Hong, Z., and Verma, D. P. S. (1992). Subcellular location of Δ1-Pyrroline-5-carboxylate reductase in root/nodule and leaf of soybean. *Plant Physiol.* 99, 1642–1649. doi: 10.1104/pp.99.4.1642

Van Wallendael, A., Soltani, A., Emery, N. C., Peixoto, M. M., Olsen, J., and Lowry, D. B. (2019). A Molecular view of plant local adaptation: incorporating stress-response networks. *Ann. Rev. Plant Biol.* 70, 559–583. doi: 10.1146/annurev-arplant-050718-100114

Verslues, P. E., and Sharma, S. (2010). Proline Metabolism and Its Implications for plant-environment interaction. *Arabidopsis Book* 3:e01401. doi: 10.1199/tab.0140

Wang, C., Liu, R., Lim, G.-H., de Lorenzo, L., Yu, K., Zhang, K., et al. (2018). Pipecolic acid confers systemic immunity by regulating free radicals. *Sci. Adv.* 4:eaar4509. doi: 10.1126/sciadv.aar4509

Wang, Y., Schuck, S., Wu, J., Yang, P., Döring, A. C., Zeier, J., et al. (2018). A MPK3/6-WRKY33-ALD1-pipecolic acid regulatory loop contributes to systemic acquired resistance. *Plant Cell* 30, 2480–2494. doi: 10.1105/tpc.18.00547

Wu, S., Tohge, T., Cuadros-Inostroza, A., Tong, H., Tenenboim, H., Kooke, R., et al. (2018). Mapping the *Arabidopsis* metabolic landscape by untargeted metabolomics at different environmental conditions. *Mol. Plant* 11, 118–134. doi: 10.1016/j.molp.2017.08.012

Yadav, A. K., Carroll, A. J., Estavillo, G. M., Rebetzke, G. J., and Pogson, B. J. (2019). Wheat drought tolerance in the field is predicted by amino acid responses to glasshouse-imposed drought. *J. Exp. Bot.* 70, 4931–4948. doi: 10.1093/jxb/erz224

Yang, J. S., Hsu, J. W., Park, S. Y., Lee, S. Y., Li, J., Bai, M., et al. (2019). ALDH7A1 inhibits the intracellular transport pathways during hypoxia and starvation to promote cellular energy homeostasis. *Nat. Commun.* 10:4068. doi: 10.1038/s41467-019-11932-11930

You, J., Zhang, Y., Liu, A., Li, D., Wang, X., Dossa, K., et al. (2019). Transcriptomic and metabolomic profiling of drought-tolerant and susceptible sesame genotypes in response to drought stress. *BMC Plant Biol.* 19:267. doi: 10.1186/s12870-019-1880-1

Yu, S., and Tian, L. (2018). Breeding major cereal grains through the lens of nutrition sensitivity. *Mol. Plant* 11, 23–30. doi: 10.1016/j.molp.2017.08.006

Zhang, C. S., Lu, Q., and Verma, D. S. (1995). Removal of feedback inhibition of Δ1-pyrroline-5-carboxylate synthetase, a bifunctional enzyme catalyzing the first two steps of proline biosynthesis in plants. *J. Biol. Chem.* 270, 20491–20496. doi: 10.1074/jbc.270.35.20491

Zhou, H., Xia, D., and He, Y. (2020). Rice grain quality—traditional traits for high quality rice and health-plus substances. *Mol. Breed.* 40:1. doi: 10.1007/s11032-019-1080-1086

Zhou, J., Wang, X., Wang, M., Chang, Y., Zhang, F., Ban, S. Z., et al. (2018). The lysine catabolite saccharopine impairs development by disrupting mitochondrial homeostasis. *J. Cell Biol.* 218, 580–597. doi: 10.1083/jcb.201807204

Conflict of Interest: The authors declare that the research was conducted in the absence of any commercial or financial relationships that could be construed as a potential conflict of interest.

Copyright © 2020 Arruda and Barreto. This is an open-access article distributed under the terms of the Creative Commons Attribution License (CC BY). The use, distribution or reproduction in other forums is permitted, provided the original author(s) and the copyright owner(s) are credited and that the original publication in this journal is cited, in accordance with accepted academic practice. No use, distribution or reproduction is permitted which does not comply with these terms.

frontiers in Plant Science

ORIGINAL RESEARCH
published: 25 May 2020
doi: 10.3389/fpls.2020.00639

Visualizing Genotypic and Developmental Differences of Free Amino Acids in Maize Roots With Mass Spectrometry Imaging

*Kelly C. O'Neill and Young Jin Lee**

Department of Chemistry, Iowa State University, Ames, IA, United States

Amino acids are essential biological compounds in plants as they store nitrogen, an essential nutrient, and are the building blocks for proteins that drive biological activity. Amino acids have been studied using a wide variety of analytical techniques in different plant systems, however, mass spectrometry imaging (MSI) is a particularly useful technique as it allows for the simultaneous collection of both chemical and spatial information. In this work, matrix-assisted laser desorption/ionization (MALDI)-MSI is used to study the different localization of free amino acids in the roots of maize inbred lines B73 and Mo17 and their reciprocal hybrids. Because amino acids are difficult to detect in mass spectrometry, especially directly on tissues, a chemical derivatization protocol is utilized to increase the ionization efficiency and improve their detection. We report differences in both abundance and localization of amino acids in B73 and Mo17 maize roots and suggest the hybrids show evidence of inheriting characteristics from both parents. Most genotypic differences are found in the cross-sections near the seed (∼2 cm away) at a later stage of development (10–11 cm in length). Here, B73 has lower amino acid abundance localized primarily to the center of the roots for most amino acids, while Mo17 has much higher abundance localized mainly to the root cortex. This difference in localization is minimized when grown in ammonium ion rich conditions. Roots grown in the presence of ^{15}N-ammonium ions provided additional insight about the amino acid synthesis. The localization of some amino acids, particularly leucine/isoleucine and glutamine, is not affected by the addition of nitrogen and is consistent regardless of the nitrogen source, either from the seeds (^{14}N-labeled) or environment (^{15}N-labeled). Nitrogen uptake from the environment is confined to glutamine, asparagine, and alanine, consistent with their roles in amino acid storage and transportation.

Keywords: mass spectrometry imaging, maize root, amino acids, nitrogen assimilation, nitrogen transportation, on-tissue derivatization

OPEN ACCESS

Edited by:
Rachel Amir,
Migal - Galilee Technology Center, Israel

Reviewed by:
Thomas Leustek,
Rutgers, The State University of New Jersey, United States
André O. Hudson,
Rochester Institute of Technology, United States

***Correspondence:**
Young Jin Lee
yjlee@iastate.edu

Specialty section:
This article was submitted to Plant Metabolism and Chemodiversity, a section of the journal Frontiers in Plant Science

Received: *10 March 2020*
Accepted: *24 April 2020*
Published: *25 May 2020*

Citation:
O'Neill KC and Lee YJ (2020) Visualizing Genotypic and Developmental Differences of Free Amino Acids in Maize Roots With Mass Spectrometry Imaging. Front. Plant Sci. 11:639. doi: 10.3389/fpls.2020.00639

INTRODUCTION

Nitrogen is an essential nutrient for crop plants that has a major impact on crop production and yields. Nitrogen has an important role in plant growth and development; therefore, understanding nitrogen uptake and metabolism can help determine how to best and most efficiently care for plants (Lemaître et al., 2008). Amino acids are responsible for the storage and transportation of nitrogen

in plants and are an important aspect of nitrogen metabolism (Pratelli and Pilot, 2014). Recently, maize roots have been used as a model species for biological studies (Paschold et al., 2010); studying roots at their early stage can provide numerous benefits. The emergence of the primary root allows early morphological, histological, and physiological analysis of the seedling, while the fast germination and growth of maize seedlings in laboratory environments allow for high-throughput experiments under controlled and standardized conditions (Paschold et al., 2010). Studying the spatial arrangement of amino acids in maize roots can shed light on nitrogen assimilation and transportation in early plant development.

Mass spectrometry imaging (MSI) has become a valuable analytical tool to visualize metabolites such as lipids and small molecules directly on plant tissues (Lee et al., 2012; Sturtevant et al., 2016). Matrix-assisted laser desorption ionization (MALDI)-MSI is a commonly used technique, particularly for cellular and sub-cellular resolution imaging, due to its combination of high-spatial resolution, high sensitivity, and chemical versatility. Recently, MALDI platforms have been optimized to reach pixel sizes from 1 to 10 μm (Zavalin et al., 2013; Korte et al., 2015), which enables the study of biological tissue at the cellular and even sub-cellular level. Recent advances in t-MALDI-2 have even allowed for spatial resolutions of less than 1 μm (Niehaus et al., 2019). Visualizing detailed metabolite information at this scale can offer unprecedented details in terms of metabolite composition and localization which can be crucial for elucidating their biological roles.

Our group has developed a MALDI-MSI platform that allows for 5–10 μm high-spatial resolution. This setup has been used for various applications including the visualization of numerous different metabolites in maize leaves (Korte et al., 2015; Dueñas et al., 2017), seeds (Dueñas et al., 2016; Feenstra et al., 2017a), and roots (Feenstra et al., 2017b). The work of Dueñas et al. has applied this platform to show that the fatty acyl localizations of some thylakoid membrane lipids such as PG 32:0 are different depending on the genotype of maize. Additionally, the hybrid maize exhibit the characteristics resembling that of the maternal parent (maternal inheritance) (Dueñas et al., 2019). Previous work out of our group has also shown the benefits of utilizing various chemical derivatization reactions to enhance the ion signals for metabolites with certain functional groups. This strategy of using multiple different chemical derivatizations on adjacent tissue sections has allowed for expanded metabolite coverage (Dueñas et al., 2019).

In this work, we used MALDI-MSI to visualize amino acids in roots of two agronomically important inbred lines of maize, B73 and Mo17, and their reciprocal hybrids, B73 × Mo17 (BxM) and Mo17 × B73 (MxB). We focus primarily on the differences in amino acid localization and abundance between the genotypes and at different developmental stages of the root. Amino acids play an essential role in plant biology; they are the building blocks for proteins and have influence in many biochemical pathways relating to growth, development, stress resistance, and signaling (Hildebrandt et al., 2015). Many research efforts have been made previously on the role of amino acids in maize, especially how they relate to nitrogen assimilation and transportation. Employed methods in these studies include colorimetry, high performance liquid chromatography (HPLC), mass spectrometry, and various assays (Fentem et al., 1983; Toro et al., 2003; Seebauer et al., 2004). Despite extensive research in this area, very little is known about the localization of amino acids in maize. Our group has done some work showing the distribution of amino acids in the maize seed during germination, however, this was rather limited due to low ion signals (Feenstra et al., 2017a).

The current study aims to determine the abundance and distribution of amino acids in maize roots under various conditions and find evidence for how hybrid maize inherit molecular characteristics relating to amino acid localization from their parents. In addition to the aforementioned benefits of working with maize roots as a model system, there are additional advantages for this particular study focusing on the early stage of root development. Once vegetative tissue begins to develop and photosynthesis starts, the transportation of nitrogen and amino acids becomes more complex. Overall, focusing on the early development of the root simplifies the study. It has been established that Mo17 has more abundant amino acids in its seeds than B73 (Feenstra et al., 2017a), but it was not well known how that is translated to the hybrids, especially as the seedlings germinate and develop. As amino acids are not easily detectable with MALDI-MSI, derivatization is often necessary in order to increase their ionization efficiency. Coniferyl aldehyde (CA) has previously been used to derivatize primary amines, including amino acids, in MALDI-MSI experiments (Seebauer et al., 2004; Manier et al., 2014; Esteve et al., 2016). This derivatization strategy is utilized here to investigate amino acid differences in B73, Mo17, and their reciprocal hybrid maize genotypes.

MATERIALS AND METHODS

Materials

Gelatin from porcine skin (300 bloom) was purchased from Electron Microscopy Sciences (Hatfield, PA, United States). 4-hydroxy-3-cinnamaldehyde (coniferyl aldehyde; CA), deuterated alanine, ammonium chloride, and 98 atom percent ^{15}N ammonium chloride were purchased from Sigma Aldrich (St. Louis, MO, United States). Potassium acetate was purchased from Fisher Scientific (Hampton, NH). The gold sputter target was purchased from Ted Pella, Inc. (Redding, CA, United States). B73, Mo17, MxB, and BxM maize seeds were obtained courtesy of Dr. Marna Yandeau-Nelson at Iowa State University.

MALDI Sample Preparation

B73, Mo17, BxM, and MxB maize seeds were grown using a method described previously (Feenstra et al., 2017b). A row of maize seeds were placed along the edge of two wetted paper towels stacked on top of one another. The paper towels were wetted with either water, 10 mM ammonium chloride, or 10 mM ^{15}N labeled ammonium chloride depending on the experiment. The seeds were then rolled up in the paper towels tightly enough to keep them in place. The paper towel rolls were then placed in a beaker filled with water, 10 mM ammonium chloride, or 10 mM ^{15}N labeled ammonium chloride for the isotope labeling

experiments. The beaker was placed in the dark while the seeds began to grow and was monitored to make sure the paper towel stayed moist throughout growth. The roots were harvested when the length of the primary root was 2.5–3 cm, 6–7 cm, or 10–11 cm as measured from the tip of the root. The length of the root at harvesting differed depending on the experiment and is stated in each section of the results.

Once the roots reached the desired length, a razor blade was used to cut the root about 2 cm below the seed. This area of interest was embedded in a 10% w/v gelatin solution and flash frozen in liquid nitrogen. The area of interest was about 2 cm from the seed regardless of the stage of development, except in the case where multiple positions on the same root were embedded. The embedded roots were stored at −20°C and allowed to thermally equilibrate. The root tissue was cryo-sectioned (CM 1850, Leica Microsystems; Buffalo Grove, IL, United States) to 10 μm thickness, collected with Cryo-Jane tape (Leica Biosystems), and attached to a pre-chilled glass slide. The prepared slides were stored at −80°C until use, when they were placed on an aluminum block stored at the same temperature and vacuum dried. The dried sample tissues were derivatized using a TM sprayer (HTX Technologies, LLC, Chapel Hill, NC, United States). A 20 mg/mL solution of CA was used for derivatization at a flow rate of 0.03 mL/min and passing 8 times over the sample tissue. After derivatization, the tissue sections were sprayed with 6.5 mM potassium acetate using the same TM sprayer method. This was done to ensure the formation of potassium adducts while limiting protonated or sodiated adducts. They were then subject to matrix deposition by sputter coating (108 Auto Sputter Coater, Ted Pella Inc., Redding, CA, United States) gold at 40 mA for 20 s. One set of experiments incorporated deuterated alanine as an internal standard. The internal standard (5 mM) was sprayed onto the sample using the same TM sprayer method as previously described.

Mass Spectrometry Imaging Analysis

A MALDI linear ion trap-Orbitrap instrument (MALDI-LTQ-Orbitrap Discovery; Thermo Finnigan, San Jose, CA, United States) was used to collect all MSI data. The instrument was modified to incorporate an external 355 nm frequency tripled Nd: YAG laser (UVFQ; Elforlight, Daventry, United Kingdom). Tuneplus and XCalibur (Thermo Finnigan) were used to develop the mass spectrometry method and acquire data, respectively. Mass spectra were acquired in positive ion mode with the Orbitrap mass analyzer for a scan range of *m/z* 100–1000.

MS images were generated using ImageQuest (Thermo Finnigan) and MSI Reader (Robichaud et al., 2013) with a mass window of ±0.003 Da. Serial tissue sections were prepared as previously described and used for MS/MS analysis. MS/MS was done using the ion trap mass analyzer and were analyzed with a mass window of 1.0 Da and normalized collision energy of 35 were used.

LCMS Sample Preparation and Analysis

Maize roots of each genotype were grown in the same manner as previously described for the MALDI-MSI analysis. Once the roots were 10–11 cm in length, they were flash frozen in liquid nitrogen, homogenized, and stored at −80°C until analysis. Only the top 4 cm of each root was homogenized (2 cm on either side of the portion embedded for MALDI). This was done in an attempt to include the portion of the root that would most resemble the imaged root sections. In order to ensure there was sufficient tissue for good analyte signals, two roots of each genotype were combined for each biological replicate. Amino acids were extracted and simultaneously derivatized with 500 μL of 20 mg/mL CA in methanol. They were vortexed for 10 min and then centrifuged at 14,000 rpm for 10 min. 100 μL of the supernatant was aliquoted out and dried down. They were then reconstituted in 100 μL of 50:50 methanol:water.

Positive mode LCMS analysis was done on an LCMS 2020 single quadrupole mass spectrometer (Shimadzu, Kyoto, Japan). 1 μL of each sample was injected onto a 4.6 × 150 mm Agilent XDB C18 column with 1.8 μm particle size. Solvent A was water with 0.1% formic and solvent B was acetonitrile with 0.1% formic acid. A flow rate of 600 μL/min was used along with the following gradient: 0% B for the first 2 min, up to 30% B over the next 18 min, 100% B over 2 min, and back down to 0% B after another 2 min, where it was held for an additional 9 min. This gradient was first used by Manier et al. to separate CA derivatized amino acids and neurotransmitters (Manier et al., 2014). Chromatograms were extracted for each of the detected amino acids and the corresponding peaks were integrated.

RESULTS AND DISCUSSION

Coniferyl Aldehyde Derivatization

Amino acids are important biological molecules that have numerous roles in plant growth and development. However, due to poor ionization efficiency, amino acids are difficult to study by mass spectrometry. For this reason, coniferyl aldehyde (CA) was employed as a chemical derivatization reagent to modify the amino acids and increase their ionization efficiency (Manier et al., 2014; Esteve et al., 2016). The reaction scheme is shown in **Scheme 1**. CA (1) reacts with primary amines, such as amino acids (2), and forms a product with an imine moiety that improves ionization efficiency (3). **Figure 1** shows representative MALDI-MS images for 12 amino acids visualized in the maize root. A total of 16 amino acids were detected with the derivatization (14 proteogenic and 2 non-proteogenic) but only those with high enough signal are displayed. As leucine and isoleucine are isomers, they are not distinguishable by mass and are shown as a mixture of the two. Without derivatization with CA, only 3 amino acids are detected in positive mode (asparagine, glutamine, and histidine) and there is no signal present at the derivatized masses. Once CA derivatization is utilized, there is significant signal improvement to generate ion images for 12 amino acids. Four more amino acids (tyrosine, glutamic acid, proline, and aminobutenoic acid) could be also detected with derivatization but had very low ion signals and could not provide meaningful localization information. This implies the utility of the adopted derivatization technique for the study of amino acids in maize root tissues. The reaction efficiency of glutamine is 80∼90%. This was calculated from dividing the ion signal

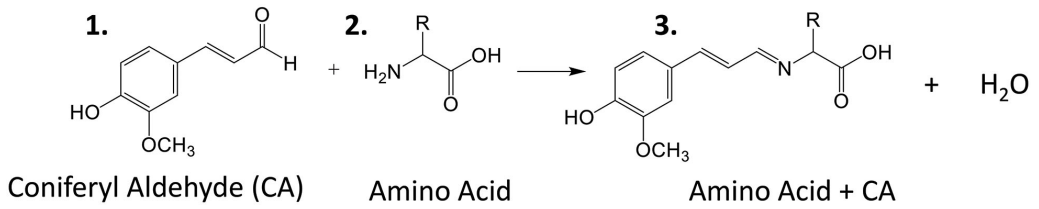

SCHEME 1 | Reaction scheme for the on-tissue derivatization of an amino acid with coniferyl aldehyde.

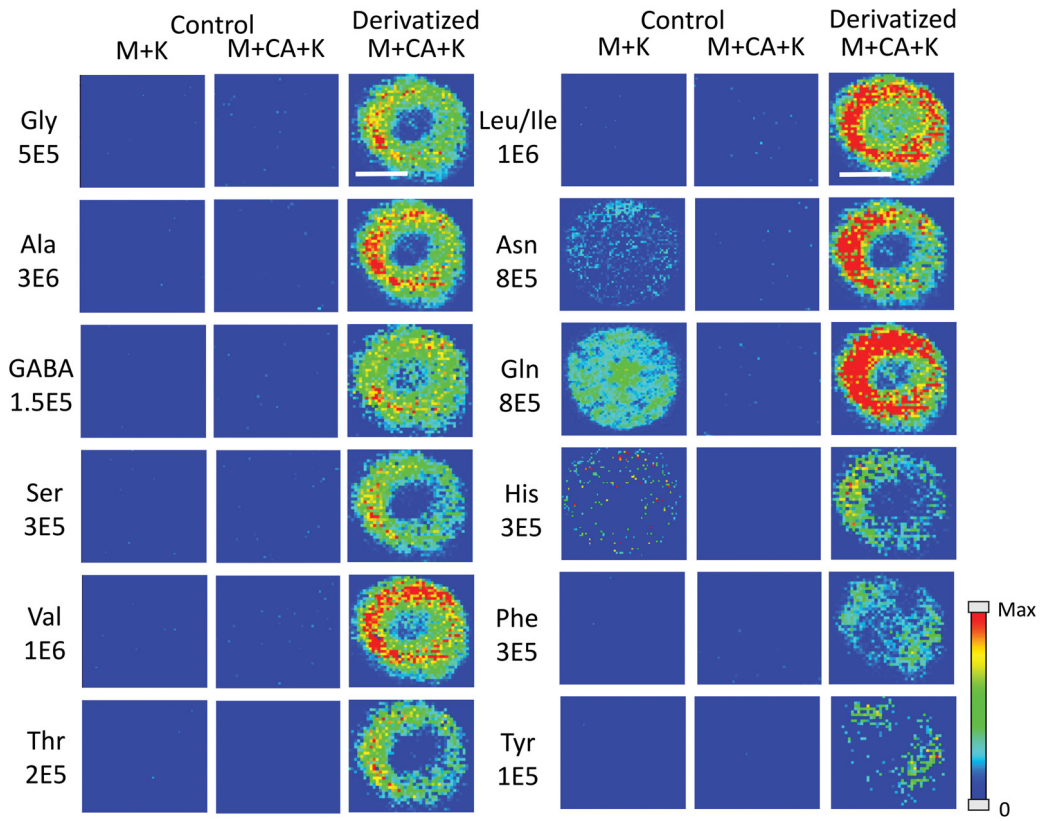

FIGURE 1 | MS images for the 12 amino acids detected in Mo17 maize roots. The first 2 columns are control roots without CA derivatization and the last column is with CA derivatization. "M + K" indicates the non-derivatized amino acids detected as potassium ion adduct. "M + CA + K" indicates the derivatized amino acids detected as potassium ion adduct. The numbers below each amino acid label correspond to the maximum intensity scale used to produce the false color image. The scale bar is 500 μm.

of derivatized glutamine by the sum of the ion signals for derivatized and underivatized glutamine. All amino acids were identified based on the exact mass of the derivatization product and three of the most abundant, alanine, valine, and leucine, were also confirmed by MS/MS and comparing with that of a CA derivatized standard.

MSI was used to explore amino acids in maize roots of inbreds B73, Mo17, and their reciprocal hybrids. Differences in abundance and localization as the roots develop and between genotypes were studied. Maize roots have a unique architecture which allows for an efficient uptake of water and nutrients (Hochholdinger, 2009). Bright-field microscope images and anatomical assignments are shown in **Supplementary Figure S1** for the cross-section of a B73 root. Maize roots exhibit a central vascular cylinder composed of the pith, xylem vessels, and the pericycle (the outermost cell layer of the inner cylinder). The ground tissue is made up of a single endodermis layer, multiple layers of cortex tissue, and a single epidermis cell layer.

Developmental Changes in the Localization of Amino Acids in Maize Roots

In order to determine how amino acids change in maize roots throughout development, roots were harvested at three different times. Harvesting times were when the total length of the root

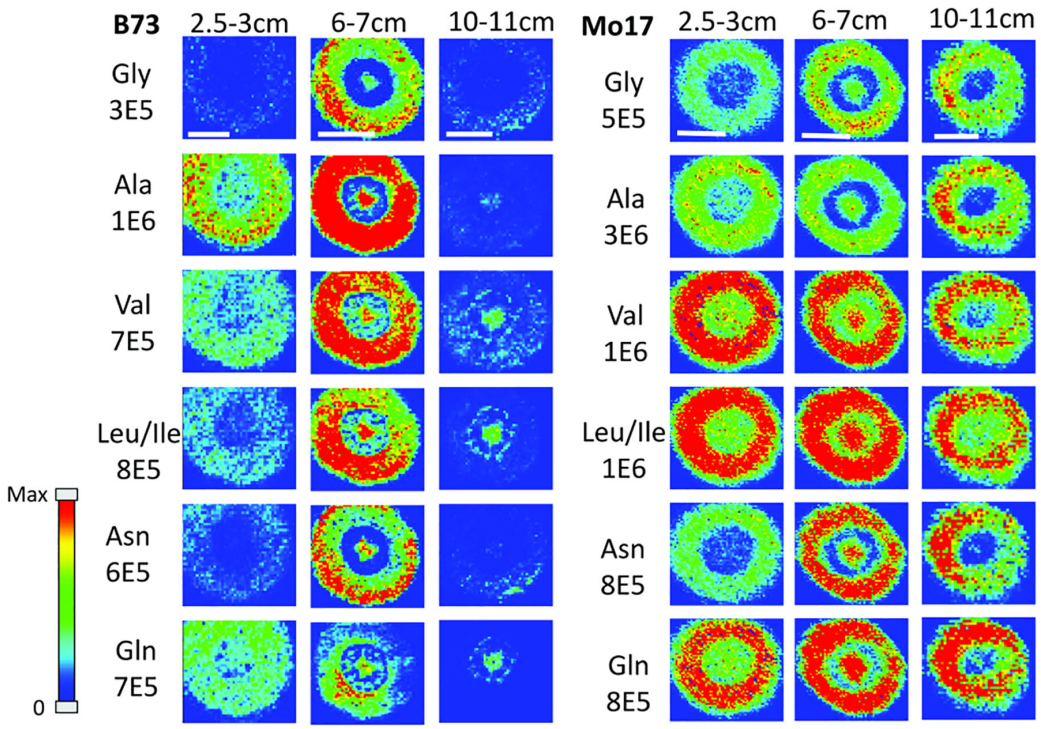

FIGURE 2 | MS images of amino acids in B73 (left) and Mo17 (right) maize roots cryosectioned at 2 cm below the seed for each different stage of development. The numbers below each amino acid label correspond to the maximum intensity scale used to produce false color image. The scale bar is 500 μm.

measured from the tip was between 2.5–3 cm, 6–7 cm, and 10–11 cm. These roots were each embedded and cryosectioned at about 2 cm away from the seed regardless of the developmental stage. The resulting images are shown in **Figure 2** comparing B73 vs. Mo17. Three biological replicates were tested at each stage with similar results, however, only one representative replicate is shown here. **Figure 2** shows localization changes in the amino acids between different developmental stages. For the purposes of this figure, only the six most abundant amino acids in the maize root tissue are shown. For B73, the early stage of root development (2.5–3 cm in length) has greater amino acid signal in the cortex. As the root develops, amino acid signals are the highest abundance at 6–7 cm in length with growing abundance at the center of the root; then, at the length of 10–11 cm, there is a significant reduction of amino acid signals, especially in the cortex. A possible explanation for this is that in the early stages of development, amino acids are synthesized in the outer cortex of the root and as the plant develops, it begins to rely more on the transportation of amino acids and/or nitrogen from other parts of the plant or the surrounding environment. These ideas are supported by evidence in literature indicating that certain amino acids flow to the root from other parts of the plant (Oaks, 1966). Another interesting note is that the intermediate root (6–7 cm in length) has a higher abundance of amino acids overall than the earlier or later stages. While there is quite a bit of biological variation between roots at the same stage of development, the mid-length roots have higher signal intensities for the derivatized amino acids on average. This is especially apparent for the B73 roots. **Supplementary Figure S2** in the supplementary information compares the average absolute signal intensities for the six most abundant amino acids at the different developmental stages.

In the case of Mo17 maize roots (right panel of **Figure 2**), the localizations are similar to that of B73 in the first two development stages. Both have the highest abundance of amino acid signal in the cortex of the root in the early stage (2.5–3 cm in length). In addition, they have a more or less even distribution between the center of the root and the cortex in the intermediate stage (6–7 cm in length). The major difference in the two genotypes occurs at the later stage of development (10–11 cm in length). While B73 loses amino acid signals in the cortex as they become concentrated to the pith and xylem, Mo17 does the opposite. Mo17 loses amino acid signals at the center of the root while those at the cortex remain similar. This suggests that B73 and Mo17 may have differences in the synthesis and/or transportation of amino acids during root development, especially at the later stage.

One hypothesis to explain the differences in localization at different developmental stages is that there is some gradient of amino acids along the length of the root, causing the localization to be different depending on the height. As a proof of concept, B73 maize roots at a later stage of development (16 cm in length) were embedded and sectioned at several different points along the length of the root. A representative data set is shown in **Supplementary Figure S3**. All amino acids are localized to the cortex near the root tips (11 or 15 cm distance from seed), similar

to the early stage of root development (2 cm cross-section for 2.5–3 cm in length in **Figure 2**). However, they are more or less evenly distributed at the mid height (5 or 8 cm distance from seed), similar to an intermediate stage (2 cm cross-section at 6–7 cm in length in **Figure 2**). Finally, some amino acids, especially leucine/isoleucine and glutamine, are primarily localized to the center of the root at the 2 cm position near the seed, similar to the later stage of root development cross-sectioned at 2 cm from the seed for the root length of 10–11 cm in **Figure 2**. Namely, there are three distinguished stages of root development in terms of amino acid localization; the early stage near the tip of the root, the mid-stage at the middle of root, and the later stage near the seed. Genotypic differences between B73 and Mo17 are minimal for the first two stages as shown in **Figure 2**, but apparent in the last stage. The cross-section 2 cm from the seed at a later stage of development was therefore used in the further study to compare their differences with the hybrids.

Genotypic Differences in Amino Acid Abundance and Localization

The hybrid roots were compared to the parents at 10–11 cm in total length cryosectioned at 2 cm from the seed. Separate B73 and Mo17 plants were grown and processed at the same time to minimize experimental variation. Signal intensities for the most abundant amino acids are displayed in **Figure 3** for each of the maize genotypes. These are the signal intensities averaged across the root areas in three biological replicates. There is a lot of biological variability in the abundance of amino acids even for the same genotype, making it difficult to determine how significant differences are; however, overall B73 and BxM have much lower amino acid signals compared to MxB and Mo17. Regardless of the genotype, alanine, valine, leucine/isoleucine, asparagine, and glutamine are the most abundant amino acids in maize root tissues. To confirm these findings with a more quantitative method, CA derivatized amino acids were also measured using LCMS for a similar region of the roots, harvested and extracted from 0 to 4 cm portion of the roots at 10–11 cm in total length. The genotypic differences are much less apparent in LCMS data due to the concentration gradient of amino acids along the root length (as seen in **Supplementary Figure S3**). The general trend of LCMS results, nonetheless, corroborated the MALDI-MSI findings; the same amino acids were found to be the most abundant and Mo17 and MxB have higher average signal levels than B73 and BxM. The LCMS data did include derivatized proline, which was detected with good signal intensity, unlike the MALDI-MSI data. We hypothesize that the on-tissue reaction might be too slow for secondary amines and does not provide high enough yield with the limited reaction time, unlike the in-solution reaction used for LCMS.

Figure 4 shows representative MS images of the six most abundant amino acids detected in maize roots (10–11 cm in length or about 8–10 days old, embedded and cryosectioned about 2 cm away from the seed) across all four genotypes. The same intensity scale is used for MS images of each amino acid to allow for a fair comparison of the relative abundances between the genotypes. Similar to the signal intensities in **Figure 3**, the

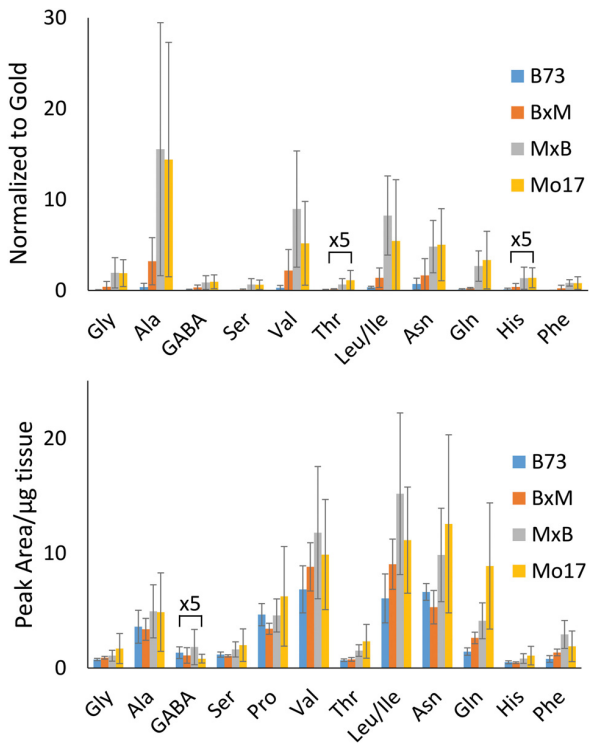

FIGURE 3 | Comparison of amino acid abundance in each genotype analyzed by MALDI-MSI of tissue section compared to LC-MS extract. MALDI-MS data presents signal intensities for selected amino acids normalized to gold matrix peak (n = 3). LC-MS data presents integrated peak areas for the extracted ion chromatogram of each amino acid normalized to the tissue weight (n = 4).

MS images show that Mo17 has much higher amino acid signal than B73 and the hybrids each have signal levels similar to that of the maternal parent. In addition to the obvious differences in overall signal and abundance, there are also more subtle differences in localization of amino acids between the two inbred lines, similar to **Figure 2**. In Mo17, most amino acids have the highest signal intensity in the cortex and minimal signal in the pith and xylem, with asparagine as a possible exception. In contrast, B73 has much of the amino acid signal localized to the center of the root and very little in the cortex, except for glycine and asparagine, which have a more even distribution. In fact, leucine/isoleucine and glutamine have almost no signal intensity in the cortex of B73. Interestingly, similar localizations are found in the hybrids, which mostly follow maternal inheritance; MxB obtains characteristics relating to amino acid localization from Mo17, whereas BxM obtains characteristics from B73. For example, leucine/isoleucine and glutamine are mostly localized at the center for BxM while significantly present in the cortex for MxB. Another example of possible maternal inheritance is the increased amino acid signal in MxB over BxM. This evidence for maternal inheritance is similar to the previous finding that the localization of thylakoid membrane lipids, specifically phosphatidylglycerols (PGs), in maize hybrids also follow characteristics of the maternal parent (Dueñas et al., 2019).

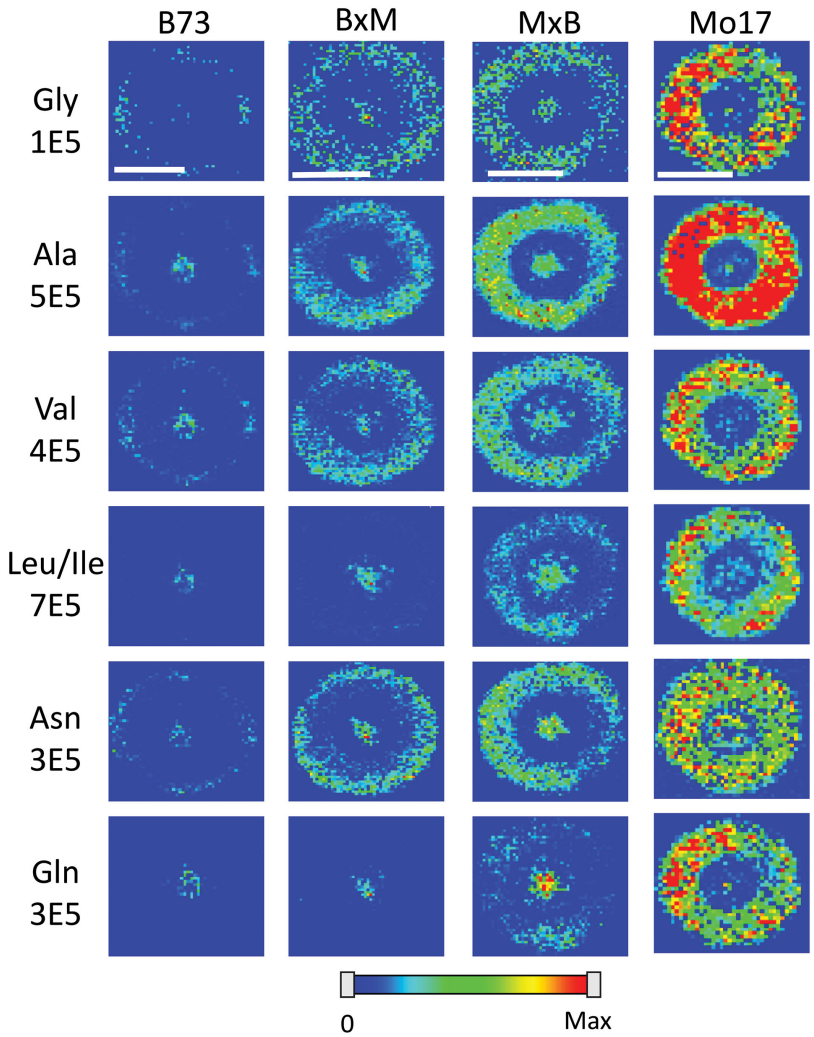

FIGURE 4 | MS images of the six most abundant amino acids in B73, BxM, MxB, and Mo17 maize roots cryosectioned at 2 cm below the seed for the development stage of 10–11 cm length. The numbers below each amino acid label correspond to the maximum intensity scale used to produce false color image. The scale bar is 500 μm.

Despite this example of maternal inheritance, there are other factors suggesting the hybrids inherit some characteristics from the paternal parent as well. For example, the increased abundance of amino acids in the center of the roots in MxB compared to Mo17 suggests characteristics of B73 in MxB.

Some may argue that these differences in localization are simply due to changes in ionization efficiency for different portions of the root if chemical composition is somewhat different between the genotypes. To address this issue, one root of each genotype was sprayed with an internal standard, deuterated alanine, and the images were created for several amino acids normalized to the deuterated alanine peak. As shown in **Supplementary Figure S4**, localizations look the same after this normalization suggesting there is no significant difference in ionization efficiency between different parts of the tissue. The localization differences described above are more apparent in **Figure 5**, which shows the signal intensity for amino acids in the pith normalized to the signal intensity in the cortex for each root. These intensities are also normalized to the overall size of the pith or cortex to account for the different tissue areas; namely, $(\Sigma_{\mathrm{Pith}}\mathrm{I}/\mathrm{Area}_{\mathrm{Pith}})/(\Sigma_{\mathrm{Cortex}}\mathrm{I}/\mathrm{Area}_{\mathrm{Cortex}})$. The y-axis of this figure is in a logarithmic scale and a ratio of one, located where the x-axis crosses the y-axis, indicates an even distribution of amino acids. With the exception of glycine, which is more abundant in the cortex than the pith in every genotype, B73 has ratios above one for every amino acid and Mo17 has ratios below one. For the most part, the hybrids have ratios in between those of the two parents, however, to varying degrees. For example, both hybrids have ratios close to one for alanine, valine, and asparagine, indicating a fairly even distribution. However, for leucine/isoleucine and glutamine, the hybrids both have ratios greater than one, but lower than that of B73. Some high standard deviations associated with asparagine and glutamine are likely due to the dramatic changes in localization along the length of the root for the two

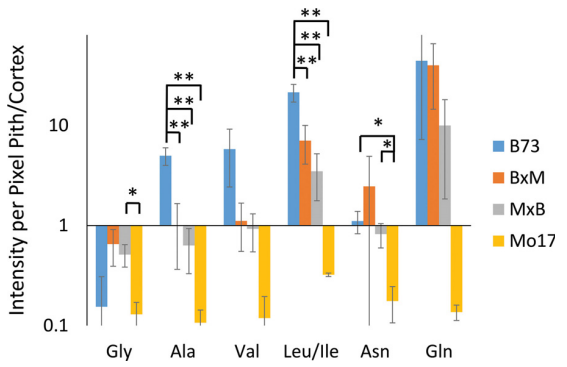

FIGURE 5 | The ratio of amino acid signals in the pith vs. cortex per unit area ($n = 3$). The * and ** indicate a $p < 0.05$ and < 0.01, respectively. The y-axis is on a logarithmic scale with the x-axis crosses the value of one, where the pith and cortex have the same signal intensity per unit area.

amino acids as shown in **Supplementary Figure S3**. Amino acids that have less biological variability exhibited some statistically significant differences. For example, the differences observed between B73 and each of the other genotypes are statistically significant for alanine and leucine/isoleucine with $p < 0.01$. For asparagine, the difference is significant only when comparing B73 to Mo17 or MxB to Mo17 with a $p < 0.05$. Overall, **Figure 5** nicely displays how the localization of most amino acids in the hybrids is a blended inheritance from both parents. The intermediate normalized intensities observed for alanine, valine, leucine/isoleucine, and asparagine especially correspond to more evenly distributed amino acids in the pith and cortex compared to the parents.

Amino acids localized primarily in the center of the root, in the pith and xylem, such as leucine/isoleucine and glutamine in B73 and BxM, may suggest these amino acids are transported to the root from other parts of the plant as opposed to being synthesized in the root itself. This would be consistent with the pith and xylem being the cells primarily responsible for the transportation of nutrients (Tegeder and Hammes, 2018). Mo17 has very little amino acid signal in the pith and xylem compared to the other maize genotypes. Therefore Mo17 may be synthesizing more amino acids in the root cortex itself and rely less on the transport of amino acids from other parts of the plant or the environment. Previous research has shown that many of the enzymes necessary for synthesizing amino acids are located in plastids and plastids achieve their highest level of development in cortical tissue (Miflin, 1974; Whatley, 1983). This supports the hypothesis that amino acids are being synthesized in the root cortex.

Changes in Amino Acid Abundance and Localization in Nitrogen Rich Conditions

All of the data shown up to this point has been from maize roots grown in pure water, which is nitrogen deficient compared to growing in soil. As plants are typically grown using fertilizer for a source of nitrogen, roots were also grown in a 10 mM solution of ammonium chloride, which acts as a nitrogen source during root development. **Figure 6** displays the representative MS images of B73 and Mo17 maize roots from three replicates grown in ammonium chloride compared to water. Not surprisingly, overall signals are higher for both B73 and Mo17 with the addition of $^{14}NH_4Cl$. Mo17 roots show changes in the localization when grown under nitrogen rich conditions with a more even distribution across the anatomy of the root. Rich nitrogen absorbed from outside might encourage the transportation of amino acids out of the roots once they are synthesized in the root cortex. In addition, the signal difference for amino acids between B73 and Mo17 maize is not as apparent when grown in the nitrogen containing solution compared to water, with the possible exception of glutamine. We hypothesize that B73 has a higher abundance of amino acids in the center of the root compared to the cortex because it relies on transportation from other parts of the plant; therefore, additional nitrogen provided from the environment may allow the B73 maize to synthesize more amino acids than would otherwise be possible. It is known that plants grown in nitrogen deficient conditions have less abundant amino acids in the roots and an altered proteome that will impact amino acid metabolism (Møller et al., 2011). Interestingly, leucine/isoleucine and glutamine are still highly enriched at the center of the B73 roots, potentially suggesting that pathways involving these amino acids are not affected by the availability of external nitrogen. Another interesting note is the increased abundance of glutamate by two orders of magnitude, which is almost invisible without additional nitrogen. This is consistent with glutamate being important for nitrogen assimilation in roots (Fentem et al., 1983).

As there are two different nitrogen sources (transported from other parts of the plant, and absorbed from environment), we performed an experiment to determine whether we can distinguish the two by growing roots in 10 mM ^{15}N-ammonium chloride. This will determine which amino acids take up nitrogen from the environment most efficiently during development. Images from this experiment are also available in **Figure 6** (two sets of images to the right). One would expect the images of amino acids with ^{14}N (labeled M in the figure) to be similar to the control because the nitrogen from the environment is ^{15}N and would appear as an isotope peak at M + 1. However, these root images look much more like the ones grown in ^{14}N ammonium chloride than the ones grown in water. This suggests that the plant does not process environmental nitrogen any different from nitrogen already present in the seed. Instead, additional nitrogen (or ammonium ion) from the environment may trigger some biological pathway that does not operate under nitrogen deficient conditions. The mass resolution of the instrument used was not high enough to resolve peaks with ^{13}C- vs. ^{15}N-amino acids. As shown in **Supplementary Figure S5**, the isotope of derivatized glutamine appears as a single peak for $^{13}C_1$- or $^{15}N_1$-isotope at "M + 1" position and $^{13}C_2$-, $^{15}N_2$-, or $^{13}C_1{}^{15}N_1$-isotope at "M + 2" position. As the ^{13}C and ^{15}N peaks were not resolved, the M + 1 peak contains both $^{13}C_1$- and $^{15}N_1$-gluatamine peaks. Considering the natural abundance of ^{13}C and ^{15}N, M + 1 peak in the maize root grown in ^{15}N-ammonium solution shown in **Supplementary Figure S5** is made up of ~90% ^{15}N from external ^{15}N-ammonium ion. The final two columns

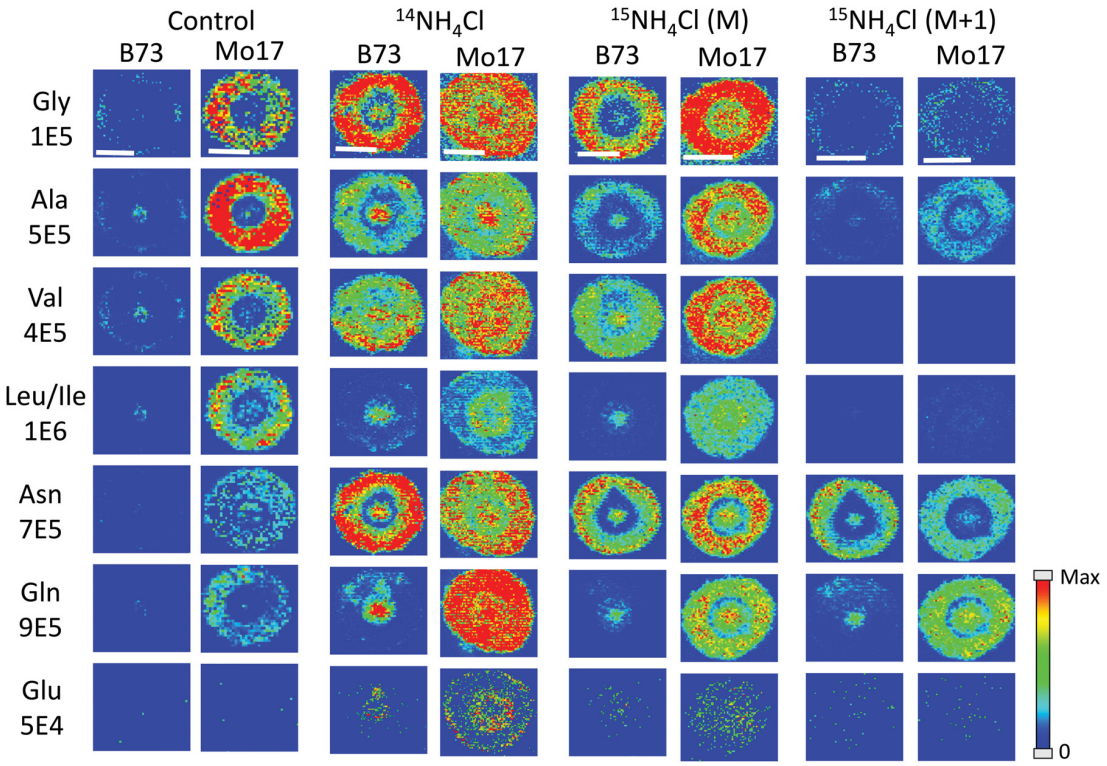

FIGURE 6 | MS images of selected amino acids in B73 and Mo17 maize root sections grown in 10 mM ammonium ion, either $^{14}NH_4Cl$ or $^{15}NH_4Cl$, compared to the control grown in water. The first three sets of images are of the monoisotopes (M peak) containing only ^{12}C and ^{14}N. The last set is of the isotope (M + 1 peak) from $^{15}NH_4Cl$ data containing one isotope of either ^{15}N or ^{13}C. The root sections were made at 2 cm below the seed when the root reached the length of 10–11 cm. The numbers below each amino acid label correspond to the maximum intensity scale used to produce false color image. The scale bar is 500 μm.

in **Figure 6** show the amino acids synthesized from nitrogen in the environment, thus ^{15}N-labeled and composing most of the M + 1 peak. They show similar localization with the ^{14}N-labeled M peak, amino acids synthesized from nitrogen already present in the seed. This provides further support for our hypothesis that environmental nitrogen only triggers a mechanism that affects abundance and localization of amino acids but does not differentiate between internal vs. external nitrogen. Some of the detected amino acids significantly incorporated ^{15}N, especially asparagine and glutamine, which is not surprising considering they are known to play the key role in nitrogen assimilation (Fentem et al., 1983).

To explore how much ^{15}N-labeled external nitrogen is incorporated for each amino acid, the peaks corresponding to each of the labeled amino acids were deconvoluted using an Excel spreadsheet developed by Gruber et al. (2007) considering the natural abundance of the isotope. The relative level of the incorporated ^{15}N from three biological replicates of each genotype are summarized in **Figure 7**. These reported results represent the percent of nitrogen in each amino acid that has come from environmental ^{15}N. Glutamine has the highest level of ^{15}N incorporation (22–35%) followed by asparagine and alanine (5–19% and 2–18%, respectively). Glutamine and asparagine are well known for nitrogen storage (Hildebrandt et al., 2015), so they would take up nitrogen from the surrounding environment and store it throughout the early development of the plant. Alanine also has been known to shuttle nitrogen between cells in crop plants, which could explain its environmental nitrogen uptake (Shrawat et al., 2008). In contrast, other amino acids, such as glycine, valine, and leucine/isoleucine, did not incorporate any appreciable amount of nitrogen from the environment. In a much later stage of development, a majority of nitrogen would be eventually replaced by ^{15}N in every amino acid; however, at this stage of development, most nitrogen still seems to be coming from the seeds except in the case of the three amino acids related with nitrogen storage or transportation.

In addition to the differences between amino acids, there also are some differences depending on the genotype of maize. There is significantly less incorporation of ^{15}N in the three amino acids in Mo17 maize than in B73, with the possible exception of glutamine. *P*-values associated with the environmental nitrogen uptake for alanine and asparagine are <0.01 and <0.05 respectively when comparing B73 and Mo17. As noted earlier, Mo17 has much higher amino acid content in seedlings (Fentem et al., 1983) and the localization of amino acids in Mo17 roots indicates it could be synthesizing most of the necessary amino acids directly in the cortex of the root. This may be the reason Mo17 is not taking in as much nitrogen from the nutrient solution in the surrounding environment. For the most part, the nitrogen incorporation in the hybrids was in between that of the

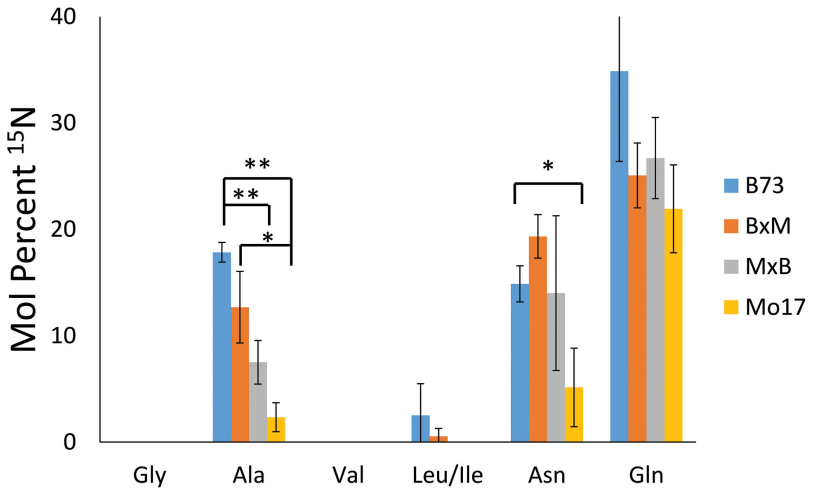

FIGURE 7 | Mol percent of ^{15}N incorporation into amino acids of maize roots grown at 10 mM ^{15}N-ammonium ion and cryosectioned at 2 cm below the seed at the root length of 10–11 cm. The error bars come from three biological replicates. The * and ** indicate a $p < 0.05$ and < 0.01, respectively.

two parents, although statistically insignificant due to the large error bars, with the exception of alanine. This is further evidence that the hybrid maize has blended traits from the two inbred lines and benefits from characteristics of both parents.

CONCLUSION

In this study, MALDI-MSI combined with CA chemical derivatization was utilized to study amino acids in maize root tissue. New insight into the localization of amino acids throughout the growth and development of maize seedlings as well as inheritance patterns of hybrid maize was observed that would not have been possible without this method. The surface imaging allowed for previously unknown differences in relative quantification between different parts of the maize root with relatively little sample preparation compared to LCMS and gas chromatography (GC)-MS. In contrast to MALDI-MSI, LC, and GCMS both require lengthy extractions, resulting in the destruction of the sample and inability to obtain spatial information. Although this study highlighted the use of MALDI-MSI for the analysis of free amino acids, the technique is versatile so other classes of compounds can be detected and visualized in the same sample. This approach, however, comes with its own limitations, most notably the difficulty in quantification compared to other techniques. An additional disadvantage due to the derivatization is the possibility of side reactions, i.e., CA reacting with compounds other than primary amines. The latter makes utilizing this technique for untargeted analyses challenging, but it may be overcome through systematic study in side reactions and more selective reagents.

While the overall abundance and localization changed in different developmental stages as well as at different points along the length of the root, locations near the seed (∼2 cm away) displayed major differences between genotypes at later stages of development. Specifically, B73 had lower amino acid abundance and showed a localization primarily in the center of the root for most amino acids. In contrast, Mo17 had higher abundance and amino acids were mostly localized to the root cortex. Both the hybrid roots grown and prepared in the same way as the parents had abundance levels that were similar to that of the maternal parent. BxM had abundance similar to or slightly higher than B73, but much lower than MxB or Mo17. Likewise, MxB had signal levels similar to Mo17. In terms of localization, a blended inheritance was observed for most amino acids, as noted by the pith/cortex signal intensity ratios, with the exception of glycine. Alanine and valine provided the best examples of blended inheritance with B73 having a signal ratio much greater than one, indicating localization primarily to the pith, Mo17 having a ratio much less than one, indicating localization primarily to the cortex, and both hybrids having a ratio close to one, indicating an even distribution. Comparing the characteristics relating amino acids in inbred lines of maize to their reciprocal hybrids gave insight into hybrid inheritance patterns. In addition, understanding the changes in amino acid localization and abundance provides essential information relating to the transportation of nutrients in the early stages of plant development.

Differences in amino acid localization and abundance were also observed for roots grown in nitrogen rich conditions compared to those grown in water. The addition of a nitrogen source in the form of an ammonium ion to the growth environment caused changes such as lessened signal discrepancy for amino acids between B73 and Mo17 compared to nitrogen deficient conditions, and more uniform distribution of amino acids, especially in Mo17. An isotope labeling experiment using $^{15}NH_4Cl$ provided some insight about nitrogen uptake from environment. First of all, there is no difference between the localization of ^{14}N-amino acid and ^{15}N-amino acid, regardless of whether they are grown in $^{14}NH_4Cl$ or $^{15}NH_4Cl$. This suggests the change in the abundance and localization due to the ammonium ion is the result of triggering a new

mechanism or biochemical pathway, and not due to different distributions of nitrogen from environment. When comparing the relative amount of ^{15}N uptake for each amino acid, only glutamine, asparagine, and alanine incorporated a significant amount of nitrogen from the environment in this early stage of root development, consistent with their major roles in nitrogen storage and transport. In terms of the amount of ^{15}N incorporation, B73 and Mo17 show the most and the least incorporation, respectively, the two hybrid maize have an intermediate level of ^{15}N incorporation between the two parents, which provides further evidence that the characteristics of the hybrids are inherited from both parents. These experiments can help shed light on nitrogen assimilation and nitrogen use efficiency in maize. Studying amino acids in maize roots has not only given insight into differences between maize genotypes and inheritance patterns, but has also shown how amino acids accumulate throughout roots as they grow and develop. Considering the success of this method for the current application, there is room to expand this work for additional applications in the future. For example, amino acids such as phenylalanine and tyrosine could be related back to the localization of defense compounds derived from the phenylpropanoid pathway.

DATA AVAILABILITY STATEMENT

The raw data supporting the conclusions of this article will be made available to any qualified researcher without any reservations.

AUTHOR CONTRIBUTIONS

KO and YL designed the experiment. KO did all of the sample preparation and data collection for the experiment. Data was analyzed by KO with the help and guidance of YL. The manuscript was prepared and written by KO and YL.

FUNDING

This work was partially supported by National Science Foundation under Grant No. 1905335.

ACKNOWLEDGMENTS

We would like to thank Dr. Marna Yandau-Nelson for providing the maize seeds for the purposes of this research and ISU Chemical Instrumentation Facility staff for assistance with the LCMS experiment.

SUPPLEMENTARY MATERIAL

The Supplementary Material for this article can be found online at: https://www.frontiersin.org/articles/10.3389/fpls.2020.00639/full#supplementary-material

REFERENCES

Dueñas, M. E., Carlucci, L., and Lee, Y. J. (2016). Matrix recrystallization for MALDI-MS imaging of maize lipids at high-spatial resolution. *J. Am. Soc. Mass Spectr.* 27, 1575–1578. doi: 10.1007/s13361-016-1422-0

Dueñas, M. E., Klein, A. T., Alexander, L. E., Yandeau-Nelson, M. D., Nikolau, B. J., and Lee, Y. J. (2017). High-spatial resolution mass spectrometry imaging reveals the genetically programmed, developmental modification of the distribution of thylakoid membrane lipids among individual cells of the maize leaf. *Plant J.* 89, 825–838. doi: 10.1111/tpj.13422

Dueñas, M. E., Larson, E. A., and Lee, Y. J. (2019). Toward mass spectrometry imaging in the metabolomics scale: increasing metabolic coverage through multiple on-tissue chemical modifications. *Front. Plant Sci.* 10:860. doi: 10.3389/fpls.2019.00860

Esteve, C., Tolner, E. A., Shyti, R., van den Maagdenberg, A. M. J. M., and McDonnell, L. A. (2016). Mass spectrometry imaging of amino neurotransmitters: a comparison of derivatization methods and application in mouse brain tissue. *Metabolomics* 12:30. doi: 10.1007/s11306-015-0926-0

Feenstra, A. D., Alexander, L. E., Song, Z., Korte, A. R., Yandeau-Nelson, M., Nikolau, B. J., et al. (2017a). Spatial mapping and profiling of metabolite distributions during germination. *Plant Physiol.* 174, 2532–2548. doi: 10.1104/pp.17.00652

Feenstra, A. D., Dueñas, M. E., and Lee, Y. J. (2017b). Five micron high resolution MALDI mass spectrometry imaging with simple, interchangeable, multi-resolution optical system. *J. Am. Soc. Mass Spectr.* 28, 434–442. doi: 10.1007/s13361-016-1577-8

Fentem, P. A., Lea, P. J., and Stewart, G. R. (1983). Ammonia assimilation in the roots of nitrate- and ammonia-grown *Hordeum vulgare* (cv Golden Promise). *Plant Physiol.* 71, 496–501. doi: 10.1104/pp.71.3.496

Gruber, C. C., Oberdorfer, G., Voss, C. V., Kremsner, J. M., Kappe, C. O., and Kroutil, W. (2007). An algorithm for the deconvolution of mass spectrosopic patterns in isotope labeling studies. evaluation for the hydrogen-deuterium exchange reaction in ketones. *J. Organ. Chem.* 72, 5778–5783. doi: 10.1021/jo070831o

Hildebrandt, T. M., Nesi, A. N., Araújo, W. L., and Braun, H.-P. (2015). Amino acid catabolism in plants. *Mol. Plant* 8, 1563–1579.

Hochholdinger, F. (2009). "The maize root system: morphology, anatomy, and genetics," in *Handbook of Maize: Its Biology*, eds J. L. Bennetzen and S. C. Hake (New York, NY: Springer), 145–160.

Korte, A., Yandeau-Nelson, M., Nikolau, B., and Lee, Y. (2015). Subcellular-level resolution MALDI-MS imaging of maize leaf metabolites by MALDI-linear ion trap-Orbitrap mass spectrometer. *Anal. Bioanal. Chem.* 407, 2301–2309. doi: 10.1007/s00216-015-8460-5

Lee, Y. J., Perdian, D. C., Song, Z., Yeung, E. S., and Nikolau, B. J. (2012). Use of mass spectrometry for imaging metabolites in plants. *Plant J.* 70, 81–95. doi: 10.19540/j.cnki.cjcmm.20191209.201

Lemaître, T., Gaufichon, L., Boutet-Mercey, S., Christ, A., and Masclaux-Daubresse, C. (2008). Enzymatic and metabolic diagnostic of nitrogen deficiency in *Arabidopsis thaliana* wassileskija accession. *Plant Cell Physiol.* 49, 1056–1065. doi: 10.1093/pcp/pcn081

Manier, M. L., Spraggins, J. M., Reyzer, M. L., Norris, J. L., and Caprioli, R. M. C. J. M. S. R. (2014). A derivatization and validation strategy for determining the spatial localization of endogenous amine metabolites in tissues using MALDI imaging mass spectrometry. *J. Mass Spectr.* 49, 665–673. doi: 10.1002/jms.3411

Miflin, B. J. (1974). The location of nitrite reductase and other enzymes related to amino acid biosynthesis in the plastids of root and leaves. *Plant Physiol.* 54, 550–555. doi: 10.1104/pp.54.4.550

Møller, A. L. B., Pedas, P. A. I., Andersen, B., Svensson, B., Schjoerring, J. K., and Finnie, C. (2011). Responses of barley root and shoot proteomes to long-term nitrogen deficiency, short-term nitrogen starvation and ammonium. *Plant Cell Environ.* 34, 2024–2037. doi: 10.1111/j.1365-3040.2011.02396.x

Niehaus, M., Soltwisch, J., Belov, M. E., and Dreisewerd, K. (2019). Transmission-mode MALDI-2 mass spectrometry imaging of cells and tissues at subcellular resolution. *Nat. Methods* 16, 925–931. doi: 10.1038/s41592-019-0536-2

Oaks, A. (1966). Transport of amino acids to the maize root. *Plant Physiol.* 41, 173–180. doi: 10.1104/pp.41.1.173

Paschold, A., Marcon, C., Hoecker, N., and Hochholdinger, F. (2010). Molecular dissection of heterosis manifestation during early maize root development. *Theor. Appl. Genet.* 120, 383–388. doi: 10.1007/s00122-009-1082-6

Pratelli, R., and Pilot, G. (2014). Regulation of amino acid metabolic enzymes and transporters in plants. *J. Exp. Bot.* 65, 5535–5556. doi: 10.1093/jxb/eru320

Robichaud, G., Garrard, K. P., Barry, J. A., and Muddiman, D. C. (2013). MSiReader: an open-source interface to view and analyze high resolving power ms imaging files on matlab platform. *J. Am. Soc. Mass Spectr.* 24, 718–721. doi: 10.1007/s13361-013-0607-z

Seebauer, J. R., Moose, S. P., Fabbri, B. J., Crossland, L. D., and Below, F. E. (2004). Amino acid metabolism in maize earshoots. implications for assimilate preconditioning and nitrogen signaling. *Plant Physiol.* 136, 4326–4334. doi: 10.1104/pp.104.043778

Shrawat, A. K., Carroll, R. T., DePauw, M., Taylor, G. J., and Good, A. G. (2008). Genetic engineering of improved nitrogen use efficiency in rice by the tissue-specific expression of alanine aminotransferase. *Plant Biotechnol. J.* 6, 722–732. doi: 10.1111/j.1467-7652.2008.00351.x

Sturtevant, D., Lee, Y.-J., and Chapman, K. D. (2016). Matrix assisted laser desorption/ionization-mass spectrometry imaging (MALDI-MSI) for direct visualization of plant metabolites in situ. *Curr. Opin. Biotechnol.* 37, 53–60. doi: 10.1016/j.copbio.2015.10.004

Tegeder, M., and Hammes, U. Z. (2018). The way out and in: phloem loading and unloading of amino acids. *Curr. Opin. Plant Biol.* 43, 16–21. doi: 10.1016/j.pbi.2017.12.002

Toro, A. A., Medici, L. O., Sodek, L., Lea, P. J., and Azevedo, R. A. (2003). Distribution of soluble amino acids in maize endosperm mutants. *Sci. Agric.* 60, 91–96.

Whatley, J. M. (1983). PLASTIDS IN THE ROOTS OF PHASEOLUSVULGARIS. *New Phytol.* 94, 381–391.

Zavalin, A., Yang, J., and Caprioli, R. (2013). Laser beam filtration for high spatial resolution MALDI imaging mass spectrometry. *J. Am. Soc. Mass Spectr.* 24, 1153–1156. doi: 10.1007/s13361-013-0638-5

Conflict of Interest: The authors declare that the research was conducted in the absence of any commercial or financial relationships that could be construed as a potential conflict of interest.

Copyright © 2020 O'Neill and Lee. This is an open-access article distributed under the terms of the Creative Commons Attribution License (CC BY). The use, distribution or reproduction in other forums is permitted, provided the original author(s) and the copyright owner(s) are credited and that the original publication in this journal is cited, in accordance with accepted academic practice. No use, distribution or reproduction is permitted which does not comply with these terms.

frontiers in Plant Science

ORIGINAL RESEARCH
published: 05 June 2020
doi: 10.3389/fpls.2020.00754

Structural Studies of Glutamate Dehydrogenase (Isoform 1) From *Arabidopsis thaliana*, an Important Enzyme at the Branch-Point Between Carbon and Nitrogen Metabolism

Marta Grzechowiak[1], Joanna Sliwiak[1], Mariusz Jaskolski[1,2] and Milosz Ruszkowski[1]*

[1] *Center for Biocrystallographic Research Institute of Bioorganic Chemistry, Polish Academy of Sciences, Poznań, Poland,*
[2] *Department of Crystallography, Faculty of Chemistry, Adam Mickiewicz University, Poznań, Poland*

OPEN ACCESS

Edited by:
Giuseppe Forlani,
University of Ferrara, Italy

Reviewed by:
Bertrand Hirel,
Institut National Français de Recherche en Agriculture, Institut National de la Recherche Agronomique (INRA), France
Paul C. Engel,
University College Dublin, Ireland

***Correspondence:**
Milosz Ruszkowski
mruszkowski@ibch.poznan.pl;
milas.poland@gmail.com

Specialty section:
This article was submitted to Plant Metabolism and Chemodiversity, a section of the journal Frontiers in Plant Science

Received: *24 March 2020*
Accepted: *12 May 2020*
Published: *05 June 2020*

Citation:
Grzechowiak M, Sliwiak J, Jaskolski M and Ruszkowski M (2020) Structural Studies of Glutamate Dehydrogenase (Isoform 1) From Arabidopsis thaliana, an Important Enzyme at the Branch-Point Between Carbon and Nitrogen Metabolism. Front. Plant Sci. 11:754. doi: 10.3389/fpls.2020.00754

Glutamate dehydrogenase (GDH) releases ammonia in a reversible NAD(P)$^+$-dependent oxidative deamination of glutamate that yields 2-oxoglutarate (2OG). In current perception, GDH contributes to Glu homeostasis and plays a significant role at the junction of carbon and nitrogen assimilation pathways. GDHs are members of a superfamily of ELFV (Glu/Leu/Phe/Val) amino acid dehydrogenases and are subdivided into three subclasses, based on coenzyme specificity: NAD$^+$-specific, NAD$^+$/NADP$^+$ dual-specific, and NADP$^+$-specific. We determined in this work that the mitochondrial *At*GDH1 isozyme from *A. thaliana* is NAD$^+$-specific. Altogether, *A. thaliana* expresses three GDH isozymes (*At*GDH1-3) targeted to mitochondria, of which *At*GDH2 has an extra EF-hand motif and is stimulated by calcium. Our enzymatic assays of *At*GDH1 established that its sensitivity to calcium is negligible. *In vivo* the *At*GDH1-3 enzymes form homo- and heterohexamers of varied composition. We solved the crystal structure of recombinant *At*GDH1 in the apo-form and in complex with NAD$^+$ at 2.59 and 2.03 Å resolution, respectively. We demonstrate also that both in the apo form and in 1:1 complex with NAD$^+$, it forms D_3-symmetric homohexamers. A subunit of *At*GDH1 consists of domain I, which is involved in hexamer formation and substrate binding, and of domain II which binds coenzyme. Most of the subunits in our crystal structures, including those in NAD$^+$ complex, are in open conformation, with domain II forming a large (albeit variable) angle with domain I. One of the subunits of the *At*GDH1-NAD$^+$ hexamer contains a serendipitous 2OG molecule in the active site, causing a dramatic (∼25°) closure of the domains. We provide convincing evidence that the N-terminal peptide preceding domain I is a mitochondrial targeting signal, with a predicted cleavage site for mitochondrial processing peptidase (MPP) at Leu17-Leu18 that is followed by an unexpected potassium coordination site (Ser27, Ile30). We also identified several MPD [(+/-)-2-methyl-2,4-pentanediol] binding sites with conserved sequence. Although *At*GDH1 is insensitive to MPD in our assays, the observation of druggable sites opens a potential for non-competitive herbicide design.

Keywords: oxidative deamination, NAD coenzyme, glutamate metabolism, 2-oxoglutarate, domain movement

INTRODUCTION

As a constituent of many important bioorganic compounds, nitrogen is one of the most essential macroelements in the biosphere. Its limited availability is thus a critical factor of plant growth and development. One of the forms of inorganic nitrogen which is directly available to plants is ammonia (Lea, 1993). Ammonia assimilation and recycling is based on the cooperative activity of three enzymes: glutamine synthetase (GS; EC 6.3.1.2), glutamate synthase (GOGAT; EC 1.4.7.1 and EC 1.4.1.14), and glutamate dehydrogenase (GDH, EC 1.4.1.2) (Lea and Miflin, 1974). GS catalyzes the ATP-dependent conversion of glutamate into glutamine by incorporating ammonia, whereas GOGAT transfers the amide group from glutamine to 2-oxoglutarate (2OG), producing two molecules of glutamate. These two enzymes function in a cycle in the cytosol and chloroplasts. The cycle intermediates, glutamine and glutamate, serve as nitrogen donors and/or acceptors in other biosynthetic pathways. GDHs release the ammonium cation from glutamate in a reversible, $NAD(P)^+$-dependent oxidative deamination reaction that yields 2OG.

For a long time, the physiological role of GDH was unclear because of uncertainty about the *in vivo* direction of its reaction (Robinson et al., 1992; Fox et al., 1995; Melo-Oliveira et al., 1996; Aubert et al., 2001; Masclaux-Daubresse et al., 2006; Purnell and Botella, 2007; Lehmann and Ratajczak, 2008; Miyashita and Good, 2008). Initially, GDH had been considered as the most important enzyme involved in the assimilation of ammonia before the discovery of the GS-GOGAT cycle. At present, the GS-GOGAT cycle is recognized as the major route of ammonia assimilation into organic molecules in plants (Lea and Miflin, 1974; Miflin and Lea, 1980). That discovery has changed the perception of the role of GDH in plants. More recent reports provide evidence that the contribution of GDH to direct NH_4^+ assimilation is negligible (5%) compared to that catalyzed by the GS-GOGAT cycle (95%) (Melo-Oliveira et al., 1996; Lea and Miflin, 2011). However, GDH provides an alternative route for the incorporation of ammonia into organic compounds only during specific environmental stimuli, when remobilization of nutrients is required (Skopelitis et al., 2006). The major role of GDH lies in fueling the tricarboxylic acid cycle (TCA cycle) with 2OG when carbon becomes the limiting factor (Fontaine et al., 2012). This way – together with GOGAT – GDH controls Glu homeostasis (Labboun et al., 2009). For that reason, GDH plays a significant role at the branch point of the carbon and nitrogen assimilation pathways (Labboun et al., 2009; Fontaine et al., 2012).

GDHs are ubiquitous enzymes that have been found in all living organisms. They belong to the family of amino acid dehydrogenases, designated ELFV (Glu/Leu/Phe/Val), that include also leucine, phenylalanine and valine dehydrogenases. Members of that family display divergent substrate specificity while preserving similarity in sequence and structure (Britton et al., 1993). Furthermore, the GDH class is divided into three subclasses, based on coenzyme specificity: NAD-specific (EC 1.4.1.2), NAD/NADP dual-specific (EC 1.4.1.3), and NADP-specific (EC 1.4.1.4) (Smith et al., 1975). For brevity, in this work we utilize the NAD or NADP abbreviations in reference to both, the oxidized and reduced forms of these coenzymes. GDHs that utilize NAD (Purnell and Botella, 2007; Fontaine et al., 2012; Oliveira et al., 2012) or NADP (Noor and Punekar, 2005; Werner et al., 2005) can be found in various combinations in plants, fungi, and microorganisms, whereas vertebrate GDHs are able to utilize both NAD and NADP with comparable efficiency, which depends on the direction of the reaction (Brunhuber and Blanchard, 1994; Engel, 2014). More precisely, NADPH is utilized in the reductive amination of 2OG while NAD^+ is utilized in the reverse reaction.

Bacterial GDHs are homohexamers while the eukaryotic enzymes have evolved into two families which differ in the oligomeric structure. Vertebrate GDHs form homohexamers, plant GDHs exist as homo- or heterohexamers composed of ∼45–50 kDa subunits, whereas tetramers of ∼115 kDa subunits were found in fungi (Britton et al., 1992). The hexameric GDHs are structurally similar and possess two domains. Domain I is involved in substrate binding while the domain II binds the coenzyme. The active site is formed in a deep groove between the two domains (Baker et al., 1992). Animal GDHs possess a third domain, called antenna, which is absent in other types of GDHs (Stillman et al., 1993, 1999; Knapp et al., 1997; Britton et al., 1999; Peterson and Smith, 1999; Werner et al., 2005; Oliveira et al., 2012). The antenna domain can bind a wide range of small molecules and this way can allosterically regulate the GDH activity (Peterson and Smith, 1999; Li et al., 2011).

Plants have distinct isozymes of GDH that are either NAD- or NADP-specific (Glevarec et al., 2004; Fontaine et al., 2006, 2012; Masclaux-Daubresse et al., 2006; Labboun et al., 2009; Qiu et al., 2009). NAD-specific GDHs are localized in mitochondria (Loulakakis and Roubelakisangelakis, 1990; Miflin and Habash, 2002; Fontaine et al., 2006), whereas NADP-specific GDHs exist in chloroplasts, where their biological function is not fully understood (Fontaine et al., 2012).

Arabidopsis thaliana possesses three genes (*GDH1, GDH2,* and *GDH3*) encoding three different NAD-dependent GDH subunits (α, β, and γ, respectively) (Fontaine et al., 2012). In this article, we will use the abbreviation *At*GDH1 to designate a homohexamer composed of the α subunits, and *At*GDH2 or *At*GDH3 for homohexamers composed of the β or γ subunits, respectively (Uniprot IDs: *At*GDH1, Q43314; *At*GDH2, Q38946; *At*GDH3, Q9S7A0). *In vivo*, the individual subunits associate in different ratios to form homo- and hetero-hexamers of ∼270 kDa. Hexamers composed of the α and β subunits are present in roots, stems, and leaves, whereas the γ-subunit assembles with the α- and β-subunits only in roots (Turano et al., 1997; Fontaine et al., 2006, 2012, 2013; Marchi et al., 2013). The *Arabidopsis* GDH isoforms have different functional properties. For example, Marchi et al. (2014) showed that *At*GDH3 is less thermostable than *At*GDH1 and *At*GDH2, and that the carboxyl terminus is involved in the stabilization of the oligomeric structure of the enzyme. It was also established that *At*GDH2, but not *At*GDH1 or *At*GDH3, has a region similar to the EF-hand loop motif that may be implicated in calcium binding. Consistently, the activity of that isoform was stimulated by Ca^{2+} ions (Loulakakis and Roubelakisangelakis, 1990; Turano et al., 1997).

So far, several structures of bacterial, archaebacterial, vertebrate, and fungal GDHs have been deposited in the Protein Data Bank (PDB). However, enzymes of plant origin have received much less attention. In the present study, we report the crystal structure of *At*GDH1 in apo form, as well as in complex with its coenzyme NAD^+ and the reaction product 2OG. The structures reveal that the enzyme undergoes an open/closed conformational change. Binding of NAD^+ is not sufficient to stabilize the closed conformation; for full open→closed transition, binding of 2OG is also necessary. The structures, together with phylogenetic, biochemical, and biophysical data, provide a complex overview of the *At*GDH1 enzyme.

RESULTS AND DISCUSSION

Phylogenetic Analysis of GDH Sequences Reveals Distinct Types in Plant Species

To provide background for functional and structural discussions, we investigated the evolutionary divergence of the GDH enzymes. The InterPro family of GDHs (IPR014362) contains 35503 sequences. We analyzed them using the EFI-ESN webserver (Zallot et al., 2019) to create sequence similarity networks (SSNs, **Figure 1**). The highest sequence variability characterizes the superkingdoms *Bacteria* and *Archaea* (**Figure 1A**). Sequences from *Eukaryota* make up only a small portion of the GDH evolution landscape. The isozymes from *Fungi*, *Metazoa*, and *Viridiplantae* are distant homologs of each other, but within each eukaryotic kingdom the sequence variability is rather minor when compared to that of prokaryotes.

We then investigated the entire family of ELFV dehydrogenases within *Streptophyta* (IPR006095) (**Figure 1B**). Our analysis shows that NAD-dependent GDHs from *Streptophyta* can be classified into discrete types. Species from the order *Brassicales* – including *A. thaliana* – contain two types of GDHs (**Figure 1B**). *At*GDH1 and *At*GDH3 belong to one type whereas *At*GDH2 is their more distant homolog. We propose to designate the cluster of sequences containing *At*GDH1 and *At*GDH3 as type I, and the cluster which contains *At*GDH2 as type II. Within the orders *Fabales* (legumes) and *Poales* (monocotyledons) there seem to exist explicit types of GDH enzymes (**Figure 1B**), but their distinct features have not been studied so far. It should be noted that the determinants of the substrate amino acid specificity within plant ELFV dehydrogenases are yet to be defined.

The divergent evolution of NAD-dependent GDHs in many plants into two types, most likely has been caused by the need to introduce a mechanism that would allow for different regulation of the activity of the isoforms. Such molecular evolution to insert regulatory sites has been shown for a number of other enzymes involved in primary metabolism (Moghe and Last, 2015). To gain more insight, we analyzed the Prosite patterns (Sigrist et al., 2013) within the two types of NAD-dependent GDHs. The first pattern, PS00074, characteristic of ELFV dehydrogenases, is present in most analyzed sequences. The second Prosite pattern, PS00018, corresponding to the EF-hand calcium-binding motif, was found in 34 type II sequences, including *At*GDH2 (residues $_{265}$DFNGGDAMNsdEL$_{277}$). It is confusing to note that the PS00018 pattern is absent in some type II sequences. This suggests that not all type II GDHs must be calcium-dependent, although it is possible that sequence variability confounds Prosite pattern recognition of protein regions that can actually bind calcium. Nonetheless, the fact that the PS00018 pattern is missing in all type I sequences strongly indicates that type I GDHs should be insensitive to calcium.

The physiological significance of calcium binding by the EF-hand motif of type II GDHs is not yet fully understood, but one can imagine links to calcium signaling and circadian clock (Clapham, 2007; Marti et al., 2018). Calcium is a universal second messenger involved in various cellular processes. Intracellular variation in free calcium concentration and its distribution in organelles are key to the plant perception of environmental changes (Xiong et al., 2006). These include the circadian rhythm, as light induces calcium influx to plant mitochondria (Hepler, 2005). As a result, the activity of type II GDHs should increase whenever calcium concentration in mitochondria is upregulated, in contrast to the activity of type I GDHs which should remain unchanged.

Biochemical and Biophysical Characterization of *At*GDH1: Metal (In)dependence and Preference for NAD Over NADP

In this work, recombinant *At*GDH1 was assayed for the oxidative deamination activity. We measured *At*GDH1 activity in the forward reaction, that is Glu→2OG, using NAD^+ as the cofactor. This direction is physiologically more relevant due to the high NAD^+/NADH ratio (3–20) in plant mitochondria (Williamson et al., 1967; Igamberdiev and Gardestrom, 2003; Fontaine et al., 2012). We also tested *At*GDH1 in the presence of $NADP^+$ instead of NAD^+, but the activity was undetectable. With NAD^+ as the coenzyme, the K_m value for L-glutamate is 2.55 ± 0.28 mM, whereas the k_{cat} is 13.3 ± 0.3 s^{-1} (**Figure 2A**). The kinetics of GDH-catalyzed oxidative deamination of glutamate was previously characterized in lupin nodules with the K_m for L-glutamate of 4.3 mM (Stone et al., 1980), and in *Pisum sativum* with K_m = 12.5 mM (Garland and Dennis, 1976).

It has been reported in the literature that the oxidative deamination activity of plant GDHs is metal-independent whereas the reverse reaction (reductive amination) could be stimulated by different divalent metal ions, such as calcium, manganese and zinc (Garland and Dennis, 1976; Turano et al., 1997). In *A. thaliana*, which possesses three GDH isoforms, it was established that the reductive amination activity of *At*GDH2 but not *At*GDH1 was stimulated by Ca^{2+} whereas the oxidative deamination of both isoforms was slightly inhibited by this cation (Turano et al., 1997). Our results are in agreement with those observations. We tested the *At*GDH1 activity also in the presence of other divalent cations and the results are summarized in **Table 1**. The *At*GDH1 enzyme was only slightly inhibited by most of the tested cations (Ca^{2+}, Zn^{2+}, Co^{2+},

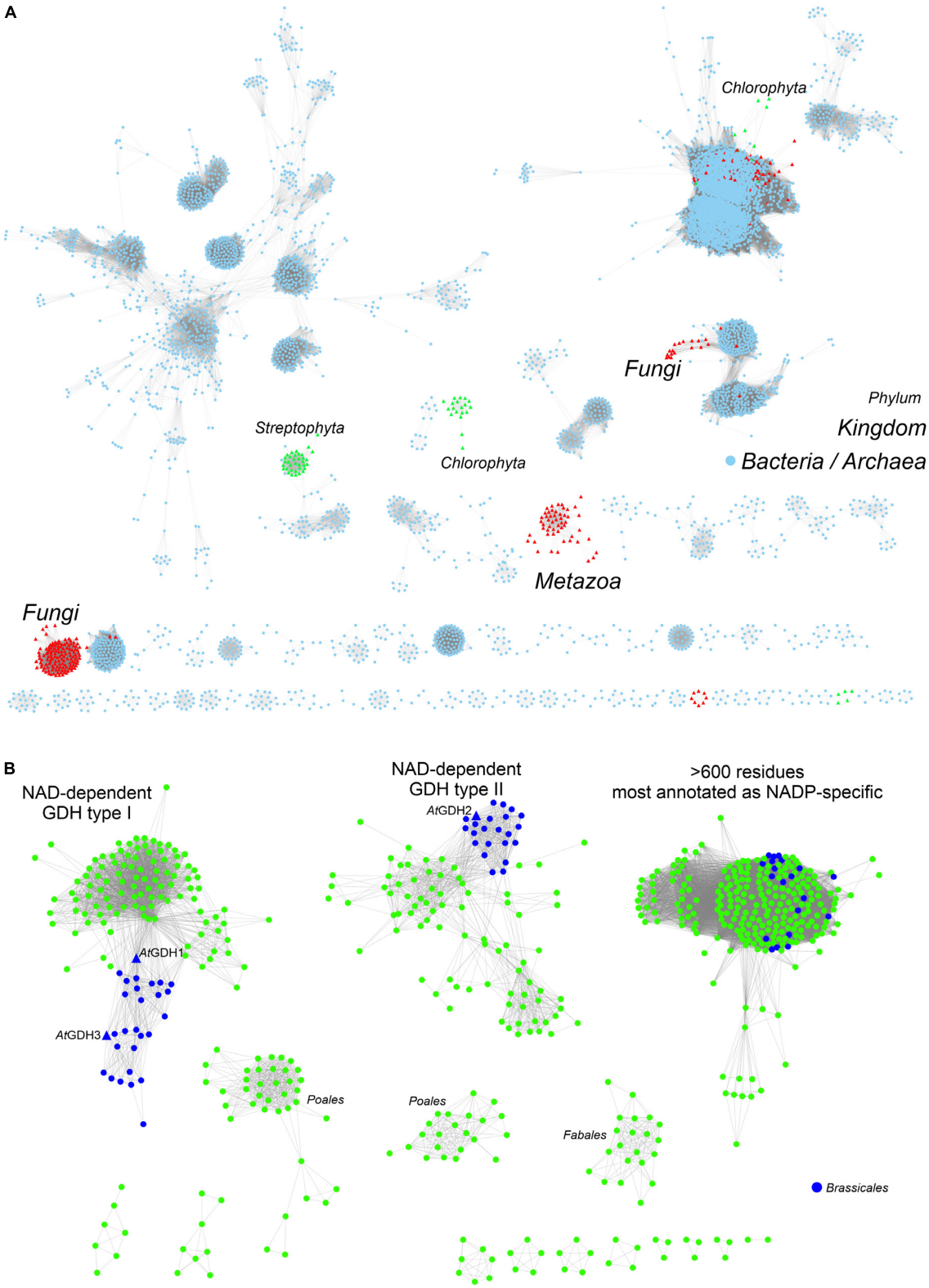

FIGURE 1 | Phylogenetic analysis. **(A)** Shows sequence similarity network of GDH sequences (InterPro family IPR014362) in all kingdoms of life. Sequences ≥ 75% identical are grouped as single, resulting in the total of 5788 nodes. Outliers (702 nodes) were rejected from the diagram. Note that sequences from *Viridiplantae* (green triangles) are divided into *Streptophyta* and *Chlorophyta* philia. **(B)** Shows the analysis of all sequences in the EFLV dehydrogenase family (IPR006095) from *Streptophyta*. Out of 804 nodes in total, 179 outliers were removed.

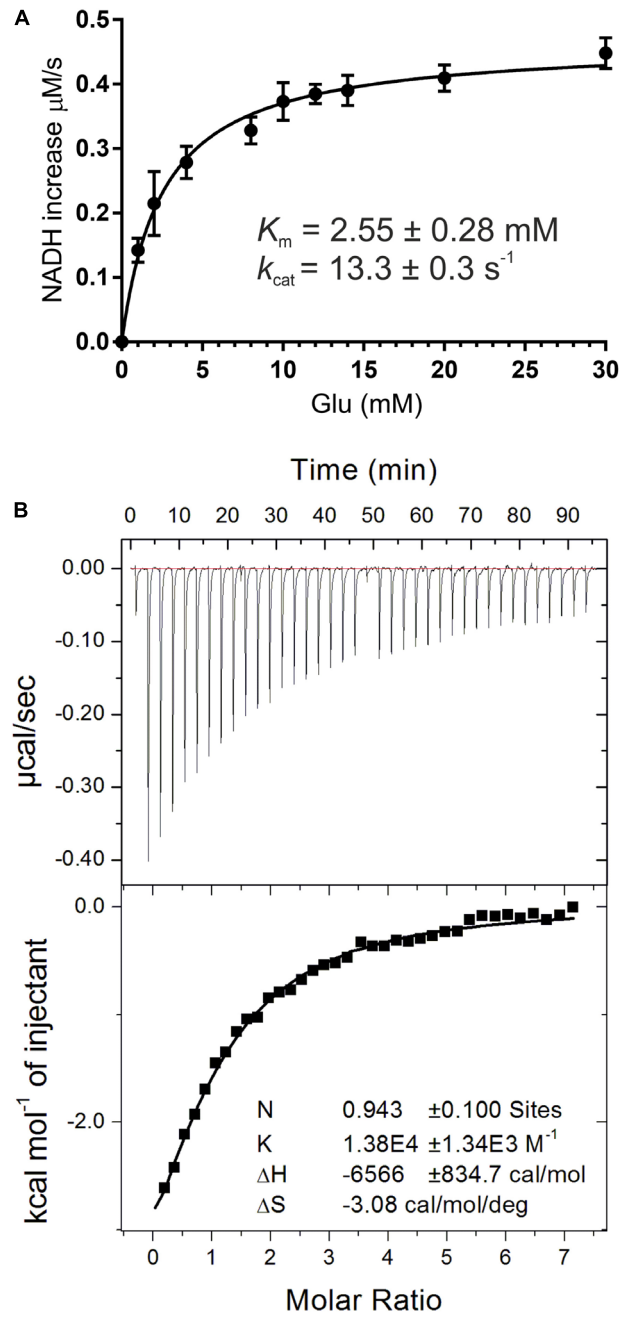

FIGURE 2 | Biochemical and biophysical characterization of *At*GDH1. Kinetic measurements **(A)** were fitted with a non-linear curve in *Prism* 6.07 software (GraphPad), based on the Michaelis-Menten equation, to calculate K_m and k_{cat}. Error bars are standard deviations calculated from three independent replicates. Isothermal titration calorimetry (ITC) experiments are presented in **(B)**. A sample raw data plot (upper panel) and the binding curve obtained after its integration (bottom panel) with the best fit of *One set of binding sites* model obtained from ITC titrations of 58 μM *At*GDH1 in the presence of 10 mM 2OG, with 1 mM NAD^+.

Cu^{2+}) with the strongest inhibitory effect of zinc. Interestingly, manganese seems to have no effect. Calcium is merely a mild inhibitor of *At*GDH1, as ∼23% inhibition was observed at 1 mM Ca^{2+}, which is physiologically irrelevant (**Table 1**). The mechanism of this inhibition is unknown. In contrast, calcium-dependent GDHs from soybean and corn are stimulated approximately twofold by calcium (Yamaya et al., 1984; Turano et al., 1997). It is worth noting that the sequence region 257–264 in *At*GDH1 and *At*GDH2, which directly precedes the EF-hand motif in *At*GDH2 (residues 265–277), is the most altered region of *At*GDH2 in comparison with *At*GDH1 (not shown). However, unlike *At*GDH2, the *At*GDH1 isoform does not have the EF-hand sequence motif which could be responsible for calcium binding, and the residues involved in inhibition must be localized elsewhere in the sequence. Since the *A. thaliana* GDH enzymes are composed *in vivo* of different ratios of the α, β, and γ subunits, each with different sensitivity to Ca^{2+} and other metal cations, this pattern of heterooligomerization suggests an interesting metal-dependent regulatory mechanism of glutamate metabolism.

TABLE 1 | Enzymatic activity of *At*GDH1.

	NAD^+-GDH activity (% of control)[a]
$NADP^+$	Not detectable
MPD (8.5 mM)	94
Mn^{2+}	99 (96)
Ca^{2+}	82 (77)
Zn^{2+}	51
Cu^{2+}	65
Co^{2+}	77

[a]*Metal cations were assayed at 100 μM concentration whereas values in parentheses refer to 1 mM concentration.*

In this study, we also evaluated NAD^+ binding by *At*GDH1. The K_d value obtained from microcalorimetric titrations in the presence of 10 mM 2OG is 72 ± 6 μM and the stoichiometry could be rounded to one NAD^+ molecule per *At*GDH1 subunit (**Figure 2B**). Our K_d value is approximately four times higher than for bacterial *Peptoniphilus asaccharolyticus* GDH with NADH (18.6 ± 0.1 μM), and about five times higher than for the same titration in the presence of 2OG (14.70 ± 0.09 μM) (Oliveira et al., 2012). The physiological concentration of NAD^+ in plant mitochondria is about 1.5 mM (Igamberdiev and Gardestrom, 2003) and is approximately an order of magnitude higher than the concentration of NADH. Thus, the obtained K_d value of 72 μM is ∼20-fold lower than the NAD^+ concentration, which ensures saturation of *At*GDH1 with the coenzyme *in vivo*. On the other hand, this rather low-affinity binding is expected in such conditions to guarantee unrestricted post-reaction release of the used coenzyme.

The Overall Structure of *At*GDH1 Bears Similarity to Bacterial Homohexameric GDHs

In this work, we determined two crystal structures of *At*GDH1, one in the apo-form and one in complex with NAD^+; 2OG is also bound in one subunit of the latter complex. In most subunits, up to five N-terminal residues were not modeled due to poor electron density, except for the closed-conformation subunit of

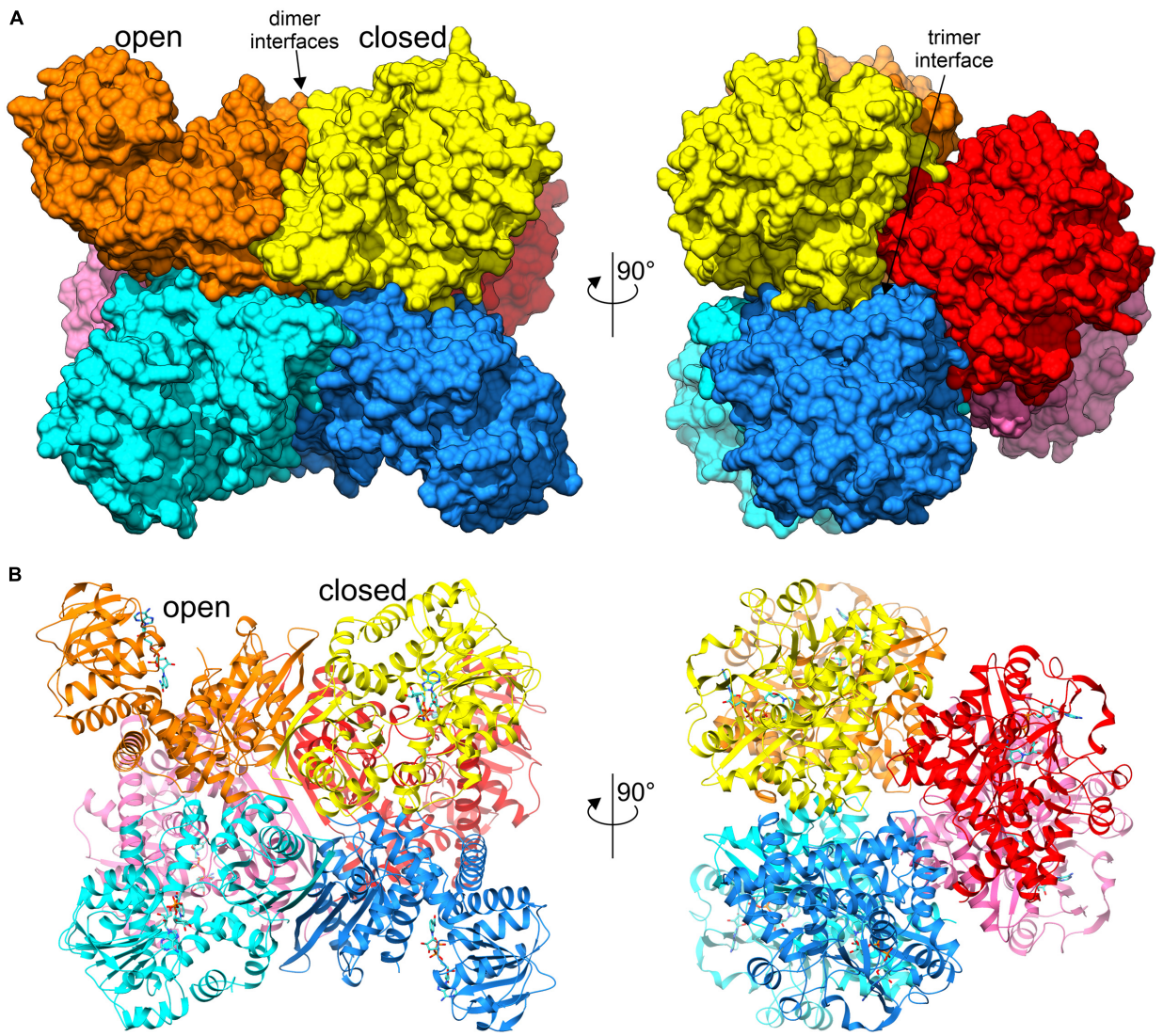

FIGURE 3 | Overall structure of *At*GDH1 homohexamer. Individual subunits of the hexameric structure in complex with NAD^+ (blue sticks) are represented by different colors. Open and closed subunits as well as dimer and trimer interfaces are indicated. **(A)** Illustrates the protein using surface representation, whereas a cartoon with secondary structure elements is shown in **(B)**. The views on the left are down one of the twofold axes of the D_3-symmetric assembly, while on the right the view is down the threefold axis.

the NAD^+ complex (see below) that was very well defined starting from Met1. The C-termini were modeled completely or are missing just the very last Ala411.

The asymmetric unit of both crystal structures is comprised of a homohexameric oligomer with non-crystallographic 32 (D_3) symmetry (**Figure 3**). The homohexameric assembly is in agreement with the size-exclusion elution profile (not shown), as well as with analysis of inter-subunit contacts by PISA (Protein Interfaces, Surfaces and Assemblies) (Krissinel, 2015), which estimated the surface area buried upon hexamer formation at 23220 $Å^2$ and the total surface area at 87480 $Å^2$ (for *At*GDH1-apo structure). The hexamer can be described as a trimer of dimers, as PISA suggests that the hypothetical dimers should be more stable than trimers (**Figure 3A**).

As mentioned in the introduction, plant GDHs have been reported to form heterohexamers comprised of different isoform subunits. However, crystallization of such a physiological heterooligomer would be very difficult if not impossible because of the low probability of capturing a homogenous heterohexamer of one particular composition and order.

A subunit of *At*GDH1 is comprised of 411 amino acid residues (44.5 kDa) and can be subdivided into two domains. Domain I, comprising residues 1–181 and 333–411, is located at the core of the D_3-symmetric hexamer. It is, therefore, key to the formation of the hexameric quaternary structure. In fact, the ten-stranded β-sheet at the twofold dimerization interface is made up from contributions of five β-strands from each subunit (**Figure 3B**). Domain II encompasses residues 182–332. It is composed of a

central, mostly parallel, seven-stranded β-sheet that is flanked by α-helices, and can be classified as a variant of Rossmann fold (Rao and Rossmann, 1973). This architecture is characteristic of proteins that bind nucleotides, including dinucleotides such as NAD(P) (Lesk, 1995).

The Dynamics of the Coenzyme Binding Domain II

Our structures of *At*GDH1 show a remarkably diversified conformation of the coenzyme binding domain II with respect to the protein core. The hinge allowing this flexibility is created by the α-helix 359–384. To measure the movement of domain II, we used the positions of the Cα atoms of three conserved residues in GDHs: Pro73, Val341 and Phe214, forming the angle χ in **Figure 4**. We note that the same points of reference were used to study the domain dynamics in other GDH proteins (Oliveira et al., 2012). In our apo-structure, all subunits are in the open conformation, even though the position of domain II varies by as much as 11.3°, with χ between 62.0° and 73.3° (**Figure 4**). In the *At*GDH1-NAD$^+$ complex, five subunits are in the open conformation (χ 70.2°–73.9°). The sixth subunit is in a closed conformation, characterized by the χ angle of 49.1°. The conformational flexibility of GDH enzymes was described for the first time by Stillman and coworkers in a study of *Clostridium symbiosum* GDH, but the reported maximum movement of the Cα atoms was 11.5 Å (Stillman et al., 1993). In *At*GDH1 the movement is more pronounced, with the Cα atom of Asp270 shifting by as much as 14.3 Å.

It is interesting to note that the most different subunits (the two most open and the closed one), whose χ angles differ by ∼25°, are situated next to each other around the threefold symmetry axis of the *At*GDH1 homohexamer (**Figure 3**). Such a feature suggests that the *At*GDH1 subunits might operate in an alternating mode, whereby opening and closing of the subunits would occur in a concerted fashion. However, we did not observe a second closed subunit. A non-uniform distribution of the open and closed forms was found in the structure of GDH from *Corynebacterium glutamicum*, an organism that secretes glutamate (Zahoor et al., 2012). In the two hexamers found in the asymmetric unit, three subunits were in the open form and nine were closed (Zahoor et al., 2012). Furthermore, the movement of domain II of *C. glutamicum* GDH was linked to catalysis (Son et al., 2015).

Our attempts to obtain a fully closed *At*GDH1 hexamer by cocrystallization with both NAD$^+$ and 2OG yielded poorly diffracting crystals. Hence, we used PDBeFOLD (Krissinel and Henrick, 2004) to search for structures that are most similar to the *At*GDH1 subunit in the closed conformation in order to investigate whether a structure of an all-closed conformer of GDH from other species has been deposited in the PDB. The best hit was the structure of *Burkholderia thailandensis* GDH in fully saturated complex with NAD and 2OG (unpublished, PDB ID: 4xgi, Seattle Structural Genomics Center for Infectious Diseases), which indeed displays the all-closed conformation. Despite only 46% sequence identity, the RMSD between the superposed Cα atoms of the closed subunits of *At*GDH1 and *B. thailandensis* GDH is as low as 1.1 Å, which suggests that we cannot exclude the possibility that *At*GDH1 might be able to close all subunits at once as well.

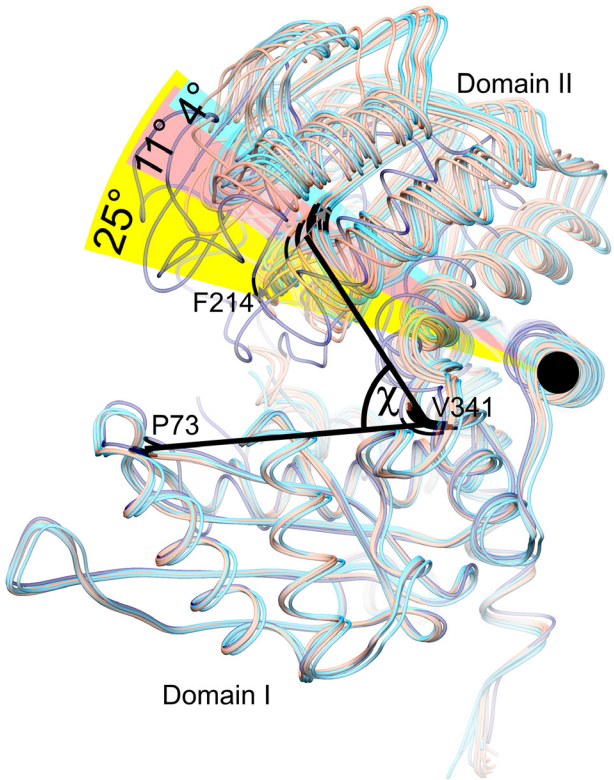

FIGURE 4 | Conformational dynamics of domain II. Twelve subunits derived from the *At*GDH1-apo structure (light red) and from the *At*GDH1-NAD$^+$ complex (open, light blue; closed, dark blue) have been superposed onto each other by matching of domain I Cα atoms. The angle χ formed by the Cα atoms of Pro73 (in domain I), Val341 (near the hinge region), and Phe314 (in domain II) is used to visualize domain II movement. The black circle indicates the "hinge" α-helix 359–384.

A very recent cryo electron microscopy (cryo-EM) study of *Thermococcus profundus* GDH further highlighted the dynamics of the GDH machine (Oide et al., 2020). The authors found a broad range of domain II conformations. Based on particle classification, they defined so-called open, half-open1, half-open2, and closed states. *At*GDH1 and *T. profundus* GDH share 45% sequence identity and we cannot be sure whether the same applies to the plant enzyme. Nonetheless, the conformational energy landscape proposed for *T. profundus* GDH is unbiased by crystal contacts that might favor some conformations more than others. On the other hand, flash-cooling may introduce other types of bias, as the authors acknowledge (Oide et al., 2020). It is also important to note that the conformational dynamic of *T. profundus* GDH was observed in the absence of NAD(P) or substrate/product. This suggests that the NAD(P)-binding domain of the GDH enzyme studied here is intrinsically very dynamic, although it remains to be confirmed if this flexibility is a universal property of GDH enzymes from other species

as well. The resolution of the reconstructed cryo-EM maps is too low (∼4 Å) for a detailed study of coenzyme binding. We propose to couple lower-resolution cryo-EM data with high-resolution crystal structures to arrive at a complete picture of GDH dynamics in future research.

The remarkably different conformation of *At*GDH1 domain II in the open and closed states is correlated with other structural features. First, the closed conformation subunit contains 2OG, the GDH reaction product, bound in the active site (see below for details). This suggests that binding of the coenzyme alone might not be sufficient to trigger the open-to-closed transition of *At*GDH1; apparently, the substrate and coenzyme must bind together to lock the closed state conformation. Notably, 2OG had not been added to the protein preparation at any stage of purification or crystallization and, therefore, must have been captured from *Escherichia coli* cells during the recombinant protein expression. The second feature that is different in the open and closed states is a bend of the N-terminal helix (not shown) that is a part of domain I. The third feature is the presence of 2-methyl-2,4-pentanediol molecules (MPD, from the crystallization solution) in the open conformation. The MPD positions are discussed in a separate section.

The Coenzyme Binding Mode Explains the Preference for NAD Over NADP

Each *At*GDH1 subunit binds one molecule of the NAD^+ coenzyme in a niche between domain I and domain II. There are no inter-subunit interactions with the NAD cofactor. Therefore, the active sites (six per one hexamer) are formed by single subunits, even though free *At*GDH1 monomers do not exist in solution. The 1:1 *At*GDH1(subunit):NAD^+ stoichiometry seen in the crystal structure is consistent with the stoichiometry estimated in our ITC experiments (**Figure 2B**).

Comparison of *At*GDH1-apo and the NAD^+ complex shows only minor rearrangements within the coenzyme binding site, which suggests that apo *At*GDH1 is already well prepared to accept the coenzyme. The description of the NAD^+ binding mode is presented here in the adenine→nicotinamide direction, which follows the orientation of the cofactor from the outside to the inside of the protein molecule. In the open *At*GDH1 conformation, the adenine moiety binds in a deep cleft, whose bottom is formed by residues Gln212, Gly213, and Ser236 (**Figures 5A,B**). The side walls of this cleft are built by Asp237 and Ile238 on one side, and by Ala289, Leu290, and Val293 on the other side. No direct H-bonds dock the adenine moiety to the protein, but there are water-mediated H-bonds connecting the adenine N1 atom to the carbonyl groups of Asp237 and Pro274 and to the Oγ atom of Ser236. There are also other interactions that involve chains of more than two water links (not discussed). The ribose moiety of the adenosine nucleoside binds to the enzyme in a solvent-exposed manner. It forms direct H-bonds between the O2′ hydroxyl and the backbone amide of Ile238, as well as between the O3′ hydroxyl and the backbone amide of Phe214. Additionally, O2′ and O3′ interact via water molecules with the carboxyl group of Asp237. The pyrophosphate moiety of the bound NAD^+ is also exposed to solvent (or to the mitochondrial matrix in the physiological milieu). It interacts directly with the backbone amides of Asn216 and Val217 and indirectly (via H_2O) with the backbone amides of Gly215 and Gly218 as well as with the carbonyl group of Ala288. The pyrophosphate binding is reinforced by the dipole moment of the α-helix that starts with Asn216. Next, the O2′ atom of the nicotinamide ribose forms a direct H-bond with the Nδ atom of Asn312. The rotamer of the Asn312 side chain can be unambiguously deduced from the H-bonding network that involves Asn337. Finally, the nicotinamide moiety binding site is created by Asn312, Asn337, Thr185 and Asn216. Positioning and orientation of the amide group of the coenzyme is ensured by a H-bond between N7 and Oδ of Asn216; Nδ of Asn216

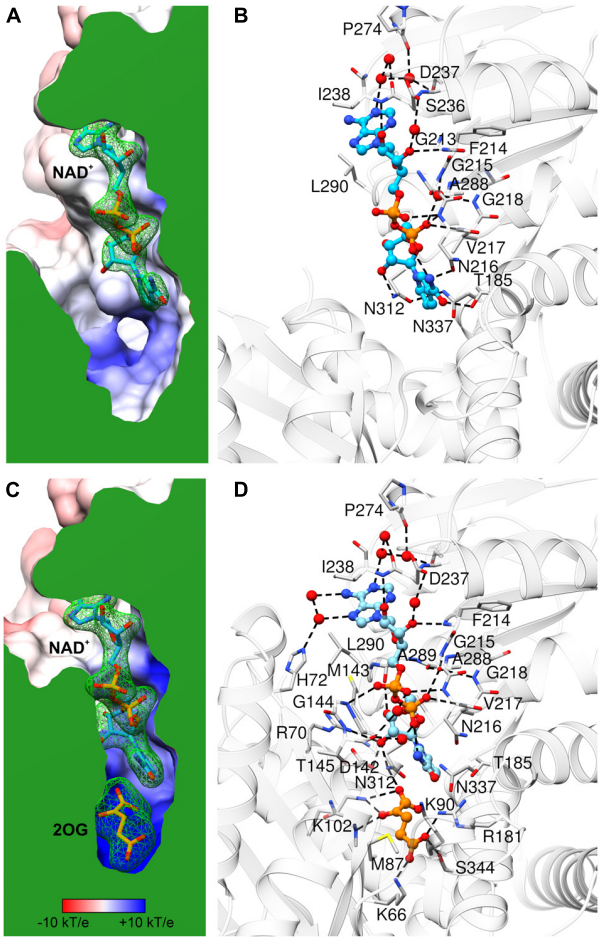

FIGURE 5 | NAD^+ binding by *At*GDH1. Each panel is shown in the same orientation with respect to domain II. The upper panels **(A,B)** illustrate the open conformation, while the lower panels **(C,D)** are for the closed conformation. The panels on the left show the protein surface colored according to electrostatic potential (legend in **C**). The surfaces are clipped (in green) to illustrate cross sections of the binding sites of NAD^+ **(A,C)** and 2OG **(C)**. The green mesh represents polder electron density maps calculated for the ligands (NAD^+ and 2OG, labeled in bold) and contoured at the 4σ level. The panels on the right visualize ligand-protein interactions, with H-bonds marked by dash lines. Water molecules that mediate the interactions are shown as red spheres.

interacts with the backbone carbonyl group of Asp182. N7 also donates an intramolecular H-bond to the NAD pyrophosphate. The nicotinamide O7 atom is in a hydrogen-bonding distance from Oγ of Thr185, but the relative positioning of these two atoms precludes such an interaction.

In the closed subunit, the NAD cofactor is significantly more buried and, therefore, less exposed to the outer environment (**Figures 5C,D**). The envelopment of NAD is primarily the result of the closing movement of domain II toward domain I, as the interactions of the coenzyme with domain II in the closed form are very similar to those in the open form. There are, however, additional bonding interactions that involve residues from domain I. Namely, the N6 and N7 atoms of the adenine moiety create additional, water-mediated H-bonds with the Nε atom of His72. A sulfur-aromatic interaction is formed with Met143 (Sδ...C8 distance 4.6 Å). The pyrophosphate moiety interacts with the backbone amide of Gly144 and, via a water molecule, with the carbonyl group of Thr145. Significantly more bonding interactions involve the nicotinamide ribose. Its O2′ hydroxyl interacts with the Nη2 atom of Arg70 and with the carboxyl group of Asp142, in addition to the bond with Nδ of Asn312 that was present in the open form. The pose of the nicotinamide moiety is different from that assumed in the open form. The N7 atom interacts via a water molecule with the carbonyl group of Thr145; in the open form, a water molecule at the same position was involved in the interaction between Thr145 and the pyrophosphate group. The plane of the nicotinamide moiety is rotated by ∼25° around the C2–C3 bond so that the C4 and C5 atoms are positioned farther from the active site. However, this conformational change is probably forced by the presence of the 2OG molecule in the closed form (see below).

Our kinetic experiments confirmed that *At*GDH1 cannot convert Glu to 2OG using $NADP^+$ (Fontaine et al., 2012). A close look into the NAD^+ binding site provides an explanation of such a strict coenzyme preference. The so-called "core fingerprint" of nucleotide-binding Rossmann-fold proteins (GXGXXG, positions P1–6) (Lesk, 1995) is in *At*GDH1 comprised of residues $_{213}$GFGNVG$_{218}$. This motif was indicated by Oliveira et al. (2012) as a determinant of coenzyme preference in a study of an NAD^+-specific GDH. NADP-specific GDHs usually have Ser or Ala at position P2, whereas NAD-dependent enzymes have a large, hydrophobic residue, typically Phe as in *At*GDH1. The second fragment responsible for coenzyme preference starts 17 residues farther down toward the C-terminus. NADP-dependent GDHs have a consensus SDS sequence there. In *At*GDH1, the fragment is $_{236}$SDI$_{238}$, which is conserved in some NAD^+-dependent GDHs from bacteria (Oliveira et al., 2012). Interestingly, the Asp237 residue of *At*GDH1 is conserved in NADP-specific enzymes. Based on our *At*GDH1-NAD^+ complex structure, Asp237 would clearly collide sterically as well as electrostatically with the 2′-phosphate of NADP. NADP-dependent GDHs are, however, capable of rearranging the conformation in this area to accommodate the 2′-phosphate. The structural data suggest that it is the third residue of this motif, Ile238, posed next to adenine, that is the most likely key player. It seems more difficult to rearrange this fragment when a hydrophobic residue is positioned next to adenine. In contrast, the SDS motif of the NADP-specific enzymes can more readily undergo a conformational change upon coenzyme binding. Nevertheless, we cannot exclude other structural elements that might (also) govern coenzyme preference.

The Open-to-Closed Conformational Transition Is Required to Form a Fully Functional Active Site

The catalytic mechanism of NAD^+-dependent GDHs has been well established in the 1990s (Stillman et al., 1993; Dean et al., 1994). In this work, we adopt it to plant isozymes using our crystal structures and structure-based sequence alignments. So far, there has been no reported structure of a tertiary GDH-NAD-Glu complex from any species. It is reasonable to assume that the overall positioning of Glu and 2OG is dictated by their carboxylic groups, and therefore should be similar. However, considering its environment in our complex, one might speculate that the amino group of Glu would be positioned differently than the carbonyl group of 2OG (**Figure 5D**).

For simplicity, we will only discuss the reaction in the Glu→2OG direction. To form a fully functional active site, the enzyme must adopt the closed conformation as only then the substrate and the coenzyme are in direct contact. In the first step, the amino group of the Glu substrate becomes deprotonated by a general base, which in the case of *At*GDH1 is Asp142. Next, a hydride anion is transferred to the *Si* prochiral face of NAD^+. In our closed-conformation subunit (with 2OG in the active site), NAD^+ is clearly oriented in a way that is compatible with hydride transfer to the *Si* face of nicotinamide. The distance between the C4 atom of NAD^+ and C2 of 2OG is 4.2 Å in the closed structure. This distance would become ∼6 Å in the open conformation based on 2OG superposition from the closed conformation (not shown). Optimally, for a direct hydride transfer the donor. . .acceptor distance should be ∼3 Å (Hammes-Schiffer, 2002). This indicates that for this stage of the reaction the substrate or/and domain II with bound NAD^+ should converge even closer. As a result of the hydride transfer, an iminoglutamate intermediate is formed. Next, Lys102 primes a water molecule for a nucleophilic attack on the imine C atom. Subsequently, Asp142 mediates proton exchange from the hydroxyl group to the newly formed amine. This is followed by ammonia elimination with simultaneous formation of the double C = O bond. Finally, NADH, 2OG and NH_4^+ are released, while Asp142 and Lys102 are deprotonated to prepare the active site for the next cycle.

Using isotope effects, a study of bovine GDH showed that a conformational change governs the rate of hydride transfer, whereas the true rate-limiting step of the reaction is product release (Wacker et al., 2010). Our structural data suggest that this model applies to *At*GDH1 as well. More precisely, a large-scale conformational change of domain II is necessary for the coenzyme to approach the substrate and accept the hydride. However, product release after the reaction must overcome at least two energy barriers linked to: (i) reopening of domain II and (ii) product dissociation from the active site.

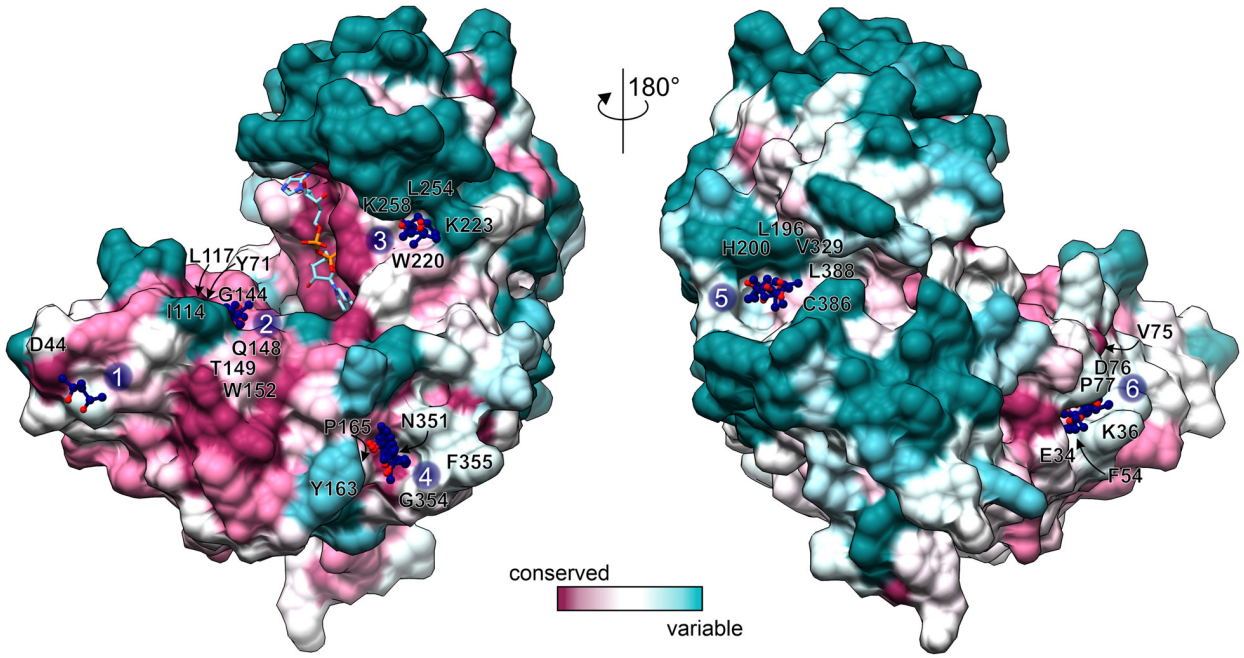

FIGURE 6 | Conservation of MPD binding sites. Conservation scores, calculated by *Consurf* (Ashkenazy et al., 2016) are mapped on the surface of an open-conformation *At*GDH1 subunit from the NAD$^+$ (sticks) complex. The coloring scheme and scale is shown at the bottom. MPD sites 1–6 are marked and the surrounding residues (within 3.5 Å of the MPD molecules) are labeled.

Conserved MPD Binding Sites as Potential Druggable Regions

GDH enzymes are important to all living organisms, which means that they could be a target for e.g., herbicide design. However, due to the redundancy of GDHs in plant species, a GDH-targeted herbicide would need to inhibit all isoforms. Moreover, as GDHs utilize Glu/2OG and NAD which are present at high concentrations *in vivo*, it seems rational to design non-competitive rather than competitive GDH inhibitors to avoid the need of using very high inhibitor concentrations. With this in mind, we analyzed the MPD binding sites in our *At*GDH1-NAD$^+$ structure. Six of those sites are conserved in all open-conformation subunits (**Figure 6**). Notably, MPD as an inhibitor (or activator) of *At*GDH1 was excluded on the basis of our enzymatic assays in which concentrations up to 8.5 mM did not change the enzymatic behavior.

We classified the six MPD binding sites by taking into account: (i) residue conservation in plant species (Consurf score $\geq$ 7; Ashkenazy et al., 2016), (ii) number of site-forming residues, (iii) proximity of the active site, and (iv) site alterations upon domain closure (**Figure 6**). Based on this analysis, sites number 2 and 6 emerge as the best candidates. In the open conformation, the MPD molecule at site 2 is positioned between the residues that form the site and NAD$^+$. In the closed conformation, access to site 2 becomes partially obscured by domain II. In that state, Gly144, which is part of site 2, interacts with the pyrophosphate moiety of NAD$^+$. In other words, a fully competent site 2 exists only in the open conformation. Site 6 is located near the dimer interface, ~24 Å from the active site. In the open conformation, the MPD molecule at site 6 separates Phe54 and Pro77 so that they are situated > 7 Å away from each other. In the closed state, the distance between Phe54 and Pro77 is reduced to ~3.6 Å, which eliminates site 6 entirely. Altogether, our structures suggest that binding of an inhibitor at sites 2 and/or 6 in the open conformation would likely interfere with closing of the enzyme, which in turn is necessary for the formation of the active site.

Overall, MPD may serve as a good indicator for sites that would be suitable for binding of hydroxyl and methyl groups, both of which are rather promiscuous in binding interactions. Therefore, it would be interesting to see whether molecules with additional, more selective functional groups could bind to the indicated sites.

A Mitochondrial Signal Peptide Has Evolved From Bacterial Ancestors, Preserved the Original Secondary Structure, and Is Able to Bind Potassium

*At*GDH1 is localized in mitochondria, as confirmed by several independent studies (Turano et al., 1997; Fontaine et al., 2012). The *GDH1* gene is coded by genomic DNA (chromosome 5) and, therefore, the *At*GDH1 protein is synthesized as a precursor in the cytosol and must be imported into mitochondria. The properties of mitochondrial target sequences have been outlined using statistical analysis, sequence alignments, and secondary structure predictions of a set of N-terminal fragments of mitochondrial proteins (Von Heijne et al., 1989; Hartl and Neupert, 1990; Claros and Vincens, 1996; Taylor et al., 2001;

Wiedemann and Pfanner, 2017). Usually, the signal peptides do not contain conserved sequence motifs but form a characteristic secondary structure. It is, therefore, difficult to deduce the presence and extent of such signal peptides unambiguously. It is usually assumed that the transit peptides should be localized within the first 40 N-terminal residues, as this is the average length, although as few as 13 or as many as 100 residues may also play a role depending on the protein (Claros and Vincens, 1996). Some common features of mitochondrial signal sequences include: (i) presence of positively charged residues, mainly Arg; (ii) absence or scarcity of negatively charged residues; (iii) enrichment in hydrophobic residues, mainly Leu and Ala; (iv) presence of hydroxylated amino acid; and (v) folding into an amphipathic α-helix (Claros and Vincens, 1996; Nielsen et al., 1997; Sjoling and Glaser, 1998; Emanuelsson and Von Heijne, 2001). An important characteristic of the α-helix is the formation of a positively charged face and a hydrophobic face that allow interaction with receptors on the outer mitochondrial membrane (Taylor et al., 2001). Most of the targeting peptides are cleaved by mitochondrial processing peptidase (MPP) to yield the mature proteins (Kitada et al., 2003; Carrie et al., 2015).

To define the probable mitochondrial targeting peptide within the amino acid sequence of *At*GDH1, we applied several online tools. *In silico* sequence-based analysis did not lead to unequivocal conclusions. MitoProtII (Claros and Vincens, 1996), MitoFates (Fukasawa et al., 2015), and iPSORT (Bannai et al., 2002) suggested that *At*GDH1 contains a putative mitochondrial transit polypeptides within 30 N-terminal residues, whereas TargetP (Armenteros et al., 2019) suggests absence of such a signal peptide. Moreover, MitoFates predicted a cleavage site after Leu17. Visual analysis of the N-terminal sequence (30 residues) of *At*GDH1 indicates that it does fit several criteria of mitochondrial targeting peptides. In particular, there are five positively charged amino acid residues (two Lys and three Arg residues), only one negatively charged residue, and three residues with hydroxyl groups. In addition, the N-terminal α helix (Leu4-Leu17) has positively charged amino acid residues on one face and hydrophobic residues on the other.

The sequence $_{12}$KLAARLLG$_{19}$ fits well into the conserved sequence pattern for recognition by MPP (Kitada et al., 2003; Carrie et al., 2015), with the putative cleavage site between Leu17 and Leu18 (**Figure 7**). Moreover, sequence conservation of this N-terminal region is very high within the family of plant NAD-dependent GDHs, with almost strict conservation of the potential cleavage site motif RXL (**Figure 7B**). In addition, this region is exposed on the surface of the protein, which makes it available for recognition by MPP. Comparison of *At*GDH1, *E. coli* GDH (PDB ID: 4bht), and human GDH (1nr1) reveals that the N-terminal fragment consisting of two helices linked by a short loop is structurally conserved (not shown). This is interesting because sequence identity within this region is low (16–34%). It is worth noting that the mitochondrial target sequence in human GDH is localized 50–60 residues upstream of the N-terminal helix (Kotzamani and Plaitakis, 2012), in a region which has no equivalent in *At*GDH1.

What is unique about *At*GDH1 and has never been observed in any GDH structure, is binding of a potassium cation

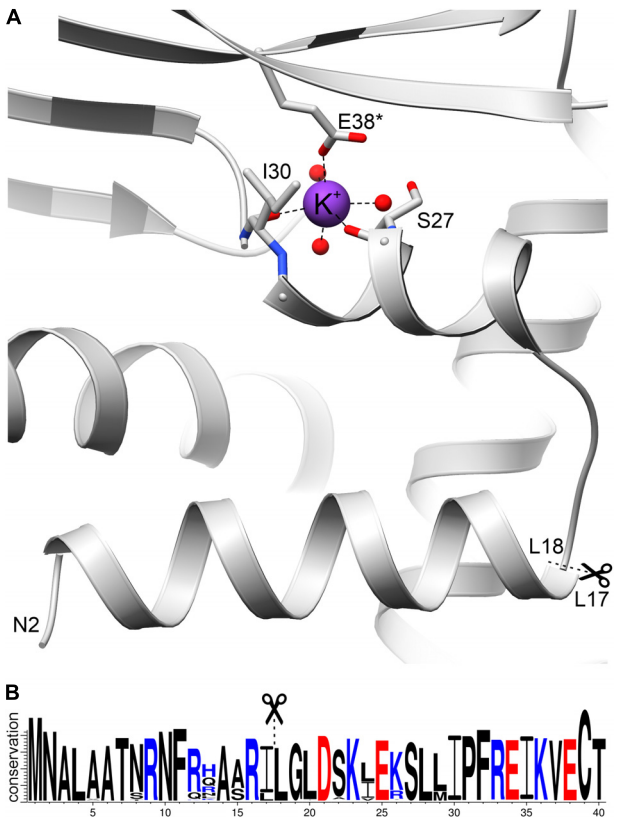

FIGURE 7 | The N-terminal fragment of *At*GDH1. **(A)** A potassium cation (purple sphere) is coordinated by the carbonyl oxygen atoms of Ser27 and Ile30, as well as by Glu38* from another subunit. Three water molecules (red spheres) complete the octahedral coordination sphere. In **(B)**, a WebLogo illustration shows residue conservation in *Viridiplantae* GDH sequences colored by charge (blue, positive; red, negative). Scissors and dash lines indicate a potential MPP cleavage site.

(**Figure 7A**), seen in both structures of *At*GDH1 presented in this work, as confirmed by the CheckMyMetal server (Zheng et al., 2017). The residues involved in potassium coordination are Ser27, Ile30, and Glu38* (from another subunit) (**Figure 7A**). Binding of potassium, which is abundant in plant cells, can alter the structure and function of the N-terminal fragment in an unpredictable way. This means that we cannot be sure whether the mitochondrial targeting peptide is indeed cleaved by MPP.

CONCLUSION

We have provided detailed structural and kinetic information about the functioning of *At*GDH1, one of three mitochondrial NAD$^+$-dependent GDHs in *A. thaliana*. Our crystal structures show that coenzyme binding does not involve any drastic conformational changes. However, formation of the active site involves a large movement (measured as angle χ) of the coenzyme binding domain II toward the substrate domain I, leading to a closed enzyme conformation. Docking of the 2OG product (and a mimic of the Glu substrate) in the

active site appears to stabilize the closed conformation. The enzyme is a D_3-symmetric hexamer, consisting of subunits with various χ conformation, including cases of extreme χ-values in one oligomer. *In vivo*, *At*GDHs form heterohexamers with variable isozyme composition. It will be difficult to reproduce such physiological oligomers in homogeneous crystals, but efforts have already been undertaken to crystallize *At*GDH3 and especially *At*GDH2, which is calcium-stimulated. On the other hand, Ca^{2+} (and several other divalent metal cations, except Zn^{2+}) has only weak inhibitory effect on *At*GDH1. We found out, however, that *At*GDH1 coordinates a potassium cation (abundant in plant cells) in a structural elbow following a purported mitochondrial targeting N-terminal peptide. This suggests an interesting follow-up study of the role of potassium in mitochondrial transport of *At*GDH1. It is also possible that the exceptional inhibitory action of Zn^{2+} is connected with coordination in the potassium site. The evidence that the Met1-Leu17 peptide is a mitochondrial signal is so far only circumstantial but strong. It will be interesting to study the properties of this peptide and the purported MPP (mitochondrial processing protease) Leu17-Leu18 cleavage site further. The crystal structures reveal several MPD binding sites, some of which have conserved sequence. Although in our tests *At*GDH1 was insensitive to MPD, the existence of such binding sites might be a good starting point for the design of non-competitive inhibitors of *At*GDH1 as potential herbicides.

MATERIALS AND METHODS

Cloning, Expression, and Purification

The full-length sequence encoding *At*GDH1 (locus: At5g18170.1, UniProt ID: Q43314) was amplified by polymerase chain reaction (PCR) with the following primers: Fw: TACTTCCAATCCAATGCCATGAGTGAAGAAACTAAAGATA ACCAGAGG and Rev: TTATCCACTTCCAATGTTATCAACGC CTCAGGGTGTGGAG, using as template the total *A. thaliana* cDNA (ecotype Col-0) from leaves. The PCR product was cloned into pMCSG68 expression vector (from the Midwest Center for Structural Genomics, Argonne, IL, United States) according to the ligase-independent cloning protocol (Kim et al., 2011).

In the next step, pMCSG68-*Atgdh1* plasmid was used to transform *E. coli* BL21-Gold (DE3) competent cells (Agilent Technologies). The transformant was cultured at 37°C in LB medium supplemented with ampicillin (150 μg/ml) until the OD_{600} reached 1.0. The temperature was then decreased to 18°C and protein expression was induced by the addition of isopropyl-β-D-thiogalactopyranoside (IPTG) to a final concentration of 0.5 mM. At that time the medium was additionally supplemented with 10 g of glucose per each liter of culture. After 16 h of induction, the cells were collected by centrifugation and the cell pellet was resuspended in binding buffer [50 mM Tris-HCl pH 7.5, 500 mM NaCl, 100 mM KCl, 20 mM imidazole, 5% v/v glycerol, 1 mM tris(2-carboxyethyl) phosphine (TCEP)]. The cells were frozen and stored at −80°C. After thawing, cells were disrupted by sonication. After sonication, benzonase (Sigma) was added to shear the DNA. The cell lysate was pelleted by centrifugation at 25,000 × *g* for 30 min at 4°C.

The clear supernatant was applied onto an affinity column packed with 3 ml of HisTrap HP resin (GE Healthcare) and equilibrated with binding buffer. The protein was eluted with 20 ml of elution buffer (50 mM Tris-HCl pH 7.5, 500 mM NaCl, 100 mM KCl, 400 mM imidazole, 5% v/v glycerol, 1 mM TCEP). His-tagged *At*GDH1 was cleaved with His-tagged TEV protease at final concentration of 0.1 mg/ml and excess of imidazole was simultaneously removed by overnight dialysis at 4°C to dialysis buffer (50 mM Tris-HCl pH 7.5, 500 mM NaCl, 100 mM KCl, 1 mM TCEP). The sample was passed again through a HisTrap column and the flow-through (containing *At*GDH1) was collected, concentrated to ∼2.5 ml and applied on HiLoad Superdex 200 16/60 column (GE Healthcare) connected to the AKTA FPLC system (Amersham Biosciences). The size exclusion chromatography was run as the final step of purification in a buffer composed of 25 mM HEPES pH 7.5, 100 mM KCl, 50 mM NaCl, and 1 mM TCEP, to yielded a homogenous protein. All homogenous protein fractions were pooled and concentrated to 3.5 mg/ml using Amicon Ultra 10 filters (Millipore). The protein concentration was estimated using UV absorbance at 280 nm and calculated molar extinction coefficients ε of 43,430 $M^{-1}\cdot cm^{-1}$. Sample purity was monitored by gel electrophoresis in 15% polyacrylamide gel in denaturing conditions (Laemmli, 1970). Pure protein samples were flash-frozen in liquid nitrogen as aliquots and stored at -80°C.

Crystallization, X-Ray Data Collection, and Processing

Initial screening for crystallization conditions was performed using the sitting drop vapor diffusion method and a screen formulated with different PEGs, buffers and salts. 1.5 μl protein samples were mixed with 0.75 μl of the reservoir solution and equilibrated against 60 μl reservoir solution. The crystallization plates were stored at 19°C. First crystals appeared after 1 day. Several crystallization conditions were selected for optimization using the sitting drop vapor diffusion method. The best *At*GDH1-apo crystals were obtained at 3.5 mg/ml protein concentration within 2 weeks, using 20% w/v PEG 4000, 100 mM Tris-HCl pH 7.5. 33% (v/v) MPD was used as cryoprotectant. Additional crystallization trials were carried out for the *At*GDH1 protein supplemented with NAD^+. Prior to the crystallization setup, the protein solution at 3.5 mg/ml (0.79 mM of subunits) was incubated overnight with 4 mM NAD^+. The best crystals were obtained using 15% w/v PEG 6000, 100 mM MES [2-(*N*-morpholino)ethanesulfonic acid] pH 6.5, 10% (v/v) MPD. 33% (v/v) MPD and 2 mM NAD^+ were included in the cryoprotectant solution. All crystals were flash-vitrified in liquid nitrogen and stored prior to synchrotron-radiation data collection.

Diffraction data were collected on the P13 beamline at the PETRA III synchrotron (Hamburg, Germany). All diffraction data were processed with *XDS* (Kabsch, 2010). The datasets

were submitted to anisotropy analysis using the *STARANISO* server (Global Phasing Ltd., Cambridge, United Kingdom)[1]. Anisotropically truncated data were used for structure solution and refinement. Data collection and processing statistics are listed in **Table 2**. The complete datasets together with raw diffraction images were deposited in the RepOD Repository with the DOI numbers: *At*GDH1-apo: 10.18150/repod.8407298; *At*GDH1-NAD$^+$: 10.18150/repod.1477886.

Determination and Refinement of the Crystal Structures

The structure of *At*GDH1-NAD$^+$ was solved by molecular replacement using *PHASER* (McCoy et al., 2007) and the *Thermotoga maritima* GDH structure (PDB ID: 1b26; 49% sequence identity) (Knapp et al., 1997) as a model. The initial model building was carried out using *Phenix.AutoBuild* (Terwilliger et al., 2008). *COOT* (Emsley et al., 2010) was used for manual fitting in the electron density maps between rounds of model refinement in *Phenix.refine* (Afonine et al., 2012) with TLS groups (Winn et al., 2003) as recommended by *Phenix.refine.* Achesym was used to place the model inside the crystallographic unit cell (Kowiel et al., 2014). A partially refined *At*GDH1-NAD$^+$ model served to solve the apo structure. During the refinement, torsion-angle non-crystallographic symmetry (NCS) restraints were applied. The refinement statistics are listed in **Table 2**.

[1]http://staraniso.globalphasing.org/cgi-bin/staraniso.cgi

Structural Analysis Software

The presence of NAD$^+$ and 2OG ligands was verified by calculating polder maps in *Phenix.Polder* (Liebschner et al., 2017), which confirmed that the ligands were present. Molecular illustrations were created with UCSF *Chimera* (Pettersen et al., 2004). Distribution of the electrostatic potential was calculated using the PDB2PQR-APBS pipeline (Baker et al., 2001; Dolinsky et al., 2004). *Consurf* (Ashkenazy et al., 2016) was used to map sequence conservation on the protein surface. Validation of the crystallographic models was carried out in *MolProbity* (Chen et al., 2010).

Kinetics of the Deamination Reaction

All enzyme activity measurements were carried out at 25.0 ± 0.1°C using an Agilent 8453 Lambda UV/Vis spectrophotometer. The time-dependent appearance of NADH was measured at 340 nm, where the increase in the measured absorbance is proportional to the NAD$^+$-dependent *At*GDH

TABLE 2 | Diffraction data and refinement statistics.

Data collection	*At*GDH1-apo			*At*GDH1-NAD$^+$		
Wavelength (Å)	0.8266			0.9763		
Space group	$P2_12_12_1$			$P2_12_12_1$		
Unit cell parameters *a, b, c* (Å)	93.6, 99.2, 318.1			93.8, 99.8, 318.0		
Resolution (Å)[a]	88.9-2.59	88.9 – 7.95	2.76 – 2.59	70.3-2.03	70.3-5.94	2.14-2.03
Unique reflections[a]	69,271	3467	3405	164,077	8204	8194
Multiplicity[a]	7.4	6.3	8.5	7.4	6.9	7.3
Ellipsoidal completeness (%)[a]	88.9	99.3	42.2	95.7	99.8	64.8
Spherical completeness (%)[a]	76.2	99.3	24.0	84.4	99.8	28.0
R_{merge} (%)[a]	19.0	4.3	107.2	7.1	2.7	80.4
R_{pim} (%)[a]	7.4	2.5	39.0	2.8	1.5	44.9
$< I/\sigma(I) >$ [a]	9.6	26.4	2.3	17.3	48.8	2.5
CC(1/2)[a]	0.995	0.998	0.581	0.999	0.999	0.781
Refinement						
R_{free} reflections	1044			1646		
No. of atoms (non-H)	18,937			19,882		
Protein	18,704			18,687		
Ligands	94			448		
Solvent	139			757		
R_{work} /R_{free} (%)	18.3/23.5			16.0/19.6		
RMSD from ideal geometry						
Bond lengths (Å)	0.006			0.008		
Bond angles (°)	0.85			0.95		
Ramachandran statistics (%)						
Favored	97.9			97.8		
Allowed	2.1			2.2		
Outliers	0.0			0.0		
PDB ID	6yeh			6yei		

[a]*Data processing statistics are given separately for: all reflections (left column), inner shell (middle column), and outer shell (right column).*

(oxidative deamination) activity. Reactions were carried out in 1 ml volumes in a buffer containing 50 mM HEPES pH 7.5, 50 mM NaCl, 1–30 mM glutamate and 1 mM NAD^+ to reach coenzyme saturation; KCl was included in protein purification buffers but had no effect on enzymatic tests (not shown). The absorbance of the cuvettes with reaction mixtures was set to 0.0 and this way they served as blanks to correct the absorbance from the reagents (NAD^+ and L-glutamate). Enzymatic reactions were initiated by the addition of 50 μl of *At*GDH1 to a final concentration of 35 nM. The final reaction solution was gently stirred to achieve homogeneity. The reaction was carried out for 2–3 min and reaction rates were obtained from the initial linear region of the curves. The measurements were made in triplicates.

The kinetic parameters were computed with the enzyme kinetics software *Prism* version 6 (GraphPad). The initial rates (NADH increase, μM/s) were plotted against substrate concentration (glutamate, mM). Non-linear least-squares regression analysis was used to fit the data to the Michaelis-Menten equation:

$$V = \frac{V_{\max}\,[S]}{K_{\mathrm{M}} + [S]} = \frac{k_{\mathrm{cat}}\,[E]_{total}\,[S]}{K_{\mathrm{M}} + [S]}$$

where [S] and [E] are the substrate and enzyme concentrations, respectively, k_{cat} is the turnover rate constant, K_{m} is Michaelis constant and $V_{\max}$ is the maximum enzyme velocity.

Additional measurements were performed to test the effect of different additives. The following basic reaction mixture (1 ml) was used: 50 mM HEPES pH 7.5, 50 mM NaCl, 10 mM L-glutamate, and 1 mM NAD^+. The following divalent metals (as chloride salts): Co^{2+}, Cu^{2+}, and Zn^{2+} were assayed at 100 μM concentration, Mn^{2+} and Ca^{2+} at 100 μM and 1 mM concentration, whereas MPD was assayed at 8.5 mM concentration. We also performed assays with 1 mM $NADP^+$ instead of NAD^+. The reactions were routinely started by the addition of the enzyme (50 μl to a final concentration of subunits of 32 nM). The effect of each additive was calculated as % of restored activity relative to sample without any additive.

Isothermal Titration Calorimetry

Microcalorimetric measurements were carried out with a MicroCal PEAQ-ITC (Malvern) calorimeter at 25°C. Titrations of NAD^+, kept at 1 mM concentration in the syringe, against *At*GDH1 protein (at 58 μM concentration, determined by biuret method at 540 mM) in the reaction cell were done in 25 mM HEPES pH 7.5, 100 mM KCl, 50 mM NaCl, and 1 mM TCEP. The protein in the reaction cell was in the presence of 10 mM 2OG (Sigma). NAD was injected in 38 aliquots of 2 μl each, in two consecutive runs, as the maximum volume of the syringe is 40 μl. Raw ITC data from these two experiments were merged and then analyzed with the *Origin* 7.0 software (OriginLab) to obtain thermodynamic parameters such as stoichiometry (N), dissociation constant (K_{d}) and changes in enthalpy (ΔH), and entropy (ΔS). *One set of binding sites* model was fitted to data. Reference power was set to 5. A stirring speed of 750 rpm and spacing of 150 s were used. Blank measurement was performed to investigate the effect of dilution of the 2OG solution in the cell with NAD^+ in the buffer. Since the integration of the peaks from the blank measurement resulted in comparable values, we decided to use Y-translation of the data points obtained from the *At*GDH1/NAD^+ titration to avoid accumulation of errors. The titration experiments were conducted in duplicate.

Sequence Similarity Network

Sequence similarity networks were calculated using the EFI-ESN webserver (Zallot et al., 2019). The InterPro family IPR014362 contains 35503 sequences as of February 2020. The size was reduced by using Uniref90 to obtain 12015 clusters. Protein sequences between 400 and 500 residues long were analyzed with alignment score of 150. To further reduce the number of nodes and edges, sequences sharing ≥ 75% identity were grouped. For the subset from *Streptophyta*, 893 sequences between 250 and 750 residues long (without Uniprot90 clustering) were analyzed based on 230 alignment score. The graphs were created in *Cytoscape* 3.3 (Shannon et al., 2003).

DATA AVAILABILITY STATEMENT

Atomic coordinates and structure factors for the crystal structures of glutamate dehydrogenase 1 (GDH1) from *Arabidopsis thaliana* (*At*) have been deposited with the Protein Data Bank (PDB) under the accession codes 6yeh (*At*GDH1 apo) (https://www.rcsb.org/structure/6YEH) and 6yei (*At*GDH1-NAD^+) (https://www.rcsb.org/structure/6YEI). PDB DOI: https://doi.org/10.2210/pdb6YEI/pdb. Raw X-ray diffraction images and processing files have been deposited in the RepOD repository of the Interdisciplinary Centre for Mathematical and Computational Modelling (ICM) of the University of Warsaw with the following DOI numbers: *At*GDH1 apo: doi: 10.18150/repod.8407298; *At*GDH1-NAD^+: doi: 10.18150/repod.1477886.

AUTHOR CONTRIBUTIONS

MG purified and crystallized the protein and tested the kinetics. MG and MR solved and refined the crystal structures. MR cloned the protein and carried out the phylogenetic analysis. JS performed and analyzed the calorimetric experiments. MG, MR, and MJ wrote the manuscript.

FUNDING

This work was supported by the National Science Centre (NCN Grant No. SONATA 2018/31/D/NZ1/03630).

ACKNOWLEDGMENTS

The diffraction data were collected at beamline P13 operated by EMBL Hamburg at the PETRA III storage ring (DESY, Hamburg, Germany; Cianci et al., 2017).

REFERENCES

Afonine, P. V., Grosse-Kunstleve, R. W., Echols, N., Headd, J. J., Moriarty, N. W., Mustyakimov, M., et al. (2012). Towards automated crystallographic structure refinement with phenix.refine. *Acta Cryst. D* 68, 352–367. doi: 10.1107/S0907444912001308

Armenteros, J. J. A., Salvatore, M., Emanuelsson, O., Winther, O., Von Heijne, G., Elofsson, A., et al. (2019). Detecting sequence signals in targeting peptides using deep learning. *Life Sci. Alliance* 2:e201900429. doi: 10.26508/lsa.201900429

Ashkenazy, H., Abadi, S., Martz, E., Chay, O., Mayrose, I., Pupko, T., et al. (2016). ConSurf 2016: an improved methodology to estimate and visualize evolutionary conservation in macromolecules. *Nucleic Acids Res.* 44, W344–W350. doi: 10.1093/nar/gkw408

Aubert, S., Bligny, R., Douce, R., Gout, E., Ratcliffe, R. G., and Roberts, J. K. (2001). Contribution of glutamate dehydrogenase to mitochondrial glutamate metabolism studied by (13)C and (31)P nuclear magnetic resonance. *J. Exp. Bot.* 52, 37–45. doi: 10.1093/jxb/52.354.37

Baker, N. A., Sept, D., Joseph, S., Holst, M. J., and Mccammon, J. A. (2001). Electrostatics of nanosystems: application to microtubules and the ribosome. *Proc. Natl. Acad. Sci. U.S.A.* 98, 10037–10041. doi: 10.1073/pnas.181342398

Baker, P. J., Britton, K. L., Engel, P. C., Farrants, G. W., Lilley, K. S., Rice, D. W., et al. (1992). Subunit assembly and active site location in the structure of glutamate dehydrogenase. *Proteins* 12, 75–86. doi: 10.1002/prot.340120109

Bannai, H., Tamada, Y., Maruyama, O., Nakai, K., and Miyano, S. (2002). Extensive feature detection of N-terminal protein sorting signals. *Bioinformatics* 18, 298–305. doi: 10.1093/bioinformatics/18.2.298

Britton, K. L., Baker, P. J., Engel, P. C., Rice, D. W., and Stillman, T. J. (1993). Evolution of substrate diversity in the superfamily of amino acid dehydrogenases prospects for rational chiral synthesis. *J. Mol. Biol.* 234, 938–945. doi: 10.1006/jmbi.1993.1647

Britton, K. L., Baker, P. J., Rice, D. W., and Stillman, T. J. (1992). Structural relationship between the hexameric and tetrameric family of glutamate-dehydrogenases. *Eur. J. Biochem.* 209, 851–859. doi: 10.1111/j.1432-1033.1992.tb17357.x

Britton, K. L., Yip, K. S., Sedelnikova, S. E., Stillman, T. J., Adams, M. W., Ma, K., et al. (1999). Structure determination of the glutamate dehydrogenase from the hyperthermophile Thermococcus litoralis and its comparison with that from *Pyrococcus furiosus*. *J. Mol. Biol.* 293, 1121–1132. doi: 10.1006/jmbi.1999.3205

Brunhuber, N. M., and Blanchard, J. S. (1994). The biochemistry and enzymology of amino acid dehydrogenases. *Crit. Rev. Biochem. Mol. Biol.* 29, 415–467. doi: 10.3109/10409239409083486

Carrie, C., Venne, A. S., Zahedi, R. P., and Soll, J. (2015). Identification of cleavage sites and substrate proteins for two mitochondrial intermediate peptidases in *Arabidopsis thaliana*. *J. Exp. Bot.* 66, 2691–2708. doi: 10.1093/jxb/erv064

Chen, V. B., Arendall, W. B. III, Headd, J. J., Keedy, D. A., Immormino, R. M., Kapral, G. J., et al. (2010). MolProbity: all-atom structure validation for macromolecular crystallography. *Acta Cryst. D* 66, 12–21. doi: 10.1107/s0907444909042073

Cianci, M., Bourenkov, G., Pompidor, G., Karpics, I., Kallio, J., Bento, I., et al. (2017). P13, the EMBL macromolecular crystallography beamline at the low-emittance PETRA III ring for high- and low-energy phasing with variable beam focusing. *J. Synchrotron Radiation* 24, 323–332. doi: 10.1107/S1600577516016465

Clapham, D. E. (2007). Calcium signaling. *Cell* 131, 1047–1058.

Claros, M. G., and Vincens, P. (1996). Computational method to predict mitochondrially imported proteins and their targeting sequences. *Eur. J. Biochem.* 241, 779–786. doi: 10.1111/j.1432-1033.1996.00779.x

Dean, J. L., Wang, X. G., Teller, J. K., Waugh, M. L., Britton, K. L., Baker, P. J., et al. (1994). The catalytic role of aspartate in the active site of glutamate dehydrogenase. *Biochem. J.* 301(Pt 1), 13–16. doi: 10.1042/bj3010013

Dolinsky, T. J., Nielsen, J. E., Mccammon, J. A., and Baker, N. A. (2004). PDB2PQR: an automated pipeline for the setup of Poisson-Boltzmann electrostatics calculations. *Nucleic Acids Res.* 32, W665–W667.

Emanuelsson, O., and Von Heijne, G. (2001). Prediction of organellar targeting signals. *Biochim. Biophys. Acta* 1541, 114–119. doi: 10.1016/s0167-4889(01)00145-8

Emsley, P., Lohkamp, B., Scott, W. G., and Cowtan, K. (2010). Features and development of Coot. *Acta Cryst. D* 66, 486–501.

Engel, P. C. (2014). Glutamate dehydrogenases: the why and how of coenzyme specificity. *Neurochem. Res.* 39, 426–432. doi: 10.1007/s11064-013-1089-x

Fontaine, J. X., Saladino, F., Agrimonti, C., Bedu, M., Terce-Laforgue, T., Tetu, T., et al. (2006). Control of the synthesis and subcellular targeting of the two GDH genes products in leaves and stems of Nicotiana plumbaginifolia and *Arabidopsis thaliana*. *Plant Cell Physiol.* 47, 410–418. doi: 10.1093/pcp/pcj008

Fontaine, J. X., Terce-Laforgue, T., Armengaud, P., Clement, G., Renou, J. P., Pelletier, S., et al. (2012). Characterization of a NADH-dependent glutamate dehydrogenase mutant of Arabidopsis demonstrates the key role of this enzyme in root carbon and nitrogen metabolism. *Plant Cell* 24, 4044–4065. doi: 10.1105/tpc.112.103689

Fontaine, J. X., Terce-Laforgue, T., Bouton, S., Pageau, K., Lea, P. J., Dubois, F., et al. (2013). Further insights into the isoenzyme composition and activity of glutamate dehydrogenase in *Arabidopsis thaliana*. *Plant Signal Behav.* 8:e23329. doi: 10.4161/psb.23329

Fox, G. G., Ratcliffe, R. G., Robinson, S. A., and Stewart, G. R. (1995). Evidence for deamination by glutamate-dehydrogenase in higher-plants-commentary. *Canad. J. Bot. Rev. Canad. Bot.* 73, 1112–1115. doi: 10.1139/b95-120

Fukasawa, Y., Tsuji, J., Fu, S. C., Tomii, K., Horton, P., and Imai, K. (2015). MitoFates: improved prediction of mitochondrial targeting sequences and their cleavage sites. *Mol. Cell. Prot.* 14, 1113–1126. doi: 10.1074/mcp.M114.043083

Garland, W. J., and Dennis, D. T. (1976). Kinetics of glutamate-dehydrogenase from pea mitochondria. *Plant Physiol.* 57, 81–81.

Glevarec, G., Bouton, S., Jaspard, E., Riou, M. T., Cliquet, J. B., Suzuki, A., et al. (2004). Respective roles of the glutamine synthetase/glutamate synthase cycle and glutamate dehydrogenase in ammonium and amino acid metabolism during germination and post-germinative growth in the model legume Medicago truncatula. *Planta* 219, 286–297. doi: 10.1007/s00425-004-1214-9

Hammes-Schiffer, S. (2002). Comparison of hydride, hydrogen atom, and proton-coupled electron transfer reactions. *Chemphyschem* 3, 33–42. doi: 10.1002/1439-7641(20020118)3:1<33::aid-cphc33>3.0.co;2-6

Hartl, F. U., and Neupert, W. (1990). Protein sorting to mitochondria: evolutionary conservations of folding and assembly. *Science* 247, 930–938. doi: 10.1126/science.2406905

Hepler, P. K. (2005). Calcium: a central regulator of plant growth and development. *Plant Cell* 17, 2142–2155. doi: 10.1105/tpc.105.032508

Igamberdiev, A. U., and Gardestrom, P. (2003). Regulation of NAD- and NADP-dependent isocitrate dehydrogenases by reduction levels of pyridine nucleotides in mitochondria and cytosol of pea leaves. *Biochim. Biophys. Acta* 1606, 117–125. doi: 10.1016/s0005-2728(03)00106-3

Kabsch, W. (2010). Xds. *Acta Cryst. D* 66, 125–132.

Kim, Y., Babnigg, G., Jedrzejczak, R., Eschenfeldt, W. H., Li, H., Maltseva, N., et al. (2011). High-throughput protein purification and quality assessment for crystallization. *Methods* 55, 12–28. doi: 10.1016/j.ymeth.2011.07.010

Kitada, S., Yamasaki, E., Kojima, K., and Ito, A. (2003). Determination of the cleavage site of the presequence by mitochondrial processing peptidase on the substrate binding scaffold and the multiple subsites inside a molecular cavity. *J. Biol. Chem.* 278, 1879–1885. doi: 10.1074/jbc.m209263200

Knapp, S., De Vos, W. M., Rice, D., and Ladenstein, R. (1997). Crystal structure of glutamate dehydrogenase from the hyperthermophilic eubacterium Thermotoga maritima at 3.0 A resolution. *J. Mol. Biol.* 267, 916–932. doi: 10.1006/jmbi.1996.0900

Kotzamani, D., and Plaitakis, A. (2012). Alpha helical structures in the leader sequence of human GLUD2 glutamate dehydrogenase responsible for mitochondrial import. *Neurochem. Int.* 61, 463–469. doi: 10.1016/j.neuint.2012.06.006

Kowiel, M., Jaskolski, M., and Dauter, Z. (2014). ACHESYM: an algorithm and server for standardized placement of macromolecular models in the unit cell. *Acta Cryst. D* 70, 3290–3298. doi: 10.1107/s1399004714024572

Krissinel, E. (2015). Stock-based detection of protein oligomeric states in jsPISA. *Nucleic Acids Res.* 43, W314–W319.

Krissinel, E., and Henrick, K. (2004). Secondary-structure matching (SSM), a new tool for fast protein structure alignment in three dimensions. *Acta Cryst. D* 60, 2256–2268. doi: 10.1107/s0907444904026460

Labboun, S., Terce-Laforgue, T., Roscher, A., Bedu, M., Restivo, F. M., Velanis, C. N., et al. (2009). Resolving the role of plant glutamate dehydrogenase. I. In vivo real time nuclear magnetic resonance spectroscopy experiments. *Plant Cell Physiol.* 50, 1761–1773. doi: 10.1093/pcp/pcp118

Laemmli, U. K. (1970). Cleavage of structural proteins during the assembly of the head of bacteriophage T4. *Nature* 227, 680–685. doi: 10.1038/227680a0

Lea, P. J. (1993). "Nitrogen metabolism," in *Plant Biochemistry and Molecular Biology*, eds P. J. Lea and R. C. Leegood (Hoboken, NJ: John Wiley & Sons Ltd), 155–180.

Lea, P. J., and Miflin, B. J. (1974). Alternative route for nitrogen assimilation in higher plants. *Nature* 251, 614–616. doi: 10.1038/251614a0

Lea, P. J., and Miflin, B. J. (2011). Nitrogen Assimilation and its relevance to crop improvement. *Ann. Plant Rev.* 42, 1–40. doi: 10.1002/9781119312994.apr0448

Lehmann, T., and Ratajczak, L. (2008). The pivotal role of glutamate dehydrogenase (GDH) in the mobilization of N and C from storage material to asparagine in germinating seeds of yellow lupine. *J. Plant Physiol.* 165, 149–158. doi: 10.1016/j.jplph.2006.12.010

Lesk, A. M. (1995). NAD-binding domains of dehydrogenases. *Curr. Opin. Struct. Biol.* 5, 775–783. doi: 10.1016/0959-440x(95)80010-7

Li, M., Li, C., Allen, A., Stanley, C. A., and Smith, T. J. (2011). The structure and allosteric regulation of glutamate dehydrogenase. *Neurochem. Int.* 59, 445–455. doi: 10.1016/j.neuint.2010.10.017

Liebschner, D., Afonine, P. V., Moriarty, N. W., Poon, B. K., Sobolev, O. V., Terwilliger, T. C., et al. (2017). Polder maps: improving OMIT maps by excluding bulk solvent. *Acta Cryst. D* 73, 148–157. doi: 10.1107/s2059798316018210

Loulakakis, C. A., and Roubelakisangelakis, K. A. (1990). Intracellular-localization and properties of nadh-glutamate dehydrogenase from vitis-vinifera l-purification and characterization of the major leaf isoenzyme. *J. Exp. Bot.* 41, 1223–1230. doi: 10.1093/jxb/41.10.1223

Marchi, L., Degola, F., Polverini, E., Terce-Laforgue, T., Dubois, F., Hirel, B., et al. (2013). Glutamate dehydrogenase isoenzyme 3 (GDH3) of Arabidopsis thaliana is regulated by a combined effect of nitrogen and cytokinin. *Plant Physiol. Biochem.* 73, 368–374. doi: 10.1016/j.plaphy.2013.10.019

Marchi, L., Polverini, E., Degola, F., Baruffini, E., and Restivo, F. M. (2014). Glutamate dehydrogenase isoenzyme 3 (GDH3) of Arabidopsis thaliana is less thermostable than GDH-1 and GDH2 isoenzymes. *Plant Physiol. Biochem.* 83, 225–231. doi: 10.1016/j.plaphy.2014.08.003

Marti, R. M. C., Hubbard, K. E., Gardner, M. J., Jung, H. J., Aubry, S., Hotta, C. T., et al. (2018). Circadian oscillations of cytosolic free calcium regulate the *Arabidopsis* circadian clock. *Nat. Plants* 4, 690–698. doi: 10.1038/s41477-018-0224-8

Masclaux-Daubresse, C., Reisdorf-Cren, M., Pageau, K., Lelandais, M., Grandjean, O., Kronenberger, J., et al. (2006). Glutamine synthetase-glutamate synthase pathway and glutamate dehydrogenase play distinct roles in the sink-source nitrogen cycle in tobacco. *Plant Physiol.* 140, 444–456. doi: 10.1104/pp.105.071910

McCoy, A. J., Grosse-Kunstleve, R. W., Adams, P. D., Winn, M. D., Storoni, L. C., and Read, R. J. (2007). Phaser crystallographic software. *J. Appl. Cryst.* 40, 658–674. doi: 10.1107/S0021889807021206

Melo-Oliveira, R., Oliveira, I. C., and Coruzzi, G. M. (1996). Arabidopsis mutant analysis and gene regulation define a nonredundant role for glutamate dehydrogenase in nitrogen assimilation. *Proc. Natl. Acad. Sci. U.S.A.* 93, 4718–4723. doi: 10.1073/pnas.93.10.4718

Miflin, B. J., and Habash, D. Z. (2002). The role of glutamine synthetase and glutamate dehydrogenase in nitrogen assimilation and possibilities for improvement in the nitrogen utilization of crops. *J. Exp. Bot.* 53, 979–987. doi: 10.1093/jexbot/53.370.979

Miflin, B. J., and Lea, P. J. (1980). "Ammonia assimilation," in *Amino Acids and Derivatives, The Biochemistry of Plants*, ed. B. J. Miflin (New York, NY: Academic Press).

Miyashita, Y., and Good, A. G. (2008). NAD(H)-dependent glutamate dehydrogenase is essential for the survival of Arabidopsis thaliana during dark-induced carbon starvation. *J. Exp. Bot.* 59, 667–680. doi: 10.1093/jxb/erm340

Moghe, G. D., and Last, R. L. (2015). Something old, something new: conserved enzymes and the evolution of novelty in plant specialized metabolism. *Plant Physiol.* 169, 1512–1523.

Nielsen, H., Engelbrecht, J., Brunak, S., and Vonheijne, G. (1997). Identification of prokaryotic and eukaryotic signal peptides and prediction of their cleavage sites. *Protein Eng.* 10, 1–6. doi: 10.1093/protein/10.1.1

Noor, S., and Punekar, N. S. (2005). Allosteric NADP-glutamate dehydrogenase from aspergilli: purification, characterization and implications for metabolic regulation at the carbon-nitrogen interface. *Microbiology* 151, 1409–1419. doi: 10.1099/mic.0.27751-0

Oide, M., Kato, T., Oroguchi, T., and Nakasako, M. (2020). Energy landscape of domain motion in glutamate dehydrogenase deduced from cryo-electron microscopy. *FEBS J.* doi: 10.1111/febs.15224 [Epub ahead of print].

Oliveira, T., Panjikar, S., Carrigan, J. B., Hamza, M., Sharkey, M. A., Engel, P. C., et al. (2012). Crystal structure of NAD+-dependent Peptoniphilus asaccharolyticus glutamate dehydrogenase reveals determinants of cofactor specificity. *J. Struct. Biol.* 177, 543–552. doi: 10.1016/j.jsb.2011.10.006

Peterson, P. E., and Smith, T. J. (1999). The structure of bovine glutamate dehydrogenase provides insights into the mechanism of allostery. *Structure* 7, 769–782. doi: 10.1016/s0969-2126(99)80101-4

Pettersen, E. F., Goddard, T. D., Huang, C. C., Couch, G. S., Greenblatt, D. M., Meng, E. C., et al. (2004). UCSF Chimera–a visualization system for exploratory research and analysis. *J. Comput. Chem.* 25, 1605–1612. doi: 10.1002/jcc.20084

Purnell, M. P., and Botella, J. R. (2007). Tobacco isoenzyme 1 of NAD(H)-dependent glutamate dehydrogenase catabolizes glutamate in vivo. *Plant Physiol.* 143, 530–539. doi: 10.1104/pp.106.091330

Qiu, X., Xie, W., Lian, X., and Zhang, Q. (2009). Molecular analyses of the rice glutamate dehydrogenase gene family and their response to nitrogen and phosphorous deprivation. *Plant Cell Rep.* 28, 1115–1126. doi: 10.1007/s00299-009-0709-z

Rao, S. T., and Rossmann, M. G. (1973). Comparison of super-secondary structures in proteins. *J. Mol. Biol.* 76, 241–256. doi: 10.1016/0022-2836(73)90388-4

Robinson, S. A., Stewart, G. R., and Phillips, R. (1992). Regulation of glutamate dehydrogenase activity in relation to carbon limitation and protein catabolism in carrot cell suspension cultures. *Plant Physiol.* 98, 1190–1195. doi: 10.1104/pp.98.3.1190

Shannon, P., Markiel, A., Ozier, O., Baliga, N. S., Wang, J. T., Ramage, D., et al. (2003). Cytoscape: a software environment for integrated models of biomolecular interaction networks. *Genome Res.* 13, 2498–2504. doi: 10.1101/gr.1239303

Sigrist, C. J. A., De Castro, E., Cerutti, L., Cuche, B. A., Hulo, N., Bridge, A., et al. (2013). New and continuing developments at PROSITE. *Nucleic Acids Res.* 41, E344–E347.

Sjoling, S., and Glaser, E. (1998). Mitochondrial targeting peptides in plants. *Trends Plant Sci.* 3, 136–140. doi: 10.1016/s1360-1385(98)01212-6

Skopelitis, D. S., Paranychianakis, N. V., Paschalidis, K. A., Pliakonis, E. D., Delis, I. D., Yakoumakis, D. I., et al. (2006). Abiotic stress generates ROS that signal expression of anionic glutamate dehydrogenases to form glutamate for proline synthesis in tobacco and grapevine. *Plant Cell* 18, 2767–2781. doi: 10.1105/tpc.105.038323

Smith, E. E., Austen, B. M., and Blumenthal, K. M. (1975). "Glutamate dehydrogenases," in *The Enzymes*, ed. Boyer (New York, NY: Academic Press), 293–367.

Son, H. F., Kim, I. K., and Kim, K. J. (2015). Structural insights into domain movement and cofactor specificity of glutamate dehydrogenase from *Corynebacterium glutamicum*. *Biochem. Biophys. Res. Commun.* 459, 387–392. doi: 10.1016/j.bbrc.2015.02.109

Stillman, T. J., Baker, P. J., Britton, K. L., and Rice, D. W. (1993). Conformational flexibility in glutamate dehydrogenase. Role of water in substrate recognition and catalysis. *J. Mol. Biol.* 234, 1131–1139. doi: 10.1006/jmbi.1993.1665

Stillman, T. J., Migueis, A. M., Wang, X. G., Baker, P. J., Britton, K. L., Engel, P. C., et al. (1999). Insights into the mechanism of domain closure and substrate specificity of glutamate dehydrogenase from *Clostridium symbiosum*. *J. Mol. Biol.* 285, 875–885. doi: 10.1006/jmbi.1998.2335

Stone, S. R., Copeland, L., and Heyde, E. (1980). Glutamate-dehydrogenase of lupin nodules-kinetics of the deamination reaction. *Arch. Biochem. Biophys.* 199, 550–559. doi: 10.1016/0003-9861(80)90313-6

Taylor, A. B., Smith, B. S., Kitada, S., Kojima, K., Miyaura, H., Otwinowski, Z., et al. (2001). Crystal structures of mitochondrial processing peptidase reveal the mode for specific cleavage of import signal sequences. *Structure* 9, 615–625. doi: 10.1016/s0969-2126(01)00621-9

Terwilliger, T. C., Grosse-Kunstleve, R. W., Afonine, P. V., Moriarty, N. W., Zwart, P. H., Hung, L. W., et al. (2008). Iterative model building, structure refinement and density modification with the PHENIX AutoBuild wizard. *Acta Cryst. D* 64, 61–69. doi: 10.1107/s090744490705024x

Turano, F. J., Thakkar, S. S., Fang, T., and Weisemann, J. M. (1997). Characterization and expression of NAD(H)-dependent glutamate dehydrogenase genes in *Arabidopsis*. *Plant Physiol.* 113, 1329–1341. doi: 10.1104/pp.113.4.1329

Von Heijne, G., Steppuhn, J., and Herrmann, R. G. (1989). Domain structure of mitochondrial and chloroplast targeting peptides. *Eur. J. Biochem.* 180, 535–545. doi: 10.1111/j.1432-1033.1989.tb14679.x

Wacker, S. A., Bradley, M. J., Marion, J., and Bell, E. (2010). Ligand-induced changes in the conformational stability and flexibility of glutamate dehydrogenase and their role in catalysis and regulation. *Protein Sci.* 19, 1820–1829. doi: 10.1002/pro.459

Werner, C., Stubbs, M. T., Krauth-Siegel, R. L., and Klebe, G. (2005). The crystal structure of Plasmodium falciparum glutamate dehydrogenase, a putative target for novel antimalarial drugs. *J. Mol. Biol.* 349, 597–607. doi: 10.1016/j.jmb.2005.03.077

Wiedemann, N., and Pfanner, N. (2017). Mitochondrial machineries for protein import and assembly. *Ann. Rev. Biochem.* 86, 685–714. doi: 10.1146/annurev-biochem-060815-014352

Williamson, D. H., Lund, P., and Krebs, H. A. (1967). The redox state of free nicotinamide-adenine dinucleotide in the cytoplasm and mitochondria of rat liver. *Biochem. J.* 103, 514–527. doi: 10.1042/bj1030514

Winn, M. D., Murshudov, G. N., and Papiz, M. Z. (2003). Macromolecular TLS refinement in REFMAC at moderate resolutions. *Methods Enzymol.* 374, 300–321. doi: 10.1016/s0076-6879(03)74014-2

Xiong, T. C., Bourque, S., Lecourieux, D., Amelot, N., Grat, S., Briere, C., et al. (2006). Calcium signaling in plant cell organelles delimited by a double membrane. *Biochim. Biophys Acta* 1763, 1209–1215. doi: 10.1016/j.bbamcr.2006.09.024

Yamaya, T., Oaks, A., and Matsumoto, H. (1984). Characteristics of glutamate dehydrogenase in mitochondria prepared from corn shoots. *Plant Physiol.* 76, 1009–1013. doi: 10.1104/pp.76.4.1009

Zahoor, A., Lindner, S. N., and Wendisch, V. F. (2012). Metabolic engineering of Corynebacterium glutamicum aimed at alternative carbon sources and new products. *Comput. Struct. Biotechnol. J.* 3:e201210004. doi: 10.5936/csbj.201210004

Zallot, R., Oberg, N., and Gerlt, J. A. (2019). The EFI web resource for genomic enzymology tools: leveraging protein, genome, and metagenome databases to discover novel enzymes and metabolic pathways. *Biochemistry* 58, 4169–4182. doi: 10.1021/acs.biochem.9b00735

Zheng, H., Cooper, D. R., Porebski, P. J., Shabalin, I. G., Handing, K. B., and Minor, W. (2017). CheckMyMetal: a macromolecular metal-binding validation tool. *Acta Cryst. D* 73, 223–233. doi: 10.1107/s2059798317001061

Conflict of Interest: The authors declare that the research was conducted in the absence of any commercial or financial relationships that could be construed as a potential conflict of interest.

Copyright © 2020 Grzechowiak, Sliwiak, Jaskolski and Ruszkowski. This is an open-access article distributed under the terms of the Creative Commons Attribution License (CC BY). The use, distribution or reproduction in other forums is permitted, provided the original author(s) and the copyright owner(s) are credited and that the original publication in this journal is cited, in accordance with accepted academic practice. No use, distribution or reproduction is permitted which does not comply with these terms.

frontiers in Plant Science

ORIGINAL RESEARCH
published: 16 June 2020
doi: 10.3389/fpls.2020.00823

Structural and Functional Characteristics of Two Molecular Variants of the Nitrogen Sensor PII in Maritime Pine

María Teresa Llebrés[1], María Belén Pascual[1†], Carolina Valle[1], Fernando N. de la Torre[1†], José Miguel Valderrama-Martin[1], Luis Gómez[2†], Concepción Avila[1†] and Francisco M. Cánovas[1†]*

[1] Grupo de Biología Molecular y Biotecnología de Plantas, Departamento de Biología Molecular y Bioquímica, Faculty of Science, Universidad de Málaga, Campus Universitario de Teatinos, Málaga, Spain, [2] Centro de Biotecnología y Genómica de Plantas, Campus de Excelencia Internacional de Montegancedo, Parque Científico y Tecnológico de la Universidad Politécnica de Madrid, Madrid, Spain

OPEN ACCESS

Edited by:
Giuseppe Forlani,
University of Ferrara, Italy

Reviewed by:
Karl Forchhammer,
University of Tübingen, Germany
Vicente Rubio,
Consejo Superior de Investigaciones Científicas (CSIC), Spain
Maurizio Chiurazzi,
National Research Council (CNR), Italy

***Correspondence:**
Francisco M. Cánovas
canovas@uma.es

†ORCID:
María Belén Pascual
orcid.org/0000-0002-7988-1204
Fernando N. de la Torre
orcid.org/0000-0002-5143-3709
Luis Gómez
orcid.org/0000-0003-0667-2302
Concepción Avila
orcid.org/0000-0001-8817-7529
Francisco M. Cánovas
orcid.org/0000-0002-4914-2558

Specialty section:
This article was submitted to Plant Metabolism and Chemodiversity, a section of the journal Frontiers in Plant Science

Received: 20 December 2019
Accepted: 22 May 2020
Published: 16 June 2020

Citation:
Llebrés MT, Pascual MB, Valle C, de la Torre FN, Valderrama-Martin JM, Gómez L, Avila C and Cánovas FM (2020) Structural and Functional Characteristics of Two Molecular Variants of the Nitrogen Sensor PII in Maritime Pine. Front. Plant Sci. 11:823. doi: 10.3389/fpls.2020.00823

High levels of nitrogen are stored as arginine during the last stages of seed formation in maritime pine (*Pinus pinaster* Aiton). The protein sensor PII regulates the feedback inhibition of arginine biosynthesis through interaction with the key enzyme *N*-acetylglutamate kinase (NAGK). In this study, the structural and functional characteristics of PII have been investigated in maritime pine to get insights into the regulation of arginine metabolism. Two different forms of PII have been identified, PpPIIa and PpPIIb, which differ in their amino acid sequence and most likely correspond to splicing variants of a single gene in the pine genome. Two PII variants are also present in other pine species but not in other conifers such as spruces. PpPIIa and PpPIIb are trimeric proteins for which structural modeling predicts similar tridimensional protein core structures. Both are located in the chloroplast, where the PII-target enzyme PpNAGK is also found. PpPIIa, PpPIIb, and PpNAGK have been recombinantly produced to investigate the formation of NAGK-PII complexes. The interaction of PpPIIa/PpPIIb and PpNAGK may be enhanced by glutamine and contribute to relieve the feedback inhibition of PpNAGK by arginine. Expression analysis of *PpPII* genes revealed that PpIIa transcripts were predominant during embryogenesis and germination. The potential roles of PpPIIa and PpPIIb in the regulation of arginine metabolism of maritime pine are discussed.

Keywords: ***Pinus pinaster*, amino acids, arginine metabolism, isoproteins, nitrogen storage**

INTRODUCTION

Plants, like other organisms, have developed mechanisms to detect and respond to changes in carbon and nitrogen levels. These mechanisms regulate the activity of proteins involved in the transport and metabolism of nitrogen and carbon compounds, allowing plants to optimize their energy sources. These processes are particularly important in trees due to their long life cycles (Cánovas et al., 2018).

The sensing mechanisms for carbon/nitrogen (C/N) balance activate genes involved in nitrogen assimilation when carbon skeletons are abundant and internal levels of organic nitrogen are low. On the other hand, they decrease the rate of nitrogen assimilation when the levels of photosynthetic products are low or the internal levels of nitrogen are relatively high. These mechanisms allow plants to adjust their energy and metabolite allocation to a shifting carbon and nitrogen availability (Coruzzi and Zhou, 2001; Gent and Forde, 2017).

The systems to sense and respond to carbon and nitrogen levels have been the subject of elegant studies on microorganisms such as *Escherichia coli* and yeast (Forchhammer and Lüddecke, 2016). In these unicellular models, signaling systems have been found to be complex and multiple (Jiang et al., 1998). These systems are even more complex in plants, which must respond to various carbon and nitrogen metabolites in different tissues, stages of development, and cell compartments (Ferrario-Méry et al., 2006, 2008). A key protein family of modulators acting in microorganisms and plants is the one of the PII signaling proteins (Selim et al., 2020a). These proteins have as targets channels, enzymes, and transcriptional regulators, influencing the activities of these targets by direct protein–protein interactions with them (Selim et al., 2020a). PII proteins sense the nitrogen, carbon, and energy richness status of the cell via interactions with allosteric effectors [ATP/ADP and 2-oxoglutarate (2OG); and, in plants, also with glutamine] and, in some bacteria, by highly specific postranslational modifications (Forchhammer and Lüddecke, 2016). In this way, PII proteins are signal transductors that play crucial roles for nitrogen/carbon and energy regulation of bacteria and also of plants. They are the main focus of the studies presented here.

PII proteins are homotrimers of a subunit presenting a well-conserved sequence which is folded according to the ferredoxin fold. This fold is made of two βαβ structural repeats, and in PII proteins, it presents three functionally important loops, called T-loop, B-loop, and a C-terminal loop. The T-loop hosts a characteristic invariant sequence motif (Motif I). This loop connects both repeats of the fold, it is long and plastic, and its conformation is influenced by the allosteric effectors of PII, also being in some bacteria the site of covalent modifications at specific residues (as exemplified by the T-loop uridylylation observed in *E. coli*, Ninfa and Atkinson, 2000). The T-loop plays a key role in the interactions of PII with its protein partners (Selim et al., 2020a). The B-loop also hosts an invariant motif (Motif II) and also participates in the interactions with PII targets (Selim et al., 2020a). The C-terminal loop of plants is called the Q-loop, it is longer than bacterial C-terminal loops, and it is the site of glutamine binding. The adenine nucleotide and 2OG effectors sit at intersubunit crevices at the root of the T-loops.

In bacteria, the signaling PII protein serves as a central processing unit to integrate signals on carbon, nitrogen, and energy abundance status, and use such information to control nitrogen uptake (Ninfa and Atkinson, 2000). The assimilation of ammonium as glutamine is regulated in response to intracellular concentrations of glutamine (a nitrogen signal) and 2-OG (a carbon signal) (Muro-Pastor et al., 2005; Robles-Rengel et al., 2019).

In plants, the PII protein is a sensor of C/N status mediated by the binding to 2-OG and glutamine. It subsequently regulates the arginine biosynthetic pathway (Chen et al., 2006; Chellamuthu et al., 2014) which is under feed-back control by arginine inhibition of *N*-acetylglutamate kinase (NAGK). However, when N is abundant, the inhibition is relieved through the interaction of NAGK with the sensor protein PII (Chen et al., 2006; Llácer et al., 2007). Increased levels of glutamine are a signal of N abundance that is sensed via the PII Q-loop and transduced into enhanced activity of NAGK (Chellamuthu et al., 2014). In this way, the connection proposed between PII and arginine-rich protein biosynthesis and deposition in seeds (Urigh et al., 2009) could be regulated by glutamine availability. Other less well-studied effects of PII on plant nitrogen metabolism include the observation made that in symbiotic nitrogen fixation PII affects the development of root nodules, the mobilization to the host of of the fixed nitrogen, and the signaling of the N nutritional status (Arcondeguy et al., 2001; D'Apuzzo et al., 2015), as well as the recent report of a potential role of PII in the biosynthetic production of NO (Parlatti et al., 2017).

In trees, when the availability of N is high, arginine is stored either as a free amino acid or as a component of storage proteins in the bark and seeds (Li and Coleman, 2019). During embryogenesis, nitrogen derived from tissue sources, mainly in the form of glutamine, is transported to developing seeds where it is used for the biosynthesis and deposition of storage proteins. In conifers, arginine is highly abundant in the seed storage proteins and represents an important source of nitrogen for developing plantlets following seed germination (Todd et al., 2001; Todd and Gifford, 2003; Cánovas et al., 2007). Therefore, the regulation of arginine metabolism has a relevant role in the store and mobilization of N during the embryogenesis and germination of pine (Llebrés et al., 2018a,b).

In vitro somatic embryogenesis in combination with cryopreservation is a major biotechnological tool for vegetative propagation of selected maritime pine varieties for different ecological and economical applications (Trontin et al., 2016). However, a fundamental understanding of how arginine metabolism is regulated during embryogenesis and germination is necessary to improve embryo quality and to generate vigorous maritime pine seedlings via somatic embryogenesis (Llebrés et al., 2018b).

In the present study, key aspects of PII regulation in maritime pine are investigated with the purpose of getting insights into the regulation of arginine biosynthesis in response to nitrogen availability in conifers, a plant group of crucial ecological and economic importance.

MATERIALS AND METHODS

Plant Material

Maritime pine embryos were excised from seeds collected from a single seed orchard (Picard, Saint-Laurent-Médoc, France) at different developmental stages (Llebrés et al., 2018b). *Pinus pinaster* Aiton seeds were provided by the Centro Nacional de Recursos Genéticos Forestales from "Ministerio de Agricultura,

Pesca, Alimentación y Medio Ambiente," Spain. Seeds were imbibed in distilled water for 24 h under continuous aeration and germinated and grown with vermiculite as a substrate under a photoperiod of 16 h light/8 h dark at 24°C. Hypocotyls of pine seedlings were collected after 2 weeks, frozen in liquid nitrogen, and stored at −80°C until use. *Nicotiana benthamiana* L. seeds were sown and grown in pots and maintained under a 16 h light/8 h dark photoperiod at 24°C for 5 weeks.

Cloning of PpPIIa, PpPIIb, and PpNAGK

The sequences of *PpPIIa*, *PpPIIb*, and *PpNAGK* were retrieved from the maritime pine (*P. pinaster*) transcriptome available at SustainPineDB v.3.0[1]. Full-length cDNAs were isolated from pine hypocotyl RNAs by reverse transcription-PCR (RT-PCR) using primers designed from *P. pinaster* sequences (Canales et al., 2014). Extraction of RNA was performed as described by Canales et al. (2012) and quantified using a NanoDrop© ND-1000 spectrophotometer. Synthesis of cDNA was performed with 5X iScript™ cDNA Synthesis Kit (Bio-Rad). The primer pairs used for specific amplification are listed in **Supplementary Table S1**. The resulting PCR products were cloned in a pJet1.2 (Thermo Fisher Scientific™) vector and completely sequenced.

Transient Expression of GFP-Proteins in *Nicotiana benthamiana*

PCR amplifications were performed as described above but the stop codons were removed from reverse primer sequences (**Supplementary Table S1**). The resulting PCR products were cloned into pDONR207 and subcloned into pGWB5 via Gateway technology (Invitrogen) to produce, under the control of the CaMV *35S* promoter, full-length proteins fused to GFP at their C-termini (El-Azaz et al., 2016). Empty pGWB5 was used for negative controls. The *Agrobacterium tumefaciens* strain C58C1 was transformed by electroporation with recombinant plasmids. *N. benthamiana* leaves (5 weeks old) were syringe infiltrated with cultures containing pGWB5 constructs mixed with cultures containing the silencing suppressor p19 protein, both with an optical density of 0.5 at 600 nm, according to previously described procedures (Liu et al., 2002). Subcellular localization of proteins was examined by confocal microscopy 36–48 h after agroinfiltration.

Transient Expression of GFP-Proteins in Pine Protoplasts

To perform transient expression assays in pine protoplasts, fusions of PpPIIa with or without its putative chloroplastic transit peptide (cTP) and the GFP reporter gene were constructed using appropriate primers. Protoplasts were prepared from maritime pine cotyledons by incubation of 1 g of freshly cutted tissue in 10 mL of a mixture containing 0.44% (w/v) K3 medium: 0.4% (w/v) cellulase, 0.4% (w/v) macerase (Calbiochem), and 0.4% sucrose. Transformation with the gene constructs was performed by electroporation essentially as previously described by Gómez-Maldonado et al. (2004). After culture in the dark for 18–24 h, the transformed protoplasts were visualized by laser confocal microscopy using a Leica CLSM microscope. Excitation was conducted with a laser beam at 488 nm. Red autofluorescence of chlorophyll was detected up to 560 nm and green fluorescence of GFP was detected between 505 and 520 nm.

Overexpression and Purification of Recombinant Proteins

Open reading frames (ORFs) corresponding to *PpPIIa* and *PpPIIb* without the cTP were PCR-amplified using primers containing appropriate restriction sites. *PpPIIa* and *PpPIIb* forward primers contained a *NdeI* restriction site and the reverse primer contain a *XhoI* restriction site. Sequences are listed in **Supplementary Table S1**. PCR products were digested and subcloned into the pET30b at *Nde*I and *Xho*I sites. Plasmid constructs were sequenced and subsequently transformed into *E. coli* strain BL21-AI (Thermo Fisher Scientific). Cells were grown at 37°C by shaking in Luria–Bertani broth containing 50 μg mL^{-1} kanamycin until OD_{600} = 0.6; 0.2% arabinose (w/v) was added, and cultures were further incubated for 5 h at 30°C with shaking. Cells were pelleted by centrifugation at 4,500 × *g* and frozen. ORF corresponding to *PpNAGK* without the cTP was amplified using a specific forward primer (**Supplementary Table S1**). The resulting PCR product was cloned into the pDONR207, subcloned into the pDest17 vector via Gateway Technology (Invitrogen), and transformed into *E. coli* strain BL21-AI (Thermo Fisher Scientific). Bacterial growth and protein induction requirements were the same as described above but the media contained 100 μg mL^{-1} ampicillin instead. Recombinant proteins were purified by binding onto Ni-agarose resin (Protino NiNTA; Macherey-Nagel). Protein concentrations were determined by the Bradford dye-binding method (Bradford, 1976) and analyzed by SDS-PAGE to verify purification.

PpNAGK Activity Assays

The activity assay based on *N*-acetylglutamylhydroxamate production was performed according to the method described by Heinrich et al. (2004). The reaction mixture consisted of 400 mM NH_2OH-HCl, pH 7, 20 mM Tris/Cl, pH 7, 20 mM $MgCl_2$, 40 mM NAG, and 10 mM ATP. Reactions were initiated by the addition of reaction mixture, the incubation was carried out at 37°C in a volume of 150 μL and terminated by the addition of 150 μL of stop mixture [1:1:1 of 5% (w/v) $FeCl_3 \cdot 6\ H_2O$ in 0.2 M HCl, 8% (w/v) trichloroacetic acid, and 0.3 M HCl]. After standing for 5 min at room temperature, the tubes were centrifuged and the absorbance was immediately measured at 540 nm. The absorbance change was linear with time of incubation in the enzyme assay for at least 30 min. Controls were carried out that did not contain *N*-acetylglutamate. There was no activity when no NAGK was added. To estimate the molar amount of *N*-acetylglutamylhydroxamate formed a molar absorption coefficient was used of 456 $M^{-1}cm^{-1}$ at 540 nm (Heinrich et al., 2004).

N-acetylglutamate kinase activity was also determined by a continuous spectrophotometric assay in which the production of ADP was coupled to NADH oxidation via pyruvate kinase

[1]http://www.scbi.uma.es/sustainpinedb/sessions/new

(PK) and lactate dehydrogenase (LDH) (Cánovas et al., 1984). The reaction mixture containing 100 mM Hepes, pH7, 10 mM $MgCl_2$, 10 mM ATP, 40 mM *N*-acetylglutamate, 1 mM phosphoenolpyruvate, 0.6 mM NADH, and 1 unit each of PK and LDH. Assays were performed in 100 μL volumes and incubated at 37°C in multi-well plates for 5 min. The blank reactions did not contain *N*-acetylglutamate.

Gel Filtration Chromatography of Purified PII Proteins

Protein samples were diluted to a concentration of 0.6 μg/μL in a solution of 25 mM Tris-HCl, pH 7.5, 150 mM NaCl, 10% (v/v) glicerol, and a 250 μL sample was then chromatographed on a ENrich^{TM} SEC 650 10 × 300 column (BioRad) equilibrated at room temperature in Tris/HCl buffer. The fast protein liquid chromatography flow rate was 0.75 mL/min, and 100 μL fractions were collected.

The column was calibrated with ribonuclease A (13.7 kDa), carbonic anhydrase (29 kDa), bovine serum albumin (66 kDa), alcohol dehydrogenase (150 kDa), ß-amylase (200 kDa), apoferritin (440 kDa), and blue dextran (void volume of the column).

Western Blot and Antibody Production

The presence of proteins in the elution fractions was detected by SDS-PAGE and western blot analysis with anti-PII antibodies as described previously (Cánovas et al., 1991). Antibodies against PpPIIa were raised in rabbits by immunization with PpPIIa recombinant protein overexpressed in *E. coli* as described by Cantón et al. (1996). The primary antibodies anti-PpPIIa were used at 1:10,000 dilution and a 1:10,000 dilution of horseradish peroxidase conjugated antirabbit serum (Sigma) was used as a secondary antibody.

Yeast Two-Hybrid Assay

Interaction assays in yeast were performed with the yeast Two-Hybrid System (YTH) of Invitrogen. PpNAGK was cloned into Gateway pDEST22 vector by LR recombination reaction to form the prey plasmid, whereas PpPIIa and PpPIIb were cloned into Gateway pDEST32 vector by LR recombination reaction to form the bait plasmids. Two mutations were produced in PpPIIa corresponding to a single change of a glutamate for lysine (Glu18Lys) and a triple amino acid change: valine, alanine, and glycine, for alanine, glycine, and alanine (Val58Ala/Ala60Gly/Gly61Ala). Site-directed mutagenesis was performed through a PCR-based strategy using iProof high-fidelity DNA polymerase (Bio-Rad) and cloned into pDEST32 vector. Specific primers were used for amplification under the following conditions: 2 min at 98°C, followed by 20 cycles (10 s at 98°C, 20 s at 60°C, and 7 min at 72°C) and a final elongation of 4 min at 72°C. Samples were treated with *Dpn*I (Thermo Scientific^{TM}) to eliminate native methylated plasmid DNA, and the PCR product was transformed into *E. coli* DH5α with selection on 100 μg mL^{-1} gentamicin. All of the constructs were verified by sequencing and co-transformed into yeast stain MAV203 using the LiAc method following the yeast transformation instructions of Invitrogen. Transformed yeasts were selected at 30°C on synthetic defined (SD) media agar plates without leucine and tryptophan.

To identify strong interactions, individual transformants were characterized on SD agar plates without leucine, tryptophan, and histidine, supplemented with 10, 25, 50, and 100 mM 3-AT (3-Amino-1, 2, 4-triazole, Sigma) and on SD agar plates without leucine, tryptophan, and uracil.

Positive colonies were grown in liquid media to the stationary phase. Aliquots of 1 mL were taken and cells were pelleted at 11,000 × *g* for 30 s, the media was removed and the cells were then washed five times with sterile distilled water (SDW). Cells were then resuspended in SDW and diluted 10, 100, and 1000 times. A volume of 10 μL from each sample was spotted onto plates containing SD media without leucine, tryptophan, and uracil. Plates were incubated at 30°C for 3 days and photographed.

Quantitative β-Galactosidase Assay

Strong YTH interactions of PpNAGK with PpPIIa and PpPIIb were quantified by the liquid β-galactosidase assay with ONPG (*o*-nitrophenyl β-D-galactopyranoside; Sigma Cat No. N-1127), following the Yeast Protocols Handbook user manual from Clontech Laboratories. All measurements were made in triplicate.

RNA Extraction and Expression Analysis

RNA extraction from maritime pine samples was performed as described by Canales et al. (2012). Synthesis of cDNA was made with 5X iScript^{TM} cDNA Synthesis Kit (Bio-Rad). The qPCR analysis was done in a thermal cycler CFX384 (Bio-Rad). Sequences of *PpPIIa* and *PpPIIb* specific primers are listed in **Supplementary Table S1**. Actin-7 was used as a reference gene. Relative expression profiles for each gene were obtained employing the R package (Ritz and Spiess, 2008) and normalized to the reference gene. For the qPCR analysis, three biological replicates and three technical replicates per sample were made.

Structural Modeling and Calculations

Structural models for PpPIIa and PpPIIb were generated with the Swiss-Model Server (Biasini et al., 2014) using as template the structure of the *Chlamydomonas* PII protein as observed in its crystal structure in complex with the NAGK from *Arabidopsis thaliana* (PDB entry 4USJ, chain C). Alternative models were generated with the I-TASSER suite (Yang et al., 2015), from which the geometry of the first 10 residues was predicted. Energy minimization and structural superpositions were performed with the 1.11.2 version of the UCSF Chimera package[2] (Pettersen et al., 2004). The electrostatic Poisson–Boltzmann (PB) potential was deduced with the 300 APBS tools in PyMol 1.7.6.7 (Schrödinger, LLC) assigning AMBER atomic charges and radii. The non-linear PB equation was solved in sequential multigrid calculations at 298 K with dielectric constants of 2 for proteins and 78.54 for water. Values of potential are given in kT units per unit charge (k, Boltzmann's constant; T, absolute temperature). PB potentials

[2]www.rbvi.ucsf.edu/chimera

mapped onto protein surfaces were rendered with PyMOL. Other figures were rendered with UCSF Chimera.

RESULTS

In silico Profile of Maritime Pine PII

Recent developments in next generation sequencing have provided a range of genomic resources for maritime pine (Canales et al., 2014; Cañas et al., 2017, 2019). The *in silico* analysis of its transcriptome revealed the existence of two different transcripts encoding putative PII proteins that were named *PpPIIa* and *PpPIIb* (**Supplementary Figure S1**). A striking characteristic of these transcripts is that their sequences mostly differ in the 5'-unstranslated region and the ORF, with minor changes in the 3'-unstranslated region (**Supplementary Figure S1**).

The ORFs of *PpPIIa* and *PpPIIb* encode polypeptides of similar size, with PpPIIa being three amino acids longer (**Supplementary Table S2**). Upon removal of the putative cTP, mature PpIIa and PpIIb proteins would have equal number of amino acids although their sequences differ in 15 amino acid residues (∼90% identity), with all the amino acid changes spread over the first half of the amino acid sequence of the mature putative proteins (**Figure 1**). Whereas most changes are conservative, a substantial change of glutamate for lysine was identified at position 18 of the mature proteins (**Figure 1A**, asterisk). Since only a single form of PII has been previously described in angiosperms, the occurrence of PII variants was further investigated in those conifers for which transcriptomic data are available. In addition to *P. pinaster*, several pine species contain two PII variants, including *Pinus taeda*, *Pinus contorta*, and *Pinus lambertiana*. However, only one PII form was found in spruce species (**Figure 1B**). Their amino acid sequences were highly conserved in pine including the aforementioned non-conservative shift at position 18. The phylogenetic analysis of PII protein variants clearly classified the pine proteins in two separate clusters, with the PIIb cluster being closer to PII proteins from other conifer species that represent an intermediate branch between pines and herbaceous plants (**Figure 1C**).

Localization of Maritime Pine PpPII

To further understand the biological roles of these proteins, their subcellular localization was determined (**Figure 2**). The ORFs of PpPIIa and PpPIIb were PCR-amplified and cloned into the Gateway vector pGWB5 and the resulting GFP fusions were transiently expressed in *N. benthamiana* leaves via agroinfiltration. The GFP fluorescence of both PpPIIa and PpPIIb fusion products was exclusively associated to chloroplasts, which were visualized by the red autofluorescence of chlorophyll. The merged images showed co-localization of chlorophyll (red) with both GFP–PpPIIa and GFP–PpPIIb (yellow) in the chloroplasts, indicating a plastidic localization for both proteins (**Figures 2A1,A2**).

To further substantiate this finding, GFP fusions for PpPIIa were constructed with and without cTP and electroporated into isolated maritime pine protoplasts. **Figure 2B** shows that GFP–PpPIIa constructs containing the cTP were appropriately targeted to the chloroplasts (**Figure 2B2**), as it was also observed for control constructs with cTP but lacking the PpPIIa coding sequence (**Figure 2B4**). However, only cytosolic GFP signals were observed for the constructs lacking cTP (**Figure 2B3**).

Structural Models of PpPIIa and PpPIIb

To gain insight into the functional significance of the amino acid differences found between mature PpPIIa and PpPIIb, their three-dimensional structures were modeled with the Swiss-Model server using as template the reported structure of Chlamydomonas PII (taken from PDB entry 4USJ, see section "Materials and Methods"), as well as by using I-TASSER, which chooses automatically model structures from the PDB database. Despite the different approaches and models used by these servers, both servers predicted essentially the same geometries for the protein cores (RMSD of 0.63–0.64 Å). The overall fold (137 residues) was remarkably similar to the X-ray structures of PII proteins previously crystallized in complex with NAGK, such as *A. thaliana* PII (AtPII; PDB entry 2RD5; Mizuno et al., 2007), *Synechococcus elongatus* PII (SePII; PDB entry 2V5H; Llácer et al., 2007), and *Chlamydomonas reinhardtii* (CrPII; PDB entry 4USJ; Chellamuthu et al., 2014) (**Figure 3A**). CrPII was the template we selected for Swiss-Model, to obtain atomic coordinates for the Q-loop residues (see below). The structural alignment of these experimentally solved proteins with PpPIIa rendered RMSD values as low as 0.29 Å (CrPII; 132 Cα pairs), 0.67 Å (AtPII; 127 Cα pairs), and 0.70 Å (105 Cα pairs), bolstering the validity of the predicted geometries. PpPIIa and PpPIIb appeared to contain all the secondary structure elements distinctive of PII proteins (reviewed by Forchhammer and Lüddecke, 2016), including the T-loop involved in Mg^{2+}. ATP binding and the C-terminal Q-loop for glutamine sensing (**Figure 3B**). PII proteins from cyanobacteria and Brassicaceae lack a glutamine binding site at the C-terminal part of the polypeptide (SePII and AtPII in **Figure 3A**). The conserved spatial positions of key residues for ligand binding allowed us to dock Mg^{2+}. ATP in the T-loop of both models, and the same is true for glutamine in the Q-loop (**Figure 3B**). Based on the known architectures for PII-NAGK complexes, we also analyzed the putative contact region with NAGK. Specific residues of the pine PIIs can be predicted to stabilize the heterodimer by interacting with complementary groups located near the end of helices αE and αG of NAGK as well as in the neighboring strands β6 and β7 (**Figure 3C**). On the PII side, the key interacting residues were located at the end of the α1-helix (W31) and in the T-loop (mainly R65, S69, and E70; numbering for PpPIIa). More specifically, W31 would participate in both hydrogen bonding (backbone) and hydrophobic contacts, whereas the T-loop residues are predicted to form hydrogen bonds and electrostatic interactions with oppositely charged residues of NAGK. While the above structural analyses are consistent with a common mechanism of action for PpPIIa and PpPIIb, calculations of the PB electrostatic potential might explain the presence of two isoforms in maritime pine. We performed a thorough comparison of the electrostatic potential projected onto the surface of both proteins and did not find

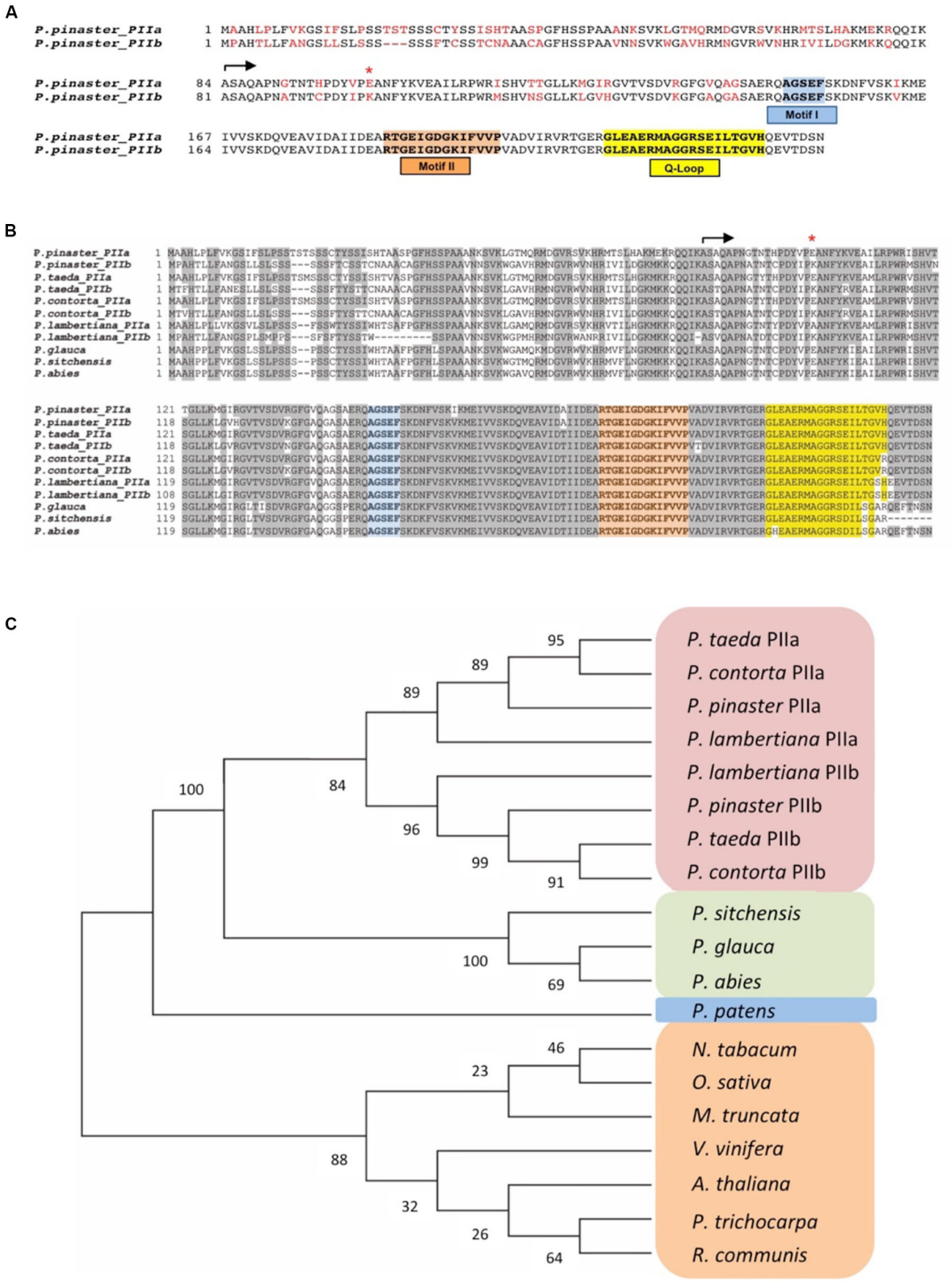

FIGURE 1 | Comparison of PII sequences. **(A)** Predicted PpPII protein sequences. The conserved sequence motifs (I and II) and the Q Loop position are boxed. The beginning of both mature polypeptides is indicated by an arrow. Residues differing in the two variants are marked in red. The red asterisk highlights a significant amino acid change at position 18 of the mature proteins (see text). **(B)** Multiple alignments of PII proteins from pine species executed with Clustal X. Conserved sequence motifs in PII proteins are highlighted: in blue Motif I, in orange Motif II, and in yellow the conserved Q-loop of plants. **(C)** Phylogenetic analysis of PII proteins in angiosperm and gymnosperm species. Alignments were imported into the Molecular Evolutionary Genetics Analyses (MEGA) software version 7.0 (Kumar et al., 2016). The phylogenetic tree was constructed with the full-length PII amino acid sequences using the neighbor-joining method. Protein sequences were obtained from the following databases: NCBI (www.ncbi.nlm.nih.gov), PlantGDB (www.plantgdb.org), TAIR (https://www.arabidopsis.org), SustainPineDB v.3.0 (http://www.scbi.uma.es/sustainpinedb/sessions/new), and PLAZA (https://bioinformatics.psb.ugent.be/plaza/versions/gymno-plaza).

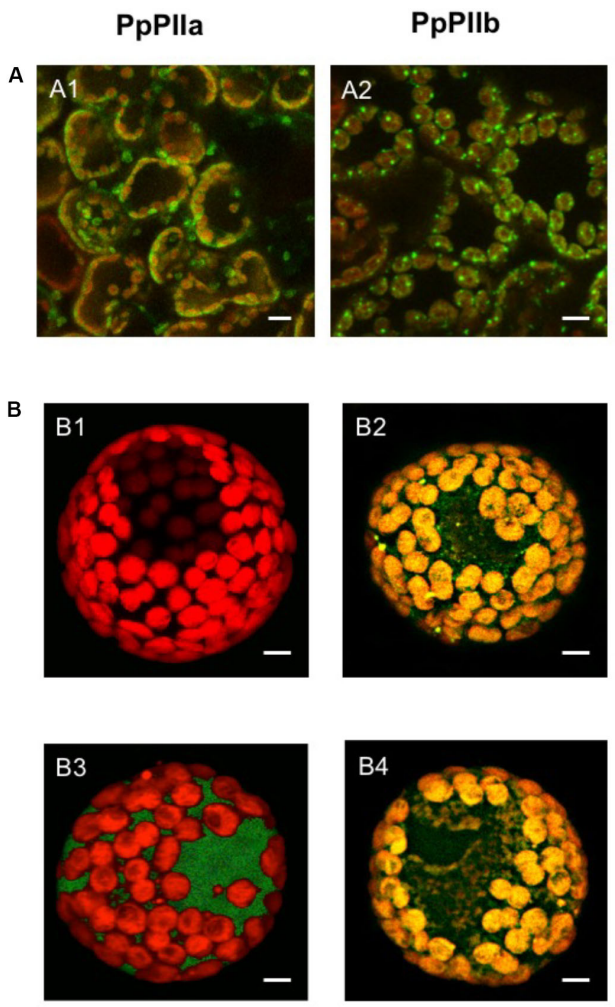

FIGURE 2 | Subcellular localization of PpPIIa and PpPIIb. **(A)** Localization in *N. benthamiana* leaves. **(A1,A2)** GFP-chlorophyll merged images showing respective localizations in the chloroplast of PpPIIa and PpPIIb. **(B)** Localization in isolated pine protoplasts. A single cell is shown containing plastids. **(B1)** control with no construct; **(B2)** GFP–PpPIIa construct containing transit peptide (cTP); **(B3)** GFP-PpPIIa construct without cTP; **(B4)** GFP-control construct without the PpPIIa protein but containing cTP. Scale bar represents 10 μm.

any significant difference for the regions involved in interacting with NAGK (**Figure 3D**, left) or PII trimerization (not shown). However, a significant effect was observed for the substitution of glutamate at position 18 of PpPIIa for lysine in PpPIIb. This notable change in the electrostatic features of the N-terminal extension (Mizuno et al., 2007) occurs in the vicinity of the Q-loop, not far from the glutamine-binding pocket (**Figure 3D** right). It has been suggested that such N-terminal extension, which maps on the opposite side of the trimer than the surface of interaction with NAGK, may be involved in protein–protein interactions and signaling (Mizuno et al., 2007; Selim et al., 2020a). Interestingly, most non-conservative mutations occur in this extension (see the alignments presented in **Figure 1**).

Activity of the Complex PpNAGK–PpPII

The mature PII isoproteins from maritime pine were recombinantly expressed in *E. coli* to raise monospecific antibodies and for further characterization (**Supplementary Figure S2**). Moreover, sufficient amounts of recombinant native proteins were necessary to perform functional studies on the interaction of PpPIIa and PpPIIb with pine NAGK (PpNAGK) and to investigate how this interaction is regulated by the availability of glutamine and 2-OG.

The native molecular mass of PpPIIa and PpPIIb was determined by gel filtration chromatography through a FPLC column calibrated with protein standards (**Figure 4**). The molecular mass of both holoproteins was estimated to be 57 kDa, a figure compatible with a trimeric structure for the native proteins.

The target enzyme of maritime pine PpPII proteins is PpNAGK, a protein of 352 amino acids. The N-terminus of the predicted polypeptide targets the protein to plastids, where the mature enzyme has been recently localized (Llebrés et al., 2018b). To examine the potential differences in the interaction of PpPIIa and PpPIIb with their target enzyme, a full-length cDNA for PpNAGK was amplified using appropriate primers. A construct encoding the mature PpNAGK enzyme (301 residues without cTP) was fused to a His-tag and overexpressed in *E. coli*. The resulting recombinant protein was purified by affinity chromatography and next used for additional studies.

The enzyme activity of PpNAGK was increased up to aproximately fivefold when any of the two PII proteins was added in increasing concentrations (**Figure 5A**). Higher concentrations of PpIIa than of PpPIIb protein appeared necessary to achieved full activation of NAGK, with the maximal activation being similar for the two isoproteins. Potential differences in the interaction of PpPII isoproteins and PpNAGK were further examined by YTH analysis (**Supplementary Figure S3**). As depicted in **Supplementary Figure S3A**, the interaction was much weaker for PpPIIb-PpNAGK than for PpPIIa-PpNAGK. To study the molecular basis of this difference, we performed mutations in the PpPIIa sequence, including the change of glutamate for lysine at position 18 (Glu18Lys) and the switch of the three amino acids near the T-loop (valine, alanine, and glycine for alanine, glycine, and alanine) at positions 58, 60, and 61, respectively (Val58Ala/Ala60Gly/Gly61Ala) (**Supplementary Figure S3B**). Quantitative comparisons using the β-galactosidase assay confirmed the observed differences in the formation of PpPII-PpNAGK complexes and showed that these amino acid changes did not affect the interaction of PpPIIa with PpNAGK.

To further characterize the sensor properties of PpPIIa and PpPIIb toward PpNAGK, the effect of glutamine was studied in the presence of varying amounts of arginine. When the PpPIIa-PpNAGK complex was allowed to form, arginine inhibition was significantly relieved by adding glutamine (**Figure 5B**). Interestingly, a similar effect of glutamine was observed for the PpPIIb–PpNAGK complex (**Figure 5C**).

Subsequent experiments were undertaken to study whether PpNAGK activity could be affected by the interaction of both PpPIIa and PpPIIb at varying levels of 2-OG. As shown in **Supplementary Figure S4**, the addition of PpPIIa and

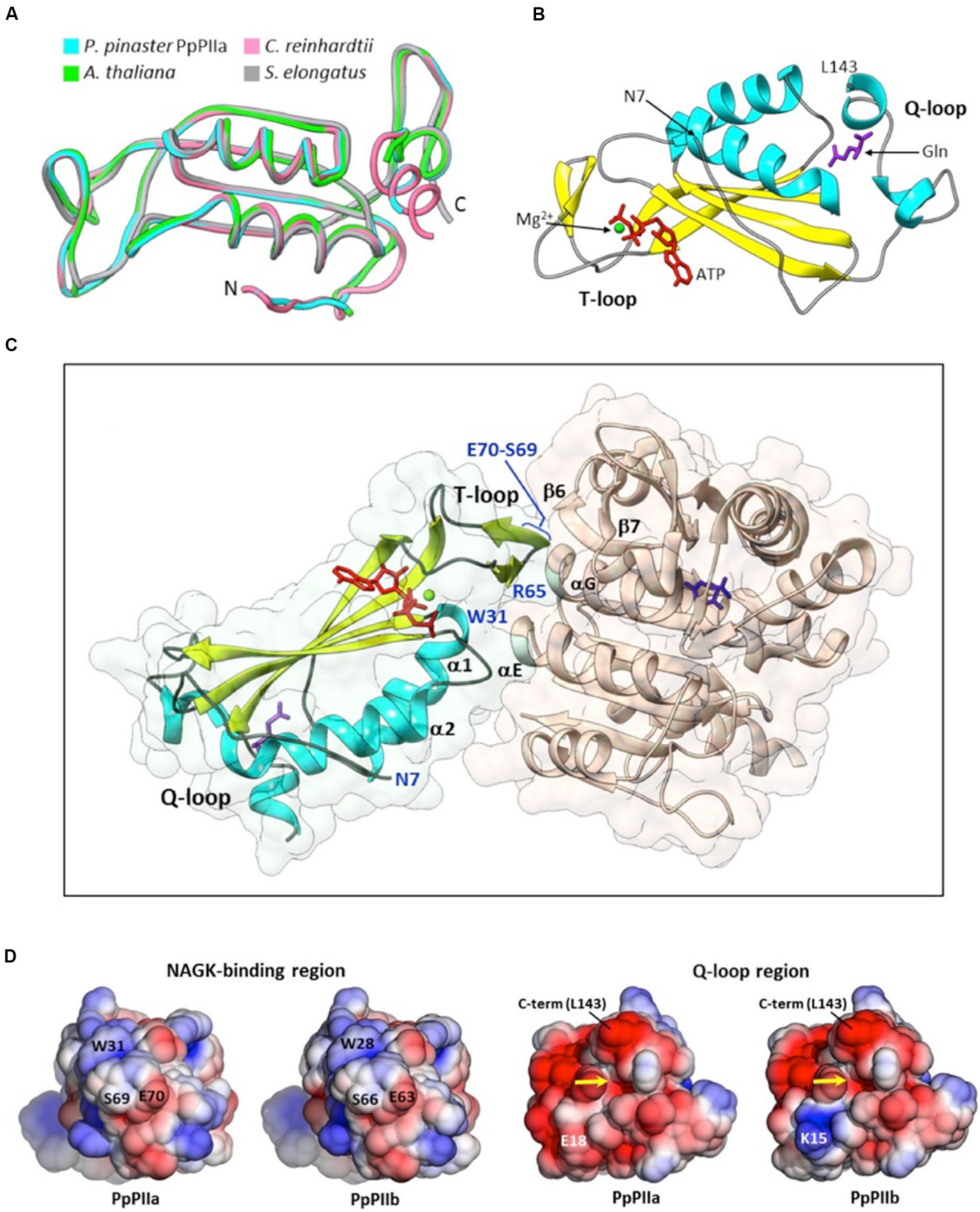

FIGURE 3 | Model structures for PpPIIa and PpPIIb. **(A)** Structural alignment of modeled PpPIIa and the experimentally solved structures for AtPII (PDB entry 2RD5), SePII (PDB entry 2V5H), and CrPII (PDB entry 4USJ), three homologous proteins crystallized in complex with NAGK and various ligands. **(B)** Cartoon representation of PpPIIa, highlighting the position of the N-terminal extension, the T-loop and the Q-loop. The position of L143 (PpPIIa numbering; C-terminal end of the model) is also indicated. Docked ligands: Mg^{2+} (green), ATP (red), and glutamine (purple). Compared to **(A)**, this view is rotated about 90° upward. **(C)** Side view of a dimer between PpPIIa and/**/NAGK from *A. thaliana* (PDB code 2RD5). The PII residues directly involved in interactions with the *Arabidopsis* enzyme are highlighted in blue, like the N-terminus of the model (N7). A molecule of *N*-acetylglutamate is shown at the active site of AtNAGK (dark blue). **(D)** Electrostatic potential distribution mapped to the solvent-accessible surfaces of PIIa and PIIb at two opposed ends: the region for NAGK binding (left pair) and the confluence of the N-terminal extension and the Q-loop (right pair). The glutamine-binding site is indicated by a yellow arrow. The potential is shown as a colored gradient from red (acidic) at -2.5 kT/e to blue (basic) at 2.5 kT/e (where k is Boltzmann's constant, T is temperature, and e is the charge on an electron).

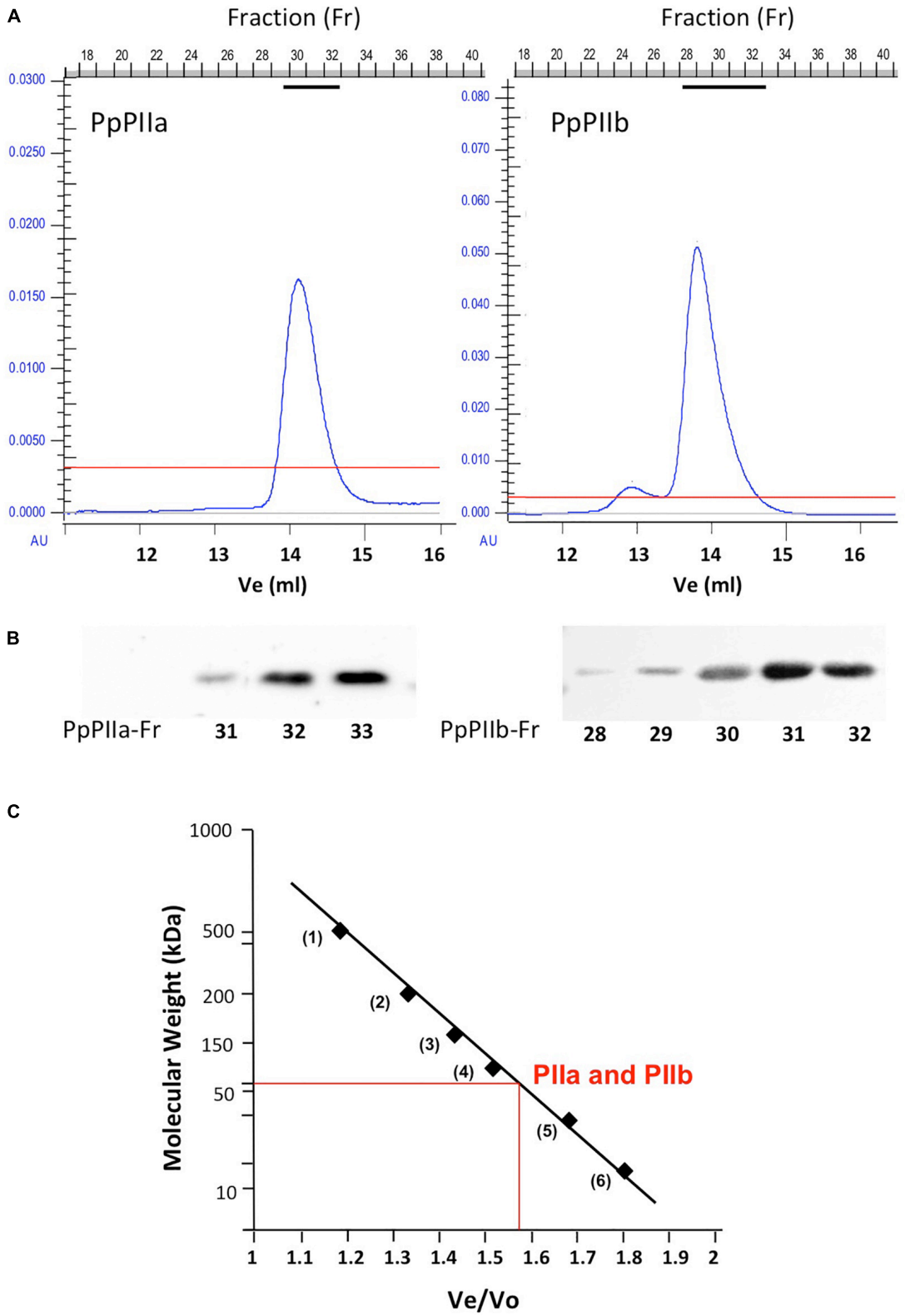

FIGURE 4 | Estimation of the molecular size of native PpPII proteins by gel filtration chromatography. **(A)** Elution profile of recombinant PpPIIa and PpPIIb proteins using gel filtration in an FPLC system. **(B)** Protein-containing fractions were tested by western blotting using monospecific antibodies against PpPIIa. **(C)** Estimation of PpPIIa and PpPIIb molecular mass using protein markers of known molecular size.

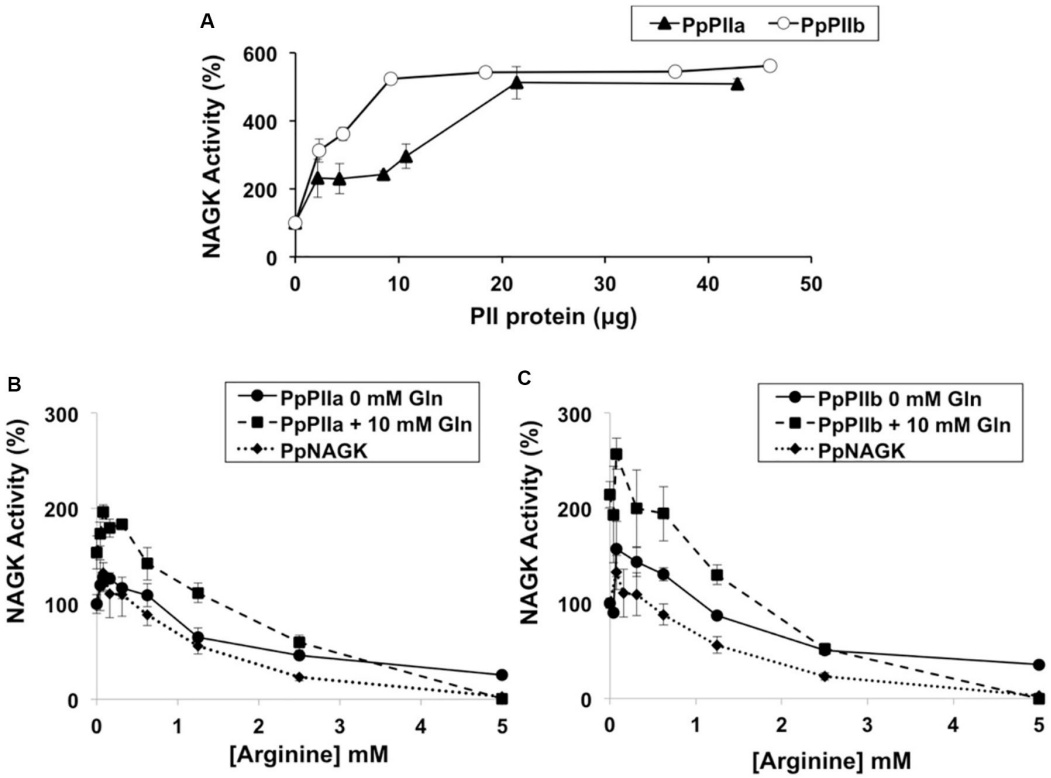

FIGURE 5 | Effects of PpPIIa and PpPIIb on the PpNAGK activity. **(A)** Effect of increasing amount of PpPIIa (black triangles) and PpPIIb (open circles) proteins on PpNAGK activity. The indicated amounts of PpPII were mixed with 0.65 µg PpNAGK, and the mixtures were placed at 4°C for 10 min to allow complex formation. The reaction was initiated by the addition of the reaction mixture into the PpNAGK-PpPII complex mixture. The *N*-acetylglutamylhydroxamate assay was used. **(B)** PpNAGK–PpPIIa complex activity inhibition by arginine with or without added glutamine. **(C)** PpNAGK–PpPIIb complex activity inhibition by arginine with or without added glutamine. Glutamine 10 mM (black squares); glutamine 0 mM (black circles). PpNAGK activity inhibition by arginine is also shown (black triangles). To test the effect of arginine on the PpNAGK–PpPII complexes, PpPII was first added into the diluted PpNAGK solution, and the two proteins were placed at 4°C for 10 min to allow complex formation followed by the addition of arginine. The arginine effect was also tested in combination with 10 mM glutamine as described above. The continuous spectrophotometric assay was used. Values are the mean ± SD of three independent determinations. NAGK activities (100%) were **(A)** 108.80 ± 14.35, **(B)** 726.15 ± 71.58, and **(C)** 563.17 ± 29.68 nkatal/mg protein. The reaction mixtures contained **(A)** 0.65, **(B)** 0.35, and **(C)** 0.35 µg of PpNAGK protein. The observed increase of PpNAGK activity with PpPIIa and PpPIIb was significant by *t*-test with a $P < 0.1$ and enhanced in presence of glutamine with a $P < 0.05$. Arginine inhibition was significantly relieved by adding glutamine ($P < 0.01$) in both PpNAGK–PpPII complexes. Each reaction mixture contained 0.35 µg of PpNAGK protein and 0.7 µg of PpPIIa and 0.7 µg PpPIIb.

PpPIIb enhanced PpNAGK activity already in the absence of glutamine. Nevertheless, under these experimental conditions, no significant differences in activity were observed at various 2-OG concentrations.

Expression of PpPIIa and PpPIIb Genes

To further explore the potential roles of PII isoproteins in maritime pine, gene expression levels were analyzed during the last stages of embryogenesis and seed germination (**Figure 6**). The relative levels of *PpPIIa* transcripts were much higher than those *PpPIIb* observed in all stages examined, with an upper abundance in the seed embryos.

DISCUSSION

A bioinformatics survey of the maritime pine transcriptome revealed the occurrence of two transcripts (*PpPIIa and PpPIIb*) encoding PII proteins (**Supplementary Figure S1**). They have similar molecular size but differ in their amino acid sequence (**Figure 1**). This finding is novel because only one form of PII has been reported to exist in other plant species (Chen et al., 2006). Interestingly, two PII homologs have also been identified in several pine species for which large transcriptomics data are available. In contrast, only one PII gene product has been found in spruce species (**Figure 1**). Taken together, our results suggest that the existence of PII variants is not a general characteristic of conifers and seems to be restricted to pines.

As the sequence of the maritime pine genome is still not available, we searched for PII homologs in the loblolly pine (*P. taeda*) genome (Neale et al., 2014). The goal was to figure out whether the two *PII* transcripts were encoded by distinct genes or they were the result of a differential splicing. The sequences for *PtPIIa* and *PtPIIb* were located in the same scaffold, but were interrupted by large gaps that prevented the retrieval of a complete gene structure.

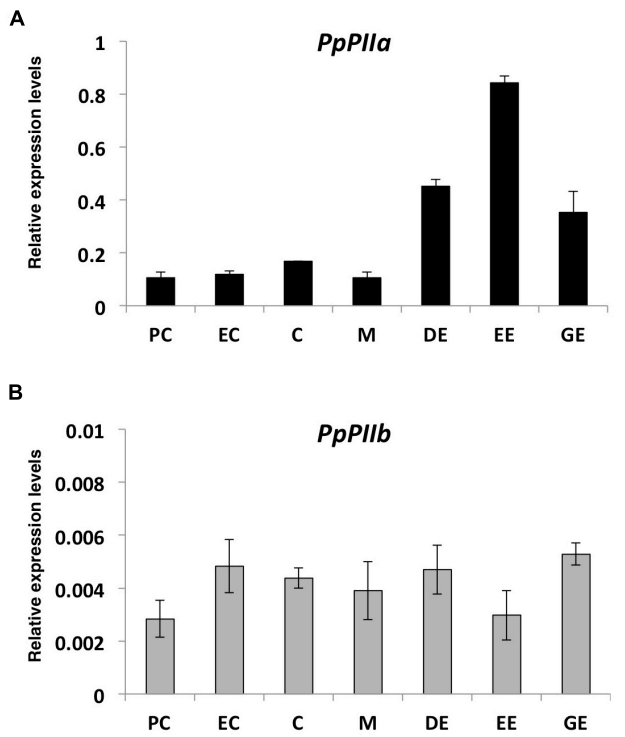

FIGURE 6 | Expression analysis of pine *PII* genes during embryogenesis and early stages of seed germination **(A)** PpIIa; **(B)** PpIIb. PC, pre-cotyledonary stage; EC, early-cotyledonary; C, cotyledonary; M, cotyledonary partially mature; DE, dry embryo; EE, embedded embryo; GE, germinated embryo. The expression level for the two genes was normalized to that of *actin-7*, used as reference gene. Bars represent mean values of three assays, with three biological replicas each ± SD. Black rectangles are used for *PpPIIa gene* and gray rectangles for the *PpPIIb* gene.

Considering the primary structure of their cDNAs, the most plausible explanation is that PtPIIa and PtPIIb are the result of alternative splicing of a single gene. No different 3'-untranslated regions were amplified from a range of different pine tissues by rapid amplification of cDNA ends (RACE). The above conclusion is reinforced by the identification of a similar pattern of hybridizing bands in a Southern blot of pine genomic DNA digested with several restriction enzymes (**Supplementary Figure S5**).

Sequence analysis of the polypeptides encoded by *PtPIIa* and *PtPIIb* identified a putative cTP in their N-terminal end. Nevertheless, the existence of two forms of PII could be related with a distinct subcellular localization in pine cells. To investigate this hypothesis, we conducted subcellular localization studies (**Figure 2**). Our results confirmed that PpPIIa and PpPIIb are located in the chloroplastic stroma, as previously reported for their *Arabidopsis* PII homolog (Chen et al., 2006). PpPIIa and PpPIIb are therefore able to interact *in vivo* with their target enzyme, PpNAGK, which is located in the same compartment in pine cells (Llebrés et al., 2018b).

The three-dimensional models of PpPIIa and PpPIIb are highly similar to the previously described crystal structures of PII proteins from *Synechococcus* and *Arabidopsis* (Mizuno et al., 2007; Llacer et al., 2008).

These two structurally characterized PII proteins lack a glutamine site, unlike PpPII proteins, judged from sequence comparisons and from the observation of activation of NAGK activity by glutamine addition to mixtures of PpNAGK and PpPII proteins (**Figures 5B,C**).

The ability to sense glutamine levels, and therefore the cellular N status, relies on a C-terminal extension of the PII polypeptide that is unique of plant proteins (Chellamuthu et al., 2014). The Q loop is disordered in the absence of glutamine, but becomes ordered when the amino acid is present, which triggers in turn a specific interaction with the basal part of the T loop. The signal is then transmitted through a conformational change that favors the interaction of PII with NAGK (Chellamuthu et al., 2014; Forchhammer and Lüddecke, 2016). The change of glutamate (PpPIIa) for lysine (PpPIIb) at position 18 is spatially close to the Q loop and therefore likely to affect the above mechanism or its regulation. As shown in **Figure 3**, it causes a major effect on the electrostatic features of this region.

Overexpression of recombinant PpPIIa and PpPIIb in *E. coli* allowed us to confirm their trimeric nature (**Figure 4**), in line with previous observations for PII proteins from plants and microorganisms (Chen et al., 2006; Forchhammer and Lüddecke, 2016). Moreover, the overproduction in *E. coli* of PpNAGK, the target enzyme of PpPII, enabled us to study the formation of PpNAGK–PpPIIa and PpNAGK–PpPIIb complexes. The binding of both PpPIIa and PpPIIb to PpNAGK increased the activity of this enzyme (**Figure 5**). A similar observation was previously reported in *Arabidopsis* (Chen et al., 2006). PpNAGK activation suggests high affinity of PpPIIa and PpPIIb for PpNAGK in the formation of regulatory complexes, what was experimentally confirmed by YTH analysis. The sequence changes between these two proteins at positions 18 (Glu18Lys) and near the T-loop (three amino acid changes) did not affect the formation of the complex with PpNAGK, as shown by site-directed mutagenesis experiments with PpPIIa (**Supplementary Figure S3**). Together, the above results suggest that the observed differences between PpPIIa and PpPIIb regarding complex formation with PpNAGK are not only based in single amino acid changes.

To better characterize PpPII proteins, we also analyzed the effects of 2-OG, arginine, and glutamine on the formation of regulatory complexes with PpNAGK. The addition of increasing amounts of 2-OG did not affect PpNAGK activity when the enzyme from maritime pine was incubated in the absence of PpPIIa or PpPIIb (**Supplementary Figure S4**). Likewise, 2-OG did not influence PpNAGK activity when complexed with any of the two PpPII proteins, suggesting that, as in other plants having glutamine-sensing PII proteins (Chellamuthu et al., 2014), 2OG did not dissociate the complex of the two proteins. Actually, glutamine proved essential for PII-NAGK complex formation in *Chlamydomonas* and some plant species studied (excepting *A. thaliana*, which does not sense glutamine) but this appears not to be the case in maritime pine for any of it two PII proteins, although it might increase the affinity of these PpPII proteins for PpNAGK, a situation that is reminescent of that recently

uncovered for the non-photoxynthetic alga *Polytomella parva* (Selim et al., 2020b).

It is well documented that the more sensitive assay for the PII-NAGK interaction is the relief of the inhibition of enzyme activity caused by arginine (Llacer et al., 2008). Chellamuthu et al. (2014) reported that glutamine is able to further relieve this feedback inhibition when NAGK is bound to PII. We have observed enhanced PpNAGK *in vitro* activity in the presence of PpPIIa and PpPIIb, when glutamine was present (**Figure 5**). The results suggest that PpPIIa and PpPIIb are equally effective in sensing glutamine and thus PII redundancy in pine does not appear to affect the sensing of glutamine. Alternatively, one may speculate that the occurrence of two PII variants might increase the dosage for sensing this amino acid, similarly as reported for enhanced glutamine biosynthesis in *Populus* (Castro-Rodríguez et al., 2015). Nevertheless, a differential role of PpPIIa and PpPIIb in other physiological conditions cannot be excluded.

In this regard, the expression patterns of both *PpPII* genes were analyzed at early stages of development to identify if each one may fulfill distinct roles during maritime pine embryogenesis and early growth (**Figure 6**). *PpPIIa* exhibited higher expression levels than *PpPIIb* suggesting its predominance, at least at these stages of development. *PpPIIa* transcripts were particularly abundant at the end of maturation and the beginning of germination when arginine metabolism is highly active. In contrast, *PpPIIb* displayed low expression levels at all stages examined (**Figure 6**). These results suggest different roles for these isoproteins, likely regulating in a different manner arginine metabolism through their interaction with PpNAGK.

CONCLUSION

In summary, we have identified two different forms of PII in maritime pine. They are most likely the splicing products of a single gene and their existence seems to be restricted to pines: a single PII has been identified in other conifer species and in angiosperms. PpPIIa and PpPIIb are trimeric proteins with similar three-dimensional structure and subcellular location. The PII-target enzyme PpNAGK is localized to the same compartment. The interactions of both recombinant PpPII variants and PpNAGK appear to be enhanced by glutamine, relieving the feedback inhibition of PpNAGK activity by arginine in the mM range. PpIIa appears to play a predominant role during maritime pine embryogenesis and germination.

DATA AVAILABILITY STATEMENT

All datasets generated for this study are included in the article/**Supplementary Material**.

AUTHOR CONTRIBUTIONS

ML, CV, FT, JV-M, and MP performed the experimental work. ML prepared the figures. LG was in charge of protein modeling. FC and CA conceived the project, supervised the work, and wrote the manuscript with contributions from FT, MP, and LG.

FUNDING

This research work was supported by grants from "Ministerio de Ciencia e Innovación" (BIO2015-69285-R and RTI2018-094041-B-I00) and Junta de Andalucía (BIO-474 and BIO-114).

ACKNOWLEDGMENTS

We are indebted to Dr. Rafael Cañas for adapting the coupled enzymatic assay to multi-well microtiter plates. We also thank Remedios Crespillo at the Molecular Biology laboratory (Universidad de Málaga Research Facilites) for excellent technical support.

SUPPLEMENTARY MATERIAL

The Supplementary Material for this article can be found online at: https://www.frontiersin.org/articles/10.3389/fpls.2020.00823/full#supplementary-material

FIGURE S1 | Primary structure of *PpPII* full-length cDNAs. Initial and stop codons are marked in red. The position of the primers utilized for the expression analysis is underlined in red.

FIGURE S2 | Purification of recombinant PpPIIa and PpPIIb proteins overproduced in *E. coli*. **(A)** Purification progress of PpPIIa. **(B)** Purification progress of PpPIIb. M, molecular makers; C, bacterial crude extract; F, flow-through eluate; W1, wash step 1; W2, wash step 2; lanes 1–5, elution of purified protein. Fractions 3 and 4 were collected for the studies performed in this work.

FIGURE S3 | Yeast two-hybrid interaction analysis. **(A)** Auxotrophic analysis of interaction of PpNAGK and PpPIIa or PpPIIb. Tranformants were analyzed in SD agar plates without tryptophan, leucine, and uracil, and several dilutions were made. **(B)** Diagram of amino acid changes performed in the isoprotein PpPIIa ($PpPIIa^{Mut1}$: Glu18Lys and $PpPIIa^{Mut2}$: Val58Ala/Ala60Gly/Gly61Ala). **(C)** β-Galactosidase activity. Bars represent mean values of three assays, with three biological replicates each ± SD; asterisk indicates significant difference between samples at $P < 0.05$.

FIGURE S4 | Effect of 2-OG concentration on PpNAGK activity. The activity of enzyme was measured in the presence of varying amounts of 2-OG, either without PpPII protein added (black triangles), or in the presence of PpPIIa (black squares) or PpPIIb (open circles) at the PpNAGK–PpPII ratios indicated. Each reaction mixture contained 0.65 μg of PpNAGK protein and 6.5 μg of PpPIIa and 6.5 μg PpPIIb. The *N*-acetylglutamylhydroxamate assay was used. Bars represent mean values of three independent experiments ± SD.

FIGURE S5 | Southern blot analysis of pine genomic DNA. Isolated genomic DNA was digested with the restriction enzymes *Eco*RI, *Hind*III y *Bam*H, and hybridized with a PpPIIa cDNA probe.

TABLE S1 | List of the gene specific primer sequences used in this work.

TABLE S2 | Characteristics of PpPIIa and PpPIIb polypeptides and processed proteins. cTP: chloroplast transit peptide. Sequences of PpPIIa and PpPIIb were available at SustainPineDB v.3.0 (http://www.scbi.uma.es/sustainpinedb/sessions/new).

REFERENCES

Arcondeguy, T., Jack, R., and Merrick, M. (2001). PII signal transduction proteins, pivotal players in microbial nitrogen control. *Microbiol. Mol. Biol. Rev.* 65, 80–105. doi: 10.1128/mmbr.65.1.80-105.2001

Biasini, M., Bienert, S., Waterhouse, A., Arnold, K., Studer, G., Schmidt, T., et al. (2014). SWISS-MODEL: modelling protein tertiary and quaternary structure using evolutionary information. *Nucleic Acids Res.* 42, W252–W258.

Bradford, M. M. (1976). A rapid and sensitive method for the quantitation of microgram quantities of protein utilizing the principle of protein-dye binding. *Anal. Biochem.* 72, 248–254. doi: 10.1016/0003-2697(76)90527-3

Canales, J., Avila, C., Cantón, F. R., Pacheco-Villalobos, D., and Díaz-Moreno, S. (2012). Gene expression profiling in the stem of young maritime pine tres: detection of ammonium stress-responsive genes in the apex. *Trees Struct. Funct.* 26, 609–619. doi: 10.1007/s00468-011-0625-z

Canales, J., Bautista, R., Label, P., Noe, F. P., Pedro, S., Celia, M., et al. (2014). De novo assembly of maritime pine transcriptome: implications for forest breeding and biotechnology. *Plant Biotechnol. J.* 12, 286–299.

Cañas, R. A., Li, Z., Pascual, M. B., Castro-Rodríguez, V., Ávila, C., Sterck, L., et al. (2017). The gene expression landscape of pine seedling tissue. *Plant J.* 91, 1064–1087. doi: 10.1111/tpj.13617

Cañas, R. A., Pascual, M. B., de la Torre, F. N., Avila, C., and Cánovas, F. M. (2019). Resources for conifer functional genomics at the omics era. *Adv. Bot. Res.* 89, 39–76. doi: 10.1016/bs.abr.2018.11.002

Cánovas, F. M., Avila, C., Cantón, F. R., Cañas, R. A., and de la Torre, F. (2007). Ammonium assimilation and amino acid metabolism in conifers. *J. Exp. Bot.* 58, 2307–2318. doi: 10.1093/jxb/erm051

Cánovas, F. M., Cañas, R. A., de la Torre, F. N., Pascual, M. B., Castro-Rodríguez, V., and Avila, C. (2018). Nitrogen metabolism and biomass production in forest trees. *Front. Plant Sci.* 9:1449. doi: 10.3389/fpls.2018.01449

Cánovas, F. M., Cantón, F. R., Gallardo, F., García-Gutiérrez, A., and de Vicente, A. (1991). Accumulation of glutamine synthetase during early development of maritime pine seedlings (*Pinus pinaster*). *Planta* 185, 372–378. doi: 10.1007/bf00201059

Cánovas, F. M., Valpuesta, V., and Núñez de Castro, I. (1984). Characterization of tomato leaf glutamine synthetase. *Plant Sci. Lett.* 37, 79–85. doi: 10.1016/0304-4211(84)90207-4

Cantón, F. R., García-Gutiérrez, A., Crespillo, R., and Cánovas, F. M. (1996). High-level expression of *Pinus sylvestris* glutamine synthetase in *Escherichia coli*. Production of polyclonal antibodies against the recombinant protein and expression studies in pine seedlings. *FEBS Lett.* 393, 205–210. doi: 10.1016/0014-5793(96)00886-1

Castro-Rodríguez, V., García-Gutiérrez, A., Cañas, R. A., Pascual, B., Avila, C., and Cánovas, F. M. (2015). Redundancy and metabolic regulation of the glutamine synthetase gene family in poplar. *BMC Plant Biol.* 15:20. doi: 10.1186/s12870-014-0365-5

Chellamuthu, V. R., Ermilova, E., Lapina, T., Luddecke, J., Minaeva, E., Herrmann, C., et al. (2014). A widespread glutamine sensing mechanism in the plant kingdom. *Cell* 159, 1188–1199. doi: 10.1016/j.cell.2014.10.015

Chen, Y. M., Ferrar, T. S., Lohmeier-Vogel, E. M., Morrice, N., Mizuno, Y., Berenger, B., et al. (2006). The PII signal transduction protein of *Arabidopsis thaliana* forms an arginine regulated complex with plastid N-acetyl glutamate kinase. *J. Biol. Chem.* 281, 5726–5733. doi: 10.1074/jbc.m510945200

Coruzzi, G. M., and Zhou, L. (2001). Carbon and nitrogen sensing and signaling in plants: emerging 'matrix effects. *Curr. Opin. Plant Biol.* 4, 247–253. doi: 10.1016/s1369-5266(00)00168-0

D'Apuzzo, E., Valkov, V. T., Parlati, A., Omrane, S., Barbulova, A., Sainz, M. W., et al. (2015). PII overexpression in Lotus japonicus affects nodule activity in permissive low nitrogen conditions and increases nodule numbers in high nitrogen treated plants. *Mol. Plant Microbe Interact.* 28, 432–442. doi: 10.1094/mpmi-09-14-0285-r

El-Azaz, J., de la Torre, F., Avila, C., and Cánovas, F. M. (2016). Identification of a small protein domain present in all plant lineages that confers high prephenate dehydratase activity. *Plant J.* 87, 215–229. doi: 10.1111/tpj.13195

Ferrario-Méry, S., Besin, E., Pichon, O., Meyer, C., and Hodges, M. (2006). The regulatory PII protein controls arginine biosynthesis in *Arabidopsis*. *FEBS Lett.* 580, 2015–2020. doi: 10.1016/j.febslet.2006.02.075

Ferrario-Méry, S., Meyer, C., and Hodges, M. (2008). Chloroplast nitrite uptake is enhanced in *Arabidopsis* PII mutants. *FEBS Lett.* 582, 1061–1066. doi: 10.1016/j.febslet.2008.02.056

Forchhammer, K., and Lüddecke, J. (2016). Sensory properties of the PII signalling protein family. *FEBS J.* 283, 425–437. doi: 10.1111/febs.13584

Gent, L., and Forde, B. (2017). How do plants sense their nitrogen status? *J. Exp. Bot.* 68, 2531–2539. doi: 10.1093/jxb/erx013

Gómez-Maldonado, J., Cánovas, F. M., and Avila, C. (2004). Molecular analysis of the 5-upstream region of a gibberellin-inducible cytosolic glutamine synthetase gene (GS1b) expressed in pine vascular tissue. *Planta* 218, 1036–1045. doi: 10.1007/s00425-003-1185-2

Heinrich, A., Maheswaran, M., Ruppert, U., and Forchhammer, K. (2004). The *Synechococcus elongatus* PII signal transduction protein controls arginine synthesis by complex formation with *N*-acetyl-l-glutamate kinase. *Mol. Microbiol.* 52, 1303–1314. doi: 10.1111/j.1365-2958.2004.04058.x

Jiang, P., Pelinska, J. A., and Ninfa, A. J. (1998). Reconstitution of the signal-transduction bicyclic cascade responsible for the regulation of Ntr gene transcription in *Escherichia coli*. *Biochemistry* 37, 12795–12801. doi: 10.1021/bi9802420

Kumar, S., Stecher, G., and Tamura, K. (2016). MEGA 7: molecular evolutionary genetic analysis version 7.0 for bigger datasets. *Mol. Biol. Evol.* 33, 1870–1874. doi: 10.1093/molbev/msw054

Li, G., and Coleman, G. D. (2019). Nitrogen storage and cycling in trees. *Adv. Bot. Res.* 89, 127–148.

Liu, Y., Schiff, M., and Dinesh-Kumar, S. P. (2002). Virus-induced gene silencing in tomato. *Plant J.* 31, 777–786. doi: 10.1046/j.1365-313x.2002.01394.x

Llácer, J. L., Contreras, A., Forchhammer, K., Marco-Marín, C., Gil-Ortiz, F., Maldonado, R., et al. (2007). The crystal structure of the complex of PII and acetylglutamate kinase revelas how PII controls the storage of nitrogen as arginine. *Proc. Natl. Acad. Sci. U.S.A.* 104, 17644–17649. doi: 10.1073/pnas.0705987104

Llacer, J. L., Fita, I., and Rubio, V. (2008). Arginine and nitrogen storage. *Curr. Opin. Struct. Biol.* 18, 673–681. doi: 10.1016/j.sbi.2008.11.002

Llebrés, M. T., Avila, C., Cánovas, F. M., and Klimaszewska, K. (2018a). Root growth of hybrid Pinus strobus (L.) and P. wallichiana (A. B. Jacks.) somatic plants is affected by the nitrogen composition of the somatic embryo germination medium. *Trees Struct. Funct.* 32, 371–381. doi: 10.1007/s00468-017-1635-2

Llebrés, M. T., Pascual, M. B., Debille, S., Trontin, J. F., Avila, C., and Cánovas, F. M. (2018b). The role of arginine metabolic pathway during embryogenesis and germination in maritime pine (*Pinus pinaster* Ait.). *Tree Physiol.* 38, 471–484. doi: 10.1093/treephys/tpx133

Mizuno, Y., Moorhead, G. B., and Ng, K. K. (2007). Structural basis for the regulation of N-acetylglutamate kinase by PII in *Arabidopsis thaliana*. *J. Biol. Chem.* 282, 35733–35740. doi: 10.1074/jbc.m707127200

Muro-Pastor, M. I., Reyes, J. C., and Florencio, F. J. (2005). Ammonium assimilation in cyanobacteria. *Photosynth. Res.* 83, 135–150. doi: 10.1007/s11120-004-2082-7

Neale, D. B., Wegrzyn, J. L., Stevens, K. A., Jill, L. W., John, D. L., Brian, Y. L., et al. (2014). Decoding the massive genome of loblolly pine using haploid DNA and novel assembly strategies. *Genome Biol.* 15:R59. doi: 10.1186/gb-2014-15-3-r59

Ninfa, A. J., and Atkinson, M. R. (2000). PII signal transduction proteins. *Trends Microbiol.* 8, 172–179. doi: 10.1016/s0966-842x(00)01709-1

Parlatti, A., Valkov, V. T., D'Apuzzo, E., Alves, L. M., Petrozza, A., Summerer, S., et al. (2017). Ectopic expression of PII induces stomatal closure in *Lotus japonicus*. *Front. Plant Sci.* 8:1299. doi: 10.3389/fpls.2017.01299

Pettersen, E. F., Goddard, T. D., Huang, C. C., Couch, G. S., Greenblatt, D. M., Meng, E. C., et al. (2004). UCSF chimera–a visualization system for exploratory research and analysis. *J. Comput. Chem.* 25, 1605–1612. doi: 10.1002/jcc.20084

Ritz, C., and Spiess, A-N. (2008). *qpcR*: an R package for sigmoidal model selection in quantitative real-time polymerase chain reaction analysis. *Bioinformatics.* 24, 1549–1551. doi: 10.1093/bioinformatics/btn227

Robles-Rengel, R., Florencio, F. J., and Muro-Pastor, M. I. (2019). Redox interference in nitrogen status via oxidative stress is mediated by 2-oxoglutarate in cyanobacteria. *New Phytol.* 224, 216–228. doi: 10.1111/nph.15979

Selim, K. A., Ermilova, E., and Forchhammer, K. (2020a). From cyanobacteria to Archaeplastida: new evolutionary insights into PII signalling in the plant kingdom. *New Phytol.* doi: 10.1111/nph.16492. [Epub ahead of print].

Selim, K. A., Lapina, T., Forchhammer, K., and Ermilova, E. (2020b). Interaction of N-acetyl-l-glutamate kinase with the PII signal transducer in the non-photosynthetic alga *Polytomella parva*: Co-evolution towards a hetero-oligomeric enzyme. *FEBS J.* 287, 465–482. doi: 10.1111/febs.14989

Todd, C. D., Cooke, J. E., Mullen, R. T., and Gifford, D. J. (2001). Regulation of loblolly pine (*Pinus taeda* L.) arginase in developing seedling tissue during germination and post-germinative growth. *Plant Mol. Biol.* 45, 555–565.

Todd, C. D., and Gifford, D. J. (2003). Loblolly pine arginase responds to arginine *in vitro*. *Planta* 217, 610–615. doi: 10.1007/s00425-003-1022-7

Trontin, J. F., Teyssier, C., Morel, A., Harvengt, J., and Lelu-Walter, M. A. (2016). "Prospects for new variety deployment through somatic embryogenesis in maritime pine," in *Vegetative Propagation of Forest Trees*, eds Y.-S. Park, J. M. Bonga, and H.-K. Moon (Seoul: Korea Forest Research Institute), 572–606.

Urigh, R. G., Ng, K. K. S., and Moorhead, G. B. G. (2009). PII in higher plants: a modern role for an ancient protein. *Trends Plant Sci.* 14, 505–511. doi: 10.1016/j.tplants.2009.07.003

Yang, J., Yan, R., Roy, A., Xu, D., Poisson, J., and Zhang, Y. (2015). The I-TASSER suite: protein structure and function prediction. *Nat. Methods* 12, 7–8. doi: 10.1038/nmeth.3213

Conflict of Interest: The authors declare that the research was conducted in the absence of any commercial or financial relationships that could be construed as a potential conflict of interest.

Copyright © 2020 Llebrés, Pascual, Valle, de la Torre, Valderrama-Martin, Gómez, Avila and Cánovas. This is an open-access article distributed under the terms of the Creative Commons Attribution License (CC BY). The use, distribution or reproduction in other forums is permitted, provided the original author(s) and the copyright owner(s) are credited and that the original publication in this journal is cited, in accordance with accepted academic practice. No use, distribution or reproduction is permitted which does not comply with these terms.

frontiers in Plant Science

ORIGINAL RESEARCH
published: 16 June 2020
doi: 10.3389/fpls.2020.00808

In *Arabidopsis thaliana* Substrate Recognition and Tissue- as Well as Plastid Type-Specific Expression Define the Roles of Distinct Small Subunits of Isopropylmalate Isomerase

*Kurt Lächler[1], Karen Clauss[1], Janet Imhof[1], Christoph Crocoll[2], Alexander Schulz[2], Barbara Ann Halkier[2] and Stefan Binder[1]**

[1] Institut für Molekulare Botanik, Fakultät für Naturwissenschaften, Universität Ulm, Ulm, Germany, [2] DynaMo Center, Department of Plant and Environmental Sciences, Faculty of Science, University of Copenhagen, Frederiksberg, Denmark

OPEN ACCESS

Edited by:
Dietmar Funck,
University of Konstanz, Germany

Reviewed by:
Soon Goo Lee,
University of North Carolina
Wilmington, United States
Sally Mackenzie,
Pennsylvania State University (PSU),
United States

***Correspondence:**
Stefan Binder
stefan.binder@uni-ulm.de

Specialty section:
This article was submitted to
Plant Metabolism
and Chemodiversity,
a section of the journal
Frontiers in Plant Science

Received: 30 January 2020
Accepted: 19 May 2020
Published: 16 June 2020

Citation:
Lächler K, Clauss K, Imhof J, Crocoll C, Schulz A, Halkier BA and Binder S (2020) In Arabidopsis thaliana Substrate Recognition and Tissue- as Well as Plastid Type-Specific Expression Define the Roles of Distinct Small Subunits of Isopropylmalate Isomerase. Front. Plant Sci. 11:808. doi: 10.3389/fpls.2020.00808

In *Arabidopsis thaliana*, the heterodimeric isopropylmalate isomerase (IPMI) is composed of a single large (IPMI LSU1) and one of three different small subunits (IPMI SSU1 to 3). The function of IPMI is defined by the small subunits. IPMI SSU1 is required for Leu biosynthesis and has previously also been proposed to be involved in the first cycle of Met chain elongation, the first phase of the synthesis of Met-derived glucosinolates. IPMI SSU2 and IPMI SSU3 participate in the Met chain elongation pathway. Here, we investigate the role of the three IPMI SSUs through the analysis of the role of the substrate recognition region spanning five amino acids on the substrate specificity of IPMI SSU1. Furthermore, we analyze in detail the expression pattern of fluorophore-tagged IPMI SSUs throughout plant development. Our study shows that the substrate recognition region that differs between IPMI SSU1 and the other two IMPI SSUs determines the substrate preference of IPMI. Expression of IPMI SSU1 is spatially separated from the expression of IPMI SSU2 and IPMI SSU3, and IPMI SSU1 is found in small plastids, whereas IMPI SSU2 and SSU3 are found in chloroplasts. Our data show a distinct role for IMPI SSU1 in Leu biosynthesis and for IMPI SSU2 and SSU3 in the Met chain elongation pathway.

Keywords: ***Arabidopsis thaliana*, plastids, leucine biosynthesis, methionine-derived glucosinolates, isopropylmalate isomerase**

INTRODUCTION

Amino acids serve as building blocks for proteins but also have other important functions. In plants for instance, they are initial substrates for the biosynthesis of specialized metabolites such as glucosinolates in the family of the Brassicaceae. According to the parent amino acid, glucosinolates are grouped into three major categories. Aromatic glucosinolates derive from Phe or Tyr whereas those synthesized from Trp represent the indole glucosinolates. The highly diversified aliphatic glucosinolates originate from Ala, from the branched-chain amino acids (Val, Leu, and

Ile) or from Met. The compounds derived from Met represent the most important subgroup of aliphatic glucosinolates in terms of quantity and diversity (Wittstock and Halkier, 2002; Halkier and Gershenzon, 2006).

Met-derived glucosinolates are synthesized in three phases (**Figure 1**). The first phase, the Met chain elongation pathway, is initiated by a transamination of Met to 4-methylthio-2-oxobutanoate (MTOB), a reaction catalyzed by the cytosolic branched chain aminotransferase 4 (BCAT4), which acts at the interphase between primary and specialized metabolism (Schuster et al., 2006). This reaction product is imported into plastids (Gigolashvili et al., 2009; Sawada et al., 2009b), where it is elongated by three-step cycles including condensation with acetyl-CoA (catalyzed by methylthioalkylmalate synthases, MAM), followed by isomerization (isopropylmalate isomerase, IPMI) and oxidative decarboxylation (isopropylmalate dehydrogenase, IPMDH). Each cycle results in a 2-oxo acid elongated by a single methylene group [i.e., 5-methylthio-2-oxopentanoate (MTOP) after a single cycle], which can now re-enter the pathway and undergo one or several additional rounds of elongation (condensation, isomerization and oxidative decarboxylation, up to eight methylene groups) (Grubb and Abel, 2006), or it is transaminated to a Met derivative. The latter metabolites are exported from the plastids to enter glucosinolate core biosynthesis along the endoplasmatic reticulum. In the last stage, various side chain modifications further increase the diversity of the Met-originating glucosinolates (Wittstock and Halkier, 2002; Halkier and Gershenzon, 2006).

Branched chain amino acids are synthesized in plastids. In a first part, two parallel pathways starting from two molecules of pyruvate or pyruvate and 2-oxobutanoate, 3-methyl-2-oxobutanoate (3MOB) and 3-methyl-2-oxopentanoate (3MOP) are formed in reactions catalyzed by three enzymes [acetohydroxyacid synthase (AHAS), ketolacid reductoisomerase (KARI) and dihydroxyacid dehydratase (DHAD)]. While 3MOP is transaminated to Ile [by a branched-chain aminotransferase (BCAT)], 3MOB can be transaminated to Val or it can be chain-elongated to 4-methyl-2-oxobutanoate (4MOP) in a reaction cascade identical to Met chain elongation demonstrating the close relationship between these pathways (condensation, isomerization and oxidative decarboxylation, **Figure 1**; Kroymann et al., 2001; Schuster et al., 2006; Binder, 2010). The close relationship is underpinned by homologous enzymes active in these reaction cascades. This is most obvious for proteins such as the large subunit of isopropylmalate isomerase (IPMI LSU1), which functions both in Leu biosynthesis and in the Met chain elongation pathway (Knill et al., 2009; Sawada et al., 2009a; He et al., 2010).

Leu and Met-derived glucosinolates are representatives of the primary and specialized metabolism, respectively, with completely different biological roles. Given the close relationship of the reaction cascades of both pathways involving homologous enzymes, the formation of Leu and the chain elongation of Met have to be kept apart. The biosynthesis of glucosinolates derived from Met occurs in cells associated with vascular tissues (Reintanz et al., 2001; Chen et al., 2003; Grubb et al., 2004; Tantikanjana et al., 2004; Schuster et al., 2006; Gigolashvili et al., 2007, 2008; He et al., 2010; Li et al., 2011; Imhof et al., 2014; Nintemann et al., 2018) and these specialized metabolites are stored in S-cells (Sulfur-rich cells) situated in close vicinity to the phloem (Koroleva et al., 2000, 2010). In contrast, very little is known where and when Leu biosynthetic proteins are expressed and therefore it is completely unknown how the biosynthesis of this amino acid is kept apart from the Met chain elongation pathway.

To address this issue, we now investigated the expression of the three small subunits of isopropylmalate isomerase (IPMI SSU1 to 3) in *Arabidopsis thaliana* (*Arabidopsis*). Using translational fusions to different fluorescent proteins, we examined the spatial expression of the small subunit 1 of isopropylmalate isomerase (IPMI SSU1, representative for Leu biosynthesis) and of the small subunits 2 and 3 (IPMI SSU2 and IPMI SSU3, representative for Met elongation) on the tissue, cell and organelle level. These investigations revealed a spatial separation of IPMI SSU1 on the one hand from IPMI SSU2 and IPMI SSU3 on the other hand. Apart from the differential accumulation of the small subunits in terms of space, distinct substrate specificities, as analyzed by converting three amino acid identities in the substrate recognition region of IPMI SSU1 to identities present in IPMI SSU3, contribute to the specialized function of isopropylmalate isomerases in *Arabidopsis*.

MATERIALS AND METHODS

Plant Lines and Cultivation

Arabidopsis plants were grown on standard soil containing 20% Vermiculite grain size 2–3 mm (Isola-Mineralwolle-Werke GmbH, Germany) and 1.5 g/l Osmocote Exact Mini fertilizer (Scotts GmbH, Germany). Plants were cultivated in a growth chamber under the following conditions: 16 h light (100–150 μmol/m^{2}s)/8 h dark at 21°C. Dual reporter lines were established by crossing characterized lines IPMI SSU1:RFP, IPMI SSU2:ECFP and IPMI SSU3:GFP according to a standard protocol (Weigel and Glazebrook, 2002). Plant lines IPMI SSU1:RFP, *ipmi ssu2/ipmi ssu3, ipmi ssu2/ipmi ssu3* + pSSU3:SSU1 and *ipmi ssu2/ipmi ssu3* + SSU3 had been described in a previous study (Imhof et al., 2014). For selection of transformants, seeds were germinated on MS medium containing 0.5% (w/v) sucrose and 50 μg/ml hygromycin.

Nucleic Acids Methods

To determine the insertion sites of the T-DNAs in the IPMI SSU1:RFP, IPMI SSU2:ECFP and IPMI SSU3:GFP reporter lines, thermal asymmetric interlaced (TAIL) PCR was performed on total DNA isolated following a previously reported protocol (Edwards et al., 1991). TAIL PCRs followed a previously established procedure (Liu and Whittier, 1994). Shortly, three T-DNA-specific oligonucleotides (TR-1 to TR-3) and the Degenerated-Primer.1 were used to amplify sequences across the T-DNA left border and adjacent genomic regions in the three nested amplification reactions. In the first PCR, total DNA was used as template while the following two nested PCRs were done on amplification products generated in the

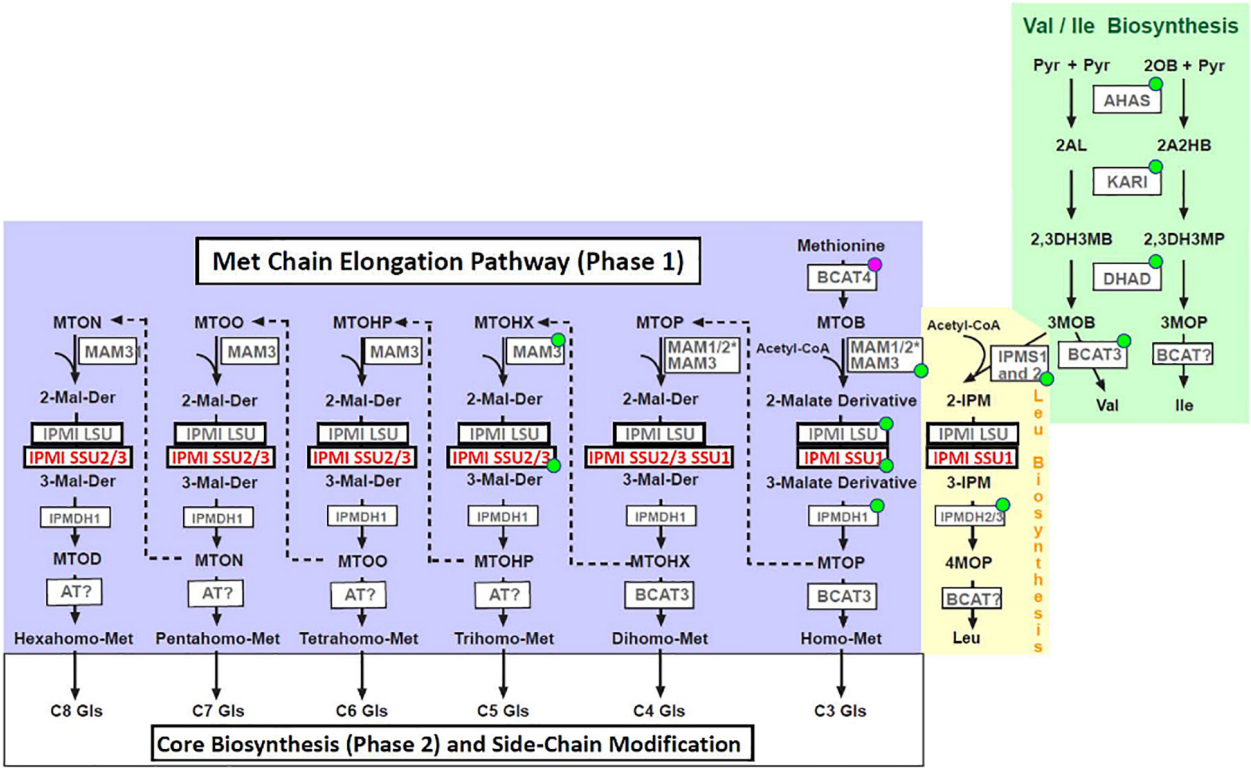

FIGURE 1 | Metabolites and enzymes of branched-chain amino acid biosynthesis (Val and Ile: green box, Leu: yellow box) and methionine chain elongation pathway (blue box). Abbreviations of metabolites: Pyr, pyruvate; 2OB, 2-oxobutanoate; 2AL, 2-acetolactate; 2A2HB, 2-aceto-2-hydroxybutyrate; 2,3DH3MB, 2,3-dihydroxy-3-methylbutanoate; 2,3DH3MP, 2,3-dihydroxy-3-methylpentanoate; 3MOB, 3-methyl-2-oxobutanoate; 3MOP, 3-methyl-2-oxopentanoate; 4MOP, 4-methyl-2-oxopentanoate; 2-IPM, 2-isopropylmalate; 3-IPM, 3-isopropylmalate; MTOB, methylthiooxobutanoate; MTOP, methylthiooxopentanoate; MTOHX, methylthiooxohexanoate; MTOHP, methylthiooxoheptanoate; MTOO, methylthiooxooctanoate; MTON, methylthiooxononanoate; MTOD, methylthiooxodecanoate, 2-Malate-Derivative, 3-Malate-Derivative; Gls, glucosinolate. Abbreviations of enzymes: AHAS, acetohydroxyacid synthase; KARI, ketolacid reductoisomerase; DHAD, dihydroxyacid dehydratase; BCAT, branched-chain aminotransferase; IPMS, isopropylmalate synthase; MAM, methylthioalkylmalate synthase; IPMI LSU, isopropylmalate isomerase large subunit; IPMI SSU, isopropylmalate isomerase small subunit; IPMDH, isopropylmalate dehydrogenase; AT, aminotransferase. Enzymes marked with a green dot localize to plastids according to SUBA4 (http://suba.live/, Hooper et al., 2017). BCAT4 is located in the cytosol. *The presence or absence of MAM1 or MAM2 is ecotype-dependent. Both enzymes are involved in early phases of Met chain elongation leading to predominantly C4 (MAM1, for instance in Col) or C3 (MAM2, for instance in Ws) glucosinolates (Kroymann et al., 2003).

previous reactions. A typical PCR program used in these experiments is given in **Supplementary Method S1**. Control reactions were done applying the same procedure but starting out from total DNA obtained from non-transformed wild-type plants. In comparison to the control reactions, specific products were selected and sequenced to determine the T-DNA insertion site. The localizations of the T-DNAs of the IPMI SSU1:RFP, IPMI SSU2:ECFP and IPMI SSU3:GFP reporter lines are given in **Supplementary Table S1**.

Construct Cloning

Cloning of the construct for the expression of the *IPMI SSU1* open reading frame under the control of the *IPMI SSU3* promoter (pSSU3:SSU1) was described in a previous report (Imhof et al., 2014). An overlap extension PCR strategy was applied to exchange amino acid identities from FLTLV (IPMI SSU1) to YGTLI (IPMI SSU3) in the *IPMI SSU1* coding region. To this end, two PCR products overlapping by 19 nucleotides were amplified with primer pairs SSU3comp.H/SSU3-1FOE.R2 and SSU1FOE.H/SSU1comp.R. These products were purified applying the GenElute Gel Extraction Kit (Sigma-Aldrich) and used as template in subsequent amplification reaction. To this end, both template PCR products were hybridized at 60°C for 5 s followed by five PCR cycles in the absence of additional primers resulting in an extension of the overlapping DNA strands. Then primers ssu3comp.H and SSU1comp.R were added and the gene with altered substrate recognition region (IPMI pSSU3:SSU1/SSU3srr) was amplified in 35 cycles. The product was finally cloned into the *Asc*I/*Pac*I sites in pMDC99 (Curtis and Grossniklaus, 2003) and the correct cloning and codon exchange was confirmed by DNA sequencing. The constructs were then used to transform *ipmi ssu2-1/ipmi ssu3-1* double knockout plants using *Agrobacterium* strain GV2260 following the floral dip procedure (Clough and Bent, 1998). The resulting line was designated *ipmi ssu2-1/ipmi ssu3-1/* + pSSU3:SSU1/SSU3srr.

To investigate the tissue-, cell and organelle-specific localization of the three IPMI SSUs the complete reading frames and promoters were fused in frame to the red fluorescent

protein *Entacmaea quadricolor* epFP611 (RFP), to the enhanced cyan fluorescent protein (ECFP) or to the soluble modified green fluorescent protein (smGFP) (Davis and Vierstra, 1998; Zacharias et al., 2002; Forner and Binder, 2007). The construct for the expression of the IPMI SSU1:RFP fusion protein had been described previously (Imhof et al., 2014) and the corresponding line is referred to as IPMI SSU1:RFP. To clone the reporter fusion construct for IPMI SSU2 and ECFP, the *IPMI SSU2* gene (−981 to +768) was amplified with oligonucleotides SSU2-ECFP.H(*Pac*I) and SSU2-ECFP.R(*Sgs*I)2 on *Arabidopsis* wild-type DNA and cloned into the corresponding sites in pMDC99. The *ECFP* reading frame was amplified with primers pSAT6.H(*Bam*HI) and pSAT6.H(*Pst*I) (Tzfira et al., 2005) and inserted into the *Bam*HI/*Pst*I restriction sites downstream of the *IPMI SSU2* gene. To follow IPMI SSU3 expression the corresponding gene (−1012 to +759) was amplified on total *Arabidopsis* DNA with oligonucleotides SSU3-GFP.H and SSU3-GFP.R, digested with *Bam*HI and *Sma*I and cloned into plasmid psmGFP4 upstream of the *GFP* reading frame (Davis and Vierstra, 1998). The fused IPMI SSU3:GFP reading frame including the IPMI SSU3 promoter was then excised from this plasmid with restriction enzymes *Bam*HI and *Eco*RI and cloned into the corresponding sites in pMDC99 (IPMI SSU3:GFP). All constructs were introduced into the *ipmi ssu2/ipmi ssu3* double knockout plants as mentioned above. After selection and inspection of different transformants by PCR, the insertion sites of the T-DNA were determined by TAIL PCR as described above and homozygous lines were established. To simultaneously follow expression of two different IPMI SSUs in single plants, the lines were crossed to generate IPMI SSU1:RFP/IPMI SSU2:ECFP, IPMI SSU1:RFP/IPMI SSU3:GFP and IPMI SSU2:ECFP/IPMI SSU3:GFP dual reporter lines. In addition, we cloned an alternative construct for the expression of fusion protein consisting of IPMI SSU1 and the ECFP, which is named IPMI SSU1:ECFP. To this end the *IPMI SSU1* gene (−431 to +753) was amplified with primer pair SSU1-ECFP.H(*Pac*I)/SSU1-ECFP.R(*Sgs*I) and the corresponding fragment was cloned into the *Pac*I/*Sgs*I sites in the above described construct IPMI SSU2:ECFP, where it replaces the *IPMI SSU2* gene. In this case, T-DNA insertion site was not determined in the transgenic plants.

For the analysis of cell-specific expression of BCAT4 an approximately 2.0 kb promoter fragment was amplified using primer pair BCAT4.Prom.hin/BCAT4.Prom.rueck. The fragment was digested with *Bam*HI and *Asc*I (sites introduced with primers) and cloned into the corresponding sites upstream of the reading frame of triple GFP containing a C-terminal nuclear localization signal (3xGFP-NLS derived from vector pJF667), that has been inserted before via *Asc*I and *Pac*I sites in pMDC99. The BCAT4 promoter:3XGFP-NLS (pBCAT4:3xGFP-NLS) construct was used to transform *Arabidopsis* as outlined in previous sections.

Microscopy

Fluorescence microscopy was done with a Leica DM5500 equipped with a Leica DFC3000 G digital camera with filter sets: RFP: RFP excitation 545/30 nm, beam splitter 570 nm, emission 610/75 nm; GFP: GFP excitation 480/40 nm, beam splitter 505 nm, emission 527/30 nm, ECFP excitation 436/20 nm, beam splitter 455 nm, emission 480/40 nm and chlorophyll autofluorescence: excitation 470/40, beamsplitter 500, emission 525/50.

In addition, images were captured with a confocal microscope Leica SP5X equipped with a HCX PL APO lambda blue 20.0 × 0.70 IMM UV objective. ECFP was excited at 458 nm. Emission was collected at 468–520 nm for ECFP and 650–695 nm for chloroplast autofluorescence. GFP was excited at 488 nm. Emission was collected at 500–530 nm for GFP and 650–695 nm for chloroplast autofluorescence. Images were analyzed using the LAS AF and LAS X software (Leica). Except for images shown in **Figures 5C,D**, **6B** and **Supplementary Figure S3**, all images were taken with wide field microscopy. Depending on the number of cell layers in the distinct cross sections, individual organelles and their shape cannot be resolved clearly in individual wide field images.

Miscellaneous Methods

Glucosinolates were analyzed following a protocol established previously (Brown et al., 2003). Twenty mg seeds were ground using a ball mill and the homogenized material was rehydrated in 1 ml 80% (v/v) methanol. After the addition of 50 μl of Sinalbin as internal standard, samples were incubated for 5 min at room temperature and then centrifuged at 13,000 rpm for 10 min. Eight hundred μl of the supernatants were recovered and loaded on equilibrated DEAE-Sephadex A 25 columns. Columns were washed with 500 μl 80% (v/v) methanol, two times with 1 ml double distilled water and 500 μl 0.02M MES buffer pH 5.2. Glucosinolates bound to the column matrix were then treated with 30 μl arylsulfatase for desulfation (sulfatase from Helix pomatia, Sigma-Aldrich) over night and finally eluted with 0.5 ml double distilled water. The eluted desulfoglucosinolates were separated using high performance liquid chromatography (Agilent 1100 HPLC system, Agilent Technologies) on a reversed phase C-18 column (Nucleodur Sphinx RP, 250 × 4.6 mm, 5 μm, Macherey-Nagel, Germany) with a water (A)-acetonitrile (B) gradient (0–1 min, 1.5% B; 1–6 min, 1.5–5% B; 6–8 min, 5–7% B; 8–18 min, 7–21% B; 18–23 min, 21–29% B; 23–23.1 min, 29–100% B; 23.1–24 min 100% B and 24.1–28 min 1.5% B; flow 1.0 ml min-1). Metabolites were detected with a photodiode array detector and peaks were integrated at 229 nm. Desulfoglucosinolates were identified by comparison of retention time and UV spectra to those of purified standards previously extracted from *Arabidopsis thaliana*.

For each line, eight seed pools each derived from seven or eight plants were analyzed and considered for calculation. Only for line *ipmi ssu2-1/ipmi ssu3-1* complemented with IPMI SSU3 (*ipmi ssu2-1/ipmi ssu3-1* + SSU3), six pools were considered for evaluation, since two lines were clear outliers. Sequencing was obtained commercially (4baselab[1], LGC Genomics[2]. Alignments

[1]http://www.4base-lab.de/index_4.html
[2]https://www.lgcgroup.com/

were done using the clustalW alignment tool[3]. Oligonucleotide sequences are given in **Supplementary Table S2**.

RESULTS

Amino Acid Identities in the Small Subunits of the IPMI Influence the Substrate Range of the Heterodimeric Enzyme

It was previously suggested that the three small subunits of isopropylmalate isomerase have different roles in Leu and/or glucosinolate metabolism in *Arabidopsis* (He et al., 2010; Imhof et al., 2014). To investigate whether the distinct functions are related to different substrate specificities influenced by the small subunits of the enzyme, we exchanged amino acid identities in a region potentially influencing the interaction with different substrates. Studies in prokaryotes identified a substrate recognition region (SRR) spanning five amino acids in the small subunit of the heterodimeric IPMI (Yasutake et al., 2004; Lee et al., 2012). A comparison of the three SSUs from *Arabidopsis* revealed differing amino acid identities within the SRR, which might be responsible for the distinct function of these proteins (**Supplementary Figure S1**). In a previously used construct, which allows the expression of the *IPMI SSU1* reading frame under the *IPMI SSU3* promoter (**Table 1**, *ipmi ssu2-1/ipmi ssu3-1* + pSSU3:SSU1), we replaced several amino acids in the substrate recognition region in the *IPMI SSU1* reading frame by amino acid residues present in this region in *IPMI SSU3* (**Figure 2**, IPMI pSSU3:SSU1/SSU3srr). This construct was introduced into a *ipmi ssu2-1/ipmi ssu3-1* double knockout mutant (**Table 1**, *ipmi ssu2-1/ipmi ssu3-1* + pSSU3:SSU1/SSU3srr). The double knockout line is unable to synthesize detectable amounts of C6, C7 and C8 aliphatic glucosinolates (**Table 1**, *ssu2-1/ipmi ssu3-1*) (Imhof et al., 2014).

Transgenic plants were selected by their resistance to hygromycin and the presence of the construct was confirmed by PCR. Glucosinolate profiling of seed samples obtained from individual T1 transformants revealed that the exchange of the amino acid identities in the SRR allowed the synthesis of 6-methylsulfinylhexylglucosinolate (6MSOH), 7-methylsulfinylheptylglucosinolate (7MSOH), 8-methylthiooctylglucosinolate (8MTO) and 8-methylsulfinyloctylglucosinolate (8MSOO), albeit they do not reach the levels seen upon the introduction of an intact IPMI SSU3 gene into the double knockout mutant. In contrast, these C6, C7 and C8 aliphatic glucosinolates were absent from the *ipmi ssu2*/*ipmi ssu3* double knockout mutant and in mutant plants containing the unchanged construct for the expression of the native *IPMI SSU1* open reading frame under the control of the *IPMI SSU3* promoter (**Table 1**). These results demonstrated that the synthesis of these long chain glucosinolate species correlates with the exchange of the amino acid identities in the SRR. Thus, this region contributes to the substrate specificity of heterodimeric IPMI in *Arabidopsis*. The clear difference in glucosinolate composition between the *ipmi ssu2-1/ipmi ssu3-1* double knockout mutant and this line containing the construct IPMI pSSU3:SSU1/SSU3srr (*ipmi ssu2-1/ipmi ssu3-1* + pSSU3:SSU1/SSU3srr) indicated that the mutated small subunit can functionally interact with the large IPMI subunit (**Table 1**).

[3]https://www.ebi.ac.uk/Tools/msa/clustalw2/

Reporter Lines Used to Analyze Spatial Expression of Small Subunits of IPMI

To investigate whether the different roles of the three small subunits of the isopropylmalate isomerase come along with differential spatial expression *in planta*, we established reporter lines expressing full length IPMI SSU proteins N-terminally fused to different fluorescent proteins in the *ipmi ssu2-1/ipmi ssu3-1* double knockout line (IPMI SSU1:RFP, IPMI SSU1:ECFP, IPMI SSU2:ECFP, and IPMI SSU3:GFP). These fusion proteins were expressed under the native promoters, which allowed a tissue-, cell-, and cell compartment-specific visualization of these proteins. For direct comparison of the different expression patterns we also established dual reporter lines, expressing two different fusion proteins (IPMI SSU1:RFP/IPMI SSU2:ECFP, IPMI SSU1:RFP/IPMI SSU3:GFP, and IPMI SSU2:ECFP/IPMI SSU3:GFP). We also generated a line expressing a nucleus-targeted triple green fluorescent protein controlled by the promoter of *BCAT4* (pBCAT4:3XGFP-NLS), a gene involved in Met chain elongation (Schuster et al., 2006). An overview of the various constructs is given in **Supplementary Figure S2**. After the establishment of the reporter lines, various tissue samples were taken from plants grown on MS medium or soil under long-day conditions.

Inspection of Different Tissues From Young Seedlings

An inspection of cotyledons from 4 to 7-day-old seedlings identified expression of IPMI subunits 1 and 2 in these organs. Consistent with previous analyses applying promoter:GUS constructs, IPMI SSU2 expression was found in tissues along the vascular bundles (Imhof et al., 2014). In addition, IPMI SSU2 also localized to isolated epidermal cells distributed over the cotyledon lamina (**Figure 3A**). Cross sections clearly confirmed the localization of IPMI SSU2 in epidermal cells and the vascular bundles (**Figures 3B,C**). IPMI SSU1:ECFP accumulated in approximately roundish, slightly elongated organelles similar to mesophyll-plastids but much smaller with a longitudinal diameter of about 4–5 μm within epidermal cells covering large parts of the lamina (**Figure 3D**). Usually no autofluorescence was seen in these organelles, but in rare instances, typical chlorophyll autofluorescence was detected, which confirmed that these organelles are indeed plastids (**Supplementary Figure S3**).

The longitudinal microscopic inspection of the hypocotyls of the different reporter lines revealed the presence of IPMI SSU2 and IPMI SSU3 in plastids of cells, which show a slight difference with respect to their location along the central vascular bundle. While IPMI SSU3 seems to be located in close vicinity to the central vasculature (**Figure 3E**), IPMI SSU2 was also

TABLE 1 | Glucosinolate content in seeds of different lines.

Gls	Glucosinolate Content in Seeds (μmol/g)					
	Col-0	Ws	*ipmi ssu2-1/ipmi ssu3-1*	*ipmi ssu2-1/ipmi ssu3-1* + pSSU3:SSU1	*ipmi ssu2-1/ipmi ssu3-1* + pSSU3:SSU1/SSU3srr	*ipmi ssu2-1/ipmi ssu3-1* + SSU3
3BZO	3.42 ± 015	10.27 ± 0.42	23.07 ± 0.67	12.16 ± 1.66	17.64 ± 2.21	5.47 ± 0.94
3OHP	0.50 ± 0.10	3.21 ± 0.26	11.43 ± 0.28	5.62 ± 0.58	4.26 ± 0.99	1.53 ± 0.37
3MTP	0.03 ± 0.03	20.88 ± 3.82	4.57 ± 0.28	0.27 ± 0.10	1.36 ± 1.12	0.08 ± 0.02
3MSOP	0.10 ± 0.03	5.15 ± 2.12	1.84 ± 0.23	0.16 ± 0.07	0.57 ± 0.46	0.11 ± 0.09
4BZO	14.17 ± 1.09	0.07 ± 0.02	2.95 ± 0.11	10.81 ± 0.98	7.69 ± 1.85	8.82 ± 0.94
4MTB	16.44 ± 1.31	n.d.	9.97 ± 0.49	25.96 ± 4.01	23.27 ± 5.15	32.74 ± 8.18
4OHB	4.39 ± 0.29	n.d.	2.74 ± 0.13	12.60 ± 0.74	5.26 ± 0.56	5.03 ± 0.31
4MSOB	2.67 ± 0.60	0.57 ± 0.14	3.59 ± 0.36	2.34 ± 0.40	2.44 ± 0.51	4.84 ± 1.64
5MSOP	0.72 ± 0.23	0.29 ± 0.21	0.49 ± 0.20	0.34 ± 0.05	0.47 ± 0.15	1.01 ± 0.31
5MTP	1.90 ± 0.29	n.d.	n.d.	0.41 ± 0.04	0.63 ± 0.33	2.14 ± 0.38
6MSOH	0.46 ± 0.14	0.19 ± 0.10	n.d.	n.d.	0.48 ± 0.18	0.66 ± 0.11
7MSOH	2.01 ± 0.48	0.88 ± 0.30	n.d.	n.d.	0.97 ± 0.26	2.79 ± 0.17
7MTH	5.76 ± 0.87	3.11 ± 0.34	n.d.	n.d.	3.73 ± 0.58	6.48 ± 0.56
8MSOO	8.95 ± 1.08	9.90 ± 1.72	n.d.	n.d.	0.57 ± 0.26	9.48 ± 0.90
8MTO	6.85 ± 0.77	14.39 ± 1.93	n.d.	n.d.	0.60 ± 0.15	4.81 ± 0.47
I3M	1.16 ± 0.12	0.31 ± 0.03	0.39 ± 0.03	0.34 ± 0.03	0.50 ± 0.08	0.64 ± 0.16
total	69.53 ± 4.35	69.24 ± 6.56	61.03 ± 1.42	71.01 ± 7.18	70.43 ± 8.89	86.64 ± 11.53

3BZO, 3-benzoyloxypropylglucosinolate; 3OHP, 3-hydroxypropylglucosinolate; 3MTP, 3-methylthiopropylglucosinolate; 3MSOP, 3-methylsulfinylpropylglucosinolate; 4BZO, 4-benzoyloxybutylglucosinolate; 4MTB, 4-methylthiobutylglucosinolate; 4OHB, hydroxybutylglucosinolate; 4MSOB, 4-methylsulfinylbutylglucosinolate; 5MSOP, 5-methylsulfinylpentylglucosinolate; 5MTP, 5-methylthiopentylglucosinolate; 6MSOH 6-methylsulfinylhexylglucosinolate; 7MSOH, 7-methylsulfinylheptylglucosinolate; 7MTH, 7-methylthioheptylglucosinolate; 8MTO, 8-methylthiooctylglucosinolate; 8MSOO, 8-methylsulfinyloctylglucosinolate and I3M, indol-3-ylmethylglucosinolate. Number of samples measured for the different lines is given in section "Materials and Methods." srr, substrate recognition region; p, promoter.

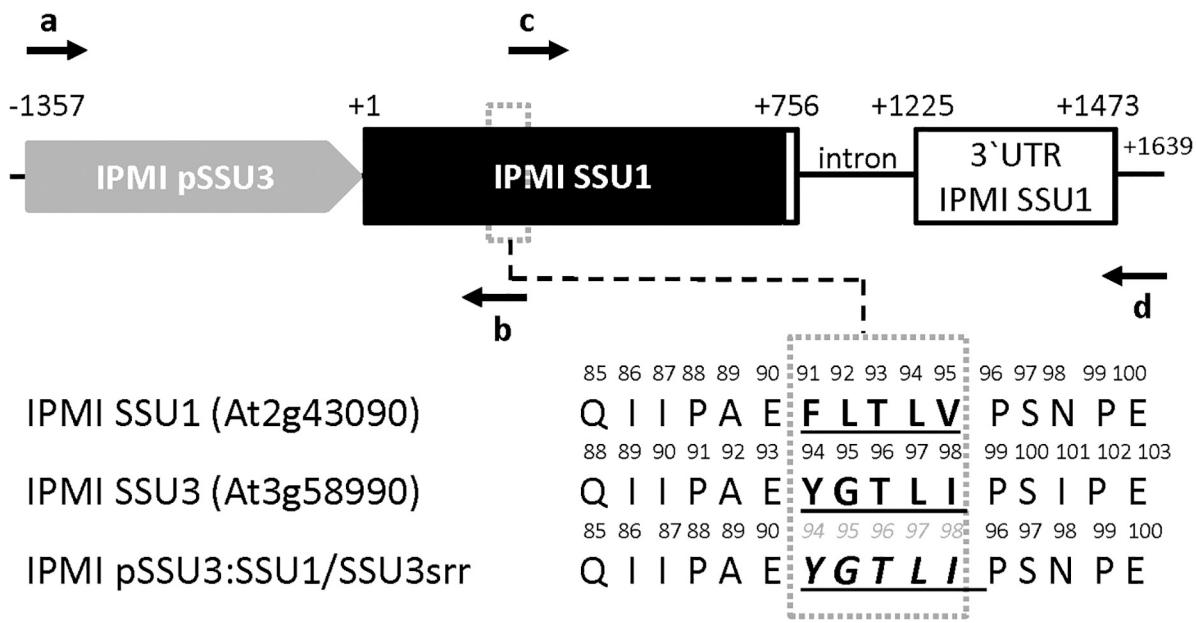

FIGURE 2 | Schema of the construct used to test the importance of distinct amino acids in the substrate recognition region (SRR) in the small subunits of IPMI. The *IPMI SSU1* reading frame (black box) including its native 3′ untranslated region (3′ UTR), white box) is expressed under the control of the *IPMI SSU3* promoter (gray box). In the SRR (dotted box) three amino acids originally present in IPMI SSU1 were substituted by the corresponding amino acid present in IPMI SSU3. Original amino acid sequences and the resulting new sequence (IPMI pSSU3:SSU1/SSU3srr) are given in the lower part of the figure. Oligonucleotides used for the generation of the construct and the amino acid replacement are indicated as horizontal arrows. Theses primers are: a, ssu3comp.H; b, SSU3/1FOE.R2, c, SSU1FOE.H and d, SSU1comp.R. Oligonucleotide sequences are given in **Supplementary Table S2**. Numbering is given with respect to the translation start codons. Schema not drawn to scale.

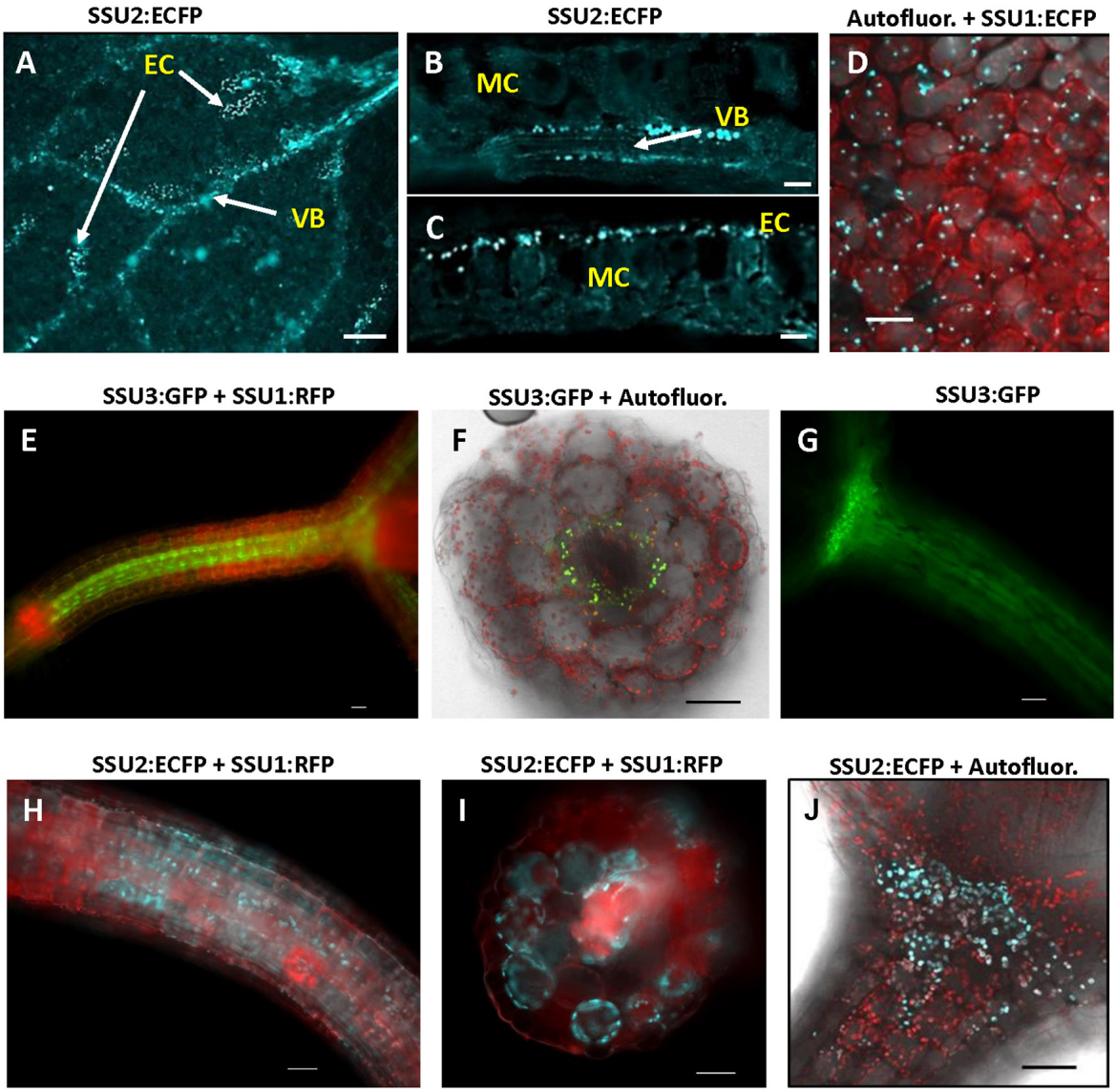

FIGURE 3 | Localization of the small subunits of IPMI in different parts of young seedlings. **(A–D)** cotyledons, **(E–J)** hypocotyls. Whole mount **(A)** and cross sections of cotyledons **(B,C)**. IPMI SSU2:ECFP (cyan) is seen in the cells along the vascular bundles (VB) in cotyledons **(A,B)** and in isolated epidermis cells [EC in **(A,C)**]. MC indicates mesophyll cells. **(D)** View onto a leaf indicating that the fluorescence of IPMI SSU1:ECFP (cyan) is mainly detected in plastids with a longitudinal diameter of approximately 4–5 μm in the epidermis. **(E–J)** IPMI SSU1-3 expression in the hypocotyl. **(D,F,H,J)** Autofluor., chlorophyll autofluorescence (red). Scale bars correspond to 20 μm **(B,C)**, 50 μm **(A,D–J)**.

seen in further peripherally located cells (**Figure 3H**) with some spatial overlap of the tissues expressing these proteins. Expression of both proteins extends up to the cotyledoneous node (**Figures 3G,J**). Cross sections through the hypocotyl confirmed that the IPMI SSU3:GFP protein localized to plastids in parenchyma cells surrounding the central vasculature, whereas IPMI SSU2 was also found in further peripheral cells (**Figures 3F,I**). These plastids containing IPMI SSU2 and IPMI SSU3 have sizes comparable to chloroplasts (**Figures 3F,J**). The localization of IPMI SSU1 differed substantially from IPMI SSU2 and IPMI SSU3. The IPMI SSU1/IPMI SSU2 and IPMI SSU1/IPMI SSU3 dual reporter lines demonstrated that IPMI SSU1 is preferentially located in peripheral cells of the hypocotyls (**Figures 3E,H,I**).

In seedling roots, IPMI SSU1 occurred in the epidermis including root hairs and throughout the cortex whereas IPMI SSU2 was found in cells along the vasculature (**Figures 4A–C** and **Supplementary Figure S4**). The IPMI SSU1:RFP/IPMI SSU2:ECFP and IPMI SSU1:RFP/IPMI SSU3:GFP dual reporter lines showed an expression of IPMI SSU1 in root parenchyma, clearly different from the localization of the other subunits involved in the Met chain elongation pathway (**Figures 4A,B**). This expression pattern observed for IPMI SSU1 is consistent with previous observations (Imhof et al., 2014). In roots, the

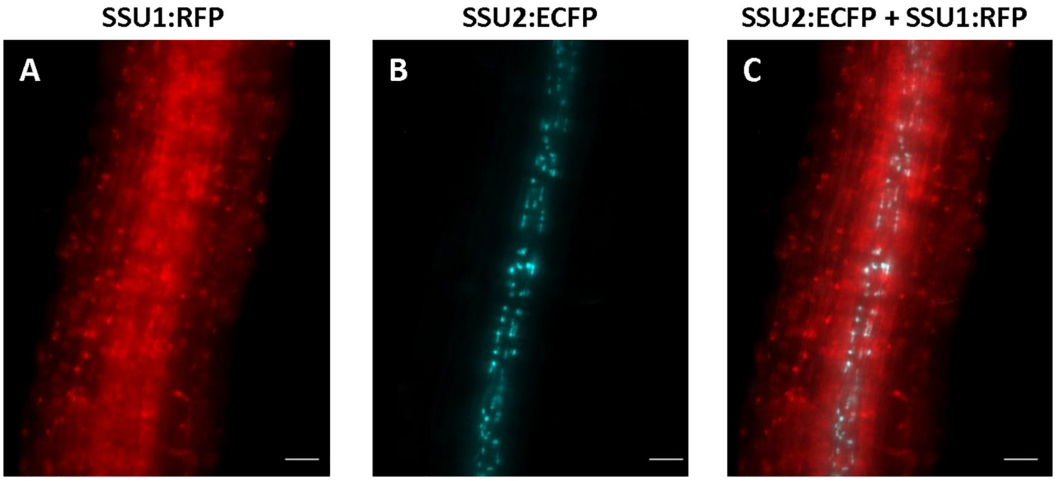

FIGURE 4 | Expression of IPMI SSU1 **(A)** and IPMI SSU2 **(B)** in roots of 6-day-old seedlings. An overlay of images is given in **(C)**. Scale bar is 20 μm **(A–C)**.

analyzed proteins are generally found in small plastids with a size as described above.

Distribution of the Different Small Subunits of IPMI in Leaves

In rosette leaves, ECFP-tagged IPMI SSU1 was found in plastids of both, the upper and lower epidermis (**Figures 5A,B**). In these cells, the fusion protein marked organelles close to the cell wall toward the mesophyll. These plastids were clearly smaller than the chloroplasts in mesophyll cells (**Figure 5B**). IPMI SSU3:GFP marked plastids in cells in the phloem and in cells close to the xylem along the vascular bundles as seen in cross sections (**Figures 5C,D**). These IPMI SSU3 containing organelles have sizes very similar to chloroplasts (highlighted by the chlorophyll autofluorescence) in the immediate vicinity.

Spatial Differentiation of IPMI SSU Expression in Roots

The three small subunits of IPMI are also expressed in roots of adult plants. IPMI SSU1 containing plastids were prevalent in the root tip and seem to be less evident in the elongation and differentiation zone (**Figures 6A,C**). Organelles with IPMI SSU1 were also found in the cortex of the mature root enclosing the stele (**Figures 6B,D,E**). These plastids formed stromules (**Figure 6A**, inset). In contrast, IPMI SSU2 and IPMI SSU3 were seen in cells closely associated with the stele (**Figures 6D,E**).

The Enzymes of Met Chain Elongation IPMI SSU2, IPMI SSU3 and BCAT4 Are Expressed in Parenchyma Cells Associated With the Phloem or the Xylem in Flowering Stalks

Expression studies of genes involved in glucosinolate biosynthesis and its regulation revealed promoter activities in or along the vascular tissues. In this context, it has been speculated that the promoter activity might co-localize with glucosinolate storing S-cells (Koroleva et al., 2000; Schuster et al., 2006). To investigate the exact cellular and subcellular localization of the IPMI SSUs, we inspected cross sections through the flowering stalk. In an IPMI SSU3/IPMI SSU1 dual reporter line, these studies provided evidence that IPMI SSU3 was expressed in two populations of cells, associated with either the phloem or the xylem (**Figure 7A**, yellow and white arrows). The cross section indicated IPMI SSU1 in the epidermis (**Figure 7A**, blue arrow). The image of this section also suggested that this protein might also be present in phloem-associated cells (**Figure 7A**, orange arrow). This localization was confirmed by a longitudinal section of a flowering stalk of IPMI SSU2/IPMI SSU1 dual reporter plant. The IPMI SSU1-containing plastids were small and found to be clearly different from the chloroplasts containing IPMI SSU2 (**Supplementary Figure S5A**). Higher magnification images localized IPMI SSU3 to a few cells located at the periphery of the phloem (**Figures 7B,C**) and in cells located proximal to the xylem (**Figures 7B,D**), here found in plastids with very similar sizes to the chloroplasts in the close vicinity (**Figure 7D**). To investigate whether the observed pattern is valid only for isopropylmalate isomerase subunits 2 and 3 or whether other proteins of the Met chain elongation pathway are also expressed in these parenchymatic cells, we analyzed BCAT4 promoter activity with a 3XGFP-NLS reporter gene (**Supplementary Figures S5B,C**). Longitudinal sections showed that BCAT4 is also expressed in cells in distal parts of the phloem and like IPMI SSU3, also in cells proximal to the xylem (**Supplementary Figures S5B,C**). Along the phloem, 3XGFP-NLS fluorescence was detected in nuclei of relatively short cells that exhibited a morphology completely different from the extremely long S-cells (**Supplementary Figure S5B**) (Koroleva et al., 2000, 2010). In addition, S-cells are located further distal to those cells expressing BCAT4, which are located very close to the phloem (**Supplementary Figure S5C**). Interestingly, nuclei indicating BCAT4 expression in the xylem parenchyma were often found to be elongated whereas those demonstrating BCAT4

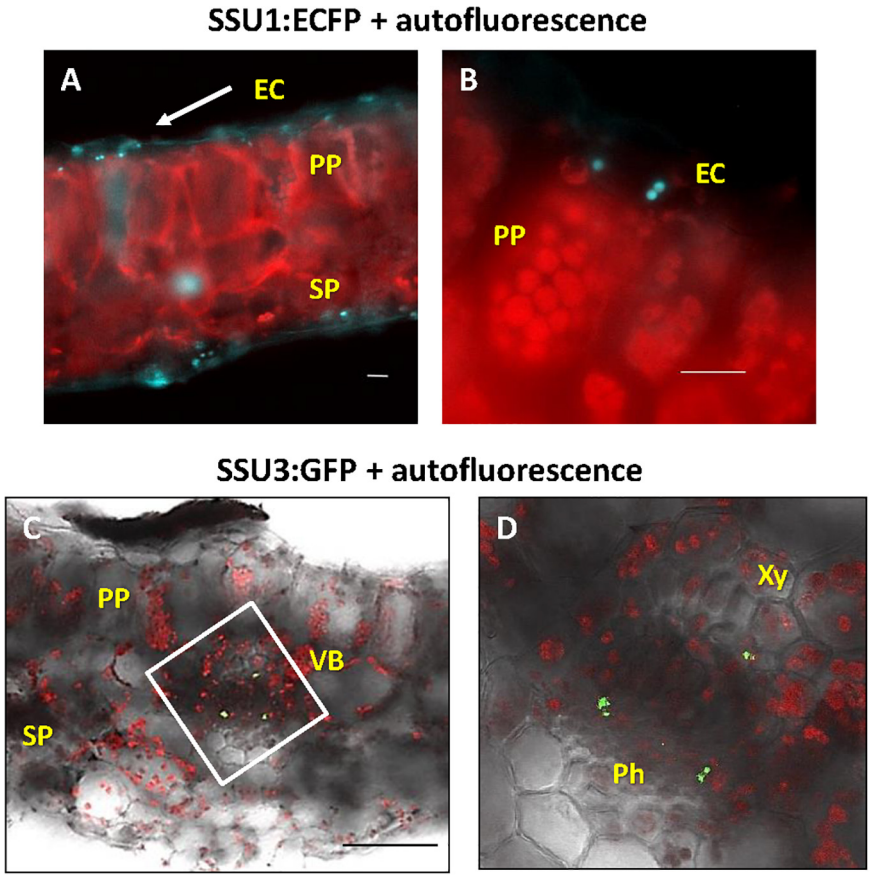

FIGURE 5 | Localization of the small IPMI subunits in leaves. **(A,B)** IPMI SSU1:ECFP-positive plastids (cyan) locate to the leaf epidermis. **(B)** the epidermal cells (EC) contain small plastids with longitudinal diameter of 4–5 μm. In comparison, chloroplasts (red autofluorescence) of mesophyll cells [palisade parenchyma (PP) and sponge parenchyma (SP)] are 7–8 μm in size. **(C,D)** Cross section through a leaf vascular bundle (VB) revealed IPMI SSU3:GFP in cells located proximal to both phloem (Ph) and xylem (Xy), respectively. Scale bars: **(A,B)** 20 μm, **(C)** 100 μm. **(D)** is a magnification of the white boxed part of the image shown in **(C)**.

expression in the cells linked to the phloem were predominantly of globular shape (**Supplementary Figure S5C**).

Occurrence of the Different Small Subunits in Generative Tissues

Finally, we examined the *in planta* distribution of the three IPMI SSUs in generative tissues. In carpels, IPMI SSU1 was found in relatively small plastids that did not exhibit detectable autofluorescence (**Figure 8A**). These plastids seemed to be located in the epidermis above a chloroplast-containing cell layer. Interestingly many of these plastids were observed in pairs indicating dividing stages (**Figure 8B**). Expression of IPMI SSU1 was neither detected in sepals, petals nor stamen, while IPMI SSU2 expression was associated with the vasculature in sepals and petals. A cross section through a maturing silique revealed the expression of IPMI SSU1 in the outermost cell layer consistent with the localization of this protein in the epidermis of the carpel (**Figure 8C**). The plastids labeled by IPMI SSU1:ECFP are clearly smaller than chloroplasts (**Figure 8D**). In pre-mature seeds, IPMI SSU1 was found in small plastids in a cell layer close to the surface very similar to what has been observed in leaves or carpels (**Figure 8D**). No autofluorescence was detected in the IPMI SSU1:ECFP-positive plastids and again a relatively large number of these organelles seemed to be in a dividing stage.

Collectively these data demonstrate an almost strict correlation of the different functions of the IPMI small subunits with distinct localizations in different plastids, cells and tissues. The localization patterns are summarized in a cartoon showing a cross section through the flowering stalk (**Figure 9**).

DISCUSSION

Sequences in the IPMI SSU Contribute to the Substrate Specificity of the Heterodimeric Enzyme

Isopropylmalate isomerase, which catalyzes the second step in Leu biosynthesis, occurs in two forms (Singh, 1999; Binder, 2010). The single subunit or monomeric enzyme is found in fungi whereas the heterodimeric form is found in bacteria and archaea as well as in plants (Knill et al., 2009; Manikandan et al., 2011; Lee et al., 2012). The heterodimer is built up of a

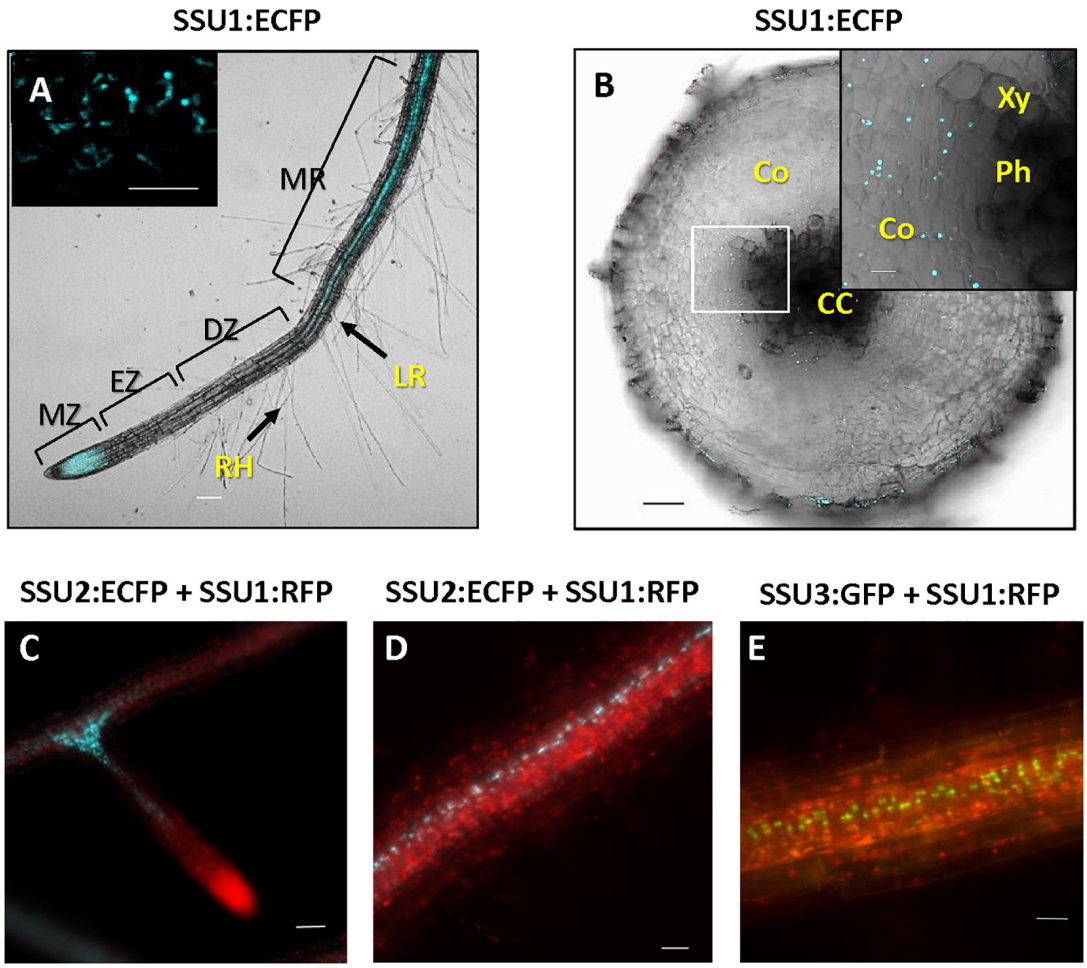

FIGURE 6 | (A) Whole mount root with IPMI SSU1:ECFP fluorescence visible in the meristematic zone (MZ) and along the stele of mature root region (MR). IPMI SSU1 is not observed in the elongation (EZ) and differentiation zones (DZ). Root hairs (RH) and an outgrowing lateral root (LR) are indicated. **(B)** In an older part of a mature root, IPMI SSU1 is also detectable in the cortex (Co) surrounding the central cylinder (CC) but not in the vascular tissue itself [xylem (Xy) and phloem (Ph)]. IPMI SSU1 containing plastids form stromules [inset in **(A)**]. **(C–E)** IPMI SSU2 and IPMI SSU3 are seen in plastids along the central cylinder, with a strong accumulation of these organelles at branches (here shown for IPMI SSU2). In contrast, IPMI SSU1 is seen in plastids throughout the cortex and in the root tip **(C)**. Scale bars: inset in **(A)** 10 μm, **(B)** 100 and 50 μm, **(C–E)** 20 μm.

large subunit, which contains an iron-sulfur cluster and a small subunit. Studies in prokaryotes showed that the active site of the enzyme is formed at the interface of both components (Lee et al., 2012). In the small subunit, two regions are critical for substrate binding. The GSSRE substrate binding motif, which is highly conserved in all small IPMI polypeptides and in related aconitases, and the substrate recognition region (SRR) located in a flexible loop of these proteins (**Supplementary Figure S1**; Frishman and Hentze, 1996; Gruer et al., 1997; Jeyakanthan et al., 2010; Lee et al., 2012). In *Arabidopsis* and rice, the GSSRE motif as well as N- and C-terminally flanking amino acids are perfectly conserved, consistent with the conserved function of this motif in substrate binding but at the same time excluding a role of this motif in substrate differentiation. Thus, the SRR determines the substrate preference of the heterodimeric enzyme consistent with previous studies of IPMI and homoaconitase (HACN) in *Methanocaldococcus jannaschii* (Jeyakanthan et al., 2010). Within the SRR, at least three amino acids differ between the three small subunits of *Arabidopsis* (**Figure 2** and **Supplementary Figure S1**). In line with the apparent function of the single small IPMI subunit from rice in Leu biosynthesis, the SRR region from this protein is almost identical to the *Arabidopsis* IPMI SSU1 that functions in Leu metabolism (**Supplementary Figure S1**; Imhof et al., 2014). The exchange of three amino acids in IPMI SSU1 to adopt the SRR sequence from IPMI SSU3 and the expression of this modified reading frame under the *IPMI SSU3* promoter in the *ipmi ssu2-1/ipmi ssu3-1* double mutant resulted in an altered glucosinolate composition. Notably, the otherwise undetectable C6, C7, and C8 glucosinolate species accumulated after the amino acid substitutions in the SRR, albeit these compounds did not reach the levels that were measured when the native IPMI SSU3 was introduced into the *ipmi ssu2-1/ipmi ssu3-1* double knockout mutant. This suggests that additional amino acids at other positions influence the substrate specificity of the

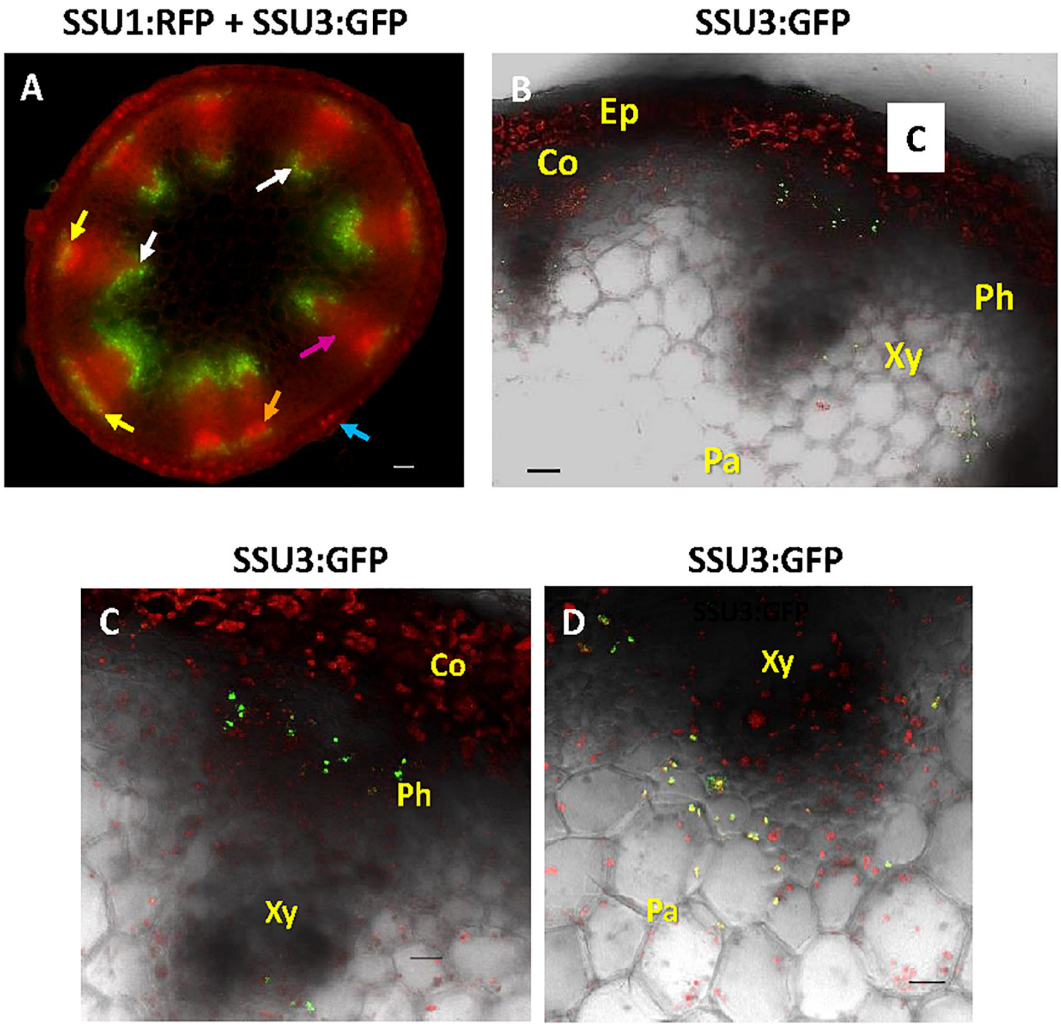

FIGURE 7 | Cross section through a flowering stalk. **(A)** In a dual reporter line, IPMI SSU3:GFP expression is seen in cells associated with the phloem (indicated by yellow arrows) but also in parenchyma cells proximal to the xylem (white arrows, with some background autofluorescence of lignin in the xylem), whereas IPMI SSU1 labeled with RFP lights up in the epidermis (blue arrow) and also in phloem-associated cells (orange arrow), although a clear resolution of the organelles is not possible in this image. Background red autofluorescence is exemplarily indicated by a purple arrow. **(B–D)** Magnified cross section shows IPMI SSU3:GFP co-expression in cells associated with the phloem (Ph) and the xylem (Xy). Other abbreviations: Co, cortex; Ep, epidermis. **(C)** IPMI SSU3:GFP in cells in close proximity to the phloem. **(D)** IPMI SSU3:GFP in cells located proximal to the xylem. Scale bars: 50 μm **(A)**, 20 μm **(B–D)**.

IPMI, but the lower levels might be also linked to differences in expression since the transgenes in the distinct lines originate from different transformation events. The differences observed in the composition in the C3 and C4 glucosinolates could be linked to a segregation of the methylthioalkylmalate synthase 1 (MAM1, Col) and MAM2 (Ws) genes in the *ipmi ssu2-1/ipmi ssu3-1* double knockout mutant. Ecotypes containing MAM1 synthesize mainly C4 short-chain glucosinolates while in those accessions with MAM2 C3 glucosinolates are dominant (**Table 1** and **Figure 1**; Kroymann et al., 2001, 2003). The generation of long-chain glucosinolates is linked to the activity of MAM3 found in all ecotypes (**Figure 1**; Kroymann et al., 2003; Textor et al., 2007). Thus, the accumulation of the long-chain glucosinolates (C6 to C8) in lines *ipmi ssu2-1/ipmi ssu3-1*/+pSSU3:SSU1/SSU3srr and *ipmi ssu2-1/ipmi ssu3-1*/+pSSU3:SSU1is independent from the genetic background of the recipient line *ipmi ssu2-1/ipmi ssu3-1*, in which no C6 to C8 glucosinolate species were detected (**Table 1**; Imhof et al., 2014), but is solely linked to the introduced transgenes.

The fact that the introduced construct for the expression of the SRR-modified IPMI SSU1 (line *ipmi ssu2-1/ipmi ssu3-1* + pSSU3:SSU1/SSU3srr) altered the glucosinolate composition in comparison to the acceptor line, i.e., the *ipmi ssu2-1/ipmi ssu3-1* double mutant, demonstrates that a functional dimerization occurred and that the introduced amino acid exchanges did not interfere with binding between this protein and the IPMI large subunit. This scenario is further supported by observations made by the analysis of bacterial and archaeal IPMI and the closely related homoaconitase (HACN), which is like IPMI composed of a small and a large subunit. Changes in the SRR

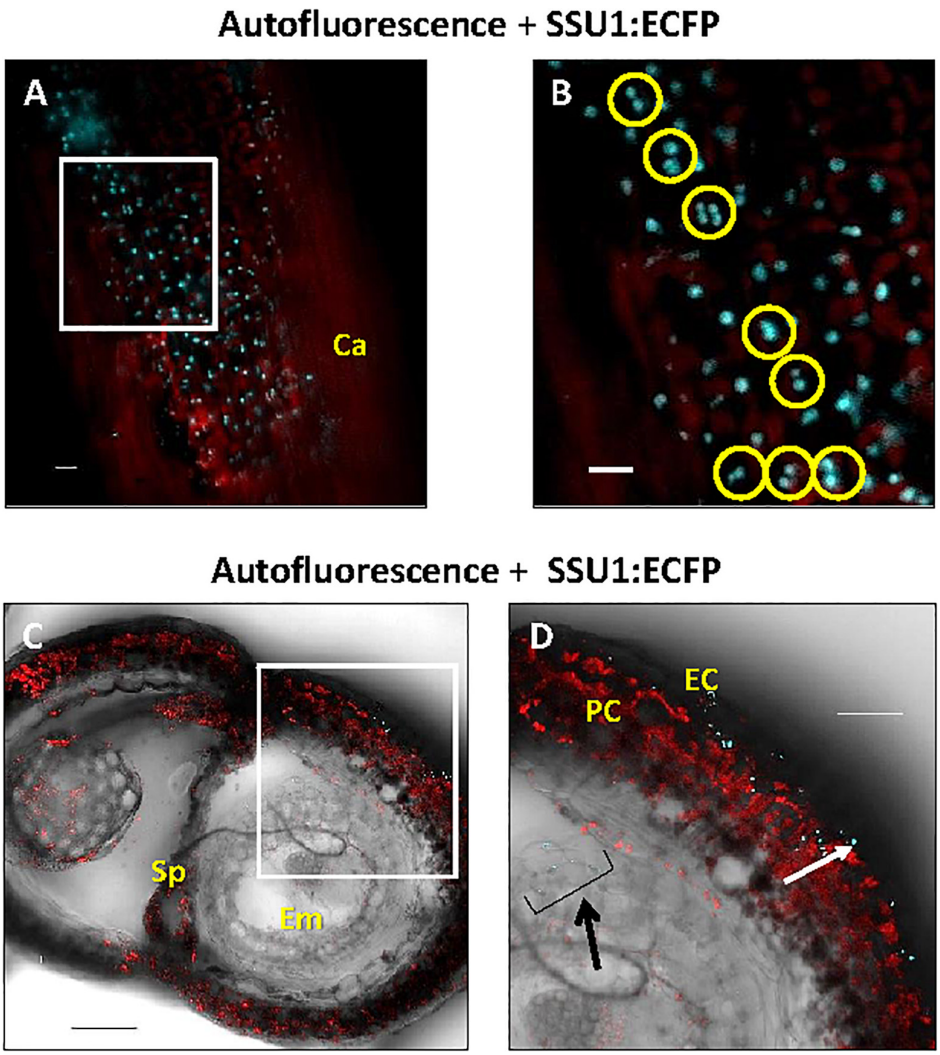

FIGURE 8 | Cellular and subcellular localization of the IPMI SSU1 protein in a premature silique. **(A)** An overlay of the fluorescence of IPMI SSU1:ECFP (cyan) and the chlorophyll autofluorescence (red) indicates that IPMI SSU1 is located in small sensory plastid-like organelles within cell layers above the chloroplast-containing cells (Ca, carpel). **(B)** A magnification of a part of the image shown in (**A,** white box) highlights the presence of IPMI SSU1 in dividing plastids (yellow circles). **(C,D)** In a cross section, IPMI SSU1:ECFP fluorescence (cyan) can be seen in small plastids (with a longitudinal diameter of approximately 4–5 μm) in epidermal cells (EC). In contrast, pericarp cells (PC) contain many chloroplasts as indicated by the chlorophyll fluorescence (red). In addition, IPMI SSU1:ECFP fluorescence is visible in outer cell layers in the developing seed (indicated by a black arrow). Sp, septum; Em, embryo. Scale bars: **(A)** 100 μm, **(B)** 10 μm and **(C,D)** 50 μm.

region of HACN in *M. jannaschii* had no negative influence on heterodimer formation. Even the exchange of 28 amino acids at the N-terminus of HACN with the sequence from the small subunit of IPMI did not interfere with higher order structure formation (Jeyakanthan et al., 2010). Furthermore, the small IPMI subunit of the archaeon *Pyrococcus horikoshii* can functionally replace the small HACN subunit when introduced into *Termus thermophilus*. This observation demonstrates that a functional dimer is formed between the large subunit HACN and the small subunit of IPMI although this small subunits shares only 43.0% identical and 62.8% similar amino acids with the small HACN subunit (Lombo et al., 2004).

Since the sequences in the SRR differ between all three IPMI subunits in *Arabidopsis* there is the potential to build IPMI enzymes with three different substrate preferences. In case of IPMI SSU1 (FLTLV), this corresponds with an expression pattern completely different from IPMI SSU2 and IPMI SSU3. In hypocotyls, there seems to be also a subtle difference between the expression pattern of IPMI subunits involved in Met chain elongation. The amino acid sequences in the SRRs are different between of IPMI SSU2 (AACTF) and IPMI SSU3 (YGTLI). While the latter contains two aliphatic amino acid at position 4 and 5 similar to IPMI SSU1, amino acid with aliphatic characteristics are present in positions 1 and 2 of IPMI SSU2. However, previous studies did not reveal clear differences in the glucosinolate quantity or composition between corresponding single mutants and wild-type lines. Likewise, amino acid profiling did not give clear hints toward the function of these proteins in the

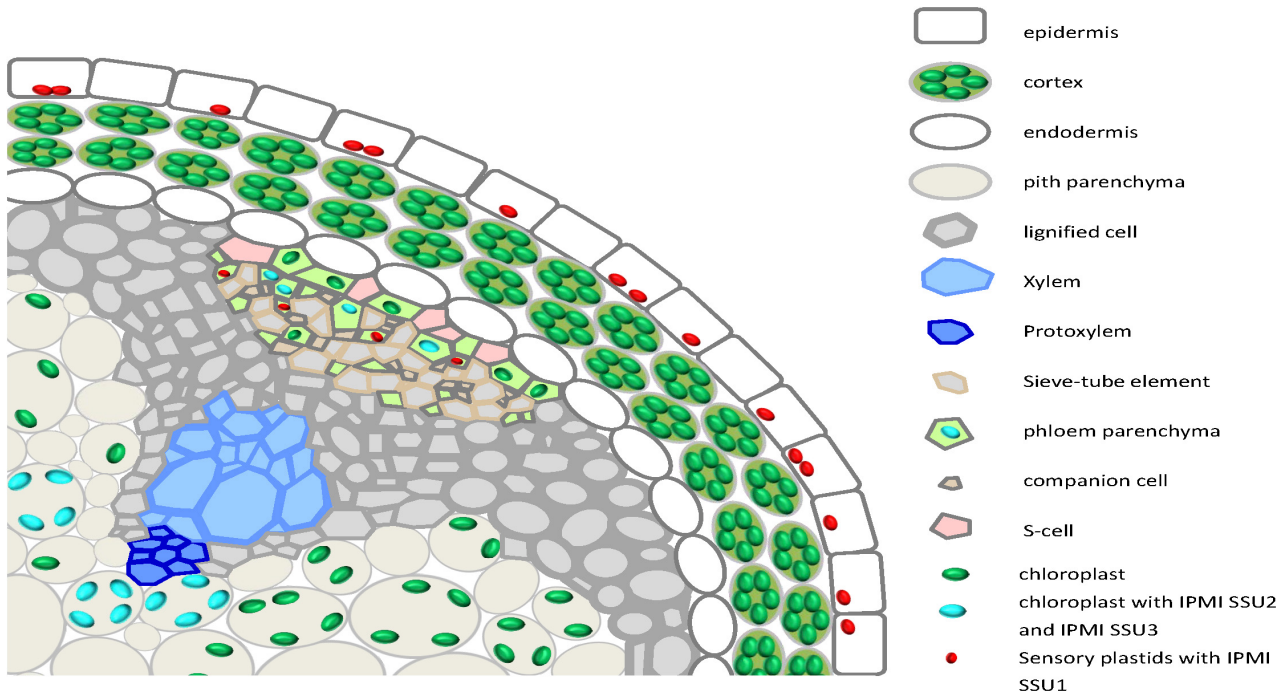

FIGURE 9 | A cartoon summarizing the expression of the different IPMI SSU proteins in a cross section through the flowering stalk.

metabolism of theses primary metabolites (Knill et al., 2009; He et al., 2010). In summary, our data demonstrate that substrate specificities of the IPMI SSU1-containing heterodimer and most likely of all IPMI heterodimers in *Arabidopsis* are determined by amino acid identities in the SRRs of the small subunit of IPMI and that this can contribute to functional specification of the holoenzymes. However, further detailed studies are required to define the exact substrate specificities of the individual IPMI SSUs in *Arabidopsis*.

Similar to IPMI, a functional specification was also observed for the isopropylmalate dehydrogenases. Here two enzymes are primarily involved in Leu biosynthesis (IPMDH2 and 3) whereas IPMDH1 catalyzes the oxidative decarboxylation step in the Met chain elongation pathway (He et al., 2009, 2011a). An amino acid substitution (Phe to Leu) in the active site severely reduces the activity of IPMDH1 toward 3-(2′-methylthio)-ethylmalate, an intermediate of Met chain elongation and enhances the conversion of 3-isopropylmalate while the reverse substitution (Leu to Phe) in IPMDH2 has the reciprocal effect. Similar to the small subunits of IPMI, the functional specification of these enzymes seems to be also influenced by spatiotemporal expression of the different IPMDH genes (He et al., 2011b).

Expression of Small Subunits of IPMI in Young Seedlings

All small IPMI subunits are expressed in young seedlings. IPMI SSU1 was found in small plastids in the epidermis similar to what was also seen in true leaves (**Figures 3A,C, 5A,B**). In most images, no natural fluorescence was detected in these small organelles with a longitudinal diameter of approximately 4 to 5 μm, but their detailed inspection revealed a weak autofluorescence linked to the presence of chlorophyll (**Supplementary Figure S3**). This is consistent with the recent detection of a set of proteins required for photosynthesis in so called sensory plastids located in vascular parenchyma cells. The sensory plastids, probably identical with what was known as leucoplasts in textbooks (Hudák, 2005), were also found in leaf epidermal cells and are morphologically very similar or even identical to the IPMI containing plastids seen in this analysis (Virdi et al., 2016; Beltran et al., 2018). Apart from cotyledons IPMI SSU1 was also found in parenchymatic cells surrounding the central vasculature in hypocotyls and roots (**Figures 3E,H,I**).

IPMI SSU2 and IPMI SSU3 were found along the vascular tissue in all parts of the seedlings. This is consistent with previous histochemical analyses of IPMI pSSU2:GUS and IPMI pSSU3:GUS reporter lines (He et al., 2010; Imhof et al., 2014). But now our analysis revealed a slightly different expression pattern of both proteins in hypocotyls, which might contribute to functional specification (**Figures 3E,H**). But as stated above, the knockout or knockdown of one or two genes in various plant lines did not result in any changes in glucosinolate quantity or composition, possibly be due to the measurement of total green tissue from adult plants, which does not detect differences between distinct tissues (Knill et al., 2009; He et al., 2010; Imhof et al., 2014).

A very peculiar expression pattern of IPMI SSU2 was seen in cotyledons. Here we found this protein in individual cells in the epidermis beside the usual association with vascular bundles (**Figures 3A–C**). Also expression of TGG1, a glucosinolate degrading myrosinase, has been found in individual epidermis

cells of cotyledons, but the pattern seems to be completely different from that of IPMI SSU2 suggesting no co-localization of this protein and the myrosinase (Husebye et al., 2002). Strikingly, the epidermal expression of IPMI SSU2 was found to be restricted to the cotyledon stage since we did not observe a similar pattern in rosette leaves as it has been seen for flavin monoxygenase $FMO_{GS\text{-}OX1}$ (Li et al., 2011).

IPMI SSU1 Expression Occurs Predominantly in Small Plastids of Epidermal Cell Layers in Green Tissues of Adult Plants

In textbooks and reviews, amino acid biosynthesis is usually described to occur in so-called leucoplasts with no details given on the localization of these organelles in distinct cell types or tissues (Hudák, 2005). Our studies of adult plants confirmed that IPMI SSU1 fusion proteins accumulate in small plastids distinguishable from chloroplasts (**Figures 3D**, **5B**). In rosette leaves, the major part of the above-ground tissue of *Arabidopsis*, IPMI SSU1-containing plastids were exclusively detected in epidermis cells. This localization in the epidermis is consistent with two other studies (Svozil et al., 2015; Beltran et al., 2018). As mentioned above, the size of these organelles and their localization in epidermis cells are consistent with so-called sensory plastids (Virdi et al., 2016; Beltran et al., 2018). A proteomic analysis of FACS separated sensory plastids from vascular parenchyma and mesophyll chloroplasts confirmed the presence of IPMI SSU1 in the proteome of sensory plastids and the absence of this protein from mesophyll chloroplasts. This applies also for other proteins of the leucine biosynthetic pathway, strongly suggesting that the complete biosynthetic pathway is present in this organelle type (Beltran et al., 2018). In addition, the localization of IPMI SSU1 both in epidermal cells and in cells associated with phloem is perfectly reflected by a targeted proteome analysis of leaf mesophyll, of epidermal and of vascular tissue of *Arabidopsis* leaves (Svozil et al., 2015). This study found IPMI SSU1 predominantly in the epidermis and to a lower extent also in vascular tissue, but not in the mesophyll, in contrast to the exclusive localization of BCAT4, IPMI SSU2 and IPMI SSU3 in the vasculature. Although sensory plastids from vascular tissue and from epidermal cells share a set of identical proteins, it is presently unclear to which extent the proteomes of these organelles from both tissues match each other (Beltran et al., 2018).

Sensory plastids contain the MutS HOMOLOG1 (MSH1) suggested to be a stress response signaling protein, highlighting the role of these organelles in tissue-specific signaling of stress response in plants. Under abiotic stress conditions, MSH1 steady state mRNA is strongly reduced, whereas downregulation or knockout of the plastid-located MSH1 proteins signal a stress state to the mutant plant, which displays enhanced tolerance to abiotic stress (MacKenzie and Kundariya, 2019). Consistent with this observation, the proteome composition of these sensory plastids reflects the function in triggering of stress and developmental responses. This function might also be linked to reticulate mutant phenotypes (Beltran et al., 2018). These phenotypes are characterized by specific aberrations in the development of mesophyll cells, while vascular tissue seems to be unaffected although most genes affected in reticulate mutants are strongly expressed in this tissue (Lundquist et al., 2014). The reticulate phenotype can be explained by two models: the "supply" and the "signaling" hypothesis. The former suggests that primary metabolites are provided to the developing mesophyll tissue. If this supply is impaired, then mesophyll development is compromised. The signaling hypothesis proposes a molecular signal to be send out from the vascular tissue to control mesophyll development. Among others, amino acids might function both as supply and/or as a signal. This is consistent with the observation that administration of aromatic amino acids rescues the reticulate phenotype in the *cue1* mutant, in which the phosphoenolpyruvate/phosphate transporter 1 (PTT1) is affected (Lundquist et al., 2014). In addition, metabolite profiling of *re* and *rer3* reticulate mutants revealed lowered levels of aromatic as well as branched chain amino acids (Pérez-Pérez et al., 2013). Interestingly, the leaves of the IPMI SSU1 knockdown mutant shows phenotypic similarities to those of reticulate mutants, with green veins and pale interveinal regions as well as small narrow chloroplasts with reduced levels of starch. But the IPMI SSU1 knockdown mutant contains elevated levels of Leu, thus, the phenotype cannot be rescued by the administration of Leu (Imhof et al., 2014). However, the reticulate-like phenotype might suggest that reduced IPMI SSU1 function and its consequences on primary metabolism might interfere with sensory plastid function in the epidermis. Whether the IPMI SSU1 knockdown plants exhibit altered fitness under abiotic stress remains to be investigated, however, these plants already suffer from a strong pleiotropic phenotype under normal cultivation conditions (Imhof et al., 2014).

Beside the potential function in the rescue of the reticulate phenotype as described above, elevated levels of aromatic amino acids play a role in broad spectrum pathogen resistance by acting as precursors for phenylpropanoids, lignin, hormones and many other compounds (Lundquist et al., 2014; Tonnessen et al., 2015). Whether leucine or the other branched chain amino acids have similar functions is unclear at present.

The epidermal localization of IPMI SSU1 also applies to other green tissues like stems, siliques and maturing seeds strongly suggesting that this cell layer is the predominant tissue which hosts the Leu biosynthetic pathway, while major parts of the green tissue including the mesophyll, the main photosynthetic tissue, is excluded from biosynthesis of this amino acid.

Beside the epidermal localization, IPMI SSU1 was also detected in the root cortex and in cells associated with the phloem (**Figure 6**), which is in line with a role of this protein in early events of aliphatic glucosinolate biosynthesis (Imhof et al., 2014). Such a role is further supported by the detection of IPMI SSU1 in a narrow stripe potentially representing a single cell layer along the phloem-associated cells in flowering stalks expressing IPMI SSU2 and IPMI SSU3 (**Supplementary Figure S5A**). The weak fluorescence was found in structures highly similar to sensory plastids and no

equivalent fluorescence was observed in non-transformed wild-type plants.

IPMI SSU2 and IPMI SSU3 Are Expressed in Both Phloem-Associated and Xylem-Associated Cells

As expected from previous expression studies of genes involved in glucosinolate biosynthesis and regulation and from in tissue-specific proteomic studies (Reintanz et al., 2001; Chen et al., 2003; Grubb et al., 2004; Tantikanjana et al., 2004; Schuster et al., 2006; Gigolashvili et al., 2007, 2008; He et al., 2010; Li et al., 2011; Imhof et al., 2014; Svozil et al., 2015; Nintemann et al., 2018), both IPMI SSU2 and IPMI SSU3 were found to be expressed along vascular tissues. In green parts of adult plants particularly in flowering stalks, these proteins were found in chloroplasts of cells located in the periphery of the phloem (**Figures 5D**, **7A**). However, we also found these proteins in parenchymatic cells situated proximal to the xylem. A similar pattern has been observed for the flavin monoxygenase $FMO_{GS\text{-}OX1}$, which is involved in side chain modification of aliphatic glucosinolates, catalyzing one of the last steps in the biosynthesis of these metabolites (Li et al., 2011) as well as for the cytochrome P450 protein CYP83A1, required for core structure formation of aliphatic glucosinolates (Nintemann et al., 2018). Additionally, such a pattern was also seen when a nucleus-targeted 3xGFP reporter protein was expressed under the control of the *BCAT4* promoter (pBCAT4:3xGFP-NLS) (**Supplementary Figures S5B,C**). BCAT4 catalyzes the committed step of Met-derived glucosinolate biosynthesis (Schuster et al., 2006). Thus, in total six different proteins involved in glucosinolate biosynthesis are expressed not only in phloem-associated cells but also in parenchymatic cells proximal to the xylem demonstrating that these cells play a role in all phases of the biosynthesis of Met-derived aliphatic glucosinolates. It is presently unknown whether these cells exhibit any additional functional specification apart from their role in specialized metabolism. The observation that biosynthesis of these specialized compounds might also occur in the proximity to the xylem fits well with the transport of glucosinolates in the xylem sap (Andersen et al., 2013; Madsen et al., 2014).

By using transcriptional/translational fusions we found that the expression of BCAT4 and IPMI SSU2/IPMI SSU3 is restricted to cells located at the proximal boundary of the phloem and at the inwards oriented side of the xylem of flowering stalks (**Figure 6** and **Supplementary Figures 5B,C**). The localization of the *BCAT4* promoter driven 3XGFP (pBCAT4:3XGFP-NLS) in the cells of the phloem periphery could potentially coincide with sulfur rich S-cells, which contain large amounts of glucosinolates. These cells are situated between the phloem parenchyma and the endodermis (Koroleva et al., 2000, 2010). However, it seems unlikely that BCAT4 and IPMI SSU2/IPMI SSU3 are expressed in these cells, since these sulfur-rich cells are biosynthetically inactive (Xu et al., 2019). This is supported by the observation that *BCAT4* promoter driven expression of GFP (pBCAT4:3XGFP-NLS) was seen in nuclei of relatively small and short cells with a morphology completely different from the extremely long S-cells (**Supplementary Figures S5B,C**). This is consistent with the conclusion drawn from the expression analysis of the above mentioned flavin monoxygenase $FMO_{GS\text{-}OX1}$ and CYP83A1, which excludes expression of these proteins in S-cells (Li et al., 2011; Nintemann et al., 2018). As suggested by Nintemann et al. (2018) for CYP83A1, we favor the presence of BCAT4 and IPMI SSU2/IPMI SSU3 in phloem parenchyma cells. Nevertheless, cells synthesizing aliphatic glucosinolates and cells storing these compounds are in close vicinity to each other. Likewise, parenchymatic cells located proximal to the xylem express these proteins suggesting that Met chain elongation and probably the complete biosynthesis of aliphatic glucosinolates occurs in this tissue. These compounds could potentially be transferred into the xylem, which serves as transport system for glucosinolates (Andersen et al., 2013). Unlike the situation in the periphery of the phloem, all of the glucosinolates synthesized near the xylem are most likely transported into other plant parts since storage of glucosinolates has not been observed in the vicinity of the xylem (Koroleva et al., 2010).

In Roots, IPMI SSU1 and IPMI SSU2/IPMI SSU3 Are Found in Tissues Surrounding the Central Cylinder

In young roots, expression of IPMI SSU2 and IPMI SSU3 was found in cells along the central cylinder, which is consistent with the biosynthesis of glucosinolates in this organ (Andersen et al., 2013). In canola, storage of glucosinolates has been demonstrated in the inner periderm of roots showing secondary growth whereas an accumulation to a far lesser extent seems to occur in phloem parenchyma of roots before secondary growth initiates (McCully et al., 2008). If a similar scenario is assumed for *Arabidopsis*, storage in the phloem parenchyma would be close to or even coincide with tissues where IPMI SSU2 and IPMI SSU3 are expressed (**Figure 6**). However, further detailed investigations of glucosinolate storage in roots of *Arabidopsis* are required to verify this assumption.

In roots, all three small IPMI subunits are found in colorless plastids. Those containing IPMI SSU1 have frequently been found to form stromules (**Figure 6A**, inset) (Köhler and Hanson, 2000). Although they are morphologically similar to each other, these plastids seem to be functionally specialized having different biological roles in plant metabolism, as suggested by the presence or absence of the different IPMI proteins and presumably also of other enzymes involved in Leu biosynthesis or Met chain elongation. The exclusion of IPMI SSU1 from large parts of the green tissue indicates that roots might also play an important role in Leu or even BCAA biosynthesis. The relatively strong expression of IPMI SSU2 and IPMI SSU3 supports a substantial role of roots in biosynthesis of Met-derived glucosinolates.

Spatial Separation of IPMI SSU1 From IPMI SSU2 and IPMI SSU3

Considering the results of our studies, two features determine the functional specification of IPMI in Leu biosynthesis (primary metabolism) and Met chain elongation (specialized metabolism)

in *Arabidopsis*. First, the different primary sequences within the SRR of the small subunits define the substrate preferences of the different heterodimers. Second, there seems to be an almost complete spatial separation of IPMI heterodimers containing either IPMI SSU1 or IPMI SSU2/IPMI SSU3 assigning distinct functions to certain cell and tissue types (**Figure 9**). IPMI SSU2 and IPMI SSU3 are apparently co-expressed in identical organelles, in almost identical cells and tissues, suggesting the heterodimers containing these proteins to have very similar or identical functions. However, two exceptions have been observed: in hypocotyls, IPMI SSU2 was found in further peripheral cells in comparison to IPMI SSU3 (**Figures 3E,F,H,I**), and in cotyledons, where IPMI SSU2 was seen in isolated epidermal cells (**Figures 3A,C**), a pattern which we never observed for IPMI SSU3. Identical expression patterns of IPMI SSU2 and IPMI SSU3 were found in many different plants from different generations, which makes it highly unlikely that the pattern are influenced by unknown regulatory loci segregating in the Col/Ws amalgam of the *ipmi ssu2-1/ipmi ssu3-1* nuclear background. In addition, for IPMI SSU1 we used two different constructs, in which the reading frame is fused to different reporter genes (IPMI SSU1:RFP/IPMI SSU2:ECFP). We obtained identical results with these different constructs also analyzed in plants from different generations.

The differential expression can be summarized as follows (**Figure 9**): In green parts of adult plants analyzed in this study, IPMI SSU1 was almost exclusively found in small plastids in epidermal cells. Interestingly, this suggests that extensive transport processes are required for a full supply of the whole plant with Leu. The small IPMI SSU1-containing plastids were also detectable in phloem associated cells in flowering stalks. With regard to size and tissue localization these plastids are identical to sensory plastids. In addition, plastids containing IPMI SSU1 exhibited weak, mostly undetectable autofluorescence typical for chlorophyll, which is consistent with the detection of proteins required for photosynthesis is these organelles (**Supplementary Figure S3**). Sensory plastids contain IPMI proteins as well as other enzymes required for Leu biosynthesis (Beltran et al., 2018). In roots, IPMI SSU1 was predominantly detected in small plastids of cortex cells surrounding the central cylinder and in roots hairs, which are part of the epidermal layer. High expression of this protein is also evident in root tips.

In above-ground parts, IPMI SSU2 and IPMI SSU3 were found in chlorophyll-containing chloroplasts of cells in the periphery of the phloem and in parenchymatic cells located proximal to the xylem (**Figures 5D**, **7A**). A very similar (or almost identical) tissue localization was found BCAT4, also active in Met chain elongation (**Supplementary Figures 5B,C**) (Schuster et al., 2006). Neither IPMI SSU2 and IPMI SSU3 nor BCAT4 were expressed in S-cells, the major storage sites of glucosinolates in the flowering stalk and leaves. In roots, IPMI SSU2 and IPMI SSU3 were seen in cells surrounding the central cylinder, where they seem to be located proximal to those cells expressing IPMI SSU1.

IPMI SSU2 and IPMI SSU3 are physically separated from IPMI SSU1 at the subcellular level. This might also hold true for the cellular level, but in case of the weak expression observed along the phloem we were not able to assign the fluorescing plastid-like structures to specific cells. Nevertheless, our studies indicate a spatial separation of Met chain elongation pathway and Leu biosynthesis. A previous study suggested an additional role of IPMI SSU1 in early phases (at least the first cycle) of Met chain elongation suggested by the accumulation of intermediates of Met chain elongation (mainly C3, less C4) and the biosynthesis of predominantly short-chain glucosinolates (C3 and C4) in the *ipmi ssu2-1/ipmi ssu3-1* double knockout mutant (Imhof et al., 2014). The involvement of IPMI SSU1 in glucosinolate biosynthesis would require intercellular transport processes of intermediates between plastids in different cells. This appears to be straightforward in the phloem, where cells expressing IPMI SSU1 were in close proximity to cells expressing IPMI SSU2 and IPMI SSU3 (**Supplementary Figure S5A**). However, the IPMI SSU1 knockdown plants show a strong pleiotropic phenotype including elevated levels of jasmonic acid (and derivatives of it). The increase of these hormones promotes glucosinolate biosynthesis and might thus lead to an "artificial" excessive accumulation of short-chain intermediates. As argued in Imhof et al. (2014), the accumulation of short-chain glucosinolates in the *ipmi ssu2-1/ipmi ssu3-1* double knockout mutant also demonstrates that IPMI SSU1 can compensate for the absence of IPMI SSU2 and -3 in the biosynthesis of these metabolites. To which extent this participation occurs in wild-type plants with three intact IPMI SSU genes, cannot be finally assessed.

We have not analyzed all tissues in all developmental stages and in some tissues there might be expression beyond detection levels. Thus, we cannot exclude additional expression patterns to the above described expression patterns. However, our study provides clear evidence that in *Arabidopsis* the SRR determines the substrate preference of the different heterodimeric enzyme Isopropylmalate isomerases and that this functional specialization is underpinned by different spatial localization of the distinct small subunits. Both features guarantee clear functions of the different heterodimers in either Leu biosynthesis or Met chain elongation albeit the large subunit participates in both pathways.

DATA AVAILABILITY STATEMENT

All datasets generated for this study are included in the article/**Supplementary Material**.

AUTHOR CONTRIBUTIONS

KL, JI, and SB planned and designed the work. KL, KC, JI, and CC performed the experiments and measurements, and analyzed the data. KL, KC AS, and CC carried out and assisted the microscopy and image analysis. KL, JI, KC, AS, CC, BH, and SB contributed to the interpretation of results. SB wrote the manuscript. All the authors made intellectual contributions to the study, read the manuscript, and approved the submission.

FUNDING

This work was supported by grant Bi 590/9-2 to SB by the Deutsche Forschungsgemeinschaft and grant 99 from Danish National Research Foundation to the DynaMo Center to BH. Universität Ulm is a Frontiers Institutional Member.

ACKNOWLEDGMENTS

We thank Uli Tengler and Conny Guha for excellent technical assistance. We are very grateful to Michael Reichelt and Jonathan Gershenzon (Max Planck Institute for Chemical Ecology, Jena, Germany) for the analysis of glucosinolates and to Birgit and Katrin Stoll (Institute Molecular Botany, Ulm University, Germany) for cloning of the pBCAT4:3xGFP-NLS construct. Providing the plasmid pJF667 with 3XGFP:NLS by Joachim Forner and Jan Lohmann (Stem Cell Biology, Centre for Organismal Studies, Heidelberg, Germany) is deeply acknowledged. Confocal images were taken at the Center for Advanced Bioimaging (CAB), University of Copenhagen.

SUPPLEMENTARY MATERIAL

The Supplementary Material for this article can be found online at: https://www.frontiersin.org/articles/10.3389/fpls.2020.00808/full#supplementary-material

REFERENCES

Andersen, T. G., Nour-Eldin, H. H., Fuller, V. L., Olsen, C. E., Burow, M., and Halkier, B. A. (2013). Integration of biosynthesis and long-distance transport establish organ-specific glucosinolate profiles in vegetative *Arabidopsis*. *Plant Cell* 25, 3133–3145. doi: 10.1105/tpc.113.110890

Beltran, J., Wamboldt, Y., Sanchez, R., LaBrant, E. W., Kundariya, H., Virdi, K. S., et al. (2018). Specialized plastids trigger tissue-specific signaling for systemic stress response in plants. *Plant Physiol.* 178, 672–683. doi: 10.1104/pp.18.00804

Binder, S. (2010). Branched-chain amino acid metabolism in *Arabidopsis thaliana*. *Arabidopsis Book* 8:e0137. doi: 10.1199/tab.0137

Brown, P. D., Tokuhisa, J. G., Reichelt, M., and Gershenzon, J. (2003). Variation of glucosinolate accumulation among different organs and developmental stages of *Arabidopsis thaliana*. *Phytochem* 62, 471–481. doi: 10.1016/s0031-9422(02)00549-6

Chen, S., Glawischnig, E., Jorgensen, K., Naur, P., Jorgensen, B., Olsen, C. E., et al. (2003). CYP79F1 and CYP79F2 have distinct functions in the biosynthesis of aliphatic glucosinolates in *Arabidopsis*. *Plant J.* 33, 923–937. doi: 10.1046/j.1365-313x.2003.01679.x

Clough, S. J., and Bent, A. F. (1998). Floral dip: a simplified method for agrobacterium-mediated transformation of *Arabidopsis thaliana*. *Plant J.* 16, 735–742.

Curtis, M. D., and Grossniklaus, U. (2003). A gateway cloning vector set for high-throughput functional analysis of genes in planta. *Plant Physiol.* 133, 462–469. doi: 10.1104/pp.103.027979

Davis, S. J., and Vierstra, R. D. (1998). Soluble, highly fluorescent variants of green fluorescent protein (GFP) for use in higher plants. *Plant Mol. Biol.* 36, 521–528.

Edwards, K., Johnstone, C., and Thompson, C. (1991). A simple and rapid method for the preparation of plant genomic DNA for PCR analysis. *Nucleic Acids Res.* 19:1349. doi: 10.1093/nar/19.6.1349

Forner, J., and Binder, S. (2007). The red fluorescent protein eqFP611: application in subcellular localization studies in higher plants. *BMC Plant Biol.* 7:28. doi: 10.1186/1471-2229-7-28

Frishman, D., and Hentze, M. W. (1996). Conservation of aconitase residues revealed by multiple sequence analysis. *Eur. J. Biochem.* 239, 197–200. doi: 10.1111/j.1432-1033.1996.0197u.x

Gigolashvili, T., Engqvist, M., Yatusevich, R., Muller, C., and Flugge, U. I. (2008). HAG2/MYB76 and HAG3/MYB29 exert a specific and coordinated control on the regulation of aliphatic glucosinolate biosynthesis in *Arabidopsis thaliana*. *New Phytol.* 177, 627–642. doi: 10.1111/j.1469-8137.2007.02295.x

Gigolashvili, T., Yatusevich, R., Berger, B., Muller, C., and Flugge, U. I. (2007). The R2R3-MYB transcription factor HAG1/MYB28 is a regulator of methionine-derived glucosinolate biosynthesis in *Arabidopsis thaliana*. *Plant J.* 51, 247–261. doi: 10.1111/j.1365-313x.2007.03133.x

Gigolashvili, T., Yatusevich, R., Rollwitz, I., Humphry, M., Gershenzon, J., and Flügge, U. I. (2009). The plastidic bile acid transporter 5 is required for the biosynthesis of methionine-derived glucosinolates in *Arabidopsis thaliana*. *Plant Cell* 21, 1813–1829. doi: 10.1105/tpc.109.066399

Grubb, C. D., and Abel, S. (2006). Glucosinolate metabolism and its control. *Trends Plant Sci.* 11, 89–100. doi: 10.1016/j.tplants.2005.12.006

Grubb, C. D., Zipp, B. J., Ludwig-Muller, J., Masuno, M. N., Molinski, T. F., and Abel, S. (2004). *Arabidopsis* glucosyltransferase UGT74B1 functions in glucosinolate biosynthesis and auxin homeostasis. *Plant J.* 40, 893–908. doi: 10.1111/j.1365-313x.2004.02261.x

Gruer, M. J., Artymiuk, P. J., and Guest, J. R. (1997). The aconitase family: three structural variations on a common theme. *Trends Biochem. Sci.* 22, 3–6. doi: 10.1016/s0968-0004(96)10069-4

Halkier, B. A., and Gershenzon, J. (2006). Biology and biochemistry of glucosinolates. *Ann. Rev. Plant Biol.* 57, 303–333. doi: 10.1146/annurev.arplant.57.032905.105228

He, Y., Chen, B., Pang, Q., Strul, J. M., and Chen, S. (2010). Functional specification of *Arabidopsis* isopropylmalate isomerases in glucosinolate and leucine biosynthesis. *Plant Cell Physiol.* 51, 1480–1487. doi: 10.1093/pcp/pcq113

He, Y., Chen, L., Zhou, Y., Mawhinney, T. P., Chen, B., Kang, B. H., et al. (2011a). Functional characterization of *Arabidopsis thaliana* isopropylmalate dehydrogenases reveals their important roles in gametophyte development. *New Phytol.* 189, 160–175. doi: 10.1111/j.1469-8137.2010.03460.x

He, Y., Galant, A., Pang, Q., Strul, J. M., Balogun, S. F., Jez, J. M., et al. (2011b). Structural and functional evolution of isopropylmalate dehydrogenases in the leucine and glucosinolate pathways of *Arabidopsis thaliana*. *J. Biol. Chem.* 286, 28794–28801. doi: 10.1074/jbc.M111.262519

He, Y., Mawhinney, T. P., Preuss, M. L., Schroeder, A. C., Chen, B., Abraham, L., et al. (2009). A redox-active isopropylmalate dehydrogenase functions in the biosynthesis of glucosinolates and leucine in *Arabidopsis*. *Plant J.* 60, 679–690. doi: 10.1111/j.1365-313x.2009.03990.x

Hooper, C. M., Castleden, I. R., Tanz, S. K., Aryamanesh, N., and Millar, A. H. (2017). SUBA4: the interactive data analysis centre for *Arabidopsis* subcellular protein locations. *Nucleic Acids Res.* 45, D1064–D1074. doi: 10.1093/nar/gkw1041

Hudák, J. (2005). "Photosynthetic apparatus," in *Handbook of Photosynthesis*, 2nd Edn, ed. M. Pessarak (London: CRC Press), 27–48.

Husebye, H., Chadchawan, S., Winge, P., Thangstad, O. P., and Bones, A. M. (2002). Guard cell- and phloem idioblast-specific expression of thioglucoside glucohydrolase 1 (myrosinase) in *Arabidopsis*. *Plant Physiol.* 128, 1180–1188. doi: 10.1104/pp.010925

Imhof, J., Huber, F., Reichelt, M., Gershenzon, J., Wiegreffe, C., Lächler, K., et al. (2014). The small subunit 1 of the *Arabidopsis* isopropylmalate isomerase is required for normal growth and development and the early stages of glucosinolate formation. *PLoS One* 9:e91071. doi: 10.1371/journal.pone.0091071

Jeyakanthan, J., Drevland, R. M., Gayathri, D. R., Velmurugan, D., Shinkai, A., Kuramitsu, S., et al. (2010). Substrate specificity determinants of the methanogen homoaconitase enzyme: structure and function of the small subunit. *Biochemistry* 49, 2687–2696. doi: 10.1021/bi901766z

Knill, T., Reichelt, H., Paetz, C., Gershenzon, J., and Binder, S. (2009). *Arabidopsis thaliana* encodes a bacterial-type heterodimeric isopropylmalate isomerase

involved in both Leu biosynthesis and the Met chain elongation pathway of glucosinolate formation. *Plant Mol. Biol.* 71, 227–239. doi: 10.1007/s11103-009-9519-5

Köhler, R. H., and Hanson, M. R. (2000). Plastid tubules of higher plants are tissue-specific and developmentally regulated. *J. Cell Sci.* 113, 81–89.

Koroleva, O. A., Davies, A., Deeken, R., Thorpe, M. R., Tomos, A. D., and Hedrich, R. (2000). Identification of a new glucosinolate-rich cell type in *Arabidopsis* flower stalk. *Plant Physiol.* 124, 599–608. doi: 10.1104/pp.124.2.599

Koroleva, O. A., Gibson, T. M., Cramer, R., and Stain, C. (2010). Glucosinolate-accumulating S-cells in *Arabidopsis* leaves and flower stalks undergo programmed cell death at early stages of differentiation. *Plant J.* 64, 456–469. doi: 10.1111/j.1365-313X.2010.04339.x

Kroymann, J., Donnerhacke, S., Schnabelrauch, D., and Mitchell-Olds, T. (2003). Evolutionary dynamics of an *Arabidopsis* insect resistance quantitative trait locus. *Proc. Natl. Acad. Sci. U.S.A.* 100(Suppl. 2), 14587–14592. doi: 10.1073/pnas.1734046100

Kroymann, J., Textor, S., Tokuhisa, J. G., Falk, K. L., Bartram, S., Gershenzon, J., et al. (2001). A gene controlling variation in *Arabidopsis* glucosinolate composition is part of the methionine chain elongation pathway. *Plant Physiol.* 127, 1077–1088. doi: 10.1104/pp.010416

Lee, E. H., Cho, Y. W., and Hwang, K. Y. (2012). Crystal structure of LeuD from *Methanococcus jannaschii*. *Biochem. Biophys. Res. Commun.* 419, 160–164. doi: 10.1016/j.bbrc.2012.01.125

Li, J., Kristiansen, K. A., Hansen, B. G., and Halkier, B. A. (2011). Cellular and subcellular localization of flavin-monooxygenases involved in glucosinolate biosynthesis. *J. Exp. Bot.* 62, 1337–1346. doi: 10.1093/jxb/erq369

Liu, Y.-G., and Whittier, R. F. (1994). Thermal asymmetric interlaced PCR: automatable amplification and sequencing of insert end fragments from pi and yac clones for chromosome walking. *Genomics* 25, 674–681. doi: 10.1016/0888-7543(95)80010-j

Lombo, T., Takaya, N., Miyazaki, J., Gotoh, K., Nishiyama, M., and Kosuge, T. (2004). Functional analysis of the small subunit of the putative homoaconitase from *Pyrococcus horikoshii* in the *Termus* lysine biosynthetic pathway. *FEMS Microbiol. Lett.* 233, 315–324. doi: 10.1111/j.1574-6968.2004.tb09498.x

Lundquist, P. K., Rosar, C., Bäutigam, A., and Weber, A. P. M. (2014). Plastid signals and the bundle sheath: mesophyll development in reticulate mutants. *Mol. Plant* 7, 14–29. doi: 10.1093/mp/sst133

MacKenzie, S. A., and Kundariya, H. (2019). Organellar protein multi-functionality and phenotypic plasticity in plants. *Phil. Trans. R. Soc. B* 20:375.

Madsen, S. R., Olsen, C. E., Nour-Eldin, H. H., and Halkier, B. A. (2014). Elucidating the role of transport processes in leaf glucosinolate distribution. *Plant Physiol.* 166, 1450–1462. doi: 10.1104/pp.114.246249

Manikandan, K., Geerlof, A., Zozulya, A. V., Svergun, D. I., and Weiss, M. S. (2011). Structural studies on the enzyme complex isopropylmalate isomerase (LeuCD) from Mycobacterium tuberculosis. *Proteins* 79, 35–49. doi: 10.1002/prot.22856

McCully, M. E., Miller, C., Sprague, S. J., Huang, C. X., and Kirkegaard, J. A. (2008). Distribution of glucosinolates and sulphur-rich cells in roots of field-grown canola (*Brassica napus*). *New Phytol.* 180, 193–205. doi: 10.1111/j.1469-8137.2008.02520.x

Nintemann, S. J., Hunziker, P., Andersen, T. G., Schulz, A., Burow, M., and Halkier, B. A. (2018). Localization of the glucosinolate biosynthetic enzymes reveals distinct spatial patterns for the biosynthesis of indole and aliphatic glucosinolates. *Physiol. Plant.* 163, 138–154. doi: 10.1111/ppl.12672

Pérez-Pérez, J. M., Esteve-Bruna, D., González-Bayón, R., Kangasjärvi, S., Caldana, C., Hannah, M. A., et al. (2013). Functional redundancy and divergence within the *Arabidopsis* RETICULATA-RELATED gene family. *Plant Physiol.* 162, 589–603. doi: 10.1104/pp.113.217323

Reintanz, B., Lehnen, M., Reichelt, M., Gershenzon, J., Kowalczyk, M., Sandberg, G., et al. (2001). bus, a bushy *Arabidopsis* CYP79F1 knockout mutant with abolished synthesis of short-chain aliphatic glucosinolates. *Plant Cell* 13, 351–367. doi: 10.1105/tpc.13.2.351

Sawada, Y., Kuwahara, A., Nagano, M., Narisawa, T., Sakata, A., Saito, K., et al. (2009a). Omics-based approaches to methionine side-chain elongation in *Arabidopsis*: characterization of the genes encoding methylthioalkylmalate isomerase and methylthioalkylmalate dehydrogenase. *Plant Cell Physiol.* 50, 1181–1190. doi: 10.1093/pcp/pcp079

Sawada, Y., Toyooka, K., Kuwahara, A., Sakata, A., Nagano, M., Saito, K., et al. (2009b). *Arabidopsis* bile acid:sodium symporter family protein 5 is involved in methionine-derived glucosinolate biosynthesis. *Plant Cell Physiol.* 50, 1579–1586. doi: 10.1093/pcp/pcp110

Schuster, J., Knill, T., Reichelt, H., Gershenzon, J., and Binder, S. (2006). BRANCHED-CHAIN AMINOTRANSFERASE 4 is part of the chain elongation pathway in the biosynthesis of methionine-derived glucosinolates in *Arabidopsis*. *Plant Cell* 18, 1–16.

Singh, B. K. (1999). "Biosynthesis of valine, leucine and isoleucine," in *Plant Amino acids: Biochemistry and Biotechnology*, ed. B. K. Singh (New York, NY: Marcel Dekker), 227–247.

Svozil, J., Gruissem, W., and Baerenfaller, K. (2015). Proteasome targeting of proteins in *Arabidopsis* leaf mesophyll, epidermal and vascular tissues. *Front. Plant Sci.* 6:376. doi: 10.3389/fpls.2015.00376

Tantikanjana, T., Mikkelsen, M. D., Hussain, M., Halkier, B. A., and Sundaresan, V. (2004). Functional analysis of the tandem-duplicated P450 genes SPS/BUS/CYP79F1 and CYP79F2 in glucosinolate biosynthesis and plant development by Ds transposition-generated double mutants. *Plant Physiol.* 135, 840–848. doi: 10.1104/pp.104.040113

Textor, S., de Kraker, J.-W., Hause, B., Gershenzon, J., and Tokuhisa, J. G. (2007). MAM3 catalyzes the formation of all aliphatic glucosinolate chain lengths in *Arabidopsis*. *Plant Physiol.* 144, 60–71.

Tonnessen, B. W., Manosalva, P., Lang, J. M., Baraoidan, M., Bordeos, A., Mauleon, R., et al. (2015). Rice phenylalanine ammonia-lyase gene OsPAL4 is associated with broad spectrum disease resistance. *Plant Mol. Biol.* 87, 273–286.

Tzfira, T., Tian, G. W., Lacroix, B., Vyas, S., Li, J., Leitner-Dagan, Y., et al. (2005). pSAT vectors: a modular series of plasmids for autofluorescent protein tagging and expression of multiple genes in plants. *Plant Mol. Biol.* 57, 503–516.

Virdi, K. S., Wamboldt, Y., Kundariya, H., Laurie, J. D., Keren, I., Kumar, K. R. S., et al. (2016). MSH1 is a plant organellar dna binding and thylakoid protein under precise spatial regulation to alter development. *Mol. Plant* 9, 245–260. doi: 10.1016/j.molp.2015.10.011

Weigel, D., and Glazebrook, J. (2002). *Arabidopsis, a Laboratory Manual.* Cold Spring Habor, NY: Cold Spring Harbor Laboratory Press.

Wittstock, U., and Halkier, B. A. (2002). Glucosinolate research in the *Arabidopsis* era. *Trends Plant Sci.* 7, 263–270.

Xu, D., Hunziker, P., Koroleva, O., Blennow, A., Crocoll, C., Schulz, A., et al. (2019). GTR-mediated radial import directs accumulation of defensive glucosinolates to sulfur-rich cells in the phloem cap of *Arabidopsis* Inflorescence stem. *Mol. Plant* 12, 1474–1484. doi: 10.1016/j.molp.2019.06.008

Yasutake, Y., Yao, M., Sakai, N., Kirita, T., and Tanaka, I. (2004). Crystal structure of the *Pyrococcus horikoshii* isopropylmalate isomerase small subunit provides insight into the dual substrate specificity of the enzyme. *J. Mol. Biol.* 344, 325–333.

Zacharias, D. A., Violin, J. D., Newton, A. C., and Tsien, R. Y. (2002). Partitioning of lipid-modified monomeric GFPs into membrane microdomains of live cells. *Science* 296, 913–916.

Conflict of Interest: The authors declare that the research was conducted in the absence of any commercial or financial relationships that could be construed as a potential conflict of interest.

Copyright © 2020 Lächler, Clauss, Imhof, Crocoll, Schulz, Halkier and Binder. This is an open-access article distributed under the terms of the Creative Commons Attribution License (CC BY). The use, distribution or reproduction in other forums is permitted, provided the original author(s) and the copyright owner(s) are credited and that the original publication in this journal is cited, in accordance with accepted academic practice. No use, distribution or reproduction is permitted which does not comply with these terms.

frontiers in Plant Science

MINI REVIEW
published: 19 June 2020
doi: 10.3389/fpls.2020.00928

Connections Between Amino Acid Metabolisms in Plants: Lysine as an Example

Qingqing Yang[1,2], *Dongsheng Zhao*[2] *and Qiaoquan Liu*[1,2*]

[1] Jiangsu Key Laboratory of Crop Genomics and Molecular Breeding, Key Laboratory of Plant Functional Genomics of the Ministry of Education, College of Agriculture, Yangzhou University, Yangzhou, China, [2] Key Laboratory of Crop Genetics and Physiology of Jiangsu Province, Jiangsu Co-Innovation Center for Modern Production Technology of Grain Crops, Yangzhou University, Yangzhou, China

Extensive efforts have been made to fortify essential amino acids and boost nutrition in plants, but unintended effects on growth and physiology are also observed. Understanding how different amino acid metabolisms are connected with other biological pathways is therefore important. In addition to protein synthesis, amino acid metabolism is also tightly linked to energy and carbohydrate metabolism, the carbon-nitrogen budget, hormone and secondary metabolism, stress responses, and so on. Here, we update the currently available information on the connections between amino acid metabolisms, which tend to be overlooked in higher plants. Particular emphasis was placed on the connections between lysine metabolism and other pathways, such as tryptophan metabolism, the tricarboxylic acid cycle, abiotic and biotic stress responses, starch metabolism, and the unfolded protein response. Interestingly, regulation of lysine metabolism was found to differ between plant species, as is the case between dicots and monocots. Determining the metabolic connection between amino acid metabolisms will help improve our understanding of the metabolic flux, supporting studies on crop nutrition.

Keywords: amino acids, metabolic connection, lysine metabolism, stress responses, tricarboxylic acid cycle, tryptophan metabolism

OPEN ACCESS

Edited by:
Maurizio Trovato,
Sapienza University of Rome, Italy

Reviewed by:
Concepcion Avila,
University of Malaga, Spain
Nishikant Wase,
University of Virginia, United States

****Correspondence:***
Qiaoquan Liu
qqliu@yzu.edu.cn

Specialty section:
This article was submitted to Plant Metabolism and Chemodiversity, a section of the journal Frontiers in Plant Science

Received: *03 April 2020*
Accepted: *08 June 2020*
Published: *19 June 2020*

Citation:
Yang Q, Zhao D and Liu Q (2020) Connections Between Amino Acid Metabolisms in Plants: Lysine as an Example. Front. Plant Sci. 11:928. doi: 10.3389/fpls.2020.00928

INTRODUCTION

Amino acids play a number of vital roles in the central metabolism of plants. Essential amino acids (EAAs), notably lysine and methionine, cannot be synthesized by humans or animals, and must therefore be acquired *via* food sources. However, imbalances in plant nutrition are often caused by a lack of certain EAAs (Galili et al., 2016). Amino acids also act as intermediates of final metabolites in certain metabolic pathways, as well as participating in the regulation of multiple metabolic pathways, and other physiological and biochemical pathways, thereby affecting numerous physiological processes in plants (Amir et al., 2018; Yang et al., 2018).

EAAs in plants have been studied extensively (Galili et al., 2016). Genetic engineering provides an effective way of improving EAA levels in plants, with numerous successful results so far, albeit with additional unexpected effects (Galili et al., 2016). Of all living organisms, higher plants are thought to exhibit the highest complexity in terms of metabolic networks, making metabolic engineering of compositional traits particularly challenging (Yang et al., 2018). This review provides an overview of the

connections between amino acid metabolisms in plants, with particular focus on new discoveries that have been made in recent years. In-depth analysis of the metabolic connections between amino acids will deepen our understanding of the genetic basis of plant genomes and metabolomes, providing new information for breeding of high-EAA crops.

METABOLIC FLUX OF AMINO ACIDS IN PLANTS

Studies have shown that regulating metabolism of a certain amino acid affects the level of other amino acids. This is mainly due to the biosynthesis and catabolism of amino acids derived from the same metabolic trunk and/or closely related to other metabolic pathways, acting as a synthetic substrate or intermediate (Long et al., 2013; Song et al., 2013).

The aspartate family pathway leads to four key EAAs, lysine, methionine, threonine and isoleucine, but is also strongly associated with homoserine, glutamate, glycine, and proline (**Figure 1A**). Engineering of lysine metabolism tends to alter other amino acids in the aspartate family, even those from other pathways, suggesting a close regulatory network in the biosynthesis of free amino acids (Yang et al., 2018). Similar findings were found during the regulation of methionine metabolism (Song et al., 2013). Interestingly, high tryptophan levels were found to be associated with high-lysine plants (Yang et al., 2018; Wang et al., 2019), while Yang et al. (2018) revealed that the accumulation of lysine induced the tryptophan synthesis and metabolism in high free lysine transgenic rice (*Oryza sativa* L.). However, few reports have documented the relationship between metabolism of different amino acid families, highlighting the need for further research.

METABOLIC CONNECTIONS BETWEEN LYSINE AND OTHER METABOLITES IN PLANTS

The lysine metabolic pathways have been well elucidated, and enhanced accumulation of lysine has been achieved *via*

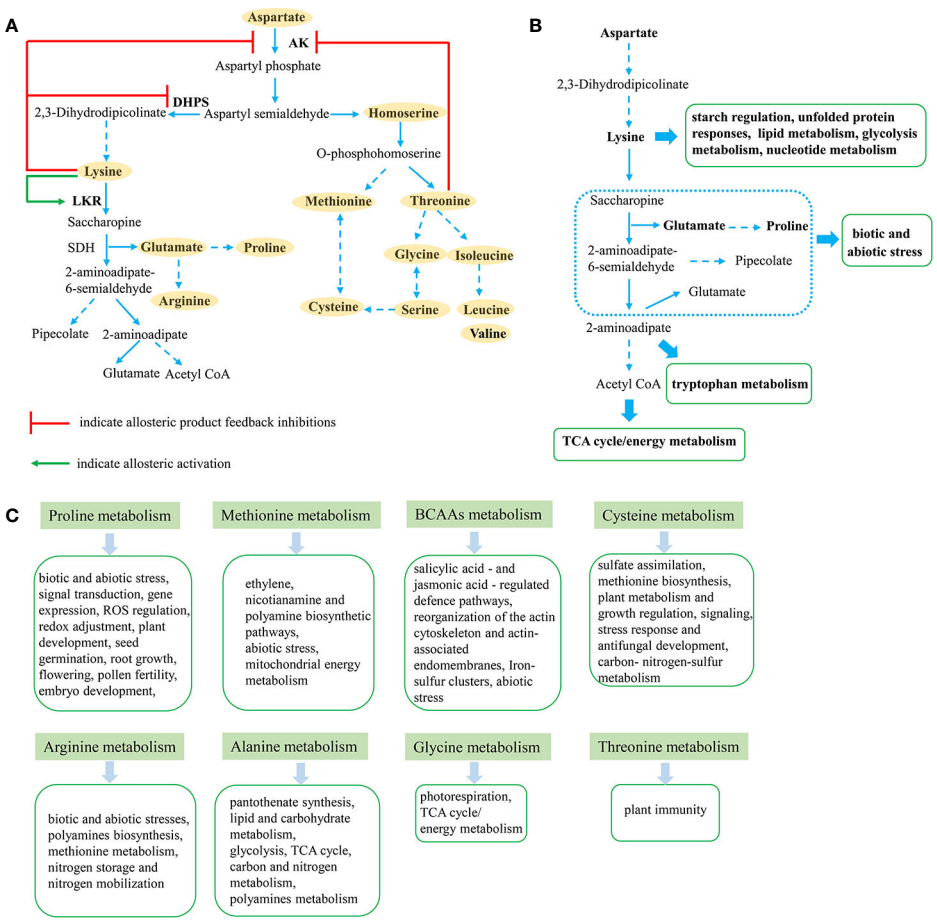

FIGURE 1 | Metabolic connections between aspartate-derived amino acids in plants. **(A)** Aspartate-derived amino acids (highlighted in orange) metabolism pathway in plants. **(B)** Brief sketch of lysine metabolism and connected metabolic pathways (green box). **(C)** Aspartate-derived amino acids connected metabolic pathways (green box).

metabolic engineering. Nevertheless, the potential connections with lysine fortification by metabolic engineering still need to be studied.

Effects of Lysine Enrichment in Plants

Efforts have been made to increase the lysine content by altering lysine metabolism or expressing high-lysine protein in plants (Sun and Liu, 2004). However, seed germination in high-lysine Arabidopsis [*Arabidopsis thaliana* (L.) Heynh.] was found to be significantly retarded and reduced (Zhu and Galili, 2004). Moreover, in soybean [*Glycine max* (Linn.) Merr.], high seed-specific expression of feedback-insensitive genes encoding dihydrodipicolinate synthase (DHPS) and aspartate kinase (AK) was found to result in wrinkled seeds and low germination rates (Falco et al., 1995), while reduced grain yield was observed in high-lysine crops (Liu et al., 2016). Studies also suggest that lysine affects starch synthesis and/or endosperm development in maize (*Zea mays* Linn.) and rice *via* biofortification (Jia et al., 2013; Liu et al., 2016). The aggravated chalkiness phenotype was also found in the seed endosperm of transgenic rice and maize (Wong et al., 2015). We recently generated transgenic rice with elevated free lysine, revealing a slight decrease in isoleucine content and enhancement of other EAAs, with a significant increase in the tryptophan content (Yang et al., 2016). Yet, a dark-brown endosperm associated with the high free lysine phenotype was also revealed in engineered mature seeds (Yang et al., 2018). The above findings suggest that an excessive increase in lysine content also affects other metabolic pathways, thereby affecting growth and development of the target plant. However, these effects also differ between different species, suggesting that differences in the metabolic flux and connections with lysine metabolism also exist.

Connections Between Lysine and Energy Metabolism

In addition to the classic role of aspartate acids in the synthesis of intracellular proteins, in the case of energy deficiency, lysine and isoleucine catabolism flux directly into the tricarboxylic acid (TCA) cycle, while threonine and methionine are converted into isoleucine (**Figure 1A**) (Wang et al., 2018). A negative effect on seed germination was also observed in high free lysine transgenic Arabidopsis expressing the *Escherichia coli dhps* gene in the *lkr* mutant (Angelovici et al., 2011). DHPS and lysine ketoglutaric acid reductase (LKR) represent two key enzymes involved in lysine biosynthesis and catabolism, respectively. Meanwhile, the results of metabolome and transcriptome analysis suggested significant increases in metabolites such as citrate, succinate, malate, and fumarate, which are involved in the TCA cycle, and the transcript of the gene encoding 2-oxoisovalerate dehydrogenase, which is associated with isoleucine catabolism in the TCA cycle, in germinated seeds with a high free lysine level, potentially affecting energy metabolism in the germinated seeds and subsequent seedling establishment (Angelovici et al., 2011). In addition, the glycine level also increased in high lysine plants, and was found to be the key intermediate metabolite during photorespiration (Schulze et al., 2016). Moreover, transcriptome analysis also revealed that the expression of photosynthesis- and photorespiration-associated genes was attenuated during seed germination in high lysine Arabidopsis (Angelovici et al., 2009; Angelovici et al., 2011).

Connection Between Lysine Metabolism and Plant Stress Response

Lysine metabolism is involved in the plant stress response in various forms. It is mainly catabolized through the saccharopine pathway, which has been shown to play a role in abiotic and biotic stress responses (**Figures 1B, C**) (Kiyota et al., 2015; Bernsdorff et al., 2016; Arruda and Barreto, 2020). Moreover, under salt and osmotic stress, *LKR*/*SDH* expression was found to increase, while downstream metabolite pipecolate was enhanced (Kiyota et al., 2015). Furthermore, pipecolate was also found to increase significantly in Arabidopsis infected with pathogenic bacteria, playing a role in plant defense responses (Bernsdorff et al., 2016).

An increase in proline is also induced by glutamate from the saccharopine pathway and in response to osmotic and salt stress (Batista-Silva et al., 2019). When tissues or cells are under osmotic stress, α-aminoadipic semialdehyde dehydrogenase (AASADH), the third enzyme in the saccharopine pathway, is significantly up-regulated, suggesting that AASADH is also related to the osmotic stress response (Brocker et al., 2010). However, in maize, the saccharopine pathway is induced by exogenous lysine and repressed by salt stress, while proline and pipecolate synthesis are significantly repressed by lysine. While AASADH accumulates in tissues under salt, osmotic and oxidative stress, LKR/SDH enzyme is not produced (Kiyota et al., 2015). Meanwhile, in developing seeds, proline is thought to play a major role in abiotic stress responses in maize, similar to the role of pipecolate in Arabidopsis and canola (*Brassica napus* L.) (Kiyota et al., 2015). Beside this, proline plays multiple functions in other biotic and abiotic stresses, signal transduction, gene expression, ROS regulation, redox adjustment, and plant development (Trovato et al., 2019) (**Figure 1C**). We recently suggested that lysine metabolism induces the jasmonate signal pathway and tryptophan metabolism during stress responses, in contrast to the primary role of pipecolate, proline, and AASADH in other plant species (Yang et al., 2018). Briefly, while lysine catabolism is involved in the plant response to abiotic and biotic stress, there are obvious differences between plant species, in line with the differing stress responses of monocot and dicot plants.

Meanwhile, isoleucine, a branched chain amino acid (BCAA) that can also be induced by the aspartate pathway, plays a pivotal role in plant stress resistance as an osmo-regulation factor (Batista-Silva et al., 2019). Homoserine and threonine are also derived from the aspartate pathway, and the amino acid imbalances associated with homoserine and threonine accumulation were found to increase plant immunity to oomycete pathogens (Zeier, 2013).

Metabolic Connections Between Lysine and Other Pathways

Starch, as an important source of carbohydrate, is also affected by lysine accumulation (Jia et al., 2013). In *opaque2* mutant maize, an increase in expression of several starch biosynthesis enzymes (GBSSI, Zpu1, SSIIa, BEI, BEIIb) was observed, leading to highly crystalline starch (Jia et al., 2013). Furthermore, Zhang et al. (2016) revealed that both *Opaque-2* and the prolamine-box binding factor network the regulation of protein and starch synthesis.

Unfolded protein responses (UPR) are characterized by the upregulation of chaperons and proteases, facilitating protein folding, and degrading unfolded protein (Ruberti and Brandizzi, 2018). In high-lysine rice with overexpression of exogenous proteins, BiP and PDI were induced in the endosperm, as well as being tightly linked to the floury/chalkiness grain phenotype, suggesting that lysine accumulation is also associated with UPR (Wong et al., 2015).

In canola and soybean, overexpression of the *Corynebacterium dapA* and *E. coli lysC* genes resulted in large increases in free lysine, but a decrease in oil production (Falco et al., 1995). Similar results have also been reported in maize (Medici et al., 2009). However, the high-lysine corn PQ15/CordapA, which was developed through reductions in lysine-poor seed storage proteins, zeins, and overexpressing *CordapA*, showed an increase in oil content in the grains (Huang et al., 2005). Furthermore, metabolome and transcriptome analysis showed a decrease in the lipid content in transgenic high lysine rice and up-regulation of mRNA levels of lipid metabolic genes (Angelovici et al., 2009; Angelovici et al., 2011; Yang et al., 2018). These findings suggest that the regulation of lysine metabolism affects lipid metabolism, but with differences between plant species.

During lysine production in microorganisms, cells produce a series of organic osmotic regulators, thereby maintaining normal osmotic pressure (Ying et al., 2014). Meanwhile, lysine production negatively interacts with acetate-associated metabolism during lysine fermentation (Anastassiadis, 2007). However, in rice and Arabidopsis, positive correlations between lysine accumulation and glycolysis metabolism were revealed (Angelovici et al., 2011; Yang et al., 2018).

Integrated metabolome and transcriptome analyses revealed that 12 genes encoding enzymes associated with nucleotide metabolism were stimulated, while levels of adenine, pseudouridine and uracil, which are related to nucleotide metabolism, were also improved in high-lysine plants (Angelovici et al., 2009; Yang et al., 2018). Lysine metabolism therefore affects the aspartate family pathway, which, in turn, may affect other metabolic pathways, confirming the complexity of the aspartate family pathway in plants.

CONNECTIONS BETWEEN OTHER AMINO ACIDS AND THEIR RELATED METABOLIC PATHWAYS

In general, amino acid metabolism is tightly linked to energy and carbohydrate metabolism, the carbon-nitrogen budget, and demands for protein synthesis and secondary metabolism (Pratelli and Pilot, 2014). Methionine is the main limiting sulfur EAA in plants, since it can be converted to cysteine in animals, thus meeting the requirements of both amino acids (Song et al., 2013). Both methionine and S-adenosylmethionine, participate in the ethylene, nicotianamine and polyamine biosynthetic pathways (Sauter et al., 2013). Moreover, the high methionine Arabidopsis was found to stimulate metabolic and transcriptomic responses associated with desiccation stress and mitochondrial energy metabolism (Cohen et al., 2014). A previous study also revealed that the higher the level of methionine in plants the higher their tolerance to abiotic stress (Ma et al., 2017). Cysteine is the first product of sulfate assimilation synthesized during the last stage of photosynthetic assimilation of sulfate (Gotor et al., 2015). It is not only a protein component, but also a source of methionine biosynthesis, and many other sulfur-containing metabolites are also involved in plant growth, signaling, stress responses, and antifungal development (Roblin et al., 2018; Kopriva et al., 2019). Furthermore, cysteine synthesis is the merging point of the three major pathways of carbon, nitrogen, and sulfur assimilation (Jobe et al., 2019).

The BCAAs isoleucine, valine and leucine are essential nutrients in humans and animals (Chen et al., 2010). BCAAs and their derivatives also contribute to plant growth, the stress response, and the production of food flavor components (Xing and Last, 2017). The BCAAs catabolism pathways have already been identified as essential during dehydration tolerance in Arabidopsis (Pires et al., 2016). They also appear to affect plant resistance to distinct pathogen classes by modulating crosstalk between salicylic acid- and jasmonic acid-regulated defense pathways (Zeier, 2013). Moreover, BCAA catabolism provides an alternative energy source under long-term dark treatment in plants (Peng et al., 2015). Recently, Cao et al. (2019) also revealed that BCAA over-accumulation leads to up-regulation of the target of rapamycin activity, which causes reorganization of the actin cytoskeleton and actin-associated endomembranes in Arabidopsis mutants. In addition, isoleucine was found to serve as a precursor for the synthesis of β-alanine in plants (Rouhier et al., 2019), while in Arabidopsis, a metabolic relationship was revealed between BCAA catabolism and iron-sulfur clusters *via* the mitochondrial homologue GRXS15 (Moseler et al., 2020).

Arginine and ornithine synthesize polyamines and are involved in plant responses to stresses. In addition, arginine constitutes a high percentage of the amino acid pool in storage proteins of conifers, while transcriptome and metabolome profiling also revealed significant genes and metabolites involved in arginine metabolism during late embryogenesis (Businge et al., 2012; Canales et al., 2014). Arginine metabolism is therefore thought to play a key role in nitrogen storage during embryogenesis and nitrogen mobilization during germination (Llebrés et al., 2018). Moreover, decarboxylated sadenosyl methionine from methionine metabolism serves as an aminopropyl donor during generation of polyamines (Gong et al., 2014). Evidence also suggests that plants synthesize β-alanine from spermine, uracil, and propionate (Parthasarathy et al., 2019). Similarly, metabolic tracing studies suggest that wheat synthesizes β-alanine from both isoleucine and propionate as in Arabidopsis

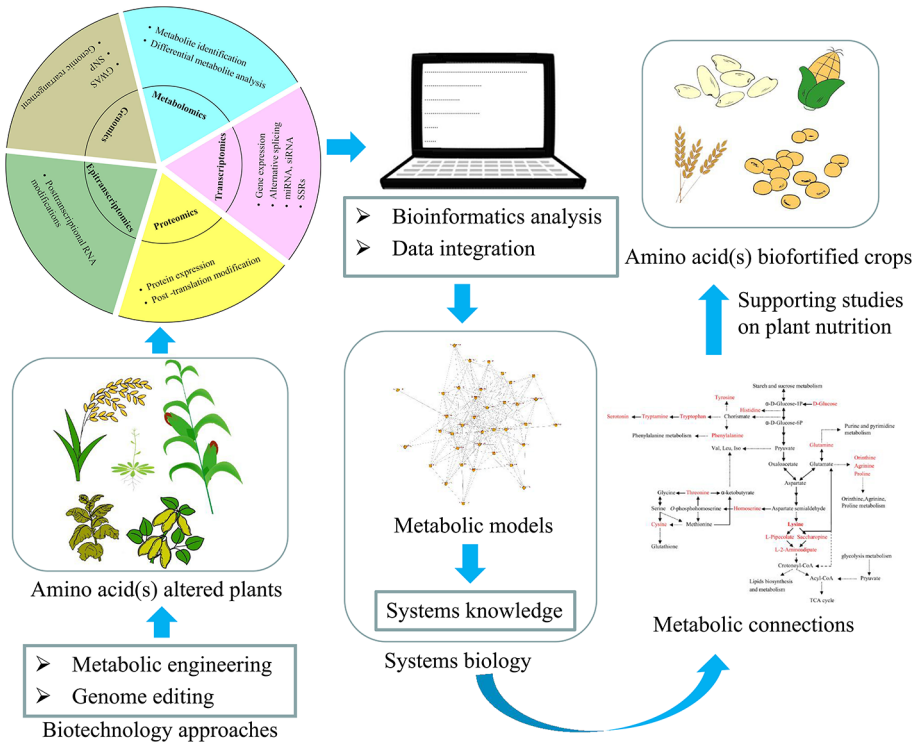

FIGURE 2 | Schematic representation of the workflow depicting the application of different approaches to acquire a systems-level understanding of amino acid(s) metabolic connections in plants, and their application to obtain amino acid(s) biofortified crops.

(Reinhart and Rouhier, 2019). In plants, β-alanine is important for the synthesis of pantothenate, and subsequently coenzyme A, which is an essential coenzyme in lipid and carbohydrate metabolism (Parthasarathy et al., 2019). Glycolysis and the TCA cycle are linked by alanine aminotransferase during hypoxia induced by waterlogging (Rocha et al., 2010). Moreover, in rice, the alanine aminotransferase 1 encoded by the *Flo12* gene was found to simultaneously regulate carbon and nitrogen metabolism, while the *flo12* mutant presented a floury white-core endosperm (Zhong et al., 2019).

In plants, the aromatic amino acids phenylalanine, tyrosine, and tryptophan are not only essential components of protein synthesis, but are also located upstream of a number of growth hormones and secondary metabolites with multiple biological functions and health-promoting properties, such as protection against abiotic and biotic stress (Tzin and Galili, 2010). Phenylalanine is required for protein biosynthesis and cell survival (Tzin and Galili, 2010), and in plants, also acts as a precursor of a large number of multi-functional secondary metabolites. Among them, lignin is a principal structural component in the supporting tissues of vascular plants and some algae (Vanholme et al., 2019). Tyrosine is the central hub to a myriad of specialized metabolic pathways, while vitamin E and plastoquinone are essential metabolites of plant nutrition, photosynthesis, and antioxidant synthesis (Schenck and Maeda, 2018). Tyrosine is also a precursor of numerous specialized metabolites with diverse physiological roles such as non-protein amino acids, attractants, and defense compounds (Schenck and Maeda, 2018). Meanwhile, tryptophan is an essential EAA in the synthesis of a large number of bioactive molecules, such as auxin, tryptamine derivatives, phytoalexins, indole glucosinolates, and terpenoid indole alkaloids, as well as playing a pivotal role in the regulation of plant growth and development and stress responses. Recently, Accordingly, these findings have all been discussed extensively (Tzin and Galili, 2010; Hildebrandt et al., 2015; Datta et al., 2016).

Little is known about histidine metabolism and its connection with other amino acids in plants. A close correlation between nickel tolerance, root histidine concentration, and ATP-PRT transcript abundance was revealed in Hyperaccumulator plants, which show constitutively high expression of the histidine biosynthetic pathway (Ingle et al., 2005). Moreover, studies of *hisn1a* mutants revealed that histidine regulates seed oil deposition and protein accumulation *via* abscisic acid biosynthesis and β-oxidation in Arabidopsis (Ma and Wang, 2016). Histidine biosynthesis is tightly linked to nucleotide metabolism *via* 5′-phosphoribosyl 1-pyrophosphate, which is intermediate metabolite of anthranilate. These findings therefore suggest a metabolic link between histidine and tryptophan, nucleotide metabolism (Koslowsky et al., 2008).

FUTURE PROSPECTIVES

Our knowledge of amino acid metabolism has increased exponentially in the past three decades. Amino acids and their derivatives have various prominent functions in plants, such as protein synthesis, growth and development, nutrition and stress responses (Hildebrandt et al., 2015). Meanwhile, metabolism is one of the most important and complex networks within biological systems, yet our understanding of metabolic regulation remains limited in terms of the modular operation of these networks. Precise and detailed information on biological and molecular mechanisms and metabolic connections is therefore essential. The recent development of omics approaches has been widely applied to studies of amino acid metabolisms and their connections (Gu et al., 2010; Angelovici et al., 2017; Xing and Last, 2017; Yang et al., 2018). Combinations of biochemistry, molecular genetics, genomics, and systems biology will continue to promote fundamental research, enabling us to develop ideas and strategies aimed at exploring new features of gene–protein–metabolite regulatory networks (**Figure 2**). Moreover, studies of epi-transcriptomics may provide a new strategy for analysis of metabolic connections in plants, giving insight into how different markers regulate a host of biological processes, from biosynthesis to catabolism and transport to function (Vandivier and Gregory, 2018). In addition, the continuously optimized gene editing technology of CRISPR-Cas has allowed the expression or activity of one or several key regulatory enzyme(s) to be altered, supporting studies aimed at improving the nutritional quality of plants (Chen et al., 2019).

In addition to technological issues, there are significant gaps in our knowledge of certain areas. Given the importance of the nutritional value of amino acids, the effects of amino acid (especially EAA) accumulation on other metabolic pathways during plant growth and development need further attention. To do so, analyses of the connections among amino acid metabolisms, transcriptional regulatory factors and post-translational modifications are essential. Thus, despite our growing knowledge of plant amino acid metabolisms and their metabolic connections, it is clear that many major discoveries have yet to be made.

AUTHOR CONTRIBUTIONS

QY and QL organized and wrote the manuscript. DZ provided critical evaluation and edited the text. All authors contributed to the article and approved the submitted version.

FUNDING

This work was supported by the National Natural Science Foundation of China (31801322 and 31701393), the Ministry of Agriculture (2016ZX08001006-005), and the Government of Jiangsu Province (BE2018357 and PAPD), China.

REFERENCES

Amir, R., Galili, G., and Cohen, H. (2018). The metabolic roles of free amino acids during seed development. *Plant Sci.* 275, 11–18. doi: 10.1016/j.plantsci.2018.06.011

Anastassiadis, S. (2007). L-Lysine fermentation. *Recent Pat. Biotechnol.* 1, 11–24. doi: 10.2174/187220807779813947

Angelovici, R., Fait, A., Zhu, X., Szymanski, J., Feldmesser, E., Fernie, A. R., et al. (2009). Deciphering transcriptional and metabolic networks associated with lysine metabolism during Arabidopsis seed development. *Plant Physiol.* 151, 2058–2072. doi: 10.1104/pp.109.145631

Angelovici, R., Fait, A., Fernie, A. R., and Galili, G. (2011). A seed high-lysine trait is negatively associated with the TCA cycle and slows down Arabidopsis seed germination. *New Phytol.* 189, 148–159. doi: 10.1111/j.1469-8137.2010.03478.x

Angelovici, R., Batushansky, A., Deason, N., Gonzalez-Jorge, S., Gore, M. A., Fait, A., et al. (2017). Network-guided GWAS improves identification of genes affecting free amino acids. *Plant Physiol.* 173, 872–886. doi: 10.1104/pp.16.01287

Arruda, P., and Barreto, P. (2020). Lysine catabolism through the saccharopine pathway: enzymes and intermediates involved in plant responses to abiotic and biotic stress. *Front. Plant Sci.* 11, 587. doi: 10.3389/fpls.2020.00587

Batista-Silva, W., Heinemann, B., Rugen, N., Nunes-Nesi, A., Araújo, W. L., Braun, H. P., et al. (2019). The role of amino acid metabolism during abiotic stress release. *Plant Cell Environ.* 42, 1630–1644. doi: 10.1111/pce.13518

Bernsdorff, F., Döring, A. C., Gruner, K., Schuck, S., Bräutigam, A., and Zeier, J. (2016). Pipecolic acid orchestrates plant systemic acquired resistance and defense priming via salicylic acid-dependent and -independent pathways. *Plant Cell* 28, 102–129. doi: 10.1105/tpc.15.00496

Brocker, C., Lassen, N., Estey, T., Pappa, A., Cantore, M., Orlova, V. V., et al. (2010). Aldehyde dehydrogenase 7A1 (ALDH7A1) is a novel enzyme involved in cellular defense against hyperosmotic stress. *J. Biol. Chem.* 285, 18452–18463. doi: 10.1074/jbc.M109.077925

Businge, E., Brackmann, K., Moritz, T., and Egertsdotter, U. (2012). Metabolite profiling reveals clear metabolic changes during somatic embryo development of Norway spruce (*Picea abies*). *Tree Physiol.* 32, 232–244. doi: 10.1093/treephys/tpr142

Canales, J., Bautista, R., Label, P., Gómez-Maldonado, J., Lesur, I., Fernández-Pozo, N., et al. (2014). *De novo* assembly of maritime pine transcriptome: implications for forest breeding and biotechnology. *Plant Biotechnol. J.* 12, 286–299. doi: 10.1111/pbi.12136

Cao, P., Kim, S. J., Xing, A., Schenck, C. A., Liu, L., Jiang, N., et al. (2019). Homeostasis of branched-chain amino acids is critical for the activity of TOR signaling in Arabidopsis. *eLife* 8, e50747. doi: 10.7554/eLife.50747

Chen, H., Saksa, K., Zhao, F., Qiu, J., and Xiong, L. (2010). Genetic analysis of pathway regulation for enhancing branched-chain amino acid biosynthesis in plants. *Plant J.* 63, 573–583. doi: 10.1111/j.1365-313X.2010.04261.x

Chen, K., Wang, Y., Zhang, R., Zhang, H., and Gao, C. (2019). CRISPR/Cas Genome Editing and Precision Plant Breeding in Agriculture. *Annu. Rev. Plant Biol.* 70, 667–697. doi: 10.1146/annurev-arplant-050718-100049

Cohen, H., Israeli, H., Matityahu, I., and Amir, R. (2014). Seed-specific expression of a feedback-insensitive form of CYSTATHIONINE-γ-SYNTHASE in Arabidopsis stimulates metabolic and transcriptomic responses associated with desiccation stress. *Plant Physiol.* 166, 1575–1592. doi: 10.1104/pp.114.246058

Datta, A., Bhattacharyya, D., Singh, S., Ghosh, A., Schmidtchen, A., Malmsten, M., et al. (2016). Role of aromatic amino acids in lipopolysaccharide and membrane interactions of antimicrobial peptides for use in plant disease control. *J. Biol. Chem.* 291, 13301–13317. doi: 10.1074/jbc.M116.719575

Falco, S. C., Guida, T., Locke, M., Mauvais, J., Sanders, C., Ward, R. T., et al. (1995). Transgenic canola and soybean seeds with increased lysine. *Nat. Biotechnol.* 13, 577–582. doi: 10.1038/nbt0695-577

Galili, G., Amir, R., and Fernie, A. R. (2016). The regulation of essential amino acid synthesis and accumulation in plants. *Annu. Rev. Plant Biol.* 67, 153–178. doi: 10.1146/annurev-arplant-043015-112213

Gong, B., Li, X., VandenLangenberg, K. M., Wen, D., Sun, S., Wei, M., et al. (2014). Overexpression of S-adenosyl-L-methionine synthetase increased tomato tolerance to alkali stress through polyamine metabolism. *Plant Biotechnol. J.* 12, 694–708. doi: 10.1111/pbi.12173

Gotor, C., Laureano-Marín, A. M., Moreno, I., Aroca, A., García, I., and Romero, L. C. (2015). Signaling in the plant cytosol: cysteine or sulfide? *Amino Acids* 47, 2155–2164. doi: 10.1007/s00726-014-1786-z

Gu, L., Jones, A. D., and Last, R. L. (2010). Broad connections in the Arabidopsis seed metabolic network revealed by metabolite profiling of an amino acid catabolism mutant. *Plant J.* 61, 579–590. doi: 10.1111/j.1365-313X.2009.04083.x

Hildebrandt, T. M., Nesi, A. N., Araújo, W. L., and Braun, H. P. (2015). Amino acid catabolism in plants. *Mol. Plant* 8, 1563–1579. doi: 10.1016/j.molp.2015.09.005

Huang, S., Kruger, D. E., Frizzi, A., D'Ordine, R. L., Florida, C. A., Adams, W. R., et al. (2005). High-lysine corn produced by the combination of enhanced lysine biosynthesis and reduced zein accumulation. *Plant Biotechnol. J.* 3, 555–569. doi: 10.1111/j.1467-7652.2005.00146.x

Ingle, R. A., Mugford, S. T., Rees, J. D., Campbell, M. M., and Smith, J. A. C. (2005). Constitutively high expression of the histidine biosynthetic pathway contributes to nickel tolerance in hyperaccumulator Plants. *Plant Cell* 17, 2089–2106. doi: 10.1105/tpc.104.030577

Jia, M., Wu, H., Clay, K. L., Jung, R., Larkins, B. A., and Gibbon, B. C. (2013). Identification and characterization of lysine-rich proteins and starch biosynthesis genes in the *opaque2* mutant by transcriptional and proteomic analysis. *BMC Plant Biol.* 13, 60. doi: 10.1186/1471-2229-13-60

Jobe, T. O., Zenzen, I., Karvansara, P. R., and Kopriva, S. (2019). Integration of sulfate assimilation with carbon and nitrogen metabolism in transition from C_3 to C_4 photosynthesis. *J. Exp. Bot.* 70, 4211–4221. doi: 10.1093/jxb/erz250

Kiyota, E., Pena, I. A., and Arruda, P. (2015). The saccharopine pathway in seed development and stress response of maize. *Plant Cell Environ.* 38, 2450–2461. doi: 10.1111/pce.12563

Kopriva, S., Malagoli, M., and Takahashi, H. (2019). Sulfur nutrition: impacts on plant development, metabolism, and stress responses. *J. Exp. Bot.* 70, 4069–4073. doi: 10.1093/jxb/erz319

Koslowsky, S., Riegler, H., Bergmüller, E., and Zrenner, R. (2008). Higher biomass accumulation by increasing phosphoribosylpyrophosphate synthetase activity in Arabidopsis thaliana and Nicotiana tabacum. *Plant Biotechnol. J.* 6, 281–294. doi: 10.1111/j.1467-7652.2007.00314.x

Liu, X., Zhang, C., Wang, X., Liu, Q., Yuan, D., Pan, G., et al. (2016). Development of high-lysine rice via endosperm-specific expression of a foreign *LYSINE RICH PROTEIN* gene. *BMC Plant Biol.* 16, 147. doi: 10.1186/s12870-016-0837-x

Llebrés, M. T., Pascual, M. B., Debille, S., Trontin, J. F., Harvengt, L., Avila, C., et al. (2018). The role of arginine metabolic pathway during embryogenesis and germination in maritime pine (*Pinus pinaster* Ait.). *Tree Physiol.* 38, 471–484. doi: 10.1093/treephys/tpx133

Long, X., Liu, Q., Chan, M., Wang, Q., and Sun, S. S. M. (2013). Metabolic engineering and profiling of rice with increased lysine. *Plant Biotechnol. J.* 11, 490–501. doi: 10.1111/pbi.12037

Ma, H., and Wang, S. (2016). Histidine regulates seed oil deposition through abscisic acid biosynthesis and β-oxidation. *Plant Physiol.* 172, 848–857. doi: 10.1104/pp.16.00950

Ma, C., Wang, Y., Gu, D., Nan, J., Chen, S., and Li, H. (2017). Overexpression of S-adenosyl-L-methionine synthetase 2 from sugar beet M14 increased Arabidopsis tolerance to salt and oxidative stress. *Int. J. Mol. Sci.* 18, 847. doi: 10.3390/ijms18040847

Medici, L. O., Gaziola, S. A., Varisi, V. A., Paula, J. A. C., Ferreira, R. R., and Azevedo, R. A. (2009). Diallelic analysis for lysine and oil contents in maize grains. *Sci. Agric.* 66, 204–209. doi: 10.1590/S0103-90162009000200009

Moseler, A., Kruse, I., Maclean, A. E., Pedroletti, L., Wagner, S., Wehler, R., et al. (2020). Branched-chain amino acid catabolism depends on GRXS15 through mitochondrial lipoyl cofactor homeostasis. *BioRxiv*. 2020.02.13.947697. doi: 10.1101/2020.02.13.947697

Parthasarathy, A., Savka, M. A., and Hudson, A. O. (2019). The synthesis and role of β-alanine in plants. *Front. Plant Sci.* 10, 921. doi: 10.3389/fpls.2019.00921

Peng, C., Uygun, S., Shiu, S. H., and Last, R. L. (2015). The impact of the branched-vhain ketoacid dehydrogenase complex on amino acid homeostasis in Arabidopsis. *Plant Physiol.* 169, 1807–1820. doi: 10.1104/pp.15.00461

Pires, M. V., Júnior, A. A. P., Medeiros, D. B., Daloso, D. M., Pham, P. A., Barros, K. A., et al. (2016). The influence of alternative pathways of respiration that utilize branched-chain amino acids following water shortage in Arabidopsis. *Plant Cell Environ.* 39, 1304–1319. doi: 10.1111/pce.12682

Pratelli, R., and Pilot, G. (2014). Regulation of amino acid metabolic enzymes and transporters in plants. *J. Exp. Bot.* 65, 5535–5556. doi: 10.1093/jxb/eru320

Reinhart, P. E., and Rouhier, K. A. (2019). Metabolic tracing and quantification of β-alanine in wheat. *FASEB J.* 33, 486.9. doi: 10.1096/fasebj.2019.33.1_supplement.486.9

Roblin, G., Octave, S., Faucher, M., Fleurat-Lessard, P., and Berjeaud, J. (2018). Cysteine: A multifaceted amino acid involved in signaling, plant resistance and antifungal development. *Plant Physiol. Bioch.* 129, 77–89. doi: 10.1016/j.plaphy.2018.05.024

Rocha, M., Licausi, F., Araújom, W. L., Nunes-Nesim, A., Sodek, L., Fernie, A. R., et al. (2010). Glycolysis and the tricarboxylic acid cycle are linked by alanine aminotransferase during hypoxia induced by waterlogging of *Lotus japonicus*. *Plant Physiol.* 152, 1501–1513. doi: 10.1104/pp.109.150045

Rouhier, K. A., Perrett, M. E., Goldfarb, M. H., Reinhart, P. E., Wilczewski-Shirai, K. C., Raymond-Schmidt, L., et al. (2019). Isoleucine serves as a precursor for the synthesis of β-alanine in plants. *FASEB J.* 33, 486.10. doi: 10.1096/fasebj.2019.33.1_supplement.486.10

Ruberti, C., and Brandizzi, F. (2018). "Methods in Molecular Biology," in *Unfolded protein response in Arabidopsis, in The Plant Endoplasmic Reticulum* (New York: Humana Press).

Sauter, M., Moffatt, B., Saechao, M. C., Hell, R., and Wirtz, M. (2013). Methionine salvage and S-adenosylmethionine: essential links between sulfur, ethylene and polyamine biosynthesis. *Biochem. J.* 451, 145–154. doi: 10.1042/BJ20121744

Schenck, C. A., and Maeda, H. A. (2018). Tyrosine biosynthesis, metabolism, and catabolism in plants. *Phytochemistry* 149, 82–102. doi: 10.1016/j.phytochem.2018.02.003

Schulze, S., Westhoff, P., and Gowik, U. (2016). Glycine decarboxylase in C3, C4 and C3-C4 intermediate species. *Curr. Opin. Plant Biol.* 31, 29–35. doi: 10.1016/j.pbi.2016.03.011

Song, S., Hou, W., Godo, I., Wu, C., Yu, Y., Matityahu, I., et al. (2013). Soybean seeds expressing feedback-insensitive cystathionine γ-synthase exhibit a higher content of methionine. *J. Exp. Bot.* 64, 1917–1926. doi: 10.1093/jxb/ert053

Sun, S. S. M., and Liu, Q. (2004). Transgenic approaches to improve the nutritional quality of plant proteins. *Vitro Cell. Dev. Pl.* 40, 155–162. doi: 10.1079/IVP2003517

Trovato, M., Forlani, G., Signorelli, S., and Funck, D. (2019). "Proline metabolism and its functions in development and stress tolerance," in *Osmoprotectant-mediated abiotic stress tolerance in plants*. Eds. M. Hossain, V. Kumar, D. Burritt, M. Fujita and P. Mäkelä. New York: Springer. doi: 10.1007/978-3-030-27423-8_2

Tzin, V., and Galili, G. (2010). New insights into the shikimate and aromatic amino acids biosynthesis pathways in plants. *Mol. Plant* 3, 956–972. doi: 10.1093/mp/ssq048

Vandivier, L. E., and Gregory, B. D. (2018). New insights into the plant epitranscriptome. *J. Exp. Bot.* 69, 4659–4665. doi: 10.1093/jxb/ery262

Vanholme, R., Meester, B. D., Ralph, J., and Boerjan, W. (2019). Lignin biosynthesis and its integration into metabolism. *Curr. Opin. Biotech.* 56, 230–239. doi: 10.1016/j.copbio.2019.02.018

Wang, W., Xu, M., Wang, G., and Galili, G. (2018). New insights into the metabolism of aspartate-family amino acids in plant seeds. *Plant Reprod.* 31, 203–211. doi: 10.1007/s00497-018-0322-9

Wang, W., Dai, Y., Wang, M., Yang, W., and Zhao, D. (2019). Transcriptome dynamics of double recessive mutant, *o2o2o16o16*, reveals the transcriptional mechanisms in the increase of its lysine and tryptophan content in maize. *Genes* 10, 316. doi: 10.3390/genes10040316

Wong, H. M., Liu, Q., and Sun, S. S. M. (2015). Biofortification of rice with lysine using endogenous histones. *Plant Mol. Biol.* 87, 235–248. doi: 10.1007/s11103-014-0272-z

Xing, A., and Last, R. L. (2017). A regulatory hierarchy of the Arabidopsis branched-vhain amino acid metabolic network. *Plant Cell* 29, 1480–1499. doi: 10.1105/tpc.17.00186

Yang, Q., Zhang, C., Chan, M. L., Zhao, D., Chen, J., Wang, Q., et al. (2016). Biofortification of rice with the essential amino acid lysine: molecular characterization, nutritional evaluation, and field performance. *J. Exp. Bot.* 67, 4285–4296. doi: 10.1093/jxb/erw209

Yang, Q., Zhao, D., Zhang, C., Wu, H., Li, Q., Gu, M., et al. (2018). A Connection between lysine and serotonin metabolism in rice endosperm. *Plant Physiol.* 176, 1965–1980. doi: 10.1104/pp.17.01283

Ying, H., He, X., Li, Y., Chen, K., and Ouyang, P. (2014). Optimization of culture conditions for enhanced lysine production using engineered *Escherichia coli*. *Appl. Biochem. Biotechnol.* 172, 3835–3843. doi: 10.1007/s12010-014-0820-7

Zeier, J. (2013). New insights into the regulation of plant immunity by amino acid metabolic pathways. *Plant Cell Environ.* 36, 2085–2103. doi: 10.1111/pce.12122

Zhang, Z., Zheng, X., Yang, J., Messing, J., and Wu, Y. (2016). Maize endosperm-specific transcription factors *O2* and *PBF* network the regulation of protein and starch synthesis. *Proc. Natl. Acad. Sci. USA.* 113, 10842–10847. doi: 10.1073/pnas.1613721113

Zhong, M., Liu, X., Liu, F., Ren, Y., Wang, Y., Zhu, J., et al. (2019). *FLOURY ENDOSPERM12* encoding alanine aminotransferase 1 regulates carbon and nitrogen metabolism in rice. *J. Plant Biol.* 62, 61–73. doi: 10.1007/s12374-018-0288-z

Zhu, X., and Galili, G. (2004). Lysine metabolism is concurrently regulated by synthesis and catabolism in both reproductive and vegetative tissues. *Plant Physiol.* 135, 129–136. doi: 10.1104/pp.103.037168

Conflict of Interest: The authors declare that this research was conducted in the absence of any commercial or financial relationships that could be construed as a potential conflict of interest.

Copyright © 2020 Yang, Zhao and Liu. This is an open-access article distributed under the terms of the Creative Commons Attribution License (CC BY). The use, distribution or reproduction in other forums is permitted, provided the original author(s) and the copyright owner(s) are credited and that the original publication in this journal is cited, in accordance with accepted academic practice. No use, distribution or reproduction is permitted which does not comply with these terms.

frontiers in Plant Science

ORIGINAL RESEARCH
published: 03 July 2020
doi: 10.3389/fpls.2020.00891

Shaping Durum Wheat for the Future: Gene Expression Analyses and Metabolites Profiling Support the Contribution of BCAT Genes to Drought Stress Response

Valentina Buffagni[1], Filippo Vurro[2], Michela Janni[2,3], Mariolina Gullì[1]*, Arturo A. Keller[4] and Nelson Marmiroli[1,5]*

[1] Department of Chemistry, Life Sciences and Environmental Sustainability, University of Parma, Parma, Italy, [2] Institute of Materials for Electronics and Magnetism (IMEM), National Research Council (CNR), Parma, Italy, [3] Institute of Bioscience and Bioresources (IBBR), National Research Council (CNR), Bari, Italy, [4] Bren School of Environmental Science & Management, University of California, Santa Barbara, Santa Barbara, CA, United States, [5] CINSA Interuniversity Consortium for Environmental Sciences, Parma/Venice, Italy

OPEN ACCESS

Edited by:
Maurizio Trovato,
Sapienza University of Rome, Italy

Reviewed by:
Marco Betti,
Universidad de Sevilla, Spain
Atsushi Fukushima,
RIKEN, Japan

***Correspondence:**
Michela Janni
michela.janni@ibbr.cnr.it
Mariolina Gullì
mariolina.gulli@unipr.it

Specialty section:
This article was submitted to Plant Metabolism and Chemodiversity, a section of the journal Frontiers in Plant Science

Received: 14 February 2020
Accepted: 29 May 2020
Published: 03 July 2020

Citation:
Buffagni V, Vurro F, Janni M, Gullì M, Keller AA and Marmiroli N (2020) Shaping Durum Wheat for the Future: Gene Expression Analyses and Metabolites Profiling Support the Contribution of BCAT Genes to Drought Stress Response. Front. Plant Sci. 11:891. doi: 10.3389/fpls.2020.00891

Global climate change, its implications for agriculture, and the complex scenario presented by the scientific community are of worldwide concern. Drought is a major abiotic stress that can restrict plants growth and yields, thus the identification of genotypes with higher adaptability to drought stress represents one of the primary goals in breeding programs. During abiotic stress, metabolic adaptation is crucial for stress tolerance, and accumulation of specific amino acids and/or as secondary metabolites deriving from amino acid metabolism may correlate with the increased tolerance to adverse environmental conditions. This work, focused on the metabolism of branched chain-amino acids (BCAAs) in durum wheat and the role of branched-chain amino acid aminotransferases (BCATs) in stress response. The role of BCATs in plant response to drought was previously proposed for *Arabidopsis*, where the levels of BCAAs were altered at the transcriptional level under drought conditions, triggering the onset of defense response metabolism. However, in wheat the role of BCAAs as a trigger of the onset of the drought defense response has not been elucidated. A comparative genomic approach elucidated the composition of the BCAT gene family in durum wheat. Here we demonstrate a tissue and developmental stage specificity of BCATs regulation in the drought response. Moreover, a metabolites profiling was performed on two contrasting durum wheat cultivars Colosseo and Cappelli resulting in the detection of a specific pattern of metabolites accumulated among genotypes and, in particular, in an enhanced BCAAs accumulation in the tolerant cv Cappelli further supporting a role of BCAAs in the drought defense response. The results support the use of gene expression and target metabolomic in modern breeding to shape new cultivars more resilient to a changing climate.

Keywords: branched-chain aminotransferase, durum wheat, drought stress, gene expression, target metabolomics

INTRODUCTION

Wheat is a major staple food, providing approximately 20% of daily calories and proteins uptake for 4.5 billion people. Durum wheat [*Triticum turgidum* L. *subsp. durum* (Desf.) Husn] in particular, is conventionally grown in semiarid environments (i.e., Mediterranean regions) where the optimization of the water resources is of major concern (Aprile et al., 2013). A recent study predicted a strong decline in wheat yields by 4.1 to 6.4% for each 1°C of temperature increase due to climate change (Liu et al., 2016). Consequently, while demand for wheat will increase of 60% by 2050, production might decrease by 29% as a result of environmental stresses imposed by climate change (Semenov et al., 2014). Drought, in particular, is a major challenge, thus improving drought tolerance in wheat varieties is of paramount importance for global food security. Depending on the onset time, duration and intensity of the stress, drought can reduce wheat yields up to 92% (Farooq et al., 2012; Sallam et al., 2019), which is enough to prompt the application of high-throughput tools to explore and exploit plant genomes to increase drought tolerance in wheat (Akpınar et al., 2013). In particular, knowledge of genomic variation and genetic basis of agronomically useful traits can be improved with the use of reference crop genome sequences (Scheben et al., 2016).

It is imperative to explain the molecular basis of drought stress defense response in durum wheat and to identify novel classes of genes for drought resistance which can be used in breeding programs: future world production of food depends to a large degree on the response of plants to drought stress (DS). The combination of target metabolite determination with enzymatic assays and gene-sequence and expression analyses represents a multi-disciplinary approach to identify favorable alleles that, when used as molecular markers, can speed and shape new crops for the future (Borrelli and Trono, 2016). To identify new genetic sources of drought tolerance, gene expression analysis may be performed with contrasting genotypes to identify candidate genes that are responsible for variations in a trait (Tuberosa and Salvi, 2006; Tuberosa and Pozniak, 2014; Borrelli and Trono, 2016; Yousfi et al., 2016; Kulkarni et al., 2017; Mahmood et al., 2020). Metabolomic is a complementary tool for selecting favorable genotypes on the basis of metabolomic variations. To date, a targeted metabolomic approach has been frequently used, focused on a restricted group of metabolites (Huang et al., 2018, 2019; Zhao et al., 2018). In our work, the starting point was the availability of the barley and common wheat genomes that have furnished new tools for mining useful genetic variation (Mayer et al., 2011; Xu et al., 2018). The syntenic relationship among the evolutionary related cereal genomes (Gale and Devos, 1998) has favored the use of a comparative genomic approach to discover new sources of drought resistance across cereals (Bolot et al., 2009).

Drought stress remodulates primary plant metabolism, as well as photosynthesis, including the production of carbohydrates, amino acids, and other osmolytes (Langridge et al., 2006).

In these conditions, plants avoid water loss via stomatal closure, which indirectly decreases the CO_2 diffusion and thus the photosynthetic rate, producing a condition of metabolic constraint. When exposed to stressful conditions, plants accumulate an array of metabolites, particularly amino acids known as precursors to and constituents of proteins playing an important role in plant metabolism and development (Hayat et al., 2012). In this respect, branched-chain amino acid aminotransferases (BCATs) may play a pivotal role in triggering the onset of defense response also in wheat. In fact, the metabolism of branched-chain amino acids (BCAAs) is closely related to the primary metabolism, as isoleucine belongs to the aspartate pathway, whereas valine and leucine are derived from pyruvate (Joshi et al., 2010). In particular, BCATs play a crucial role in the metabolism of BCAAs (Binder, 2010), since they catalyze the last step of the synthesis and/or the initial step of the degradation of this class of amino acids. In plants, BCAAs are synthesized in the chloroplasts, whereas the degradation occurs in the mitochondria (Binder et al., 2007). BCATs have been previously characterized in *Arabidopsis* (Diebold et al., 2002; Urano et al., 2009; Binder, 2010; Angelovici et al., 2013), in tomato (Maloney et al., 2010), maize (Witt et al., 2012) and wheat (Bowne et al., 2012).

Several studies also indicate that a pool of these amino acids accumulates in leaves of barley (Templer et al., 2017) and wheat (Bowne et al., 2012) under water-limiting conditions. This hypothesis is supported by the fact that in *Triticeae* species, the most significant changes under drought stress can be observed in amino acids, organic acids and sugars content (Ullah et al., 2017) along with other compatible solute accumulation (Obata and Fernie, 2012). Moreover, an accumulation of BCAAs, following a regulation at the transcriptional level was observed under water-limiting conditions in *Arabidopsis* (Urano et al., 2009). The involvement of BCATs in stress response has been reported in *Arabidopsis* (Huang and Jander, 2017; Batista-Silva et al., 2019), and other plant species (Lanzinger et al., 2015; Ullah et al., 2017). Increased levels of BCAAs under drought conditions lead to higher protein degradation (Huang and Jander, 2017) or initiate a defense mechanism which stimulates the catabolic activity of BCAT and prevents the accumulation of toxic metabolites, as shown in sugarcane (Vital et al., 2017; Ali et al., 2019). In *Arabidopsis* and in other plant species both BCAAs biosynthesis and degradation occur, and these contrasting pathways must be carefully balanced to maintain homeostasis of the pool of this important group of amino acids. This is particularly true under stress conditions and critical in conditions of energy deprivation (Binder, 2010). It has also been proposed that BCAAs under conditions of energy shortage are catabolized in the TCA cycle to generate energy (Galili et al., 2016). Thus, an up-regulation of the anabolic enzyme could contribute to keep at a constant level this alternative fuel of the primary metabolism under DS conditions in wheat flag leaves.

A clear correlation between the accumulation of BCAAs under DS and their *de novo* synthesis has not been demonstrated yet, but based on the evidences in the literature (Scarpeci et al., 2016) it can be argued that the gene *BCAT3* contributes to acquire a higher tolerance as well as a good yield under DS in *Arabidopsis*. In barley, a comparative genomic approach was used to characterize the *HvBCAT-1* gene, involved in the drought defense response (Malatrasi et al., 2006).

The variation in levels observed in the pool of free amino acids correlates with the level of drought stress tolerance of the cultivars. BCAAs, in particular, increase as a consequence of the upregulation of catabolic enzymes including BCAT (Lanzinger et al., 2015). Moreover, BCAAs can work as alternative respiratory substrate under stress conditions (Araújo et al., 2011).

Nevertheless, the role of BCAAs in water-deficit stress tolerance is still unknown, as well as the molecular involvement of BCAT enzymes.

The increasing availability of the genomic sequences of many crops allows for the analysis of allelic variation within germplasm collection with the aim to discover useful alleles for subsequent breeding. In particular, the most common forms of nucleotide variations are single nucleotide polymorphisms (SNPs) and small insertions and deletions (indels), which may be significantly associated with phenotypic variations and plant adaptation to environmental constraints (Xia et al., 2017; Liu et al., 2018).

In this work, the molecular characterization of BCATs was performed in two durum wheat cultivars Cappelli and Colosseo, characterized by contrasting phenotypes for drought tolerance. Colosseo is more susceptible (Rampino et al., 2006) and Cappelli is more tolerant (Aprile et al., 2013) to drought. Taking advantage of a comparative genomic approach, this study aimed to: (i) identify the homoeologs of the chloroplast *BCAT* in Cappelli and Colosseo; (ii) characterize gene expression in response to drought stress during flowering and grain filling, as the most sensitive stages for grain set development and yield; and (iii) perform a targeted metabolic profiling employing nuclear magnetic resonance (NMR) spectroscopy.

MATERIALS AND METHODS

Seed Materials and Germination Conditions

Seeds of Cappelli were provided by the Institute of Biosciences and Bioresources (IBBR) of Bari (Italy); Colosseo, by Council for Agricultural Research and Economics (CREA) of the Research centre for Genomics & Bioinformatics at Fiorenzuola d'Arda (Italy); Kronos, was kindly provided by Prof. Cristobal Uauy (John Innes Center, Norwich, United Kingdom); and Primadur, Simeto, Messapia, Ciccio, Creso, Saragolla, and Svevo, by the Center of Cereal Research (CREA-CER) of Foggia (Italy).

Seeds were surface-sterilized with 0.5% (v/v) sodium hypochlorite for 5 min with gentle agitation, then rinsed in distilled sterile water, and germinated on wet filter paper for 9 days at 6°C under dark conditions.

Genomic DNA Isolation and Sequencing

Genomic isolation of genomic *TdBCAT* genes was carried out in the durum wheat cultivars Cappelli and Colosseo. Genomic DNA was extracted with the GenElute™ Plant Genomic DNA Miniprep Kit (SIGMA-ALDRICH, St. Louis, MO, United States) from 100 mg of frozen leaves of Cappelli and Colosseo. DNA quality and quantity were assessed with Nanodrop 2000 (Thermo Scientific, Wilmington, DE, United States). The DNA integrity and quantity were also checked with agarose gel electrophoresis (1% agarose w/v, 1X TAE buffer, GelRed™ as Nucleic Acid gel stain) by comparison to a λ genomic DNA ladder.

End-point PCR amplification of the full *TdBCAT-A* and *TdBCAT-B* gene sequences was carried out in a final volume of 20 μl, containing 10–20 ng of DNA, and 0.2 μM of each forward and reverse primers, 2X GoTaq® Colorless Master Mix (Promega, Madison, WI, United States), in a TC-512 Thermal cycler (Techne, Duxford, Cambridge, United Kingdom). PCR conditions were optimized for different groups of primers (**Supplementary Table S1**):

- For primer pairs (PP) PP1-PP6, PCR amplification was performed with 2 min initial denaturation at 94°C followed by 35 cycles with 30 s denaturation at 94°C, 30 s annealing, and elongation at 72°C for 60 s/kb; 5 min final extension at 72°C.
- For PP7 and PP8 PCR amplifications were performed applying a touch-down PCR applying 2 min initial denaturation at 95°C followed by 10 cycles with 30 s denaturation at 94°C, 30 s annealing at 65°C with a drop −0.5°C/cycle, and elongation at 72°C for 60 s/kb, then followed by 35 cycles with 10 cycles with 30 s denaturation at 94°C, 30 s annealing, and elongation at 72°C for 60 s/kb; 5 min final extension at 72°C.

The optimized annealing temperatures for each primer pair are reported in **Supplementary Table S1**.

Amplicons of the expected size (**Supplementary Table S1**) were recovered from the agarose gel using NZYGelpure kit (NZYtech, Lisbon, Portugal) and sequenced (Eurofins Genomics, Ebersberg, Germany).

Plant Growth and Stress Conditions

For the expression analysis during the germination phase (Experiment 1), seeds of ten durum wheat cultivars were used as experimental material: Kronos, Primadur, Simeto, Colosseo, Messapia, Ciccio, Creso, Saragolla, Svevo, and Cappelli. For the expression analysis during the reproductive stage (Experiment 2), only the two contrasting cultivars Cappelli and Colosseo were tested.

Experiment 1: After germination at 6°C, 8-days old coleoptiles (Z0.9, Zadoks scale) were dehydrated for 8 h (stress condition), or kept well-hydrated on wet paper (control condition). Ten coleoptiles from each cultivar and for each condition were sampled and immediately frozen in liquid N_2 and kept at −80°C until RNA extraction (**Figure 1A**).

Experiment 2: After germination, three plants for each cultivar (Colosseo and Cappelli), stage and treatment (18 plants in total) were grown in a growth chamber (Light/Dark 16:8 h, T = 20°C, RH = 80%) under well-watered conditions until the late tilling stage (Z30, Zadoks scale) and then transplanted, with three plants per pot (4.5 L). Each pot had the same amount of soil medium mixture 8:4:1 (v/v/v) soil:peat:perlite. After transplanting, the relative Soil Water Content (RSWC) was monitored until the end of the experiment. To calculate RSWC, dry weight (DW), field capacity (FC) and the current fresh weight (FW) of soil were monitored before transplanting and during the entire

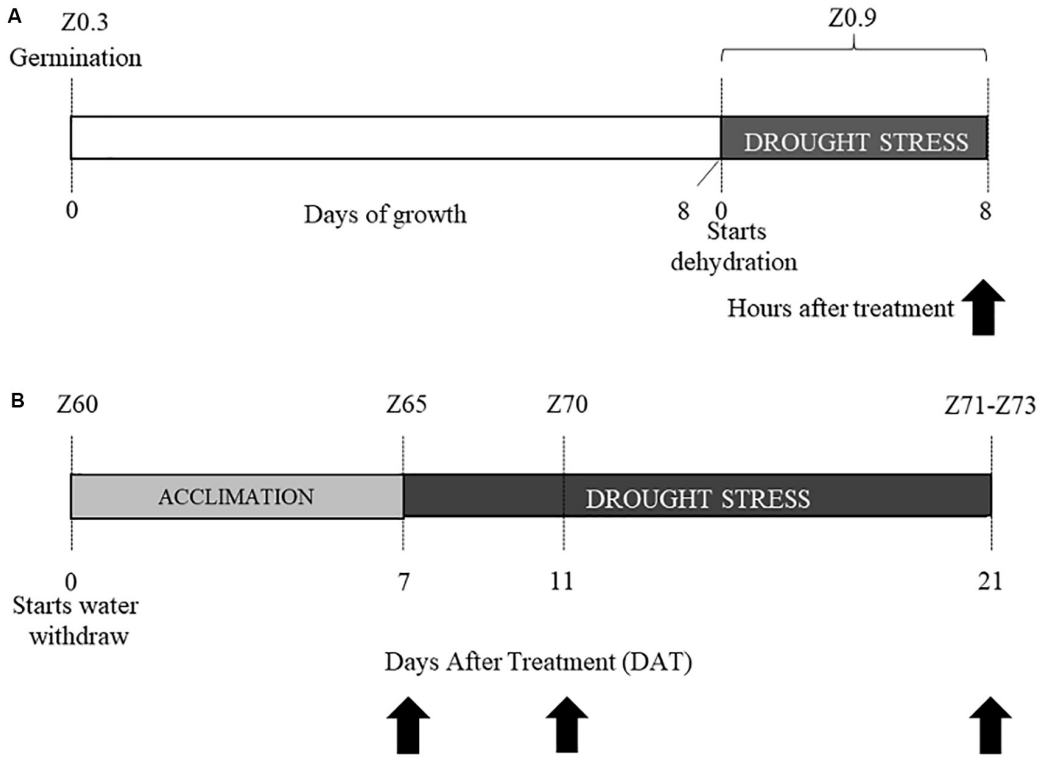

FIGURE 1 | Experimental design. Experiment 1 **(A)** and experiment 2 **(B)**. Stages are indicated according to Zadoks classification as Z followed by a number. Black arrows indicate the time-points in which tissues were sampled for transcriptional analysis.

experiment, as described in Aprile et al. (2013). The experimental values were entered into the formula RSWC = [(FW-DW)/(FC-DW)] × 100. Weight of the pots and plant biomass were considered for this estimation. Each pot was weighted twice a day to measure the FW, and consequently proper amounts of water were added to maintain RSWC for all the duration of the experiment. All plants were kept at 80% RSWC (control condition) until the end of the heading phase (Z60, Zadoks scale), when the water withdrawal started to reach the stress condition (30% of the RSWC) 7 days after treatment (DAT). When plants reached RSWC 30% this was considered as the acclimation to drought stress (DS). Tissue sampling for the physiological and transcriptional analysis were performed 2 h after the beginning of the light-period at three time-points: (1) 7 DAT or acclimation to DS; (2) 11 DAT; (3) and 21 DAT (**Figure 1B**).

For each time-point spikes and flag leaves were harvested and immediately frozen in liquid nitrogen to be kept at −80°C until RNA extraction and NMR metabolomic analysis. The leaf below the flag leaf was used for the physiological evaluation. For each cultivar and time-point, 3 plants were sampled (biological replicates; **Figure 1B**).

Physiological Analyses

Physiological response to drought was investigated on three plants for each cultivar, stage and treatment during Experiment 2 by measuring leaf relative water content (RWC) and the chlorophyll content. The leaf immediately below the flag leaf was considered. Both analyses were performed immediately after the sampling for the transcriptional analysis, at the same time of the day (2 h after the start of the light period), for each time-point, condition and genotype. Leaf RWC (%) was measured in control and stressed leaves of both Cappelli and Colosseo. Five disks (Ø = 1 cm) were clipped from each leaf of 3 plants, placed in 1.5 mL tubes. Fresh weight (FW) was immediately recorded then leaf-disks were soaked in distilled water for 4 h at room temperature under constant light. The turgid leaf disks were then rapidly blotted to remove surface water and weighed to obtain turgid weight (TW). Tissues were dried in the oven at 80°C for 24 h to record the dry weight (DW). The RWC was calculated according to the formula: RWC (%) = [FW-DW)/(TW-DW] × 100 (Barrs and Weatherley, 1962).

Chlorophyll content was measured in control and stressed leaves of both Cappelli and Colosseo with a SPAD-502 Minolta (Spectrum Technologies Inc., Plainfield, IL, United States) following the manufacturer instructions. Ten measures for each leaf of 3–4 plants were recorded along the leaf length (technical replicates).

RNA Isolation and Gene Expression Analyses by RT-qPCR

Total RNA was extracted from flag leaves or spikes of three plants with RNeasy Plant Mini Kit (Qiagen, Hilden, Germany). Plant samples were collected, pooled and homogenized in liquid

nitrogen and 100 mg were used for the extraction. The total RNA was displayed on agarose gel (1% agarose w/v, 1X TAE buffer, GelRed™ as Nucleic Acid gel stain) to assess its integrity. For each sample, 1 μg of total RNA was retro-transcribed into cDNA with QuantiTect Reverse Transcription Kit (Qiagen) according to the manufacturer instructions.

The expression analysis of each target gene was performed as a two-step real-time quantitative PCR (RT-qPCR). 1 μL (dilution 1:10) of cDNA was used for the analysis with a ABI PRISM 7000 Sequence Detection System (Applied Biosystems, Foster City, CA, United States). Reactions were set up in 10 μL volume with 2X PowerUp SybrGreen Master Mix (Life Technologies, Carlsbad, CA, United States) and 300 nM of gene-copy specific forward and reverse primers (**Supplementary Table S1**).

TaActin gene (AB181991, Rocchi et al., 2012) was used as house-keeping gene for normalization whereas the expression of durum wheat drought-related gene *TdDHN15.3* (AM180931.1, Rampino et al., 2006) was used to evaluate the stress conditions in the tissues. The mean Ct measured for the reference gene actin varied by less than 2.2%. All qPCR data were analyzed using the $2^{-\Delta\Delta Ct}$ method using control samples as calibrator (Livak and Schmittgen, 2001). The qPCR data are presented as the mean values calculated from three biological replicates with three technical replicates.

Bioinformatic Analysis

The genomic sequence of *TdBCAT* isolated and sequenced in cv. Cappelli and cv. Colosseo were compared with the reference sequence of *T. durum* cv. Svevo[1], using BLASTn algorithm (Altschul et al., 1990). The proximal promoter region (up to 1000 bp upstream start codon ATG) were analyzed using PlantPan 3.0 (Chow et al., 2019) considering *Oryza sativa* as a model species for *Triticeae*.

The gene topography and the putative transcription starting site were inferred using the FGENESH + (Solovyev et al., 2006) of the Softberry suites (Softberry Inc., Mount Kisco, NY, United States) starting from a similar protein HvBCAT (CAE00460.2). The predicted protein sequences were deduced and used for the following analyses. The protein localization was hypothesized exploiting the WOLF pSORT predictor (Horton et al., 2007).

Molecular evolution of BCATs was inferred by using the Maximum Likelihood method based on the Poisson correction model, on multiple alignment performed with the MUSCLE algorithm (Edgar, 2004) and the tree with the highest log likelihood was considered, (Maximum Likelihood method, 1000 Bootstrap Replications) using the Poisson model as substitution model (Zuckerkandl and Pauling, 1965). Initial tree(s) for the heuristic search were obtained automatically as described in Tamura et al. (2011) by applying Neighbor-Join and BioNJ algorithms (Saitou and Nei, 1987; Gascuel, 1997) to a matrix of pairwise distances estimated using a JTT model, and then selecting the topology with superior log likelihood value. The analysis involved 39 amino acid sequences. All positions with less than 95% site coverage were eliminated; fewer than 5% alignment gaps, missing data, and ambiguous bases were allowed at any position. The tree sketched to scale, with branch lengths measured in the number of substitutions per site. Evolutionary analyses were conducted in MEGA6 (Tamura et al., 2013).

[1]https://d-data.interomics.eu/blast/nucleotide/nucleotide

Metabolomic Through NMR and Data Analyses

Comparative metabolic profiling was performed on flag leaves tissues derived from the Experiment 2 (**Figure 1B**), collected from Cappelli and Colosseo at 7, 11, and 21 DAT both in control and drought stressed conditions. Leaves and spikes tissues previously sampled and stored at −80°C were ground to a fine powder in liquid N_2 with a pestle and mortar, then freeze-dried at a vacuum level of 0.2 mbar and −50°C (Lio5P, 5Pascal, Milan, Italy). Samples were prepared for the NMR analysis according to Kim et al. (2010). In particular, 50 mg of ground samples were transferred into an Eppendorf tube and extracted with a mixture of 1:1 v/v CH_3OH-d4:KH_2PO_4 (Acros Organics, Thermo, United States) at pH 6.0, containing 0.1% (wt/wt) sodium trimethylsilyl propionate (TSP). Samples were vortexed for 1 min and sonicated for 20 min at room temperature, then centrifuged at 17,000 × *g* for 10 min. Centrifugation was repeated until a clear supernatant was obtained. The supernatants were then transferred separately into the NMR tubes for NMR measurements. Samples were immediately processed after extraction using the following method: one-dimensional 1H-NMR spectra (three replicates for each time point, treatment and cultivar) were acquired with JEOL – ECZ600R/M3 (Joel, Japan) spectrometer at the proton frequency of 600.1723 MHz using the following parameter: 128 scans, sweep window 15 ppm, 64 k points and a calibrated 90° pulse length of 8.86 μs at 25°C using Carr-Purcell-Meiboom-Gill (CPMG) pulse sequence with a constant time CPMG delay, Trelax, of 20 ms. A 10 s relaxation delay was found to be adequate for the acquisition of quantitative data.

These parameters gave a total analysis time of 36 m 22 s. The spectra were processed and analyzed with Chenomx NMR suite 8.1 (Chenomx Inc., Edmonton, AB, Canada), zero-filing to 128 k points and line broadening 0.5 Hz22. All data were referenced to the TSP peak at 0 ppm.

Spectral matching, metabolites assignment and identification were performed with Chenomx NMR Analysis Software libraries that automatically fit the experimental spectrum to the Spectral Reference Library. The software automatically adjusts the Reference Library and allows the user to adjust peak intensity and define the exact location to determine the concentration values. Then, the intensity and position of the peak (**Supplementary Table S2**) were manually adjusted to generate concentrations of the selected primary metabolites detected in the plant samples.

Statistical Analyses

Student's *t*-test was applied to compare data of control and stressed plants for the analyses of physiological traits.

Nuclear magnetic resonance data were statistically analyzed applying the one-way homoskedastic Student's *t*-test and standard error (SE) was calculated between replicas using

Office Excel 365 ProPlus (Microsoft Corporation, Redmond, WA, United States). To overcome a recurrent limitation in metabolomic experiments which is the small number of replicates, *p*-values have been adjusted applying the corrected FDR-adjusted *p*-values for multiple comparisons following the method proposed by Benjamini and Hochberg, 1995. The application of the FDR correction to adjust the *p*-values is expected not only to reduce false positives, but also to minimize false negatives; the p.adjust function (R stat package)[2] was used (Jafari and Ansari-Pour, 2019; Piasecka et al., 2019; Fukushima et al., 2020).

RESULTS

Identification and Genomic Characterization of TdBCAT

A comparative genomic approach was utilized to identify *TdBCAT-A* and *TdBCAT-B* genes in Colosseo and Cappelli, using the barley *HvBCAT-1* (AJ574850) gene as reference. First of all, the *HvBCAT-1* matching sequences in either A and B genomes of *Triticum aestivum* were considered, on the basis of the IWGSC-CSS assembly (IWGSC, 2014). Top-score matches were used to reconstruct *in silico* the bread wheat sequences of *TaBCAT* including chromosome position, and transcript annotation (Traes), if available (**Supplementary Table S3**).

TaBCAT sequence localized on chromosomes group 4 of *T. aestivum* cv. Chinese Spring, in particular on the short arm of chromosome 4A (4AS), and on the long arm of both chromosome 4B (4BL) and 4D (4DL). This is in agreement with previously reported pericentric inversion on chromosome 4A, which caused the partial transfer of 4AL to 4AS (Devos et al., 1995) and the reported localization of *HvBCAT-1* on chromosome 4H in barley (Malatrasi et al., 2006). The chromosomal location was further verified and confirmed by investigating the durum wheat genome of Svevo[3], matching an identical sequence on chromosomes 4A and 4B (identity >99.8%, *E*-value 0.0).

Locus-specific primer pairs allow the *in vivo* identification of the *TdBCAT-A* and *TdBCAT-B* genes in Colosseo and Cappelli. Two different alleles for *TdBCAT-A* (MK648150 and MK648149) were identified sharing 99.87% identity, while a common *TdBCAT-B* allele (MK648151) was identified in both cultivars. The analysis of *TdBCAT-A* sequence in the two cultivars showed for the Colosseo allele a 100% identity with the *–A* sequence retrieved in the Svevo reference genome. Moreover, five SNPs explaining the 0,13% variation, were found in the *TdBCAT-A* sequence. Three SNPs were located in the promoter region at 809 (T/G), 705 (T/C) and 681 (A/G) bp downstream of the ATG, and two SNPs (G/T and T/A) were observed in the first intron 218 and 219 bp downstream of the ATG, respectively. Although the presence of SNPs was retrieved only in non-coding regions of *TdBCAT-A* genes, they can impact on the gene expression thus on the phenotypic variation (Fiume et al., 2004; Webb et al., 2009; Trujillo-Moya et al., 2018). The overall conservation of *BCAT* genes is shown in the multiple sequence alignment (**Supplementary Figure S1**).

A full list of the genes identified and their coordinates in three different wheat genome assemblies, CSS assembly (IWGSC, 2014), the TGAC v.1 (Clavijo et al., 2017) and the RefSeq v.1 (IWGSC, 2019) are reported in **Supplementary Table S4**. The gene's topography predicted by the *in silico* analysis (**Figure 2**) confirms the 7 exons-structure previously reported for *HvBCAT-1* (Malatrasi et al., 2006). The coding sequences (CDSs) of 1200 bp-long, encoded a protein of 399 amino acids for both *TdBCAT-A* and *TdBCAT-B*. A transcriptional start site (TSS) was predicted at 156 bp and 248 bp upstream the starting codon in *TdBCAT-A* and *TdBCAT-B,* respectively, and a PolyA site was retrieved 2085 bp and 2066 bp downstream of the ATG.

Promoter Analysis

The promoter sequences of *TdBCAT-A and TdBCAT-B* were analyzed with Plant PAN 3.0 database (Chow et al., 2019). The complete list of the Transcription factors binding sites (TFBS) identified is reported in **Supplementary Table S6**. Here the TFBS related to drought stress are reported in **Table 1**.

One Dehydration-Responsive Element-Binding (DREB) is predicted in either A and B gene promoters as targeted by DREB2 subunits of the AP2/ERF family, which are key regulators in many abiotic stress responses including drought, high salinity and heat stress (Zhang et al., 2009; Yousfi et al., 2016; Xie et al., 2019). The two genes show a different number of Abscisic-acid Responsive Elements (ABRE) targeted by ABF3 and several TFs of the bHLH family. In particular, *TdBCAT-B* has the highest number of ABREs elements as compared to *TdBCAT-A*.

A conserved triplet of motifs targeted by EIN3 was identified in both *-A* and *-B* genes. EIN3 is a TF that regulates primary plant response to ethylene, a well-known stress-response hormone and regulator of plant growth and development (Khan et al., 2017).

Phylogenetic Analysis and Subcellular Localization of BCATs

The BLASTp analysis of the protein sequences identified TdBCAT proteins as a chloroplastic-like Branched-Chain Amino Acid Amino-Transferase, since the first 100 score matched only to chloroplast or to chloroplastic-like proteins, in accordance with the WoLFPSORT prediction (score: *k*-nearest neighbors = 14) (Horton et al., 2007). Only three sequences showing a 66% of identity were annotated as mitochondrial BCATs: BCAT1 of *Morus notabilis* (XP_024029919.1), BCAT1 of *Ziziphus jujuba* (XP_015885109.1) and BCAT1 of *Momordica charantia* (XP_022132131.1).

A multiple alignment was performed on 39 sequences, including previously isolated BCATs and all the AtBCAT isoforms of *Arabidopsis thaliana* described as mitochondrial, chloroplastic and cytosolic.

The clustering (**Figure 3**) placed TdBCAT-A and TdBCAT-B in the same subtree with three chloroplastic BCATs of *Arabidopsis* (AtBCAT-2, AtBCAT-3, AtBCAT-5) (Diebold et al., 2002). As expected, all the cytosolic and the mitochondrial BCATs clustered in two distinct subtrees, although the mitochondrial BCATs fell

[2]http://www.R-project.org
[3]https://d-data.interomics.eu/

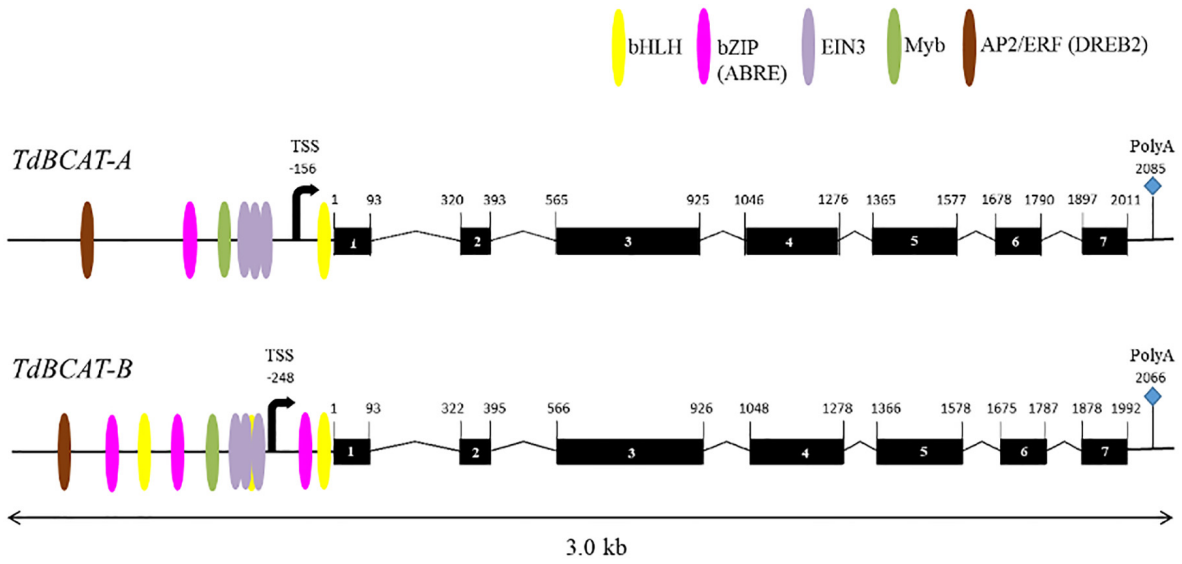

FIGURE 2 | Schematic representations of TdBCAT homoeolog genes. Exons are represented as black boxes. The most relevant TFs binding site on the promoter regions are shown: Basic Helix-Loop-Helix (bHLH), Basic Leucine Zipper Domain (bZIP; ABRE), Ethylene Insensitive 3 (EIN3); Apetala2/Ethylene Responsive Factor (AP2/ERF, DREB2). The predicted sites for transcription start (TSS) and termination (PolyA) are shown.

TABLE 1 | List of some regulatory elements in TdBCAT promoters.

TF family	TF(s)	Position[(a)]		Binding sequence		TFBS ID[(b)]
		TdBCAT-A	*TdBCAT-B*	*TdBCAT-A*	*TdBCAT-B*	
AP2/ERF	DREB2	−758 (+)	−817 (−)	(+) gCACCGaca	(−) gggCGGTGa	TFmatrixID_0066
bHLH			−584 (±)		(+) GCTCGttc	TFmatrixID_0174;
			−218 (±)		(+) aacACTTGc	TFmatrixID_0176
			−20 (±)		(+) GCCCGggc	
		−12 (±)	−12 (±)	(+) GTACGtgc	(+) GTACGtgc	
bZIP	ABF3		−673 (±)	(+) CCACGggt	(+) AGACGtat	TFmatrixID_0193
		−455 (±)	−507 (±)		(+) CCACGggt	
			−93 (±)		(+) AAACGtat	
EIN3	EIN3	−280 (±)	−329 (±)	(+) taATGCAtgt	(+) taATGCAtgt	TFmatrixID_0256
		−250 (±)	−299 (±)	(+) caATGCAtgt	(+) caATGCAtgt	
		−229 (±)	−265 (±)	(+) caATGCAtgt	(+) caATGCAtgt	
MyB			−709 (±)		(+) atAATATttt	TFmatrixID_0334;
			−683 (±)		(+) atAATATtat	TFmatrixID_0320;
		−313 (±)	−372 (±)	(+) caaATATCt	(+) caaATATCt	TFmatrixID_0357

The relative transcription factors (TFs) predicted to bind the Transcription Factors Binding Sites (TFBS) are indicated. (a) Positions consider as + 1 the A of the start codon (ATG) of the corresponding gene. In brackets the position on the plus(+) and/or minus(−) strand; (b) TFBS ID from PlantPan3.0 database.

into the chloroplast subtree, indicating a possible mis-annotation of these sequences. The phylogenetic analysis reveals high similarity between the isolated TdBCATs and the *Triticum urartu* BCAT; moreover, high identity was observed within the BCATs in the *Triticeae* tribe and in general between *Gramineae*, followed in order of similarity by *Brachypodium distachyon*, *O. sativa, Setaria italica, Sorghum bicolor,* and finally *Zea mays.*

Physiological Traits Analyses

The effects of drought stress on Cappelli and Colosseo, were evaluated in Experiment 2 considering the leaf immediately below the flag leaf. Three-time points were considered: 7, 11, and 21 DAT.

A significant progressive reduction of the RWC starting from 11 DAT (Z65) was observed in both cultivars (p-*value* $\leq$ 0.01), more consistent in the sensitive genotype Colosseo confirming its higher susceptibility to drought stress. Two weeks after the stress imposition the RWC was 50% in Colosseo compared with the 71% detected in Cappelli (**Figure 4A**).

The relative chlorophyll content measured with SPAD confirmed the overall health status of the plants, and

TABLE 2 | | Relative expression of TdDHN15.3 and TdBCAT genes in coleoptiles of dehydrated plantlets.

	Creso	Kronos	Messapia	Primadur	Ciccio	Simeto	Saragolla	Svevo	Colosseo	Cappelli
TdDHN15.3	317.4	1, 946.50	406.37	1, 016.93	421.68	661.68	1, 072.43	1, 930.82	789.61	301.29
TdBCAT-A	0.84	0.92	0.84	1.09	0.46	0.87	1.02	0.69	1.78	1.33
TdBCAT-B	1.24	1.44	2.35	1.84	0.67	1.18	1.42	0.9	1.47	2.43

Ten durum wheat cultivars were considered. Values represent fold-change (FC) mean values of dehydrated samples in comparison with the regularly irrigated once.

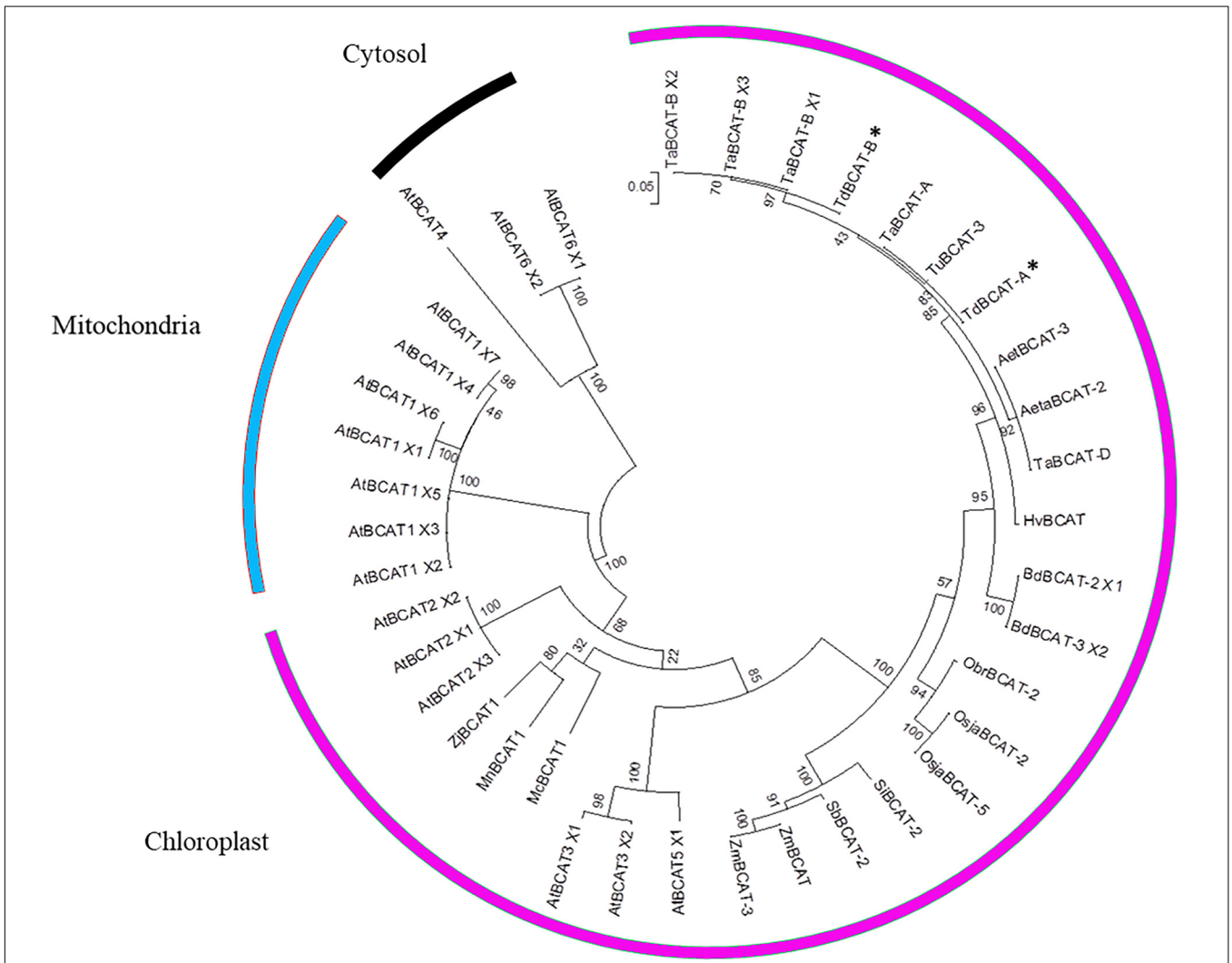

FIGURE 3 | Phylogenetic tree. The TdBCAT-A and –B deduced protein sequences were used to design the phylogenetic tree. The tree was obtained by Maximum Likelihood method using MEGA 6 (Tamura et al., 2013); the highest log likelihood (–3956.0220) is shown. Asterisks indicate the newly isolated TdBCATs (*). TuBCAT-3 (*Triticum urartu*, EMS62409.1), HvBCAT (*Hordeum vulgare* CAE00460.2), Aeta BCAT-2 (*Aegilops tauschii,* XP_020159191.1), AetBCAT-3 (*Aegilops tauschii*, XP 020173856.1), BdBCAT-2 × 1 (*Brachypodium distachyon*, XP_003558433.1), BdBCAT-3_X2 (*B. distachyon*, XP_010228932.1), OsjaBCAT-2 (*Oryza sativa* Japonica group, XP_015630708.1), OsjaBCAT-5 (*O. sativa* Japonica group, ABF94786.1), ObrBCAT-2 (*Oryza brachyantha*, XP_006651192.1), SiBCAT-2 (*Setaria italica*, XP_004985120.1), SbBCAT-2 (*Sorghum bicolor*, XP_021317757.1), ZmBCAT (*Zea mays*, XP_008674369.1), ZmBCAT-3 (*Z. mays*, PWZ58251.1). The only three BCATs descripted as mitochondrial are MnBCAT1 (*Morus notabilis*, XP_024029919.1), ZjBCAT1 (*Ziziphus jujuba*, XP_015885109.1) and McBCAT1 (*Momordica charantia,* XP_022132131.1). Sequences retrieved from Ensembl Plant database are the *Triticum aestivum* TaBCAT-A (TraesCS4A01G059800.1), TaBCAT-B_X1, X2 and X3 (TraesCS4B01G235400.1, 0.2, 0.3), TaBCAT-D (TraesCS4D01G236800.1), and the *Arabidopsis thaliana* AtBCAT1_X1, X2, X3, X4, X5, X6, X7 (AT1G10060.1, 0.2, 0.3, 0.4, 0.5, 0.6, 0.7), AtBCAT2_X1, X2, X3 (AT1G10070.1, 0.2, 0.3), AtBCAT3_X1, X2 (AT3G49680.1, 0.2), AtBCAT5_X1, X2 (AT5G65780.1, 0.2), AtBCAT6_X1, X2 (AT1G50110.1, 0.2), AtBCAT4 (AT3G19710).

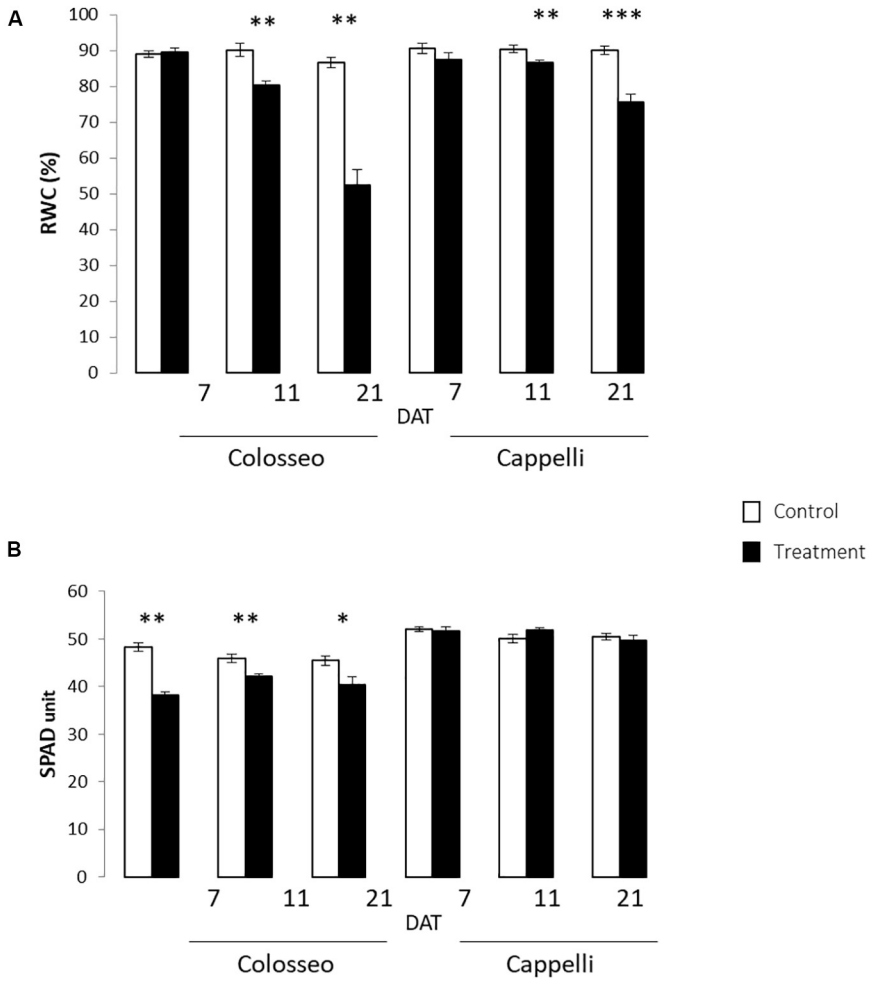

FIGURE 4 | Physiological analyses. Were performed on leaves of Colosseo and Cappelli at three time-points: 7, 11, and 21 days after treatment (DAT) in control (white) and treated (black) plants. Three plants each time point for each treatment have been considered. **(A)** Relative Water Content (RWC) values are presented as the mean (±SE) of ten leaf disks. **(B)** Chlorophyll content values are presented as the mean (±SE) of ten measures for 3–4 leaves. Significantly different values are indicated with asterisks (***p-value $\leq$ 0.001; **p-value $\leq$ 0.01; *p-value $\leq$ 0.05 evaluated with Student's t-test.).

showed in Colosseo stronger significant reduction of chlorophyll content in particular at 7 DAT (p-value $\leq$ 0.01) (**Figure 4B**).

The physiological analyses confirmed the higher DS tolerance of Cappelli, which, in drought conditions, maintains a higher RWC in leaves and a higher photosynthetic capacity.

Gene Expression Analyses

The modulation of *TdBCAT* genes in response to DS was monitored under water-limiting conditions in two relevant phases of durum wheat development: germination (Experiment 1) and reproductive stages (Experiment 2). The dehydrin gene *TdDHN15.3* (AM180931.1), was used as control since is known to be strongly up-regulated in dehydrated durum wheat coleoptiles and in barley flag leaves under terminal drought (Rampino et al., 2006; Karami et al., 2013). This set of experiments showed strong homoeologs and cultivar-specificity in the expression profile of the newly identified *TdBCAT* genes (**Figure 5**).

During germination *TdBCAT-A* is not significantly modulated in response to DS in all cultivars tested, while *TdBCAT-B* is up-regulated, though moderately, in most of the cultivars tested, with the exception of Ciccio and Svevo in which the down-regulation is still below 2-fold as compared to controls (**Table 2**). In Cappelli, *TdBCAT-B* expression increases about 2-fold in dehydrated coleoptiles. *TdDHN15.3* shows the highest up-regulation from 300-fold to almost 1946-fold, depending on the cultivar (**Table 2**). This is consistent with the observation reported by Rampino et al. (2006) in durum wheat cultivars exposed to severe drought stress conditions, which observed comparable expression levels of many dehydrin genes, including *TdDHN15.3.*

In plants subjected to a prolonged stress from the end of heading phase to the early grain-filling stage (Experiment 2) *TdDHN15.3* showed a strong up-regulation at all-time points, mainly in Cappelli (**Supplementary Table S5**). In particular, the highest fold change (FC) values were observed at 7 DAT both in flag leaves (FC 19.84) and in spikes (FC 8.63), while

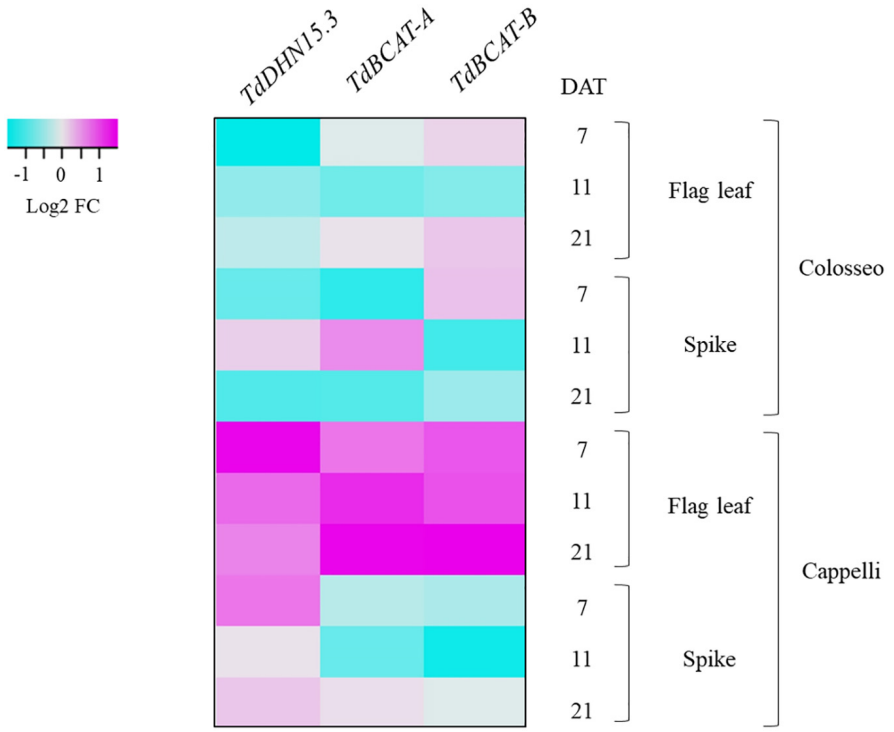

FIGURE 5 | Heat-map showing the relative expression of *TdBCAT-A*, *TdBCAT-B*, and *TdDHN15.3* in response to drought stress in the flag leaf and spike. Three different time-points (7, 11, and 21 days after treatment, DAT) in the reproductive stage in three plants for each treatment of drought-sensitive (Colosseo) and drought-tolerant (Cappelli) durum wheat cultivars were considered. Data are expressed as log2 Fold-change (FC).

lower values were observed at 21 DAT (early post-anthesis) n leaves (FC 7.73) and spike (FC 4.63). Our data agree with the results of Karami et al. (2013) of a remarkable higher induction of this gene in barley flag leaf, in tolerant genotypes (**Supplementary Table S5**). On the other hand, in Colosseo, *TdDHN15.3* expression is consistently lower as compared to Cappelli, with the maximum level of induction in spike tissues at 11 DAT (FC 4.40), while in flag leaves the highest over-expression was recorded at 21 DAT (FC 2.55, **Supplementary Table S5**).

TdBCAT-A and *TdBCAT-B* were up-regulated in the flag leaves under DS, reaching the maximum in Cappelli at 21 DAT, with FC 13.5 and 16.37, respectively (**Figure 5** and **Supplementary Table S5**). In Colosseo, the up-regulation was less consistent and followed a different trend: in flag leaves both genes had similar level of expression at 7 and 21 DAT (FC 2.0–2.4 and FC 3.21–3.54), with no relevant changes at 11 DAT; in spikes *TdBCAT-A* was induced at 11 DAT (FC 4.62), while *TdBCAT-B* was progressively down regulated from 7 to 21 DAT (FC from 3.61 to 1.47, **Figure 5** and **Supplementary Table S5**). In Cappelli, both genes were strongly over-expressed in flag leaves, supporting the hypothesis of a higher relevance of the gene expression of this gene in leaves than in spikes under drought.

Moreover, these data highlight strong tissue specificity in the expression of *TdDHN15.3* in response to drought. In the stressed coleoptiles the highest expression was observed in the cultivar Kronos (FC 1946.50 **Table 2**), while in Cappelli the maximum of expression was observed in flag leaves, even if with lower extent (FC 20) (**Supplementary Table S5** and **Figure 5**).

Metabolic Characterization of Drought Stress Response

Plant samples from each genotype collected at 7, 11, and 21 DAT were analyzed using a targeted metabolomic approach by selecting 12 metabolites among those known to be affected by drought. These metabolites are distributed into three classes: amino acids (with a focus on BCAAs), organic acids and sugars. During DS the intracellular osmotic potential is decreased by accumulating compatible solutes such as proline (Pro), ɣ-aminobutyric acid (GABA) and glutamate (Hildebrandt, 2018; Fàbregas and Fernie, 2019; Kang et al., 2019). Moreover, the production of sucrose, and malic acid and glutamic acid are promoted during drought stress (Marček et al., 2019).

Our results showed that Pro synthesis is increased during drought, but new insights were found regarding differences in the accumulation of other metabolites between the two durum wheat varieties.

Branched chain-amino acids are positively accumulated during drought stress in durum wheat. Leucine, isoleucine, and valine, increased significantly under stress conditions in both Colosseo and Cappelli with a maximum at 21 DAT (**Figure 6**) which correlates with the expression level of both *TdBCAT-A* and *B* in Cappelli. Analyses of the level of BCAAs have already

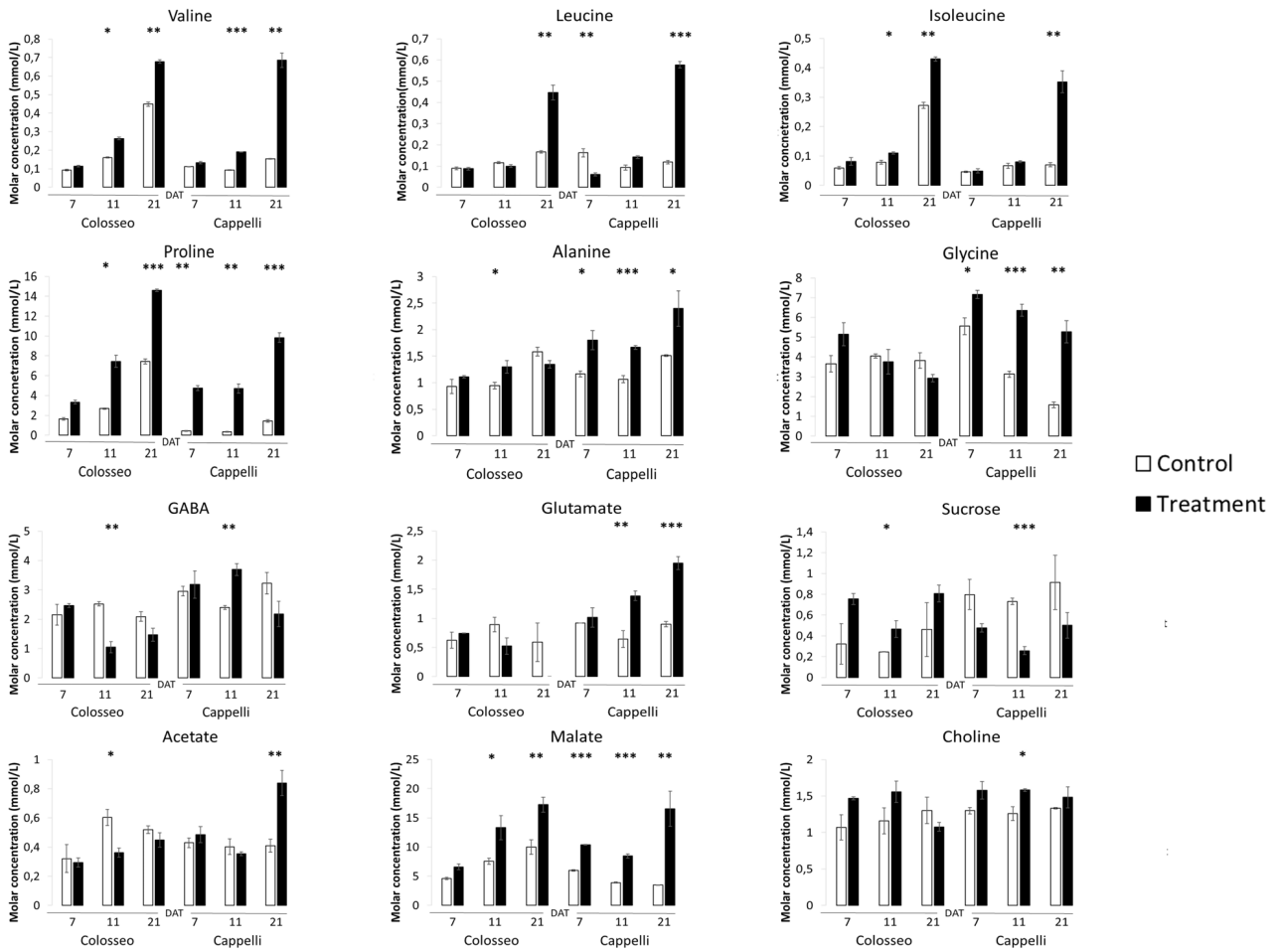

FIGURE 6 | Targeted NMR metabolite profiling. The analyses were conducted on Cappelli and Colosseo leaves at three time-points: 7, 11, and 21 days after treatment (DAT) in control (white) and treated (black) plants. Three plants have been considered for the analyses. Values expressed as molar concentration (mmol/L) represent the mean (± SE) of three independent samplings. Significantly different values are labeled with asterisks (*FDR-adjusted p-value ≤ 0.05; **FDR-adjusted p-value ≤ 0.01; ***FDR-adjusted p-value ≤ 0.001 evaluated with Student's t-test adjusted to control the false discovery rate (FDR).

demonstrated that valine were present at higher levels than isoleucine and leucine in stems, leaves, and flowers (Maloney et al., 2010; Kochevenko et al., 2012).

A subset of metabolites, including three amino acids (alanine, glycine), choline and glutamate and three organic acids (GABA, malate, and acetate) increased only in Cappelli which, on the contrary, exhibited a lower accumulation of sucrose. In Colosseo, drought stress induced the higher accumulation of sucrose during DS (**Figure 6**).

In Cappelli, the content of Pro was positively regulated during the stress with no increase at 11 DAT and a maximum at 21 DAT (**Figure 6**), while Colosseo showed a progressive increase reaching higher content at 21 DAT. In addition, the basal levels of Pro in the non-stressed Colosseo plants were higher than in Cappelli.

GABA, as part of the compatible osmolytes, was upregulated in the early phases of the drought response in Cappelli but was downregulated in Colosseo, confirming the hypothesis of an involvement of GABA in increasing drought tolerance in Cappelli, acting as ROS scavenger (Hildebrandt, 2018). Among the genotypes, the organic acids content was higher in the case of malate, which was accumulated in Colosseo (at 11 and at 21 DAT) and at all-time points in Cappelli. Acetate was significantly accumulated only in Cappelli at 21 DAT. The content of choline, the precursor of glycine-betaine slightly increased in early phases of the defense response in Cappelli (11 DAT); choline is involved in the defense response correlated with the osmoregulation process (**Figure 6**). A summary of the metabolic responses of Cappelli and Colosseo to drought is reported in **Figure 7**.

DISCUSSION

This paper describes the genomic characterization of the *TdBCAT*s in *T. durum* obtained through a combination of *in silico* and *in vivo* analyses that also led to the cellular localization of the *TdBCATs*. As previously reported for other plant species, the N-terminal extensions of *TdBCAT* genes

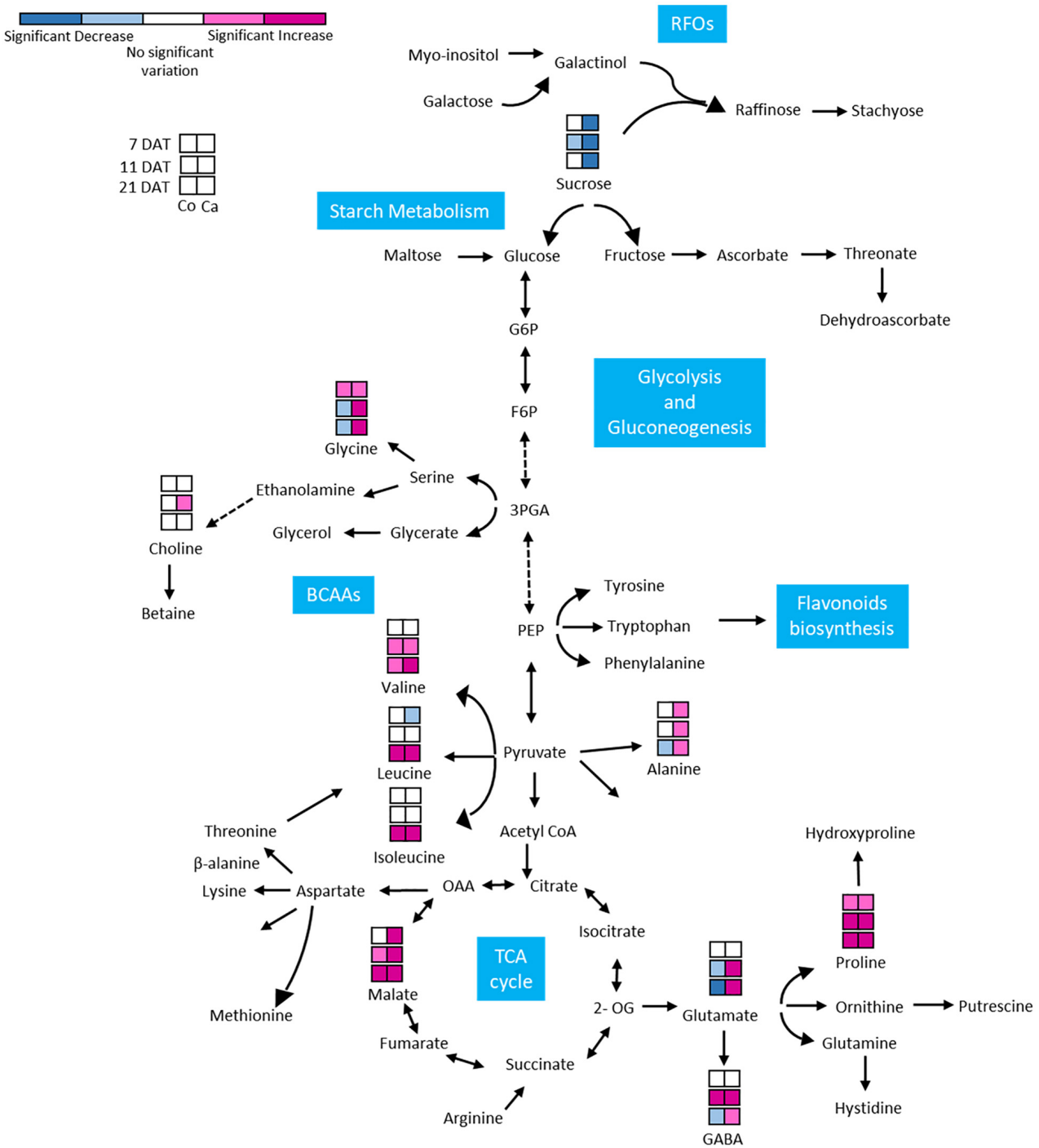

FIGURE 7 | Metabolic response of Colosseo (Co) and Cappelli (Ca) plants to drought. Boxes represent the three time points analyzed (7, 11, and 21 DAT). Colors depict the relative accumulation levels of the analyzed metabolites in stressed samples as compared to the control. Metabolites with magenta and pink boxes denote significant increases while sky blue or dark blue boxes denote significant decreases. White boxes indicate no significant change. The level of significance was set at *p-value* $\leq$ 0.05. BCAAs, branched-chain aminoacids; RFOs, raffinose family oligosaccharides.

targeted the protein in chloroplasts in durum wheat, suggesting a specialized enzymatic activity to complete the synthesis of either Val, Leu, and Ile. The regulation of the homeologs A and B alleles in response to DS in leaves and spikes, suggests a tissue specific function, considering their higher expression in leaves but lower in reproductive organs. In addition, a strong cultivar specificity was observed, with these transcripts more abundant in Cappelli (tolerant) than in Colosseo (susceptible). This expression pattern

during drought may reflect a higher demand for amino acids in vegetative organs to counteract the effects of water deprivation.

The distinct localization patterns and the drought specific over-expression of *TdBCATs* was also confirmed by the expression of *TdBCAT-A* and *-B* in coleoptiles in eight (Creso, Kronos, Messapia, Primadur, Simeto, Saragolla, and Cappelli) out of ten cultivars tested (excluding Svevo and Ciccio) and demonstrated that BCATs participate in early phases of the DS defense response and an extremely low expression at basal levels in normal growth conditions.

The targeted NMR analysis of the metabolomic alteration of leaves in both Cappelli and Colosseo (**Figure 7**) indicated important alteration to the levels of several metabolites. Previous studies linked the involvement of several defense mechanisms, such as ROS balance, and signaling pathways with increased levels of metabolites in different plant species (Urano et al., 2009; Kochevenko et al., 2012; Pires et al., 2016; Todaka et al., 2017; Fàbregas and Fernie, 2019; Fukushima et al., 2020). In this study the metabolomic analysis was targeted to define the contrasting metabolic changes in leaves of two cultivars with different tolerance to DS and to search for correlations between the changes in metabolites classes and levels and the regulation of the newly identified *TdBCAT* genes.

An enhanced level of amino acids have been found in several plant species as *Arabidopsis*, wheat, soybean, bean, rice and chickpea in DS conditions (Sassi et al., 2010; Silvente et al., 2012; Rahman et al., 2017; Todaka et al., 2017; Hildebrandt, 2018; Batista-Silva et al., 2019; Kang et al., 2019). As expected, BCAAs (Leu, Ile, and Val) levels increased under water deficit at higher extent in the tolerant Cappelli and the increase seems regulated at a transcriptional level with a dehydration inducible specificity.

This is also consistent with the presence in the *TdBCAT-A* and *–B* promoters of typical ABRE motifs. It is well established that during abiotic stress low abundant amino acids like BCAAs are not synthesized but they accumulate due to an increased protein turnover in conditions of carbohydrate starvation (dehydration, salt stress, darkness) and then are degraded (Hildebrandt, 2018). Similarly, the activities of some enzymes related to the catabolism of BCAAs showed rapid increase in response to abiotic stresses, and therefore it is reasonable to assume an important role in the metabolism of BCAAs under stress (Mata et al., 2016) possibly due to the onset of BCAAs catabolism in the tolerance mechanism as suggested also by Mata et al. (2016). Moreover, it has been proposed that BCAAs under energy shortage are catabolized by the TCA cycle to generate energy (Galili et al., 2016), thus an up-regulation of the anabolic enzyme could contribute to keep at constant level this alternative fuel for the primary metabolism under DS condition in wheat flag leaves.

Proline (Pro) plays a pivotal role in mitigating drought stress by reducing ROS level and by preserving the integrity of plant membrane and proteins (Hayat et al., 2012) and its accumulation under stress has been associated with drought tolerance in many plants (Kishor et al., 2005). In a previous study, it was observed that Pro was highly accumulated in the leaves of a drought tolerant wheat cultivar at a higher concentration than in a sensitive one (Kang et al., 2019). In this analyses, a higher accumulation of Pro in leaves of the susceptible cv Colosseo was observed contrasting with previous result (Kang et al., 2019).

GABA, showed a higher accumulation in Cappelli at 21 DAT than in Colosseo where a strong reduction during the stress was observed. Glutamate, as expected, showed a similar trend since it is a precursor of GABA (Marček et al., 2019), and is accumulated in Cappelli while its content strongly decreases in Colosseo during drought stress, as previously observed in another drought sensitive wheat genotype (Michaletti et al., 2018).

Finally, the accumulation of compounds as GABA, malate and amino acids may reflect disruption of export of these compounds or their precursors from source to sink under stress conditions, since both organic acids and amino acids are common constituents of sap exudates in diverse plant species (Bialczyk and Lechowski, 1992; Hildebrandt, 2018).

In this work we observed that the choline accumulation was significantly enhanced in the early phases of the response to DS (11 DAT) in Cappelli (Gou et al., 2015), supporting for this variety increased capacity of osmoregulation during drought response and that the accumulation of compatible osmolytes such as glycinebetaine (GB) and choline is significantly involved in osmotic adjustment and protection of essential biomolecules under various environmental stresses including DS (Ashraf and Foolad, 2007; Ashraf et al., 2011).

Sugars are known to play a pivotal role as signaling molecules of many metabolic networks in plants. Drought stress is known to disrupt carbohydrate metabolism and to decrease sucrose level in leaves, presumably due to an induced increase of invertase activity (Ruan et al., 2010; Gagné-Bourque et al., 2016), hampering the rate of sucrose export to the sink organs. This hypothesis was confirmed because sugar accumulated mostly in the susceptible Colosseo, and was decreased strongly in the tolerant Cappelli. The lower abundance of sugars and the higher amount of BCAAs observed is consistent with the severity of DS imposed (Fàbregas and Fernie, 2019).

The abundance of organic acids in the drought tolerant Cappelli was increased by DS supporting its greater capacity in regulating drought stress. The relative abundance of malate correlates more with environmental factors than with water availability, and may reflect the enhancement of a malate-oxaloacetate transport to prevent over-reduction of photosynthetic electron chain components, leading to the accumulation of malate in vacuoles (Scheibe, 2004). The ability of C3 plants to store malate was likely to reflect genetic variation in key pathways, being more evident in a susceptible cultivar.

Also, the content of acetate increased specifically in Cappelli at 21 DAT. Its role seems to be as an initial factor that promotes and connects fundamental metabolism, epigenetic regulation and hormone signaling, ultimately leading to the plant drought tolerance (Kim et al., 2017).

The metabolic profiling allowed for comprehensive analyses of a range of metabolites that have great value in both phenotyping and plant genotyping. In fact, a set of water stress related metabolic biomarkers for wheat was identified as differently accumulated in contrasting cultivars opening new perspectives to select superior performing lines in breeding programs, employing targeted metabolomic as a fast and low-cost diagnostic tool.

DATA AVAILABILITY STATEMENT

The data set generated for this study can be found in the Genomic sequences are available on NCBI repository. NMR data are available upon request to the authors, and will be soon available in MetaboLights (http://www.ebi.ac.uk/metabolights/).

AUTHOR CONTRIBUTIONS

MJ, VB, MG, and NM conceived and designed the experiments. VB performed genomic and gene expression experiments and analyzed the data. FV performed the NMR analyses and analyzed the data under the supervision of AK. NM and MJ coordinated the entire project and preparation of the manuscript. All authors contributed to the article and approved the submitted version.

FUNDING

This work was supported by Emilia Romagna Region under the ERDF project "SmartWheat" (POR FESR 2014–2020 program – Action 1.2.2. PG/2015/732409). NM and MG acknowledge contributions from the SIMBA project, funded by the European Union's Horizon 2020 Research and Innovation Program under grant agreement No. 818431 (SIMBA). This output reflects only the authors view, and the European Union cannot be held responsible for any use that may be made of the information contained therein.

ACKNOWLEDGMENTS

The authors wish to thank Consortium CINSA for the financial support and Dr. R. Baricchi and Prof. T. A. Pertinhez for the help with the NMR data.

SUPPLEMENTARY MATERIAL

The Supplementary Material for this article can be found online at: https://www.frontiersin.org/articles/10.3389/fpls.2020.00891/full#supplementary-material

REFERENCES

Akpınar, B. A., Lucas, S. J., and Budak, H. (2013). Genomics approaches for crop improvement against abiotic stress. *Sci. World J.* 2013:361921. doi: 10.1155/2013/361921

Ali, A., Khan, M., Sharif, R., Mujtaba, M., and Gao, S.-J. (2019). Sugarcane omics: an update on the current status of research and crop improvement. *Plants* 8:344. doi: 10.3390/plants8090344

Altschul, S. F., Gish, W., Miller, W., Myers, E. W., and Lipman, D. J. (1990). Basic local alignment search tool. *J. Mol. Biol.* 215, 403–410.

Angelovici, R., Lipka, A. E., Deason, N., Gonzalez-Jorge, S., Lin, H., Cepela, J., et al. (2013). Genome-wide analysis of branched-chain amino acid levels in *Arabidopsis* seeds. *Plant Cell* 25, 4827–4843. doi: 10.1105/tpc.113.119370

Aprile, A., Havlickova, L., Panna, R., Marč, C., Borrelli, G. M., Marone, D., et al. (2013). Different stress responsive strategies to drought and heat in two durum wheat cultivars with contrasting water use efficiency. *BMC Genomics* 14:821. doi: 10.1186/1471-2164-14-821

Araújo, W. L., Tohge, T., Ishizaki, K., Leaver, C. J., and Fernie, A. R. (2011). Protein degradation – an alternative respiratory substrate for stressed plants. *Trends Plant Sci.* 16, 489–498. doi: 10.1016/j.tplants.2011.05.008

Ashraf, M., Akram, N. A., Al-Qurainy, F., and Foolad, M. R. (2011). Drought tolerance. Roles of organic osmolytes, growth regulators, and mineral nutrients. *Adv. Agron.* 111, 249–296. doi: 10.1016/B978-0-12-387689-8.00002-3

Ashraf, M., and Foolad, M. R. (2007). Roles of glycine betaine and proline in improving plant abiotic stress resistance. *Environ. Exp. Bot.* 59, 206–216. doi: 10.1016/j.envexpbot.2005.12.006

Barrs, H. D., and Weatherley, P. E. (1962). A re-examination of the relative turgidity technique for estimating water cleficits in leaves. *Aust. J. Biol. Sci.* 15, 413–428.

Batista-Silva, W., Heinemann, B., Rugen, N., Nunes-Nesi, A., Araújo, W. L., Braun, H.-P., et al. (2019). The role of amino acid metabolism during abiotic stress release. *Plant Cell Environ.* 42, 1630–1644. doi: 10.1111/pce.13518

Benjamini, Y., and Hochberg, Y. (1995). Controlling the false discovery rate: a practical and powerful approach to multiple testing. *J. R. Stat. Soc. Ser. B Methodol.* 57, 289–300. doi: 10.1111/j.2517-6161.1995.tb02031.x

Bialczyk, J., and Lechowski, Z. (1992). Absorption of HCO3 - by roots and its effect on carbon metabolism of tomato. *J. Plant Nutr.* 15, 293–312. doi: 10.1080/01904169209364320

Binder, S. (2010). Branched-chain amino acid metabolism in *Arabidopsis thaliana*. *Arabidopsis Book* 8:e0137. doi: 10.1199/tab.0137

Binder, S., Knill, T., and Schuster, J. (2007). Branched-chain amino acid metabolism in higher plants. *Physiol. Plant.* 129, 68–78. doi: 10.1111/j.1399-3054.2006.00800.x

Bolot, S., Abrouk, M., Masood-Quraishi, U., Stein, N., Messing, J., Feuillet, C., et al. (2009). The 'inner circle' of the cereal genomes. *Curr. Opin. Plant Biol.* 12, 119–125. doi: 10.1016/j.pbi.2008.10.011

Borrelli, G. M., and Trono, D. (2016). Molecular approaches to genetically improve the accumulation of health-promoting secondary metabolites in staple crops—a case study: the lipoxygenase-B1 genes and regulation of the carotenoid content in pasta products. *Int. J. Mol. Sci.* 17:1177. doi: 10.3390/ijms17071177

Bowne, J. B., Erwin, T. A., Juttner, J., Schnurbusch, T., Langridge, P., Bacic, A., et al. (2012). Drought responses of leaf tissues from wheat cultivars of differing drought tolerance at the metabolite level. *Mol. Plant* 5, 418–429. doi: 10.1093/mp/ssr114

Chow, C.-N., Lee, T.-Y., Hung, Y.-C., Li, G.-Z., Tseng, K.-C., Liu, Y.-H., et al. (2019). PlantPAN3.0: a new and updated resource for reconstructing transcriptional regulatory networks from ChIP-seq experiments in plants. *Nucleic Acids Res.* 47, D1155–D1163. doi: 10.1093/nar/gky1081

Clavijo, B. J., Venturini, L., Schudoma, C., Accinelli, G. G., Kaithakottil, G., Wright, J., et al. (2017). An improved assembly and annotation of the allohexaploid wheat genome identifies complete families of agronomic genes and provides genomic evidence for chromosomal translocations. *Genome Res.* 27, 885–896. doi: 10.1101/gr.217117.116

Devos, K. M., Dubcovsky, J., Dvořák, J., Chinoy, C. N., and Gale, M. D. (1995). Structural evolution of wheat chromosomes 4A, 5A, and 7B and its impact on recombination. *TAG Theor. Appl. Genet. Theor. Angew. Genet.* 91, 282–288. doi: 10.1007/bf00220890

Diebold, R., Schuster, J., Däschner, K., and Binder, S. (2002). The branched-chain amino acid transaminase gene family in Arabidopsis encodes plastid and mitochondrial proteins. *Plant Physiol.* 129, 540–550. doi: 10.1104/pp.001602

Edgar, R. C. (2004). MUSCLE: multiple sequence alignment with high accuracy and high throughput. *Nucleic Acids Res.* 32, 1792–1797. doi: 10.1093/nar/gkh340

Fàbregas, N., and Fernie, A. R. (2019). The metabolic response to drought. *J. Exp. Bot.* 70, 1077–1085. doi: 10.1093/jxb/ery437

Farooq, M., Hussain, M., Wahid, A., and Siddique, K. H. M. (2012). "Drought stress in plants: an overview," in *Plant Responses to Drought Stress*, ed. R. Aroca (Berlin: Springer), 1–33. doi: 10.1007/978-3-642-32653-0_1

Fiume, E., Christou, P., Gianì, S., and Breviario, D. (2004). Introns are key regulatory elements of rice tubulin expression. *Planta* 218, 693–703.

Fukushima, A., Kuroha, T., Nagai, K., Hattori, Y., Kobayashi, M., Nishizawa, T., et al. (2020). Metabolite and phytohormone profiling illustrates metabolic

reprogramming as an escape strategy of deepwater rice during partially submerged stress. *Metabolites* 10:68. doi: 10.3390/metabo10020068

Gagné-Bourque, F., Bertrand, A., Claessens, A., Aliferis, K. A., and Jabaji, S. (2016). Alleviation of drought stress and metabolic changes in timothy (*Phleum pratense* L.) colonized with *Bacillus subtilis* B26. *Front. Plant Sci.* 7:584. doi: 10.3389/fpls.2016.00584

Gale, M. D., and Devos, K. M. (1998). Comparative genetics in the grasses. *Proc. Natl. Acad. Sci. U.S.A.* 95, 1971–1974.

Galili, G., Amir, R., and Fernie, A. R. (2016). The regulation of essential amino acid synthesis and accumulation in plants. *Annu. Rev. Plant Biol.* 67, 153–178.

Gascuel, O. (1997). BIONJ: an improved version of the NJ algorithm based on a simple model of sequence data. *Mol. Biol. Evol.* 14, 685–695. doi: 10.1093/oxfordjournals.molbev.a025808

Gou, W., Tian, L., Ruan, Z., Zheng, P., Chen, F., Zhang, L., et al. (2015). Accumulation of choline and glycinebetaine and drought stress tolerance induced in maize (*Zea mays*) by three plant growth promoting rhizobacteria (PGPR) strains. *Pak. J. Bot.* 47, 581–586.

Hayat, S., Hayat, Q., Alyemeni, M. N., Wani, A. S., Pichtel, J., and Ahmad, A. (2012). Role of proline under changing environments. *Plant Signal. Behav.* 7, 1456–1466. doi: 10.4161/psb.21949

Hildebrandt, T. M. (2018). Synthesis versus degradation: directions of amino acid metabolism during Arabidopsis abiotic stress response. *Plant Mol. Biol.* 98, 121–135.

Horton, P., Park, K.-J., Obayashi, T., Fujita, N., Harada, H., Adams-Collier, C. J., et al. (2007). WoLF PSORT: protein localization predictor. *Nucleic Acids Res.* 35, W585–W587. doi: 10.1093/nar/gkm259

Huang, T., and Jander, G. (2017). Abscisic acid-regulated protein degradation causes osmotic stress-induced accumulation of branched-chain amino acids in *Arabidopsis thaliana*. *Planta* 246, 737–747.

Huang, Y., Adeleye, A. S., Zhao, L., Minakova, A. S., Anumol, T., and Keller, A. A. (2019). Antioxidant response of cucumber (*Cucumis sativus*) exposed to nano copper pesticide: quantitative determination via LC-MS/MS. *Food Chem.* 270, 47–52. doi: 10.1016/j.foodchem.2018.07.069

Huang, Y., Li, W., Minakova, A. S., Anumol, T., and Keller, A. A. (2018). Quantitative analysis of changes in amino acids levels for cucumber (*Cucumis sativus*) exposed to nano copper. *Nanoimpact* 12, 9–17. doi: 10.1016/j.impact.2018.08.008

IWGSC (2014). A chromosome-based draft sequence of the hexaploid bread wheat (*Triticum aestivum*) genome. *Science* 345:1251788. doi: 10.1126/science.1251788

IWGSC (2019). *IWGSC RefSeq v1.0. Int. Wheat Genome Seq. Consort.* Available online at: https://www.wheatgenome.org/News/Latest-news/All-IWGSC-data-related-to-the-reference-sequence-of-bread-wheat-IWGSC-RefSeq-v1.0-publicly-available-at-URGI (accessed July 16, 2019).

Jafari, M., and Ansari-Pour, N. (2019). Why, when and how to adjust your P values? *Cell J. Yakhteh* 20, 604–607. doi: 10.22074/cellj.2019.5992

Joshi, V., Joung, J.-G., Fei, Z., and Jander, G. (2010). Interdependence of threonine, methionine and isoleucine metabolism in plants: accumulation and transcriptional regulation under abiotic stress. *Amino Acids* 39, 933–947.

Kang, Z., Babar, M. A., Khan, N., Guo, J., Khan, J., Islam, S., et al. (2019). Comparative metabolomic profiling in the roots and leaves in contrasting genotypes reveals complex mechanisms involved in post-anthesis drought tolerance in wheat. *PLoS One* 14:e0213502. doi: 10.1371/journal.pone.0213502

Karami, A., Shahbazi, M., Niknam, V., Shobbar, Z. S., Tafreshi, R. S., Abedini, R., et al. (2013). Expression analysis of dehydrin multigene family across tolerant and susceptible barley (*Hordeum vulgare* L.) genotypes in response to terminal drought stress. *Acta Physiol. Plant.* 35, 2289–2297.

Khan, N. A., Khan, M. I. R., Ferrante, A., and Poor, P. (2017). Editorial: ethylene: a key regulatory molecule in plants. *Front. Plant Sci.* 8:1782. doi: 10.3389/fpls.2017.01782

Kim, H. K., Choi, Y. H., and Verpoorte, R. (2010). NMR-based metabolomic analysis of plants. *Nat. Protoc.* 5, 536–549. doi: 10.1038/nprot.2009.237

Kim, J.-M., To, T. K., Matsui, A., Tanoi, K., Kobayashi, N. I., Matsuda, F., et al. (2017). Acetate-mediated novel survival strategy against drought in plants. *Nat. Plants* 3:17097. doi: 10.1038/nplants.2017.97

Kishor, P. B. K., Sangam, S., Amrutha, R. N., Laxmi, P. S., and Naidu, K. R. (2005). Regulation of proline biosynthesis, degradation, uptake and transport in higher plants: its implications in plant growth and abiotic stress tolerance. *Curr. Sci.* 88, 424–438.

Kochevenko, A., Araújo, W. L., Maloney, G. S., Tieman, D. M., Do, P. T., Taylor, M. G., et al. (2012). Catabolism of branched chain amino acids supports respiration but not volatile synthesis in tomato fruits. *Mol. Plant* 5, 366–375. doi: 10.1093/mp/ssr108

Kulkarni, M., Soolanayakanahally, R., Ogawa, S., Uga, Y., Selvaraj, M. G., and Kagale, S. (2017). Drought response in wheat: key genes and regulatory mechanisms controlling root system architecture and transpiration efficiency. *Front. Chem.* 5:106. doi: 10.3389/fchem.2017.00106

Langridge, R., Christian-Smith, J., and Lohse, K. A. (2006). Access and resilience: analyzing the construction of social resilience to the threat of water scarcity. *Ecol. Soc.* 11:18.

Lanzinger, A., Frank, T., Reichenberger, G., Herz, M., and Engel, K.-H. (2015). Metabolite profiling of barley grain subjected to induced drought stress: responses of free amino acids in differently adapted cultivars. *J. Agric. Food Chem.* 63, 4252–4261. doi: 10.1021/acs.jafc.5b01114

Liu, B., Asseng, S., Müller, C., Ewert, F., Elliott, J., Lobell, D. B., et al. (2016). Similar estimates of temperature impacts on global wheat yield by three independent methods. *Nat. Clim. Change* 6, 1130–1136. doi: 10.1038/nclimate3115

Liu, M., Wang, Z., Xiao, H.-M., and Yang, Y. (2018). Characterization of TaDREB1 in wheat genotypes with different seed germination under osmotic stress. *Hereditas* 155:26.

Livak, K. J., and Schmittgen, T. D. (2001). Analysis of relative gene expression data using real-time quantitative PCR and the 2-ΔΔCT method. *Methods* 25, 402–408. doi: 10.1006/meth.2001.1262

Mahmood, T., Khalid, S., Abdullah, M., Ahmed, Z., Shah, M. K. N., Ghafoor, A., et al. (2020). Insights into drought stress signaling in plants and the molecular genetic basis of cotton drought tolerance. *Cells* 9:105. doi: 10.3390/cells9010105

Malatrasi, M., Corradi, M., Svensson, J. T., Close, T. J., Gulli, M., and Marmiroli, N. (2006). A branched-chain amino acid aminotransferase gene isolated from *Hordeum vulgare* is differentially regulated by drought stress. *Theor. Appl. Genet.* 113, 965–976.

Maloney, G. S., Kochevenko, A., Tieman, D. M., Tohge, T., Krieger, U., Zamir, D., et al. (2010). Characterization of the branched-chain amino acid aminotransferase enzyme family in tomato1[W][OA]. *Plant Physiol.* 153, 925–936. doi: 10.1104/pp.110.154922

Marček, T., Hamow, Á., Végh, B., Janda, T., and Darko, E. (2019). Metabolic response to drought in six winter wheat genotypes. *PLoS One* 14:e0212411. doi: 10.1371/journal.pone.0212411

Mata, A. T., Jorge, T. F., Pires, M. V., and Antonio, C. (2016). "Drought stress tolerance in plants: insights from metabolomics," in *Drought Stress Tolerance in Plants, Vol 2: Molecular and Genetic Perspectives*, eds M. A. Hossain, S. H. Wani, S. Bhattacharjee, D. J. Burritt, and L.-S. P. Tran (Cham: Springer International Publishing), 187–216. doi: 10.1007/978-3-319-32423-4_7

Mayer, K. F. X., Martis, M., Hedley, P. E., Šimková, H., Liu, H., Morris, J. A., et al. (2011). Unlocking the barley genome by chromosomal and comparative genomics[W][OA]. *Plant Cell* 23, 1249–1263. doi: 10.1105/tpc.110.082537

Michaletti, A., Naghavi, M. R., Toorchi, M., Zolla, L., and Rinalducci, S. (2018). Metabolomics and proteomics reveal drought-stress responses of leaf tissues from spring-wheat. *Sci. Rep.* 8:5710.

Obata, T., and Fernie, A. R. (2012). The use of metabolomics to dissect plant responses to abiotic stresses. *Cell. Mol. Life Sci.* 69, 3225–3243.

Piasecka, A., Kachlicki, P., and Stobiecki, M. (2019). Analytical methods for detection of plant metabolomes changes in response to biotic and abiotic stresses. *Int. J. Mol. Sci.* 20:379. doi: 10.3390/ijms20020379

Pires, M. V., Júnior, A. A. P., Medeiros, D. B., Daloso, D. M., Pham, P. A., Barros, K. A., et al. (2016). The influence of alternative pathways of respiration that utilize branched-chain amino acids following water shortage in *Arabidopsis*. *Plant Cell Environ.* 39, 1304–1319. doi: 10.1111/pce.12682

Rahman, M. A., Akond, M., Babar, M. A., Beecher, C., Erickson, J., Thomason, K., et al. (2017). LC-HRMS based non-targeted metabolomic profiling of wheat (*Triticum aestivum* L.) under post-anthesis drought stress. *Am. J. Plant Sci.* 8, 3024–3061. doi: 10.4236/ajps.2017.812205

Rampino, P., Pataleo, S., Gerardi, C., Mita, G., and Perrotta, C. (2006). Drought stress response in wheat: physiological and molecular analysis of resistant and sensitive genotypes. *Plant Cell Environ.* 29, 2143–2152. doi: 10.1111/j.1365-3040.2006.01588.x

Rocchi, V., Janni, M., Bellincampi, D., Giardina, T., and D'Ovidio, R. (2012). Intron retention regulates the expression of pectin methyl esterase inhibitor (Pmei) genes during wheat growth and development: isolation and functional characterisation of wheat Pmei genes. *Plant Biol.* 14, 365–373. doi: 10.1111/j.1438-8677.2011.00508.x

Ruan, Y.-L., Jin, Y., Yang, Y.-J., Li, G.-J., and Boyer, J. S. (2010). Sugar input, metabolism, and signaling mediated by invertase: roles in development, yield potential, and response to drought and heat. *Mol. Plant* 3, 942–955. doi: 10.1093/mp/ssq044

Saitou, N., and Nei, M. (1987). The neighbor-joining method: a new method for reconstructing phylogenetic trees. *Mol. Biol. Evol.* 4, 406–425. doi: 10.1093/oxfordjournals.molbev.a040454

Sallam, A., Alqudah, A. M., Dawood, M. F. A., Baenziger, P. S., and Börner, A. (2019). Drought stress tolerance in wheat and barley: advances in physiology, breeding and genetics research. *Int. J. Mol. Sci.* 20:3137. doi: 10.3390/ijms20133137

Sassi, S., Aydi, S., Hessini, K., González, E. M., Arrese-Igor, C., and Abdelly, C. (2010). Long-term mannitol-induced osmotic stress leads to stomatal closure, carbohydrate accumulation and changes in leaf elasticity in *Phaseolus vulgaris* leaves. *Afr. J. Biotechnol.* 9, 6061–6069. doi: 10.5897/AJB09.1783

Scarpeci, T. E., Frea, V. S., Zanor, M. I., and Valle, E. M. (2016). Overexpression of *AtERF019* delays plant growth and senescence and improves drought tolerance in Arabidopsis. *J. Exp. Bot.* 68, 673–685. doi: 10.1093/jxb/erw429

Scheben, A., Yuan, Y., and Edwards, D. (2016). Advances in genomics for adapting crops to climate change. *Curr. Plant Biol.* 6, 2–10. doi: 10.1016/j.cpb.2016.09.001

Scheibe, R. (2004). Malate valves to balance cellular energy supply. *Physiol. Plant.* 120, 21–26. doi: 10.1111/j.0031-9317.2004.0222.x

Semenov, M. A., Stratonovitch, P., Alghabari, F., and Gooding, M. J. (2014). Adapting wheat in Europe for climate change. *J. Cereal Sci.* 59, 245–256. doi: 10.1016/j.jcs.2014.01.006

Silvente, S., Sobolev, A. P., and Lara, M. (2012). Metabolite adjustments in drought tolerant and sensitive soybean genotypes in response to water stress. *PLoS One* 7:e38554. doi: 10.1371/journal.pone.0038554

Solovyev, V., Kosarev, P., Seledsov, I., and Vorobyev, D. (2006). Automatic annotation of eukaryotic genes, pseudogenes and promoters. *Genome Biol.* 7, S10.1–S10.12. doi: 10.1186/gb-2006-7-s1-s10

Tamura, K., Peterson, D., Peterson, N., Stecher, G., Nei, M., and Kumar, S. (2011). MEGA5: molecular evolutionary genetics analysis using maximum likelihood, evolutionary distance, and maximum parsimony methods. *Mol. Biol. Evol.* 28, 2731–2739. doi: 10.1093/molbev/msr121

Tamura, K., Stecher, G., Peterson, D., Filipski, A., and Kumar, S. (2013). MEGA6: molecular evolutionary genetics analysis version 6.0. *Mol. Biol. Evol.* 30, 2725–2729. doi: 10.1093/molbev/mst197

Templer, S. E., Ammon, A., Pscheidt, D., Ciobotea, O., Schuy, C., McCollum, C., et al. (2017). Metabolite profiling of barley flag leaves under drought and combined heat and drought stress reveals metabolic QTLs for metabolites associated with antioxidant defense. *J. Exp. Bot.* 68, 1697–1713. doi: 10.1093/jxb/erx038

Todaka, D., Zhao, Y., Yoshida, T., Kudo, M., Kidokoro, S., Mizoi, J., et al. (2017). Temporal and spatial changes in gene expression, metabolite accumulation and phytohormone content in rice seedlings grown under drought stress conditions. *Plant J.* 90, 61–78. doi: 10.1111/tpj.13468

Trujillo-Moya, C., George, J.-P., Fluch, S., Geburek, T., Grabner, M., Karanitsch-Ackerl, S., et al. (2018). Drought sensitivity of Norway spruce at the species' warmest fringe: quantitative and molecular analysis reveals high genetic variation among and within provenances. *G3* 8, 1225–1245. doi: 10.1534/g3.117.300524

Tuberosa, R., and Pozniak, C. (2014). Durum wheat genomics comes of age: introduction to the special issue on durum wheat genomics. *Mol. Breed.* 34, 1527–1530. doi: 10.1007/s11032-014-0188-y

Tuberosa, R., and Salvi, S. (2006). Genomics-based approaches to improve drought tolerance of crops. *Trends Plant Sci.* 11, 405–412. doi: 10.1016/j.tplants.2006.06.003

Ullah, N., Yüce, M., Neslihan, Öztürk Gökçe, Z., and Budak, H. (2017). Comparative metabolite profiling of drought stress in roots and leaves of seven Triticeae species. *BMC Genomics* 18:969. doi: 10.1186/s12864-017-4321-2

Urano, K., Maruyama, K., Ogata, Y., Morishita, Y., Takeda, M., Sakurai, N., et al. (2009). Characterization of the ABA-regulated global responses to dehydration in Arabidopsis by metabolomics. *Plant J.* 57, 1065–1078. doi: 10.1111/j.1365-313X.2008.03748.x

Vital, C. E., Giordano, A., de Almeida Soares, E., Rhys Williams, T. C., Mesquita, R. O., Vidigal, P. M. P., et al. (2017). An integrative overview of the molecular and physiological responses of sugarcane under drought conditions. *Plant Mol. Biol.* 94, 577–594. doi: 10.1007/s11103-017-0611-y

Webb, E., Broderick, P., Lubbe, S., Chandler, I., Tomlinson, I., and Houlston, R. S. (2009). A genome-wide scan of 10 000 gene-centric variants and colorectal cancer risk. *Eur. J. Hum. Genet.* 17, 1507–1514. doi: 10.1038/ejhg.2009.92

Witt, S., Galicia, L., Lisec, J., Cairns, J., Tiessen, A., Araus, J. L., et al. (2012). Metabolic and phenotypic responses of greenhouse-grown maize hybrids to experimentally controlled drought stress. *Mol. Plant* 5, 401–417. doi: 10.1093/mp/ssr102

Xia, Y., Li, R., Bai, G., Siddique, K. H. M., Varshney, R. K., Baum, M., et al. (2017). Genetic variations of HvP5CS1 and their association with drought tolerance related traits in barley (*Hordeum vulgare* L.). *Sci. Rep.* 7:7870.

Xie, Z., Nolan, T. M., Jiang, H., and Yin, Y. (2019). AP2/ERF transcription factor regulatory networks in hormone and abiotic stress responses in *Arabidopsis*. *Front. Plant Sci.* 10:228. doi: 10.3389/fpls.2019.00228

Xu, X., Sharma, R., Tondelli, A., Russell, J., Comadran, J., Schnaithmann, F., et al. (2018). Genome-wide association analysis of grain yield-associated traits in a pan-European barley cultivar collection. *Plant Genome* 11:170073. doi: 10.3835/plantgenome2017.08.0073

Yousfi, S., Márquez, A. J., Betti, M., Araus, J. L., and Serret, M. D. (2016). Gene expression and physiological responses to salinity and water stress of contrasting durum wheat genotypes. *J. Integr. Plant Biol.* 58, 48–66. doi: 10.1111/jipb.12359

Zhang, Z., Zhang, H., Quan, R., Wang, X.-C., and Huang, R. (2009). Transcriptional regulation of the ethylene response factor LeERF2 in the expression of ethylene biosynthesis genes controls ethylene production in tomato and tobacco. *Plant Physiol.* 150, 365–377. doi: 10.1104/pp.109.135830

Zhao, L., Huang, Y., Paglia, K., Vaniya, A., Wancewicz, B., and Keller, A. A. (2018). Metabolomics reveals the molecular mechanisms of copper induced cucumber leaf (*Cucumis sativus*) senescence. *Environ. Sci. Technol.* 52, 7092–7100. doi: 10.1021/acs.est.8b00742

Zuckerkandl, E., and Pauling, L. (1965). "Evolutionary divergence and convergence in proteins," in *Evolving Genes and Proteins*, eds V. Bryson and H. J. Vogel (Cambridge, MA: Academic Press), 97–166. doi: 10.1016/B978-1-4832-2734-4.50017-6

Conflict of Interest: The authors declare that the research was conducted in the absence of any commercial or financial relationships that could be construed as a potential conflict of interest.

Copyright © 2020 Buffagni, Vurro, Janni, Gullì, Keller and Marmiroli. This is an open-access article distributed under the terms of the Creative Commons Attribution License (CC BY). The use, distribution or reproduction in other forums is permitted, provided the original author(s) and the copyright owner(s) are credited and that the original publication in this journal is cited, in accordance with accepted academic practice. No use, distribution or reproduction is permitted which does not comply with these terms.

frontiers in Plant Science

ORIGINAL RESEARCH
published: 10 July 2020
doi: 10.3389/fpls.2020.00987

The Neighboring Subunit Is Engaged to Stabilize the Substrate in the Active Site of Plant Arginases

Bartosz Sekula *

Synchrotron Radiation Research Section of Macromolecular Crystallography Laboratory, National Cancer Institute, Argonne, IL, United States

OPEN ACCESS

Edited by:
Giuseppe Forlani, University of Ferrara, Italy

Reviewed by:
Krzysztof Brzezinski, University of Białystok, Poland
Paul F. Morris, Bowling Green State University, United States

***Correspondence:**
Bartosz Sekula
bartosz.sekula@nih.gov; sekula.bartosz@gmail.com

Specialty section:
This article was submitted to Plant Metabolism and Chemodiversity, a section of the journal Frontiers in Plant Science

Received: *12 February 2020*
Accepted: *17 June 2020*
Published: *10 July 2020*

Citation:
Sekula B (2020) The Neighboring Subunit Is Engaged to Stabilize the Substrate in the Active Site of Plant Arginases. Front. Plant Sci. 11:987. doi: 10.3389/fpls.2020.00987

Arginine acts as a precursor of polyamines in plants in two known pathways, agmatine and ornithine routes. It is decarboxylated to agmatine by arginine decarboxylase, and then transformed to putrescine by the consecutive action of agmatine iminohydrolase and N-carbamoylputrescine amidohydrolase. Alternatively, it can be hydrolyzed to ornithine by arginase and then decarboxylated by ornithine decarboxylase to putrescine. Some plants lack a functional ornithine pathway, but all have one or two arginases that can have dual cellular localization, in mitochondria and plastids. It was recently shown that arginases from *Arabidopsis thaliana* and soybean act also as agmatinases, thus they can produce putrescine directly from agmatine. Therefore, arginase (together with arginine decarboxylase) can complement putrescine production in plastids, providing a third polyamine biosynthesis pathway in plants. Phylogenetic analysis suggests that arginases, highly conserved in the plant kingdom, create the only group of enzymes recognized in the family of ureohydrolases in plants. Arginases are metalloenzymes with binuclear manganese cluster in the active site. In this work, two arginases from *A. thaliana* and *Medicago truncatula* are structurally characterized and their binding properties are discussed. Crystal structures with bound ornithine show that plant hexameric arginases engage a long loop from the neighboring subunit to stabilize α-amino and carboxyl groups of the ligand. This unique ligand binding mode is unobserved in arginases from other domains of life. Structural analysis shows that substrate binding by residues from two neighboring subunits might also characterize some prokaryotic agmatinases. This feature of plant arginases is most likely the determinant of their ability to recognize not only arginine but also agmatine as their substrates, thus, to act as arginase and agmatinase.

Keywords: polyamine biosynthesis, urea cycle, agmatinase, ureohydrolases, arginine amidinohydrolase

INTRODUCTION

Arginine has the highest nitrogen to carbon ratio of all proteinogenic amino acids which makes it an effective storage form for organic nitrogen in plants; it may be responsible for up to half of the stored nitrogen in plant seeds (Winter et al., 2015). Therefore, arginine plays a critical role in nitrogen metabolism and recycling in plants (Slocum, 2005). Plants, unlike animals, rather recycle nitrogen in the form of urea instead of excreting it (Sirko and Brodzik, 2000). Except for being a building block for proteins, arginine (or its derivatives) is a potential source of nitric oxide (Flores et al., 2008). Moreover, under high nitrogen supply, arginine may secure proline production through degradation to ornithine (Forlani et al., 2015). Arginine can also be converted to putrescine, γ-aminobutyric acid, or nicotine, playing a key role in development and stress management in plants (Siddappa et al., 2018). Therefore, arginine catabolism is used not only to mobilize nitrogen reserves but also it is used as a part of plant defensive mechanism (Siddappa et al., 2018).

As an essential part of polyamine biosynthesis in plants, arginine can be used as a precursor of putrescine in several ways (Michael, 2016; Patel et al., 2017). In the first route, arginine undergoes decarboxylation by arginine decarboxylase to agmatine, which is then transformed to putrescine in two steps. The first reaction is catalyzed by agmatine iminohydrolase, the enzyme built of two subunits characterized by an αββαβ five-bladed propeller fold (Sekula and Dauter, 2019). The second step is carried out by N-carbamoylputrescine amidohydrolase, which in plants forms characteristic octamers with four pairs of subunits arranged helically (Sekula et al., 2016). An alternative route for putrescine production is the ornithine pathway. In this route, ornithine is obtained from arginine by the action of arginase (arginine amidinohydrolase, ARGAH). Then, putrescine is produced by ornithine decarboxylase. However, ornithine decarboxylase is missing in some plants (Hanfrey et al., 2001), therefore, a functional ornithine pathway is also absent in these species. The studies on ARGAH from *Arabidopsis thaliana* and soybean have also shown that concerted action of ARGAH and one of the arginine decarboxylases may complement the putrescine biosynthesis as the third route (Patel et al., 2017). Therefore, arginine is initially decarboxylated to agmatine and then, through the hydrolytic action of ARGAH on agmatine (agmatinase activity), putrescine is produced. These findings overturn earlier results (Chen et al., 2004) which indicated that tomato ARGAH (evolutionary closer related to *A. thaliana* ARGAH than soybean ARGAH), does not convert agmatine at high substrate concentration. ARGAHs in the plant kingdom are highly conserved and it was suggested that dual arginase and agmatinase activity of ARGAHs is common in plants (Patel et al., 2017). Moreover, ARGAH has high *Km* for arginine (Patel et al., 2017).Therefore, in plant tissues (or some cell compartments, like plastids), with low arginine concentration, arginine would be preferentially converted to agmatine by arginine decarboxylase, thus enabling the third putrescine biosynthesis pathway through agmatinase activity of ARGAH.

A. thaliana has two ARGAH isoforms encoded by genes *ARGAH1* (At4g08900) and *ARGAH2* (At4g08870), which most likely appeared by gene duplication (Brownfield et al., 2008). *Arabidopsis* ARGAHs present dual localization; they are localized in the mitochondrial matrix (Flores et al., 2008), but they can also be targeted to plastids (Patel et al., 2017). Only *ARGAH1* is actively transcribed in pollen (Brownfield et al., 2008), which likely secures the high demand of proline in pollen. In stress conditions (drought, oxidative stress, wounding) and upon methyl jasmonate treatment, *ARGAH2* expression is increased in a concerted manner with arginine decarboxylase 2 (Patel et al., 2017). Similarly, expression and activity of only one ARGAH isoform are alleviated as a response to wounding and methyl jasmonate in tomato leaves (Chen et al., 2004). ARGAH activity during germination is highly increased, which clearly shows that in plant seedlings arginine is used to recover nitrogen and carbon (Tiburcio et al., 1990). Thus, in germinating seeds (where most of the nitrogen is in the form of arginine), increased arginase activity (increased conversion of arginine to ornithine) is involved in the recovery of nitrogen and carbon from arginine to translocate it to growing points.

Similarly to other eukaryotic (Di Costanzo et al., 2010) and prokaryotic (Bewley et al., 1999) orthologues, plant ARGAHs, are binuclear manganese metalloenzymes. Together with agmatinase, formiminoglutamase, and proclavaminate aminohydrolase, ARGAHs are grouped with the Ureohydrolase Superfamily. This family of enzymes has a highly conserved fold (Dowling et al., 2008) with α/β/α sandwich. It also shares the mechanism of guanidine moiety hydrolysis (Christianson and Cox, 1999). However, it was suggested that plant arginases are unique in that they are phylogenetically more similar to the bacterial agmatinases, than to bacterial or mammalian arginases (Patel et al., 2017). A few ARGAHs have been described in plants (Boutin, 1982; Desai, 1983; Martin-Falquina and Legaz, 1984; Kang and Cho, 1990; Hwang et al., 2001; Dabir et al., 2005), however, the structure of any plant ureohydrolase is still unknown.

In this work, ARGAHs from two model plant species, *A. thaliana* (*At*ARGAH1) and *Medicago truncatula* (*Mt*ARGAH), are structurally characterized by X-ray crystallography and small-angle X-ray scattering (SAXS). Based on the crystal structures of *At*ARGAH1 and *Mt*ARGAH complexes with ornithine combined with the analysis of sequence conservation of the key residues of plant ARGAHs their dual arginase/agmatinase function in plants is discussed.

MATERIALS AND METHODS

Cloning, Overexpression, and Purification of *Mt*ARGAH and *At*ARGAH1

Complementary DNA (cDNA) of *M. truncatula* and *A. thaliana* was obtained with the use of SuperScript II reverse transcriptase (Life Technologies), as well as oligo dT (15 and 18) primers and total RNA isolated from leaves with an RNeasy Plant Mini Kit (Qiagen). The open reading frames (ORF) of *At*ARGAH1 (Ordered Locus Name: At4g08900) and *Mt*ARGAH (Ordered Locus Name: MTR_4g024960) were isolated by polymerase

chain reaction. Primers were designed to clone full ORF of *Mt*ARGAH and *At*ARGAH1 starting from codon 25. The following primers were used: TACTTCCAATCCAATGCCTCT GCTTCTTCAATCGAGAAAGGGCAAA (*At*ARGAH1-forward), TTATCCACTTCCAATGTTATCATTTCGAGATTT TCGCAGCTAATTCTCTAA (*At*ARGAH1-reverse), TACT TCCAATCCAATGCCATGTCGACTATAGCACGCAGAGG (*Mt*ARGAH-forward), TTATCCACTTCCAATGTTATCATTT TGACATCTTTGCAGCCAATTCTCT (*Mt*ARGAH-reverse).

A ligase-independent cloning (Kim et al., 2011) protocol was applied to incorporate *Mt*ARGAH and *At*ARGAH1 genes into a pMCSG68 vector (Midwest Center for Structural Genomics). The vectors with *At*ARGAH1 and *Mt*ARGAH were used to transform BL21 Gold *Escherichia coli* competent cells (Agilent Technologies). The correctness of the cloned sequences was checked by DNA sequencing of the isolated plasmids from the overnight culture in LB medium with 150 μg/ml of ampicillin. The pMCSG68 vector is used to express the construct with an N-terminal His_6-tag followed by the tobacco etch virus (TEV) protease cleavage site.

Overexpression of the protein started with inoculation of 1 L of fresh lysogeny broth medium (with 150 μg/ml of ampicillin) with 15 ml of overnight culture. Then the medium was shaken at 37°C until OD_{600} reached value 1.0. Afterward, the culture was cooled to 10°C for 1 h and 0.5 mM of isopropyl-β-D-thiogalactopyranoside was added. After 16 h of overexpression at 18°C, the culture was cooled to 4°C. The cells were pelleted in the centrifuge (3,500×*g* for 20 min). The cell pellets were resuspended in 35 ml of the binding buffer (50 mM HEPES pH 7.8; 500 mM NaCl; 20 mM imidazole; 1 mM tris(2-carboxyethyl)phosphine, TCEP) and frozen at −80°C. Thawed samples were placed in an ice/water bath and subjected to sonication (60 four-second sonication bursts in 26-second intervals). Cell debris was pelleted in a centrifuge (25,000×*g* for 30 min at 4°C). The first step of protein purification was performed on HisTrap HP resin (GE Healthcare). The supernatant was transferred to the columns packed with 5 ml of resin which were coupled to Vac-Man (Promega). Then, the resin with bound *At*ARGAH1 and *Mt*ARGAH was washed five times with 40 ml of the binding buffer. *At*ARGAH1 or *Mt*ARGAH were eluted with 20 ml of elution buffer (50 mM HEPES pH 7.8, 500 mM NaCl, 400 mM imidazole, 1 mM TCEP). Cleavage of the His_6-tag from *At*ARGAH1 and *Mt*ARGAH by His_6-tagged TEV protease (final concentration of 0.1 mg/ml) was performed in parallel to overnight dialysis at 4°C against the buffer: 50 mM HEPES pH 7.8, 500 mM NaCl, 1 mM TCEP. Cleaved His_6-tag and His_6-tagged TEV protease were separated from *At*ARGAH1 and *Mt*ARGAH on HisTrap HP resin. Size-exclusion chromatography on a HiLoad Superdex 200 16/60 column (GE Healthcare) coupled to the AKTA FPLC system (Amersham Biosciences) was the last step of purification. The running buffer was as follows: 50 mM HEPES pH 7.8, 100 mM KCl, 50 mM NaCl, 1 mM TCEP.

Crystallization and Data Collection

*At*ARGAH1 and *Mt*ARGAH were concentrated with Amicon concentrators (Millipore) to the final concentration of approximately 18 and 6 mg/ml, respectively. Concentration was determined by the absorbance measurement at 280 nm with the following extinction coefficients: 18,910 $M^{-1} \times cm^{-1}$ (*Mt*ARGAH) and 14,440 $M^{-1} \times cm^{-1}$ (*At*ARGAH1). Proteins were crystallized by the hanging drop method; the best crystals were obtained with streak seeding. *Mt*ARGAH was crystallized in conditions optimized from initial screening in Morpheus Screen (Molecular Dimensions): 55 mM $CaCl_2$, 55 mM $MgCl_2$, 80 mM HEPES/MOPS buffer at pH 7.5, 30% ethylene glycol; 15% polyethylene glycol 8000. *At*ARGAH1-ORN was crystallized in conditions optimized from initial screening in BCS screen (Molecular Dimensions): 50 mM L-arginine, 50 mM L-glutamic acid, 22% PEG Smear Broad, 5% glycerol. The complex of *Mt*ARGAH-ORN was obtained by cocrystallization with 50 mM L-arginine. Crystal of *At*ARGAH1-ORN was cryoprotected with glycerol.

The diffraction data were collected at the SER-CAT 22-ID and SBC 19-ID beamlines at the Advanced Photon Source (APS), Argonne National Laboratory, USA. The diffraction data were processed with *XDS* (Kabsch, 2010) and *HKL-3000* (Otwinowski and Minor, 1997); for details see **Table 1**.

Structure Determination and Refinement

The structure of unliganded *Mt*ARGAH was solved in *Phaser* (McCoy et al., 2007). The structure of putative agmatinase from *C. difficile* (PDB ID: 3LHL) was used as the search model. The initial solution was rebuilt in *PHENIX AutoBuild* (Terwilliger et al., 2008). Then, the structure underwent the subsequent steps of manual and automatic refinement with *Coot* (Emsley et al., 2010) and *REFMAC* (Murshudov et al., 2011). Unliganded *Mt*ARGAH was used as the search model for the determination of *Mt*ARGAH-ORN and *At*ARGAH1-ORN structures. TLS parameters (Winn et al., 2001; Winn et al., 2003) were used in the later stages of the structure refinement. Standard CCP4 libraries (Winn et al., 2011) were used for the refinement of ligands in *REFMAC* or *PHENNIX* (Adams et al., 2010). Polder omit maps (Liebschner et al., 2017) were used to validate the position of bound ornithine in *Mt*ARGAH-ORN and *At*ARGAH1-ORN (**Figures 5A, B**). The quality of refined structures was controlled by R_{work}, R_{free} (Brunger, 1992) and geometric parameters. Evaluation of the final models was done in *MolProbity* (Chen et al., 2010). CheckMyMetal (Zheng et al., 2017) was used for the evaluation of the geometry of bound Mn^{2+} ions. The final refinement statistics are given in **Table 1**.

Small-Angle X-Ray Scattering (SAXS) Measurements

SAXS data were collected from *At*ARGAH1 (5.5 mg/ml) and *Mt*ARGAH (5 mg/ml) at the BioCAT 18-ID beamline (Fischetti et al., 2004) at APS with the in-line size exclusion chromatography setup and Pilatus3 1M detector (Dectris). Prior to the SAXS data collection, the sample was applied to the WTC-015S5 column (Wyatt Technologies) coupled to the Infinity II HPLC (Agilent Technologies) system. Directly after the separation on the column samples were analyzed with the Agilent UV detector, a Multi-Angle Light Scattering (MALS) detector and a Dynamic Light Scattering (DLS) detector (DAWN Helios

TABLE 1 | Data collection and refinement statistics.

Structure:	*Mt*ARGAH	*Mt*ARGAH-ORN	*At*ARGAH1-ORN
Data collection			
Beamline	19-ID	22-ID	22-ID
Wavelength (Å)	0.979	1.00	1.00
Temperature (K)	100	100	100
Space group	$P2_1$	$P2_1$	$I4_1$
Unit cell parameters			
a b c (Å)	79.3 142.9 90.0	83.7 166.1 150.9	267.3 267.3 262.9
β (°)	115.9	94.5	90.0
Oscillation range (°)	0.3	0.5	0.25
Resolution (Å)	44.55–1.93 (2.04–1.93)	50–2.12 (2.25–2.12)	30–2.25 (2.33–2.25)
Reflections collected/unique	457,132/130,001	971,248/231,608	1,434,604/429,624
Completeness (%)	95.7 (93.6)	99.7 (98.9)	99.0 (99.9)
Multiplicity	3.5 (3.4)	4.2 (4.0)	3.3 (3.4)
R_{merge} (%)	7.5 (62.6)	5.6 (71.4)	6.4 (48.3)
$<I/\sigma(I)>$	10.9 (2.1)	15.5 (1.9)	17.1 (2.5)
Refinement			
R_{free} reflections	1,040	1,019	2,236
No. of atoms (non-H)			
protein	14,733	29,581	58,189
ligands	12	87	368
solvent	547	1,331	4,951
R_{work}/R_{free} (%)	18.2/21.8	16.0/19.9	15.9/19.7
Mean ADP[a] (Å^2)	36.0	51.0	41.3
RMSD from ideal geometry			
bond lengths (Å)	0.01	0.01	0.01
bond angles (°)	1.9	0.9	1.8
Ramachandran statistics (%)			
favored	96	98	97
allowed	4	2	3
outliers	0	0	0
PDB code	6VSS	6VST	6VSU

[a]*ADP, atomic displacement parameter.*
Values in parentheses refer to the highest-resolution shell.

II, Wyatt Technologies), and a RI detector (Optilab T-rEX, Wyatt), and then the samples were directed to the SAXS flow cell (1.5 mm quartz capillary). The scattering data were collected at 1.03 Å wavelength at room temperature with 0.5 s exposure every 2 s. The sample-to-detector distance was 3.5 m and the collected q-range was 0.004–0.4 Å^{-1}. Data reduction and analysis were performed in *BioXTAS RAW* 1.5.1 (Hopkins et al., 2017). Several frames from the elution peak and were averaged, which increased the signal-to-noise ratio. Then, the buffer signal from averaged frames proximal to the sample peak was subtracted from the averaged scattering data of the elution peak. The *Rg* values calculated from the Guinier and distance distribution analysis were 36 Å for both analyzed proteins. The calculated maximum dimensions of the particles (D_{max}) for *At*ARGAH1 and *Mt*ARGAH were almost identical, 104 and 105 Å, respectively. Further calculations were done with the following *qRg* limits: 0.45–1.31 (*At*ARGAH1) and 0.36–1.31 (*Mt*ARGAH). *DAMMIF* (Franke and Svergun, 2009), *DAMAVER* (Volkov and Svergun, 2003), *DAMMIN* (Svergun, 1999) and *DAMFILT* were consecutively used for the calculation of the *ab initio* envelopes, averaging, refinement and filtration. Threefold symmetry restraints were applied during the envelope generation. SAXS envelopes were superposed with the crystallographic hexamers of *At*ARGAH1 and *Mt*ARGAH in *SUPCOMB*.

Phylogenetic Analysis

The first set of sequences of *Viridiplantae* protein sequences, annotated as a Superfamily of ureohydrolases (IPR006035) in the *InterPro* database (Finn et al., 2017), was filtered by *ElimDupes* (www.hiv.lanl.gov) to obtain a set of unique sequences. Then, sequences were sorted in *BioEdit* (Hall, 1999); sequences with the length of 300–430 residues were used for further analysis. This set was aligned by *MUSCLE* (Edgar, 2004) in *MEGA7* (Kumar et al., 2016). Clear outliers and incomplete sequences were removed manually. The final set contained 141 sequences, which were re-aligned in *MUSCLE* and conservation of each residue was analyzed.

The second set was created by the search of non-redundant protein sequences database in protein *BLAST* (Altschul et al., 1997) with the sequence of *At*ARGAH1 without predicted signal peptide (UNIPROT ID: P46637). Results with E value lower than 0.005 were further analyzed analogically to the Set 1. Final set consisted of 226 sequences (the full list of the accession numbers of analyzed sequences can be found in the **Supplementary Material**).

Other Software Used

Molecular illustrations were created with UCSF *Chimera* (Pettersen et al., 2004) and *PyMOL* (Schrödinger, LLC). The secondary structure was recognized with ProMotif (Hutchinson and Thornton, 1996) within the *PDBsum* server (de Beer et al., 2014). Sequence alignments were edited in *BioEdit* (Hall, 1999).

RESULTS AND DISCUSSION

The Structure of *At*ARGAH1 and *Mt*ARGAH

In *A. thaliana*, there are two ARGAHs (*At*ARGAH1 and *At*AR GAH2), while *M. truncatula* has only one isoform, *Mt*ARGAH. The subunits of these plant ARGAHs have 342 (*At*ARGAH1), 344 (*At*ARGAH2), 338 (*Mt*ARGAH) residues. *At*ARGAH1 and *At*ARGAH2 share almost 85% identity. *Mt*ARGAH presents 76 and 72% sequence identity to *At*ARGAH1 and *At*ARGAH2, respectively. They all have signal peptide (21-residue long in *At*ARGAH1, 26 residues in *At*ARGAH2, and 15 residues in *Mt*ARGAH) (Almagro Armenteros et al., 2019) that is predicted to target proteins to mitochondria. However, the studies show that *Arabidopsis* ARGAHs present dual localization, they can also be targeted to plastids (Patel et al., 2017). In fact, about 20 N-terminal residues are disordered in the structures of full-length *Mt*ARGAH and they were not modeled in the final models.

*At*ARGAH1 and *Mt*ARGAH share the arginase/deacetylase fold (Andreeva et al., 2008). The subunit architecture in both

proteins is the three-layer α/β/α sandwich where the eight-stranded parallel β-sheet is buried between two helical bundles (**Figure 1A**). Five helices cover one face of the β-sheet and the set of six helices is placed on the other side. Structures of both ARGAHs are very similar, with about 0.7 Å RMSD of the superposed Cα atoms of corresponding monomers. Both proteins have two *cis*-peptide bonds (Glu150-Pro1151 and Gly158-Gly159 in *At*ARGAH1; Asp146-Pro147 and Gly154-Gly155 in *Mt*ARGAH). The *cis*-peptide bond between two Gly residues is highly conserved in ureohydrolases, it is in the conserved Gly-Gly-Asp-His motif (Ahn et al., 2004), which contributes to the region responsible for manganese binding within ARGAH active site (see below). A characteristic feature of plant ARGAHs is the protruding loop region (*L2**, **Figure 1A**), which shapes the active site entrance of the neighboring subunit within the oligomer (see below).

The crystal structures of both ARGAH enzymes indicate that they also share the same symmetrical hexameric assembly (32 symmetry, **Figure 1B**); RMSD of the Cα atoms of superposed hexamers of *At*ARGAH1-ORN and *Mt*ARGAH-ORN is ~1 Å. The analysis with PISA server (Krissinel, 2015) shows that both ARGAHs present similar total buried area (~21,000 $Å^2$). The hexamer is formed by a pair of three subunits (ABC and DEF, each with the threefold symmetry, center panel of **Figure 1B**) which are stacked with one another in a way that each subunit from one triplet (A, B, C) interacts with only one subunit from another triplet (D, E, F, respectively). In fact, the pair of triplets in *Mt*ARGAH seems to be tighter than it is in *At*ARGAH1; the buried area between interacting monomers A/D, B/E, C/F in *Mt*ARGAH is in average ~1,600 $Å^2$, while in in *At*ARGAH1 it is ~1,200 $Å^2$. SAXS results for both proteins (**Figures 2A, B**) are very similar, with identical *Rg* and nearly identical D_{max}, and confirm that plant ARGAHs are also hexamers in solution. The estimated molecular weight of *At*ARGAH1 from SAXS data (211 kDa) matches almost ideally the hexameric *At*ARGAH1 (calculated molecular weight of the expressed hexameric construct is 209 kDa). Although the predicted molecular weight of *Mt*ARGAH from SAXS (191 kDa) differs from the theoretical hexamer mass based on the sequence of expressed *Mt*ARGAH (224 kDa), the calculated *ab initio* SAXS envelope of *Mt*ARGAH still represents the *Mt*ARGAH hexamer (**Figure 2C**). It is, in fact, more detailed than the SAXS envelope of *At*ARGAH1 (**Figure 2D**) and slightly more resembles the crystal structure.

Active Site

The active site with a double manganese cluster is formed in each ARGAH subunit by loop regions (*L1*, *L3*, *L4*, *L5*, *L7*, and *L8*) placed on the C-terminal ends of six β-stands (**Figure 3**). Additionally, the entrance of the active site is complemented by the loop *L2** from the neighboring subunit in the triplet. The amino acid composition of these loops is very similar in described ARGAHs (**Figure 3A**). Moreover, based on the phylogenetic analysis (see *Materials and Methods* section) these loops exhibit highly conserved features in all plant ureohydrolases (**Figure 3B**, see below). Thus, the structural characteristics of the active site of *At*ARGAH1 and *Mt*ARGAH can be transferred with high probability to other plant ARGAHs,

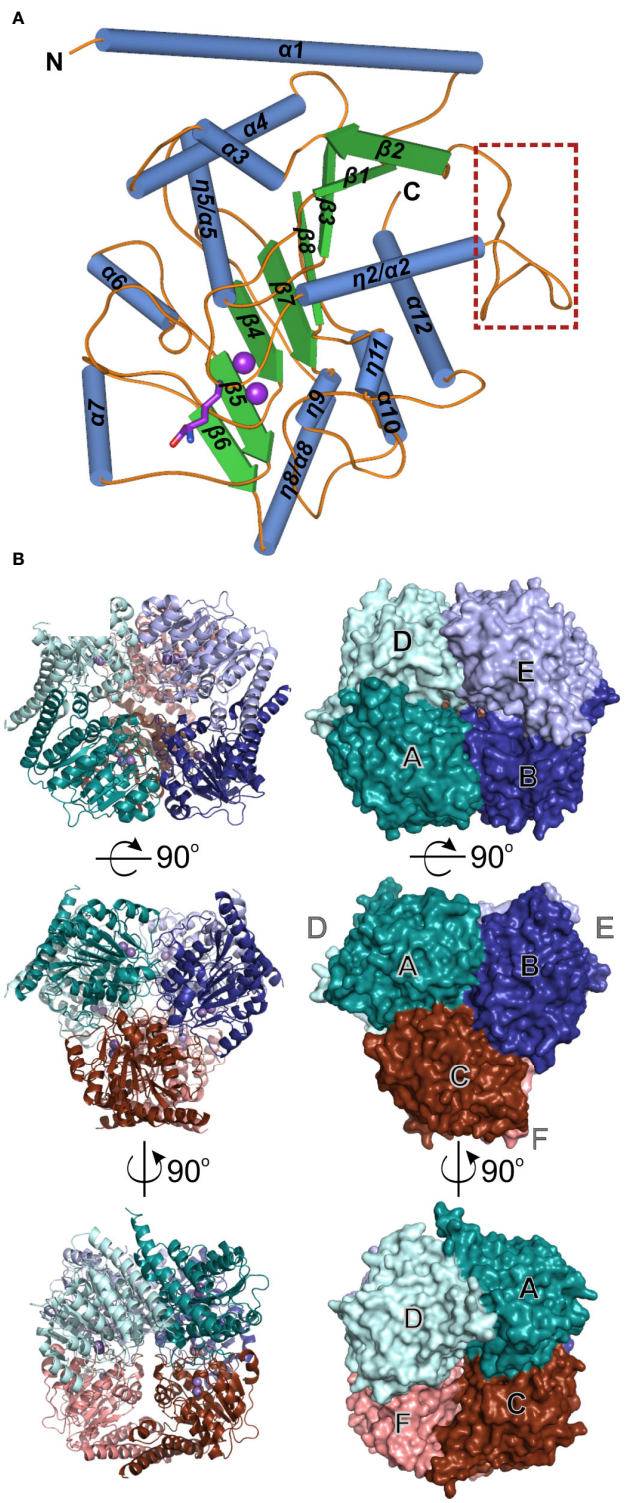

FIGURE 1 | ARGAH crystal structure. **(A)** Architecture of *At*ARGAH1 monomer, secondary structure elements are color-coded as follows: helices (blue cylinders), sheets (green arrows), and coil regions (orange lines); the loop L2* (engaged in substrate binding in the neighboring subunit) is marked with a brown square. **(B)** *At*ARGAH1 hexameric assembly shown in cartoon (left) and surface (right) representation; each subunit is depicted with different color.

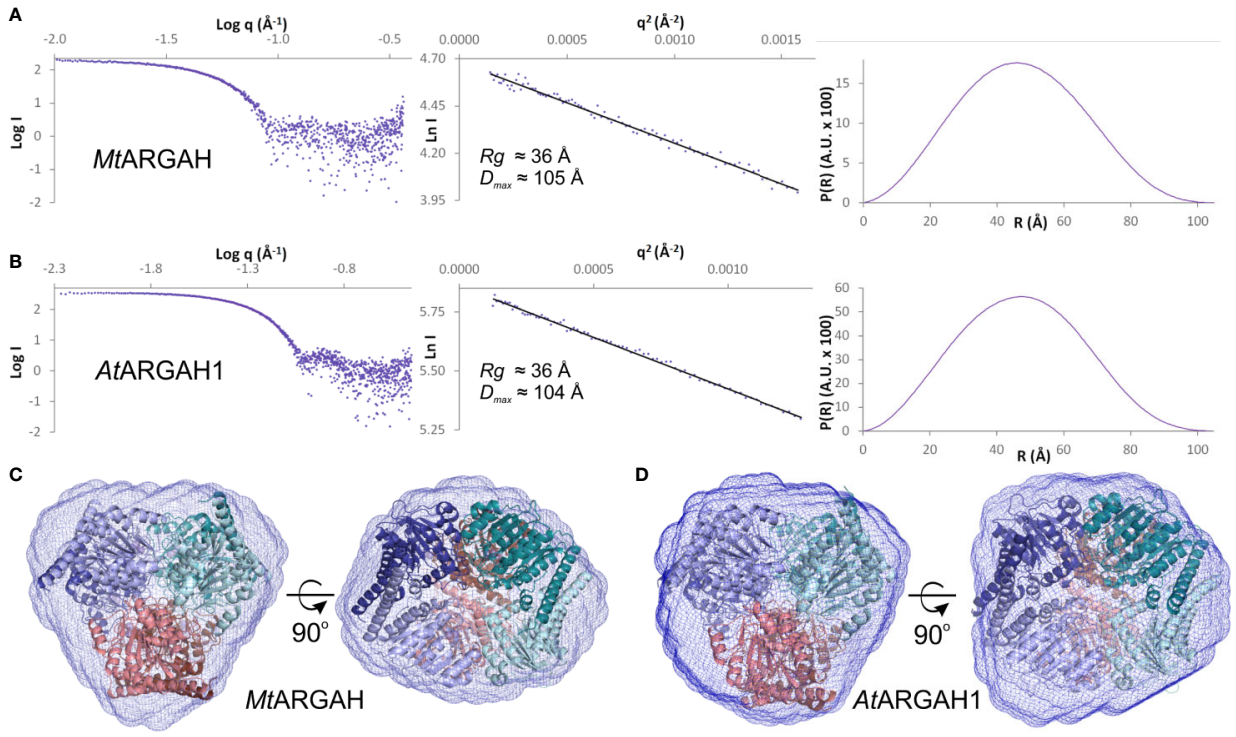

FIGURE 2 | ARGAH solution structure. SAXS data for *Mt*ARGAH **(A)** and *At*ARGAH1 **(B)**; left chart presents the experimental SAXS curve; Guinier plots of the scattering curve with the best fit shown as a black line are shown in the center; pair-distance distribution function for SAXS data, P(R), is shown on the right. *Ab initio* averaged SAXS envelopes (blue mesh) of *Mt*ARGAH **(C)** and *At*ARGAH1 **(D)**; envelopes are superposed with *Mt*ARGAH and *At*ARGAH1 crystallographic hexamers.

as well. The manganese cluster is placed deep inside the active site, close to the C-terminal ends of β4 and β7 on one face of the core β-sheet (**Figures 3B** and **4**). Two Mn^{2+} ions are bridged together in *Mt*ARGAH by Asp181, Asp266, and the catalytic hydroxide ion (**Figure 4**, see below). In *At*ARGAH1 the bridging residues are Asp185 and Asp270. The general coordination geometry of Mn^{2+} ions in ARGAH active site is square pyramidal and distorted octahedral (Christianson and Cox, 1999). In *Mt*ARGAH, Mn^{2+} ions present the same coordination geometry (**Figure 4**). Square pyramid around one Mn^{2+} is formed by OD2 of Asp185, ND1 of His157, OD2 of Asp266, OD1 of Asp181, and the bridging hydroxide ion (OD2 of Asp181 is perpendicular to the plane formed by the other four ligands). Octahedral coordination of the other Mn^{2+} is created by OD1 of Asp181, ND1 of His183, OD2 of Asp266, OD1 of Asp268, OD2 of Asp268, and the bridging hydroxide ion. The architecture of the region responsible for Mn^{2+} binding is the same in *At*ARGAH1 (**Figure 3A**), and it is highly conserved not only in plant ARGAHs (**Figure 3B**) but also in arginases from other domains of life (Christianson and Cox, 1999). In some structures of ARGAHs with ligands (Ahn et al., 2004), both Mn^{2+} have disordered octahedral coordination geometry with an additional water molecule, which is also observed in some subunits in *At*ARGAH1-ORN structure.

Plant arginases are likely not different from other manganese ureohydrolases regarding the catalytic mechanism, widely accepted for these enzymes (Christianson and Cox, 1999). Catalytic hydroxide ion (the one which coordinates both Mn^{2+}), initially is H-bonded to Asp185 in *Mt*ARGAH structure. The substrate (arginine or agmatine) enters the active site with guanidine moiety placed above the manganese cluster. Glu309 in *Mt*ARGAH (Glu313 in *At*ARGAH1), localized at the back wall of the catalytic cavity, likely H-bonds the substrate so it can be oriented in a way that the center carbon atom of the guanidine moiety is in close vicinity to the catalytic hydroxide ion. Eventually, the hydroxide ion performs a nucleophilic attack on the central carbon of the substrate to create a tetrahedral intermediate, similar in geometry to ARGAH inhibitors (Di Costanzo et al., 2005). After a proton transfer, likely from Asp185, to the amino group of created ornithine (or putrescine), the intermediate is broken down with the release of reaction products: ornithine (putrescine) and urea.

Plant ARGAHs Engage Second Subunit to Stabilize the Substrate in the Active Site

Structures of *At*ARGAH1-ORN and *Mt*ARGAH-ORN with the reaction product, ornithine, were obtained as a result of *in vitro* arginine hydrolysis. Although the hydrolysis took place before the crystal growth (there is no trace of urea molecule in the active site, and ornithine is not uniformly bound in all ARGAH active sites), the structures clearly correspond to the post-catalytic state of the enzyme. This inhomogeneity in ornithine binding can be

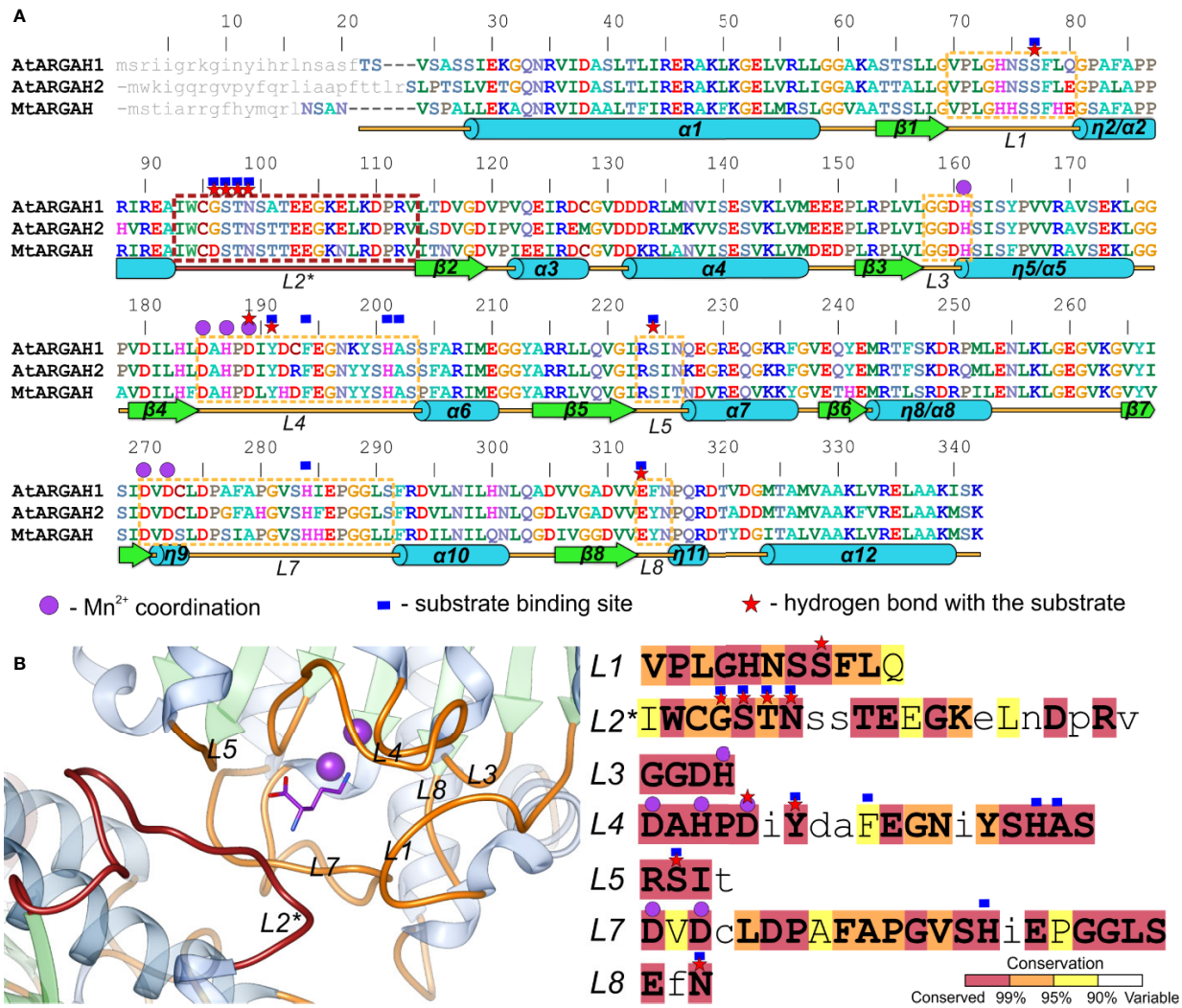

FIGURE 3 | ARGAH structure. **(A)** Sequence alignment of *At*ARGAH1, *At*ARGAH2, and *Mt*ARGAH; residues are color-coded by type; secondary structure elements are shown below the alignment: helices (cylinders), sheets (arrows), and coil regions (lines); dashed lines mark sequence regions of the active site vicinity; loop L2* (engaged in substrate binding in the neighboring subunit) is marked in brown; purple circles denote residues engaged in coordination of the manganese cluster; red stars mark residues that are involved in the hydrogen bonding interactions with the substrate; blue squares indicate the residues that build the substrate binding site (in 5 Å radius of ornithine bound in ARGAH structures); grey small letters mark the predicted signal peptides; sequence positions above the alignment refer to *At*ARGAH1 sequence. **(B)** Architecture of the substrate binding site in *At*ARGAH1 structure (left) and sequence conservation of plant ureohydrolases (calculation is based on a set of set of 226 unique sequences, see *Materials and Methods*) in the loop regions that build the active site entrance; residues are highlighted accordingly to the presented conservation score; small letters depict less conserved residues.

explained by insufficient concentration of the ligand, since ARGAHs should present relatively low affinity to the reaction product. However, in subunits where electron density maps are more clear and indicate ornithine binding (**Figures 5A, B**), the position of the ligand in the model explains the ligand binding mode of plant ARGAHs.

Ornithine penetrates the active site with Nϵ amino group pointed towards the manganese cluster. Therefore, α-amino and carboxyl groups of the ligand are stabilized by residues from *L*1, *L*4, *L*5, *L*7 coil regions of one subunit, and *L*2* from the neighboring subunit of ARGAH hexamer (**Figures 5A, B**). At the active site entrance of *Mt*ARGAH, carboxyl group of ornithine creates two direct hydrogen bonds with the hydroxyl group of Tyr187 and the amino group of Asn95 from the neighboring subunit (Tyr191 and Asn95 in *At*ARGAH1). Additionally, it creates a couple of water-mediated H-bonds with Ser220, with Asp185 (Ser224, with Asp189 in *At*ARGAH1). The amino group of ornithine is more exposed to the solvent region. As a result, it is H-bonded to three water molecules that mediate the interactions with Ser73, Ser220, Asp92*, and Thr94* (Ser77, Ser224, Gly96*, Ser97*, and Thr98* in *At*ARGAH1; asterisk denotes residue from the

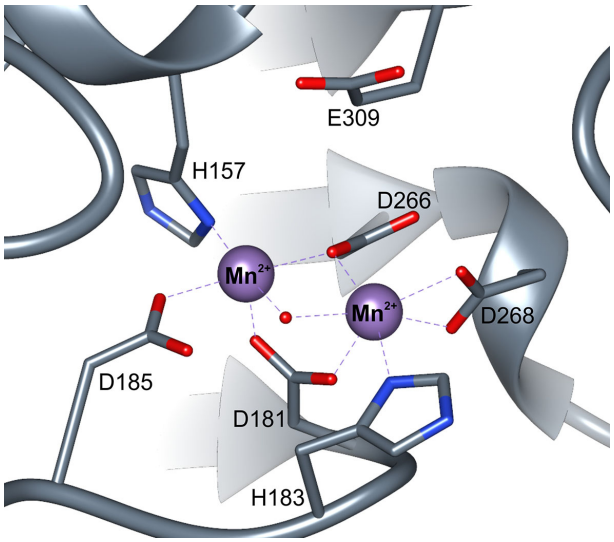

FIGURE 4 | ARGAH active site. Coordination of manganese ions (purple spheres) in the active site of *Mt*ARGAH structure; red dot represents the catalytic hydroxide ion.

neighboring subunit). In some monomers of *Mt*ARGAH, the interatomic distances also suggest direct H-bond interaction of an amino group of ornithine with Ser93*. Somewhat limited resolution of the structures and partial disorder in the solvent region does not allow of an unambiguous assignment of the interactions of α-amino group of ARGAH substrate with the main chain of *L2** region (Asp92*, Ser93*, and Thr94* of *Mt*ARGAH; Gly96*, Ser97*, and Thr98* of *At*ARGAH1). The interactions could also vary depending on the conditions (pH or ionic strength). Therefore, when agmatine (lacking a carboxyl group) would be the bound ligand, this substrate would not interact with Tyr187 and Asn95 (Tyr191 and Asn99 in *At*ARGAH1). Thus, the amino group of agmatine could be moved closer to residues from *L2**, where it could possibly create direct hydrogen bonds with their carbonyl oxygen atoms. Interestingly, orientation and interactions with the surrounding residues of the α-amino and carboxyl groups of bound ornithine in plant ARGAHs are nowhere near orientation of ornithine in human arginase (**Figure 6**) (Ilies et al., 2011) and other arginases (see below).

Plant ARGAHs Present Highly Conserved Features Around the Active Site Entrance

InterPro database (Finn et al., 2017) contains only five sequences of *Viridiplantae* proteins annotated as arginases. Therefore, to investigate the sequence conservation of plant ARGAHs, a set of 226 unique sequences were used in the analysis (see *Materials and Methods*). This set contained nearly all sequences assigned to the superfamily of *Viridiplantae* ureohydrolases (IPR006035). It was used to analyze the conservation of residues from *L1*–*L5*, *L7* and *L8* regions that build the ARGAH active site and its entrance (**Figure 3B**). These are residues that are responsible for the substrate specificity of plant ureohydrolases.

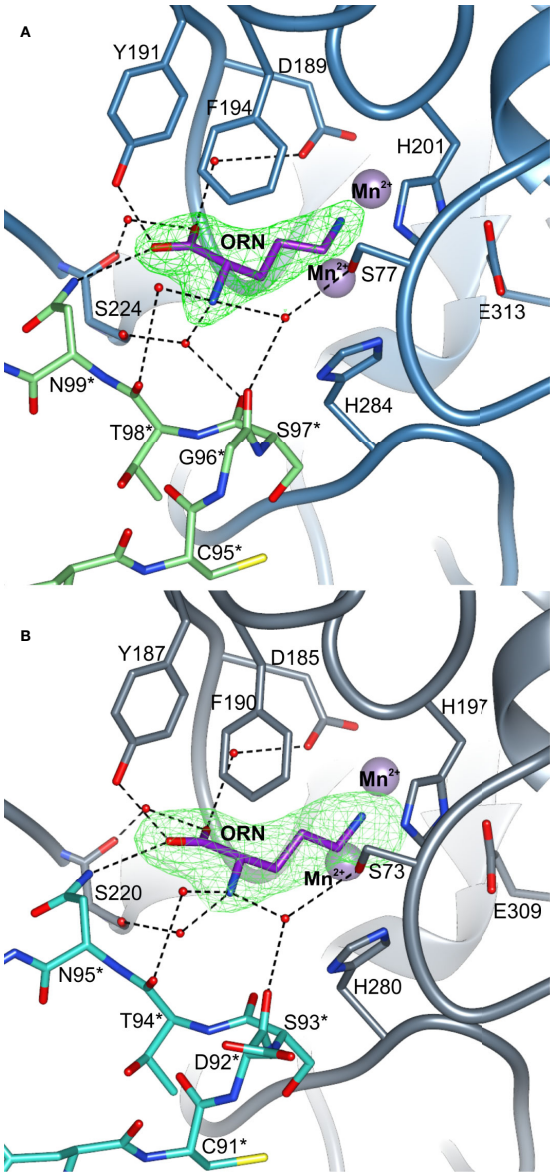

FIGURE 5 | The ligand binding mode of plant ARGAHs. The binding mode of ornithine (ORN) in the active site of **(A)** *At*ARGAH1 and **(B)** *Mt*ARGAH; dashed lines indicate hydrogen bonds; residues are numbered accordingly to the sequence positions of presented proteins; green mesh represents Polder omit maps (contoured at 6 σ) around bound ornithine calculated in *Phenix* (Liebschner et al., 2017); residues from the neighboring subunit are marked with asterisk.

It is no surprise that the sequence of plant ureohydrolases is fully conserved in the region responsible for the interactions with double manganese cluster since they hydrolyze guanidine moiety of the substrate. More unexpected is that almost all residues from the vicinity (5 Å radius) of bound ornithine in presented plant ARGAHs structures (*At*ARGAH1-ORN and *Mt*ARGAH-ORN) are highly conserved (conservation >99%, **Figure 3B**). Only two residues in *L2**, corresponding to Gly96* and Thr98* of *At*ARGAH1, and one in *L4* (Phe194 of *At*ARGAH1) present

lower conservation (these positions are identical in >95% of analyzed sequences). However, the slight variability of Gly96-Ser97-Thr98 fragment concerns the region that interacts with ornithine *via* carbonyl oxygens of the main chain. In this case the overall conformation of the *L2** loop is more important than the type of side chains of amino acids which build the loop.

The helix η2/α2 in the ARGAH structure is followed by a pair of hydrophobic residues (Ile or Met in position equivalent to residue 93 of *At*ARGAH1, and the fully conserved Trp94) which bends the main chain to begin the β-turn, just before the Ser97-Thr98-Asn99 motif. In that way, Asn99 and carbonyl oxygens of the preceding residues are positioned close to the entrance of the active site to bind the substrate. Comparison of *At*ARGAH1 with *Mt*ARGAH shows that substitution of glycine to aspartic acid (**Figures 5A, B**) does not affect the conformation of the loop *L2**. Therefore, evolutionary pressure in this region is to preserve the overall conformation of the main chain rather than to conserve side chains. Additionally, the residue which H-bonds carboxyl group of ornithine (Asn99 in *At*ARGAH1 and Asn95 in *Mt*ARGAH) is fully conserved in all plant ARGAHs.

Another important region for ARGAH specificity is loop *L4* with fully conserved Tyr191 that also binds carboxyl group of the substrate. In this case, two consecutive β-turns position Phe194 and Tyr191 close to each other and in the vicinity of the substrate. Phe194 from *L4* in 16 sequences from the analyzed set is substituted with tyrosine. Therefore, this position requires an aromatic residue which limits the size of the active site. Interestingly, Tyr191 is flanked by more variable residues in plant ureohydrolases; positions 192 and 193 present especially high variability. However, in both, *At*ARGAH1 and *Mt*ARGAH, substitution of the side chains of residues corresponding to positions 192 and 193 has minor effect on the position of the main chain in this region and side chains of Phe194 and Tyr191.

Overall, the conservation of loop regions around the active site is very high in all plant ureohydrolases, not only in terms of amino acid composition but also in terms of their length. No examples of deletions or insertions were found. Therefore, it can be assumed that all analyzed sequences of plant ureohydrolases, and sequences in the *InterPro* superfamily of ureohydrolases (IPR006035) are in fact the same ARGAHs. They should present not only very similar structure to *At*ARGAH1 and *Mt*ARGAH but also they should share the same substrate binding mode and the same substrate specificity, as previously suggested (Patel et al., 2017).

Comparison With Other Ureohydrolases

Examples of structures of other ureohydrolases with ornithine are found in the Protein Data Bank (PDB), e.g., for bacterial arginase from *Bacillus caldovelox* (PDB ID: 4CEV) (Bewley et al., 1999) or human arginase, *Hs*ARG1 (PDB ID: 3GMZ) (Ilies et al., 2011). Although bacterial arginases are usually hexamers and eukaryotic are trimers (Ahn et al., 2004), they bind ornithine in a very similar fashion. However, the binding mode is very different to that observed in plant ARGAHs (**Figure 6B**). The carboxyl group of ornithine in plant ARGAHs occupies the position of the amino group of ornithine in mammalian and bacterial arginases. This significant difference in the ligand binding mode is a consequence of the difference of loop *L4* architecture. In *At*ARGAH1 there is Phe194 that fills this part of the pocket (**Figure 6B**). Additionally, bacterial and mammalian arginases basically lack *L2** coil region. In *Hs*ARG1 this fragment is 9-residue shorter in comparison to *L2** of *At*ARGAH1 and it forms a helix, which does not interact with a substrate. Therefore, the active sites of mammalian and bacterial arginases are independent in each subunit. Looking only at this comparison, it is no surprise that plant ARGAHs are not phylogenetically

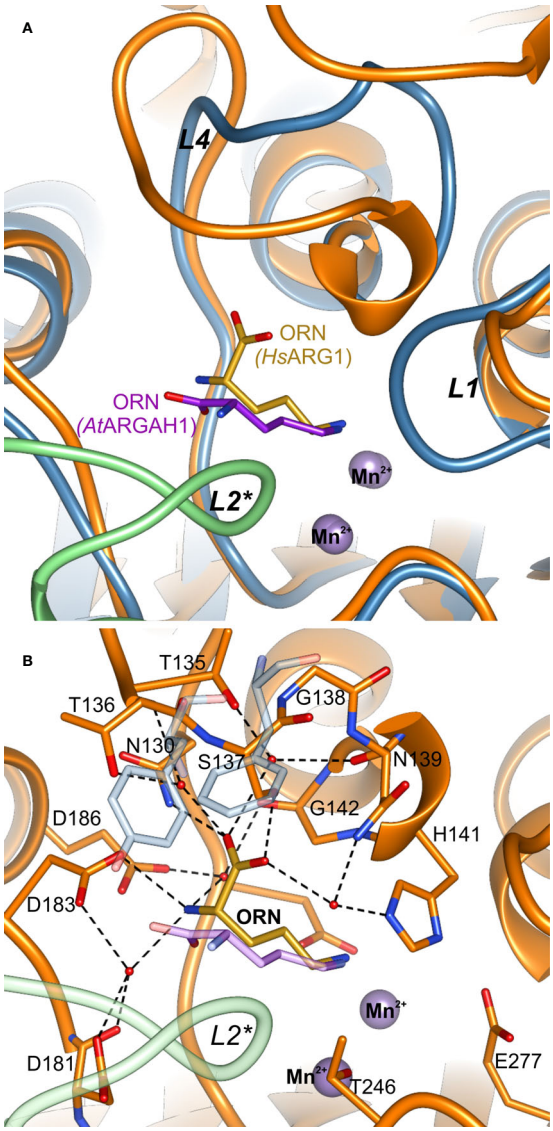

FIGURE 6 | Comparison of ornithine binding mode in *At*ARGAH1 and *Hs*AGS1. **(A)** Cartoon representation of the superposed *At*ARGAH1-ORN and *Hs*ARG1-ORN (PDB ID: 3GMZ) structures; the chain of subunit A and B of *At*ARGAH1 is light blue and green, while the chain of *Hs*ARG1 is orange; **(B)** interactions of bound ornithine (yellow) in the structure of *Hs*ARG1-ORN (orange, PDB ID: 3GMZ); to highlight structural differences of plant ARGAHs *Hs*ARG1 some structural features (the loop *L2**, ornithine, Phe191, and F194) of the superposed *At*ARGAH1 structure are shown in semi-transparent representation.

closer related to arginases from other domains of life than to bacterial agmatinases (Chen et al., 2004).

There are 36 structures of different proteins in the PDB that present the arginase topology annotated by CATH (Sillitoe et al., 2015); 25 of them are actual or putative ureohydrolases. Unfortunately, there is no structural data about ligand binding in other proteins than, already mentioned, arginases. It is worth noting that the structure of agmatinase from *Deinococcus radiodurans* (PDB ID: 1WOG) (Ahn et al., 2004) is annotated as the complex with product analogue, 1,6-diaminohexane, but a close look at the available electron density maps puts the interpretation of this ligand as highly doubtful. Therefore, information about this ligand was omitted in further analysis. Search across the PDB identified only a few proteins that might engage a neighboring subunit for the purpose of ligand binding, similarly to plant ARGAH. These are: procalvaminate amidinohydrolase from *Streptomyces clavuligerus* (PDB ID: 1GQ6), guanidinobutyrase from *Pseudomonas aeruginosa* (PDB ID: 3NIO) (Lee et al., 2011), 3-guanidinopropionase from *P. aeruginosa* (PDB ID: 3NIP) (Lee et al., 2011), putative agmatinase from *Clostridioides difficile* (*Cd*AGM, PDB ID: 3LHL), agmatinase from *Thermoplasma volcanium* (*Tv*AGM, PDB ID: 3PZL), and agmatinase from *Burkholderia thailandensis* (*Bt*AGM, PDB ID: 4DZ4).

The active site vicinity of *Cd*AGM and *Tv*AGM is very similar to plant ARGAHs (especially the conformation of *L4*, **Figure 7A**), but none of the mentioned proteins share the same ligand-binding residues that are conserved in plant ARGAHs (Ser97-Thr98-Asn99 motif in *L2** or Tyr191 in *L4* of *At*ARGAH1). Therefore, they would most likely differ considerably from plant ARGAHs in terms of the ligand binding mode. This is also true for *Bt*AGM, which significantly differs from plant ARGAHs in *L4*. It has Trp165 in position corresponding to Tyr191 in *At*ARGAH1, and Glu78 instead of Asn99 (**Figure 7B**). Glu78 of *Bt*AGM in the region corresponding to *L2** of *At*ARGAH1 would be ideal binding counterpart for terminal amine of agmatine. These proteins do not seem to have residues that would easily interact with carboxyl group of the substrate; thus, they would be specific strictly to agmatine as a substrate. Therefore, the conserved features of plant ARGAHs put them as truly unique ureohydrolases.

CONCLUSIONS

The presented crystal structures of *At*ARGAH1 and *Mt*ARGAH revealed the ligand binding mode in these hexameric enzymes. The conformation of all loop regions around the active site of both proteins is very similar. Therefore, it is not surprising that interactions with the reaction product inside the active site are nearly identical for both ARGAHs. Both enzymes engage the loop region *L2** from the neighboring subunit to stabilize the ligand inside the active site. Combining these results with highly conserved features of plant ARGAHs, it is likely that all ARGAHs in the plant kingdom recognize their ligands in a similar fashion. Although the mechanism of guanidine moiety hydrolysis is universal among ureohydrolases of different

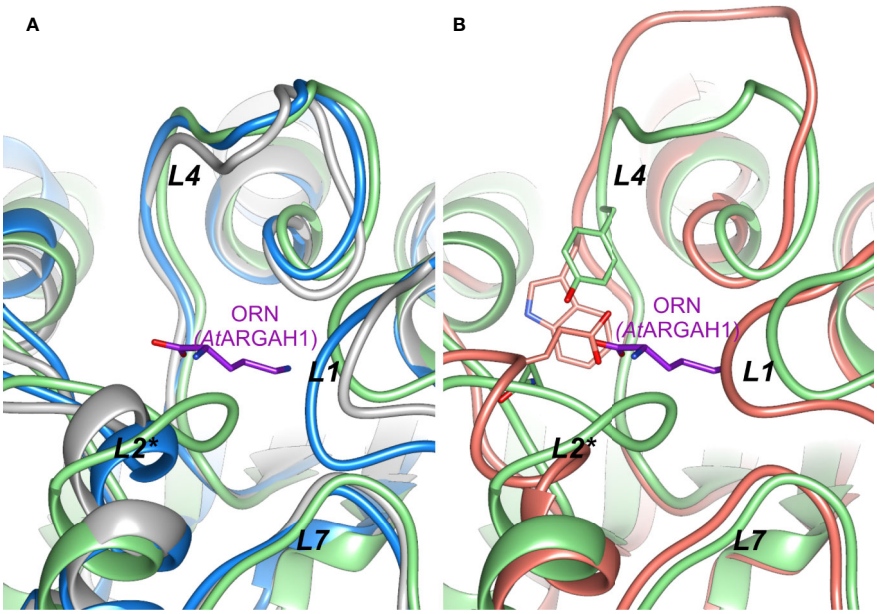

FIGURE 7 | Comparison of plant AGAH with agmatinases. **(A)** Superposition of *At*ARGAH1 (light green) with agmatinase from *Clostridioides difficile* (grey, PDB ID: 3LHL), agmatinase from *Thermoplasma volcanium* (blue, PDB ID: 3PZL); **(B)** superposition of *At*ARGAH1 (light green) with agmatinase from *Burkholderia thailandensis* (salmon, PDB ID: 4DZ4); ornithine bound in *At*ARGAH1 is shown as violet sticks; positions of Tyr191, Asn99 (both *At*ARGAH1), and corresponding to them Trp165 and Glu78 (both residues from *Burkholderia thailandensis* agmatinase) are shown as sticks representation.

domains of life, the characteristic ligand binding mode distinguishes plant ARGAHs from other eukaryotic and prokaryotic arginases and agmatinases. These features seem to be an accommodation for the dual arginase/agmatinase activity of plant ARGAHs.

DATA AVAILABILITY STATEMENT

The coordinates and structure factors of the related structures were deposited in the Protein Data Bank (PDB): 6VSS (*Mt*ARGAH), 6VST (*Mt*ARGAH-ORN), 6VSU (*At*ARGAH1-ORN).

AUTHOR CONTRIBUTIONS

The author confirms being the sole contributor of this work and has approved it for publication.

FUNDING

This project was supported in part by the Intramural Research Program of the National Cancer Institute, Center for Cancer Research.

ACKNOWLEDGMENTS

The author would like to acknowledge Zbigniew Dauter, NCI, for guidance, advice, and supervision, and Srinivas Chakravarthy, BioCAT, for assistance during SAXS experiments. Diffraction data were collected at the Advanced Photon Source (APS), Argonne National Laboratory (ANL), at the SER-CAT beamline 22-ID (supported by the U.S. Department of Energy [DOE], Office of Basic Energy Sciences, under contract W-31-109-Eng-38) and the 19-ID beamline of the Structural Biology Center (operated by UChicago Argonne, LLC, for the DOE, Office of Biological and Environmental Research, under contract DE-AC02-06CH11357). SAXS research on the 18-ID BioCAT beamline used resources of APS, a DOE Office of Science User Facility operated by ANL (contract DE-AC02-06CH11357), a project supported by grant 9P41 GM103622 from the National Institute of General Medical Sciences (NIGMS). The use of the PILATUS 3 1M detector was provided by grant 1S10OD018090-01 from NIGMS.

SUPPLEMENTARY MATERIAL

The Supplementary Material for this article can be found online at: https://www.frontiersin.org/articles/10.3389/fpls.2020.00987/full#supplementary-material

REFERENCES

Adams, P. D., Afonine, P. V., Bunkoczi, G., Chen, V. B., Davis, I. W., Echols, N., et al. (2010). PHENIX: a comprehensive Python-based system for macromolecular structure solution. *Acta Crystallogr. D Biol. Crystallogr.* 66, 213–221. doi: 10.1107/S0907444909052925

Ahn, H. J., Kim, K. H., Lee, J., Ha, J.-Y., Lee, H. H., Kim, D., et al. (2004). Crystal Structure of Agmatinase Reveals Structural Conservation and Inhibition Mechanism of the Ureohydrolase Superfamily. *J. Biol. Chem.* 279, 50505–50513. doi: 10.1074/jbc.M409246200

Almagro Armenteros, J. J., Salvatore, M., Emanuelsson, O., Winther, O., von Heijne, G., Elofsson, A., et al. (2019). Detecting sequence signals in targeting peptides using deep learning. *Life Sci. Alliance* 2, e201900429. doi: 10.26508/lsa.201900429

Altschul, S. F., Madden, T. L., Schaffer, A. A., Zhang, J., Zhang, Z., Miller, W., et al. (1997). Gapped BLAST and PSI-BLAST: a new generation of protein database search programs. *Nucleic Acids Res.* 25, 3389–3402. doi: 10.1093/nar/25.17.3389

Andreeva, A., Howorth, D., Chandonia, J.-M., Brenner, S. E., Hubbard, T. J. P., Chothia, C., et al. (2008). Data growth and its impact on the SCOP database: new developments. *Nucleic Acids Res.* 36, D419–D425. doi: 10.1093/nar/gkm993

Bewley, M. C., Jeffrey, P. D., Patchett, M. L., Kanyo, Z. F., and Baker, E. N. (1999). Crystal structures of Bacillus caldovelox arginase in complex with substrate and inhibitors reveal new insights into activation, inhibition and catalysis in the arginase superfamily. *Structure* 7, 435–448. doi: 10.1016/S0969-2126(99)80056-2

Boutin, J. P. (1982). Purification, properties and subunit structure of arginase from Iris bulbs. *Eur. J. Biochem.* 127, 237–243. doi: 10.1111/j.1432-1033.1982.tb06861.x

Brownfield, D. L., Todd, C. D., and Deyholos, M. K. (2008). Analysis of Arabidopsis arginase gene transcription patterns indicates specific biological functions for recently diverged paralogs. *Plant Mol. Biol.* 67, 429–440. doi: 10.1007/s11103-008-9336-2

Brunger, A. T. (1992). Free R value: a novel statistical quantity for assessing the accuracy of crystal structures. *Nature* 355, 472–475. doi: 10.1038/355472a0

Chen, H., McCaig, B. C., Melotto, M., He, S. Y., and Howe, G. A. (2004). Regulation of plant arginase by wounding, jasmonate, and the phytotoxin coronatine. *J. Biol. Chem.* 279, 45998–46007. doi: 10.1074/jbc.M407151200

Chen, V. B., Arendall, W. B., Headd, J. J., Keedy, D. A., Immormino, R. M., Kapral, G. J., et al. (2010). MolProbity: all-atom structure validation for macromolecular crystallography. *Acta Crystallogr. D* 66, 12–21. doi: 10.1107/S0907444909042073

Christianson, D. W., and Cox, J. D. (1999). Catalysis By Metal-Activated Hydroxide in Zinc and Manganese Metalloenzymes. *Annu. Rev. Biochem.* 68, 33–57. doi: 10.1146/annurev.biochem.68.1.33

Dabir, S., Dabir, P., and Somvanshi, B. (2005). Purification, properties and alternate substrate specificities of arginase from two different sources: Vigna catjang cotyledon and buffalo liver. *Int. J. Biol. Sci.* 1, 114–122. doi: 10.7150/ijbs.1.114

de Beer, T. A., Berka, K., Thornton, J. M., and Laskowski, R. A. (2014). PDBsum additions. *Nucleic Acids Res.* 42, D292–D296. doi: 10.1093/nar/gkt940

Desai, H. V. (1983). Purification & properties of arginase from Arachis hypogea L. seedlings. *Indian J. Biochem. Biophys.* 20, 236–237.

Di Costanzo, L., Sabio, G., Mora, A., Rodriguez, P. C., Ochoa, A. C., Centeno, F., et al. (2005). Crystal structure of human arginase I at 1.29-Å resolution and exploration of inhibition in the immune response. *Proc. Natl. Acad. Sci. U. S. A.* 102, 13058–13063. doi: 10.1073/pnas.0504027102

Di Costanzo, L., Ilies, M., Thorn, K. J., and Christianson, D. W. (2010). Inhibition of human arginase I by substrate and product analogues. *Arch. Biochem. Biophys.* 496, 101–108. doi: 10.1016/j.abb.2010.02.004

Dowling, D. P., Di Costanzo, L., Gennadios, H. A., and Christianson, D. W. (2008). Evolution of the arginase fold and functional diversity. *Cell. Mol. Life Sci.* 65, 2039–2055. doi: 10.1007/s00018-008-7554-z

Edgar, R. C. (2004). MUSCLE: multiple sequence alignment with high accuracy and high throughput. *Nucleic Acids Res.* 32, 1792–1797. doi: 10.1093/nar/gkh340

Emsley, P., Lohkamp, B., Scott, W. G., and Cowtan, K. (2010). Features and development of Coot. *Acta Crystallogr. D Biol. Crystallogr.* 66, 486–501. doi: 10.1107/S0907444910007493

Finn, R. D., Attwood, T. K., Babbitt, P. C., Bateman, A., Bork, P., Bridge, A. J., et al. (2017). InterPro in 2017-beyond protein family and domain annotations. *Nucleic Acids Res.* 45, D190–D199. doi: 10.1093/nar/gkw1107

Fischetti, R., Stepanov, S., Rosenbaum, G., Barrea, R., Black, E., Gore, D., et al. (2004). The BioCAT undulator beamline 18ID: a facility for biological non-crystalline diffraction and X-ray absorption spectroscopy at the Advanced Photon Source. *J. Synchrotron. Radiat.* 11, 399–405. doi: 10.1107/S0909049504016760

Flores, T., Todd, C. D., Tovar-Mendez, A., Dhanoa, P. K., Correa-Aragunde, N., Hoyos, M. E., et al. (2008). Arginase-negative mutants of Arabidopsis exhibit increased nitric oxide signaling in root development. *Plant Physiol.* 147, 1936–1946. doi: 10.1104/pp.108.121459

Forlani, G., Bertazzini, M., Zarattini, M., Funck, D., Ruszkowski, M., and Nocek, B. (2015). Functional properties and structural characterization of rice delta(1)-pyrroline-5-carboxylate reductase. *Front. Plant Sci.* 6, 565. doi: 10.3389/fpls.2015.00565

Franke, D., and Svergun, D. I. (2009). DAMMIF, a program for rapid ab-initio shape determination in small-angle scattering. *J. Appl. Crystallogr.* 42, 342–346. doi: 10.1107/S0021889809000338

Hall, T. A. (1999). BioEdit: a user-friendly biological sequence alignment editor and analysis program for Windows 95/98/NT. *Nucl. Acids Symp. Ser.* 41, 95–98.

Hanfrey, C., Sommer, S., Mayer, M. J., Burtin, D., and Michael, A. J. (2001). Arabidopsis polyamine biosynthesis: absence of ornithine decarboxylase and the mechanism of arginine decarboxylase activity. *Plant J.* 27, 551–560. doi: 10.1046/j.1365-313X.2001.01100.x

Hopkins, J. B., Gillilan, R. E., and Skou, S. (2017). BioXTAS RAW: improvements to a free open-source program for small-angle X-ray scattering data reduction and analysis. *J. Appl. Crystallogr.* 50, 1545–1553. doi: 10.1107/S1600576717011438

Hutchinson, E. G., and Thornton, J. M. (1996). PROMOTIF–a program to identify and analyze structural motifs in proteins. *Protein Sci.* 5, 212–220. doi: 10.1002/pro.5560050204

Hwang, H. J., Kim, E. H., and Cho, Y. D. (2001). Isolation and properties of arginase from a shade plant, ginseng (Panax ginseng C.A. Meyer) roots. *Phytochemistry* 58, 1015–1024. doi: 10.1016/s0031-9422(01)00392-2

Ilies, M., Di Costanzo, L., Dowling, D. P., Thorn, K. J., and Christianson, D. W. (2011). Binding of alpha,alpha-disubstituted amino acids to arginase suggests new avenues for inhibitor design. *J. Med. Chem.* 54, 5432–5443. doi: 10.1021/jm200443b

Kabsch, W. (2010). XDS. *Acta Crystallogr. D Biol. Crystallogr.* 66, 125–132. doi: 10.1107/S0907444909047337

Kang, J. H., and Cho, Y. D. (1990). Purification and Properties of Arginase from Soybean, Glycine max, Axes. *Plant Physiol.* 93, 1230–1234. doi: 10.1104/pp.93.3.1230

Kim, Y., Babnigg, G., Jedrzejczak, R., Eschenfeldt, W. H., Li, H., Maltseva, N., et al. (2011). High-throughput protein purification and quality assessment for crystallization. *Methods* 55, 12–28. doi: 10.1016/j.ymeth.2011.07.010

Krissinel, E. (2015). Stock-based detection of protein oligomeric states in jsPISA. *Nucleic Acids Res.* 43, W314–W319. doi: 10.1093/nar/gkv314

Kumar, S., Stecher, G., and Tamura, K. (2016). MEGA7: Molecular Evolutionary Genetics Analysis version 7.0 for bigger datasets. *Mol. Biol. Evol.* 33, 1870–1874. doi: 10.1093/molbev/msw054

Lee, S. J., Kim, D. J., Kim, H. S., Lee, B. I., Yoon, H. J., Yoon, J. Y., et al. (2011). Crystal structures of Pseudomonas aeruginosa guanidinobutyrase and guanidinopropionase, members of the ureohydrolase superfamily. *J. Struct. Biol.* 175, 329–338. doi: 10.1016/j.jsb.2011.05.002

Liebschner, D., Afonine, P. V., Moriarty, N. W., Poon, B. K., Sobolev, O. V., Terwilliger, T. C., et al. (2017). Polder maps: improving OMIT maps by excluding bulk solvent. *Acta Crystallogr. D* 73, 148–157. doi: 10.1107/s2059798316018210

Martin-Falquina, A., and Legaz, M. E. (1984). Purification and Properties of the Constitutive Arginase of Evernia prunastri. *Plant Physiol.* 76, 1065–1069. doi: 10.1104/pp.76.4.1065

McCoy, A. J., Grosse-Kunstleve, R. W., Adams, P. D., Winn, M. D., Storoni, L. C., and Read, R. J. (2007). Phaser crystallographic software. *J. Appl. Crystallogr.* 40, 658–674. doi: 10.1107/s0021889807021206

Michael, A. J. (2016). Biosynthesis of polyamines and polyamine-containing molecules. *Biochem. J.* 473, 2315–2329. doi: 10.1042/bcj20160185

Murshudov, G. N., Skubak, P., Lebedev, A. A., Pannu, N. S., Steiner, R. A., Nicholls, R. A., et al. (2011). REFMAC5 for the refinement of macromolecular crystal structures. *Acta Crystallogr. D* 67, 355–367. doi: 10.1107/S0907444911001314

Otwinowski, Z., and Minor, W. (1997). Processing of X-ray diffraction data collected in oscillation mode. *Methods Enzymol.* 276, 307–326. doi: 10.1016/S0076-6879(97)76066-X

Patel, J., Ariyaratne, M., Ahmed, S., Ge, L., Phuntumart, V., Kalinoski, A., et al. (2017). Dual functioning of plant arginases provides a third route for putrescine synthesis. *Plant Sci.* 262, 62–73. doi: 10.1016/j.plantsci.2017.05.011

Pettersen, E. F., Goddard, T. D., Huang, C. C., Couch, G. S., Greenblatt, D. M., Meng, E. C., et al. (2004). UCSF Chimera–a visualization system for exploratory research and analysis. *J. Comput. Chem.* 25, 1605–1612. doi: 10.1002/jcc.20084

Sekula, B., and Dauter, Z. (2019). Structural study of agmatine iminohydrolase from Medicago truncatula, the second enzyme of the agmatine route of putrescine biosynthesis in plants. *Front. Plant Sci.* 10, 320. doi: 10.3389/fpls.2019.00320

Sekula, B., Ruszkowski, M., Malinska, M., and Dauter, Z. (2016). Structural investigations of N-carbamoylputrescine amidohydrolase from Medicago truncatula: insights into the ultimate step of putrescine biosynthesis in plants. *Front. Plant Sci.* 7, 350. doi: 10.3389/fpls.2016.00350

Siddappa, S., Basrur, V., Ravishankar Rai, V., and Marathe, G. K. (2018). Biochemical and functional characterization of an atypical plant l-arginase from Cilantro (Coriandrum sativam L.). *Int. J. Biol. Macromol.* 118, 844–856. doi: 10.1016/j.ijbiomac.2018.06.096

Sillitoe, I., Lewis, T. E., Cuff, A., Das, S., Ashford, P., Dawson, N. L., et al. (2015). CATH: comprehensive structural and functional annotations for genome sequences. *Nucleic Acids Res.* 43, D376–D381. doi: 10.1093/nar/gku947

Sirko, A., and Brodzik, R. (2000). Plant ureases: roles and regulation. *Acta Biochim. Pol.* 47, 1189–1195. doi: 10.18388/abp.2000_3972

Slocum, R. D. (2005). Genes, enzymes and regulation of arginine biosynthesis in plants. *Plant Physiol. Biochem.* 43, 729–745. doi: 10.1016/j.plaphy.2005.06.007

Svergun, D. I. (1999). Restoring Low Resolution Structure of Biological Macromolecules from Solution Scattering Using Simulated Annealing. *Biophys. J.* 76, 2879–2886. doi: 10.1016/S0006-3495(99)77443-6

Terwilliger, T. C., Grosse-Kunstleve, R. W., Afonine, P. V., Moriarty, N. W., Zwart, P. H., Hung, L. W., et al. (2008). Iterative model building, structure refinement and density modification with the PHENIX AutoBuild wizard. *Acta Crystallogr. D* 64, 61–69. doi: 10.1107/S090744490705024X

Tiburcio, A. F., Kaur–Sawhney, R., and Galston, A. W. (1990). "7 - Polyamine Metabolism," in *Intermediary Nitrogen Metabolism*. Eds. B. J. Miflin and P. J. Lea (San Diego: Academic Press), 283–325. doi: 10.1016/B978-0-08-092616-2.50013-9

Volkov, V. V., and Svergun, D. I. (2003). Uniqueness of ab initio shape determination in small-angle scattering. *J. Appl. Crystallogr.* 36, 860–864. doi: 10.1107/S0021889803000268

Winn, M. D., Isupov, M. N., and Murshudov, G. N. (2001). Use of TLS parameters to model anisotropic displacements in macromolecular refinement. *Acta Crystallogr. D* 57, 122–133. doi: 10.1107/S0907444900014736

Winn, M. D., Murshudov, G. N., and Papiz, M. Z. (2003). Macromolecular TLS refinement in REFMAC at moderate resolutions. *Methods Enzymol.* 374, 300–321. doi: 10.1016/S0076-6879(03)74014-2

Winn, M. D., Ballard, C. C., Cowtan, K. D., Dodson, E. J., Emsley, P., Evans, P. R., et al. (2011). Overview of the CCP4 suite and current developments. *Acta Crystallogr. D* 67, 235–242. doi: 10.1107/S0907444910045749

Winter, G., Todd, C. D., Trovato, M., Forlani, G., and Funck, D. (2015). Physiological implications of arginine metabolism in plants. *Front. Plant Sci.* 6, 534. doi: 10.3389/fpls.2015.00534

Zheng, H., Cooper, D. R., Porebski, P. J., Shabalin, I. G., Handing, K. B., and Minor, W. (2017). CheckMyMetal: a macromolecular metal-binding validation tool. *Acta Crystallogr. D Struct. Biol.* 73, 223–233. doi: 10.1107/S2059798317001061

Conflict of Interest: The author declares that the research was conducted in the absence of any commercial or financial relationships that could be construed as a potential conflict of interest.

Copyright © 2020 Sekula. This is an open-access article distributed under the terms of the Creative Commons Attribution License (CC BY). The use, distribution or reproduction in other forums is permitted, provided the original author(s) and the copyright owner(s) are credited and that the original publication in this journal is cited, in accordance with accepted academic practice. No use, distribution or reproduction is permitted which does not comply with these terms.

frontiers in Plant Science

ORIGINAL RESEARCH
published: 22 July 2020
doi: 10.3389/fpls.2020.01118

Cysteine and Methionine Biosynthetic Enzymes Have Distinct Effects on Seed Nutritional Quality and on Molecular Phenotypes Associated With Accumulation of a Methionine-Rich Seed Storage Protein in Rice

*Sarah J. Whitcomb[1], Apidet Rakpenthai[1], Franziska Brückner[1], Axel Fischer[2], Saroj Parmar[3], Alexander Erban[4], Joachim Kopka[4], Malcolm J. Hawkesford[3] and Rainer Hoefgen[1]**

[1] Laboratory of Amino Acid and Sulfur Metabolism, Department of Molecular Physiology, Max Planck Institute of Molecular Plant Physiology, Potsdam, Germany, [2] Bioinformatics Infrastructure Group, Max Planck Institute of Molecular Plant Physiology, Potsdam, Germany, [3] Plant Sciences Department, Rothamsted Research, Harpenden, United Kingdom, [4] Applied Metabolome Analysis Infrastructure Group, Max Planck Institute of Molecular Plant Physiology, Potsdam, Germany

OPEN ACCESS

Edited by:
Sakiko Okumoto,
Texas A&M University, United States

Reviewed by:
Naoko Ohkama-Ohtsu,
Tokyo University of Agriculture and Technology, Japan
Enrique Martinez Force,
Instituto de la Grasa (IG), Spain

***Correspondence:**
Rainer Hoefgen
hoefgen@mpimp-golm.mpg.de

Specialty section:
This article was submitted to Plant Metabolism and Chemodiversity, a section of the journal Frontiers in Plant Science

Received: 28 April 2020
Accepted: 07 July 2020
Published: 22 July 2020

Citation:
Whitcomb SJ, Rakpenthai A, Brückner F, Fischer A, Parmar S, Erban A, Kopka J, Hawkesford MJ and Hoefgen R (2020) Cysteine and Methionine Biosynthetic Enzymes Have Distinct Effects on Seed Nutritional Quality and on Molecular Phenotypes Associated With Accumulation of a Methionine-Rich Seed Storage Protein in Rice. Front. Plant Sci. 11:1118. doi: 10.3389/fpls.2020.01118

Staple crops in human and livestock diets suffer from deficiencies in certain "essential" amino acids including methionine. With the goal of increasing methionine in rice seed, we generated a pair of "Push × Pull" double transgenic lines, each containing a methionine-dense seed storage protein (2S albumin from sunflower, HaSSA) and an exogenous enzyme for either methionine (feedback desensitized cystathionine gamma synthase from Arabidopsis, AtD-CGS) or cysteine (serine acetyltransferase from *E. coli*, EcSAT) biosynthesis. In both double transgenic lines, the total seed methionine content was approximately 50% higher than in their untransformed parental line, *Oryza sativa* ssp. *japonica* cv. Taipei 309. HaSSA-containing rice seeds were reported to display an altered seed protein profile, speculatively due to insufficient sulfur amino acid content. However, here we present data suggesting that this may result from an overloaded protein folding machinery in the endoplasmic reticulum rather than primarily from redistribution of limited methionine from endogenous seed proteins to HaSSA. We hypothesize that HaSSA-associated endoplasmic reticulum stress results in redox perturbations that negatively impact sulfate reduction to cysteine, and we speculate that this is mitigated by EcSAT-associated increased sulfur import into the seed, which facilitates additional synthesis of cysteine and glutathione. The data presented here reveal challenges associated with increasing the methionine content in rice seed, including what may be relatively low protein folding capacity in the endoplasmic reticulum and an insufficient pool of sulfate available for additional cysteine and methionine synthesis. We propose that future approaches to

further improve the methionine content in rice should focus on increasing seed sulfur loading and avoiding the accumulation of unfolded proteins in the endoplasmic reticulum. *Oryza sativa* ssp. *japonica*: urn:lsid:ipni.org:names:60471378-2.

Keywords: methionine, cysteine, nutritional quality, seed storage protein, serine acetyltransferase, cystathionine gamma-synthase, endoplasmic reticulum, *Oryza sativa*

INTRODUCTION

Unlike plants, all animals lack the enzymatic machinery to synthesize *de novo* some of the 20 proteinaceous amino acids. These so called "essential amino acids" must be consumed in their diet. Further, for optimal growth, these essential amino acids must be consumed in the right balance for the animal's metabolic needs. Amino acids that are in excess of amount defined by the first limiting amino acid will be catabolized, and the effective protein content of the feed will be reduced.

Methionine (Met) is one such essential amino acid, but the amount present in plant-based animal feed blends is typically insufficient optimal livestock growth and health. Cysteine (Cys) is not strictly considered an essential amino acid in the diets of animals because it can be synthesized from methionine, but in dietary situations where methionine is limited, cysteine becomes conditionally essential. Increasing the methionine and cysteine content of commodity cereals and grain legumes would benefit farmers by elevating the value of their crop and would be of benefit to livestock rearing by reducing the need for synthetic amino acid supplementation of animal feed.

Crops differ dramatically in how they store methionine. For example, in potato tubers 90% of the methionine is soluble (Dancs et al., 2008), while in alfalfa leaves (Amira et al., 2005) and cereal grains (Amir et al., 2018) almost all methionine is incorporated into protein. In tissues such as seeds that store Met predominantly in protein, a relatively direct approach to elevate the Met content is to increase the protein sink strength fraction by introducing genes for methionine-rich seed storage proteins (SSP). This approach assumes that the sink strength for methionine in endogenous seed proteins is relatively low, and this limits methionine accumulation in the seed. As seeds contain only low levels of free amino acids (Amir et al., 2018), this approach also assumes that the synthesis and/or metabolism of methionine is sensitive to signaled demand from SSPs. In order to achieve meaningful increases in protein-incorporated Met, the transgene needs to be highly expressed and the peptide/protein stable in the targeted tissue. Typically accumulation of foreign proteins is enhanced by targeting to the endoplasmic reticulum (ER) (Twyman et al., 2003). However, this can have the undesired consequence of overloading the protein folding and processing capacity of the ER (Oono et al., 2010; De Wilde et al., 2013).

Metabolic engineering of methionine biosynthesis is an alternative approach to increase methionine in the seed. The choice of which enzyme(s) to modify in which tissue(s) is complex and based on species-specific knowledge (or assumptions), such as where the methionine used in seed tissue for protein translation is synthesized, and in species capable of *de novo* Met synthesis in seeds, whether all steps of the sulfur assimilation pathway are also active in seeds as opposed to a pathway intermediate being transported into the seed. Additionally, one must consider if biosynthetic and transport pathways in other tissues can compensate for bottlenecks and limitations in the seed. The main assumption behind this metabolic engineering approach is that the pool size of free methionine and/or metabolic flux to methionine in the seed influence the profile of proteins synthesized.

Over the past several decades the general methods described above have been successfully used to substantially increase the methionine content of maize, soybean, and several other grain legumes (Molvig et al., 1997; Chiaiese et al., 2004; Song et al., 2013; Kim et al., 2014; Xiang et al., 2018; Amir et al., 2019). Although the quantity of rice used in livestock feed is currently dwarfed by other commodity crops (Global Rice Science Partnership, 2013), it is important to address improvement of rice protein quality. Among the major cereals, rice has the highest net protein utilization by livestock (Juliano, 1992). Furthermore, the regions of the world that cultivate maize and rice are globally distinct, and the development of rice varieties with increased methionine content would allow livestock farmers in rice-focused regions to reduce their reliance on blending higher methionine maize with soybeans for their livestock feed.

The sunflower seed albumin 2A, HaSSA, has attributes that make it an attractive choice for transgenic methods to study the effect of increased protein sink strength for sulfur amino acids (S-AA): it is remarkably dense in methionine and cysteine (16 and 8% by length, respectively) (Kortt et al., 1991), and it has been shown to be processed correctly in the seeds of several crops, which is important for transgene protein accumulation. Furthermore, it is rumen stable (Spencer et al., 1988; McNabb et al., 1994), making it suitable for blended sheep feeds, which need to be particularly rich in methionine for wool growth (Qi and Lupton, 1994). Based on positive results in lupin seed (Molvig et al., 1997), the *HaSSA* gene was introduced into rice under the control of a wheat glutelin (SSP gene) promoter and targeted to the endoplasmic reticulum (ER), where endogenous SSPs are post-translationally modified by disulfide bond formation and glycosylation (Hagan et al., 2003). By expressing HaSSA the goal was to "pull" additional S-AA, Met, and Cys into the seed protein fraction. Hagan and colleagues achieved high levels of HaSSA accumulation (to approximately 7% of total seed protein) in their transformed rice line, hereafter referred to as SSA (Hagan et al., 2003). At this level of accumulation, if the methionine incorporated into HaSSA was simply an additive to endogenous seed proteins at parental accumulation levels, then a 40% increase in total seed methionine would be expected in SSA

seeds. However, only a 25% increase in total seed methionine was observed, and due to high intra-line variation this increase was not considered statistically significant (Hagan et al., 2003). In addition to the gap between predicted and observed change in total seed methionine, the profile of expressed proteins in SSA seeds was clearly different from the parental rice cultivar, Taipei 309 (Hagan et al., 2003). Several of the major changes were consistent with the hypothesis that free methionine became strongly limiting in the SSA seeds and the heterologous protein diverted free methionine away from endogenous protein translation. These results suggested that sink strength is not the primary factor limiting methionine content in rice seeds and that subsequent efforts in rice should focus on increasing the supply of methionine in the seed.

To address the assumed deficiency in methionine supply in rice, two enzymes in the methionine biosynthetic pathway have been targeted for modification: cystathionine-gamma-synthase (CGS) catalyzes the first of three enzymatic steps to synthesize methionine from cysteine (Hesse et al., 2004); serine acetyl-transferase (SAT) catalyzes the formation of O-acetyl serine (OAS) which provides the carbon backbone for cysteine, the thiol precursor for methionine (Watanabe et al., 2015). In rice it is not known to what extent methionine for protein synthesis is synthesized *de novo* in the seed and to what extent it (or a precursor) is imported from another tissue such as leaves. With this in mind, a ubiquitin promoter was chosen to drive expression of heterologous transgenes coding for these key enzymes in S-AA biosynthesis (Nguyen et al., 2012; Whitcomb et al., 2018).

In the case of CGS, a feedback-desensitized version of the enzyme from Arabidopsis (AtD-CGS) was chosen. Heterologous expression *AtD-CGS* in tobacco (Hacham et al., 2008; Matityahu et al., 2013), soybean (Song et al., 2013), and azuki bean (Hanafy et al., 2013) resulted in large increases in free methionine in vegetative tissues and in seeds. However, heterologous expression of *AtD-CGS* in rice did not result in increased methionine in leaves or seeds despite persistently elevated CGS activity in leaves (enzymatic activity in seeds was not tested) (Whitcomb et al., 2018). We suggested that flux to methionine was increased in the *AtD-CGS* transgenic lines (hereafter referred to simply as CGS), but in rice the concentration of free methionine may be homeostatically regulated and the additional synthesized methionine catabolized, similar to results for lysine (Karchi et al., 1994).

Ubiquitin promoter-driven expression of *cysE* from *E. coli* (*EcSAT*) was found to be more successful in rice than ubiquitin promoter-driven expression of *AtD-CGS* (Nguyen et al., 2012; Whitcomb et al., 2018). While the concentration of free methionine remained unchanged in the seeds of the *EcSAT* transgenic lines (hereafter referred to simply as SAT), total methionine was significantly increased in some of the generated lines. These results suggested that methionine accumulation in SSA seeds (Hagan et al., 2003) may not be limited primarily by insufficient methionine synthesis but rather by insufficient cysteine synthesis.

Here we generated double transgenic lines, containing both increased sink strength ("pull") for methionine and increased cystine/methionine biosynthetic enzyme activity ("push"), to test whether combining these traits would result in a synergistic increase in rice seed methionine. This combinatorial approach has proved successful in maize, narbon bean, and potato (Demidov et al., 2003; Dancs et al., 2008; Planta et al., 2017), but to our knowledge, this is the first report to combine increased sink and source strength for methionine in rice. Specifically, we crossed SSA transgenic plants with the SAT transgenic line or the CGS transgenic line that we deemed most promising. Among the SAT rice lines generated by Nguyen et al. (2012), all had similarly high free cysteine (Cys) levels in their seeds. SAT47 was chosen for our "PushxPull" study because it showed the greatest increase in protein-incorporated methionine. Among the CGS lines generated by Whitcomb et al. (2018), CgSx4 was chosen because it had the highest measured CGS activity and marginally higher free methionine in seeds.

RESULTS

Expression of *AtD-CGS*, *EcSAT*, and *HaSSA* Transcripts and Accumulation of HaSSA Protein in Seeds

As a first step to characterize the seeds of the five transgenic lines used in this study we used RNA-seq data to determine transcript abundances of the *AtD-CGS* transgene and endogenous *CGS* genes, the *EcSAT* transgene and endogenous *SAT* genes, and the *HaSSA* transgene. The *AtD-CGS* and *EcSAT* transgenes are both driven by a maize ubiquitin promoter, and their transcripts were highly abundant in milkripe seeds, even after at least five generations post-transformation (**Figures 1A, B**). Considering only expressed genes in milkripe seeds, the *AtD-CGS* and *EcSAT* transgenes were expressed in the 97th and 99th percentiles, respectively, in this tissue. We identified one expressed endogenous *CGS* transcript (Os03g0376100, 76th percentile) and three expressed endogenous *SAT* transcripts (Os03g0133900, Os03g0196600, and Os05g0533500, 81st, 21st, and 24th percentiles, respectively) in milkripe seeds. The endogenous *CGS* transcript level was not significantly affected in any of the transgenic lines, but we did observe moderate upregulation of one of the endogenous *SAT* isoforms (Os05g0533500) in SSA seeds (1.6-fold relative to Taipei, padj < 0.001) and CGS × SSA seeds (1.4-fold relative to Taipei, padj < 0.02). We did not find any compensatory reduction in endogenous *CGS* or *SAT* transcripts in seeds expressing the *AtD-CGS* or *EcSAT* transgenes. These data show that at least one endogenous isoform of *CGS* and *SAT* is highly expressed in milkripe seeds. Therefore, transgene expression is likely to increase total enzymatic activity of the relevant methionine or cysteine biosynthetic step rather than to bring a new biosynthetic "trait" into the seeds.

Transcripts of the *HaSSA* transgene were also highly abundant in milkripe seeds (>99th percentile) (**Figure 1C**), but as a sink for methionine and cysteine, HaSSA protein levels are of greater importance. Equal quantities of the SDS-soluble protein fraction from mature seeds were separated by SDS-PAGE and Coomassie stained (**Figure 1D**). Hagan et al., 2003

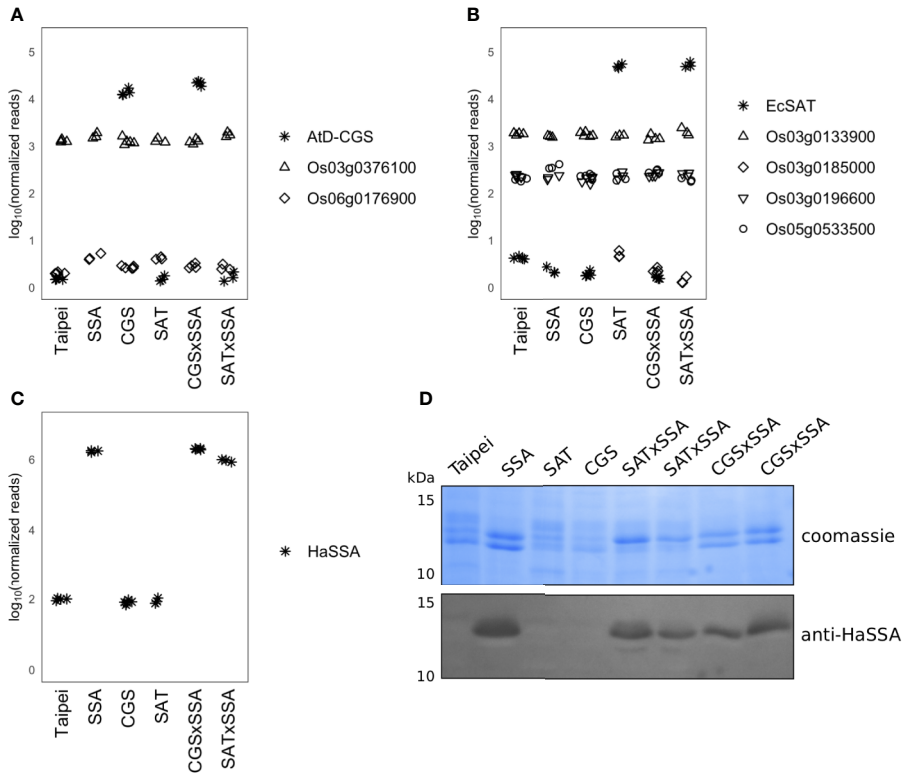

FIGURE 1 | Expression of CGS, SAT, and SSA transcripts and accumulation of SSA protein in seeds. Normalized RNAseq read counts in milkripe seeds for **(A)** the *AtD-CGS* transgene and rice *CGS* isoforms, **(B)** the *EcSAT* transgene and rice *SAT* isoforms, and **(C)** the *HaSSA* transgene are plotted on a $\log_{10}$ y-axis to facilitate comparison of expression levels between transgenes and endogenous isoforms. Each symbol in the plotting area **(A–C)** represents the reads from the milkripe stage seeds of an individual plant. Biological replicates: Taipei n = 4, SSA n = 3, CGS n = 5, SAT n = 3, CGS × SSA n = 4, SAT × SSA n = 3. Significance testing is presented in **Supplemental Table 1**. **(D)** The SDS-soluble protein fraction from mature seeds was subjected to 15% acrylamide SDS-PAGE followed by western blotting with a polyclonal anti-SSA antibody. Each lane contains 20 μg of protein extracted from the seeds of an individual plant. The western blot was performed at least three times. The data shown are representative.

reported HaSSA accumulation equivalent to approximately 7% of salt extracted seed protein (Hagan et al., 2003), but we were not able to clearly identify the HaSSA protein band in SDS-solubilized seed protein by Coomassie staining alone. Identification of the HaSSA protein band was achieved by western blotting with a polyclonal HaSSA antibody. We observed a similar level of HaSSA protein accumulation in the CGS × SSA and SAT × SSA seeds, but it did not appear to be higher than in the parental SSA line (**Figure 1D**), despite the increased expression of the S-amino acid biosynthetic enzyme transgenes (**Figures 1A, B**).

Seed Protein Profiles

The protein profile of SSA seeds is different from that of the parental Taipei as the abundance of several major SSPs is altered: reduction in glutelin acidic and basic subunits, reduction in alpha-globulin, and accumulation of prolamin 7/14 (Hagan et al., 2003; Islam et al., 2005). Since total S-AA and protein content of seeds was not significantly changed in SSA seeds, the authors concluded that production of HaSSA protein diverted the limited supply of free cysteine and methionine from endogenous relatively S-AA rich SSPs.

Based on these data, we expected *EcSAT* and/or *AtD-CGS* to suppress the altered protein profile phenotype of *HaSSA* in double transgenic seeds. However, the protein profiles of CGS × SSA and SAT × SSA seeds look very similar to SSA (**Figure 2**). In contrast to SSA, the 1D SDS-PAGE protein profiles of SAT and CGS appeared indistinguishable from Taipei (**Figure 2**). These data suggest that either additional S-AA production in EcSAT- and AtD-CGS-containing lines is insignificant or other factors besides S-AA limitation contribute to the altered seed protein profile of HaSSA-containing seeds.

Expression of Endoplasmic Reticulum Quality Control Genes

Other examples in rice seeds of highly expressed foreign proteins targeted to the secretory pathway have also resulted in significant changes in endogenous protein accumulation that partially overlap with those we observe in HaSSA-containing seeds (Takagi et al., 2005; Yasuda et al., 2005; Oono et al., 2010). Notably, the foreign proteins in these studies were not particularly rich in methionine or cysteine. More generally, strong expression of secretory pathway-targeted transgenes puts a heavy demand on the quality control machinery of the

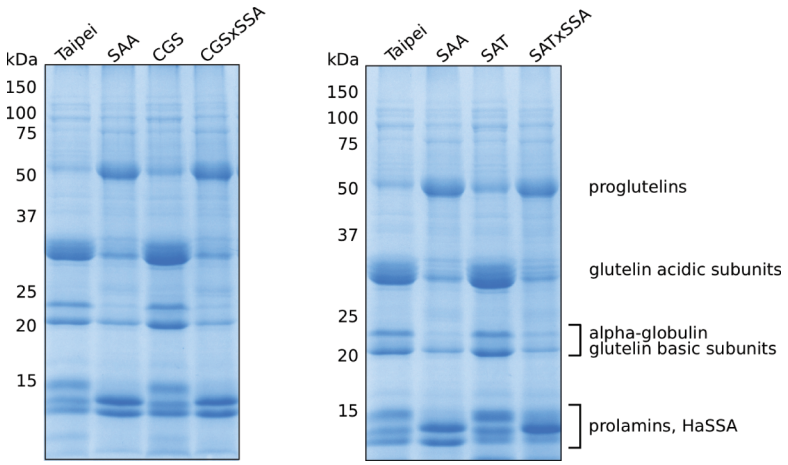

FIGURE 2 | Seed protein profiles of mature seeds. The SDS-soluble protein fraction from mature seeds was subjected to 13% acrylamide SDS-PAGE followed by Coomassie staining. Each lane contains 10 μg of protein extracted from the seeds of an individual plant. Protein band labeling is based on previously published data (Hagan et al., 2003; Yasuda et al., 2009). The protein extraction and SDS-PAGE were performed three times. The data shown are representative.

ER and can induce the unfolded protein response (UPR) in an attempt to maintain protein folding and modification fidelity as well as timely transport of proteins out of the ER to other destinations in the secretory pathway (Oono et al., 2010; De Wilde et al., 2013; Liu and Howell, 2016). The accumulation of glutelin precursors in the HaSSA-containing seeds (**Figure 2**) could indicate retention of proglutelin in the ER due to misfolding or insufficient trafficking of proglutelin out of the ER *via* COPII vesicles to the Golgi and eventually to protein storage vacuoles where it is proteolytically cleaved into acidic and basic subunits (Satoh-Cruz et al., 2010; Tian et al., 2013; Qian et al., 2015). Therefore, we investigated whether the altered protein profile in HaSSA-containing seeds may be associated with activation of an unfolded protein response (UPR) due to an overloaded ER protein processing machinery.

Specific changes characteristic of the UPR include increases in ER resident chaperone, co-chaperone, and protein disulfide isomerase expression (Liu and Howell, 2016). The most abundant chaperone system in the ER lumen is composed of ATP-regulated Hsp70 family chaperones (BiP), ATP-independent co-chaperones of the Hsp40 family (DnaJ) and a nucleotide exchange factor. Additional important chaperones include the Hsp90 family (GRP94) and the calnexin/calreticulin (CNX/CRT) proteins. Protein disulfide isomerases (PDIs) mediate disulfide bond formation, dissolution, and reformation and are critical for protein folding. Differential expression analysis of these chaperones, co-chaperones, and protein disulfide isomerases revealed a general upregulation in seeds of the three HaSSA-containing lines and only minor expression changes in seeds of SAT and CGS lines (**Figure 3**). Further, the major isoform in milkripe seeds of each enzyme family (BiP1 Os02g0115900, GRP94 Os06g0716700, CNX Os04g0402100, CRT Os07g0246200, and PDIL1-1 Os11g00199200) is strongly and significantly upregulated specifically in the HaSSA-containing lines. Minor isoforms BiP4 Os05g0428600 and PDIL2-3 Os09g0451500, the nucleotide exchange factor for Hsp70 chaperones (NEF Os09g0512700), and the electron acceptor for PDI-mediated disulfide bond formation (ERO1 Os03g0733800) were also found to be upregulated, further supporting a functional increase in ER protein folding capacity in HaSSA-containing seeds. Notably, we observed little if any attenuation of UPR gene upregulation in the CGS × SSA and SAT × SSA seeds, as might be expected if S-AA limitation for HaSSA translation were the cause of the increased chaperone expression.

Methionine, Cysteine, and Glutathione Levels in Mature Seeds

Published results from our group and others suggest that methionine content in rice is limited by both sink strength (the proportion of methionine codons in SSP transcripts) and by source strength (synthetic flux to S-AA) (Hagan et al., 2003; Lee et al., 2003; Nguyen et al., 2012; Whitcomb et al., 2018). Total seed methionine in SSA seeds was not significantly different from parental Taipei despite the strong accumulation of HaSSA protein (Hagan et al., 2003). We measured a comparable increase (25% compared to Hagan's 30%), but due to much lower intra-line variation in our data, the calculated p-value (<0.005) was found to be highly significant (**Figure 4A**). Our selected SAT line also showed increased total methionine relative to parental Taipei, but this increase was lower than reported by Nguyen et al. (2012) (1.45 fold compared to 4.75 fold) (**Figure 4A**). This disparity may be due to a different technical method for determining total amino acid concentration in the seed. We chose here a standard method used in food quality control and employed a company to run the respective analyses. Consistent with Whitcomb et al. (2018), ubiquitin promoter-driven

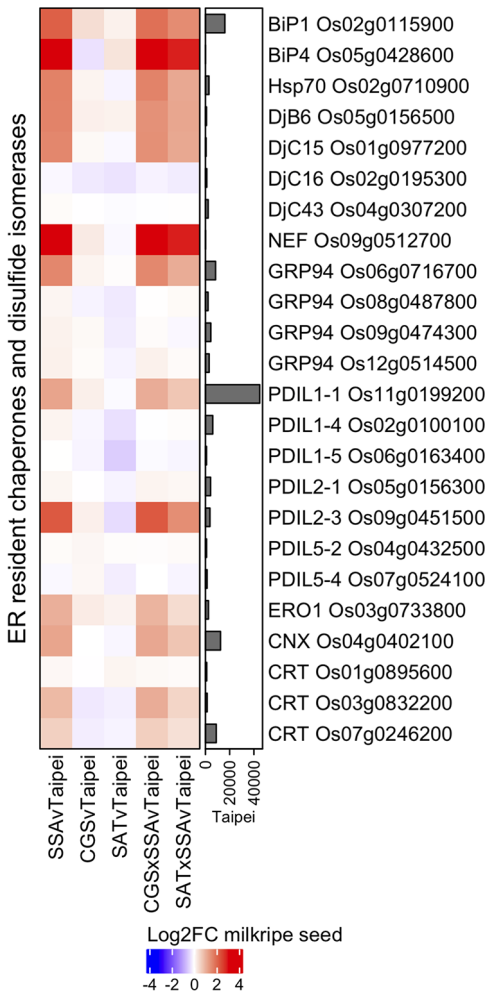

FIGURE 3 | Differential expression of ER chaperones, co-chaperones, and protein disulfide isomerases in milkripe seeds. Differential expression data are presented in a heatmap matrix of Log_2-fold change (Log2FC) relative to Taipei. The mean normalized read count in Taipei for each gene is presented in a bar graph annotation of the heatmap. Those ER resident chaperones (BiP, Hsp70, GRP94, CNX, CRT), co-chaperones (NEF, DjB, DjC), and protein disulfide isomerase (PDIL, ERO1) genes with a mean normalized read count > 1000 in at least one line are shown. Biological replicates: Taipei n = 4, SSA n = 3, CGS n = 5, SAT n = 3, CGS × SSA n = 4, SAT × SSA n = 3. Significance testing is presented in **Supplemental Table 1**.

expression of feedback-desensitized *AtD-CGS* did not result in an appreciable increase in total seed methionine (**Figure 4A**).

The primary question of our study was whether push and pull traits would synergistically interact when combined in the same rice plant to allow increased accumulation of methionine in the seed. The data give a different answer to this question depending on which "push" trait is used: increased activity in the cysteine biosynthesis pathway, or farther downstream in the methionine pathway specifically. Combining *EcSAT* and *HaSSA* in seeds, both of which successfully increased total Met individually, did not lead to a further increase. However, co-expression of *AtD-CGS* with *HaSSA* in the seed was found to synergistically affect total seed methionine: CGS × SSA seeds had higher total methionine than either parent and higher than the sum of total methionine level in each parent, but accumulation was not higher than in SAT and SAT × SSA seeds. Three transgenic lines (SAT, SAT × SSA and CGS × SSA) had total methionine levels comparable to those in IR64, a "high protein" variety, reflecting an increase of approximately 50% over the parental Taipei line (**Figure 4A**).

In our transgenic lines, the magnitude of changes in total cysteine in the seed was found to be smaller than those for methionine (**Figure 4B**). The HaSSA protein is extremely methionine-rich (16% by length), but it also has a higher proportion of cysteine residues (8%) than most rice seed proteins. Despite this characteristic, total cysteine was actually lower in SSA seeds than in Taipei; the observed increases in total methionine seemed to come at the expense of total cysteine in this line. Hagan et al., 2003 also observed a decrease in total cysteine in SSA seeds. SAT catalyzes the formation of OAS, the carbon backbone for cysteine synthesis, and as expected, expression of *EcSAT* resulted in an increase in total cysteine in the seed (Hagan et al., 2003). Combining *HaSSA* with *EcSAT* relieved the decrease in total Cys found in SSA seeds but did not lead to a further increase above *EcSAT* alone (as is true for total Met), and although cysteine is a substrate for AtD-CGS, no decrease in total cysteine was observed in CGS seeds.

The observed increase in S-AA content in SAT × SSA and CGS × SSA seeds (**Figure 4C**) could be explained by especially high HaSSA levels, but based on the SSA western blot (**Figure 1D**), HaSSA protein accumulation in the double transgenic lines was if anything slightly lower than in SSA alone. The total S-AA data (**Figure 4C**) taken together with the seed protein profiles (**Figure 2**) and ER chaperone gene expression patterns (**Figure 3**) argue for an ER-stress based mechanism for seed protein profile change in HaSSA-containing seeds, rather than a redistribution of dramatically limited S-AA supply.

In rice seeds the proportion of S-amino acids that remain free rather than incorporated into polypeptides is extremely small. In the case of methionine, the average total pool size in Taipei was measured to be 2 g/kg dry weight (DW), which is equivalent to approximately 13,000 pmol/mg DW, while the average measured free methionine concentration was only approximately 1.4 pmol/mg DW. Highly significant differences in free methionine concentration were observed, but given how small the pool of free methionine is relative to the total pool size it is unclear whether these differences have any biological relevance (**Figure 4D**). While the total quantity of methionine and cysteine stored in the rice seed are very similar (both approximately 2 g/kg DW) (**Figures 4D, E**), the proportion that remains soluble is approximately 10-fold higher for Cys than for Met. We found a strong accumulation of free Cys in EcSAT-containing lines, as expected from literature. However, the level of accumulation was not attenuated by the presence of the strong sink for S-AA in the form of HaSSA protein (**Figure 4E**).

Glutathione (GSH), a tripeptide of cysteine, glutamic acid, and glycine, is a major metabolic product of cysteine, and is at least an order of magnitude more abundant in mature rice seeds

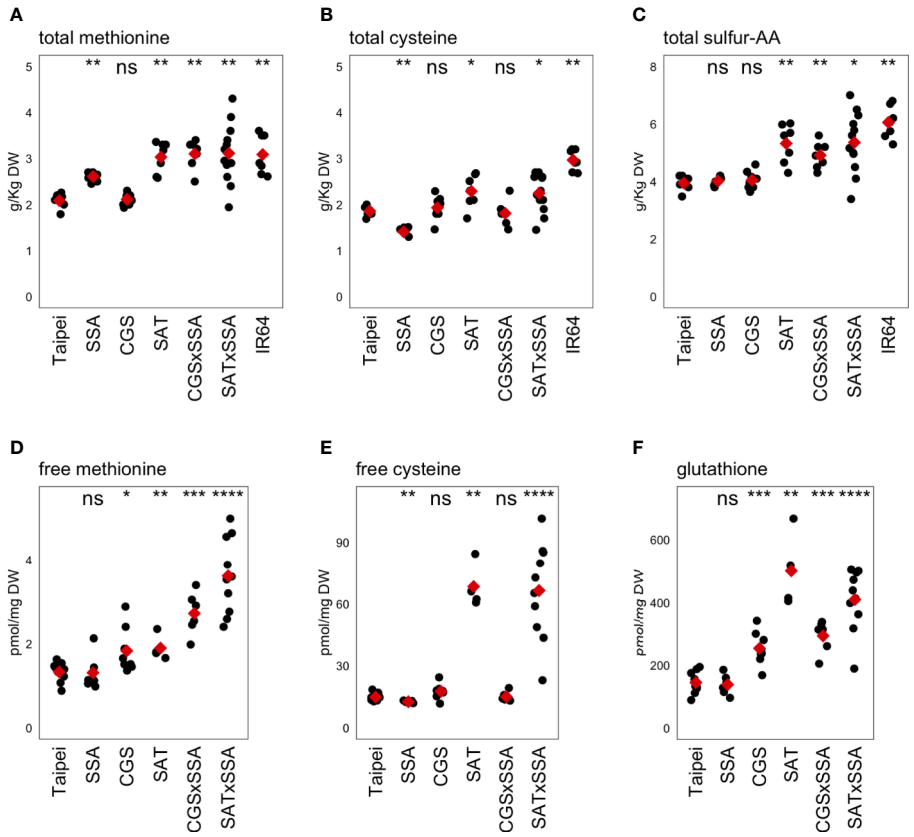

FIGURE 4 | Methionine, cysteine, and glutathione levels in mature seeds. The concentrations of the sulfur-containing amino acids methionine **(A, D)** and cysteine **(B, E)** as well as the cysteine-containing tripeptide glutathione **(F)** were determined in mature seeds. The concentration of total sulfur-amino acids (S-AA) was determined by adding the total concentration of methionine and cysteine in the same seed sample **(C)**. Each black dot indicates the measured concentration in the seeds from an individual plant. The mean concentration in each line is indicated by a red diamond. The data presented are from two independent experiments. Wilcoxon rank-sum test was performed to compare the median concentration in each line to the median of Taipei. The significance level of each test is designated: ns (not significant) for $p > 0.05$, * for $p \leq 0.05$, ** for $p \leq 0.01$, *** for $p \leq 0.001$, and **** for $p \leq 0.0001$.

than free cysteine. The two transgenic lines with the highest total cysteine and free cysteine, SAT and SAT × SSA, also had the highest GSH levels (**Figure 4F**). Interestingly, GSH also accumulated somewhat in AtD-CGS-containing lines, despite no increase in cysteine concentration, suggesting that increased cysteine synthesis occurs in AtD-CGS-containing seeds, but that it is diverted to downstream products such as GSH.

Sulfate Levels and Sulfur Pools

Unexpectedly, the sulfate concentration in mature seeds was found to be approximately four-fold higher in EcSAT-containing seeds than in all other lines (**Figure 5A**). SAT and SAT × SSA plants also had approximately four to seven-fold higher sulfate levels in their leaves (**Figures 5B, C**).

Our goal was to generate rice seeds enriched in S-AA. This either requires the seed to import more sulfur from other parts of the plant for assimilation into cysteine and methionine or to redistribute the existing sulfur pools to S-AA, or a combination of these two mechanisms. To assess whether redistribution of sulfur or additional import was driving the significantly elevated S-AA levels in SAT, SAT × SSA, and CGS × SSA seeds, we measured the total sulfur content. SAT and SAT × SSA seeds showed large increases in total sulfur (56 and 41% respectively). Although more subtle, CGS × SSA seeds also contained elevated total sulfur, and the size of that increase (13%) was comparable in size to the increase in S-AA in this line (**Figure 5D**). These data suggest that increased import of sulfur into the seed, rather than redistribution, underlies the increase in total Cys and Met in the seed of SAT, CGS × SSA, and SAT × SSA plants. In the case of EcSAT-containing seeds, the increase in total sulfur is substantially greater than the increase in S-AA, indicating that there are other sulfur-compound pools in these seeds that experience an increase. Although SAT and SAT × SSA seeds had large relative increases in sulfate and GSH, both major transport forms of sulfur, the magnitude of these pool size changes do not account for the large increase in total sulfur in these seeds. In fact, the *EcSAT* transgene had a larger effect on the size of the "sulfur-other" pool (sulfur not contained in the sulfate, GSH, or S-AA pools) than on sulfate, GSH, or S-AA (**Figure 5E**). Resolution of the identity of the differentially accumulating

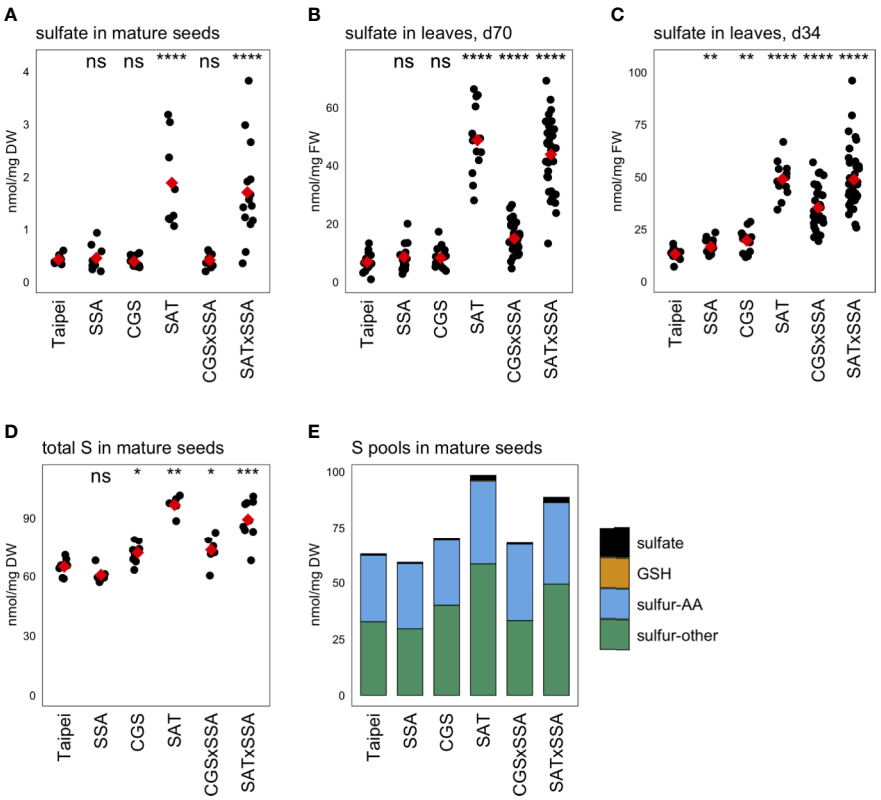

FIGURE 5 | Sulfur pools. The concentration of sulfate was determined in **(A)** mature seeds and leaves from plants **(B)** 70 days (d70) after transplantation and **(C)** 34 days (d34) after transplantation. The total sulfur (S) in mature seeds was also determined **(D)**. Each black dot indicates the measured concentration in the specified tissue from an individual plant. The mean concentration in each line is indicated by a red diamond. The data presented are from two independent experiments. Wilcoxon rank-sum test was performed to compare the median concentration in each line to the median of Taipei. The significance level of each test is designated: ns (not significant) for $p > 0.05$, * for $p \leq 0.05$, ** for $p \leq 0.01$, *** for $p \leq 0.001$, and **** for $p \leq 0.0001$. For those mature seed samples for which total S, sulfate, GSH, total Met, and total Cys were determined, the mean concentration of each of these sulfur pools was calculated for each line. The S-other pool is the remainder of the sulfate, GSH, total Met, and total Cys concentrations subtracted from the total S concentration in each sample. The absolute and relative sizes of sulfur pools in mature seeds are visualized in a stacked bar graph **(E)**. Biological replicates for the S pools analyses: n = 12 for all lines except SAT × SSA, for which n = 28.

sulfur-containing metabolites in this pool was beyond the scope of our study and remains an interesting open question.

Relative Transcript Abundance of Sulfate Transporters, S-Assimilatory Enzymes, and S-Methylmethionine Degradation Enzymes

Various S-compounds are known to be transported between tissues in different plant species (Gigolashvili and Kopriva, 2014). One of the most mobile S-compounds is sulfate. Sulfate transporters (SULTRs) are a family of proteins that can be classified into four groups based on specifics of their function and localization (Takahashi et al., 2011). The rice genome contains 13 SULTRs, the expression of which were determined in milkripe rice seeds in order to assess whether transcriptional regulation of these genes might provide evidence that increased sulfate import contributes to the observed differences in total sulfur in mature seeds (**Figure 6A**). Among the 13 rice SULTRs, we found the highest expressed were group 3 and group 4 transporters, which are responsible for intracellular sulfate transport (into plastids and out of vacuoles, respectively). High-affinity, plasma membrane-localized transporters in the SULTR group 1, which could be expected to contribute to sulfate import from source tissues, were notably expressed at much lower levels, with SULTR1;1 Os03g0195800 and SULTR1;2 Os03g0196000 close to the detection limit. This may explain the remarkably low level of sulfate in rice seeds. Three SULTRs were found to be differentially expressed in transgenic lines: SULTR4;1 Os09g0240500, SULTR1;3 Os08g0406400 and SULTR1;1 Os03g0195800. While the two group 1 SULTRs are likely plasma membrane-localized and were strongly and significantly induced, their absolute expression remained very low, and neither were upregulated in EcSAT-containing seeds. This suggests that additional S in these seeds is not due to increased transcription of plasma membrane localized transporters. However, these data do not exclude the possibility that SULTR activity may be differentially regulated post-transcriptionally or that sulfate flux into the seed may vary based on the concentration of sulfate in the phloem. In fact, the

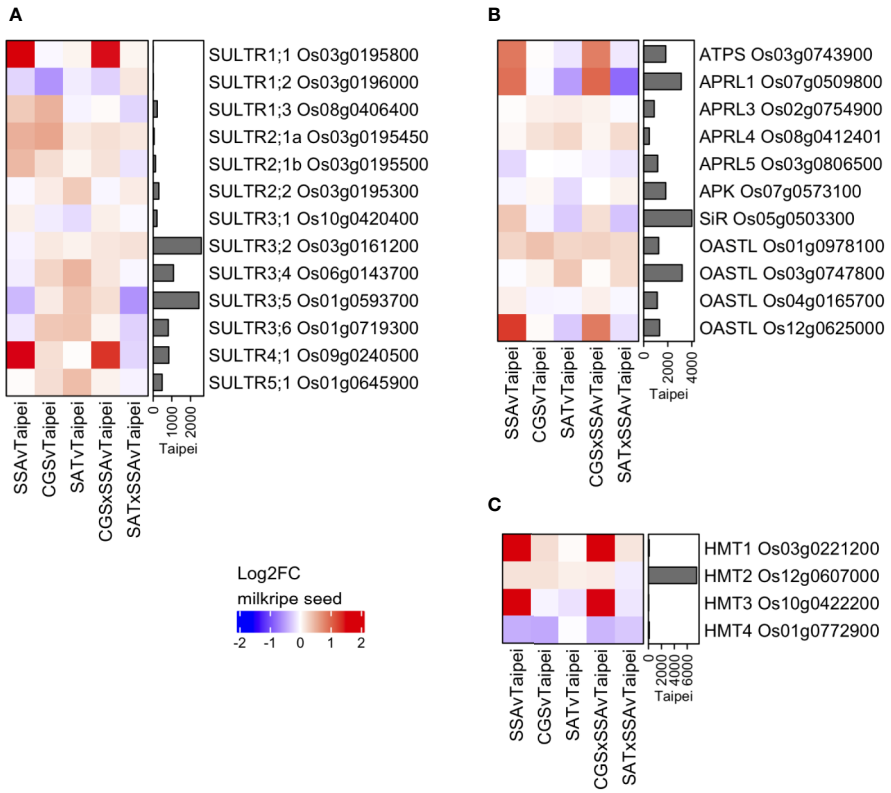

FIGURE 6 | Differential expression of genes for sulfate transporters, S-assimilatory enzymes, and SMM degradation enzymes in milkripe seeds. Differential expression data are presented as heatmap matrices of Log_2-fold change (Log2FC) relative to Taipei. The mean normalized read count in Taipei for each gene is presented in a bar graph annotation of the heatmap. All 13 genes annotated as sulfate transporters (SULTRs) in rice **(A)** and all four genes annotated as homocysteine methyltransferases (HMT) in rice **(C)** are shown. Annotated ATP sulfurylase, APR reductase, APR kinase, sulfite reductase, and OAS-thiol-lyase genes with a mean normalized read count > 500 in at least one line are shown **(B)**. Biological replicates: Taipei n = 4, SSA n = 3, CGS n = 5, SAT n = 3, CGS × SSA n = 4, SAT × SSA n = 3. Significance testing is presented in **Supplemental Table 1**.

measured sulfate concentration in leaves from SAT and SAT × SSA plants was found to be 6 to 7-fold higher than Taipei (**Figures 5B, C**). Notably, we observed strong upregulation of SULTR4;1, but only in SSA and CGS × SSA (**Figure 6A**). SULTR4;1 has been shown to be localized to the tonoplast and is likely involved in sulfate efflux from this intracellular storage compartment (Kataoka et al., 2004; Zuber et al., 2010). Sulfate, whether imported across the plasma membrane or released from vacuolar storage, is reduced and assimilated into cysteine or adenosine 3′-phospho 5′-phosphosulfate (PAPS) in several enzymatic steps. Mirroring the differential expression pattern of SULTR4;1, at least one isoform of each enzyme in the sulfate assimilation pathway is transcriptionally upregulated in both SSA and CGS × SSA milkripe seeds: ATP sulfurylase (ATPS) Os03g0743900, adenosine 5′-phosphosulfate reductase 1 (APRL1) Os07g0509800, sulfite reductase (SiR) Os05g0503300, O-acetylserine (thiol) lyase (OASTL) Os12g0625000 (**Figure 6B**). Transcriptional upregulation of these enzymes and the vacuolar SULTR in SSA and CGS × SSA seeds could be the result of especially high unmet demand for reduced sulfate in these lines.

Another major inter-tissue transport form of sulfur is GSH (Kuzuhara et al., 2000). Two GSH transporters have been identified thus far in rice, OsOPT3 and OsOPT6 (Zhang et al., 2004; Wongkaew et al., 2018). OsOPT6 transcripts were below the detection limit in milkripe seeds, and OsOPT3 transcripts were expressed at an extremely low level (data not shown). Unless their expression strongly increases later in seed maturation, GSH is unlikely to be more than a very minor form of sulfur transported into the seed and cannot explain the differential accumulation of sulfur.

Two methionine-derived sulfur-containing metabolites, S-methylmethionine (SMM) and S-adenosylmethionine (SAM), are also potential forms of sulfur imported into the seed. SMM is readily detected in rice seedlings (Menegus et al., 2004), and the importance of SMM in inter-tissue sulfur transport has long been suggested (Bourgis et al., 1999; Tan et al., 2010; Cohen et al., 2017). Thus far there are no transmembrane transporters identified for SMM in plants (Gigolashvili and Kopriva, 2014), and therefore their expression pattern in seeds cannot be checked. But if increased SMM import underlies the differential accumulation of sulfur, then one might expect

enzymes involved in SMM metabolism to be differentially regulated. Methionine can be generated from SMM and homocysteine in one step *via* the action of homocysteine S-methyltransferase (HMT). Of the four annotated HMTs in rice, two are strongly upregulated in SSA and CGS × SSA seeds, but are expressed at much lower levels than the major HMT isoform in seeds, HMT2, which showed only very minor expression changes in all our transgenic lines (**Figure 6C**). Whether upregulation of the minor isoforms, HMT1, and HMT3 results in higher flux of SMM to methionine in these seeds remains unclear, and the transcript data provide no evidence that differential SMM transport into the seed is relevant for the observed sulfur accumulation. SAM transmembrane transporters are represented by a family of seven genes in rice (GO:0000095). However, transcripts for all seven were expressed at only low levels in milkripe seeds, and none were deemed differentially regulated relative to Taipei (data not shown).

Taken together, expression patterns of S-compound transporters do not point to a specific S-compound that is increasingly imported into seeds with elevated S-AA contents. Of course, it remains possible that the import activity of specific S-compound transporters is increased in the absence of mRNA accumulation. Given the very high levels of sulfate in SAT and SAT × SSA leaves, these lines may have higher phloem concentrations of sulfate and thereby increased import of sulfate into the seed.

OAS and OAS-Cluster Gene Expression in Milkripe Seeds

OAS is often considered an indicator of sulfur deficiency or, alternatively, a signaling molecule responsive to sulfur deficiency. In the seeds of SSA and CGS × SSA lines exists an interesting situation where OAS (**Figure 7A**) and many transcriptional markers of sulfur deficiency (**Figure 6**) accumulate while the sulfate and total sulfur concentration in these seeds is not reduced relative to Taipei (**Figures 5A, D**). Since EcSAT catalyzes the formation of OAS, it was initially surprising that OAS does not accumulate in SAT seeds and that *EcSAT* expression suppresses HaSSA-associated OAS accumulation in the double transgenic seeds.

Hubberten et al., 2012 identified a cluster of six genes in Arabidopsis whose expression is highly correlated with OAS accumulation in a variety of conditions, including sulfur-deficiency and oxidative stress (Hubberten et al., 2012). The so-called OAS-cluster in Arabidopsis is composed of APR3, SDI1, SDI2, LSU1, SHM7/MSA1, and ChaC-like. With the exception of SDI1 and SDI2, multiple orthologs of each Arabidopsis gene are annotated in the rice genome. At least one ortholog of each OAS-cluster member was found in our data to be strongly and significantly upregulated in SSA and CGS × SSA seeds but not in SAT or SAT × SSA (**Figure 7B**), *i.e.* specifically in those lines with elevated OAS levels (**Figure 7A**).

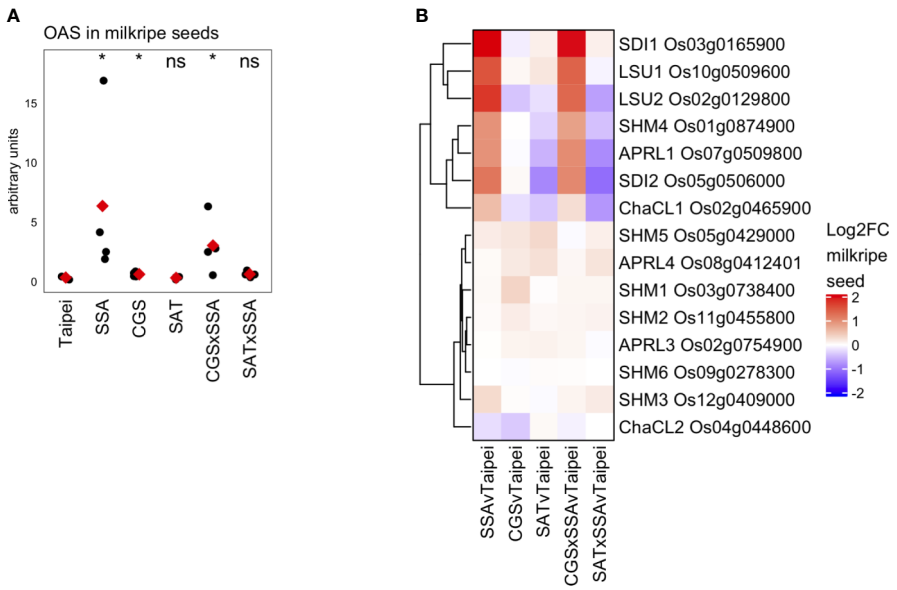

FIGURE 7 | OAS accumulation and differential expression of OAS-cluster genes in milkripe seeds **(A)** The relative abundance (arbitrary units) of O-acetylserine (OAS) in milkripe seeds is presented. Each black dot indicates the determined relative abundance in the seeds of independent individual plants (n = 4). The mean abundance in each line is indicated by a red diamond. Wilcoxon rank-sum test was performed to compare the median accumulation in each line to the median of Taipei. The significance level of each test is designated: ns (not significant) for $p > 0.05$, * for $p \leq 0.05$. **(B)** Differential expression data for the 15 putative orthologs in rice of the 7 so-called "OAS-cluster" genes in *Arabidopsis thaliana* are presented as a heatmap of Log_2-fold change (Log2FC) relative to Taipei with genes clustered hierarchically using Euclidean distance metric and average linkage. Biological replicates: Taipei n = 4, SSA n = 3, CGS n = 5, SAT n = 3, CGS × SSA n = 4, SAT × SSA n = 3. Significance testing is presented in **Supplemental Table 1**.

DISCUSSION

The HaSSA-Associated Seed Protein Profile May Result From Insufficient ER Folding Capacity Rather Than Insufficient S-AA Provision

We generated so-called "Push × Pull" lines by combining a strong S-AA sink with cysteine or methionine biosynthesis transgenes with the idea that increased production of S-AA would allow for high levels of HaSSA accumulation without downregulation of endogenous relatively S-rich SSP. However, the seed protein profile phenotype of SSA was not reverted to control composition by co-expression with either *AtD-CGS* or *EcSAT* (**Figure 2**), despite higher total S-AA levels in both double transgenic lines (**Figure 4C**). Specifically, total methionine was determined to be 20% higher in CGS × SSA and SAT × SSA seeds than in SSA (**Figure 4A**), and total cysteine was found to be 30 and 60% higher, in CGS × SSA and SAT × SSA, respectively, than in SSA (**Figure 4B**). These data suggest that the seed protein profile phenotype observed by Hagan et al. (2003) and Islam et al. (2005) in SSA rice seeds was not necessarily the result of insufficient S-AA supply and preferential incorporation into HaSSA.

Perhaps the most noticeable change in the SSA seed protein profile is to the glutelin component. Glutelins are referred to in Islam et al. (2005) as being relatively S-AA rich and their decrease in SSA seeds is used as evidence of S-AA redistribution. But with only 0.1–2.4% S-AA, we would instead characterize glutelins as having merely low or intermediate S-AA density, falling on the left side of the S-AA density distribution of SSPs and proteins coded for by the top 1% expressed transcripts in rice seeds (**Supplemental Figure 1**). Furthermore, it is not clear from data presented in Hagan et al. (2003) or Islam et al. (2005) whether the total glutelin content (proglutelin plus proteolytically cleaved glutelin subunits) of SSA seeds is altered. Given the lack of clear reduction in total glutelin levels and its low to intermediate S-AA density, we considered the possibility that accumulation of proglutelins and the reduction in glutelin subunits were symptoms of insufficient protein processing in the ER rather than a consequence of S-AA limitation. Direct reduction of the folding capacity of the rice endosperm ER has been achieved by deficiency in a primary chaperone in the ER lumen, PDIL1-1. In PDIL1-1-deficient seeds, proglutelin strongly accumulated and processed glutelin subunits were strongly reduced (Satoh-Cruz et al., 2010). Proglutelin also accumulated in seeds with a genetic block to secretory protein transport out of the ER to the Golgi *via* COPII vesicles (Tian et al., 2013; Qian et al., 2015).

In addition to differential accumulation of proglutelin and glutelin subunits, alpha-globulin levels are reduced in HaSSA-containing seeds. Unlike glutelins, alpha-globulin is S-AA dense, with 5.9% methionine and 4.3% cysteine by length (**Supplemental Figure 1**). But reduction in this S-AA rich SSP is also consistent with overloaded ER protein folding capacity due to high *HaSSA* expression. High expression of other foreign proteins and peptides targeted to the ER in rice seeds can produce seed protein profiles very similar to that of SSA, irrespective of the S-AA content of the highly expressed foreign protein. For example, transgenic rice seeds expressing dimers of 42 amino acid beta-amyloid peptides (Ab1-42) have strong accumulation in proglutelins and reductions in alpha-globulin levels despite the transgenic peptide containing zero cysteine residues and having only intermediate methionine density (2.4% by length) (Oono et al., 2010). Transgenic rice expressing seven tandem human T-cell epitopes to Japanese Cedar pollen (7Crp) also show increased proglutelins and decreased alpha-globulin (Takagi et al., 2005). The transgenic peptide contains zero methionines and is 3% cysteine by length. Importantly, the seed protein profile phenotype in 7Crp seeds depends upon the expression strength of the 7Crp peptide. At low expression levels, the seed protein profile looks very similar to untransformed seeds (Takaiwa et al., 2007), while at five-times higher expression, proglutelin accumulated and alpha-globulin was clearly reduced (Takagi et al., 2005). Not only were the seed protein profiles of the beta-amyloid and 7Crp rice seeds similar to SSA, CGS × SSA, and SAT × SSA, but a similar set of ER resident chaperones and co-chaperones is upregulated, including BiP1 Os02g0115900, BiP4 Os05g0428600, Hsp70 Os02g0710900, NEF Os09g0512700, GRP96 Os06g0716700, CNX Os04g0402100 and CRT Os03g0832200, presumably as a response to increased demand for folding capacity in the ER. Based on the data above, we propose that the seed protein profile phenotype in HaSSA-containing seeds is primarily a non-specific effect of ER protein folding capacity overload, rather than S-AA limitation.

Lupin seeds have also been targeted for high HaSSA accumulation (Molvig et al., 1997), and despite similar relative levels of exogenous protein accumulation (5% of total protein in lupin, 7% in rice), the authors did not observe a large change in the seed protein profile. This raises the question, is rice particularly susceptible to ER overloading? Rice has the lowest grain protein content amongst major cereals (Juliano, 1992) which perhaps limits the seed's capacity to synthesize foreign proteins without producing stress in the ER. Rice seeds also have extremely low levels of available sulfur (in the form of sulfate) in comparison to some other crops (Molvig et al., 1997; Chiaiese et al., 2004; Shinmachi et al., 2010) which may prevent meaningful increases in GSH synthesis when there is greater than normal protein folding load in the ER. The precise role of GSH in the ER is still under investigation, but there are strong indications that GSH may be critical for reduction and PDI-mediated isomerization of non-native disulfide bonds (Chakravarthi et al., 2006). Misfolded proteins containing non-native disulfide bonds would be expected to accumulate in situations where the ER protein-folding machinery is under heavy load due to strong expression of ER targeted foreign transgenes such as *HaSSA*. Furthermore, some level of oxidative stress due to H_2O_2 production is intrinsic to disulfide bond formation in the ER (Harding et al., 2003). An overloaded ER that is not able to sufficiently correct and resolve misfolded proteins can result in H_2O_2 production significant enough to alter the glutathione redox state (Ozgur et al., 2014; Dietz et al., 2016) and to influence the cytosolic redox potential (Lai et al., 2018). Therefore, in the context of an overloaded ER protein folding

machinery, it might be adaptive to specifically downregulate expression of SSPs with very high S-AA density, such as S-rich 10kDa prolamin (Hagan et al., 2003), so that cysteine could then be repurposed for GSH synthesis.

HaSSA Provokes a Sulfur Deficiency-Like Molecular Phenotype in Rice Seeds That Is Suppressed by Co-Expression With *EcSAT* but Not *AtD-CGS*

In addition to the seed protein profile phenotype described above, we also found an association between the *HaSSA* transgene and a S-deficiency-like molecular phenotype (**Figure 6**, **Figure 7**), despite no reduction in total sulfur (**Figure 5D**). The strongest gene expression changes include upregulation of S-assimilation pathway genes SULTR1;1 Os03g0195800, SULTR4;1 Os09g0240500, ATPS 0s03g0743900, APRL1 Os07g0509800, SAT Os05g0533500, and OASTL Os12g0625000. OAS and the OAS-cluster genes (Hubberten et al., 2012) also accumulated specifically in the same set of lines. OAS has previously been shown to accumulate in chickpea seeds expressing high levels of HaSSA protein (Chiaiese et al., 2004). The HaSSA-associated S-deficiency molecular phenotype described here is presumably the result of signaling of especially high S-AA demand for seed protein translation or of ER protein folding overload and moderate oxidative stress, both of which generate a higher need for cysteine.

Unlike the seed protein profile phenotype, the main features of the HaSSA-associated S-deficiency molecular phenotype are suppressed by co-expression of *EcSAT* (**Figures 6** and **7**). Notably, OAS, the product of SAT enzymatic activity, does not accumulate in the seeds of EcSAT-containing plants (**Figure 7A**) despite very strong expression of the transgene and no compensatory reduction in endogenous SAT transcript levels in this tissue (**Figure 1B**). While initially surprising, these results are very similar to other published studies that also used a Cys-sensitive isoform of SAT as their transgene. Transgenic Arabidopsis that highly expressed a Cys-sensitive SAT from watermelon also had no OAS accumulation despite high measured SAT activity and increased GSH concentration, suggesting that additional OAS was synthetized but it was readily converted to Cys, which was then incorporated into GSH (Noji and Saito, 2002). Similarly, Hopkins et al. measured OAS levels in *EcSAT* (Cys-sensitive) transgenic potato that were similar to WT (Hopkins et al., 2005). Our EcSAT isoform is cysteine-inhibited and indeed the concentration of free cysteine is significantly higher in SAT and SAT × SSA seeds. This suggests that OAS production is essentially buffered by negative feedback at the level of EcSAT activity and additional OAS synthesized by EcSAT is quantitatively consumed by OASTL activity and converted to cysteine. Such complete conversion to cysteine of the additional OAS produced by the same *EcSAT* transgene has already been shown *in vitro* (Harms et al., 2000). OASTL Os030747800, the highest expressed OASTL isoform in milkripe seeds, is moderately yet significantly (padj < 0.0001) upregulated, specifically in SAT-containing seeds, perhaps facilitating the conversion of the additional OAS produced in these transgenic lines.

OAS is expected to accumulate in situations where the supply of sulfide is insufficient for the OAS available for formation of cysteine by OASTL. The production of sulfide from sulfate requires the contribution of eight electrons from reductants. As shown in **Figure 3**, seeds from all three of our HaSSA-containing lines showed signs of ER stress in the form of strong upregulation of UPR genes. Conditions that result in an overloaded protein folding machinery in the ER have been linked to perturbed redox status (Ozgur et al., 2014), and OAS is known to accumulate in situations of oxidative stress, such as menadione treatment (Lehmann et al., 2009). We propose that strong *HaSSA* expression may result in reduced availability of reductant (GSH and ferredoxin) for APR and SiR, a lower sulfide: OAS ratio than in non-HaSSA-containing seeds, and as a consequence, OAS accumulation. Furthermore, we suggest that the *EcSAT* transgene results in a large enough increase in sulfur import into the seed (**Figure 5D**) for the sulfate reduction pathway to produce enough sulfide to keep OAS from accumulating in SAT × SSA seeds (**Figure 7A**). Expression of the *AtD-CGS* transgene also increases S-import into the seed, but not enough to keep the flux to sulfide high enough for the additional S-AA demanded by HaSSA translation and folding. Flux from sulfate to sulfide may also be increased in SAT × SSA seeds compared to SSA and CGS × SSA due to additional synthesis of GSH (the electron donor for APR) (Bick et al., 1998) (**Figure 4F**) and ferredoxin (the electron donor for SiR) (Krueger and Siegel, 1982) made possible by a larger pool of synthesized cysteine.

Given the importance of thiol-based antioxidant systems in mitigating oxidative stress (Ulrich and Jakob, 2019), it is reasonable that sulfur assimilation, and cysteine synthesis in particular, would be enhanced under such conditions. In fact, the activities of both APR and SAT have been shown to increase during oxidative stress. The activity of the Arabidopsis APR1 isoform increases under oxidative conditions, probably *via* disulfide bond formation (Bick et al., 2001). Soybean plastidic SAT has been shown to be phosphorylated under oxidative stress, resulting in a loss of feedback inhibition by cysteine and increased activity (Liu et al., 2006). Although there is no evidence of SAT regulation by phosphorylation in Arabidopsis, the chloroplast cyclophilin CYP20-3 participates in folding of AtSAT1 in a redox-dependent fashion, to enhance the activity of AtSAT1 and to affect thiol contents (Dominguez-Solis et al., 2008). Additionally, it was recently shown that the availability of (reduced) GSH in Arabidopsis and tobacco positively affects S-assimilation downstream of APR activity, including the steady state concentration of cysteine and methionine (Cohen et al., 2020). The data presented in this study support that redox regulation of sulfate assimilation and cysteine synthesis also occurs in rice.

Improving Nutritional Quality of Seeds

Using a set of S-AA "push", "pull" and "Push × Pull" lines, we show that multiple paths can lead to higher seed methionine in rice. First, ubiquitin promoter-driven *EcSAT* is sufficient on its

own to produce rice seeds with 50% higher total methionine content (**Figure 4A**). This demonstrated that there is an accessible path in rice seeds to higher methionine that does not require increasing the protein sink for methionine. This transgenic line was produced to "push" cysteine synthesis, but unexpectedly, we found that the transgene had the effect of increasing sulfur content in the seed (**Figure 5D**). As indicated above, rice seeds have very little available sulfate relative to some other cereals (Shinmachi et al., 2010) and grain legumes (Molvig et al., 1997; Chiaiese et al., 2004), and this characteristic may influence the capacity for increased accumulation of S-AA and GSH in the tissue. The relative contribution of increased SAT activity and increased sulfur supply to the resultant improvement in seed protein quality in SAT transgenic seeds remains to be investigated.

Second, while ubiquitin promoter-driven *AtD-CGS* and glutenin promoter-driven *HaSSA* are ineffective on their own, in combination they synergistically interact to result in seeds with higher seed methionine (**Figure 4A**). Like *EcSAT*, but to a lesser extent, the *AtD-CGS* transgene results in increased seed sulfur content, some of which is incorporated into cysteine (**Figure 5D**). AtD-CGS is ineffective on its own because the cysteine available as a substrate for CGS might be tightly regulated in the plastid and flux to GSH might be prioritized over methionine (**Figure 4F**). Translation of the large number of *HaSSA* transcripts produced in the developing seed has the potential to "pull" significant quantities of additional methionine into the seed. In fact, the *HaSSA* transgene has been successfully used to increase the methionine content of lupin seeds (Molvig et al., 1997) and chickpeas (Chiaiese et al., 2004). In both cases, total seed sulfur remained nearly constant, but the concentration of sulfate in the seed dropped significantly, suggesting that the additional methionine demanded by HaSSA protein accumulation required increased assimilation of the existing sulfate pool. In rice seed, the concentration of sulfate relative to total sulfur is remarkably low relative to both lupin and chickpea (approximately 1, 30, and 20% of total S in rice, lupin, and chickpea, respectively) (Molvig et al., 1997; Chiaiese et al., 2004). Introduction of the new sink HaSSA seems insufficient to induce S-AA biosynthesis in the seed or to trigger sulfate uptake. Further, the load HaSSA puts on the ER for its folding appears to generate significant stress, including oxidative stress. In particular, the high number of Cys residues in HaSSA may amplify the folding load since formation of incorrect disulfide bridges (which need to be resolved and the correct bridges formed) compounds with each additional cysteine in the peptide. Because oxidizing environments promote disulfide bond formation this effect may be especially strong when the ER is experiencing stress since the stress produces ROS. Dissolution of incorrect disulfide bonds oxidizes GSH to GSSG (Chakravarthi et al., 2006), reducing the pool of reductants available for sulfate to sulfide reduction for eventual Cys and Met amino acid synthesis. *AtD-CGS* and *HaSSA* are effective in combination because they relieve deficiencies in the other. *AtD-CGS*-mediated increase in S-import results in additional flux to Cys, which is further pulled into Met synthesis due to strong sink in the form in HaSSA (**Figure 4A**). In the context of this strong sink for Met, the relative prioritization of synthesized Cys for GSH synthesis is weaker. HaSSA-associated decrease in reductant supply for sulfate reduction is complemented by increased supply of S for assimilation to Cys and Met.

In contrast to *AtD-CGS*, when *EcSAT* is co-expressed with *HaSSA* it does not synergistically increase methionine content in the seed. In fact, the increase in total methionine and cysteine are nearly equivalent in both SAT and SAT × SSA. However, the seed protein profiles in these two lines look very different from each other, with the SAT × SSA seeds having the ER stress protein profile phenotype and SAT seeds having a profile very similar to untransformed Taipei (**Figure 2**). The additional S-AA in SAT seeds are likely distributed into many seed proteins, or into a few proteins with very high S-AA content that are expressed at low levels, both of which would make perceiving differences by 1D SDS-PAGE difficult. Taken together these results suggest that the total S-AA level is not a reliable determinant of the seed protein profile in rice.

Limited Seed Sulfate Availability/Intake/Loading Limits S-AA Related Nutritional Quality in Rice

A common feature of all three transgenic lines in this study with increased S-AA content is elevated total sulfur in the seed. This indicates that sulfur loading is a factor that can limit grain cysteine and methionine content in rice and that the seed is able to assimilate additional sulfur into organic molecules including S-AA. However, we were unable to determine what form or forms of sulfur are differentially imported into high S-AA lines. Transcript data from milkripe seeds did not reveal clear candidates based on annotated transporter expression or expression of enzymes that would be responsible for metabolizing specific imported S-species into major branch point metabolites, such as cysteine. Some indirect evidence points to sulfate as being the major differentially imported form of sulfur. In EcSAT-containing lines sulfate levels were considerably higher than in Taipei in all tissues tested, i.e. leaves from plants 34 and 70 days after germination, and mature seeds (**Figures 5A–C**). And it was previously shown that total CGS activity (sum of activity from endogenous isoforms and *AtD-CGS* transgene) was positively correlated with sulfate content in leaves (Whitcomb et al., 2018). Therefore, phloem loading with sulfate may be increased in our S-AA "push" lines. Higher levels of sulfate in the phloem would likely translate into greater sulfate unloading into seed tissues, even in the absence of transcriptional upregulation of well-expressed plasma membrane-localized SULTRs in the seed. There is also evidence that SULTR activity can be regulated both post-transcriptionally and post-translationally (Hopkins et al., 2005; Rouached et al., 2005; Yoshimoto et al., 2007; Shibagaki and Grossman, 2010). OASTL has been shown to inhibit sulfate transport across the plasma membrane by direct interaction with the STAS domain of SULTR1;2 (Shibagaki and Grossman, 2010). OASTL also interacts with SAT, forming the cysteine synthase complex (Hell and Wirtz, 2011), and one could speculate that high

EcSAT accumulation could bind-up enough OASTL to reduce OASTL binding with SULTR1;2 and thereby reduce OASTL-mediated inhibition of sulfate transport *via* SULTR1;2. In future studies, flux analysis with labeled S would be required to confidently identify the S-species that are differentially imported into EcSAT and to a lesser extent, AtD-CGS containing seeds.

In conclusion, the set of five transgenic lines presented here provides insight into the factors that limit cysteine and methionine accumulation in rice seed and suggest different approaches to produce even greater increases than those achieved here. First, seed sulfur loading is strongly implicated as a critical factor, although which transport form of sulfur is differentially imported is still unknown. Additionally, experiments to separate the effect of EcSAT's serine acetyl transferase activity from its effect on seed sulfur loading should be performed in order to design the next iteration of rice transgenic lines. Notably, both *EcSAT* and *AtD-CGS* expression in our transgenic lines are driven by ubiquitin promoters. It would be helpful to know whether seed-specific or leaf – specific expression of these enzymes would be sufficient to increase import of S into the seed. Second, the very high expression level and S-AA density of HaSSA may actually inhibit its effectiveness as a method to "pull" S-AA in to rice seeds. The data here suggest that rice seeds possess insufficient protein folding capacity in the ER for the very high levels of HaSSA accumulation, which results in oxidative stress. Translation of *HaSSA* transcripts may capture enough synthesized cysteine (for translation and for conversion into methionine for translation) to shortchange other uses of cysteine, such as synthesis of GSH and other antioxidants that are particularly important in the context of accumulated unfolded proteins in the ER and altered redox state in other cellular compartments. Therefore, a SSP with more moderate S-AA density and/or expressed at more moderate levels may be more effective for increasing total methionine in rice seeds. For example, 2S albumin from sesame (S2SA) has approximately 3-fold lower S-AA density than HaSSA, but low copy number transformation resulted in a large increase in both total cysteine and methionine in rice seed and no major changes in the endogenous seed protein profile were observed (Lee et al., 2003). We interpret this as a sign that the seeds are experiencing less ER unfolded protein stress than the SSA rice line used here.

Improving the nutritive quality of commodity crops remains an important goal. In this study we provided a deeper understanding of the processes underlying rice seed protein accumulation and outlined a basis for overcoming hurdles to further increase protein-bound S-AA content to meet nutritional needs.

MATERIALS AND METHODS

Rice Lines

The line Taipei, *Oryza sativa* ssp. *japonica* cv. Taipei 309, IRGC accession 42576, served as the untransformed control line for the single and double transgenic lines in this study. The line IR64, *Oryza sativa* ssp. *indica* cv. IR64, served as a high-protein reference line. Generation of the line SSA was previously described in Hagan et al. (2003). Briefly, Taipei was transformed by microparticle bombardment with a transgene construct containing the coding region of the 2S albumin SFA8 from sunflower, *HaSSA*, and the KDEL ER retention sequence driven by Bx17 wheat high molecular weight glutenin promoter. Generation of the line CGS was previously described in Whitcomb et al. (2018), and the line CgSx4 from that study is simply referred to here as line CGS. Briefly, Taipei was transformed by *Agrobacterium tumefaciens* with a transgene construct containing the coding region for a feedback desensitized variant of *Arabidopsis thaliana* cystathionine-gamma-synthase, *AtD-CGS* and the chloroplast-targeting transit peptide from *Pisum sativum*, driven by the maize ubiquitin 1 promoter. Generation of the line SAT was previously described in Nguyen et al. (2012), and the line SAT47 from that study is simply referred to here as line SAT. Briefly, Taipei was transformed by *Agrobacterium tumefaciens* with a transgene construct containing the *cysE* gene from *Escherichia coli*, *EcSAT*, and the Arabidopsis rbcS 5′ signal sequence for chloroplastic targeting, driven by the maize ubiquitin 1 promoter. The CGS × SSA and SAT × SSA lines were generated by crossing homozygous T2 SAT and CGS plants with the SSA line. In these crosses, SSA served as the pollen donor. F1 plants were screened by PCR for the presence of the *HaSSA* transgene. Double transgenic plants in the F2 generation were screened by PCR for both *AtD-CGS* and *HaSSA* or *EcSAT* and *HaSSA*, and two segregants from each cross were chosen for further analysis. Single seed decent was used to propagate the lines to the F3, F4, or F5 generation depending on the assay (see *Plant Material Sampling*). Data from the two lines derived from each of the initial Push × Pull crosses were analyzed separately and found to have substantively similar molecular and metabolic phenotypes. For visualization and significance testing, data from these lines were combined and presented as simply CGS × SSA or SAT × SSA. PCR primers for screening: AtD-CGS_F 5′ agg atc cgt ccg tca gct gag cat taa agc and AtD-CGS_R 5′ aaa gct tga tgg ctt cga gag ctt gaa g; EcSAT_F 5′ gac gct act caa gca cga aa and EcSAT_R 5′ ccc atc ccc ata ctc aaa tg; HaSSA_F 5′ atg gca agg ttt tcg atc gt and HaSSA_R 5′ att tgg cat ggt tgg gac at.

Growth Conditions

Seeds were germinated at 28°C in the dark on tap water-soaked paper towels. After 10 days, seedlings were transferred to a growth chamber with the following conditions: 12 h day length with a photon flux density set at 600 μE m^{-2} s^{-1} (Lamps: Iwasaki Eye MT 400 DL/BH E40, DHL Licht, Wülfrath, Germany); 26°C in the light and 22°C in the dark; relative humidity of 75% in the light and 70% in the dark. Single seedlings were transplanted into individual pots (18 cm deep, 10 cm diameter) of waterlogged soil after seven days of acclimation to the growth chamber. Soil was a mixture of two parts potting soil (70% white moss peat, 30% clay), and one-part sand. One gram of slow-release fertilizer (Plantacote Depot 4 M; Lanxess, Langenfeld, Germany) and 0.1 g Fetrilon Combi (Compo, Münster, Germany) were mixed into

the soil in each pot. Pots were kept partially submerged in water until seeds ripened, then all water was withdrawn, and the plants were allowed to dry out.

Plant Material Sampling

Milkripe and mature seeds were harvested 10 days and 21 days after anthesis, respectively. Unfilled seeds and those with fungus-infected hulls were excluded. Milkripe seeds were flash frozen in liquid nitrogen, and mature seed samples were dried at 50°C for 2 days prior to storage at −80°C. Seed samples from double transgenic plants that were used for RNAseq and sulfur-containing metabolite analyses were of the F5 generation and the F4 generation, respectively. The 2nd and 3rd mature leaves on the main tiller were harvested at 34 and 70 days after transplantation and flash frozen. Leaf samples from double transgenic plants were from the F3 generation.

Seed Protein Extraction and Western Blotting

100 mg finely ground mature seed samples were thawed on ice in 600 µl of protein extraction buffer [62.5 mM Tris-HCL pH 6.8, 2% SDS, 10% glycerol]. The protein concentration of the supernatant after centrifugation was determined by Bradford assay with BSA as a standard. Western blotting for HaSSA was performed with an anti-HaSSA polyclonal antibody kindly donated by Linda Tabe, CSIRO and an anti-sheep HRP-conjugated antibody from Thermo Scientific (Pierce).

Total Sulfur Content

Whole mature seed samples with husks were milled with a Retsch Ultra-Centrifugal Mill ZM200 and dried overnight at 80°C. 250 mg aliquots of milled and dried sample were digested in 5 ml of trace analysis grade 65% nitric acid:perchloric acid (15:85, v/v) for 8.5 h at increasing temperatures [2 h at room temperature, 3 h at 60°C, 1 h at 100°C, 1 h at 120°C, 1.5 h at 175°C]. After cooling, 4 ml of 25% (v/v) nitric acid was added and the tubes were reheated to 80°C for 1 h. 13 ml of ultra-pure water was added, the solutions mixed well, and then heated again at 80°C for 30 min. After cooling, these solutions were brought up to 20 ml with 5% nitric acid (v/v) and filtered (Whatman, no. 42 from GE Healthcare). Solutions were analyzed by inductively coupled plasma optical emission spectroscopy (ICP-OES) on an Optima 7300 DV ICP-OES (Perkin Elmer LAS Ltd., Seer Green, UK) using appropriate quality control checks, *e.g.* calibration verification standards, in house standards, and certified reference materials.

Total Methionine and Cysteine Content

Dry, mature seed samples of approximately 1 g were were oxidized with ice-cooled performic acid. Oxidation reactions were stopped with hydrobromic acid and then dried in a vacuum rotary evaporator. Residues were resuspended in 6N hydrochloric acid, and hydrolysis was allowed to proceed for 24 h at 110°C. After drying the samples in a vacuum rotary evaporator, the hydrolyzed residue was resuspended in demineralized water. The HPLC method for derivatization, separation, and quantification of methionine and cysteine content was performed essentially as previously described (Algermissen et al., 1989). Briefly, immediately prior to injection into the HPLC, samples were derivatized with ortho-phthaldehyde (OPA) in methanol with addition of borate buffer pH 9.5 and mercaptoethanol. HPLC was performed using a Merck LiChrospher® 5 µm RP-18 100 Å, 250 × 3 mm ID column connected to an HPLC system from Agilent in combination with a fluorescence detector from Shimadzu. Acetate buffer solutions with different methanol concentrations were used as HPLC eluents for the separation of amino acids by a gradient method.

Glutathione and Free Cysteine Concentration

50 mg aliquots of frozen, finely ground mature seed tissue were suspended in 500 µl 100 mM HCl, vortexed, and cleared by centrifugation. 60 µl of supernatant was then reduced by incubation at room temperature with 35 µl of 10 mM DTT in 100 µl of 0.25 M CHES, pH 9.4. The samples where then derivatized for 15 min in the dark with 5 µl of 25 mM monobromobimane in acetonitrile. The derivatization was stopped by adding 110 µl of 100 mM methanesulfonic acid, and the major soluble thiols were quantified by HPLC as previously described (Kreft et al., 2003). HPLC was performed using a Eurospher 100-5 C18, Column 250 × 4 mm connected to a Dionex HPLC system, and data were collected and processed with Chromeleon software version 6.8 from Dionex.

Free Methionine Determination

50 mg aliquots of frozen, finely ground mature seed tissue were resuspended in 300 µl ice cold methanol followed by 15 min of shaking at 950 rpm at 70°C. As a second extraction step, 167 µl of chloroform was added, and samples were shaken at 950 rpm for 5 min at 37°C. 333 µl of water was vortexed into the samples, and then they were centrifuged for 5 min at 20,800 g. 100 µl aliquots of the upper polar phase were dried overnight in a vacuum concentrator. The dried polar phase was resuspended in 70 µl of 5 mM sodium phosphate buffer pH 6.2 and subjected to HPLC analysis with pre-column, online ortho-phthaldehyde (OPA) derivatization in combination with fluorescence detection (Lindroth and Mopper, 1979). HPLC was performed using a Phenomenex HyperClone™ 3 µm ODS (C18) 120 Å, LC column 150 × 4.6 mm connected to a Dionex HPLC system, and data were processed with Chromeleon software version 6.8 from Dionex.

Sulfate Concentration Determination

Dried polar phase aliquots from methanol:chloroform extraction (see above, *Free Methionine Determination*) were resuspended in 1 ml ULC/MS grade de-ionized water, vortexed, and spun at 4°C for 15 min at full speed in a tabletop microcentrifuge. Sulfate concentration was determined by anion exchange chromatography using an ICS-3000 from Dionex. Data were collected and processed with Chromeleon software version 6.8 from Dionex.

O-Acetyl Serine Determination

Metabolite profiling of milkripe seed tissue by gas chromatography–mass spectrometry (GC–MS) was performed

essentially as previously described (Erban et al., 2007; Erban et al., 2019). To enrich for polar primary metabolites and small secondary products, 60 mg samples were extracted with methanol and chloroform as described above for free methionine determination but with the following changes for GC–MS analysis: extraction volumes were scaled to the larger initial sample mass, $^{13}C_6$-sorbitol at 17 mg/L was added to the methanol extraction step to allow later correction of analytical variance, and 160 µl, rather than 100 µl, polar phase aliquots were taken for analysis. Dried polar phase aliquots were chemically derivatized by methoxyamination and trimethylsilylation. A mixture of n-alkanes was added to the derivatized samples to serve as retention index standards. Gas chromatography coupled to electron impact ionization time-of-flight mass spectrometry was performed using an Agilent 6890N24 gas chromatograph and a Pegasus III mass spectrometer from LECO Instruments. ChromaTOF software (LECO, St. Joseph, MI, USA) was used to process the chromatograms. For metabolite identification TagFinder (Luedemann et al., 2008), NIST mass spectral library and search software (https://www.nist.gov/srd/nist-standard-reference-database-1a-v17), and the mass spectral and retention time index reference collection of the Golm Metabolome Database (http://gmd.mpimp-golm.mpg.de/) were used. Data were annotated and curated manually. Mass spectral intensity was normalized to sample fresh weight and $^{13}C_6$-sorbitol. The twice silylated (2TMS) derivative of O-acetylserine (MPIMP ID, A141001; http://gmd.mpimp-golm.mpg.de/Analytes/b4a42a07-e58c-4fb3-83e5-21fc5dc3330a.aspx) was chosen for relative quantification of OAS levels in milkripe seeds.

Differential Gene Expression Analysis

Milkripe seed samples were harvested 10 days after flowering on an individual panicle basis. Total RNA was prepared from approximately 100 mg of frozen, finely ground tissue with Ribospin™ Seed/Fruit kit (GeneAll Biotechnology, Korea) followed by two rounds of DNase treatment (first round with Riboclear™ plus! from GeneAll, second round with TURBO DNA-*free* Kit from Invitrogen), and PCR was performed to assess possible remaining genomic DNA contamination. Only those total RNA samples with RIN quality scores greater than 7.3 by Bioanalyzer were submitted for RNA sequencing. Library preparation and sequencing were performed at the Max Planck Genome Center, Cologne, Germany (https://mpgc.mpipz.mpg.de/home). rRNA depletion was performed on 1,000 ng total RNA samples with the Ribo-Zero™ rRNA Removal Kit (seed/root) from Illumina. Subsequent library preparation was performed with NEBNext® Ultra™ Directional RNA Library Prep Kit for Illumina® (New England Biolabs) according to the manufacturer's instructions. Quality and quantity were assessed at all steps *via* capillary electrophoresis (TapeStation, Agilent Technologies) and fluorometry (Qubit, Thermo Fisher Scientific). Libraries were immobilized and processed onto a flow cell with cBot (Illumina) and subsequently sequenced on HiSeq3000 system (Illumina) with approximately 50×10^6 strand-specific 150 bp single-end reads for each milkripe seed sample. The quality of the raw fastq sequence data was assessed by FastQC (http://www.bioinformatics.babraham.ac.uk/projects/fastqc/). Raw data were mapped first against the rice genome and then against a set of transgenes. In detail, sequence data were mapped using STAR (Dobin et al., 2013; Dobin and Gingeras, 2015) version 2.7.1a with the parameters –quantMode TranscriptomeSAM GeneCounts, –outSAMtype BAM Unsorted, and –outReadsUnmapped Fastx. Ensembl version 43 (IRGSP 1.0) genome reference in FASTA format (ftp://ftp.ensemblgenomes.org/pub/release-43/plants/fasta/oryza_sativa/dna/Oryza_sativa.IRGSP-1.0.dna.toplevel.fa.gz) and Ensembl version 43 cDNA Annotation in GTF format (ftp://ftp.ensemblgenomes.org/pub/release-43/plants/gtf/oryza_sativa/Oryza_sativa.IRGSP-1.0.43.gtf.gz) were used for genome indexing (–sjdbOverhang 149 –genomeSAindexNbases 13). In order to determine RNA read counts for the *AtD-CGS*, *EcSAT*, and *HaSSA* transgenes, reads unmapped to the rice genome were used as input for mapping against a fasta file containing the sequences X56686.1, M15745.1, and NM_110977.3, downloaded from NCBI), which was indexed with bwa version 7.17 in "is" mode. Reads were mapped against it in backtrack ("aln") mode (Li and Durbin, 2009) and converted to sam format with bwa samse. Afterwards samtools version 1.8 was used to convert sam to bam format (samtools view -bS), sort (samtools sort), and index (samtools index) the resulting bam alignment files in order to create read counts per input sequence (samtools idxstats) (Li et al., 2009). Anti-strand read counts from the ReadsPerGene files of all 22 samples were merged in order to perform differential expression analysis. Reads that could be unambiguously mapped to either a rice gene or transgene were retained for further analysis in R version 3.6.1 with the package DESeq2 (Love et al., 2014) version 1.24.0. Differences in sequencing depth between samples were accounted for in DESeq2 with median-of-ratio normalization. Differential expression analysis was performed using dispersion and log fold change estimates after shrinkage with the DESeq2 *maximum a posteriori* option. To determine the significance level of estimated Log_2-fold change, Wald tests were performed, and genes were considered differentially expressed relative to Taipei if the Benjamini–Hochberg adjusted p-value was less than 0.01. Genes were considered "expressed" in milkripe seeds if their average normalized counts were greater than 100. The empirical cumulative distribution function ecdf from the R stats package version 3.6.1 was used to calculate the expression strength percentile among all "expressed" genes in milkripe seeds.

Data Visualization

Quantitative data visualizations were prepared in R version 3.6.1. Univariate scatter plots and the stacked bar plot were generated with the R package ggplot2 version 3.2.1. Significance testing results were added to the plots with the R package ggpubr version 0.2.3. Heatmaps were prepared with the R packages ComplexHeatmap version 2.0.0 and circlize version 0.4.7.

DATA AVAILABILITY STATEMENT

The RNA-seq dataset generated for this study has been deposited in NCBI's Gene Expression881 Omnibus (Edgar et al., 2002) and are accessible through GEO series accession number GSE149252882 (https://www.ncbi.nlm.nih.gov/geo/query/acc.cgi?acc=GSE149252).

AUTHOR CONTRIBUTIONS

RH and SW contributed to the conception and design of the study. SW, AR, and FB grew all plants, harvested samples, and processed them for analytical measurements. FB performed the crosses and selected transgenic lines. SP and MH performed the ICP-OES analysis. AE and JK performed analysis of the GC–MS data. SW and AF performed the RNA-seq analysis. SW performed the statistical analysis and prepared all visualizations. SW took the lead in interpreting the data and wrote the first draft of the manuscript. All authors contributed to the article and approved the submitted version.

FUNDING

The primary funding sources for this study were the Max Planck Society (Germany) and the EU RTN BIONUT (BIOchemical and genetic dissection of control of plant mineral NUTrition) FP7: 264296. Rothamsted Research receives grant-aided support from the Biotechnology and Biological Sciences Research Council (BBSRC) through the Designing Future Wheat programme [BB/P016855/1].

ACKNOWLEDGMENT

We are grateful to Ines Fehrle in the Applied Metabolome Analysis Infrastructure Group at the Max Planck Institute for Molecular Plant Physiology (Germany) for performing the GC–MS measurements. We thank Linda Tabe at CSIRO (Australia) for kindly providing Taipei and SSA seeds and the anti-HaSSA antibody used in this study. We thank the Max Planck-Genome-centre Cologne (http://mpgc.mpipz.mpg.de/home/) for performing the RNA sequencing in this study and the Institut für Getreideverarbeitung GmbH, Nuthetal, Germany for performing the total methionine and cysteine determination.

SUPPLEMENTARY MATERIAL

The Supplementary Material for this article can be found online at: https://www.frontiersin.org/articles/10.3389/fpls.2020.01118/full#supplementary-material

SUPPLEMENTARY TABLE 1 | Significance testing results for genes presented in **Figures 1**, **3**, **6**, and **7**.

REFERENCES

Algermissen, B., Nündel, M., and Riedel, E. (1989). Analytik von Aminosäuren mit Fluoreszenz-HPLC. *GIT Labor-Fachzeitschrift* 33 (9), 783–790.

Amir, R., Galili, G., and Cohen, H. (2018). The metabolic roles of free amino acids during seed development. *Plant Sci.* 275, 11–18. doi: 10.1016/j.plantsci.2018.06.011

Amir, R., Cohen, H., and Hacham, Y. (2019). Revisiting the attempts to fortify methionine contents in plant seeds. *J. Exp. Bot.* 70 (16), 4105–4114. doi: 10.1093/jxb/erz134

Amira, G., Ifat, M., Tal, A., Hana, B., Shmuel, G., and Rachel, A. (2005). Soluble methionine enhances accumulation of a 15 kDa zein, a methionine-rich storage protein, in transgenic alfalfa but not in transgenic tobacco plants. *J. Exp. Bot.* 56 (419), 2443–2452. doi: 10.1093/jxb/eri237

Bick, J. A., Aslund, F., Chen, Y., and Leustek, T. (1998). Glutaredoxin function for the carboxyl-terminal domain of the plant-type 5'-adenylylsulfate reductase. *Proc. Natl. Acad. Sci. U. S. A.* 95 (14), 8404–8409. doi: 10.1073/pnas.95.14.8404

Bick, J. A., Setterdahl, A. T., Knaff, D. B., Chen, Y., Pitcher, L. H., Zilinskas, B. A., et al. (2001). Regulation of the plant-type 5'-adenylyl sulfate reductase by oxidative stress. *Biochemistry* 40 (30), 9040–9048. doi: 10.1021/bi010518v

Bourgis, F., Roje, S., Nuccio, M. L., Fisher, D. B., Tarczynski, M. C., Li, C., et al. (1999). S-methylmethionine plays a major role in phloem sulfur transport and is synthesized by a novel type of methyltransferase. *Plant Cell* 11 (8), 1485–1498. doi: 10.1105/tpc.11.8.1485

Chakravarthi, S., Jessop, C. E., and Bulleid, N. J. (2006). The role of glutathione in disulphide bond formation and endoplasmic-reticulum-generated oxidative stress. *EMBO Rep.* 7 (3), 271–275. doi: 10.1038/sj.embor.7400645

Chiaiese, P., Ohkama-Ohtsu, N., Molvig, L., Godfree, R., Dove, H., Hocart, C., et al. (2004). Sulphur and nitrogen nutrition influence the response of chickpea seeds to an added, transgenic sink for organic sulphur. *J. Exp. Bot.* 55 (404), 1889–1901. doi: 10.1093/jxb/erh198

Cohen, H., Salmon, A., Tietel, Z., Hacham, Y., and Amir, R. (2017). The relative contribution of genes operating in the S-methylmethionine cycle to methionine metabolism in Arabidopsis seeds. *Plant Cell Rep.* 36 (5), 731–743. doi: 10.1007/s00299-017-2124-1

Cohen, A., Hacham, Y., Welfe, Y., Khatib, S., Avice, J.-C., and Amir, R. (2020). Evidence of a significant role of glutathione reductase in the sulfur assimilation pathway. *Plant J.* 102 (2), 246–261. doi: 10.1111/tpj.14621

Dancs, G., Kondrak, M., and Banfalvi, Z. (2008). The effects of enhanced methionine synthesis on amino acid and anthocyanin content of potato tubers. *BMC Plant Biol.* 8, 65. doi: 10.1186/1471-2229-8-65

De Wilde, K., De Buck, S., Vanneste, K., and Depicker, A. (2013). Recombinant antibody production in Arabidopsis seeds triggers an unfolded protein response. *Plant Physiol.* 161 (2), 1021–1033. doi: 10.1104/pp.112.209718

Demidov, D., Horstmann, C., Meixner, M., Pickardt, T., Saalbach, I., Galili, G., et al. (2003). Additive effects of the feed-back insensitive bacterial aspartate kinase and the Brazil nut 2S albumin on the methionine content of transgenic narbon bean (Vicia narbonensis L.). *Mol. Breed.* 11 (3), 187–201. doi: 10.1023/a:1022814506153

Dietz, K. J., Turkan, I., and Krieger-Liszkay, A. (2016). Redox- and Reactive Oxygen Species-Dependent Signaling into and out of the Photosynthesizing Chloroplast. *Plant Physiol.* 171 (3), 1541–1550. doi: 10.1104/pp.16.00375

Dobin, A., and Gingeras, T. R. (2015). Mapping RNA-seq Reads with STAR. *Curr. Protoc. Bioinf.* 51, 11 14 11–19. doi: 10.1002/0471250953.bi1114s51

Dobin, A., Davis, C. A., Schlesinger, F., Drenkow, J., Zaleski, C., Jha, S., et al. (2013). STAR: ultrafast universal RNA-seq aligner. *Bioinformatics* 29 (1), 15–21. doi: 10.1093/bioinformatics/bts635

Dominguez-Solis, J. R., He, Z., Lima, A., Ting, J., Buchanan, B. B., and Luan, S. (2008). A cyclophilin links redox and light signals to cysteine biosynthesis and stress responses in chloroplasts. *Proc. Natl. Acad. Sci. U. S. A.* 105 (42), 16386–16391. doi: 10.1073/pnas.0808204105

Edgar, R., Domrachev, M., and Lash, A. E. (2002). Gene Expression Omnibus: NCBI gene expression and hybridization array data repository. *Nucleic Acids Res.* 30 (1), 207–210. doi: 10.1093/nar/30.1.207

Erban, A., Schauer, N., Fernie, A. R., and Kopka, J. (2007). Nonsupervised construction and application of mass spectral and retention time index

libraries from time-of-flight gas chromatography-mass spectrometry metabolite profiles. *Methods Mol. Biol.* 358, 19–38. doi: 10.1007/978-1-59745-244-1_2

Erban, A., Fehrle, I., Martinez-Seidel, F., Brigante, F., Mas, A. L., Baroni, V., et al. (2019). Discovery of food identity markers by metabolomics and machine learning technology. *Sci. Rep.* 9 (1), 9697. doi: 10.1038/s41598-019-46113-y

Gigolashvili, T., and Kopriva, S. (2014). Transporters in plant sulfur metabolism. *Front. Plant Sci.* 5:442. doi: 10.3389/fpls.2014.00442

Global Rice Science Partnership (2013). *Rice Almanac. 4th ed* (Los Baños, Philippines: International Rice Research Institute).

Hacham, Y., Matityahu, I., Schuster, G., and Amir, R. (2008). Overexpression of mutated forms of aspartate kinase and cystathionine gamma-synthase in tobacco leaves resulted in the high accumulation of methionine and threonine. *Plant J.* 54 (2), 260–271. doi: 10.1111/j.1365-313X.2008.03415.x

Hagan, N. D., Upadhyaya, N., Tabe, L. M., and Higgins, T. J. (2003). The redistribution of protein sulfur in transgenic rice expressing a gene for a foreign, sulfur-rich protein. *Plant J.* 34 (1), 1–11. doi: 10.1046/j.1365-313X.2003.01699.x

Hanafy, M. S., Rahman, S. M., Nakamoto, Y., Fujiwara, T., Naito, S., Wakasa, K., et al. (2013). Differential response of methionine metabolism in two grain legumes, soybean and azuki bean, expressing a mutated form of Arabidopsis cystathionine gamma-synthase. *J. Plant Physiol.* 170 (3), 338–345. doi: 10.1016/j.jplph.2012.10.018

Harding, H. P., Zhang, Y., Zeng, H., Novoa, I., Lu, P. D., Calfon, M., et al. (2003). An integrated stress response regulates amino acid metabolism and resistance to oxidative stress. *Mol. Cell* 11 (3), 619–633. doi: 10.1016/s1097-2765(03)00105-9

Harms, K., von Ballmoos, P., Brunold, C., Hofgen, R., and Hesse, H. (2000). Expression of a bacterial serine acetyltransferase in transgenic potato plants leads to increased levels of cysteine and glutathione. *Plant J.* 22 (4), 335–343. doi: 10.1046/j.1365-313x.2000.00743.x

Hell, R., and Wirtz, M. (2011). Molecular Biology, Biochemistry and Cellular Physiology of Cysteine Metabolism in Arabidopsis thaliana. *Arabidopsis Book* 9, e0154. doi: 10.1199/tab.0154

Hesse, H., Kreft, O., Maimann, S., Zeh, M., and Hoefgen, R. (2004). Current understanding of the regulation of methionine biosynthesis in plants. *J. Exp. Bot.* 55 (404), 1799–1808. doi: 10.1093/jxb/erh139

Hopkins, L., Parmar, S., Blaszczyk, A., Hesse, H., Hoefgen, R., and Hawkesford, M. J. (2005). O-acetylserine and the regulation of expression of genes encoding components for sulfate uptake and assimilation in potato. *Plant Physiol.* 138 (1), 433–440. doi: 10.1104/pp.104.057521

Hubberten, H. M., Klie, S., Caldana, C., Degenkolbe, T., Willmitzer, L., and Hoefgen, R. (2012). Additional role of O-acetylserine as a sulfur status-independent regulator during plant growth. *Plant J.* 70 (4), 666–677. doi: 10.1111/j.1365-313X.2012.04905.x

Islam, N., Upadhyaya, N. M., Campbell, P. M., Akhurst, R., Hagan, N., and Higgins, T. J. (2005). Decreased accumulation of glutelin types in rice grains constitutively expressing a sunflower seed albumin gene. *Phytochemistry* 66 (21), 2534–2539. doi: 10.1016/j.phytochem.2005.09.002

Juliano, B. O. (1992). Structure, chemistry, and function of the rice grain and its fractions. *Cereal Foods World* 37, 772–774.

Karchi, H., Shaul, O., and Galili, G. (1994). Lysine synthesis and catabolism are coordinately regulated during tobacco seed development. *Proc. Natl. Acad. Sci. U. S. A.* 91 (7), 2577–2581. doi: 10.1073/pnas.91.7.2577

Kataoka, T., Watanabe-Takahashi, A., Hayashi, N., Ohnishi, M., Mimura, T., Buchner, P., et al. (2004). Vacuolar sulfate transporters are essential determinants controlling internal distribution of sulfate in Arabidopsis. *Plant Cell* 16 (10), 2693–2704. doi: 10.1105/tpc.104.023960

Kim, W. S., Jez, J. M., and Krishnan, H. B. (2014). Effects of proteome rebalancing and sulfur nutrition on the accumulation of methionine rich delta-zein in transgenic soybeans. *Front. Plant Sci.* 5:633. doi: 10.3389/fpls.2014.00633

Kortt, A. A., Caldwell, J. B., Lilley, G. G., and Higgins, T. J. (1991). Amino acid and cDNA sequences of a methionine-rich 2S protein from sunflower seed (Helianthus annuus L.). *Eur. J. Biochem.* 195 (2), 329–334. doi: 10.1111/j.1432-1033.1991.tb15710.x

Kreft, O., Hoefgen, R., and Hesse, H. (2003). Functional analysis of cystathionine gamma-synthase in genetically engineered potato plants. *Plant Physiol.* 131 (4), 1843–1854. doi: 10.1104/pp.102.015933

Krueger, R. J., and Siegel, L. M. (1982). Spinach siroheme enzymes: Isolation and characterization of ferredoxin-sulfite reductase and comparison of properties with ferredoxin-nitrite reductase. *Biochemistry* 21 (12), 2892–2904. doi: 10.1021/bi00541a014

Kuzuhara, Y., Isobe, A., Awazuhara, M., Fujiwara, T., and Hayashi, H. (2000). Glutathione levels in phloem sap of rice plants under sulfur deficient conditions. *Soil Sci. Plant Nutr.* 46 (1), 265–270. doi: 10.1080/00380768.2000.10408782

Lai, Y. S., Renna, L., Yarema, J., Ruberti, C., He, S. Y., and Brandizzi, F. (2018). Salicylic acid-independent role of NPR1 is required for protection from proteotoxic stress in the plant endoplasmic reticulum. *Proc. Natl. Acad. Sci. U. S. A.* 115 (22), E5203–E5212. doi: 10.1073/pnas.1802254115

Lee, T. T., Wang, M. M., Hou, R. C., Chen, L. J., Su, R. C., Wang, C. S., et al. (2003). Enhanced methionine and cysteine levels in transgenic rice seeds by the accumulation of sesame 2S albumin. *Biosci. Biotechnol. Biochem.* 67 (8), 1699–1705. doi: 10.1271/bbb.67.1699

Lehmann, M., Schwarzlander, M., Obata, T., Sirikantaramas, S., Burow, M., Olsen, C. E., et al. (2009). The metabolic response of Arabidopsis roots to oxidative stress is distinct from that of heterotrophic cells in culture and highlights a complex relationship between the levels of transcripts, metabolites, and flux. *Mol. Plant* 2 (3), 390–406. doi: 10.1093/mp/ssn080

Li, H., and Durbin, R. (2009). Fast and accurate short read alignment with Burrows-Wheeler transform. *Bioinformatics* 25 (14), 1754–1760. doi: 10.1093/bioinformatics/btp324

Li, H., Handsaker, B., Wysoker, A., Fennell, T., Ruan, J., Homer, N., et al. (2009). The Sequence Alignment/Map format and SAMtools. *Bioinformatics* 25 (16), 2078–2079. doi: 10.1093/bioinformatics/btp352

Lindroth, P., and Mopper, K. (1979). High-Performance Liquid-Chromatographic Determination of Subpicomole Amounts of Amino-Acids by Precolumn Fluorescence Derivatization with Ortho-Phthaldialdehyde. *Anal. Chem.* 51 (11), 1667–1674. doi: 10.1021/ac50047a019

Liu, J. X., and Howell, S. H. (2016). Managing the protein folding demands in the endoplasmic reticulum of plants. *New Phytol.* 211 (2), 418–428. doi: 10.1111/nph.13915

Liu, F., Yoo, B. C., Lee, J. Y., Pan, W., and Harmon, A. C. (2006). Calcium-regulated phosphorylation of soybean serine acetyltransferase in response to oxidative stress. *J. Biol. Chem.* 281 (37), 27405–27415. doi: 10.1074/jbc.M604548200

Love, M. I., Huber, W., and Anders, S. (2014). Moderated estimation of fold change and dispersion for RNA-seq data with DESeq2. *Genome Biol.* 15 (12):550. doi: 10.1186/s13059-014-0550-8

Luedemann, A., Strassburg, K., Erban, A., and Kopka, J. (2008). TagFinder for the quantitative analysis of gas chromatography–mass spectrometry (GC-MS)-based metabolite profiling experiments. *Bioinformatics* 24 (5), 732–737. doi: 10.1093/bioinformatics/btn023

Matityahu, I., Godo, I., Hacham, Y., and Amir, R. (2013). Tobacco seeds expressing feedback-insensitive cystathionine gamma-synthase exhibit elevated content of methionine and altered primary metabolic profile. *BMC Plant Biol.* 13, 206. doi: 10.1186/1471-2229-13-206

McNabb, W. C., Spencer, D., Higgins, T. J., and Barry, T. N. (1994). In-vitro rates of rumen proteolysis of ribulose-1,5-bisphosphate carboxylase (rubisco) from lucerne leaves, and of ovalbumin, vicilin and sunflower albumin 8 storage proteins. *J. Sci. Food Agric.* 64 (1), 53–61. doi: 10.1002/jsfa.2740640109

Menegus, F., Lilliu, I., Brambilla, I., Bonfa, M., and Scaglioni, L. (2004). Unusual accumulation of S-methylmethionine in aerobic-etiolated and in anoxic rice seedlings: an 1H-NMR study. *J. Plant Physiol.* 161 (6), 725–732. doi: 10.1078/0176-1617-01081

Molvig, L., Tabe, L. M., Eggum, B. O., Moore, A. E., Craig, S., Spencer, D., et al. (1997). Enhanced methionine levels and increased nutritive value of seeds of transgenic lupins (Lupinus angustifolius L.) expressing a sunflower seed albumin gene. *PNAS* 94 (16), 8393–8398. doi: 10.1073/pnas.94.16.8393

Nguyen, H. C., Hoefgen, R., and Hesse, H. (2012). Improving the nutritive value of rice seeds: elevation of cysteine and methionine contents in rice plants by ectopic expression of a bacterial serine acetyltransferase. *J. Exp. Bot.* 63 (16), 5991–6001. doi: 10.1093/jxb/ers253

Noji, M., and Saito, K. (2002). Molecular and biochemical analysis of serine acetyltransferase and cysteine synthase towards sulfur metabolic engineering in plants. *Amino Acids* 22 (3), 231–243. doi: 10.1007/s007260200011

Oono, Y., Wakasa, Y., Hirose, S., Yang, L., Sakuta, C., and Takaiwa, F. (2010). Analysis of ER stress in developing rice endosperm accumulating beta-amyloid peptide. *Plant Biotechnol. J.* 8 (6), 691–718. doi: 10.1111/j.1467-7652.2010.00502.x

Ozgur, R., Turkan, I., Uzilday, B., and Sekmen, A. H. (2014). Endoplasmic reticulum stress triggers ROS signalling, changes the redox state, and regulates the antioxidant defence of Arabidopsis thaliana. *J. Exp. Bot.* 65 (5), 1377–1390. doi: 10.1093/jxb/eru034

Planta, J., Xiang, X., Leustek, T., and Messing, J. (2017). Engineering sulfur storage in maize seed proteins without apparent yield loss. *Proc. Natl. Acad. Sci. U. S. A.* 114 (43), 11386–11391. doi: 10.1073/pnas.1714805114

Qi, K., and Lupton, C. J. (1994). A Review of the Effects of Sulfur Nutrition on Wool Production and Quality. *Sheep Goat Res. J.* 10 (2), 133–140.

Qian, D., Tian, L., and Qu, L. (2015). Proteomic analysis of endoplasmic reticulum stress responses in rice seeds. *Sci. Rep.* 5:14255. doi: 10.1038/srep14255

Rouached, H., Berthomieu, P., El Kassis, E., Cathala, N., Catherinot, V., Labesse, G., et al. (2005). Structural and functional analysis of the C-terminal STAS (sulfate transporter and anti-sigma antagonist) domain of the Arabidopsis thaliana sulfate transporter SULTR1.2. *J. Biol. Chem.* 280 (16), 15976–15983. doi: 10.1074/jbc.M501635200

Satoh-Cruz, M., Crofts, A. J., Takemoto-Kuno, Y., Sugino, A., Washida, H., Crofts, N., et al. (2010). Protein disulfide isomerase like 1-1 participates in the maturation of proglutelin within the endoplasmic reticulum in rice endosperm. *Plant Cell Physiol.* 51 (9), 1581–1593. doi: 10.1093/pcp/pcq098

Shibagaki, N., and Grossman, A. R. (2010). Binding of cysteine synthase to the STAS domain of sulfate transporter and its regulatory consequences. *J. Biol. Chem.* 285 (32), 25094–25102. doi: 10.1074/jbc.M110.126888

Shinmachi, F., Buchner, P., Stroud, J. L., Parmar, S., Zhao, F. J., McGrath, S. P., et al. (2010). Influence of sulfur deficiency on the expression of specific sulfate transporters and the distribution of sulfur, selenium, and molybdenum in wheat. *Plant Physiol.* 153 (1), 327–336. doi: 10.1104/pp.110.153759

Song, S. K., Hou, W. S., Godo, I., Wu, C. X., Yu, Y., Matityahu, I., et al. (2013). Soybean seeds expressing feedback-insensitive cystathionine -synthase exhibit a higher content of methionine. *J. Exp. Bot.* 64 (7), 1917–1926. doi: 10.1093/jxb/ert053

Spencer, D., Higgins, T. J., Freer, M., Dove, H., and Coombe, J. B. (1988). Monitoring the fate of dietary proteins in rumen fluid using gel electrophoresis. *Br. J. Nutr.* 60 (2), 241–247. doi: 10.1079/bjn19880096

Takagi, H., Saito, S., Yang, L., Nagasaka, S., Nishizawa, N., and Takaiwa, F. (2005). Oral immunotherapy against a pollen allergy using a seed-based peptide vaccine. *Plant Biotechnol. J.* 3 (5), 521–533. doi: 10.1111/j.1467-7652.2005.00143.x

Takahashi, H., Kopriva, S., Giordano, M., Saito, K., and Hell, R. (2011). Sulfur assimilation in photosynthetic organisms: molecular functions and regulations of transporters and assimilatory enzymes. *Annu. Rev. Plant Biol.* 62, 157–184. doi: 10.1146/annurev-arplant-042110-103921

Takaiwa, F., Takagi, H., Hirose, S., and Wakasa, Y. (2007). Endosperm tissue is good production platform for artificial recombinant proteins in transgenic rice. *Plant Biotechnol. J.* 5 (1), 84–92. doi: 10.1111/j.1467-7652.2006.00220.x

Tan, Q., Zhang, L., Grant, J., Cooper, P., and Tegeder, M. (2010). Increased phloem transport of S-methylmethionine positively affects sulfur and nitrogen metabolism and seed development in pea plants. *Plant Physiol.* 154 (4), 1886–1896. doi: 10.1104/pp.110.166389

Tian, L., Dai, L. L., Yin, Z. J., Fukuda, M., Kumamaru, T., Dong, X. B., et al. (2013). Small GTPase Sar1 is crucial for proglutelin and alpha-globulin export from the endoplasmic reticulum in rice endosperm. *J. Exp. Bot.* 64 (10), 2831–2845. doi: 10.1093/jxb/ert128

Twyman, R. M., Stoger, E., Schillberg, S., Christou, P., and Fischer, R. (2003). Molecular farming in plants: host systems and expression technology. *Trends Biotechnol.* 21 (12), 570–578. doi: 10.1016/j.tibtech.2003.10.002

Ulrich, K., and Jakob, U. (2019). The role of thiols in antioxidant systems. *Free Radic. Biol. Med.* 140, 14–27. doi: 10.1016/j.freeradbiomed.2019.05.035

Watanabe, M., Hubberten, H. M., Saito, K., and Hoefgen, R. (2015). "Serine Acetyltransferase," in *Amino Acids in HIgher Plants*. Ed. J. P. F. D'Mello (Wallingford, Oxfordshire, United Kingdom: CAB International), 195–218.

Whitcomb, S. J., Nguyen, H. C., Bruckner, F., Hesse, H., and Hoefgen, R. (2018). Cystathionine Gamma-Synthase activity in rice is developmentally regulated and strongly correlated with sulfate. *Plant Sci.* 270, 234–244. doi: 10.1016/j.plantsci.2018.02.016

Wongkaew, A., Asayama, K., Kitaiwa, T., Nakamura, S. I., Kojima, K., Stacey, G., et al. (2018). AtOPT6 Protein Functions in Long-Distance Transport of Glutathione in Arabidopsis thaliana. *Plant Cell Physiol.* 59 (7), 1443–1451. doi: 10.1093/pcp/pcy074

Xiang, X., Wu, Y., Planta, J., Messing, J., and Leustek, T. (2018). Overexpression of Serine Acetyltransferase in Maize Leaves Increases Seed-Specific Methionine-Rich Zeins. *Plant Biotechnol. J* 16 (5), 1057–1067. doi: 10.1111/pbi.12851

Yasuda, H., Tada, Y., Hayashi, Y., Jomori, T., and Takaiwa, F. (2005). Expression of the small peptide GLP-1 in transgenic plants. *Transgenic Res.* 14 (5), 677–684. doi: 10.1007/s11248-005-6631-4

Yasuda, H., Hirose, S., Kawakatsu, T., Wakasa, Y., and Takaiwa, F. (2009). Overexpression of BiP has inhibitory effects on the accumulation of seed storage proteins in endosperm cells of rice. *Plant Cell Physiol.* 50 (8), 1532–1543. doi: 10.1093/pcp/pcp098

Yoshimoto, N., Inoue, E., Watanabe-Takahashi, A., Saito, K., and Takahashi, H. (2007). Posttranscriptional regulation of high-affinity sulfate transporters in Arabidopsis by sulfur nutrition. *Plant Physiol.* 145 (2), 378–388. doi: 10.1104/pp.107.105742

Zhang, M. Y., Bourbouloux, A., Cagnac, O., Srikanth, C. V., Rentsch, D., Bachhawat, A. K., et al. (2004). A novel family of transporters mediating the transport of glutathione derivatives in plants. *Plant Physiol.* 134 (1), 482–491. doi: 10.1104/pp.103.030940

Zuber, H., Davidian, J. C., Wirtz, M., Hell, R., Belghazi, M., Thompson, R., et al. (2010). Sultra4;1 mutant seeds of Arabidopsis have an enhanced sulphate content and modified proteome suggesting metabolic adaptations to altered sulphate compartmentalization. *BMC Plant Biol.* 10, 78. doi: 10.1186/1471-2229-10-78

Conflict of Interest: The authors declare that the research was conducted in the absence of any commercial or financial relationships that could be construed as a potential conflict of interest.

Copyright © 2020 Whitcomb, Rakpenthai, Brückner, Fischer, Parmar, Erban, Kopka, Hawkesford and Hoefgen. This is an open-access article distributed under the terms of the Creative Commons Attribution License (CC BY). The use, distribution or reproduction in other forums is permitted, provided the original author(s) and the copyright owner(s) are credited and that the original publication in this journal is cited, in accordance with accepted academic practice. No use, distribution or reproduction is permitted which does not comply with these terms.

frontiers in Plant Science

REVIEW
published: 23 July 2020
doi: 10.3389/fpls.2020.01127

How Does Proline Treatment Promote Salt Stress Tolerance During Crop Plant Development?

Ahmed El Moukhtari[1,2], *Cécile Cabassa-Hourton*[1], *Mohamed Farissi*[2] *and Arnould Savouré*[1*]

[1] Sorbonne Université, UPEC, CNRS, IRD, INRA, Institut d'Ecologie et Sciences de l'Environnement de Paris, IEES, Paris, France, [2] Laboratory of Biotechnology & Sustainable Development of Natural Resources, Polydisciplinary Faculty, Sultan Moulay Slimane University, Beni Mellal, Morocco

Soil salinity is one of the major abiotic stresses restricting the use of land for agriculture because it limits the growth and development of most crop plants. Improving productivity under these physiologically stressful conditions is a major scientific challenge because salinity has different effects at different developmental stages in different crops. When supplied exogenously, proline has improved salt stress tolerance in various plant species. Under high-salt conditions, proline application enhances plant growth with increases in seed germination, biomass, photosynthesis, gas exchange, and grain yield. These positive effects are mainly driven by better nutrient acquisition, water uptake, and biological nitrogen fixation. Exogenous proline also alleviates salt stress by improving antioxidant activities and reducing Na^+ and Cl^- uptake and translocation while enhancing K^+ assimilation by plants. However, which of these mechanisms operate at any one time varies according to the proline concentration, how it is applied, the plant species, and the specific stress conditions as well as the developmental stage. To position salt stress tolerance studies in the context of a crop plant growing in the field, here we discuss the beneficial effects of exogenous proline on plants exposed to salt stress through well-known and more recently described examples in more than twenty crop species in order to appreciate both the diversity and commonality of the responses. Proposed mechanisms by which exogenous proline mitigates the detrimental effects of salt stress during crop plant growth are thus highlighted and critically assessed.

Keywords: salinity, proline, plant development, photosynthesis, biological nitrogen fixation, nutrient uptake, water nutrition, antioxidants

OPEN ACCESS

Edited by:
Maurizio Trovato, Sapienza University of Rome, Italy

Reviewed by:
Magdy Fahim Mansour, Ain Sham University, Egypt
Naser A. Anjum, Aligarh Muslim University, India

***Correspondence:**
Arnould Savouré
arnould.savoure@sorbonne-universite.fr

Specialty section:
This article was submitted to Plant Metabolism and Chemodiversity, a section of the journal Frontiers in Plant Science

Received: *20 April 2020*
Accepted: *08 July 2020*
Published: *23 July 2020*

Citation:
El Moukhtari A, Cabassa-Hourton C, Farissi M and Savouré A (2020) How Does Proline Treatment Promote Salt Stress Tolerance During Crop Plant Development? Front. Plant Sci. 11:1127. doi: 10.3389/fpls.2020.01127

INTRODUCTION

Salinity is a major abiotic stress that severely affects crop plant growth and development from seed germination to harvest. In recent years, increasing deleterious effects on agricultural productivity have been observed especially in arid and semiarid regions where rainfall is low and evapotranspiration is high (Jha et al., 2019). It is estimated that more than 7% of total land and almost 20% of arable land are affected by salinity with affected areas increasing at an annual rate of

1–2% (Zhu and Gong, 2014; Rizwan et al., 2015). It is indeed predicted that more than 50% of arable land will be rendered unproductive by 2050 due to the levels of salt stress induced in crops (Vinocur and Altman, 2005; Bianco and Defez, 2009). This trend coincides with the increasing challenge of ensuring global food security, so it is even more urgent to be able to exploit more arable land and increase crop productivity even in infertile soil by developing efficient and tolerant crops able to grow in salty conditions (Rengasamy, 2006; Safdar et al., 2019). Thus, new alternative approaches to allow crops to efficiently tolerate salt stress are needed. Indeed, the use of exogenous compounds, which are both ecofriendly and easily available, such as silicon (Zhu and Gong, 2014; Rizwan et al., 2015), trehalose (Nounjan et al., 2012), glycine betaine (Hossain and Fujita, 2010), and proline (Hoque et al., 2008; Deivanai et al., 2011; Wani et al., 2016), is a sustainable approach to overcoming the negative effects of salt stress on seed germination, plant growth, and productivity.

Proline is the most common endogenous osmolyte accumulated under various abiotic stresses including salinity (Szabados and Savouré, 2010; Slama et al., 2015). When applied as an exogenous compound to crops, proline can improve salt tolerance (Heuer, 2010). For example, in salt-stressed *Zea mays*, foliar application of proline increased plant growth with a positive effect on yield characteristics (Alam et al., 2016). The beneficial effects of exogenous proline application on salt stress tolerance has been the subject of several reviews. For example, Ashraf and Foolad (2007) focused on the effect of exogenous proline on seed germination, seedling growth and Na^+/K^+ ratio. More recently Meena et al. (2019) considered some beneficial effects of exogenous proline on plant tolerance to varying environments. Some of the latest progress in the subject addresses aspects related to ionic toxicity reduction, biological nitrogen fixation, and salt tolerance related-gene expression. Therefore, this review integrates this most recent research with current thinking on proline and plant salt tolerance in the context of some key developmental stages of crop growth.

IMPACTS OF SALINITY ON DEVELOPMENTAL PHYSIOLOGY OF CROP PLANTS

With the exception of halophytes, which represent 1–3% of the flowering plants, most plants, and especially crops, are salt-sensitive during their life cycle. Salt stress reduces plant growth and productivity (for review see van Zelm et al., 2020) and may be a direct effect due to the accumulation of Na^+ and Cl^- or an indirect effect due to water deprivation (Ghars et al., 2008; Safdar et al., 2019).

Seed germination may be drastically affected by salinity in both glycophytes and halophytes (Ghoulam and Fares, 2001; Liu et al., 2018). Salinity inhibits *Lens culinaris* seed germination by disturbing hydrolytic enzyme activities such as α-amylase, β-amylase and α-glucosidase (Sidari et al., 2008). Salt-inhibited *Medicago sativa* seed germination is correlated with the inhibition of the seed reserve mobilization (Farissi et al., 2011). Furthermore, salinity is known to inhibit seed germination by disturbing the homeostasis of plant growth regulators such as abscisic acid and gibberellic acid, the two of the main phytohormones participating in the regulation of germination (Holdsworth et al., 2008; Skubacz et al., 2016). Salinity causes secondary stress, known as oxidative stress, when reactive oxygen species (ROS) accumulate in cells. At high levels, ROS disturb normal metabolism by peroxidating proteins, lipids, and nucleic acids (Hayat et al., 2012; Farissi et al., 2014). Salinity-induced oxidative stress and membrane damage during germination and seedling growth have been described in several plant species and explain some of the deleterious effects of salt stress on seed germination (Wang et al., 2010; Zhang et al., 2015). The proposed effects of salinity on plant during seed germination are summarized in **Figure 1**.

As the radicle and later the roots emerge, the presence of salt triggers osmotic stress which makes water uptake more difficult. In addition, high salt concentrations in soil disrupt mineral nutrition leading to ion imbalance in the cells. Accumulation of excess sodium in plant cells has a toxic effect as it leads to precipitation or partial denaturation of proteins, phytohormone imbalances, generation of ROS, and changes in membrane permeability (**Figure 2**). Salinity was also reported to affect N metabolism at different steps including N uptake, NO_3^- reduction and NH_4^+ assimilation by disturbing the activities of the main enzymes involved in nitrogen metabolism such as nitrate reductase, nitrite reductase, glutamate synthetase, and glutamate synthase (Ashraf et al., 2018).

As the seedling establishes itself to become autotrophic, photosynthesis, essential for growth, is very vulnerable to salt stress (**Figure 2**) (Safdar et al., 2019). Numerous studies have reported that photosynthesis is suppressed by salinity in several plant species. Smaller leaf area, fewer photosynthesis pigments, lower quantum efficiency of photosystem II (*Fv/Fm*) and less gas exchange were reported under salty conditions, which clearly contributed to the reduction observed in length and biomass of both shoots and roots (Ben Ahmed et al., 2011; Wani et al., 2016). Likewise, salinity was reported to induce the activity of some enzymes that degrade chlorophyll (Jamil et al., 2007). As a consequence of chlorophyllase induction, the total amount of chlorophyll decreases and chloroplast structure is disturbed, which directly influence photosynthesis rate and hence plant growth. Under osmotic stress, plants close their stomata to prevent water loss by transpiration (Yang et al., 2006). However, this mechanism also limits the assimilation of CO_2, which then slows the photosynthesis rate and limits plant growth and productivity. High levels of salt may also affect cell division (Munns and Tester, 2008).

Legume–rhizobium symbiosis is a specific relationship established between legumes and nitrogen-fixing bacteria such as rhizobia. During this mutualistic symbiosis, inside a newly formed organ called a nodule, rhizobia are able to provide enough nitrogen to the host legume through the specific activity of nitrogenase and in return they receive a variety of

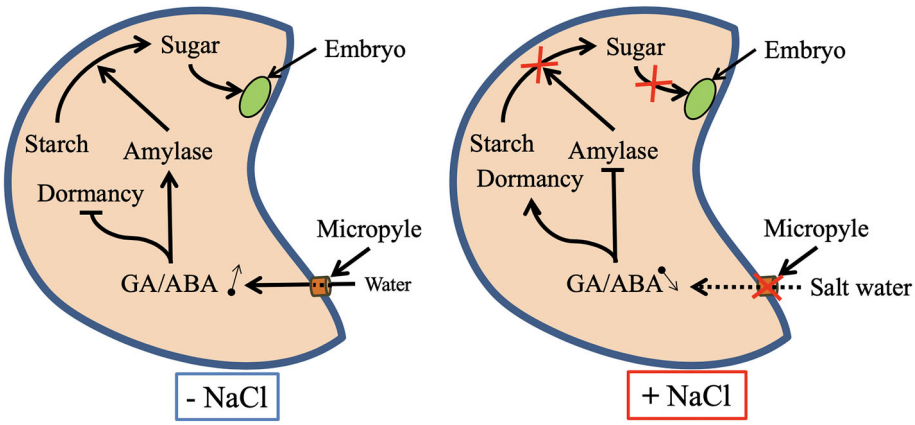

FIGURE 1 | Proposed mechanisms for the regulation of seed dormancy release and seed reserve mobilization under salt-stressed and unstressed conditions. Abbreviations: ABA, abscisic acid; GA, gibberellic acid.

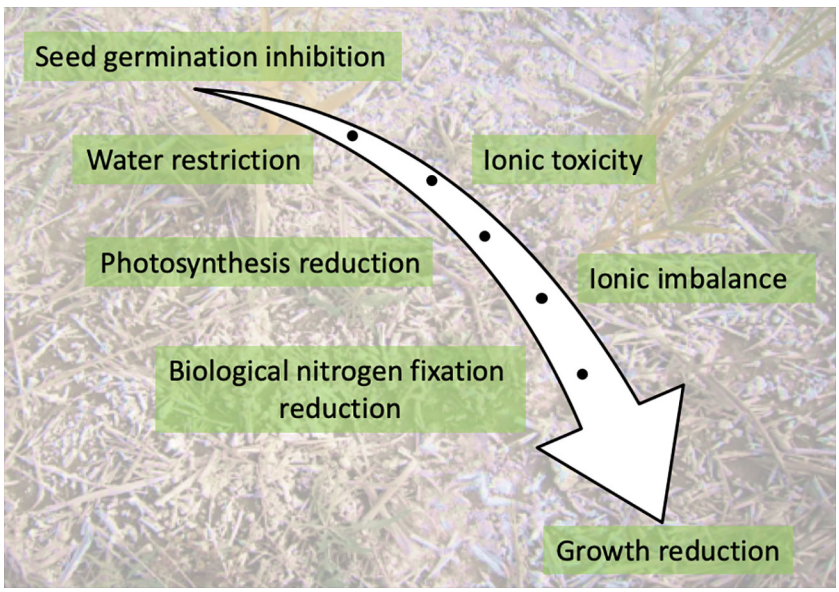

FIGURE 2 | Key impacts of salinity on a developing plant.

carbon-based compounds from photosynthates and some micronutrients *e.g.*, Fe, S, Mo (Checcucci et al., 2017). Legume–rhizobium symbiosis represents one of the main ecological processes in the agroecosystem due to its benefits on soil fertility (Farissi et al., 2014). However, this symbiotic process is drastically limited by salt stress, affecting both the micro- and macro-symbiont. Indeed, depending on their sensitivity, salinity affects the survival and distribution of rhizobia in the soil (Zahran, 1999). Salinity was also reported to inhibit legume–rhizobium symbiosis establishment by reducing the number of root hairs containing infection threads (Zahran and Sprent, 1986). In addition, if symbiosis is already established, salinity decreases symbiotic performance by reducing leghemoglobin synthesis and nitrogenase activity (López et al., 2008). Studies also showed that salt stress limits the supply of carbon sources to the bacteroids by reducing the activity of phosphoenolpyruvate carboxylase and malate dehydrogenase, and so the number of bacteroids inside the nodule (López et al., 2008). The main effects of salt stress on legume–rhizobium symbiosis are summarized in **Figure 3**.

PROLINE METABOLISM IN PLANTS

In higher plants, biosynthesis of proline occurs *via* two pathways depending on the relative availability of the alternative

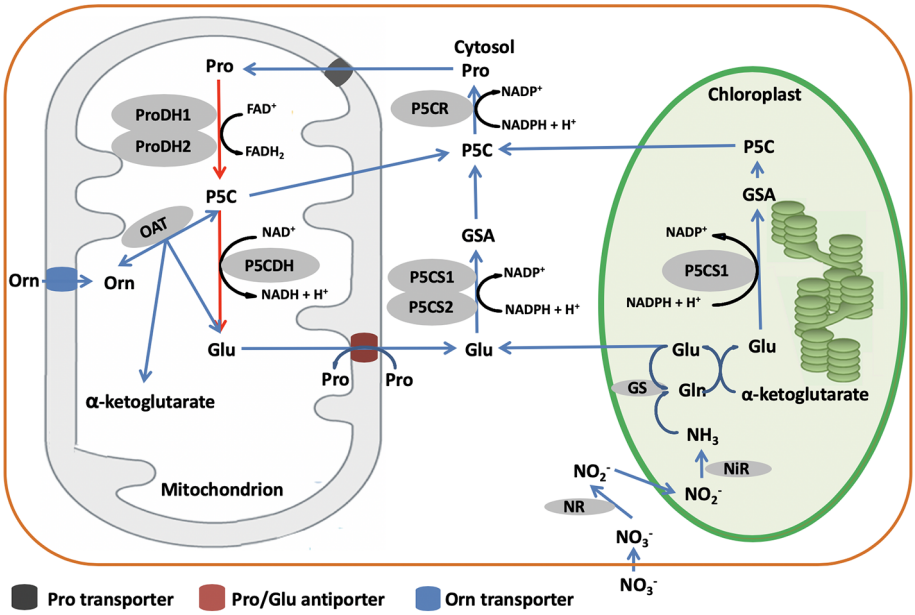

FIGURE 3 | Proposed proline metabolism pathways in higher plants. Biosynthesis (blue lines) and catabolism (red lines) are shown. Abbreviations: Pro, proline; Glu, glutamate; Orn, ornithine; NR, nitrate reductase; NiR, nitrite reductase.

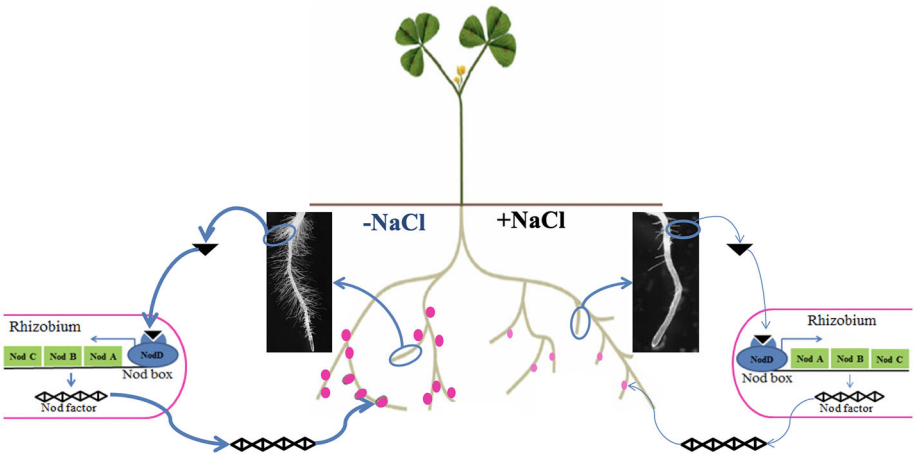

FIGURE 4 | Conceptual illustration of the effect of salt stress on the establishment and functioning of legume–rhizobium symbiosis. Under nitrogen deficiency, without salt stress the legume emits many (bold arrow) chemical cues in the form of isoflavonoids (black triangle) to specifically attract rhizobia, which in turn secrete Nod factors allowing recognition between the two partners and formation of functional nodules (dark pink dots). However, salt stress negatively affects the legume–rhizobium dialogue by reducing isoflavonoid secretion (thin arrow) leading to less nodulation (number and biomass) and nodule function (pale pink dots).

substrates, glutamate (Glu) and ornithine (Orn) (**Figure 4**). The Glu pathway starts with pyrroline-5-carboxylate synthetase (P5CS) that uses ATP and NAD(P)H+H^+ to reduce Glu to glutamate-semialdehyde (GSA), which spontaneously converts to pyrroline-5-carboxylate (P5C) (Szabados and Savouré, 2010). Then, P5C is reduced to proline by the action of P5C reductase (P5CR) using NADPH and H^+ (Szabados and Savouré, 2010). In most plant species, P5CS is encoded by two genes, *P5CS1* and *P5CS2*, while P5CR is encoded by only one gene (Szabados and Savouré, 2010). However, in some species like *Medicago truncatula*, P5CS is possibly encoded by three genes (Kim and Nam, 2013; Nguyen et al., 2013). The Orn pathway has mostly been considered as an alternative pathway for proline biosynthesis. Ornithine-δ-aminotransferase (OAT) transaminates Orn to produce GSA and P5C, which is then reduced to proline by the action of P5CR (Mansour and Ali, 2017). According to You et al.

(2012), transgenic lines of rice constitutively overexpressing *OAT* produce higher levels of proline than wild type, pointing to a more pivotal role of the Orn pathway in proline biosynthesis.

Although the genes and enzymes involved in proline biosynthesis have been well studied, the preferential use of Glu or Orn as substrate is still unclear. Some authors have reported that the preferred pathway is dependent on the developmental stage, the Orn pathway having a particularly crucial role in seedling development (Schmid et al., 2005; Hayat et al., 2012). Others however, have documented that the pathway preference is species-dependent. Indeed, AbdElgawad et al. (2015) noted that the Glu pathway involving P5CS and P5CR is predominant in grass, while the Orn pathway with OAT and P5CR is predominant in legumes. This difference may be related to the N nutritional status. In fact, Delauney et al. (1993) found that OAT is nitrogen-dependent. Another aspect to consider is the environmental control over which proline biosynthetic pathway is used. Zhen and Ma (2009) showed that P5CS activity (Glu pathway) increased upon salt stress treatment, while OAT activity (Orn pathway) appeared not to be affected, suggesting that the Glu pathway rather than the Orn pathway plays a more significant role in proline accumulation during osmotic regulation. In *Vigna aconitifolia*, Delauney et al. (1993) showed that salt stress induced the accumulation of *P5CS* mRNA while *OAT* mRNA levels were suppressed. Lei et al. (2016) and Mansour and Ali (2017) confirmed that the accumulation of proline under salt stress is related to the up-regulation of *P5CS* (Glu pathway) genes and down-regulation of *Proline dehydrogenase* (*PDH*) genes. In comparison, Funck et al. (2008) demonstrated that OAT is localized in mitochondria and it is not essential for proline biosynthesis.

For catabolism, proline is converted back to Glu in the mitochondria by the sequential action of PDH and P5C dehydrogenase (P5CDH). Although the Nomenclature Committee of The International Union of Biochemistry and Molecular Biology (IUBMB) recommended the name glutamate γ-semialdehyde dehydrogenase (GSALDH), an enzyme name derived from its substrate, for the second enzyme of proline catabolism, the name P5CDH is kept in the review for clarity for the research community. PDH oxidizes proline to P5C which is converted to Glu by P5CDH using NAD^+ as electron acceptor (Servet et al., 2012; Schertl et al., 2014). In some plant species including *Arabidopsis thaliana*, *Nicotiana tabacum*, and *M. sativa*, PDH is encoded by two genes, whereas P5CDH is encoded by a single gene (Miller et al., 2005; Ribarits et al., 2007; Servet et al., 2012).

INFLUENCES OF PROLINE METABOLISM ON PHYSIOLOGICAL AND BIOCHEMICAL PROCESSES

Proline has been widely reported to be a multifunctional amino acid that acts at different plant growth stages (Szabados and Savouré, 2010). Indeed, proline metabolism plays a key role in the oxidative pentose phosphate pathway (OPPP) by generating $NAD(P)^+$ in the cytosol (Signorelli, 2016). Since the OPPP is involved in triggering seed germination, it is believed that proline metabolism has a beneficial effect on seed germination (Kavi Kishor and Sreenivasulu, 2014). When stomata are closed under osmotic stress to avoid water losses by transpiration, CO_2 assimilation is limited (Yang et al., 2006). This phenomenon reduces carbon fixation and NAD(P)H consumption by the Calvin cycle and leads to accumulation of ROS by electrolyte leakage. However, proline biosynthesis requires the oxidation of two $NAD(P)H^+$ molecules to $NADP^+$ (**Figure 4**), which helps to reduce NAD(P)H and recycle $NAD(P)^+$. Furthermore, the oxidation of NAD(P)H to $NADP^+$ during proline biosynthesis increases $NADP^+$ which will be reduced in the pentose phosphate pathway to $NAD(P)H^+$ generating one molecule of CO_2 (**Figure 5**). Thus, the CO_2 generated allows carbon reduction to continue under stressful conditions, while the NAD(P)H will be used in proline biosynthesis to prevent ROS production (Verslues and Sharma, 2010; Signorelli et al., 2015). Proline was also reported to contribute to photosynthesis improvement by protecting RuBisCo activity and mitochondrial

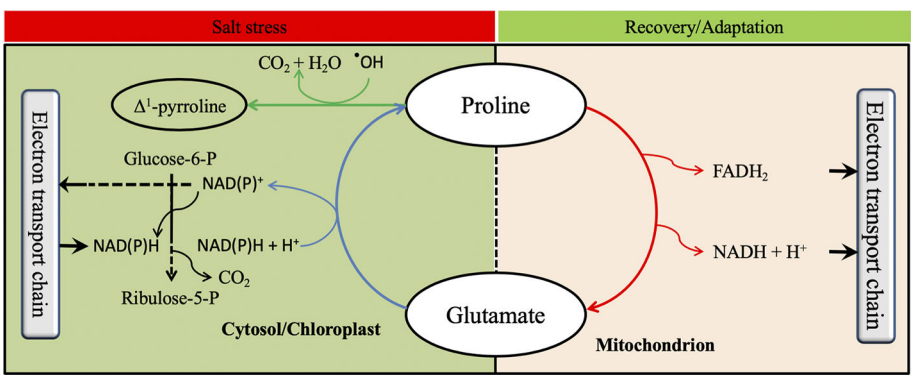

FIGURE 5 | Possible influence of proline metabolism on physiological and biochemical processes. The oxidative pentose phosphate pathway is shown by black lines, the proline anabolic pathway with blue lines, the proline catabolic pathway with red lines, and proline scavenging reactive oxygen species with green lines.

electron transport chain complex II (Solomon et al., 1994; Hamilton and Heckathorn, 2001). Furthermore, proline anabolism allows plants to adjust their osmotic homeostasis which helps to restore plant water content particularly under osmotic stress (Misra and Gupta, 2005). Proline metabolism has also been documented to play an important role during biological nitrogen fixation (BNF) particularly under stressed conditions. Indeed, a high positive correlation between the expression of *StP5CS* and two nodulation-related genes and one leghemoglobin gene was reported by Ren et al. (2018). Likewise, proline catabolism was reported to provide energy to the bacteroids during the BNF (Kohl et al., 1988) suggesting that both proline anabolism and catabolism improved BNF efficiency. In addition, proline has been reported in several studies to play a role in non-enzymatic antioxidant activities (Matysik et al., 2002; Signorelli et al., 2015). These proposed roles of proline metabolism in key physiological and biochemical are illustrated in **Figure 5**.

EFFECT OF EXOGENOUS PROLINE DURING SALT STRESS

Exogenous Proline Application and Proline Metabolism Under Salt Stress

Many studies show that salt stress triggers the induction of genes involved in proline biosynthesis, which leads to proline accumulation (Armengaud et al., 2004; Kim and Nam, 2013; Nguyen et al., 2013). According to Székely et al. (2008), knocking out the function of P5CS in *A. thaliana* indicates a key role for this enzyme in plant salt tolerance because the *p5cs1* plants are hypersensitive to salt. Exogenous application of proline can effectively improve tolerance of plants to salt stress through the regulation of endogenous proline metabolism, partly achieved through differential expression of specific proline-related genes. For example, de Freitas et al. (2018) demonstrated that foliar application of proline to *Z. mays* resulted in a decrease in P5CS activity and an increase in PDH under salt stress. Similar results in salt stressed *Sorghum bicolor* were reported more recently (de Freitas et al., 2019). Adding exogenous proline led to a decrease in P5CS activity in both stressed and unstressed *Eurya emarginata*, but to an increase in PDH activity only in unstressed plants (Zheng et al., 2015). Under salt stress, *Triticum aestivum* seed priming with exogenous proline significantly decreased the content of proline and P5C with a reduction in the activity of P5CS, while PDH activity was significantly increased (Rady et al., 2019). The effect of exogenous proline on *PDH* expression was also reported by Kiyosue et al. (1996) and Nakashima et al. (1998) in *A. thaliana*. Deuschle et al. (2001) reported that, in addition to PDH, exogenous proline increased *P5CDH* transcript levels, and suggested that this response may protect plants against proline toxicity. However, other authors like Nounjan et al. (2012) have shown that applying exogenous proline significantly increased expression of *P5CS* and *P5CR* in salt-stressed *Oryza sativa*.

Effect of Proline Treatment on Seed Germination Under Salt Stress

Seed germination is one of the most critical stages in the plant life cycle (Hubbard et al., 2012) because it is very sensitive to abiotic stress. In particular, salt stress causes osmotic stress that limits seed water absorption and ion toxicity due to the high accumulation of Na^+ and Cl^- (Murillo-Amador et al., 2002; Farissi et al., 2011). In recent years, there have been numerous papers about the effect of exogenous compounds like hormones, mineral elements, and amino acids in alleviating salinity stress during seed germination (Atia et al., 2009; Dallali et al., 2012; Rizwan et al., 2015; Coskun et al., 2016). However, the effect of exogenous proline on seed germination under salt stress is poorly understood as only a few studies have been published. Deivanai et al. (2011) demonstrated that exogenous proline had a positive concentration-dependent effect on seed germination under salt stress. Application of 1 mM proline alleviates the negative effect of 400 mM NaCl, but 100 mM proline did not have a significant effect. Similarly, 50 mM proline treatment improved seed germination of two cultivars of *S. bicolor* under salt conditions (Nawaz et al., 2010). Therefore exogenous proline application at suitable concentrations may alleviate the negative effect of salt stress by regulating cellular osmotic balance, but detailed studies behind these data are still needed to better understand the molecular mechanisms involved.

Effects of Proline Treatment on Plant Growth and Biomass Under Salt Stress

It is well documented that certain concentrations of exogenous proline regulate different aspects of plant growth and development under salt stress including rises in biomass and productivity (Huang et al., 2009; Nawaz et al., 2010; Nounjan et al., 2012; Wu et al., 2017). Addition of exogenous proline improved the growth of calli from two *Medicago sativa* cultivars upon salt stress, but dry weight and proline contents between the two were different with a better salt tolerance correlated with higher proline accumulation (Ehsanpour and Fatahian, 2003). Khan et al. (2014) tested the effects of 30 and 60 mM proline applied as a foliar spray to *Helianthus annuus*, concentrations that induced tolerance to 60 and 120 mM NaCl. They found that exogenous proline mitigates the salt stress effects on plant growth as proven by longer shoots and roots, and greater fresh and dry weights of shoots and roots, and this positive effect was more pronounced at the lower proline concentration (30 mM). Similarly, Wani et al. (2016) reported that a foliar spray of 20 mM proline alleviates the negative effects of salt stress on *Brassica juncea* by increasing lengths and fresh and dry masses of both shoots and roots, and the area of leaves. In addition, exogenous proline supply significantly increased plant height and number of roots in salt stressed *O. sativa* (Teh et al., 2016). Likewise, application of proline increased dry mass of leaves and roots and their soluble protein contents in salt stressed *Z. mays* (de Freitas et al., 2018). In some cases, exogenous proline stimulates yield under salt stress. Exogenous proline increased fresh and dry biomasses, grain yield and 1000-grain weight of salt-stressed *T. aestivum* (Rady et al., 2019). In salt-stressed *Z.*

mays, foliar-applied proline increased the number of seeds per plant, total grain weight and the 100-grain weight (Alam et al., 2016). In general, exogenous application of proline increased plant growth and productivity under salt-induced stress but the underlying mechanisms, probably linked to some hormonal regulation, still remain elusive.

Exogenous Proline Alters Stress-Responsive Gene Expression Under Salt Stress

Evidence for the mechanisms by which exogenous proline improves plant salt tolerance is still scarce. In order to gain some insight into such mechanisms at the gene level, Nounjan et al. (2012) studied the effect of exogenous proline on the expression of proline metabolism-related genes *P5CS* and *P5CR* as well as genes encoding antioxidant enzymes, superoxide dismutases (*Cu/ZnSOD, MnSOD*), ascorbate peroxidase (*CytAPX*), and catalase (*CatC*), in salt-stressed *O. sativa* seedlings. Results showed that after six days of salt treatment, exogenous proline upregulated *P5CS* and *P5CR* transcript levels. Likewise, the genes encoding antioxidant-related enzymes were upregulated by exogenous proline added to the salt-stressed rice plants. In a different study on salt-stressed *N. tabacum*, exogenous proline was found to increase transcript levels of genes encoding SOD, cationic peroxidase (POX) and CAT (Hoque et al., 2008). To understand more about the mechanistic role of gene regulation in exerting the effect of exogenous proline as plant salt tolerance, additional genetic experiments are required to particularly investigate the expression of genes related to the transport and translocation of Na^+ and Cl^-. More needs to be known about the relationship between the addition of proline and the expression of aquaporin-related genes under salt stress.

Exogenous Proline Influences Plant–Water Relations Under Salt Stress

Much research has documented how exogenous proline substantially alleviates salt stress by increasing leaf water potential, water content and restoring water use efficiency (**Table 1**). In *Brassica juncea*, Wani et al. (2016) noted that the leaf water potential was reduced under salt stress, but 20 mM proline applied as a foliar spray completely reversed the loss in water potential. Similarly, Huang et al. (2009) demonstrated that, under saline conditions, exogenous proline could alleviate the growth inhibition of salt-sensitive *Cucumis sativus*, and this was accompanied with leaves having higher water content. Studying salt-stressed *O. europaea* plants, Ben Ahmed et al. (2011) found that the relative water content is 1.05 and 1.09-fold higher under 25 and 50 mM of exogenous proline, respectively, than in the absence of proline. In the same way, 20 mM exogenous proline significantly alleviated the negative effects of 200 mM NaCl and raised the leaf water content in *Eurya emarginata* (Zheng et al., 2015). The role of exogenous proline in maintaining higher plant water content under salinity was also reported in *Onobrychis viciifolia* (Wu et al., 2017) and *S. bicolor* (de Freitas et al., 2019).

Many authors have suggested that the increase in water content and water potential of leaves in response to exogenous proline under salt stress could be because the proline triggers the accumulation of some organic and inorganic compounds such as proline, glycine betaine, soluble sugars and K^+ that help plants adjust their cellular osmotic potential and hence maintain higher water content (Ben Ahmed et al., 2011; Nounjan et al., 2012; Khan et al., 2014; Zheng et al., 2015). Another possibility is that maintaining a favorable water content under osmotic stress may be attributed to the regulation of the expression of root aquaporin genes in response to exogenous proline. These possible mechanisms for mediating osmotic stress tolerance and improving plant water content need to be studied in more detail at the molecular level.

Exogenous Proline Balances Mineral Nutrient Uptake and Assimilation Under Salt Stress

Salinity not only increases Na^+ and Cl^- in plants but also induces decreases in Ca^{2+}, K^+, Mg^{2+}, NO_3^-, S, and other essential nutrients leading to overall nutrient deficiency (Manchanda and Garg, 2008; Farissi et al., 2014). The positive effects of exogenous proline on plant tolerance to salt stress have been linked to increased assimilation of nutrients in many studies. Abdelhamid et al. (2013) reported that exogenous proline application increased P, K, NO_3^- and NO_2^- contents in *Phaseolus vulgaris* under different levels of salinity (three fields with electrical conductivities of 1.84, 6.03, or 8.97 dS m^{-1}). Similarly, exogenous proline increased leaf N, Ca^{2+} and K^+ contents in *Cucumis melo* exposed to stress from 150 mM salt (Kaya et al., 2007). Also under salty conditions, exogenous proline increased Ca^{2+} and K^+ in *S. bicolor* (de Freitas et al., 2019) and *O. europaea* (Ben Ahmed et al., 2011). Alam et al. (2016) suggested that exogenous proline may increase the uptake of N, P, K^+ and S in *Z. mays* under salinity. As well as nutrient uptake, the activities of some enzymes involved in nutrient assimilation are triggered by exogenous proline under salty conditions. Nitrate reductase is one of the most important enzymes involved in nitrogen assimilation and exogenous proline stimulates its activity in *H. annuus* (Khan et al., 2014) and *C. melo* (Yan et al., 2011) exposed to salt stress. Recently, Teh et al. (2016) reported that exogenous proline alleviated the negative effects of salt stress and enhanced nitrate reductase and Glu synthase activities in *O. sativa*. Some authors have suggested that proline may provide a good way to store and recycle nitrogen under stress conditions (Heuer, 2010; Szabados and Savouré, 2010; Verslues and Sharma, 2010; Ben Rejeb et al., 2014; Mansour and Ali, 2017). Consistent with this line of reasoning is evidence that PDH is stimulated in *P. vulgaris* under nitrogen deficiency suggesting that proline may be used as a nitrogen source for growth (Hayat et al., 2012). Similarly, exogenous proline was also used as a source of nitrogen by *Vigna radiata* L. seedlings under stress conditions (Posmyk and Janas, 2007).

The above studies provide preliminary evidence that exogenous proline alleviates the negative effects of salt by

TABLE 1 | Effects of exogenous proline on seed germination, plant growth, photosynthesis, nutrient acquisition, water uptake, ionic toxicity, proline metabolism, gene expression, antioxidant activities, and biological nitrogen fixation in different plant species under salt stress.

Plant name	Salt concentration	Exogenous proline concentration	Application method	Variable	Effect of exogenous proline		
					Without stress	With stress	References
Cucumis melo	150 mM	10 mM	Foliar spray	Growth		+	Kaya et al. (2007)
				Chlorophyll content		+	
				Electrolyte leakage		+	
				Proline content	Not shown	+	
				Relative water content		+	
				Stomatal density		+	
				Nutrient acquisition and Na/K ratio		+	
	100 mM	10 mM	Foliar spray	Growth	–	+	Huang et al. (2009)
				Proline content	+	+	
Cucumis sativus				Relative water content	–	+	
				MDA	+	+	
				Antioxidant enzyme activities	+	+	
				Na^+, Cl^- and K^+ content	–	–	
	200 mM	10 mM	Nutrient solution	Growth	–	–	Zheng et al. (2015)
				MDA	–	+	
Eurya emarginata				Na^+/K^+ ratio	–	+	
				Antioxidant enzyme activities	–	+	
				P5CS activity	–	+	
				PDH activity	+	–	
	15 mM	25 mM	Not shown	Number of nodules	–	+	Sabagh et al. (2017)
Glycine				Biological nitrogen fixation	–	+	
				Nitrogenase activity	+	+	
Helianthus annus	60 mM	30 mM	Foliar spray	Growth	+	+	Khan et al. (2014)
	120 mM	60 mM		Chlorophyll content	+	+	
				Na+ and K+ content	+	+	
				Nitrate reductase activity	-	+	
				Protein content	+	+	
				Total amino acids	+	+	
				Total sugars	–	-	
Mung bean	300 mM	15 mM	Nutrient solution	Glutathione	Not shown		Hossain and Fujita (2010)
				Antioxidant enzyme activities			
				MDA and H2O2			
Nicotiana tabacum	200 mM	20 mM	Medium solution	Non enzymatic antioxidant activities	Not shown	+	Hoque et al. (2008)
				Antioxidant enzyme activities		+	
				Carbonyl content		+	
Olea europaea	100 mM	25 mM	Nutrient solution	Relative water content and leaf water	Not shown	+	Ben Ahmed et al. (2011)
	200 mM	50 mM		potential		+	
				Gas exchange		+	
				Photosynthetic pigment		+	
				Compatible solute		-	
				Mineral ion contents		+	
				Na^+/K^+ and $Na^+/Ca2^+$ ratio			
Onobrychi sviciaefolia	25 mM	2.5 mM	Nutrient solution	Growth	-	+	Wu et al. (2017)
	100 mM			Water content	-	+	
				MDA	-	-	
				Na^+/K^+ ratio	-	+	
				Proline content	+	+	
Oryza sativa	100 mM	1 mM	Seed pretreatment	Seed germination	-	+	Deivanai et al. (2011)
	200 mM	5 mM		Growth	-	+	
	300 mM	10 mM		Chlorophyll content	+	+	
	400 mM			Proline content	+	-	
				Protein content	+	+	
	100 mM	10 mM	Nutrient solution	Growth	-	-	Nounjan et al. (2012)
				Na^+/K^+ ratio	+	+	
				Proline content	+	+	
				H2O2 content	+	+	
				Antioxidant enzyme activities	+	+	
				P5CS gene expression	+	+	

(Continued)

TABLE 1 | Continued

Plant name	Salt concentration	Exogenous proline concentration	Application method	Variable	Effect of exogenous proline		
					Without stress	With stress	References
				P5CR gene expression	+	+	
				Antioxidant enzyme gene expression	+	+	
	150 mM	5 mM 10 mM	Growth medium	Growth	+	+	Teh et al. (2016)
				Nitrogen-metabolism enzyme activities	-	+	
				Nitrogen content	-	+	
Pisum sativum	100 mM	60 mM	Foliar spray	Growth	+	+	Shahid et al. (2014)
				Gas exchange	+	+	
				Chlorophyll content	+	+	
				Relative water content	+	+	
				Compatible solute	+	+	
				H2O2, MDA and electrolyte leakage	-	+	
Sorghum bicolor	75 mM	30 mM	Foliar spray	Growth	-	+	de Freitas et al. (2019)
				Membrane damage	-	+	
				Relative water content	-	+	
				Gas exchange	-	+	
				Nutrient uptake	-	+	
				K^+/Na^+ ratio	-	+	
				Amino acids	-	+	
				Proline content	+	+	
				P5CS activity	-	+	
				OAT activity	-	-	
				ProDH activity	+	+	
				P5CS gene expression	-	+	
				OAT gene expression	+	+	
				ProDH gene expression	+	+	
Triticum durum	120 mM	12 mM	Seed pretreatment	Growth	-	+	Rady et al. (2019)
				Photosynthetic activities	-	+	
				K^+/Na^+ ratio	-	+	
				Proline content	-	+	
				Proline metabolism enzyme activities	-	+	
				MDA and H2O2 content	-	+	
				Antioxidant enzyme activities	-	+	
				Non-enzymatic antioxidant activities	-	+	
Zea mays	25 mM 50 mM	25 mM 50 mM 100 mM	Foliar spray	Growth	Not shown	+	Alam et al. (2016)
				Grain yield		+	
				Chlorophyll		+	
				Nutrient uptake		+	
				K^+/Na^+ ratio		+	
	80 mM	30 mM	Foliar spray	Growth	-	+	de Freitas et al. (2018)
				Ion content	-	-	
				K^+/Na^+ ratio	-	-	
				Proline content	+	+	
				P5CS activity	-	+	
				ProDH activity	+	+	
				Antioxidant enzyme activities	-	+	
				Non enzymatic antioxidant activities	-	-	
				MDA and H2O2 content	-	+	

+ and - indicate positive and negative effects, respectively.

improving uptake of some nutrients as well as stimulating the activity of some enzymes involved in nutrient assimilation. However, research into the effect of exogenous proline on the translocation of micronutrients is limited.

Proline Treatment Mediates Reduction in Ion Toxicity Due to Salt Stress

High salt concentrations increase Na^+ and Cl^- contents in plants and decrease the abundance of other cations such as K^+ and Ca^{2+}, which leads to mineral nutrient imbalance (Zhu and Gong, 2014). Indeed, under salty conditions, sustaining ion homeostasis is one of the adaptive strategies that tolerant plants use to cope with salt stress. These strategies may help the plant to prevent potentially toxic effects of the build-up of ions like Na^+ and Cl^- that cause various types of damage to lipids, proteins and nucleic acids (Zhu and Gong, 2014; Bargaz et al., 2015; Rizwan et al., 2015). Application of 5 mM proline in a foliar spray decreased Na^+ content and increased K^+/Na^+ ratio in *P. vulgaris*

(Abdelhamid et al., 2013). More recently, de Freitas et al. (2018) reported that external application of proline decreased both Na^+ and Cl^- contents, but increased the K^+ content and the K^+/Na^+ ratio in salt-stressed *Z. mays*. Similar results have been reported in *S. bicolor* (de Freitas et al., 2019). Khan et al. (2014) demonstrated that exogenous proline alleviated the negative effect of 120 mM salt, and enhanced K^+ content, and reduced Na^+ concentration in *H. annuus*. In salt-stressed *O. europaea*, exogenous proline improved salt tolerance through maintaining a low Na^+ content, a high K^+ content and lowered Na^+/K^+ and Na^+/Ca^{2+} ratios in both young and old leaves (Ben Ahmed et al., 2011). Compared to salt-stressed plants, exogenous proline application increased the K^+/Na^+ ratio in *O. sativa* under 100 mM NaCl (Sobahan et al., 2012) and in *Z. mays* under 50 mM NaCl (Alam et al., 2016). Recently, Wu et al. (2017) reported that 2.5 mM exogenous proline decreased the Na^+/K^+ ratio in *Onobrychis viciifolia* Scop under 100 mM NaCl.

Removing Na^+ from the cytosol and compartmentalizing it in the vacuole are important strategies to maintain a low Na^+ concentration (Bargaz et al., 2015). Transgenic *Saccharum officinarum* overexpressing the *P5CS1* gene had a low Na^+ content compared to wild type (Guerzoni et al., 2014). Ben Ahmed et al. (2011) had previously suggested that the lower accumulation of Na^+ in proline-treated *O. europaea* under salt stress may be due to the effect of exogenous proline on the ability of root to exclude the salt ions Na^+ and Cl^- from the xylem to the shoot. The activity of some transporters, like a plasma membrane Na^+/H^+ antiporter encoded by the *SALT overly sensitive* (*SOS*) gene, facilitates the export of Na^+ from the cytosol to the leaves, protecting the plant from its toxicity (Zhu, 2003; Bargaz et al., 2015). Proline does not always act in this way to induce salt tolerance. Indeed, in *C. sativus*, exogenous proline has no significant effect on Na^+ and K^+ concentrations in leaves but improves leaf water content under 100 mM NaCl (Huang et al., 2009). This higher water content due to the exogenous application of proline may dilute the salt and therefore limit salt toxicity leading to better plant growth. This was confirmed by Ben Ahmed et al. (2011) who reported that the large reduction in Na^+ accumulation in leaves and roots in response to exogenous proline application was due to its interference in osmotic adjustment and/or its dilution. Additional studies on the effect of exogenous proline on membrane transporters, such as Na^+/H^+ antiporters and K^+/H^+ symporters, are needed to investigate the mechanism by which exogenous proline reduces salt ion toxicity.

Exogenous Proline Improves Photosynthesis Under Salt Stress

Abiotic stresses, including salt stress, cause stomata to close and chlorophyll synthesis to slow down (Hayat et al., 2012), while activating chlorophyllase activities (Jamil et al., 2007), damaging chloroplast structure and destabilizing pigment protein complexes (Singh and Dubey, 1995). These effects lead to a reduction in photosynthesis and, as a result, plant growth inhibition (Farissi et al., 2018). The beneficial effect of exogenous proline on plant growth under salt stress has often been associated with a change in photosynthesis parameters (**Table 1**) (Hayat et al., 2012; Mansour and Ali, 2017). Ben Ahmed et al. (2011) found that proline supplements to two-year-old *O. europaea* exposed to 100 or 200 mM NaCl resulted in higher levels of net photosynthesis, chlorophyll *a* and *b* and carotenoid contents as compared to salt-stressed plants without supplements. In a similar study, Wani et al. (2016) reported that exogenous proline increased various photosynthetic attributes including net photosynthesis, leaf area, stomatal conductance, intercellular CO_2, transpiration rate, and quantum efficiency of photosystem II (Fv/Fm) in two salt-stressed *B. juncea* cultivars. Similar results were obtained in *Solanum melongena* (Shahbaz et al., 2013) and in *Pisum sativum* (Shahid et al., 2014). Nawaz et al. (2010) also reported a positive effect of exogenous proline on chlorophyll *a* and total chlorophyll contents in salt-stressed *S. bicolor*. However there was no equivalent significant difference in chlorophyll b content under 50 and 100 mM of NaCl. These findings strongly suggest that exogenous proline influences plant growth under salt stress by enhancing photosynthetic processes.

Exogenous Proline Application Reduces Oxidative Stress in Salt-Stressed Plants

ROS are continuously generated in stressed plants due to the incomplete reduction of oxygen. Some of them can play a role as second messengers to trigger tolerance to abiotic stresses (Ben Rejeb et al., 2014). Proline has been considered to be a molecular chaperone due to its capacity to scavenge ROS, to stabilize protein and other macromolecular complexes, and to provide cellular redox potential (Szabados and Savouré, 2010; Ben Rejeb et al., 2014). Furthermore, under salt stress, exogenous proline increases enzymatic and non-enzymatic antioxidant activities, which improves plant tolerance. Indeed, Hossain and Fujita (2010) reported that exogenous application of 15 mM proline to the growth medium of mung bean exposed to 300 mM NaCl significantly decreased malondialdehyde (MDA) and H_2O_2 contents, and this decrease correlated significantly with an increase in glutathione content and glutathione peroxidase, glutathione-S-transferase and glutathione reductase activities. In the previously cited study by Wani et al. (2016), 20 mM proline sprayed on two *B. juncea* cultivars growing under three different concentrations of salt (2.8, 4.2, and 5.6 $dS.m^{-1}$), reduced electrolyte leakage and increased the activities of some antioxidant enzymes like CAT, SOD and POX. At the same time, proline itself can contribute to ROS scavenging and hence to plant salt tolerance, including when it is supplied exogenously (Ben Rejeb et al., 2014). However, Nounjan et al. (2012) showed that exogenous application of 10 mM proline to salt stressed *O. sativa* seedlings decreased the activity of SOD, POX, and CAT and increased H_2O_2 content. In agreement with those results, Huang et al. (2009) reported that foliar spray of proline lowered the MDA content and the SOD activity in a salt-sensitive *C. sativus* cultivar under 100 mM NaCl. An increase in POX activity in response to exogenous proline was also measured in the salt-stressed cucumber. Mansour and Ali (2017) suggested that the decrease in antioxidant activities under salt stress in response to exogenous proline may be involved in the improvement

of salt tolerance through ROS signaling. Species-specific differences may explain these contradictory results on proline effects.

Symbiotic Nitrogen Fixation Is Enhanced by Proline Treatment Under Salt Stress Conditions

Soil inorganic nitrogen deficiency is one of the most limiting factors for plant growth. However, the biological reduction of atmospheric nitrogen to ammonium by rhizobia-legume symbiosis can provide enough nitrogen to maximize growth and yield (Zahran, 1999; Kraiser et al., 2011). Encouraging rhizobia–legume symbiosis is a sustainable approach to increasing crop production, while decreasing dependency on chemical nitrogen fertilizer in traditional agriculture, which causes widespread environmental pollution (Ferguson et al., 2019). Salt stress limits the distribution, survival, and infectivity of rhizobia by decreasing the number and the biomass of nodules, and diminishing leghemoglobin synthesis and nodule respiration leading to a decrease in nitrogenase activity and nitrogen fixation rate (Zahran, 1999; Faghire et al., 2011; Monica et al., 2013). Improving BNF under salt stress is considered to be a major goal for crop scientists. Several strategies have been adopted to improve BNF under high-salt conditions including the selection of the most tolerant rhizobium–legume combinations, use of arbuscular mycorrhizal fungi, improvement of agricultural practice, genetic breeding and plant genetic modification, seed priming and exogenous application of compounds like hormones and osmoprotectants (Faghire et al., 2011; Faghire et al., 2013; Sabagh et al., 2017; Farooq et al., 2017).

Although positive correlations between endogenous proline and BNF under salt stress have been reported in many studies (Tejera et al., 2005; Verdoy et al., 2006; Fahmi et al., 2011; Kim and Nam, 2013; Bargaz et al., 2015), very few studies have focused on the effect of exogenous proline. Sabagh et al. (2017) studied salt-stressed *Glycine max* induced by 15 mM NaCl, and supplied 25 mM proline in the growing medium. The result was an increase in nodule number and biomass. Furthermore, the loss in nitrogenase activity caused by salinity was overcome when proline was applied (Sabagh et al., 2017). Similar results were observed in *Cicer arietinum* growing under conditions of cadmium toxicity, where 20 mM exogenous proline alleviated the negative effect of cadmium (25 mg/kg) and increased the number of nodules, the leghemoglobin content and the nitrogenase activity (Alyemeni et al., 2016). Moreover, the positive effect of exogenous proline on nitrogenase activity under salt stress has been reported not only in plants but also in some bacterial strains like *Klebsiella pneumonia* (Le Rudulier et al., 1982). Investigating the relationship between proline metabolism and BNF, Ren et al. (2018) demonstrated that overexpression of *StP5CS* enhanced the relative expression of two nodulation-related genes and one leghemoglobin gene. This was reflected by an increase in nodulation and nitrogen fixation under salt stress. Furthermore, overexpression of *P5CS* from *Vigna aconitifolia* in *M. truncatula* enhanced tolerance to salt stress and improved nitrogenase activity (Verdoy et al., 2006). In addition, Kim and Nam (2013) demonstrated that *P5CS3* regulated *M. truncatula* nodule number under salt stress. The above studies show that exogenous proline may improve BNF under salt stress, but the detailed mechanisms behind this relationship are still not clear as well as its relevance to field conditions.

Proline Toxicity in Salt-Stressed Plants

Despite the protective roles of exogenous proline on salt-stressed plants, several papers reported that its positive effect is concentration-dependent, high concentration could cause a toxic effect in plants (Hellmann et al., 2000; Maggio et al., 2002). For example, while low concentrations (20–33 mM) alleviated the deleterious effect of salt stress, external supplementation of high proline concentration (50 and 100 mM) was found to be toxic for both salt-stressed and unstressed callus culture of mung bean (Kumar and Sharma, 1989). In agreement with that, Rodriguez and Heyser (1988) demonstrated that 10 mM of exogenous proline seriously inhibited the normal growth of Distichlis suspension cultures under 260 mM of salt stress. Similarly, in salt stressed *Oryza sativa*, while low concentrations (20–30 mM) of proline were effective in mitigating the adverse effect of 100 mM NaCl on growth, higher concentrations (40 to 50 mM) resulted in growth reduction (Roy et al., 1993). In addition, in contrast to 1 mM, the external supplementation of 10 mM of proline to salt stressed *Solanum lycopersicum* decreased leaf and root fresh weights, even leading to plant death if proline is added in high concentration (Heuer, 2003). Furthermore, Rajendrakumar et al. (1997) showed that proline at high concentration could destabilize the DNA helix, lower the DNA melting point, increase susceptibility to S1 nuclease and insensitivity to DNAase1. Interestingly *p5cdh* and *prodh* mutants were shown to be more sensitive to proline treatments (Mani et al., 2002; Nanjo et al., 2003; Deuschle et al., 2004; Cabassa-Hourton et al., 2016), indicating the importance of proline catabolism in the regulation proline level for plants. However, the underlying mechanism of proline toxicity remains elusive.

CONCLUSIONS AND PROSPECTS

Exogenous proline application can improve salt tolerance by regulating physiological, biochemical and enzymatic processes and have a positive effect on plant growth, development and productivity under salt stress conditions. To focus on where potential solutions will be found in future crop research, the proposed beneficial effects of exogenous proline on salt stress tolerance in developing plants are summarized in **Figure 6**.

Exogenous proline reduces Na^+ and Cl^- content and increases K^+/Na^+ ratio in many plant species (**Table 1**) (*e.g.* Abdelhamid et al., 2013; de Freitas et al., 2018; de Freitas et al., 2019). Na^+/H^+ is an antiporter plasma membrane transporter, encoded by an

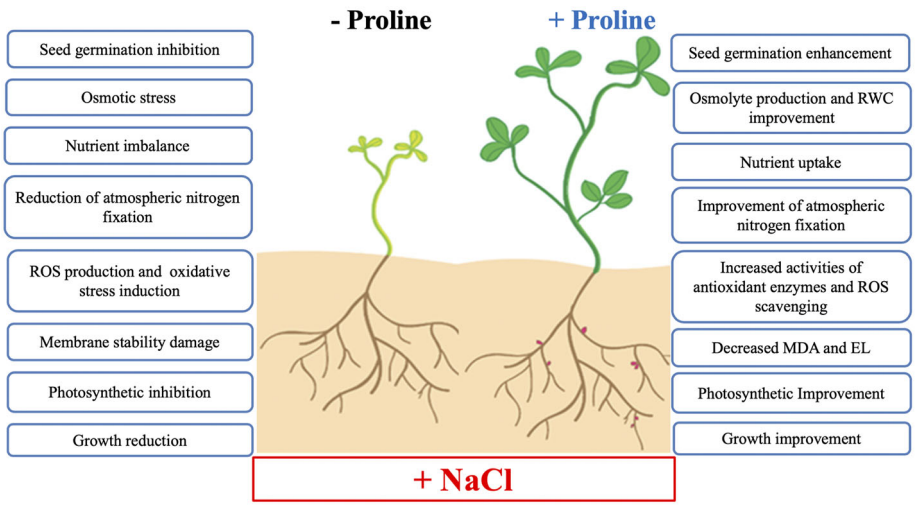

FIGURE 6 | Summary of the main effects of exogenous proline in plant salt tolerance. Abbreviations: RWC, relative water content; ROS, reactive oxygen species; MDA, malondialdehyde; EL, electrolyte leakage.

SOS1 gene, that pumps Na^+ from root cells to leaves, boosting salt stress tolerance (Zhu and Gong, 2014; Bargaz et al., 2015). High-affinity K^+ transporter (HKT) is another transporter that mediates salt tolerance in various plant species through regulation of the transport of salt ions from root to shoot (Kaundal et al., 2019; Thouin et al., 2019). In view of the important roles of these two transporters in plant salt tolerance, it would be interesting to investigate how exogenous proline can regulate the *SOS1* and *HKT* gene expression under salt stress and their relationship with salt tolerance.

Water restriction is one of the main effects of salt stress in plants (Farissi et al., 2014). Exogenous proline was widely reported to increase plant water content under salt stress (**Table 1**), and this may contribute to salt dilution and as a result plant growth improvement (Huang et al., 2009; Zheng et al., 2015). Aquaporins are a group of transporters that facilitate absorption of water by plant from soil. Under salt stress, there is a positive correlation between the expression of aquaporin genes and salt tolerance of *Eutrema salsugineum* (Qin et al., 2019). To better understand the mechanism by which exogenous proline improves plant water relations under salt stress, the effect of this osmoprotectant on the expression of aquaporin genes under salt stress will be interesting to investigate.

BNF is an important process that improves soil fertility but it is very sensitive to salt stress from the establishment of the symbiosis to nitrogen fixation (Zahran, 1999; Monica et al., 2013). The ability of exogenous proline to improve nitrogen acquisition under salt conditions was reported in several species (Kaya et al., 2007; Abdelhamid et al., 2013; Alam et al., 2016). The beneficial effect of this molecule in nitrogen nutrition of legumes through nitrogenase activity, however, is poorly understood and very few studies have been done. It will be important to focus on the effect of exogenous proline on nitrogenase gene expression under salt stress to better understand the effect of this multifunctional amino acid on BNF.

The effect of exogenous proline in alleviating the negative impact of salt stress appears to be both dose- and species-dependent. It is still not clear how proline works in reducing the detrimental effect of salt stress and further research is needed. Omics approaches can provide a more holistic molecular perspective of biological systems compared to traditional approaches. Transcriptome analysis has been widely applied to explore genes that are differentially expressed in response to abiotic stresses. These data are essential to identify and potentially manipulate genes that impact stress tolerance under diverse environmental conditions. Increasing amounts of data suggest that proline has certain regulatory functions. Using transcript profiling, Oono et al. (2003) showed that proline can also trigger expression of one third of rehydration-inducible plant genes. Most of the known proline-responsive genes have the conserved PRE cis-acting element in their promoter regions, which is a target of specific bZIP-type transcriptional activators (Oono et al., 2003; Satoh et al., 2004; Weltmeier et al., 2006). From this starting point, the proline-related signaling pathway requires further elucidation using multiomics technologies that dissect the multiple corresponding genes or metabolites. Therefore, further large-scale analyses of transcript, protein and metabolite responses are required to understand how plants respond to proline and the adaptive value of proline in plant stress adaptation.

AUTHOR CONTRIBUTIONS

AEM proposed and wrote the review. CC-H and MF commented on the content of the review and revised the text. AS revised the text at different stages of the writing process and contributed to

the final version of the manuscript. All authors contributed to the article and approved the submitted version.

FUNDING

This work was supported by the Hubert Curien Maghreb Partnership—PHC Maghreb, No. 19MAG41/41482RL—governed by the agreement signed between the French Ministry of Europe and Foreign Affairs and the Algerian, Moroccan and Tunisian Ministries of Higher Education and Scientific Research.

ACKNOWLEDGMENTS

We thank the APCE team for constructive discussions and inspiring ideas. The authors would like to thank the two reviewers and Editor for their constructive comments that helped to improve the manuscript.

REFERENCES

AbdElgawad, H., De Vos, D., Zinta, G., Domagalska, M. A., Beemster, G. T. S., and Asard, H. (2015). Grassland species differentially regulate proline concentrations under future climate conditions: an integrated biochemical and modelling approach. *New Phytol.* 208, 354–369. doi: 10.1111/nph.13481

Abdelhamid, M., Rady, M. M., Osman, A. S., and Abdalla, M. A. (2013). Exogenous application of proline alleviates salt-induced oxidative stress in *Phaseolus vulgaris* L. plants. *J. Hortic. Sci. Biotechnol.* 88, 439–446. doi: 10.1080/14620316.2013.11512989

Alam, R., Das, D., Islam, M., Murata, Y., and Hoque, M. (2016). Exogenous proline enhances nutrient uptake and confers tolerance to salt stress in maize (*Zea mays* L.). *Progr. Agric.* 27, 409–417. doi: 10.3329/pa.v27i4.32120

Alyemeni, M. N., Hayat, Q., Hayat, S., Faizan, M., and Faraz, A. (2016). Exogenous proline application enhances the efficiency of nitrogen fixation and assimilation in chickpea plants exposed to cadmium. *Legume Res.* 39, 221–227. doi: 10.18805/lr.v0iOF.9291

Armengaud, P., Thiery, L., Buhot, N., March, G. G., and Savouré, A. (2004). Transcriptional regulation of proline biosynthesis in *Medicago truncatula* reveals developmental and environmental specific features. *Physiol. Plant* 120, 442–450. doi: 10.1111/j.0031-9317.2004.00251.x

Ashraf, M. F. M. R., and Foolad, M. R. (2007). Roles of glycine betaine and proline in improving plant abiotic stress resistance. *Environ. Exp. Bot.* 59 (2), 206–216. doi: 10.1016/j.envexpbot.2005.12.006

Ashraf, M., Shahzad, S. M., Imtiaz, M., and Rizwan, M. S. (2018). Salinity effects on nitrogen metabolism in plants-focusing on the activities of nitrogen metabolizing enzymes: A review. *J. Plant Nutr.* 41, 1065–1081. doi: 10.1016/j.crvi.2009.03.009

Atia, A., Debez, A., Barhoumi, Z., Smaoui, A., and Abdelly, C. (2009). ABA, GA3, and nitrate may control seed germination of *Crithmum maritimum* (Apiaceae) under saline conditions. *C. R. Biol.* 332, 704–710. doi: 10.1016/j.crvi.2009.03.009

Bargaz, A., Zaman-Allah, M., Farissi, M., Lazali, M., Drevon, J.-J., Maougal, R., et al. (2015). Physiological and molecular aspects of tolerance to environmental constraints in grain and forage legumes. *Int. J. Mol. Sci.* 16, 18976–19008. doi: 10.3390/ijms160818976

Ben Ahmed, C., Magdich, S., Ben Rouina, B., Sensoy, S., Boukhris, M., and Ben Abdullah, F. (2011). Exogenous proline effects on water relations and ions contents in leaves and roots of young olive. *Amino Acids* 40, 565–573. doi: 10.1007/s00726-010-0677-1

Ben Rejeb, K., Abdelly, C., and Savouré, A. (2014). How reactive oxygen species and proline face stress together. *Plant Physiol. Biochem.* 80, 278–284. doi: 10.1016/J.PLAPHY.2014.04.007

Bianco, C., and Defez, R. (2009). *Medicago truncatula* improves salt tolerance when nodulated by an indole-3-acetic acid-overproducing *Sinorhizobium meliloti* strain. *J. Exp. Bot.* 60, 3097–3107. doi: 10.1093/jxb/erp140

Cabassa-Hourton, C., Schertl, P., Bordenave-Jacquemin, M., Saadallah, K., Guivarc'h, A., Lebreton, S., et al. (2016). Proteomic and functional analysis of proline dehydrogenase 1 link proline catabolism to mitochondrial electron transport in *Arabidopsis thaliana*. *Biochem. J.* (2016), 2623–2634. doi: 10.1042/BCJ20160314

Checcucci, A., DiCenzo, G. C., Bazzicalupo, M., and Mengoni, A. (2017). Trade, diplomacy, and warfare: the quest for elite rhizobia inoculant strains. *Front. Microbial.* 8:2207. doi: 10.3389/fmicb.2017.02207

Coskun, D., Britto, D. T., Huynh, W. Q., and Kronzucker, H. J. (2016). The role of silicon in higher plants under salinity and drought stress. *Front. Plant Sci.* 7:1072. doi: 10.3389/fpls.2016.01072

Dallali, H., Maalej, E. M., Ghanem Boughanmi, N., and Haouala, R. (2012). Salicylic acid priming in *Hedysarum carnosum* and *Hedysarum coronarium* reinforces NaCl tolerance at germination and the seedling growth stage. *AJCS* 6, 407–414.

de Freitas, P. A. F., de Souza Miranda, R., Marques, E. C., Prisco, J. T., and Gomes-Filho, E. (2018). Salt Tolerance Induced by Exogenous Proline in Maize Is Related to Low Oxidative Damage and Favorable Ionic Homeostasis. *J. Plant Growth Regul.* 37, 911–924. doi: 10.1007/s00344-018-9787-x

de Freitas, P. A. F., de Carvalho, H. H., Costa, J. H., Miranda, R., de, S., da, C. K. D., et al. (2019). Salt acclimation in sorghum plants by exogenous proline: physiological and biochemical changes and regulation of proline metabolism. *Plant Cell Rep.* 38, 403–416. doi: 10.1007/s00299-019-02382-5

Deivanai, S., Xavier, R., Vinod, V., Timalata, K., and Lim, O. (2011). Role of Exogenous Proline in Ameliorating Salt Stress at Early Stage in Two Rice Cultivars. *J. Stress Physiol. Biochem.* 7, 158–174.

Delauney, A. J., Hu, C.-A. A., Kishor, P. B. K., Pal, D., and Verma, S. (1993). Cloning of Ornithine delta-Aminotransferase cDNA from *Vigna aconitifolia* by Trans-complementation in Escherichia coli and Regulation of Proline Biosynthesis. *J. Biol. Chem.* 268, 18673–18676.

Deuschle, K., Funck, D., Forlani, G., Stransky, H., Biehl, A., Leister, D., et al. (2004). The role of Δ1-pyrroline-5-carboxylate dehydrogenase in proline degradation. *Plant Cell* 16, 3413–3425. doi: 10.1105/tpc.104.023622

Deuschle, K., Funck, D., Hellmann, H., Däschner, K., Binder, S., and Frommer, W. B. (2001). A nuclear gene encoding mitochondrial Δ1-pyrroline-5-carboxylate dehydrogenase and its potential role in protection from proline toxicity. *Plant J.* 27, 345–356. doi: 10.1046/j.1365-313X.2001.01101.x

Ehsanpour, A. A., and Fatahian, N. (2003). Effects of salt and proline on *Medicago sativa* callus. *Plant Cell Tiss. Org. Cult.* 73, 53–56. doi: 10.1023/A:1022619523726

Faghire, M., Bargaz, A., Farissi, M., Palma, F., Mandri, B., Lluch, C., et al. (2011). Effect of salinity on nodulation, nitrogen fixation and growth of common bean (Phaseolus vulgaris) inoculated with rhizobial strains isolated from the Haouz region of Morocco. *Symbiosis* 55, 69–75. doi: 10.1007/s13199-011-0144-0

Faghire, M., Farissi, M., Taoufiq, K., Fghire, R., Bargaz, A., Mandri, B., et al. (2013). Genotypic variation of nodules' enzymatic activities in symbiotic nitrogen fixation among common bean (*Phaseolus vulgaris* L.) genotypes grown under salinity constraint. *Symbiosis* 60, 115–122. doi: 10.1007/s13199-013-0247-x

Fahmi, A.II, Nagaty, H. H., Eissa, R. A., and Hassan, M. M. (2011). Effects of salt stress on some nitrogen fixation parameters in Faba Bean. *Pakistan J. Biol. Sci.* 14, 385–391. doi: 10.3923/pjbs.2011.385.391

Farissi, M., Bouizgaren, A., Faghire, M., Bargaz, A., and Ghoulam, C. (2011). Agro-physiological responses of Moroccan alfalfa (*Medicago sativa* L.) populations to salt stress during germination and early seedling stages. *Seed Sci. Technol.* 39, 389–401. doi: 10.15258/sst.2011.39.2.11

Farissi, M., Aziz, F., Bouizgaren, A., and Ghoulam, C. (2014). Legume-rhizobia symbiosis under saline conditions: Agro-physiological and biochemical aspects of tolerance. *Int. J. Innov. Sci. Res.* 11, 96–104.

Farissi, M., Mouradi, M., Farssi, O., Bouizgaren, A., and Ghoulam, C. (2018). Variations in leaf gas exchange, chlorophyll fluorescence and membrane potential of Medicago sativa root cortex cells exposed to increased salinity:

The role of the antioxidant potential in salt tolerance. *Arch. Biol. Sci.* 70, 413–423. doi: 10.2298/ABS171019001F

Farooq, M., Gogoi, N., Hussain, M., Barthakur, S., Paul, S., Bharadwaj, N., et al. (2017). Effects, tolerance mechanisms and management of salt stress in grain legumes. *Plant Physiol. Biochem.* 118, 199–217. doi: 10.1016/J.PLAPHY.2017.06.020

Ferguson, B. J., Mens, C., Hastwell, A. H., Zhang, M., Su, H., Jones, C. H., et al. (2019). Legume nodulation: The host controls the party. *Plant Cell Environ.* 42, 41–51. doi: 10.1111/pce.13348

Funck, D., Stadelhofer, B., and Koch, W. (2008). Ornithine-δ-aminotransferase is essential for Arginine Catabolism but not for Proline Biosynthesis. *BMC Plant Biol.* 8:40. doi: 10.1186/1471-2229-8-40

Ghars, M. A., Parre, E., Debez, A., Bordenave, M., Richard, L., Leport, L., et al. (2008). Comparative salt tolerance analysis between *Arabidopsis thaliana* and *Thellungiella halophila*, with special emphasis on K^+/Na^+ selectivity and proline accumulation. *J. Plant Physiol.* 165, 588–599. doi: 10.1016/j.jplph.2007.05.014

Ghoulam, C., and Fares, K. (2001). Effect of salinity on seed germination and early seedling growth of sugar beet (*Beta vulgaris* L.). *Seed Sci. Technol.* 29, 357–364.

Guerzoni, J. T. S., Belintani, N. G., Moreira, R. M. P., Hoshino, A. A., Domingues, D. S., Filho, J. C. B., et al. (2014). Stress-induced Δ1-pyrroline-5-carboxylate synthetase (P5CS) gene confers tolerance to salt stress in transgenic sugarcane. *Acta Physiol. Plant* 36, 2309–2319. doi: 10.1007/s11738-014-1579-8

Hamilton, E. W., and Heckathorn, S. A. (2001). Mitochondrial adaptations to NaCl. Complex I is protected by anti-oxidants and small heat shock proteins, whereas complex II is protected by proline and betaine. *Plant Physiol.* 126 (3), 1266–1274. doi: 10.1104/pp.126.3.1266

Hayat, S., Hayat, Q., Alyemeni, M. N., Wani, A. S., Pichtel, J., Ahmad, A., et al. (2012). Role of proline under changing environments: A review. *Plant Signal. Behav.* 7, 1–11. doi: 10.4161/psb.21949

Hellmann, H., Funck, D., Rentsch, D., and Frommer, W. B. (2000). Hypersensitivity of an Arabidopsis sugar signaling mutant toward exogenous proline application. *Plant Physiol.* 122, 357–368. doi: 10.1104/pp.122.2.357

Heuer, B. (2003). Influence of exogenous application of proline and glycinebetaine on growth of salt-stressed tomato plants. *Plant Sci.* 165, 693–699. doi: 10.1016/S0168-9452(03)00222-X

Heuer, B. (2010). "Role of proline in plant response to drought and salinity," in *Handbook of Plant and Crop Stress*, *3rd ed*. Ed. A. Pessarakli (Boca Raton: CRC Press), 213–238.

Holdsworth, M. J., Bentsink, L., and Soppe, W. J. (2008). Molecular networks regulating Arabidopsis seed maturation, after-ripening, dormancy and germination. *New Phytol.* 179, 33–54. doi: 10.1111/j.1469-8137.2008.02437.x

Hoque, M. A., Banu, M. N. A., Nakamura, Y., Shimoishi, Y., and Murata, Y. (2008). Proline and glycinebetaine enhance antioxidant defense and methylglyoxal detoxification systems and reduce NaCl-induced damage in cultured tobacco cells. *J. Plant Physiol.* 165, 813–824. doi: 10.1016/J.JPLPH.2007.07.013

Hossain, M. A., and Fujita, M. (2010). Evidence for a role of exogenous glycinebetaine and proline in antioxidant defense and methylglyoxal detoxification systems in mung bean seedlings under salt stress. *Physiol. Mol. Biol. Plants* 16, 19–29. doi: 10.1007/s12298-010-0003-0

Huang, Y., Bie, Z., Liu, Z., Zhen, A., and Wang, W. (2009). Protective role of proline against salt stress is partially related to the improvement of water status and peroxidase enzyme activity in cucumber. *Soil Sci. Plant Nutr.* 55, 698–704. doi: 10.1111/j.1747-0765.2009.00412.x

Hubbard, M., Germida, J., and Vujanovic, V. (2012). Fungal endophytes improve wheat seed germination under heat and drought stress. *Botany* 90, 137–149. doi: 10.1139/b11-091

Jamil, M., Rehman, S., Lee, K. J., Kim, J. M., Kim, H.-S., and Rha, E. S. (2007). Salinity reduced growth PS2 photochemistry and chlorophyll content in radish. *Sci. Agric.* 64, 111–118. doi: 10.1590/S0103-90162007000200002

Jha, U. C., Bohra, A., Jha, R., and Parida, S. K. (2019). Salinity stress response and "omics" approaches for improving salinity stress tolerance in major grain legumes. *Plant Cell Rep.* 38, 255–277. doi: 10.1007/s00299-019-02374-5

Kaundal, A., Sandhu, D., Duenas, M., and Ferreira, J. F. S. (2019). Expression of the high-affinity K+ transporter 1 (PpHKT1) gene from almond rootstock "Nemaguard" improved salt tolerance of transgenic Arabidopsis. *PloS One* 14, e0214473. doi: 10.1371/journal.pone.0214473

Kavi Kishor, P. B., and Sreenivasulu, N. (2014). Is proline accumulation per se correlated with stress tolerance or is proline homeostasis a more critical issue? *Plant Cell Environ.* 37, 300–311. doi: 10.1111/pce.12157

Kaya, C., Tuna, A. L., Ashraf, M., and Altunlu, H. (2007). Improved salt tolerance of melon (*Cucumis melo* L.) by the addition of proline and potassium nitrate. *Environ. Exp. Bot.* 60, 397–403. doi: 10.1016/j.envexpbot.2006.12.008

Khan, A., Iqbal, I., Ahmed, I., Nawaz, H., and Nawaz, M. (2014). Role of proline to induce salinity tolerance in sunflower (*Helianthus annus* L.). *Sci. Technol. Dev.* 33, 88–93.

Kim, G. B., and Nam, Y. W. (2013). A novel Δ1-pyrroline-5-carboxylate synthetase gene of *Medicago truncatula* plays a predominant role in stress-induced proline accumulation during symbiotic nitrogen fixation. *J. Plant Physiol.* 170, 291–302. doi: 10.1016/j.jplph.2012.10.004

Kiyosue, T., Yoshiba, Y., Yamaguchi-Shinozaki, K., and Shinozaki, K. (1996). A nuclear gene encodinq mitochondrial Proline Dehydrogenase, an enzyme involved in proline metabolism, is upregulated by proline but downregulated by dehydration in Arabidopsis. *Plant Cell* 8, 1323–1335. doi: 10.1105/tpc.8.8.1323

Kohl, D. H., Schubert, K. R., Carter, M. B., Hagedorn, C. H., and Shearer, G. (1988). Proline metabolism in N2-fixing root nodules: energy transfer and regulation of purine synthesis. *Proc. Natl. Acad. Sci.* 85, 2036–2040. doi: 10.1073/pnas.85.7.2036

Kraiser, T., Gras, D. E., Gutiérrez, A. G., González, B., and Gutiérrez, R. A. (2011). A holistic view of nitrogen acquisition in plants. *J. Exp. Bot.* 62, 1455–1466. doi: 10.1093/jxb/erq425

Kumar, V., and Sharma, D. R. (1989). Effect of exogenous proline on growth and ion content in NaCl stressed and monstressed cells of mungbean, *Vigna radiata* var. radiata. *Indian J. Exp. Biol.* 27, 813–815.

Le Rudulier, D., Yang, S. S., and Csonka, L. N. (1982). Nitrogen fixation in *Lebsiella pneumoniae* during osmotic stress Effect of exogenous proline or proline overproducing plasmid. *Biochim. Biophys. Acta* 719, 273–283. doi: 10.1016/0304-4165(82)90099-X

Lei, P., Xu, Z., Liang, J., Luo, X., Zhang, Y., Feng, X., et al. (2016). Poly(γ-glutamic acid) enhanced tolerance to salt stress by promoting proline accumulation in *Brassica napus* L. *Plant Growth Regul.* 78, 233–241. doi: 10.1007/s10725-015-0088-0

Liu, R., Wang, L., Tanveer, M., and Song, J. (2018). Seed Heteromorphism: An Important Adaptation of Halophytes for Habitat Heterogeneity. *Front. Plant Sci.* 9:1515:1515. doi: 10.3389/fpls.2018.01515

López, M., Herrera-Cervera, J. A., Iribarne, C., Tejera, N. A., and Lluch, C. (2008). Growth and nitrogen fixation in *Lotus japonicus* and *Medicago truncatula* under NaCl stress: nodule carbon metabolism. *J. Plant Physiol.* 165 (6), 641–650. doi: 10.1016/j.jplph.2007.05.009

Maggio, A., Miyazaki, S., Veronese, P., Fujita, T., Ibeas, J.II, Damsz, B., et al. (2002). Does proline accumulation play an active role in stress-induced growth reduction? *Plant J.* 31, 699–712. doi: 10.1046/j.1365-313X.2002.01389.x

Manchanda, G., and Garg, N. (2008). Salinity and its effects on the functional biology of legumes. *Acta Physiol. Plant* 30, 595–618. doi: 10.1007/s11738-008-0173-3

Mani, S., Van De Cotte, B., Van Montagu, M., and Verbruggen, N. (2002). Altered levels of proline dehydrogenase cause hypersensitivity to proline and its analogs in Arabidopsis. *Plant Physiol.* 128, 73–78. doi: 10.1104/pp.010572

Mansour, M. M. F., and Ali, E. F. (2017). Evaluation of proline functions in saline conditions. *Phytochemistry* 140, 52–68. doi: 10.1016/J.PHYTOCHEM.2017.04.016

Matysik, J., Alia, B. B., and Mohanty, P. (2002). Molecular mechanisms of quenching of reactive oxygen species by proline under stress in plants. *Curr. Sci.* 82, 525–532.

Meena, M., Divyanshu, K., Kumar, S., Swapnil, P., Zehra, A., Shukla, V., et al. (2019). Regulation of L-proline biosynthesis, signal transduction, transport, accumulation and its vital role in plants during variable environmental conditions. *Heliyon* 5, e02952. doi: 10.1016/j.heliyon.2019.e02952

Miller, G., Stein, H., Honig, A., Kapulnik, Y., and Zilberstein, A. (2005). Responsive modes of *Medicago sativa* proline dehydrogenase genes during salt stress and recovery dictate free proline accumulation. *Planta* 222, 70–79. doi: 10.1007/s00425-005-1518-4

Misra, N., and Gupta, A. K. (2005). Effect of salt stress on proline metabolism in two high yielding genotypes of green gram. *Plant Sci.* 169 (2), 331–339. doi: 10.1016/j.plantsci.2005.02.013

Monica, N., Vidican, R., Pop, R., and Rotar, I. (2013). Stress factors affecting symbiosis activity and nitrogen fixation by Rhizobium cultured *in vitro*. *ProEnvironment* 6, 42–45.

Munns, R., and Tester, M. (2008). Mechanisms of salinity tolerance. Annu. *Rev. Plant Biol.* 59, 651–681. doi: 10.1146/annurev.arplant.59.032607.092911

Murillo-Amador, B., Lopez-Aguilar, R., Kaya, C., Larrinaga-Mayoral, J., and Flores-Hernandez, A. (2002). Comparative effects of NaCl and polyethylene glycol on germination, emergence and seedling growth of Cowpea. *J. Agron. Crop Sci.* 188, 235–247. doi: 10.1046/j.1439-037X.2002.00563.x

Nakashima, K., Satoh, R., Kiyosue, T., Yamaguchi-Shinozaki, K., and Shinozaki, K. (1998). A gene encoding proline dehydrogenase is not only induced by proline and hypoosmolarity, but is also developmentally regulated in the reproductive organs of Arabidopsis. *Plant Physiol.* 118, 1233–1241. doi: 10.1104/pp.118.4.1233

Nanjo, T., Fujita, M., Seki, M., Kato, T., Tabata, S., and Shinozaki, K. (2003). Toxicity of free proline revealed in an Arabidopsis T-DNA-tagged mutant deficient in proline dehydrogenase. *Plant Cell Physiol.* 44, 541–548. doi: 10.1093/pcp/pcg066

Nawaz, K., Talat, A., Hussain, K.II, and Majeed, A. (2010). Induction of salt tolerance in two cultivars of Sorghum (*Sorghum bicolor* L.) by exogenous application of proline at seedling stage. *World Appl. Sci. J.* 10, 93–99.

Nguyen, M. L., Kim, G. B., Hyun, S. H., Lee, S. Y., Lee, C. Y., Choi, H. K., et al. (2013). Physiological and metabolomic analysis of a knockout mutant suggests a critical role of MtP5CS3 gene in osmotic stress tolerance of *Medicago truncatula*. *Euphytica* 193, 101–120. doi: 10.1007/s10681-013-0957-4

Nounjan, N., Nghia, P. T., and Theerakulpisut, P. (2012). Exogenous proline and trehalose promote recovery of rice seedlings from salt-stress and differentially modulate antioxidant enzymes and expression of related genes. *J. Plant Physiol.* 169, 596–604. doi: 10.1016/J.JPLPH.2012.01.004

Oono, Y., Seki, M., Nanjo, T., Narusaka, M., Fujita, M., Satoh, R., et al. (2003). Monitoring expression profiles of Arabidopsis gene expression during rehydration process after dehydration using ca. 7000 full-length cDNA microarray. *Plant J.* 34, 868–887. doi: 10.1046/j.1365-313X.2003.01774.x

Posmyk, M. M., and Janas, K. M. (2007). Effects of seed hydropriming in presence of exogenous proline on chilling injury limitation in *Vigna radiata* L. seedlings. *Acta Physiol. Plant* 29, 509–517. doi: 10.1007/s11738-007-0061-2

Qin, S., Liu, Y., Han, Y., Xu, G., Wan, S., Cui, F., et al. (2019). Aquaporins and their function in root water transport under salt stress conditions in *Eutrema salsugineum*. *Plant Sci.* 287, 110199. doi: 10.1016/j.plantsci.2019.110199

Rady, M., Kusvuran, A., Alharby, H. F., Alzahrani, Y., and Kusvuran, S. (2019). Pretreatment with proline or an organic bio-stimulant induces salt tolerance in wheat plants by improving antioxidant redox state and enzymatic activities and reducing the oOxidative stress. *J. Plant Growth Regul.* 38, 449–462. doi: 10.1007/s00344-018-9860-5

Rajendrakumar, C. S., Suryanarayana, T., and Reddy, A. R. (1997). DNA helix destabilization by proline and betaine: possible role in the salinity tolerance process. *FEBS Lett.* 410, 201–205. doi: 10.1016/S0014-5793(97)00588-7

Ren, X. W., Yu, D. W., Yang, S. P., Gai, J. Y., and Zhu, Y. L. (2018). Effects of *StP5CS* gene overexpression on nodulation and nitrogen fixation of vegetable soybean under salt stress conditions. *Legume Res.* 41, 675–680. doi: 10.18805/LR-386

Rengasamy, P. (2006). World salinization with emphasis on Australia. *J. Exp. Bot.* 57, 1017–1023. doi: 10.1093/jxb/erj108

Ribarits, A., Abdullaev, A., Tashpulatov, A., Richter, A., Heberle-Bors, E., and Touraev, A. (2007). Two tobacco proline dehydrogenases are differentially regulated and play a role in early plant development. *Planta* 225, 1313–1324. doi: 10.1007/s00425-006-0429-3

Rizwan, M., Ali, S., Ibrahim, M., Farid, M., Adrees, M., Bharwana, S. A., et al. (2015). Mechanisms of silicon-mediated alleviation of drought and salt stress in plants: a review. *Environ. Sci. Pollut. Res.* 22, 15416–15431. doi: 10.1007/s11356-015-5305-x

Rodriguez, M. M., and Heyser, J. W. (1988). Growth inhibition by exogenous proline and its metabolism in saltgrass (*Distichlis spicata*) suspension cultures. *Plant Cell Rep.* 7, 305–308. doi: 10.1007/BF00269924

Roy, D., Basu, N., Bhunia, A., and Banerjee, S. K. (1993). Counteraction of exogenous L-proline with NaCl in salt-sensitive cultivar of rice. *Biol. Plant* 35 (1), 69. doi: 10.1007/BF02921122

Sabagh, E. L., Sorour, S., Ragab, A., Saneoka, H., and Islam, M. (2017). The effect of exogenous application of proline and glycine betaine on the nodule activity of soybean under saline condition. *J. Agric. Biotechnol.* 2, 1–5. .

Safdar, H., Amin, A., Shafiq, Y., Ali, A., and Yasin, R. (2019). A review: Impact of salinity on plant growth. *Nat. Sci.* 17, 34–40. doi: 10.7537/marsnsj170119.06

Satoh, R., Fujita, Y., Nakashima, K., Shinozaki, K., and Yamaguchi-Shinozaki, K. (2004). A novel subgroup of bZIP proteins functions as transcriptional activators in hypoosmolarity-responsive expression of the *ProD*H gene in Arabidopsis. *Plant Cell Physiol.* 45, 309–317. doi: 10.1093/pcp/pch036

Schertl, P., Cabassa, C., Saadallah, K., Bordenave, M., Savouré, A., and Braun, H. P. (2014). Biochemical characterization of proline dehydrogenase in Arabidopsis mitochondria. *FEBS J.* 281, 2794–2804. doi: 10.1111/febs.12821

Schmid, M., Davison, T. S., Henz, S. R., Pape, U. J., Demar, M., Vingron, M., et al. (2005). A gene expression map of *Arabidopsis thaliana* development. *Nat. Genet.* 37 (5), 501–506. doi: 10.1038/ng1543

Servet, C., Ghelis, T., Richard, L., Zilberstein, A., and Savouré, A. (2012). Proline dehydrogenase: a key enzyme in controlling cellular homeostasis. *Front. Biosci.* 17, 607–620. doi: 10.2741/3947

Shahbaz, M., Mushtaq, Z., Andaz, F., and Masood, A. (2013). Does proline application ameliorate adverse effects of salt stress on growth, ions and photosynthetic ability of eggplant (*Solanum melongena* L.)? *Sci. Hortic.* 164, 507–511. doi: 10.1016/J.SCIENTA.2013.10.001

Shahid, M. A., Balal, R. M., Pervez, M. A., Abbas, T., Aqeel, M. A., Javaid, M. M., et al. (2014). Exogenous proline and proline-enriched *Lolium perenne* leaf extract protects against phytotoxic effects of nickel and salinity in *Pisum sativum* by altering polyamine metabolism in leaves. *Turk. J. Bot.* 38, 914–926. doi: 10.3906/bot-1312-13

Sidari, M., Santonoceto, C., Anastasi, U., Preiti, G., and Muscolo, A. (2008). Variations in four genotypes of lentil under NaCl-Salinity stress. *Am. J. Agric. Biol. Sci.* 3, 410–416. doi: 10.3844/ajabssp.2008.410.416

Signorelli, S., Dans, P. D., Coitiño, E. L., Borsani, O., and Monza, J. (2015). Connecting proline and γ-aminobutyric acid in stressed plants through nonenzymatic Reactions. *PloS One* 10, e0115349. doi: 10.1371/journal.pone.0115349

Signorelli, S. (2016). The fermentation analogy: a point of view for understanding the intriguing role of proline accumulation in stressed plants. *Front. Plant Sci.* 7:1339. doi: 10.3389/fpls.2016.01339

Singh, A. K., and Dubey, R. S. (1995). Changes in chlorophyll a and b contents and activities of photosystems 1 and 2 in rice seedlings induced by NaCl. *Photosynth* 31, 489–499. .

Skubacz, A., Daszkowska-Golec, A., and Szarejko, I. (2016). The role and regulation of ABI5 (ABA-Insensitive 5) in plant development, abiotic stress responses and phytohormone crosstalk. *Front. Plant Sci.* 7:1884. doi: 10.3389/fpls.2016.01884

Slama, S., Bouchereau, A., Flowers, T., Abdelly, C., and Savouré, A. (2015). Diversity, distribution and roles of osmoprotective compounds accumulated in halophytes under abiotic stress. *Ann. Bot.* 115, 433–447. doi: 10.1093/aob/mcu239

Sobahan, M. A., Akter, N., Ohno, M., Okuma, E., Hirai, Y., Mori, I. C., et al. (2012). Effects of exogenous proline and glycinebetaine on the salt tolerance of rice cultivars. *Biosci. Biotechnol. Biochem.* 76, 1568–1570. doi: 10.1271/bbb.120233

Solomon, A., Beer, S., Waisel, Y., Jones, G. P., and Paleg, L. G. (1994). Effects of NaCl on the carboxylating activity of Rubisco from *Tamarix jordanis* in the presence and absence of proline-related compatible solutes. *Physiol. Plant* 90, 198–204. . doi: 10.1111/j.1399-3054.1994.tb02211.x

Szabados, L., and Savouré, A. (2010). Proline: a multifunctional amino acid. *Trends Plant Sci.* 15, 89–97. doi: 10.1016/J.TPLANTS.2009.11.009

Székely, G., Ábrahám, E., Cséplő, Ã., Rigó, G., Zsigmond, L., Csiszár, J., et al. (2008). Duplicated *P5CS* genes of Arabidopsis play distinct roles in stress regulation and developmental control of proline biosynthesis. *Plant J.* 53, 11–28. doi: 10.1111/j.1365-313X.2007.03318.x

Teh, C.-Y., Shaharuddin, N. A., Ho, C.-L., and Mahmood, M. (2016). Exogenous proline significantly affects the plant growth and nitrogen assimilation enzymes activities in rice (*Oryza sativa*) under salt stress. *Acta Physiol. Plant* 38, 151. doi: 10.1007/s11738-016-2163-1

Tejera, N. A., Campos, R., Sanjuan, J., and Lluch, C. (2005). Effect of sodium chloride on growth, nutrient accumulation, and nitrogen fixation of common bean plants in symbiosis with isogenic strains. *J. Plant Nutr.* 28, 1907–1921. doi: 10.1080/01904160500306458

Thouin, J., Guo, M. Y., Zribi, I., Pauly, N., Mouradi, M., Cherki, G., et al. (2019). The *Medicago truncatula* HKT family: Ion transport properties and regulation of expression upon abiotic stresses and symbiosis. *bioRxiv*, 720474. doi: 10.1101/720474

van Zelm, E., Zhang, Y., and Testerink, C. (2020). Salt tolerance mechanisms of plants. *Annu. Rev. Plant Biol.* 71, 1–24. doi: 10.1146/annurev-arplant-050718-100005

Verdoy, D., Coba de la Pena, T., Redondo, F. J., Lucas, M. M., and Pueyo, J. J. (2006). Transgenic *Medicago truncatula* plants that accumulate proline display nitrogen-fixing activity with enhanced tolerance to osmotic stress. *Plant Cell Environ.* 29, 1913–1923. doi: 10.1111/j.1365-3040.2006.01567.x

Verslues, P. E., and Sharma, S. (2010). *Proline metabolism and its implications for plant-environment interaction. Arabidopsis Book*, Vol. 8. (American Society of Plant Biologists), e0140. doi: 10.1199/tab.0140

Vinocur, B., and Altman, A. (2005). Recent advances in engineering plant tolerance to abiotic stress: achievements and limitations. *Curr. Opin. Biotechnol.* 16, 1–10. doi: 10.1016/j.copbio.2005.02.001

Wang, X.-D., Chao, O.-Y., Fan, Z.-R., Gao, S., and Tang, L. (2010). Effects of exogenous silicon on seed germination and antioxidant enzyme activities of *Momordica charantia* under salt stress. *J. Anim. Plant Sci.* 6 (3), 700–708.

Wani, A. S., Ahmad, A., Hayat, S., and Tahir, I. (2016). Is foliar spray of proline sufficient for mitigation of salt stress in *Brassica juncea* cultivars? *Environ. Sci. Pollut. Res.* 23, 13413–13423. doi: 10.1007/s11356-016-6533-4

Weltmeier, F., Ehlert, A., Mayer, C. S., Dietrich, K., Wang, X., Schütze, K., et al. (2006). Combinatorial control of Arabidopsis proline dehydrogenase transcription by specific heterodimerisation of bZIP transcription factors. *EMBO J.* 25, 3133–3143. doi: 10.1038/sj.emboj.7601206

Wu, G.-Q., Feng, R.-J., Li, S.-L., and Du, Y.-Y. (2017). Exogenous application of proline alleviates salt-induced toxicity in sainfoin seedlings. *J. Anim. Plant Sci.* 27, 246–251. doi: 10.17221/665/2017-PSE

Yan, Z., Sun, J., and Guo, S. (2011). Effects of exogenous proline on nitrate reduction in melon seedlings under salt stress. *Plant Sci. J.* 29, 118–123. doi: 10.3724/SP.J.1142.2011.10118

Yang, X., Chen, X., Ge, Q., Li, B., Tong, Y., Zhang, A., et al. (2006). Tolerance of photosynthesis to photoinhibition, high temperature and drought stress in flag leaves of wheat: a comparison between a hybridization line and its parents grown under field conditions. *Plant Sci.* 171, 389–397. doi: 10.1016/j.plantsci.2006.04.010

You, J., Hu, H., and Xiong, L. (2012). An *ornithine d-aminotransferase* gene OsOAT confers drought and oxidative stress tolerance in rice. *Plant Sci.* 197, 59–69. doi: 10.1016/j.plantsci.2012.09.002

Zahran, H. H., and Sprent, J.II (1986). Effects of sodium chloride and polyethylene glycol on root-hair infection and nodulation of *Vicia faba* L. plants by *Rhizobium leguminosarum*. *Planta* 167 (3), 303–309. doi: 10.1007/BF00391332

Zahran, H. H. (1999). Rhizobium-legume symbiosis and nitrogen fixation under severe conditions and in an arid climate. *Microbiol. Mol. Biol. Rev.* 63 (4), 968–989. doi: 10.1128/MMBR.63.4.968-989.1999

Zhang, X. H., Zhou, D., Cui, J. J., Ma, H. L., Lang, D. Y., Wu, X. L., et al. (2015). Effect of silicon on seed germination and the physiological characteristics of *Glycyrrhiza uralensis* under different levels of salinity. *J. Hortic. Sci. Biotechnol.* 90, 439–443. doi: 10.1080/14620316.2015.11513207

Zhen, W. B., and Ma, Q. H. (2009). Proline metabolism in response to salt stress in common reed [*Phragmites australis* (Cav.) Trin. *Ex Steud. Bot. Mar.* 52, 341–347. doi: 10.1515/BOT.2009.007

Zheng, J. L., Zhao, L. Y., Wu, C. W., Shen, B., and Zhu, A. Y. (2015). Exogenous proline reduces NaCl-induced damage by mediating ionic and osmotic adjustment and enhancing antioxidant defense in *Eurya emarginata*. *Acta Physiol. Plant* 37, 181. doi: 10.1007/s11738-015-1921-9

Zhu, Y., and Gong, H. (2014). Beneficial effects of silicon on salt and drought tolerance in plants. *Agron. Sustain. Dev.* 34, 455–472. doi: 10.1007/s13593-013-0194-1

Zhu, J.-K. (2003). Regulation of ion homeostasis under salt stress. *Curr. Opin. Plant Biol.* 6, 441–445. doi: 10.1016/S1369-5266(03)00085-2

Conflict of Interest: The authors declare that the research was conducted in the absence of any commercial or financial relationships that could be construed as a potential conflict of interest.

Copyright © 2020 El Moukhtari, Cabassa-Hourton, Farissi and Savouré. This is an open-access article distributed under the terms of the Creative Commons Attribution License (CC BY). The use, distribution or reproduction in other forums is permitted, provided the original author(s) and the copyright owner(s) are credited and that the original publication in this journal is cited, in accordance with accepted academic practice. No use, distribution or reproduction is permitted which does not comply with these terms.

frontiers in Plant Science

ORIGINAL RESEARCH
published: 05 August 2020
doi: 10.3389/fpls.2020.01136

The Level of Methionine Residues in Storage Proteins Is the Main Limiting Factor of Protein-Bound-Methionine Accumulation in Arabidopsis Seeds

Aiswarya Girija[1†], *David Shotan*[1,2†], *Yael Hacham*[1,2] *and Rachel Amir*[1,2*]

[1] Department of Plant Science, MIGAL—Galilee Research Center, Kiryat Shmona, Israel, [2] Department of Biotechnology, Tel-Hai College, Upper Galilee, Israel

OPEN ACCESS

Edited by:
Supaart Sirikantaramas,
Chulalongkorn University, Thailand

Reviewed by:
Enrique Martinez Force,
Instituto de la Grasa (IG), Spain
Thomas Leustek,
The State University of New Jersey,
United States
Dwayne Hegedus,
Agriculture and Agri-Food Canada
(AAFC), Canada

***Correspondence:**
Rachel Amir
rachel@migal.org.il

[†]These authors have contributed
equally to this work

Specialty section:
This article was submitted to
Plant Metabolism
and Chemodiversity,
a section of the journal
Frontiers in Plant Science

Received: 07 May 2020
Accepted: 13 July 2020
Published: 05 August 2020

Citation:
Girija A, Shotan D, Hacham Y and
Amir R (2020) The Level of Methionine
Residues in Storage Proteins Is the
Main Limiting Factor of Protein-
Bound-Methionine Accumulation in
Arabidopsis Seeds.
Front. Plant Sci. 11:1136.
doi: 10.3389/fpls.2020.01136

The low level of methionine, an essential sulfur-containing amino acid, limits the nutritional quality of seeds. Two main factors can control the level of protein-bound methionine: the level of free methionine that limits protein accumulation and the methionine residues inside the storage proteins. To reveal the main limiting factor, we generated transgenic *Arabidopsis thaliana* seed-specific plants expressing the methionine-rich sunflower seed storage (*SSA*) protein (A1/A2). The contents of protein-bound methionine in the water-soluble protein fraction that includes the SSA in A1/A2 were 5.3- and 10.5-fold, respectively, compared to control, an empty vector (EV). This suggests that free methionine can support this accumulation. To elucidate if the level of free methionine could be increased further in the protein-bound methionine, these lines were crossed with previously characterized plants having higher levels of free methionine in seeds (called SSE). The progenies of the crosses (A1S, A2S) exhibited the highest level of protein-bound methionine, but this level did not differ significantly from A2, suggesting that all the methionine residues of A2 were filled with methionine. It also suggests that the content of methionine residues in the storage proteins is the main limiting factor. The results also proposed that the storage proteins can change their content in response to high levels of free methionine or SSA. This was assumed since the water-soluble protein fraction was highest in A1S/A2S as well as in SSE compared to EV and A1/A2. By using these seeds, we also aimed at gaining more knowledge about the link between high free methionine and the levels of metabolites that usually accumulate during abiotic stresses. This putative connection was derived from a previous analysis of SSE. The results of metabolic profiling showed that the levels of 29 and 20 out of the 56 metabolites were significantly higher in SSE and A1, respectively, that had higher level of free methionine, compared A1S/A2S, which had lower free methionine levels. This suggests a strong link between high free methionine and the accumulation of stress-associated metabolites.

Keywords: 2S sunflower albumin, cystathionine-γ-synthase, metabolic profiling, metabolism, methionine, seed storage proteins

INTRODUCTION

The low levels of methionine, an essential sulfur-containing amino acid, limit the nutritional quality of a plant-based diet (Hesse and Hoefgen, 2003; Amir et al., 2012). Methionine, in addition to its role in protein synthesis, plays a vital role in growth and development processes of plants, but also in humans and animals (Amir et al., 2019). To meet the increasing demand for methionine in humans and animal food and feed, four main approaches have been tested previously in both vegetative and seed tissues: i) upregulating key methionine biosynthesis enzymes to elevate the level of free methionine; ii) expressing methionine-rich storage proteins to incorporate more free methionine into the protein fraction; iii) reducing methionine-poor storage proteins inside the plants to support the accumulation of methionine-rich proteins; and iv) silencing methionine catabolic enzymes [reviewed by Galili and Amir (2013) and Amir et al. (2019)]. In the current study, we tested a combination of the first two approaches in order to determine the rate-limiting factor of protein-bound methionine in *Arabidopsis thaliana* seeds that were used as a model plant.

One of the approaches previously tested to elevate protein-bound methionine was elevating free methionine with the goal of promoting the accumulation of methionine-rich storage proteins. Previous studies have shown that one of the main regulatory enzymes controlling the level of free methionine is its first biosynthesis unique enzyme, cystathionine-γ-synthase (CGS). CGS combines the carbon/amino skeleton from the aspartate pathway with sulfur moiety derived from cysteine (Kim et al., 2002) (**Figure 1**). Indeed, overexpressing the *A. thaliana CGS* (*AtCGS*), or seed-specific expression of *AtCGS*, leads to significantly higher levels of free methionine (Kim et al., 2002; Di et al., 2003; Dancs et al., 2008; Hanafy et al., 2013; Song et al., 2013; Cohen et al., 2014; Cohen et al., 2016b). High elevations of free methionine in seeds were also obtained when other genes from the biochemical pathways of the aspartate family and the sulfur assimilation pathway were used (Karchi et al., 1993; Demidov et al., 2003; Kim et al., 2012; Nguyen et al., 2012; Planta et al., 2017; Xiang et al., 2018). In order to achieve a high expression in seeds during the production of proteins, the heterologous genes were fused to the promoters of seed-storage proteins that express the genes in the last stage of seed development when most of the amino acids are formed (e.g., Karchi et al., 1993; Kim et al., 2012; Nguyen et al., 2012; Matityahu et al., 2013; Amir et al., 2018). The highest level of free methionine (sixfold) was detected in the seeds of *A. thaliana* [called SSE plants (Cohen et al., 2014)], expressing the feedback-insensitive form of *AtCGS*, *AtD-CGS* (Hacham et al., 2006).

In addition to high levels of free methionine, the metabolic profile of SSE seeds resembles a profile of plants that suffer from abiotic stress (Cohen et al., 2014). The levels of most of the amino acids, polyols, and sugars increased significantly in these seeds compared to control wild type (WT) seeds. Also, the expression levels of genes associated with abiotic stresses such as early response to dehydration, drought, and osmotic stresses were significantly upregulated in these SSE seeds (Cohen et al., 2014). This phenotype suggests that a high level of methionine causes stress.

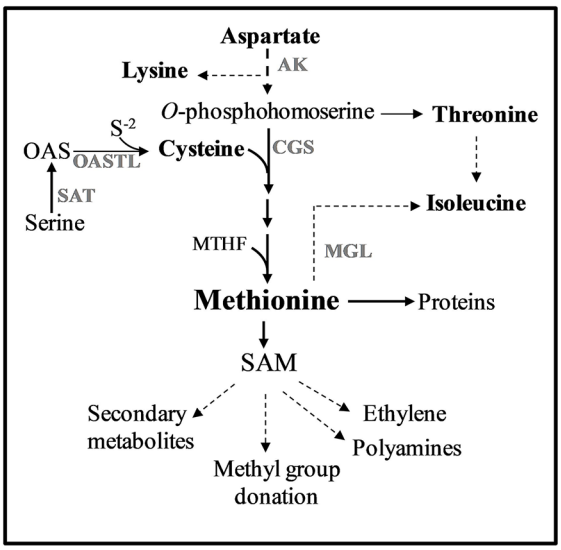

FIGURE 1 | Methionine metabolism in plants. Only some of the enzymes and metabolites are specified. Solid arrows represent one metabolic step while dashed arrows represent multiple metabolic steps. Abbreviations: AK, aspartate kinase; CGS, cystathionine γ-synthase; MGL, methionine γ-lase; SAM, S-adenosyl-methionine; S^{-2}, sulfide; OAS, *O*-acetylserine; SAT, serine acetyl transferase; OASTL, *O*-acetylserine thiol lyase.

The second approach to elevate methionine, which was based on experimental evidence, indicates that although the steady-state level of free methionine is relatively low, the flux towards its degraded metabolites is relatively high. By using radiolabeled isotope in *Lemna punctata* and *A. thaliana*, it was revealed that about 80% and 50% of the methionine was catabolized to its main catabolic product, *S*-adenosyl methionine (SAM) and to its related metabolites, respectively (Giovanelli et al., 1985; Ranocha et al., 2001) (**Figure 1**). SAM is the major methyl donor for methyltransferases and a precursor for various essential metabolites such as ethylene, vitamins, and polyamines (Roje, 2006). Based on the understanding that most of the free methionine drives towards SAM and its associated metabolites, the researchers suggest that increasing the expression level of heterologous genes encoded to methionine-rich seed-storage proteins would compete with that vast degradation and would trap the free methionine into storage proteins. Several methionine-rich storage proteins were used to increase protein-bound methionine. These include the 2S albumin of sunflower (having 16% methionine residues from the total amino acids), 15 kDa zein (having 11%), and the 2S albumin of Brazil nut (having 18%) [reviewed by Tabe et al. (1993) and Galili and Amir (2013)]. Seed-specific expression of these methionine-rich proteins revealed that

the levels of protein-bound methionine that incorporates into proteins increased in the transgenic seeds of soybean by 16% (Zhang et al., 2014), 33% in canola (Altenbach et al., 1992), and about 90% in lupin and chickpea seeds (Molvig et al., 1997; Chiaiese et al., 2004). However, in studying the consequences of these manipulations, it was found that these elevations were mostly at the expense of other sulfur-containing metabolites and/or endogenous methionine-rich proteins (Jung, 1997; Molvig et al., 1997; Muntz et al., 1998; Tabe and Droux, 2002; Hagan et al., 2003). Based on these findings, the researchers assume that the low pool of free methionine in seeds limits the accumulation of methionine-rich proteins during grain filling.

In the current study, we aim at i) revealing the main limiting factor that controls the accumulation of protein-bound methionine in *A. thaliana* seeds, which could be either the content of free methionine or the level of methionine residues inside the seed-storage proteins; ii) determining if a combination of increasing methionine biosynthesis with the expression of methionine-rich storage proteins in seeds [also known as the "push–pull" strategy (Tabe et al., 2010)] will lead to higher levels of protein-bound methionine compared to their parents; iii) studying the effect of high methionine levels on the content of water-soluble protein fraction; and iv) gaining more knowledge about the relationship between high free methionine content in seeds and the accumulation of stress-related metabolites.

MATERIALS AND METHODS

Generation of Transgenic *A. thaliana* Plants Expressing Seed-Specific Sunflower Albumin (*SSA*)

The *SSA* gene (GenBank Accession. no: X56686) controlled by the seed-specific vicilin promoter [originating from pea (*Pisum sativum* L.)] and the vicilin terminator in pLT4 plasmid was kindly obtained from Linda Tabe (Molvig et al., 1997). The fragment containing the promoter, the *SSA* gene, and the terminator was then digested from the pLT4 vector using *EcoRI* and introduced into the binary Ti plasmid pGPTV-BAR. This latter plasmid has the *bar* resistance gene for the Basta herbicide. This plasmid was used to transform *Agrobacterium tumefaciens* EHA105 cells. *A. tumefaciens* EHA105 harboring pGPTV-SSA-BAR was used to transform *A. thaliana* Columbia-0 ecotype using the floral dip method. Transformed seeds were selected on medium supplemented with Basta (5 μg ml^{-1}). Thirteen independent transformation events were selected and planted in an enriched soil medium. Seeds were collected from the T_1 generation and then analyzed for a 3:1 segregation based on the presence of the transgene and the observed resistant phenotype to Basta. Segregated T_1 lines were then regrown, and the T_2 generation was examined for non-segregating lines to produce T_2 and further T_3 homozygous lines. Two T_3 homozygous lines designated as A1 and A2, showing the highest levels of SSA protein accumulation by immunoblot analysis, were chosen for further analysis.

Generation of Transgenic *A. thaliana* Plants Co-expressing the Seed-Specific *SSA* and the Feedback-Insensitive Form of Cystathionine-γ-Synthase *(AtD-CGS)*

The selected homozygous transgenic plants (A1 & A2) were crossed with the fifth generation of SSE lines expressing the seed-specific *AtD-CGS* (Cohen et al., 2014). For the crossing events, the unopened flowers were hand-pollinated and the seeds were harvested after maturation. A plant having an empty vector (EV) was used as the experimental control (Cohen and Amir, 2017). The progenies resulted from the independent crosses, A1 x SSE and A2 x SSE, referred to as A1S and A2S, were grown on a 0.5% Murashige and Skoog (MS) medium (Duchefa) containing 0.5% sucrose and 7 mg ml^{-1} plant Agar (Duchefa). T_1 and T_2 lines of seeds expressing *SSA* alone (A1, A2) and crosses (A1S, A2S) were selected on media supplemented with 5 μg ml^{-1} Basta. Since the SSE seeds lost their kanamycin resistance during the generation, the presence of *AtD-CGS* gene was confirmed by PCR analysis. Genomic DNA was extracted from the leaves of 30 independent progenies of each A1S and A2S line and was screened by PCR using gene-specific primers (**Supplementary Table S1**). Seedlings were transferred to fertilized soil after 12 days of germination and grown at 22 ± 2°C under a 16 h/8 h light/dark photoperiod. T_3 generations of all genotypes including the control EV plants were grown at the same time in an environmentally controlled growth chamber. Mature dry seeds were harvested followed by drying and were stored at 4°C.

Quantitative Real-Time PCR and Immunoblot Analyses

For transcript determination, total RNA was extracted from 50 mg of mature dry seeds using the Spectrum Plant Total RNA kit (Sigma). One microgram of RNA was used for cDNA biosynthesis using the Verso cDNA biosynthesis kit (Thermo Scientific) according to the manufacturer's protocol. The expression of mRNA levels of *AtD-CGS* and *SSA* in EV and transgenic plants was quantified using quantitative real-time PCR (qRT-PCR). To normalize variance among samples, protein phosphatase 2A subunit A3 (*AtPP2A-A3*) transcript level was used as an endogenous control (Cohen et al., 2014). The values presented are means of five biological replicates. All primers used for qRT-PCR analyses are listed in **Supplementary Table S1**.

For the immunoblot analysis, water-soluble protein fraction was extracted from 20 mg dry seeds of EV and transgenic seeds, A1, A2, A1S and A2S, as previously described (Matityahu et al., 2013). The seeds were ground in 400 μl of 25 mM Na phosphate buffer pH = 7.8 with a protease inhibitor cocktail (Sigma, P9599). After two centrifugation cycles (20,000 g at 4°C for 20 min), the upper phase was collected and 20 μl was loaded onto the gel. The expression level of the *SSA* (6.5 kDa) protein was detected with *SSA* anti-serum that was kindly obtained from Rainer Hoefgen (Max Planck Institute of Molecular Plant Physiology, Germany).

Primary Metabolic Profiling, Free and Protein-Bound Amino Acids Determination Using GC-MS

Mature dry seeds from different transgenic sets were collected separately from eight distinct plants. Twenty milligrams of mature dry seeds from control and transgenic lines were ground into a fine powder using liquid nitrogen and a Restch MM 301 homogenizer, as previously described (Cohen et al., 2014; Cohen et al., 2016b). The crude extract was separated into polar and non-polar phases with methanol/water/chloroform. The upper polar phase was vacuum-dried and dissolved in 40 µl of 20 mg ml^{-1} methoxyamine hydrochloride in pyridine for 2 h, followed by derivatization for 30 min in N-methyl-N (trimethylsilyl)-trifluoroacetamide at 37°C for 2 h with vigorous shaking. One microliter of sample was injected into a GC-MS system with a split ratio of 1:1, together with the amino acid standards of 5, 10, 25, 50, 100 and 200 µM. For the free amino acid, the single-ion mass method was used with the RXI-5-Sil MS capillary column (RESTEK; 30 m, 0.25-mm i.d., and 0.25-mm thickness), while the total-ion-count method was used for metabolic profiling and separation using the VF-5ms capillary column (Agilent; 30 m + 10 m EZ-guard, 0.25-mm i.d., and 0.25-mm thicknesses). All analyses were carried out on a GC-MS system (Agilent 7890A) coupled with a mass selective detector (Agilent 5975c) and a Gerstel multipurpose sampler (MPS2; Cohen et al., 2014). Norleucine (2 mg ml^{-1} in HPLC grade water) and Ribitol (2 mg ml^{-1} in HPLC grade water) were used as internal standards. The peak areas were calculated from the standard calibration curves and normalized to the internal controls (norleucine and ribitol) signal.

For the analysis of water-soluble protein-bound amino acid content, 20 mg of seeds was ground into powder using a Restch MM 301 homogenizer suspended in 400 µl of water containing 2 mg ml^{-1} norleucine and vigorously vortexed. After two centrifugation cycles (20,000 g at 4°C for 20 min), the water-soluble protein fraction was determined from the upper phase. Forty microliter of water-soluble protein was dried under vacuum and sent for protein hydrolysis (Department of Chemical Research Support, Weizmann Institute of Science, Rehovot, Israel). Samples of the hydrolyzed proteins were separated using 300 µl of water and 300 µl of chloroform. From the aqueous phase, 200 µl of the sample was dried under vacuum and derivatized, as described for the free amino acid analysis. The data were collected from five biological replicates and analyzed according to the standard curve for each amino acid.

Quantification of the Content of the Water-Soluble Proteins

To quantify the water-soluble protein, 20 mg of seeds was ground into powder using a Restch MM 301 homogenizer suspended in 400 µl of 25 mM Na phosphate buffer pH = 7.8 and vigorously vortexed. After two centrifugation cycles (20,000 g at 4°C for 20 min), the water-soluble protein fraction was determined from the upper phase using a Bradford reagent. Bovine serum albumin was used as a standard.

Determination of Seed Weight and Germination Assay

The dry seed weight was determined from exactly 100 seeds of each genotype in four biological replicates. For the germination assay, 30 seeds from each of these genotypes in five replicates were placed on the same day in a petri dish having 0.5% MS medium (Duchefa), supplemented with 0.5% sucrose (J.D. Baker) and 7 mg ml^{-1} plant agar (Duchefa). After 48 h in a cold room (4°C), the plates were transferred to a growth room (22 ± 2°C, 16/8-h light/dark cycle at 100 µmol m^{-2} s^{-1}). The rate of germination was determined by observing the emergence of radicals 2 days post-transferring to the growth room.

Statistical Analysis

The normalized data were used for multivariate statistical analysis, including principal component analysis (PCA). Heat maps were used to visualize metabolite responses and were generated based on the average of each metabolite in five biological replicates. PCAs and heat maps were done using the Metaboanalyst 4.0 software (https://www.metaboanalyst.ca/; Chong et al., 2018). The graphs for the experiments were performed using the GraphPad Prism 8 scientific software. Student's t-test and analysis of variance (ANOVA) were done using the JMP 8 software: a P value of <0.05 was considered statistically significant for the experiments.

RESULTS

Seeds of Transgenic *A. thaliana* Plants Expressing a Methionine-Rich Sunflower Albumin Had a Higher Level of Protein-Bound Methionine

To introduce the "push–pull" strategy in seeds, we generated *A. thaliana* plants expressing the methionine-rich 6.5 kDa 2S albumin from sunflower (*SSA*) under the control of the seed-specific vicilin promoter. The seeds of 13 independent Basta-resistant transgenic lines were screened for their SSA protein content using immunoblot analysis. Two homozygous lines designated as A1 and A2, having the highest expression levels of SSA, were chosen for further study (**Figure 2A**). Quantitative real-time PCR (qRT-PCR) analyses showed that A2 has 2.1-fold higher expression levels of the transgene *SSA* compared to A1 (**Figure 2B**), which is in accordance with the results obtained from the immunoblot analysis (**Figure 2A**). Plants having an empty vector (EV) were used as a control for this study (Cohen and Amir, 2017).

To determine if a high level of SSA would lead to increased incorporation of free methionine into the water-soluble protein fraction, which also included the albumin fraction, this protein fraction was extracted from A1/A2 seeds. This fraction was subjected to protein hydrolysis, and the level of methionine was measured. The results showed that the levels of protein-bound methionine in this fraction had increased significantly up to 5.3- and 10.5-fold in the seeds of A1 and A2, respectively, compared to the control EV seeds (**Table 1**). The accumulation

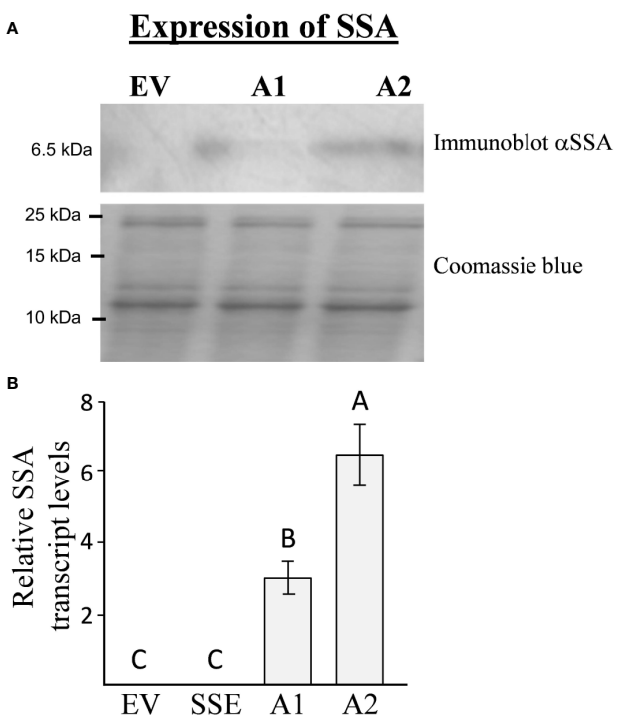

FIGURE 2 | The expression levels of *SSA* in transgenic seeds**. (A)** Immunoblot analysis of *SSA* in A1/A2 transgenic seeds expressing this gene. The upper panel represents the signal using antibodies against the *SSA* protein, while the bottom panel represents crude protein extracts counterstained with coomassie brilliant blue used for equal loading. The marker size is shown on the left. **(B)** qRT-PCR analysis of *SSA* transcript levels in lines expressing the *SSA* gene (A1, A2) and in the empty vector (EV) line used as a control. The results are normalized according to the expression of constitutive gene *AtPP2A-A3*. The data are presented as the mean ± SD of five individual plants per line. Statistically significant changes (Tukey-Kramer HSD test, $P \leq 0.05$) between plants are identified by different letters.

of protein-bound methionine in A1/A2 seeds correlated well with the expression levels of SSA both at the transcript and protein levels (**Figure 2**).

Seeds of the Transgenic Plants Showed Differences in Their *AtD-CGS* and *SSA* Expression Levels Compared to EV

With the aim of understanding whether the levels of free methionine are a limiting factor in the accumulation of methionine in the storage proteins of A1/A2 seeds, and if so, whether the methionine level could be increased further in these seeds, we crossed between the homozygous lines expressing *SSA* with the fifth generation of homozygous SSE plants. This latter plant expressed *AtD-CGS* under the control of the seed-specific phaseolin promoter and had a high level of free methionine (Cohen et al., 2014). Two independent crossing events were carried out: A1 x SSE (termed A1S) and A2 x SSE (termed A2S). Since SSE lines lost their kanamycin resistance after several generations (but they had the NptII gene and the *AtD-CGS*), the progenies of these crosses were germinated on half-MS media with Basta, and 15 Basta-resistant plants from each line of the crosses were screened by PCR for the presence of both genes, *SSA* and *AtD-CGS*. The seeds from T_3 homozygous progenies were used for further analysis.

The transcript expression levels of the *SSA* and *AtD-CGS* in the parents and those expressing the two heterologous genes were measured using quantitative real-time PCR (qRT-PCR) (for details, see **Supplementary Figure S1**; **Supplementary Text**). To reveal if the level of free methionine limits the accumulation of *SSA*, an immunoblot analysis was carried out using anti-*SSA* antibodies on the water-soluble protein fraction. If that limitation exists, the protein level of *SSA* is expected to increase in the progenies of the crosses (A1S, A2S) above the level of their parents, A1 and A2. The results showed that the *SSA* level was higher in two lines of A1S (by about 50–100%) than in

TABLE 1 | The level of protein-bound amino acids in dry seeds expressing *AtD-CGS* (SSE), *SSA* (A1, A2), those expressing the two genes (A1S, A2S), and the control EV after protein hydrolysis[#].

	EV	SSE	A1	A2	A1S	A2S
Alanine	8.01 ± 1.60 a	12.53 ± 2.82 a	11.32 ± 1.61 a	13.23 ± 2.38 a	14.24 ± 4.34 a	14.88 ± 4.70 a
Valine	5.76 ± 1.43 a	8.46 ± 1.74 a	8.80 ± 1.99 a	8.36 ± 1.29 a	6.19 ± 1.53 a	7.13 ± 1.84 a
Serine	4.38 ± 0.93 b	6.80 ± 1.33 b	7.00 ± 0.96 b	8.88 ± 1.47 a	7.927 ± 2.199 b	8.98 ± 2.77 a
Leucine	5.30 ± 0.89 c	9.41 ± 2.00 bc	11.00 ± 1.71 bc	17.32 ± 3.24 a	15.32 ± 4.64 b	17.35 ± 5.04 a
Threonine	4.70 ± 0.96 a	7.72 ± 1.59 a	6.43 ± 0.75 a	8.17 ± 1.57 a	7.76 ± 2.35 a	8.56 ± 2.54 a
Isoleucine	2.99 ± 0.50 b	4.63 ± 0.86 b	4.68 ± 0.57 b	5.90 ± 0.95 a	5.48 ± 1.85 ab	6.24 ± 1.73 a
Proline	6.89 ± 2.23 a	7.92 ± 1.57 a	10.75 ± 2.27 a	10.13 ± 1.65 a	9.44 ± 2.32 a	10.20 ± 3.19 a
Glycine	3.45 ± 0.17 c	6.28 ± 1.39 bc	6.66 ± 0.68 a	11.72 ± 1.50 b	9.29 ± 5.00 bc	13.78 ± 4.33 a
Methionine	0.75 ± 0.16 c	1.46 ± 0.46 b	3.99 ± 0.20 b	7.93 ± 1.14 a	7.82 ± 0.95 a	8.71 ± 2.01 a
Aspartate	28.46 ± 12.84 a	39.56 ± 9.26 a	42.60 ± 7.26 a	56.81 ± 8.22 a	41.30 ± 25.69 a	54.20 ± 19.19 a
Phenylalanine	2.87 ± 0.47 b	5.01 ± 1.09 b	4.26 ± 0.60 b	5.95 ± 1.23 a	5.40 ± 1.81 b	6.50 ± 2.42 a
Glutamate	27.71 ± 7.37 b	46.51 ± 9.74 b	49.13 ± 7.69 b	73.39 ± 13.42 a	63.97 ± 19.99 a	79.72 ± 29.88 a
Lysine	13.06 ± 3.07 b	27.70 ± 6.80 b	25.27 ± 6.14 b	32.45 ± 4.98 a	23.37 ± 9.60 b	32.91 ± 11.60 a
Tyrosine	1.35 ± 0.38 b	2.79 ± 0.63 b	2.78 ± 0.41 b	4.01 ± 0.65 a	2.74 ± 1.19 b	4.07 ± 1.84 a
Total AA's	115.71 ± 32.67 b	186.81 ± 39.05 ab	194.71 ± 29.65 ab	264.31 ± 42.26 a	219.13 ± 63.77ab	273.25 ± 93.12 a

[#]*The levels of amino acids after protein hydrolysis. The quantities of amino acids were analyzed using GC-MS, and their levels were normalized to norleucine and calculated as μmol per g dry weight of seeds. Values are the mean ± standard deviation of five biological replicates of 20 mg seeds isolated from five plants per line. Significance between plants was calculated according to the Turkey-Kramer HSD test (p < 0.05) and is identified by different letters.*

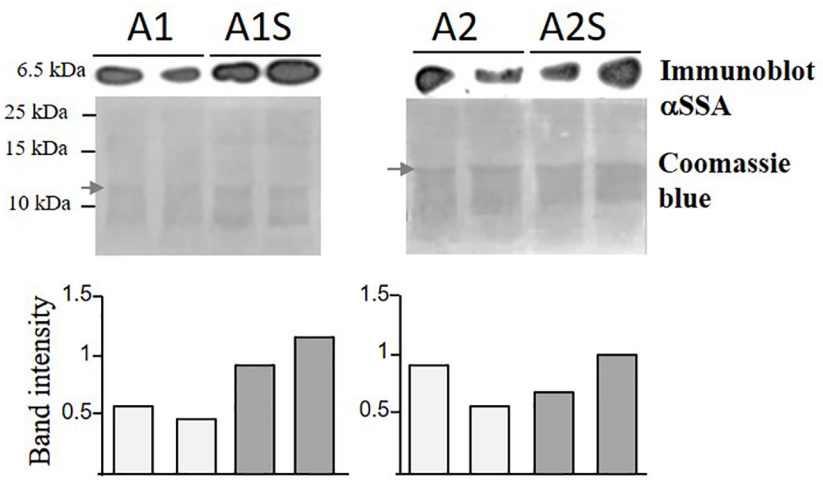

FIGURE 3 | Immunoblot analysis of *SSA* in transgenic seeds expressing *SSA* alone (A1, A2) and in seeds expressing *SSA* and *AtD-CGS* (A1S, A2S). For the analysis, water-soluble proteins were extracted from an equal amount of 20 mg seeds from each sample with the addition of an equal amount of extraction buffer. Two lines for each genotype were tested. Upper panels: immunoblot analysis using antibodies against the protein of *SSA*. Lower panel: coomassie brilliant blue staining used for equal loading. The marker size is shown on the left. The graph represents band intensity of the SSA normalized to a band from coomassie (marked by an arrow) as measured by ImageJ. The two gels were run separately.

its parent, A1, but such an elevation was not observed in A2S, which exhibited a level of *SSA* similar to its parent, A2 (**Figure 3**). In addition, coomassie-brilliant blue staining showed a higher level of other water-soluble storage proteins in A1S, compared to A1 (**Figure 3**). These results indicated that the seed-specific expression of *AtD-CGS* led at least in A1S to higher levels of *SSA*, which in turn also supported the accumulation of other storage proteins in this line. The observation that A2S had a level of *SSA* similar to A2 (**Figure 3**) indicates that the capacity for methionine residues was fulfilled in the A2 line (which has a twofold higher expression level of *SSA* compared to A1), and thus, a higher level of free methionine (caused by the expression of *AtD-CGS*) failed to raise the level of *SSA* significantly beyond that detected in A2 in the water-soluble protein fraction.

A Bradford assay was used to determine if a higher expression of SSA affects the total water-soluble protein fraction. This fraction (which also includes SSA) is the second major fraction after the 12S globulins (cruciferin), and it accounts for about 20% of the total proteins in seeds of *A. thaliana* (Fujiwara et al., 2002). The results showed that the seeds of A1 and A2 had 24% and 38% higher levels of water-soluble protein, respectively, compared to EV (**Figure 4**), suggesting that the expression of SSA can increase the level of this fraction. The results also demonstrated that the SSE seeds had the highest water-soluble protein abundance of 69% compared to EV, while those of A1S and A2S had 51% and 58% higher levels, respectively, compared to EV, which did not differ significantly from SSE (**Figure 4**). This suggests that the co-expression of *AtD-CGS* and *SSA* in *A. thaliana* seeds does not elevate the level of water-soluble proteins fraction beyond the level detected in SSE seeds expressing *AtD-CGS* alone. Together, the results showed that a combination of *SSA* and *AtD-CGS* led to higher water-soluble protein levels in A1S compared to A1, while A2S had an insignificant elevation of 16% compared to A2.

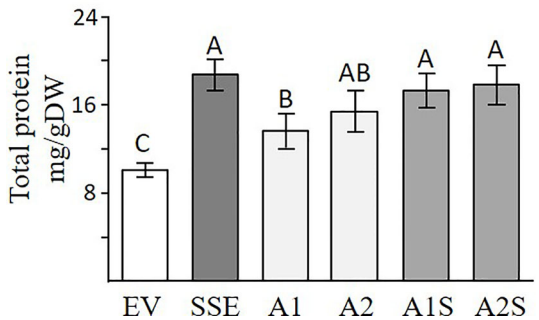

FIGURE 4 | Total water-soluble protein fractions analyzed by Bradford assay. Water-soluble proteins fractions in seeds expressing the *SSA* gene (A1, A2), in seeds expressing *SSA* and *AtD-CGS* (A1S, A2S), and in SSE and EV. The assay was done on extracts from 20 mg seeds/dry weight. The data are presented as the mean ± SD from four individual plants. Statistically significant changes (Tukey-Kramer HSD test, $P \leq 0.05$) between plants are identified by different letters.

Effect of Co-expression of *AtD-CGS* and *SSA* on the Levels of Free and Protein-Bound Methionine, and on the Other Amino Acids in the Transgenic Seeds

Based on the accumulation of SSA in the progenies of A1S (**Figure 3**), and the high level of the water-soluble protein

fraction in the seeds of A1S/A2S, we assume that most of the free methionine in these lines was incorporated into SSA, and thus, the levels of protein-bound methionine would increase. To test these assumptions, the water-soluble protein fraction was isolated from the seeds of the different lines and was used for protein hydrolysis followed by GC-MS analysis. The results showed that the level of protein-bound methionine increased significantly in A1S/A2S (**Figure 5A**). By comparing the level of protein-bound methionine in the seeds of the progenies of the crosses lines with their parents A1/A2, it was found that proteinbound methionine increased significantly by 96% in A1S compared to A1, but in A2S, the elevation (10%) was insignificant compared to A2 (**Figure 5A**). The SSE seeds showed a twofold increase in the level of protein-bound methionine compared to EV (**Figure 5A**), which is consistent with the previous report showing a 1.6-fold increase in the levels of protein-bound methionine of the SSE seeds (Cohen et al., 2014). In comparison to the SSE seeds, the levels of protein-bound methionine contents in the A1S and A2S seeds increased 5.4- and 5.9-fold, respectively, and compared to EV, their levels increased 10.4- and 11.5-fold, respectively (**Figure 5A**; **Table 1**). Together, the results showed that the level of protein-bound methionine increased significantly in A1S compared to A1, suggesting a potential of the "pull–push" approach. However, the results obtained from A2S and A2 suggest that they reach their maximum capacity to incorporate free methionine, and that the methionine residues in the storage proteins become the main limiting factor of the protein-bound methionine content.

The higher levels of water-soluble proteins in the A1S and A2S transgenic lines (**Figure 4**) and the previous findings that higher levels of free methionine in SSE affect the levels of other amino acids (free and protein-bound) (Cohen et al., 2014) suggest a possible elevation of other amino acids in the water-soluble protein fraction in the progenies of the crosses. Indeed, our results showed that the water-soluble protein bound amino acids were significantly higher in A2, A1S, and A2S compared to A1, SSE, and EV. Compared to EV, the accumulation of protein-bound amino acids was highest in A2S (2.36-fold), while A1S showed an elevation of only 89%. The level in A2, however, was not significantly altered compared to A2S and had a 2.28-fold higher level compared to EV (**Figure 5B**; **Table 1**). The levels in SSE and A1 were 61% and 68% higher compared to EV. The amino acids that showed the highest elevations in A2 and A2S were leucine, serine, isoleucine, lysine, glutamate, phenylalanine, and tyrosine, while the levels of most of the other amino acids did not differ significantly between the different sets of seeds (**Table 1**). The results showed that a higher expression level of *AtD-CGS* and/or *SSA* increased the total levels of other amino acids in addition to methionine.

In *A. thaliana* seeds, about 7% of the amino acids were found in their free form (Cohen et al., 2014). Therefore, we next studied how their levels in the different transgenic lines with the assumption that their levels would decrease compared to the SSE seeds. To test this assumption, the levels of free methionine and other amino acids were determined using GC-MS. In all the transgenic lines A2, A1S, and A2S, the level of free methionine was significantly reduced compared to EV. As expected from our previous study (Cohen et al., 2014), the level of free methionine in SSE increased 1.8-fold, while in A1S and A2, the levels were similar to those detected in EV, and A2S showed a reduction of about twofold compared to EV. Notably, compared to SSE, the seeds of A1S and A2S showed a significant 1.7- and 3.6-fold

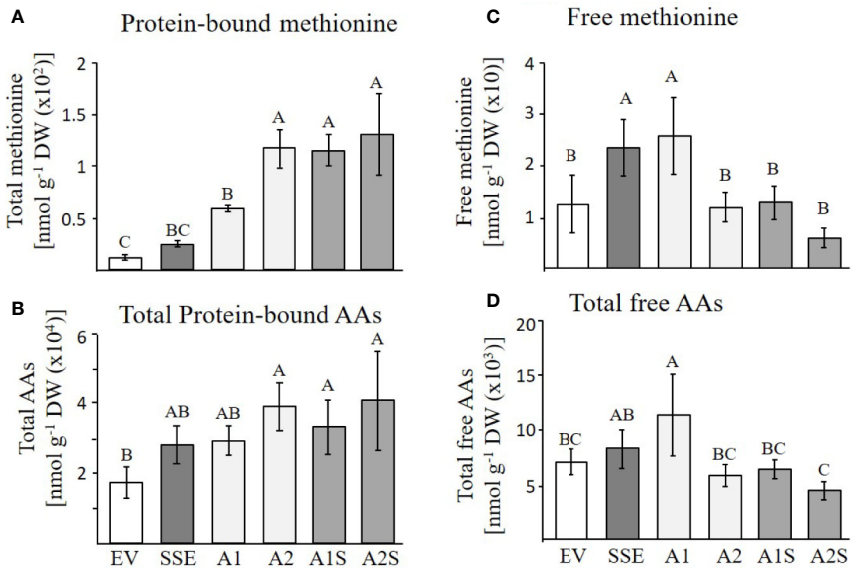

FIGURE 5 | GC-MS analyses of free and protein-bound methionine and other amino acids. **(A, B)** Protein-bound levels of methionine and total amino acids in the transgenic dry seeds of A1S, A2S, A1, A2, SSE, and EV followed by protein hydrolysis; **(C, D)** Free levels of methionine and total amino acids in the same set of seeds. Data shown are means ± SD of five biological replicates. Statistically significant changes (Tukey-Kramer HSD test, $P \leq 0.05$) between plants are identified by different letters.

reduction in free methionine content, respectively (**Figure 5C**), suggesting that most of the free methionine incorporated into the seed proteins and mostly to SSA. However, A1 showed an approximately twofold higher free methionine level compared to EV, which is similar to that detected in SSE (**Figure 5C**; **Table 2**).

Next, the effects of these manipulations were tested on the levels of the other free amino acids. A similar effect of reduction was observed in A2, A1S, and A2S. The levels of total free amino acids were 19% higher in SSE compared to EV, but were 11% and 60% lower in the progenies of the crosses A1S and A2S, respectively (**Figure 5D**). Compared to EV, A1 had 62% higher content of total free amino acids, but A2 showed a 21% lower level. Furthermore, the low content of free amino acids in A2, A1S, and A2S (**Figure 5D**) compared to SSE strongly suggests that these amino acids incorporated into *SSA* and other seed proteins (**Figure 5B**).

Taken together, the results showed that the contents of protein-bound methionine and other amino acids increased significantly in A1S, A2S, and A2. This shows that a higher level of methionine in A2 does not support the further accumulation of methionine, where apparently most of the methionine residues in the proteins of this line were filled with methionine, which is unlike A1. The levels of free methionine and other free amino acids in A2 and A1S were similar to EV, and in A2S, it decreased to about twofold compared to EV, suggesting that most of the free amino acids incorporated into the storage proteins.

Evidence of Metabolic Changes in the Different Sets of Transgenic Seeds

Changes in methionine and amino acid contents can affect the accumulation of other metabolites in plants (Galili et al., 2016; Amir et al., 2019). Having seeds that co-express *AtD-CGS* and *SSA* with a lower level of free methionine than that detected in SSE can enable us to examine our fourth goal, which is to reveal the link between high free methionine and the metabolic stress phenotype. The presence of such a link was assumed from measurements carried out in *A. thaliana* and soybean seeds expressing the *AtD-CGS* (Song et al., 2013; Cohen et al., 2014; Cohen et al., 2016b). These seeds had higher levels of free methionine, and their primary metabolic profiles resembled plants suffering from abiotic stress with high levels of amino acids, polyols, and sugars. These seeds also showed up-regulation of genes related to abiotic stress (Cohen et al., 2014; Cohen and Amir, 2017). We hypothesized that this phenotype was due to the presence of high levels of free methionine in these transgenic seeds. If this is the case, then in the seeds of A1S/A2S where the levels of free methionine were reduced compared to SSE and A1, the levels of stress-related metabolites are expected to decrease. To examine this assumption, global primary metabolic profiling was performed on the seeds of the different transgenic lines. A total of 56 metabolites were detected by GC-MS, and the metabolic overview of the seeds was plotted onto a principal component analysis (PCA) to visualize the relationship between the samples (**Figure 6A**). The PCA analysis showed that A1 and A2 were separated from the A1S and A2S crosses lines; that SSE and A1, which had higher levels of free methionine, were relatively closed; and that A2 and EV were also relatively closed (**Figure 6A**; **Supplementary Figure S2**).

The heat-map analysis showed that most of the metabolites were higher in SSE and A1, which had higher levels of free methionine compared to other sets of seeds (**Figure 6B**). Twenty-nine metabolites showed relatively higher levels in SSE compared to A1S and A2S: sugars (arabinose, glucose, fructose, galactose, glucopyranose, xylose, talose, and cellobiose); sugar acids and organic acids (citric, malic, propanedioic, gluconic, hexadecanoic, and octadecanoic acids); amino acids (glutamate, serine, leucine, isoleucine, threonine, tryptophan, glycine, and proline); and polyols (myo-inisitol, xylitol, sorbitol, mannitol, and arabitol) (**Table 2**; **Supplementary Table S2**). Moreover, the

TABLE 2 | The level of free amino acids in dry seeds expressing *AtD-CGS* (SSE), *SSA* (A1, A2), those expressing the two genes (A1S, A2S), and the control EV[#].

	EV	SSE	A1	A2	A1S	A2S
Alanine	0.26 ± 0.24 c	0.52 ± 0.16 a	0.53 ± 0.11 a	0.30 ± 0.02 bc	0.56 ± 0.07 a	0.47 ± 0.08 ab
Valine	1.02 ± 0.18 b	1.58 ± 0.44 b	2.38 ± 1.10 a	1.16 ± 0.30 b	1.25 ± 0.19 b	0.98 ± 0.17 b
Serine	1.76 ± 0.06 ab	1.81 ± 0.39 ab	2.23 ± 0.54 a	1.42 ± 0.16 bc	1.31 ± 0.17 c	1.07 ± .0.18 c
Leucine	0.34 ± 0.04 bc	0.58 ± 0.25 b	0.77 ± 0.37 a	0.28 ± 0.11 c	0.33 ± 0.05 c	0.22 ± 0.06 c
Threonine	1.08 ± 0.18 a	0.97 ± 0.19a	1.09 ± 0.17 a	0.67 ± 0.12 b	0.95 ± 0.14 a	0.55 ± 0.09 c
Isoleucine	0.44 ± 0.02 c	0.79 ± 0.38 b	1.18 ± 0.59 a	0.45 ± 0.16 c	0.43 ± 0.06 c	0.32 ± 0.07 c
Proline	0.24 ± 0.11 b	0.33 ± 0.24 ab	0.56 ± 0.40 a	0.14 ± 0.05 b	0.10 ± 0.02 c	0.10 ± 0.03 c
Glycine	0.19 ± 0.03 c	0.29 ± 0.15 b	0.35 ± 0.14 a	0.20 ± 0.08 c	0.18 ± 0.03 c	0.17 ± 0.07 c
Homoserine	0.10 ± 0.04 b	0.19 ± 0.16 ab	0.25 ± 0.07 a	0.12 ± 0.04 ab	0.14 ± 0.04 ab	0.07 ± 0.01 b
Methionine	0.12 ± 0.06 b	0.23 ± 0.06 a	0.26 ± 0.09 a	0.12 ± 0.03 b	0.13 ± 0.04 b	0.06 ± 0.01 b
Aspartate	0.54 ± 0.25 ab	0.51 ± 0.14 b	0.82 ± 0.27 a	0.48 ± 0.06 b	0.47 ± 0.12 b	0.19 ± 0.04 c
Phenylalanine	0.27 ± 0.17 ab	0.22 ± 0.07 ab	0.28 ± 0.11 a	0.13 ± 0.02 bc	0.22 ± 0.05 ab	0.03 ± 0.01 c
Glutamate	0.47 ± 0.31 a	0.21 ± 0.09 a	0.36 ± 0.23 a	0.13 ± 0.04 ab	0.05 ± 0.03 c	0.02 ± 0.01 c
Tyrosine	0.07 ± 0.05 c	0.75 ± 0.4 bc	0.14 ± 0.03 ab	0.08 ± 0.02 bc	0.14 ± 0.04 a	0.07 ± 0.02 c
Tryptophan	0.12 ± 0.05 b	0.11 ± 0.06 b	0.21 ± 0.10 a	0.08 ± 0.01 bc	0.06 ± 0.01 c	0.03 ± 0.01 d
Total AA's	7.08 ± 1.25 bc	8.45 ± 1.98 b	11.45 ± 3.84 a	5.82 ± 1.10 bc	6.36 ± 0.89 bc	4.42 ± 0.71 c

[#]*The quantities of free amino acids were analyzed using GC-MS, and their levels were normalized to norleucine and calculated as μmol per g dry weight of seeds. Values are the mean ± standard deviation of five biological repetitions of 20 mg seeds isolated from five plants per line. Significance between plants was calculated according to the Turkey-Kramer HSD test ($p < 0.05$) and is identified by different letters.*

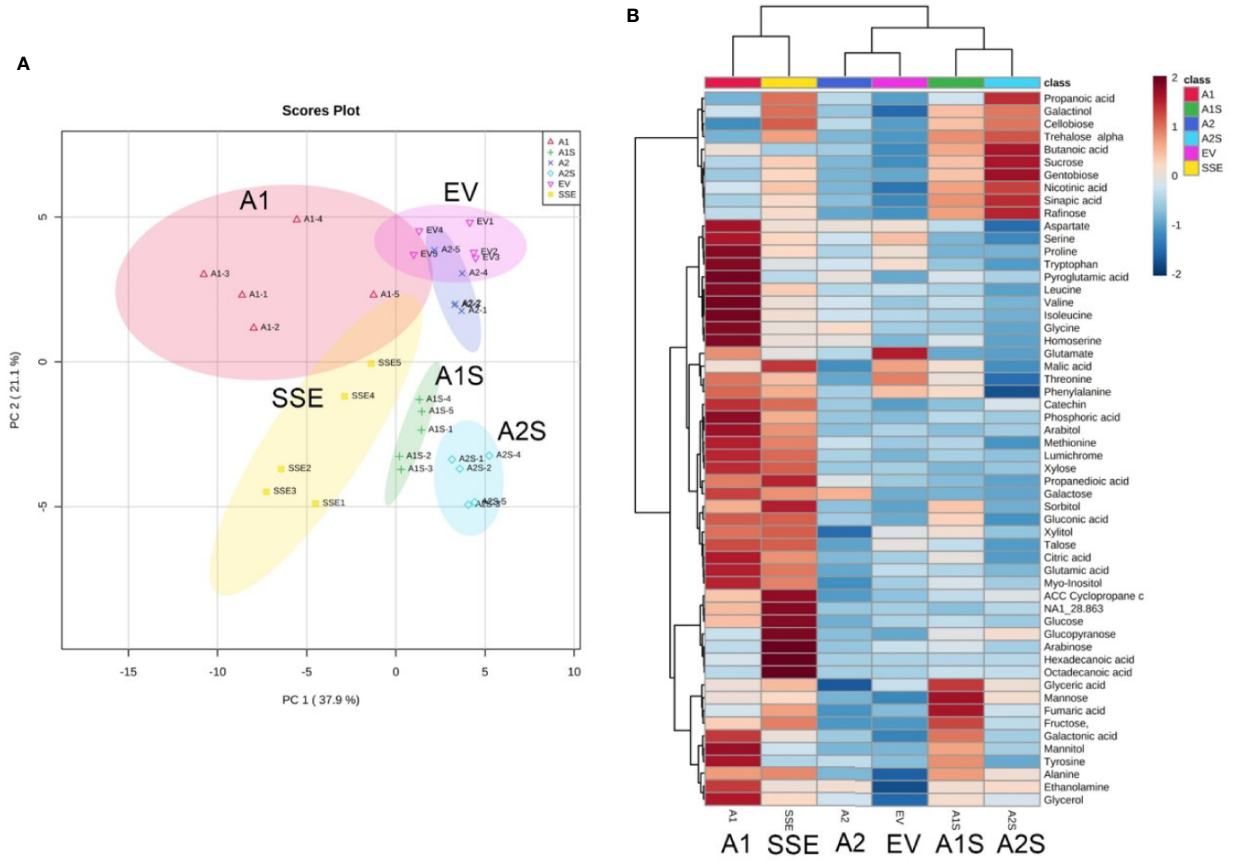

FIGURE 6 | Graphical representation of changes in metabolite profiles in the transgenic seeds. **(A)** Principal component analysis (PCA) according to their entire primary metabolome set of 56 metabolites measured by GC-MS analysis. The data points are displayed as projections onto the two primary axes (eigenvectors). Variances explained by the first two components (PC1 and PC2) appear in parentheses. **(B)** Schematic representation of these metabolites in a heat map. The intensity of blue or red represents the value of the coefficient, as indicated on the color scale. The data are represented as the average value of five biological replicates.

level of catechin, which associated with abiotic stress responses, was significantly reduced in A1S and A2S compared to SSE (**Supplementary Table S2**). In addition, 20 metabolites increased significantly in A1 compared to the other lines where 18 metabolites overlapped with SSE. Compered to SSE, A1 had significantly higher levels of valine, phosphoric acid, and aspartate (**Table 2**; **Supplementary Table S2**).

To determine if these low levels of metabolites are correlated to methionine, a correlation analysis was made of all transgenic sets. All of the top 25 metabolites that correlated to methionine had a positive correlation (**Supplementary Figure S3**): the amino acids leucine, isoleucine, valine, serine, homoserine aspartate, glycine, proline, tryptophan, threonine, and phenylalanine; the sugars xylose, galactose, talose, and glucose; the organic acids citrate, phosphoric acid, propanedioate, pyroglutamate, and gluconate; and the polyols sorbitol, myo-inisitol, arabitol and mannitol, and catechin.

In order to present an overview map of the correlations, to detect other metabolites that correlated to methionine, and to explore the metabolites that were negatively correlated to methionine, a Pearson's pairwise correlation coefficients analysis for each pair of the 56 different metabolites was performed (**Supplementary Figure S4**). This analysis showed that 43 metabolites were positively correlated to methionine, and only 13 metabolites were negatively correlated to methionine: mannose, raffinose, sucrose, gentobiose, trehalose, cellobiose, glycerate, fumarate, butanoic acid, nicotinic acid, sinapic acid, fructose, and galactinol (**Supplementary Figure S4**). Notably, all of these 13 metabolites showed higher levels in A1S and A2S compared to A2 and EV, while the other metabolites were similar to those detected in A2 and EV (**Figure 6B**; **Supplementary Table S2**).

Together, the results from metabolic profiling showed that most of the annotated metabolites decreased significantly in crosses lines that have low levels of free methionine compared to SSE and A1 seeds that had higher levels of free methionine. Our results strengthen the link between high free methionine and the accumulation of metabolites related to stress.

Seed Weight and Germination Rate of Transgenic Seeds

Changes in protein accumulation and cellular ingredients could affect seed yield, seed weight, and germination rate. Since we did not find any significant changes in the yield between the different transgenic lines, the total weight of 100 seeds was determined for each set to reveal that SSE has a significantly higher level (6%), while A1 has a significantly lower weight of 23% compared to that detected in EV. The weights of the other lines did not change significantly compared to EV (**Figure 7A**).

The germination rate was determined by the emergence of radicals, and it was measured 1 and 2 days after the cold imbibition treatment for all of these genotypes. The results showed that there was no difference in germination rate for both progenies of crosses (A1S/A2S) compared to seeds expressing *AtD-CGS* and *SSA* alone, but all of these lines germinated better than EV and reached the maximum germination rate by the second day following imbibition (**Figure 7B**).

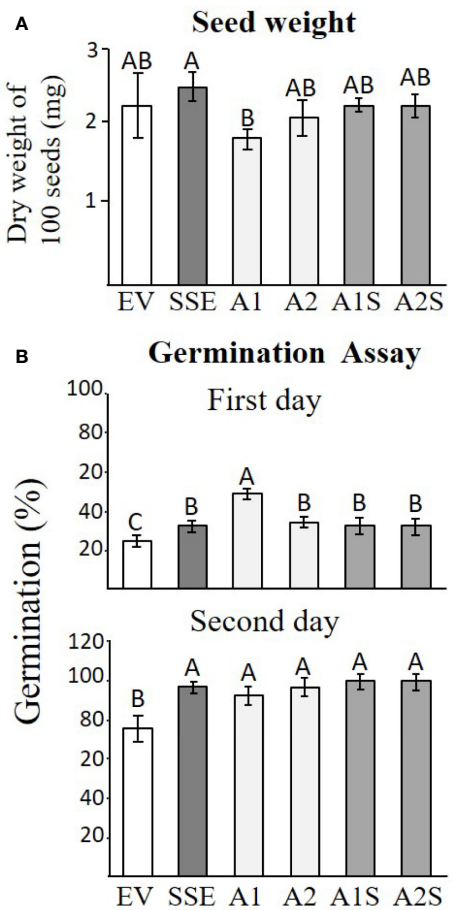

FIGURE 7 | Seed weight and germination efficiency. **(A)** The seed weight of 100 seeds of the different transgenic lines of EV, SSE, A1, A2, A1S, and A2S. Data shown are means of four biological replicates. **(B)** The germination rate on the first and second days after the plates were placed for 2 days in a cold room and were then transferred to a culture room. The rate of germination was determined by observing the emergence of radicals. Data shown are means of five replicates, each composed of 30 seeds from each genotype. Statistically significant changes (Tukey-Kramer HSD test, $P \leq 0.05$) between plants are identified by different letters.

DISCUSSION

Revealing the Factor/s Controlling the Accumulation of Protein-Bound Methionine in *A. thaliana* Seeds

The low levels of protein-bound methionine in cereals and legume crops limit the nutritional quality of seeds (Galili and Amir, 2013); therefore, an important biotechnological goal is to find approaches for increasing its levels. Generally, the low level of protein-bound methionine in seeds can result mainly from the low content of free methionine that restricts the synthesis of proteins and their accumulation, or from the number of methionine residues inside the endogenous seed-storage proteins [reviewed by Tabe et al. (1993); Galili and Amir (2013), and Amir et al. (2019)]. The previous observation that protein-bound methionine content increased by 65% in the water-soluble protein fraction of SSE suggested that higher levels of free methionine limit methionine accumulation in *A. thaliana* seeds (Cohen et al., 2014). The higher methionine content also affects the levels of proteins in the water-soluble fraction, which increased significantly by 10% in SSE seeds (Cohen et al., 2014).

However, the results of this study indicate that the level of protein-bound methionine in *A. thaliana* seeds is mainly limited by the methionine residues within the endogenous seed proteins. This suggestion is based on the following findings obtained from previous studies and the current study: i) Seed-specific expression of *AtD-CGS* in the first generation of SSE seeds, which led to a high level of free methionine (six-fold), elevated the level of protein-bound methionine in the water-soluble protein fraction only by 1.65-fold compared to EV (Cohen et al., 2014), while the level of protein-bound methionine in this fraction in *A. thaliana* seeds expressing the *SSA* alone (A1 and A2) increased significantly by 5.3- and 10.5-fold, respectively, compared to EV. This suggests that the *A. thaliana* seeds have enough free methionine content to support this accumulation; (ii) in seeds of SSE, the level of free methionine remained high (sixfold; Cohen et al., 2014), proposing that the capacity of methionine residues in the endogenous proteins came to saturation; iii) the increased level of the water-soluble protein fraction in seeds expressing SSA, A1, and A2 (24% and 38%, respectively) compared to EV (**Figure 4**) also suggests that there is enough free methionine in *A. thaliana* that can support this elevation; and iv) differences were detected between A1 and A2 in their protein-bound methionine in the water-soluble fraction. Compared to A1, A2 showed an approximately twofold higher expression level of *SSA* at the transcript and protein levels, which was in accordance to the twofold higher level of protein-bound methionine in the water-soluble fraction and about twofold lower level in its free

methionine (**Figure 5**). This observation strongly implies that if the expression level of SSA in A1 would increase further, the level of free methionine would still support the accumulation of SSA. We assume that in A1, the expression level of SSA triggered the synthesis or accumulation of free methionine (**Figure 5**), but since the expression level of SSA in this line did not reach that of A2 (**Figure 2**), the free methionine did not succeed to incorporating into the SSA protein and thus remained at a high level (**Figure 5A**). All of these lines of evidence support the assumption that the protein-bound methionine in the water-soluble fraction in *A. thaliana* seeds is limited mainly by methionine residues in the seed proteins. Despite these lines of evidence, it should be stated that the results and assumptions are based on only two transgenic lines expressing the SSA gene (A1 and A2) and two progenies from a single cross with SSE (A1S and A2S).

The higher level of protein-bound methionine that was detected in *A. thaliana* seeds expressing *SSA* (5.3- and 10.5-fold in A1 and A2, respectively) was higher than other transgenic seeds expressing the same gene. The level detected in grains of lupins was twofold (Tabe et al., 2010) and 90% (Molvig et al., 1997), in chickpea grains by 90% (Chiaiese et al., 2004), while in rice, it increased by 75% (Lee et al., 2003) or changed insignificantly (Hagan et al., 2003) compared to control seeds. The proteins of *A. thaliana* seeds most probably have the lowest endogenous methionine residues in their proteins. However, the differences in the results could also be explained by sulfur availability, as was previously shown, for example, in chickpea and lupin growing with low and regular levels of sulfur (Tabe and Droux, 2001; Tabe and Droux, 2002; Chiaiese et al., 2004). Yet, the selected gene and the promoter also played a major role in methionine accumulation in seeds. This, for example, was shown in rice when the sesame 2S albumin was expressed under the control of a rice seed-specific glutelin promoter, in which the level of protein-bound methionine increased by 75% (Lee et al., 2003), but when *SSA* was expressed under the wheat's high molecular weight of glutenin promoter, no significant changes were detected compared to the control seeds (Hagan et al., 2003).

In addition to the content of the methionine residues inside proteins, the level of free methionine could also be a limiting factor for the content of protein-bound methionine in seeds. To test this possibility, the levels of free methionine increased by the seed-specific expression of genes related to methionine biosynthesis pathway. The expression of these genes led to a range between non-significant elevations in azuki beans expressing *mto1-AtCGS* (Hanafy et al., 2013) up to a fourfold increase in maize expressing serine acetyltransferase (Xiang et al., 2018). The level of free methionine in these seeds increased twofold in azuki bean seeds, while in maize, it increased fourfold compared to the control seeds (Hanafy et al., 2013; Xiang et al., 2018). In between this range, one can find tobacco seeds expressing the bacterial aspartate kinas or *AtCGS* whose protein-bound methionine increased by 6.5% or 97%, with threefold and twofold elevations in their free methionine (Karchi et al., 1993; Matityahu et al., 2013), and also two soybean strains expressing the *AtD-CGS* having 2.3- to 3-fold elevations in their protein-bound methionine and 91% and 3.2-fold elevation in their free methionine (Song et al., 2013; Cohen et al., 2016b). In the current study, expression of *AtD-CGS* in *A. thaliana* SSE seeds increased free methionine 1.8-fold and protein-bound methionine 2-fold compared to EV. These results, as well as others [reviewed by Galili and Amir (2013) and Amir et al. (2019)], suggest that each genotype has a different methionine synthesis ability and/or different methionine residues in their endogenous proteins. Some genotypes are limited mainly by the methionine residues in their proteins (as in *A. thaliana*, azuki beans) and others by their free methionine content (as in tobacco). The results also suggest that many different factors could be at play in regulating the protein-bound methionine in seeds, and thus, each approach should be empirically tested separately in the seeds of each genotype.

Revealing Whether the Combination of the Two Approaches ("Push–Pull") Increases the Level of Protein-Bound Methionine in Transgenic Seeds

In the current study, it was detected that A2 expressing *SSA* alone and progenies of the "push–pull" approach (A1S, A2S) showed similar high levels of protein-bound methionine in the water-soluble protein fraction, which were 10.4- to 11.5-fold higher than EV (**Figure 5A**). As mentioned above, this suggests that A2 reached the maximum capacity of methionine residues for methionine incorporation. The observation that a higher production of free methionine did not affect the level of protein-bound methionine was also reported in lupin seeds expressing serine acetyltransferase (in the sulfur assimilation pathway; **Figure 1**) together with the 2S albumin of Brazil nut. The level of protein-bound methionine in these seeds did not increase beyond the levels detected in their parents (Tabe et al., 2010). However, this is unlike the results found in narbon bean seeds, which expressed the feedback-insensitive bacterial aspartate kinase and the 2S albumin of Brazil nut (Demidov et al., 2003). In these seeds, the level of methionine increased up to 2.4-fold compared to control seeds, and they also had more methionine than their parents: 10–12% more than those expressing the aspartate kinase and 80% more than those expressing Brazil nut (Demidov et al., 2003).

This combined approach was also tested in vegetative tissues, showing that unlike tobacco plants over-expressing *AtD-CGS* and 15 kDa zein in which the level of zein did not alter compared to plants over-expressing only 15 kDa zein (Golan et al., 2005), the level of this latter protein increased significantly in alfalfa transgenic plants expressing the same genes (Bagga et al., 2005; Golan et al., 2005). This elevation was concurrent with a reduction in the level of free methionine when compared to plants expressing *AtD-CGS* alone, implying that more free methionine was incorporated into the zein in the crossed alfalfa plants (Bagga et al., 2005; Golan et al., 2005). This strategy using the same enzymes was also tested in transgenic potatoes, leading to a sixfold increase in free and protein-bound methionine in the zein-containing protein fraction of the transgenic tubers (Dancs

et al., 2008). The results from different studies trying the "push–pull" approach suggest that the successes depend on the genotype and the selection of genes. Remarkably, the results are promising and suggest that in certain seeds, this approach can lead to higher levels of protein-bound methionine, which is a very important aspect regarding the nutritional quality of seeds.

The Effect of High Protein-Bound Methionine on the Levels of Storage Proteins

It was previously detected that a high expression level of *AtD-CGS* and thus a high level of methionine in SSE seeds increased the content of total proteins (Cohen et al., 2014; Cohen et al., 2016a). A high content of protein was also reported in the seeds of two transgenic lines of soybean (Song et al., 2013; Cohen et al., 2016b) and in tobacco seeds expressing the same *AtD-CGS* (Matityahu et al., 2013). These results suggest that the level of free methionine limits protein accumulation. These elevations are most probably also related to the high levels of other free amino acids whose levels were found to increase in these transgenic lines. High elevation of amino acids was also detected in the leaves of two *A. thaliana* lines having 1.75- and 2.25-fold higher contents of free methionine (Kim and Leustek, 2000). At least in the transgenic seeds, the total protein-bound amino acids also increased (Song et al., 2013; Cohen et al., 2014; Cohen et al., 2016b).

The high content of water-soluble proteins in SSE seeds (**Figure 4**; Cohen et al., 2014) suggests that high levels of free methionine change the levels of several storage proteins. It was indeed previously shown using 2D-gels and MALDI-MS that the accumulation of major storage proteins 12S-globulins and 2S-albumins changed in SSE (obtained from the first generation of SSE). It was also revealed that these changes were induced only from a certain threshold of free methionine, regardless of their methionine residue contents (Cohen et al., 2016a). The ability of the protein profile of seeds to change was also observed in A1S/A2S when the water-soluble proteins fraction was detected. The higher level of protein in this fraction in A1S compared to A1 (**Figure 3**) suggests that significant effects occurred when the level of methionine increased. However, this elevation in A1S was not reflected in the levels of water-soluble protein fractions (**Figure 4**), which were similar to those detected in SSE. We assume that this happens because the levels of some of the other storage proteins increased in A1S (in addition to SSA) as it occurred in SSE. In addition, the observation that the level of the water-soluble protein fraction obtained in SSE was similar to that measured in A2S suggests that SSA accumulation was at the expense of other endogenous proteins in the seeds. The results also propose that the seeds have a compensatory response to maintain stationary protein levels. This response might occur through the activities of promoters. In the current study, the heterologous genes are driven by the vicilin (SSA) and phaseolin (SSE) promoters, both of which drive genes encoding seed storage proteins, and thus may inherently be subject to the influences of amino acid and protein contents. However, these assumptions require further study. In any case, these assumptions are in accordance with other studies showing that while heterologous methionine-rich storage proteins accumulate in transgenic seeds, the level of other endogenous proteins had decreased. These include observations in rice, maize, soybean, and lupin seeds expressing methionine-rich storage proteins (SSA, 10 kDa zein, or the 2S Brazil nut) whereby the seeds did not show an increase in the level of protein-bound methionine, while instead the endogenous seed protein composition was markedly altered in such a way that the sulfur-poor proteins became over-abundant, while endogenous sulfur-rich proteins were down-regulated (e.g., Jung, 1997; Tabe and Droux, 2002; Hagan et al., 2003). These fluctuations might result due to alternation at the transcript expression level of seed-storage proteins. It was previously reported that high expression levels of SSA and serine acetyltransferase that increased the level of cysteine alter the transcript expression levels of several lupin seed storage proteins (Tabe and Droux, 2002). In addition, the transcript expression levels of sulfur-poor proteins were up-regulated when the level of *O*-acetyl serine (metabolite from the sulfur assimilation pathway; **Figure 1**) increased, and down-regulated when the level of free methionine increased (Hirai et al., 2002; Chiaiese et al., 2004), suggesting a direct effect of these metabolites on the transcript level of sulfur-poor storage proteins. The studies showing that the level of protein-bound methionine does not increase when the level of methionine-rich storage protein is expressed, together with studies showing that the levels of sulfur-containing metabolites decreased in several transgenic seeds (Molvig et al., 1997; Muntz et al., 1998), suggest that the level of free methionine limits the accumulation of proteins, and thus, they suggest examining the "push–pull" approach.

Transgenic Seeds With Lower Free Methionine Content Exhibited Less Accumulation of Stress-Associated Metabolites Compared to Seeds With High Levels of Free Methionine

The fourth goal of the current study was to gain more evidence of the relationship between a high level of free methionine and the accumulation of stress-related metabolites. In a prior study, it was reported that SSE seeds with high levels of free methionine are accompanied by higher levels of other free amino acids (62% more than in EV) (Cohen et al., 2014). Such elevations were also reported in transgenic *A. thaliana* seeds expressing *RNAi-AtCGS* that have a high level of free methionine (Cohen and Amir, 2017; Cohen et al., 2017). In these transgenic seeds, the levels of other stress-related metabolites were also increased significantly, and the expression levels of genes related to drought and osmotic stresses were significantly up-regulated (Cohen et al., 2014; Cohen and Amir, 2017). The reasons for these elevations are not yet clear, but the positive correlation between higher levels of free methionine to higher levels of other amino acids and stress metabolites was also shown in two varieties of soybean seeds expressing *AtD-CGS* (Song et al., 2013; Cohen et al., 2016b), in tobacco leaves over-expressing *AtCGS* (Hacham et al., 2017), and

A. thaliana leaves having higher levels of methionine (Kim and Leustek, 2000).

We hypothesized that if high levels of free methionine cause this effect in *A. thaliana* seeds, then a reduction in its level due to higher incorporation of methionine into seed proteins should reduce the levels of these metabolites. Indeed, the metabolic profiling that was conducted on the different sets of seeds shows that compared to SSE, the three sets of seeds, A2, A1S, and A2S, which show lower levels of free methionine (similar to EV), have lower levels of 29 out of 56 metabolites. These reduced metabolites are considered to be associated with stress responses such as sugars, free amino acids, organic acids, polyols, and several other metabolites (Ingram and Bartels, 1996; Angelovici et al., 2009; ElSayed et al., 2014). Moreover, the level of catechin, which is associated with abiotic stress responses, was reduced significantly in A2, A1S, and A2S compared to SSE (**Supplementary Table S2**).

A1 seeds expressing *SSA* alone also have a significant higher level of free methionine. Twenty metabolites increased significantly in this line compared to A2, A1S, A2S, and EV, most of which were related to abiotic stress (**Supplementary Table S2**; **Table 2**) (Ingram and Bartels, 1996). In addition, all of the top 25 metabolites that were found to be correlated with methionine were positively correlated (**Supplementary Figure S3**), and only 13 out of 56 metabolites had a negative correlation (**Supplementary Figure S4**). High positive correlation between high elevation of 21 out of 66 metabolites with methionine was also detected in soybean seeds (Cohen et al., 2016b). Taken together, our findings considerably strengthen the assumption that high levels of free methionine lead to higher accumulation of metabolites related to stress responses. The reason for this connection is yet unknown and definitely requires further studies.

The Effect of Various Manipulations on Seed Weight and Germination Efficiency

The seeds of progenies of the crosses A1S and A2S, as well as SSE, exhibited significantly higher levels of water-soluble protein fraction compared to EV (**Figure 4**), and they also had similar seed dry weights (**Figure 7A**). This indicated that higher levels of water-soluble protein and protein-bound methionine in these seeds contributed to the significant increase in seed weight. This is in accordance with the results obtained for the seeds of A1, which exhibit relatively lower water-soluble protein content, and the protein-bound methionine was lower compared to A1S, A2S, and SSE.

The higher germination rate of SSE, A1, A2, A1S, and A2S seeds compared to EV suggests that the higher levels of proteins and other soluble metabolites contribute to improved germination efficiency (**Figure 7B**). This is unlike the first generation of SSE that shows the same germinate rate as the control seeds. However, SSE seeds show better germination rates under osmotic and salt stresses than WT seeds (Cohen et al., 2014). The results also differ from tobacco seeds expressing *AtD-CGS*, whose germination rates were significantly lower than that of the WT (Matityahu et al., 2013). Taken together, our results imply that the manipulation leads to a high level of proteins and to a better germination rate.

CONCLUSION

Four objectives were addressed in this study; all were related to methionine metabolism in seeds. The first was to obtain more knowledge about the factor/s limiting the accumulation of protein-bound methionine content in *A. thaliana* seeds that are used as a model plant for *Brassicaceae*, as well as for other plants. The second goal was to reveal if the level of methionine could be increased further by using the "push–pull" approach. The third goal was to study how high levels of SSA and methionine affect the level of total water-soluble proteins in seeds. The fourth goal was to strengthen the assumption that an association exists between higher levels of free methionine and the accumulation of stress-related metabolites in seeds.

The results showed that free methionine levels in Arabidopsis seeds can increase the protein-bound methionine in seeds as shown in the seeds of SSE. However, expressing *SSA* led to a significantly higher level of protein-bound methionine compared to SSE (about 5-fold), suggesting that the content of methionine residues in the storage protein is the main limiting factor of methionine accumulation in Arabidopsis seeds as shown in A2 plants. Moreover, the "push–pull" approach obtained by crossing plants expressing seed-specific *AtD-CGS* and those expressing the *SSA* did not lead to significantly higher levels of protein-bound methionine beyond the level obtained by A2 expressing the *SSA* alone. This indicates that the methionine residues in A2 line reach a maximum threshold for the incorporation of free methionine. More than that, it also proposed that expression levels of SSA in A1 increased the methionine biosynthesis pathway and elevated the free methionine content. The results achieved in A1 and A1S suggested that the "push–pull" strategy should be tested in other seeds, since its applicability could lead to methionine improvement that could increase the nutritional value of these seeds. The results obtained from the water-soluble proteins measurements showed that their levels were similar in SSE and in the progenies of the crosses (A1S, A2S), suggesting that the accumulation of *SSA* in seeds was at the expense of other endogenous proteins that accumulate in SSE. The results of this study also suggested a link between higher free methionine content and accumulation of other amino acids, sugars, polyols, and metabolites that accumulate in plants during stress. This link is interesting but the reason is still unknown and thus requires further studies.

DATA AVAILABILITY STATEMENT

All datasets presented in this study are included in the article/ **Supplementary Material**.

AUTHOR CONTRIBUTIONS

YH and RA: Experimental design. AG, DS, and YH: Conducted the experiments. AG, DS, and YH: Data analysis. AG, YH, and RA: Manuscript preparation. All authors have read and approved the manuscript.

FUNDING

This work was supported by grants from the Israeli Science Foundation (grant no. 1004/15).

ACKNOWLEDGMENTS

This research was carried out in the Plant Metabolism Laboratory of MIGAL—Galilee Research Institute in Kiryat Shmona, Israel. We thank Linda Tabe for the plasmid carrying the *SSA* gene and Rainer Hofgen for the SSA antibodies.

SUPPLEMENTARY MATERIAL

The Supplementary Material for this article can be found online at: https://www.frontiersin.org/articles/10.3389/fpls.2020.01136/full#supplementary-material

REFERENCES

Altenbach, S. B., Kuo, C. C., Staraci, L. C., Pearson, K. W., Wainwright, C., Georgescu, A., et al. (1992). Accumulation of a Brazil nut albumin in seeds of transgenic canola results in enhanced levels of seed protein methionine. *Plant Mol. Biol.* 18 (2), 235–245. doi: 10.1007/BF00034952

Amir, R., Han, T., and Ma, F. (2012). Bioengineering approaches to improve the nutritional values of seeds by increasing their methionine content. *Mol. Breed* 29, 915–924. doi: 10.1007/s11032-011-9690-7

Amir, R., Galili, G., and Cohen, H. (2018). The metabolic roles of free amino acids during seed development. *Plant Sci.* 275, 11–18. doi: 10.1016/j.plantsci.2018.06.011

Amir, R., Cohen, H., and Hacham, Y. (2019). Revisiting the attempts to fortify methionine content in plant seeds. *J. Exp. Bot.* 70, 4105–4114. doi: 10.1093/jxb/erz134

Angelovici, R., Fait, A., Zhu, X., Szymanski, J., Feldmesser, E., Fernie, A. R., et al. (2009). Deciphering transcriptional and metabolic networks associated with lysine metabolism during Arabidopsis seed development. *Plant Physiol.* 151 (4), 2058–2072. doi: 10.1104/pp.109.145631

Bagga, S., Ponteza, C., Ross, J., Martin, M. N., Luestek, T., and Sengupta-Gopalan, C. (2005). A transgene for high methionine protein is post transcriptionally regulated by methionine. *Vitro Cell Dev. Biol. Plant* 41, 731–741. doi: 10.1079/IVP2005709

Chiaiese, P., Ohkama-Ohtsu, N., Molvig, L., Godfree, R., Dove, H., Hocart, C., et al. (2004). Sulphur and nitrogen nutrition influence the response of chickpea seeds to an added, transgenic sink for organic sulphur. *J. Exp. Bot.* 55 (404), 1889–1901. doi: 10.1093/jxb/erh198erh198

Chong, J., Soufan, O., Li, C., Caraus, I., Li, S., Bourque, G., et al. (2018). MetaboAnalyst 4.0: towards more transparent and integrative metabolomics analysis. *Nucleic Acids Res.* 46 (W1), W486–W494. doi: 10.1093/nar/gky310

Cohen, H., and Amir, R. (2017). Dose-dependent effects of higher methionine levels on the transcriptome and metabolome of transgenic Arabidopsis seeds. *Plant Cell Rep.* 36 (5), 719–730. doi: 10.1007/s00299-016-2003-1

Cohen, H., Israeli, H., Matityahu, I., and Amir, R. (2014). Seed-specific expression of a feedback-insensitive form of CYSTATHIONINE-gamma-SYNTHASE in Arabidopsis stimulates metabolic and transcriptomic responses associated with desiccation stress. *Plant Physiol.* 166 (3), 1575–1592. doi: 10.1104/pp.114.246058

Cohen, H., Pajak, A., Pandurangan, S., Amir, R., and Marsolais, F. (2016a). Higher endogenous methionine in transgenic Arabidopsis seeds affects the composition of storage proteins and lipids. *Amino Acids* 48 (6), 1413–1422. doi: 10.1007/s00726-016-2193-4

Cohen, H., Shir, O. M., Yu, Y., Hou, W., Sun, S., Han, T., et al. (2016b). Genetic background and environmental conditions drive metabolic variation in wild type and transgenic soybean (Glycine max) seeds. *Plant Cell Environ.* 39 (8), 1805–1817. doi: 10.1111/pce.12748

Cohen, H., Hacham, Y., Panizel, I., Rogachev, I., Aharoni, A., and Amir, R. (2017). Repression of CYSTATHIONINE gamma-SYNTHASE in Seeds Recruits the S-Methylmethionine Cycle. *Plant Physiol.* 174 (3), 1322–1333. doi: 10.1104/pp.17.00579

Dancs, G., Kondrak, M., and Banfalvi, Z. (2008). The effects of enhanced methionine synthesis on amino acid and anthocyanin content of potato tubers. *BMC Plant Biol.* 8, 65, 1471–2229. doi: 10.1186/1471-2229-8-65

Demidov, D., Horstmann, C., Meixner, M., Pickard, T., Saalbach, I., Galili, G., et al. (2003). Additive effects of the feed-back insensitive bacterial aspartate kinase and the Brazil nut 2S albumin on the methionine content of transgneic narbon bean (Vicia narbonensis L.). *Mol. Breed* 11, 187–201. doi: 10.1023/A:1022814506153

Di, R., Kim, J., Martin, M. N., Leustek, T., Jhoo, J., Ho, C. T., et al. (2003). Enhancement of the primary flavor compound methional in potato by increasing the level of soluble methionine. *J. Agric. Food Chem.* 51 (19), 5695–5702. doi: 10.1021/jf030148c

ElSayed, A. I., Rafudeen, M. S., and Golldack, D. (2014). Physiological aspects of raffinose family oligosaccharides in plants: protection against abiotic stress. *Plant Biol. (Stuttg)* 16 (1), 1–8. doi: 10.1111/plb.12053

Fujiwara, T., Nambara, E., Yamagishi, K., Goto, D. B., and Naito, S. (2002). Storage proteins. *Arabidopsis Book* 1, e0020. doi: 10.1199/tab.0020

Galili, G., and Amir, R. (2013). Fortifying plants with the essential amino acids lysine and methionine to improve nutritional quality. *Plant Biotechnol. J.* 11 (2), 211–222. doi: 10.1111/pbi.12025

Galili, G., Amir, R., and Fernie, A. R. (2016). The Regulation of Essential Amino Acid Synthesis and Accumulation in Plants. *Annu. Rev. Plant Biol.* 67, 153–178. doi: 10.1146/annurev-arplant-043015-112213

Giovanelli, J., Mudd, S. H., and Datko, A. H. (1985). In vivo regulation of de novo methionine biosynthesis in a higher plant (Lemna). *Plant Physiol.* 77, 450–455. doi: 10.1104/pp.77.2.450

Golan, A., Matitiyho, I., Avraham, T., Badani, H., Galili, S., and Amir, R. (2005). Soluble methionine enhances accumulation of a 15 kDa zein, a methionine-rich storage protein, in transgenic alfalfa but not in transgenic tobacco plants. *J. Exp. Bot.* 56 (419), 2443–2452. doi: 10.1093/jxb/eri237

Hacham, Y., Schuster, G., and Amir, R. (2006). An in vivo internal deletion in the N-terminus region of Arabidopsis cystathionine gamma-synthase results in CGS expression that is insensitive to methionine. *Plant J.* 45 (6), 955–967. doi: 10.1111/j.1365-313X.2006.02661.x

Hacham, Y., Matityahu, I., and Amir, R. (2017). Transgenic tobacco plants having a higher level of methionine are more sensitive to oxidative stress. *Physiol. Plant* 160 (3), 242–252. doi: 10.1111/ppl.12557

Hagan, N. D., Upadhyaya, N., Tabe, L. M., and Higgins, T. J. (2003). The redistribution of protein sulfur in transgenic rice expressing a gene for a foreign, sulfur-rich protein. *Plant J.* 34 (1), 1–11. doi: 10.1046/j.1365-313X.2003.01699.x

Hanafy, M. S., Rahman, S. M., Nakamoto, Y., Fujiwara, T., Naito, S., Wakasa, K., et al. (2013). Differential response of methionine metabolism in two grain legumes, soybean and azuki bean, expressing a mutated form of Arabidopsis cystathionine gamma-synthase. *J. Plant Physiol.* 170 (3), 338–345. doi: 10.1016/j.jplph.2012.10.018

Hesse, H., and Hoefgen, R. (2003). Molecular aspects of methionine biosynthesis. *Trends Plant Sci.* 8 (6), 259–262. doi: 10.1016/S1360-1385(03)00107-9

Hirai, Y., Kim, H., Hayashi, H., Chino, M., Naito, S., and Fujiwara, T. (2002). Independent roles of methionine and O-acetyl-l-serine in the regulation of the β subunit gene of β-conglycinin. *Soil Sci. Plant Nutr.* 48, 87–94. doi: 10.1080/00380768.2002.10409175

Ingram, J., and Bartels, D. (1996). The Molecular Basis of Dehydration Tolerance in Plants. *Annu. Rev. Plant Physiol. Plant Mol. Biol.* 47, 377–403. doi: 10.1146/annurev.arplant.47.1.377

Jung, R. (1997). "Expression of a 2S albumin from Bertholletia excelsain soybean," in *The 39th NIBB Conference: Dynamic aspects of seed maturation and germination* (Okazaki: National Institute for Basic Biology).

Karchi, H., Shaul, O., and Galili, G. (1993). Seed specific expression of a bacterial desensitized aspartate kinase increases the production of seed threonine and methionine in transgenic tobacco. *Plant J.* 3, 721–727. doi: 10.1111/j.1365-313X.1993.00721.x

Kim, H., and Leustek, T. (2000). Repression of cystathionine g-synthase in Arabidopsis thaliana produces partial methionine auxotrophy and developmental abnormalities. *Plant Sci.* 151, 9–18. doi: 10.1016/S0168-9452(99)00188-0

Kim, J., Lee, M., Chalam, R., Martin, M. N., Leustek, T., and Boerjan, W. (2002). Constitutive overexpression of cystathionine gamma-synthase in Arabidopsis leads to accumulation of soluble methionine and S-methylmethionine. *Plant Physiol.* 128 (1), 95–107. doi: 10.1104/pp.101801

Kim, W. S., Chronis, D., Juergens, M., Schroeder, A. C., Hyun, S. W., Jez, J. M., et al. (2012). Transgenic soybean plants overexpressing O-acetylserine sulfhydrylase accumulate enhanced levels of cysteine and Bowman-Birk protease inhibitor in seeds. *Planta* 235 (1), 13–23. doi: 10.1007/s00425-011-1487-8

Lee, T. T., Wang, M. M., Hou, R. C., Chen, L. J., Su, R. C., Wang, C. S., et al. (2003). Enhanced methionine and cysteine levels in transgenic rice seeds by the accumulation of sesame 2S albumin. *Biosci. Biotechnol. Biochem.* 67 (8), 1699–1705. doi: 10.1271/bbb.67.1699

Matityahu, I., Godo, I., Hacham, Y., and Amir, R. (2013). Tobacco seeds expressing feedback-insensitive cystathionine gamma-synthase exhibit elevated content of methionine and altered primary metabolic profile. *BMC Plant Biol.* 13, 206. doi: 10.1186/1471-2229-13-206

Molvig, L., Tabe, L. M., Eggum, B. O., Moore, A. E., Craig, S., Spencer, D., et al. (1997). Enhanced methionine levels and increased nutritive value of seeds of transgenic lupins (Lupinus angustifolius L.) expressing a sunflower seed albumin gene. *Proc. Natl. Acad. Sci. U.S.A.* 94 (16), 8393–8398. doi: 10.1073/pnas.94.16.8393

Muntz, K., Christov, V., Saalbach, G., Saalbach, I., Waddell, D., Pickardt, T., et al. (1998). Genetic engineering for high methionine grain legumes. *Nahrung* 42 (3-4), 125–127. doi: 10.1002/(SICI)1521-3803(199808)42:03/04<125::AID-FOOD125>3.3.CO;2-1

Nguyen, H. C., Hoefgen, R., and Hesse, H. (2012). Improving the nutritive value of rice seeds: elevation of cysteine and methionine contents in rice plants by ectopic expression of a bacterial serine acetyltransferase. *J. Exp. Bot.* 63 (16), 5991–6001. doi: 10.1093/jxb/ers253

Planta, J., Xiang, X., Leustek, T., and Messing, J. (2017). Engineering sulfur storage in maize seed proteins without apparent yield loss. *Proc. Natl. Acad. Sci. U.S.A.* 114 (43), 11386–11391. doi: 10.1073/pnas.1714805114

Ranocha, P., McNeil, S. D., Ziemak, M. J., Li, C., Tarczynski, M. C., and Hanson, A. D. (2001). The S-methylmethionine cycle in angiosperms: ubiquity, antiquity and activity. *Plant J.* 25 (5), 575–584. doi: 10.1046/j.1365-313x.2001.00988.x

Roje, S. (2006). S-Adenosyl-L-methionine: beyond the universal methyl group donor. *Phytochemistry* 67 (15), 1686–1698. doi: 10.1016/j.phytochem.2006.04.019

Song, S., Hou, W., Godo, I., Wu, C., Yu, Y., Matityahu, I., et al. (2013). Soybean seeds expressing feedback-insensitive cystathionine gamma-synthase exhibit a higher content of methionine. *J. Exp. Bot.* 64 (7), 1917–1926. doi: 10.1093/jxb/ert053

Tabe, L. M., and Droux, M. (2001). Sulfur assimilation in developing lupin cotyledons could contribute significantly to the accumulation of organic sulfur reserves in the seed. *Plant Physiol.* 126 (1), 176–187. doi: 10.1104/pp.126.1.176

Tabe, L. M., and Droux, M. (2002). Limits to sulfur accumulation in transgenic lupin seeds expressing a foreign sulfur-rich protein. *Plant Physiol.* 128 (3), 1137–1148. doi: 10.1104/pp.010935

Tabe, L. M., Higgins, C. M., McNabb, W. C., and Higgins, T. J. (1993). Genetic engineering of grain and pasture legumes for improved nutritive value. *Genetica* 90 (2-3), 181–200. doi: 10.1007/bf01435039

Tabe, L., Wirtz, M., Molvig, L., Droux, M., and Hell, R. (2010). Overexpression of serine acetlytransferase produced large increases in O-acetylserine and free cysteine in developing seeds of a grain legume. *J. Exp. Bot.* 61 (3), 721–733. doi: 10.1093/jxb/erp338

Xiang, X., Wu, Y., Planta, J., Messing, J., and Leustek, T. (2018). Overexpression of serine acetyltransferase in maize leaves increases seed-specific methionine-rich zeins. *Plant Biotechnol. J.* 16 (5), 1057–1067. doi: 10.1111/pbi.12851

Zhang, Y., Schernthaner, J., Labbe, N., Hefford, M. A., Zhao, J., and Simmonds, D. H. (2014). Improved protein quality in transgenic soybean expressing a de novo synthetic protein, MB-16. *Transgenic Res.* 23 (3), 455–467. doi: 10.1007/s11248-013-9777-5

Conflict of Interest: The authors declare that the research was conducted in the absence of any commercial or financial relationships that could be construed as a potential conflict of interest.

Copyright © 2020 Girija, Shotan, Hacham and Amir. This is an open-access article distributed under the terms of the Creative Commons Attribution License (CC BY). The use, distribution or reproduction in other forums is permitted, provided the original author(s) and the copyright owner(s) are credited and that the original publication in this journal is cited, in accordance with accepted academic practice. No use, distribution or reproduction is permitted which does not comply with these terms.

frontiers in Plant Science

REVIEW
published: 04 September 2020
doi: 10.3389/fpls.2020.577980

Challenges and Prospects of New Plant Breeding Techniques for GABA Improvement in Crops: Tomato as an Example

Pietro Gramazio[1], *Mariko Takayama*[1,2] *and Hiroshi Ezura*[1,2*]

[1] Faculty of Life and Environmental Sciences, University of Tsukuba, Tsukuba, Japan, [2] Tsukuba Plant Innovation Research Center (T-PIRC), University of Tsukuba, Tsukuba, Japan

OPEN ACCESS

Edited by:
Sakiko Okumoto,
Texas A&M University, United States

Reviewed by:
Estela M. Valle,
CONICET Instituto de Biología Molecular y Celular de Rosario (IBR), Argentina
Christine Helen Foyer,
University of Birmingham, United Kingdom

***Correspondence:**
Hiroshi Ezura
ezura.hiroshi.fa@u.tsukuba.ac.jp

Specialty section:
This article was submitted to Plant Metabolism and Chemodiversity, a section of the journal Frontiers in Plant Science

Received: 30 June 2020
Accepted: 20 August 2020
Published: 04 September 2020

Citation:
Gramazio P, Takayama M and Ezura H (2020) Challenges and Prospects of New Plant Breeding Techniques for GABA Improvement in Crops: Tomato as an Example. Front. Plant Sci. 11:577980. doi: 10.3389/fpls.2020.577980

Over the last seven decades, γ-aminobutyric acid (GABA) has attracted great attention from scientists for its ubiquity in plants, animals and microorganisms and for its physiological implications as a signaling molecule involved in multiple pathways and processes. Recently, the food and pharmaceutical industries have also shown significantly increased interest in GABA, because of its great potential benefits for human health and the consumer demand for health-promoting functional compounds, resulting in the release of a plethora of GABA-enriched products. Nevertheless, many crop species accumulate appreciable GABA levels in their edible parts and could help to meet the daily recommended intake of GABA for promoting positive health effects. Therefore, plant breeders are devoting much effort into breeding elite varieties with improved GABA contents. In this regard, tomato (*Solanum lycopersicum*), the most produced and consumed vegetable worldwide and a fruit-bearing model crop, has received much consideration for its accumulation of remarkable GABA levels. Although many different strategies have been implemented, from classical crossbreeding to induced mutagenesis, new plant breeding techniques (NPBTs) have achieved the best GABA accumulation results in red ripe tomato fruits along with shedding light on GABA metabolism and gene functions. In this review, we summarize, analyze and compare all the studies that have substantially contributed to tomato GABA breeding with further discussion and proposals regarding the most recent NPBTs that could bring this process to the next level of precision and efficiency. This document also provides guidelines with which researchers of other crops might take advantage of the progress achieved in tomato for more efficient GABA breeding programs.

Keywords: γ-aminobutyric acid, GABA metabolism, tomato, health-promoting food, breeding strategies, new plant breeding techniques, CRISPR/Cas, *cis*-engineering

INTRODUCTION

Consumer preferences are shifting towards health-promoting and functionally enriched food products that could translate into healthier lifestyles. Therefore, industry and producers are encouraged to develop and design new products to target this growing market and promote studies to test their dietary functional claims (Diana et al., 2014; Ramos-Ruiz et al., 2018). Γ-Aminobutyric acid (GABA) is widely recognized as a bioactive and functional compound thanks to a plethora of *in vitro* and *in vivo* studies reporting its beneficial effects in treating many metabolic disorders (Yoshimura et al., 2010; Yang et al., 2012). In humans, GABA functions as an inhibitory neurotransmitter (Owens and Kriegstein, 2002), and it has been reported that the intake of GABA is effective in lowering the blood pressure of hypertensive patients (Inoue et al., 2003), inducing relaxation (Abdou et al., 2006), reducing psychological stress (Nakamura et al., 2009), and shortening sleep latency (Yamatsu et al., 2016), among other health benefits. Consequently, in recent decades, the food industry has focused on releasing and developing new GABA-enriched products such as tea, yogurt, bread, cheese and fermented foods (Park and Oh, 2007; Poojary et al., 2017; Quílez and Diana, 2017). However, the GABA concentration of these products is often insufficient to confer health-promoting effects and prevent lifestyle-related disorders. Many crop plants, including fresh vegetables, have high GABA levels. Hence, plant breeders have devoted considerable efforts to developing new and improved varieties of vegetables with increased GABA contents (Lee et al., 2018). However, classical breeding is often limited by the capacity to either identify or produce (i.e., through processes such as random mutagenesis) suitable parental germplasms, apart from being time- and resource-consuming. New plant breeding techniques (NPBTs) can overcome this barrier to obtain remarkable achievements in a safer and faster way. On the other hand, GABA and other GABA genes are involved in the metabolism of many important plant species, and their modulation could be exploited to develop more well-adapted and resilient varieties.

Here, we provide an overview of the main aspects of GABA metabolism and how NPBTs could help to increase plant GABA contents using tomato as a model fruit-bearing crop.

GABA CONTENTS IN CROP SPECIES

After its first detection in potato tubers in 1949 (Steward et al., 1949), GABA has been found and measured in almost all economically important and model crop species, apart from bacteria, fungi and animals (Ramos-Ruiz et al., 2018). Some crops, at the harvest stage, accumulate considerable GABA levels that can substantially contribute to the daily recommended intake of GABA (10–20 mg) to generate positive health effects (Fukuwatari et al., 2001; Kazami et al., 2002; Inoue et al., 2003; Nishimura et al., 2016). The GABA content in crops varies across species and varieties and depends on a multitude of factors, such as the plant developmental stage, environmental conditions, response to biotic and abiotic stresses, and postharvest treatments (Ham et al., 2012; Kim et al., 2013; Chalorcharoenying et al., 2017) (**Table 1**). Among fresh vegetables, tomato is one of the crops that accumulates a significant amount of GABA in its edible parts, even though its content increases until the

TABLE 1 | GABA content in crops.

Crop	GABA content	Reference
Apple	0.003–0.004 mg g^{-1}	Deewatthanawong and Watkins, 2010; Deyman et al., 2014
Artichoke	0.011 mg g^{-1}	Dosi et al., 2013
Asparagus	0.15 mg g^{-1}	Zhao et al., 2007
Banana	0.023 mg g^{-1}	Wang et al., 2016
Blueberry	0.079–0.089 mg g^{-1}	Zhang et al., 2014; Lee et al., 2015
Broccoli	0.031 mg g^{-1}	Murcia et al., 2001
Cabbage	0.032–0.071 mg g^{-1}	Park et al., 2014
Carrot	0.00014 mg g^{-1}	Fan et al., 1986
Cherimoya	0.005 mg g^{-1}	Merodio et al., 1998
Eggplant	0.23–0.38 mg g^{-1}	Mori et al., 2013
Kiwi	0.077–0.141 mg g^{-1}	Macrae and Redgwell, 1992
Loquat	0.018 mg g^{-1}	Cao et al., 2012
Lychee	1.7–3.5 mg g^{-1}	Wu et al., 2016
Mulberry	0.86–1.86 mg g^{-1}	Kim et al., 2010
Muskmelon	0.103–0.722 mg mL^{-1}	Biais et al., 2010
Onion	0.001 mg g^{-1}	Oh et al., 2003
Orange	0.344 mg mL–1	Zazzeroni et al., 2009
Peach	0.008 mg mL^{-1}	Jia et al., 2000
Potato	0.16–0.61 mg g^{-1}	Nakamura et al., 2006
Pumpkin	3.71–15.53 mg g^{-1}	Qi et al., 2012
Radish	0.28 mg g^{-1}	Kato et al., 2015
Raspberry	0.101–0.194 mg g^{-1}	Lee et al., 2015
Spinach	0.043 mg g^{-1}	Oh et al., 2003
Strawberry	0.0155–0.036 mg g^{-1}	Deewatthanawong et al., 2010b
Tomato	0.35–2.01 mg g^{-1}	Loiudice et al., 1995; Saito et al., 2008
Zucchini	0.026–0.040 mg g^{-1}	Palma et al., 2014

mature green stage and then rapidly decreases during ripening (Akihiro et al., 2008; Saito et al., 2008; Sánchez Pérez et al., 2011). It has been found that the GABA content in tomato also varies greatly depending on the genotype or cultivar assessed. Saito et al. (2008) reported a range of 39.6 to 102.5 mg/100 g fresh weight (FW) (0.39–1.02 mg g^{-1}) of GABA in 11 fresh market cultivars and a range of 35.4 to 93.3 mg/100 g FW (0.35–0.93 mg g^{-1}) in 38 processing cultivars. Higher values for processing tomatoes were reported previously by Loiudice et al. (1995), where 11 lines of San Marzano cultivars showed a range of 132 to 201 mg/100 g FW (1.32–2.01 mg g^{-1}) of GABA. On the other hand, even though few genotypes have been examined, tomato wild relatives generally seem to accumulate less GABA than modern cultivars (Anan et al., 1996; Saito et al., 2008; Deewatthanawong and Watkins, 2010). This is probably due to a positive selection for the "umami" flavor, which is linked to the glutamate content.

GABA PATHWAY IN PLANTS

GABA is a ubiquitous four-carbon nonproteinogenic amino acid that is widely distributed throughout the animal, plant and bacterial kingdoms. In plants, GABA is mainly metabolized *via* a short pathway called the GABA shunt, which is linked with several pathways, such as the TCA cycle (Bouché and Fromm, 2004; Shelp et al., 2017; **Figure 1**). In the cytosol, GABA is irreversibly synthesized from L-glutamate *via* the H^+-dependent glutamate decarboxylase (GAD) enzyme, or alternatively by polyamine (putrescine and spermidine) degradation or a nonenzymatic reaction from proline under oxidative stress (Shelp et al., 2012; Signorelli et al., 2015; Yang et al., 2015). A wide range of GAD copies, which are differentially expressed according to organ types, growth stages and environmental conditions, has been identified in different plant species (Bouché and Fromm, 2004; Ramos-Ruiz et al., 2019). GAD usually presents a calcium/calmodulin (Ca^{2+}/CaM) binding domain (CaMBD) at the C-terminus (30–50 amino acids) that modulates its activity in the presence of Ca^{2+} at acidic pH (Snedden et al., 1996; Gut et al., 2009). Under physiological cell conditions (pH 7.0), CaMBD inhibits GAD activity by folding its active site. Increases in cytosolic Ca^{+2} and H^+ ions, usually as a stress response, unfold and bind CaMBD, releasing the GAD active site and stimulating its activity (Snedden et al., 1995).

The GABA shunt and the TCA cycle are connected by a transmembrane protein, GABA permease (GABA-P), that allows GABA flux from the cytosol into mitochondria (Michaeli et al., 2011). Subsequently, GABA is catabolized to succinic semialdehyde (SSA) by the transaminase enzyme GABA-T. Depending on the substrate affinity, two GABA-T enzymes can catalyze the reaction: α-ketoglutarate-dependent GABA-TK or pyruvate-dependent GABA-TP. GABA-TK receives an amino group from a-ketoglutarate and generates SSA and glutamate, while GABA-TP requires pyruvate or glyoxylate that are converted into alanine or glycine (Shimajiri et al., 2013; Trobacher et al., 2013). However, the latter has been found exclusively in plants, usually showing a higher activity than GABA-TK, while the rest of the organisms use primarily GABA-TK (Narayan and Nair, 1990; Van Cauwenberghe et al., 2002; Bartyzel et al., 2003).

Finally, SSA is catabolized in succinate, a TCA component, and NADH plus a hydrogen ion is generated from NAD^+ by the succinic semialdehyde dehydrogenase (SSADH) enzyme (Bouché et al., 2003). Succinate and NADH are electron donors to the mitochondrial electron transport chain that produces ATP as a final outcome (Ramos-Ruiz et al., 2019). Alternatively, SSA can be converted to γ-hydroxybutyric acid (GHB) and $NAD(P)^+$ in the presence of NAD(P) and a hydrogen ion by succinic semialdehyde reductase (SSR) in the cytosol or chloroplast, usually as a response to stresses (Simpson et al., 2008; Hildebrandt et al., 2015). When the NAD^+:NADH ratio is low, the SSADH route is inhibited, as it depends on the energy balance in mitochondria, resulting in the accumulation of SSA due to the consequent GABA-T inhibition (Van Cauwenberghe and Shelp, 1999; Podlešáková et al., 2019).

GABA GENES IN TOMATO

In the latest version of the tomato reference genome (Heinz 1706, version SL 4.0, Hosmani et al., 2019), five GAD genes have been annotated (Solyc11g011920, Solyc04g025530, Solyc05g054050, Solyc01g005000 and Solyc03g098240). The first GAD gene, *ERT D1* (Solyc03g098240), was predicted in 1995 from the screening of the "Ailsa Craig" tomato fruit cDNA library, showing peak expression at the fruit breaker stage and slowly declining during ripening (Gallego et al., 1995). Subsequently, from immature fruits of "MicroTom", three GAD genes were characterized during fruit development: *SlGAD1* (Solyc03g098240, allelic to *ERD D1*), which reaches its highest expression at mature fruit stages, and *SlGAD2* (Solyc11g011920) and *SlGAD3* (Solyc01 g005000), which increase their expression during fruit development and rapidly decline during ripening (Akihiro et al., 2008). However, while *SlGAD1* did not exhibit a clear correlation with the GABA content during fruit ripening, *SlGAD2* and *SlGAD3* showed a positive correlation, suggesting a main role of the latter in GABA biosynthesis. This was confirmed by Takayama et al. (2015) by suppressing the three *SlGAD* genes through the RNAi approach, resulting in a significant GABA reduction for *SlGAD2* and *SlGAD3*-suppressed lines in mature green fruit, while *SlGAD1* GABA levels were similar to those of the wild type (WT).

In tomato, three GABA-TP genes were suggested to catabolize GABA to SSA: *SlGABA-T1* (Solyc07g043310) found in mitochondria, *SlGABA-T2* (Solyc12g006470) in the cytosol and *SlGABA-T3* (Solyc12g006450) in plastids (Akihiro et al., 2008; Clark et al., 2009). By RNAi loss-of-function analyses, Koike et al. (2013) suppressed the three *SlGABA-T* genes and observed an increase in GABA of up 9-fold in red mature fruits of *SlGABA-T1*-suppressed lines, while no significant correlation was observed between the GABA content and *SlGABA-T2* and *SlGABA-T3* expression. In light of these results and the fact that

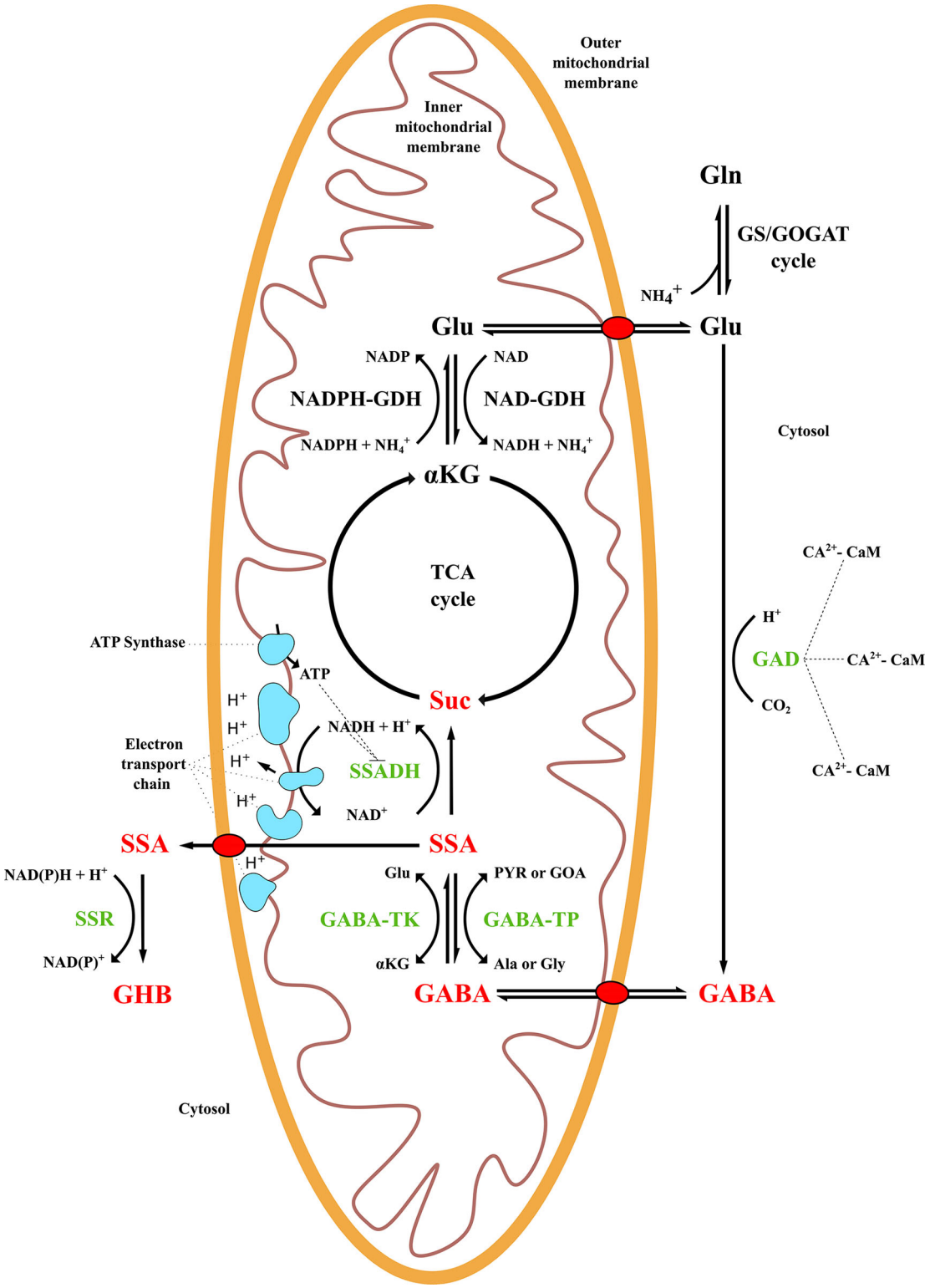

FIGURE 1 | γ-Aminobutyric acid (GABA) shunt metabolism and related pathways in plant species. TCA, tricarboxylic acid cycle; GS/GOGAT, glutamine-synthetase/glutamate-synthase cycle; GAD, glutamate decarboxylase; GABA-TK, α-ketoglutarate-dependent GABA transaminase; GABA-TP, pyruvate-dependent GABA transaminase; SSADH, succinic semialdehyde dehydrogenase; SSR, succinic semialdehyde reductase; GDH, glutamate dehydrogenase; SSA, succinic semialdehyde; Suc, succinate; GHB, γ-hydroxybutyric acid; αKG, alpha-ketoglutarate; Glu, glutamate; Ala, alanine; Gly, glycine, PYR, pyruvate, GOA, glyoxylic acid.

SlGABA-T1 is expressed at a higher level than *SlGABA-T2* and *SlGABA-T3* during fruit ripening (Clark et al., 2009), *SlGABA-T1* was suggested as the major *GABA-T* gene responsible for GABA catabolism. These results were confirmed by Li et al. (2018) by a multiplex CRISPR/Cas9 system targeting the three *SlGABA-Ts*. The last steps of the GABA shunt in tomato are not yet well characterized. To date, one SSADH gene (*SlSSADH*, probably Solyc09g090700) has been identified in tomato as responsible for SSA catabolism in succinate, and it was expressed in fruits across all developmental stages even though it showed a low correlation with the GABA content (Akihiro et al., 2008). On the other hand, two SSR genes have been isolated in tomato (*SlSSR1* and *SlSSR2*, probably Solyc09g018790 and Solyc03g121720) (Akihiro et al., 2008). The expression of *SlSSR1* has been found to be slightly higher in mature red fruits than in breaker fruits, while *SlSSR2* showed the opposite expression pattern (Deewatthanawong et al., 2010a). Further studies are required to fully characterize the two alternative routes of SSA catabolism in the tomato GABA shunt and to determine how they are linked with GABA biosynthesis.

ROLES OF GABA METABOLISM

Across the kingdoms, a plethora of processes, functions, and pathways that are directly or indirectly involved in GABA metabolism have been identified (Seifikalhor et al., 2019). In plants, GABA plays important roles in pH and redox regulation, energy production, carbon/nitrogen balance maintenance, plant growth regulation and development, senescence, pollen germination, and fruit ripening, among other functions (Kinnersley and Turano, 2000; Bouché and Fromm, 2004; Fait et al., 2008; Renault et al., 2011; Yu et al., 2014; Carillo, 2018; Podlešáková et al., 2019). Similar to many other plant molecules, such as calcium, jasmonates, abscisic or salicylic acid, GABA rapidly accumulates in response to environmental stress (Kinnersley and Turano, 2000; Gill et al., 2016). Plants have developed highly dynamic mechanisms to face unfavorable and stressful conditions to maximize their chances to survive, modulating their responses according to the stress severity and growth stage (Podlešáková et al., 2019). Many studies on different species have reported the involvement of GABA in many abiotic stresses, such as salinity, drought, hypoxia, high/low temperature or light and nutrient deficiency/excess (Kinnersley and Turano, 2000; Renault et al., 2010; Al-Quraan et al., 2013; Espasandin et al., 2014; Wang et al., 2014; Daş et al., 2016). GABA also has inhibitory effects on biotic defenses, especially against insects and fungi (Sánchez-López et al., 2016a; Sánchez-López et al., 2016b; Scholz et al., 2017). Undoubtedly, any change affecting the genes involved in GABA metabolism, both at the sequence or expression level, could either potentiate or disrupt functions (Seifikalhor et al., 2019). In tomato, the potential roles of GABA metabolism have been investigated using, among other approaches, reverse genetics. The three *SlGAD* genes were suppressed individually and simultaneously by RNAi, demonstrating that *SlGADs* are key genes for GABA production in tomato (Takayama et al., 2015). However, the downregulation of GABA biosynthesis through SlGAD knockdown did not show a significant effect on plant growth and fruit development under stress-free conditions. In contrast, the loss-of-function of *SlGABA-T* genes resulting in drastic changes and abnormal phenotypes (Koike et al., 2013). Two out of three *SlGABA-T* mutants, *SlGABA-T1* and *SlGABA-T3*, showed severe dwarfism with a plant height half or less than that of the Micro-Tom wild type, probably due to defects in cell elongation. Additionally, *SlGABA-T1* also exhibited infertility and flower abscission, while no remarkable changes were observed in *SlGABA-T2*. Similarly, the suppression of *SlSSADH* by VIGS led to a dwarf phenotype with curled leaves, probably due to enhanced ROS accumulation (Bao et al., 2015). However, under 200 mM NaCl treatment, *SlSSADH*-suppressed plants exhibited superior salt resistance compared to that of the WT, showing a higher shoot biomass level and significantly higher chlorophyll content and photosynthesis rate. In contrast, under the same stress conditions, *SlGAD*- and *SlGABA-T*-suppressed plants showed severe salt sensitivity (Bao et al., 2015). These results suggested that tomato GABA metabolism is involved in salt stress tolerance.

More recently, Li et al. (2018), using a multiplex CRISPR/Cas9 system, targeted four GABA genes (*SlGABA-T1*, *SlGABA-T2*, *SlGABA-T3* and *SlSSADH*) and *CAT9*, a protein that transports GABA from vacuoles to mitochondria for catabolism (Snowden et al., 2015), constructing a pYLCRISPR/Cas9 plasmid with six sgRNA cassettes. Almost all edited plants with multiple mutations exhibited severe dwarfism with heights from 32.5 to 95.6% shorter than the WT. Moreover, the plants that presented higher GABA contents also showed pale green and curled compound leaves, and some of them developed a secondary axis and more leaflets with visible leaf necrosis. When analyzed by scanning electron microscopy, the leaf tissues of those mutants exhibited smaller and more compressed cells than those of the WT that were larger and stretched, confirming previous study results that suggested that GABA may be involved in plant cell elongation in vegetative tissues and leaf development regulation (Renault et al., 2011). Leaf necrosis was especially severe in *SlSSADH*-knockout lines, probably due to the increase in H_2O_2 levels and GHB accumulation, similar to *Arabidopsis SSADH*-deficient mutants (Bouché et al., 2003). Furthermore, some mutants also exhibited bud necrosis and fewer flowers, and only a few mutants set fruit, some of which were teratogenic (Li et al., 2018).

As in other plant species, GABA is involved in stress tolerance in tomato (Seifikalhor et al., 2019). Seifi et al. (2013) observed that the overactivation of the GABA shunt in the *sitiens* tomato mutant played a vital role in resistance to *Botrytis cinerea*, maintaining cell viability and slowing senescence at the site of primary invasion. The authors hypothesized that the H_2O_2-mediated defense *via* GABA in response to *B. cinerea* might have restricted the extent of cell death in the vicinity of the pathogen penetration sites.

More recently, it has been reported that GABA is highly involved in plant-pathogen interactions under *Ralstonia solanacearum* attack (Wang et al., 2019). Proteomic and transcriptomic profiles revealed that *SlGAD2* was downregulated, whereas *SlGABA-Ts* and *SlSSADH* were upregulated during infection. The silencing of *SlSSADH* by

VIGS did not result in significant changes under *R. solanacearum* infection, while hypersusceptibility was observed for *SlGAD2*-suppressed lines, suggesting that *SlGAD2* participates in the plant defense response. However, further studies are required to understand the molecular mechanisms underlying GABA metabolism in response to pathogen attack. Thus far, it is clear that GABA levels rapidly increase under stress conditions (Shelp et al., 1999; Ramesh et al., 2017).

Recently, GABA has gained attention as a priming agent (Jalil and Ansari, 2020). Plant priming or conditioning is a promising strategy in which the plant's physiological state is intentionally altered by natural products or synthetic chemicals to promote a more effective defense response in the case of subsequent harsher stresses (Kerchev et al., 2020). When the plant reaches the "primed" state, broad-spectrum defense is partially induced by activating defense genes, changing the proteome profile and accumulating defense compounds, among other processes, minimizing the corresponding negative effects on crop productivity (Vijayakumari et al., 2016). GABA and its synthetic isomer β-aminobutyric acid (BABA) have been reported as effective priming agents (Kerchev et al., 2020). Their application prior to pathogen infection or abiotic stress, by foliar spraying or seed soaking, triggers a similar response as endogenous GABA, modulating the latter and significantly improving the plant immune system, defense response and vigor (Malekzadeh et al., 2014; Li et al., 2017). Yang et al. (2017) reported remarkable resistance to alternaria rot (*Alternaria alternata*) after applying 100 μg ml^{-1} of exogenous GABA to tomato fruits. Although GABA did not show direct antifungal activity, it induced host-mediated resistance at the right time by activating antioxidant enzymes such as peroxidase, superoxide dismutase and catalase and reducing cell death caused by reactive oxygen species. During GABA treatment, *SlGABA-T* and *SlSSADH* were found to be upregulated. Applications of exogenous GABA at 500 and 750 μmol L^{-1} to tomato seedlings under cold stress significantly reduced electrolyte leakage, an indirect cause of chilling injury (Malekzadeh et al., 2014). GABA reduced germination under chilling stress by increasing the activity of antioxidant enzymes and the concentration of osmolytes such as proline and soluble sugars compared to those of untreated seedlings; additionally, the malondialdehyde content, an indicator of plant oxidative stress, was reduced, which results in the maintenance of membrane integrity. Similarly, 0.5 mM exogenous GABA added to a solution of 200 mM NaCl improved seedling tolerance to salt stress, enhancing the contents of antioxidant compounds such as phenolics and endogenous GABA (Çekiç, 2018). In addition to those on tomato, a plethora of studies have reported the successful usage of GABA as a priming agent in other crops, demonstrating its suitability for enhancing the innate plant immune system after stress exposure without deploying excessive energy expenses (Priya et al., 2019; Sheteiwy et al., 2019; Tarkowski et al., 2019). However, even though the success of GABA as a priming agent is compelling, the exact mechanisms of action are still puzzling.

PROS AND CONS OF INCREASING GABA CONTENTS

Undoubtedly, the most important advantage to increasing the GABA content in crops and food matrices is the great potentially beneficial effect on human health, especially the antihypertensive effects (Inoue et al., 2003). Increasing the daily dietary intake of GABA might, in the long run, prevent and alleviate high blood pressure effects. In this regard, tomato is of special interest since it is the most produced and consumed vegetable worldwide and is consumed daily produce for a large part of the human population. Tomato accumulates one of the highest GABA contents among fruit and vegetables, and unlike processed food products, its taste and chemical compounds are not manipulated by additional ingredients such as sugar, salt or fat, whose excess promotes side effects. Thus, a tomato with an enhanced GABA content would benefit many people through daily dietary consumption.

However, this is not an easy task since endogenous GABA intensively accumulates from flowering to the mature green stage, being the predominant free amino acid, but rapidly declines during fruit ripening (Sorrequieta et al., 2010; Sánchez Pérez et al., 2011). Most importantly, high accumulation of GABA could provoke a severe imbalance of amino acids in cells that leads to aberrant phenotypes. Koike et al. (2013) successfully increased GABA levels by suppressing *SlGABA-T1 via* RNA interference. However, the transgenic plants showed dwarf phenotypes, with heights less than half of that of the WT, and infertility coupled with severe flower abscission. Similarly, the *Arabidopsis* GABA-T-deficient mutant *pop2* showed defectiveness in pollen tube growth and cell elongation in hypocotyls and primary roots (Palanivelu et al., 2003; Renault et al., 2011). Recently, Li et al. (2018) succeeded in increasing GABA levels up to 19-fold by a multiplex CRISPR/Cas9 system targeting the three *SlGABA-Ts* and *SlSSADH*. However, the edited plants barely set fruit, some of which were teratogenic, and showed severe dwarfism, pale green and curled compound leaves and necrosis on leaves and buds. Interestingly, Bao et al. (2015) suppressed the main genes involved in GABA metabolism by VIGS and observed a 40% reduction in GABA contents for *SlGADs*-suppressed lines and an increase of 1.5- and 2.0-fold for *SlGABA-Ts* and *SlSSADH* gene expression levels, respectively. However, only *SlSSADH*-edited plants showed defective phenotypes with curled leaves and severe dwarfism, probably due to GHB accumulation, as in the *Arabidopsis ssadh*-deficient mutant (Bouché et al., 2003).

On the other hand, attempts to increase GABA contents by manipulating *SlGADs* have resulted in less disruptive phenotypes. Takayama et al. (2015) overexpressed *SlGAD3* and observed an increase in its mRNA levels of more than 20-fold in mature green and 200-fold in red fruits that translated to an increase in the GABA content. However, those plants did not show abnormal fruits or vegetative organs. The same authors succeeded in further increasing GABA levels in red-ripe fruits compared to their previous *SlGAD3*-overexpression line by overexpressing the coding sequence of *SlGAD3*, lacking 87

nucleotides from the end in the C-terminal domain with a fruit-specific promoter (Takayama et al., 2017). Similar to other species, the removal of the GAD C-terminal domain, which is autoinhibitory, led to a significant increase in the GABA content (Baum et al., 1996; Akama and Takaiwa, 2007). Despite no morphological abnormalities observed in the new transgenic lines, defects were observed during fruit ripening. The fruits never turned red and remained orange even 30 days after the breaker stage, along with a reduction in lycopene contents and lower mRNA levels of carotenoid genes. The authors hypothesized that the removal of the C-terminal domain provoked a metabolic disturbance due to the overexpression of *SlGAD3*. At 10 days after the breaker stage, GABA accounted for up to 81% of the total free amino acids in overexpression lines compared to 6.2% in the WT, whereas low levels of aspartate and glutamate were recorded. Aberrant phenotypes were also observed in similar studies where the GAD C-terminal autoinhibitory domain was removed and significantly higher levels of GABA were accompanied by low levels of glutamate. Transgenic tobacco plants expressing a truncated GAD from petunia exhibited plant growth abnormalities coupled with reduced cell elongation in the stem (Baum et al., 1996). Similarly, dwarfism, sterility and etiolated leaves were observed in transgenic rice plants expressing a truncated *OsGAD2* (Akama and Takaiwa, 2007). These authors suggested that abnormalities could be the result of an amino acid imbalance in cells, especially low glutamate levels, due to its direct or indirect involvement in many fundamental pathways, such as gibberellin biosynthesis or posttranslational modification of cell wall proteins. Similarly, transgenic tomato fruits obtained by Bemer et al. (2012), where FUL1 and FUL2 transcription factors were simultaneously suppressed, showed orange-ripe phenotypes, two-fold higher GABA and eight-fold lower glutamate levels than the WT. The enhanced GABA fruits obtained by Takayama et al. (2017) also showed a delay in ethylene production, which peaked 10 days after the breaker stage compared with three days in the WT, and possibly a reduced ethylene sensitivity when the fruits were exposed to equivalent high levels of ethylene as the WT fruits. The authors also reported altered expression levels of transcription factors, such as TAGL1, FUL1, FUL2, RIN and ERF6, which play a major role in regulating ethylene biosynthesis, and lycopene accumulation genes, such as *ACS2*, *PSY1* and *CRTISO* (Bemer et al., 2012; Shima et al., 2013; Fujisawa et al., 2014).

Finally, overaccumulation of GABA in tomato fruit could lead to a reduction in glutamate, which is linked to the umami flavor (Yamaguchi, 1998), since glutamate is a GABA precursor. Indeed, significantly lower levels of glutamate in the high GABA tomato lines were observed, such as in *SlGABA-T1*-suppressed plants (Koike et al., 2013) and *SlGAD3ΔC*-overexpression plants (Takayama et al., 2017). Compared to the WT, the former showed an up to 11.7 times higher GABA content (13.59 vs 1.16 μmol/g FW of the WT) and 31.2% less glutamate (1.26 vs 1.83 μmol/g FW of the WT), while the latter showed an up to 18 times higher GABA content (28.56 vs 1.58 μmol/g FW of the WT) and 92.5% less glutamate (0.15 vs 2.00 μmol/g FW of the WT) in the red stage fruit. However, we have confirmed that a mild increase in GABA by 2–4 times does not dramatically affect the glutamate content, even though the effects vary among varieties (Lee et al., 2018). In addition, other molecules, such as some ribonucleotides (e.g., inosine and guanosine monophosphates), could synergistically potentiate, by a factor of 100, the umami taste in the presence of glutamate (Ninomiya, 1998; Yamaguchi, 1998; Chew et al., 2017). However, tomato flavor is the sum of complex interactions among sugars, acids and volatiles perceived between taste and olfaction, and preferences change among consumers, countries and cultures (Tieman et al., 2017).

STRATEGIES DEPLOYED FOR IMPROVING GABA LEVELS

In recent years, many strategies have been implemented to identify or breed materials to enhance GABA levels in crop species. In tomato, one of the first approaches was classical breeding through the identification of promising materials with higher GABA contents by screening the natural diversity of tomatoes for the subsequent development of new improved lines by crossing those materials with elite cultivars. Saito et al. (2008) screened 61 tomato varieties, including 38 processing and 11 fresh market cultivars, six wild species and six wild derivatives, for two years to identify naturally occurring GABA-enriched materials. However, even though an interesting variation in GABA content was found among the accessions, the results were poorly reproducible between the tested years, suggesting that GABA levels were highly influenced by the cultivation conditions. In fact, the average GABA content in red mature fruit was 50.3 mg/100 g FW in 2005 when the cultivars were screened in an open field and 66.8 mg/100 g FW in 2006 when tested in a plastic house. Nevertheless, the cultivar 'DG03-9' exhibited high GABA levels in both years and under saline stress (104.4 mg/100 g FW), showing its suitability to be used to breed new enhanced GABA-rich cultivars. Notably, the six wild accessions from three tomato-related species (*S. pimpinellifolium* [25.2 mg/100 g FW], *S. cheesmanii* [8.8–53.0 mg/100 g FW] and *S. lycopersicum* var. *cerasiforme* [11.0 mg/100 g FW]) exhibited a low average GABA content. Similar results were observed by Anan et al. (1996) screening accessions from *S. peruvianum* (9.8 - 10.1 mg/100 g FW), *S. pimpinellifolium* (34.2–49.7 mg/100 g FW) and *S. hirsutum* (25.5 mg/100 g FW), whereas accessions from *S. esculentum* showed appreciable GABA levels (52.4–107.7 mg/100 g FW). On the other hand, three of the six wild derivates screened by Saito et al. (2008) that reported high average GABA contents (106.4–114.7 mg/100 g FW) were bred from *S. chmielewskii*. However, so far, the highest GABA content reported from a tomato wild relative was found in *S. pennellii* at approximately 200 mg/100 g FW (Schauer et al., 2005; Takayama et al., 2017). Despite the few studies that screened for natural variations in GABA contents in tomato germplasms, which are often difficult to compare due to the tissue or stage analyzed and/or the protocol used for the GABA measurements, a wide diversity can be found across cultivated, heirloom and wild materials that

can be used for GABA breeding. Classical breeding has achieved quantum leaps in crop improvement but entails some drawbacks. The development of a new variety can take up to 10 years with a classical breeding program, while that can be shortened when coupled with molecular marker selection. This makes the process time- and resource-consuming. In addition, the result is not always guaranteed when the aim is delimited to introgression of a specific alleles or traits while maintaining the genetic background and fitness of the elite variety. Furthermore, when the donor parent is a wild relative, additional challenges must be overcome, such as linkage drag of undesirable traits, crossing barriers or offspring infertility (Prohens et al., 2017).

For these reasons, alternative approaches were explored to overcome these difficulties. One of them was by screening a TILLING population generated in the background of Micro-Tom (Saito et al., 2011). However, even though approximately 4,500 EMS lines were evaluated to isolate *SlGAD3* mutant alleles, no significant mutations were found that were translated in lines with enhanced GABA levels (Ezura et al., unpublished results).

Fortunately, a wide spectrum of new technologies has emerged to sort out some of the disadvantages of conventional crossbreeding and induced mutagenesis by radiation or chemical agents. These are labeled NPBTs, which include the development of genetically modified organisms (GMOs) and genome editing. Even though there is no consensus or ultimate definition of what NPBTs are, it is an umbrella term to define several techniques that make use of a genetic modification step where the final result does not include the presence of a foreign gene (i.e., a gene that is not present in the species or cannot be obtained by traditional cross-breeding from related species) (Schaart et al., 2016). Nevertheless, every country has a different regulatory definition of NPBTs, and the list of identified NPBT technologies greatly varies from one legislation to another, being constantly under revision and discussion by policymakers. For the sake of brevity and because of the complexity and dynamic evolution of this topic, we recommend the following reviews to provide an overview of the wide range of NPBTs available and their regulation in several countries (Schaart et al., 2016; Purnhagen et al., 2018; Kleter et al., 2019; Hartung, 2020; Schiemann et al., 2020; Zhang et al., 2020).

Although GMO technologies have been used since the 1980s, first-generation GMOs cannot exactly reflect the transgene position in recipient plants. Thus, multiple transgenic events must be performed and screened to select transgenic plants with the pursued trait without undesired off-target effects (Qaim, 2020). Second- and third-generation sequencing platforms have allowed unprecedented knowledge of plant genomes and genomic regions controlling QTLs and major genes, fostering precision and speed in genome editing and breeding (Hickey et al., 2019). Since then, a new generation of mutation breeding techniques has started to target specific genomic regions, increasing specificity and reducing potential off-target effects along with saving time and resources. In fact, the greater specificity and precision of NPBTs is their main advantage over classical breeding and random mutagenesis that do not allow for specific targeting or cannot control potential additional genetic changes that might be introduced due to the linkage associated with the latter. NPBTs allow for targeting the individual genes controlling traits, allowing preservation of the genetic background of an elite variety and avoiding the undesirable effects of linkage drag.

In tomato, NPBTs have been used for understanding GABA metabolism and gene actions and investigating how to enhance GABA levels in red ripe fruits. The latter was achieved by applying two different strategies: increasing *SlGADs* activities and consequently GABA biosynthesis; and decreasing or silencing *SlGABA-Ts* activity and thus reducing GABA degradation. Although three copies of *SlGADs* and three of *SlGABA-Ts* were found in tomato, it is currently clear that *SlGAD3* and *SlGABA-T1* are mainly involved in GABA accumulation during fruit ripening. The first attempt to increase GABA content using genetic engineering was made by Koike et al. (2013), who targeted *SlGABA-T1* by an RNA interference approach under the control of the constitutive CaMV 35S in Micro-Tom. The *35S::SlGABA-T1*^{RNAi}-suppressed lines exhibited 1.3-fold (118.6 mg/100 g FW) higher GABA content than the WT at the mature green stage, 2.0-fold (126.8 mg/100 g FW) higher at the yellow stage and 6.8-fold (106.2 mg/100 g FW) higher at the mature red stage. *SlGABA-T1* suppression reduced the catabolism of GABA to SSA in the ripening stage, limiting its degradation from the peak reached at the breaker stage. While in the WT, the GABA content dropped 83.1% from the mature green to red stage, the decrease in *35S::SlGABA-T1*^{RNAi} lines was only 3% on average. However, as reported above, those plants exhibited severe abnormalities. Nevertheless, when they replaced the 35S promoter with E8, a strong inducible promoter specific to tomato fruit ripening, to avoid the systemic suppression of *SlGABA-Ts* by the CaMV 35S promoter, the *E8::SlGABA-T1*^{RNAi}-suppressed lines showed a similar WT phenotype with no evidence of dwarfism or infertility. Although the GABA levels of *E8::SlGABA-T1*^{RNAi} lines were similar to those of the WT at the mature green stage (71.1–87.6 mg/100 g FW), their content was 2.5-fold higher than that of WT (45.3–59.8 mg/100 g FW) at the red stage, dropping 29.0% versus 72.4% in the WT, although their GABA content was almost half of that of *35S::SlGABA-T1*^{RNAi}. These results suggested that the systemic knockout of *SlGABA-Ts*, especially *SlGABA-T1*, led to abnormal phenotypes, whereas a fruit-specific knockout, knockdown or less severe gene expression reduction produced normal phenotypes with enhanced GABA levels.

The opposite approach was attempted by Takayama et al. (2015), who overexpressed *SlGAD3* by generating transgenic plants under the control of the CaMV 35S promoter in Micro-Tom. The *OX-SlGAD3*-overexpression lines exhibited 2.7- to 3.3-fold higher GABA contents than the WT at the mature green stage and 4.0- to 5.2-fold higher GABA contents at the red stage. Despite the much higher GABA content, the *OX-SlGAD3* lines did not show significant visible phenotypic changes. The same authors, to further increase GABA levels in red-ripe fruits, overexpressed the full-length coding sequence of *SlGAD3* (*SlGAD3*^{OX}) and were missing the same 87 nucleotides from the end in the C-terminal domain (*SlGAD3ΔC*^{OX}), substituting CaMV35S for the fruit-specific E8 promoter and the NOS terminator for *Arabidopsis* heat shock protein 18.2 (HSP) (Takayama et al., 2017). At 10 days after the breaker stage,

SlGAD3ΔC^{OX} lines exhibited 11- to 12-fold higher GABA levels than the WT (237.1–268 mg/100 g FW) and almost double those of *SlGAD3*^{OX} lines (123.7–154.6 mg/100 g FW). Although the latter displayed substantially higher mRNA levels than the previously generated *OX-SlGAD3* lines (Takayama et al., 2015), probably due to the *Arabidopsis* HSP terminator, which is more effective than the NOS terminator in enhancing mRNA expression (Kurokawa et al., 2013), their GABA levels were similar. This result suggested that even though increased mRNA expression translates into a higher GABA content, it does not linearly increase with the mRNA level, and other factors are involved in regulating GABA levels, such as the C-terminal domain. In fact, the *SlGAD3*^{OX} and *SlGAD3ΔC*^{OX} lines exhibited similar mRNA levels, but the GABA content was almost doubled in the latter, implying that the C-terminus also acts as an autoinhibitory domain in tomato. However, even though the lines of both constructs did not display any morphological abnormalities, probably by virtue of replacing CaMV35S for the fruit-specific E8 promoter, the *SlGAD3ΔC*^{OX} lines exhibited a delay in ethylene production and ethylene sensitivity along with an orange-ripe phenotype that never turned completely red.

In light of these results, Nonaka et al. (2017) further investigated the effects of the C-terminal region in *SlGAD3* to breed an enhanced GABA line without defects, targeting the autoinhibitory domain by the CRISPR/Cas9 system. After comparing the amino acid sequence of *SlGAD* orthologs from five species for the conserved tryptophan, lysine and glutamate residues involved in CaM binding, the 37th amino acid at the C-terminal domain was selected as the target to induce a premature stop codon in *SlGAD3*. This target was different from the 29th amino acid (87 nucleotides) selected by Takayama et al. (2017). The T_1 regenerated plants of *TG3C37* that had a stop codon at 34, 36 and 40 amino acids at the C-terminal, thus upstream of the autoinhibitory domain and close to the target at the 37th amino acid, and exhibited a higher GABA content at the red mature stage of up to 15 times more (125.73 mg/100 g FW) than that of the WT. Although some lines were slightly smaller than the WT, flowering and fruit yield were not affected, and no significant phenotypic defects were observed. Considering the absence of visible morphological and physiological abnormalities and the range of GABA levels obtained, these results were similar to those obtained by overexpressing the full coding length of *SlGAD3* (*SlGAD3*^{OX}). The authors stated that even though targeted mutagenesis by CRISPR/Cas9 is as effective a strategy as the transgenic approach in increasing GABA contents, CRISPR/Cas9 could be more publicly accepted than conventional transgenesis in the near future.

The latest attempt to develop improved GABA tomato lines was made by Li et al. (2018) using a multiplex CRISPR/Cas9 vector with six gRNA cassettes to target the three *SlGABA-Ts* along with *SlSSADH* and *CAT9* that were transformed in the Ailsa Craig cultivar. The edited plants were divided into six groups based on the mutation patterns from single to quadruple mutated targets. However, only the single *SlGABA-T1* and the double *SlGABA-T1* and *SlGABA-T3* mutants set fruits due to the severe infertility of the rest of the combinations. The *SlGABA-T1* edited lines exhibited 1.43-fold higher GABA levels (102.80 mg/100 g FW) than the WT at the mature green stage and 2.95-fold higher (73.83 mg/100 g FW) levels at the red stage. Even though those fruits did not show differences in size, shape and color with the WT, the plants experienced abnormalities in leaf development and plant growth. Once again, these results demonstrated that *SlGABA-T1* is deeply involved in GABA metabolism, but its severe mRNA expression reduction by suppression or mutation leads to deficient plants not suitable for breeding.

ADVANTAGES OF THE USE OF NPBTs IN CROP BREEDING AND THEIR SOCIETAL ACCEPTANCE

Genome editing is a technology that enables precise mutagenesis only in targeted genes. Therefore, using this technology, we can significantly reduce the labor and time required to introduce desirable mutations, which is a challenge for conventional mutagenesis techniques using chemical or irradiation treatments. This property would be a major advantage in breeding crops that have strong consumer preferences, require a large number of varieties in a single crop and have rapidly changing needs because to breed more varieties, more labor and time would be required. Tomatoes are one such example. They are consumed all over the world, and preferred shapes, colors, flavors and uses vary by region. Since genome editing technology can directly reproduce useful genetic mutations in breeding parents, we would be able to improve the traits of familiar varieties more rapidly and efficiently. In the case of improving the GABA content in tomato, genome editing would be effective not only in experimental cultivars but also in commercial cultivars. Indeed, we succeeded in reproducing the mutation that confers an increased GABA content in fruit in several commercial cultivars by applying the CRISPR/Cas9 system as used in experimental cultivars (Nonaka et al., 2017). It took only half a year to obtain null-segregant (T-DNA free) plants with homozygote mutations. Even though an additional selfing or backcross step would be needed to select elite lines as in conventional breeding, it can reduce the time to develop breeding material considerably when compared to conventional cross breeding, which takes 3–5 years.

However, frequently, NPBTs are confused or associated with the first generation of modified crops, where the use of foreign DNA to develop new and improved crops allows society and policymakers to perceive health and environmental risks associated with their cultivation and consumption. Even though three decades of GMO cultivation and dozens of studies reported no more human health risks than those posed by conventional agriculture (Nicolia et al., 2014; Zaidi et al., 2019), the general perception of GMO technologies remains negative, with large differences among countries. The emergence of genome editing technologies such as CRISPR/Cas has generated great expectations among scientists, breeding companies and the food industry regarding the possibility of changing consumer perceptions of food biotechnology. However, even though the societal acceptance of NPBTs is higher than that

of the first GMO crops, currently, "food technology neophobia" still affects many consumers and not only high-income countries (Farid et al., 2020; Siegrist and Hartmann, 2020). Often, this confusion is promoted by the same lawmakers that legislatively, as in the case of the European Court of Justice, equate genome-edited crops with the first generation of GMOs, negatively influencing the public perceptions of NPBT products (Callaway, 2018; Zaidi et al., 2019). Nevertheless, there are grounds for cautious optimism due to the policy relaxation of some countries that are considering opening their markets to NPBT products such as China and Russia. Currently, in seven countries (Argentina, Brazil, Chile, Colombia, Israel, Paraguay and the US, plus India, Uruguay, Honduras, Guatemala and El Salvador, which are under consideration), genome-edited crops that do not incorporate foreign DNA are regulated as conventional plants with no additional restrictions, while Japan, Canada and Australia have stricter regulation of genome-edited products than conventional ones but less stringent regulation than that of GMOs that incorporate DNA from other species (https://crispr-gene-editing-regs-tracker.geneticliteracyproject.org/). In contrast, other countries such as New Zealand, Mexico or the EU strictly regulate NPBT products, basically banning their development and introduction.

ALTERNATIVE PROSPECTS FOR GABA IMPROVEMENT USING NBPTs

New NPBT approaches and techniques have been launched at a frantic pace in the last two decades, especially for genome editing. However, the first-generation of gene-editing methods, such as zinc-finger nuclease or TALEN, have been totally eclipsed by the CRISPR/Cas9 system. Since the first evidence of its powerful applications in 2012 (Jinek et al., 2012), the CRISPR/Cas9 system and its subsequent variants have become the most widely used NPBTs due to their simplicity, reliability and versatility. Many of these variants are focused on improving the genome editing process from the first monoguide CRISPR/Cas9 versions towards multiplexed and multilocus strategies (Vad-Nielsen et al., 2016; Zetsche et al., 2017), enhanced Cas enzymes and new ribonucleoprotein complexes (Bernabé-Orts et al., 2019; McCarty et al., 2020) and cleavage patterns (Komor et al., 2016; Shimatani et al., 2017), among others.

Apart from the performance of the genome editing system *per se*, interesting CRISPR/Cas9 applications and approaches have been proposed and validated in plants. One of the most promising is *cis*-regulatory region engineering (*cis*-engineering), which targets the noncoding sequences controlling gene transcription. Many examples have reported that mutations in *cis*-regulatory elements (CREs) produce significant phenotypic and morphological changes that have been selected during domestication (Meyer and Purugganan, 2013; Swinnen et al., 2016). In tomato, changes in CREs and promoter regions were translated in elongated (*SlSUN*) and larger fruits (*FW2.2*, *FW3.2*, *SlWUS*) or those with improved β-carotene contents (*Slcys-B*) (van der Knaap et al., 2014; Li et al., 2020) as just a few relevant examples. However, despite the great potential of this approach, currently, the vast majority of CRISPR/Cas9 studies focus on targeting coding sequences for null allele editing or controlling transcription by activation (CRISPRa) or inhibition (CRISPRi), and only 15 studies so far have reported successful applications of *cis*-engineering (Li et al., 2020). One of them was successfully conducted in tomato by *cis*-engineering the promoters of genes controlling fruit size, inflorescence branching and plant architecture, achieving multiple *cis*-regulatory alleles with a continuum of quantitative variation (Rodríguez-Leal et al., 2017). The scarcity of *cis*-engineering studies might be due to the lack of information on CRE functions and the regulatory complexity and redundancy of transcriptional control. Additionally, in contrast to targeting the coding regions that could produce substantial and pleiotropic effects, the effects of *cis*-regulatory allele targeting are often more subtle and discrete (Wittkopp and Kalay, 2012).

Perfect examples of detrimental pleiotropic effects in GABA studies were reported by Koike et al. (2013) and Li et al. (2018) who suppressed and edited, respectively, the coding sequences of *SlGABA-Ts*. In both studies, the regenerated plants showed multiple abnormalities, making them useless for breeding despite the higher GABA levels achieved. To overcome these drawbacks, the authors of this review are currently *cis*-engineering the promoter region of *SlGABA-T1* (**Figure 2**). The aim of this study was to modulate *SlGABA-T1* gene expression to achieve the best balance between reduced enzyme activity and a higher GABA content without detrimental pleiotropic effects that cause plant abnormalities. This can be theoretically achieved by producing many *cis*-engineering promoter alleles that exhibit a continuum of gene expression and CRE combinations. However, like most plant species, almost no knowledge has been generated regarding the structure of promoters and other regulatory sequences in tomato, and no prior information is currently available for CREs and their interactions in the promoter of *SlGABA-T1*. Even though prior knowledge would facilitate and speed the process, *cis*-engineering could be implemented if a multiplexed CRISPR/Cas9 system was developed (Li et al., 2020). For this, we assembled a vector containing four gRNAs that was designed within a region 2 kbp upstream of the *SlGABA-T1* start codon and transformed in Micro-Tom (**Figure 2A**). Furthermore, the same vector was also used to transform the high GABA line SlGAD3ΔC37 developed by Nonaka et al. (2017) to exploit the potential synergistic effects between the *cis*-engineering promoters in *SlGABA-T1* alleles and *SlGAD3* without the autoinhibitory domain (**Figure 2B**). A complementary approach could also involve *cis*-engineering the promoter of SlGAD3ΔC37, combining the effects of removing the autoinhibitory domain and modulating the gene expression level by *cis*-engineering (**Figure 2C**). Apart from achieving improved GABA lines, this study may provide useful information on GABA gene promoters that will open the path to future strategies that are currently unavailable.

For example, if CREs and their interactions with regulatory elements are sufficiently characterized, the multiplex unspecific gRNA approach could be replaced by site-specific promoter editing. A step further in this direction would be the upgraded precision

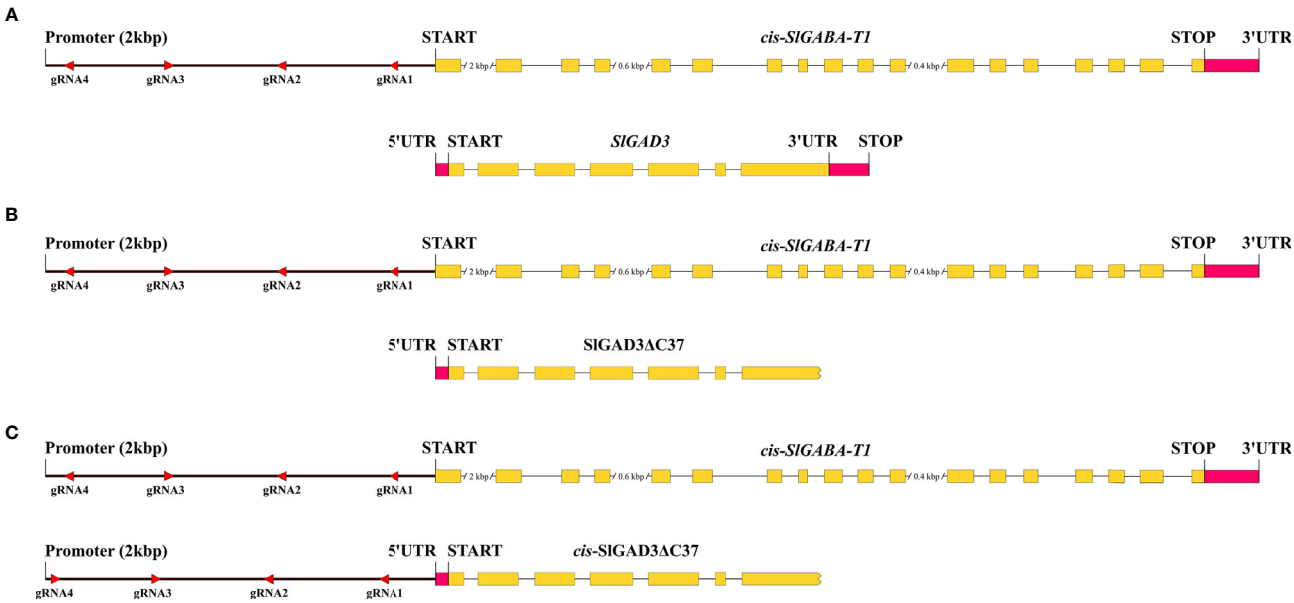

FIGURE 2 | *Cis*-engineering approaches of *SlGABA-T1* and *SlGAD3* promoters to enhance the GABA content in tomato. **(A)** *Cis*-engineering of the promoter region of *SlGABA-T1* while *SlGAD3* remained the wild type to observe the effects of *SlGABA-T1* CRE editing. **(B)** *Cis*-engineering the promoter regions of *SlGABA-T1* of the SlGAD3ΔC37 GABA improved line to exploit the potential synergistic effects of the *cis*-engineering and coding sequence targeting approaches. **(C)** *Cis*-engineering of the promoter regions of *SlGABA-T1* and SlGAD3ΔC37 to maximize GABA accumulation.

from genome editing to base editing or the groundbreaking prime editing strategy that has recently been demonstrated to be feasible in higher plants (Rees and Liu, 2018; Anzalone et al., 2019; Lin et al., 2020).

However, other NPBT strategies could be more challenging to implement for GABA breeding until their technical limitations and low efficiency are overcome. Among those, a fascinating approach is promoter insertion or promoter swapping that allows introduction or replacement of CREs or entire promoters. However, these approaches rely on the homology-directed repair (HDR) pathway, which has exhibited low efficiency in plants (Chen et al., 2019). Nevertheless, in tomato Čermák et al. (2015) succeeded in inserting a 35S promoter upstream of the gene controlling anthocyanin biosynthesis (ANT1), resulting in enhanced anthocyanin accumulation.

FINAL REMARKS

The ubiquity of GABA across the kingdoms and its involvement in many fundamental pathways has captivated the interest of scientists for several decades. More recently, after uncovering its potential benefit for human health, the food industry and plant breeders are devoting efforts and resources to improving the GABA levels in food matrices and crops. In plant breeding, NPBTs have demonstrated a higher efficiency and precision than classical crossbreeding for achieving this goal, and studies using induced mutagenesis unlabeled the genetic basis of GABA regulatory pathways, some of which also lead to an increased GABA content in some cases. Nevertheless, large room for improvement exists that can be harnessed *via* the new generation of NPBTs that are emerging at an incredible speed. The progress achieved in tomato could potentially transfer to other crops, taking advantage of the knowledge generated to shorten GABA breeding programs.

AUTHOR CONTRIBUTIONS

Idea conceptualization: HE. Writing—original draft preparation: PG. Writing—review and editing: PG, MT and HE.

FUNDING

PG is grateful to the Japanese Society for the Promotion of Science for the JSPS postdoctoral grant FY2019-P19105.

REFERENCES

Abdou, A. M., Higashiguchi, S., Horie, K., Kim, M., Hatta, H., and Yokogoshi, H. (2006). Relaxation and immunity enhancement effects of γ-Aminobutyric acid (GABA) administration in humans. *BioFactors* 26, 201–208. doi: 10.1002/biof.5520260305

Akama, K., and Takaiwa, F. (2007). C-terminal extension of rice glutamate decarboxylase (*OsGAD2*) functions as an autoinhibitory domain and overexpression of a truncated mutant results in the accumulation of extremely high levels of GABA in plant cells. *J. Exp. Bot.* 58, 2699–2707. doi: 10.1093/jxb/erm120

Akihiro, T., Koike, S., Tani, R., Tominaga, T., Watanabe, S., Iijima, Y., et al. (2008). Biochemical mechanism on GABA accumulation during fruit development in tomato. *Plant Cell Physiol.* 49, 1378–1389. doi: 10.1093/pcp/pcn113

Al-Quraan, N. A., Sartawe, F.A.b., and Qaryouti, M. M. (2013). Characterization of γ-aminobutyric acid metabolism and oxidative damage in wheat (*Triticum aestivum* L.) seedlings under salt and osmotic stress. *J. Plant Physiol.* 170, 1003–1009. doi: 10.1016/j.jplph.2013.02.010

Anan, T., Ito, H., and Monma, S. (1996). Chemical contents in fruits of transgenic tomato carrying the TMV coat protein gene, nontransgenic tomato, and other *Lycopersicon* species. *J. Japanese Soc Hortic. Sci.* 65, 635–644. doi: 10.2503/jjshs.65.635

Anzalone, A. V., Randolph, P. B., Davis, J. R., Sousa, A. A., Koblan, L. W., Levy, J. M., et al. (2019). Search-and-replace genome editing without double-strand breaks or donor DNA. *Nature* 576, 149–157. doi: 10.1038/s41586-019-1711-4

Bao, H., Chen, X., Lv, S., Jiang, P., Feng, J., Fan, P., et al. (2015). Virus-induced gene silencing reveals control of reactive oxygen species accumulation and salt tolerance in tomato by γ-aminobutyric acid metabolic pathway. *Plant Cell Environ.* 38, 600–613. doi: 10.1111/pce.12419

Bartyzel, I., Pelczar, K., and Paszkowski, A. (2003). Functioning of the γ-aminobutyrate pathway in wheat seedlings affected by osmotic stress. *Biol. Plant* 47, 221–225. doi: 10.1023/B:BIOP.0000022255.01125.99

Baum, G., Lev-Yadun, S., Fridmann, Y., Arazi, T., Katsnelson, H., Zik, M., et al. (1996). Calmodulin binding to glutamate decarboxylase is required for regulation of glutamate and GABA metabolism and normal development in plants. *EMBO J.* 15, 2988–2996. doi: 10.1002/j.1460-2075.1996.tb00662.x

Bemer, M., Karlova, R., Ballester, A. R., Tikunov, Y. M., Bovy, A. G., Wolters-Arts, M., et al. (2012). The tomato FRUITFULL homologs TDR4/FUL1 and MBP7/FUL2 regulate ethylene-independent aspects of fruit ripening. *Plant Cell* 24, 4437–4451. doi: 10.1105/tpc.112.103283

Bernabé-Orts, J. M., Casas-Rodrigo, I., Minguet, E. G., Landolfi, V., Garcia-Carpintero, V., Gianoglio, S., et al. (2019). Assessment of Cas12a-mediated gene editing efficiency in plants. *Plant Biotechnol. J.* 17, 1971–1984. doi: 10.1111/pbi.13113

Biais, B., Beauvoit, B., William Allwood, J., Deborde, C., Maucourt, M., Goodacre, R., et al. (2010). Metabolic acclimation to hypoxia revealed by metabolite gradients in melon fruit. *J. Plant Physiol.* 167, 242–245. doi: 10.1016/j.jplph.2009.08.010

Bouché, N., and Fromm, H. (2004). GABA in plants: Just a metabolite? *Trends Plant Sci.* 9, 110–115. doi: 10.1016/j.tplants.2004.01.006

Bouché, N., Fait, A., Bouchez, D., Møller, S. G., and Fromm, H. (2003). Mitochondrial succinic-semialdehyde dehydrogenase of the γ-aminobutyrate shunt is required to restrict levels of reactive oxygen intermediates in plants. *Proc. Natl. Acad. Sci. U. S. A.* 100, 6843–6848. doi: 10.1073/pnas.1037532100

Callaway, E. (2018). CRISPR plants now subject to tough GM laws in European Union. *Nature* 560, 16. doi: 10.1038/d41586-018-05814-6

Cao, S., Cai, Y., Yang, Z., and Zheng, Y. (2012). MeJA induces chilling tolerance in loquat fruit by regulating proline and γ-aminobutyric acid contents. *Food Chem.* 133, 1466–1470. doi: 10.1016/j.foodchem.2012.02.035

Carillo, P. (2018). GABA shunt in durum wheat. *Front. Plant Sci.* 9, 100. doi: 10.3389/fpls.2018.00100

Çekiç, F. (2018). Exogenous GABA stimulates endogenous GABA and phenolic acid contents in tomato plants under salt stress. *Celal Bayar Üniversitesi Fen Bilim. Derg.* 14, 61–64. doi: 10.18466/cbayarfbe.348935

Čermák, T., Baltes, N. J., Čegan, R., Zhang, Y., and Voytas, D. F. (2015). High-frequency, precise modification of the tomato genome. *Genome Biol.* 16, 232. doi: 10.1186/s13059-015-0796-9

Chalorcharoenying, W., Lomthaisong, K., Suriharn, B., and Lertrat, K. (2017). Germination process increases phytochemicals in corn. *Int. Food Res. J.* 24, 552–558.

Chen, K., Wang, Y., Zhang, R., Zhang, H., and Gao, C. (2019). CRISPR/Cas genome editing and precision plant breeding in agriculture. *Annu. Rev. Plant Biol.* 70, 667–697. doi: 10.1146/annurev-arplant-050718-100049

Chew, B. L., Fisk, I. D., Fray, R., Tucker, G. A., Bodi, Z., Ferguson, A., et al. (2017). The effect of adenosine monophosphate deaminase overexpression on the accumulation of umami-related metabolites in tomatoes. *Plant Cell Rep.* 36, 81–87. doi: 10.1007/s00299-016-2058-z

Clark, S. M., Di Leo, R., Van Cauwenberghe, O. R., Mullen, R. T., and Shelp, B. J. (2009). Subcellular localization and expression of multiple tomato γ-aminobutyrate transaminases that utilize both pyruvate and glyoxylate. *J. Exp. Bot.* 60, 3255–3267. doi: 10.1093/jxb/erp161

Daş, Z. A., Dimlioğlu, G., Bor, M., and Özdemir, F. (2016). Zinc induced activation of GABA-shunt in tobacco (*Nicotiana tabaccum* L.). *Environ. Exp. Bot.* 122, 78–84. doi: 10.1016/j.envexpbot.2015.09.006

Deewatthanawong, R., and Watkins, C. B. (2010). Accumulation of γ-Aminobutyric acid in apple, strawberry and tomato fruit in response to postharvest treatments. in. *Acta Hortic.* 877, 947–952. doi: 10.17660/ActaHortic.2010.877.127

Deewatthanawong, R., Rowell, P., and Watkins, C. B. (2010a). γ-Aminobutyric acid (GABA) metabolism in CO2 treated tomatoes. *Postharvest Biol. Technol.* 57, 97–105. doi: 10.1016/j.postharvbio.2010.03.007

Deewatthanawong, R., Nock, J. F., and Watkins, C. B. (2010b). γ-Aminobutyric acid (GABA) accumulation in four strawberry cultivars in response to elevated CO2 storage. *Postharvest Biol. Technol.* 57, 92–96. doi: 10.1016/j.postharvbio.2010.03.003

Deyman, K. L., Brikis, C. J., Bozzo, G. G., and Shelp, B. J. (2014). Impact of 1-methylcyclopropene and controlled atmosphere storage on polyamine and 4-aminobutyrate levels in "Empire" apple Fruit. *Front. Plant Sci.* 5, 144. doi: 10.3389/fpls.2014.00144

Diana, M., Quílez, J., and Rafecasa, M. (2014). Gamma-aminobutyric acid as a bioactive compound in foods: a review. *J. Funct. Foods* 10, 407–420. Foods, M. R.-J. of F., and 2014, U. doi: 10.1016/j.jff.2014.07.004

Dosi, R., Daniele, A., Guida, V., Ferrara, L., Severino, V., and Di Maro, A. (2013). Nutritional and metabolic profiling of the globe artichoke (*Cynara scolymus* L. cv. '*Capuanella*' heads) in province of Caserta, Italy. *Aust. J. Crop Sci.* 7, 1927–1934.

Espasandin, F. D., Maiale, S. J., Calzadilla, P., Ruiz, O. A., and Sansberro, P. A. (2014). Transcriptional regulation of 9-*cis*-epoxycarotenoid dioxygenase (NCED) gene by putrescine accumulation positively modulates ABA synthesis and drought tolerance in *Lotus tenuis* plants. *Plant Physiol. Biochem.* 76, 29–35. doi: 10.1016/j.plaphy.2013.12.018

Fait, A., Fromm, H., Walter, D., Galili, G., and Fernie, A. R. (2008). Highway or byway: the metabolic role of the GABA shunt in plants. *Trends Plant Sci.* 13, 14–19. doi: 10.1016/j.tplants.2007.10.005

Fan, T. W. M., Higashi, R. M., Lane, A. N., and Jardetzky, O. (1986). Combined use of 1H-NMR and GC-MS for metabolite monitoring and in vivo 1H-NMR assignments. *BBA - Gen. Subj.* 882, 154–167. doi: 10.1016/0304-4165(86)90150-9

Farid, M., Cao, J., Lim, Y., Arato, T., and Kodama, K. (2020). Exploring factors affecting the acceptance of genetically edited food among youth in Japan. *Int. J. Environ. Res. Public Health* 17:2935. doi: 10.3390/ijerph17082935

Fujisawa, M., Shima, Y., Nakagawa, H., Kitagawa, M., Kimbara, J., Nakano, T., et al. (2014). Transcriptional regulation of fruit ripening by tomato FRUITFULL homologs and associated MADS box proteins. *Plant Cell* 26, 89–101. doi: 10.1105/tpc.113.119453

Fukuwatari, Y., Sato, N., Kawamori, R., Watanabe, Y., Yoshida, K., Ying, R., et al. (2001). A study on the antihypertensive action and safety of tablets containing γ-aminobutyric acid (GABA). *East. Med.* 17, 1–17.

Gallego, P. P., Whotton, L., Picton, S., Grierson, D., and Gray, J. E. (1995). A role for glutamate decarboxylase during tomato ripening: the characterisation of a cDNA encoding a putative glutamate decarboxylase with a calmodulin-binding site. *Plant Mol. Biol.* 27, 1143–1151. doi: 10.1007/BF00020887

Gill, S. S., Anjum, N. A., Gill, R., and Tuteja, N. (2016). Abiotic stress signaling in plants-an overview. *Abiotic Stress Response Plants* (Hoboken, New Jersey, USA: Wley), 1–12. doi: 10.1002/9783527694570.ch1

Gut, H., Dominici, P., Pilati, S., Astegno, A., Petoukhov, M. V., Svergun, D.II, et al. (2009). A common structural basis for pH and calmodulin-mediated regulation in plant glutamate decarboxylase. *J. Mol. Biol.* 392, 334–351. doi: 10.1016/j.jmb.2009.06.080

Ham, T. H., Chu, S. H., Han, S. J., and Ryu, S. N. (2012). γ-aminobutyric acid metabolism in plant under environment stressses. *Korean J. Crop Sci.* 57, 144–150. doi: 10.7740/kjcs.2012.57.2.144

Hartung, U. (2020). Inside lobbying on the regulation of new plant breeding techniques in the European Union: Determinants of Venue Choices. *Rev. Policy Res.* 37, 92–114. doi: 10.1111/ropr.12366

Hickey, L. T., Hafeez, N., Robinson, H., Jackson, S. A., Leal-Bertioli, S. C. M., Tester, M., et al. (2019). Breeding crops to feed 10 billion. *Nat. Biotechnol.* 37, 744–754. doi: 10.1038/s41587-019-0152-9

Hildebrandt, T. M., Nunes Nesi, A., Araújo, W. L., and Braun, H. P. (2015). Amino acid catabolism in plants. *Mol. Plant* 8, 1563–1579. doi: 10.1016/j.molp.2015.09.005

Hosmani, P. S., Flores-Gonzalez, M., Geest, H., van de, Maumus, F., Bakker, L. V., Schijlen, E., et al. (2019). An improved de novo assembly and annotation of the tomato reference genome using single-molecule sequencing, Hi-C proximity ligation and optical maps. *bioRxiv* 767764. doi: 10.1101/767764

Inoue, K., Shirai, T., Ochiai, H., Kasao, M., Hayakawa, K., Kimura, M., et al. (2003). Blood-pressure-lowering effect of a novel fermented milk containing γ-aminobutyric acid (GABA) in mild hypertensives. *Eur. J. Clin. Nutr.* 57, 490–495. doi: 10.1038/sj.ejcn.1601555

Jalil, S. U., and Ansari, M.II (2020). "Physiological Role of Gamma Aminobutyric Acid (GABA) in Salt Stress Tolerance," in *Plant Ecophysiology and Adaptation under Climate Change: Mechanisms and Perspectives II* (Singapore: Springer Singapore), 399–413. doi: 10.1007/978-981-15-2172-0_13

Jia, H., Okamoto, G., and Hirano, K. (2000). Effect of amino acid composition on the taste of 'Hakuho' peaches (*Prunus persica* Batsch) grown under different fertilizer levels. *J. Japanese Soc Hortic. Sci.* 69, 135–140. doi: 10.2503/jjshs.69.135

Jinek, M., Chylinski, K., Fonfara, I., Hauer, M., Doudna, J. A., and Charpentier, E. (2012). A programmable dual-RNA-guided DNA endonuclease in adaptive bacterial immunity. *Sci. (80-.).* 337, 816–821. doi: 10.1126/science.1225829

Kato, R., Hayashi, S., Kobayashi, T., Takahashi, H., Kimura, N., Takahashi, A., et al. (2015). Behavior analysis of γ-aminobutyrate and glutamate decarboxylase activity in salted radish roots (Takuan-zuke). *Nippon Shokuhin Kagaku Kogaku Kaishi* 62, 492–500. doi: 10.3136/nskkk.62.492

Kazami, D., Ogura, N., Fukuchi, T., Tsuji, K., Anazawa, M., and Maeda, H. (2002). Antihypertensive effect of Japanese taste seasoning containing γ-amino butyric acid on mildly hypertensive and high-normal blood pressure subjects and normal subjects. *Nippon Shokuhin Kagaku Kogaku Kaishi* 49, 409–415. doi: 10.3136/nskkk.49.409

Kerchev, P., van der Meer, T., Sujeeth, N., Verlee, A., Stevens, C. V., Van Breusegem, F., et al. (2020). Molecular priming as an approach to induce tolerance against abiotic and oxidative stresses in crop plants. *Biotechnol. Adv.* 40:107503. doi: 10.1016/j.biotechadv.2019.107503

Kim, E. O., Lee, Y. J., Leem, H. H., Seo, I. H., Yu, M. H., Kang, D. H., et al. (2010). Comparison of nutritional and functional constituents, and physicochemical characteristics of mulberrys from seven different *Morus alba* L. cultivars. *J. Korean Soc Food Sci. Nutr.* 39, 1467–1475. doi: 10.3746/jkfn.2010.39.10.1467

Kim, S. L., Lee, J. E., Kwon, Y. U., Kim, W. H., Jung, G. H., Kim, D. W., et al. (2013). Introduction and nutritional evaluation of germinated soy germ. *Food Chem.* 136, 491–500. doi: 10.1016/j.foodchem.2012.08.022

Kinnersley, A. M., and Turano, F. J. (2000). Gamma aminobutyric acid (GABA) and plant responses to stress. *CRC Crit. Rev. Plant Sci.* 19, 479–509. doi: 10.1080/07352680091139277

Kleter, G. A., Kuiper, H. A., and Kok, E. J. (2019). Gene-edited crops: Towards a harmonized safety assessment. *Trends Biotechnol.* 37, 443–447. doi: 10.1016/j.tibtech.2018.11.014

Koike, S., Matsukura, C., Takayama, M., Asamizu, E., and Ezura, H. (2013). Suppression of γ-aminobutyric acid (GABA) transaminases induces prominent GABA accumulation, dwarfism and infertility in the tomato (*Solanum lycopersicum* L.). *Plant Cell Physiol.* 54, 793–807. doi: 10.1093/pcp/pct035

Komor, A. C., Kim, Y. B., Packer, M. S., Zuris, J. A., and Liu, D. R. (2016). Programmable editing of a target base in genomic DNA without double-stranded DNA cleavage. *Nature* 533, 420–424. doi: 10.1038/nature17946

Kurokawa, N., Hirai, T., Takayama, M., Hiwasa-Tanase, K., and Ezura, H. (2013). An E8 promoter-HSP terminator cassette promotes the high-level accumulation of recombinant protein predominantly in transgenic tomato fruits: A case study of miraculin. *Plant Cell Rep.* 32, 529–536. doi: 10.1007/s00299-013-1384-7

Lee, Y., Lee, J. H., Kim, S. D., Chang, M. S., Jo, I. S., Kim, S. J., et al. (2015). Chemical composition, functional constituents, and antioxidant activities of berry fruits produced in Korea. *J. Korean Soc Food Sci. Nutr.* 44, 1295–1303. doi: 10.3746/jkfn.2015.44.9.1295

Lee, J., Nonaka, S., Takayama, M., and Ezura, H. (2018). Utilization of a genome-edited tomato (*Solanum lycopersicum*) with high gamma aminobutyric acid content in hybrid breeding. *J. Agric. Food Chem.* 66, 963–971. doi: 10.1021/acs.jafc.7b05171

Li, Y., Fan, Y., Ma, Y., Zhang, Z., Yue, H., Wang, L., et al. (2017). Effects of exogenous γ-aminobutyric acid (GABA) on photosynthesis and antioxidant system in pepper (*Capsicum annuum* L.) seedlings under low light stress. *J. Plant Growth Regul.* 36, 436–449. doi: 10.1007/s00344-016-9652-8

Li, R., Li, R., Li, X., Fu, D., Zhu, B., Tian, H., et al. (2018). Multiplexed CRISPR/Cas9-mediated metabolic engineering of γ-aminobutyric acid levels in *Solanum lycopersicum*. *Plant Biotechnol. J.* 16, 415–427. doi: 10.1111/pbi.12781

Li, Q., Sapkota, M., and van der Knaap, E. (2020). Perspectives of CRISPR/Cas-mediated cis-engineering in horticulture: unlocking the neglected potential for crop improvement. *Hortic. Res.* 7, 1–11. doi: 10.1038/s41438-020-0258-8

Lin, Q., Zong, Y., Xue, C., Wang, S., Jin, S., Zhu, Z., et al. (2020). Prime genome editing in rice and wheat. *Nat. Biotechnol.* 38, 582–585. doi: 10.1038/s41587-020-0455-x

Loiudice, R., Impembo, M., Laratta, B., Villari, G., Lo Voi, A., Siviero, P., et al. (1995). Composition of San Marzano tomato varieties. *Food Chem.* 53, 81–89. doi: 10.1016/0308-8146(95)95791-4

Macrae, E. A., and Redgwell, R. J. (1992). Amino acids in kiwifruit 1. Distribution within the fruit during fruit maturation. *New Zeal. J. Crop Hortic. Sci.* 20, 329–336. doi: 10.1080/01140671.1992.10421775

Malekzadeh, P., Khara, J., and Heydari, R. (2014). Alleviating effects of exogenous gamma-aminobutiric acid on tomato seedling under chilling stress. *Physiol. Mol. Biol. Plants* 20, 133–137. doi: 10.1007/s12298-013-0203-5

McCarty, N. S., Graham, A. E., Studená, L., and Ledesma-Amaro, R. (2020). Multiplexed CRISPR technologies for gene editing and transcriptional regulation. *Nat. Commun.* 11, 1–13. doi: 10.1038/s41467-020-15053-x

Merodio, C., Muñoz, M. T., Del Cura, B., Buitrago, D., and Escribano, M.II (1998). Effect of high CO2 level on the titres of γ-aminobutyric acid, total polyamines and some pathogenesis-related proteins in cherimoya fruit stored at low temperature. *J. Exp. Bot.* 49, 1339–1347. doi: 10.1093/jxb/49.325.1339

Meyer, R. S., and Purugganan, M. D. (2013). Evolution of crop species: Genetics of domestication and diversification. *Nat. Rev. Genet.* 14, 840–852. doi: 10.1038/nrg3605

Michaeli, S., Fait, A., Lagor, K., Nunes-Nesi, A., Grillich, N., Yellin, A., et al. (2011). A mitochondrial GABA permease connects the GABA shunt and the TCA cycle, and is essential for normal carbon metabolism. *Plant J.* 67, 485–498. doi: 10.1111/j.1365-313X.2011.04612.x

Mori, T., Umeda, T., Honda, T., Zushi, K., Wajima, T., and Matsuzoe, N. (2013). Varietal differences in the chlorogenic acid, anthocyanin, soluble sugar, organic acid, and amino acid concentrations of eggplant fruit. *J. Hortic. Sci. Biotechnol.* 88, 657–663. doi: 10.1080/14620316.2013.11513021

Murcia, M. A., López-Ayerra, B., Martínez-Tomé, M., and García-Carmona, F. (2001). Effect of industrial processing on amino acid content of broccoli. *J. Sci. Food Agric.* 81, 1299–1305. doi: 10.1002/jsfa.942

Nakamura, K., Nara, K., Noguchi, T., Ohshiro, T., and Koga, H. (2006). Contents of γ-aminobutyric acid (GABA) in potatoes and processed potato products. *Nippon Shokuhin Kagaku Kogaku Kaishi* 53, 514–517. doi: 10.3136/nskkk.53.514

Nakamura, H., Takishima, T., Kometani, T., and Yokogoshi, H. (2009). Psychological stress-reducing effect of chocolate enriched with γ-aminobutyric acid (GABA) in humans: Assessment of stress using heart rate variability and salivary chromogranin A. *Int. J. Food Sci. Nutr.* 60, 106–113. doi: 10.1080/09637480802558508

Narayan, V. S., and Nair, P. M. (1990). Metabolism, enzymology and possible roles of 4-aminobutyrate in higher plants. *Phytochemistry* 29, 367–375. doi: 10.1016/0031-9422(90)85081-P

Nicolia, A., Manzo, A., Veronesi, F., and Rosellini, D. (2014). An overview of the last 10 years of genetically engineered crop safety research. *Crit. Rev. Biotechnol.* 34, 77–88. doi: 10.3109/07388551.2013.823595

Ninomiya, K. (1998). Umami: natural occurence. *Food Rev. Int.* 14, 177–211. doi: 10.1080/87559129809541157

Nishimura, M., Yoshida, S.II, Haramoto, M., Mizuno, H., Fukuda, T., Kagami-Katsuyama, H., et al. (2016). Effects of white rice containing enriched gamma-

aminobutyric acid on blood pressure. *J. Trad. Complement. Med.* 6, 66–71. doi: 10.1016/j.jtcme.2014.11.022

Nonaka, S., Arai, C., Takayama, M., Matsukura, C., and Ezura, H. (2017). Efficient increase of γ-aminobutyric acid (GABA) content in tomato fruits by targeted mutagenesis. *Sci. Rep.* 7, 7057. doi: 10.1038/s41598-017-06400-y

Oh, S. H., Moon, Y. J., and Oh, C.-H. (2003). γ -aminobutyric acid (GABA) content of selected uncooked foods. *Prev. Nutr. Food Sci.* 8, 75–78. doi: 10.3746/jfn.2003.8.1.075

Owens, D. F., and Kriegstein, A. R. (2002). Is there more to GABA than synaptic inhibition? *Nat. Rev. Neurosci.* 3, 715–727. doi: 10.1038/nrn919

Palanivelu, R., Brass, L., Edlund, A. F., and Preuss, D. (2003). Pollen tube growth and guidance is regulated by POP2, an *Arabidopsis* gene that controls GABA levels. *Cell* 114, 47–59. doi: 10.1016/S0092-8674(03)00479-3

Palma, F., Carvajal, F., Jamilena, M., and Garrido, D. (2014). Contribution of polyamines and other related metabolites to the maintenance of zucchini fruit quality during cold storage. *Plant Physiol. Biochem.* 82, 161–171. doi: 10.1016/j.plaphy.2014.06.001

Park, K. B., and Oh, S. H. (2007). Production of yogurt with enhanced levels of gamma-aminobutyric acid and valuable nutrients using lactic acid bacteria and germinated soybean extract. *Bioresour. Technol.* 98, 1675–1679. doi: 10.1016/j.biortech.2006.06.006

Park, S., Valan Arasu, M., Lee, M. K., Chun, J. H., Seo, J. M., Lee, S. W., et al. (2014). Quantification of glucosinolates, anthocyanins, free amino acids, and vitamin C in inbred lines of cabbage (*Brassica oleracea* L.). *Food Chem.* 145, 77–85. doi: 10.1016/j.foodchem.2013.08.010

Podlešáková, K., Ugena, L., Spíchal, L., Doležal, K., and De Diego, N. (2019). Phytohormones and polyamines regulate plant stress responses by altering GABA pathway. *N. Biotechnol.* 48, 53–65. doi: 10.1016/j.nbt.2018.07.003

Poojary, M. M., Dellarosa, N., Roohinejad, S., Koubaa, M., Tylewicz, U., Gómez-Galindo, F., et al. (2017). Influence of innovative processing on γ-aminobutyric acid (GABA) contents in plant food materials. *Compr. Rev. Food Sci. Food Saf.* 16, 895–905. doi: 10.1111/1541-4337.12285

Priya, M., Sharma, L., Kaur, R., Bindumadhava, H., Nair, R. M., Siddique, K. H. M., et al. (2019). GABA (γ-aminobutyric acid), as a thermo-protectant, to improve the reproductive function of heat-stressed mungbean plants. *Sci. Rep.* 9, 1–14. doi: 10.1038/s41598-019-44163-w

Prohens, J., Gramazio, P., Plazas, M., Dempewolf, H., Kilian, B., Díez, M. J., et al. (2017). Introgressiomics: a new approach for using crop wild relatives in breeding for adaptation to climate change. *Euphytica* 213, 158. doi: 10.1007/s10681-017-1938-9

Purnhagen, K. P., Kok, E., Kleter, G., Schebesta, H., Visser, R. G. F., and Wesseler, J. (2018). EU court casts new plant breeding techniques into regulatory limbo. *Nat. Biotechnol.* 36, 799–800. doi: 10.1038/nbt.4251

Qaim, M. (2020). Role of new plant breeding technologies for food security and sustainable agricultural development. *Appl. Econ. Perspect. Policy* 42, 129–150. doi: 10.1002/aepp.13044

Qi, H., Yang, Y., Wang, L., Xu, Y., and Qu, S. (2012). Determination of bioactive ingredients in five pumpkin seeds cultivars. *Adv. Mater. Res.* 554–556, 985–989. doi: 10.4028/www.scientific.net/AMR.554-556.985

Quílez, J., and Diana, M. (2017). "Gamma-aminobutyric acid-enriched fermented foods," in *Fermented foods in health and disease prevention*. Eds. J. Frías, C. Martínez-Villaluenga and E. Peñas (Cambridge, USA: Academic Press), 85–103.

Ramesh, S. A., Tyerman, S. D., Gilliham, M., and Xu, B. (2017). γ-aminobutyric acid (GABA) signalling in plants. *Cell. Mol. Life Sci.* 74, 1577–1603. doi: 10.1007/s00018-016-2415-7

Ramos-Ruiz, R., Poirot, E., and Flores-Mosquera, M. (2018). GABA, a non-protein amino acid ubiquitous in food matrices. *Cogent Food Agric.* 4, 1534323. doi: 10.1080/23311932.2018.1534323

Ramos-Ruiz, R., Martinez, F., and Knauf-Beiter, G. (2019). The effects of GABA in plants. *Cogent Food Agric.* 5, 1670553. doi: 10.1080/23311932.2019.1670553

Rees, H. A., and Liu, D. R. (2018). Base editing: precision chemistry on the genome and transcriptome of living cells. *Nat. Rev. Genet.* 19, 770–788. doi: 10.1038/s41576-018-0059-1

Renault, H., Roussel, V., El Amrani, A., Arzel, M., Renault, D., Bouchereau, A., et al. (2010). The *Arabidopsis* pop2-1 mutant reveals the involvement of GABA transaminase in salt stress tolerance. *BMC Plant Biol.* 10:20. doi: 10.1186/1471-2229-10-20

Renault, H., El Amrani, A., Palanivelu, R., Updegraff, E. P., Yu, A., Renou, J. P., et al. (2011). GABA accumulation causes cell elongation defects and a decrease in expression of genes encoding secreted and cell wall-related proteins in *Arabidopsis thaliana*. *Plant Cell Physiol.* 52, 894–908. doi: 10.1093/pcp/pcr041

Rodríguez-Leal, D., Lemmon, Z. H., Man, J., Bartlett, M. E., and Lippman, Z. B. (2017). Engineering quantitative trait variation for crop improvement by genome editing. *Cell* 171, 470–480.e8. doi: 10.1016/j.cell.2017.08.030

Saito, T., Matsukura, C., Sugiyama, M., Watahiki, A., Ohshima, I., Iijima, Y., et al. (2008). Screening for γ-aminobutyric acid (GABA)-rich tomato varieties. *J. Japanese Soc Hortic. Sci.* 77, 242–250. doi: 10.2503/jjshs1.77.242

Saito, T., Ariizumi, T., Okabe, Y., Asamizu, E., Hiwasa-Tanase, K., Fukuda, N., et al. (2011). TOMATOMA: A novel tomato mutant database distributing Micro-Tom mutant collections. *Plant Cell Physiol.* 52, 283–296. doi: 10.1093/pcp/pcr004

Sánchez Pérez, E. M., García López, J., Iglesias, M. J., López Ortiz, F., Toresano, F., and Camacho, F. (2011). HRMAS-nuclear magnetic resonance spectroscopy characterization of tomato "flavor varieties" Almería (Spain). *Food Res. Int.* 44, 3212–3221. doi: 10.1016/j.foodres.2011.08.012

Sánchez-López, Á.M., Bahaji, A., De Diego, N., Baslam, M., Li, J., Muñoz, F. J., et al. (2016a). *Arabidopsis* responds to *Alternaria alternata* volatiles by triggering plastid phosphoglucose isomerase-independent mechanisms. *Plant Physiol.* 172, 1989–2001. doi: 10.1104/pp.16.00945

Sánchez-López, Á.M., Baslam, M., De Diego, N., Muñoz, F. J., Bahaji, A., Almagro, G., et al. (2016b). Volatile compounds emitted by diverse phytopathogenic microorganisms promote plant growth and flowering through cytokinin action. *Plant Cell Environ.* 39, 2592–2608. doi: 10.1111/pce.12759

Schaart, J. G., van de Wiel, C. C. M., Lotz, L. A. P., and Smulders, M. J. M. (2016). Opportunities for products of new plant breeding techniques. *Trends Plant Sci.* 21, 438–449. doi: 10.1016/j.tplants.2015.11.006

Schauer, N., Zamir, D., and Fernie, A. R. (2005). Metabolic profiling of leaves and fruit of wild species tomato: A survey of the *Solanum lycopersicum* complex. in. *J. Exp. Bot.* 56, 297–307. doi: 10.1093/jxb/eri057

Schiemann, J., Robienski, J., Schleissing, S., Spök, A., Sprink, T., and Wilhelm, R. A. (2020). Plant genome editing – Policies and governance. *Front. Plant Sci.* 11, 284. doi: 10.3389/fpls.2020.00284

Scholz, S. S., Malabarba, J., Reichelt, M., Heyer, M., Ludewig, F., and Mithöfer, A. (2017). Evidence for GABA-induced systemic GABA accumulation in *Arabidopsis* upon wounding. *Front. Plant Sci.* 8:388:388. doi: 10.3389/fpls.2017.00388

Seifi, H. S., Curvers, K., De Vleesschauwer, D., Delaere, I., Aziz, A., and Höfte, M. (2013). Concurrent overactivation of the cytosolic glutamine synthetase and the GABA shunt in the ABA-deficient sitiens mutant of tomato leads to resistance against *Botrytis cinerea*. *New Phytol.* 199, 490–504. doi: 10.1111/nph.12283

Seifikalhor, M., Aliniaeifard, S., Hassani, B., Niknam, V., and Lastochkina, O. (2019). Diverse role of γ-aminobutyric acid in dynamic plant cell responses. *Plant Cell Rep.* 38, 847–867. doi: 10.1007/s00299-019-02396-z

Shelp, B. J., Bown, A. W., and McLean, M. D. (1999). Metabolism and functions of gamma-aminobutyric acid. *Trends Plant Sci.* 4, 446–452. doi: 10.1016/S1360-1385(99)01486-7

Shelp, B. J., Bozzo, G. G., Trobacher, C. P., Chiu, G., and Bajwa, V. S. (2012). Strategies and tools for studying the metabolism and function of γ-aminobutyrate in plants. I. Pathway structure. *Botany* 90, 651–668. doi: 10.1139/B2012-030

Shelp, B. J., Bown, A. W., and Zarei, A. (2017). 4-Aminobutyrate (GABA): A metabolite and signal with practical significance. *Botany* 95, 1015–1032. doi: 10.1139/cjb-2017-0135

Sheteiwy, M. S., Shao, H., Qi, W., Hamoud, Y. A., Shaghaleh, H., Khan, N. U., et al. (2019). GABA-alleviated oxidative injury induced by salinity, osmotic stress and their combination by regulating cellular and molecular signals in rice. *Int. J. Mol. Sci.* 20, 5709. doi: 10.3390/ijms20225709

Shima, Y., Kitagawa, M., Fujisawa, M., Nakano, T., Kato, H., Kimbara, J., et al. (2013). Tomato FRUITFULL homologues act in fruit ripening via forming

MADS-box transcription factor complexes with RIN. *Plant Mol. Biol.* 82, 427–438. doi: 10.1007/s11103-013-0071-y

Shimajiri, Y., Ozaki, K., Kainou, K., and Akama, K. (2013). Differential subcellular localization, enzymatic properties and expression patterns of γ-aminobutyric acid transaminases (GABA-Ts) in rice (*Oryza sativa*). *J. Plant Physiol.* 170, 196–201. doi: 10.1016/j.jplph.2012.09.007

Shimatani, Z., Kashojiya, S., Takayama, M., Terada, R., Arazoe, T., Ishii, H., et al. (2017). Targeted base editing in rice and tomato using a CRISPR-Cas9 cytidine deaminase fusion. *Nat. Biotechnol.* 35, 441–443. doi: 10.1038/nbt.3833

Siegrist, M., and Hartmann, C. (2020). Consumer acceptance of novel food technologies. *Nat. Food* 1, 343–350. doi: 10.1038/s43016-020-0094-x

Signorelli, S., Dans, P. D., Coitiño, E. L., Borsani, O., and Monza, J. (2015). Connecting proline and γ-aminobutyric acid in stressed plants through non-enzymatic reactions. *PloS One* 10, e0115349. doi: 10.1371/journal.pone.0115349

Simpson, J. P., Di Leo, R., Dhanoa, P. K., Allan, W. L., Makhmoudova, A., Clark, S. M., et al. (2008). Identification and characterization of a plastid-localized *Arabidopsis* glyoxylate reductase isoform: Comparison with a cytosolic isoform and implications for cellular redox homeostasis and aldehyde detoxification. *J. Exp. Bot.* 59, 2545–2554. doi: 10.1093/jxb/ern123

Snedden, W. A., Arazi, T., Fromm, H., and Shelp, B. J. (1995). Calcium/calmodulin activation of soybean glutamate decarboxylase. *Plant Physiol.* 108, 543–549. doi: 10.1104/pp.108.2.543

Snedden, W. A., Koutsia, N., Baum, G., and Fromm, H. (1996). Activation of a recombinant petunia glutamate decarboxylase by calcium/calmodulin or by a monoclonal antibody which recognizes the calmodulin binding domain. *J. Biol. Chem.* 271, 4148–4153. doi: 10.1074/jbc.271.8.4148

Snowden, C. J., Thomas, B., Baxter, C. J., Smith, J. A. C., and Sweetlove, L. J. (2015). A tonoplast Glu/Asp/GABA exchanger that affects tomato fruit amino acid composition. *Plant J.* 81, 651–660. doi: 10.1111/tpj.12766

Sorrequieta, A., Ferraro, G., Boggio, S. B., and Valle, E. M. (2010). Free amino acid production during tomato fruit ripening: A focus on L-glutamate. *Amino Acids* 38, 1523–1532. doi: 10.1007/s00726-009-0373-1

Steward, F., Thompson, J., and Dent, C. (1949). γ-aminobutyric acid: a constituent of the potato tuber? *Science* 110, 439–440.

Swinnen, G., Goossens, A., and Pauwels, L. (2016). Lessons from domestication: targeting cis-regulatory elements for crop improvement. *Trends Plant Sci.* 21, 506–515. doi: 10.1016/j.tplants.2016.01.014

Takayama, M., Koike, S., Kusano, M., Matsukura, C., Saito, K., Ariizumi, T., et al. (2015). Tomato glutamate decarboxylase genes *SlGAD2* and *SlGAD3* play key roles in regulating γ-Aminobutyric acid levels in tomato (*Solanum lycopersicum*). *Plant Cell Physiol.* 56, 1533–1545. doi: 10.1093/pcp/pcv075

Takayama, M., Matsukura, C., Ariizumi, T., and Ezura, H. (2017). Activating glutamate decarboxylase activity by removing the autoinhibitory domain leads to hyper γ-aminobutyric acid (GABA) accumulation in tomato fruit. *Plant Cell Rep.* 36, 103–116. doi: 10.1007/s00299-016-2061-4

Tarkowski, Ł.P., de Poel, B., Van, Höfte, M., and Van den Ende, W. (2019). Sweet immunity: Inulin boosts resistance of lettuce (*lactuca sativa*) against grey mold (*botrytis cinerea*) in an ethylene-dependent manner. *Int. J. Mol. Sci.* 20, 1052. doi: 10.3390/ijms20051052

Tieman, D., Zhu, G., Resende, M. F. R., Lin, T., Nguyen, C., Bies, D., et al. (2017). A chemical genetic roadmap to improved tomato flavor. *Sci. (80-.).* 355, 391–394. doi: 10.1126/science.aal1556

Trobacher, C. P., Clark, S. M., Bozzo, G. G., Mullen, R. T., DeEll, J. R., and Shelp, B. J. (2013). Catabolism of GABA in apple fruit: Subcellular localization and biochemical characterization of two γ-aminobutyrate transaminases. *Postharvest Biol. Technol.* 75, 106–113. doi: 10.1016/j.postharvbio.2012.08.005

Vad-Nielsen, J., Lin, L., Bolund, L., Nielsen, A. L., and Luo, Y. (2016). Golden Gate Assembly of CRISPR gRNA expression array for simultaneously targeting multiple genes. *Cell. Mol. Life Sci.* 73, 4315–4325. doi: 10.1007/s00018-016-2271-5

Van Cauwenberghe, O. R., and Shelp, B. J. (1999). Biochemical characterization of partially purified gaba: Pyruvate transaminase from *Nicotiana tabacum*. *Phytochemistry* 52, 575–581. doi: 10.1016/S0031-9422(99)00301-5

Van Cauwenberghe, O. R., Makhmoudova, A., McLean, M. D., Clark, S. M., and Shelp, B. J. (2002). Plant pyruvate-dependent gamma-aminobutyrate transaminase: Identification of an *Arabidopsis* cDNA and its expression in *Escherichia coli*. *Can. J. Bot.* 80, 933–941. doi: 10.1139/b02-087

van der Knaap, E., Chakrabarti, M., Chu, Y. H., Clevenger, J. P., Illa-Berenguer, E., Huang, Z., et al. (2014). What lies beyond the eye: The molecular mechanisms regulating tomato fruit weight and shape. *Front. Plant Sci.* 5, 227. doi: 10.3389/fpls.2014.00227

Vijayakumari, K., Jisha, K. C., and Puthur, J. T. (2016). GABA/BABA priming: a means for enhancing abiotic stress tolerance potential of plants with less energy investments on defence cache. *Acta Physiol. Plant* 38, 230. doi: 10.1007/s11738-016-2254-z

Wang, C., Fan, L., Gao, H., Wu, X., Li, J., Lv, G., et al. (2014). Polyamine biosynthesis and degradation are modulated by exogenous gamma-aminobutyric acid in root-zone hypoxia-stressed melon roots. *Plant Physiol. Biochem.* 82, 17–26. doi: 10.1016/j.plaphy.2014.04.018

Wang, Y., Luo, Z., Mao, L., and Ying, T. (2016). Contribution of polyamines metabolism and GABA shunt to chilling tolerance induced by nitric oxide in cold-stored banana fruit. *Food Chem.* 197, 333–339. doi: 10.1016/j.foodchem.2015.10.118

Wang, G., Kong, J., Cui, D., Zhao, H., Niu, Y., Xu, M., et al. (2019). Resistance against *Ralstonia solanacearum* in tomato depends on the methionine cycle and the γ-aminobutyric acid metabolic pathway. *Plant J.* 97, 1032–1047. doi: 10.1111/tpj.14175

Wittkopp, P. J., and Kalay, G. (2012). Cis-regulatory elements: Molecular mechanisms and evolutionary processes underlying divergence. *Nat. Rev. Genet.* 13, 59–69. doi: 10.1038/nrg3095

Wu, Z. C., Yang, Z. Y., Li, J. G., Chen, H., Huang, X. M., and Wang, H. C. (2016). Methyl-inositol, γ-aminobutyric acid and other health benefit compounds in the aril of litchi. *Int. J.* 67, 762–772. doi: 10.1080/09637486.2016.1198888

Yamaguchi, S. (1998). Basic properties of umami and its effects on food flavor. *Food Rev. Int.* 14, 139–176., 762–772. doi: 10.1080/09637486.2016.1198888

Yamatsu, A., Yamashita, Y., Pandharipande, T., Maru, I., and Kim, M. (2016). Effect of oral γ-aminobutyric acid (GABA) administration on sleep and its absorption in humans. *Food Sci. Biotechnol.* 25, 547–551. doi: 10.1007/s10068-016-0076-9

Yang, N. C., Jhou, K. Y., and Tseng, C. Y. (2012). Antihypertensive effect of mulberry leaf aqueous extract containing γ-aminobutyric acid in spontaneously hypertensive rats. *Food Chem.* 132, 1796–1801. doi: 10.1016/j.foodchem.2011.11.143

Yang, R., Yin, Y., and Gu, Z. (2015). Polyamine degradation pathway regulating growth and GABA accumulation in germinating fava bean under hypoxia-NaCl stress. *J. Agric. Sci. Technol.* 17, 311–320.

Yang, J., Sun, C., Zhang, Y., Fu, D., Zheng, X., and Yu, T. (2017). Induced resistance in tomato fruit by γ-aminobutyric acid for the control of alternaria rot caused by *Alternaria alternata*. *Food Chem.* 221, 1014–1020. doi: 10.1016/j.foodchem.2016.11.061

Yoshimura, M., Toyoshi, T., Sano, A., Izumi, T., Fujii, T., Konishi, C., et al. (2010). Antihypertensive effect of a γ-aminobutyric acid rich tomato cultivar "DG03-9" in spontaneously hypertensive rats. *J. Agric. Food Chem.* 58, 615–619. doi: 10.1021/jf903008t

Yu, G. H., Zou, J., Feng, J., Peng, X. B., Wu, J. Y., Wu, Y. L., et al. (2014). Exogenous γ-aminobutyric acid (GABA) affects pollen tube growth via modulating putative Ca2+-permeable membrane channels and is coupled to negative regulation on glutamate decarboxylase. *J. Exp. Bot.* 65, 3235–3248. doi: 10.1093/jxb/eru171

Zaidi, S. S., Vanderschuren, H., Qaim, M., Mahfouz, M. M., Kohli, A., Mansoor, S., et al. (2019). New plant breeding technologies for food security. *Sci. (80-.).* 363, 1390–1391. doi: 10.1126/science.aav6316

Zazzeroni, R., Homan, A., and Thain, E. (2009). Determination of γ-aminobutyric acid in food matrices by isotope dilution hydrophilic interaction chromatography coupled to mass spectrometry. *J. Chromatogr. Sci.* 47, 564–568. Chromatographic, E. T.-J. of, and 2009, U. doi: 10.1093/chromsci/47.7.564

Zetsche, B., Heidenreich, M., Mohanraju, P., Fedorova, I., Kneppers, J., Degennaro, E. M., et al. (2017). Multiplex gene editing by CRISPR-Cpf1 using a single crRNA array. *Nat. Biotechnol.* 35, 31–34. doi: 10.1038/nbt.3737

Zhang, H., Wang, Z. Y., Yang, X., Zhao, H. T., Zhang, Y. C., Dong, A. J., et al. (2014). Determination of free amino acids and 18 elements in freeze-dried

strawberry and blueberry fruit using an Amino Acid Analyzer and ICP-MS with micro-wave digestion. *Food Chem.* 147, 189–194. doi: 10.1016/j.foodchem.2013.09.118

Zhang, D., Hussain, A., Manghwar, H., Xie, K., Xie, S., Zhao, S., et al. (2020). Genome editing with the CRISPR-Cas system: an art, ethics and global regulatory perspective. *Plant Biotechnol. J.* 18, 1651–1669. doi: 10.1111/pbi.13383

Zhao, Y., and Jiang, Y. J. (2007). Primary study on factors affecting the biosynthesis of γ-Aminobutyric acid in harvested asparagus. *Food Res. Dev.* 9. Development, Y. J.-F. R. and, and 2007.

Conflict of Interest: The authors declare that the research was conducted in the absence of any commercial or financial relationships that could be construed as a potential conflict of interest.

Copyright © 2020 Gramazio, Takayama and Ezura. This is an open-access article distributed under the terms of the Creative Commons Attribution License (CC BY). The use, distribution or reproduction in other forums is permitted, provided the original author(s) and the copyright owner(s) are credited and that the original publication in this journal is cited, in accordance with accepted academic practice. No use, distribution or reproduction is permitted which does not comply with these terms.

frontiers in Plant Science

ORIGINAL RESEARCH
published: 25 September 2020
doi: 10.3389/fpls.2020.565134

Differential Contribution of P5CS Isoforms to Stress Tolerance in Arabidopsis

Dietmar Funck[1], Lukas Baumgarten[1], Marc Stift[1], Nicolaus von Wirén[2] and Luise Schönemann[1]*

[1] Department of Biology, University of Konstanz, Konstanz, Germany, [2] Molecular Plant Nutrition, Leibniz Institute of Plant Genetics and Crop Plant Research, Gatersleben, Germany

Proline accumulation is a widespread response of plants to salt stress as well as drought and cold stress. In most plant species, two isoforms of pyrroline-5-carboxylate synthetase (P5CS) catalyze the first step in proline biosynthesis from glutamate. In Arabidopsis, these isoforms differ in their spatial and temporal expression patterns, suggesting sub-functionalization. P5CS1 has been identified as the major contributor to stress-induced proline accumulation, whereas P5CS2 has been considered important for embryo development and growth. In contrast to previous results, our analysis of P5CS1- and P5CS2-GFP fusion proteins indicates that both enzymes were exclusively localized in the cytosol. The comparison of the susceptibility of *p5cs1* and *p5cs2* mutants to infection with *Pseudomonas syringae* and salt stress provided novel information on the contribution of the two P5CS isoforms to proline accumulation and stress tolerance. In agreement with previous studies, salt-stressed *p5cs1* mutants accumulated very little proline, indicating that P5CS1 contributed more to stress-induced proline accumulation, whereas its impact on stress tolerance was rather weak. Germination and establishment of *p5cs2* mutants were impaired under ambient conditions, further supporting that P5CS2 is most important for growth and development, whereas its contribution to stress-induced proline accumulation was smaller than that of P5CS1. In contrast to *p5cs1* mutants or wildtype plants, *p5cs2* mutants were only weakly affected by sudden exposure to a high NaCl concentration. These findings show that proline content, which was intermediate in leaves of *p5cs2* mutants, was not directly correlated with stress tolerance in our experiments. In rosettes of NaCl-exposed *p5cs2* mutants, nearly no accumulation of Na^+ was observed, and the plants showed neither chlorosis nor reduction of photosynthesis. Based on these data, we suggest a function of P5CS2 or P5CS2-mediated proline synthesis in regulating Na^+ accumulation in leaves and thereby salt stress tolerance.

Keywords: proline biosynthesis, pyrroline-5-carboxylate synthetase, salt stress, compatible solutes, subcellular localization, seedling development, *Pseudomonas syringae*

OPEN ACCESS

Edited by:
Supaart Sirikantaramas, Chulalongkorn University, Thailand

Reviewed by:
László Szabados, Hungarian Academy of Sciences (MTA), Hungary
Severine Planchais, Université Pierre et Marie Curie, France

****Correspondence:***
Dietmar Funck
Dietmar.Funck@uni-konstanz.de

Specialty section:
This article was submitted to Plant Metabolism and Chemodiversity, a section of the journal Frontiers in Plant Science

Received: *27 May 2020*
Accepted: *09 September 2020*
Published: *25 September 2020*

Citation:
Funck D, Baumgarten L, Stift M, von Wirén N and Schönemann L (2020) Differential Contribution of P5CS Isoforms to Stress Tolerance in Arabidopsis. Front. Plant Sci. 11:565134. doi: 10.3389/fpls.2020.565134

INTRODUCTION

Worldwide, soil salinity is a major problem for plant productivity in irrigation-dependent cultivation systems as well as in coastal areas. A high soluble ion content in the soil constitutes two problems for plant growth: First, water uptake is inhibited due to its dependence on a higher concentration of osmotically active solutes inside the cells. Second, some ions, especially Na^+, exert toxic effects when they accumulate inside cells (Munns and Tester, 2008; Zörb et al., 2019). Since Na^+ and Cl^- are usually the most abundant ions in saline soil, most experimental studies use NaCl-induced stress as a proxy for salt stress in general. Numerous efforts have been made to improve the salt tolerance of crop plants while at the same time maintaining high productivity under non-stress conditions (Agarwal et al., 2013; Liang et al., 2018). However, the progress achieved so far is rather limited, emphasizing the need for a more detailed analysis of the natural tolerance mechanisms that plants have evolved to cope with salt stress.

Arabidopsis and many other plant species accumulate free proline in response to salt stress or similar environmental stress factors causing cellular water deprivation (Liang et al., 2013; Kavi Kishor and Sreenivasulu, 2014). Stress-dependent accumulation of proline is achieved by induced biosynthesis from glutamate in combination with proline transport between different tissues or cell types as well as repression of proline degradation in mitochondria (Szabados and Savoure, 2010; Trovato et al., 2019). Stress-induced alterations of protein biosynthesis and degradation rates may also affect free amino acid concentrations, but are not expected to cause a specific increase in proline (Hildebrandt, 2018). High concentrations of proline can stabilize proteins and membranes, and it has been suggested that proline accumulation stimulates the antioxidant defense system (Forlani et al., 2019b; Zouari et al., 2019). Direct contributions of proline to radical scavenging and osmotic adjustment have also been proposed but the evidence is controversial (Forlani et al., 2019a). At present, it is not fully understood whether high proline concentrations or the synthesis of proline mediate the protective effects.

Proline biosynthesis is a two-step process, in which the intermediate pyrroline-5-carboxylate (P5C) is synthesized by the bifunctional enzyme P5C-synthetase (P5CS), combining both glutamate kinase and γ-glutamylphosphate reductase activities in a single polypeptide. Like many other plant species, Arabidopsis has two isoforms of P5CS, which apparently are sub-functionalized in the stress-responsive P5CS1 (At2g39800) and the housekeeping P5CS2 (At3g55610; (Székely et al., 2008; Turchetto-Zolet et al., 2009). Analysis of GFP fusion proteins suggested that both P5CS isoforms are mainly cytosolic but may be localized in plastids under stress conditions (Székely et al., 2008). The second step of proline biosynthesis is catalyzed by P5C reductase (P5CR), which is encoded by a single-copy gene in Arabidopsis and most other plant species. The expression pattern of *P5CR* did not provide conclusive evidence for a limiting role in proline biosynthesis, giving rise to the assumption that P5CS is the key enzyme for proline accumulation (Szabados and Savoure, 2010). However, the detailed characterization of post-translational mechanisms of enzyme activity modulation provided evidence that also P5CR activity may be regulating proline synthesis rates according to the cellular redox status and cytosolic ion concentrations (Giberti et al., 2014). A P5CR:GFP fusion protein was exclusively localized in the cytosol in Arabidopsis, raising the question whether plastids can indeed be the site of proline synthesis in stressed plants (Funck et al., 2012).

Several independent T-DNA insertion mutants lacking P5CS1 have shown strongly reduced proline levels both under normal growth conditions and in response to stress. This had been revealed by increased levels of reactive oxygen species in leaves of stressed *p5cs1* mutants, and by root growth being more sensitive to NaCl- or PEG-induced osmotic stress compared to wildtype plants (Székely et al., 2008; Sharma et al., 2011). Expression of P5CR and at least one isoform of P5CS are essential for sexual reproduction in Arabidopsis, indicating that plants have no alternative pathways to synthesize proline (Funck et al., 2012; Mattioli et al., 2012; Mattioli et al., 2018). Homozygous *p5cs1* mutants that were additionally heterozygous for a *p5cs2* mutation had very low proline content and root growth was reduced due to fewer cell divisions in the meristematic zone of the root tip (Biancucci et al., 2015). In contrast to single mutants lacking P5CS1, which develop normally and are fertile, homozygous embryos of two recessive T-DNA insertion mutants lacking P5CS2 are conditionally aborted in heterozygous plants (Székely et al., 2008; Mattioli et al., 2009; Funck et al., 2012). When immature, homozygous *p5cs2* seeds were fed with proline, they germinated *in vitro* and the resulting seedlings were shown to be devoid of functional *P5CS2* transcripts (Székely et al., 2008). We succeeded to cultivate rescued, homozygous *p5cs2* seedlings on soil, where they produced viable seeds under short-day conditions (Funck et al., 2012). The stress tolerance of *p5cs2* mutants has not been analyzed so far.

Besides salt and osmotic stress, also biotic stress leads to alterations in proline metabolism. *P5CS1* expression did not change considerably in response to bacterial infections, whereas an upregulation of *P5CS2* during the hypersensitive response to an avirulent *Pseudomonas syringae* strain was observed in Arabidopsis (Fabro et al., 2004). Multiple lines of evidence suggest a role of proline degradation in the orchestration of the hypersensitive response to incompatible pathogens (Ayliffe et al., 2002; Fabro et al., 2004; Mitchell et al., 2006; Cecchini et al., 2011). Especially proline dehydrogenase (ProDH)-dependent generation of reactive oxygen species in mitochondria seems to contribute to the regulation of cell death or survival, but also signaling functions or toxicity of mitochondrial P5C, or a proline-P5C cycle across the mitochondrial membrane were proposed (Deuschle et al., 2004; Miller et al., 2009; Cecchini et al., 2011; Monteoliva et al., 2014). The individual contributions of P5CS1 and P5CS2 to pathogen defense have not yet been reported.

In this study, we revisited the subcellular localization of the two P5CS isoforms in Arabidopsis and used *p5cs1* and *p5cs2* mutants to perform a detailed analysis of their importance for germination and seedling development. Additionally, we tested the pathogen susceptibility of mature plants and analyzed their

sensitivity to salt and excess light stress alone or in combination. Our results indicate that *P5CS2* expression does not contribute to the defense against *P. syringae* but has a regulatory function for NaCl stress tolerance.

MATERIALS AND METHODS

Plant Material and DNA Constructs

Arabidopsis (*Arabidopsis thaliana* (L.) Heynh., ecotype Col-0, seed stock Col-8 from NASC) and T-DNA insertion lines were obtained from the NASC (GABI452_G01, *p5cs2-1*; Salk_063517, *p5cs1-4*) or from the INRA Versailles Resource Centre (FLAG_139H07, *p5cs2-2*). Backcrossing of the mutants and generation of homozygous plants is described in (Funck et al., 2012). Expression constructs for P5CS:GFP fusion proteins were generated by inserting the coding sequences without stop codon of *P5CS1* (from ABRC clone U14433) or *P5CS2* (from ABRC clone G2E1) *via* pENTR into the plant transformation vector pUBC-GFP-Dest (Grefen et al., 2010) and verified by Sanger sequencing. *Agrobacterium tumefaciens* strain GV3101 was used to transform Col-0 plants by the floral dip method (Clough and Bent, 1998).

Confocal Microscopy

Protoplasts were isolated from leaves of P5CS1:GFP or P5CS2:GFP expressing and wildtype plants by overnight incubation in protoplast medium (0.45 M sorbitol, ½ strength MS salt mixture) supplemented with 10 mg ml^{-1} cellulase and 2.5 mg ml^{-1} macerozyme. Spectral images were recorded with a Zeiss LSM880 equipped with a 63× water immersion lens. The samples were excited at 488 nm and images were recorded with 20 spectral channels (9 nm bandwidth) between 490 and 668 nm. A chlorophyll spectrum was obtained from WT protoplasts and a GFP spectrum from a P5CS2:GFP expressing epidermis protoplast that did not contain chloroplasts. Linear unmixing with background subtraction was performed with the ZEN software (Zeiss). Channel overlay, false coloring and adjustment to identical gain, offset and contrast settings were performed in ImageJ and Adobe Photoshop.

Growth Conditions and Stress Treatments

For germination assays, the assessment of seedling development or root growth and RNA extraction, plants were cultivated axenically as described in (Funck et al., 2010). Germination was scored as radicle protrusion and seeds that did not germinate were excluded from the assessment of further development. Approximately fifty seeds of each genotype were placed in a common Petri dish (9 cm diameter) and per condition, 4 plates with seeds from different parental plants were analyzed. To monitor root growth, 4-day-old seedlings were transferred to vertically placed Petri dishes (15 cm diameter) containing 50 ml of ½ x MS medium with the indicated supplements and 15 g/l of agar. Per condition, two plates with six seedlings of each genotype were analyzed. Seedlings were excluded from the analysis if their roots did not reach half of the length of the longest root from the same genotype and plate.

For salt stress experiments, plants were cultivated on soil ("Einheitserde", type P, Gebr. Patzer, Sinntal-Altengronau, Germany) in a climate chamber with a light period of 9 h with day/night temperatures of 21°C/17°C and 50% relative humidity at a photon flux density of 120 ± 10 μmol m^{-2} s^{-1} from metal halide lamps (Clean Ace MT400DL/BH, Iwasaki, Tokyo, Japan). To induce salt stress, individual 9 cm pots with a single plant were twice soaked from the bottom with 25 ml of a 0.3 M NaCl solution at a two-day interval. Control plants received the same amount of water. To induce light stress, the plants were exposed for 1 h to 1,000 ± 100 μmol m^{-2} s^{-1} from metal halide lamps (Powerstar HQI-E bulb, 400 W/D; Osram, Germany) placed approximately 30 cm above the rosettes. Excess heat was removed by a fan directed mainly against the lamps.

Northern Blot Analysis

RNA isolation, Northern blotting and detection with DIG-labeled probes (DIG-probe synthesis kit, Roche, Basel, Switzerland) was carried out as described in (Funck et al., 2008; Funck et al., 2010). A *P5CS2*-specific probe comprising primarily the 3′-UTR sequence was produced with the primers described in (Strizhov et al., 1997).

Pathogen Defense Assays

Pseudomonas syringae pv. *tomato* strain DC3000 was cultivated in NGA medium (5 g L^{-1} peptone, 3 g L^{-1} yeast extract, 2% (V/V) glycerol, pH 7) with 50 μg ml^{-1} rifampicin. The medium for the strain carrying the avrRPM1 gene on a plasmid contained additionally 50 μg ml^{-1} kanamycin. Pathogen growth assays were carried out essentially as described in (Debener et al., 1991). Briefly, an exponentially growing *P. syringae* culture was harvested by centrifugation, resuspended to the desired density in 10 mM $MgCl_2$ and used to infiltrate 5 leaves per plant trough the stomata of the lower epidermis with a 1 ml syringe. Leaf samples for the determination of bacterial titers were collected immediately after infiltration as well as 2 and 4 days post inoculation. After brief rinsing, three disks from independent leaves were macerated in 10 mM $MgCl_2$ and a series of 5-fold dilutions was spotted in triplicates on NGA plates supplemented with rifampicin.

Pigment and Proline Content Determination

For pigment extraction, fresh or freeze-dried leaves were ground under dim light in liquid nitrogen and pigments were extracted in 80% acetone (for simplicity, the entire fresh weight of the leaves was considered to be water). Quantification of pigments was carried out by determining the OD of suitable dilutions of the crude extracts at 470 nm, 647 nm and 663 nm according to (Lichtenthaler, 1987). Proline content of leaves was determined by a modification of the assay originally developed by (Bates et al., 1973) as described in (Funck et al., 2008).

Leaf Sap Osmolality and Ion Concentrations

Crude leaf extracts were produced by macerating fresh leaves for 30 s at 30 Hz in a Tissue Lyser (Eppendorf, Hilden, Germany), heating the slurry to 96°C followed by centrifugation for 10 min

at 4°C and 25,000 *g*. The extracts were diluted with double-distilled water to be within the linear range for determination of osmolality or ion concentrations. Osmolality was measured with a freeze point osmometer (Osmomat 30, Gonotech GmbH, Berlin, Germany) with distilled water and a NaCl solution with 0.3 Osm kg^{-1} as references. Concentrations of individual ions in the leaf sap were determined by inductively coupled plasma optical emission spectroscopy (ICP-OES) as described in (Gruber et al., 2013).

Measurement of Photosynthetic Parameters

The ImagingWin software and an Imaging PAM (Walz, Effeltrich, Germany) equipped with standard measuring head were used to record chlorophyll fluorescence and absorptivity of excised leaves placed with the maximal recommended distance to the camera on moist filter paper. F_0 was determined after 5 min dark adaptation at measuring light intensity and frequency settings of 1. After an initial saturating flash to determine F_m, the leaves were exposed for 8 min to actinic blue light (86 μmol m^{-2} s^{-1}) prior to the determination of F' and F_m' before and during an additional saturating flash for the calculation of ΦPSII ((F_m'-F')/F_m'). Absorptivity of the leaves was estimated according to the recommendations of the manufacturer from the difference between pictures with red and near infrared illumination and used to calculate rates of linear electron transport, assuming an equal distribution of absorbed photons between PS II and PS I. The NPQ parameter for inducible non-photochemical quenching is calculated by the ImagingWin software as (F_m-F_m')/F_m'. Fluorescence intensities and absorptivity were averaged over 2 circular areas per leaf with 2 mm diameter each.

Statistical Analysis

Unless otherwise mentioned, statistical analyses were performed in R (R core team, 2020). The effects of proline and NaCl addition to the medium on the proportion of germinated seeds and established seedlings of the two *p5cs2* mutants at day 10 was assessed by binomial generalized linear mixed models as implemented in the *glmer* function from the *lme4* package (Bates et al., 2015). Models included genotype and either proline concentration (0, 2 and 10 mM) or NaCl concentration (0, 50, 100 and 200 mM) as fixed effects, and plate identity as a random effect. Because germination and establishment of wildtype and *p5cs1-4* seeds was at or very near to 100%, they could not be included into the model. Therefore, Fisher's exact test was used to compare the proportions of germinated seeds or established seedlings under each condition to the wildtype using the RealStatistics Excel add-in (Zaiontz, 2020).

The effects of proline and NaCl in the medium on root growth of wildtype and mutant genotypes were assessed by a Gaussian linear mixed model as implemented in the *lmer* function from the *lme4* package in R (Bates et al., 2015). Models included genotype (wildtype, *p5cs1-4*, *p5cs2-1*, and *p5cs2-2*), proline concentration (0 and 2 mM), NaCl concentration (0 and 150 mM) and their interactions as fixed effects, and plate identity as a random effect. Photosynthetic parameters were appropriately transformed to obtain normal distribution of the model residuals and homogeneity of variance before the analysis with linear models (*lm* function in R). Post hoc pairwise comparisons between treatments or between genotypes were performed using the *glht* function of the *multcomp* package (Hothorn et al., 2008).

Other physiological parameters and bacterial titers were analyzed by one-way or two-way ANOVA with Tukey's HSD test for multiple post-hoc pairwise comparisons using SigmaPlot (V13).

RESULTS

P5CS1:GFP and *P5CS2*:GFP Fusion Proteins Are Localized in the Cytosol

A previous report suggested that both P5CS1 and P5CS2 from Arabidopsis can be localized in chloroplasts of stressed cells or isolated protoplasts despite the absence of recognizable transit peptides in the amino acid sequences (Székely et al., 2008). We re-visited the subcellular localization in transgenic plants stably expressing P5CS1:GFP and P5CS2:GFP fusion constructs under control of the constitutive Ubiquitin10 promoter. We used the Ubiquitin10 promoter, because it produces moderate expression levels and is less prone to silencing than other constitutive promoters (Grefen et al., 2010). When introduced into *p5cs1-4/p5cs1-4 p5cs2-1/P5CS2* sesquimutants, both constructs allowed the selection of plants in which all endogenous *P5CS* genes were inactivated by T-DNA insertions (**Supplementary Figure S1A**). With both constructs, we observed aggregation of the GFP fusion proteins in strongly expressing lines and frequently, the expression was partially or completely silenced (data not shown). Only lines with stable and moderate expression were used for microscopic analysis. In multi-wavelength confocal fluorescence images of leaf protoplasts, spectral unmixing showed that GFP signals from both P5CS1:GFP and P5CS2:GFP fusion proteins were exclusively detectable in the cytosol (**Figure 1** and **Supplementary Figure S1**). When the same images were processed to mimic channel splitting, it became evident that chlorophyll autofluorescence was also detectable in the GFP channel and generated the impression of dual localization of P5CS:GFP fusion proteins in the cytosol and in chloroplasts (**Supplementary Figures S1B, C**). Additionally, the images show that, despite identical microscope settings, chlorophyll fluorescence intensity in both the green and the red spectral range varied between individual protoplasts. The exclusive detection of both P5CS1:GFP and P5CS2:GFP in the cytosol indicates that sub-functionalization of the two P5CS isoforms in Arabidopsis is not depending on differential subcellular localization.

Homozygous *p5cs2* Mutants Are Impaired in Germination and Seedling Development

To differentiate the roles of P5CS1 and P5CS2 in plant development and their contribution to stress tolerance, we compared single mutants lacking either isoform with wildtype plants under

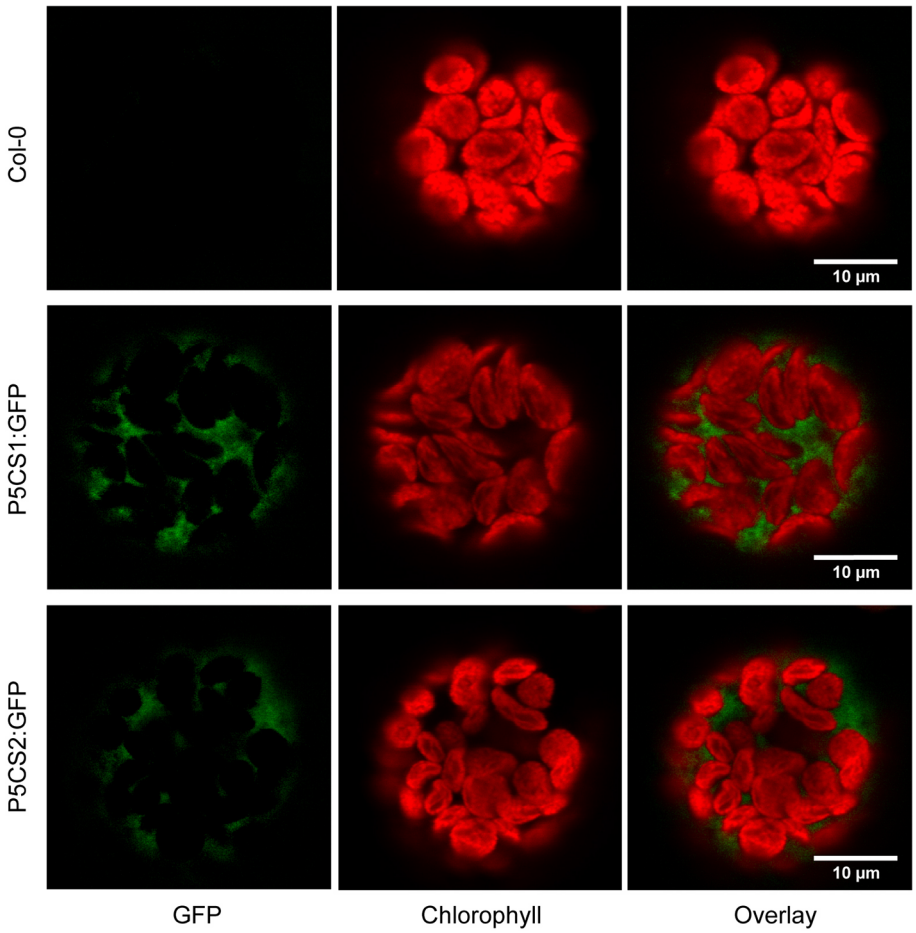

FIGURE 1 | Subcellular localization of P5CS1 and P5CS2. GFP and chlorophyll fluorescence images of mesophyll protoplasts isolated from wildtype and P5CS1:GFP or P5CS2:GFP expressing plants. Spectrally resolved confocal fluorescence images with 20 channels spanning 490 to 668 nm emission wavelength were used for spectral unmixing with GFP and chlorophyll reference spectra. The GFP images and the overlay demonstrate that fluorescence emission from chloroplasts was entirely attributable to chlorophyll, and GFP fluorescence was exclusively detected in the cytosol. Compare with the simulated channel splitting mode images in **Supplementary Figure S1**.

different cultivation conditions. Previous reports have shown that several /*p5cs1*/T-DNA insertion lines are phenotypically equivalent (Székely et al., 2008; Sharma et al., 2011) and therefore we chose to use the representative null-allele *p5cs1-4* for our experiments. Seed viability of two *p5cs2* null-mutants showed strong batch-to-batch variability and on average only 83% (*p5cs2-1*) and 73% (*p5cs2-2*) of the seeds had germinated after 10 d in sterile culture on half-strength Murashige and Skoog (1/2 MS) medium supplemented with 30 mM sucrose, compared to nearly 100% in *p5cs1-4* mutants and the wildtype (**Figure 2A**, **Supplementary Figure S2**). Nearly all wildtype and *p5cs1-4* seeds had germinated after two days, whereas a larger proportion among the seeds of both *p5cs2* mutant lines took three or more days to germinate. The presence of proline in the growth medium had no significant effect on the final proportion of germinated seeds of *p5cs2* mutants (**Figure 2B**, **Supplementary Table S1**). Similarly, application of mild salt stress (50 mM NaCl), which is sufficient to increase the expression of *P5CS1* in seedlings (see **Figure 5**), had no significant effect on germination (**Supplementary Figure S2B**). The presence of 100 mM and 200 mM NaCl in the medium delayed germination in all genotypes. While nearly all wildtype and *p5cs1-4* seeds eventually germinated, only 50% and 25% of the *p5cs2* mutant seeds had germinated after 10 days in the presence of 100 mM and 200 mM NaCl, respectively (**Figures 2C, D**).

In the presence of external proline, nearly all successfully germinated seedlings of all four genotypes developed elongated hypocotyls and green, expanded cotyledons (which we scored as successful seedling establishment). These seedlings continued to grow and developed true leaves later on (**Figure 3**, **Supplementary Figure S2**). Compared to wildtype and *p5cs1* mutant seedlings, development of *p5cs2* mutant seedlings was a few days delayed during this early phase of development even in the presence of external proline. Without external supply of proline, only around 25% of the *p5cs2* mutant seedlings established successfully, despite the presence of

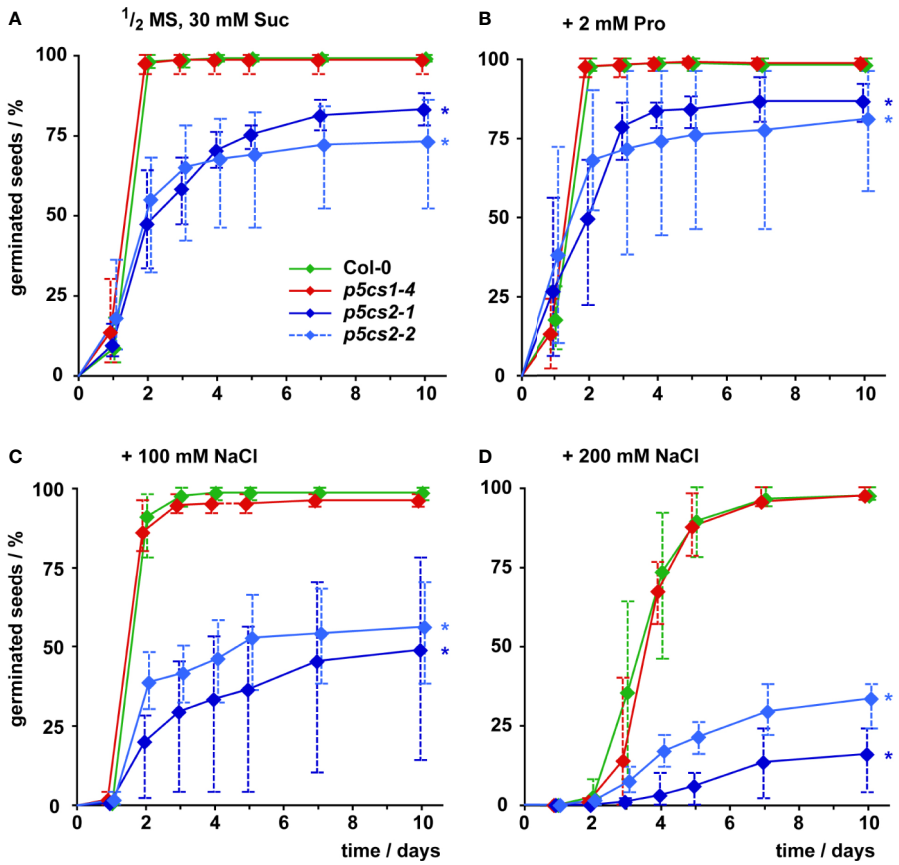

FIGURE 2 | Influence of proline and NaCl on germination of *p5cs1* and *p5cs2* mutants. Germination (scored as radicle protrusion) was followed for 10 days after plating seeds on axenic half-strength MS medium containing 30 mM sucrose (Suc) without supplements **(A)**, supplemented with 2 mM proline **(B)**, 100 mM NaCl **(C)**, or 200 mM NaCl **(D)**. Diamonds represent mean proportions of germinated seeds from 4 batches, consisting of 50 seeds each, from individual parental plants. Whiskers extend to the highest and lowest values in each sample and asterisks indicate values that were significantly different from Col-0 at day 10 ($p < 0.05$ by Fisher's exact test).

30 mM sucrose in the medium to promote germination and development (**Figure 3A**, **Supplementary Figure S2D**). The presence of 50 or 100 mM NaCl in the cultivation medium also significantly increased the proportion of *p5cs2* seedlings that successfully de-etiolated and expanded their cotyledons (**Supplementary Table S1**). At 200 mM NaCl, seedlings of all four genotypes failed to establish (**Supplementary Figure S2D**).

Székely et al. (2008) described enhanced sensitivity of root elongation to NaCl stress in *p5cs1* mutants. Therefore, we also compared the effects of proline, NaCl, or both on root growth of *p5cs2* mutants, wildtype and *p5cs1-4* seedlings (**Figure 4**, **Supplementary Figure S3**, **Supplementary Table S2**). To minimize the influence of differences in establishment, all seedlings were initially germinated in the presence of 2 mM proline and transferred to fresh plates 4 days after sowing. When transferred to plates without external proline, roots of wildtype seedlings and *p5cs1-4* mutants elongated at a nearly linear rate to 8 cm on day 19 after plating (**Figure 4A**). Roots of *p5cs2* mutants continued to grow at the same rate as wildtype and *p5cs1-4* roots for 2 to 3 days, but then nearly completely stopped growing. When the seedlings were transferred to plates containing 2 mM proline, root growth of wildtype and *p5cs1-4* seedlings was reduced to approximately 60%. In contrast, the presence of 2 mM proline stimulated root growth of *p5cs2* mutants resulting in similar rates of root elongation in seedlings of all genotypes (**Figure 4B**). Similarly, supplementing the medium with 100 or 150 mM NaCl stimulated root growth of *p5cs2* mutants, but inhibited root growth of wildtype seedlings and even more of *p5cs1-4* mutants (**Figure 4C**, **Supplementary Figure S3**). The simultaneous supply with 2 mM proline slightly reduced the inhibitory effect of 150 mM NaCl in wildtype plants and /*p5cs1-4*/ mutants (**Figure 4D**).

In summary, both 2 mM proline or 150 mM NaCl had opposite effects on *p5cs2* mutants compared to wildtype plants or *p5cs1* mutants. On medium with 200 mM NaCl, which was lethal during germination (**Supplementary Figure S2D**), some of the transferred seedlings survived, but root growth was very poor in all genotypes (**Supplementary Figure S3**).

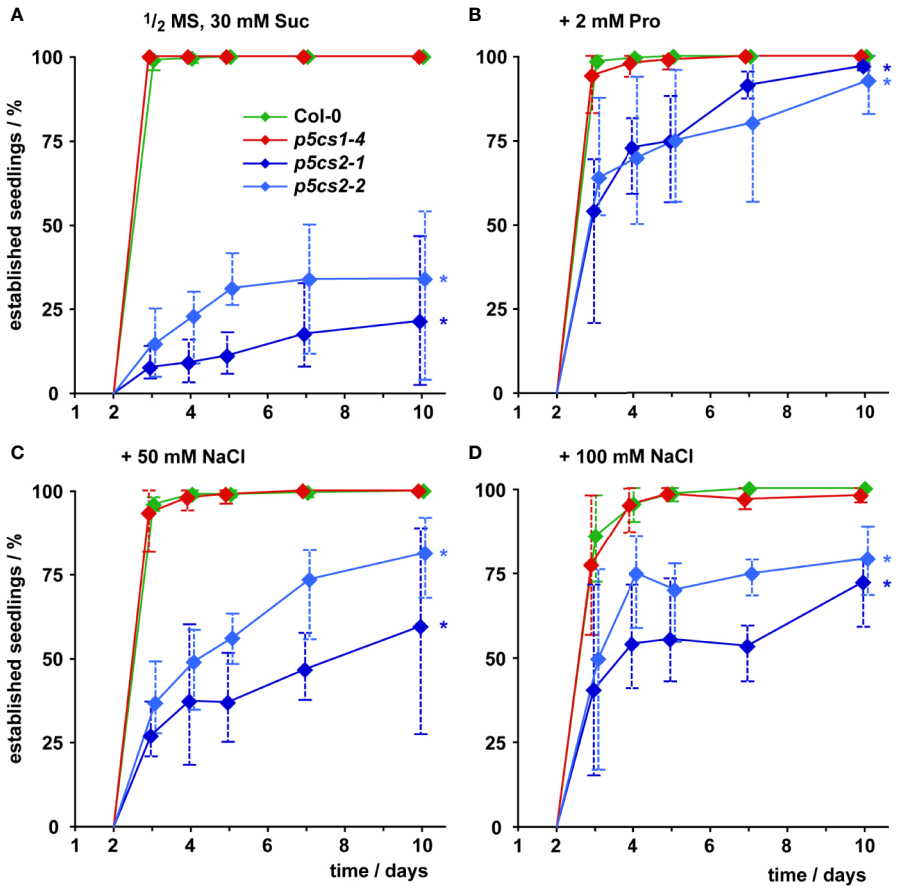

FIGURE 3 | Seedling establishment of *p5cs1* and *p5cs2* mutants. Seedling establishment was determined between 2 and 10 days after plating of seeds on axenic half-strength MS medium containing 30 mM sucrose (Suc, **A**) supplemented with either 2 mM proline (Pro, **B**) or 50 mM **(C)** and 100 mM NaCl **(D)**. Seeds that had not germinated were excluded from the analysis and only seedlings with fully expanded, green cotyledons were scored as "established". Diamonds represent mean proportions of established seedlings among the germinated seeds from 4 batches, consisting of 50 seeds each, from individual parental plants. Whiskers extend to the highest and lowest values in each sample and asterisks indicate values that were significantly different from Col-0 at day 10 ($p < 0.05$ by Fisher's exact test).

The Influence of *p5cs* Mutations on Transcript Levels of Proline Metabolism-Related Genes Is Weak

To determine if a mutation in one isoform of *P5CS* was compensated by altered expression of other enzymes involved in proline metabolism, we compared transcript levels by Northern blot analysis (**Figure 5**). The plants were cultivated for 2 weeks on half-strength MS medium supplemented with 30 mM sucrose and 50 mM NaCl or 2 mM proline. In *p5cs1-4* and *p5cs2-1* mutants, no transcripts of the corresponding genes were detected, while we detected large amounts of aberrant *P5CS2* transcripts in *p5cs2-2* mutants with a 3′UTR-specific probe. As expected, 50 mM NaCl induced *P5CS1* expression and repressed *ProDH1*-expression, but this effect was independent of *p5cs1* or *p5cs2* mutations. *P5CS1* transcript levels did not show differences between wildtype and *p5cs2* mutant seedlings, irrespective of the cultivation conditions. Transcript levels of *ProDH1* showed strong variability in all genotypes and under all conditions, but except for the repression by NaCl, no consistent pattern was detectable across the three repetitions of the experiment (**Supplementary Figure S4**). *P5C dehydrogenase (P5CDH)* reproducibly showed the highest transcript levels in *p5cs2* mutants in the absence of proline or NaCl. This may be a consequence of the developmental arrest during de-etiolation of *p5cs2* mutant seedlings. In none of the conditions and genotypes tested, a strong change in the level of *P5CR* or *Ornithine-δ-aminotransferase (δOAT)* transcripts was observed.

p5cs2 Mutants Are Not Impaired in Defense Against Virulent or Avirulent *Pseudomonas syringae* Strains

In Arabidopsis, *P5CS2* is considered as the "housekeeping" isoform with a prominent contribution to proline biosynthesis in rapidly growing tissues. Additionally, Fabro et al. (2004) reported a specific upregulation of *P5CS2* expression during the hypersensitive response in Arabidopsis leaves after

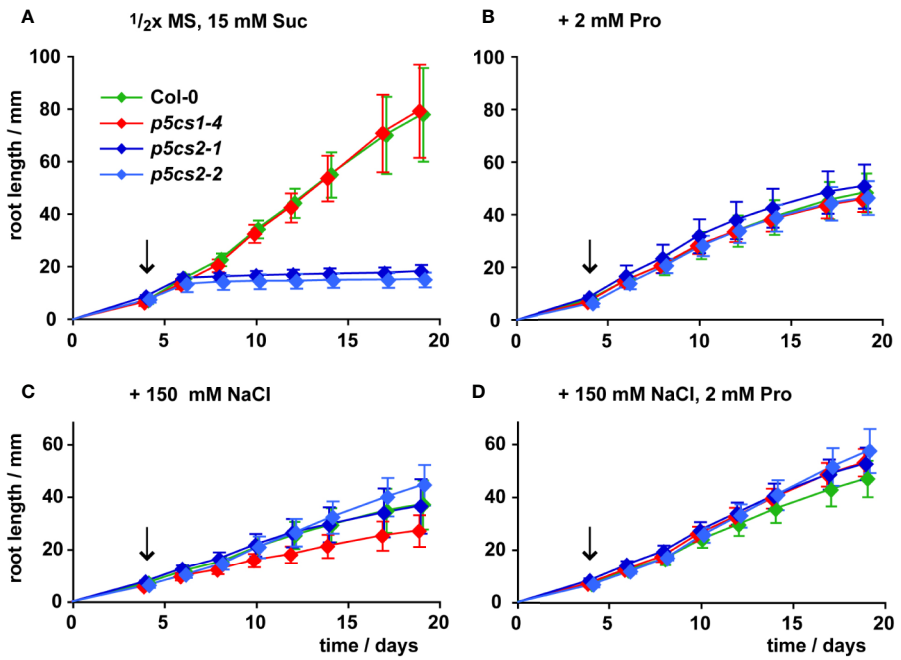

FIGURE 4 | Influence of proline and NaCl on root growth of *p5cs1* and *p5cs2* mutants. Seedlings were pre-cultivated for 4 days on plates with half-strength MS medium supplemented with 15 mM sucrose (Suc) and 2 mM proline (Pro) to support establishment of *p5cs2* mutant seedlings. Then, established seedlings were transferred to vertical plates containing half-strength MS medium with 15 mM Suc without supplements **(A)**, or supplemented with 2 mM Pro **(B)**, 150 mM NaCl **(C)**, or both **(D)**. Arrows indicate time point of seedling transfer, after which root length was monitored for further 15 days. Diamonds represent the mean ± SD of 5 to 10 seedlings per genotype that developed continuously until day 19. The response of *p5cs2* mutants to the individual or combined treatments was significantly different from that of wildtype plants and *p5cs1-4* mutants (**Supplementary Table S2**).

infection with incompatible strains of *Pseudomonas syringae* pv. *tomato*. To test for a contribution of *P5CS1* and *P5CS2* to defense responses, we compared the pathogen susceptibility between wildtype plants and *p5cs1-4* or *p5cs2* mutants. We infected mature leaves of wildtype, *p5cs1-4* and *p5cs2* plants with virulent *P. syringae* DC3000 and with avirulent *P. syringae* DC3000 avrRpm1 (**Supplementary Figure S5**). The virulent bacteria multiplied more than 300-fold during the first two days, whereas the titers of viable bacteria started to decline between day two and day four, when disease symptoms became macroscopically visible. The avirulent, Rpm1-expressing bacteria multiplied less than 100-fold during the first two days and the plants started to show signs of HR-based defense already at that time (data not shown). Although the avirulent bacteria multiplied three to six times between day two and day four, they did not reach the same titers as the virulent bacteria. We did not observe significant differences in the bacterial titer between wildtype plants and *p5cs1-4* or *p5cs2* mutants infected with virulent *P. syringae* DC3000 (**Supplementary Table S3**). The avirulent *P. syringae* DC3000 avrRpm1 reached a slightly higher titer in *p5cs1-4* mutants and a slightly lower cell density in *p5cs2-1* mutant leaves, but in both mutants, the bacterial cell density differed less than a factor of 2 from the one reached in wildtype leaves. Obviously, the lack of *P5CS2* induction in late phases of an infection with avirulent bacteria did not compromise the defense in *p5cs2-1* mutants.

p5cs2 Mutants Are More Tolerant to NaCl Stress Than *p5cs1* Mutants or Wildtype Plants

Since we found no indication of altered susceptibility to bacterial infection in mature *p5cs1-4* and *p5cs2* mutants, we focused on their response to abiotic stress. To induce salt stress, we watered six-week-old plants twice with 300 mM NaCl solution, 4 and 2 days before sampling and analysis. This treatment caused the collapse of the oldest leaves of wildtype and *p5cs1-4* mutant plants and a slight curling and chlorosis of the younger leaves (**Figure 6**). Surprisingly, *p5cs2* mutants showed no visible symptoms of stress. Free proline content of the unstressed control plants was slightly lower in *p5cs2* mutants than in wildtype plants and significantly reduced in *p5cs1-4* mutants (**Figure 7A**, **Supplementary Table S4**). In response to stress, wildtype leaves showed an approximately 30-fold increase in proline content, reaching 16.5 μmol g^{-1} FW. While *p5cs2-1* mutants still reached 8.7 μmol g^{-1} FW, *p5cs1-4* were the least able to induce proline accumulation, reaching only 2.7 μmol g^{-1} FW. To get an idea of the importance of proline accumulation in osmotic adjustment, we determined the osmolality of crude, boiled leaf extracts. Under control conditions, wildtype leaf extract had an osmolality of 303 mOsm and *p5cs1-4* or *p5cs2-1* mutants were not significantly different (**Figure 7B**, **Supplementary Table S4**). After 4 days of NaCl stress, the osmolality increased to 1042 mOsm in wildtype and 1117 mOsm in *p5cs1-4* leaves, while *p5cs2-1* mutant

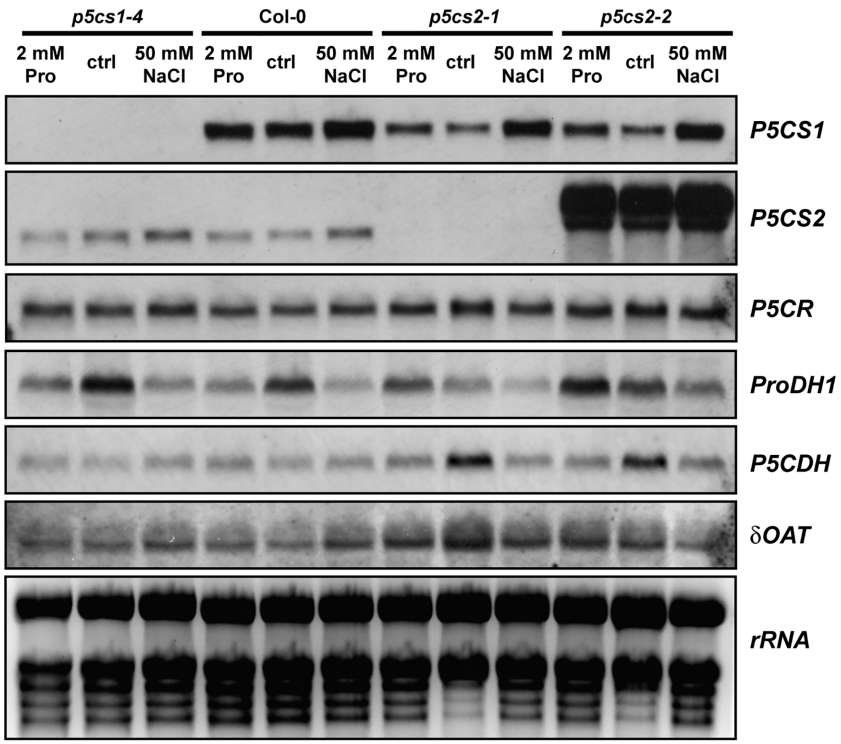

FIGURE 5 | Transcript levels of proline metabolism-related genes. Wildtype (Col-0) seedlings and *p5cs1* or *p5cs2* mutants were harvested after 2 weeks of growth on half-strength MS medium with 30 mM sucrose (ctrl) supplemented with 50 mM NaCl or 2 mM proline (Pro). Total RNA was extracted and subjected to northern blotting by consecutively hybridizing the same membrane with specific probes for the genes indicated to the right of the panels. Ethidium bromide stained *rRNA* is shown as a loading control in the last panel. Two additional sets of Northern blots from independent experiments gave very similar results for all genes except *ProDH1* (See **Supplementary Figure S4**). For full names of the analyzed genes, please refer to the main text.

leaves showed significantly lower values (472 mOsm), demonstrating that the extent of proline accumulation was not correlated to the overall osmotic adjustment.

Since changes in proline content could not account for the large differences in leaf sap osmolality, we analyzed the concentrations of different cations in the leaf sap (**Figure 7C**). In leaf sap of both wildtype and *p5cs1-4* mutant plants, an increase by more than 350 mM Na^+ became evident after 4 days of salt treatment, whereas the Na^+ concentration in *p5cs2-1* leaves did not increase significantly (1.3 mM in control conditions and 7.6 mM in NaCl stressed plants). The other analyzed ions (K^+, Ca^{++} and Mg^{++}) did not show major changes. The sum of all cation concentrations accounted for roughly 50% of the leaf sap osmolality in all three genotypes under both stress and non-stress conditions, indicating that the contribution of uncharged solutes to total osmolality was presumably rather small.

To determine if the brighter color of the stressed wildtype and *p5cs1-4* plants was the result of pigment breakdown, we determined the chlorophyll (Chl) and carotenoid content of the leaves. In the absence of stress, pigment content was indistinguishable between all three genotypes (**Figure 8A** and **Supplementary Table S5**). After stress, leaves of wildtype and *p5cs1-4* plants showed an approximately 20% decrease in total pigment content, whereby the decrease of Chl *a* was more pronounced than Chl *b* or total carotenoids. Consequently, the Chl *a*/Chl *b* ratio was significantly reduced by NaCl stress in wildtype and *p5cs1-4* plants. In accordance with the visual appearance, the total pigment content did not change much in *p5cs2-1* mutant leaves. The slight increase in pigment content per fresh weight in *p5cs2-1* mutants was due to a reduced water content, as evidenced in parallel experiments, in which pigment contents were determined on a dry weight basis from freeze-dried leaves (data not shown).

We also analyzed the effect of NaCl stress and altered pigmentation on the performance of the photosynthetic electron transport by *in vivo* Chl fluorescence imaging (**Figures 8B, C**; **Supplementary Table S6**). Székely et al. (2008) had observed increased production of reactive oxygen species in leaves of NaCl stressed *p5cs1* mutants. Chloroplasts are known as the main source for reactive oxygen species in illuminated plant cells, therefore we wondered if the accumulation of reactive oxygen species in *p5cs1* mutants could be caused by deteriorated photosynthetic electron transport. Since NaCl stress alone induced only minor changes in photosynthetic parameters, we additionally exposed the plants for 1 h to excess light stress (1,000 ± 100 μE) to enhance potential differences in stress tolerance. In the absence of NaCl stress, the photosynthetic electron transport rate (ETR) decreased by

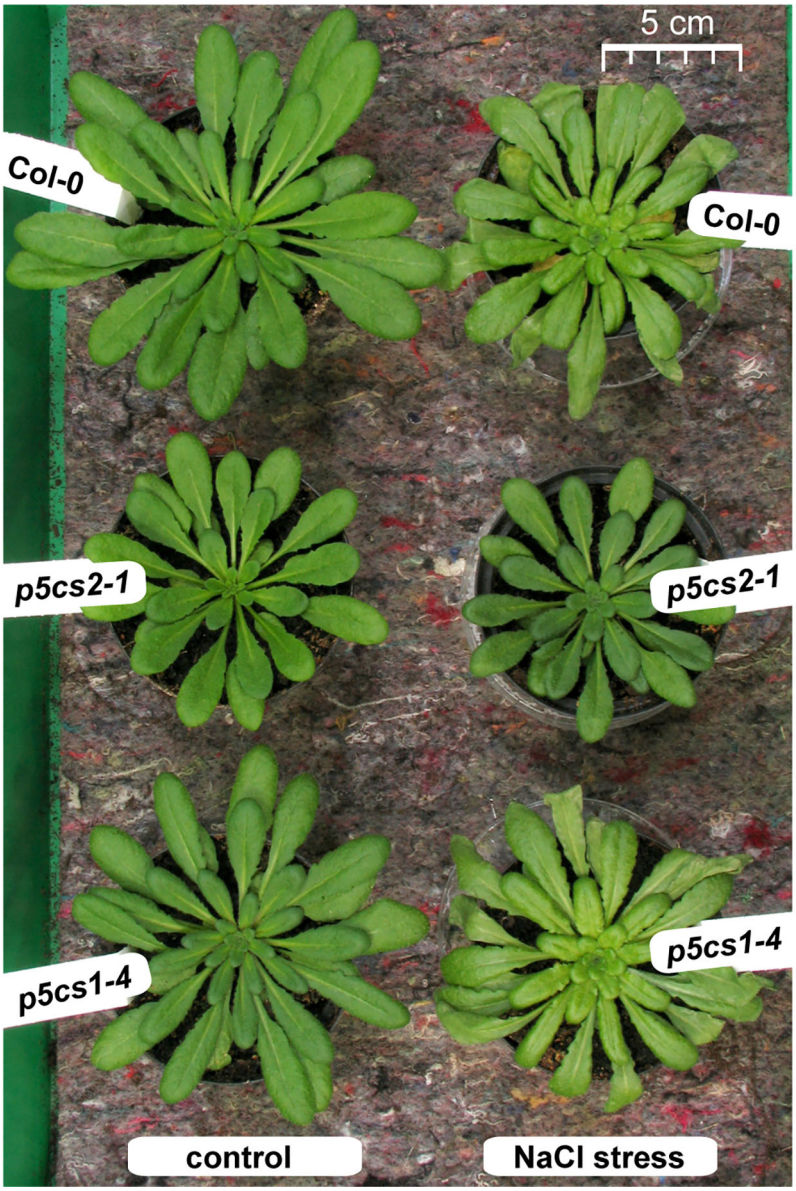

FIGURE 6 | Phenotype of *p5cs* mutant plants after salt stress. Six-week-old plants were stressed 4 and 2 days before the picture was taken with 25 ml per pot of a 300 mM NaCl solution whereas control plants received normal tap water. Note that the left half of the picture with the control plants was already published as **Supplementary Figure S4** in (Funck et al., 2012) to illustrate the reduced rosette size of *p5cs2-1* mutants.

approximately 15% in all lines after light stress (**Figure 8B**). NaCl-stressed plants showed a similar reduction in ETR as light-stressed control plants, whereby *p5cs2-1* plants showed the smallest decrease in ETR. When NaCl-stressed plants were exposed to excess light stress, ETR dropped by 41% and 35% in wildtype and *p5cs1-4* leaves, respectively, whereas the decline in leaves of *p5cs2-1* mutants was only 13%. Absorptivity of photosynthetically active radiation (PAR), the maximum photochemical efficiency of PS II (F_v/F_m) and the photochemical efficiency in the light acclimated state (Φ_{PSII}) showed nearly identical variations as ETR in dependence on genotype and treatment (**Supplementary Figure S6**). Similar results in experiments with *p5cs2-2* mutant plants confirmed the reduced sensitivity of *p5cs2* mutants to combined NaCl and excess light stress. In a minority of the repetitions of the NaCl stress experiment, an increased sensitivity of *p5cs1-4* mutants compared to wildtype plants was observed (data not shown). Overall, the visual appearance, ion and pigment content as well as the analysis of photosynthesis indicated that the tolerance towards NaCl stress was improved in *p5cs2* mutants, rendering them less susceptible to combined NaCl and excess light stress.

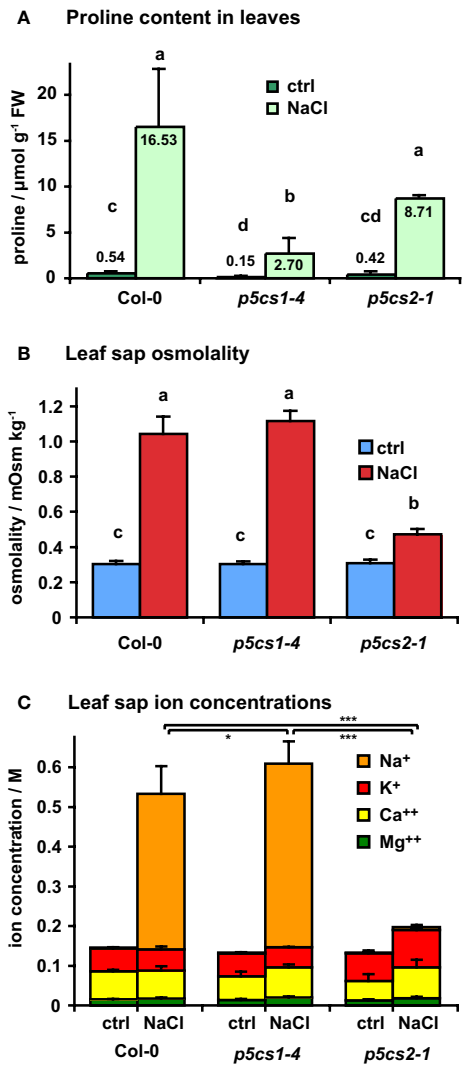

FIGURE 7 | Salt accumulation and osmotic adjustment in *p5cs1* and *p5cs2* mutants. Six-week-old plants were stressed with 300 mM NaCl 4 and 2 days before the analysis of free proline content **(A)**, leaf sap osmolality **(B)**, and leaf sap cation concentrations **(C)**. Bars represent the average +SD of 4 or 5 replicates per condition and genotype. Two-way ANOVA detected significant differences depending on treatment and genotype in all three datasets (**Supplementary Table S4**). Leaf sap osmolality and Na^+ concentrations under NaCl stress were indistinguishable between Col-0 and *p5cs1-4* mutants, but significantly lower in *p5cs2-1* mutants. Different letters above the columns in **(A)** and **(B)** indicate significantly different values ($p < 0.05$). Asterisks in **(C)** indicate significant difference between genotypes under NaCl stress (*, ***: $p < 0.05$ and < 0.001, respectively, see **Supplementary Table S4**).

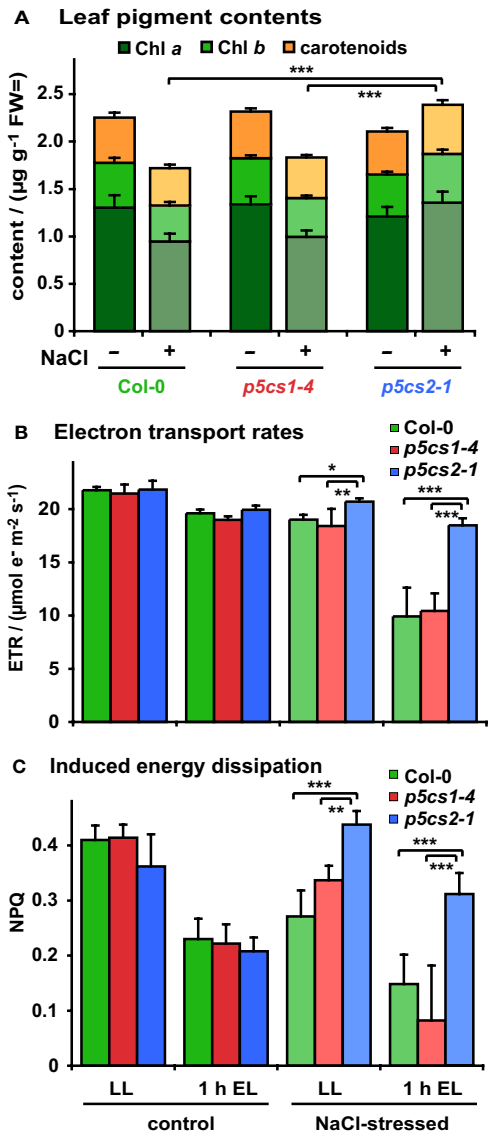

FIGURE 8 | Influence of salt stress and excess light on photosynthetic performance of *p5cs1* and *p5cs2* mutants. Six-week-old plants were stressed with 300 mM NaCl 4 and 2 days before the analysis. **(A)** Pigment content of mature leaves. **(B)** Chlorophyll fluorescence analysis combined with red and near infrared reflection measurements was used to estimate electron transport rates prior to and after 1 h exposure to excess light stress (EL, 1,000 ± 100 µmol photons m^{-2} s^{-1}). **(C)** Inducible energy dissipation (NPQ) measured on the same leaves as in **(B)**. Bars represent the average +SD of 4 or 5 replicates per condition and genotype. ANOVA analysis revealed significant differences depending on treatment, genotype and treatment x genotype interaction in all three data sets (**Supplementary Tables S5**, **S6**). Pairwise comparisons showed that NaCl stress caused reduced pigment contents in Col-0 and *p5cs1-4* mutants, but increased pigment contents in *p5cs2-1* mutants. Both NaCl stress and excess light treatment reduced ETR in all genotypes, but *p5cs2-1* mutants were significantly less affected. Inducible energy dissipation (NPQ) was decreased by NaCl stress and excess light treatment in Col-0 and *p5cs1-4* mutants, but increased by NaCl stress in *p5cs2-1* mutants. Asterisks indicate significant differences between genotypes within one condition (*, **, ***: $p < 0.5$, < 0.01, and < 0.001, respectively).

DISCUSSION

We used Arabidopsis *p5cs1* and *p5cs2* mutants to get a better understanding of the function of proline biosynthesis and accumulation in the stress tolerance of plants. The data presented here demonstrate that the two P5CS isoforms have different functions in stress defense, although both contribute to stress-induced proline accumulation and our results indicate that they

are both localized in the cytosol. P5CS1 activity mediated the major part of proline accumulation, whereas P5CS2 activity was required for normal seedling development and especially root growth under non-stressed conditions. The developmental defects of *p5cs2* mutants were attenuated by external proline or mild salt stress and unexpectedly, the absence of P5CS2 made the plants more tolerant to salt stress and prevented the accumulation of Na^+ ions in the leaves.

By careful spectral analysis of P5CS1:GFP and P5CS2:GFP expressing protoplasts (**Figure 1** and **Supplementary Figure S1B**), we did not find any evidence for chloroplast localization of P5CS1 or P5CS2, as it had been suggested in an earlier report (Székely et al., 2008). In our plants, the GFP fusion constructs consisted of a constitutive promoter and the cDNAs of *P5CS1* or *P5CS2*, whereas Székely et al. (2008) used the endogenous promoters and the full gene sequences. Complementation of *p5cs1-4/p5cs2-1* double mutants by our GFP constructs demonstrated that they confer functional P5CS1 or P5CS2 expression (**Supplementary Figure S1A**). We have previously demonstrated the utility of spectrally resolved fluorescence imaging to resolve ambiguous reports on dual localization of proteins in Arabidopsis (Huber et al., 2019). Especially when the GFP signals are weak and the experimental conditions are likely to influence chlorophyll fluorescence, as *e.g.* during the isolation of protoplasts, classical channel separation cannot efficiently distinguish between the small green component of chlorophyll autofluorescence and true GFP signals. Because Székely et al. (2008) used exclusively wavelength-based separation of GFP and chlorophyll fluorescence, and did not include pictures of wildtype cells, it remains ambiguous if the signals they detected in chloroplasts were true GFP signals. For Arabidopsis, our spectrally deconvoluted confocal images of protoplasts expressing P5CS1:GFP or P5CS2:GFP fusion proteins, together with the exclusively cytosolic localization of P5CR (Funck et al., 2012), strongly indicate that plastids do not contribute to P5CS-mediated proline biosynthesis. Contrasting reports on the subcellular localization of P5CS and P5CR in other plant species underline that this topic requires further attention (Rayapati et al., 1989; Szoke et al., 1992; Murahama et al., 2001; Kim and Nam, 2013).

Previous work had demonstrated that the T-DNA insertions in the two *p5cs2* mutant lines prevent the formation of functional *P5CS2* transcripts and cause conditional embryo lethality, especially when mutant seeds develop side by side with wildtype and heterozygous seeds in the same silique (Székely et al., 2008; Mattioli et al., 2009; Funck et al., 2012). *In vitro* cultivation of immature seeds allowed the rescue of fertile, homozygous *p5cs2* mutants (Funck et al., 2012). The seeds harvested from homozygous *p5cs2* mutants showed strong batch-to-batch variation in vitality, presumably depending on the physiological state of the parent plant (**Figure 2**). On average, seeds from *p5cs2* mutants germinated more slowly than wildtype seeds and the proportion of non-viable seeds was higher, irrespective of the presence of external proline in the medium. After germination, *p5cs2* mutant seedlings frequently failed to de-etiolate and establish vegetative growth in axenic culture in the absence of stress (**Figure 3**). Despite the presence of 15 mM sucrose in our cultivation medium, roots of *p5cs2* mutants barely elongated (**Figure 4**). Previous studies have highlighted the requirement of proline for the stimulation of cell division and growth in the root meristem (Wang et al., 2014; Biancucci et al., 2015). Supplementing the growth medium with 2 or 10 mM proline improved development of *p5cs2* seedlings, demonstrating the predominant role of P5CS2 in providing proline for growth and development. In contrast, external proline inhibited root growth of wildtype and *p5cs1* mutant seedlings. Inhibitory effects of external proline on plants have been described previously and underline the importance of proline homeostasis for optimal growth and development (Bonner et al., 1996; Hellmann et al., 2000; Hare et al., 2002).

An additional function of P5CS2 in defense against an incompatible pathovar of *P. syringae* had been proposed based on the upregulation of *P5CS2* expression in late phases of the hypersensitive defense response (Fabro et al., 2004). Other reports suggested that rather than proline biosynthesis, proline degradation by ProDH and the associated production of reactive oxygen species was important for pathogen defense (Miller et al., 2009; Monteoliva et al., 2014). In our experiments, disease symptoms and pathogen proliferation were very similar in wildtype plants and *p5cs2* or *p5cs1* mutants, irrespective of the use of compatible or incompatible *P. syringae* strains (**Supplementary Figure S5**). Therefore, it appears that *P5CS2* induction and proline accumulation are rather consequences of a HR-based defense than an active part of the defense mechanism.

In contrast to unchanged sensitivity of *p5cs1-4* and *p5cs2-1* mutants to biotic stress, their differential tolerance to abiotic stress, specifically NaCl-induced salt stress, revealed unexpected functions of P5CS2 in stress defense. Confirming previous studies, *p5cs1-4* mutants showed strongly reduced proline accumulation in response to NaCl stress, indicating that P5CS1 mediates the major part of proline accumulation in leaves (**Figure 7A**). P5CS1-mediated proline accumulation had been found to limit the production of reactive oxygen species in leaves and was proposed to provide an energy source (by means of proline transport and degradation) for sustained root growth during osmotic stress (Székely et al., 2008; Sharma et al., 2011). The presence of sucrose as a carbon and energy source in our culture medium may explain why the tolerance of *p5cs1-4* mutants to NaCl stress was only slightly compromised in our sterile culture setup. However, also soil-grown *p5cs1-4* mutants were phenotypically indistinguishable from wildtype plants under non-stressed conditions and despite the strongly reduced proline accumulation, they showed nearly unchanged stress sensitivity in our experiments.

In contrast, loss of *P5CS2* expression in the *p5cs2* mutants impaired their growth under non-stressed conditions, whereas mild salt stress improved seedling development, but not germination, of *p5cs2* mutants similar to the external supply of proline and abolished the differences to wildtype seedlings in root growth (**Figures 3**, **4**). The induction of *P5CS1* expression by NaCl and the resulting increase in proline content probably explain why mild salt stress and external proline both had a positive effect on the development of *p5cs2* seedlings (**Figures 5**, **7**). Northern blot analyses of *p5cs2* mutants grown from mature seeds revealed that *p5cs2-1* contained no detectable transcripts of the 3′-part of the *P5CS2* gene, while *p5cs2-2* mutants contained increased levels of aberrant, longer transcripts (**Figure 5**). These

are presumably hybrid molecules with the 5′-end derived from the T-DNA inserted in the second exon of *P5CS2*. Both *p5cs2* mutant lines showed a similar increase of *P5CS1* transcript levels in response to NaCl treatment as wildtype seedlings. *Vice versa*, the expression of *P5CS2* was unaffected by the mutation in *p5cs1-4*, indicating little or no crosstalk or feedback in the regulation of expression of the two *P5CS* genes. The changes in transcript levels of other proline metabolism-related genes in response to NaCl or external proline also were very similar to wildtype plants in both *p5cs1* and *p5cs2* mutants.

Analyzing the rosettes of mature, soil grown plants, we found no consistent evidence for a contribution of *P5CS1* to the tolerance towards short-term salt stress, although in a subset of the experiments, *p5cs1-4* mutant plants were more severely affected by the stress treatment. Overall, NaCl accumulation, pigment loss and inhibition of photosynthetic electron transport were not significantly different between wildtype plants and *p5cs1-4* mutants, despite the strongly reduced proline accumulation in *p5cs1-4* mutants (**Figures 7**, **8**, **Supplementary Figure S6**). Notably, the reduced proline content did not result in an altered osmolality of crude leaf extracts from *p5cs1-4* mutants (**Figure 7B**), supporting previous estimations that the function of proline accumulation cannot be primarily the osmotic adjustment during stress (Hare and Cress, 1997; Forlani et al., 2019b). However, partitioning studies indicated that the predominant accumulation of proline in the cytosol and in chloroplasts of osmotically stressed potato leaves and in salt-stressed sugar beet may account for a relevant osmotic function of proline in these compartments (Büssis and Heineke, 1998; Hossain et al., 2017). Compartment-specific metabolite analyses in cold-stressed or high-light-exposed Arabidopsis rosettes confirmed that the distribution of proline within the cells changes in response to stress and is additionally dependent on changes in carbon metabolism (Fürtauer et al., 2016; Hörmiller et al., 2017; Küstner et al., 2019). Genetically encoded nanosensors for *in vivo* analysis of proline concentrations and osmotic potential, as they are already available for other amino acids and the subcellular redox potential, will need to be developed and used to determine the precise contribution of proline to osmotic adjustment (Bogner and Ludewig, 2007; Schwarzländer et al., 2016; Sanford and Palmer, 2017).

In sharp contrast to *p5cs1-4* mutants, soil-grown *p5cs2-1* mutant plants were much more tolerant to NaCl stress. Leaves of NaCl-treated *p5cs2-1* mutants showed no reduction in pigment content or photosynthetic electron transport (**Figure 8** and **Supplementary Figure S6**). This observation undermines the prevailing dogma that an increased content of compatible solutes is a direct measure and cause of stress tolerance, because proline accumulation was intermediate in *p5cs2-1* mutants compared to wildtype plants and *p5cs1-4* mutants. Stress perception was obviously not affected, since *p5cs2* mutants showed a similar degree of *P5CS1* induction as wildtype plants (**Figure 5**). The relative increase in proline content in *p5cs2-1* mutants (21-fold) was also intermediate between *p5cs1-4* mutants (19-fold) and wildtype plants (31-fold). Thus, other factors than overall proline synthesis or content must be the reason for the reduced stress sensitivity of *p5cs2-1* mutants.

The most striking difference between wildtype plants and *p5cs1-4* mutants on the one side and *p5cs2-1* mutants on the other side was observed in the osmolality and ion concentrations of crude leaf extracts after treatment with NaCl (**Figures 7B, C**). Wildtype plants and *p5cs1-4* mutants accumulated 390 and 460 mM Na^+, respectively, in the leaves, whereas in leaves of *p5cs2-1* mutants the Na^+ concentrations was not elevated. The largely unchanged levels of the other analyzed cations (K^+, Ca^{++}, Mg^{++}) indicated that the stress symptoms observed in the leaves were mainly caused by osmotic effects or by toxicity of high Na^+, and presumably also Cl^-, concentrations. The presence of large amounts of Na^+ ions in the rosettes of wildtype plants and *p5cs1-4* mutants after application of salt solution to the soil demonstrated that Na^+ entered the roots and was efficiently transferred to the shoot. The mutation of *P5CS2* prevented the accumulation of Na^+ in the leaves or delayed it beyond the time of our analyses and thereby protected the *p5cs2-1* mutants from Na^+ toxicity.

As in many previous reports, especially on the genetic engineering of stress tolerance, the increased resistance of *p5cs2-1* mutant plants comes at the cost of reduced growth under non-stress conditions (Lawlor, 2013). We propose that three factors can, individually or in combination, explain the reduced salt accumulation and thus increased tolerance of *p5cs2* mutants and these hypotheses can be tested in future experiments: First, the smaller rosettes of *p5cs2* mutants (Funck et al., 2012) could result in lower transpiration rates and consequently a reduced uptake of water and solutes from the soil. Second, the shorter roots of *p5cs2* mutants under non-stressed conditions provide a lower contact area to the substrate with a reduced absolute number of membrane proteins, through which Na^+ ions can enter the root cells. Third, the reduced proline synthesis and content especially in the meristematic tissue of the root tips, where *P5CS2* is predominantly expressed in wildtype plants (Székely et al., 2008), could pre-adapt the *p5cs2* mutants to prevent excessive Na^+ uptake or transfer to the leaves. This could be achieved by increased expression of Na^+/H^+ antiporters like SOS1 and NHX1 or by limiting the entry of Na^+ into the xylem by increased HKT1 expression (Zhang and Shi, 2013). Our preliminary analyses gave inconsistent results for the regulation of these genes in roots of *p5cs2-1* mutants. Future experiments will additionally show whether temporally or spatially confined suppression of *P5CS2* expression can be used to enhance salt tolerance without compromising plant productivity and fitness under non-stressful conditions.

DATA AVAILABILITY STATEMENT

The raw data supporting the conclusions of this article will be made available by the authors, without undue reservation.

AUTHOR CONTRIBUTIONS

DF designed the study, performed or supervised the majority of the experiments, and wrote the initial version of the manuscript. LB and LS performed the analyses of stressed plants. NvW performed the ion quantifications. MS contributed to the experimental design and the statistical analyses. All authors contributed to the article and approved the submitted version.

FUNDING

This work was funded by the Excellence Initiative of the University of Konstanz (Young Scholar Fund). LS received a fellowship from the Heinz Böckler Foundation (390471).

ACKNOWLEDGMENTS

We would like to thank Silvia Kuhn, Roswitha Miller and Susanne Reiner for technical assistance in the lab and the gardeners of the University of Konstanz for excellent plant care. We thank Martin Stöckl and the Bioimaging Centre of the University of Konstanz for help with spectrally resolved confocal microscopy. LS received a fellowship from the Heinz-Böckler Stiftung for her PhD project. We are especially grateful to Iwona Adamska and the University of Konstanz for the long-standing support of this project.

SUPPLEMENTARY MATERIAL

The Supplementary Material for this article can be found online at: https://www.frontiersin.org/articles/10.3389/fpls.2020.565134/full#supplementary-material

REFERENCES

Agarwal, P. K., Shukla, P. S., Gupta, K., and Jha, B. (2013). Bioengineering for salinity tolerance in plants: state of the art. *Mol. Biotechnol.* 54 (1), 102–123. doi: 10.1007/s12033-012-9538-3

Ayliffe, M. A., Roberts, J. K., Mitchell, H. J., Zhang, R., Lawrence, G. J., Ellis, J. G., et al. (2002). A plant gene up-regulated at rust infection sites. *Plant Physiol.* 129 (1), 169–180. doi: 10.1104/pp.010940

Bates, L. S., Waldren, R. P., and Teare, I. D. (1973). Rapid determination of free proline for water-stress studies. *Plant Soil* 39 (1), 205. doi: 10.1007/BF00018060

Bates, D., Mächler, M., Bolker, B., and Walker, S. (2015). Fitting linear mixed-effects models using lme4. *J. Stat. Software* 1 (1), 1–48. doi: 10.18637/jss.v067.i01

Biancucci, M., Mattioli, R., Moubayidin, L., Sabatini, S., Costantino, P., and Trovato, M. (2015). Proline affects the size of the root meristematic zone in Arabidopsis. *BMC Plant Biol.* 15, 263. doi: 10.1186/s12870-015-0637-8

Bogner, M., and Ludewig, U. (2007). Visualization of arginine influx into plant cells using a specific FRET-sensor. *J. Fluoresc.* 17 (4), 350–360. doi: 10.1007/s10895-007-0192-2

Bonner, C. A., Williams, D. S., Aldrich, H. C., and Jensen, R. A. (1996). Antagonism by L-glutamine of toxicity and growth inhibition caused by other amino acids in suspension cultures of *Nicotiana silvestris*. *Plant Sci.* 113 (1), 43–58. doi: 10.1016/0168-9452(95)04284-9

Büssis, D., and Heineke, D. (1998). Acclimation of potato plants to polyethylene glycol-induced water deficit II. Contents and subcellular distribution of organic solutes. *J. Exp. Bot.* 49 (325), 1361–1370. doi: 10.1093/jxb/49.325.1361

Cecchini, N. M., Monteoliva, M. I., and Alvarez, M. E. (2011). Proline dehydrogenase contributes to pathogen defense in Arabidopsis. *Plant Physiol.* 155 (4), 1947–1959. doi: 10.1104/pp.110.167163

Clough, S. J., and Bent, A. F. (1998). Floral dip: a simplified method for *Agrobacterium*-mediated transformation of *Arabidopsis thaliana*. *Plant J.* 16 (6), 735–743. doi: 10.1046/j.1365-313x.1998.00343.x

Debener, T., Lehnackers, H., Arnold, M., and Dangl, J. L. (1991). Identification and molecular mapping of a single *Arabidopsis thaliana* locus determining resistance to a phytopathogenic *Pseudomonas syringae* isolate. *Plant J.* 1 (3), 289–302. doi: 10.1046/j.1365-313X.1991.t01-7-00999.x

Deuschle, K., Funck, D., Forlani, G., Stransky, H., Biehl, A., Leister, D., et al. (2004). The role of δ^1-pyrroline-5-carboxylate dehydrogenase in proline degradation. *Plant Cell* 16 (12), 3413–3425. doi: 10.1105/tpc.104.023622

Fabro, G., Kovacs, I., Pavet, V., Szabados, L., and Alvarez, M. E. (2004). Proline accumulation and *AtP5CS2* gene activation are induced by plant-pathogen incompatible interactions in Arabidopsis. *Mol. Plant Microbe Interact.* 17 (4), 343–350. doi: 10.1094/MPMI.2004.17.4.343

Forlani, G., Bertazzini, M., and Cagnano, G. (2019a). Stress-driven increase in proline levels, and not proline levels themselves, correlates with the ability to withstand excess salt in a group of 17 Italian rice genotypes. *Plant Biol. (Stuttg)* 21 (2), 336–342. doi: 10.1111/plb.12916

Forlani, G., Trovato, M., Funck, D., and Signorelli, S. (2019b). "Regulation of Proline Accumulation and Its Molecular and Physiological Functions in Stress Defence," in *Osmoprotectant-Mediated Abiotic Stress Tolerance in Plants: Recent Advances and Future Perspectives*. Eds. M. A. Hossain, V. Kumar, D. J. Burritt, M. Fujita and P. S. A. Mäkelä (Cham: Springer International Publishing), 73–97. doi: 10.1007/978-3-030-27423-8_3

Funck, D., Stadelhofer, B., and Koch, W. (2008). Ornithine-δ-aminotransferase is essential for arginine catabolism but not for proline biosynthesis. *BMC Plant Biol.* 8, 40. doi: 10.1186/1471-2229-8-40

Funck, D., Eckard, S., and Müller, G. (2010). Non-redundant functions of two proline dehydrogenase isoforms in Arabidopsis. *BMC Plant Biol.* 10, 70. doi: 10.1186/1471-2229-10-70

Funck, D., Winter, G., Baumgarten, L., and Forlani, G. (2012). Requirement of proline synthesis during Arabidopsis reproductive development. *BMC Plant Biol.* 12, 191. doi: 10.1186/1471-2229-12-191

Fürtauer, L., Weckwerth, W., and Nägele, T. (2016). A benchtop fractionation procedure for subcellular analysis of the plant metabolome. *Front. Plant Sci.* 7, 1912. doi: 10.3389/fpls.2016.01912

Giberti, S., Funck, D., and Forlani, G. (2014). Δ^1-Pyrroline-5-carboxylate reductase from Arabidopsis thaliana: stimulation or inhibition by chloride ions and feedback regulation by proline depend on whether NADPH or NADH acts as co-substrate. *New Phytol.* 202 (3), 911–919. doi: 10.1111/nph.12701

Grefen, C., Donald, N., Hashimoto, K., Kudla, J., Schumacher, K., and Blatt, M. R. (2010). A ubiquitin-10 promoter-based vector set for fluorescent protein tagging facilitates temporal stability and native protein distribution in transient and stable expression studies. *Plant J.* 64 (2), 355–365. doi: 10.1111/j.1365-313X.2010.04322.x

Gruber, B. D., Giehl, R. F., Friedel, S., and von Wiren, N. (2013). Plasticity of the Arabidopsis root system under nutrient deficiencies. *Plant Physiol.* 163 (1), 161–179. doi: 10.1104/pp.113.218453

Hare, P. D., and Cress, W. A. (1997). Metabolic implications of stress-induced proline accumulation in plants. *Plant Growth Regul.* 21 (2), 79–102. doi: 10.1023/A:1005703923347

Hare, P. D., Cress, W. A., and van Staden, J. (2002). Disruptive effects of exogenous proline on chloroplast and mitochondrial ultrastructure in Arabidopsis leaves. *S. Afr. J. Bot.* 68 (3), 393–396. doi: 10.1016/S0254-6299(15)30405-1

Hellmann, H., Funck, D., Rentsch, D., and Frommer, W. B. (2000). Hypersensitivity of an Arabidopsis sugar signaling mutant toward exogenous proline application. *Plant Physiol.* 123 (2), 779–789. doi: 10.1104/pp.123.2.779

Hildebrandt, T. M. (2018). Synthesis versus degradation: directions of amino acid metabolism during Arabidopsis abiotic stress response. *Plant Mol. Biol.* 98 (1-2), 121–135. doi: 10.1007/s11103-018-0767-0

Hörmiller, I. I., Nägele, T., Augustin, H., Stutz, S., Weckwerth, W., and Heyer, A. G. (2017). Subcellular reprogramming of metabolism during cold acclimation in *Arabidopsis thaliana*. *Plant Cell Environ.* 40 (5), 602–610. doi: 10.1111/pce.12836

Hossain, M. S., Persicke, M., ElSayed, A. I., Kalinowski, J., and Dietz, K. J. (2017). Metabolite profiling at the cellular and subcellular level reveals metabolites associated with salinity tolerance in sugar beet. *J. Exp. Bot.* 68 (21-22), 5961–5976. doi: 10.1093/jxb/erx388

Hothorn, T., Bretz, F., and Westfall, P. (2008). Simultaneous inference in general parametric models. *Biom. J.* 50 (3), 346–363. doi: 10.1002/bimj.200810425

Huber, C. V., Jakobs, B. D., Mishra, L. S., Niedermaier, S., Stift, M., Winter, G., et al. (2019). DEG10 contributes to mitochondrial proteostasis, root growth, and seed yield in Arabidopsis. *J. Exp. Bot.* 70 (19), 5423–5436. doi: 10.1093/jxb/erz294

Kavi Kishor, P. B., and Sreenivasulu, N. (2014). Is proline accumulation per se correlated with stress tolerance or is proline homeostasis a more critical issue? *Plant Cell Environ.* 37 (2), 300–311. doi: 10.1111/pce.12157

Kim, G.-B., and Nam, Y.-W. (2013). A novel Δ^1-pyrroline-5-carboxylate synthetase gene of *Medicago truncatula* plays a predominant role in stress-induced proline accumulation during symbiotic nitrogen fixation. *J. Plant Physiol.* 170 (3), 291–302. doi: 10.1016/j.jplph.2012.10.004

Küstner, L., Fürtauer, L., Weckwerth, W., Nägele, T., and Heyer, A. G. (2019). Subcellular dynamics of proteins and metabolites under abiotic stress reveal deferred response of the *Arabidopsis thaliana* hexokinase-1 mutant *gin2-1* to high light. *Plant J.* 100 (3), 456–472. doi: 10.1111/tpj.14491

Lawlor, D. W. (2013). Genetic engineering to improve plant performance under drought: physiological evaluation of achievements, limitations, and possibilities. *J. Exp. Bot.* 64 (1), 83–108. doi: 10.1093/jxb/ers326

Liang, X., Zhang, L., Natarajan, S. K., and Becker, D. F. (2013). Proline mechanisms of stress survival. *Antioxid. Redox Signal.* 19 (9), 998–1011. doi: 10.1089/ars.2012.5074

Liang, W., Ma, X., Wan, P., and Liu, L. (2018). Plant salt-tolerance mechanism: A review. *Biochem. Biophys. Res. Commun.* 495 (1), 286–291. doi: 10.1016/j.bbrc.2017.11.043

Lichtenthaler, H. K. (1987). "Chlorophylls and carotenoids: Pigments of photosynthetic biomembranes," in *Methods Enzymol.* Eds. L. Packer and R. Douce (Cambridge, MA: Academic Press), 350. doi: 10.1016/0076-6879(87)48036-1

Mattioli, R., Falasca, G., Sabatini, S., Altamura, M. M., Costantino, P., and Trovato, M. (2009). The proline biosynthetic genes *P5CS1* and *P5CS2* play overlapping roles in Arabidopsis flower transition but not in embryo development. *Physiol. Plant* 137 (1), 72–85. doi: 10.1111/j.1399-3054.2009.01261.x

Mattioli, R., Biancucci, M., Lonoce, C., Costantino, P., and Trovato, M. (2012). Proline is required for male gametophyte development in Arabidopsis. *BMC Plant Biol.* 12, 236. doi: 10.1186/1471-2229-12-236

Mattioli, R., Biancucci, M., El Shall, A., Mosca, L., Costantino, P., Funck, D., et al. (2018). Proline synthesis in developing microspores is required for pollen development and fertility. *BMC Plant Biol.* 18 (1), 356. doi: 10.1186/s12870-018-1571-3

Miller, G., Honig, A., Stein, H., Suzuki, N., Mittler, R., and Zilberstein, A. (2009). Unraveling δ^1-pyrroline-5-carboxylate-proline cycle in plants by uncoupled expression of proline oxidation enzymes. *J. Biol. Chem.* 284 (39), 26482–26492. doi: 10.1074/jbc.M109.009340

Mitchell, H. J., Ayliffe, M. A., Rashid, K. Y., and Pryor, A. J. (2006). A rust-inducible gene from flax (*fis1*) is involved in proline catabolism. *Planta* 223 (2), 213–222. doi: 10.1007/s00425-005-0079-x

Monteoliva, M. I., Rizzi, Y. S., Cecchini, N. M., Hajirezaei, M. R., and Alvarez, M. E. (2014). Context of action of proline dehydrogenase (ProDH) in the hypersensitive response of Arabidopsis. *BMC Plant Biol.* 14 (1), 21. doi: 10.1186/1471-2229-14-21

Munns, R., and Tester, M. (2008). Mechanisms of salinity tolerance. *Annu. Rev. Plant Biol.* 59, 651–681. doi: 10.1146/annurev.arplant.59.032607.092911

Murahama, M., Yoshida, T., Hayashi, F., Ichino, T., Sanada, Y., and Wada, K. (2001). Purification and characterization of Δ^1-pyrroline-5-carboxylate reductase isoenzymes, indicating differential distribution in spinach (*Spinacia oleracea* L.) leaves. *Plant Cell Physiol.* 42 (7), 742–750. doi: 10.1093/pcp/pce093

R core team (2020). *R: A language and environment for statistical computing* (Vienna, Austria: R Foundation for Statistical Computing). Available at: https://www.R-project.org/. Downloaded 2020-03-27.

Rayapati, P. J., Stewart, C. R., and Hack, E. (1989). Pyrroline-5-carboxylate reductase is in pea (*Pisum sativum* L.) leaf chloroplasts. *Plant Physiol.* 91 (2), 581–586. doi: 10.1104/pp.91.2.581

Sanford, L., and Palmer, A. (2017). "Recent advances in development of genetically encoded fluorescent sensors," in *Methods Enzymol.* Eds. R. B. Thompson and C. A. Fierke (San Diego: Academic Press), 1–49. doi: 10.1016/bs.mie.2017.01.019

Schwarzländer, M., Dick, T. P., Meyer, A. J., and Morgan, B. (2016). Dissecting redox biology using fluorescent protein sensors. *Antioxid. Redox Signal.* 24 (13), 680–712. doi: 10.1089/ars.2015.6266

Sharma, S., Villamor, J. G., and Verslues, P. E. (2011). Essential role of tissue-specific proline synthesis and catabolism in growth and redox balance at low water potential. *Plant Physiol.* 157 (1), 292–304. doi: 10.1104/pp.111.183210

Strizhov, N., Ábrahám, E., Ökrész, L., Blickling, S., Zilberstein, A., Schell, J., et al. (1997). Differential expression of two *P5CS* genes controlling proline accumulation during salt-stress requires ABA and is regulated by ABA1, ABI1 and AXR2 in Arabidopsis. *Plant J.* 12 (3), 557–569. doi: 10.1046/j.1365-313x.1997.00557.x

Szabados, L., and Savoure, A. (2010). Proline: a multifunctional amino acid. *Trends Plant Sci.* 15 (2), 89–97. doi: 10.1016/j.tplants.2009.11.009

Székely, G., Ábrahám, E., Cséplő, A., Rigó, G., Zsigmond, L., Csiszár, J., et al. (2008). Duplicated *P5CS* genes of Arabidopsis play distinct roles in stress regulation and developmental control of proline biosynthesis. *Plant J.* 53 (1), 11–28. doi: 10.1111/j.1365-313X.2007.03318.x

Szoke, A., Miao, G. H., Hong, Z., and Verma, D. P. (1992). Subcellular location of δ^1-pyrroline-5-carboxylate reductase in root/nodule and leaf of soybean. *Plant Physiol.* 99 (4), 1642–1649. doi: 10.1104/pp.99.4.1642

Trovato, M., Forlani, G., Signorelli, S., and Funck, D. (2019). "Proline metabolism and its functions in development and stress tolerance," in *Osmoprotectant-Mediated Abiotic Stress Tolerance in Plants: Recent Advances and Future Perspectives*. Eds. M. A. Hossain, V. Kumar, D. J. Burritt, M. Fujita and P. S. A. Mäkelä (Cham: Springer International Publishing), 41–72. doi: 10.1007/978-3-030-27423-8_2

Turchetto-Zolet, A. C., Margis-Pinheiro, M., and Margis, R. (2009). The evolution of pyrroline-5-carboxylate synthase in plants: a key enzyme in proline synthesis. *Mol. Genet. Genomics* 281 (1), 87–97. doi: 10.1007/s00438-008-0396-4

Wang, G., Zhang, J., Wang, G., Fan, X., Sun, X., Qin, H., et al. (2014). Proline responding1 plays a critical role in regulating general protein synthesis and the cell cycle in Maize. *Plant Cell* 26 (6), 2582–2600. doi: 10.1105/tpc.114.125559

Zaiontz, C. (2020). *Real statistics resource pack Release 6.8*. (Charles Zaiontz). Available at: www.real-statistics.com, Downloaded 2020-03-27.

Zhang, J. L., and Shi, H. (2013). Physiological and molecular mechanisms of plant salt tolerance. *Photosyn. Res.* 115 (1), 1–22. doi: 10.1007/s11120-013-9813-6

Zörb, C., Geilfus, C. M., and Dietz, K. J. (2019). Salinity and crop yield. *Plant Biol. (Stuttg)* 21 (Suppl 1), 31–38. doi: 10.1111/plb.12884

Zouari, M., Hassena, A. B., Trabelsi, L., Rouina, B. B., Decou, R., and Labrousse, P. (2019). "Exogenous proline-mediated abiotic stress tolerance in plants: Possible mechanisms," in *Osmoprotectant-Mediated Abiotic Stress Tolerance in Plants: Recent Advances and Future Perspectives*. Eds. M. A. Hossain, V. Kumar, D. J. Burritt, M. Fujita and P. S. A. Mäkelä (Cham: Springer International Publishing), 99–121. doi: 10.1007/978-3-030-27423-8_4

Conflict of Interest: The authors declare that the research was conducted in the absence of any commercial or financial relationships that could be construed as a potential conflict of interest.

Copyright © 2020 Funck, Baumgarten, Stift, von Wirén and Schönemann. This is an open-access article distributed under the terms of the Creative Commons Attribution License (CC BY). The use, distribution or reproduction in other forums is permitted, provided the original author(s) and the copyright owner(s) are credited and that the original publication in this journal is cited, in accordance with accepted academic practice. No use, distribution or reproduction is permitted which does not comply with these terms.

frontiers in Plant Science

ORIGINAL RESEARCH
published: 22 October 2020
doi: 10.3389/fpls.2020.582026

A Specific and Sensitive Enzymatic Assay for the Quantitation of L-Proline

Giuseppe Forlani[1] and Dietmar Funck[2]*

[1] Department of Life Science and Biotechnology, University of Ferrara, Ferrara, Italy, [2] Laboratory of Plant Physiology and Biochemistry, Department of Biology, University of Konstanz, Konstanz, Germany

Because proline accumulates rapidly in response to several stress conditions such as drought and excess salt, increased intracellular levels of free proline are considered a hallmark of adaptive reactions in plants, particularly in response to water stress. Proline quantitation is easily achievable by reaction with ninhydrin, since under acidic conditions peculiar red or yellow reaction products form with this unique cyclic amino acid. However, little attention has been paid to date to cross-reaction of ninhydrin with other amino acids at high levels, or with structurally related compounds that may also be present at significant concentrations in plant tissues, possibly leading to proline overestimation. *In vitro* at high pH values, δ^1-pyrroline-5-carboxylate reductase, the enzyme catalyzing the second and last step in proline synthesis from glutamate, was early found to catalyze the reverse oxidation of proline with the concomitant reduction of $NAD(P)^+$ to NAD(P)H. Here we characterized this reverse reaction using recombinant enzymes from *Arabidopsis thaliana* and *Oryza sativa*, and demonstrated its utility for the specific quantification of L-proline. By optimizing the reaction conditions, fast, easy, and reproducible measurement of L-proline concentration was achieved, with similar sensitivity but higher specificity than the commonly used ninhydrin methods.

Keywords: proline measurement, chemical assay, enzymatic assay, specificity, sensitivity

OPEN ACCESS

Edited by:
Omar Borsani,
Universidad de la República, Uruguay

Reviewed by:
László Szabados,
Biological Research Centre,
Hungarian Academy of Sciences (MTA), Hungary
Maria Grazia Annunziata,
Max Planck Institute of Molecular Plant Physiology, Germany

****Correspondence:***
Giuseppe Forlani
flg@unife.it

Specialty section:
This article was submitted to Plant Abiotic Stress, a section of the journal Frontiers in Plant Science

Received: *10 July 2020*
Accepted: *30 September 2020*
Published: *22 October 2020*

Citation:
Forlani G and Funck D (2020) A Specific and Sensitive Enzymatic Assay for the Quantitation of L-Proline. Front. Plant Sci. 11:582026. doi: 10.3389/fpls.2020.582026

INTRODUCTION

Water stress tolerance is in the focus of many research projects and also a major goal for plant breeding to secure crop productivity in the face of ongoing climate change (Ahanger et al., 2017). Accumulation of free proline (this term referring to the L-isomer, if not specified otherwise) is a common response of plants to diverse stress factors, mainly drought and high salinity, but also to cold or pathogen attack (Hayat et al., 2012). Therefore, rapid and cost-efficient assays to determine tissue proline content are useful to monitor plant stress responses or to assess stress tolerance. Chinard (1952) reported that at approximately pH 1.0 ninhydrin reacts with only a few amino acids, and that this reaction can be used to quantify proline, ornithine, lysine, and hydroxylysine in pure solution. Later on, a modification of this method was described in which lysine and hydroxylysine do not react (Bates et al., 1973), establishing a quick assay for proline in plant extracts that has become the most widely adopted reference method (cited by more than 12,000 articles) and is used with minor modifications until today. This assay takes advantage of the formation of a red, hydrophobic reaction product from proline and ninhydrin at very low pH and high temperature (100°C), while all other proteinogenic amino acids produce little or no color. Extraction of the reaction product with toluene avoids interference from hydrophilic red plant pigments like anthocyanins, but constitutes an additional, potentially harmful handling step that produces toxic waste. Moreover ornithine, an intermediate in the synthesis and degradation of

arginine (Winter et al., 2015), reacts under these conditions with the same efficiency, and some other amino acids like glutamine show 1–2% color yield of equivalent amounts of proline (Bates et al., 1973). The interference of these ninhydrin-positive substances is negligible in those cases in which proline content in plant tissues is found to increase hundredfold in response to hyperosmotic stress (e.g., Handa et al., 1983; Binzel et al., 1987; Santos-Díaz and Ochoa-Alejo, 1994). However, during recent years increasing evidence has been reported that suggests a more faceted protective role of intracellular free proline (Sharma et al., 2011; Shinde et al., 2016; Signorelli, 2016), and even slight increases of its intracellular content, well below those required for effective osmotic compensation, were found beneficial under stress. The exact mechanisms underlying these positive effects are still a matter of debate (Forlani et al., 2019b), and some data also suggest that an increase in proline metabolic rates, more than its absolute concentration, may help the cell to counteract abiotic stress conditions (Kavi Kishor and Sreenivasulu, 2014; Forlani et al., 2019a). To allow a deeper insight in these metabolic plant responses, there would consequently be a need of methods able to reliably detect even minor variations in proline levels.

In another variant of the acid ninhydrin assay, in which the reaction is carried out at lower temperature (50°C) and less acidic conditions (about pH 3.0), proline yields a peculiar yellow product, whereas most primary amines – like the other proteinogenic amino acids and ornithine – produce red to purple adducts (Williams and Frank, 1975). Conveniently, the reaction mixture can be read as it is, without the need of extracting the chromophore with an organic solvent. However, this protocol has been specifically developed for the quantitation of pure δ^1-pyrroline-5-carboxylic acid (P5C), an intermediate in all the plant routes for proline biosynthesis and catabolism (Trovato et al., 2019), and its specificity when used for proline determination has not been thoroughly investigated. Therefore, in this case as well, standard solutions for calibration should comprise a mixture of amino acids similar to their abundance in the plant extracts, and reaction blanks without ninhydrin are required to subtract various plant compounds able to absorb at the same wavelength.

The limitations inherent to both these established protocols could be overcome by the availability of a robust and specific enzymatic assay for proline quantification. Proline dehydrogenase (ProDH, EC 1.5.5.2), the enzyme that oxidizes proline to P5C in plant mitochondria, is attached to the inner mitochondrial matrix and is very difficult to purify. Moreover, it is believed to transfer electrons directly to quinones of the respiratory electron transfer chain (Cabassa-Hourton et al., 2016), and is unable to catalyze *in vitro* the reduction of $NAD(P)^+$ (Lanfranchi et al., manuscript in preparation). The opposite reaction, *i.e.,* the NAD(P)H-dependent reduction of P5C to proline, is catalyzed *in vivo* by P5C reductase (P5CR, EC 1.5.1.2; Forlani et al., 2015b). During early purification attempts, a single protein was found to possess both P5CR and proline dehydrogenase activities (Rena and Splittstoesser, 1975), and later on a purified P5CR was shown to catalyze the reverse reaction at alkaline pH (Szoke et al., 1992). A protocol to assay P5CR following the proline-dependent reduction of NAD^+ at pH 10 was then reported (Chilson et al., 1992) and, because P5C is not commercially available, in many subsequent papers this reaction (or even the oxidation of proline analogs such as thiaproline) was used to assay the enzyme (e.g., Nocek et al., 2005; Meng et al., 2006), though it does not represent a physiological feature. We have previously described P5CRs from *Arabidopsis thaliana*, *Oryza sativa*, and *Medicago truncatula* as very stable enzymes that can easily be stored at 4°C over prolonged periods with negligible loss of activity (Funck et al., 2012; Giberti et al., 2014; Forlani et al., 2015a; Ruszkowski et al., 2015). Based on these premises, we established the reverse reaction of P5CR under optimized conditions as a simple, specific and reliable method for proline quantification.

MATERIALS AND METHODS

Heterologous Expression and Affinity Purification of Plant P5CRs

Cloning and functional characterization of Arabidopsis and rice P5CRs have been previously described (Giberti et al., 2014; Forlani et al., 2015a). Overexpression was carried out in *Escherichia coli* BL21 (DE3) pLysS cells. The bacteria were grown at 24 °C in 2-L Erlenmeyer flasks with shaking at 100 rpm in 400 mL LB medium supplemented with 100 μg mL^{-1} ampicillin and 50 μg mL^{-1} chloramphenicol. At an OD_{600} of 0.5, expression of P5CR was induced with 1 mM isopropyl-β-D-thiogalactopyranoside. The culture was further incubated for 6 h, then cells were harvested by centrifugation at 3,000 *g* for 10 min and pellets were weighed and frozen at −20 °C. The samples (about 1 g) were thawed and extracted in an ice-cold mortar with 2 g g^{-1} alumina powder, then the homogenate was resuspended in 25 mL g^{-1} of extraction buffer (50 mM sodium phosphate, pH 7.5, 200 mM NaCl and 20 mM imidazole) containing 0.5 mM DTT. Cell debris was pelleted by centrifugation at 12,000 *g* for 10 min at 4 °C. The supernatant was applied at a constant flow of 10 mL h^{-1} to a 0.1 mL His SpinTrap column (GE Healthcare). After binding, the column was washed with 5 mL of extraction buffer and eluted stepwise with 3-mL aliquots of buffer containing increasing concentrations of imidazole (50, 100, 200, 350, and 500 mM), while collecting 1-mL fractions. Both Arabidopsis and rice P5CR eluted reproducibly and quantitatively at about 350 mM imidazole (**Supplementary Figure S1**). The His_6-tag was not cleaved, as it has been shown to have no influence on the functional properties of the enzymes (Giberti et al., 2014; Forlani et al., 2015a). Protein concentration was determined by the method of Bradford (1976), using bovine serum albumin as the standard. Homogeneity of purified preparations was checked by discontinuous SDS-PAGE (12% acrylamide separating gel). Enzyme preparations were filter-sterilized (0.2 μm) and stored at 4 ± 2°C in the dark.

P5CR Assays

Assays were performed in either 1 cm/0.2 cm path cuvettes (UVette; Eppendorf, Milan, Italy) in a final volume of 1 mL, or 96-microwell plates in a final volume of 0.2 mL. In the former case, OD_{340} was determined with a Novaspec plus spectrophotometer (Amersham Biosciences, Milan, Italy) equipped with a Peltier

device set to 37°C and a UVette adaptor. In the latter case, the plate was equilibrated at 37°C prior to enzyme addition, and absorbance was measured using a Ledetect plate reader (Labexim, Lengau, Austria) equipped with a LED plugin at 340 nm. Each sample was carried out in triplicate (technical replications). Each determination was repeated with at least three different enzyme preparations (biological replications), obtaining almost identical patterns. Presented data refer to a single enzyme preparation, and are means ± SE over technical replicates. Linear and non-linear regressions of data were computed using Prism 6 for Windows, version 6.03 (GraphPad Software, San Diego, CA, United States).

Forward Assay

The physiological activity of P5CR was routinely measured at pH 7.5 as the P5C-dependent oxidation of NAD(P)H. P5C was synthesized by the periodate oxidation of δ-*allo*-hydroxylysine (Sigma H0377), purified by cation exchange chromatography on a 200–400 mesh Dowex AG50W-X4 column, and quantified as described (Williams and Frank, 1975). P5C solutions in 1 M HCl were stored at 4°C in the dark, and brought to neutral pH just before the assay using proper aliquots of a 1 M Tris base solution. Unless otherwise specified, the assay mixture contained 2 mM DL-P5C and 0.4 mM of either NADH or NADPH in 50 mM Tris-HCl buffer, pH 7.5. Parallel blanks were performed in which P5C had been omitted.

Reverse Assay

The reverse activity of P5CR was routinely measured at pH 10.2 as the proline-dependent reduction of $NAD(P)^+$. Unless otherwise specified, the assay mixture contained 10 mM L-proline and 5 mM of either NAD^+ or $NADP^+$ in 100 mM glycine-NaOH buffer, pH 10.2. Parallel blanks were performed in which proline had been omitted. Kinetic analyses were performed by varying a single substrate while maintaining the invariable substrate at 10 mM $NADP^+$ or 20 mM NAD^+, and 50 mM (with NAD^+) or 5 mM (with $NADP^+$) proline in the case of *O. sativa* P5CR; at 3 mM $NADP^+$ or 15 mM NAD^+, and 2 mM proline in the case of the enzyme from *A. thaliana*. K_M and V_{max} values and their confidence intervals were computed using the corresponding functions in the Prism 6 software.

Ninhydrin Assays

Assays were performed using either the protocols described by Bates et al. (1973) or Williams and Frank (1975). No changes were introduced, but volumes were reduced while maintaining proportion and composition of the solutions. Solutions of pure proline in water were used to calibrate the assays. In all cases samples were carried out in triplication, and mean values ± SE are reported. Each experiment was repeated twice.

Bates Protocol

Ninhydrin was dissolved at 25 mg mL^{-1} in 60% (v/v) acetic acid – 13.8% (w/v) phosphoric acid. Samples (100 μL) were mixed with the same volume of both ninhydrin solution and glacial acetic acid, and incubated at 100°C for 60 min. After cooling, the formed chromophore was extracted with 200 μL toluene by vortexing a few times. Following centrifugation at 10,000 *g* for 3 min, the organic phase was read at 520 nm in quartz or PMMA cuvettes using an Ultrospec 1100 pro spectrophotometer (Amersham Biosciences).

Williams and Frank Protocol

Ninhydrin was dissolved at 1.5 mg mL^{-1} in glacial acetic acid. Samples (15 μL) were sequentially mixed with 15 μL of 3 M Na acetate and 200 μL ninhydrin solution, and immediately read in PS cuvettes with the Ultrospec 1100 pro spectrophotometer, or in 96-microwell plates with the Ledetect plate reader equipped with LED plugins at 352, 520 or 540 nm. After incubation at 50°C for 12.5 min, samples were cooled to room temperature and read again. The difference of absorbance between final reading and time-zero value was considered.

Cell Culture, Growth Conditions and Amino Acid Extraction

Nicotiana plumbaginifolia Viviani suspension cultured cells were grown heterotrophycally at 24°C in the dark, as described previously (Forlani et al., 1996). Cultures were treated with 175 mM NaCl three days after subculturing, when cells had entered the exponential phase of growth. At increasing time after the treatment, culture aliquots were withdrawn, and cells were harvested on nylon filters (2 μm) under vacuum. Cells were split into two samples, which were resuspended with 2 mL g^{-1} of either 3% (w/v) 5-sulfosalicylic acid solution or 100 mM glycine-NaOH buffer, pH 10.5, and extracted with a teflon-in-glass Potter homogenizer with 20 strokes. The homogenates were centrifuged 3 min at 12,000 *g*, and the supernatants were stored at −20°C until analyzed. Just before the analysis, extracts in glycine-NaOH buffer were treated 5 min at 95°C to completely inactivate endogenous enzymes, and then further centrifuged.

RESULTS

Ninhydrin-Based Methods Can Significantly Overestimate Proline Content

To get an estimate of the errors introduced by the commonly used ninhydrin assays for proline quantification, their specificity and possible interference from other amino acids were re-investigated. We confirmed that the Bates assay detects ornithine with almost the same sensitivity as proline, and also pipecolate, which differs from proline by an additional C-atom in the ring, was detected, although with a sensitivity one order of magnitude lower (**Figure 1A**). The four-atom ring analog azetidin-2-carboxylate (A2CA) was not detected. D-proline and DL-P5C produced about 60% and 50% of the absorbance at 520 nm compared to equivalent concentrations of L-proline, while hydroxyproline reacted with similar efficiency as pipecolate (**Figure 1B**). The modified assay by Williams and Frank showed a somehow higher specificity, but equally suffered from some interferences. Ornithine produced only 5% of the absorption at 352 nm compared to equimolar concentrations of proline, and the absorbance obtained with the same levels of pipecolate and

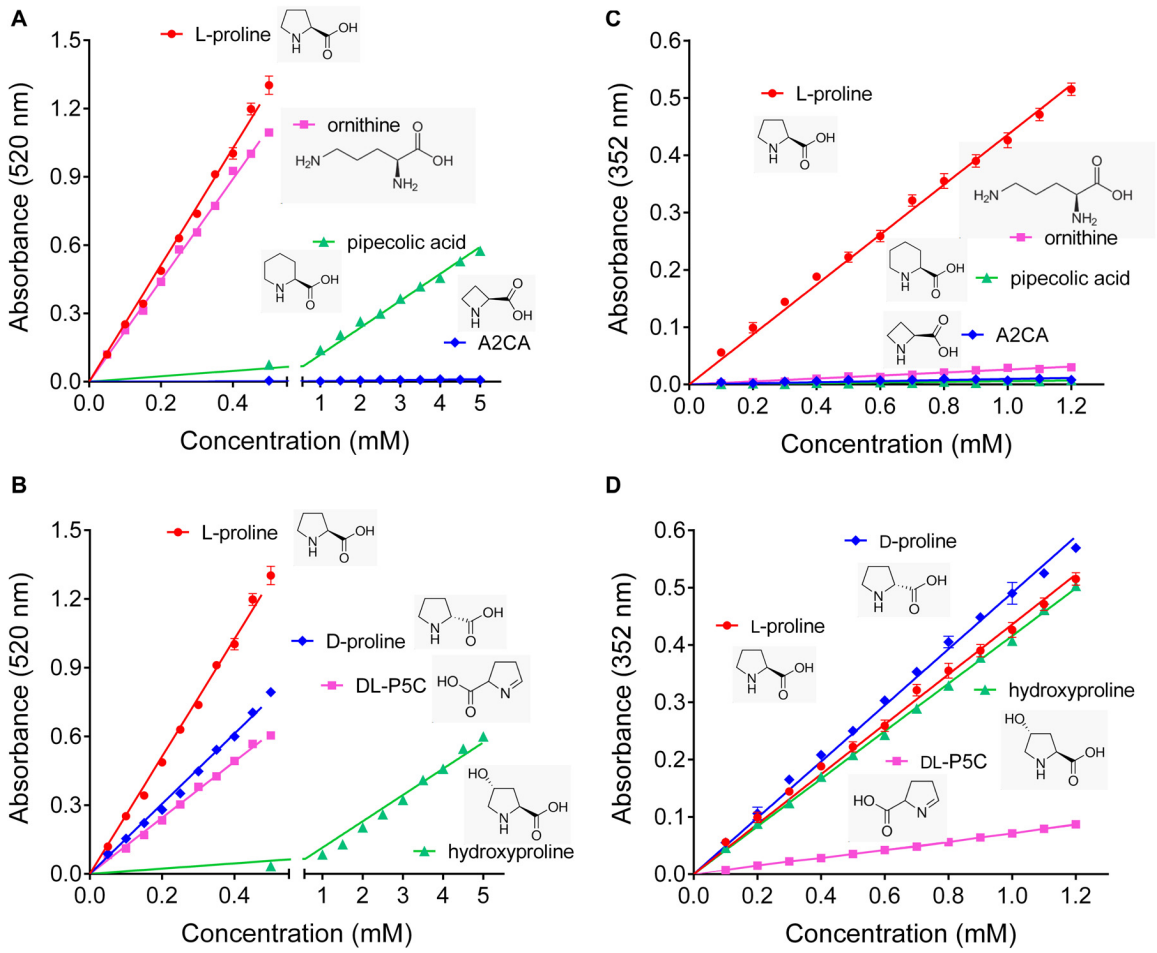

FIGURE 1 | Specificity of the established ninhydrin-based methods for proline quantification. **(A,B)** In the assay developed by Bates et al. (1973), ninhydrin reacts also with ornithine, D-proline and DL-pyrroline-5-carboxylate (P5C), while pipecolate and hydroxyproline produce only low absorbances, and azetidin-2-carboxylate (A2CA) is undetectable. **(C,D)** The modified assay by Williams and Frank (1975) shows less interference by ornithine, pipecolate and DL-P5C, but the absorbance yield with D-proline and hydroxyproline is almost the same as for proline. All data are means ± SE over four replicates.

A2CA was negligible (**Figure 1C**). However, P5C gave rise to 10% of the optical density obtained with proline, and D-proline and hydroxyproline produced a yellow adduct with nearly the same absorbance intensities as L-proline (**Figure 1D**).

Visually, the products formed by the Williams and Frank assay from proline, P5C and primary amino acids were clearly different, yielding yellow, red or purple color, respectively (**Figure 2A**). However, when we analyzed the absorption spectra, it became evident that also the products formed from P5C and glutamate absorb – even if slightly – at 352 nm, the wavelength that is typically used to quantify proline. Changing the measuring wavelength would strongly impair the sensitivity of the assay without much gain in specificity. Because the reaction of proline with ninhydrin produces color with much higher efficiency, the error produced by the contribution of primary amino acids is negligible when proline constitutes 10% or more of the total amino acids. However, when proline was only 1% of the total amino acids, the absorption at 352 nm was approximately twice as high as for pure proline (**Figure 2B**). Since the amino acid composition of an unknown sample is virtually impossible to predict, none of the two ninhydrin-based assays is satisfactory to obtain a precise measure of proline content in plant tissues, and a novel method would be required.

At Alkaline pH, Plant P5CR Mediates Proline-Dependent NAD(P)$^+$ Reduction

Plants produce a plethora of metabolites, thus the specificity of any chemistry-based colorimetric assay is difficult to predict or confirm. An enzyme-based assay is supposed to have a much narrower range of substrates, and appears as a possible solution for a specific assay for L-proline. Isolation and purification of ProDH from plants has not been reported so far, but an alternative is represented by the reverse reaction of P5CR at high pH (**Figure 3**). We purified His-tagged recombinant Arabidopsis and rice P5CRs after expression in *E. coli* by Ni-affinity chromatography (**Supplementary Figure S1**). Starting from 400 mL of bacterial culture, about 400–500 and 800–900 μg

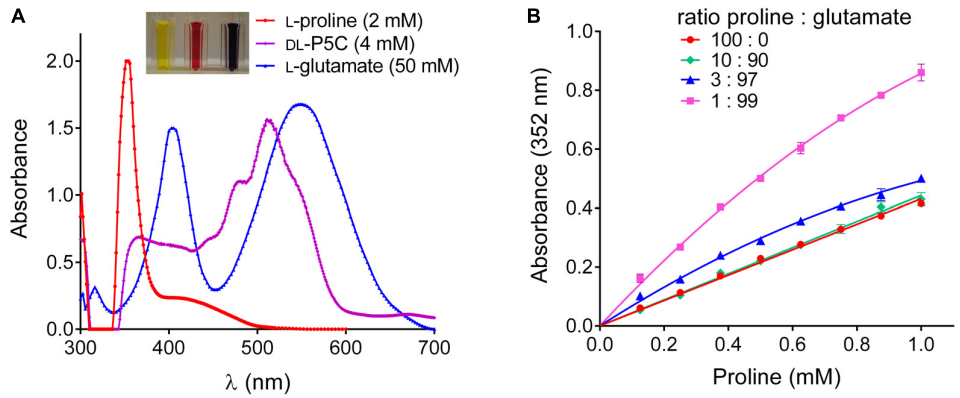

FIGURE 2 | Overestimation of proline content by the Williams and Frank assay in samples containing high levels of other amino acids. **(A)** Absorption spectra of the reaction products of proline, P5C and glutamate under the conditions described by Williams and Frank (1975) show different intensities and absorption maxima, but all contribute to OD at 352 nm, which is used to quantify proline. **(B)** In extracts in which proline represents a minor component of the pool of free amino acids, this overlap leads to a significant overestimation of its content. Data in panel **(B)** refer to samples in which proline has been analyzed alone, or in combination with glutamate, as indicated, and are means ± SE over four replicates.

of purified protein were obtained, respectively. At pH 7.5 *in vitro*, the conversion of P5C to proline by P5CR appeared as a virtually unidirectional reaction, which proceeded without product inhibition until the NAD(P)H/NAD(P)$^+$ ratio became unfavorable (**Figure 3B**) (Giberti et al., 2014; Forlani et al., 2015a). However, under more alkaline conditions the reaction was found to proceed also in the reverse direction, and kinetic analysis revealed that both the initial rate of NAD$^+$ reduction and the NADH level at equilibrium were increasing between pH 8 and 10 (**Figure 3C**). However, even at pH 10.2 the resulting rates were found significantly lower than those of the physiological reaction at neutral pH, were not proportional to the amount of enzyme, and rapidly lost linearity, yielding only semiquantitative results (**Figure 3D**).

To obtain a comprehensive picture of the pH dependence of the reactions catalyzed by plant P5CR, the initial rates of the forward and the reverse reaction were measured over a wide range of pH values, using either NAD(P)$^+$ or NAD(P)H as cofactors (**Figures 3E,F**). With NADH as the electron donor, the forward reaction became undetectable above pH 10.2, and with NADPH above pH 11.0. The reverse reaction with NADP$^+$ had a rather narrow pH optimum around pH 11.8, whereas with NAD$^+$ as electron acceptor, a broad optimum between pH 9.5 and 12 was observed.

Based on the pH-dependence of the initial reaction rates, we reasoned that the reverse P5CR reaction could be employed for a quantitative assay for L-proline. A thorough kinetic analysis of the reverse reactions of Arabidopsis and rice P5CRs was performed to determine the constraints for the optimal assay conditions (**Supplementary Figure S2**). The results, summarized in **Table 1**, showed that both enzymes have a higher affinity for NADP$^+$ than for NAD$^+$, and that the affinity for proline is also higher when NADP$^+$ is used as the electron acceptor. However, with NADP$^+$ as the cofactor, proline concentrations higher than 2–3 mM in the case of the enzyme from Arabidopsis, or higher than 5–7 mM for that from rice, were found inhibitory (data not shown). Moreover, with NAD$^+$ as cofactor, both enzymes showed much higher V_{max} values, and reached maximal catalytic efficiencies around 25 μkat (mg protein)$^{-1}$. We concluded that both enzymes could be used for quantitative assays of proline in the micromolar range when a saturating concentration of NAD$^+$ was provided.

At pH 10.5 ± 0.1 the Reverse P5CR Reaction Allows Reliable Quantitation of L-Proline

Based on the kinetic data, a large excess of rice P5CR was incubated at pH 10.2 with a nearly saturating NAD$^+$ concentration and increasing levels of proline in the micromolar range. Under this condition, NADH production reached a plateau within 10 min, and its level was proportional to the initial proline concentration (**Figure 4A**). However, at concentrations exceeding 150 μM proline, the reaction appeared not to proceed to completion, and less than equimolar concentrations of NADH were produced (**Figure 4B**). Because the results presented in **Figure 3** imply that at pH 10.2 an equilibrium between forward and reverse reaction determines the final NADH yield, we carefully tested the influence of pH in the range from 10.0 to 11.1 on the initial rate and final NADH yield of the reverse reaction (**Figures 4C,D**). Between pH 10.0 and pH 10.4, the initial rate was very similar, but the final NADH yield increased steadily. Above pH 10.6 the reaction was considerably slower, and above pH 10.8 a plateau of NADH was not reached within 20 min. We concluded that pH 10.5 ± 0.1 would be the optimal condition for a quantitative assay. Lowering either the NAD$^+$ or the enzyme concentration at pH 10.5 progressively slowed down the reaction but had no influence on the amount of NADH formed in the plateau phase (**Figures 4E,F**). Very similar results were obtained with Arabidopsis P5CR (data not shown). Despite the higher affinity of both P5CR enzymes for NADP$^+$, less reliable results were obtained with NADP$^+$ as cofactor (not shown), most likely

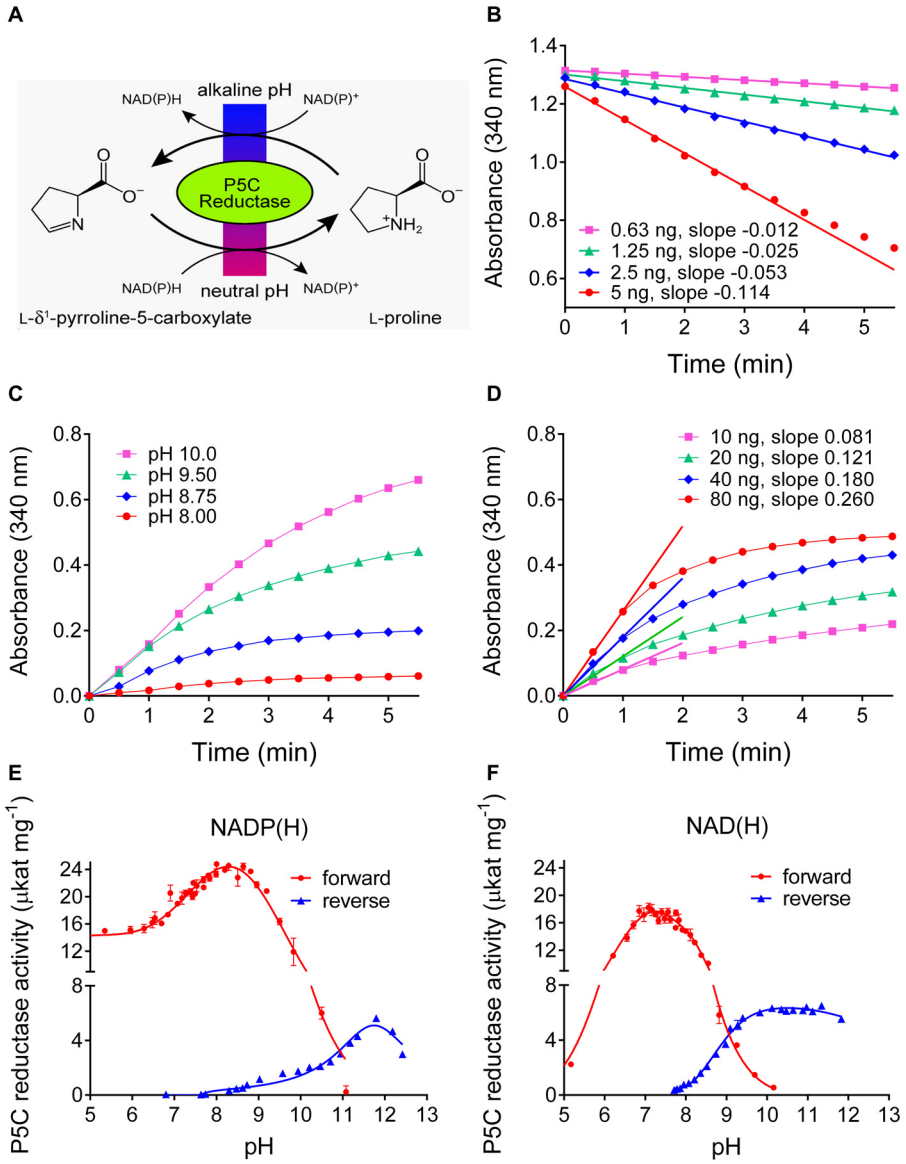

FIGURE 3 | Forward and reverse reactions of Arabidopsis P5CR. **(A)** *In vivo* the enzyme catalyzes the reduction of P5C to proline, using either NADH or NADPH as the electron donor. However, at alkaline pH *in vitro*, also the reverse reaction takes place. **(B)** At pH 7.5, the P5C-dependent oxidation of NADH is linear over long times, and proportional to the amount of enzyme. **(C)** Proline-dependent NAD^+ reduction by 100 ng P5CR is detectable only at pH ≥ 8.0, is strongly dependent on the pH of the assay mixture, and rapidly reaches a plateau. **(D)** Even at pH 10.2, no clear linear phase of NAD^+ reduction is evident and the estimated slopes are not proportional to the amount of enzyme and less steep compared to the forward reaction. Same conditions as in panel **(C)** were used, but pH 10.2. **(E,F)** The pH-activity relationship of the forward and the reverse reaction was characterized by incubating 100 ng P5CR in 50 mM Hepes mixed with increasing concentrations of KOH, and using either NADP(H) **(E)** or NAD(H) **(F)** as cofactor. The actual pH value in each sample was measured at the end of the reaction with a microelectrode. Values refer to the initial, quasi-linear rates, and are the mean ± SE over three replicates. Similar results were obtained with rice P5CR.

due to the lower reaction rate and the higher pH optimum of the forward reaction (**Figure 3E**).

Having determined the optimal conditions for proline quantification with the reverse P5CR reaction, we investigated the range of linearity, sensitivity, and specificity of this method. For proline concentrations between 100 and 500 µM, the plateau of NADH production was consistently reached after 15 min (**Figure 5A**), and up to 350 µM proline the reaction was virtually complete (**Figure 5B**). Above this level, the relationship between proline and NADH concentration gradually lost linearity, yet the use of a non-linear fit for absorbance values obtained from known proline concentrations allowed reliable measurement up to 1 mM (data not shown). When the performance of this enzymatic method was compared with the ninhydrin-based assay of Williams and Frank (1975), a similar sensitivity was found. In terms of color development per absolute proline

TABLE 1 | Kinetic properties of the reverse reaction of P5CR.

	Rice P5CR	Arabidopsis P5CR	
V_{max} (NAD^+)	25.64 ± 0.90	33.92 ± 0.45	μkat (mg protein)$^{-1}$
V_{max} (Pro, with NAD^+ as the co-substrate)	21.00 ± 0.80	25.57 ± 0.70	μkat (mg protein) $^{-1}$
V_{max} ($NADP^+$)	0.376 ± 0.003	3.94 ± 0.66	μkat (mg protein) $^{-1}$
V_{max} (Pro, with $NADP^+$ as the co-substrate)	0.387 ± 0.005	3.77 ± 0.12	μkat (mg protein) $^{-1}$
K_M(app) for L-Pro (NAD^+)	4.86 ± 0.49	2.38 ± 0.18	mM
K_M(app) for L-Pro ($NADP^+$)	0.223 ± 0.016	0.378 ± 0.038	mM
K_M(app) for NAD^+	15.01 ± 1.05	7.17 ± 0.21	mM
K_M(app) for $NADP^+$	0.321 ± 0.016	0.517 ± 0.034	mM

Data used for calculating kinetic constants are reported in ***Supplementary Figure S2****.*

amount, the ninhydrin assay yielded approximately two-fold higher absorbance values (ΔA_{352} = 0.0284 ± 0.0006 nmol^{-1} with ninhydrin vs ΔA_{340} = 0.0141 ± 0.0001 nmol^{-1} for the enzymatic assay) (**Figure 5C**). However, because the ninhydrin assay uses larger sample volumes, the enzymatic assay is three times more sensitive with respect to proline concentration in the sample (ΔA_{340} = 1.452 ± 0.009 mM^{-1} compared to ΔA_{352} = 0.450 ± 0.006 mM^{-1} with ninhydrin). Concerning specificity, neither D-proline nor hydroxyproline at similar levels induced any NAD^+ reduction by P5CR (**Figure 5D**). Similar assay characteristics were obtained with Arabidopsis P5CR, and both enzymes showed no NADH production with P5C, ornithine, pipecolate, or A2CA as substrates (data not shown).

Based on these results, a protocol for the quantitation of free proline in extracts from plant materials was set down (**Table 2**). This protocol was applied in an experiment in which a *Nicotiana plumbaginifolia* cell culture was treated with salt, and the consequent increase of intracellular free proline was determined at increasing time after the treatment. Cells were also extracted in sulfosalicylic acid and analyzed with the acidic ninhydrin method of Williams and Frank (1975), and the results obtained with the two protocols were compared (**Figure 6**). When extracts in sulfosalicylic acid were analyzed with either ninhydrin or the enzymatic method, substantially identical results were evident (**Figure 6A**). A very similar pattern was obtained also with extracts in glycine-NaOH buffer that were analyzed with the enzymatic method. On the contrary, when extracts in glycine-NaOH buffer were analyzed with the ninhydrin method, the amount of proline was overestimated in samples with low proline content, most likely due to the residual presence of proteins (**Figure 6B**).

DISCUSSION

A careful analysis of established ninhydrin-based methods for proline quantification revealed that these assays are unreliable, when structurally related compounds or a 30-fold excess of α-amino acids are present in a sample. With our newly developed enzymatic assay, which is specific for L-proline, we present a simple and robust solution for this problem. In extracts from plant cells grown under normo-osmotic conditions, proline typically accounts for only 2–4% of total free amino acids (*e.g.,* Forlani et al., 2013; Giberti et al., 2017). Additionally, depending on the assay conditions, ninhydrin reacts equally well with D-proline or ornithine, but also P5C, hydroxyproline, and pipecolate contribute significantly to the output of the assays. We are not aware of any reports describing the natural occurrence of D-proline in plants, but transporters with the capacity to import D-proline from the growth substrate have been described (Breitkreuz et al., 1999; Lehmann et al., 2011). In contrast, ornithine is both a precursor and a degradation product of arginine (Winter et al., 2015), and in leaves of salt-stressed cashew plants ornithine content reached almost 50% of L-proline concentration (da Rocha et al., 2012). Monteoliva et al. (2014) detected P5C levels below 2 nmol g^{-1} FW in control and pathogen-infected Arabidopsis plants without specifying potential losses of P5C during extraction. By extraction under strongly acidic conditions, which minimizes the loss of P5C prior to analysis, we found that P5C levels are, even after exposure to high concentrations of external proline, undetectable in wild-type Arabidopsis plants, with a detection limit corresponding to 50 nmol g^{-1} FW or 5% of the typical proline content in leaves (Deuschle et al., 2004). Hydroxyproline is typically formed post-translationally by proline hydroxylases and is highly abundant in proline-rich cell wall proteins (Kavi Kishor et al., 2015; Marzol et al., 2018). Free *trans*-4-hydroxy-L-proline was found at low levels in oak and pepper plants and its content changed similarly to L-proline in response to stress (Oufir et al., 2009; del Amor et al., 2010; Florencio-Ortiz et al., 2018). Free *cis*-4-hydroxy-L-proline seems to be a specialty of sandal (*Santalum album* L) and related species, where it constitutes up to 10% of the dry weight in some tissues (Radhakrishnan and Giri, 1954; Kuttan et al., 2015). Pipecolate is a degradation intermediate of lysine and its content was found to be four times higher than L-proline in Arabidopsis leaves after infection with *Pseudomonas syringae* pv *maculicola* (Návarová et al., 2012). Similarly, Thomason et al. (2018) reported an almost 6-fold increase of pipecolate content in heat-stressed wheat leaves. All these examples illustrate the possibility that in several cases the use of the established ninhydrin-based assays would provide inaccurate results and lead to a significant overestimate of proline content and/or an incorrect evaluation of its homeostatic levels under stress.

The results presented in this study show that the reverse reaction of recombinant plant P5CR can be used as a robust

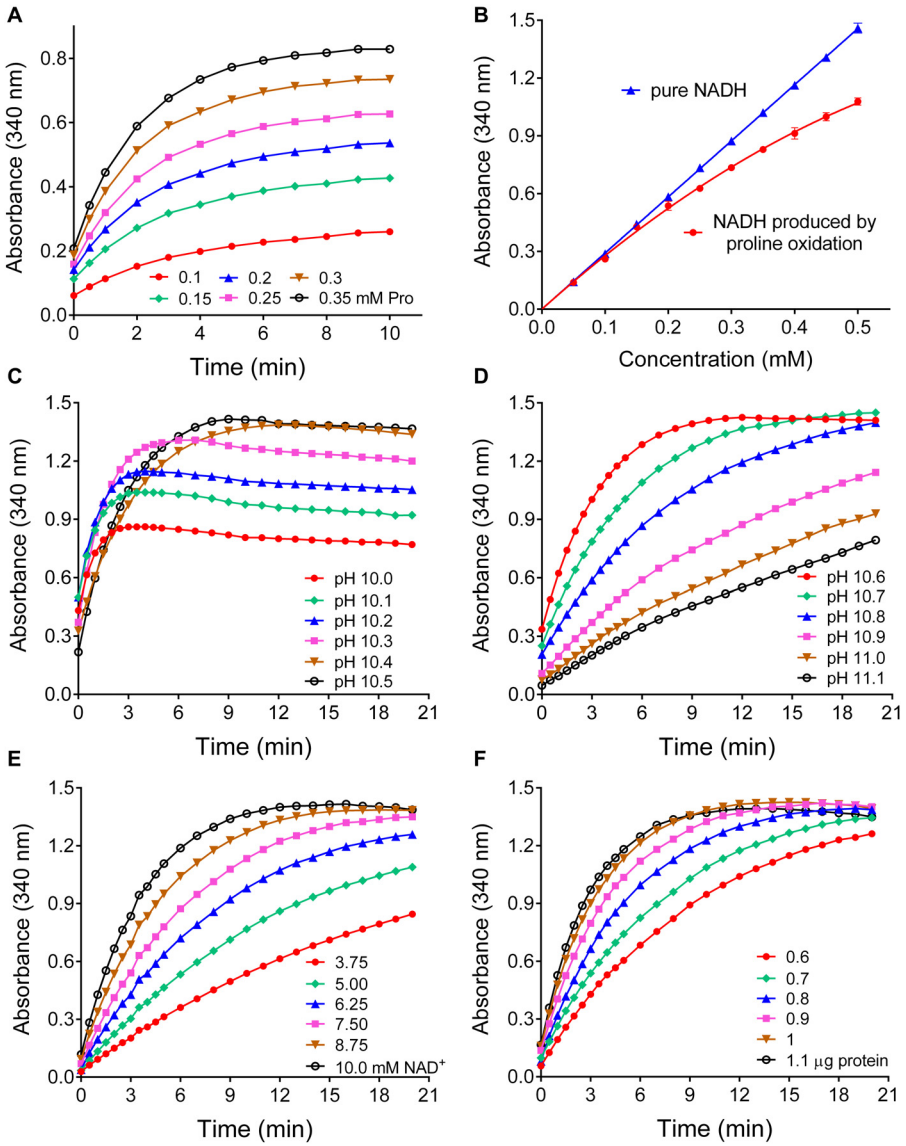

FIGURE 4 | Effects of various parameters on the sensitivity and the linearity of a proline assay based on the reverse reaction of P5CR. **(A)** When increasing concentrations of proline were incubated at pH 10.2 in the presence of 10 mM NAD^+ and a large excess of P5CR (1 µg protein), the production of NADH reached a proline concentration-dependent plateau in about 10 min. **(B)** Under these conditions, the reverse P5CR reaction yielded sub-stoichiometric concentrations of NADH above 150 µM proline. **(C)** When the pH of the reaction mixture was gradually varied, the optimal yield of NADH from 0.5 mM proline was reached at pH values exceeding 10.3. **(D)** Above pH 10.6 the time required for the completion of the reaction increased gradually. **(E,F)** Lowering NAD^+ **(E)** or enzyme concentration **(F)** at pH 10.5 reduced the reaction velocity with little effect on the final NADH concentration. Presented results are means ± SE over at least three replicates, and were obtained with P5CR from rice. The experiment was repeated twice with the same results, and very similar patterns were found also with the enzyme from Arabidopsis.

and highly specific assay for L-proline. The enzyme that catalyzes proline oxidation under physiological conditions, ProDH, could not be exploited with this aim, since it does not use $NAD(P)^+$ as the electron acceptor (Lanfranchi et al., manuscript in preparation). In contrast to previous publications describing the reverse P5CR reaction with NAD^+ as an assay for quantification of P5CR activity (Chilson et al., 1992; Nocek et al., 2005; Meng et al., 2006), the use for L-proline quantification required slightly more alkaline reaction conditions (pH ≥ 10.5 rather than pH 10 or pH 10.2; **Figure 4C**). This difference can be explained by the energetics and stoichiometry of the reaction. At pH 7.5, the standard redox potential (E_0') of (P5C + 3 H^+)/proline is −123 mV (Becker and Thomas, 2001), whereas E_0' of (NAD^+ + H^+)/NADH is −335 mV. Thus, under physiological pH conditions, the reverse reaction is only possible when virtually no NADH is present in the reaction mixture. The asymmetric involvement of protons results in a pH-dependence of the redox potential for (P5C + 3 H^+)/proline of approximately −90 mV

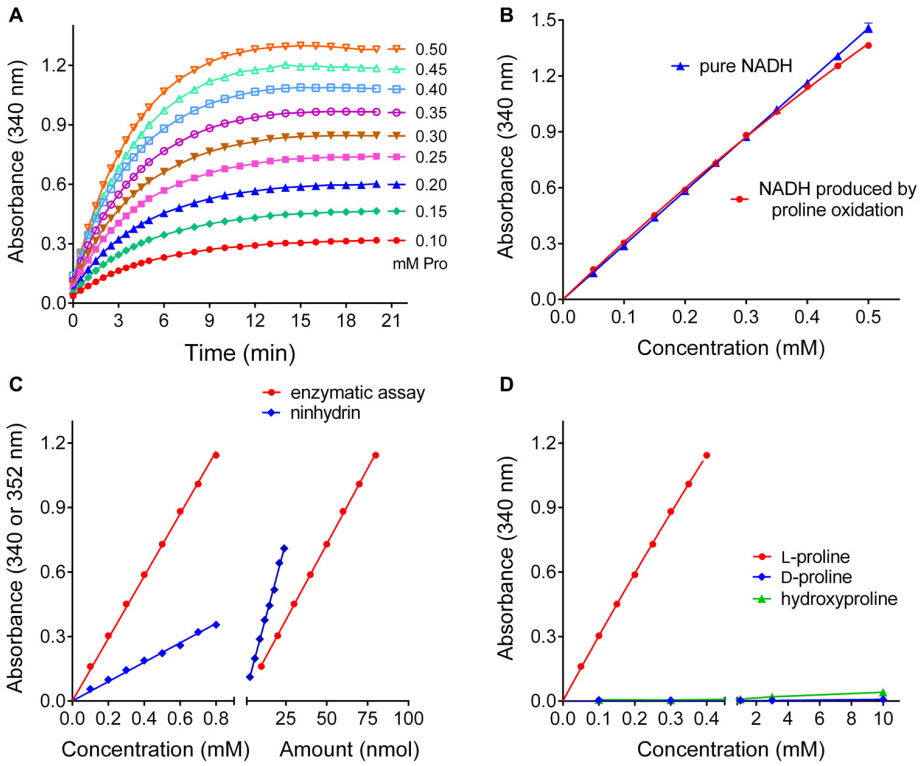

FIGURE 5 | Performance of the optimized P5CR reaction for proline quantification. **(A)** Time- and proline-dependent NADH production by 1 μg rice P5CR at pH 10.5 in the presence of 10 mM NAD^+ was followed by determining the increase of optical density at 340 nm. **(B)** The comparison of the absorbance of pure NADH and the proline-dependent NADH produced after 15 min under these conditions demonstrated a stoichiometric relationship up to 350 μM proline. **(C)** Sensitivity was compared for the enzymatic assay and the acetate/ninhydrin assay on the basis of either proline concentration, or proline amount in the assayed solution. **(D)** Neither D-proline nor L-hydroxyproline in the micro to millimolar range induced significant NADH formation by P5CR. All data are means ± SE over at least three replicates.

TABLE 2 | Step-by-step protocol for the enzymatic determination of free proline content.

1. Homogenize plant material in 1–5 mL g^{-1} of 100 mM glycine-NaOH buffer, pH 10.5[a]
2. Centrifuge 3–5 min at 10–12,000 *g* at RT, discarding the pellet
3. Treat samples for 5 min at 95°C to inactivate endogenous enzymes
4. In a 96-well plate, put 5–100 μL aliquots of extract in duplicate in a final volume of 100 μL; include reference samples containing 5–100 μL of a standard solution with 1 mM L-Pro
5. Add 100 μL of a pre-warmed 2x reaction mixture containing 10 mM NAD^+ and 2 μg P5CR in 100 mM glycine-NaOH buffer, pH 10.5 to one of the duplicate samples, to the second sample add 100 μL of an identical mixture without P5CR
6. Follow the increase in absorbance at 340 nm in the P5CR-containing samples until a maximum value is reached (usually 20 to 30 min) and subtract the absorbance value of the samples without P5CR
7. Select the range in which the change in OD_{340} is proportional to the volume of extract and calculate the slope of a regression line
8. Divide the slope of the regression line for a given sample by that of the reference solution: the result represents the concentration of free proline in the extract (in mmol L^{-1}); multiply this value for the number of mL extraction buffer g^{-1}, to obtain the concentration in μmol g^{-1}

[a]*As an alternative, plant material can be extracted with 70% ethanol. In this case, following centrifugation, extracts should be brought to dryness at room temperature in a centrifugal vacuum concentrator to remove ethanol, and residues resuspended in 100 mM glycine-NaOH buffer, pH 10.5. This would allow concentration of extracts from samples with very low proline content, and makes step 3 unnecessary.*

[$-2.303 \times (RT/zF) \times n$, with z as the number of transferred electrons and n as the number of incorporated protons] per pH unit, yielding −485 mV at pH 10.5. The redox potential of (NAD^+ + H^+)/NADH only changes by −30 mV per pH unit, reaching −425 mV at pH 10.5. With a sufficiently large excess of NAD^+, low concentrations of proline can therefore be quantitatively converted to P5C at this high pH. The slower reaction of P5CR found at pH values exceeding 10.5 (**Figure 4D**) might depend on a gradual inactivation or denaturation of the enzyme. An additional factor that may promote the reverse reaction at high pH values is the spontaneous equilibrium between cyclic P5C and linear glutamate-5-semialdehyde, which is shifted toward glutamate-5-semialdehyde under alkaline conditions (Mezl and Knox, 1976). According to structural data, only P5C but not glutamate-5-semialdehyde will bind efficiently to the active site of P5CR (Ruszkowski et al., 2015).

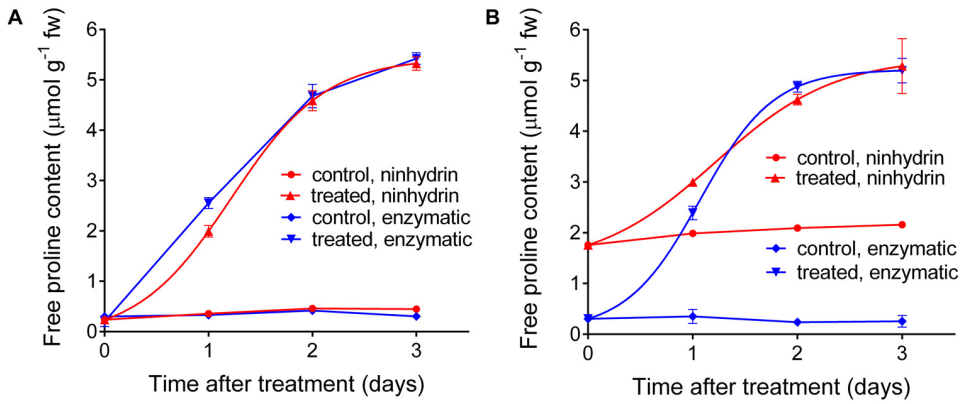

FIGURE 6 | Comparison between the results obtained with the enzymatic and the acidic ninhydrin method according to Williams and Frank (1975). Cell suspension cultures of wild tobacco were treated with 175 mM NaCl. At increasing time after the treatment, culture aliquots were withdrawn and cells were extracted in either 3% (v/v) sulfosalicylic acid **(A)** or in 100 mM glycine-NaOH buffer, pH 10.5 **(B)**. Proline in the two series of extracts was quantified with both the enzymatic and the ninhydrin methods. Data are means ± SE over three biological replicates.

Similar to the forward reaction of P5CR, also the reverse reaction was much faster with NAD^+ than with $NADP^+$, and both analyzed enzymes had a higher affinity toward $NADP^+$ (Giberti et al., 2014; Forlani et al., 2015a). The additional phosphate group of $NADP^+$ is tightly bound by several hydrogen bonds in the crystal structure of *Medicago truncatula* P5CR (Ruszkowski et al., 2015). This stronger binding of $NADP^+$ nicely explains both a higher affinity and a slower exchange rate, resulting in the lower maximal reaction rate. Modifications in the structure of the active site of P5CR induced by binding to the phosphate of $NADP^+$ may also account for the increased affinity toward proline when $NADP^+$ is used as cofactor. Similarly, the affinity of both Arabidopsis and rice P5CR toward P5C was much higher with $NADP^+$ as cofactor, which might additionally contribute to the slower reaction rate and inhibition by proline concentrations exceeding 3 and 7 mM, respectively (Giberti et al., 2014; Forlani et al., 2015a). Despite the slower reaction rate, the reverse reaction with $NADP^+$ might be useful for the quantification of very low concentrations of proline, although – according to the pH profile of the forward and the reverse reaction – at least pH 11 would be required to eliminate interference from the forward reaction.

We are not aware of any commercial source of plant P5CR, but recombinant expression and affinity purification by FPLC or benchtop columns should be possible in any molecular biology laboratory, and the expression constructs for Arabidopsis or rice P5CR are available upon request. Except a photometer, no special equipment is needed and no harmful chemicals have to be used for this novel assay. When a microplate reader is available, large numbers of samples can be processed in parallel and even automation of the assay would be feasible. By the use of a microvolume photometer, tiny amounts of sample will be sufficient for reliable proline quantification. In contrast to the ninhydrin-based assays, the enzymatic assay operates at moderate temperatures, thereby reducing the risk of volume change by evaporation. We performed all assays at 37°C, but with slightly longer incubation times, also lower temperatures will give reliable results. The sensitivity of the enzymatic assay for proline is very similar to the ninhydrin-based assays and the linear range spans almost one order of magnitude. Therefore, up to a 10-fold increase in proline content can be quantified using identical extraction and measurement conditions. For plants with very high proline content, dilution of the samples may be required. In our hands, a single enzyme preparation from 400 mL of induced *E. coli* culture was enough to perform hundreds of assays with the described protocol. Moreover, the purified enzyme is substantially stable, with less than 10% activity loss after 3 months of storage at 4°C. The source of the enzyme can be selected according to cDNA availability, while the slightly higher V_{max} of P5CR from Arabidopsis can be exploited to shorten the incubation time. We did not test the reverse reaction of P5CR from other plant species, but we can speculate that they will have similar biochemical and kinetic properties.

In times of non-biased metabolomics, fast and cost-efficient assays to specifically quantify a selected metabolite are still valuable tools for the phenotypic analysis of large populations. Our newly designed assay can be used for both relative and absolute quantification of proline content. In comparison to the traditional, ninhydrin-based assays, it is very similar with respect to sensitivity and dynamic range, but highly superior with respect to specificity.

DATA AVAILABILITY STATEMENT

The raw data supporting the conclusions of this article will be made available by the authors, without undue reservation.

AUTHOR CONTRIBUTIONS

GF designed the study and performed the majority of the experiments. DF prepared the expression plasmids. All authors have contributed to the manuscript and approved its final version.

FUNDING

This work was supported by a grant from the University of Ferrara (FAR 2019).

ACKNOWLEDGMENTS

We thank Dr. Andrea Straforini for technical assistance during enzyme purification.

SUPPLEMENTARY MATERIAL

The Supplementary Material for this article can be found online at: https://www.frontiersin.org/articles/10.3389/fpls.2020.582026/full#supplementary-material

Supplementary Figure 1 | Affinity purification of heterologously expressed rice and Arabidopsis δ^1-pyrroline-5-carboxylate reductase (P5CR). 6×-His-tagged P5CRs from Arabidopsis (32.5 kDa) and rice (33.5 kDa) were expressed in *Escherichia coli* as previously described (Giberti et al., 2014; Forlani et al., 2015a). Soluble protein extracts from IPTG-induced cells were loaded onto His SpinTrap columns (GE Healthcare) and bound proteins were eluted with increasing concentrations of imidazole, as indicated. Proteins were determined by the method of Bradford (1976), and activity was measured as the P5C-dependent oxidation of NADPH. Selected fractions (E, crude extract; ft, flow through) were analyzed by SDS-PAGE (12% separating gel) and Coomassie staining. The arrows indicate the position of the recombinant enzymes in the crude extracts. *, molecular weight markers.

Supplementary Figure 2 | Kinetic analysis of the reverse reaction of rice and Arabidopsis P5C reductase (P5CR). The purified enzymes (25 and 50 ng for Arabidopsis and rice P5CR, respectively) were incubated at 37°C in 100 mM glycine-NaOH buffer, pH 10.2. The proline-dependent reduction of $NAD(P)^+$ was measured photometrically at 340 nm. The invariable substrates were fixed at 10 mM $NADP^+$ or 20 mM NAD^+ **(A)**; 50 mM (with NAD^+) or 5 mM (with $NADP^+$) proline **(B)**; 3 mM $NADP^+$ or 15 mM NAD^+ **(C)**; 2 mM proline **(D)**. One unit of enzyme activity is herein defined as the corresponding forward reaction rate measured at pH 7.5 under saturating substrate conditions (1 mM L-P5C and 0.4 mM NADPH). Data are mean ± SE over three replicates.

REFERENCES

Ahanger, M. A., Akram, N. A., Ashraf, M., Alyemeni, M. N., Wijaya, L., and Ahmad, P. (2017). Plant responses to environmental stresses-from gene to biotechnology. *AoB Plants* 9:lx025. doi: 10.1093/aobpla/plx025

Bates, L. S., Waldren, R. P., and Teare, I. D. (1973). Rapid determination of free proline for water-stress studies. *Plant Soil* 39, 205–207. doi: 10.1007/BF00018060

Becker, D. F., and Thomas, E. A. (2001). Redox properties of the PutA protein from *Escherichia coli* and the influence of the flavin redox state on PutA-DNA interactions. *Biochemistry* 40, 4714–4721. doi: 10.1021/bi0019491

Binzel, M., Hasegawa, P., Rhodes, D., Handa, S., Handa, A., and Bressan, R. (1987). Solute accumulation in tobacco cells adapted to NaCl. *Plant Physiol.* 84, 1408–1415. doi: 10.1104/pp.84.4.1408

Bradford, M. M. (1976). A rapid and sensitive method for the quantitation of microgram quantities of protein utilizing the principle of protein-dye binding. *Anal. Biochem.* 72, 248–254. doi: 10.1016/0003-2697(76)90527-3

Breitkreuz, K. E., Shelp, B. J., Fischer, W. N., Schwacke, R., and Rentsch, D. (1999). Identification and characterization of GABA, proline and quaternary ammonium compound transporters from *Arabidopsis thaliana*. *FEBS Lett.* 450, 280–284. doi: 10.1016/s0014-5793(99)00516-5

Cabassa-Hourton, C., Schertl, P., Bordenave-Jacquemin, M., Saadallah, K., Guivarc'h, A., Lebreton, S., et al. (2016). Proteomic and functional analysis of proline dehydrogenase 1 link proline catabolism to mitochondrial electron transport in *Arabidopsis thaliana*. *Biochem. J.* 473, 2623–2634. doi: 10.1042/BCJ20160314

Chilson, O. P., Kelly-Chilson, A. E., and Schneider, J. D. (1992). Pyrroline-5-carboxylate reductase in soybean nodules: comparison of the enzymes in host cytosol, *Bradyrhizobium japonicum* bacteroids, and cultures. *Plant Physiol.* 99, 119–123. doi: 10.1104/pp.99.1.119

Chinard, F. P. (1952). Photometric estimation of proline and ornithine. *J. Biol. Chem.* 199, 91–95.

da Rocha, I. M. A., Vitorello, V. A., Silva, J. S., Ferreira-Silva, S. L., Viégas, R. A., Silva, E. N., et al. (2012). Exogenous ornithine is an effective precursor and the δ-ornithine amino transferase pathway contributes to proline accumulation under high N recycling in salt-stressed cashew leaves. *J. Plant Physiol.* 169, 41–49. doi: 10.1016/j.jplph.2011.08.001

del Amor, F. M., Cuadra-Crespo, P., Walker, D. J., Camara, J. M., and Madrid, R. (2010). Effect of foliar application of antitranspirant on photosynthesis and water relations of pepper plants under different levels of CO_2 and water stress. *J. Plant Physiol.* 167, 1232–1238. doi: 10.1016/j.jplph.2010.04.010

Deuschle, K., Funck, D., Forlani, G., Stransky, H., Biehl, A., Leister, D., et al. (2004). The role of δ^1-pyrroline-5-carboxylate dehydrogenase in proline degradation. *Plant Cell* 16, 3413–3425. doi: 10.1105/tpc.104.023622

Florencio-Ortiz, V., Selles-Marchart, S., Zubcoff-Vallejo, J., Jander, G., and Casas, J. L. (2018). Changes in the free amino acid composition of *Capsicum annuum* (pepper) leaves in response to *Myzus persicae* (green peach aphid) infestation. A comparison with water stress. *PLoS One* 13:e0198093. doi: 10.1371/journal.pone.0198093

Forlani, G., Berlicki, Ł, Duò, M., Dziędzioła, G., Giberti, S., Bertazzini, M., et al. (2013). Synthesis and evaluation of effective inhibitors of plant δ^1-pyrroline-5-carboxylate reductase. *J. Agric. Food Chem.* 61, 6792–6798. doi: 10.1021/jf401234s

Forlani, G., Bertazzini, M., and Cagnano, G. (2019a). Stress-driven increase in proline levels, and not proline level itself, correlates with the ability to withstand excess salt in a group of 17 Italian rice genotypes. *Plant Biol.* 21, 336–342. doi: 10.1111/plb.12916

Forlani, G., Trovato, M., Funck, D., and Signorelli, S. (2019b). "Regulation of proline accumulation and its molecular and physiological functions in stress defense," in *Osmoprotectant-Mediated Abiotic Stress Tolerance in Plants: Recent Advances and Future Perspectives*, eds M. A. Hossain, V. Kumar, D. J. Burritt, M. Fujita, and P. Mäkelä (Switzerland: Springer Nature).

Forlani, G., Bertazzini, M., Zarattini, M., Funck, D., Ruszkowski, M., and Nocek, B. (2015a). Functional properties and structural characterization of rice δ^1-pyrroline-5-carboxylate reductase. *Front. Plant Sci.* 6:565. doi: 10.3389/fpls.2015.00565

Forlani, G., Makarova, K., Ruszkowski, M., Bertazzini, M., and Nocek, B. (2015b). Evolution of plant δ^1-pyrroline-5-carboxylate reductases from phylogenetic and structural perspectives. *Front. Plant Sci.* 6:567. doi: 10.3389/fpls.2015.00567

Forlani, G., Lejczak, B., and Kafarski, P. (1996). *N*-pyridyl-aminomethylene-bisphosphonic acids inhibit the first enzyme in the shikimate pathway, 3-deoxy-D-*arabino*-heptulosonate-7-phosphate synthase. *Pestic. Biochem. Physiol.* 55, 180–188. doi: 10.1006/pest.1996.0047

Funck, D., Winter, G., Baumgarten, L., and Forlani, G. (2012). Requirement of proline synthesis during Arabidopsis reproductive development. *BMC Plant Biol.* 12:191. doi: 10.1186/1471-2229-12-191

Giberti, S., Bertazzini, M., Liboni, A., Berlicki, Ł, Kafarski, P., and Forlani, G. (2017). Phytotoxicity of aminobisphosphonates targeting both δ^1-pyrroline-5-carboxylate reductase and glutamine synthetase. *Pest. Manag. Sci.* 73, 435–443. doi: 10.1002/ps.4299

Giberti, S., Funck, D., and Forlani, G. (2014). Δ^1-pyrroline-5-carboxylate reductase from *Arabidopsis thaliana*: stimulation or inhibition by chloride ions and feedback regulation by proline depend on whether NADPH or NADH acts as co-substrate. *New Phytol.* 202, 911–919. doi: 10.1111/nph.12701

Handa, S., Bressan, R., Handa, K., Carpita, N. C., and Hasegawa, P. M. (1983). Solutes contributing to osmotic adjustment in cultured plant cells

adapted to water stress. *Plant Physiol.* 73, 834–8431. doi: 10.1104/pp.73.3.834

Hayat, S., Hayat, Q., Alyemeni, M. N., Wani, A. S., Pichtel, J., and Ahmad, A. (2012). Role of proline under changing environments: a review. *Plant Signal. Behav.* 7, 1456–1466. doi: 10.4161/psb.21949

Kavi Kishor, P. B., Hima Kumari, P., Sunita, M. S., and Sreenivasulu, N. (2015). Role of proline in cell wall synthesis and plant development and its implications in plant ontogeny. *Front. Plant Sci.* 6:544. doi: 10.3389/fpls.2015.00544

Kavi Kishor, P. B., and Sreenivasulu, N. (2014). Is proline accumulation per se correlated with stress tolerance or is proline homeostasis a more critical issue? *Plant Cell Environ.* 37, 300–311. doi: 10.1111/pce.12157

Kuttan, R., Panikkar, B., and Binitha, P. P. (2015). Amino acids in sandal (*Santalum album* L) with special reference to cis-4-hydroxy-L-proline and sym. homospermidine. *Springerplus* 4:546. doi: 10.1186/s40064-015-1303-1

Lehmann, S., Gumy, C., Blatter, E., Boeffel, S., Fricke, W., and Rentsch, D. (2011). *In planta* function of compatible solute transporters of the AtProT family. *J. Exp. Bot.* 62, 787–796. doi: 10.1093/jxb/erq320

Marzol, E., Borassi, C., Bringas, M., Sede, A., Rodriguez Garcia, D. R., Capece, L., et al. (2018). Filling the gaps to solve the extensin puzzle. *Mol. Plant* 11, 645–658. doi: 10.1016/j.molp.2018.03.003

Meng, Z., Lou, Z., Liu, Z., Li, M., Zhao, X., Bartlam, M., et al. (2006). Crystal structure of human pyrroline-5-carboxylate reductase. *J. Mol. Biol.* 395, 1364–1377. doi: 10.1016/j.jmb.2006.04.053

Mezl, V. A., and Knox, W. E. (1976). Properties and analysis of a stable derivative of pyrroline-5-carboxylic acid for use in metabolic studies. *Anal. Biochem.* 74, 430–440. doi: 10.1016/0003-2697(76)90223-2

Monteoliva, M. I., Rizzi, Y. S., Cecchini, N. M., Hajirezaei, M. R., and Alvarez, M. E. (2014). Context of action of proline dehydrogenase (ProDH) in the hypersensitive response of Arabidopsis. *BMC Plant Biol.* 14:21. doi: 10.1186/1471-2229-14-21

Návarová, H., Bernsdorff, F., Döring, A.-C., and Zeier, J. (2012). Pipecolic acid, an endogenous mediator of defense amplification and priming, is a critical regulator of inducible plant immunity. *Plant Cell* 24, 5123–5141. doi: 10.1105/tpc.112.103564

Nocek, B., Chang, C., Li, H., Lezondra, L., Holzle, D., Collart, F., et al. (2005). Crystal structures of δ^1-pyrroline-5-carboxylate reductase from human pathogens *Neisseria meningitides* and *Streptococcus pyogenes*. *J. Mol. Biol.* 354, 91–106. doi: 10.1016/j.jmb.2005.08.036

Oufir, M., Schulz, N., Sha Vallikhan, P. S., Wilhelm, E., Burg, K., Hausman, J. F., et al. (2009). Simultaneous measurement of proline and related compounds in oak leaves by high-performance ligand-exchange chromatography and electrospray ionization mass spectrometry for environmental stress studies. *J. Chromatogr. A* 1216, 1094–1099. doi: 10.1016/j.chroma.2008.12.030

Radhakrishnan, A. N., and Giri, K. V. (1954). The isolation of allohydroxy-L-proline from sandal (*Santalum album* L.). *Biochem. J.* 58, 57–61. doi: 10.1042/bj0580057

Rena, A. B., and Splittstoesser, W. E. (1975). Proline dehydrogenase and pyrroline-5-carboxylate reductase from pumpkin cotyledons. *Phytochemistry* 14, 657–661. doi: 10.1016/0031-9422(75)83010-X

Ruszkowski, M., Nocek, B., Forlani, G., and Dauter, Z. (2015). The structure of *Medicago truncatula* δ^1-pyrroline-5-carboxylate reductase provides new insights into regulation of proline biosynthesis in plants. *Front. Plant Sci.* 6:869. doi: 10.3389/fpls.2015.00869

Santos-Díaz, M., and Ochoa-Alejo, N. (1994). PEG-tolerant cell clones of chili pepper: growth, osmotic potentials and solute accumulation. *Plant Cell Tissue Organ Cult.* 37, 1–8. doi: 10.1007/BF00048110

Sharma, S., Villamor, J. G., and Verslues, P. E. (2011). Essential role of tissue-specific proline synthesis and catabolism in growth and redox balance at low water potential. *Plant Physiol.* 157, 292–304. doi: 10.1104/pp.111.183210

Shinde, S., Villamor, J. G., Lin, W.-D., Sharma, S., and Verslues, P. E. (2016). Proline coordination with fatty acid synthesis and redox metabolism of chloroplast and mitochondria. *Plant Physiol.* 172, 1074–1088. doi: 10.1104/pp.16.01097

Signorelli, S. (2016). The fermentation analogy: a point of view for understanding the intriguing role of proline accumulation in stressed plants. *Front. Plant Sci.* 7:1339. doi: 10.3389/fpls.2016.01339

Szoke, A., Miao, G.-H., Hong, Z., and Verma, D. P. S. (1992). Subcellular location of δ^1-pyrroline-5-carboxylate reductase in root/nodule and leaf of soybean. *Plant Physiol.* 99, 1642–1649. doi: 10.1104/pp.99.4.1642

Thomason, K., Babar, M. A., Erickson, J. E., Mulvaney, M., Beecher, C., and MacDonald, G. (2018). Comparative physiological and metabolomics analysis of wheat (*Triticum aestivum* L.) following post-anthesis heat stress. *PLoS One* 13:e0197919. doi: 10.1371/journal.pone.0197919

Trovato, M., Forlani, G., Signorelli, S., and Funck, D. (2019). "Proline metabolism and its functions in development and stress tolerance," in *Osmoprotectant-Mediated Abiotic Stress Tolerance in Plants: Recent Advances and Future Perspectives*, eds M. A. Hossain, V. Kumar, D. J. Burritt, M. Fujita, and P. Mäkelä (Switzerland: Springer Nature).

Williams, I., and Frank, L. (1975). Improved chemical synthesis and enzymatic assay of δ^1-pyrroline-5-carboxylic acid. *Anal. Biochem.* 64, 85–97. doi: 10.1016/0003-2697(75)90408-x

Winter, G., Todd, C., Trovato, M., Forlani, G., and Funck, D. (2015). Physiological implications of arginine metabolism in plants. *Front. Plant Sci.* 6:534. doi: 10.3389/fpls.2015.00534

Conflict of Interest: The authors declare that the research was conducted in the absence of any commercial or financial relationships that could be construed as a potential conflict of interest.

Copyright © 2020 Forlani and Funck. This is an open-access article distributed under the terms of the Creative Commons Attribution License (CC BY). The use, distribution or reproduction in other forums is permitted, provided the original author(s) and the copyright owner(s) are credited and that the original publication in this journal is cited, in accordance with accepted academic practice. No use, distribution or reproduction is permitted which does not comply with these terms.

frontiers in Plant Science

PERSPECTIVE
published: 28 October 2020
doi: 10.3389/fpls.2020.582877

Proline Accumulation in Pollen Grains as Potential Target for Improved Yield Stability Under Salt Stress

*Roberto Mattioli[1,2], Noemi Palombi[1], Dietmar Funck[3] and Maurizio Trovato[1]**

[1] Department of Biology and Biotechnology, Sapienza University of Rome, Rome, Italy, [2] Department of Science, Roma Tre University, Rome, Italy, [3] Department of Plant Physiology and Biochemistry, University of Konstanz, Konstanz, Germany

Seed yield, a major determinant for the commercial success of grain crops, critically depends on pollen viability, which is dramatically reduced by environmental stresses, such as drought, salinity, and extreme temperatures. Salinity, in particular, is a major problem for crop yield known to affect about 20% of all arable land and cause huge economic losses worldwide. Flowering plants are particularly sensitive to environmental stress during sexual reproduction, and even a short exposure to stressing conditions can severely hamper reproductive success, and thus reduce crop yield. Since proline is required for pollen fertility and accumulates in plant tissues in response to different abiotic stresses, a role of proline in pollen protection under salt stress conditions can be envisaged. In this perspective, we analyze old and new data to evaluate the importance of pollen development under saline conditions, and discuss the possibility of raising proline levels in pollen grains as a biotechnological strategy to stabilize seed yield in the presence of salt stress. The overall data confirm that proline is necessary to preserve pollen fertility and limit seed loss under stressful conditions. However, at present, we have not enough data to conclude whether or not raising proline over wildtype levels in pollen grains can effectively ameliorate seed yield under saline conditions, and further work is still required.

Keywords: proline, pollen, seed yield, salt stress, *P5CS2*, stress tolerance

OPEN ACCESS

Edited by:
Vasileios Fotopoulos, Cyprus University of Technology, Cyprus

Reviewed by:
Saddam Hussain, University of Agriculture, Faisalabad, Pakistan
Nafees A. Khan, Aligarh Muslim University, India

***Correspondence:**
Maurizio Trovato
maurizio.trovato@uniroma1.it

Specialty section:
This article was submitted to Plant Physiology, a section of the journal Frontiers in Plant Science

Received: *13 July 2020*
Accepted: *12 October 2020*
Published: *28 October 2020*

Citation:
Mattioli R, Palombi N, Funck D and Trovato M (2020) Proline Accumulation in Pollen Grains as Potential Target for Improved Yield Stability Under Salt Stress. Front. Plant Sci. 11:582877. doi: 10.3389/fpls.2020.582877

INTRODUCTION

Abiotic stresses like extreme temperatures, drought, and high salinity are responsible for strong losses in crop production worldwide and are expected to worsen in the future because of the ongoing climate change (IPPC, 2019). High soil salinity inhibits plant growth and productivity mainly by limiting water uptake, promoting the intracellular accumulation of Na^+ and Cl^-, which in turn cause the accumulation of reactive oxygen species (ROS; Rengasamy, 2006; Munns and Tester, 2008; van Zelm et al., 2020). Numerous studies have addressed stress tolerance in plants mainly focusing on germination or the vegetative phase with comparatively little attention paid to the reproductive stage. In flowering plants, however, the reproductive phase is highly sensitive to abiotic stresses (Dolferus et al., 2011; Senapati et al., 2019).

POLLEN FERTILITY AND STRESS TOLERANCE

Most of the yield reduction caused by heat and drought stress are caused by hampered pollen viability and reduced ovule fertilization (Barnabas et al., 2008). The sensitivity of the reproductive phase to drought is especially evident in rice, where water stress caused incomplete anther and pollen development, incomplete anther dehiscence, a strong reduction in grain set, and precocious grain abortion soon after fertilization (Namuco and O'Toole, 1986; Ekanayake et al., 1989; Garrity and O'Toole, 1994; Guo et al., 2016). A positive relationship between grain yield and pollen fertility under drought or heat conditions also has been described in wheat (Lalonde et al., 1997; Yu et al., 2019). However, ovule and embryo development can also be involved in stress-induced sterility and reduced seed setting of grain crops (Wilkinson et al., 2018).

Salt stress experienced during the reproductive phase dramatically impedes pollen development and viability, as shown by *in vitro* pollen viability and germination tests from Petunia, maize, and carrot plants grown under saline conditions (Reddy and Goss, 1971; Dhingra and Varghese, 1985; El Sayed and Kirkwood, 1992; Kiełkowska et al., 2019). Reduced seed set as a consequence of hampered pollen fertility was also reported in rice (Abdullah et al., 2001; Gerona et al., 2019) and wheat (Abdullah et al., 1978) grown in saline soils. Direct experimental evidence for a decisive role of pollen quality in maintaining fertility and yield under salinity conditions was obtained in barley: The lower yield of a salt-sensitive cultivar was overcome by cross-pollination with pollen from a salt-tolerant cultivar (Hirasawa et al., 2017; Kodama et al., 2018).

PROLINE AND STRESS TOLERANCE

Although stress tolerance in plants is a complex process brought about by the coordinated action of different mechanisms (Munns and Gilliham, 2015), the accumulation of single compatible solutes has been reported to confer stress tolerance in several plant species (Biancucci et al., 2015; Hossain et al., 2019). Proline has long been known to accumulate upon abiotic and, to a lesser extent, biotic stresses, and the accumulation of this amino acid has been frequently correlated with improved stress tolerance (Forlani et al., 2019). More recently, transcriptomic and proteomic studies (Gupta et al., 2016; Hoermiller et al., 2017; Batista-Silva et al., 2019), genetic analyses (Xia et al., 2017) and meta-analyses of publicly available datasets (Hildebrandt, 2018; Guo et al., 2019), have corroborated the importance of proline metabolism in stress tolerance.

The molecular mechanisms by which proline exerts its effects on stress tolerance are not fully understood, and different functions may act together or in parallel (**Figure 1**). As a highly soluble zwitterionic molecule, proline can accumulate to high concentrations in plant cells and contribute to the osmotic potential. In this way, proline could limit the loss of water from cells during drought or salt stress conditions. While proline accumulation can significantly contribute to the osmotic pressure in halophytes, the biological significance of this mechanism has been questioned in glycophytes and might be only marginal (Munns and Tester, 2008; Forlani et al., 2019). With its kosmotropic properties, proline can facilitate the correct folding of proteins or counteract protein denaturation caused by water stress (Kumar, 2009; Forlani et al., 2019; Mojtabavi et al., 2019). Additionally, proline can prevent protein aggregation at low water availability or high ionic strength by modulating surface charges and Coulomb interactions (Govrin et al., 2018; Rydeen et al., 2018; Govrin et al., 2019). Alternatively or in addition, proline synthesis might improve stress tolerance in plants by modulating the $NADP^+$/NADPH ratio in the cytosol, resulting in crosstalk with other stress-related pathways like the oxidative pentose phosphate pathway (Sharma et al., 2011; Esposito, 2016). Last but not least, proline might also behave as a second messenger participating in signal transduction pathways leading to stress tolerance (Hayat et al., 2012; Liang et al., 2013).

A secondary effect of salinity, following osmotic and ionic stress, is oxidative stress, which leads to accumulation of reactive oxygen species (ROS), the removal of which represents an important mechanism of stress tolerance. Although a particular action of proline as ROS scavenger is unlikely (Signorelli et al., 2014), proline has been reported to reduce the accumulation of hydrogen peroxide, limit the peroxidation of cell lipids, and enhance the activities of antioxidant enzymes (Banu et al., 2009; Ben Rejeb et al., 2014, 2015; Guo et al., 2020; Hanif et al., 2020; Liu et al., 2020). Both the stabilization of antioxidant enzymes and the induction of gene expression have been suggested. A direct sensor for proline has so far not been identified in plants, but proline catabolism in mitochondria was shown to increase the production of ROS, which may in turn act to induce antioxidant enzyme expression (Liang et al., 2013; Ben Rejeb et al., 2014). Interestingly, proline degradation was also shown to induce the activity of plasma membrane NADPH oxidases, which in turn stimulates proline biosynthesis, potentially generating a feed-forward loop (Ben Rejeb et al., 2015; Fabro et al., 2016).

Intriguingly, proline also accumulates under non-stressed conditions after floral transition, mainly in reproductive tissues and organs, and is thought to contribute to the regulation and success of reproduction. The role of proline in plant sexual reproduction seems particularly important for pollen grains, where it accumulates in large amounts and is essential for pollen development and fertility (Trovato et al., 2019). Proline accumulation is mainly achieved by synthesis from glutamate through the sequential action of δ^1-pyrroline-carboxylate synthetase (P5CS) and δ^1-pyrroline-carboxylate reductase (P5CR). Like many seed crops, the model plant Arabidopsis contains two P5CS isoforms coded for by *P5CS1*, and *P5CS2*, respectively, while P5CR is encoded by a single *P5CR* gene (Turchetto-Zolet et al., 2009; Funck et al., 2012; Rai and Penna, 2013). Mitochondrial degradation mediated by proline dehydrogenase (ProDH) and δ^1-pyrroline-carboxylate dehydrogenase (P5CDH/GSALDH) can limit proline accumulation (Trovato et al., 2019). ProDH is also present in two isoforms in Arabidopsis, encoded by *ProDH1* and *ProDH2*, whereas P5CDH, which is also required for arginine degradation, is encoded by a single copy gene (Deuschle et al., 2001; Funck et al., 2010).

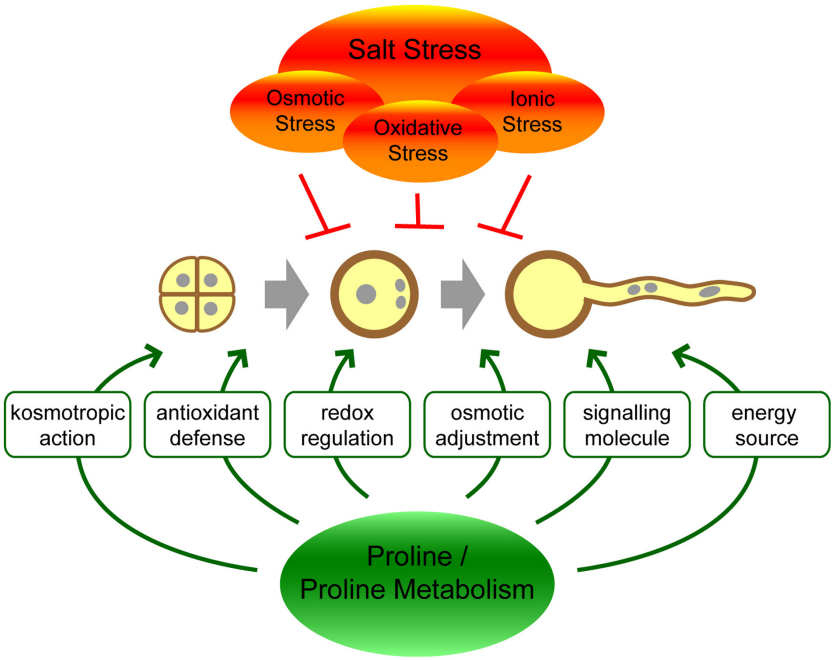

FIGURE 1 | Hypothetical functions of proline or proline metabolism in the protection of pollen against salt stress.

Despite the rapid and massive increase of proline after water stress, the causal connection between proline accumulation and stress tolerance remains a matter of debate. Although an overwhelming number of reports claim that proline accumulation leads to stress tolerance (Forlani et al., 2019), some authors have raised concerns hypothesizing that proline metabolism, rather than proline accumulation, might be responsible for stress tolerance (Bhaskara et al., 2015), or have challenged the notion that proline confers stress tolerance (Kim et al., 2016; Mwadzingeni et al., 2016; Mansour and Ali, 2017; Forlani et al., 2019). Signorelli (2016) proposed that the accumulation of proline during stress could be a mere consequence of the metabolic adaptation of plant cells to stress. Toxic effects of external proline application suggested that high proline content is not *per se* beneficial for plants under all conditions (Hellmann et al., 2000).

PROLINE AND STRESS TOLERANCE DURING SEED PRODUCTION

Some lines of evidence, however, may suggest a special role for proline in protecting reproductive processes under stressful conditions. In a study from Mwadzingeni et al. (2016) on ninety-six bread wheat (*Triticum aestivum* L.) genotypes, conducted under both greenhouse and field conditions, a weak but positive correlation between grain yield and proline content in vegetative tissue was detected. Strikingly, the beneficial role for proline accumulation in maintaining productivity was only evident when the drought stress was applied during flowering and grain-filling periods. Essential or beneficial roles of high proline contents were reported in several aspects of plant reproduction, such as flowering time, embryogenesis, and pollen development and fertility (Székely et al., 2008; Trovato et al., 2019). Also exogenous proline has been reported to stimulate yield under salt stress, although the mechanisms by which external proline treatment can mitigate the negative effects of salt remain elusive and may not be identical to those of endogenous proline accumulation (Farooq et al., 2017; Meena et al., 2019; El Moukhtari et al., 2020). In wheat grown in the presence of 120 mM NaCl, for example, pretreatment with proline increased fresh and dry biomass, grain yield and grain weight (Rady et al., 2019). In maize treated with different concentrations of NaCl, proline solutions sprayed on maize leaves improved growth and grain yield at 25 mM and 50 mM NaCl (Alam et al., 2016). To the best of our knowledge, the economic feasibility of using external proline application as an agricultural practice has never been analyzed.

The increased abundance of proline observed in reproductive tissues after floral transition in Arabidopsis (Chiang and Dandekar, 1995) may reflect the specific need for stress protection during the reproductive phase. In support of this hypothesis, Sulpice et al. (2003) reported that treatment of Arabidopsis plants with 100 mM NaCl caused both pollen and ovule sterility, leading to a strong reduction of the number of seeds per silique. These defects were partially rescued in transgenic Arabidopsis engineered to accumulate glycine betaine, a non-proteinogenic amino acid with similar properties as proline (Sulpice et al., 2003; Waditee et al., 2005).

To verify a possible correlation between grain yield and proline content, we carried out a series of experiments with the proline deficient sesquimutant *p5cs1 p5cs2/P5CS2* (homozygous for a *p5cs1* mutation and heterozygous for *p5cs2*), and

analyzed the number of seeds per silique under moderate salt stress conditions (For experimental details see **Supplementary Methods S1**). Similar to Sulpice et al. (2003), we found that salt stress treatment, administered after floral transition, led to a significant and proportional reduction in the number of seeds per silique of wildtype plants (**Figure 2A** and **Supplementary Table S2**). When we exposed the *p5cs1 p5cs2/P5CS2* mutant to 150 mM NaCl, the detrimental effect was even more pronounced than in wildtype plants, and we recorded significantly stronger reduction in the number of seeds per silique (**Figure 2B** and **Supplementary Table S3**), supporting, in the converse argument, the hypothesis that proline may reduce salinity damages on seed production. While these data confirm the importance of proline for seed set under salt stress conditions, they do not clarify whether or not it is specifically important for pollen protection, because all tissues of a *p5cs1 p5cs2/P5CS2* mutant are poor in proline. The content of free proline measured in *p5cs1 p5cs2/P5CS2* mutants varies depending on different tissues and growth conditions, but, on average, these sesquimutants have from one-third to one-fourth as much proline as wildtype plants (Funck et al., 2012; Mattioli et al., 2012, 2018).

Data from *p5cs1 p5cs2/P5CS2* p_{17340}*:P5CS2,* a *p5cs1 p5cs2/P5CS2* mutant expressing an additional copy of the proline biosynthesis gene *P5CS2* under the control of the pollen-specific promoter of the *At5g17340* gene, encoding a putative membrane lipoprotein (Honys and Twell, 2004; Mattioli et al., 2018), though, provided further support for the hypothesis that proline is especially important in pollen protection under stress. The number of seeds per silique in a *p5cs1 p5cs2/P5CS2* p_{17340}*:P5CS2* line was significantly higher compared to the parental *p5cs1 p5cs2/P5CS2* sesquimutants under stress conditions, and close to wildtype numbers (**Figure 2B** and **Supplementary Table S2**). Since the pollen-specific expression of *p5cs1 p5cs2/P5CS2* p_{17340}*:P5CS2* can complement the defect of proline synthesis in pollen grains but not in other tissues (Mattioli et al., 2018), the fewer seeds found in sesquimutant siliques are likely caused by insufficient proline in pollen grains. At present, however, we cannot rule out a possible contribution of ovule fertility in the overall process of seed production under the tested conditions, and further investigations are clearly needed.

DOES ENHANCED PROLINE ACCUMULATION IN POLLEN GRAINS IMPROVE SEED PRODUCTION UNDER SALT STRESS?

Despite the encouraging indications coming from the literature, and from our experiments with mutants defective in proline synthesis, clear-cut evidence that enhanced proline accumulation in pollen grains can sustain seed production under stress is still lacking. In an attempt to clarify this point, we introduced the pollen-specific p_{17340}*:P5CS2* construct in wildtype Arabidopsis plants and analyzed the resulting transgenic plants for the number of seeds per silique. In preliminary results from heterozygous T1 progeny directly after the selection, most

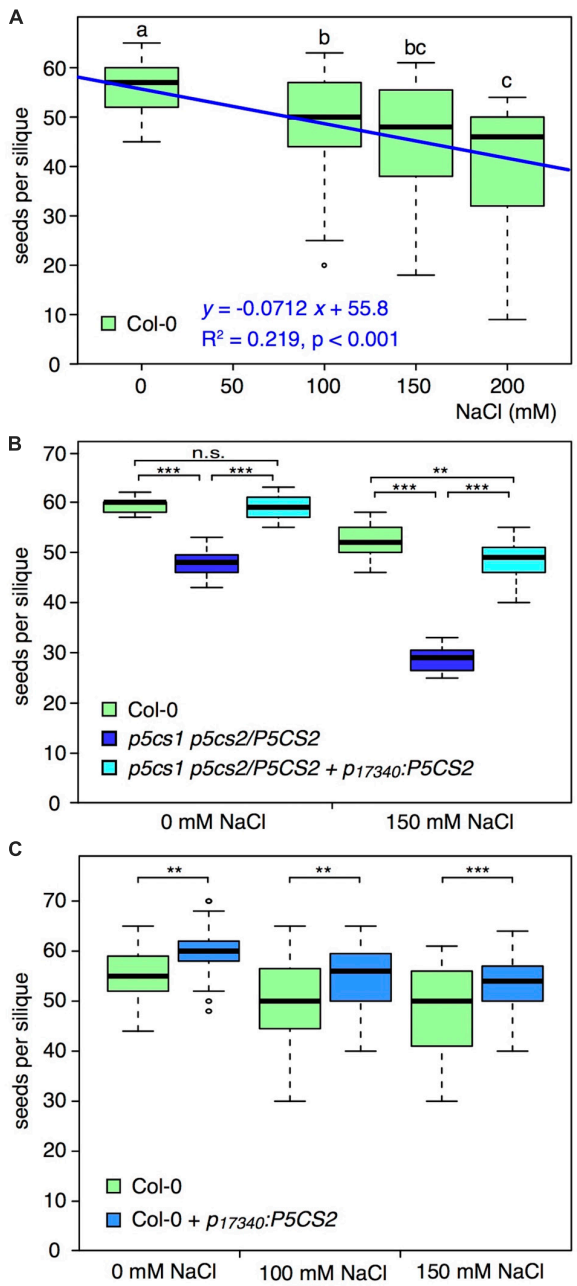

FIGURE 2 | Effects of salt on the number of seeds per silique in different genotypes. **(A)** Box plot and regression line (blue) showing the effects of different NaCl concentrations on the number of seeds per silique in wildtype (Col-0) plants. Different letters indicate significant differences ($p < 0.05$, $n = 31$ siliques per salt concentration) between groups calculated by all-pairwise Mann-Whitney-Wilcoxon tests. **(B)** Box plot of the numbers of seeds per silique in wildtype (green), *p5cs1 p5cs2/P5CS2* sesquimutants (dark blue), and *p5cs1 p5cs2/P5CS2* + p_{17340}*:P5CS2* (light blue), treated without or with 150 mM NaCl. Asterisks indicate significant differences between genotypes (**: $p < 0.01$, ***: $p < 0.001$, n.s.: not significant; $n = 15$ siliques per genotype and condition). All genotypes had significantly reduced numbers of seeds per silique under salt stress and there was a significant interaction between salt stress and genotype. **(C)** Box plot showing the numbers of seeds per silique in wildtype (green) and p_{17340}*:P5CS2* (blue) treated with 0, 100, and 150 mM

(Continued)

FIGURE 2 | Continued
NaCl. Asterisks indicate significant differences between genotypes (**: $p < 0.01$, ***: $p < 0.001$; $28 < n < 74$ siliques per genotype and condition). Both genotypes showed significantly reduced numbers of seeds per silique in response to salt stress but there was no significant interaction between salt stress and genotype. In all the panels, boxes indicate the lower and upper quartiles, and the solid horizontal line shows the median. Whiskers above and below the box display the 90th and 10th percentile, respectively, and outliers are shown as open circles. Representative data sets from at least three replicates with independent transgenic lines are shown. For details about statistical analyses please refer to **Supplementary Tables 1–3**.

transgenic lines produced more seeds per silique. In the T2 generation, we found several homozygous lines bearing significantly more seeds per silique than wildtype, while others produced similar or even lower seed numbers. However, when we exposed the plants with more seeds per silique to 100 or 150 mM NaCl after floral transition, we observed a decline in seed numbers both in wildtype and in p_{17340}*:P5CS2* transgenic plants (**Figure 2C** and **Supplementary Table S4**), with similar trendline slopes of −0.046 for wildtype and −0.044 for p_{17340}*:P5CS2.* At 200 mM NaCl, the seed numbers per silique were on average lower in the p_{17340}*:P5CS2* transgenic plants but the data were too variable for both genotypes and could not be meaningfully included in the statistical analysis (data not shown).

At this stage, we can say that expression of an additional copy of *P5CS2* in pollen during late stages of development, as mediated by the *At5g17340* promoter, improves pollination and fertilization success. However, we cannot draw a final conclusion whether enhanced proline accumulation in pollen could improve the yield stability under salt stress conditions.

Although this result may corroborate the hypothesis that proline accumulation is not causal for salt stress tolerance, there are still good reasons for further investigations. A possible reason for the unchanged salt sensitivity of our p_{17340}*:P5CS2* transgenic plants could be that we chose a wrong pollen-specific promoter. Although very effective in a proline-deficient mutant, this promoter might not be strong enough to provide a significant proline surplus in a wildtype background subjected to salt stress, when the expression of the endogenous *P5CS1* gene is already induced (Strizhov et al., 1997). Alternatively, the protective capacity of proline accumulation or biosynthesis could already be exhausted in pollen and any further increase may draw resources from other protective mechanisms.

FUTURE PERSPECTIVES

Proline accumulation, especially in pollen, has undoubtedly a major role in the critical phase of seed development under stress, as it has been shown earlier and was reinforced in this work. At present, direct experimental proof is still lacking that it is possible to raise proline levels in pollen grains above physiological levels, and that such an increase could effectively improve seed yield under (salt) stress conditions. The *At5g17340* promoter used in this study is expressed in gametophytic, but not in sporophytic tissues of the anther during late phases of pollen maturation (da Costa-Nunes, 2013; Mattioli et al., 2018). It is possible that, under salt stress conditions, increased proline content or biosynthesis would additionally be required during meiosis and early microspore development or in sporophytic tissues, particularly the tapetum, to improve pollen development and quality. Alternative or artificially enhanced promoters may be used to boost P5CS expression in the male reproductive tissue.

Feedback regulation of both proline biosynthesis and degradation have been demonstrated and may prevent or limit the further increase in proline levels in pollen. In particular, the feedback inhibition exerted by proline on the activity of P5CS1 and P5CS2 (Zhang et al., 1995) can potentially limit proline accumulation in pollen grains and might be removed by mutagenesis of a critical, conserved phenylalanine residue (Zhang et al., 1995; Hong et al., 2000), through gene editing. Both, the expression of *ProDH1* and, to a lesser extent, *ProDH2* were shown to be upregulated by proline in Arabidopsis via the transcription factor bZIP11 (Satoh et al., 2004; Hanson et al., 2008). The binding sites of bZIP11 in the promoters of *ProDH1* and *ProDH2* are known and could be modified or blocked by an artificial binding protein. Alternatively, *DFR1,* encoding a mitochondrial protein potentially inhibiting proline degradation (Ren et al., 2018) might be overexpressed in pollen. In addition, it is known that different plant species, and even different natural mutants of a same species, can use different post-transcriptional, post-translational and epigenetic regulatory mechanisms to adjust proline homeostasis, including alternative splicing (Kesari et al., 2012), ubiquitination (Ju et al., 2013; Kim et al., 2017), histone trimethylation (Feng et al., 2016) and microRNA-mediated regulation (Gupta, 2020).

To improve the chances of successfully modifying stress tolerance of pollen development, a better knowledge of the metabolites and metabolic processes important for microspore development will be required. In a recent work, Wada et al. (2020) used on-site cell-specific mass spectrometry to analyze the metabolome of single pollen grains under normal and heat stress conditions, and found proline as one of the most abundant metabolites. This new technology might be used to identify mutants with increased proline content and to determine if proline accumulation is at some point limited by precursor availability or may interfere with other metabolic pathways. In parallel, the recent improvements of single-cell transcriptomics will facilitate the comparison between different developmental phases of pollen in the absence or presence of stress, and may help to identify additional genes that are essential for pollen viability under stress. All experiments that aim to enhance the stress tolerance of pollen should be carried out and verified in different stress conditions and carefully designed, not only *in vitro* but also in field conditions, to evaluate in real conditions the feasibility of this strategy to improve crop resilience to salinity stress.

DATA AVAILABILITY STATEMENT

The original contributions presented in the study are included in the article/**Supplementary Material**, further inquiries can be directed to the corresponding author.

AUTHOR CONTRIBUTIONS

MT and DF organized and wrote the manuscript and performed the statistical analyses. RM generated the transgenic plants. NP performed the stress experiments and the count of seeds. All authors have read and approved the manuscript.

FUNDING

This work was funded by Sapienza University of Rome and by the University of Konstanz.

ACKNOWLEDGMENTS

We thank Rosi Miller and the gardener team of the University of Konstanz for help with plant cultivation and propagation. Marc Stift from the ecology group of the University of Konstanz provided help with the statistical analyses.

SUPPLEMENTARY MATERIAL

The Supplementary Material for this article can be found online at: https://www.frontiersin.org/articles/10.3389/fpls.2020.582877/full#supplementary-material

REFERENCES

Abdullah, Z., Ahmad, R., and Ahmed, J. (1978). Salinity induced changes in the reproductive physiology of wheat plants. *Plant Cell Physiol.* 19, 99–106. doi: 10.1093/oxfordjournals.pcp.a075584

Abdullah, Z., Khan, M. A., and Flowers, T. J. (2001). Causes of Sterility in seed set of rice under Salinity stress. *J. Agron. Crop Sci.* 187, 25–32. doi: 10.1046/j.1439-037X.2001.00500.x

Alam, R., Das, D., Islam, M., Murata, Y., and Hoque, M. (2016). Exogenous proline enhances nutrient uptake and confers tolerance to salt stress in maize (*Zea mays L.*). *Progr. Agric.* 27, 409–417. doi: 10.3329/pa.v27i4.32120

Banu, N. A., Hoque, A., Watanabe-Sugimoto, M., Matsuoka, K., Nakamura, Y., Shimoishi, Y., et al. (2009). Proline and glyclinebetaine induce antioxidant defense gene expression and suppress cell death in cultured tobacco cells under salt stress. *J. Plant Physiol.* 166, 146–156. doi: 10.1016/j.jplph.2008.03.002

Barnabas, B., Jager, K., and Feher, A. (2008). The effect of drought and heat stress on reproductive processes in cereals. *Plant Cell Environ.* 31, 11–38. doi: 10.1111/j.1365-3040.2007.01727.x

Batista-Silva, W., Heinemann, B., Rugen, N., Nunes-Nesi, A., Araújo, W. L., Braun, H.-P., et al. (2019). The role of amino acid metabolism during abiotic stress release. *Plant Cell Environ.* 42, 1630–1644. doi: 10.1111/pce.13518

Ben Rejeb, K., Abdelly, C., and Savoure, A. (2014). How reactive oxygen species and proline face stress together. *Plant Physiol. Biochem.* 80, 278–284. doi: 10.1016/j.plaphy.2014.04.007

Ben Rejeb, K., Lefebvre-De Vos, D., Le Disquet, I., Leprince, A.-S., Bordenave, M., Maldiney, R., et al. (2015). Hydrogen peroxide produced by NADPH oxidases increases proline accumulation during salt or mannitol stress in *Arabidopsis thaliana*. *New Phytol.* 208, 1138–1148. doi: 10.1111/nph.13550

Bhaskara, G. B., Yang, T. H., and Verslues, P. E. (2015). Dynamic proline metabolism: importance and regulation in water limited environments. *Front. Plant Sci.* 6:484. doi: 10.3389/fpls.2015.00484

Biancucci, M., Mattioli, R., Forlani, G., Funck, D., Costantino, P., and Trovato, M. (2015). Role of proline and GABA in sexual reproduction of angiosperms. *Front. Plant Sci.* 6:680. doi: 10.3389/fpls.2015.00680

Chiang, H. H., and Dandekar, A. M. (1995). Regulation of proline accumulation in *Arabidopsis thaliana* (L) Heynh during development and in response to desiccation. *Plant Cell Environ.* 18, 1280–1290. doi: 10.1111/J.1365-3040.1995.Tb00187.X

da Costa-Nunes, J. A. (2013). A novel *Arabidopsis* marker line that strongly labels uninucleate microspores and the subsequent male gametophyte development stages. *SpringerPlus* 2:237. doi: 10.1186/2193-1801-2-237

Deuschle, K., Funck, D., Hellmann, H., Daschner, K., Binder, S., and Frommer, W. B. (2001). A nuclear gene encoding mitochondrial Delta-pyrroline-5-carboxylate dehydrogenase and its potential role in protection from proline toxicity. *Plant J.* 27, 345–356. doi: 10.1046/j.1365-313x.2001.01101.x

Dhingra, H. R., and Varghese, T. M. (1985). Effect of Salt Stress on Viability. *Germination and Endogenous Levels of Some Metabolites and Ions in Maize (Zea-Mays-L) Pollen. Ann. Bot.* 55, 415–420. doi: 10.1093/oxfordjournals.aob.a086920

Dolferus, R., Ji, X., and Richards, R. A. (2011). Abiotic stress and control of grain number in cereals. *Plant Sci.* 181, 331–341. doi: 10.1016/j.plantsci.2011.05.015

Ekanayake, I. J., De Datta, S. K., and Steponkus, P. L. (1989). Spikelet sterility and flowering response of rice to water stress at anthesis. *Ann. Bot.* 63, 257–264. doi: 10.1093/oxfordjournals.aob.a087740

El Moukhtari, A., Cabassa-Hourton, C., Farissi, M., and Savouré, A. (2020). How does proline treatment promote salt stress tolerance during crop plant development? *Front. Plant Sci.* 11:1127. doi: 10.3389/fpls.2020.01127

El Sayed, H., and Kirkwood, R. C. (1992). Effects of NaCl salinity and hydrogel polymer treatment on viability, germination and solute content in maize (Zea mays) pollen. *Phyton Ann. Rei Bot. Horn* 32, 143–157.

Esposito, S. (2016). Nitrogen assimilation, Abiotic stress and Glucose 6-Phosphate dehydrogenase: the Full Circle of Reductants. *Plants (Basel)* 5:24. doi: 10.3390/plants5020024

Fabro, G., Rizzi, Y. S., and Alvarez, M. E. (2016). *Arabidopsis* proline dehydrogenase contributes to flagellin-mediated PAMP-triggered immunity by affecting RBOHD. *Mol. Plant Microbe. Interact.* 29, 620–628. doi: 10.1094/MPMI-01-16-0003-R

Farooq, M., Nawaz, A., Chaudhry, M. A. M., Indrasti, R., and Rehman, A. (2017). Improving resistance against terminal drought in bread wheat by exogenous application of proline and gamma-aminobutyric acid. *J. Agron. Crop Sci.* 203, 464–472. doi: 10.1111/jac.12222

Feng, X. J., Li, J. R., Qi, S. L., Lin, Q. F., Jin, J. B., and Hua, X. J. (2016). Light affects salt stress-induced transcriptional memory of P5CS1 in *Arabidopsis*. *Proc. Natl. Acad. Sci. U.S.A.* 113, E8335–E8343. doi: 10.1073/pnas.1610670114

Forlani, G., Trovato, M., Funck, D., and Signorelli, S. (2019). "Regulation of proline accumulation and its molecular and physiological functions in stress defence," in *Osmoprotectant-Mediated Abiotic Stress Tolerance in Plants: Recent Advances and Future Perspectives*, eds M. A. Hossain, V. Kumar, D. Burritt, M. Fujita, and P. Mäkelä (New York, NY: Springer Press), 73–97. doi: 10.1007/978-3-030-27423-8_3

Funck, D., Eckard, S., and Muller, G. (2010). Non-redundant functions of two proline dehydrogenase isoforms in *Arabidopsis*. *BMC Plant Biol.* 10:70. doi: 10.1186/1471-2229-10-70

Funck, D., Winter, G., Baumgarten, L., and Forlani, G. (2012). Requirement of proline synthesis during *Arabidopsis* reproductive development. *BMC Plant Biol.* 12:191. doi: 10.1186/1471-2229-12-191

Garrity, D. P., and O'Toole, J. C. (1994). Screening rice for drought resistance at the reproductive phase. *Field Crops Res.* 39, 99–110. doi: 10.1016/0378-4290(94)90012-4

Gerona, M. B., Deocampo, M. P., Egdane, J. A., Ismail, A. M., and Dionisio-Sese, M. L. (2019). Physiological responses of contrasting rice genotypes to salt stress at reproductive stage. *Rice Sci.* 26, 207–219. doi: 10.1016/j.rsci.2019.05.001

Govrin, R., Obstbaum, T., and Sivan, U. (2019). Common source of cryoprotection and osmoprotection by osmolytes. *J. Am. Chem. Soc.* 141, 13311–13314. doi: 10.1021/jacs.9b06727

Govrin, R., Tcherner, S., Obstbaum, T., and Sivan, U. (2018). Zwitterionic osmolytes resurrect electrostatic interactions screened by salt. *J. Am. Chem. Soc.* 140, 14206–14210. doi: 10.1021/jacs.8b07771

Guo, C., Yao, L., You, C., Wang, S., Cui, J., Ge, X., et al. (2016). MID1 plays an important role in response to drought stress during reproductive development. *Plant J.* 88, 280–293. doi: 10.1111/tpj.13250

Guo, M., Liu, X., Wang, J., Li, L., Zhang, W., Gong, B., et al. (2019). Investigation on salt-response mechanisms in *Arabidopsis thaliana* from UniProt protein knowledgebase. *J. Plant Interact.* 14, 21–29. doi: 10.1080/17429145.2018.1551581

Guo, M., Zhang, X., Liu, J., Hou, L., Liu, H., and Zhao, X. (2020). OsProDH negatively regulates thermotolerance in rice by modulating proline metabolism and reactive oxygen species scavenging. *Rice* 13:61. doi: 10.1186/s12284-020-00422-3

Gupta, A. (2020). *ath-miR164c* influences plant responses to the combined stress of drought and bacterial infection by regulating proline metabolism. *Environ. Exp. Bot.* 172:103998. doi: 10.1016/j.envexpbot.2020.103998

Gupta, A., Sarkar, A. K., and Senthil-Kumar, M. (2016). Global transcriptional analysis reveals unique and shared responses in *Arabidopsis thaliana* exposed to combined drought and pathogen stress. *Front. Plant Sci.* 7:686. doi: 10.3389/fpls.2016.00686

Hanif, S., Saleem, M. F., Sarwar, M., Irshad, M., Shakoor, A., Wahid, M. A., et al. (2020). Biochemically triggered heat and drought stress tolerance in rice by proline application. *J. Plant Growth Regul.* doi: 10.1007/s00344-020-10095-3

Hanson, J., Hanssen, M., Wiese, A., Hendriks, M. M., and Smeekens, S. (2008). The sucrose regulated transcription factor bZIP11 affects amino acid metabolism by regulating the expression of *ASPARAGINE SYNTHETASE1* and *PROLINE DEHYDROGENASE2*. *Plant J.* 53, 935–949. doi: 10.1111/j.1365-313X.2007.03385.x

Hayat, S., Hayat, Q., Alyemeni, M. N., Wani, A. S., Pichtel, J., and Ahmad, A. (2012). Role of proline under changing environments: a review. *Plant Signal Behav.* 7, 1456–1466. doi: 10.4161/psb.21949

Hellmann, H., Funck, D., Rentsch, D., and Frommer, W. B. (2000). Hypersensitivity of an *Arabidopsis* sugar signaling mutant toward exogenous proline application. *Plant Physiol.* 123, 779–789. doi: 10.1104/pp.123.2.779

Hildebrandt, T. M. (2018). Synthesis versus degradation: directions of amino acid metabolism during *Arabidopsis* abiotic stress response. *Plant Mol. Biol.* 98, 121–135. doi: 10.1007/s11103-018-0767-0

Hirasawa, T., Sato, K., Yamaguchi, M., Narita, R., Kodama, A., Adachi, S., et al. (2017). Differences in dry matter production, grain production, and photosynthetic rate in barley cultivars under long-term salinity. *Plant Prod. Sci.* 20, 288–299. doi: 10.1080/1343943x.2017.1343647

Hoermiller, I. I., Naegele, T., Augustin, H., Stutz, S., Weckwerth, W., and Heyer, A. G. (2017). Subcellular reprogramming of metabolism during cold acclimation in *Arabidopsis thaliana*. *Plant Cell Environ.* 40, 602–610. doi: 10.1111/pce.12836

Hong, Z., Lakkineni, K., Zhang, Z., and Verma, D. P. S. (2000). Removal of feedback inhibition of Δ1-Pyrroline-5-Carboxylate synthetase results in increased proline accumulation and protection of plants from osmotic stress. *Plant Physiol.* 122, 1129–1136. doi: 10.1104/pp.122.4.1129

Honys, D., and Twell, D. (2004). Transcriptome analysis of haploid male gametophyte development in *Arabidopsis*. *Genome Biol.* 5:R85. doi: 10.1186/gb-2004-5-11-r85

Hossain, M. A., Kumar, V., Burritt, D., Fujita, M., and Mäkelä, P. (eds) (2019). *Osmoprotectant-Mediated Abiotic Stress Tolerance In Plants: Recent Advances And Future Perspectives*. New York, NY: Springer Nature.

IPPC (2019). *Climate Change and Land: An IPCC Special Report on Climate Change, Deserti Cation, Land Degradation, Sustainable Land Management, Foodsecurity, and Greenhouse Gas Fluxes in Terrestrial Ecosystems*, eds P. R. Shukla, J. Skea, E. Calvo Buendia, V. Masson-Delmotte, H.-O. Pörtner, D. C. Roberts, et al. (Geneva: IPCC).

Ju, H.-W., Min, J.-H., Chung, M.-S., and Kim, C. S. (2013). The *atrzf1* mutation of the novel RING-type E3 ubiquitin ligase increases proline contents and enhances drought tolerance in *Arabidopsis*. *Plant Sci.* 20, 1–7. doi: 10.1016/j.plantsci.2012.12.007

Kesari, R., Lasky, J. R., Villamor, J. G., Des Marais, D. L., Chen, Y.-J. C., Liu, T.-W., et al. (2012). Intron-mediated alternative splicing of *Arabidopsis P5CS1* and its association with natural variation in proline and climate adaptation. *Proc. Natl. Acad. Sci. U.S.A.* 109, 9197–9202. doi: 10.1073/pnas.1203433109

Kiełkowska, A., Grzebelus, E., Lis-Krzyścin, A., and Maćkowska, K. (2019). Application of the salt stress to the protoplast cultures of the carrot (*Daucus carota* L.) and evaluation of the response of regenerants to soil salinity. *Plant Cell Tissue Organ. Cult.* 137, 379–395. doi: 10.1007/s11240-019-01578-7

Kim, A.-R., Min, J.-H., Lee, K.-H., and Kim, C. S. (2017). PCA22 acts as a suppressor of *atrzf1* to mediate proline accumulation in response to abiotic stress in *Arabidopsis*. *J. Exp. Bot.* 68, 1797–1809. doi: 10.1093/jxb/erx069

Kim, J., Liu, Y., Zhang, X., Zhao, X., and Childs, K. L. (2016). Analysis of salt-induced physiological and proline changes in 46 switchgrass (*Panicum virgatum*) lines indicates multiple response modes. *Plant Physiol. Biochem.* 105, 203–212. doi: 10.1016/j.plaphy.2016.04.020

Kodama, A., Narita, R., Yamaguchi, M., Hisano, H., Adachi, S., Takagi, H., et al. (2018). QTLs maintaining grain fertility under salt stress detected by exome QTL-seq and interval mapping in barley. *Breeding Sci.* 68, 561–570. doi: 10.1270/jsbbs.18082

Kumar, R. (2009). Role of naturally occurring osmolytes in protein folding and stability. *Arch. Biochem. Biophys.* 491, 1–6. doi: 10.1016/j.abb.2009.09.007

Lalonde, S., Beebe, D. U., and Saini, H. S. (1997). Early signs of disruption of wheat anther development associated with the induction of male sterility by meiotic-stage water deficit. *Sex. Plant Reprod.* 10, 40–48. doi: 10.1007/s004970050066

Liang, X., Zhang, L., Natarajan, S. K., and Becker, D. F. (2013). Proline mechanisms of stress survival. *Antioxid. Redox Signal.* 19, 998–1011. doi: 10.1089/ars.2012.5074

Liu, L., Huang, L., Lin, X., and Sun, C. (2020). Hydrogen peroxide alleviates salinity-induced damage through enhancing proline accumulation in wheat seedlings. *Plant Cell Rep.* 39, 567–575. doi: 10.1007/s00299-020-02513-3

Mansour, M. M. F., and Ali, E. F. (2017). Evaluation of proline functions in saline conditions. *Phytochemistry* 140, 52–68. doi: 10.1016/j.phytochem.2017.04.016

Mattioli, R., Biancucci, M., El Shall, A., Mosca, L., Costantino, P., Funck, D., et al. (2018). Proline synthesis in developing microspores is required for pollen development and fertility. *BMC Plant Biol.* 18:356. doi: 10.1186/s12870-018-1571-3

Mattioli, R., Biancucci, M., Lonoce, C., Costantino, P., and Trovato, M. (2012). Proline is required for male gametophyte development in *Arabidopsis*. *BMC Plant Biol.* 12:236. doi: 10.1186/1471-2229-12-236

Meena, M., Divyanshu, K., Kumar, S., Swapnil, P., Zehra, A., Shukla, V., et al. (2019). Regulation of L-proline biosynthesis, signal transduction, transport, accumulation and its vital role in plants during variable environmental conditions. *Heliyon* 5:e02952. doi: 10.1016/j.heliyon.2019.e02952

Mojtabavi, S., Samadi, N., and Faramarzi, M. A. (2019). Osmolyte-Induced folding and stability of proteins: concepts and Characterization. *Iran J. Pharm. Res.* 18(Suppl.1), 13–30. doi: 10.22037/ijpr.2020.112621.13857

Munns, R., and Gilliham, M. (2015). Salinity tolerance of crops–what is the cost? *New Phytol.* 208, 668–673. doi: 10.1111/nph.13519

Munns, R., and Tester, M. (2008). Mechanisms of salinity tolerance. *Annu. Rev. Plant Biol.* 59, 651–681. doi: 10.1146/annurev.arplant.59.032607.092911

Mwadzingeni, L., Shimelis, H., Tesfay, S., and Tsilo, T. J. (2016). Screening of bread wheat genotypes for drought tolerance using phenotypic and proline analyses. *Front. Plant Sci.* 7:1276. doi: 10.3389/fpls.2016.01276

Namuco, O. S., and O'Toole, J. C. (1986). Reproductive Stage Water Stress and Sterility. I. Effect of Stress during Meiosis1. *Crop Sci.* 26, 317–321. doi: 10.2135/cropsci1986.0011183X002600020022x

Rady, M., Kusvuran, A., Alharby, H. F., Alzahrani, Y., and Kusvuran, S. (2019). Pretreatment with proline or an organic bio-stimulant induces salt tolerance in wheat plants by improving antioxidant redox state and enzymatic activities and reducing the oxidative stress. *Growth Regul.* 38, 449–462. doi: 10.1007/s00344-018-9860-5

Rai, A. N., and Penna, S. (2013). Molecular evolution of plant P5CS gene involved in proline biosynthesis. *Mol. Biol. Rep.* 40, 6429–6435. doi: 10.1007/s11033-013-2757-2

Reddy, P. R., and Goss, G. A. (1971). Effect of salinity on pollen viability as altered by increasing osmotic pressure with NaCl. $MgCl_2$ and $CaCl_2$. *Am. J. Bot.* 58, 721–725. doi: 10.1002/j.1537-2197.1971.tb10025.x

Ren, Y., Miao, M., Meng, Y., Cao, J., Fan, T., Yue, J., et al. (2018). DFR1-mediated inhibition of proline degradation pathway regulates drought and freezing tolerance in *Arabidopsis*. *Cell Rep.* 23, 3960–3974. doi: 10.1016/j.celrep.2018.04.011

Rengasamy, P. (2006). World salinization with emphasis on Australia. *J. Exp. Bot.* 57, 1017–1023. doi: 10.1093/jxb/erj108

Rydeen, A. E., Brustad, E. M., and Pielak, G. J. (2018). Osmolytes and protein-protein interactions. *J. Am. Chem. Soc.* 140, 7441–7444. doi: 10.1021/jacs.8b03903

Satoh, R., Fujita, Y., Nakashima, K., Shinozaki, K., and Yamaguchi-Shinozaki, K. (2004). A novel subgroup of bZIP proteins functions as transcriptional activators in hypoosmolarity-responsive expression of the ProDH Gene in *Arabidopsis*. *Plant Cell Physiol.* 45, 309–317. doi: 10.1093/pcp/pch036

Senapati, N., Stratonovitch, P., Paul, M. J., and Semenov, M. A. (2019). Drought tolerance during reproductive development is important for increasing wheat yield potential under climate change in Europe. *J. Exp. Bot.* 70, 2549–2560. doi: 10.1093/jxb/ery226

Sharma, S., Villamor, J. G., and Verslues, P. E. (2011). Essential role of tissue-specific proline synthesis and catabolism in growth and redox balance at low water potential. *Plant Physiol.* 157, 292–304. doi: 10.1104/pp.111.183210

Signorelli, S. (2016). The fermentation analogy: a point of view for understanding the intriguing role of proline accumulation in stressed plants. *Front. Plant Sci.* 7:1339. doi: 10.3389/fpls.2016.01339

Signorelli, S., Coitino, E. L., Borsani, O., and Monza, J. (2014). Molecular mechanisms for the reaction between (OH)-O-center dot radicals and proline: insights on the role as reactive oxygen species scavenger in plant stress. *J. Phys. Chem. B* 118, 37–47. doi: 10.1021/jp407773u

Strizhov, N., Ábrahám, E., Ökrész, L., Blickling, S., Zilberstein, A., Schell, J., et al. (1997). Differential expression of two *P5CS* genes controlling proline accumulation during salt-stress requires ABA and is regulated by ABA1. ABI1 and AXR2 *in Arabidopsis*. *Plant J.* 12, 557–569. doi: 10.1046/j.1365-313x.1997.00557.x

Sulpice, R., Tsukaya, H., Nonaka, H., Mustardy, L., Chen, T. H., and Murata, N. (2003). Enhanced formation of flowers in salt-stressed *Arabidopsis* after genetic engineering of the synthesis of glycine betaine. *Plant J.* 36, 165–176. doi: 10.1046/j.1365-313x.2003.01873.x

Székely, G., Ábrahám, E., Cséplő, A., Rigó, G., Zsigmond, L., Csiszár, J., et al. (2008). Duplicated *P5CS* genes of *Arabidopsis* play distinct roles in stress regulation and developmental control of proline biosynthesis. *Plant J.* 53, 11–28. doi: 10.1111/j.1365-313X.2007.03318.x

Trovato, M., Forlani, G., Signorelli, S., and Funck, D. (2019). "Proline Metabolism and its Functions in Development and Stress Tolerance," in *Osmoprotectant-Mediated Abiotic Stress Tolerance in Plants: Recent Advances and Future Perspectives*, eds M. A. Hossain, V. Kumar, D. Burritt, M. Fujita, and P. Mäkelä (New York, NY: Springer Press).

Turchetto-Zolet, A. C., Margis-Pinheiro, M., and Margis, R. (2009). The evolution of pyrroline-5-carboxylate synthase in plants: a key enzyme in proline synthesis. *Mol. Genet. Genomics* 281, 87–97. doi: 10.1007/s00438-008-0396-4

van Zelm, E., Zhang, Y., and Testerink, C. (2020). Salt tolerance mechanisms of plants. *Annu. Rev. Plant Biol.* 71, 403–433. doi: 10.1146/annurev-arplant-050718-100005

Wada, H., Hatakeyama, Y., Nakashima, T., Nonami, H., Erra-Balsells, R., Hakata, M., et al. (2020). On-site single pollen metabolomics reveals varietal differences in phosphatidylinositol synthesis under heat stress conditions in rice. *Sci. Rep.* 10:2013. doi: 10.1038/s41598-020-58869-9

Waditee, R., Bhuiyan, M. N., Rai, V., Aoki, K., Tanaka, Y., Hibino, T., et al. (2005). Genes for direct methylation of glycine provide high levels of glycinebetaine and abiotic-stress tolerance in Synechococcus and *Arabidopsis*. *Proc. Natl. Acad. Sci. U.S.A.* 102, 1318–1323. doi: 10.1073/pnas.0409017102

Wilkinson, L. G., Bird, D. C., and Tucker, M. R. (2018). "Exploring the Role of the Ovule in cereal grain development and reproductive stress tolerance," in *Annual Plant Reviews Online*, ed. J. A. Roberts (Hoboken, NJ: John Wiley and Sons).

Xia, Y., Li, R., Bai, G., Siddique, K. H. M., Varshney, R. K., Baum, M., et al. (2017). Genetic variations of *HvP5CS1* and their association with drought tolerance related traits in barley (*Hordeum vulgare* L.). *Sci. Rep.* 7:7870. doi: 10.1038/s41598-017-08393-0

Yu, J., Jiang, M., and Guo, C. (2019). Crop pollen development under drought: from the phenotype to the mechanism. *Int. J. Mol. Sci.* 20:1550. doi: 10.3390/ijms20071550

Zhang, C. S., Lu, Q., and Verma, D. P. (1995). Removal of feedback inhibition of delta 1-pyrroline-5-carboxylate synthetase, a bifunctional enzyme catalyzing the first two steps of proline biosynthesis in plants. *J. Biol. Chem.* 270, 20491–20496. doi: 10.1074/jbc.270.35.20491

Conflict of Interest: The authors declare that the research was conducted in the absence of any commercial or financial relationships that could be construed as a potential conflict of interest.

Copyright © 2020 Mattioli, Palombi, Funck and Trovato. This is an open-access article distributed under the terms of the Creative Commons Attribution License (CC BY). The use, distribution or reproduction in other forums is permitted, provided the original author(s) and the copyright owner(s) are credited and that the original publication in this journal is cited, in accordance with accepted academic practice. No use, distribution or reproduction is permitted which does not comply with these terms.

frontiers in Plant Science

REVIEW
published: 03 December 2020
doi: 10.3389/fpls.2020.546213

Lysine, Lysine-Rich, Serine, and Serine-Rich Proteins: Link Between Metabolism, Development, and Abiotic Stress Tolerance and the Role of ncRNAs in Their Regulation

P. B. Kavi Kishor[1], Renuka Suravajhala[2], Guddimalli Rajasheker[3], Nagaraju Marka[4], Kondle Kavya Shridhar[3], Divya Dhulala[3], Korubothula Prakash Scinthia[3], Kummari Divya[3], Madhavi Doma[3], Sujatha Edupuganti[5], Prashanth Suravajhala[6] and Rathnagiri Polavarapu[7]*

[1]Department of Biotechnology, Vignan's Foundation for Science, Technology and Research (Deemed to be University), Guntur, India, [2]Department of Chemistry, Manipal University Jaipur, Jaipur, India, [3]Department of Genetics, Osmania University, Hyderabad, India, [4]Biochemistry Division, National Institute of Nutrition-ICMR, Hyderabad, India, [5]Department of Botany, Osmania University, Hyderabad, India, [6]Department of Biotechnology and Bioinformatics, Birla Institute of Scientific Research, Jaipur, India, [7]Genomix CARL, Pulivendula, India

OPEN ACCESS

Edited by:
Giuseppe Forlani, University of Ferrara, Italy

Reviewed by:
Sara Rosa-Téllez, University of Valencia, Spain
Balasubramani Subramani Paranthaman, Florida Agricultural and Mechanical University, United States

***Correspondence:**
P. B. Kavi Kishor
pbkavi@yahoo.com

Specialty section:
This article was submitted to Plant Metabolism and Chemodiversity, a section of the journal Frontiers in Plant Science

Received: *27 March 2020*
Accepted: *30 October 2020*
Published: *03 December 2020*

Citation:
Kishor PBK, Suravajhala R, Rajasheker G, Marka N, Shridhar KK, Dhulala D, Scinthia KP, Divya K, Doma M, Edupuganti S, Suravajhala P and Polavarapu R (2020) Lysine, Lysine-Rich, Serine, and Serine-Rich Proteins: Link Between Metabolism, Development, and Abiotic Stress Tolerance and the Role of ncRNAs in Their Regulation. Front. Plant Sci. 11:546213. doi: 10.3389/fpls.2020.546213

Lysine (Lys) is indispensable nutritionally, and its levels in plants are modulated by both transcriptional and post-transcriptional control during plant ontogeny. Animal glutamate receptor homologs have been detected in plants, which may participate in several plant processes through the Lys catabolic products. Interestingly, a connection between Lys and serotonin metabolism has been established recently in rice. 2-Aminoadipate, a catabolic product of Lys appears to play a critical role between serotonin accumulation and the color of rice endosperm/grain. It has also been shown that expression of some lysine-methylated proteins and genes encoding lysine-methyltransferases (KMTs) are regulated by cadmium even as it is known that Lys biosynthesis and its degradation are modulated by novel mechanisms. Three complex pathways co-exist in plants for serine (Ser) biosynthesis, and the relative preponderance of each pathway in relation to plant development or abiotic stress tolerance are being unfolded slowly. But the phosphorylated pathway of L-Ser biosynthesis (PPSB) appears to play critical roles and is essential in plant metabolism and development. Ser, which participates indirectly in purine and pyrimidine biosynthesis and plays a pivotal role in plant metabolism and signaling. Also, L-Ser has been implicated in plant responses to both biotic and abiotic stresses. A large body of information implicates Lys-rich and serine/arginine-rich (SR) proteins in a very wide array of abiotic stresses. Interestingly, a link exists between Lys-rich K-segment and stress tolerance levels. It is of interest to note that abiotic stresses largely influence the expression patterns of SR proteins and also the alternative splicing (AS) patterns. We have checked if any lncRNAs form a cohort of differentially expressed genes from the publicly available PPSB, sequence read archives of NCBI GenBank. Finally, we discuss the link between Lys and Ser synthesis, catabolism, Lys-proteins, and SR proteins during plant development and their myriad roles in response to abiotic stresses.

Keywords: lysine metabolism, serine metabolism, abiotic stress, plant ontology, stress tolerance

INTRODUCTION

Amino acids are organic compounds, which contain amine ($-NH_2$) and carboxyl C(=O)OH) functional groups along with a side chain (R group). As amino acids are building blocks of proteins, they participate in the synthesis of hormones in animals and in peptide hormone synthesis in plants (Hirakawa et al., 2017). In the case of plants, amino acids also take part in the synthesis of several secondary plant products. Amino acids that cannot be synthesized by some mammals and humans are generally known as "essential," and lysine (Lys) is one among them (Bright and Shewry, 1983). The pathway of Lys is always a target for the development of herbicides in addition to increasing nutritional value in cereals. Lys is entangled in histone modifications and, therefore, is associated with epigenome and stress biology in plants (Yuan et al., 2013). Lys is the most limiting in all major cereal grains and is therefore considered as a nutritionally significant amino acid (Wenefrida et al., 2009; Galili and Amir, 2013). This is precisely the reason why Lys is a target for crop improvement. Poor people suffer from deficiencies in the essential amino acids like Lys and methionine. If crop plants contain less Lys, the nutritional value of such crops is also reduced by more than 50% and leads to imbalances in the amino acids. But breeding methods have led to the accumulation of Lys in vegetative tissues, which is in fact deleterious to the growth of plants (Ghislain et al., 1995). Therefore, pathways for Lys synthesis in plants have been identified and also the corresponding genes that encode them, keeping in view of their genetic transformation as an alternative approach. But such an effort requires identification of seed specific promoters, which help in the accumulation of more Lys in seeds/grains (Amir and Tabe, 2006). Most importantly, Lys acts as a precursor for the metabolic pathway implicated in plant stress response and also its development as revealed from the studies of Arruda et al. (2000) and Galili et al. (2001). Negrutiu et al. (1984) isolated for the first time, a Lys over-producing mutant from the protoplast cultures of *Nicotiana sylvestris*. This mutant was a result of altered expression of one of the biosynthetic pathway genes encoding a dihydrodipicolinate synthase (DHDPS). Reduced sensitivity to feedback inhibition in transgenic plants with overexpressed bacterial DHDPS (Perl et al., 1992; Shaul and Galili, 1992, 1993) helped to discover the Lys biosynthetic pathway and its modulation. Further, Karchi et al. (1995) dissected out that Lys biosynthesis and catabolism are coordinately regulated during the development of a seed in tobacco. Thus, for the first time the amino acid Lys has been correlated with plant development. Galili et al. (2001) later reviewed the catabolic events of Lys and implicated them not only to development but also to abiotic stress tolerance. A large body of information suggests that the regulatory networks associated with Lys biosynthesis and catabolism are intertwined largely with plant tissues and organ specificity and interactions between diverse metabolic fluxes.

Another important amino acid in the body of plants is serine (Ser), which helps to form the phospholipids necessary for signal transduction. L-Ser is not only a proteinogenic amino acid, but also it participates in catalytic functions of diverse enzymatic reactions in plants. Importantly, Ser takes an active part in the biosynthesis of many biomolecules such as amino acids, phospholipids, and sphingolipids that are obligatory for cell proliferation (Kalhan and Hanson, 2012). Ser gets phosphorylated by kinases and participates in signaling mechanisms (Chaneton et al., 2012). In plants, multiple biosynthetic pathways exist for Ser. The photorespiratory glycolate pathway appears as the major one, but non-photorespiratory phosphorylated pathway also exists.

This review discusses dehydration proteins known as dehydrins (DHNs), which are members of the LEA protein family group 2 or D-11 (Close, 1997). Since they do not have proper tertiary structures, they are described as "protein clouds" or "cooked spaghetti" (Uversky, 2013, 2016). DHNs are hydrophobic, with more than 50% of the residues being charged or polar in nature and 25% being either alanine or glycine. DHNs contain Lys- and Ser-rich residue and are associated with stress tolerance (Malik et al., 2017). Both Lys and Ser are essential, the former for humans, and the later for plants. Interestingly, both of them are important in plants as a link between metabolism and development. This review focuses on the climacteric links that have been established in recent times about Lys and Ser biosynthesis and catabolism, their association with plant growth and development, abiotic stress tolerance, and also Lys- and Ser-rich proteins, functional significance, and their remarkable ability to bestow stress tolerance in plants.

TWO Lys BIOSYNTHETIC PATHWAYS EXIST IN PLANTS BUT DIFFER FROM THAT OF PROKARYOTES

In nature, two pathways namely diaminopimelate (DAP) pathway (**Figure 1A**) and α-aminoadipate (AAA) have been identified for biosynthesis of Lys (**Figure 1B**). The first pathway belongs to the aspartate derived biosynthetic family, involved also in the synthesis of threonine, methionine, and isoleucine (Galili, 1995; Velasco et al., 2002; Hudson et al., 2005). The second pathway is part of the glutamate biosynthetic family, involving α-ketoglutarate and acetyl coenzyme A (as seen in *Thermus thermophilus*; Miyazaki et al., 2004; Xu et al., 2006). While the DAP pathway operates in prokaryotes and plants, the AAA pathway in yeast, protists, and higher fungi. In the DAP pathway, aspartate and pyruvate act as precursors for the biosynthesis of Lys *via* the intermediate DAP. This pathway adds carbon groups to aspartate to yield Lys (**Figure 1A**), but exhibits feedback regulation either by Lys or by threonine (Velasco et al., 2002; Hudson et al., 2005). Both pathways are not known to operate in any single organism/plant till date. In higher plants, Lys is synthesized in plastids and no evidence exists for its cytosolic synthesis (Hudson et al., 2006). Glutamate first gets converted to aspartate by aspartate aminotransferase enzyme (AAT). Aspartate kinase (AK), the first enzyme of the pathway catalyzes aspartate to 3-aspartic semialdehyde (3-ASA). While light and photosynthetic activity in the daytime positively affect 3-ASA biosynthesis especially in young leaves

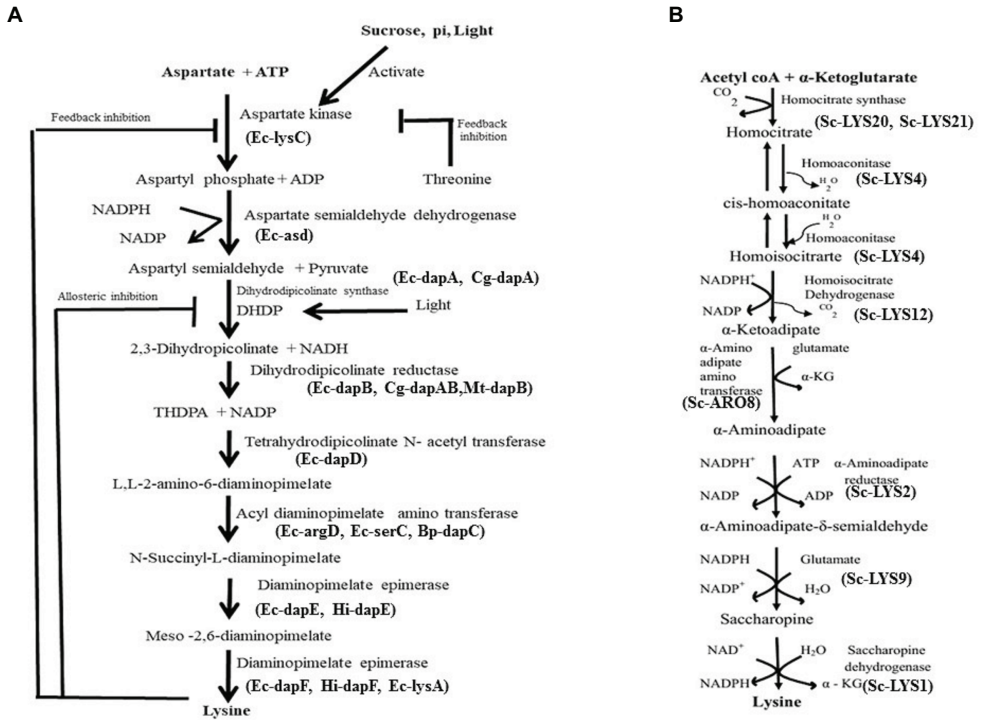

FIGURE 1 | (A) Lysine biosynthesis pathway and its feedback regulation in plants. Ec, *Escherichia coli*; Sc, *S. cerevisiae*; Hi, *Haemophilus influenzae*. **(B)** Biosynthesis pathway of lysine *via* aminoadipate. The pathway operates mostly in fungi.

(**Figure 1A**), darkness stimulates the degradation of aspartate to asparagine. Isoenzymes of AK exist as monofunctional polypeptides, which have the Lys-sensitive kinase activity. Interestingly, the bifunctional enzymes AK/homoserine dehydrogenase (HSD) contain threonine-sensitive AK as well as HSD isozymes linked on a single polypeptide. Threonine partially feedback regulates HSD enzyme and, therefore, Lys production is affected (Galili, 2002; **Figure 1A**). Some of the factors affecting Lys biosynthesis in plants are shown in **Table 1**. Vauterin et al. (1999) have shown that activity of DHDPS is high in meristems, in the vasculature of leaves, roots, stems, carpels, styles, stigma, pollen, and young embryos. In line with this, they demonstrated that DHDPS promoter exhibits cell type-specific expressions, indicating its multiple functions in diverse tissues. Synthesis of Lys by transcriptional activation in a tissue specific manner clearly implicates regulation of the enzyme at the RNA level. The enzyme *L,L*-diaminopimelate aminotransferase ($_{LL}$-DAP-AT) is a novel variant that catalyzes tetrahydrodipicolinate to *L,L*-DAP and then helps in the synthesis of Lys in lower plants (*Physcomitrella patens*) as well as higher plants like *A. thaliana*, soybean, and spinach (Hudson et al., 2006). This indicates that the enzyme is highly conserved among diverse plant species. Further, in *A. thaliana*, this enzyme catalyzes a reversible reaction. DHDPS and dihydrodipicolinate reductase (DHDPR) enzymes catalyze the two vital steps in Lys biosynthesis (**Figure 1A**). It is arguable, however, if it has a tetrameric or dimeric arrangement since it is not yet distinctly known. Tetrahydrodipicolinate (THDPA) is converted to *meso*-2,6-diaminopimelate (*m*-DAP) catalyzed by different enzymes. Hudson et al. (2006) reported a novel and specific $_{LL}$-DAP-AT that directly converts THDPA to $_{LL}$-DAP in *A. thaliana* (regarded as DAP-AT pathway). Interestingly, $_{LL}$-DAP-AT operates efficiently in the forward/biosynthetic direction in plants (Hudson et al., 2006). Diaminopimelate epimerase is the last enzyme in the pathway, which converts *m*-DAP to Lys (**Figure 1A**).

TRANSGENIC PLANTS ACCUMULATE HIGH Lys CONTENT

Transgenic lines were generated by over expressing bacterial Lys biosynthetic pathway genes in several plants. While seeds were wrinkled in high-Lys producing transgenic *Glycine max* (Falco et al., 1995), seed germination retarded in *A. thaliana* (Zhu and Galili, 2003, 2004), and the endosperm hardened in the *QPM* mutant of maize (Gibbon et al., 2003). Long et al. (2013), and Yang et al. (2016) generated transgenic rice by overexpressing a combination of bacterial genes that encode AK and DHDPS and also by inhibiting Lys ketoglutarate (α-KG) reductase/saccharopine dehydrogenase (LKR/SDH). These transgenic lines of rice displayed 60-fold increase in Lys and thus biofortified, but endosperm color was dark-brown. Surprisingly, the seed germination and subsequent performance of these plants when evaluated in the field conditions did not

TABLE 1 | Factors affecting the biosynthesis of Lys and Ser in plants.

Lysine	Serine	References
Two pathways exist in plants for the biosynthesis of Lys.	Three (glycolate linked to photorespiration and two non-photorespiratory) pathways exist for Ser biosynthesis.	Galili (2002), Zhu and Galili (2004), Ros et al. (2014), Dellero et al. (2016), Igamberdiev and Kleczkowski (2018).
Synthesized in plastids.	Synthesized in chloroplasts and mitochondrial matrix.	Ho and Saito (2001).
Feedback regulation by Lys controls its own synthesis. Further, threonine also affects Lys synthesis. Thus, two amino acids control its biosynthesis. Lys also inhibits DHDPS and arrests thereby its own biosynthesis.	Feedback regulation by Ser controls its biosynthesis, but activated by another amino acid L-homocysteine unlike Lys, suggesting an allosteric mechanism.	Galili (2002), Velasco et al. (2002), Ros et al. (2014), Zhu and Galili (2004), Okamura and Hirai (2017).
Lys production is concurrently regulated by both synthesis and degradation in reproductive and vegetative tissues.	Ser production in photosynthetic tissues is mostly regulated by high atmospheric CO_2 concentration.	Zhu and Galili (2004), Ros et al. (2014).
Light and photosynthetic activities affect the first enzyme AK in the pathway positively, and darkness stimulates degradation of aspartate to asparagine. Lys inhibits its synthesis by inhibiting the activity of AK. AK is also sensitive to threonine. Lys allosterically inhibits DHDPS, thereby arresting its own synthesis.	Interaction of Fd-GOGAT has been found essential for photorespiratory SHMT activity. Therefore, a complex regulation occurs in this high flux pathway, and Ser biosynthesis.	Galili (2002), Hudson et al. (2006).
Two genes in the pathway are light-regulated. AK is also modulated by sucrose and inorganic phosphate (Pi), thus affect Lys biosynthesis.	Expression of only *PGDH1* is modulated by high CO2, but not by *PGDH2*. Both *PGDH1* and *PGDH3* genes are regulated by light-dark regimes in photosynthetic tissues. In non-photosynthetic tissues, PGDH genes are expressed under light-dark regimes. Thus, PPSP pathway appears critical for both types tissues and affects thereby Ser biosynthesis.	Zhu-Shimoni and Galili (1998), Vauterin et al. (1999), Galili (2002). Benstein et al. (2013), Toujani et al. (2013).

show any change in their nutrition. Overexpression of tryptophan decarboxylase 3, an enzyme involved in serotonin (sometimes called the happy chemical, seen in human brain mostly) biosynthesis proved that tryptophan (a remote precursor of serotonin) and serotonin are responsible for dark-brown phenotype of endosperm in high-Lys producing lines (Kanjanaphachoat et al., 2012; Yang et al., 2016, 2018). They also proposed that 2-aminoadipate (an intermediate in Lys catabolism) might play a role between jasmonate signaling, elevated serotonin levels, and the endosperm color. Using a seed-specific promoter, Zhu and Galili (2003, 2004) overexpressed a bacterial *DHDPS* gene in a knockout *A. thaliana* mutant lacking the bifunctional enzyme α-aminoadipic semialdehyde synthase (AASS) that contains both LKR/SDH activities (in bacteria and fungi, the two enzymes are encoded by separate genes; Zhu et al., 2002). Transgenic *A. thaliana* seeds displayed 64-fold increase in free Lys levels. Houmard et al. (2007) achieved significant increase in the amount of Lys in transgenic maize kernels by RNA interference technique through endosperm specific suppression of *LKR/SDH* gene. Possibilities exist therefore for attaining high Lys containing crop plants as nutrient/food supplements to both animals and humans using its degradative pathway genes. In the light of the above facts, a deeper understanding of the metabolism and its networks are needed before we create Lys/nutrient-rich crop plants acceptable to the consumers.

Lys CATABOLISM PRODUCES GLUTAMATE AND STRESS-RELATED METABOLITES, WHICH HELP TO OVERCOME ABIOTIC STRESS

If amino acids (cysteine or Lys for example) are accumulated in high concentrations, they may be toxic to the plants (Zhu and Galili, 2004), hence, they must be degraded. The saccharopine pathway (**Figure 2**) is the primary pathway for Lys degradation, which occurs in the liver (in animals) specifically within mitochondria (Galili et al., 2001). This is the reverse of the AAA pathway (**Figure 1B**), and in plants and animals, the first two steps in the catabolism are catalyzed by LKR/SDH activities. Lys combines with α-KG to form saccharopine by the enzyme LKR (**Figure 2**), which ultimately generates glutamate and other stress-related metabolites. Also, Lys has been found vital during seed germination, where it serves as a source of carbon and energy by feeding the intermediates (like α-KG) of TCA cycle to the growing seedlings (Afendi et al., 2012). Thus, the mechanistic insights into Lys degradation and its intermediates serving as the precursors for generation of energy (NADH) *via* the electron transport chain have been furnished (Araujo et al., 2010).

Lys serves as an alternative respiratory substrate under a variety of stresses, including drought, and senescence under extended darkness (Urano et al., 2009; Joshi et al., 2010). Flexibility/remobilization of molecules are necessary since it helps the plants to maintain metabolic homeostasis and supply energy, the primary necessity to survive. Consistent with this, under salinity and drought stress conditions, contents of Lys and other amino acids increased in wheat, potato, and safflower, which displayed tolerance to stress (Saeedipour and Moradi, 2012; Muttucumaru et al., 2015; Zafari and Ebadi, 2016) and high expression of *LKR/SDH* and aminoadipic semialdehyde dehydrogenase (*AASADH*) genes involved in saccharopine pathway (Brocker et al., 2010; Less et al., 2011).

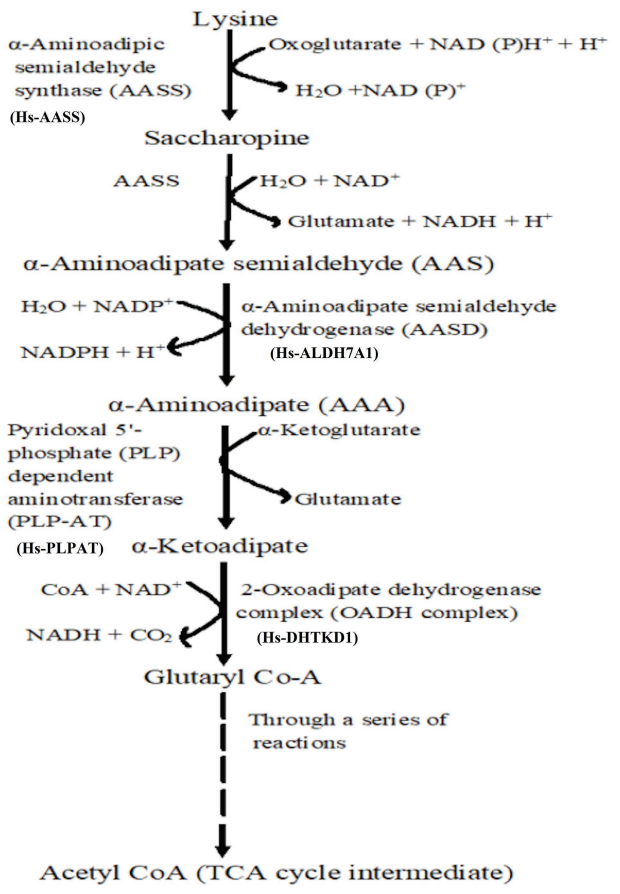

FIGURE 2 | Lysine catabolism *via* saccharopine is the prominent pathway. Broken line indicates that through several reactions, glutaryl Co-A is converted to TCA cycle intermediate acetyl coenzyme A for energy generation.

Further, ectopic expression of *AASADH* resulted in the generation of stress-tolerant plants (Rodrigues et al., 2006). In radish, drought stress was relieved with Lys application in chelation with Zn as seed priming (Noman et al., 2018). Supporting such studies, Wang et al. (2013) observed higher Lys and protein contents in transgenic maize lines in comparison with wild type plants. Such transgenics exhibited not only substantial growth but also salt stress tolerance. Upregulation of saccharopine pathway genes directs Lys to degrade to α-aminoadipate semialdehyde (AAS) and glutamate, which in turn regulates homologs of animal glutamate receptors involved in plant development (Galili et al., 2001). Arruda et al. (2000) pointed out that the saccharopine pathway described above might be accountable for the biosynthesis of several regulatory molecules implicated in root growth and senescence under both biotic and abiotic stresses. Further, Rizwan et al. (2017) demonstrated the alleviation of metal stress in wheat upon foliar spray of Lys. It has been found that variability exists among different populations of *A. halleri* for Cd accumulation (Stein et al., 2017; Corso et al., 2018). Such an intraspecific variability has prompted Serre et al. (2020) to investigate the molecular mechanisms associated with metal tolerance, especially the Lys-methylated proteins in plants. The effect of Cd on Lys-methylated proteins and KMTs were studied in *A. thaliana*, *A. lyrata*, and *A. halleri*, which have differential tolerance to Cd. Gene expression, protein mass spectrometric, and immunoblotting techniques revealed significant expressions in Lys-methylated proteins and regulation of genes coding KMTs by Cd (Serre et al., 2020). Interruption of KMT gene in *A. thaliana* displayed a significant increase in Cd tolerance in comparison with wild type plants. Further, a knock-out mutant of the calmodulin Lys methyltransferase gene exhibited enhanced Cd tolerance. These results suggest that the regulation of nonhistone proteins by Lys methylation play pivotal roles in *A. thaliana* plants to Cd stress. The results are novel and unexpected, hinting us to explore more about lysine-methylated proteins and KMTs in future to generate plants for phytoremediation. But in the developing maize endosperm, saccharopine pathway is induced by exogenous supply of lysine and repressed by salt stress. In young maize coleoptiles, *LKR/SDH* and *AASADH* were induced at the transcript level by abiotic stress. Only the AASADH protein accumulates in the stressed tissues, but not the LKR/SDH. These results indicate that in the developing seeds, the saccharopine pathway is used for pipecolic acid synthesis, although proline plays a role in abiotic stress response. Thus, saccharopine pathways in maize seed development and stress response differ from dicots (Kiyota et al., 2015). Batista-Silva et al. (2019) demonstrated rapid detoxification of Lys in the leaves of *A. thaliana* during initial stages of stress recovery. Their results indicate that amino acid-derived secondary metabolites increase when the stress is being relieved and further showed an increase in the levels of amino acids that act as precursors for secondary plant product biosynthesis.

MULTIPLE PATHWAYS CO-EXIST FOR Ser BIOSYNTHESIS IN PLANTS

Ser participates in the biosynthetic pathways of several key biomolecules essential for synthesis of other nitrogen bases (purines, pyrimidines, and thymidine), amino acids (cysteine, glycine, and tryptophan), phospholipids, sphingolipids, and cell proliferation (Ros et al., 2014; Mattaini et al., 2016). Cysteine in turn is needed for the biosynthesis of both methionine and homocysteine. Ser biosynthesis in plants proceeds *via* different pathways: glycolate pathway, which is associated with photorespiration and two non-photorespiratory pathways and the phosphorylated and the glycerate pathways. Existence or coexistence of three distinct pathways in plants for Ser biosynthesis reveals the complex nature of its regulatory processes. Out of the three, glycolate pathway (**Figure 3A**) has been considered as the prime pathway (Tolbert, 1980; Douce et al., 2001). Photorespiration has been considered as the main source of Ser in plants since this pathway is associated with it; therefore, it has been assumed that, at least, in photosynthetic tissues the quantitative contribution of this pathway to Ser pool would be higher. For this reason, the non-photorespiratory pathways

have been considered of minor importance to date. Ser is synthesized through glycolate, glycerate, and PPSB pathways, which are described below.

BIOSYNTHESIS OF Ser IN PLANTS

Through the glycolate pathway, L-Ser is synthesized during plant photorespiration within the mitochondrial matrix. In this pathway, one molecule of glycine is decarboxylated and deaminated by a fascinating complex enzyme called glycine decarboxylase (GDC). Both carbon dioxide (CO_2) and ammonia (NH_3) are formed with the release of NADH from NAD^+ (Douce et al., 2001). In a complex reaction, the methylene carbon of glycine molecule is transferred to tetrahydrofolate (THF) to form methylene tetrahydrofolate (5,10-CH_2-THF). Methylene THF now combines with the second molecule of glycine to form L-Ser catalyzed by a Ser hydroxymethyltransferase (SHMT) enzyme (**Figure 3A**). This is a pyridoxal 5'-phosphate-dependent enzyme, which catalyzes the reversible reaction of Ser to glycine in either a tetrahydrofolate-dependent or tetrahydrofolate-independent manner. One-carbon units that result from the activity of SHMT, have been found vital in proliferating cells (Wu et al., 2017). The glycolate pathway has also biological significance like the other two. For instance, *Arabidopsis* SHMT mutant (*shm1-1*) was isolated by Somerville and Ogren (1981), which shows a strong photorespiratory phenotype that is rescued under high CO_2 (Voll et al., 2006). One of the *SHMT1*-deficient mutants defective in *GLU1* gene has been reported in *A. thaliana* (Jamai et al., 2009), which encodes ferredoxin-dependent glutamate synthase located in chloroplasts (Fd-GOGAT). This enzyme is associated with the photorespiratory reassimilation of NH_3 and primary nitrogen assimilation. An important observation made by Jamai et al. (2009) shows that Fd-GOGAT is targeted to the mitochondria as well as chloroplasts. Interaction of Fd-GOGAT has been found essential for photorespiratory SHMT activity (**Table 1**). Thus, a complex regulation occurs in this high flux pathway. Both SHM1 and SHM2 are targeted to the mitochondria and operate redundantly in one carbon metabolism of non-photorespiring especially during lignification of vascular cells. Interestingly, double mutant lacking both mitochondrial SHMTs shows a lethal phenotype even under non-photorespiratory conditions, which point out the non-redundant role(s) of both isoforms and the importance of C1 metabolism for plant development (Engel et al., 2011). Five more SHM isoforms were predicted and targeted to different subcellular compartments like cytosol, plastids, and nucleus. Functional information is available for the plastidic isoform SHM3 (Zhang et al., 2010), which is believed to be involved in general one-carbon metabolism along with cytosolic isoforms SHM4 and SHM5 (Engel et al., 2011).

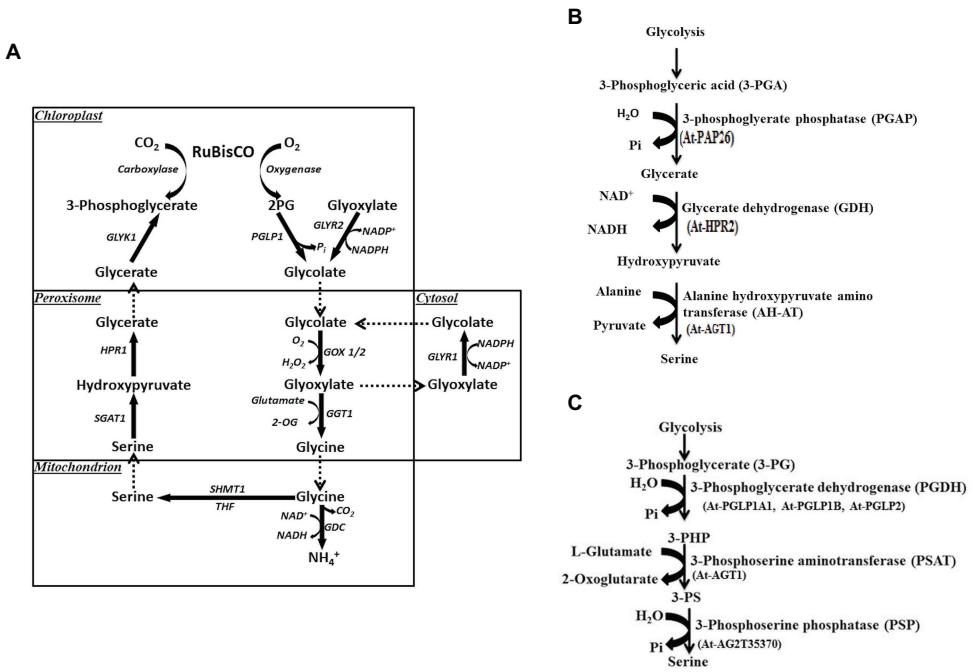

FIGURE 3 | (A) Biosynthesis of serine *via* glycolate pathway during photorespiration. 2PG, 2-phosphoglycolate; PGLP1, 2PG phosphatase 1; GLYR1/2, glyoxylate reductase 1/2, glutamate glyoxylate aminotransferase 1; GDC, glycine decarboxylase complex; THF, tetrahydrofolate; SHMT1, serine hydroxymethyl transferase 1; SGAT1, serine glyoxylate aminotransferase 1; HPR, hydroxypyruvate reductase 1; GLYK1, glycerate kinase 1. **(B)** Serine biosynthesis *via* glycerate pathway. At, *Arabidopsis thaliana*. **(C)** Phosphorylated pathway of L-serine biosynthesis (PPSB). 3-PG, 3-phosphoglycerate; 3-PHP, 3-phosphohydroxypyruvate; 3-PS, 3-phosphoserine; and At, *Arabidopsis thaliana*.

Ser is also synthesized in leaves through glycerate pathway. It is well-known that 3-phosphoglycerate (3-PG) is synthesized during glycolytic pathway (**Figure 3B**). L-Ser is formed from 3-PG by a dephosphorylation reaction (Kleczkowski and Givan, 1988) and includes part of the reverse sequence of the photorespiratory cycle. 3-PG forms glycerate and the reaction is catalyzed by 3-phosphoglycerate phosphatase (PGAP). Glycerate is then converted to hydroxypyruvate by glycerate dehydrogenase (GDH) enzyme (**Figure 3B**). In the last reaction, alanine-hydroxypyruvate aminotransferase (AH-AT) enzyme and glycine hydroxypyruvate aminotransferase (GH-AT) convert hydroxypyruvate to L-Ser. While one reaction takes place in the cytosol (PGAP), the remaining three (GDH, AH-AT, and GH-AT) take place in peroxisomes through enzymatic pathways (Kleczkowski and Givan, 1988; Greenler et al., 1989). To date, several genes involved in the glycerate pathway have been identified. However, no specific genes have been characterized and/or cloned to account specifically for glycerate pathway, so its functional significance remains little unclear (Ros et al., 2013; Igamberdiev and Kleczkowski, 2018).

One of the Ser biosynthetic pathways, PPSB, is conserved across bacteria, plants, and animals (Fell and Snell, 1988; Ho and Saito, 2001) and operates in plastids in plants. 3-PG generated *via* plastidial glycolysis and Calvin cycles acts as a precursor for the synthesis of Ser (**Figure 3C**). In the three sequential reactions, 3-PG is first converted to 3-phosphohydroxypyruvate (3-PHP) by the enzyme D-3-phosphoglycerate dehydrogenase 1 (PGDH1), EC 1.1.1.95; Slaughter and Davies, 1968). In this conversion, the cofactor NAD^+ is reduced to NADH. 3-PHP is then converted to 3-phosphoserine (3-PS) by a transamination reaction catalyzed by 3-phosphoserine aminotransferase (PSAT, EC2.6.1.52; Hanford and Davies, 1958). Wulfert and Krueger (2018) for the first time provided the genetic evidences for the *PSAT* genes. *PSAT1*-silenced lines displayed a strong inhibition of shoot and root growth and hypersensitivity to the inhibition of the photorespiratory Ser biosynthesis at higher CO_2 levels (**Table 1**). Such lines also showed accumulation of certain amino acids, due to increased assimilation of NH_3. Knockdown of *PSAT1* alters the amino acid metabolism in plants (Wulfert and Krueger, 2018). PSAT catalyzes the transfer of the amino group of glutamate to 3-hydroxypyruvate, resulting in 2-oxoglutarate and 3-phosphoserine. It is interesting to note that *PSAT1* is essential for light and sugar-dependent growth promotion in *A. thaliana* (Wulfert and Krueger, 2018). During this biosynthetic pathway, glutamate is converted to 2-oxoglutarate, an intermediate in the TCA cycle that generates energy. 3-PS is finally catalyzed by 3-phosphoserine phosphatase (PSP, EC 3.1.3.3) to form Ser (**Figure 3C**). The enzymatic and genetic evidence for these enzymes were achieved by Benstein et al. (2013), Cascales-Miñana et al. (2013), and Toujani et al. (2013). While three genes for PGDHs were described, two genes encoding for PSAT noticed in the TAIR,[1] cloned and observed to have activity *in vitro* (Ho et al., 1998, 1999a,b; Ho and Saito, 2001). Coexistence of multiple genes for PPSB and the presence of corresponding enzymes in different tissues indicate that they may perform diverse functions. This fact needs to be further investigated, but there is evidence supporting it (Ho and Saito, 2001; Waditee et al., 2007; Benstein et al., 2013). The genes associated with PPSB are expressed in several tissues (Ros et al., 2014) based on which it is argued that this pathway acts as a link between metabolism and development. It has been demonstrated that *PGDH1* expression has been modulated by high CO_2 levels (Benstein et al., 2013). They demonstrate that the content of Ser is reduced in *PGDH1*-silenced plants exposed to high CO_2. They are of the opinion that expression of $PGDH_2$ is not modulated by high CO_2. Furthermore, *PGDH1* and *PGDH3* genes have been found regulated in *A. thaliana* by light-dark regimes in photosynthetic tissues (Toujani et al., 2013; **Table 1**). On the other hand, in non-photosynthetic tissues, *PGDH* family of genes are equally expressed under light-dark regimes indicating that PPSB pathway (**Figure 3C**) may be critical for both photosynthetic and non-photosynthetic tissues (**Table 1**). Unlike *PGDH* family of genes, where their expression pattern is tightly regulated at organ level, *PSP1* gene is expressed in all organs (Cascales-Miñana et al., 2013; Toujani et al., 2013). This could be due to the presence of a unique *PSP1* gene. Thus, several pieces of evidence point out that the PPSB pathway is highly relevant in photosynthetic tissues during dark conditions, when photorespiration does not operate.

Ser METABOLISM IS ESSENTIAL FOR PLANT DEVELOPMENT AND ABIOTIC STRESS TOLERANCE

Though biological significance of PPSB has been demonstrated and found essential for the development of male gametophyte, pollen, embryo, and postembryonic root growth (Cascales-Miñana et al., 2013; Toujani et al., 2013; Ros et al., 2014, and the references therein), its metabolic implications have not been completely understood. In PPSB-deficient mutants, adenosine 5'-phosphosulfate reductase genes, sulfate transporters were upregulated (Anoman et al., 2019) with enhanced flux of ^{35}S into thiol biosynthesis, mostly in root tissues, and also their transport and allocation. Thus, deficiency of PPSB activity perturbs sulfur homeostasis between photosynthetic and non-photosynthetic tissues (Anoman et al., 2019). Besides supplying carbon to the one-carbon pool (necessary for the biosynthesis of thymidylate and methionine), Ser is implicated in signaling mechanisms (Ser is phosphorylated by kinases; Antonov et al., 2014; Ros et al., 2014; Mattaini et al., 2016). Double mutants of *gapcp1gapcp2* arrested not only primary root growth, but also showed defects in pollen development. Supplementation of L-Ser to the *gapcp1gapcp2* mutant roots resulted in the recovery of root growth (Muñoz-Bertomeu et al., 2009). Further, it has been noticed that embryo and male gametophyte become lethal in mutant plants lacking Ser palmitoyltransferase, an enzyme associated with sphingolipid biosynthesis (Chen et al., 2006; Dietrich et al., 2008). Associated with the above, in *psp1* and *pgdh1* homozygous mutant, development of embryo in *Arabidopsis* is totally arrested inferring

[1]http://www.arabidopsis.org/

the importance of Ser in all the above cases (Benstein et al., 2013; Cascales-Miñana et al., 2013; Toujani et al., 2013). Similarly, in *PSP1*- and *PGDH1*-deficient *Arabidopsis* mutants, root development was inhibited, indicating poor auxin biosynthesis in such mutants. In plants, tryptophan (produced by condensation of Ser and indole) acts as a precursor for auxin biosynthesis (Tzin and Galili, 2010; Dunn, 2012), so lack of Ser in the cells leads to root developmental defects. Benstein et al. (2013) further noticed inhibition of leaf initiation when plants containing reduced levels of PGDH activity were grown under elevated levels of CO_2. Ser is also implicated in folate metabolism. Mutants deficient in tetrahydrofolate metabolism show defects both in root and embryo development. It is however opined that Ser is not solely responsible for root development, and multiple factors/processes might be involved along with Ser. Interestingly, D-Ser (a derivative of L-Ser) has been found to act as a signaling molecule between male gametophyte and pistil communications (Michard et al., 2011). Thus, these observations infer that Ser metabolic pathways are critical for plant ontogeny. Alterations in *PPSB* gene expressions perturb not only the TCA cycle but also amino acid biosynthesis (Cascales-Miñana et al., 2013; Toujani et al., 2013).

SHMT1 functions in the photorespiratory pathway and play a critical role in controlling cell damage provoked by high light (photooxidative stress) and salt stresses and in restricting pathogen-induced cell death (Moreno et al., 2005). Further, SHMT1, located in mitochondria, converts glycine to Ser, and Liu et al. (2019) reported complementation of *A. thaliana shm1-1* (photorespiratory growth phenotype) by SHMT1 wild type plants. They found that reduced SHMT activity led to a decreased stomatal closure in response to ABA and salt stress. Transgenic lines, which showed reduced *SHMT* activity, were not only more sensitive to salt stress but also to drought stress recovery. In line with this, Batool et al. (2018) propose that cysteine is the limiting factor for ABA biosynthesis in the early stages of drought conditions in guard cells and potentially in other cell types of the leaf. Thus, its explicit glycolate pathway has a role to play in plant abiotic stress. Glycerate pathway has been linked to γ-aminobutyric acid (GABA) shunt, which affects plant growth as well as development throughout life cycle and accumulates rapidly and contributes in response to biotic and abiotic stresses (Ramos-Ruiz et al., 2019). Ser formed in glycerate and PPSB pathways acts as a precursor of glycine, formate, and glycolate, which accumulate under stress conditions (Igamberdiev and Kleczkowski, 2018). A hypothesis has been presented by Igamberdiev and Kleczkowski (2018) on the regulation of redox balance in stressed plant cells *via* participation of the reactions connected with glycerate and PPSB pathways. Thus, a link between carbon and nitrogen metabolism exists, which is regarded as vital in maintaining cellular redox and energy levels under stress conditions.

Accumulation of Ser was noticed in plants exposed to low and high temperatures, flooding, and high salt stress levels (Stewart and Larher, 1980; Kaplan et al., 2004; Bocian et al., 2015; Li et al., 2017) as well as combined stresses of drought and heat (Hossain et al., 2017). Overexpression of *PGDH* gene isolated from *Aphanothece halophytica* (a cyanobacterial species) lead to elevated salt and cold stress tolerance in *A. thaliana* (Waditee et al., 2007), indicating the involvement of PGDH enzyme in abiotic stresses. In line with this, studies conducted by Rosa-Téllez et al. (2020) have demonstrated that the response observed to salt stress depends on the isoform studied. Thus, while *PGDH1* activity could be relevant for plant tolerance to salinity, the function of *PGDH3* seems detrimental under such environmental conditions. Lines overexpressing *PGDH1* (*OexPGDH1*) accumulate less proline and raffinose (stress markers) in roots under salt stress than lines overexpressing *PGDH3* (*OexPGDH3*). Moreover, the levels of oxidized glutathione (GSSG; derived from Cys) increased under salt stress in *OexPGDH3* as compared to both *OexPGDH1* and wild type plants. Ser is utilized in many biosynthetic pathways and thereby contributes to nucleotide synthesis, methylation reactions, and production of the reducing power. Both glutathione and NADPH help in antioxidant defense in plants (Yang and Vousden, 2016). Glutathione acts as a precursor of phytochelatins and helps in chelating toxic metals, and needed for the detoxification of methylglyoxal, a cytotoxic and an emerging signaling molecule in plant abiotic stress responses and tolerance. Further, glutathione has been found to impact translation and subsequent changes. Interestingly, PPSB could affect the ABA signal transduction and thus trigger the downstream genes under cold and salt stress conditions. In support of this statement, double mutants like *gapcp1gapcp2*, which have an impaired phosphorylation pathway are insensitive to ABA (Muñoz-Bertomeu et al., 2011a,b), suggesting that Ser pathway somehow triggers ABA signals for environmental stress tolerance. Ser acts as a precursor for the synthesis of glycine betaine, an important osmotic agent, and a scavenger of ROS. Some species like rice and *Arabidopsis* do not produce glycine betaine, but in such a case, glutathione (a derivative of cysteine) scavenges ROS generated during abiotic stress (Rosa-Téllez et al., 2020). The relevance and importance of catabolism of amino acids as an alternative respiratory substrate has been demonstrated during drought or short light periods (Araujo et al., 2010; Engqvist et al., 2011; Krüßel et al., 2014). It appears therefore that a tight relationship exists between Lys and Ser metabolism during abiotic stress recovery.

DHNs CONTAIN LYSINE-RICH RESIDUES INVOLVED IN ABIOTIC STRESS TOLERANCE

Late embryogenesis abundant proteins (LEAs) are hydrophilic and thermostable in nature. This property helps them to interact not only with biomolecules, but also metal ions (Liu et al., 2013; Cuevas-Velazquez et al., 2017). DHNs are group II LEA proteins and are widely distributed in bryophytes, gymnosperms, and angiosperms (Yu et al., 2018), accumulate during embryogenesis and induced in vegetative tissues following exposure to diverse environmental stresses (Battaglia et al., 2008). They are low molecular weight (ranging 9–200 kD), modular, intrinsically disordered proteins (IDPs), and lack

well-defined three-dimensional structures (Riley et al., 2019). But SbDHN5 (from *Sorghum bicolor*) has been discovered as an ordered protein with phosphorylation sites (Nagaraju et al., 2018). Hence, it would be of interest to find out the overexpression of *SbDHN5* in crop plants and their resistance to abiotic stresses. Proximate *in vitro* evidences exist that DHNs protect plants in myriad ways, such as buffering of ion sequestration (Alsheikh et al., 2003), hydrate water (Bokor et al., 2005), chaperone activity (Abedini et al., 2017), membrane binding and stabilization (Xing et al., 2011), enzyme cryoprotection (Hughes and Graether, 2011; Drira et al., 2013), and in scavenging ROS (Hara et al., 2013). DHNs contain Lys-rich K-segment, which is prevalent in all DHNs with EKKGIMDKIKEKLPG (15 amino acids) and located near the C-terminus (Close, 1996; Malik et al., 2017). K-segments participate in forming class A2 amphipathic α-helix that protect both enzymes and membranes (Baker et al., 1988). More than one K-segment is also noticed in few DHN proteins, but with several conserved residues (Koag et al., 2009; Graether and Boddington, 2014). DHNs have four different types of conserved sequence motifs namely K-, S-, Y-, ([V/T]D] [E/Q] YGNP), and ϕ segments. Quite intriguing is that no position in the K-segment is conserved totally (Graether and Boddington, 2014). Without any exception, all DHNs contain a minimum of one copy of Lys-rich K-segment located near the C-terminal. In some DHNs, more than one K-segment, but with distinct amino acid sequences may be present. The conserved residues among the K-segment include Lys-Ile-Lys-Glu in the core, Lys-Leu-Pro-Gly in the C-terminal, and Glu-Lys-Lys in the N-terminal regions (Graether and Boddington, 2014). However, the amino acid residues in K-segment among lower and higher plants may differ. In gymnosperms, K-segment shares a variable sequence like (Q/E)K(P/A)G(M/L)LDKIK(A/Q)(K/M)(I/L)PG, while in higher plants, it has EKKGIMDKIKEKLPG (Close, 1996; Jarvis et al., 1996). While K-segment is associated with plant development besides stress tolerance, the conserved sequence of Y is homologous to that of chaperone molecules (Martin et al., 1993). On the other hand, S-segment contains Ser cascade sequence SSSSSSSD, and this segment is observed mostly as a single copy in DHNs. S-segment is a phosphorylatable patch of 4–10 Ser residues and can transfer DHNs from cytoplasm to the nucleus (Goday et al., 1994). Stretches of sequence with a variable length are usually noticed and S-segment also participates in plant development alongside abiotic stress tolerance. It is also of interest to note that in Y_nSK_n-type DHNs, the K- and S-segments are linked by a fixed motif GXGGRRKK (where X can be any amino acid), indicating a functional linkage between K- and S-segments. While the motif GXGG is highly pliable and interacts with negatively charged phosphoserines with K-segment, motif RRKK appears to be a nuclear localization signal (Jensen et al., 1998; Malik et al., 2017). In between the conserved motifs, there are ϕ segments with small, polar, and charged amino acids. Φ-segments are stretches of sequences with variable lengths of amino acids. Based on the sequence and the number of K, S, and Y segments, DHNs have been further classified in five subfamilies/subgroups such as K_nS, Y_nSK_n, K_n, Y_nK_n, and SK_n (Mundy and Chua, 1988). While Y_nSK_n-type DHNs are expressed mostly under desiccation and salt stresses, K_n, SK_n, and K_nS are upregulated by cold, desiccation, and salt stresses (Graether and Boddington, 2014). The presence of S (Ser) motif preceding the K (Lys) motif (Y_nSK_n, SK_n, and S_nKS) and also frequent occurrence of one of such subclasses Y_nSK_n in monocots has been noticed by Abedini et al. (2017). Interestingly, out of 13 HvDHNs, 10 Y_nSK_n members were noticed in a drought-tolerant barley (Kosová et al., 2011), and three in *Sorghum bicolor* out of six detected (Nagaraju et al., 2018). DHNs have been observed in vegetative tissues grown under control conditions, inferring that they play a key role in plant growth. The Y2K4-type DHN MtCAS31 (from *Medicago truncatula*) by interacting with AtICE1 (induces CBF expression 1) has been shown to associate with stomatal development, increasing the drought tolerance by decreasing the stomatal density of transgenic *A. thaliana* (Xie et al., 2012). DHN5 when overexpressed in *A. thaliana* showed different responses to biotic (as an antibacterial and antifungal factor) and abiotic stresses (Drira et al., 2015, 2016) besides protecting lactate dehydrogenase, β-glucosidase, and glucose oxidase from cold and heat stresses (Brini et al., 2010; Drira et al., 2013).

The DHNs are localized mostly in the cytoplasm, nucleus, plasma membrane, and mitochondria (Hara et al., 2013). It is interesting to note that many S-segment-containing DHNs are localized to the nucleus inferring that the S-segment moves to nucleus besides K_n and Y_nK_n types (Wisniewski et al., 1999; Lin et al., 2012). Graether and Boddington (2014) discovered that several of K_n, SK_n, K_nS, Y_nSK_n, and Y_nK_n DHNs were upregulated during low temperature (cold), desiccation, and salt stresses. The His-flanking K-segments (the major functional component) have been found to bind to membranes and play a major role during stress response (Eriksson et al., 2011). Further, a correlation exists between the number of K-segments and abiotic stress tolerance. In line with this statement, K-segment of wheat DHN WZY2 has been found to protect plants from temperature stress (Yang et al., 2015). In this regard, it is interesting to note that the derivative containing two K-segments (WZY2) displays remarkable cold and heat stress tolerance than the truncated derivative without K-segments. This implies that K-segment is the major functional component of WZY2 (Yang et al., 2015). Interestingly, among the spliced DHN1a_s (YSK2) and unspliced DHN1a_u (YS), only the spliced variant exhibited resistance to cold and drought stresses and to *Botrytis cinerea* (Rosales et al., 2014).

Ser-RICH PROTEINS ARE IMPLICATED IN ABIOTIC STRESS AS WELL AS IN PLANT DEVELOPMENT

Lazar et al. (1995) first identified serine/arginine-rich (SR) proteins using monoclonal antibodies raised against a Ser phospho epitope in the arginine/serine-rich (RS) domain. SR proteins now appear as a highly conserved family of RNA-binding protein members in eukaryotes and regarded as crucial alternative splicing (AS) regulators of pre-mRNAs (Palusa et al., 2010),

thereby increasing the transcript complexity. SR proteins range in size from 21 to 41 kDa in *A. thaliana*, and have two RNA recognition motifs at the N- and C-terminal RS domains, rich in SR dipeptides. AS has been recognized as a means of plant adaptation to a changing environment and is controlled in a tissue- and development-specific manner especially under abiotic stress conditions. These proteins play crucial roles in maintaining genome stability (Xiao et al., 2007), promoting transcriptional elongation (Lin et al., 2008), and cell cycle progression (Zhong et al., 2009). Many environmental stresses modulate AS patterns of SR proteins, phosphorylation status, and subcellular distribution in plants. In the promoter regions, Chen et al. (2019) found 92 development-, stress-, and hormone-related *cis*-elements. This implies that SR proteins play an important role during plant development and in response to environmental stresses. SR proteins were predicted to interact with other SR and non-SR proteins, inferring their association in other functions. Developmental defects were noticed with the overexpression of *Arabidopsis* SRp30, RSZ33, or mutations in SC35 and SCL genes (Lopato et al., 1999; Maria et al., 2003; Yan et al., 2017), implying the involvement of SR proteins in plant development. The number of SR proteins may vary in different taxa (16 in *Physcomitrella patens*, 18 in *Brachypodium*, 22 in rice, 25 in *Brassica rapa*, and 40 in wheat; Melo et al., 2020), which are divided into many subfamilies. Expression levels of the SCL30a, SCL28, and SCL33 genes were altered upon treatment with ABA (Cruz et al., 2014), indicating that SR proteins respond to ABA. Zhang et al. (2014) noticed that splicing factor SR34b mutation reduces cadmium tolerance in *Arabidopsis* by regulating iron-regulated transporter 1 gene. Besides its response to high light intensities (Tanabe et al., 2008), *Arabidopsis* SR45 participates as a suppressor to innate immunity (Zhang et al., 2017). Likewise, SR protein RSZ21 obtained from *Arachis* has been found to play a role in plant defense and HR-like cell death (Kumar and Kirti, 2012). Yoon et al. (2018) discovered altered expression levels of 78.6% genes (22 out of 28) and 60.7% of AS patterns in *Brassica rapa* in response to abiotic stresses. The highest expressions were detected when plants were exposed to oxidative, cold, and heat treatments. Interestingly, cold and heat stresses caused the most AS events. These studies point out that type of abiotic stress largely influences the expression patterns of SR proteins and also the AS patterns. Using CRISPR/Cas9-mediated plant genome engineering, Butt et al. (2019) targeted each rice SR locus and produced single knockouts. Such a study is extremely vital and forms a useful resource material to understand the role of SR proteins in plant development as well as abiotic stresses.

DO ncRNAs HAVE A ROLE IN THE REGULATION OF Lys AND Ser PATHWAYS AND ITS INTERACTIONS?

Major part of the genome is non-coding and is transcribed into non-coding RNAs (ncRNAs) only, which is known to play a regulatory role. Among these ncRNAs, long non-coding RNAs (lncRNAs) are known to be involved in regulation of gene expression. However, very little is known about the role of ncRNAs in providing tolerance against biotic stress including plant diseases. The interactions of lncRNAs with proteins in plants using a system genomic approach is promising and is relevant to ascertain characteristic trait biology relationships. In the recent past, several databases for genes encoding lncRNAs in plants have become available, which include greeNC (Gallart et al., 2016), CantataDB (Szczesniak et al., 2016), PLncDB (Jin et al., 2013) etc. However, these databases lack *bona fide* entries and have poor annotations. In plants, lncRNAs are known to perform multiple biological functions, which include the following: phosphate homeostasis (Bazin and Bailey-Serres, 2015), flowering (Swiezewski et al., 2009), photomorphogenesis (Wang et al., 2014), stress response (Yuan et al., 2018), fertility (Liu et al., 2017), etc. The lncRNAs are also known to function as target mimics of miRNAs (Aung et al., 2006; Pant et al., 2008) and regulate post-translational processes *via* protein modifications and protein-protein interactions (PPIs; Liu et al., 2015), etc. Song and Zhang (2017) have extensively reviewed the characteristics, identification, and functions of lncRNAs in response to various stresses. The authors delve into a greater understanding and need of nutrient deficiency and the factors associated with abiotic stress. We also argue that the identification of regulatory elements associated with a disease and validating them through NGS has been a routine task. In this process, distinct signatures in the form of lncRNAs in plants would be ideal candidates for studying agronomically important traits. It is a challenge to identify ncRNAs that were not characterized earlier and to find if they are specific to any trait/genotype. For example, the miRNA target analysis also divulged that *DHNs* are targeted by 51 miRNAs responsive to abiotic stress. The gene expressions are common and well-coordinated under diverse abiotic stress conditions and *DHNs* are no exception. The role of DHNs under different abiotic stress conditions, the regulatory networks of *DHN* genes, and their physiological functions have been discussed (Yu et al., 2018). In *S. bicolor*, transcript expressions were higher in roots, stems, and leaves in comparison with inflorescences (Nagaraju et al., 2018). While all *DHN* genes exhibited high expressions in stems under cold, heat, salt, and drought stresses, *SbDHN2* displayed the highest expression under multiple stresses in all the tissues of *S. bicolor* (Nagaraju et al., 2018). These results infer that the involvement of SbDHN2 of YnS group in a wide array of stresses. In the recent past, studies on proteome diversity revealed that lncRNAs play a very important role in serine/arginine (SR) regulations (Fesenko et al., 2017). Furthermore, the role of lncRNAs in nonsense-mediated mRNA decay was identified under differential alternative splicing in relation to altitude, not the abiotic stress, which is beyond the scope of this review. Furthermore, Ser and Lys metabolism together are not explicitly known.

CONCLUSIONS AND OUTLOOK

Both Lys and Ser are key amino acids, involved in plant ontogeny and also connected with abiotic stress tolerance. The biosynthetic pathways are multiple and complex. Among the

pathways that exist, the PPSB appears to play a critical role during growth and development. Diverse mechanisms associated with biosynthesis and catabolism of these two important amino acids however, need to be elucidated and also their interaction with other pathways. Attempts were made to enrich the seeds of rice and others with Lys, but still problems exist with regard to seed morphology. These shortcomings need to be overcome in future in order to make high Lys-containing lines available to the public. Further, it is concluded that Lys is catabolized to serve as an alternative respiratory substrate since photosynthetic activity is impaired under abiotic stress conditions. Thus, plants get detoxified by supplementing the much-needed energy during the time of abiotic stress recovery. This vital function of Lys is in addition to its regular participation in protein synthesis and other metabolic activities. Such functions to the amino acids are novel and were not predicted earlier. Many functions of Lys and Ser during growth and development have come into light recently, though the mechanistic explanations are not clear. Further, Lys- and Ser-rich proteins and their induction during abiotic stress reveals the crucial role they play in a wide spectrum of abiotic stresses. Identification of the *cis*- and *trans*-acting elements associated with the activation/suppression of the biosynthetic pathway genes and subsequent events that take place in the downstream remains elucidated. Finally, lncRNAs appear to play a role in these processes by interacting with serine kinase and several novel proteins. Mapping those miRNAs and lncRNAs, their interaction and the key roles they play during the regulation of these processes is certainly the biggest challenge for future research.

AUTHOR CONTRIBUTIONS

PBK wrote the first draft with sections on Serine and split by all other authors. RS developed the figures. PS wrote sections on lncRNAs. PBK, PS, and RP proofread the manuscript before all the agreeing to submission. All authors contributed to the revisions and approved the submitted version.

REFERENCES

Abedini, R., Golmohammadi, F. G., PishkamRad, R., Pourabedi, E., Jafarnezhadi, A., Shobbar, Z. S., et al. (2017). Plant dehydrins: shedding light on structure and expression patterns of dehydrin gene family in barley. *J. Plant Res.* 130, 747–763. doi: 10.1007/s10265-017-0941-5

Afendi, F. M., Okada, T., Yamazaki, M., Hirai-Morita, A., Nakamura, Y., Ikeda, S., et al. (2012). KNApSAcK family databases: integrated metabolite-plant species databases for multifaceted plant research. *Plant Cell Physiol.* 53:e1. doi: 10.1093/pcp/pcr165

Alsheikh, M. K., Heyen, B. J., and Randall, S. K. (2003). Ion binding properties of the dehydrin ERD14 are dependent upon phosphorylation. *J. Biol. Chem.* 278, 40882–40889. doi: 10.1074/jbc.M307151200

Amir, R., and Tabe, L. (2006). "Molecular approaches to improving plant methionine content" in *Plant genetic engineering. Metabolic engineering and molecular farming II. Vol. 8.* eds. P. K. Jaiwal and R. P. Singh (Huston, Texas, USA: Studium Press LLC), 1–26.

Anoman, A. D., Flores-Tornero, M., Benstein, R. M., Blau, S., Rosa-Téllez, S., Bräutigam, A., et al. (2019). Deficiency in the phosphorylated pathway of serine biosynthesis perturbs sulfur assimilation. *Plant Physiol.* 180, 153–170. doi: 10.1104/pp.18.01549

Antonov, A., Agostini, M., Morello, M., Minieri, M., Melino, G., and Amelio, I. (2014). Bioinformatics analysis of the serine and glycine pathway in cancer cells. *Oncotarget* 5, 11004–11013. doi: 10.18632/oncotarget.2668

Araujo, W. L., Ishizaki, K., Nunes-Nesi, A., Larson, T. R., Tohge, T., Krahnert, I., et al. (2010). Identification of the 2-hydroxyglutarate and isovaleryl-CoA dehydrogenases as alternative electron donors linking lysine catabolism to the electron transport chain of *Arabidopsis* mitochondria. *Plant Cell* 22, 1549–1563. doi: 10.1105/tpc110075630

Arruda, P., Kemper, E. L., Papes, F., and Leite, A. (2000). Regulation of lysine catabolism in higher plants. *Trends Plant Sci.* 5, 324–330. doi: 10.1016/S1360-1385(00)01688-5

Aung, K., Lin, S., Wu, C. C., Huang, Y. T., Su, C. L., and Chiou, T. J. (2006). pho2, a phosphate over accumulator, is caused by a nonsense mutation in a microRNA399 target gene. *Plant Physiol.* 141, 1000–1011. doi: 10.1104/pp.106.078063

Baker, J., Van Dennsteele, C., and Dure, L. (1988). Sequence and characterization of 6 lea proteins and their genes from cotton. *Plant Mol. Biol.* 11, 277–291. doi: 10.1007/BF00027385

Batista-Silva, W., Rugen, B., Nunes-Nesi, A., Arruda, W. L., Braun, H., and Hildebrandt, T. M. (2019). The role of amino acid metabolism during abiotic stress release. *Plant Cell Environ.* 42, 1630–1644. doi: 10.1111/pce.13518

Batool, S., Uslu, V. V., Rajab, H., Ahmad, N., Waadt, R., Geiger, D., et al. (2018). Sulfate is incorporated into cysteine to trigger ABA production and stomatal closure. *Plant Cell* 30, 2973–2987. doi: 10.1105/tpc.18.00612

Battaglia, M., Olvera-Carrillo, Y., Garciarrubio, A., Campos, F., and Covarrubias, A. A. (2008). The enigmatic LEA proteins and other hydrophilins. *Plant Physiol.* 148, 6–24. doi: 10.1104/pp108120725

Bazin, J., and Bailey-Serres, J. (2015). Emerging roles of long non-coding RNA in root developmental plasticity and regulation of phosphate homeostasis. *Front. Plant Sci.* 6:400. doi: 10.3389/fpls.2015.00400

Benstein, R. M., Ludewig, K., Wulfert, S., Wittek, S., Gigolashvili, T., Frerigmann, H., et al. (2013). *Arabidopsis* phosphoglycerate dehydrogenase1 of the phosphoserine pathway is essential for development and required for ammonium assimilation and tryptophan biosynthesis. *Plant Cell* 25, 5011–5029. doi: 10.1105/tpc.113.118992

Bocian, A., Zwierzykowski, Z., Rapacz, M., Koczyk, G., Ciesiolka, D., and Kosmala, A. (2015). Metabolite profiling during cold acclimation of *Lolium perenne* genotypes distinct in the level of frost tolerance. *J. Appl. Genet.* 56, 439–449. doi: 10.1007/s13353-015-0293-6

Bokor, M., Csizmók, V., Kovács, D., Bánki, P., Friedrich, P., Tompa, P., et al. (2005). NMR relaxation studies on the hydrate layer of intrinsically unstructured proteins. *Biophys. J.* 88, 2030–2037. doi: 10.1529/biophysj.104.051912

Bright, S. W. J., and Shewry, P. R. (1983). Improvement of protein quality in cereals. *CRC Crit. Rev. Plant Sci.* 1, 49–93. doi: 10.1080/07352688309382171

Brini, F., Saibi, W., Amara, I., Gargouri, A., Masmoudi, K., and Hanin, M. (2010). Wheat dehydrin DHN-5 exerts a heat-protective effect on β-glucosidase and glucose oxidase activities. *Biosci. Biotechnol. Biochem.* 74, 1050–1054. doi: 10.1271/bbb.90949

Brocker, C., Lassen, N., Estey, T., Pappa, A., Cantore, M., Orlova, V. V., et al. (2010). Aldehyde dehydrogenase 7A1 (ALDH7A1) is a novel enzyme involved in cellular defense against hyperosmotic stress. *J. Biol. Chem.* 285, 18452–18463. doi: 10.1074/jbc.M109.077925

Butt, H., Piatek, A., Li, L., Reddy, A. S. N., and Mahfouz, M. M. (2019). Multiplex CRISPR mutagenesis of the serine/arginine-rich (SR) gene family in rice. *Genes* 10:596. doi: 10.3390/genes10080596

Cascales-Miñana, B., Muñoz-Bertomeu, J., Flores-Tornero, M., Anoman, A. D., Pertusa, J., Alaiz, M., et al. (2013). The phosphorylated pathway of serine biosynthesis is essential both for male gametophyte and embryo development and for root growth in *Arabidopsis*. *Plant Cell* 25, 2084–2101. doi: 10.1105/tpc.113.112359

Chaneton, B., Hillmann, P., Zheng, L., Martin, A. C., Maddocks, O. D., Chokkathukalam, A., et al. (2012). Serine is a natural ligand and allosteric activator of pyruvate kinase M2. *Nature* 491, 458–462. doi: 10.1038/nature11540

Chen, M., Han, G., Dietrich, C. R., Dunn, T. M., and Cahoon, E. B. (2006). The essential nature of sphingolipids in plants as revealed by the functional

identification and characterization of the *Arabidopsis* LCB1 subunit of serine palmitoyltransferase. *Plant Cell* 18, 3576–3593. doi: 10.1105/tpc.105.040774

Chen, S., Li, J., Liu, Y., and Li, H. (2019). Genome-wide analysis of serine/arginine-rich protein family in wheat and *Brachypodium distachyon*. *Plan. Theory* 8:188. doi: 10.3390/plants8070188

Close, T. J. (1996). Dehydrins: emergence of a biochemical role of a family of plant dehydration proteins. *Physiol. Plant.* 97, 795–803. doi: 10.1111/j.1399-3054.1996.tb00546.x

Close, T. J. (1997). Dehydrins: a commonalty in the response of plants to dehydration and low temperature. *Physiol. Plant.* 100, 291–296. doi: 10.1111/j1399-30541997tb04785x

Corso, M., Schvartzman, M. S., Guzzo, F., Souard, F., Malkowski, E., Hanikenne, M., et al. (2018). Contrasting cadmium resistance strategies in two metallicolous populations of *Arabidopsis halleri*. *New Phytol.* 218, 283–297. doi: 10.1111/nph.14948

Cruz, T. M. D., Carvalho, R. F., Richardson, D. N., and Duque, P. (2014). Abscisic acid (ABA) regulation of *Arabidopsis* SR protein gene expression. *Int. J. Mol. Sci.* 15, 17541–17564. doi: 10.3390/ijms151017541

Cuevas-Velazquez, C. L., Reyes, J. L., and Covarrubias, A. A. (2017). Group 4 late embryogenesis abundant proteins as a model to study intrinsically disordered proteins in plants. *Plant Signal. Behav.* 12, 10893–10903. doi: 10.1080/15592324.2017.1343777

Dellero, Y., Jossier, M., Glab, N., Oury, C., Tcherkez, G., and Hodges, M. (2016). An *Arabidopsis thaliana* photorespiratory glycolate oxidase mutant exhibits altered carbon allocation and leaf senescence after a transfer from high CO_2 to air. *J. Exp. Bot.* 67, 3149–3163. doi: 10.1093/jxb/erw054

Dietrich, C. R., Han, G., Chen, M., Berg, R. H., Dunn, T. M., and Cahoon, E. B. (2008). Loss-of-function mutations and inducible RNAi suppression of *Arabidopsis* LCB2 genes reveal the critical role of sphingolipids in gametophytic and sporophytic cell viability. *Plant J.* 54, 284–298. doi: 10.1111/j.1365-313X.2008.03420.x

Douce, R., Bourguignon, J., Neuburger, M., and Rébeillé, F. (2001). The glycine decarboxylase system: a fascinating complex. *Trends Plant Sci.* 6, 167–176. doi: 10.1016/S1360-1385(01)01892-1

Drira, M., Hanin, M., Masmoudi, K., and Brini, F. (2016). Comparison of full-length and conserved segments of wheat dehydrin DHN-5 overexpressed in *Arabidopsis thaliana* showed different responses to abiotic and biotic stress. *Funct. Plant Biol.* 43, 1048–1060. doi: 10.1071/FP16134

Drira, M., Saibi, W., Amara, I., Masmoudi, K., Hanin, M., and Brini, F. (2015). Wheat dehydrin K-segments ensure bacterial stress tolerance, antiaggregation and antimicrobial effects. *Appl. Biochem. Biotechnol.* 175, 1–12. doi: 10.1007/s12010-015-1502-9

Drira, M., Saibi, W., Brini, F., Gargouri, A., Masmoudi, K., and Hanin, M. (2013). The K-segments of the wheat dehydrin DHN-5 are essential for the protection of lactate dehydrogenase and β-glucosidase activities *in vitro*. *Mol. Biotechnol.* 54, 643–650. doi: 10.1007/s12033-012-9606-8

Dunn, M. F. (2012). Allosteric regulation of substrate channeling and catalysis in the tryptophan synthase bienzyme complex. *Arch. Biochem. Biophys.* 519, 154–166. doi: 10.1016/j.abb.2012.01.016

Engel, N., Ewald, R., Gupta, K. J., Zrenner, R., Hagemann, M., and Bauwe, H. (2011). The presequence of *Arabidopsis* serine hydroxymethyltransferase SHM2 selectively prevents import into mesophyll mitochondria. *Plant Physiol.* 157, 1711–1720. doi: 10.1104/pp.111.184564

Engqvist, M. K., Kuhn, A., Wienstroer, J., Weber, K., Jansen, E. E. W., Jakobs, C., et al. (2011). Plant D-2-hydroxyglutarate dehydrogenase participates in the catabolism of lysine especially during senescence. *J. Biol. Chem.* 286, 11382–11390. doi: 10.1074/jbc.M110.194175

Eriksson, S. K., Kutzer, M., Procek, J., Grobner, G., and Harryson, P. (2011). Tunable membrane binding of the intrinsically disordered dehydrin Lti30, a cold-induced plant stress protein. *Plant Cell* 23, 2391–2404. doi: 10.1105/tpc.111.085183

Falco, S. C., Guida, T., Locke, M., Mauvais, J., Sanders, C., Ward, R. T., et al. (1995). Transgenic canola and soybean seeds with increased lysine. *Biotechnology* 13, 577–582. doi: 10.1038/nbt0695-577

Fell, D. A., and Snell, K. (1988). Control analysis of mammalian serine biosynthesis. Feedback inhibition on the final step. *Biochem. J.* 256, 97–101. doi: 10.1042/bj2560097

Fesenko, I., Khazigaleeva, R., Kirov, I., Kniazev, A., Glushenko, O., Babalyan, K., et al. (2017). Alternative splicing shapes transcriptome but not proteome diversity in *Physcomitrella patens*. *Sci. Rep.* 7:2698. doi: 10.1038/s41598-017-02970-z

Galili, G. (1995). Regulation of lysine and threonine synthesis. *Plant Cell* 7, 899–906. doi: 10.2307/3870045

Galili, G. (2002). New insights into the regulation and functional significance of lysine metabolism in plants. *Annu. Rev. Plant Biol.* 53, 27–43. doi: 10.1146/annurevarplant53091401110929

Galili, G., and Amir, R. (2013). Fortifying plants with the essential amino acids lysine and methionine to improve nutritional quality. *Plant Biotechnol. J.* 11, 211–222. doi: 10.1111/pbi.12025

Galili, G., Tang, G., Zhu, X., and Gakiere, B. (2001). Lysine catabolism: a stress and development super-regulated metabolic pathway. *Curr. Opin. Plant Biol.* 4, 261–266. doi: 10.1016/S1369-5266(00)00170-9

Gallart, P. A., Pulido, H., de Lagran, I. A. M., Sanseverino, W., and Cigliano, A. (2016). GREENC: a Wiki-based database of plant lncRNAs. *Nucleic Acids Res.* 44, D1161–D1166. doi: 10.1093/nar/gkv1215

Ghislain, M., Frankard, V., and Jacobs, M. (1995). A dinucleotide mutation in dihydrodipicolinate synthase of *Nicotiana sylvestris* leads to lysine overproduction. *Plant J.* 8, 733–743. doi: 10.1046/j.1365-313X.1995.08050733.x

Gibbon, B. C., Wang, X., and Larkins, B. A. (2003). Altered starch structure is associated with endosperm modification in quality protein maize. *Proc. Natl. Acad. Sci. U. S. A.* 100, 15329–15334. doi: 10.1073/pnas.2136854100

Goday, A., Jensen, B., Culiañez-Macià, F., Mar Albà, M., Figueras, M., Serratosa, J., et al. (1994). The maize abscisic acid-responsive protein Rab17 is located in the nucleus and interacts with nuclear localization signals. *Plant Cell* 6, 351–360. doi: 10.1105/tpc.6.3.351

Graether, S. P., and Boddington, K. F. (2014). Disorder and function: a review of the dehydrin protein family. *Front. Plant Sci.* 5:576. doi: 10.3389/fpls.2014.00576

Greenler, J. M., Sloan, J. S., Schwartz, B. W., and Becker, W. M. (1989). Isolation, characterization and sequence analysis of a full-length cDNA clone encoding NADH-dependent hydroxypyruvate reductase from cucumber. *Plant Mol. Biol.* 13, 139–150. doi: 10.1007/BF00016133

Hanford, J., and Davies, D. D. (1958). Formation of phosphoserine from 3-phosphoglycerate in higher plants. *Nature* 182, 532–533. doi: 10.1038/182532a0

Hara, M., Kondo, M., and Kato, T. A. (2013). KS-type dehydrin and its related domains reduce cu-promoted radical generation and the histidine residues contribute to the radical-reducing activities. *J. Exp. Bot.* 64, 1615–1624. doi: 10.1093/jxb/ert016

Hirakawa, Y., Torii, K. U., and Uchida, N. (2017). Mechanisms and strategies shaping plant peptide hormones. *Plant Cell Physiol.* 58, 1313–1318. doi: 10.1093/pcp/pcx069

Ho, C. L., Noji, M., and Saito, K. (1999a). Plastidic pathway of serine biosynthesis molecular cloning and expression of 3-phosphoserine phosphatase from *Arabidopsis thaliana*. *J. Biol. Chem.* 274, 11007–11012. doi: 10.1074/jbc.274.16.11007

Ho, C. L., Noji, M., Saito, M., and Saito, K. (1999b). Regulation of serine biosynthesis in *Arabidopsis* crucial role of plastidic 3-phosphoglycerate dehydrogenase in non-photosynthetic tissues. *J. Biol. Chem.* 274, 397–402. doi: 10.1074/jbc.274.1.397

Ho, C. L., Noji, M., Saito, M., Yamazaki, M., and Saito, K. (1998). Molecular characterization of plastidic phosphoserine aminotransferase in serine biosynthesis from *Arabidopsis*. *Plant J.* 16, 443–452. doi: 10.1046/j.1365-313x.1998.00313.x

Ho, C. L., and Saito, K. (2001). Molecular biology of the plastidic phosphorylated serine biosynthetic pathway in *Arabidopsis thaliana*. *Amino Acids* 20, 243–259. doi: 10.1007/s007260170042

Hossain, M. S., Persicke, M., ElSayed, A. I., Kalinowski, J., and Dietz, K. J. (2017). Metabolite profiling at the cellular and subcellular level reveals metabolites associated with salinity tolerance in sugar beet. *J. Exp. Bot.* 68, 5961–5976. doi: 10.1093/jxb/erx388

Houmard, N. M., Mainville, J. L., Bonin, C. P., Huang, S., Luethy, M. H., and Malvar, T. M. (2007). High-lysine corn generated by endosperm-specific suppression of lysine catabolism using RNAi. *Plant Biotechnol. J.* 5, 605–614. doi: 10.1111/j.1467-7652.2007.00265.x

Hudson, A. O., Bless, C., Macedo, P., Chatterjee, S. P., Singh, B. K., Gilvarg, C., et al. (2005). Biosynthesis of lysine in plants: evidence for a variant of the known bacterial pathways. *Biochim. Biophys. Acta* 1721, 27–36. doi: 10.1016/j.bbagen.2004.09.008

Hudson, A. O., Singh, B. K., Leustek, T., and Gilvarg, C. (2006). An LL-diaminopimelate aminotransferase defines a novel variant of the lysine biosynthesis pathway in plants. *Plant Physiol.* 140, 292–301. doi: 10.1104/pp.105.072629

Hughes, S., and Graether, S. P. (2011). Cryoprotective mechanism of a small intrinsically disordered dehydrin protein. *Protein Sci.* 20, 42–50. doi: 10.1002/pro.534

Igamberdiev, A. U., and Kleczkowski, L. A. (2018). The glycerate and phosphorylated pathways of serine synthesis in plants: the branches of plant glycolysis linking carbon and nitrogen metabolism. *Front. Plant Sci.* 9:318. doi: 10.3389/fpls.2018.00318

Jamai, A., Salome, P. A., Schilling, S. H., Weber, A. P. M., and McClung, C. R. (2009). *Arabidopsis* photorespiratory serine hydroxymethyltransferase activity requires the mitochondrial accumulation of ferredoxin dependent glutamate synthase. *Plant Cell* 21, 595–606. doi: 10.1105/tpc.108.063289

Jarvis, S. B., Taylor, M. A., MacLeod, M. R., and Davies, H. V. (1996). Cloning and characterisation of the cDNA clones of three genes that are differentially expressed during dormancy-breakage in the seeds of douglas fir (*Pseudotsuga menziesii*). *J. Plant Physiol.* 147, 559–566. doi: 10.1016/S0176-1617(96)80046-0

Jensen, A. B., Goday, A., Figueras, M., Jessop, A. C., and Pages, M. (1998). Phosphorylation mediates the nuclear targeting of the maize Rab17 protein. *Plant J.* 13, 691–697. doi: 10.1046/j.1365-313X.1998.00069.x

Jin, J., Liu, J., Wang, H., Wong, L., and Chua, N. M. (2013). PLncDB: plant long non-coding RNA database. *Bioinformatics* 29, 1068–1071. doi: 10.1093/bioinformatics/btt107

Joshi, V., Joung, J. G., Fei, Z., and Jander, G. (2010). Interdependence of threonine, methionine and isoleucine metabolism in plants: accumulation and transcriptional regulation under abiotic stress. *Amino Acids* 39, 933–947. doi: 10.1007/s00726-010-0505-7

Kalhan, S. C., and Hanson, R. W. (2012). Resurgence of serine: an often neglected but indispensable amino acid. *J. Biol. Chem.* 287, 19786–19791. doi: 10.1074/jbc.R112.357194

Kanjanaphachoat, P., Wei, B. Y., Lo, S. F., Wang, I. W., Wang, C. S., Yu, S. M., et al. (2012). Serotonin accumulation in transgenic rice by over-expressing tryptophan decarboxlyase results in a dark brown phenotype and stunted growth. *Plant Mol. Biol.* 78, 525–543. doi: 10.1007/s11103-012-9882-5

Kaplan, F., Kopka, J., Haskell, D. W., Zhao, W., Schiller, K. C., Gatzke, N., et al. (2004). Exploring the temperature-stress metabolome of *Arabidopsis*. *Plant Physiol.* 136, 4159–4168. doi: 10.1104/pp.104.052142

Karchi, H., Miron, D., Ben-Yaacov, S., and Galili, G. (1995). The lysine-dependent stimulation of lysine catabolism in tobacco seed requires calcium and protein phosphorylation. *Plant Cell* 7, 1963–1970. doi: 10.1105/tpc.7.11.1963

Kiyota, E., Pena, I. A., and Arruda, P. (2015). The saccharopine pathway in seed development and stress response of maize. *Plant Cell Environ.* 38, 2450–2461. doi: 10.1111/pce.12563

Kleczkowski, L. A., and Givan, C. V. (1988). Serine formation in leaves by mechanisms other than the glycolate pathway. *J. Plant Physiol.* 132, 641–652. doi: 10.1016/S0176-1617(88)80223-2

Koag, M. C., Wilkens, S., Fenton, R. D., Resnik, J., Vo, E., and Close, T. J. (2009). The K-segment of maize DHN1 mediates binding to anionic phospholipid vesicles and concomitant structural changes. *Plant Physiol.* 150, 1503–1514. doi: 10.1104/pp109136697

Kosová, K., Vítámvás, P., Prášil, I. T., and Renaut, J. (2011). Plant proteome changes under abiotic stress-contribution of proteomics studies to understanding plant stress response. *J. Proteomics* 74, 1301–1322. doi: 10.1016/j.jprot.2011.02.006

Krüßel, L., Junemann, J., Wirtz, M., Birke, H., Thornton, J. D., Browning, L. W., et al. (2014). The mitochondrial sulfur dioxygenase ETHYLMALONIC ENCEPHALOPATHY PROTEIN1 is required for amino acid catabolism during carbohydrate starvation and embryo development in *Arabidopsis*. *Plant Physiol.* 165, 92–104. doi: 10.1104/pp.114.239764

Kumar, K. R. R., and Kirti, P. B. (2012). Novel role for a serine/arginine-rich splicing factor, AdRSZ21 in plant defense and HR-like cell death. *Plant Mol. Biol.* 80, 461–476. doi: 10.1007/s11103-012-9960-8

Lazar, G., Schaal, T., Maniatis, T., and Goodman, H. M. (1995). Identification of a plant serine-arginine-rich protein similar to the mammalian splicing factor SF2/ASF. *Proc. Natl. Acad. Sci. U. S. A.* 92, 7672–7676. doi: 10.1073/pnas.92.17.7672

Less, H., Angelovici, R., Tzin, V., and Galili, G. (2011). Coordinated gene networks regulating *Arabidopsis* plant metabolism in response to various stresses and nutritional cues. *Plant Cell* 23, 1264–1271. doi: 10.1105/tpc.110.082867

Li, M., Guo, R., Jiao, Y., Jin, X., Zhang, H., and Shi, L. (2017). Comparison of salt tolerance in soja based on metabolomics of seedling roots. *Front. Plant Sci.* 8:1101. doi: 10.3389/fpls.2017.01101

Lin, S., Coutinho-Mansfield, G., Wang, D., Pandit, S., and Fu, X. D. (2008). The splicing factor SC35 has an active role in transcriptional elongation. *Nat. Struct. Mol. Biol.* 15, 819–826. doi: 10.1038/nsmb.1461

Lin, C. H., Peng, P. H., Ko, C. Y., Markhart, A. H., and Lin, T. Y. (2012). Characterization of a novel Y2K-type dehydrin *VrDhn1* from *Vigna radiata*. *Plant Cell Physiol.* 53, 930–942. doi: 10.1093/pcp/pcs040

Liu, Y., Mauve, C., Lamothe-Sibold, M., Guerard, F., and Glab, N. (2019). Photorespiratory serine hydroxymethyltransferase 1 activity impacts abiotic stress tolerance and stomatal closure. *Plant Cell Environ.* 42, 2567–2583. doi: 10.1111/pce.13595

Liu, Y., Wang, L., Xing, X., Sun, L., Pan, J., Kong, X., et al. (2013). ZmLEA3, a multifunctional group 3 LEA protein from maize (*Zea mays* L.) is involved in biotic and abiotic stresses. *Plant Cell Physiol.* 54, 944–959. doi: 10.1093/pcp/pct047

Liu, Y., Wang, L., Zhang, T., Yang, X., and Li, D. (2017). Functional characterization of KS-type dehydrin ZmDHN13 and its related conserved domains under oxidative stress. *Sci. Rep.* 7:7361. doi: 10.1038/s41598-017-07852-y

Liu, H., Yu, C., Li, H., Ouyang, B., Wang, T., Zhang, J., et al. (2015). Overexpression of *ShDHN*, a dehydrin gene from *Solanum habrochaites* enhances tolerance to multiple abiotic stresses in tomato. *Plant Sci.* 231, 198–211. doi: 10.1016/j.plantsci.2014.12.006

Long, X., Liu, Q., Chan, M., Wang, Q., and Sun, S. S. (2013). Metabolic engineering and profiling of rice with increased lysine. *Plant Biotechnol. J.* 11, 490–501. doi: 10.1111/pbi.12037

Lopato, S., Kalyna, M., Dorner, S., Kobayashi, R., Krainer, A. R., and Barta, A. (1999). atSRp30, one of two SF2/ASF-like proteins from *Arabidopsis thaliana*, regulates splicing of specific plant genes. *Genes Dev.* 13, 987–1001. doi: 10.1101/gad.13.8.987

Malik, A. A., Veltri, M., Boddington, K. F., Singh, K. K., and Graether, S. P. (2017). Genome analysis of conserved dehydrin motifs in vascular plants. *Front. Plant Sci.* 8:709. doi: 10.3389/fpls.2017.00709

Maria, K., Sergiy, L., and Andrea, B. (2003). Ectopic expression of *atRSZ33* reveals its function in splicing and causes pleiotropic changes in development. *Mol. Biol. Cell* 14, 3565–3577. doi: 10.1091/mbc.e03-02-0109

Martin, J., Geromanos, S., Tempest, P., and Hartl, F. U. (1993). Identification of nucleotide-binding regions in the chaperonin proteins GroEL and GroES. *Nature* 366, 279–282. doi: 10.1038/366279a0

Mattaini, K. R., Sullivan, M. R., and Heiden, M. G. V. (2016). The importance of serine metabolism in cancer. *J. Cell Biol.* 214, 249–257. doi: 10.1083/jcb.201604085

Melo, J. P., Kalyna, M., and Duque, P. (2020). Current challenges in studying alternative splicing in plants: the case of *Physcomitrella patens* SR proteins. *Front. Plant Sci.* 11:286. doi: 10.3389/fpls.2020.00286

Michard, E., Lima, P. T., Borges, F., Silva, A. C., Portes, M. T., Carvalho, J. E., et al. (2011). Glutamate receptor-like genes form Ca^{2+} channels in pollen tubes and are regulated by pistil D-serine. *Science* 332, 434–437. doi: 10.1126/science.1201101

Miyazaki, T., Miyazaki, J., Yamane, H., and Nishiyama, M. (2004). α-Aminoadipate aminotransferase from an extremely thermophilic bacterium, *Thermus thermophilus*. *Microbiology* 150, 2327–2334. doi: 10.1099/mic.0.27037-0

Moreno, J. I., Martin, R., and Castresana, C. (2005). *Arabidopsis* SHMT1, a serine hydroxymethyltransferase that functions in the photorespiratory pathway influences resistance to biotic and abiotic stress. *Plant J.* 41, 451–463. doi: 10.1111/j.1365-313X.2004.02311.x

Mundy, J., and Chua, N. H. (1988). Abscisic acid and water-stress induce the expression of a novel rice gene. *EMBO J.* 7, 2279–2286. doi: 10.1002/j.1460-2075.1988.tb03070.x

Muñoz-Bertomeu, J., Anoman, A. D., Toujani, W., Cascales-Miñana, B., Flores-Tornero, M., and Ros, R. (2011a). Interactions between abscisic acid and plastidial glycolysis in *Arabidopsis*. *Plant Signal. Behav.* 6, 157–159. doi: 10.4161/psb.6.1.14312

Muñoz-Bertomeu, J., Bermúdez, M. A., Segura, J., and Ros, R. (2011b). *Arabidopsis* plants deficient in plastidial glyceraldehyde-3-phosphate dehydrogenase show alterations in abscisic acid (ABA) signal transduction: interaction between

ABA and primary metabolism. *J. Exp. Bot.* 62, 1229–1239. doi: 10.1093/jxb/erq353

Muñoz-Bertomeu, J., Cascales-Miñana, B., Mulet, J. M., Baroja-Fernández, E., Pozueta-Romero, J., Kuhn, J. M., et al. (2009). Plastidial glyceraldehyde-3-phosphate dehydrogenase deficiency leads to altered root development and affects the sugar and amino acid balance in *Arabidopsis*. *Plant Physiol.* 151, 541–558. doi: 10.1104/pp.109.143701

Muttucumaru, N., Powers, S. J., Elmore, J. S., Mottram, D. S., and Halford, N. G. (2015). Effects of water availability on free amino acids, sugars, and acrylamide-forming potential in potato. *J. Agric. Food Chem.* 63, 2566–2575. doi: 10.1021/jf506031w

Nagaraju, M., Reddy, P. S., Kumar, S. A., Kumar, A., Suravajhala, P., Ali, A., et al. (2018). Genome-wide *in silico* analysis of dehydrins in *Sorghum bicolor*, *Setaria italica* and *Zea mays* and quantitative analysis of dehydrin gene expressions under abiotic stresses in *Sorghum bicolor*. *Plant Gene* 13, 64–75. doi: 10.1016/j.plgene.2018.01.004

Negrutiu, I., Cattoir-Reynearts, A., Verbruggen, I., and Jacobs, M. (1984). Lysine overproducer mutants with an altered dihydrodipicolinate synthase from protoplast culture of *Nicotiana sylvestris* (Spegazzini and Comes). *Theor. Appl. Genet.* 68, 11–20. doi: 10.1007/BF00252303

Noman, A., Ali, Q., Maqsood, J., Iqbal, N., Javed, M. T., Rasool, N., et al. (2018). Deciphering physio-biochemical, yield, and nutritional quality attributes of water-stressed radish (*Raphanus sativus* L.) plants grown from Zn-Lys primed seeds. *Chemosphere* 195, 175–189. doi: 10.1016/j.chemosphere.2017.12.059

Okamura, E., and Hirai, M. Y. (2017). Novel regulatory mechanism of serine biosynthesis associated with 3-phosphoglycerate dehydrogenase in *Arabidopsis thaliana*. *Sci. Rep.* 7:3533. doi: 10.1038/s41598-017-03807-5

Palusa, S. G., Ali, G. S., and Reddy, A. S. (2010). Alternative splicing of pre-mRNAs of *Arabidopsis* serine/arginine-rich proteins: regulation by hormones and stresses. *Plant J.* 49, 1091–1107. doi: 10.1111/j.1365-313X.2006.03020.x

Pant, B. D., Buhtz, A., Kehr, J., and Scheible, W. R. (2008). MicroRNA399 is a long-distance signal for the regulation of plant phosphate homeostasis. *Plant J.* 53, 731–738. doi: 10.1111/j.1365-313X.2007.03363.x

Perl, A., Shaul, O., and Galili, G. (1992). Regulation of lysine synthesis in transgenic potato plants expressing a bacterial dihydrodipicolinate synthase in their chloroplasts. *Plant Mol. Biol.* 19, 815–823. doi: 10.1007/BF00027077

Ramos-Ruiz, R., Martinez, F., and Knauf-Beiter, G. (2019). The effects of GABA in plants. *Cogent Food Agric.* 5:1670553. doi: 10.1080/23311932.2019.1670553

Riley, A. C., Ashlock, D. A., and Graether, S. P. (2019). Evolution of the modular, disordered stress proteins known as dehydrins. *PLoS One* 14:e0211813. doi: 10.1371/journal.pone.0211813

Rizwan, M., Ali, S., Hussain, A., Ali, Q., Shakoor, M. B., Zia-ur-Rehman, M., et al. (2017). Effect of zinc-lysine on growth, yield and cadmium uptake in wheat (*Triticum aestivum* L.) and health risk assessment. *Chemosphere* 187, 35–42. doi: 10.1016/j.chemosphere.2017.08.071

Rodrigues, S. M., Andrade, M. O., Gomes, A. P. S., DaMatta, F. M., Baracat-Pereira, M. C., and Fontes, E. P. B. (2006). *Arabidopsis* and tobacco plants ectopically expressing the soybean antiquitin-like ALDH7 gene display enhanced tolerance to drought, salinity, and oxidative stress. *J. Exp. Bot.* 57, 1909–1918. doi: 10.1093/jxb/erj132

Ros, R., Cascales-Miñana, B., Segura, J., Anoman, A. D., Toujani, W., Flores-Tornero, M., et al. (2013). Serine biosynthesis by photorespiratory and non-photorespiratory pathways: an interesting interplay with unknown regulatory networks. *Plant Biol.* 15, 707–712. doi: 10.1111/j.1438-8677.2012.00682.x

Ros, R., Muñoz-Bertomeu, J., and Krueger, S. (2014). Serine in plants: biosynthesis, metabolism, and functions. *Trends Plant Sci.* 19, 564–569. doi: 10.1016/j.tplants.2014.06.003

Rosales, R., Romero, I., Escribano, M. I., Merodio, C., and Sanchez-Ballesta, M. T. (2014). The crucial role of ϕ and K-segments in the *in vitro* functionality of *Vitis vinifera* dehydrin DHN1a. *Phytochemistry* 108, 17–25. doi: 10.1016/j.phytochem.2014.10.006

Rosa-Téllez, S., Anoman, A. D., Alcantara-Enguidanos, A., Garza-Aguirre, R. A., Alseekh, S., and Ros, R. (2020). PGDH family genes differentially affect *Arabidopsis* tolerance to salt stress. *Plant Sci.* 290:110284. doi: 10.1016/j.plantsci.2019.110284

Saeedipour, S., and Moradi, F. (2012). Stress-induced changes in the free amino acid composition of two wheat cultivars with difference in drought resistance. *Afr. J. Biotechnol.* 11, 9559–9565. doi: 10.5897/AJB11.3870

Serre, N. B. C., Sarthou, M., Gigarel, O., Figuet, S., Corso, M., Choulet, J., et al. (2020). Protein lysine methylation contributes to modulating the response of sensitive and tolerant *Arabidopsis* species to cadmium stress. *Plant Cell Environ.* 43, 760–774. doi: 10.1111/pce.13692

Shaul, O., and Galili, G. (1992). Increased lysine synthesis in tobacco plants that express high levels of bacterial dihydrodipicolinate synthase in their chloroplasts. *Plant J.* 2, 203–209. doi: 10.1111/j.1365-313X.1992.00203.x

Shaul, O., and Galili, G. (1993). Concerted regulation of lysine and threonine synthesis in tobacco plants expressing bacterial feedback-insensitive aspartate kinase and dihydrodipicolinate synthase. *Plant Mol. Biol.* 23, 759–768. doi: 10.1007/BF00021531

Slaughter, J. C., and Davies, D. D. (1968). The isolation and characterization of 3-phosphoglycerate dehydrogenase from peas. *Biochem. J.* 109, 743–748. doi: 10.1042/bj1090743

Somerville, C. R., and Ogren, W. L. (1981). Photorespiration-deficient mutants of *Arabidopsis thaliana* lacking mitochondrial serine transhydroxymethylase activity. *Plant Physiol.* 67, 666–671. doi: 10.1104/pp.67.4.666

Song, Y., and Zhang, D. (2017). The role of long noncoding RNAs in plant stress tolerance. *Methods Mol. Biol.* 1631, 41–68. doi: 10.1007/978-1-4939-7136-7_3

Stein, R. J., Höreth, S., de Melo, J. R., Syllwasschy, L., Lee, G., Garbin, M. L., et al. (2017). Relationships between soil and leaf mineral composition are element-specific, environment-dependent and geographically structured in the emerging model *Arabidopsis halleri*. *New Phytol.* 213, 1274–1286. doi: 10.1111/nph.14219

Stewart, G. R., and Larher, F. (1980). "Accumulation of amino acids and related compounds in relation to environmental stress" in *Amino acids and derivatives*. Springer Berlin Heidelberg: Academic Press, 609–635.

Swiezewski, S., Liu, F., Magusin, A., and Dean, C. (2009). Cold-induced silencing by long antisense transcripts of an *Arabidopsis* polycomb target. *Nature* 462, 799–802. doi: 10.1038/nature08618

Szczesniak, M. W., Rosikiewicz, W., and Makałowska, I. (2016). CANTATAdb: a collection of plant long non-coding RNAs. *Plant Cell Physiol.* 57:e8. doi: 10.1093/pcp/pcv201

Tanabe, N., Kimura, A., Yoshimura, K., and Shigeoka, S. (2008). "Identification of interacting factors with a high-light responsible SR protein, atSR45a, involved in the regulation of alternative splicing in *Arabidopsis*" in *Photosynthesis. Energy from the Sun*. Dordrecht, The Netherlands: Springer, 1347–1350.

Tolbert, N. E. (1980). "Photorespiration" in *The biochemistry of plants. Vol. 2.* ed. D. D. Davis (New York: Academic Press), 487–523.

Toujani, W., Muñoz-Bertomeu, J., Flores-Tornero, M., Rosa-Téllez, S., Anoman, A. D., Alseekh, S., et al. (2013). Functional characterization of the plastidial 3-phosphoglycerate dehydrogenase family in *Arabidopsis*. *Plant Physiol.* 163, 1164–1178. doi: 10.1104/pp.113.226720

Tzin, V., and Galili, G. (2010). New insights into the shikimate and aromatic amino acids biosynthesis pathways in plants. *Mol. Plant* 3, 956–972. doi: 10.1093/mp/ssq048

Urano, K., Maruyama, K., Ogata, Y., Morishita, Y., Takeda, M., Sakurai, N., et al. (2009). Characterization of the ABA-regulated global responses to dehydration in *Arabidopsis* by metabolomics. *Plant J.* 57, 1065–1078. doi: 10.1111/j.1365-313X.2008.03748.x

Uversky, V. N. (2013). A decade and a half of protein intrinsic disorder: biology still waits for physics. *Protein Sci.* 22, 693–724. doi: 10.1002/pro.2261

Uversky, V. N. (2016). Dancing protein clouds: the strange biology and chaotic physics of intrinsically disordered proteins. *J. Biol. Chem.* 291, 6681–6688. doi: 10.1074/jbc.R115.685859

Vauterin, M., Frankard, V., and Jacobs, M. (1999). The *Arabidopsis thaliana* dhdps gene encoding dihydrodipicolinate synthase, key enzyme of lysine biosynthesis, is expressed in a cell-specific manner. *Plant Mol. Biol.* 39, 695–708. doi: 10.1023/A:1006132428623

Velasco, A. M., Leguina, J. I., and Lazcano, A. (2002). Molecular evolution of the lysine biosynthetic pathways. *J. Mol. Evol.* 55, 445–449. doi: 10.1007/s00239-002-2340-2

Voll, L. M., Jamai, A., Renne, P., Voll, H., McClung, C. R., and Weber, A. P. (2006). The photorespiratory *Arabidopsis* shm1 mutant is deficient in SHM1. *Plant Physiol.* 140, 59–66. doi: 10.1104/pp.105.071399

Waditee, R., Bhuiyan, N. H., Hirata, E., Hibino, T., Tanaka, Y., Shikata, M., et al. (2007). Metabolic engineering for betaine accumulation in microbes and plants. *J. Biol. Chem.* 282, 34185–34193. doi: 10.1074/jbc.M704939200

Wang, Y., Fan, X., Lin, F., He, G., Terzaghi, W., Zhu, D., et al. (2014). *Arabidopsis* noncoding RNA mediates control of photomorphogenesis by red light. *Proc. Natl. Acad. Sci. U. S. A.* 111, 10359–10364. doi: 10.1073/pnas.1409457111

Wang, M., Liu, C., Li, S., Zhu, D., Zhao, Q., and Yu, J. (2013). Improved nutritive quality and salt resistance in transgenic maize by simultaneously overexpression of a natural lysine-rich protein gene, SBgLR, and an ERF transcription factor gene, TSRF1. *Int. J. Mol. Sci.* 14, 9459–9474. doi: 10.3390/ijms14059459

Wenefrida, I., Utomo, H. S., Blanche, S. B., and Linscombe, S. D. (2009). Enhancing essential amino acids and health benefit components in grain crops for improved nutritional values. *Recent Pat. DNA Gene Seq.* 3, 219–225. doi: 10.2174/187221509789318405

Wisniewski, M., Webb, R., Balsamo, R., Close, T. J., Yu, X. M., and Griffith, M. (1999). Purification, immunolocalization, cryoprotective, and antifreeze activity of PCA60: A dehydrin from peach (*Prunus persica*). *Physiol. Plant.* 105, 600–608. doi: 10.1034/j.1399-3054.1999.105402.x

Wu, M., Wanggou, S., Li, X., Liu, Q., and Xie, Y. (2017). Overexpression of mitochondrial serine hydroxyl-methyltransferase 2 is associated with poor prognosis and promotes cell proliferation and invasion in gliomas. *Onco Targets Ther.* 10, 3781–3788. doi: 10.2147/OTT.S130409

Wulfert, S., and Krueger, S. (2018). Phosphoserine aminotransferase1 is part of the phosphorylated pathways for serine biosynthesis and essential for light and sugar-dependent growth promotion. *Front. Plant Sci.* 9:1712. doi: 10.3389/fpls.2018.01712

Xiao, R., Sun, Y., Ding, J. H., Lin, S., Rose, D. W., Rosenfeld, M. G., et al. (2007). Splicing regulator SC35 is essential for genomic stability and cell proliferation during mammalian organogenesis. *Mol. Cell. Biol.* 27, 5393–5402. doi: 10.1128/MCB.00288-07

Xie, C., Zhang, R. X., Qu, Y. T., Miao, Z. Y., Zhang, Y. Q., Shen, X. Y., et al. (2012). Overexpression of *MtCAS31* enhances drought tolerance in transgenic *Arabidopsis* by reducing stomatal density. *New Phytol.* 195, 124–135. doi: 10.1111/j.1469-8137.2012.04136.x

Xing, X., Liu, Y., Kong, X., Liu, Y., and Li, D. (2011). Overexpression of a maize dehydrin gene, ZmDHN2b, in tobacco enhances tolerance to low temperature. *Plant Growth Regul.* 65, 109–118. doi: 10.1007/s10725-011-9580-3

Xu, H., Andi, B., Qian, J., West, A. H., and Cook, P. F. (2006). The α-aminoadipate pathway for lysine biosynthesis in fungi. *Cell Biochem. Biophys.* 46, 43–64. doi: 10.1385/CBB:46:1:43

Yan, Q., Xia, X., Sun, Z., and Fang, Y. (2017). Depletion of *Arabidopsis* SC35 and SC35-like serine/arginine-rich proteins affects the transcription and splicing of a subset of genes. *PLoS Genet.* 13:e1006663. doi: 10.1371/journal.pgen.1006663

Yang, M., and Vousden, K. H. (2016). Serine and one-carbon metabolism in cancer. *Nat. Rev. Cancer* 16, 650–662. doi: 10.1038/nrc.2016.81

Yang, Q. Q., Zhang, C. Q., Chan, M. L., Zhao, D. S., Chen, J. Z., Wang, Q., et al. (2016). Biofortification of rice with the essential amino acid lysine: molecular characterization, nutritional evaluation, and field performance. *J. Exp. Bot.* 67, 4285–4296. doi: 10.1093/jxb/erw209

Yang, W., Zhang, L., Lv, H., Li, H., Zhang, Y., Xu, Y., et al. (2015). The K-segments of wheat dehydrin WZY2 are essential for its protective functions under temperature stress. *Front. Plant Sci.* 6:406. doi: 10.3389/fpls.2015.00406

Yang, Q. Q., Zhao, D. S., Zhang, C. Q., Wu, H. Y., Li, Q. F., Gu, M. H., et al. (2018). A connection between lysine and serotonin metabolism in rice endosperm. *Plant Physiol.* 176, 1965–1980. doi: 10.1104/pp.17.01283

Yoon, E. K., Krishnamurthy, P., Kim, J. A., Jeong, M. J., and Lee, S. I. (2018). Genome-wide characterization of *Brassica rapa* genes encoding serine/arginine-rich proteins: expression and alternative splicing events by abiotic stresses. *J. Plant Biol.* 61, 198–209. doi: 10.1007/s12374-017-0391-6

Yu, Z., Wang, X., and Zhang, L. (2018). Structural and functional dynamics of dehydrins: a plant protector protein under abiotic stress. *Int. J. Mol. Sci.* 19:3420. doi: 10.3390/ijms19113420

Yuan, J., Li, J., Yang, Y., Tan, C., Zhu, Y., Hu, L., et al. (2018). Stress-responsive regulation of long non-coding RNA polyadenylation in *Oryza sativa*. *Plant J.* 93, 814–827. doi: 10.1111/tpj.13804

Yuan, L., Liu, X., Luo, M., Yang, S., and Wu, K. (2013). Involvement of histone modifications in plant abiotic stress responses. *J. Integr. Plant Biol.* 55, 892–901. doi: 10.1111/jipb.12060

Zafari, M., and Ebadi, A. (2016). Effects of water strass and brassinosteroid (24-epibrassinolide) on changes of some amino acids and pigments in safflower (*Cartamus tinctorius* L.). *J. Curr. Res. Sci.* 1:711.

Zhang, W., Du, B., Liu, D., and Qi, X. (2014). Splicing factor SR34b mutation reduces cadmium tolerance in *Arabidopsis* by regulating iron-regulated transporter 1 gene. *Biochem. Biophys. Res. Commun.* 455, 312–317. doi: 10.1016/j.bbrc.2014.11.017

Zhang, X. N., Shi, Y., Powers, J. J., Gowda, N. B., Zhang, C., Ibrahim, H. M. M., et al. (2017). Transcriptome analyses reveal SR45 to be a neutral splicing regulator and a suppressor of innate immunity in *Arabidopsis thaliana*. *BMC Genomics* 18:772. doi: 10.1186/s12864-017-4183-7

Zhang, Y., Sun, K., Sandoval, F. J., Santiago, K., and Roje, S. (2010). One-carbon metabolism in plants: characterization of a plastid serine hydroxymethyltransferase. *Biochem. J.* 430, 97–105. doi: 10.1042/BJ20100566

Zhong, X. Y., Wang, P., Han, J., Rosenfeld, M. G., and Fu, X. D. (2009). SR proteins in vertical integration of gene expression from transcription to RNA processing to translation. *Mol. Cell* 35, 1–10. doi: 10.1016/j.molcel.2009.06.016

Zhu, X., and Galili, G. (2003). Increased lysine synthesis coupled with a knockout of its catabolism synergistically boosts lysine content and also transregulates the metabolism of other amino acids in *Arabidopsis* seeds. *Plant Cell* 15, 845–853. doi: 10.1105/tpc.009647

Zhu, X., and Galili, G. (2004). Lysine metabolism is concurrently regulated by synthesis and catabolism in both reproductive and vegetative tissues. *Plant Physiol.* 135, 129–136. doi: 10.1104/pp.103.037168

Zhu, X., Tang, G., and Galili, G. (2002). The activity of the *Arabidopsis* bifunctional lysine-ketoglutarate reductase/saccharopine dehydrogenase enzyme of lysine catabolism is regulated by functional interaction between its two enzyme domains. *J. Biol. Chem.* 277, 49655–49661. doi: 10.1074/jbc.M205466200

Zhu-Shimoni, J. X., and Galili, G. (1998). Expression of an *Arabidopsis* aspartate kinase/homoserine dehydrogenase gene is metabolically regulated by photosynthesis-related signals but not by nitrogenous compounds. *Plant Physiol.* 116, 1023–1028. doi: 10.1104/pp.116.3.1023

Conflict of Interest: The authors declare that the research was conducted in the absence of any commercial or financial relationships that could be construed as a potential conflict of interest.

Copyright © 2020 Kishor, Suravajhala, Rajasheker, Marka, Shridhar, Dhulala, Scinthia, Divya, Doma, Edupuganti, Suravajhala and Polavarapu. This is an open-access article distributed under the terms of the Creative Commons Attribution License (CC BY). The use, distribution or reproduction in other forums is permitted, provided the original author(s) and the copyright owner(s) are credited and that the original publication in this journal is cited, in accordance with accepted academic practice. No use, distribution or reproduction is permitted which does not comply with these terms.

frontiers in Plant Science

ORIGINAL RESEARCH
published: 23 December 2020
doi: 10.3389/fpls.2020.602939

Appropriate Activity Assays Are Crucial for the Specific Determination of Proline Dehydrogenase and Pyrroline-5-Carboxylate Reductase Activities

Sandrine Lebreton[1†], Cécile Cabassa-Hourton[1†], Arnould Savouré[1], Dietmar Funck[2] and Giuseppe Forlani[3]*

[1] Sorbonne Université, UPEC, CNRS, IRD, INRAE, Institute of Ecology and Environmental Sciences—Paris, IEES, Paris, France, [2] Department of Biology, University of Konstanz, Konstanz, Germany, [3] Department of Life Sciences and Biotechnology, University of Ferrara, Ferrara, Italy

OPEN ACCESS

Edited by:
Han Asard,
University of Antwerp, Belgium

Reviewed by:
Hamada AbdElgawad,
Beni-Suef University, Egypt
Donald Becker,
University of Nebraska-Lincoln, United States

***Correspondence:**
Dietmar Funck
Dietmar.Funck@uni-konstanz.de

[†] These authors have contributed equally to this work

Specialty section:
This article was submitted to Plant Abiotic Stress, a section of the journal Frontiers in Plant Science

Received: 04 September 2020
Accepted: 03 December 2020
Published: 23 December 2020

Citation:
Lebreton S, Cabassa-Hourton C, Savouré A, Funck D and Forlani G (2020) Appropriate Activity Assays Are Crucial for the Specific Determination of Proline Dehydrogenase and Pyrroline-5-Carboxylate Reductase Activities. Front. Plant Sci. 11:602939. doi: 10.3389/fpls.2020.602939

Accumulation of proline is a widespread plant response to a broad range of environmental stress conditions including salt and osmotic stress. Proline accumulation is achieved mainly by upregulation of proline biosynthesis in the cytosol and by inhibition of proline degradation in mitochondria. Changes in gene expression or activity levels of the two enzymes catalyzing the first reactions in these two pathways, namely pyrroline-5-carboxylate (P5C) synthetase and proline dehydrogenase (ProDH), are often used to assess the stress response of plants. The difficulty to isolate ProDH in active form has led several researchers to erroneously report proline-dependent NAD^+ reduction at pH 10 as ProDH activity. We demonstrate that this activity is due to P5C reductase (P5CR), the second and last enzyme in proline biosynthesis, which works in the reverse direction at unphysiologically high pH. ProDH does not use NAD^+ as electron acceptor but can be assayed with the artificial electron acceptor 2,6-dichlorophenolindophenol (DCPIP) after detergent-mediated solubilization or enrichment of mitochondria. Seemingly counter-intuitive results from previous publications can be explained in this way and our data highlight the importance of appropriate and specific assays for the detection of ProDH and P5CR activities in crude plant extracts.

Keywords: proline dehydrogenase, pyrroline-5-carboxylate reductase, enzyme activity assay, electron acceptor, protein extraction, mitochondria

INTRODUCTION

Many prokaryotes and eukaryotes accumulate free proline as a compatible solute in response to abiotic or biotic stress (Forlani et al., 2019; Trovato et al., 2019). Therefore, in order to improve crop performance under stress conditions, a lot of research has been dedicated to understand the molecular basis of proline accumulation and the role of this amino acid in plant acclimation and stress tolerance (Szabados and Savoure, 2010; Forlani et al., 2019;

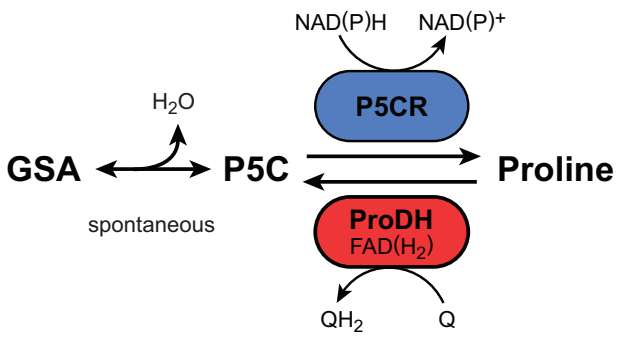

FIGURE 1 | Reactions and enzymes known to produce or degrade proline in plants. GSA, glutamate-5-semialdehyde; P5C, pyrroline-5-carboxylate; P5CR: P5C reductase; ProDH, proline dehydrogenase, Q/QH_2, oxidized/reduced ubiquinone.

El Moukhtari et al., 2020). Multi-level analyses and flux modeling demonstrated that different plant species rely on different regulatory mechanisms of either transcriptional regulation or modulation of enzyme activities to shift the balance between proline biosynthesis, consumption, and degradation toward proline accumulation (AbdElgawad et al., 2015; Hildebrandt, 2018; Dellero et al., 2020). Proline is synthesized from glutamate and also degraded to glutamate via the common intermediate glutamate-5-semialdhyde (GSA), which is in spontaneous equilibrium with pyrroline-5-carboxylate (P5C, **Figure 1**). Proline production is catalyzed by the sequential action of P5C synthetase and P5C reductase (P5CR), the latter being the only known enzyme to synthesize proline in plants (Trovato et al., 2019). P5CR can utilize both NADH and NADPH as the electron donor for P5C reduction (Giberti et al., 2014). Proline degradation occurs in mitochondria by the sequential action of proline dehydrogenase (ProDH) and P5C dehydrogenase (P5CDH; Trovato et al., 2019). Whereas P5CDH is a soluble enzyme in the mitochondrial matrix and uses NAD^+ as the preferential electron acceptor (Forlani et al., 1997, 2015a), ProDH is a membrane bound flavoenzyme that seems to donate electrons directly to ubiquinone in the mitochondrial inner membrane (Elthon and Stewart, 1981; Servet et al., 2012; Schertl et al., 2014; Cabassa-Hourton et al., 2016). To account for the frequent observation of oxygen consumption in conjunction with proline oxidation, ProDH was and is occasionally also referred to as proline oxidase, but good evidence for direct electron transfer to molecular oxygen has not been obtained so far.

Most of the molecular data about proline metabolism has been obtained with Arabidopsis, but genes for proline metabolic enzymes have also been cloned from other model species and their expression has been analyzed. Numerous studies have analyzed the correlation between stress tolerance and proline content as well as transcript and activity levels of proline metabolic enzymes (Per et al., 2017). Two activities can be easily detected in crude extracts of soluble proteins from plants: P5C-dependent oxidation of NAD(P)H with a pH-optimum at 7–8 (with NADH) or 8–9 (with NADPH; Giberti et al., 2014), and proline-dependent NAD^+-reduction at pH > 9 (Rena and Splittstoesser, 1975). Early purification attempts already indicated that both activities may be mediated by the same protein, i.e., P5CR (Rena and Splittstoesser, 1975), and later on purified P5CRs were shown to catalyze both reactions (Krueger et al., 1986; Szoke et al., 1992). Because P5C is unstable in neutral solutions and not commercially available, many subsequent papers used proline-dependent NAD^+ reduction at high pH to assay P5CR activity, although it does not represent a physiological feature (Nocek et al., 2005; Meng et al., 2006).

Analysis of proline-dependent respiration in isolated corn mitochondria showed that the respiration rates were insensitive to NAD^+ addition and that ProDH is bound to the inner mitochondrial membrane (Elthon and Stewart, 1981, 1982). Solubilization of membrane-bound proteins from corn or Arabidopsis mitochondria allowed the detection of ProDH activity as proline-dependent reduction of decylubiquinone, 2,6-dichlorophenolindophenol (DCPIP), cytochrome *c*, or iodonitrotetrazolium (Rayapati and Stewart, 1991; Schertl et al., 2014). These activities were nearly completely absent in mitochondria isolated from Arabidopsis *prodh1/prodh2* double mutants (Cabassa-Hourton et al., 2016). Structural and functional studies on ProDH from bacteria (PutA), yeast (Put1) or human showed that they all contain a tightly bound FAD cofactor and transfer electrons to a membrane-localized quinone (Wanduragala et al., 2010; Tallarita et al., 2012; Singh et al., 2014; Tanner, 2019).

Against this large body of evidence, following early reports claiming the occurrence of an NAD-linked "ProDH" in wheat (Mazelis and Creveling, 1974) and *Chlorella pyrenoidosa* (McNamer and Stewart, 1974), numerous publications have assigned proline-dependent NAD^+ reduction at high pH to ProDH activity. Our detailed characterization of recombinant proteins, plant protein extracts, and isolated mitochondria from Arabidopsis wildtype and mutants clearly shows that only P5CR mediates this activity. ProDH activity can be specifically quantified as proline-dependent DCPIP reduction, but requires membrane-solubilizing agents for extraction or enrichment of mitochondria.

MATERIALS AND METHODS

Plant Material and Cultivation Conditions

Arabidopsis [*Arabidopsis thaliana* (L.) Heynh.], ecotype Col-0 and T-DNA insertion lines were obtained from the NASC and the GABI-KAT project as described previously (Funck et al., 2010; Kleinboelting et al., 2012; Cabassa-Hourton et al., 2016). A *prodh1-4/prodh2-2* double mutant was obtained by crossing *prodh1-4* and *prodh2-2* and was described by Cabassa-Hourton et al. (2016). Surface-sterilized seeds were sown on grids placed on solid half-strength Murashige and Skoog medium (0.8% agar) in Petri dishes and cultivated under a long-day light regime (16 h photoperiod; 90 $\mu mol\ m^{-2}\ s^{-1}$ at 21°C). With the aid of the grids, entire batches of seedlings were transferred to fresh Petri dishes containing sterile water and incubated for 3 days in darkness at 21°C.

For mitochondria isolation, seedlings were sown and grown on soil (16 h photoperiod at 80–100 μmol photons m^{-2} s^{-1} at 21°C).

Protein Extraction and Mitochondria Enrichment

Seedlings were ground in a cold mortar with 2 mL of grinding buffer [50 mM Tris-HCl pH 7.5, 0.5 mM EDTA, 0.5 mM $MgCl_2$, 0.5 mM DTT, 1% (w/v) polyvinylpyrrolidone 30, ± 0.5% (v/v) triton-X-100 and 1 × protease inhibitor cocktail (Sigma P2714)]. Soluble protein extracts were centrifuged for 15 min at 20,000 g at 4°C to remove insoluble plant debris. Supernatants were then desalted into the buffer used for the subsequent enzymatic activity on PD10 Sephadex G25 columns (GE healthcare). Soluble protein concentration was determined according to Bradford (1976) with BSA as standard.

Mitochondria were enriched by several differential centrifugation steps as described by Cabassa-Hourton et al. (2016) from detached leaves of 1-month-old plants that had been incubated in darkness for 5 days prior to mitochondria isolation. Mitochondrial protein concentration was determined according to Lowry et al. (1951) with BSA as standard.

DNA Constructs and Recombinant Protein Production

Bacterial expression constructs for Arabidopsis ProDH1 and ProDH2 including or excluding the putative mitochondrial transit peptides and with an N-terminal GST tag were generated by amplifying the coding sequence from cDNA with primers that introduce suitable restriction sites (**Supplementary Table S1**). The resulting PCR products were digested and inserted into pGEX-4T-1 or pGEX-6P-1. Protein expression in *E. coli* BL21(λDE3) star cells was induced with 1 mM IPTG at 18°C overnight. The cells were lysed by sonication in extraction buffer [50 mM Tris pH7.5, 5 mM $MgCl_2$, 50 mM KCl, 0.5 mM FAD, 0.5 mM DTT ± 0.1% (w/v) dodecyl maltoside] and the GST fusion proteins were purified with Protino™ Glutathione-Agarose 4B (Macherey-Nagel) according to the recommendations of the supplier. Glutathione was removed from the purified proteins by passage through PD SpinTrap G-25 columns (GE lifescience) equilibrated with extraction buffer.

Expression and purification of 6xHis-tagged Arabidopsis and rice P5CR were performed as described previously (Giberti et al., 2014; Forlani et al., 2015b). Protein concentrations were determined according to Bradford (1976) with BSA as standard. All activity assays were performed with enzymes purified from at least three independent bacterial cultures.

Enzyme Activity Assays

ProDH activity was calculated from the difference in the rates of DCPIP reduction before and after the addition of 150 mM proline (Huang and Cavalieri, 1979; Schertl et al., 2014). Variable amounts of protein extracts or purified enzymes were incubated at 25°C in 850 μl reaction buffer until a linear decrease of the OD_{600} was observed (typically 2–3 min). Then the reaction was started by adding 150 μl of a 1 M proline solution and the decrease in the OD_{600} was followed until at least 1 min of linear reaction was observed. The final reaction mix contained 100 mM Tris-HCl, pH 7.5, 2.5 mM $MgCl_2$, 1 mM KCN, 0.5 mM FAD, 0.5 mM phenazine methosulfate, and 60 μM DCPIP. The activity of P5CR in the physiological forward reaction was calculated from the difference in the rates of NADPH oxidation at pH 7.5 and 25°C in the presence or absence of DL-P5C as described previously (Forlani et al., 2007). DL-P5C was kept as a stock in 1 M HCl and neutralized with 1 M Tris-base immediately before the reaction was started. The final reaction mixture contained 200 mM Tris-HCl, 0.4 mM NADPH, 1 mM DL-P5C and variable amounts of protein extract or purified enzymes. The activity of P5CR in the reverse reaction was calculated from the difference in the rates of NAD^+ reduction at pH 10 and 25°C before and after the addition of 50 mM proline (from a 1 M stock solution) as described in Forlani and Funck (2020). The final reaction mixture contained 60 mM Na carbonate buffer or 60 mM Glycine-NaOH buffer, pH 10, 10 mM NAD^+ and variable amounts of protein extract or purified enzymes. In all assays, the amount of enzyme was adjusted to ensure linear reaction rates over at least 1 min. Extinction coefficients of ε_{600} = 19.1 mM^{-1} cm^{-1} for DCPIP (Basford and Huennekens, 1955) and ε_{340} = 6.22 mM^{-1} cm^{-1} for NADH and NADPH were used to calculate specific activities.

RESULTS

Expression of Arabidopsis ProDH1 or ProDH2 in *E. coli* Confers the Ability to Catalyze Proline-Dependent DCPIP Reduction, but Not Proline-Dependent NAD^+ Reduction at High pH

Analysis of mitochondrial protein extracts from Arabidopsis seedlings by mass spectrometry identified N-terminal peptides of ProDH1 and ProDH2 lacking the first 12 and 13 amino acids, respectively, indicating processing of the N-termini during import into mitochondria (Launay et al., 2019; and data not shown). When the deduced mature polypeptides (ProDH1ΔN12 and ProDH2ΔN13) or the pre-proteins of Arabidopsis ProDH1 and ProDH2 were expressed as GST-fusion proteins in *E. coli*, very little soluble protein of the expected size was obtained by expression over night at 10–18°C (**Figure 2A**). This notwithstanding, crude protein extracts of the *E. coli* cultures expressing ProDH1 or ProDH2, but not from cells carrying an empty vector or expressing Arabidopsis P5CR, showed clearly detectable rates of proline-dependent DCPIP reduction (**Figure 2B**). These rates were slightly higher in cells expressing the mature forms of ProDH1 and ProDH2 compared to the pre-proteins (data not shown) and therefore, all subsequent experiments were carried out exclusively with the mature proteins. The rates of P5C-dependent NADPH-oxidation at pH 7.5 and of proline-dependent NAD^+ reduction at pH 10 were very similar in cells carrying the empty vector or expressing ProDH1 or ProDH2, but increased more than 180-fold in cells expressing P5CR (**Figure 2B**). These

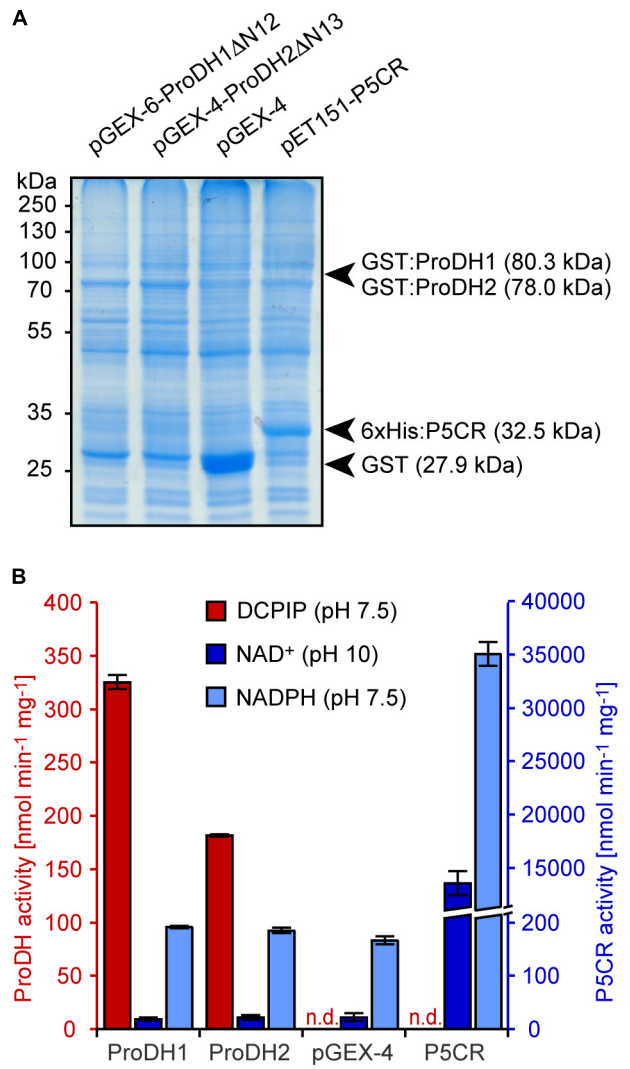

FIGURE 2 | Enzyme activities in bacterial extracts. Soluble protein extracts from *E. coli* cells carrying an empty vector or overexpressing either GST:ProDH1ΔN12, GST:ProDH2ΔN13 or 6xHis:P5CR were used for different enzyme assays. **(A)** Coomassie-stained gel with the positions of molecular weight markers and those expected for the recombinant proteins. **(B)** Proline-dependent 2,6-dichlorophenolindophenol (DCPIP) reduction (red columns) and P5C-dependent NADPH oxidation (light blue columns) were measured at pH 7.5, while proline-dependent NAD^+ reduction (blue columns) was measured at pH 10. Data are the average (±SD) of technical triplicates. Independent protein preparations gave very similar results; n.d., not detected.

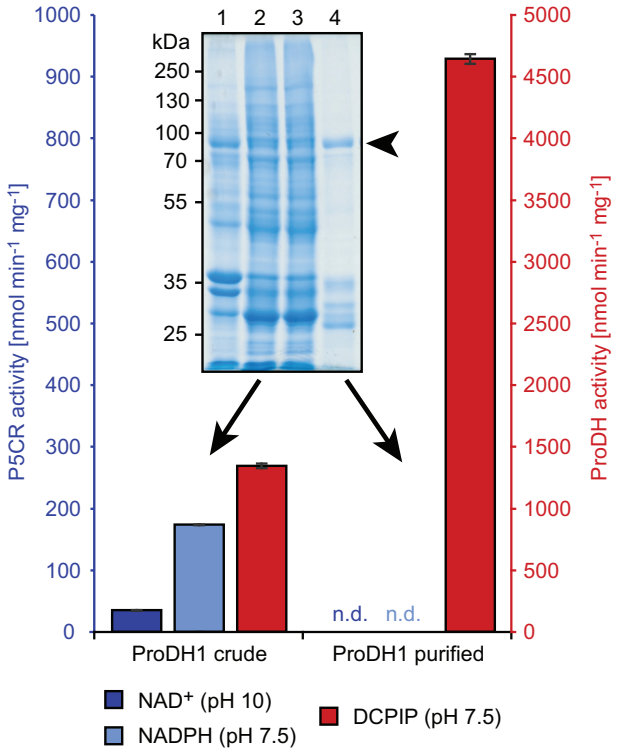

FIGURE 3 | Activities of purified recombinant GST:ProDH1ΔN12. Crude protein extract of bacteria overexpressing GST:ProDH1ΔN12 and affinity-purified GST:ProDH1ΔN12 (indicated by an arrowhead, calculated molecular weight is 80.3 kDa) were assayed for proline-dependent 2,6-dichlorophenolindophenol (DCPIP) reduction and P5C-dependent NADPH oxidation at pH 7.5, as well as for proline-dependent NAD^+ reduction at pH 10. Note that the scales of the two *y*-axes are in an opposite ratio than in **Figure 2**. Data are the average (±SD) of technical triplicates. Two further, independent protein preparations gave very similar results; n.d., not detected. The inset shows a Coomassie-stained, denaturing protein gel of the assayed fractions. Lane 1: insoluble proteins, lane 2: soluble extract [in the presence of 0.1% (w/v) dodecyl maltoside], lane 3: flow-through of the glutathione agarose column, lane 4: purified GST:ProDH1ΔN12.

observations strongly suggest that only DCPIP reduction can be attributed to ProDH activity and that PutA, the bi-functional ProDH/P5CDH from *E. coli*, was not expressed under our cultivation conditions or was not present in the soluble protein fraction. As expected, P5CR on the other hand seems to mediate both the oxidation of NADPH at pH 7.5 and the reduction of NAD^+ at pH 10. ProC, the P5CR of *E. coli*, was presumably present in all soluble protein extracts and conferred low rates of proline-dependent NAD^+ reduction, as well as P5C-dependent NADPH oxidation.

Purified Recombinant ProDH1 and ProDH2 Do Not Reduce NAD^+

Addition of 0.1% (w/v) dodecyl maltoside to the extraction buffer increased the DCPIP reduction activity in the soluble fraction of ProDH expressing *E. coli* cells and allowed binding of the recombinant proteins to glutathione agarose beads (**Figure 3** and **Supplementary Figure S1**). Proteins with the expected molecular weight of 80.3 kDa for GST:ProDH1ΔN12 and 78.0 kDa for GST:ProDH2ΔN13 were strongly enriched in the glutathione-eluted fraction together with additional smaller proteins. These smaller proteins were recognized by anti-GST antibodies (data not shown), and were different between GST:ProDH1 and GST:ProDH2 preparations, indicating that they are fragments of the recombinant fusion proteins. Overall, a large fraction of the proline-dependent DCPIP reduction activity was lost during the purification, but the specific activity was strongly increased. Neither proline-dependent NAD^+

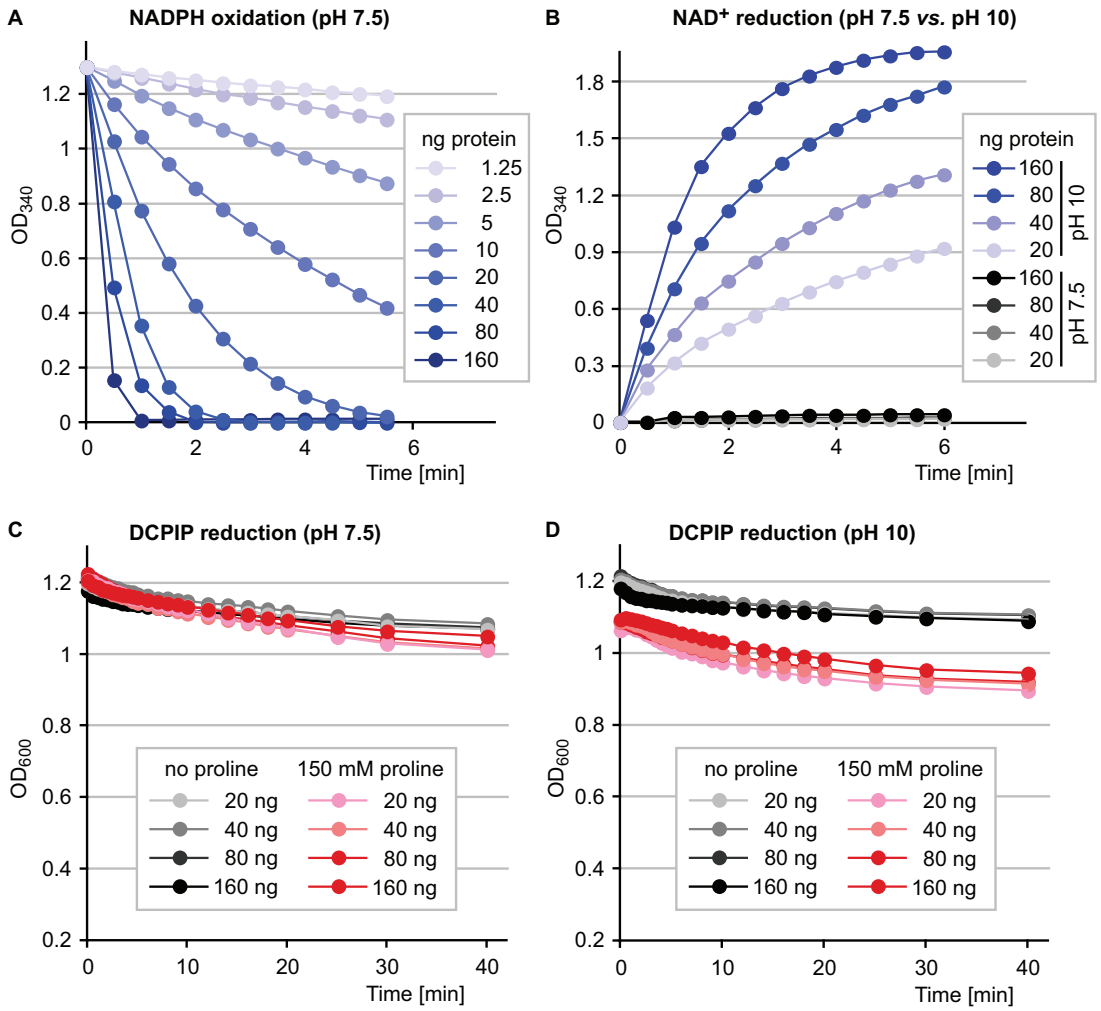

FIGURE 4 | Enzymatic activities of purified P5CR. 6xHis:P5CR was purified and its activity was analyzed photometrically under various conditions. **(A)** P5C-dependent oxidation of NADPH at pH 7.5, the physiological forward-reaction of P5CR, was followed over time with different amounts of enzyme in the assay. **(B)** Proline-dependent reduction of NAD^+, the reverse reaction of P5CR, was monitored at two different pH values and with different amounts of enzyme. **(C)** Reduction of 2,6-dichlorophenolindophenol (DCPIP) at pH 7.5 with various amounts of enzyme in the presence or absence of proline. **(D)** Reduction of DCPIP at pH 10 with various amounts of enzyme in the presence or absence of proline. All data are from single kinetic analyses. Very similar results were obtained with at least three independently purified enzyme preparations.

reduction at pH 10 nor P5C-dependent NADPH oxidation were consistently detected in the fractions containing the purified ProDHs.

Purified Recombinant P5CR Reduces NAD^+ at High pH, but Does Not Reduce DCPIP

We have shown previously, that recombinant Arabidopsis or rice P5CR can easily be purified to electrophoretic homogeneity after overexpression as 6xHis fusion proteins in *E. coli* (Giberti et al., 2014; Forlani et al., 2015b). Purified Arabidopsis P5CR showed rates of P5C-dependent oxidation of NADPH at pH 7.5 and of proline-dependent reduction of NAD^+ at pH 10 that were proportional to the amount of enzyme in the assay (**Figures 4A,B**). At physiological pH, however, P5CR did not mediate detectable proline-dependent NAD^+ reduction. Proline-dependent DCPIP reduction was not detected at either pH 7.5 or pH 10. Only a residual DCPIP reduction that was not proportional to the amount of enzyme was observed in both the presence and absence of proline in the assay (**Figures 4C,D**). Very similar results were obtained with purified recombinant P5CR from rice (data not shown).

Soluble Protein Extracts Contain P5CR but Not ProDH Activity

Having demonstrated with purified, recombinant plant proteins that only DCPIP reduction truly reflects ProDH activity, we analyzed the distribution of ProDH and P5CR activities in plant extracts. In soluble protein extracts of plants grown under normal conditions, proline-dependent

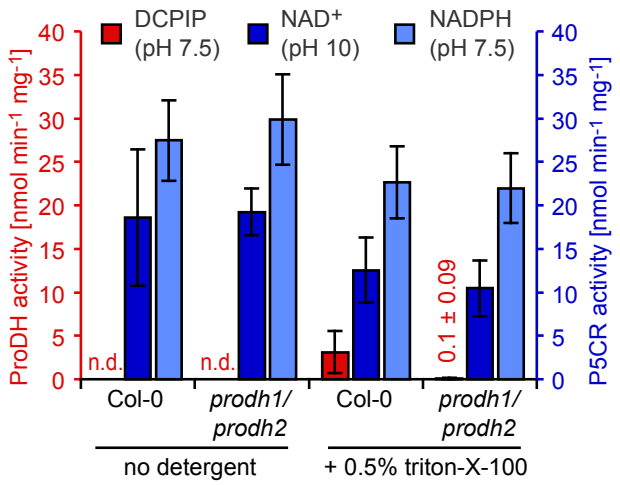

FIGURE 5 | ProDH and P5CR activity levels in Arabidopsis seedlings in response to dark-induced senescence. Twelve-day-old Arabidopsis seedlings grown on 0.5x Murashige and Skoog solid medium were transferred to water and darkness for 3 days to trigger senescence and *ProDH1* and *ProDH2* expression. Enzyme activities were measured in soluble protein extracts prepared with or without 0.5% (v/v) triton-X-100 from wildtype (Col-0) seedlings and *prodh1-4/prodh2-2* double mutants. ProDH activity (red bars) was calculated from the proline-dependent reduction of the artificial electron acceptor 2,6-dichlorophenolindophenol (DCPIP) at pH 7.5. P5CR activity (light blue bars) was measured through P5C-dependent oxidation of NADPH at pH 7.5. Reverse P5CR activity (blue bars) was detected based on proline-dependent NAD^+ reduction at pH 10. Data are means (±SD) of three independent biological replicates. n.d.: ProDH activity not detected.

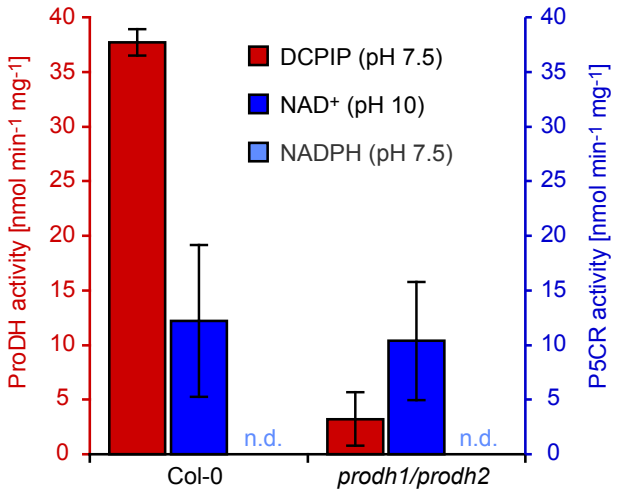

FIGURE 6 | ProDH and P5CR activities in isolated mitochondria. Crude mitochondrial fractions were prepared from Arabidopsis wildtype (Col-0) and *prodh1-4/prodh2-2* double mutant leaves after 5 days of dark treatment. Isolated mitochondria were assayed for proline-dependent 2,6-dichlorophenolindophenol (DCPIP) reduction at pH 7.5 (red columns) and proline-dependent NAD^+ reduction at pH 10 (blue columns). P5C-dependent NADPH oxidation at pH 7.5 was not detected (n.d.). Data are means (±SD) of three independent preparations of mitochondria.

reduction of DCPIP was not detected, whereas proline-dependent reduction of NAD^+ at pH 10 and P5C-dependent oxidation of NADPH at pH 7.5 were readily measured in extracts prepared with or without 0.5% (v/v) triton-X-100 (**Supplementary Figure S2**).

When Arabidopsis seedlings were placed for 3–5 days in darkness, a condition known to induce ProDH expression (Kovács et al., 2019; Launay et al., 2019), soluble protein extracts without detergent in the extraction buffer did not show proline-dependent DCPIP reduction at pH 7.5 (**Figure 5**). When the extraction buffer contained 0.5% (v/v) triton-X-100, a low rate of DCPIP reduction (3.1 nmol min^{-1} mg^{-1}) was detected in extracts from wildtype seedlings, but this activity was nearly undetectable in extracts from *prodh1-4/prodh2-2* double mutants. In contrast, proline-dependent NAD^+ reduction at pH 10 as well as P5C-dependent NADPH oxidation at pH 7.5 were detected at similar rates in extracts from wildtype plants and *prodh1-4/prodh2-2* double mutants. The specific activity of proline-dependent NAD^+ reduction at pH 10 decreased from 18.6 to 12.6 nmol min^{-1} mg^{-1} in extracts of wildtype seedlings when 0.5% (v/v) triton-X-100 was added to the extraction buffer, reflecting a higher total protein concentration in the triton-containing extracts. Very similar results were obtained with 0.1% (w/v) dodecyl maltoside in the extraction buffer and *prodh1-1/prodh2-1* double mutants (data not shown).

ProDH Activity Is Enriched in Isolated Mitochondria

When mitochondria were partially purified by differential centrifugation of extracts from detached mature leaves kept for 5 days in darkness to induce ProDH expression, proline-dependent DCPIP reduction was detected with specific activity of 37.7 nmol min^{-1} mg^{-1} in wildtype mitochondria, which was more than 10 times higher than in total protein extracts of dark-treated seedlings (**Figure 6**). When mitochondria were isolated from dark-treated leaves of a *prodh1-4/prodh2-2* double mutant line, the specific activity of proline-dependent DCPIP reduction was less than 10% of the activity in wildtype mitochondria. Proline-dependent NAD^+ reduction at pH 10 was detected with a rate of 12.2 nmol min^{-1} mg^{-1} and this activity was not significantly different between wildtype mitochondria and mitochondria isolated from leaves of *prodh1-4/prodh2-2* double mutants (10.4 nmol min^{-1} mg^{-1}). P5C-dependent NADPH oxidation at pH 7.5 was near or below the detection limit in isolated mitochondria, irrespective of the genotype of the seedlings.

DISCUSSION

By our detailed comparisons of extracts or purified mitochondria from wildtype plants and *prodh1/prodh2* double mutants, as well as recombinant enzymes expressed in *E. coli*, we demonstrate that both ProDH1 and ProDH2 from Arabidopsis catalyze the proline-dependent reduction of DCPIP in the presence of

FAD and phenazine methosulfate, but do not mediate proline-dependent NAD^+ reduction at pH 10.

When Arabidopsis ProDH1 and ProDH2 were expressed as GST fusion proteins in *E. coli*, expression of the mature proteins without the mitochondrial transit peptides slightly improved expression or solubility of the GST:ProDH fusion proteins, yielding higher specific DCPIP reduction activities in soluble extracts. Additionally, both the forward (P5C-dependent NADPH oxidation) and the reverse (proline-dependent NAD^+ reduction) activity of P5CR were detected in crude *E. coli* extracts (**Figure 2**). Because the latter two activities were detected at similar levels in extracts from bacteria harboring an empty vector, they are most likely mediated by ProC, the P5CR from *E. coli*. We did not notice any interference from PutA, the bi-functional ProDH/P5CDH from *E. coli*, in the activity assays. This was to be expected, because the expression of the *putA* gene is under catabolite repression in rich media, and additionally PutA represses its own transcription in the absence of external proline (Nakao et al., 1988). Purification of the GST:ProDH fusion proteins strongly increased the specific activity of proline-dependent DCPIP reduction, whereas the proline-dependent reduction of NAD^+ at pH 10 was depleted (**Figure 3** and **Supplementary Figure S1**). The specific activities of the purified GST:ProDH1ΔN12 and GST:ProDH2ΔN13 were similar to the activities reported recently for ProDH1ΔN39 and ProDH2ΔN29 expressed as fusion proteins with the maltose binding protein (Fabro et al., 2020).

Conversely, purified P5CRs did not reduce DCPIP, but mediated both proline-dependent NAD^+ reduction and P5C-dependent NADPH oxidation, depending on the pH of the assay mixture (**Figure 4**). The same picture was obtained with crude extracts from *E. coli* cells overexpressing Arabidopsis P5CR (**Figure 2**). Above pH 6.2, P5C dominates in the equilibrium between GSA and P5C (Bearne and Wolfenden, 1995) and in the physiological pH range, the energy of NAD(P)H oxidation drives the reaction catalyzed by P5CR mainly toward proline. At high pH values, the free energy favors the reaction toward P5C because three protons are released during the conversion of proline to P5C. A detailed characterization and discussion of the pH-dependence of the reaction catalyzed by P5CR can be found in Forlani and Funck (2020), where the authors demonstrate that at pH 10.5, the proline-dependent reduction of NAD^+ by purified P5CR can be used as a specific method for proline quantification.

As reported many times before, both P5C-dependent NADPH oxidation at pH 7.5 and proline-dependent NAD^+ reduction at pH 10 were readily detectable in crude plant protein extracts, irrespective of the use of mild detergents (**Figure 5** and **Supplementary Figure S2**). These activities were at the same level in *prodh1/prodh2* double mutants as in wildtype plants, demonstrating that they are not related to the native ProDH proteins. Because *P5CR* is an essential gene in Arabidopsis and homozygous mutants are aborted very early during embryo development, it is not possible to use *p5cr* mutants to confirm the origin of these activities (Funck et al., 2012). Detection of proline-dependent DCPIP reduction in crude plant extracts required both the use of a mild detergent in the extraction buffer and the induction of *ProDH1* or *ProDH2* expression (**Figure 5** and **Supplementary Figure S2**). Well-characterized experimental systems for the induction of *ProDH1* and *ProDH2* expression are feeding with external proline or induction of senescence and autophagy by exposure to prolonged periods of darkness (Cabassa-Hourton et al., 2016; Kovács et al., 2019; Launay et al., 2019). We chose dark-induced starvation as the more physiologically relevant treatment. After 3 days of dark induction, the specific activity of proline-dependent DCPIP reduction in extracts of wildtype seedlings was roughly one tenth of the specific P5CR forward or reverse activity. DCPIP reduction was nearly undetectable in extracts from *prodh1/prodh2* double mutants, confirming that this activity is mediated specifically by ProDHs. It has been noted previously that both the *prodh1-4* and the *prodh2-2* mutants contain low levels of native transcripts (Funck et al., 2010) that may explain the residual DCPIP reduction activity even though both ProDH1 and ProDH2 protein levels were below the detection limit of Western blotting (Launay et al., 2019).

Cell fractionation, GFP-tagging and immunodetection in electron micrographs showed that ProDHs are localized in mitochondria (Elthon and Stewart, 1981; Funck et al., 2010; Launay et al., 2019). In mitochondrial preparations from dark-induced wildtype plants, the specific rate of proline-dependent DCPIP reduction was more than three times higher than the proline-dependent reduction of NAD^+, whereas the latter activity was typically at least fourfold higher than DCPIP reduction in total protein extracts (**Figures 5**, **6**). Again, specifically the DCPIP reduction activity was lower in mitochondria isolated from *prodh1/prodh2* double mutants, confirming that ProDHs mediate this activity. In contrast, NAD^+ reduction was not affected and can therefore not be mediated by ProDHs. It was unexpected to detect proline-dependent NAD^+ reduction at pH 10 in isolated mitochondria, because analysis of plants expressing a P5CR:GFP fusion protein did not provide any evidence for mitochondrial import or association of P5CR in Arabidopsis (Funck et al., 2012). However, co-fractionation of P5CR activity with organelles, namely plastids, has been observed previously in other plant species (Rayapati et al., 1989; Szoke et al., 1992; Murahama et al., 2001). The exclusive detection of the reverse activity of P5CR in isolated mitochondria could be explained by a high content of P5CDH, which is also a mitochondrial enzyme in Arabidopsis (Deuschle et al., 2001). An excess of P5CDH will compete with P5CR for P5C and since P5CDH accepts both NAD^+ or $NADP^+$ as electron acceptor, any $NADP^+$ formed by P5CR would be instantly re-reduced by P5CDH (Forlani et al., 1997).

We are aware that numerous previous publications have assigned proline-dependent NAD^+ reduction at pH 9 or higher in plant extracts or recombinant proteins to ProDH. Our data clearly demonstrate that the conclusions based on this erroneous assignment may be at least partially wrong or misleading. It is beyond the scope of this article to try to provide a comprehensive list of these publications or to provide a detailed discussion of previous conclusions that may no longer be valid. However, we urge all researchers in the field of proline metabolism to be aware of this pitfall and help to ensure, both in their roles as researchers

and as reviewers, that only suitable enzyme assays will be applied in future studies.

DATA AVAILABILITY STATEMENT

The raw data supporting the conclusions of this article will be made available by the authors, without undue reservation, to any qualified researcher.

AUTHOR CONTRIBUTIONS

DF initiated the study, performed assays with recombinant ProDH and plant protein extracts, and drafted the manuscript. GF performed the assays with recombinant P5CR. SL, CC-H, and AS performed the experiments with plant extracts and isolated mitochondria. All authors contributed to the data evaluation and the final manuscript.

FUNDING

This work was supported by the Sorbonne Université, CNRS, the University of Konstanz, and the University of Ferrara (FAR 2020).

ACKNOWLEDGMENTS

We would like to thank Roswitha Miller for technical assistance with protein expression and activity assays. Further thanks to Régine Lebrun and Brigitte Meunier-Gontero from the proteomic platform from the Mediterranean Institute of Microbiology of the Aix Marseille University for the determination of the transit peptide of ProDH1 by N-terminal Edman degradation.

SUPPLEMENTARY MATERIAL

The Supplementary Material for this article can be found online at: https://www.frontiersin.org/articles/10.3389/fpls.2020.602939/full#supplementary-material

Supplementary Figure 1 | Specific activity of purified recombinant GST:ProDH2ΔN13. Crude protein extract of bacteria overexpressing GST:ProDH2ΔN13 and affinity-purified GST:ProDH2ΔN13 (indicated by an arrowhead, calculated molecular weight is 78.0 kDa) were assayed for proline-dependent 2,6-dichlorophenolindophenol (DCPIP) reduction (red columns) and P5C-dependent NADPH oxidation at pH 7.5 (light blue columns), as well as for proline-dependent NAD^+ reduction at pH 10 (dark blue columns). Note that the scales of the two *y*-axes are in an opposite ratio than in **Figure 2**. Data are the average (±SD) of technical triplicates. Two further, independent protein preparations gave very similar results; n.d., not detected. The inset shows a Coomassie-stained, denaturing protein gel of the assayed fractions. Lane 1: soluble extract [in the presence of 0.1% (w/v) dodecyl maltoside], lane 2: flow-through of the glutathione agarose column, lane 3: purified GST:ProDH2ΔN13.

Supplementary Figure 2 | ProDH and P5CR activities in Arabidopsis seedlings. Twelve-days-old Arabidopsis wildtype (Col-0) seedlings grown on 0.5x Murashige and Skoog solid medium were used to prepare soluble protein extracts either with or without 0.5% triton-X-100. ProDH activity, assayed as proline-dependent reduction of 2,6-dichlorophenolindophenol (DCPIP) at pH 7.5, was not detected (n.d.). P5CR activity (light blue bars) was measured as P5C-dependent oxidation of NADPH at pH 7.5. Reverse P5CR activity (blue bars) was detected as proline-dependent NAD^+ reduction at pH 10. Data are means (±SD) of three independent batches of seedlings.

Supplementary Table 1 | Primers used for cloning of ProDH expression constructs.

REFERENCES

AbdElgawad, H., De Vos, D., Zinta, G., Domagalska, M. A., Beemster, G. T., and Asard, H. (2015). Grassland species differentially regulate proline concentrations under future climate conditions: an integrated biochemical and modelling approach. *New Phytol.* 208, 354–369. doi: 10.1111/nph.13481

Basford, R. E., and Huennekens, F. M. (1955). Studies on Thiols. I. Oxidation of Thiol groups by 2, 6-Dichlorophenol Indophenol1. *J. Am. Chem. Soc.* 77, 3873–3877. doi: 10.1021/ja01619a058

Bearne, S. L., and Wolfenden, R. (1995). Glutamate γ-semialdehyde as a natural transition state analogue inhibitor of *Escherichia coli* glucosamine-6-phosphate synthase. *Biochemistry* 34, 11515–11520. doi: 10.1021/bi00036a026

Bradford, M. M. (1976). A rapid and sensitive method for the quantitation of microgram quantities of protein utilizing the principle of protein-dye binding. *Anal. Biochem.* 72, 248–254. doi: 10.1006/abio.1976.9999

Cabassa-Hourton, C., Schertl, P., Bordenave-Jacquemin, M., Saadallah, K., Guivarc'h, A., Lebreton, S., et al. (2016). Proteomic and functional analysis of proline dehydrogenase 1 link proline catabolism to mitochondrial electron transport in *Arabidopsis thaliana*. *Biochem. J.* 473, 2623–2634. doi: 10.1042/bcj20160314

Dellero, Y., Heuillet, M., Marnet, N., Bellvert, F., Millard, P., and Bouchereau, A. (2020). Sink/source balance of leaves influences amino acid pools and their associated metabolic fluxes in winter oilseed rape (*Brassica napus* L.). *Metabolites* 10:150. doi: 10.3390/metabo10040150

Deuschle, K., Funck, D., Hellmann, H., Däschner, K., Binder, S., and Frommer, W. B. (2001). A nuclear gene encoding mitochondrial Δ^1-pyrroline-5-carboxylate dehydrogenase and its potential role in protection from proline toxicity. *Plant J.* 27, 345–356. doi: 10.1046/j.1365-313X.2001.01101.x

El Moukhtari, A., Cabassa-Hourton, C., Farissi, M., and Savouré, A. (2020). How does proline treatment promote salt stress tolerance during crop plant development? *Front. Plant Sci.* 11:1127. doi: 10.3389/fpls.2020.01127

Elthon, T. E., and Stewart, C. R. (1981). Submitochondrial location and electron transport characteristics of enzymes involved in proline oxidation. *Plant Physiol.* 67, 780–784. doi: 10.1104/pp.67.4.780

Elthon, T. E., and Stewart, C. R. (1982). Proline oxidation in corn mitochondria : involvement of NAD, relationship to ornithine metabolism, and sidedness on the inner membrane. *Plant Physiol.* 70, 567–572. doi: 10.1104/pp.70.2.567

Fabro, G., Cislaghi, A. P., Condat, F., Deza Borau, G., and Alvarez, M. E. (2020). The N-terminal domain of *Arabidopsis* proline dehydrogenase affects enzymatic activity and protein oligomerization. *Plant Physiol. Biochem.* 154, 268–276. doi: 10.1016/j.plaphy.2020.04.019

Forlani, G., Bertazzini, M., Zarattini, M., and Funck, D. (2015a). Functional characterization and expression analysis of rice δ^1-pyrroline-5-carboxylate dehydrogenase provide new insight into the regulation of proline and arginine catabolism. *Front. Plant Sci.* 6:591. doi: 10.3389/fpls.2015.00591

Forlani, G., Bertazzini, M., Zarattini, M., Funck, D., Ruszkowski, M., and Nocek, B. (2015b). Functional properties and structural characterization of rice δ^1-pyrroline-5-carboxylate reductase. *Front. Plant Sci.* 6:565. doi: 10.3389/fpls.2015.00565

Forlani, G., and Funck, D. (2020). A specific and sensitive enzymatic assay for the quantitation of L-proline. *Front. Plant Sci.* 11:582026. doi: 10.3389/fpls.2020.582026

Forlani, G., Giberti, S., Berlicki, L., Petrollino, D., and Kafarski, P. (2007). Plant P5C reductase as a new target for aminomethylenebisphosphonates. *J. Agric. Food Chem.* 55, 4340–4347. doi: 10.1021/jf0701032

Forlani, G., Scainelli, D., and Nielsen, E. (1997). Δ^1-Pyrroline-5-carboxylate dehydrogenase from cultured cells of potato (Purification and properties). *Plant Physiol.* 113, 1413–1418. doi: 10.1104/pp.113.4.1413

Forlani, G., Trovato, M., Funck, D., and Signorelli, S. (2019). "Regulation of proline accumulation and its molecular and physiological functions in stress defence," in *Osmoprotectant-Mediated Abiotic Stress Tolerance in Plants*, eds M. A. Hossain, V. Kumar, D. Burritt, M. Fujita, and P. Mäkelä (Cham: Springer International Publishing), doi: 10.1007/978-3-030-27423-8

Funck, D., Eckard, S., and Müller, G. (2010). Non-redundant functions of two proline dehydrogenase isoforms in *Arabidopsis*. *BMC Plant Biol.* 10:70. doi: 10.1186/1471-2229-10-70

Funck, D., Winter, G., Baumgarten, L., and Forlani, G. (2012). Requirement of proline synthesis during *Arabidopsis* reproductive development. *BMC Plant Biol.* 12:191. doi: 10.1186/1471-2229-12-191

Giberti, S., Funck, D., and Forlani, G. (2014). Δ^1-Pyrroline-5-carboxylate reductase from *Arabidopsis thaliana*: stimulation or inhibition by chloride ions and feedback regulation by proline depend on whether NADPH or NADH acts as co-substrate. *New Phytol.* 202, 911–919. doi: 10.1111/nph.12701

Hildebrandt, T. M. (2018). Synthesis versus degradation: directions of amino acid metabolism during *Arabidopsis* abiotic stress response. *Plant Mol. Biol.* 98, 121–135. doi: 10.1007/s11103-018-0767-0

Huang, A. H. C., and Cavalieri, A. J. (1979). Proline oxidase and water stress-induced proline accumulation in spinach leaves. *Plant Physiol.* 63, 531–535. doi: 10.1104/pp.63.3.531

Kleinboelting, N., Huep, G., Kloetgen, A., Viehoever, P., and Weisshaar, B. (2012). GABI-Kat SimpleSearch: new features of the *Arabidopsis thaliana* T-DNA mutant database. *Nucleic Acids Res.* 40, D1211–D1215. doi: 10.1093/nar/gkr1047

Kovács, H., Aleksza, D., Baba, A. I., Hajdu, A., Király, A. M., Zsigmond, L., et al. (2019). Light control of salt-induced proline accumulation is mediated by ELONGATED HYPOCOTYL 5 in *Arabidopsis*. *Front. Plant Sci.* 10:1584. doi: 10.3389/fpls.2019.01584

Krueger, R., Jäger, H.-J., Hintz, M., and Pahlich, E. (1986). Purification to homogeneity of pyrroline-5-carboxylate reductase of barley. *Plant Physiol.* 80, 142–144. doi: 10.1104/pp.80.1.142

Launay, A., Cabassa-Hourton, C., Eubel, H., Maldiney, R., Guivarc'h, A., Crilat, E., et al. (2019). Proline oxidation fuels mitochondrial respiration during dark-induced leaf senescence in *Arabidopsis thaliana*. *J. Exp. Bot.* 70, 6203–6214. doi: 10.1093/jxb/erz351

Lowry, O. H., Rosebrough, N. J., Farr, A. L., and Randall, R. J. (1951). Protein measurement with the folin phenol reagent. *J. Biol. Chem.* 193, 265–275.

Mazelis, M., and Creveling, R. K. (1974). L-proline dehydrogenase of *Triticum vulgare* germ: purification, properties and cofactor interactions. *Phytochemistry* 13, 559–565. doi: 10.1016/S0031-9422(00)91353-0

McNamer, A. D., and Stewart, C. R. (1974). Nicotinamide adenine dinucleotide-dependent proline dehydrogenase in *Chlorella*. *Plant Physiol.* 53, 440–444. doi: 10.1104/pp.53.3.440

Meng, Z., Lou, Z., Liu, Z., Li, M., Zhao, X., Bartlam, M., et al. (2006). Crystal structure of human pyrroline-5-carboxylate reductase. *J. Mol. Biol.* 359, 1364–1377. doi: 10.1016/j.jmb.2006.04.053

Murahama, M., Yoshida, T., Hayashi, F., Ichino, T., Sanada, Y., and Wada, K. (2001). Purification and characterization of Δ^1-pyrroline-5-carboxylate reductase isoenzymes, indicating differential distribution in Spinach (*Spinacia oleracea* L.) leaves. *Plant Cell Physiol.* 42, 742–750. doi: 10.1093/pcp/pce093

Nakao, T., Yamato, I., and Anraku, Y. (1988). Mapping of the multiple regulatory sites for *putP* and *putA* expression in the *putC* region of *Escherichia coli*. *Mol. Gen. Genet.* 214, 379–388. doi: 10.1007/BF00330470

Nocek, B., Chang, C., Li, H., Lezondra, L., Holzle, D., Collart, F., et al. (2005). Crystal structures of Δ^1-pyrroline-5-carboxylate reductase from human pathogens *Neisseria meningitides* and *Streptococcus pyogenes*. *J. Mol. Biol.* 354, 91–106. doi: 10.1016/j.jmb.2005.08.036

Per, T. S., Khan, N. A., Reddy, P. S., Masood, A., Hasanuzzaman, M., Khan, M. I. R., et al. (2017). Approaches in modulating proline metabolism in plants for salt and drought stress tolerance: phytohormones, mineral nutrients and transgenics. *Plant Physiol. Biochem.* 115, 126–140. doi: 10.1016/j.plaphy.2017.03.018

Rayapati, P. J., and Stewart, C. R. (1991). Solubilization of a proline dehydrogenase from maize (*Zea mays* L.) mitochondria. *Plant Physiol.* 95, 787–791. doi: 10.1104/pp.95.3.787

Rayapati, P. J., Stewart, C. R., and Hack, E. (1989). Pyrroline-5-carboxylate reductase is in pea (*Pisum sativum* L.) leaf chloroplasts. *Plant Physiol.* 91, 581–586. doi: 10.1104/pp.91.2.581

Rena, A. B., and Splittstoesser, W. E. (1975). Proline dehydrogenase and pyrroline-5-carboxylate reductase from pumpkin cotyledons. *Phytochemistry* 14, 657–661. doi: 10.1016/0031-9422(75)83010-X

Schertl, P., Cabassa, C., Saadallah, K., Bordenave, M., Savoure, A., and Braun, H. P. (2014). Biochemical characterization of proline dehydrogenase in *Arabidopsis* mitochondria. *FEBS J.* 281, 2794–2804. doi: 10.1111/febs.12821

Servet, C., Ghelis, T., Richard, L., Zilberstein, A., and Savoure, A. (2012). Proline dehydrogenase: a key enzyme in controlling cellular homeostasis. *Front. Biosci. (Landmark Ed.)* 17:607–620. doi: 10.2741/3947

Singh, H., Arentson, B. W., Becker, D. F., and Tanner, J. J. (2014). Structures of the PutA peripheral membrane flavoenzyme reveal a dynamic substrate-channeling tunnel and the quinone-binding site. *Proc. Natl. Acad. Sci. U.S.A.* 111, 3389–3394. doi: 10.1073/pnas.1321621111

Szabados, L., and Savoure, A. (2010). Proline: a multifunctional amino acid. *Trends Plant Sci.* 15, 89–97. doi: 10.1016/j.tplants.2009.11.009

Szoke, A., Miao, G. H., Hong, Z., and Verma, D. P. (1992). Subcellular location of δ^1-pyrroline-5-carboxylate reductase in root/nodule and leaf of soybean. *Plant Physiol.* 99, 1642–1649. doi: 10.1104/pp.99.4.1642

Tallarita, E., Pollegioni, L., Servi, S., and Molla, G. (2012). Expression in *Escherichia coli* of the catalytic domain of human proline oxidase. *Protein Expr. Purif.* 82, 345–351. doi: 10.1016/j.pep.2012.01.021

Tanner, J. J. (2019). Structural biology of proline catabolic enzymes. *Antioxid. Redox Signal.* 30, 650–673. doi: 10.1089/ars.2017.7374

Trovato, M., Forlani, G., Signorelli, S., and Funck, D. (2019). "Proline metabolism and its functions in development and stress tolerance," in *Osmoprotectant-Mediated Abiotic Stress Tolerance in Plants*, eds M. A. Hossain, V. Kumar, D. Burritt, M. Fujita, and P. Mäkelä (Cham: Springer International Publishing), doi: 10.1007/978-3-030-27423-8

Wanduragala, S., Sanyal, N., Liang, X., and Becker, D. F. (2010). Purification and characterization of Put1p from *Saccharomyces cerevisiae*. *Arch. Biochem. Biophys.* 498, 136–142. doi: 10.1016/j.abb.2010.04.020

Conflict of Interest: The authors declare that the research was conducted in the absence of any commercial or financial relationships that could be construed as a potential conflict of interest.

Copyright © 2020 Lebreton, Cabassa-Hourton, Savouré, Funck and Forlani. This is an open-access article distributed under the terms of the Creative Commons Attribution License (CC BY). The use, distribution or reproduction in other forums is permitted, provided the original author(s) and the copyright owner(s) are credited and that the original publication in this journal is cited, in accordance with accepted academic practice. No use, distribution or reproduction is permitted which does not comply with these terms.

frontiers in Plant Science

ORIGINAL RESEARCH
published: 07 January 2021
doi: 10.3389/fpls.2020.581234

Physiological, Nutritional and Metabolomic Responses of Tomato Plants After the Foliar Application of Amino Acids Aspartic Acid, Glutamic Acid and Alanine

*Marina Alfosea-Simón[1], Silvia Simón-Grao[1,2], Ernesto Alejandro Zavala-Gonzalez[3], Jose Maria Cámara-Zapata[1], Inmaculada Simón[1], Juan José Martínez-Nicolás[1], Vicente Lidón[1] and Francisco García-Sánchez[2]**

[1] Escuela Politécnica Superior de Orihuela, Universidad Miguel Hernández, Orihuela, Spain, [2] Centro de Edafología y Biología Aplicada del Segura, Consejo Superior de Investigaciones Científicas, Murcia, Spain, [3] Investigador Asociado al Departamento I+D Atlantica Agricola, Villena, Spain

OPEN ACCESS

Edited by:
Sakiko Okumoto,
Texas A&M University, United States

Reviewed by:
Guillaume Pilot,
Virginia Tech, United States
Luigi Lucini,
Catholic University of the Sacred Heart, Italy
Hiroshi Ezura,
University of Tsukuba, Japan

***Correspondence:**
Francisco García-Sánchez
fgs@cebas.csic.es

Specialty section:
This article was submitted to Plant Physiology, a section of the journal Frontiers in Plant Science

Received: 08 July 2020
Accepted: 07 December 2020
Published: 07 January 2021

Citation:
Alfosea-Simón M, Simón-Grao S, Zavala-Gonzalez EA, Cámara-Zapata JM, Simón I, Martínez-Nicolás JJ, Lidón V and García-Sánchez F (2021) Physiological, Nutritional and Metabolomic Responses of Tomato Plants After the Foliar Application of Amino Acids Aspartic Acid, Glutamic Acid and Alanine. Front. Plant Sci. 11:581234. doi: 10.3389/fpls.2020.581234

Agriculture is facing a great number of different pressures due to the increase in population and the greater amount of food it demands, the environmental impact due to the excessive use of conventional fertilizers, and climate change, which subjects the crops to extreme environmental conditions. One of the solutions to these problems could be the use of biostimulant products that are rich in amino acids (AAs), which substitute and/or complement conventional fertilizers and help plants adapt to climate change. To formulate these products, it is first necessary to understand the role of the application of AAs (individually or as a mixture) in the physiological and metabolic processes of crops. For this, research was conducted to assess the effects of the application of different amino acids (Aspartic acid (Asp), Glutamic acid (Glu), L-Alanine (Ala) and their mixtures Asp + Glu and Asp + Glu + Ala on tomato seedlings (*Solanum lycopersicum* L.). To understand the effect of these treatments, morphological, physiological, ionomic and metabolomic studies were performed. The results showed that the application of Asp + Glu increased the growth of the plants, while those plants that received Ala had a decreased dry biomass of the shoots. The greatest increase in the growth of the plants with Asp + Glu was related with the increase in the net CO_2 assimilation, the increase of proline, isoleucine and glucose with respect to the rest of the treatments. These data allow us to conclude that there is a synergistic effect between Aspartic acid and Glutamic acid, and the amino acid Alanine produces phytotoxicity when applied at 15 mM. The application of this amino acid altered the synthesis of proline and the pentose-phosphate route, and increased GABA and trigonelline.

Keywords: metabolites, nutrients, minerals, gas exchange parameters, ^{1}H-NMR, organic acids, sugars

INTRODUCTION

The tomato (*Solanum lycopersicum* L.) is one of the most-consumed and demanded crops worldwide due to its great nutritional and antioxidant properties. This high demand makes it one of the most important crops at the social and economic levels. In agreement with the statistics from the Food and Agriculture Organization [FAO] (2020), more than 180 million tons of tomato have been grown in the past year worldwide, of which 24 million come from Europe. Spain is the second-most important producer in Europe, with an approximate production of 5 million tons per year.

Due to the increase in the world's population since the industrial revolution, the performance of the crops has had to increase fast and exponentially to provide and answer to the demand for food; however, in the past few years, the production and quality of the harvest of various crops, among which we find tomatoes, have been greatly affected as a result of climate change. The high temperatures and periods of drought, which have become more intense and prolonged, have affected crop production (Wallace et al., 2003; Parry, 2019; Mutale-Joan et al., 2020). Aside from the challenge faced by agriculture for increasing production in an era of climate change, we also find another important challenge, such as the practice of sustainable agriculture that affects the environment the least. Thus, at present, new agronomic strategies are being designed and evaluated, which could help take on these challenges, starting with the acquisition of basic scientific knowledge about the physiological and metabolic processes of crops. As an alternative to conventional agronomic strategies, such as the application of synthetic inorganic fertilizers, which could have damaging effects on the environment, other more ecological alternatives are being adopted (Foley et al., 2011; Tilman et al., 2002; Mutale-Joan et al., 2020). Among these new agronomic strategies, we find the use of biostimulants (Lucini et al., 2015). It has been observed that the use of these products significantly improves the performance of crops, as they have beneficial effects on the physiological processes of plants, such as the absorption of water and nutrients, among others (Mutale-Joan et al., 2020).

Biostimulants are composed of bioactive compounds such as humic acids, hydrolyzed proteins, seaweed and microorganism extracts, among others (Rouphael et al., 2018). The hydrolyzed proteins and seaweed extracts are a rich source of amino acids, and these compounds tend to be added freely to enrich the biostimulant products, as they have very beneficial effects on the crops due to their role in the synthesis of proteins, vitamins, nucleotides and alkaloids, aside from having effects as elicitors (Khan et al., 2019). Some of the most important effects described in the past few years are: (i) they palliate the negative impact of certain environmental stresses such as drought (L-methionine in bitter gourd, *Momordica charantia* L.; Akram et al., 2020), salinity (mixture of amino acids in tomato plants; Tantawy et al., 2009), Cd toxicity (Glutamate in rice; Jiang et al., 2020), (ii) they induce hormonal responses and improve the absorption of nitrogen (mixture of amino acids and polypeptides in tomato, corn and peas; Colla et al., 2014), (iii) they regulate the antioxidant metabolism (Glutamate, Cysteine, Phenylalanine, Glycine in soy Teixeira et al., 2017).

Despite the fact that as of today no doubts exist about the positive effects of the application of amino acids, as mentioned above, little is known about the role played by each of these amino acids on the physiological and metabolic processes of plants. On many occasions, the biostimulant products are formulated from the chemical hydrolysis of raw materials rich in amino acids (residues from the agro-food industry), but there is a lack of knowledge on their amino acid profile or what specific function they play in crops. Also, the application of biostimulant products rich in amino acids can vary depending on the species, cultivar, climate, dose used, origin and application time (Parađiković et al., 2019). Therefore, to create highly efficient biostimulant products, it is indispensable to understand what role the different amino acids play on the physiological and metabolic processes of crops, and the possible antagonistic, neutral and synergistic effects between them.

Amino acids such as Glutamic acid, Aspartic acid and Alanine are three of the amino acids used in the formulation of biostimulant products (Colla et al., 2015). These are added in their free form or as part of the raw materials from hydrolyzed proteins. **Glutamic acid** is important in the metabolism of nitrogen, as it intervenes in the assimilation of nitrogen in plants and in the reactions of amino transferases (Lea and Ireland, 1999; Cao et al., 2010). This amino acid, aside from its intrinsic value as an amino acid itself, is the precursor of other amino acids such as Aspartic acid, Serine, Alanine, Lysine and Proline, among others. **Alanine** is synthesized from Glutamic acid, and its transamination with oxoglutarate produces glutamate and pyruvate, a reversible reaction, granting this amino acid a dual function between carbon and nitrogen metabolism (Kendziorek et al., 2012). Lastly, this amino acid is linked with the synthesis of chlorophylls and photosynthetic activity (Sánchez-Pale, 2017). **Aspartic acid** is obtained from a transamination reaction between glutamate and oxaloacetate in plants, and is metabolized to produce the amino acids lysine, threonine, methionine, and isoleucine, in a series of reactions known as the Aspartic acid metabolic pathway. The application of these three amino acids to plants helps them to endure adverse environmental conditions such as drought, salinity and heavy metal toxicity (Rai, 2002). However, up to the present, the effects of the individual application of these amino acids on the physiology and the primary metabolism of plants, or the antagonistic or synergistic effects that could result from the mixture of amino acids, are unknown. This knowledge could be essential when designing biostimulants that contain amino acids, or even when selecting the raw materials for which the profile of amino acids is better adapted to the requirements of a specific crop. For this, the objectives of the study were to understand the effects of the application of the amino acids Glutamic acid, Aspartic acid and Alanine, applied individually or as a mixture, on the physiological and metabolic processes, and the nutritional state of tomato plants of the 'Optima' variety; and to discover if these changes stimulate the vegetative growth of the plants. To characterize the metabolic state of the plants, the ^{1}H-NMR omics technique was utilized, as it

allows analyzing a great quantity of primary metabolites in a fast and simple manner.

MATERIALS AND METHODS

Growth Conditions and Plant Material

The experiment was performed on tomato plants (*Solanum lycopersicum* L.) of the 'Optima' variety, obtained from a commercial seedling nursery (Babyplant S.L., Santomera, Murcia, Spain), and planted in a tunnel greenhouse in an experimental field from the CEBAS-CSIC, located in the municipality of Santomera (18 Km from Murcia, Spain). The climatic conditions in the interior of the greenhouse were: temperature day/nigh 32/19 ± 3°C, photosynthetically active radiation (PAR) of 1000 μmol m^{-2} s^{-1}, relative humidity of 52/80 ± 5% and a 15 h photoperiod.

The tomato seedlings, selected according to height and the number of completely developed true leaves, were transplanted to 3.5 L pots with a fine-grained "Universal" substrate, free of pathogens and weed seeds, composed of yellow and black peat, coconut fiber and perlite, in a ratio of 5:4:1 (Projar professional, 2018, Spain) The irrigation was applied through of dripper system of rate of 4 L h^{-1}.

With regards to fertigation management, Hoagland's nutrient solution, composed of KNO_3 (27 g 100 L^{-1}), $Ca(NO_3)_2$ (42 g 100 L^{-1}), KH_2PO_4 (7 g 100 L^{-1}), $MgSO_4$ (13 g 100 L^{-1}), Fe-EDTA (1 g 100 L^{-1}), and micronutrients (1 g 100 L^{-1}; Hidromix S, Valagro) was used in the irrigation. During the first week after the transplantation, plants were irrigated with 50% Hoagland solution one minute per day. After this week, plants were irrigated with 100% Hoagland solution two times per day, 5 min during the morning and 5 min during the afternoon. The tap water utilized for the preparation of the nutrient solution came from Tajo-Segura water transfer, with an electrical conductivity (EC) of 0.9 dS m^{-1} and pH of 8.2. When drainage in every irrigation event was less than 15% irrigation time was increased.

Amino Acids Utilized and Preparation

The AAs utilized for the assays were Glutamic acid (Glu), Aspartic acid (Asp) and Alanine (L-Ala) from Caldic Ibérica (Barcelona, Spain). The selection of these three AAs and its doses was made according to previous experiments within the framework of project RTC-2016-4568-2 carried out at the CEBAS-CSIC. The aim of this project was to study every one of the 22 amino acids in different doses and mixtures in tomato plants. For each individual amino acid, a stock solution was first prepared with a final concentration of 7%. For this, 7 g of each amino acid were added to 100 mL of ultrapure water; in the case of Glutamic acid and Aspartic acid, drops of 50% KOH were added to facilitate their dilution in water. After the preparation of the individual AAs (7%), the following treatments were prepared: 15 mM Aspartic acid (Asp), 15 mM Glutamic acid (Glu), 15 mM Alanine (Ala), 15 mM Aspartic acid + 15 mM Glutamic acid (Asp + Glu) and 15 mM Aspartic acid + 15 mM Glutamic acid + 15 mM Alanine (Asp + Glu + Ala). For each formulation, before their application, Tween-20 was added to a concentration of 0.1% (a surfactant compound that improves the adherence of the formulation to the leaves), and the pH was adjusted to be 5.5 to 6.5. Therefore, the treatments applied were: (1) Control treatment (without AAs, in which only ultrapure water was pulverized on the tomato plants); and treatments with the foliar application of the amino acids: (2) Asp, (3) Glu, (4) L-Ala, (5) Asp + Glu, and (6) Asp + Glu + L-Ala. For each of the treatments, the concentrations of the equivalent nitrogen (mg L^{-1}) were: Asp 0.22, Glu 0.20, L-Ala 0.33, Asp + Glu 0.42, and Asp + Glu + L-Ala 0.75.

Application of the Treatments

The application of the treatments was performed foliarly, and was done after two weeks of acclimation of the tomato plants. Each treatment was pulverized on the aerial part of the plants, so that the greatest foliar area was covered with the preparation. Within the greenhouse, the plants were divided into four blocks, and within each block, the treatments were applied to four plants, which were considered as an experimental unit.

Gas Exchange Parameters

After a week of treatment the following parameters were measured: the net CO_2 assimilation rate (A_{CO2}), stomatal conductance (g_s), the water use efficiency (WUE = A_{CO2}/E_{leaf}, where E_{leaf} corresponds to the value of leaf transpiration obtained in each measurement), and the Ci/Ca ratio (where Ci corresponds to the substomatal CO_2 and Ca corresponds to external CO_2). These parameters were measured in two plants per treatment and block, in leaves that were completely developed and healthy, in the morning (8:30am - 11:00am, using a portable gas analyzer for the measurement of gas exchange parameters (PP System Ciras2, United Kingdom). During the measurements, the equipment was configured to maintain constant light (PAR: 1200 mmol m^{-2} s^{-1}) and CO_2 concentration (400 ppm) in the measurement chamber.

Chlorophyll Fluorescence and Concentration Parameters

The chlorophyll fluorescence parameters were measured in the same plants utilized for the gas exchange measurements, utilizing a portable pulse-modulated fluorometer FMS-2 (Hansatech Instruments Ltd., United Kingdom). The chlorophyll fluorescence parameters measured were: the quantum efficiency of PSII, (ΦPSII = $(F_m'-F_s)/F_m'$; the antennae efficiency of PSII, F_v'/F_m' = $(F_m'-F_0')/F_m'$; and the photochemical quenching co-efficient, qP = $(F_m'-F_s)/(F_m'-F_0')$, where F_s is the steady-state fluorescence yield, F_m' is the maximal value when all reaction centers are closed after a pulse of saturating light (12,000 μmol m^{-2} s^{-1} for 0.8 s), and F_0' is the minimal fluorescence in the light-adapted state that is obtained by turning off the actinic light temporarily and applying a pulse of far-red light (735 nm) to drain the electrons from PSII. The chlorophylls were also measured with a portable meter CL-01 (SPAD units- Hansatech).

Growth Parameters

After the gas exchange and chlorophyll fluorescence measurements, the following measurements were taken: height and diameter of the stem at three different points in all

the plants. Also, the number of flowers of each plant and the percent of open flowers, after which the plants were harvested. In this sampling, the shoots of the plants were measured with a precision Sartorius scale (Acculab), after which they were dried in an oven at 60°C for at least 48 h (g dw shoot). From the shoots, eight leaflets were collected from each plant, which were washed with de-ionized water; four of them were dry-processed for the nutritional study, and the other four were processed fresh for the metabolomics study. The leaflets samples were taken from leaves that were completely developed, located mid-height of the plant.

Determination of the Mineral Nutrients Concentration in Leaf Tissue

For the nutritional study, the previously dried and ground samples were analyzed. The concentration of Na, K, Mg, Ca, P, S, Fe, Cu, Mn, Zn and B was analyzed with inductively coupled plasma spectrometry (Iris Intrepid II, Thermo Electron Corporation, Franklin, United States), after digestion with HNO_3:H_2O_2 (5:3 by volume), utilizing a microwave (CERM Mars Xpress, North Carolina, United States) with a temperature ramp that reached 200°C in 20 min, and maintaining this temperature for 2 h. The total N and C was measured with a C/N elemental analyzer Thermo Finnigan (Milan, Italy).

Metabolic Analysis of Leaf Tissue

A "non-targeted" metabolic analysis was conducted in the fresh leaf samples. These samples were ground with liquid nitrogen with a mortar and pestle and lyophilized. Afterwards, the samples were prepared for analysis according with the protocol by Van der Sar et al. (2013). For this analysis, a Nuclear Magnetic Resonance (NMR) system coupled to a 500 MHz Bruker spectrometer (Bruker Biospin, Rheinstetten, Germany) equipped with a broadband 5 mm N_2 CryoProbe Prodigy BBO. All the tomato leaf extracts were measured at 300.1 ± 0.1 K without rotation and with 4 test scans before the 32 scans performed for the experiment.

The acquisition parameters were set in the following manner: the size of the FID = 64K, spectral band = 12.4345 ppm, receiver gain = 28.5, acquisition time = 2.18 s, relaxation delay = 2s, and line broadening = 0.50 Hz. The acquisition of data was performed through the NOESY pulse sequence of pre-saturation (Bruker 1D, noesypr1d) with water suppression through the irradiation of the water frequency during the recycling and mixing times. In the procession of the samples and for each spectrum separately, a reduction of noise is produced, based on the deconvolution of the multi-level signal. Afterwards, a correction is performed of the baseline, and to complete the process, an interpolation technique of the areas of the signal is utilized.

All of this provides us with a "fingerprint" of the sample, a general view of the metabolites that are most represented produced by the cells at time of harvest, expressing the chemical shifts (δ) in parts per million (ppm). The NMR equipment detects the signals and records them as frequency vs intensity graphic, known as the "acquisition spectrum".

The resulting ^{1}H-NMR spectra were processed with the Chenomx NMR Suite program version 8.3 (Chenomx, Edmonton, Canada), in order to identify and quantify the metabolites of interest. All the samples were calibrated with the signal from the internal standard (IS), the deuterated Trimethylsilylpropionic acid sodium salt (TSP-d_4) and the pH was set to a value of around 6. The software utilized includes a broad range of spectrum data which can be utilized to detect the metabolites that are over 5–10 μM: among the metabolites that were found and/or quantified, the following are highlighted: Aspartate, Glutamate, Alanine, Glutamine, Isoleucine, Valine, Tyrosine, Proline, Phenylalanine, Citrate, Formate, Fumarate, Malate, Fructose, Glucose, Sucrose, GABA, and Trigonelline (Duynhoven et al., 2013; Becerra-Martínez et al., 2017).

Statistical Analysis

In this assay, the experimental design was one-factor (foliar application of the formulations) with a total of four experimental units (n = 4), which consisted of 4 biological units each. The statistical analysis included a one-way ANOVA with the SPSS program v24. When the ANOVA was significant ($p < 0.05$), Duncan's HSD test for the separation of means was applied for $p < 0.05$. On the other hand, with the same statistics software, a Pearson's correlation matrix was performed, which measured the degree of linear relationship between the variables. Also, to establish the existence or not of significant differences between the percent of metabolites compared with the control, a Student's t-test was performed, for which the data were previously transformed through the arcsine of the root square of the value divided by one hundred.

A principal component analysis (PCA) and a cluster analysis (CA) were also performed. The cluster analysis was applied to the standardized data for hierarchical associations employing Ward's method for agglomeration and the squared Euclidean distance as the dissimilarity measure.

RESULTS

Vegetative Growth Parameters

The vegetative growth parameters were significantly affected by the treatments applied. Without the exogenous application of the AAs (control), the growth values were: a height of 37.5 cm, a stem diameter of 9.8 mm, and a dry weight of 19.1 g, respectively. The plants from the Asp + Glu treatment had a shoot dry weight that was significantly greater than the rest of the treatments, increasing by 25% with respect to the control plants. The plants with the least growth were those that were treated with the mixture of Asp + Glu + Ala, with a decrease in growth of 76%. The dry weight of the shoot decreased with the treatments in the following order: Asp + Glu > Control = Asp > Glu = Ala > Asp + Glu + Ala. As for the height, the plants treated with the Asp + Glu mixture were the tallest, but significant differences were only observed with the Asp and Asp + Glu + Ala treatments. The plants

with the thickest stems were those that were treated with Glu, but significant differences were only observed with Asp and Asp + Glu + Ala (**Figure 1**).

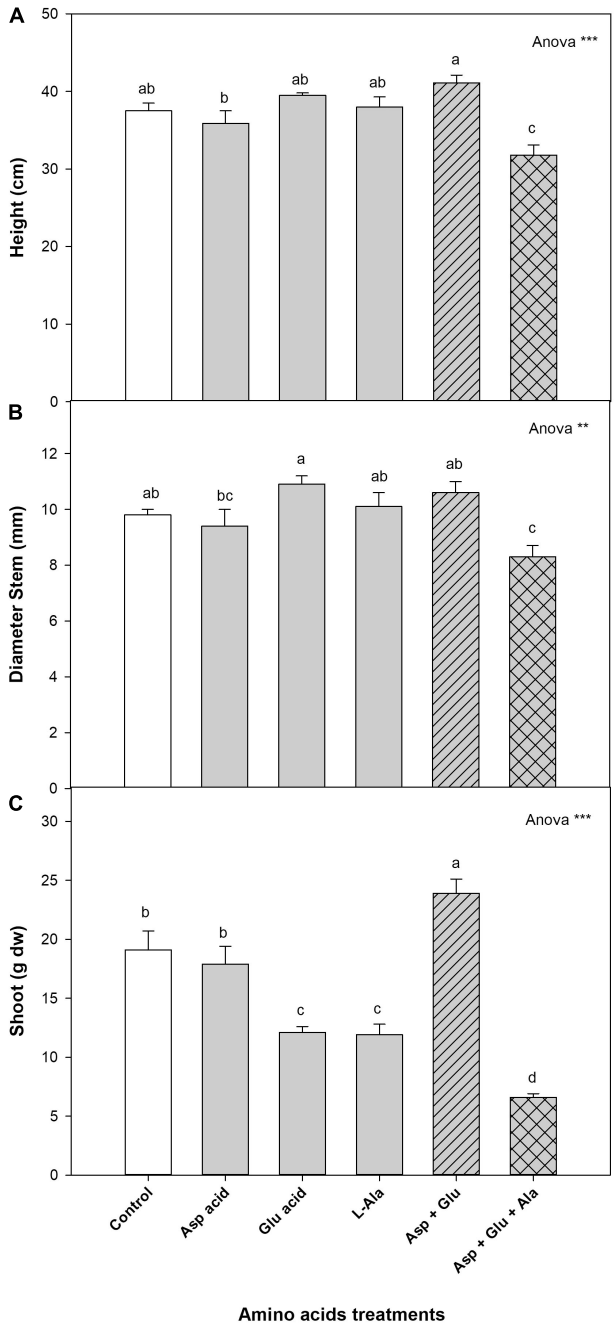

FIGURE 1 | Growth parameters: height (cm) **(A)**, diameter stem (mm) **(B)** and shoot (g dw) **(C)**, measured in the 'Optima' variety of tomato after a week from the exogenous application of the treatment with AAs: Control (without AAs), Aspartic acid (Asp ac.), Glutamic acid (Glu ac.), L-Alanine (L-Ala), combination Asp + Glu and combination Asp + Glu + Ala. In the ANOVA: ** and *** indicate significant differences at $p < 0.01$ and $p < 0.001$, respectively. The different *lower case letters* indicate significant differences ($p < 0.05$) between the means established by Duncan's test ($n = 4$).

Physiological Study

For the parameters of gas exchange, it was observed that the plants without the exogenous application of AAs had the following values: A_{CO2} 14.4 μmol m^{-2} s^{-1}, g_s 231.9 mmol m^{-2} s^{-1}, Ci/Ca 0.65, and WUE 6.09 μmol $mmol^{-1}$ (**Figure 2**). In all the parameters assayed, significant differences were observed with the treatments. The plants with the greatest net CO_2 assimilation rate were those from the Asp + Glu treatment, although without significant differences found with respect to the Glu-treated plants. The lowest values were found in plants from the Asp + Glu + Ala treatments (although not significant with respect to the control and L-Ala). With respect to the g_s and Ci/Ca parameters, the control plants and those treated with Asp had values that were significantly lower than those from the rest of the treatments, while for WUE, the lowest values were found in plants treated with Glu, L-Ala and Asp + Glu + Ala.

The exogenous application of AAs did not affect neither the quantum efficiency of PSII (Φ_{PSII}) nor the photochemical quenching co-efficient (qP). However, significant differences were observed between the treatments for the antennae efficiency parameter, in that the plants from the Asp treatment had the highest value, being significant with respect to those found in the Glu and Ala treatments.

As for the concentration of chlorophylls, for the completely developed leaves (DL) as well as the buds (LB), significant differences were observed among the treatments (**Figure 3**). The control plants had chlorophyll values for DL and LB of 33.9 and 47.0 (SPAD values), respectively. The plants that were treated with Asp acid had the highest values of DL and LB, being significant for all the treatment in DL, and as compared to the control plants, and the Ala and Asp + Glu + Ala treatments for LB.

Ionomic Study

For the plants that were not foliarly treated with AAs, the concentration of the macronutrients Ca, K, Mg, Na and P were 2.66, 2.95, 0.72, 0.19, 0.31, and 3.97 g 100 g^{-1} dw, respectively (**Table 1**). The concentration of Ca and Mg did not change due to the application of the AAs treatments with respect to the control treatment. However, significant differences were observed for K, P and N. These differences were due to the concentration of these nutrients increasing in the Ala and Asp + Glu + Ala treatments with respect to the other treatments with AAs and the control.

The micronutrients results showed that for the control plants, the concentrations of B, Cu, Fe, Mn, and Zn were 47.8, 8.7, 171.2, 71.7, and 23.1 ppm, respectively (**Table 1**). In this case, there were significant differences in the concentrations of Cu, Fe, Mn and Zn. For Cu, these differences were due to the two-fold increase in concentration of the plants treated with Asp + Glu + Ala as compared to the rest of the treatments. The concentration of Fe oscillated between 171.2 ppm (control) and 104.85 (Glu and Asp + Glu), of Mn between 93.3 (Asp) and 67.5 (L-Ala), and of Zn between 36.8 (L-Ala and Asp + Glu + Ala) and

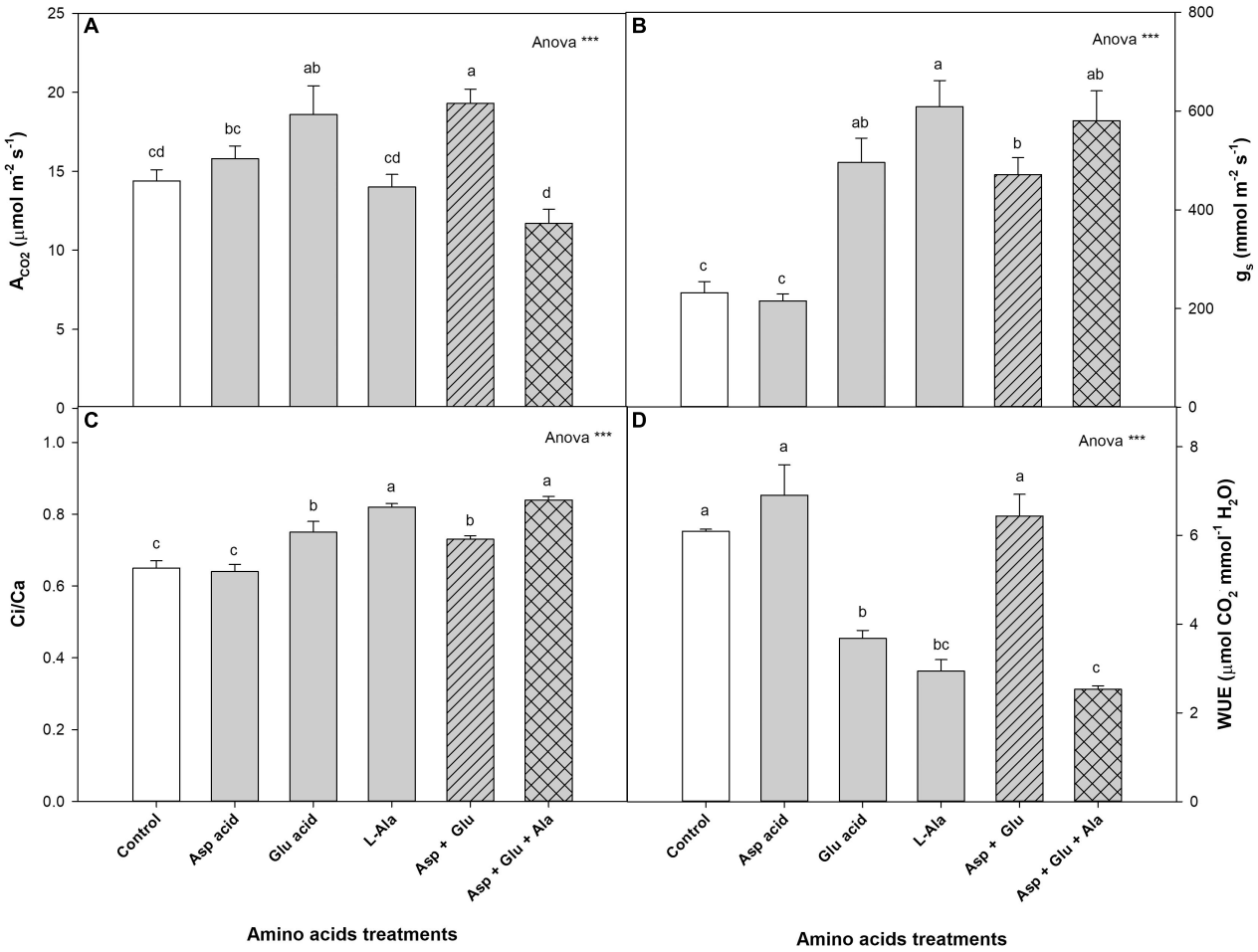

FIGURE 2 | Gas exchange parameters: net CO_2 assimilation rate (A_{CO2}) **(A)**, stomatal conductance (g_s) **(B)**, Ci/Ca ratio (Ci corresponds to the substomatal CO_2 and Ca correspond to external CO_2) **(C)** and water use efficiency (WUE) **(D)**, measured in the 'Optima' variety of tomato after a week from the exogenous application of the treatment with AAs: Control (without AAs), Aspartic acid (Asp ac.), Glutamic acid (Glu ac.), L-Alanine (L-Ala), combination Asp + Glu and combination Asp + Glu + Ala. In the ANOVA: *** indicate significant differences for $p < 0.001$. The different *lower case letters* indicate significant differences ($p < 0.05$) between the means established by Duncan's test ($n = 4$).

23.1 (Control), with significant differences observed between the maximum and minimum values.

Metabolomic Study

Amino Acids

The AAs detected with ^{1}H-NMR in tomato plants were Aspartate, Glutamate, Alanine, Tyrosine, Valine, Glutamine, Isoleucine, Phenylalanine and Proline. Of these AAs, in the control plants, the ones that added up to 98% of the total AAs detected were, in decreasing order, Glutamate (38%), Proline (30%), Glutamine (20%) and Aspartate (10%) (**Table 2**, **Supplementary Figure 1**). Of all the AAs measured, significant differences were observed with the treatments assayed, for Glutamate, Proline, Alanine, Tyrosine and Isoleucine. In the case of glutamate, it was observed that the application of L-Ala, Asp + Glu and Asp + Glu + Ala decreased its concentration with respect to the control, with the lowest values observed in plants treated with Asp + Glu + Ala. In the case of Proline, the treatments which included L-Ala (L-Ala and the Asp + Glu + Ala mixture) decreased its concentration, moving from 6.83 mg g^{-1} dw from the control plants to 2.5 mg g^{-1} dw, while the treatments Asp, Glu and their mixture (Asp + Glu) increased it, reaching the highest concentration in the mixture of 10.02 mg g^{-1} dw. The concentration of Alanine increased in the plants treated with this AA foliarly (L-Ala and Asp + Glu + Ala), and the Asp + Glu mixture, with the highest concentration measured in the plants treated with L-Ala. The concentration of Tyrosine decreased with the application of L-Ala and Asp + Glu + Ala. Likewise, the concentration of Isoleucine decreased with the application of Asp + Glu, in relation to the control plants (**Table 2**).

As for the relative distribution of the AAs, it was observed that in general, the treatments followed a model that was similar to the control plants, as previously commented, with some differences. The application of Asp, Glu and their mixture resulted in the % proline being higher than that of glutamate; and in the Asp + Glu

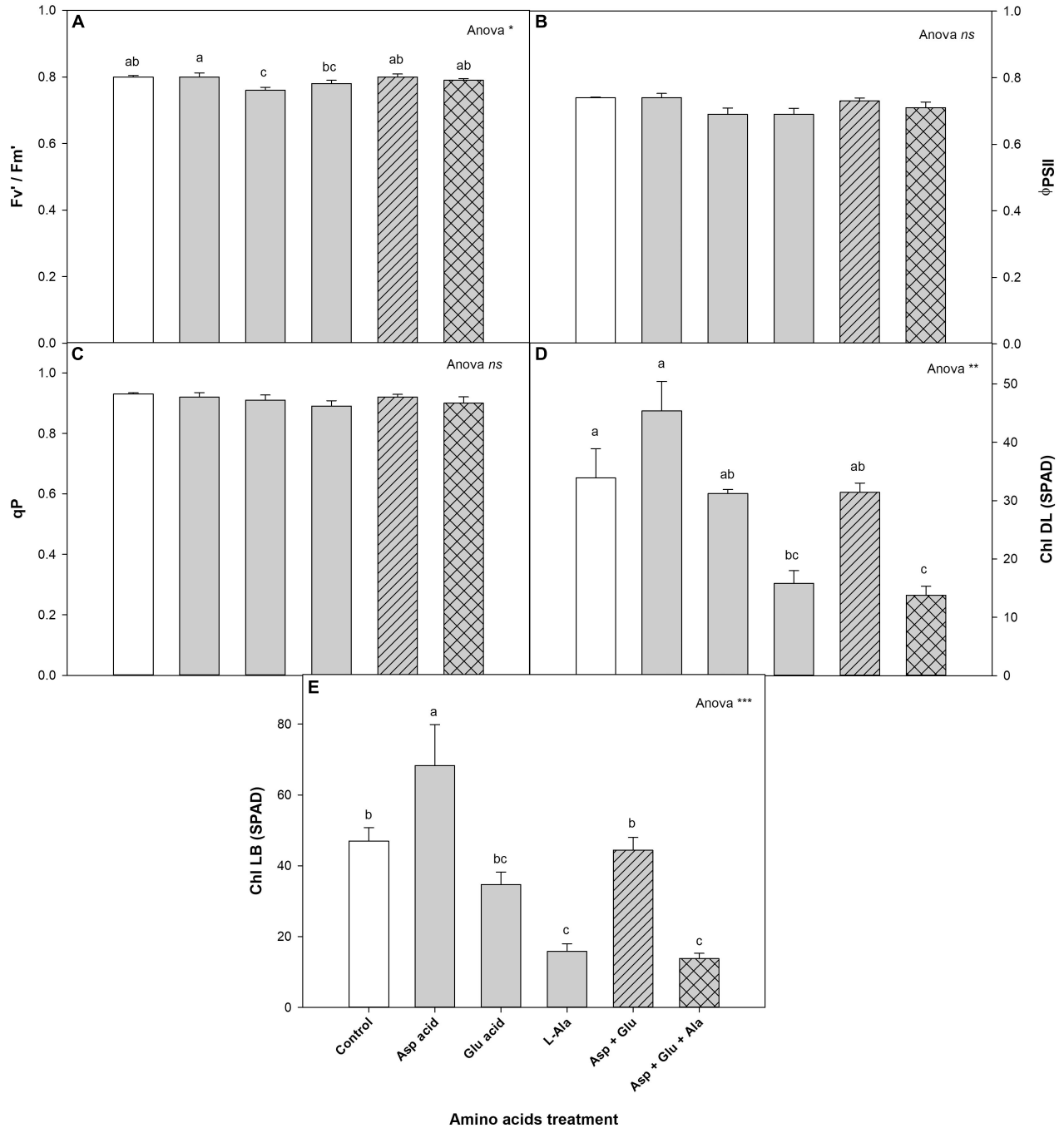

FIGURE 3 | Chlorophyll fluorescence: antennae efficiency of PSII (Fv′/Fm′) **(A)**, quantum efficiency of PSII (Φ_{PSII}) **(B)**, photochemical quenching co-efficient (qP) **(C)** and chlorophylls (Chl) measured in completely developed leaves (DL) **(D)** and leaf buds (LB) **(E)**, parameters measured in the 'Optima' variety of tomato after a week from the exogenous application of the treatment with AAs: Control (without AAs), Aspartic acid (Asp ac.), Glutamic acid (Glu ac.), L-Alanine (L-Ala), combination Asp + Glu and combination Asp + Glu + Ala. In the ANOVA: '*ns*' indicates non-significant differences for a confidence interval of 95%; on their part, *, **, and *** indicate significant differences at $p < 0.05$, $p < 0.01$, and $p < 0.001$, respectively. The different *lower case letters* indicate significant differences ($p < 0.05$) between the means established by Duncan's test ($n = 4$).

mixture, the % of L-Ala overcame that of Glutamine (**Supplementary Figure 1**). On the other hand, the percentage of glutamine was higher than that of proline in the L-Ala and Asp + Glu + Ala treatments.

Organic Acids

The organic acids quantified with ^{1}H-NMR were malate, citrate, fumarate and formate (**Figure 4**, **Supplementary Figure 2**). Among these, the most common was malate, whose

TABLE 1 | Concentration of macro (g 100 g^{-1} dw) and micronutrients (ppm) quantified in leaves from the 'Optima' variety of tomato after a week from the exogenous application of the treatment with AAs: Control (without AAs), Aspartic acid (Asp ac.), Glutamic acid (Glu ac.), L-Alanine (L-Ala), combination Asp + Glu and combination Asp + Glu + Ala.

	Macronutrients (g 100 g^{-1} dw)				
Treatments	**Ca**	**K**	**Mg**	**P**	**N**
Control (without AAs)	2.66 ± 0.06	2.95 ± 0.04 cd	0.72 ± 0.03	0.31 ± 0.02bc	3.97 ± 0.15b
Asp Ac.	2.73 ± 0.19	2.85 ± 0.19 cd	0.67 ± 0.07	0.39 ± 0.04b	4.49 ± 0.43b
Glu Ac.	2.62 ± 0.20	2.72 ± 0.01d	0.71 ± 0.03	0.28 ± 0.01*c*	3.88 ± 0.27b
L-Ala	2.92 ± 0.23	4.50 ± 0.12b	0.66 ± 0.05	0.63 ± 0.04a	6.08 ± 0.24a
Asp + Glu	2.66 ± 0.21	3.33 ± 0.22*c*	0.71 ± 0.04	0.40 ± 0.04*b*	4.77 ± 0.17b
Asp + Glu + Ala	2.05 ± 0.16	5.42 ± 0.25a	0.64 ± 0.08	0.70 ± 0.02a	6.47 ± 0.30a
ANOVA	*ns*	***	*ns*	***	***
	Micronutrients (ppm)				
Treatments	**B**	**Cu**	**Fe**	**Mn**	**Zn**
Control (without AAs)	47.8 ± 1.3	8.7 ± 1.3b	171.2 ± 22.2a	71.7 ± 0.9bc	23.1 ± 0.7c
Asp Ac.	45.4 ± 1.2	11.8 ± 0.6b	121.9 ± 12.5bc	93.3 ± 2.3a	29.3 ± 1.7b
Glu Ac.	43.7 ± 0.7	9.3 ± 0.9b	104.7 ± 2.9c	84.8 ± 1.9ab	29.8 ± 1.9b
L-Ala	38.8 ± 2.8	11.3 ± 1.0b	125.5 ± 8.3bc	67.5 ± 2.6c	37.1 ± 2.7a
Asp + Glu	40.9 ± 4.7	8.9 ± 0.9b	105.0 ± 9.5c	76.6 ± 6.7bc	30.2 ± 3.1b
Asp + Glu + Ala	45.5 ± 5.2	22.7 ± 2.5a	154.2 ± 14.2ab	83.4 ± 6.5ab	36.4 ± 1.6a
ANOVA	*ns*	***	**	**	**

*In the ANOVA: 'ns' indicates non-significant differences for a confidence interval of 95%; on their part, ** and *** indicate significant differences at $p < 0.01$ and $p < 0.001$, respectively. The different lower case letters indicate significant differences ($p < 0.05$) between the means established by Duncan's test (n = 4).*

TABLE 2 | Concentration of amino acids (mg g^{-1} dw) quantified by NMR in leaves from the 'Optima' variety of tomato after a week from the exogenous application of the treatment with AAs: Control (without AAs), Aspartic acid (Asp ac.), Glutamic acid (Glu ac.), L-Alanine (L-Ala), combination Asp + Glu and combination Asp + Glu + Ala.

	Amino Acids (mg g^{-1} dw)								
Treatments	**Glutamate**	**Proline**	**Glutamine**	**Aspartate**	**Alanine**	**Phenylalanine**	**Valine**	**Tyrosine**	**Isoleucine**
Control (without AAs)	7.85 ± 0.68a	6.83 ± 0.26c	4.68 ± 0.46	2.50 ± 0.26	0.60 ± 0.05cd	0.26 ± 0.03	0.25 ± 0.03	0.19 ± 0.03a	0.15 ± 0.03b
Asp Ac.	6.58 ± 0.42abc	8.63 ± 0.37b	4.89 ± 0.58	2.43 ± 0.23	0.56 ± 0.01cd	0.22 ± 0.03	0.24 ± 0.02	0.18 ± 0.04a	0.14 ± 0.03b
Glu Ac.	6.75 ± 0.70ab	8.13 ± 0.71b	4.02 ± 0.57	2.36 ± 0.23	0.48 ± 0.02d	0.30 ± 0.03	0.22 ± 0.03	0.15 ± 0.04ab	0.21 ± 0.04b
L-Ala	5.05 ± 0.19cd	2.47 ± 0.17d	3.15 ± 0.48	2.31 ± 0.16	1.44 ± 0.07a	0.18 ± 0.02	0.21 ± 0.02	0.06 ± 0.01b	0.20 ± 0.04b
Asp + Glu	5.54 ± 0.26bcd	10.02 ± 0.22a	2.82 ± 0.47	3.55 ± 0.42	0.66 ± 0.01c	0.27 ± 0.02	0.31 ± 0.03	0.13 ± 0.03ab	0.34 ± 0.04a
Asp + Glu + Ala	4.31 ± 0.43d	2.59 ± 0.04d	3.33 ± 0.40	2.53 ± 0.25	0.93 ± 0.03b	0.25 ± 0.02	0.21 ± 0.03	0.07 ± 0.01c	0.21 ± 0.04b
ANOVA	**	***	*ns*	*ns*	***	*ns*	*ns*	*	*

*In the ANOVA: 'ns' indicates non-significant differences for a confidence interval of 95%; on their part, *, **, and *** indicate significant differences at $p < 0.05$, $p < 0.01$, and $p < 0.001$, respectively. The different lower case letters indicate significant differences ($p < 0.05$) between the means established by Duncan's test (n = 4).*

concentration comprised 80% of the total acids quantified, followed by citrate with 12%, with fumarate and formate being minor constituents. Thus, the concentration of malate increased with the application of Glu, and decreased in the plants from the L-Ala, Asp + Glu and Asp + Glu + Ala treatments, with respect to the control plants, reaching a concentration that was lower in the last treatment (**Figure 4**). The concentration of citrate decreased in all the treatments except for L-Ala, where no significant differences were found with respect to the control. The concentration of fumarate increased with the application of all the amino acids, with the highest value reached with the Asp + Glu mixture. The same trend was observed in the shoot concentration of formate, which increased in all the AAs treatments except for Asp. The greatest concentration was found for the Asp + Glu + Ala mixture, without significant differences observed with Asp + Glu and L-Ala. Despite the changes produced by the application of the AAs, the relative distribution of these in each treatment followed the same model as the one described previously for the control plants (**Supplementary Figure 2**).

Sugars

The sugars quantified with ^{1}H-NMR in the leaves of the tomato plants were fructose, sucrose and glucose. Of these, the most commonly quantified was fructose (44.5%), followed by sucrose (31.5%) and glucose (24.0%) (**Figure 5**,

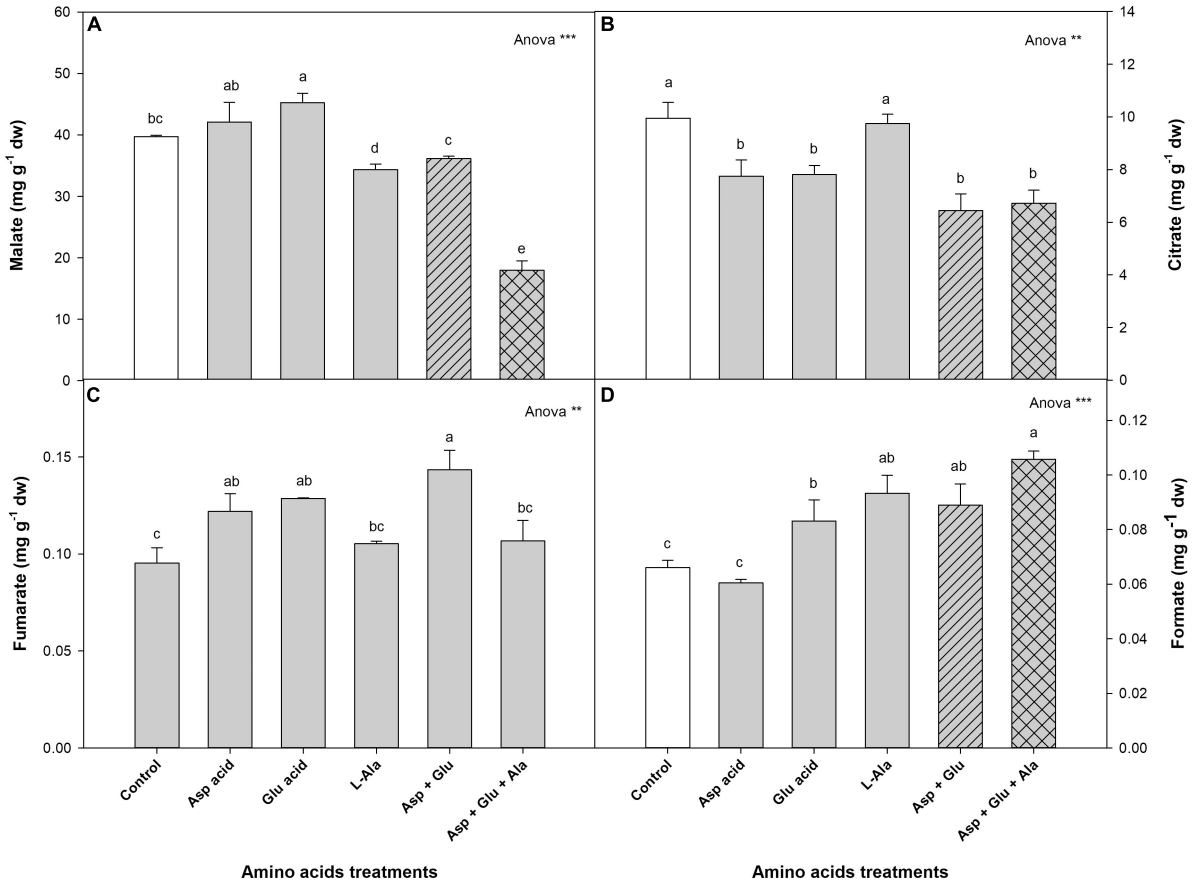

FIGURE 4 | Concentration of organic acids (mg g^{-1} dw): malate **(A)**, citrate **(B)**, fumarate **(C)**, and formate **(D)**, quantified by NMR in tomato leaves from the 'Optima' variety of tomato after a week from the exogenous application of the treatment with AAs: Control (without AAs), Aspartic acid (Asp ac.), Glutamic acid (Glu ac.), L-Alanine (L-Ala), combination Asp + Glu and combination Asp + Glu + Ala. In the ANOVA: ** and *** indicate significant differences for $p < 0.01$ and 0.001, respectively. The different *lower case letters* indicate significant differences ($p < 0.05$) between the means established by Ducan's test. The vertical bar indicates the standard error of the mean ($n = 4$).

Supplementary Figure 3). For all of them, it was observed that all the treatments affected their concentration. For fructose, the concentration increased with the application of Glu, while it decreased with the application of L-Ala and Asp + Glu + Ala, as compared to the control plants. For sucrose, the only significant difference observed between the treatments was the increase in its concentration in plants from the Asp treatment, as compared to the application of Asp + Glu + Ala. The concentration of glucose decreased with the application of Asp, Glu, L-Ala and Asp + Glu + Ala, with the L-Ala treatment having the lowest value. The relative distribution of these three sugars did not change in the AAs treatments with respect to the control treatment, as commented previously, except for the application of L-Ala, which resulted in a greater percentage of sucrose as compared to the percentage of fructose (**Supplementary Figure 3**).

Other Metabolites

The ^{1}H-NMR analysis also detected and quantified 4-Aminobutyrate (GABA) and Trigonelline (**Figure 6**). In normal conditions, without the application of AAs, the tomato plants have values of 0.92 mg g^{-1} dw for GABA and 0.71 mg g^{-1} dw for Trigonelline. In both cases, it was observed that the ANOVA was significant for the treatments. The application of the Asp + Glu + Ala mixture increased the concentration of GABA with respect to the rest of the treatments, increasing from 1.15 mg g^{-1} dw for the control treatment to 1.82 mg g^{-1} dw for this treatment. The concentration of Trigonelline decreased with the application of L-Ala and Asp + Glu + Ala, with the concentration being the lowest in the latter treatment.

Principal Components Analysis (PCA) and Cluster Analysis

For a better and simpler visual interpretation of all the data, a principal component analysis and a cluster analysis were conducted (**Figure 7**). The first four components explained 93.75% of the variability, and the first three, represented by PC1, PC2 and PC3, explained 84%. The PC1 component explained 53.35% of the variability observed, thus showing that the variability was fundamentally due to WUE, qP, K, Mg, P,

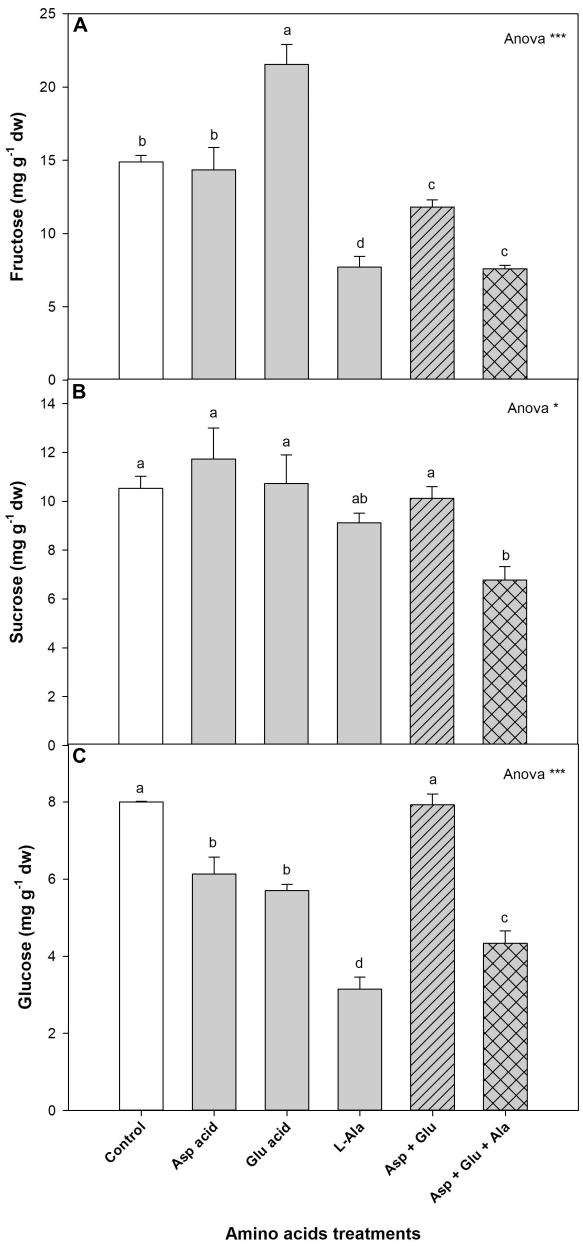

FIGURE 5 | Concentration of sugars (mg g^{-1} dw): fructose **(A)**, Sucrose **(B)**, and glucose **(C)**, quantified by NMR in tomato leaves from the 'Optima' variety of tomato after a week from the exogenous application of the treatment with AAs: Control (without AAs), Aspartic acid (Asp ac.), Glutamic acid (Glu ac.), L-Alanine (L-Ala), combination Asp + Glu and combination Asp + Glu + Ala. In the ANOVA: * and *** indicate significant differences for $p < 0.05$ and 0.001, respectively. The different *lower case letters* indicate significant differences ($p < 0.05$) between the means established by Ducan's test. The vertical bar indicates the standard error of the mean ($n = 4$).

N, Glutamic acid, Proline, Tyrosine, Sucrose, GABA, Formate, and Trigonelline. The cluster analysis showed that L-Ala, and Asp + Glu + Ala treatments were more different to the rest of treatments.

DISCUSSION

Amino acids in plants are involved in primary and secondary metabolism, and participate in a wide range of cellular enzymatic reactions as constituents of different enzymes such as aminotransferases, dehydrogenases, lyases and decarboxylases. Therefore, they can have an influence on diverse phenological and physiological processes such as vegetative development of the plants, seed germination, fruit maturation, signaling and activation of defense systems against abiotic and biotic stresses, osmotic adjustment, deactivation of reactive oxygen species, and as a reserve source of nitrogen, among others (Teixeira et al., 2017). These important functions of the AAs in plants lead to the application of biostimulant products containing AAs, either added in their free form or added as botanical and seaweed extracts and hydrolyzed proteins, becoming a common practice in agriculture (Khan et al., 2019). Nevertheless, in order for the biostimulant products to become more efficient in the improvement of the agronomic performance of the crops, and so that they can be specifically formulated depending on the crop varieties, it necessary to understand the function of each amino acid in each crop, to identify antagonistic, synergistic or neutral effects among the amino acid mixtures, and to determine the doses and the best time of application.

In our experiment, it was observed that the foliar application of AAs can alter the vegetative growth of the plants. However, this effect was dependent on the AAs utilized for the preparation of the products applied. According to the shoot dry weight data (**Figure 1**), the best treatment found from all those applied was the Asp + Glu mixture. And, taking account that the application of these two AAs individually did not affect this parameter or even decreased it, as in the Glu treatment, relative to the control plants, it was concluded that there was a synergistic effect these two AAs. The opposite behavior was found for the plants to which L-Ala was applied individually or as part of a mixture. In this case, it became apparent that L-Ala was harmful to tomato plants when applied at a concentration of 15 mM. In addition, when mixed with Asp + Glu, its negative effect was enhanced, as observed in the decrease in dry weight of the shoot as well as the appearance of damage to the leaves (**Figure 1**). Some synergic effects between AAs has been previously reported. In an experiment conducted with this same tomato variety under saline conditions (Alfosea-Simón et al., 2020), it was observed that the Pro + Glu and Met + Trp mixtures were more efficient in palliating the effects of salinity as compared to the individual application of these AAs. Despite the positive effects of the application of Glutamic or Aspartic acids being observed on several occasions, such as in Kimchi plants grown in low temperatures (Lee et al., 2017) or rice under an excess of Cd (Rizwan et al., 2017), the positive effects of these two AAs applied simultaneously had never been previously described. On the other hand, plants from Asp + Glu + Ala applications received three times more amino acid content compared to those from individual Asp, Glu and Ala spraying, and 1.8 time more relative to Asp + Glu treatment. Thus, the excess of aminoacid content in the spraying Asp + Glu + Ala solution could have damaged the plants. In several cases, for instance, in Arabidopsis plants, it has been shown that amino

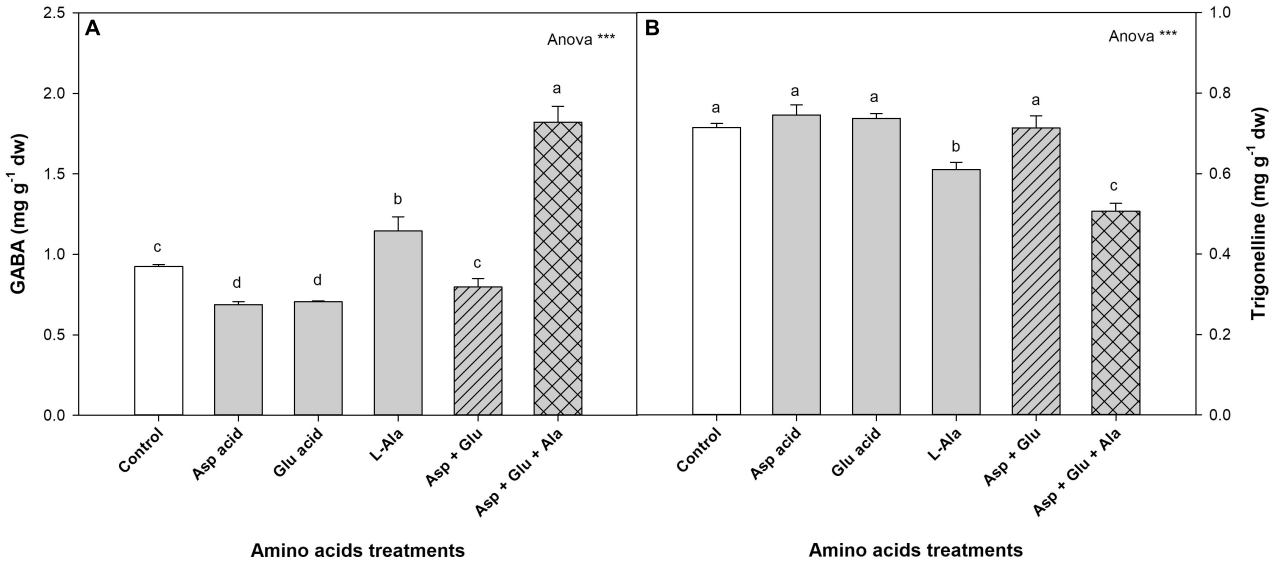

FIGURE 6 | Concentration of GABA **(A)** and Trigonelline **(B)** (mg g^{-1} dw) quantified by NMR in tomato leaves from the 'Optima' variety of tomato after a week from the exogenous application of the treatment with AAs: Control (without AAs), Aspartic acid (Asp ac.), Glutamic acid (Glu ac.), L-Alanine (L-Ala), combination Asp + Glu and combination Asp + Glu + Ala. In the ANOVA: *** indicates significant differences for $p < 0.001$. The different *lower case letters* indicate significant differences ($p < 0.05$) between the means established by Ducan's test. The vertical bar indicates the standard error of the mean ($n = 4$).

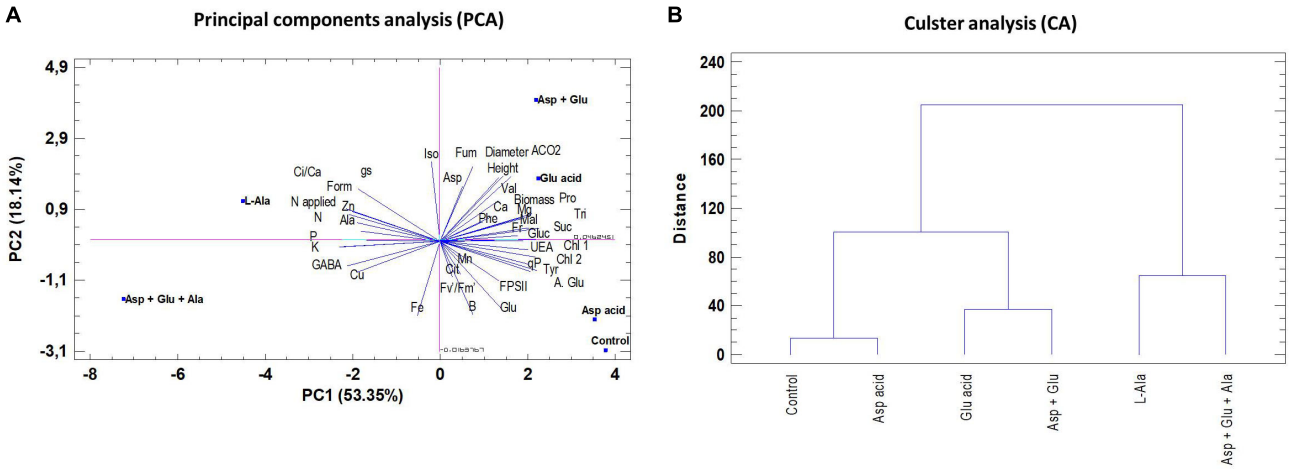

FIGURE 7 | Principal component analysis (PC1 and PC2) **(A)** and Cluster analysis (CA) **(B)** in tomato leaves from the 'Optima' variety of tomato after a week from the exogenous application of the treatment with AAs: Control (without AAs), Aspartic acid (Asp ac.), Glutamic acid (Glu ac.), L-Alanine (L-Ala), combination Asp + Glu and combination Asp + Glu + Ala.

acids as low as 100 μM applied via root caused damage in the root growth (Ravelo-Ortega et al., 2021). Thus, low concentrations of amino acids in some plant species can have un-expected effects.

One of the reasons why the plants treated with Asp + Glu had a greater growth can be found in the results from the physiological study. In this study (**Figure 8**), it was observed that one of the common responses of the plants when treated with any AAs treatment was the increase in stomatal conductance (g_s). However, this generalized response was not observed in the A_{CO2}. The only plants that had an increase in the CO_2 assimilation rate, in parallel to the opening of stomata, were those from the Asp + Glu treatment. Thus, the simultaneous effect of Asp + Glu could have enhanced the biochemical reactions of photosynthesis. This has already been reported by Lee et al. (2017) with the foliar application of Glutamic acid, with positive effects observed on the photosynthetic rate and stomatal conductance. In an experiment carried out in rice plants under conditions of cadmium stress, it was determined that the foliar application of Asp also improved the photosynthetic rate and stomatal conductance (Rizwan et al., 2017). In our experiment in tomato plants, the simultaneous application of Asp + Glu was necessary to enhance A_{CO2}. In addition, in these

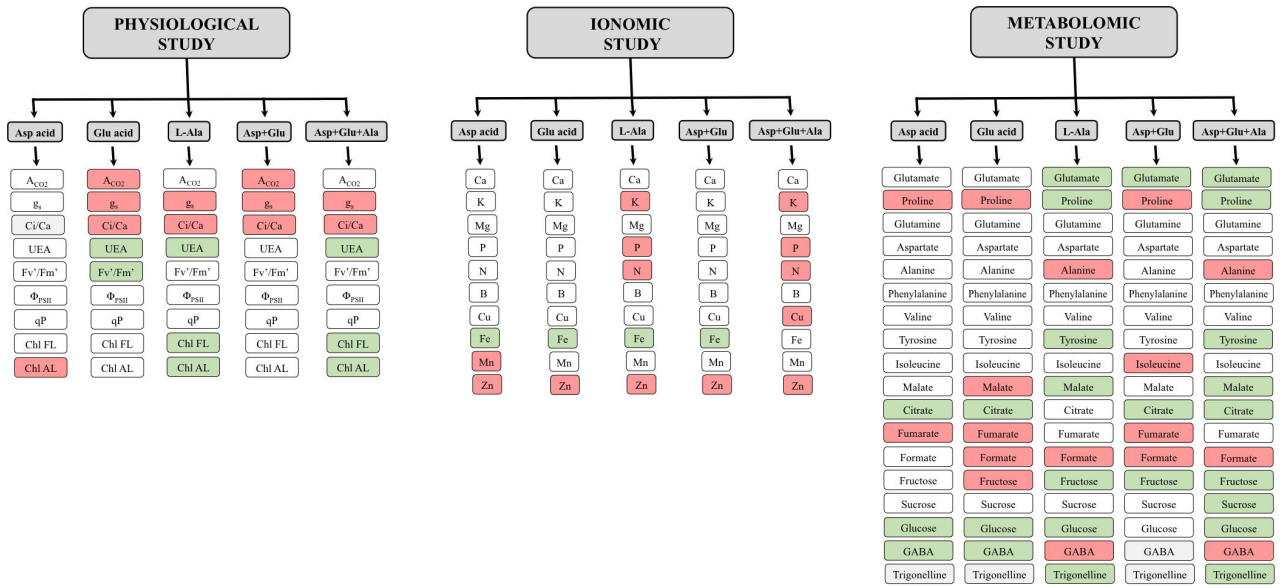

FIGURE 8 | Summary of the relative results with respect to the control obtained after the foliar application of the AA treatments: Control (without AAs), Aspartic acid (Asp ac.), Glutamic acid (Glu ac.), L-Alanine (L-Ala), combination Asp + Glu and combination Asp + Glu + Ala. The red or green color indicate a significant increase or reduction, respectively, of the concentration of the metabolite in plants from the AA treatments compared with the control treatment. The white color indicates that no significant differences were found between the control and the corresponding AA treatment.

plants, A_{CO2} and g_s had similar increases (as a percentage), relative to control plants. Thus, the WUE was maintained similar to the control plants, resulting in the maintenance of a good balance between the CO_2 captured and water lost by the plants. On the other hand, the application of L-Ala seems to have altered the non-stomatal factors of photosynthesis (biochemical factors), as indicated by the decrease in the assimilation rate of CO_2 in plants treated with L-Ala and Asp + Glu + Ala in parallel to the decrease in the Ci/Ca ratio (Farquhar and Sharkey, 1982). In plant cell culture studies, evidence has been shown about the harmful effects of L-Alanine. Chen et al. (2006) in cell cultures of *V. labrusca* and *V. vinifera* observed that the application of L-Ala to the growth media caused the death of cells due to the activation of Phenylalanine ammonium lyase, 4-hydroxylase cinnamic acid, the expression of the stilbene synthase gene, and the accumulation of stilbenes. Nevertheless, the applications of L-Ala to crops has barely been studied, except in the *Plumbago indica* crop, where the application of Alanine (5mM) combined with chitosan (150 mg L^{-1}) improved its production (Jaisi and Panichayupakaranant, 2020).

The ionomics study indicated that the AAs applied to the tomato plants of the variety 'Optima' did not induce changes in the absorption of nutrients relative to control plants, as the concentrations of macronutrients and micronutrients in plants from any of the treatments were within the normal range for this crop (Watanabe et al., 2016). However, some foliar treatments with amino acids are able to increase or decrease the absorption of diverse macronutrients and micronutrients as indicated by Sainju et al. (2003). The data from our experiment showed that the plants treated with L-Ala (L-Ala and Asp + Glu + Ala) had an altered nutritional status as in these plants it was increased the K, P and N concentration. This could be due to a concentration effect, as the dry weight of the shoot decreased. However, as this effect was not observed in the concentration of Ca and Mg, it should not be discarded that the L-Ala amino acid could have influenced the absorption and transport of the nutrients in plants. Nevertheless, the increase in K, P and N with respect to Ca and Mg could have created nutritional imbalances which may have caused a decrease in the growth of the shoots. Another possible reason for the highest leaf N concentration observed in the Asp + Glu + Ala treated plants could be due to the high N concentration (0.75 mg N L^{-1}) of the solution sprayed relative to the rest of treatments.

In the metabolomics study, it was observed that the most significant change observed after the application of the AAs Aspartic acid, Glutamic acid and their Asp + Glu mixture, occurred in the concentration of Proline. The Asp and Glu treatments, and their Asp + Glu mixture increased the concentration of this amino acid, and this increase was greater with the Asp + Glu mixture. Proline is an AA with multiple functions. It has the ability to act as an osmoprotector, and plays a role in osmotic adjustment, deactivation of free oxygen radicals, regulation of the absorption of nutrients, and can also induce the CO_2 assimilation rate (Pervaiz et al., 2019). These functions are especially important when the plants suffer adverse environmental conditions. In the Mediterranean area, the typical greenhouse conditions can make temperature be a limiting factor in tomato cultivation. Therefore, the increase of proline in these plants could have exerted a protective role that favored the increase in the CO_2 assimilation rate and the plant's growth. In addition, glutamate, aside from being a precursor of proline, is also related to the production of glutathione

and arginine. These two compounds are involved in oxidative metabolism, directly as glutathione or indirectly as arginine, as they activate PAL activity (Ben-Rejeb et al., 2014; Zheng et al., 2011). On the contrary, the application of L-Ala and Asp + Glu + Ala decreased the concentration of proline, and this response coincided with a decrease of A_{CO2} and decreased shoot growth. These results suggest that Asp + Glu improved the physiological and morphological parameters of the plants through the synthesis of proline, while Ala altered the metabolism of the plants by reducing the concentration of proline, and therefore reducing their growth.

In plants, the AAs Glutamate and Aspartate are precursors of up to eleven AAs. The reaction of Glutamate + Oxaloacetate produces Aspartate + α-ketoglutarate. This reaction is reversible, so that in the biosynthesis pathways, the AAs from glutamate (such as Alanine, Valine, Leucine, Glutamine, Proline and Arginine) are connected with those from Aspartate (such as Asparagine, Methionine, Threonine, Isoleucine and Lysine) (Forde and Lea, 2007). The application of Glutamate and Aspartate and their mixture did not increase the foliar concentration of these AAs, but were metabolized to increase the concentration of proline. Instead, the application of L-Ala individually or in a mixture increased the concentration of L-Ala in leaves. This AA was not metabolized, so that the increase in concentration could have caused damages to the cells, as observed in Chen et al. (2006) in cell cultures. Another of the alterations produced by the application of L-Ala was the decrease in Tyrosine. This AA is the precursor of secondary metabolites derived from the p-Coumaroyl-CoA pathway, which produces compounds such as coumarins, flavonoids, isoflavonoids, stilbenes, aurones, cutin, suberin, sporopollenin, catechins, proanthocyanidins, lignans, lignins, phenylpropenes, acylated polyamines and many other alkaloid derivatives. These compounds are related with the antioxidant protection capacity of the cells and with the mechanisms of protection of plants against plagues and diseases.

In the metabolomics study it was also observed that some compounds from the pentose phosphate pathway, such as fructose, sucrose, glucose and formate, as well as the tricarboxylic acid pathway (citrate, malate and fumarate), were affected. For the individual application of Asp, Glu and L-Ala and their mixture Asp + Glu, different responses were observed in the pentose phosphate pathway and the tricarboxylic acid one, which demonstrate that the mix of amino acids has a different effect than the AA applied individually. The mixtures that contained L-Ala produced a decrease in the concentration of fructose, sucrose and glucose, malate and citrate. This could suggest that the L-Ala applied at a concentration of 15mM produces alterations in the metabolism of C such as in A_{CO2}, which could have caused a decrease in the growth of the shoot. Therefore, the causes of L-Ala toxicity in tomato plants should be studied further, using as the report from Chen et al. (2006) a reference, where it was observed that AAs can activate the enzymes Phenylalanine ammonium lyase, 4-hydroxylase cinnamic acid, the expression of the stilbene synthase gene, and the accumulation of stilbenes. In the case of Asp, Glu, and their mixture, it was observed that while the mixture maintained the concentration of glucose at similar values as those of the control, the individual application decreased its concentration. This could indicate that the simultaneous application of Asp + Glu improved the capture and assimilation of CO_2 in the plants, improving the growth of these plants, where proline could have played an important role in increasing the performance of the photosynthetic system. For the tricarboxylic acid pathway, it was observed that the application of this Asp + Glu treatment induced a reduction in the concentration of citrate, and an increase in the concentration of fumarate, which could have modulated the A_{CO2} and g_s regulation in plants under this treatment. Some studies have revealed a negative correlation between the concentrations of fumarate and gas exchange through the opening of stomata (Nunes-Nesi et al., 2007; Araújo et al., 2012).

Another of the responses that differentiated the treatments that contained L-Ala with those that did not have this AA, was observed in the concentrations of GABA and Trigonelline. The GABA increased while the Trigonelline decreased with respect to the control, and this response was greater when L-Ala was applied with the Asp + Glu mixture. GABA is a non-protein amino acid with multiple functions in plants, playing an important role in metabolic processes such as signaling, interconnection between Carbon and Nitrogen metabolisms and the tolerance to different stresses such as low light intensity, salinity, and lack of nitrogen, drought or temperature (Ramos-Ruiz et al., 2019). The increase in GABA observed in plants treated with L-Ala could be the result of some type of stress produced by this amino acid, unchaining a protection response related with GABA. In these plants, this response was not enough to counter the stress created, and therefore, led to a decrease in growth. The concentration of Trigonelline also increases in the plant as a response to different stresses, mainly salinity, drought or UV light (Cho et al., 1999; Cho et al., 2003; Willmon et al., 2017). However, the application of L-Ala in this experiment decreased its concentration. It is important to point out that the increased in GABA and the decrease of Trigonelline are found in plants suffering some abiotic stress, so that these metabolites could be used as biomarkers to detect the possible negative effects of these AAs in tomato plants. However, more research is needed to verify this hypothesis.

The different changes observed in the metabolic processes of the plants utilized in the present research could be due that the AAs, aside from having physiological functions, may also be involved in the metabolism of plants in signaling processes (Häusler et al., 2014). It has been described that plants have glutamate receptors (GLRs) that could be activated not only by glutamate, but also by other AAs such as Serine, Alanine, Methionine, Tryptophan, Phenylalanine, Leucine, Asparagine, Threonine, Cysteine, Glycine, Tyrosine, and Peptides (Vincill et al., 2012; Forde and Roberts, 2014). The activation of these receptors could unchain a series of signaling mechanisms in processes related to the absorption of nitrogen by the roots (Miller et al., 2008), growth and architecture of the roots (Weiland et al., 2016), antioxidant metabolism (Hildebrandt et al., 2015; Weiland et al., 2016), regulation of

transcription factors (Santi et al., 2017), regulation of stomas and photosynthesis, and plant defense (Weiland et al., 2016), as well as balances between C and N metabolism (Kang and Turano, 2003; Price et al., 2012).

CONCLUSION

In this experiment, it was observed that the application of AA to tomato plants could be beneficial for increasing their vegetative development, but this application should be first optimized. To increase the efficiency of biostimulant products in agriculture, much research is needed that may reveal: i) the effects of the AAs on physiological and metabolic processes of plants, either applied individually or as a mixture; in this experiment it was observed that the combined application of the AAs (in this case Asp and Glu) had better effects that their individual application, and ii) what dose needs to be applied; in this experiment, it was observed that the application of 15 mM of Alanine is toxic to tomato plants, and it is not reversed by the simultaneous application of the Asp + Glu + Ala mixture. The application of AAs to plants resulted in changes in their ionomic, physiological and metabolomic profiles; however, as these compounds have many different functions in plants, a systems biology approach that integrates metabolomics, proteomic, genomic and hormonal studies to delve into these changes, is necessary.

DATA AVAILABILITY STATEMENT

The raw data supporting the conclusions of this article will be made available by the authors, without undue reservation.

AUTHOR CONTRIBUTIONS

FG-S and EZ-G conceived and designed the research. MA-S, SS-G, IS, and VL conducted the experiments and collected the data in the field and in the lab. JC-Z and JM-N analyzed the data and did tables and figures. FG-S and MA-S wrote the manuscript. SS-G and EZ-G commented and revised the manuscript. All authors contributed to the article and approved the submitted version.

FUNDING

This research was funded by State R&D Program Oriented to the Challenges of the Society, Innovation and Science Ministerial (Spain Government), grant number RTC-2016-4568-2.

ACKNOWLEDGMENTS

We acknowledge support of the publication fee by the CSIC Open Access Publication Support Initiative through its Unit of Information Resources for Research (URICI).

SUPPLEMENTARY MATERIAL

The Supplementary Material for this article can be found online at: https://www.frontiersin.org/articles/10.3389/fpls.2020.581234/full#supplementary-material

Supplementary Figure 1 | Profile of the concentration of AAs (%) quantified with Nmr in tomato plant leaves from the 'Optima' variety after a week from the exogenous application of the treatment with AAs: Control (without AAs), Aspartic acid (Asp ac.), Glutamic acid (Glu ac.), L-Alanine (L-Ala), combination Asp + Glu and combination Asp + Glu + Ala. * indicates significant differences at $p < 0.05$ between the means established by Student's *t-test* ($n = 4$).

Supplementary Figure 2 | Profile of the concentration of organic acids (%) quantified by RMN in tomato leaves from the 'Optima' variety of tomato after a week from the exogenous application of the treatment with AAs: Control (without AAs), Aspartic acid (Asp ac.), Glutamic acid (Glu ac.), L-Alanine (L-Ala), combination Asp + Glu and combination Asp + Glu + Ala. * indicates significant differences at $p < 0.05$ between the means established by Student's *t-test* ($n = 4$).

Supplementary Figure 3 | Profile of the concentration of sugars (%) quantified by Nmr in tomato leaves from the 'Optima' variety of tomato after a week from the exogenous application of the treatment with AAs: Control (without AAs), Aspartic acid (Asp ac.), Glutamic acid (Glu ac.), L-Alanine (L-Ala), combination Asp + Glu and combination Asp + Glu + Ala. * indicates significant differences at $p < 0.05$ between the means established by Student's *t-test* ($n = 4$).

REFERENCES

Akram, N. A., Umm, E. H., Ashraf, M., Ashraf, M., and Sadiq, M. (2020). Exogenous application of L-methionine mitigates the drought-induced oddities in biochemical and anatomical responses of bitter gourd (*Momordica charantia* L.). *Sci. Hortic.* 267:109333. doi: 10.1016/j.scienta.2020.109333

Alfosea-Simón, M., Zavala-Gonzalez, E. A., Camara-Zapata, J. M., Martínez-Nicolás, J. J., Simón, I., and Simón-Grao, S. (2020). Effect of foliar application of amino acids on the salinity tolerance of tomato plants cultivated under hydroponic system. *Sci. Hortic* 272:109509. doi: 10.1016/j.scienta.2020.109509

Araújo, W., Nunes-Nesi, A., Nikoloski, Z., Sweetlove, L., and Fermie, A. (2012). Metabolic control and regulation of the tricarboxylic acid cycle in photosynthetic and heterotrophic plant tissues. *Plant Cell Environ.* 35, 1–21. doi: 10.1111/j.1365-3040.2011.02332.x

Becerra-Martínez, E., Florentino-Ramos, E., Pérez-Hernández, N., Zepeda-Vallejo, L. G., Villa-Ruano, N., Velázquez-Ponce, M., et al. (2017). 1H NMR-based metabolomic fingerprinting to determine metabolite levels in serrano peppers (*Capsicum annum* L.) *grown in two different regions*. *Food Res. Int.* 102, 163–170. doi: 10.1016/j.foodres.2017.10.005

Ben-Rejeb, K., Abdelly, C., and Savouré, A. (2014). How reactive oxygen species and proline face stress together. *Plant Physiol. Biochem.* 80, 278–284. doi: 10.1016/j.plaphy.2014.04.007

Cao, M., Song, C., Jin, Y., Liu, L., Liu, J., Xie, H., et al. (2010). Synthesis of poly(γ-glutamic acid) and heterologous expression of *pgsBCA* genes. *J. Mol. Catal. B Enzym.* 67, 111–116. doi: 10.1016/j.molcatb.2010.07.014

Chen, J., Hall, D. E., Murata, J., and De Luca, V. (2006). L-Alanine induces programmed cell death in V. *labrusca cell suspension cultures*. *Plant Sci.* 171, 734–744. doi: 10.1016/j.plantsci.2006.07.003

Cho, Y., Lightfoot, D., and Wood, A. J. (1999). Trigonelline concentrations in salt stressed leaves of cultivated *Glycine max*. *Phytochemistry* 52, 1235–1238.

Cho, Y., Njiti, V. N., Chen, X., Lightfoot, D. A., and Wood, A. J. (2003). Trigonelline concentration in field-grown soybean in response to irrigation. *Biol. Plant.* 46, 405–410. doi: 10.1023/A:1024390522259

Colla, G., Nardi, S., Cardarelli, M., Ertani, A., Lucini, L., Canaguier, R., et al. (2015). Protein hydrolysates as biostimulants in horticulture. *Sci. Hortic.* 196, 28–38. doi: 10.1016/j.scienta.2015.08.037

Colla, G., Rouphael, Y., Canaguier, R., Svecova, E., and Cardarelli, M. (2014). Biostimulant action of a plant-derived protein hydrolysate produced through enzymatic hydrolysis. *Front. Plant Sci.* 5, 1–6. doi: 10.3389/fpls.2014.00448

Duynhoven, J. V., Van As, H., Belton, P. S., and Webb, G. A. (2013). *Magnetic Resonance in Food Science: Food for Thought*, 1st Edn. Cambridge: RSC Publishing.

Farquhar, G. D., and Sharkey, T. D. (1982). Stomatal conductance and photosynthesis. *Annu. Rev. Plant Physiol.* 33, 317–345. doi: 10.1146/annurev.pp.33.060182.001533

Foley, J. A., Ramankutty, N., Brauman, K. A., Cassidy, E. S., Gerber, J. S., Jonhnston, M., et al. (2011). Solutions for a cultivated planet. *Nature* 478:337. doi: 10.1038/nature10452

Food and Agriculture Organization [FAO] (2020). *Datos Sobre Alimentación en Agricultura – FAOSTAT*. Rome: FAO.

Forde, B. G., and Lea, P. J. (2007). Glutamate in plants: metabolism, regulation, and signalling. *J. Exp. Bot.* 58, 2339–2358. doi: 10.1093/jxb/erm121

Forde, B. G., and Roberts, M. R. (2014). Glutamate receptor-like channels in plants: a role as amino acid sensors in plant defence? *F1000Prime Rep.* 6:37. doi: 10.12703/P6-37

Häusler, R. E., Ludewing, F., and Krueger, S. (2014). Amino acids – A life beteween metabolism and signalling. *Plant Sci.* 229, 225–237. doi: 10.1016/j.plantsci.2014.09.011

Hildebrandt, T. M., Nunes Nesi, A., Araújo, W. L., and Braun, H. P. (2015). Amino Acid Catabolism in Plants. *Mol. Plant* 8, 1563–1579. doi: 10.1016/j.molp.2015.09.005

Jaisi, A., and Panichayupakaranant, P. (2020). Enhanced plumbagin production in Plumbago indica root culture by simultaneous and sequential dual elicitations using chitosan with ?-alanine and methyl-β-cyclodextrin. *Bioresour. Bioprocess* 7:10. doi: 10.1186/s40643-020-0298-9

Jiang, M., Jiang, J., Li, S., Li, M., Tan, Y., Song, S., et al. (2020). Glutamate alleviates cadmium toxicity in rice via suppressing cadmium uptake and translocation. *J. Hazard. Mater.* 384:121319. doi: 10.1016/j.jhazmat.2019.121319

Kang, J., and Turano, F. J. (2003). The putative glutamate receptor 1.1 *(AtGLR*1.1) functions as a regulator of carbon and nitrogen metabolism in Arabidopsis thaliana. *Proc. Natl. Acad. Sci. U.S.A.* 100, 6872–6877. doi: 10.1073/pnas.1030961100

Kendziorek, M., Paszkowski, A., and Zagdanska, B. (2012). Differential regulation of alanine aminotransferase homologues by abiotic stresses in wheat (*Triticum aestivum* L.) *seedlings*. *Plant Cell Rep.* 31, 1105–1117. doi: 10.1007/s00299-012-1231-2

Khan, S., Yu, H., Li, Q., Gao, Y., Sallam, B. N., Wang, H., et al. (2019). Exogenous application of amino acids improves the growth and yield of lettuce by enhancing photosynthetic assimilation and nutrient availability. *Agronomy* 9:5. doi: 10.3390/agronomy9050266

Lea, P. J., and Ireland, R. J. (1999). "*Nitrogen Metabolism Inhigher Plants*," in *Plant Amino Acids: Biochemistry and Biotechnology*," ed. B. K. Singh (New York, NY: Marcel Dekker), 1–4.

Lee, H. J., Kim, J. S., Lee, S. G., Kim, S. K., Mun, B., and Choi, C. S. (2017). Glutamic acid foliar application enhances antioxidant enzyme activities in kimchi cabbages leaves treated with low air temperature. *Hortic. Sci. Technol.* 35, 700–706.

Lucini, L., Rouphael, Y., Cardarelli, M., Canaguier, R., Kumar, P., and Colla, G. (2015). The effect of a plant-derived biostimulant on metabolic profiling andcrop performance of lettuce grown under saline conditions. *Sci. Hortic.* 182, 124–133. doi: 10.1016/j.scienta.2014.11.022

Miller, A. J., Fan, X., Shen, Q., and Smith, S. J. (2008). Amino acids and nitrate as signals for the regulation of nitrogen acquisition. *J. Exp. Bot.* 59, 111–119. doi: 10.1093/jxb/erm208

Mutale-Joan, C., Redouane, B., Najib, E., Yassine, K., Lyamlouli, K., Laila, S., et al. (2020). Screening of microalgae liquid extracts for their bio stimulant properties on plant growth, nutrient uptake and metabolite profile of Solanum lycopersicum L. *Sci. Rep.* 10:1. doi: 10.1038/s41598-020-59840-4

Nunes-Nesi, A., Carrari, F., Gibon, Y., Sulpice, R., Lytovchnko, A., Fisahn, J., et al. (2007). Deficiency of mitochondrial fumarase activity in tomato plants impairs photosynthesis via an effect on stomatal function. *Plant J.* 50, 1093–1106. doi: 10.1111/j.1365-313X.2007.03115.x

Parađiković, N., Teklić, T., Zeljković, S., Lisjak, M., and Špoljarević, M. (2019). Biostimulants research in some horticultural plant species—A review. *Food Energy Secur.* 8:2. doi: 10.1002/fes3.162

Parry, M. L. (2019). *Climate Change and World Agriculture*. Abingdon: Routledge.

Pervaiz, A., Iqbal, A., Khalid, A., Manzoor, A., Noreen, S., Ayaz, A., et al. (2019). Proline induced modulation in physiological responses in wheat plants. *J. Agric. Environ. Sci.* 8, 112–119. doi: 10.15640/jaes.v8n1a11

Price, M. B., Jelesko, J., and Okumoto, S. (2012). Glutamate receptor homologs in plants: functions and evolutionary origins. *Front. Plant Sci.* 3:235. doi: 10.3389/fpls.2012.00235

Rai, V. K. (2002). Role of amino acids in plant responses to stresses. *Biologia Plant.* 45, 481–487. doi: 10.1023/A:1022308229759

Ramos-Ruiz, R., Martínez, F., and Knauf-Beiter, G. (2019). The effects of GABA in plants. *Cogent Food Agric.* 5:1670553. doi: 10.1080/23311932.2019.1670553

Ravelo-Ortega, G., López-Bucio, J. S., Ruiz-Herrera, L. F., Pelagio-Flores, R., Ayala-Rodríguez, J. A., Reyes de la Cruz, H., et al. (2021). The growth of Arabidopsis primary root is repressed by several and diverse amino acids through auxin-dependent and independent mechanisms and MPK6 kinase activity. *Plant Sci.* 302:110717. doi: 10.1016/j.plantsci.2020.110717

Rizwan, M., Ali, S., Akbar, M. Z., Shakoor, M. B., Mahmood, A., Ishaque, W., et al. (2017). Foliar application of aspartic acid lowers cadmium uptake and Cd-induced oxidative stress in rice under Cd stress. *Environ. Sci. Pollut. Res. Int.* 24, 21938–21947. doi: 10.1007/s11356-017-9860-1

Rouphael, Y., Spíchal, L., Panzarová, K., Casa, R., and Colla, G. (2018). High-Throughput plant phenotyping for developing novel biostimulants: from lab to field or From Field to lab? *Front. Plant Sci.* 9:1197. doi: 10.3389/fpls.2018.01197

Sánchez-Pale, J. R. (2017). *Evaluación del efecto de humics- 95 y amynofol, en el desarrollo y crecimiento de Impatiens waller*aina Hook. *F. VAR. LILLICOP*. Doctoral Thesis. Toluca: Universidad Autónoma del Estado de México, 14.

Sainju, U. M., Dris, R., and Singh, B. (2003). Mineral nutrition of tomato. *J. Food Agric. Environ.* 1, 176–183.

Santi, C., Molesini, B., Gluzzo, F., Pii, Y., Vitulo, N., and Pandolfini, T. (2017). Genome-wide transcriptional changes and lipid profile modifications induced by medicago truncatula N5 overexpression at an early stage of the symbiotic interaction with sinorhizobium meliloti. *Genes* 8:396. doi: 10.3390/genes8120396

Tantawy, A. S., Abdel-Mawgoud, A. M. R., El-Nemr, M. A., and Chamoun, Y. G. (2009). Alleviation of salinity effects on tomato plants by application of amino acids and growth regulators. *Eur. J. Sci. Res.* 30, 484–494.

Teixeira, W. F., Fagan, E. B., Soares, L. H., Umburanas, R. C., Reichardt, K., and Neto, D. D. (2017). Foliar and seed application of amino acids affects the antioxidant metabolism of the soybean crop. *Front. Plant Sci.* 8:327. doi: 10.3389/fpls.2017.00327

Tilman, D., Cassman, K. G., Matson, P. A., Naylor, R., and Polasky, S. (2002). Agricultural sustainability and intensive production practices. *Nature* 418:671. doi: 10.1016/j.jclepro.2020.121656

Van der Sar, S., Kim, H. K., Meissner, A., Verpoorte, R., and Choi, Y. H. (2013). "Nuclear Magnetic Resonance spectroscopy for plant metabolite profiling," in *The Handbook of Plant Metabolomics*, eds W. Weckwerth and G. Kahl, 57–76. doi: 10.1002/9783527669882.ch3

Vincill, E. D., Bieck, A. M., and Spalding, E. P. (2012). Ca2+ conduction by an amino acid-gated ion channel related to glutamate receptors. *Plant Physiol.* 159, 40–46. doi: 10.1104/pp.112.197509

Wallace, J. S., Acreman, M. C., and Sullivan, C. A. (2003). The sharing of water between society and ecosystems: from conflict to catchment–based co–management. *Philos. Trans. R. Soc. London. Ser. B: Biol. Sci.* 358, 2011–2026. doi: 10.1098/rstb.2003.1383

Watanabe, T., Maejima, E., Yoshiruma, T., Urayama, M., Yamauchi, A., Owadano, M., et al. (2016). The ionomic study of vegetable crops. *PLoS One* 11:e0160273. doi: 10.1371/journal.pone.0160273

Weiland, M., Mancuso, S., and Baluska, F. (2016). Signalling via glutamate and GLRs in *Arabidopsis thaliana*. *Funct. Plant Biol.* 43, 1–25. doi: 10.1071/FP15109

Willmon, D., Devireddy, A. R., Inupakutikal, M., Puppala, N., and Chol, Y. (2017). Stress Responses of Peanut (*Arachis hypogaea* L.) Genotypes as Measured by Trigonelline Content after Exposure to UV-B Radiation. *Am. J. Plant Sci.* 8, 998–1010. doi: 10.4236/ajps.2017.85066

Zheng, Y., Sheng, J., Zhao, R., Zhang, R., Lv, S., Liu, L., et al. (2011). Preharvest l-arginine treatment induced postharvest disease resistance to botrysis cinerea in tomato fruits. *J. Agric. Food Chem.* 59, 6543–6549. doi: 10.1021/jf2000053

Conflict of Interest: EZ-G was employed by the company Atlantica Agricola.

The remaining authors declare that the research was conducted in the absence of any commercial or financial relationships that could be construed as a potential conflict of interest.

Copyright © 2021 Alfosea-Simón, Simón-Grao, Zavala-Gonzalez, Cámara-Zapata, Simón, Martínez-Nicolás, Lidón and García-Sánchez. This is an open-access article distributed under the terms of the Creative Commons Attribution License (CC BY). The use, distribution or reproduction in other forums is permitted, provided the original author(s) and the copyright owner(s) are credited and that the original publication in this journal is cited, in accordance with accepted academic practice. No use, distribution or reproduction is permitted which does not comply with these terms.

frontiers in Plant Science

ORIGINAL RESEARCH
published: 12 January 2021
doi: 10.3389/fpls.2020.604349

Enhanced Production of Aromatic Amino Acids in Tobacco Plants Leads to Increased Phenylpropanoid Metabolites and Tolerance to Stresses

Moran Oliva[1†], Aviv Guy[2,3†], Gad Galili[1], Evgenia Dor[4], Ron Schweitzer[3], Rachel Amir[2,3] and Yael Hacham[2,3]*

[1] Department of Plant and Environmental Sciences, Weizmann Institute of Science, Rehovot, Israel, [2] Laboratory of Plant Science, MIGAL – Galilee Research Institute, Kiryat Shmona, Israel, [3] Tel-Hai College, Upper Galilee, Israel, [4] Department of Weed Research, Agriculture Research Organization, Newe Ya'ar Research Center, The Volcani Center, Ramat Yishay, Israel

OPEN ACCESS

Edited by:
Stefan Martens,
Fondazione Edmund Mach, Italy

Reviewed by:
André O. Hudson,
Rochester Institute of Technology,
United States
Joseph Lynch,
Purdue University, United States

***Correspondence:**
Rachel Amir
rachel@migal.org.il

[†] These authors have contributed equally to this work

Specialty section:
This article was submitted to Plant Metabolism and Chemodiversity, a section of the journal Frontiers in Plant Science

Received: 09 September 2020
Accepted: 03 December 2020
Published: 12 January 2021

Citation:
Oliva M, Guy A, Galili G, Dor E, Schweitzer R, Amir R and Hacham Y (2021) Enhanced Production of Aromatic Amino Acids in Tobacco Plants Leads to Increased Phenylpropanoid Metabolites and Tolerance to Stresses. Front. Plant Sci. 11:604349. doi: 10.3389/fpls.2020.604349

Aromatic amino acids (AAAs) synthesized in plants via the shikimate pathway can serve as precursors for a wide range of secondary metabolites that are important for plant defense. The goals of the current study were to test the effect of increased AAAs on primary and secondary metabolic profiles and to reveal whether these plants are more tolerant to abiotic stresses (oxidative, drought and salt) and to *Phelipanche egyptiaca* (Egyptian broomrape), an obligate parasitic plant. To this end, tobacco (*Nicotiana tabacum*) plants were transformed with a bacterial gene (AroG) encode to feedback-insensitive 3-deoxy-D-arabino-heptulosonate 7-phosphate synthase, the first enzyme of the shikimate pathway. Two sets of transgenic plants were obtained: the first had low expression of the AroG protein, a normal phenotype and minor metabolic changes; the second had high accumulation of the AroG protein with normal, or deleterious morphological changes having a dramatic shift in plant metabolism. Metabolic profiling analysis revealed that the leaves of the transgenic plants had increased levels of phenylalanine (up to 43-fold), tyrosine (up to 24-fold) and tryptophan (up to 10-fold) compared to control plants having an empty vector (EV) and wild type (WT) plants. The significant increase in phenylalanine was accompanied by higher levels of metabolites that belong to the phenylpropanoid pathway. AroG plants showed improved tolerance to salt stress but not to oxidative or drought stress. The most significant improved tolerance was to *P. aegyptiaca*. Unlike WT/EV plants that were heavily infected by the parasite, the transgenic AroG plants strongly inhibited *P. aegyptiaca* development, and only a few stems of the parasite appeared above the soil. This delayed development of *P. aegyptiaca* could be the result of higher accumulation of several phenylpropanoids in the transgenic AroG plants and in *P. aegyptiaca,* that apparently affected its growth. These findings indicate that high levels of AAAs and their related metabolites have the potential of controlling the development of parasitic plants.

Keywords: aromatic amino-acids, aroG, parasitic plant, *Phelipanche aegyptiaca*, salt stress, shikimate pathway, tobacco (*Nicotiana tabacum*)

INTRODUCTION

The shikimate pathway is initiated by combining phosphoenolpyruvate (PEP) and erythrose-4-phosphate (E4P) with the activity of 3-deoxy-D-arabino-heptulosonate 7-phosphate synthase (DAHPS). Following six enzymatic steps, it ends with the production of chorismate, which is then used to generate three aromatic amino acids (AAAs): tryptophan, phenylalanine, and tyrosine (Yoo et al., 2013). These AAAs are used for protein synthesis and for the synthesis of different secondary metabolites that play a major role in protecting plants from biotic and abiotic stresses (**Supplementary Figure S1**).

Studies have shown that the levels of AAAs are mainly regulated by: (i) the expression levels of genes encoding enzymes in the pathway that are controlled by both developmental and environmental signals (reviewed by Maeda and Dudareva, 2012); (ii) the levels of precursors of the shikimate pathway (PEP and E4P) (Maeda and Dudareva, 2012); (iii) the rate of AAAs catabolism that leads to biosynthesis of their downstream metabolites (Galili et al., 2016); and (iv) the activity of key enzymes in the shikimate and AAAs pathways, namely, DAHPS, chorismate mutase (CM), arogenate dehydratase (ADT), anthranilate synthate (AS), and arogenate dehydrogenase (ADH) that were shown to be regulated allosterically by products of the pathway (Li and Last, 1996; Huang et al., 2010; Tzin and Galili, 2010; Westfall et al., 2014; **Supplementary Figure S1**).

Studies have also shown that under abiotic stresses, the expression levels of genes in the AAAs biosynthesis pathway are up-regulated, leading to higher levels of AAAs and their secondary metabolites, including flavonoids, anthocyanins, betalains, and phenolic acids (reviewed by Tzin and Galili, 2010; Maeda and Dudareva, 2012). Indeed, abiotic stresses such as drought, heavy metal, salinity, high/low temperature, ultraviolet radiation, nutrient deficiencies, wounding, pathogen attacks, and herbicide treatment promote the phenylpropanoids pathway that produced most of these metabolites (Solecka, 1997; Sharma et al., 2012). In addition, high levels of AAAs and their related secondary metabolites were associated with a high tolerance ability of plants to biotic and abiotic stresses (Maeda and Dudareva, 2012; Sharma et al., 2019; Francini et al., 2019). Moreover, salicylate, a product of the shikimate pathway, is involved in the adaptation of plants to the stress conditions (Loake and Grant, 2007; Khan et al., 2015). Thus, the induction of AAAs could potentially contribute directly and indirectly to the stress tolerance of the plants.

A mutant of bacterial DAHPS enzyme (called AroG) that has a substitute of leucine at position 175 with glutamine ($AroG_{175}$) led to the production of phenylalanine feedback-insensitive enzyme (Tzin et al., 2012). Overexpression of this gene led to significantly higher levels of AAAs and their specific secondary metabolites in transgenic *Arabidopsis thaliana*, purple Petunia hybrida V26, tomato *(Solanum lycopersicum)* fruits and grape (*Vitis vinifera*) cell culture (Tzin et al., 2012, 2013; Manela et al., 2015; Oliva et al., 2015).

The objectives of the current study were to study the effect of AroG overexpression on the phenotype of tobacco (*Nicotiana tabacum*) plants and on their metabolic profiling, and to test the ability of AroG transgenic plants in coping with abiotic stresses (salt, drought, and oxidative) and biotic stresses caused by the parasitic plant, *Phelipanche aegyptiaca*.

MATERIALS AND METHODS

Plasmid Construction, Plant Transformation, and Growth

The feedback-insensitive $AroG_{175}$ construct that was used previously to transform *A. thaliana*, petunia, tomato, and grape cells (Tzin et al., 2012, 2013; Manela et al., 2015; Oliva et al., 2015) was used to transform tobacco WT (*Nicotianata tobacum* cv Samsun NN) plants (**Supplementary Figure S2**). Control plants having an empty vector (EV) were generated by transforming WT plants with the plasmid used for AroG cloning (pBART; Tzin et al., 2012) that contain only the kanamycin-resistant gene. For the plant transformation, sterile tobacco seeds were grown on Nitsch media (Duchefa, Netherlands) with 2% (w/v) sucrose in a growth chamber under a 16/8 h light/dark cycle at 25°C. After 4 weeks, leaves from the sterile tobacco plants were transformed, as previously described (Horsch et al., 1985). Transgenic plants were selected on Nitsch media containing 100 mg L^{-1} kanamycin and 400 mg L^{-1} carbenicillin, and the kanamycin-resistant plants were transferred to soil for further growth. To obtained propagate plants, T_0 transgenic AroG and control plants (WT and EV) were propagated from leaves using 2 μM benzyl adenine (BA) and 0.01 μM indole acetic acid (IAA) in MS medium with 3% sucrose. After 4 weeks, developing shoots were removed from the calli to allow rooting in MS medium with 150 mg/L kanamycin. The developing shoots from WT plants were transferred to MS medium without antibiotics. Rooted shoots of similar size and having a similar root system were transferred to soil in 1L pots and were grown in a growth chamber under a 16/8 h light/dark cycle at 25 ± 3°C. For the abiotic stress, 1L pots were grown in a greenhouse during the spring with 20–28°C with no artificial light.

Quantitative Real-Time PCR and Immunoblot Analyses

The protein expression levels of the bacterial AroG were measured in the leaves of 10-week-old transgenic AroG plants that were resistant to kanamycin and in the leaves of WT and EV using immunoblot and antibodies against the three copies of hemagglutinin (3xHA) epitope tag that fused to the AroG gene (**Supplementary Figure S2**). The transcript expression level was measured by quantitative real-time PCR (qRT-PCR), as previously described (Matityahu et al., 2013). Primers used for (qRT-PCR) analyses are listed in **Supplementary Table S2**.

Extraction and Analysis of Primary Metabolites Using Gas Chromatography-Mass Spectrometry (GC-MS)

Primary metabolites were extracted from 20 mg of dried powder from the leaves of the tobacco AroG and the control WT and EV plants. The extraction and derivatization method was employed using norleucine as internal standard (0.2 mg mL^{-1}), as previously described (Cohen et al., 2016). Volumes of 1 μL were injected into the GC-MS column. A set of retention time standards consisting of alkanes of increasing molecular mass dissolved in pyridine were injected after each set of 10 samples. Metabolites were detected using GC-MS, as previously described (Malitsky et al., 2008; Mintz-Oron et al., 2008). The Xcalibur software v.3.1 (Thermo Finnigan) was used for data analysis, and compounds were identified by comparing their retention index (RI) and mass spectrum to those generated by standards and analyzed using the same column and under similar conditions. When standards were not available, compounds were identified putatively by comparing their RI and mass spectrum to those present in the mass spectra GMD VAR5 library of the Max Planck Institute for Plant Physiology, Golm, Germany, and the commercial mass spectra library NIST05[1].

Total Phenolic Compounds Content Determination

For total phenolic compounds content determination, 20 mg dried powder from leaves were ground in 0.5 mL water, and the colorimetric method (Ben Nasr et al., 1996) was employed. Ten microliter of the extraction sample were loaded on a 96 well ELISA plate. To each well, 50 μL of 10% Folin-Ciocalteu reagent and 40 μL of 7.5% (w/v) Na_2CO_3 were added. The plate was incubated for 40 min at 37°C and then read at 765 nm (Infinite M200PRO, Tecan, Grodig, Austria). A standard curve was created using gallic acid in a range of 0.5–10 μ g.

Detection of Phenolic Compounds in Tobacco Leaves Using uHPLC-DAD

Twenty mg of dry tissue were ground in 1 mL distilled water. The extraction was shaken for 40 min at 50°C, then centrifuged for 20 min at 20,000 g. The supernatant was filtered through 0.45 μm filters (Millipore) and kept frozen at −70°C until used. The chromatographic analysis was performed using UltiMate 3000 modules consisting of a solvent delivery module LG-980-02, pump LPG-3400SD, autosampler WP53000TSL, column compartment TCC3000SD and detector DAD3000 UV/vis (Ultimate 3000, Thermo Fisher Scientific). Ten microliter from the water extraction were injected into a Hydro-RP-C18 Synergi column (3 mm × 100 mm, particle size = 2.5 μm, Phenomenex, United Kingdom). Elution was performed at a flow rate of 0.8 mL/min using a mixture of water/Formic acid (99:1 v/v) (A) and acetonitrile (B) as a mobile phase. The run time was 35 min, and the samples were eluted by the following gradient: 100% A and 0% B at time 0, followed by 96% A and 4% B at 3.6 min, 85% A and 15% B for 22 min, 50% A and 50% B at 23 min, 20% A and 80% B from 25 to 28 min, 100% A and 0% B at 32 min until 35 min. Detection was performed at 280 nm.

Detection of Phenylpropanoids Compound in *P. aegyptiaca* and Tobacco Roots Using HPLC and LC-MS/MS Analysis

For phenylpropanoids determination by HPLC, 20 mg of dry tissue were extracted in 80% methanol. The samples were analyzed by injecting 5 μL of the extracted solutions into an uHPLC connected to a photodiode array detector (Dionex Ultimate 3000) with a reverse-phase column (Phenomenex RP-18, 100 mm, 3.0 mm, 2.5 μm). The mobile phase consisted of (A) DDW containing 0.1% formic acid and (B) acetonitrile containing 0.1% formic acid. The gradient started with 5% B for 2 min, then increased to 98% B in 20 min and maintained at 98% B for another 3 min. Phase B was returned to 5% for 2 min and the column was allowed to equilibrate at 5% B for 5 min before the next injection. The flow rate was 0.4 mL/min. The LC-MS/MS analysis was performed with a Heated Electrospray ionization (HESI-II) source connected to a Q Exactive™ Plus Hybrid Quadrupole-Orbitrap™ Mass Spectrometer Thermo Scientific™. ESI capillary voltage was set to 3,500 V, capillary temperature to 300°C, gas temperature to 350°C and gas flow to 35 mL/min. The mass spectra (m/z 100–1,000) were acquired in both negative-ion and positive-ion modes with high resolution (FWHM = 70,000). For MS^2 analysis, the collision energy was set to 15, 50 and 100 EV. For data preprocessing, the peak area integration was performed with Compound Discoverer 3.1 (Thermo Fisher Scientific, Version 3.1.0.305). Several of the compounds, vanillin, ferulic acid, cinnamic acid, chlorogenic acid, caffeic acid, and 4-coumaric acid, were identified based on standards (all standards were purchased from Sigma, except for trans-ferulic acid, which was purchased from TCI, Tokyo Chemical Industry). Other compounds were identified based on the MzCloud database using MS^2 data and the ChemSpider database using HRMS (**Supplementary Table S4**).

Abiotic Tolerance Assays

For the salt tolerance examination, the propagated plants having 6–8 leaves were acclimated in a greenhouse for 2 weeks, and plants of similar size were used for the stress experiments. The experiments were conducted under greenhouse conditions at 20–28°C. The plants were irrigated every 2 days with 250 mL of 150 mM NaCl solution for 21 days. After 21 days of salt stress, the height (cm), total dry biomass (mg) of aerial parts, senescence level (number of yellow and senescing leaves out of total leaves number) and plant vigor score were measured. The vigor score is based on phenotype, whereby "1" is the score for plants having wilting

[1]www.nist.gov

and senescing leaves that were out of full turgor, and "9" is the score for plants that look normal with full turgor. Each line tested was compared to control EV plants under the same stress conditions.

For the oxidative stress assay, 8 mm of discs from the leaves of T_0 propagated transgenic and control plants that were grown in a greenhouse were placed in plates with 0, 1, 2, 5 μM methyl viologen (paraquate) under 80–110 μE light conditions for 20 h. The chlorophyll content of the leaf discs was then measured using ImageJ software[2]. Change was calculated and marked as green level (in%) compared to control (distilled water).

For the drought stress assay, propagated plants were moved to 1L posts in a greenhouse and were irrigated normally for 3 weeks (six developed leaves). To generate the first period of drought stress, irrigation was stopped for 10 days. After 10 days of drought when early morning wilting was observed, senescence level and plant vigor score were measured. The plants were then watered fully for 3 days to full recovery. Followed recovery, a second drought period was applied for 10 days. At the end of the second drought, parameters of height, dry biomass and relative water content (RWC) were measured. For relative water content (RWC), leaf samples (8 mm discs) were floated overnight in deionized water. Turgid weight was determined, and all of the samples were dried at a constant temperature. Dry weight was measured and percent relative water content (RWC,%) was calculated 100* (fresh weight – dry weight/turgid weight – dry weight). RWC was measured with 4–8 biological repetitions.

P. aegyptiaca Tolerance Experiments

Homozygous seeds of WT, EV, AroG lines 2.1 and 3.1 were germinated and grown on Nitsh media (Duchefa) for 3 weeks. Seedlings were transferred to 2-L pots (Tefen Nachsholim, Israel) using medium heavy clay-loam soil containing a dry weight basis of 55% clay, 23% silt, 20% sand, 2% organic matter, pH 7.1 (one plant per pot). Slow-release fertilizer at a concentration of 0.6% (w/v) (Osmocote, Scotts Miracle-Gro, Marysville, OH) and *P. aegyptiaca* seeds at a concentration of 15 ppm (15 mg seeds kg^{-1} soil ∼2,250 seeds kg^{-1}) were added to the soil (Hacham et al., 2016). The above-mentioned components were mixed to homogeneity in a cement mixer for 10 min. The pots were placed in a net house and drip-irrigated. When the tobacco plants were fully developed and flowered, the shoots were cut at the soil surface. The roots were washed gently, removing the soil under tap water, and dried on a paper towel. *P. aegyptiaca* at all developmental stages were collected from each plant, and their numbers and biomasses were recorded. The biomass of the tobacco roots and shoots were also measured.

Statistical Analyses

The data represent the mean of the independent replicates. Statistical significance was evaluated using JMP software version 8.0 (SAS Institute Inc., Cary, NC). Significant differences between treatments were calculated according to the Tukey-Kramer HSD test or the student t-test ($p < 0.05$). Principal component analysis (PCA) was conducted using the MetaboAnalyst 3.0 comprehensive tool[3] (Xia et al., 2015) with auto scaling manipulations. Graphs were compiled using GraphPad Prism 5.01 scientific software[4].

RESULTS

Several Tobacco Plants Having a High Expression of the *E. coli* Feedback-Insensitive $AroG_{175}$ Exhibited a Severe Abnormal Phenotype

To study the impact of high AAAs levels on primary metabolic profile and on the ability of tobacco plants to cope with stresses, we overexpressed the *E. coli* $AroG_{175}$ gene targeted to the chloroplast under the control of the 35S CaMV promoter and octopine synthase terminator (Tzin et al., 2012; **Supplementary Figure S2**). Thirty kanamycin-resistant T_0 tobacco lines were screened for expression of the AroG gene by immunoblot analysis using antibodies against the 3HA epitope-tag that was fused to the AroG gene (**Supplementary Figure S2**). Out of the 30 lines, 22 plants showed a band of the expected 42 kDa polypeptide (**Supplementary Figure S3**). Fifteen plants exhibited a morphological phenotype similar to the empty vector (EV) and wild type (WT) plants that were used as controls. However, seven transgenic lines (**Supplementary Figure S3**) exhibited a severe abnormal phenotype, including slow developmental rate, failure to produce flowers, narrow curled pale leaves and loss of apical dominance (**Figure 1A**). Based on these phenotypes we chose for further analysis, three lines (marked as lines #1–3) that exhibited a normal phenotype and three lines (marked as lines #4–6) that had abnormal phenotypes compared to the EV and WT plants. Due to the inability of the plants having the abnormal phenotype to produce flowers, we propagated the plants using a tissue culture and generated shoots from the leaves of T_0 AroG transgenic plants and from EV and WT plants. The regenerated plants exhibited a phenotype similar to their original transgenic lines. The growth rate of the different propagated plants was measured to show that lines #4–6 have severe growth retardation compared to lines #1–3 and the control plants (**Figure 1B**). To reveal the relationship between the morphological phenotype of the transgenic plants to the AroG protein accumulation, immunoblot analysis was made for comparison of the six selected lines. The immunoblot analysis showed that transgenic lines #4–6 had high protein accumulation, about 7- to 10-fold compared to lines #2–3 (**Figure 2**). Notably, line #1 that showed a high expression level of protein exhibited a normal morphological phenotype.

The severe abnormal phenotype of lines #4–6 could be attributed to the high auxin levels produced from tryptophan. To test this assumption, the expressions levels of two auxin

[2]https://imagej.nih.gov/ij/

[3]http://metaboanalyst.ca/

[4]http://www.graphpad.com/

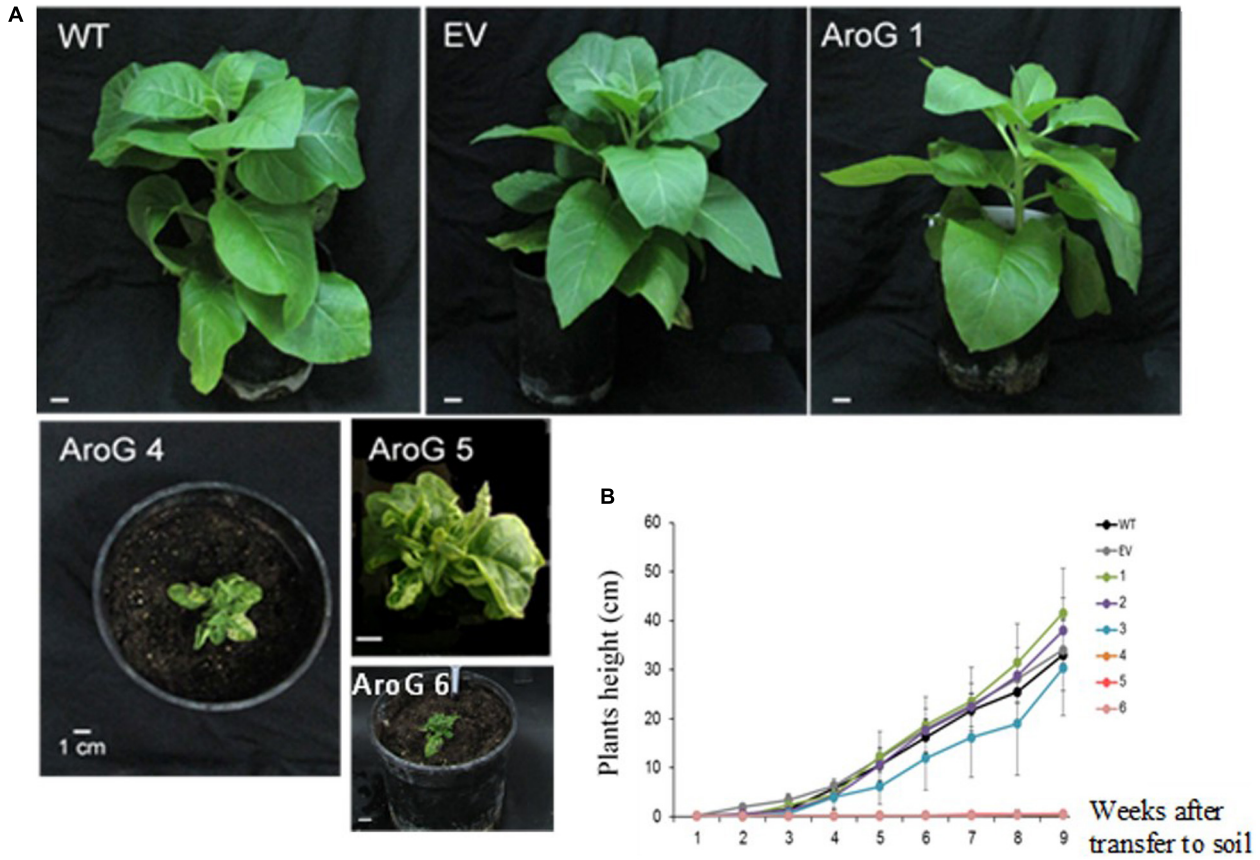

FIGURE 1 | Phenotype of transgenic plants expressing the bacterial AroG gene. **(A)** The photos were taken 9 weeks after transferring to soil. **(B)** Growth rate measurements. Four-week propagated plants were transferred to soil; shoot height was measured every 7 days for a period of nine additional weeks. Data are presented as mean ± SE (n = 4–7). WT, wild type plants; EV, transgenic plants having an empty vector; AroG, plants overexpressing the bacterial AroG gene; that had a normal phenotype (lines #1–3) and an abnormal phenotype (lines #4–6).

response genes were measured using qRT-PCR, but the changes were insignificant compared to those having a normal phenotype. Moreover, feeding experiments carried out on WT plants having different auxin contents did not suggest that the phenotype was due to the higher auxin content (see **Supplementary Text S4** for more details; **Supplementary Figures S4**, **S5)**.

The Levels of Aromatic Amino Acids and Their Associated Metabolites Increased in the Transgenic Plants

To study the effect of higher expression levels of AroG on plant metabolic profiling, GC-MS analysis was used on extracts from the leaves of 10-week-old propagated tobacco plants. Seventy-six metabolites were detected using GC-MS (**Supplementary Table S1**). Principal component analysis (PCA) showed that lines #2–3 having a low AroG protein accumulation were grouped close to the control plants (WT/EV), while lines #1, #4–6 were grouped separately (**Figure 3**). The observation that line #1 was grouped together with lines #4–6, which exhibited an abnormal phenotype, suggested that a high accumulation of AroG protein resulted in a significantly altered metabolic profile. These four lines had significantly higher levels of AAAs compared to WT/EV. The level of phenylalanine increased up to 43-fold, tyrosine up to 24-fold and tryptophan up to 10-fold compared to EV (**Figure 4** and **Supplementary Table S1**). Lines #2–3 had slightly increased levels of AAAs, but with no significant difference compared to EV (**Figure 4** and **Supplementary Table S1**). In addition to AAAs, the levels of shikimate, quinate, and phenylpyruvate (that related to the AAA pathway), significantly increased in lines #1, #4–6 compared to WT/EV (**Figure 4** and **Supplementary Table S1**). The levels of phenylalanine downstream metabolite, 4-hydroxybenzoate, also increased significantly in these lines (**Figure 4** and **Supplementary Table S1**), while phenyllactate and phenylethylamine increased significantly only in lines #4–6, which exhibited an abnormal phenotype (**Figure 4** and **Supplementary Table S1**).

Since the shikimate pathway contributes to the production of phenolic compounds in plants, total phenolic content (TPC) was measured in young leaves. All of the transgenic lines had higher TPC by about 2- to 2.8-fold compared to EV, but with no significant difference between transgenic lines having high AroG expression (lines #1, #4–6) and those with low expression

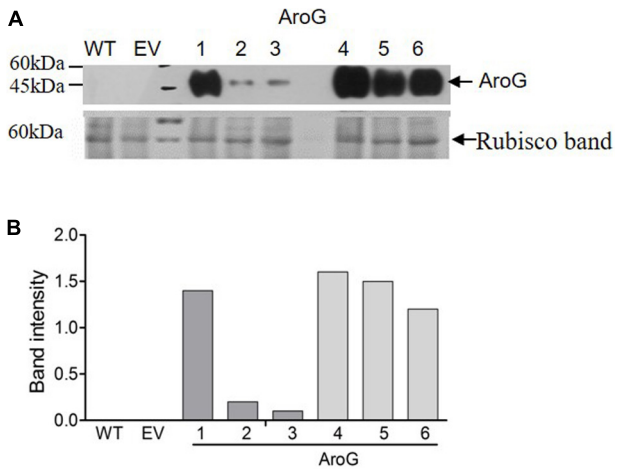

FIGURE 2 | Expression level of bacterial AroG in transgenic tobacco plants. **(A)** Immunoblot analysis of protein extracts from the leaves of WT, EV and transgenic plants expressing AroG using anti-HA antibodies. Lower panel: coomassie brilliant blue staining used for equal loading; the rubisco band is marked by an arrow. The marker size is shown on the left. **(B)** The graph represents band intensity obtained from the immunoblot analysis that was normalized to the rubisco band as measured by ImagJ.

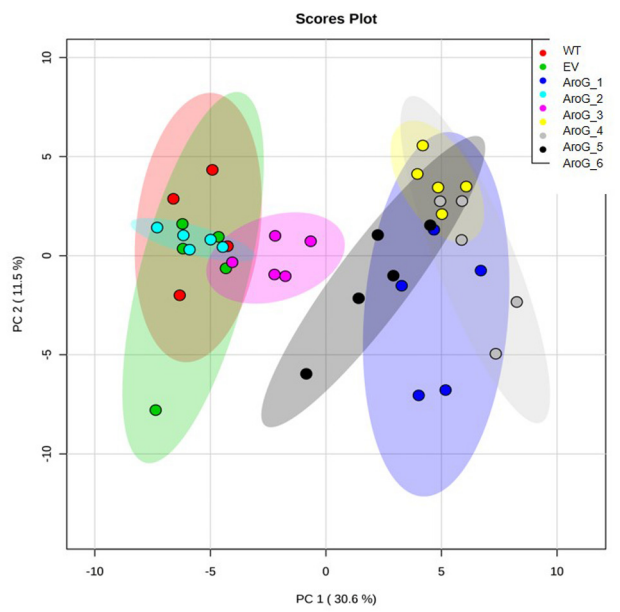

FIGURE 3 | PCA plot of GC-MS data set obtained from the leaves of WT, EV, and transgenic AroG lines #1–6. Variances explained by the first two components (PC1 and PC2) appear in parentheses. WT (n = 4), EV and AroG plants (n = 5).

(lines #2, #3) (**Figure 5**). The similar TPC level in the different AroG lines was unexpected since these lines differ at the levels of AAAs and their associated metabolites. Therefore, we examined the differences between profiles of the phenols using HPLC-DAD at 280 nm. As was shown for the TPC, the HPLC-DAD analysis revealed that AroG lines had higher levels of phenols compared to WT/EV. However, this analysis showed that different phenols increased in the different AroG lines. Lines #4–6 had higher levels of phenols no. 1, 4 and 8, lines #2 and #3 had higher levels of phenol no. 5, and lines #1 and #2 had higher levels of phenol 2 (see **Supplementary Text S6** for more detail; **Supplementary Figure S6**).

The Levels of Most of the Primary Metabolites Did Not Change Significantly in the Transgenic Plants

Since the shikimate pathway and its associated metabolites used about 30% of the photo- assimilate carbon (Maeda and Dudareva, 2012; Galili et al., 2016), we next studied the effect of AroG expression on a wide range of primary metabolites. GC-MS analysis revealed that the changes in AAAs levels in the transgenic lines did not affect most of the other amino acids, with the exception of serine that decreased in lines #1, #4–6, methionine that decreased in lines #4–6, aspartate that increased in line #3, cysteine that increased in lines #1 and #4, and lysine that increased in line #6 (**Figure 6** and **Supplementary Table S1**).

In lines #1, #4–6 having a high AroG protein level, several differences in sugars levels were observed. The levels of threose and xylose were reduced in lines #4–6 compared to WT/EV, while the levels of the other sugars increased, including fructose, glucose, melibiose, β-D-galactopyranoside (in lines #1 and #4), trehalsoe (in lines #1 and #3) and gentabiose (in lines #1, #4 and #6) (**Figure 6** and **Supplementary Table S1**). An increase was also detected in sugar acids, threonate (in lines #4 and #6) and glycerate (in lines #1, #4, and #6) (**Figure 6** and **Supplementary Table S1**). Citrate increased significantly in lines #1, #4–6 while other TCA intermediates didn't change significantly compared to WT/EV (**Figure 6** and **Supplementary Table S1**). The results of the primary metabolites analysis imply that the induction of the shikimate pathway by a high expression of the AroG protein resulted in mild changes in the plants' primary metabolism. Most of the changes were detected in the sugars content.

The Effect of a High Expression Level of AroG on the Ability of the Plants to Cope With Abiotic Stresses

Studies have shown that in response to environmental stresses, plants induce the shikimate pathway and produce higher levels of AAAs and phenolic metabolites (Dixon and Paiva, 1995; Dixon, 2001; Francini et al., 2019; You et al., 2019). However, it is not yet clear if plants having higher levels of these metabolites can be more tolerant to abiotic stress. To obtain more knowledge on this possibility, tobacco lines #1–3, which had higher TPC and a normal phenotype, were tested for their abilities to cope with salt, oxidative and drought stresses.

To test tolerance to salt stress, 3-week-old propagated transgenic lines and EV that were grown on soil were supplemented with 150 mM NaCl. After 21 days, plant height, senescence level, plant vigor (see "Materials and Methods" section) and total dry biomass of the shoots were measured. The results showed that line #1 was more tolerant to 150 mM NaCl compared to EV since it accumulated

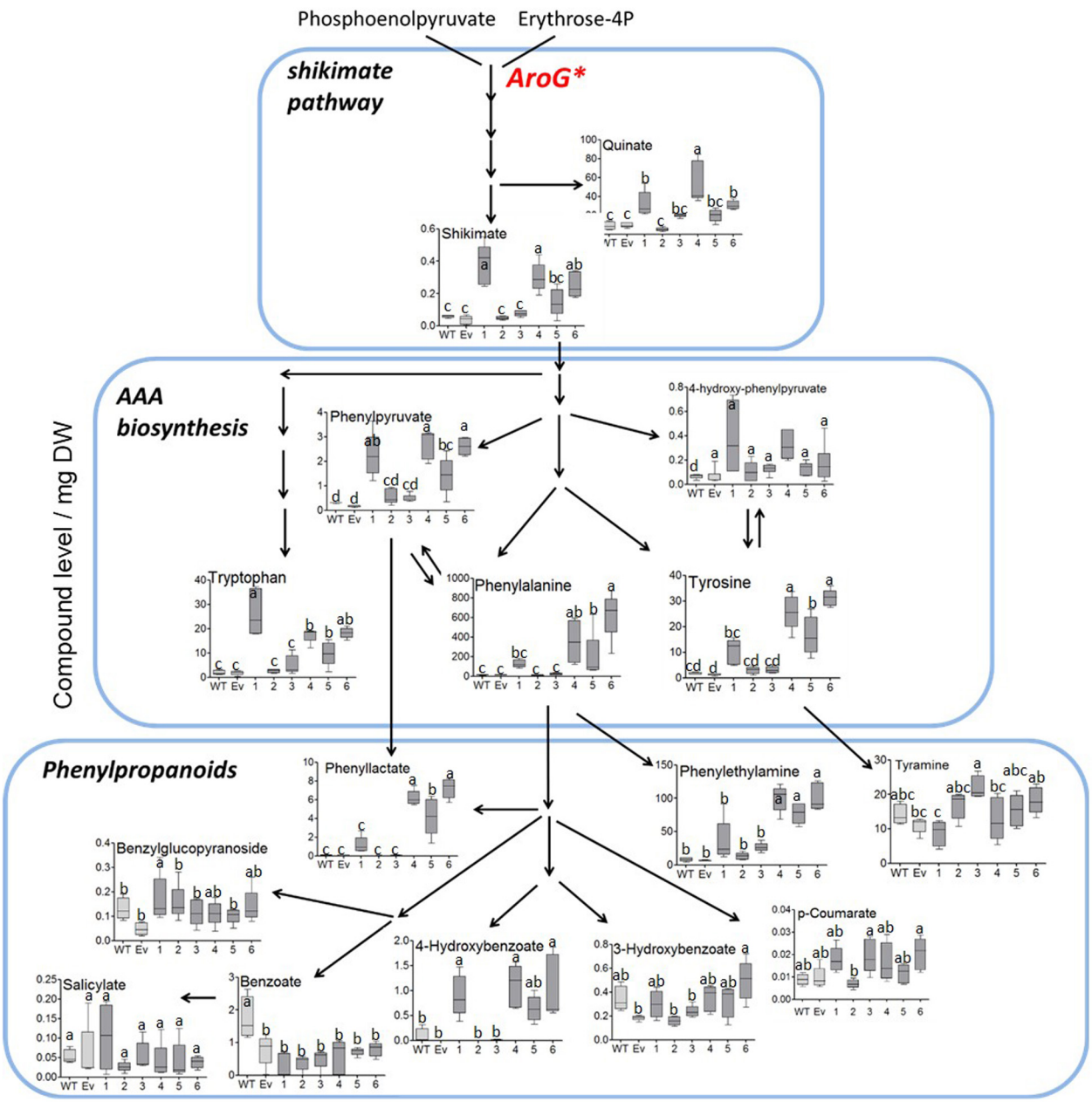

FIGURE 4 | Levels of AAAs and their associated metabolites as detected by GC-MS in the leaves of WT (n = 4), EV (n = 5) and transgenic tobacco AroG lines #1–6 (n = 5). Results are presented on a pathway scheme with the graph representing compound level as the peak area normalized to the internal standard (norleucine) and calculated for 1 mg of dry weight (DW).

3.5-fold more biomass, had improved vigor (2-fold), and had less senescence phenotype (3-fold lower) compared to EV (**Figure 7**). Although lines #2 and #3 had a biomass similar to EV, line #2 showed significantly higher tolerance in the height and plant vigor parameters (1.7-fold higher in both) (**Figure 7B**).

The ability to cope with oxidative stress was also examined in the leaves. The transgenic lines showed high TPC, which could function as scavengers of reactive oxygen species (Das and Roychoudhury, 2014). Leaf discs were exposed to oxidative stress caused by methyl viologen. Bleaching content resulting from chlorophyll degradation was calculated and marked as% of green level compared to non-oxidative conditions. Leaf discs of line #1 had similar bleaching to EV discs in 1 μM methyl viologen (labeled pq), but when exposed to 2 μM and 5 μM methyl viologen, they were less bleached [95 and 90% green level of that detected in the control of non-treated plants (0 pq)], compared to EV (having 80% green level of its control)

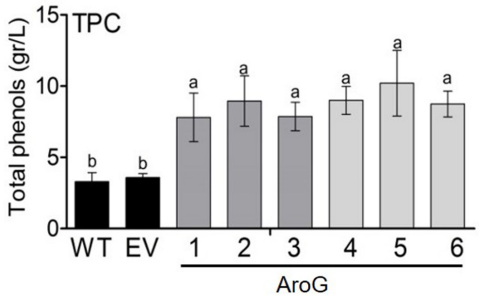

FIGURE 5 | Total polyphenol content (TPC) in the leaves of transgenic plants overexpressing the bacterial AroG gene and EV/WT. TPC is represented as g gallic acid equivalents per liter of water extract. Data are presented as the mean ± SE of four biological repetitions. Different letters represent statistical significance ($p \leq 0.05$) which was determined using the Tukey-Kramer test.

(**Supplementary Figure S7**). At 2 and 5 μM methyl viologen, line #2 had 84 and 87% green level of its control, and line #3 had 93 and 87% green level of its control, but these values were insignificant compared to the bleaching of EV at 2 and 5 μM methyl viologen (**Supplementary Figure S7**).

For drought stress experiments, we used plants of similar size and age. The plants were irrigated normally for 3 weeks (4–6 developed leaves), afterward the irrigation was stopped for 10 days. Parameters of senescence level and plant vigor score were measured (**Supplementary Figure S8**). The plants were then watered fully for 3 days to full recovery, and a second drought period commenced for 10 days. At the end of the second drought, parameters of height, dry biomass and relative water content (RWC) were measured (**Supplementary Figure S8**). The data showed that AroG lines did not exhibit improved tolerance to drought compared to EV, as lines #1 and #2 resembled EV in all of the parameters that were measured. Line #3 had an improved vigor score by 1.6-fold compared to EV and a 40% lower senescence level (**Supplementary Figure S8**).

The Transgenic AroG Plants Were More Tolerant to the Parasitic Plant, *P. aegyptiaca*

It had been found previously that the application of higher levels of certain amino acids can inhibit the germination of the obligate parasite, *Orobanche ramosa* seeds (Vurro et al., 2006; Fernández-Aparicio et al., 2013, 2017). This suggests that high levels of amino acids can alter the parasite metabolism and cause growth inhibition. These findings encouraged us to determine whether the AroG lines would be more tolerant to *P. aegyptiaca*, a close relative of *O. ramosa*. *P. aegyptiaca* is an obligatory root parasite lacking chlorophyll that parasitizes many dicotyledonous crops, causing tremendous losses in crop yield and quality worldwide (Joel et al., 2007).

To test the tolerance of the transgenic plants to *P. aegyptiaca* infection, homozygous plants of the second generation, offspring of line #2 (#2.1) and line #3 (#3.1) with normal phenotypes, were used. Although the levels of AAAs were not significantly altered in the parents of these lines compared to WT/EV (**Figure 4**), in the leaves of these homozygous lines, #2.1 and #3.1, the level of tyrosine significantly increased by 3.3- to 3.5-fold, and the level of phenylalanine significantly increased by 2- to 3.8-fold compared to EV (**Supplementary Table S3**). The level of tryptophan, however, did not significantly changed. Since *P. aegyptiaca* is a root parasite, we also measured the levels of these AAAs in the roots of lines #2.1, #3.1, to define that compared to the roots of EV, the levels of tryptophan increased by 1.5- to 2-fold, tyrosine by 4- to 6-fold, and phenylalanine by 5- to 6-fold, respectively (**Figure 8**). The levels of AAAs were similar in WT and EV plants (**Supplementary Table S3**). Four-week-old transgenic plants and their controls (WT/EV) were transferred to soil mixed with seeds of *P. aegyptiaca*. Twelve weeks later, *P. aegyptiaca* inflorescence started to emerge from the ground. The numbers of *P. aegyptiaca* inflorescence that emerged from the ground were counted every week over a period of 4 weeks. The results showed that at the first week of measurement, the numbers of parasites in the pots of lines #2.1 and #3.1 were 30 and 20% lower, respectively, compared to those detected in the pots of WT/EV (**Figure 9A**). At week 4, the numbers of parasites were 60 and 40% lower, respectively, compared to the WT/EV pots (**Figure 9A**). A difference was also detected in the developmental state of the parasite that had delayed development on the AroG lines. *P. aegyptiaca* that developed on AroG lines were at a stage of underground pre-emergent or post-emergent shoots with flower buds, while most of the *P. aegyptiaca* that developed on WT/EV were fully flowered (**Figure 9B**).

At the end of the experiment (4 weeks from the time that *P. aegyptiaca* inflorescence started to emerge from the soil), the roots of the tobacco plants were washed from the soil in order to count the total number of *P. aegyptiaca* that were attached to the roots, including those that remained underground. The results showed that the total *P. aegyptiaca* number in lines #2.1 and #3.1 pots was lower by 42–61%, respectively, compared to EV but did not differ from WT (**Figure 9C**). Due to the observation that the *P. aegyptiaca* grown on lines #2.1 and #3.1 were less developed than those grown on WT/EV, the biomass of total *P. aegyptiaca* was measured. The biomass was lower by 54–73% in pots of lines #2.1 and #3.1, respectively, compared to the control (**Figures 9C,D**). Notably, some of the edges of the parasites' inflorescences attached to the roots of these AroG lines exhibited a brown/black color and looked damaged, and they were unable to develop further (**Figure 9E**). These data demonstrate that *P. aegyptiaca* growth was significantly inhibited when it was attached to AroG plants.

To show indications of reasons for the inhibition effect, the shoots of *P. aegyptiaca* were analyzed for the levels of AAAs by GC-MS. The level of tryptophan was significantly higher by 1.9- and 2-fold in *P. aegyptiaca* that were grown on lines #2.1 and #3.1, respectively, compared to those grown on EV. However, the level of

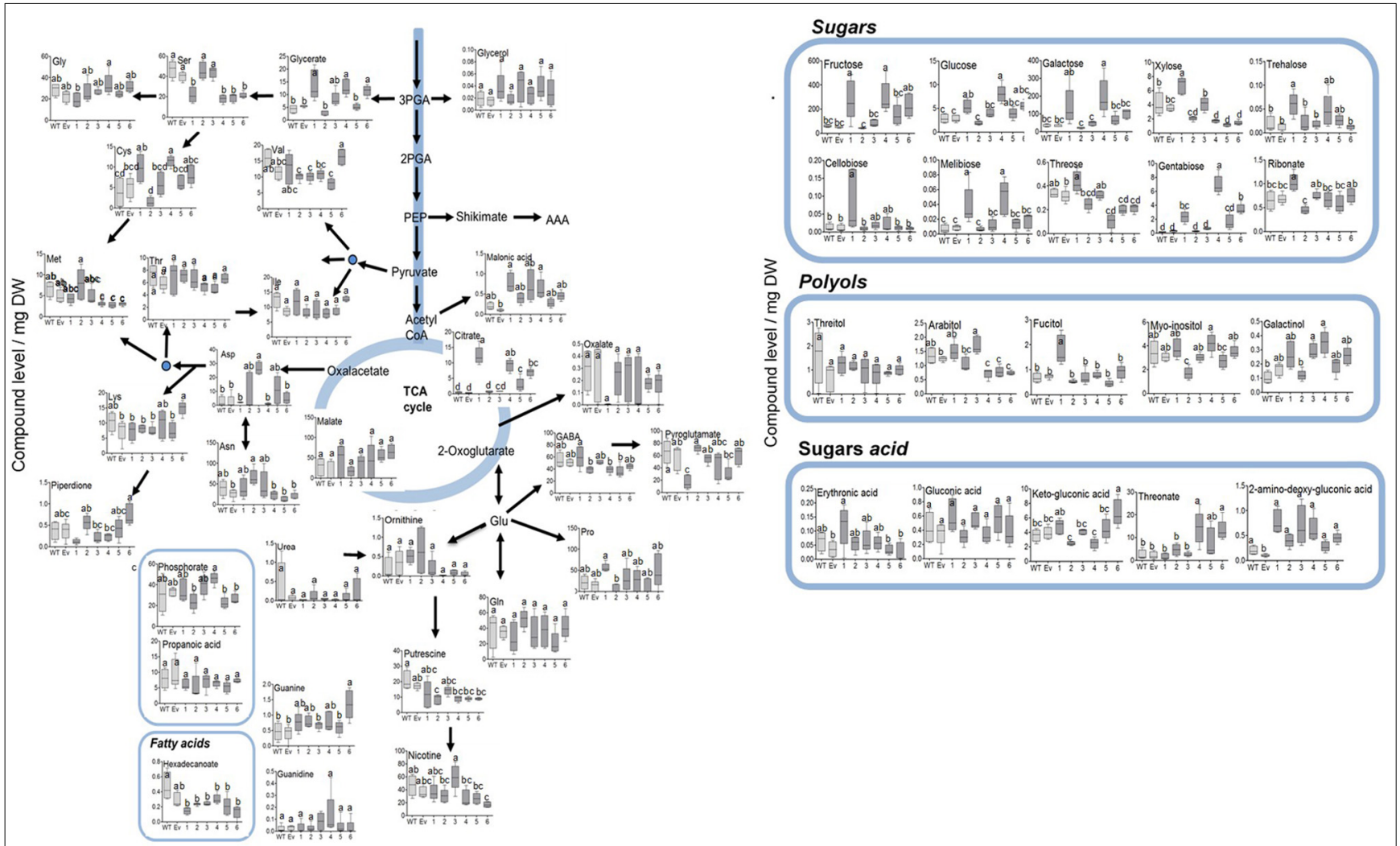

FIGURE 6 | Primary metabolites profile of plants overexpressing the bacterial AroG gene. Metabolites analysis was performed using GC-MS in the leaves of WT (n = 4), EV (n = 5), and transgenic tobacco AroG lines #1–6 (n = 5). Data represent compound level as the peak area normalized to the internal standard (norleucine) and calculated for 1 mg of dry weight (DW).

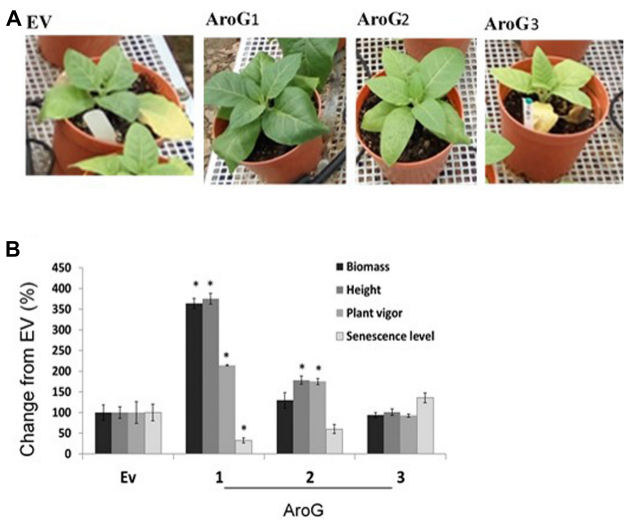

FIGURE 7 | The ability of the transgenic plants overexpressing the bacterial AroG to cope with salt stress. **(A)** The phenotype of representative plants from each group 21 days after the salt-stress (150 mM) period. **(B)** The graph shows the% changes in different growth parameters of AroG lines #1, #2, #3 (n = 8–10) from EV (n = 7) 21 days after irrigation with 150 mM salt. EV is marked as 100%. Data are presented as the mean (±) SE. Significance ($p \leq 0.05$) compared to EV is marked by asterisks.

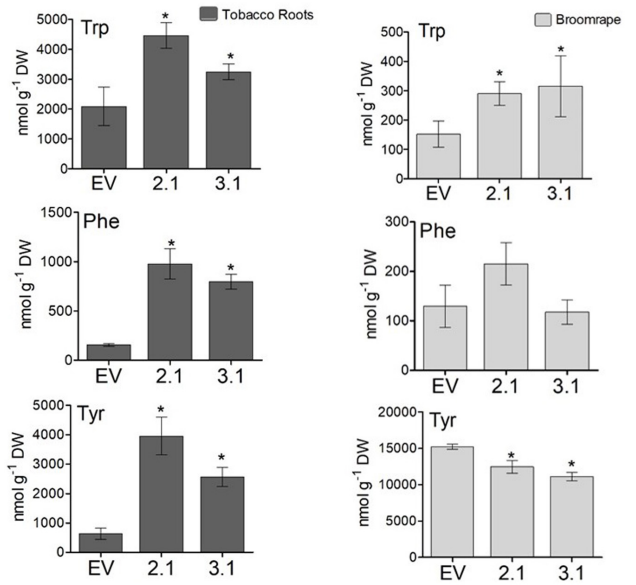

FIGURE 8 | The levels of aromatic amino acids in the roots of the transgenic plants overexpressing the bacterial AroG gene and in *P. egyptiaca*. The levels of AAAs were detected by GC-MS analysis in the roots of AroG lines #2.1 and #3.1, in EV (dark gray) and in *P. aegyptiaca* (light gray). Data are presented as the mean ± SE of five different tobacco plants or of *P. aegyptiaca* that were collected from five different pots. Asterisks represent statistical significance ($p \leq 0.05$) compared to the control (EV) was determined using the Student's t-test.

phenylalanine did not differ significantly between these lines, and the level of tyrosine decreased slightly but significantly by 19 and 26% in *P. aegyptiaca* grown on #2.1 and #3.1 plants, respectively (**Figure 8**). The levels of AAAs were similar in *P. aegyptiaca* grown on WT and EV (**Supplementary Table S3**).

The AAAs can be used in *P. aegyptiaca* to produce phenols and other metabolites that might accumulate and thus inhibit the growth of the parasite. Hydroxycinnamic acid compounds that belong to the phenylpropanoids may affect growth retardation, since feeding analysis with these compounds showed that they can reduce the radicle growth of *O. crenata* (Fernández-Aparicio et al., 2013). Therefore, we measured the levels of several phenylpropanoids in the tobacco roots and in *P. aegyptiaca* plants using LC-MS/MS. The results showed that the levels of several phenylpropanoids contents were changed. Compared to EV roots, the roots of line #3.1 had a significant increase in the levels of caffeic acid (1.9-fold), quinic acid (1.7-fold), chlorogenic acid (1.9-fold) and ferulic acid isomer (1.9-fold). The levels of these compounds also increased in the roots of line #2.1, although the elevation did not differ significantly from WT/EV (**Figure 10** and **Supplementary Table S4**). We assumed that the high levels of AAAs and phenylpropanoids found in the #3.1 roots could affect the levels of phenylpropanoids in *P. aegyptiaca* grown on this line. To test this assumption, this analysis was also performed on the parasite shoots. *P. aegyptiaca* grown on line #3.1 showed significantly higher levels of two isomers of caffeic acid (3.4- and 4.1-fold), 4-hydroxycinnamaldehyde (2.9-fold), coumarin (2.3-fold), and comaric acid (2.7-fold) compared to those grown on EV (**Figure 10** and **Supplementary Table S4**). *P. aegyptiaca* that were grown on line #2.1 showed a similar trend, although the elevation was not significant compared to those grown on WT/EV (**Figure 10** and **Supplementary Table S4**). Unlike these elevations, the level of two isomers of sinapinic acid decreased significantly by 65 and 77% for isomer a, respectively, and 35 and 53% for isomer b in *P. aegyptiaca* that were grown on transgenic lines #2.1 and #3.1, respectively, compared to the EV control (**Figure 10**). Although these changes in phenylpropanoids levels, the levels of total phenols content (TPC) inside the parasite was not significantly altered in *P. aegyptiaca* that were grown on AroG lines and those grown on WT/EV (**Supplementary Figure S9**).

The normal development of the host plants is usually impaired when they are infected by *P. aegyptiaca*. Therefore, we measured the weights of the tobacco plants to find out that the shoots and roots weights of lines #2.1 and #3.1 were similar to WT/EV (**Figure 11A**). However, the infected WT/EV plants developed a small number of abnormal flowers (**Figure 11B**), unlike lines #2.1 and #3.1 that developed normal inflorescences and flowers (**Figures 10B**, **11B**). Accordingly, total flower weight was 10- to 25-fold higher, at these transgenic lines compared to WT/EV (**Figure 11C**). This phenotype, together with the lower levels of inflorescence shoots of the parasite that emerged from the ground, suggest that the transgenic lines are more tolerant to the parasite than the WT/EV control plants.

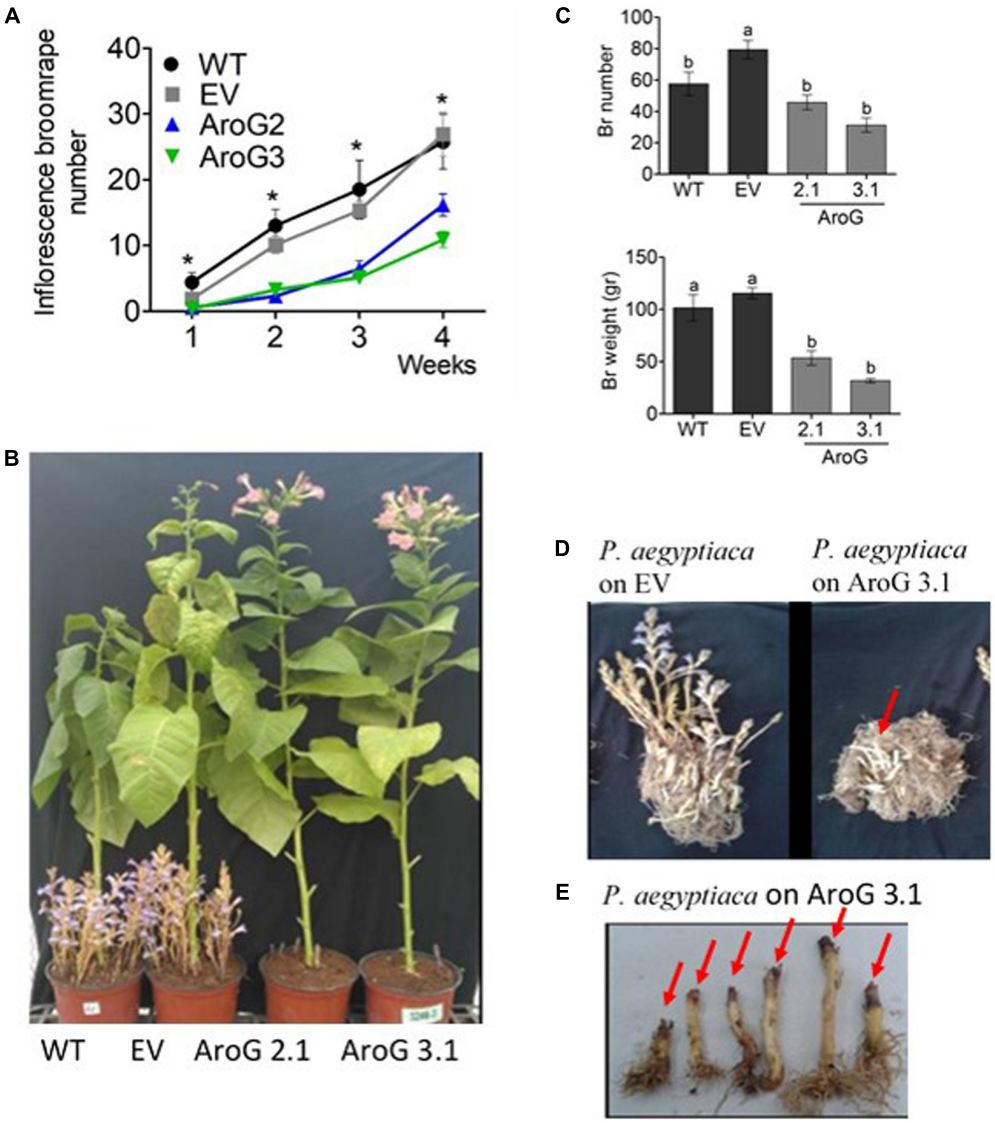

FIGURE 9 | Phenotype of *Phelipanche aegyptiaca* that grew on homozygous AroG lines #2.1 and #3.1. **(A)** Inflorescence *P. aegyptiaca* number emerging from the soil per pot over 4 weeks. The count begins when the first *P. aegyptiaca* shoot emerged from the soil. Significant difference between WT/EV and AroG lines was determined using the Student's *t*-test ($p < 0.05$) and is marked by asterisks. **(B)** Representative of photos showing the phenotype of *P. aegyptiaca* grown on AroG lines #2.1 and #3.1 and the control WT/EV at the end of the experiment (4 weeks from the time that *P. aegyptiaca* inflorescence started to emerge from the soil). **(C)** Weight and number of *P. aegyptiaca* per pot. Measurements were taken after the roots of the tobacco plants were washed from the soil and all of the *P. aegyptiaca* were collected. Different letters represent statistical significance ($p \leq 0.05$) using the Tukey-Kramer test. Data are presented as the mean ± SE of *P. aegyptiaca* that were collected from 6 to 8 different tobacco plants for each set. **(D)** The phenotype represents tobacco roots and *P. aegyptiaca* developed on EV and on transgenic tobacco line #3.1. The red arrow marks *P. aegyptiaca* attached to the roots that did not emerge from the soil. **(E)** The phenotype represents inflorescence shoots of *P. aegyptiaca* grown on line #3.1. The red arrow marks the black edges of *P. aegyptiaca*.

DISCUSSION

The Effect of High Expression Level of AroG on the Phenotype of Tobacco Plants

Unlike transgenic *A. thaliana* and petunia plants overexpressing the bacterial AroG gene, which showed a similar morphological phenotype to their control plants (Tzin et al., 2012; Oliva et al., 2015), about 30% of the transgenic tobacco plants showed a severely abnormal phenotype (**Figure 1**). All of the plants with an abnormal phenotype (lines #4–6) had high protein expression levels of AroG, while plants with a normal phenotype were divided into two sub-set: those with low expression of AroG protein (e.g., lines #2–3); and those with high expression (e.g., line #1). The reason for the abnormal phenotype is still unknown, but since the level of tryptophan, the precursor for auxin synthesis, significantly increased in

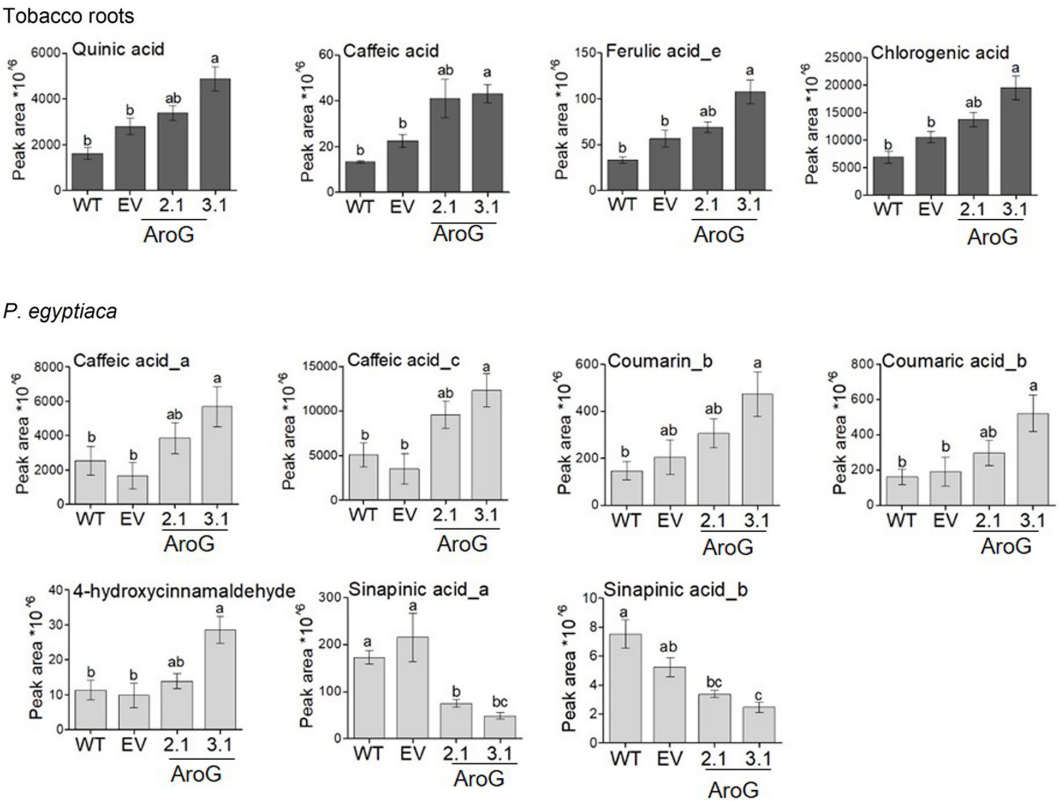

FIGURE 10 | Levels of phenylpropanoids as detected by LC–MS/MS analysis in roots and in the parasite. Levels of the compounds in transgenic AroG lines #2.1 and 3.1, EV and WT (dark gray) and *Phelipanche aegyptiaca* attached to the roots of these plants (light gray). Data are presented as the mean ± SE of six different plants. Different letters represent statistical significance ($p \leq 0.05$), which was determined using the Tukey-Kramer test. The figure shows only the phenylpropanoids that changed significantly.

transgenic lines #4–6 (**Figure 4**), we tried to determine if auxin is involved. No significant evidence was found for a higher level of auxin in AroG tobacco lines. Thus, we assumed that the abnormal phenotype in lines #4–6 results from a high accumulation of AAAs and their associated secondary metabolites (**Figure 4**). This assumption was supported by an analysis of transgenic *A. thaliana* plants expressing a mutated gene of arogenate dehydratase 2 (ADT2), the last enzyme in the phenylalanine biosynthesis pathway called *padt*2-1D. These plants had a 70-fold increase in phenylalanine, 67-fold increase in tryptophan and 9.8-fold increase in tyrosine levels compared to WT. In addition, the levels of salicylic acid and several metabolites related to phenylpropanoid increased significantly (Huang et al., 2010). The *padt*2-1D transgenic plants exhibited a relatively similar phenotype to transgenic tobacco lines #4–6, which included an altered rosette leaf morphology as the leaves were narrower with curled edges, and some plants in the segregating populations also had a dwarf phenotype and didn't produce seeds (Huang et al., 2010). A similar morphological phenotype was also exhibited in *A. thaliana* plants that overexpressed ADT4 or ADT5, as they had a dwarf phenotype with narrow, small and curled leaves, and some plants were sterile (Chen et al., 2016).

The Effect of High Expression Level of AroG on the Metabolic Profile of Tobacco Plants

The primary and secondary metabolites that were detected on tobacco leaves showed a positive correlation between AroG protein accumulation and metabolites that related to the shikimate pathway, AAAs, and their derived metabolites (**Figure 4**). Similar results were obtained when AroG was overexpressed in other plants and tissues (*A. thaliana*, petunia, tomato fruit and grape cell culture; Tzin et al., 2012, 2013; Manela et al., 2015; Oliva et al., 2015). As we had found for tobacco lines #1 and #4–6, the levels of all three AAAs increased significantly in the leaves of transgenic AroG petunia plants compared to control plants (**Table 1**; Oliva et al., 2015). Expressing this heterologous gene in *A. thaliana* and red tomato fruits resulted in significantly increased levels of phenylalanine and tryptophan compared to control, while tyrosine was not altered significantly (**Table 1**; Tzin et al., 2012, 2013). In the grape cell culture, only phenylalanine and tyrosine increased (**Table 1**; Manela et al., 2015). These data show that the expression of AroG mostly affected the level of phenylalanine. In addition to the accumulation of AAAs, the increased levels of shikimate in tobacco, *A. thaliana* and

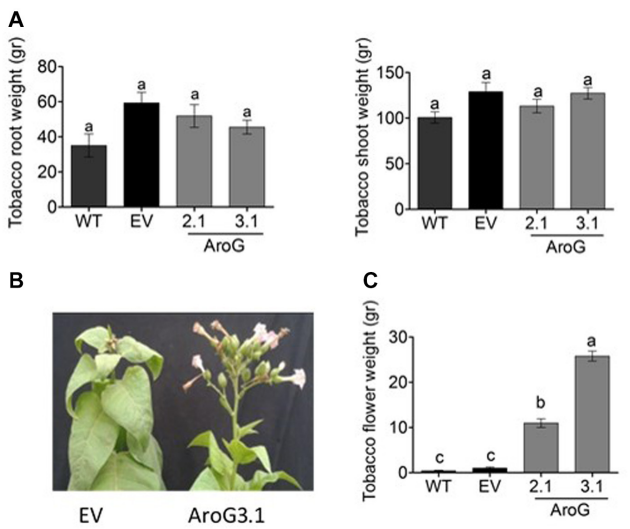

FIGURE 11 | Phenotype of homozygotes AroG lines # 2.1 and #3.1 and WT/EV that were infected by *Phelipanche aegyptiaca*. **(A)** Weights of shoots and roots of the tobacco plants. **(B)** Represents the edge of the shoots and inflorescence of the tobacco EV and AroG line #3.1 plants. **(C)** Weight of tobacco flowers. Data are presented as the mean ± SE of total flowers that were collected from 6 to 8 plants for each set. Different letters represent statistical significance ($p \leq 0.05$), which was determined using the Tukey-Kramer test.

ripe red tomato fruits that expressed AroG (**Table 1**) indicate that DAHPS serves as a major regulator of flux throughout the shikimate pathway.

The high levels of AAAs found in AroG tobacco plants affected the levels of their downstream secondary metabolites since the levels of the phenylalanine-derived metabolites, phenyllactate, 4-hydroxybenzoate and phenylethylamine, accumulated in AroG plants compared to the control (**Figure 4**). This is in accordance with other transgenic plants and tissues overexpressing the AroG gene, although in each plant species or tissue type, different metabolites that are driven from the AAAs were altered (**Table 1**). Taken together, the data suggest that the overexpression of the bacterial AroG gene significantly enhanced flux toward the shikimate pathway, resulting in higher levels of AAAs and their associated secondary metabolites, which change depending on the different regulatory points and the biosynthesis genes found in these plants.

The primary metabolic profile of tobacco plants showed that although transgenic lines #1 and #4–6 had a significant increase in AAAs, only mild changes were observed in the contents of other amino acids (**Figure 6** and **Supplementary Table S1**). Most of the soluble amino acids did not change significantly compared to WT/EV, with the exception of serine, which decreased, most probably since it is used for the tryptophan biosynthetic pathway as a nitrogen source (Tzin and Galili, 2010), and methionine, a member of the aspartate family amino acids, which decreased in lines #4–6, indicating a possible interaction between the aspartate family and AAA metabolic networks. The mild effect of increased AAAs content on other amino acids was also detected in *A. thaliana* and petunia, which overexpressed AroG. In *A. thaliana* seedlings, only alanine increased significantly (Tzin et al., 2012), while in petunia leaves, the levels of glutamine and asparagine decreased (Oliva et al., 2015). These two amino acids are nitrogen donors in the final step of keto-acid conversion into

TABLE 1 | The effect of AroG expression on the levels of shikimate pathway metabolites and AAAs secondary metabolites in different transgenic plants.

	Shikimate	Phenylalanine	Tryptophan	Tyrosine	Shikimate metabolites and AAAs derivatives secondary metabolites	
Tobacco leaves	> 7	>43	> 10	>24	Quinate, Phenylpyruvate, 4-hydroxybenzoate, Phenyllactate and Phenylethylamine	
A. thaliana Seedling	> 30	>180	> 2.6	NS	Prephenate, Phenylacetonitrile, homogentisate, 4-Hydroxybenzoate, Coumarate hexose derivatives, Ferulate hexose derivatives, Ferulic acid derivatives, Sinapoyl hexose derivative, sinapate, Sinapyl alcohol, Coniferin, 2-phenylethyl glucosinolate, 4-Methoxyindole glucosinolate	Tzin et al., 2012
Petunia leaves	NR	> 122	>8	>14	Phenyllactate, Prephenate, 5 trans Caffeoyl quinate, 4 Caffeoyl Quinate, rosmarinate, Salysilate Glucopyranoside, Sinapate, trans- Caffeate, 1 Benzylglucopyranoside, 3,4-Hydroxyphenyllactate, Tocopherol, Pyrogallol, Dihydroxyphenylalanine, Ferulate, Hydroquinone	Oliva et al., 2015
Tomato fruits Ripe red	> 62	> 88	> 4	>171	3-Caffeoylquinic acid, 4-Caffeoylquinic acid, Coumaric acid, Coumaric acid hexoside or derivative, Kaempferol-glucose-rhamnose, Naringenin chalcone, Tricaffeoylquinic acid	Tzin et al., 2013
Grape cell culture	> 3.5	>40	ND	> 800	Phenylpyruvate, 3-hydroxy phenylacetate, Hydroquinone, 4-Hydroxyphenyl b-glucopiranoside, Coumarate, Resveratrol, 4-Hydroxy-benzoate, Dihydroquerccetin, Epicatechin	Manela et al., 2015

Data are given in fold change above the control. NS, not significant; NR, not reported.

phenylalanine and tyrosine (Oliva et al., 2015). Mild changes in the levels of amino acids were also detected in transgenic *padt2-1D A. thaliana* lines, in which the increased levels of AAAs were accompanied by elevated levels of arginine, valine, and leucine (Huang et al., 2010).

The expression of AroG had a more significant effect on the sugars profile. In tobacco lines that highly expressed AroG, there was an increase in the levels of several sugars such as fructose, glucose, trehalose, melibiose, β-D-galactopyranoside, and gentabiose (**Figure 6** and **Supplementary Table S1**). All of the above-mentioned sugars and additional sugars increased in the leaves of two petunia lines that overexpressed AroG (Oliva et al., 2015). Unlike tobacco and petunia, transgenic *A. thaliana* seedlings showed no significant changes in their sugars levels (Tzin et al., 2012).

Overall, the data of the primary metabolic profile indicate that enhanced shikimate pathway activity in tobacco plants mostly increase the carbon metabolites (e.g., sugar, TCA cycle and shikimate) and less the nitrogen metabolites (e.g., amino acid and polyamines). Based on the results obtained from other transgenic plants, the effect of AroG on the metabolic profiling varies between different genotypes.

Contribution of High AAA Levels to Abiotic Stress Tolerance

Plants, in response to abiotic stresses (such as salt, drought or oxidative), induce the shikimate pathway and its downstream metabolites (AAAs and phenylpropanoids) to gain better adaptability to the stress (Dixon and Paiva, 1995; Pandey et al., 2015; Francini et al., 2019; Sharma et al., 2019). An example of the effect of a high level of AAAs in stress response comes from a recent study showing that the direct or indirect application of phenylalanine can increase tolerance to the fungal pathogen *Botrytis cinerea* in tomato and petunia leaves by enhancing the levels of anti-fungal phenylalanine-derived metabolites (Oliva et al., 2019). Also, when tryptophan was added to the growth medium of *A. thaliana* seedlings, it was revealed that they were more tolerant to stress caused by cadmium (Cd), a phytotoxic metal in soils (Sanjaya et al., 2008). In accordance, tryptophan-overproducing *trp5-1* plants were more tolerant to Cd while tryptophan auxotroph *trp2-1* was more sensitive to Cd (Sanjaya et al., 2008).

To determine if AroG tobacco plants would be more tolerant to abiotic stress, we tested lines #1–3 for their ability to cope with salt, oxidative and drought stresses. Line #1, which accumulated a high level of AroG protein and high contents of AAAs and their derivatives, showed improved salt tolerance in all tested parameters, line #2 exhibited higher levels of only two parameters, and line #3 did not show an advantage over the control WT/EV plants (**Figure 7**). The higher ability of AroG line #1 might be related to the observation that it had slightly higher levels of proline and sugars (**Figure 6**), which are known to function as osmolytes (Bolouri-Moghaddam et al., 2010; Verslues and Sharma, 2010). *A. thaliana* transgenic plants that overexpressed the mutant gene of *adt2* and accumulated high levels of phenylalanine also exhibited enhanced tolerance to salt stress as detected by its root length (Huang et al., 2010), suggesting that higher levels of phenylalanine contributed in some manner to salt tolerance. An efficient response in a plant to salt stress demands a multifactor response (Francini et al., 2019), therefore, it could be that changes in several metabolites that associated to the phenylpropanoids together contributed to better performance of AroG line #1 under stress.

In response to oxidative stress, the data indicate that AroG plants could have a minor advantage over WT/EV. This could be the result of increased TPC levels found in AroG plants, since phenols have ROS scavenging activity (Das and Roychoudhury, 2014). The response to drought stress did not show a significant advantage of AroG lines over the control plants, suggesting that the metabolic changes in tobacco AroG are less effective in adaptation to this stress.

The Transgenic Plants Were More Tolerant to Infection Caused by *P. aegyptiaca*

Infection of AroG plants with *P. aegyptiaca* showed that plants with a high level of AAAs can inhibit the development of the parasitic plant. The inhibitory activity of certain amino acids on the germination and growth of broomrape (*P. ramose*, *Orobanche crenata,* and *Orobanche minor*) has been previously studied by adding certain amino acids to the growth media (Vurro et al., 2006; Fernández-Aparicio et al., 2013, 2017). For example, the application of exogenous methionine to the soil caused a strong reduction in the number of emerged *P. aegyptiaca* shoots, as well as in their dry and fresh weights, without causing a significant effect to the tomato plants host (Vurro et al., 2006). Similarly, when applied to tomato roots, methionine strongly reduced the number of developed tubercles of *P. ramosa* (Vurro et al., 2006). The inhibitory effect on germination and radicle growth was also found when each of the AAAs were added to the growth medium of *O. minor* (Fernández-Aparicio et al., 2017). Field experiments showed that irrigation with 20 mM tryptophan led to a 39% reduction in *O. minor* emergence above soil compared to the control (Fernández-Aparicio et al., 2017). Tryptophan added to the growth medium also inhibited *O. crenata* radical growth (Fernández-Aparicio et al., 2013). These findings suggest that certain amino acids applied exogenously can inhibit the growth of the parasitic plants. However, these previous studies used feeding experiments and not plants that have higher endogenous levels of amino acids.

In the current study, we demonstrated the potential of plants having a high level of AAAs to inhibit the growth of the parasitic plant *P. aegyptiaca*, without significantly affecting the phenotype of the host. The transgenic tobacco AroG lines were more tolerant to the parasitic plants, since, unlike EV and WT, the infected AroG lines had normal development and they had flowers. The growth of the parasitic plants was inhibited in the AroG lines as they had a significantly lower number of inflorescent shoots compared to WT/EV. Moreover, part of the *P. aegyptiaca* apical meristem turned black and their development ceased.

Although AroG roots accumulated higher levels of all three AAAs compared to WT/EV plants, the parasitic plants accumulated higher amounts only of tryptophan, while the level of phenylalanine remain unchanged and that of tyrosine decreased (**Figure 9**). Therefore, we assume that the inhibition of *P. aegyptiaca* development is due to changes in AAAs-derived metabolites. Support of this assumption comes from observations that *O. cumana* that grow on resistant sunflower plants accumulated higher phenolic compounds compared to *O. cumana* that grow on susceptible sunflower plants (Echevarría-Zomeno et al., 2006). Furthermore, the addition of scopoletin to the growth medium inhibits *O. crenata* seed germination and radicle growth and causes cell necrotic-like darkening in young radicles (Fernández-Aparicio et al., 2013). This metabolite is derived from the phenylpropanoid pathway and synthesized via cinnamates, and can accumulate in different plant species such as *A. thaliana* and cereal roots (Baghestani et al., 1999; Kai et al., 2008). The inhibitory effect of shikimate pathway-derived metabolites on plant growth was also seen when exogenous applications of three hydroxycinnamic acids, caffeic acid, p-coumaric acid and ferulic acid, induced a reduction in *O. crenata* radicle growth (Fernández-Aparicio et al., 2013). The roots of lines #3.1, which exhibit the highest tolerance to *P. aegyptiaca*, had significant higher levels of caffeic acid, ferulic acid, quinic acid and chlorogenic acid compared to WT/EV roots, indicating that the accumulation of these metabolites in the roots of the host plants can affect the growth of the parasitic plants. In addition, caffeic acid, coumarin, coumaric acid and 4-hydroxycinnamaldehyde were elevated in *P. aegyptiaca*, which was attached to the roots of line #3.1. This suggests that these compounds can be involved in *P. aegyptiaca* growth inhibition. Some of these metabolites can cause growth inhibition in different plant species, as reported previously for caffeic acid, coumaric acid and cinnamic acid derivatives that were applied exogenously (Zanardo et al., 2009; Orcaray et al., 2011; Fernández-Aparicio et al., 2013).

The increased levels of hydroxycinnamic acid were accompanied by a significant reduction in the levels of sinapinic acid (also called sinapic acid) in *P. aegyptiaca* that grow on lines #3.1 and #2.1. The relationship between accumulations of hydroxycinnamic acid, p-coumaric acid, caffeic acid and ferulic acid in the roots and lower levels of sinapinic acid was previously detected in pea plants that were treated with herbicides chlorsulfuron and imazethapyr, which inhibit acetolactate synthase (ALS) (Orcaray et al., 2011).

Taken together, the results show that higher expression levels of AroG in the host plant (tobacco) can inhibit the growth of the parasitic plant *P. aegyptiaca* and bring a novel potential way to manage such parasitic weeds.

CONCLUSION

This study aimed at gaining more knowledge about the effect of increasing the AroG gene encoded to feedback-insensitive 3-deoxy-D-arabino-heptulosonate 7-phosphate synthase (DAHPS), the first enzyme of the shikimate pathway, on the accumulation of AAAs and their associated metabolites in tobacco plants. We also aimed at revealing the effect on the primary metabolic profile, tolerance to abiotic stress, and the ability to cope with *P. aegyptiaca*, a parasite plant. Our study is in agreement with previous studies, indicating that DAHPS serves as a major regulator of flux throughout the shikimate pathway and that most of the carbon flux goes toward phenylalanine, whose level increased up to 43-fold. The significant increase in phenylalanine resulted in increased levels of metabolites that belong to the phenylpropanoid pathway, including 4-hydroxybenzoate, phenyllactate and phenylethylamine. These changes were accompanied by mild changes in the plants' primary metabolites, most of which were in sugars content. In addition, our results provide evidence that plants with high levels of AAAs and their related metabolites have improved tolerance to salt stress and the potential to inhibit the development of the parasitic plant, *P. aegyptiaca*.

DATA AVAILABILITY STATEMENT

The datasets presented in this study can be found in online repositories. The names of the repository/repositories can be found in the article/**Supplementary Material**.

AUTHOR CONTRIBUTIONS

YH, MO, and RA: experimental design and manuscript preparation. AG, ED, and MO: conducting the experiments. AG, MO, RS, and YH: data analysis. All authors have read and approved the manuscript.

FUNDING

This work was supported by a grant from the Ministry of Agriculture and Rural Development (grant no. 21-01-0036).

ACKNOWLEDGMENTS

This research was carried out in the Plant Metabolism Laboratory of MIGAL—Galilee Research Institute in Kiryat Shmona, Israel, and the Weizmann Institute of Science in Rehovot, Israel. We thank Prof. Soliman Khatib from MIGAL and Tel-Hai College for his technical support in the LC-MS/MS analysis of the phenylpropanoids.

SUPPLEMENTARY MATERIAL

The Supplementary Material for this article can be found online at: https://www.frontiersin.org/articles/10.3389/fpls.2020.604349/full#supplementary-material

Supplementary Figure 1 | Schematic diagram of the aromatic amino acid (AAAs) biosynthesis pathway in plants. The main related metabolites from each of the AAAs are indicated in the blue framed box. Only regulatory enzymes are mentioned. DAHPS, 3-deoxy-d-arabino-2-heptulosonate 7-phosphate synthase;

CM, chorismate mutase; ADT, arogenate dehydratase; AS, anthranilatesynthate; ADH, arogenate dehydrogenase.

Supplementary Figure 2 | Schematic diagram of the constructs used in the current study. Upper panel: the construct used to express the AroG gene. Lower panel: an empty vector (EV) used as a control. 35S Omega, cauliflower mosaic virus 35S promoter fused to the omega translation enhancer; TP, RuBisCO small subunit-3A plastid transit peptide; AroG, the bacterial feedback-insensitive AroG encoded to 3-deoxy-d-arabino-2-heptulosonate 7-phosphate synthase with a mutation at amino acid number 175; 3HA, three copies of the hemagglutinin epitope tag; OCS ter, octopine synthase terminator; LB, left border; RB, right border.

Supplementary Figure 3 | Screening of the protein expression level of DAHPS in the T_0 tobacco transgenic plants. The upper panel shows the immunoblot analysis made for the leaves of 12-week-old transgenic plants using antibodies against the 3HA epitope-tag that was fused to the AroG gene. The size of the DAHPS is 42 kDa. The lower panel shows Coomassie-blue staining of the protein profiles of tobacco leaves. Proteins (20 μg) extracted from the leaves were fractionated by SDS-PAGE. M, marker size; EV, empty vector. Each of these gels was run separately. Lines #1–3 (in the text) are plants No. 3, 8, and 10, respectively, and lines #4–6 are plants No. 16, 17, and 26. Plants that had abnormal shoot phenotype are marked by antistrike.

Supplementary Figure 4 | Expression levels of two auxin response genes at WT, EV, and AroG transgenic tobacco lines as detected by qRT-PCR. Data are given as relative to protein phosphatase 2A subunit (PP2A) expression. Data are presented as the mean ± SE of three different biological repetitions. Asterisks represent statistical significance ($p \leq 0.05$) of each AroG line from EV plants (using the Student's *t*-test).

Supplementary Figure 5 | Effect of auxin treatment on plant phenotype. **(A)** The phenotype of WT plants grown for 8 weeks on Nitsch medium supplemented with aphthaleneacetic acid (NAA) or phenylacetic acid (PAA). **(B)** The phenotype of 3-week-old tobacco WT plants sprayed with increasing concentrations (0.1, 1, 10, 100 μM) of indole-3-butyric acid (IBA), indole-3-acetic acid (IAA), indole-3-propionic acid (IPA), or tryptophan (TRP) for 10 days. Spraying with double-distilled water (DDW) was used as a control.

Supplementary Figure 6 | Phenolic compounds found in leaves of AroG lines #1–6 and in EV/WT plants as measured at a wavelength of 280 nm using HPLC-DAD. Data are presented as the mean ± SE of four biological repetitions. Different letters represent statistical significance ($p \leq 0.05$), which was determined using the Tukey-Kramer test.

Supplementary Figure 7 | The response of AroG lines to oxidative stress. Eight mm discs (n = 8–12) of transgenic AroG #1, #2, #3, and EV leaves (n = 7) were exposed to different levels of in 0, 1, 2,5 μM methyl viologen (pq) for 20 h under 80–110 μE light conditions, and bleaching level was measured by ImageJ. Data are presented as a change (in%) from green level under the non-stress condition (0 pq) that was marked as 100%. Significance ($p \leq 0.05$) from EV at the same condition is marked by asterisks.

Supplementary Figure 8 | The response of AroG lines to drought stress. The plants were grown in a greenhouse as described in "Materials and Methods" section. Parameters of senescence level and plant vigor were measured after the first drought period of 10 days, and parameters of height, dry biomass and relative water content (RWC) were measured at the end of the second drought period of 10 days. Data are presented as the mean ± SE of six biological replicates. Significance ($p \leq 0.05$) of each line compared to EV under the same conditions is marked by asterisks.

Supplementary Figure 9 | Total polyphenol content (represented as g gallic acid equivalents per liter of water extract) in *P. aegyptiaca* grown on WT, EV, and AroG lines. Data are presented as the mean ± SE of *P. aegyptiaca* that were collected from five different pots. Different letters represent statistical significance ($p \leq 0.05$), which was determined using the Tukey-Kramer test.

Supplementary Table 1 | GCMS-metabolite dataset as detected in WT and transgenic plants.

Supplementary Table 2 | List of primers used in the qRT-PCR analyses.

Supplementary Table 3 | (A) The levels of aromatic amino acids in homozygous lines #2.1, #3.1, WT, EV and in P. aegyptiaca. **(B)** The levels of aromatic amino acid in the roots of WT and EV and in *P. aegyptiaca.*

Supplementary Table 4 | Levels of phenylpropanoids detected by LC-MS/MS in *Phelipanche aegyptiaca (P. aegyptiaca)* and the roots of WT and transgenic plants.

Supplementary Text 4 | Feeding experiments with auxin suggest that the phenotype of lines #4–6 is not related to high auxin levels.

Supplementary Text 6 | Profile of phenolic compounds found in the leaves of AroG lines and WT/EV.

REFERENCES

Baghestani, A., Lemieux, C., and Leroux, G. D. (1999). Determination of allelochemicals in spring cereal cultivars of different competitiveness. *Weed Sci.* 47, 498–504 doi: 10.1017/s0043174500092171

Ben Nasr, C., Ayed, N., and Metche, M. (1996). Quantitative determination of the polyphenolic content of pomegranate peel. *Z. Lebensm. Unters. Forsch.* 203,374–378 doi: 10.1007/bf01231077

Bolouri-Moghaddam, M. R., Le Roy, K., Xiang, L., Rolland, F., and Van den Ende, W. (2010). Sugar signaling and antioxidant network connections in plant cells. FEBS J. 277, 2022–37 doi: 10.1111/j.1742-4658.2010.07633.x

Chen, Q., Man, C., Li, D., Tan, H., Xie, Y., and Huang, J. (2016). Arogenate Dehydratase Isoforms Differentially Regulate Anthocyanin Biosynthesis in Arabidopsis thaliana. *Mole. Plant* 9, 1609–1619. doi: 10.1016/j.molp.2016.09.010

Cohen, H., Pajak, A., Pandurangan, S., Amir, R., and Marsolais, F. (2016). Higher endogenous methionine in transgenic Arabidopsis seeds affects the composition of storage proteins and lipids. *Amino Acids* 48, 1413–1422. doi: 10.1007/s00726-016-2193-4

Dargeviciute, A., Roux, C., Decreux, A., Sitbon, F., and Perrot-Rechenmann, C. (1998). Molecular cloning and expression of the early Auxin-responsive Aux/IAA gene family in Nicotiana tabacum. *Plant Cell Physiol.* 39, 993–1002.

Das, K., and Roychoudhury, A. (2014). Reactive oxygen species (ROS) and response of antioxidants as ROS-scavengers during environmental stress in plants. *Front. Environ. Sci.* 2:53. doi: 10.3389/fenvs.2014.00053

Dixon, R. A. (2001). Natural products and plant disease resistance. *Nature* 411, 843–7. doi: 10.1038/35081178

Dixon, R. A., and Paiva, N. (1995). Stress-induced phenylpropanoid metabolism. *Plant Cell* 7, 1085–1097. doi: 10.1105/tpc.7.7.1085

Echevarría-Zomeno, S., Perez-de-Luque, A., Jorrın, J., and Maldonado, A. M. (2006). Pre-haustorial resistance to broomrape (Orobanche cumana) in sunflower (Helianthus annuus): cytochemical studies. *J. Exp. Bot.* 57, 4189–4200. doi: 10.1093/jxb/erl195

Fernández-Aparicio, M., Bernard, A., Falchetto, L., Marget, P., Chauvel, B., Steinberg, C. (2017). Investigation of Amino Acids As Herbicides for Control of Orobanche minor Parasitism in Red Clover. *Front. Plant Sci.* 8:842. doi: 10.3389/fpls.2017.00842

Fernández-Aparicio, M., Cimmino, A., Evidente, A., and Rubiales, D. (2013). Inhibition of Orobanche crenata seed germination and radicle growth by allelochemicals identified in cereals. *J. Agric. Food Chem.* 61, 9797–803. doi: 10.1021/jf403738p

Francini, A., Giro, A., and Ferrante, A. (2019). Biochemical and Molecular Regulation of Phenylpropanoids Pathway Under Abiotic Stresses. *Plant Sign. Mole.* 2019, 183–192. doi: 10.1016/B978-0-12-816451-8.00011-3

Galili, G., Amir, R., and Fernie, A. R. (2016). The Regulation of Essential Amino Acid Synthesis and Accumulation in Plants. *Annu. Rev. Plant Biol.* 67, 153–78. doi: 10.1146/annurev-arplant-043015-112213

Hacham, Y., Hershenhorn, J., Dor, E., and Amir, R. (2016). Primary metabolic profiling of Egyptian broomrape (Phelipanche aegyptiaca) compared to its host tomato roots. *J. Plant Physiol.* 205, 11–19. doi: 10.1016/j.jplph.2016.08.005

Horsch, R. B., Fry, J. E., Hoffman, N. L., Eichholtz, D., Rogers, S. G., and Fraley, R. T. (1985). A Simple and General Method for Transferring Genes into Plants. *Science* 227, 1229–1231 doi: 10.1126/science.227.4691.1229

Huang, T., Tohge, T., Lytovchenko, A., Fernie, A. R., and Jander, G. (2010). Pleiotropic physiological consequences of feedback-insensitive phenylalanine biosynthesis in Arabidopsis thaliana. *Plant J.* 63, 823–835. doi: 10.1111/j.1365-313X.2010.04287

Joel, D. M., Hershenhorn, J., Eizenberg, H., Aly, R., Ejeta, G., Rich, P. J., Ransom, J. K., Sauerborn, J., and Rubiales, D. (2007). *Biology and management of weedy root parasites*. *Horticultural Reviews*. Hoboken, NJ: John Wiley & Sons,, 267–349.

Kai, K., Mizutani, M., Kawamura, N., Yamamoto, R., Tamai, M., Yamaguchi, H., Sakata, K., and Shimizu, B. (2008). Scopoletin is biosynthesized via ortho-hydroxylation of feruloyl CoA by a 2-oxoglutarate-dependent dioxygenase in Arabidopsis thaliana. Plant J. 55, 989–99. doi: 10.1111/j.1365-313X.2008.03568.x

Khan, M., Fatma, M., Per, T., Anjum, N., and Khan, N. (2015). Salicylic acid-induced abiotic stress tolerance and underlying mechanisms in plants. *Front. Plant Sci.* 6:465. doi: 10.3389/fpls.2015.00462

Li, J., and Last, R. L. (1996). The Arabidopsis thaliana trp5 mutant has a feedback-resistant anthranilate synthase and elevated soluble tryptophan. *Plant Physiol.* 110, 51–59. doi: 10.1104/pp.110.1.51

Loake, G., and Grant M. (2007). Salicylic acid in plant defence - the players and protagonists. *Curr. Opin. Plant Biol.* 10:466–472. doi: 10.1016/j.pbi.2007.08.008

Maeda, H., and Dudareva, N. (2012). The shikimate pathway and aromatic amino Acid biosynthesis in plants. *Annu. Rev. Plant Biol.* 63, 73–105. doi: 10.1146/annurev-arplant-042811-105439

Malitsky, S., Blum, E., Less, H., Venger, I., Elbaz, M., Morin, S., Eshed, Y., and Aharoni, A. (2008). The transcript and metabolite networks affected by the two clades of Arabidopsis glucosinolate biosynthesis regulators. *Plant Physiol.* 148, 2021–2049. doi: 10.1104/pp.108.124784

Manela, N., Oliva, M., Ovadia, R., Sikron-Persi, N., Ayenew, B., Fait, A., Galili, G., Perl, A., Weiss, D., and Oren-Shamir, M. (2015). Phenylalanine and tyrosine levels are rate-limiting factors in production of health promoting metabolites in Vitisvinifera cv. Gamay Red cell suspension. *Front. Plant Sci.* 6:538. doi: 10.3389/fpls.2015.00538

Matityahu, I., Godo, I., Hacham, Y., and Amir, R. (2013). Tobacco seeds expressing feedback-insensitive cystathionine gamma-synthase exhibit elevated content of methionine and altered primary metabolic profile. *BMC Plant Biol.* 13:206. doi: 10.1186/1471-2229-13-206

Mintz-Oron, S., Mandel, T., Rogachev, I., Feldberg, L., Lotan, O., Yativ, M., Wang, Z., Jetter, R., Venger, I., Adato, A., and Aharoni, A. (2008). Gene expression and metabolism in tomato fruit surface tissues. *Plant Physiol.* 147, 823–851. doi: 10.1104/pp.108.116004

Oliva, M., Hatan, E., Kumar, V., Galsurker, O., Nisim-Levi, A., Ovadia, R., Galili, G., Lewinsohn, E., Elad, Y., Alkan, N., and Oren-Shamir, M. (2019). Increased phenylalanine levels in plant leaves reduces susceptibility to *Botrytis cinerea*. *Plant Sci.* 290:110289. doi: 10.1016/j.plantsci.2019.110289

Oliva, M., Ovadia, R., Perl, A., Bar, E., Lewinsohn, E., Galili, G., and Oren-Shamir, M. (2015). Enhanced formation of aromatic amino acids increases fragrance without affecting flower longevity or pigmentation in Petunia × hybrida. *Plant Biotechnol. J.* 13, 125–136. doi: 10.1111/pbi.12253

Orcaray, L., Igal, M., Zabalza, A., and Royuela, M., (2011). Role of Exogenously Supplied Ferulic and p-Coumaric Acids in Mimicking the Mode of Action of Acetolactate Synthase inhibiting Herbicides. *J. Agric. Food Chem.* 59, 10162–10168. doi: 10.1021/jf2025538

Pandey, P., Ramegowda, V., and Senthil-Kumar, M. (2015). Shared and unique responses of plants to multiple individual stresses and stress combinations: physiological and molecular mechanisms. *Front. Plant Sci.* 6:723. doi: 10.3389/fpls.2015.00723

Sanjaya, A., Hsiao, P. Y., Su, R. C., Ko, S. S., Tong, C. G., Yang, R. Y., and Chan, M. T. (2008). Overexpression of Arabidopsis thaliana tryptophan synthase beta 1 (AtTSB1) in Arabidopsis and tomato confers tolerance to cadmium stress. *Plant Cell Environ.* 31, 1074–85. doi: 10.1111/j.1365-3040.2008.01819

Sharma, A., Shahzad, B., Rehman, A., Bhardwaj, R., Landi, M., and Zheng, B. (2019). Response of Phenylpropanoid Pathway and the Role of Polyphenols in Plants under Abiotic Stress. *Molecules* 24:3462. doi: 10.3390/molecules24132452

Sharma, P., Jha, A. B., Dubey, R. S., and Pessarakli, M. (2012). Reactive Oxygen Species, Oxidative Damage, and Antioxidative Defense Mechanism in Plants under Stressful Conditions. *J. Bot.* 2012:217037.

Solecka, D. (1997). Role of phenylpropanoid compounds in plant responses to different stress factors. *Acta Physiol. Plant.* 19, 257–268. doi: 10.1007/s11738-997-0001-1

Sugawara, S., Mashiguchi, K., Tanaka, K., Hishiyama, S., Sakai, T., Hanada, K., et al. (2015). Distinct Characteristics of Indole-3-Acetic Acid and Phenylacetic Acid, Two Common Auxins in Plants. *Plant Cell Physiol.* 56, 1641–1654. doi: 10.1093/pcp/pcv088

Tzin, V., and Galili, G. (2010). New Insights into the Shikimate and Aromatic Amino Acids Biosynthesis Pathways in Plants. *Mole. Plant.* 3, 956–972. doi: 10.1093/mp/ssq048

Tzin, V., Malitsky, S., Ben Zvi, M. M., Bedair, M., Sumner, L., Aharoni, A., and Galili, G. (2012). Expression of a bacterial feedback-insensitive 3-deoxy-D-arabino-heptulosonate 7-phosphate synthase of the shikimate pathway in Arabidopsis elucidates potential metabolic bottlenecks between primary and secondary metabolism. *N. Phytol.* 194, 430–439. doi: 10.1111/j.1469-8137.2012.04052.x

Tzin, V., Rogachev, I., Meir, S., Zvi, M. M. B., Masci, T., Vainstein, A., Aharoni, A., and Galili, G. (2013). Tomato fruits expressing a bacterial feedback-insensitive 3-deoxy-d-arabino-heptulosonate 7-phosphate synthase of the shikimate pathway possess enhanced levels of multiple specialized metabolites and upgraded aroma. *J. Exp. Bot.* 64, 4441–4452. doi: 10.1093/jxb/ert250

Verslues, P. E., and Sharma, S., (2010). Proline Metabolism and Its Implications for Plant-Environment Interaction. *Arabidop. Book* 2010:e0140. doi: 10.1199/tab.0140

Vurro, M., Boari, A., Pilgeram, A. L., and Sands, D. C. (2006). Exogenous amino acids inhibit seed germination and tubercle formation by Orobanche ramose. *Biol. Contr.* 36, 258–265. doi: 10.1016/j.biocontrol.2005.09.017

Westfall, C. S., Xu, A., and Jez, J. M. (2014). Structural Evolution of Differential Amino Acid Effector Regulation in Plant Chorismate Mutases. *J. Biol. Chem.* 289, 28619–28628. doi: 10.1074/jbc.M114.591123

Xia, J., Sinelnikov, I.V., Han, B., and Wishart, D. S. (2015). MetaboAnalyst 3.0-making metabolomics more meaningful. *Nucleic Acids Res.* 43, W251–W257. doi: 10.1093/nar/gkv380

Yoo, H., Widhalm, J. R., Qian, Y., Maeda, H., Cooper, B. R., Jannasch, A. S., Gonda, I., Lewinsohn, A., Rhodes, D., and Dudareva, N. (2013). An alternative pathway contributes to phenylalanine biosynthesis in plants via a cytosolic tyrosine: phenylpyruvate aminotransferase. *Nat. Commun,.* 4:2833. doi: 10.1038/ncomms3833

You, J., Zhang, Y., Liu, A., Li, D., Wang, X., Dossa, K., Zhou, R., Yu, J., Zhang, Y. (2019). Transcriptomic and metabolomic profiling of drought-tolerant and susceptible sesame genotypes in response to drought stress. *BMC Plant Biol.* 19:267. doi: 10.1186/s12870-019-1880-1

Zanardo, D. I. L., Lima, R. B., Ferrarese, M. D. L., Bubna, G. A., and Ferrarese-Filho, O. (2009). Soybean root growth inhibition and lignification induced by *p*-coumaric acid. *Environ. Exp. Bot.* 66, 25–30. doi: 10.1016/j.envexpbot.2008.12.014

Zhu, Q., Li, B., Mu, S., Han, B., Cui, R., Xu, M., You, Z., and Dong, H. (2013). TTG2-regulated development is related to expression of putative auxin response factor genes in tobacco. *BMC Genom.* 14:806. doi: 10.1186/1471-2164-14-806

Conflict of Interest: The authors declare that the research was conducted in the absence of any commercial or financial relationships that could be construed as a potential conflict of interest.

Copyright © 2021 Oliva, Guy, Galili, Dor, Schweitzer, Amir and Hacham. This is an open-access article distributed under the terms of the Creative Commons Attribution License (CC BY). The use, distribution or reproduction in other forums is permitted, provided the original author(s) and the copyright owner(s) are credited and that the original publication in this journal is cited, in accordance with accepted academic practice. No use, distribution or reproduction is permitted which does not comply with these terms.

frontiers in Plant Science

ORIGINAL RESEARCH
published: 26 January 2021
doi: 10.3389/fpls.2020.606386

Increased Expression of UMAMIT Amino Acid Transporters Results in Activation of Salicylic Acid Dependent Stress Response

*Julien Besnard[1,2], Unnati Sonawala[1], Bal Maharjan[2], Eva Collakova[3], Scott A. Finlayson[2,4], Guillaume Pilot[3], John McDowell[3] and Sakiko Okumoto[1,2]**

[1] Department of Plant Pathology, Physiology and Weed Science, Virginia Tech, Blacksburg, VA, United States, [2] Department of Soil and Crop Sciences, Texas A&M AgriLife Research, Texas A&M University, College Station, TX, United States, [3] School of Plant and Environmental Sciences, Virginia Tech, Blacksburg, VA, United States, [4] Faculty of Molecular and Environmental Plant Sciences, Texas A&M University, College Station, TX, United States

OPEN ACCESS

Edited by:
Daniel Roberts,
The University of Tennessee,
Knoxville, United States

Reviewed by:
Yangdou Wei,
University of Saskatchewan, Canada
Shimpei Uraguchi,
Kitasato University, Japan

***Correspondence:**
Sakiko Okumoto
sokumoto@tamu.edu

Specialty section:
This article was submitted to
Plant Membrane Traffic and Transport,
a section of the journal
Frontiers in Plant Science

Received: 14 September 2020
Accepted: 17 December 2020
Published: 26 January 2021

Citation:
Besnard J, Sonawala U,
Maharjan B, Collakova E,
Finlayson SA, Pilot G, McDowell J
and Okumoto S (2021) Increased
Expression of UMAMIT Amino Acid
Transporters Results in Activation
of Salicylic Acid Dependent Stress
Response.
Front. Plant Sci. 11:606386.
doi: 10.3389/fpls.2020.606386

In addition to their role in the biosynthesis of important molecules such as proteins and specialized metabolites, amino acids are known to function as signaling molecules through various pathways to report nitrogen status and trigger appropriate metabolic and cellular responses. Moreover, changes in amino acid levels through altered amino acid transporter activities trigger plant immune responses. Specifically, loss of function of major amino acid transporter, over-expression of cationic amino acid transporter, or over-expression of the positive regulators of membrane amino acid export all lead to dwarfed phenotypes and upregulated salicylic acid (SA)-induced stress marker genes. However, whether increasing amino acid exporter protein levels lead to similar stress phenotypes has not been investigated so far. Recently, a family of transporters, namely USUALLY MULTIPLE ACIDS MOVE IN AND OUT TRANSPORTERS (UMAMITs), were identified as amino acid exporters. The goal of this study was to investigate the effects of increased amino acid export on plant development, growth, and reproduction to further examine the link between amino acid transport and stress responses. The results presented here show strong evidence that an increased expression of UMAMIT transporters induces stress phenotypes and pathogen resistance, likely due to the establishment of a constitutive stress response via a SA-dependent pathway.

Keywords: membrane transport, amino acid transport, amino acid metabolism, stress response, salicylic acid

INTRODUCTION

Plants absorb nitrogen (N) mostly in its two major inorganic forms, ammonium and nitrate ions. These ions are eventually assimilated into glutamine, then the N is transferred through transamination reactions to all other organic N molecules including other amino acids. In addition to the critical role as the central metabolites, amino acids serve as the N carrier between different organelles, tissues and organs. Distribution of assimilated N from the source (typically photosynthetic leaves) to sink tissues is mainly achieved through translocation of amino acids. To meet such needs, plant genomes encode numerous amino acid transporters

(∼100 identified members of transporter families in Arabidopsis, Tegeder and Hammes, 2018), which function in transporting amino acids across the plasma membrane, as well as across organelle membranes.

Given the central role of amino acids in cellular metabolism and N balance between organs, it is not surprising that multiple mechanisms seem to exist to monitor the levels of amino acids. For example, TARGET OF RAPAMYCIN Complexes (TORCs) are cytosolic kinases that are activated by branched chain amino acids and are conserved among fungi, metazoans and plants (Nakajo et al., 2004; Fumarola et al., 2005; Kingsbury et al., 2015; Shimobayashi and Hall, 2016; Cao et al., 2019; Schaufelberger et al., 2019). Another cytosolic kinase, GENERAL CONTROL NON-REPRESSIBLE 2 (GCN2), is important for sensing N deficiency and is also conserved in fungi, metazoans, and plants. GCN2 does not sense amino acids *per se*, however it is activated when bound to de-acetylated tRNAs, which are more abundant when the cell is deprived of amino acids. Activated GCN2 represses protein synthesis by deactivating EUKARYOTIC ELONGATION INITIATION FACTOR 2α (eIF2α) through phosphorylation (Chantranupong et al., 2015). Therefore, TORC and GCN2 monitor the cytosolic amino acid sufficiency and deficiency, respectively. Additionally, GLUTAMATE RECEPTOR-LIKE (GLR) proteins, which structurally resemble the neuronal glutamate receptors from metazoans, seem to be involved in the perception of extracellular amino acids (Qi et al., 2006; Stephens et al., 2008; Vincill et al., 2012; Tapken et al., 2013; Kong et al., 2016; Goto et al., 2020). In addition to the proteogenic amino acids sensed by the above pathways, specialized non-proteogenic amino acids, such as β-aminobutyric acid (Luna et al., 2014) and pipecolic acid (PIP) and its derivative N-hydroxypipecolic acid (NHP) (Huang et al., 2020), function as defense signaling molecules, both of which activate the SA-dependent defense pathway.

The existence of amino acid sensing mechanisms in plants suggests that alteration of amino acid levels via altered amino acid metabolism or transport might trigger pleiotropic responses. Indeed, several independent studies in which the transport of amino acids has been enhanced or altered seem to confirm this possibility. A study using knockout lines for the amino acid importer LYSINE HISTIDINE TRANSPORTER 1 (LHT1) revealed that amino acid contents within the tissue and the extracellular fluid were both altered, and these mutants showed a constitutive stress response mediated by salicylic acid (SA) (Hirner et al., 2006; Liu et al., 2010). Similarly, overexpression of CATIONIC AMINO ACID TRANSPORTER 1 (CAT1) caused a stunted phenotype, associated with increased SA levels, resistance against *Pseudomonas synringae*, and the upregulation of genes associated with the development of systemic acquired resistance (pathogenesis- related genes or *PR*) (Yang et al., 2014). Similar observations were reported upon over-expression of GLUTAMINE DUMPER 1 (GDU1), a single-transmembrane protein which promotes amino acid export through an unknown mechanism (Pilot et al., 2004; Pratelli et al., 2010). Similar to *lht1* knockouts and CAT1 overexpressor mutants, SA levels in GDU1 overexpressing plants were elevated (Liu et al., 2010).

Recent discovery of UMAMITs which are bidirectional facilitators of amino acid transport, offer the possibility to interrogate the response of plants to increased amino acid export directly. The goal of this study was to investigate the effects of overexpressing UMAMIT genes that were shown to promote amino acid transport in plants (UMAMIT14, 18, 24, and 25, Ladwig et al., 2012; Müller et al., 2015; Besnard et al., 2016, 2018) on plant development, growth, and reproduction to further examine the link between amino acid transport and stress responses. The results presented here show strong evidence that amino acid export activity positively correlates with stress phenotypes and pathogen resistance, most likely due to the establishment of a constitutive SA-mediated stress response.

MATERIALS AND METHODS

Plant Culture

Arabidopsis plants (Col-0) for observing phenotypes, mRNA and protein levels were grown in long days (16 h light at 50 μmol m^{-2} s^{-1} at the soil surface, 50% humidity, 22°C) in soil composed of 2:1 Sunshine Mix™: vermiculite. Plants were watered with 0.15 g/L MiracleGro™ fertilizer (24/8/16, N:P:K) three times a week. For *Hyaloperonospora arabidopsidis* infection, plants were grown under 8 h of light at 22°C and 16 h of dark at 20°C For kanamycin selection, seeds were sown on half-strength MS medium (1/2 Murashige and Skoog salt supplemented with 30 mM sucrose and 0.8% agarose with pH adjusted to 5.8 with KOH) containing 50 μg/ml kanamycin. Kanamycin-resistant plants were transferred to the long day conditions described above after 1 week of selection. Wild type Arabidopsis plants were transformed using the floral dip method using *Agrobacterium tumefaciens* strain GV3101 (pMP90) (Clough and Bent, 1998) to generate the overexpressor lines for UMAMIT14, UMAMIT18, UMAMIT24 and UMAMIT25.

DNA Constructs

UMAMIT14 genomic sequence (from ATG to the amino acid before the stop codon) was PCR-amplified from Col-0 genomic DNA with primers carrying *attb1* and *attb2* sequences flanking the genomic region. The PCR fragments were cloned into pDONRZeo vector using BP clonase II (Life Technologies, United States), and all entry clones were sequenced prior to use. *UMAMIT14* genomic sequence was transferred to the destination vector pPWYTkan (Besnard et al., 2016) using LR clonase II (Life Technologies, United States) to generate the 35S:UMAMIT14 lines. The same cloning steps were used for the creation of the lines over-expressing the genomic sequences of UMAMIT18, UMAMIT24, and UMAMIT25. A list of primers used for cloning is available in **Supplementary Table 1**.

Protein Electrophoresis and Western Blotting

Leaf protein was extracted from rosette leaves of plants about 3-weeks old. The leaves were ground in liquid nitrogen, then vortexed for 5 min in the extraction buffer [250 mM

Tris-HCl, pH. 8.5, 25 mM EGTA, 0.88 M sucrose, 5 mM DTT, Complete Proteinase Inhibitor (Roche, United States) at 1 tablet/50 mL volume], added at 3:1 v/w to the ground leaves. The soluble protein fraction was isolated from debris by centrifuging at 14,000 rpm for 10 min twice. Protein concentrations were determined using the Bradford assay (Coomassie Protein Assay Kit, Pierce, United States), following the procedure recommended by the manufacturer. Ten μg of extracted leaf proteins were denatured at 50°C for 15 min in an equivalent volume of loading buffer (62.5 mM Tris-HCl pH 6.8 adjusted with KOH, 2.7 M glycerol, 150 μM bromophenol blue and 70 mM SDS). Proteins were separated by SDS-PAGE and transferred to a Hybond^{TM} ECL (GE Healthcare, United Kingdom) nitrocellulose membrane following the manufacturer's recommendations. UMAMIT14-c-myc was detected using anti-cmyc rabbit polyclonal IgG (Santa Cruz Biotechnology, clone sc-789; 1/4,000) and anti-rabbit IgG conjugated to horseradish peroxidase (1/10,000). Antibodies were detected by reaction with the ECL^{TM} Prime Kit (GE Healthcare, United Kingdom) using the manufacturer's recommendations.

RNA Extraction and qRT-PCR

RNA was extracted using the RNAeasy plant kit (Qiagen, United States) according to the manufacturer's recommendation. Two μg of total RNA was used for cDNA synthesis with random primers using the iScript advanced cDNA synthesis kit (Bio-rad, United States). The list of primers used for qRT-PCR are described in **Supplementary Table 1**. QRT-PCR was performed using iTAQ Universal SYBR Green Supermix (Bio-rad), according to the manufacturer's recommendation. Fold change relative to WT was calculated using the pcr package in R, using standard curves obtained with serial dilution of cDNA samples (Ahmed and Kim, 2018).

Sporangiophore Assay and Trypan Blue Staining for *Hyaloperonospora arabidopsidis* Infection

The sporangiophore assay was performed using *Hyaloperonospora arabidopsidis* isolate Noco2 on 12-day-old seedlings. Trypan staining was performed to visualize hyphal growth and cell death on samples collected at 7 dpi (days post-inoculation). Both the sporangiophore assay and trypan staining were performed as described in Mcdowell et al. (2011).

Analysis of Amino Acid Levels

Amino acid extractions and analyses in wild type and *35S:UMAMIT14-4* leaves were performed in wild type and *35S:UMAMIT14-4* leaves using Waters ultra-performance liquid chromatography coupled to fluorescent detection (UPLC-FLD) as described (Besnard et al., 2016; Schneider et al., 2016). Briefly, leaves of 5-week-old Arabidopsis plants were extracted after lyophilization and pulverization using biphasic extractions. Norvaline (0.5 μM final concentration) was used as an internal standard. Aqueous phase was derivatized using Waters AccQ•Tag ^{TM} Ultra Amino Acid kit and injected on a Waters H-class Acquity UPLC-FLD equipped with a 10 cm Waters AccQ•Tag^{TM} Ultra C18 column (1.7 μm, 2.1 mm × 100 mm; Waters, Milford, MA). Waters 10.2 min free amino cell culture chromatographic method was used to separate different amino acids (Waters). Data analysis was performed as described (Collakova et al., 2013).

Quantification of Plant Hormones

SA, indole-3-acetic acid (IAA) and abscisic acid (ABA) were extracted and quantified using LC-MS/MS-based multiple reaction monitoring and isotope dilution based on the method of Liu and Finlayson, 2019). SA was quantified in negative ion mode monitoring the transitions 137.0–93.10 (endogenous) and 141.0–97.10 (labeled standard) with a cone voltage of 29 V and a collision energy of 16 eV.

Statistical Analyses

One-way ANOVA followed by Tukey's test, or two- tailed *t*-tests were used to determine significant differences ($p < 0.05$) between samples in Prism (Graphpad, United States).

RESULTS

Expression of UMAMIT Amino Acid Exporters Induces a Stunted Phenotype in Arabidopsis

Previous studies have shown that *gdu1-1D* plants, in which amino acid export activity is enhanced, show pleiotropic stress phenotypes including smaller plant sizes and increased stress marker expression (Pilot et al., 2004; Liu et al., 2010; Pratelli et al., 2012; Besnard et al., 2016). In order to investigate a direct relationship between amino acid export and a stress phenotype, we sought to over-express an amino acid exporter. UMAMIT14, which functions as an exporter for charged (His, Glu, Asp), polar (Gln, Asn, Ser, Thr) and non-polar (Ala, Val, Ile, Leu, Phe) amino acids when expressed in yeasts, was chosen for the study (Müller et al., 2006; Besnard et al., 2016). Transgenic Arabidopsis lines that over-express *UMAMIT14-cmyc* under the control of the 35S promoter were constructed.

The observed phenotype was indeed reminiscent of *gdu1-1D*, showing stunted growth after 3 weeks (**Figure 1A**). The degree of dwarfism varied widely among the T1 and T2 plants, and for the individuals with most severe phenotypes we were unable to establish a homozygous line. Quantification of UMAMIT14-cMyc protein revealed that the phenotypic severity in T2 generation plants was positively correlated with the level of c-Myc-tagged UMAMIT14 protein expression (**Figures 1A,B**), similar to GDU1 over-expressors (Pilot et al., 2004). To further confirm that the phenotype is caused by amino acid export, three additional UMAMIT proteins, UMAMIT18, 24, and 25 (Ladwig et al., 2012; Besnard et al., 2016, 2018) were expressed under the control of the 35S promoter. UMAMIT14, 18, 24, and 25 share multiple substartes (Gln, Ala, Thr, Val, Ile), although the substrate specificity for other amino acids differ slightly; for example, Asp and GABA secretion is not increased in yeasts

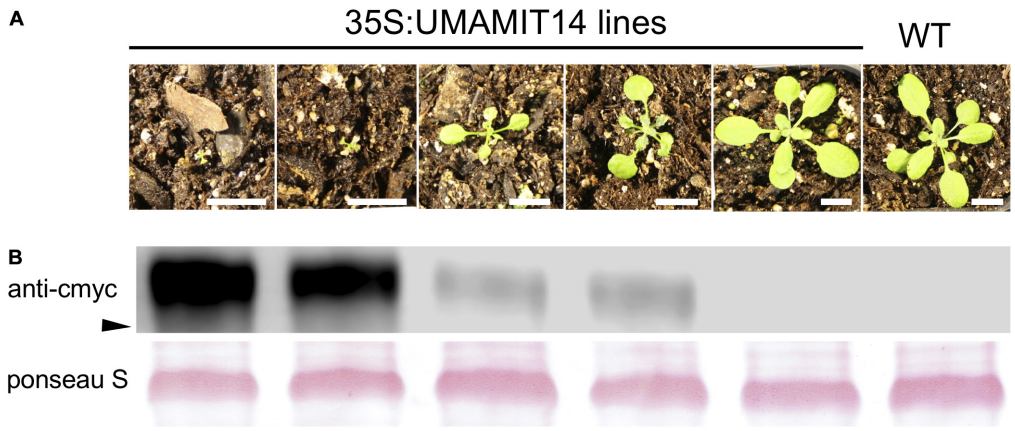

FIGURE 1 | Constitutive expression of UMAMIT14 leads to a stunted phenotype. **(A)** Macroscopic phenotypes of 3-week-old Arabidopsis plants from T2 generation, expressing UMAMIT1-cMyc fusion under 35S promoter, compared to the wild type plant (right). Scale bar: 1 cm. **(B)** Top: Western blot targeting UMAMIT14-c-myc from corresponding lines shown in **(A)**. Each lane contained 10 μg of proteins extracted from 4-week-old wild type and 35S:UMAMIT14 leaves. Arrowhead indicates 40 kDa. Bottom: RubisCO protein visualized with Ponseau S staining of the membrane used for the Western blot shown in the top panel.

by UMAMIT14 expression, but is increased by UMAMIT24 and 25 (Besnard et al., 2016, 2018). Similar stunted phenotypes were observed for plants overexpressing UMAMIT 18, 24, and 25 (**Supplementary Figure 1**). Taken together, the results indicate that over-expression of UMAMIT transporters induces a pleiotropic phenotype including growth retardation.

From the UMAMIT14 overexpressor lines, two representative lines, *35S:UMAMIT14-4 and 35S:UMAMIT14-6,* which show moderate and strong growth retardation phenotypes, respectively, were selected for further analysis (**Figure 2A**). *35S:UMAMIT14-4* and *35S:UMAMIT14-6* lines accumulated about 130- and 220-fold more *UMAMIT14* mRNA in leaves compared to the wild type, respectively, reflecting the severity of the phenotypes (**Figure 2B**). Western blot analysis showed that the difference in the mRNA amount between the lines is reflected in the amount of UMAMIT14 protein expressed (**Figure 2C**).

In addition to the stunted phenotype, *35S:UMAMIT14-4* and *35S:UMAMIT14-6* lines showed pleiotropic changes in various growth parameters. Under long day conditions, *35S:UMAMIT14-4* and *35S:UMAMIT14-6* displayed reduced plant biomass, silique length, and seeds per silique compared to the wild type (**Table 1**). In addition, plant height and seed weight were decreased in *35S:UMAMIT14-6* compared to the wild type.

SA-Mediated Stress Responses Are Upregulated in *35S:UMAMIT14* Lines

Previous studies have shown that alteration of membrane amino acid transport induces SA-mediated stress responses (Liu et al., 2010; Yang et al., 2014). To evaluate whether similar responses are induced in overexpression lines, we quantified the expression of *PR1*, a marker gene for the SA pathway (Van Loon et al., 2006). *PR1* mRNA content was greatly increased in the leaves of both *35S:UMAMIT14-4* and *35S:UMAMIT14-6* plants (**Figure 3A**). In addition, the expression of *AGD2-LIKE DEFENSE RESPONSE PROTEIN 1 (ALD1)*, which encodes the enzyme catalyzing the first committed step of pipecolic acid (PIP) and NHP biosynthesis, was also increased in *35S:UMAMIT14-4* and *35S:UMAMIT14-6* plants (**Figure 3B**). The SA content in leaves of *35S:UMAMIT14-4* and *35S:UMAMIT14-6* plants was also significantly higher compared to the WT (**Figure 4**). No consistent trends for other plant hormones tested (IAA,ABA and JA) were found between *35S:UMAMIT14-4* and *35S:UMAMIT14-6* plants (**Supplementary Figure 2**).

Transgenic Lines Overexpressing UMAMIT14 Gene Displayed Enhanced Disease Resistance

We reasoned that if the SA-dependent defense pathway is activated in *35S:UMAMIT14* plants, their resistance to the pathogens known to activate the SA pathway would be bolstered (Mcdowell et al., 2011; Wei et al., 2015). Indeed, *35S:UMAMIT14-4* plants were found to be resistant to the biotrophic pathogen *Hyaloperonospora arabidopsidis* (*Hpa*), while the wild type remained sensitive. At 7 days post-inoculation, cotyledons of wild type plants developed sporangiophores whereas no sporangiophores were detected on *35S:UMAMIT14-4* plants (**Figures 5A–D**). The cotyledons of *35S:UMAMIT14-4* plants also showed macroscopic lesions caused by cell death, similar to those that have been observed in *gdu1-D* plants (**Figure 5B**; Liu et al., 2010). Hyphal growth within the leaf tissue is inhibited, concomitant with the increased cell death in the leaves of *35S:UMAMIT14-4* plants (**Figures 5D–G**). These results suggest that over-expression of *UMAMIT14* disrupts amino acid homeostasis leading to a constitutive immune response against *Hpa*.

DISCUSSION

In the present study, it has been shown that over-expressing four independent UMAMITs that function as amino acid

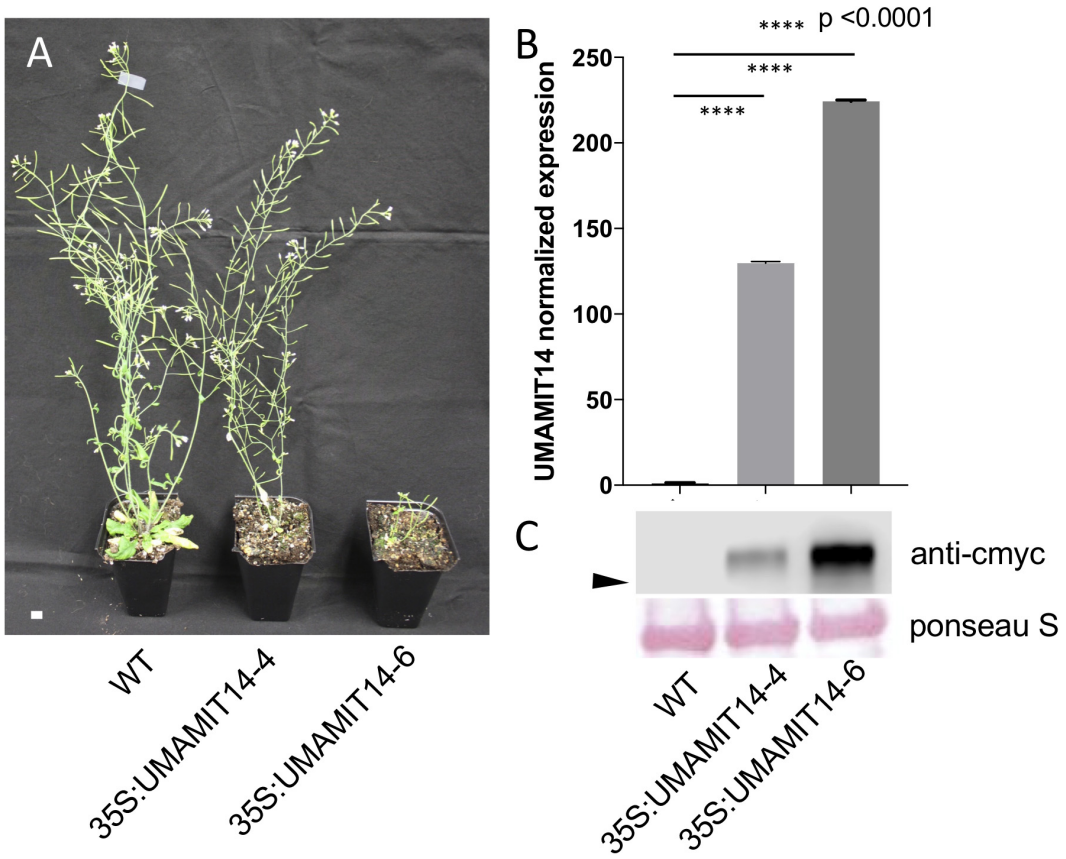

FIGURE 2 | Phenotypes of 35S:UMAMIT14-4 and 14–6 lines. **(A)** Appearance of WT, 35S:UMAMIT14-4 and 35S:UMAMIT14-6 plants at maturity (12-weeks-old). Scale bar: 1 cm. **(B)** Relative *UMAMIT14* expression levels in 2-week-old seedlings of 35S:UMAMIT14-4 and 35S:UMAMIT14-6 lines compared to the wild type. Statistical significance at $p < 0.05$ is shown (asterisk) using one-way ANOVA and Tukey's *post hoc* tests. Error bars: standard deviation, $n = 4$.

TABLE 1 | Characteristics of 9-week-old Arabidopsis plants grown in soil under long day conditions.

	Plant height (cm)	Biomass* (g)	Seed weight (mg)	Silique length (mm)	Seeds per silique
WT	34.6 ± 2.9 (a)	0.490 ± 0.021 (a)	94.32 ± 25.61 (a)	17.5 ± 1.0 (a)	58.7 ± 8.1 (a)
35S:UMAMIT14-1	28.7 ± 2.8 (a)	0.273 ± 0.116 (b)	104.84 ± 37.80 (a)	8.7 ± 1.5 (b)	16.7 ± 4.7 (b)
35S:UMAMIT14-4	3.6 ± 2.2 (b)	0.031 ± 0.007 (c)	16.28 ± 5.59 (b)	9.5 ± 1.7 (b)	25.6 ± 6.2 (c)

Biomass represents all plant tissue collected from the aerial parts, minus the seeds. Significant differences ($p < 0.05$) are indicated by different letters according to one-way ANOVA followed by Tukey's test ($n = 4$ biological replicates).

exporters causes a stunted growth phenotype (**Figures 1**, **2** and **Supplementary Figure 1**). Further studies of two such over-expressor lines, *35S:UMAMIT14-4* and *35S:UMAMIT14-6*, showed altered physiological traits such as a decrease in biomass and seed yield (**Table 1**). *UMAMIT14* over-expression also led to accumulation of SA and upregulation of a marker gene responding to the SA-dependent signaling pathway, *PR1* (Malamy et al., 1990; Van Loon and Van Strien, 1999). *ALD1* expression was also increased, indicating that the PIP/NHP-mediated pathway was also activated. Corroborating the activation of SA and PIP/NHP pathways, increased resistance to an SA-responsive pathogen was also observed (**Figures 4**, **5**). Thus, a variety of elevated immune response hallmarks were observed.

The results from our study are in agreement with previous reports in which the mis-regulation of amino acid transport led to stress responses (Pilot et al., 2004; Hirner et al., 2006; Yang et al., 2014; Liu et al., 2016). Additionally, a forward genetics screen revealed that the *RESISTANCE TO PHYTOPHTHORA PARASITICA 1* (*RTP1*) mutant, which shows an elevated SA-mediated stress response, is caused by a defect in the *UMAMIT36* gene, although amino acid transport activity for UMAMIT36 has yet to be established (Pan et al., 2016). It is worthwhile noting that such defense-inducing phenotypes are likely associated with both increased (in case of *CAT1* over-expression and RTP1 loss-of-function) and decreased (*LHT1* knock-out, *GDU1-D, UMAMIT14, UMAMIT 18, UMAMIT 24, UMAMIT 25* over-expression) amino acid retention in the cytosol. In cases where

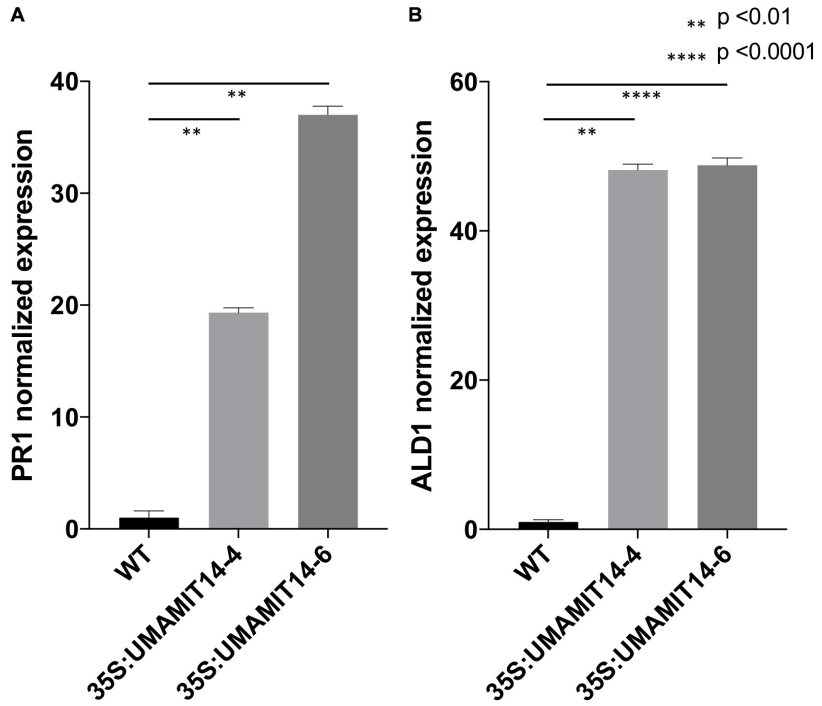

FIGURE 3 | Relative expression levels of PR1 **(A)** and ALD1 **(B)** in 35S:UMAMIT14 lines. The expression levels of PR1 and ALD1 genes in 2-week-old 35S:UMAMIT14 plants were normalized to the expression levels in the wild type. Error bars: standard deviation, $n = 4$. Significant difference compared to the wild type are indicated by stars according to one-way ANOVA and Tukey's *post hoc* tests.

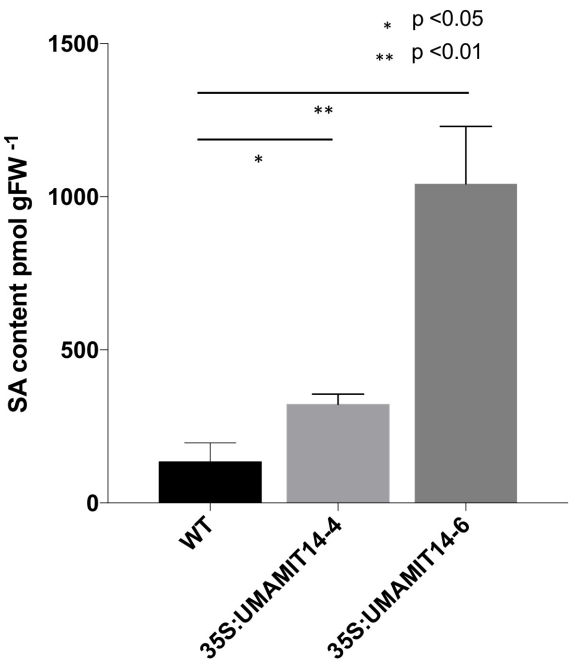

FIGURE 4 | SA content in 35S:UMAMIT14-4 and 35S:UMAMIT14-6 plants. Total SA was extracted from the leaves of 3-week-old 35S:UMAMIT14-4 or 35S:UMAMIT14-6 plants. Student's *t*-test was conducted to evaluate the statistical difference (indicated by an asterisk). Error bars: standard deviation, $n \geq 4$.

amino acid profiles of the mutants were investigated, there was no clear common trend for the contents of specific amino acids being altered (Pilot et al., 2004; Hirner et al., 2006). Examination of amino acid profiles in 35S-UMAMIT14-4 line corroborates with these results, showing some amino acid composition changes but with no general trend common with *lht1* or *GDU1-D* mutants (**Supplementary Figure 3**). This is similar to the results from multiple studies reporting the amino acid contents in various mutants of amino acid biosynthesis genes (Van Damme et al., 2009; Hwang et al., 2011; Stuttmann et al., 2011; Alvarez et al., 2012). While all mutants showed enhanced defenses responses, they all displayed different amino acid accumulations and profiles, without any clear correlation between single amino acid contents or phenotypes.

The exact mechanism through which the SA-mediated defense pathway is triggered in these amino acid transporter or metabolic enzyme mutants is unknown. One potential pathway is via pipecolic acid (PIP) and its derivative, N-hydroxypipecolic acid (NHP). PIP and NHP are generated in the tissue attacked by biotrophic pathogens, and NHP functions as a long-distance signal to induce systemic resistance in distal leaves (Bernsdorff et al., 2016; Chen et al., 2018). PIP is generated from Lys; therefore a change in Lys metabolism might trigger an overproduction of PIP/NHP. In addition, PIP is also an analog of the proteogenic amino acid Pro. Currently there is no evidence showing that any of these amino acid transporters transport PIP/NHP at a physiologically relevant concentration. If they do function as PIP/NHP transporters, at least some of the phenotypes might

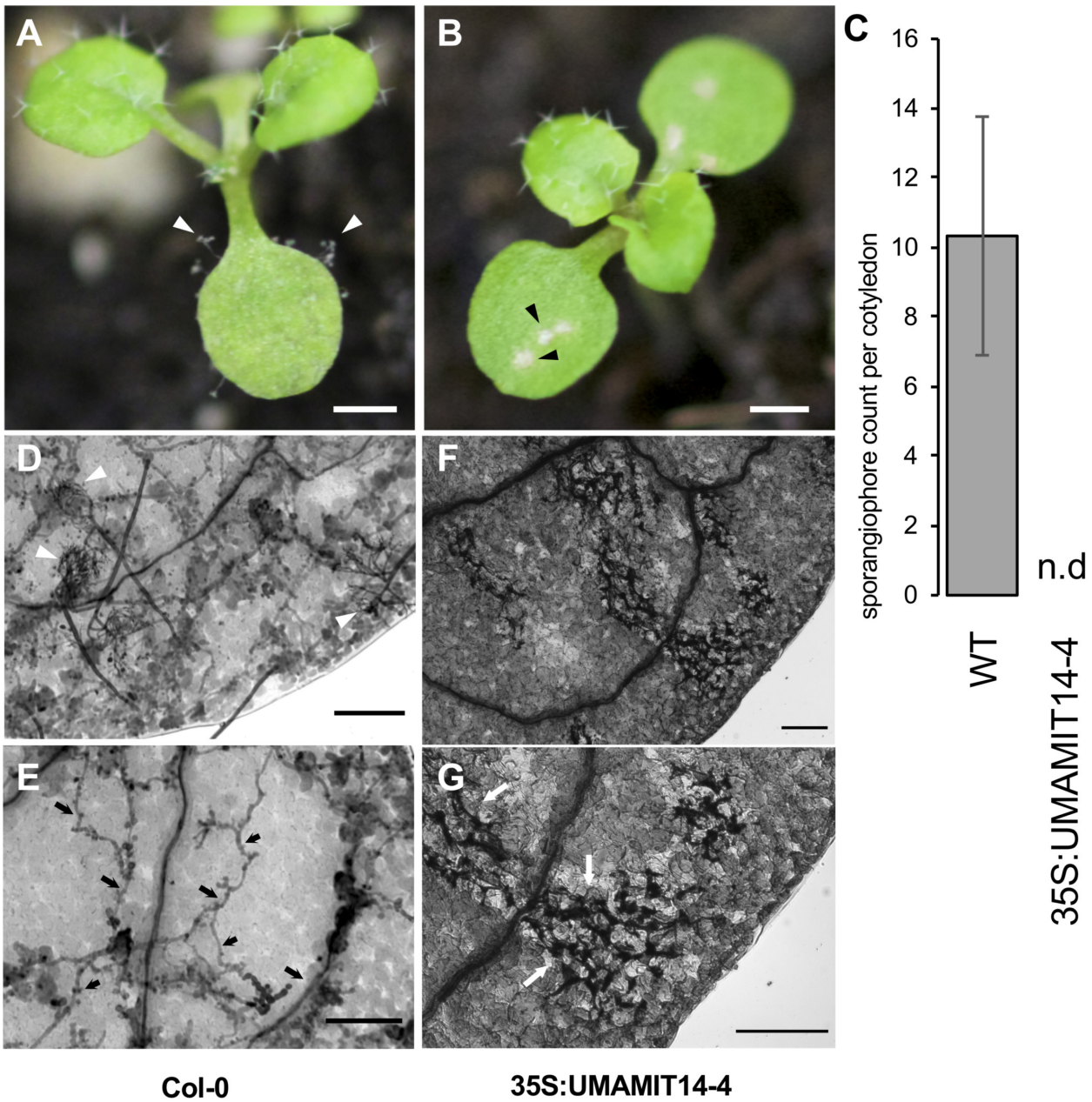

FIGURE 5 | Responses of WT and 35S:UMAMIT14-4 to *Hyaloperonospora arabidopsidis* infection. **(A)** Col-0 (left) and **(B)** 35S:UMAMIT14 (right) inoculated with *Hyaloperonospora arabidopsidis* (Noco2), 7 days post-inoculation. Col-0 cotyledons display asexual reproductive structures (sporangiophores) whereas 35S:UMAMIT14 cotyledons display macroscopic lesions indicating cell death/necrosis. Scale bar: 1 mm. **(C)** Sporangiophore counts on 11-day-old cotyledons. The cotyledons were inoculated with 5×10^4 spores per ml and counted after 7 day post-inoculation. N.d. no sporangiophores were detected on cotyledons. **(D–G)** Trypan blue-stained cotyledons of Col-0 **(D,E)** and 35S:UMAMIT14 **(F,G)** inoculated with *Hyaloperonospora arabidopsidis* (Noco2), 7 days post-inoculation. **(D)** Multiple sporangiophores (white arrows) are visible on the surface. **(E)** Hyphal growth (black arrows) are visible within the leaf tissue. **(F)** No sporangiophore is visible on the leaf surface. **(G)** Areas of cell death are visible by trypan blue staining (white arrows). Note the absence of hyphae within the leaf tissue. Scale bars: 100 μm.

be explained by mis-localization of these signaling molecules. Another potential pathway could be via GCN2; amino acid deficiency caused by transporter misregulation could increase the concentration of free tRNA, which is perceived by GCN2 to induce stress responses (Li et al., 2013). Additionally, the change in the concentration of extracellular amino acids might trigger the responses of GLRs (reviewed in Forde and Roberts, 2014). Deciphering the exact mechanism will be complex, because these pathways are interconnected. For example, PIP/NHP induces the production of SA (Navarova et al., 2012), which, in turn,

induces GCN2-dependent eIF2 phosphorylation (Lageix et al., 2008). Although the downstream components of GLRs are not well known, AtGLR3;3 seems to be required for defense responses against biotrophic pathogens, which is dependent on the SA pathway (Manzoor et al., 2013). Genetic experiments conferring altered transporter activities, defects in PIP/NHP synthesis, and/or defects in GCN2- or GLR-mediated signaling could help to elucidate the canonical components required for the immune responses triggered by misregulation of amino acid transporters.

SA is also known to interact with other plant hormones. For example, there is a well-characterized reciprocal antagonism between SA and JA pathways (Ikemura et al., 1990). SA also suppresses the function of auxin by downregulating the auxin receptor, TIR1 (Wang et al., 2007). MYB96, a transcription factor downstream of ABA signaling is also known to induce SA response, and activation tagging line *myb97-1* shows a dwarf phenotype which is dependent of SA production (Seo and Park, 2010). Therefore, it is possible that other hormones are involved in triggering the stress response observed in UMAMIT14 overexpressing plants. In our current study, however, we did not observe any consistent increase or decrease of other plant hormones (IAA, ABA, and JA) in the UMAMIT14 overexpression lines. Therefore, it is likely that the phenotypic responses we observe is primarily due to the activation of SA pathway.

While constitutive activation of the SA pathway via loss or gain of function of amino acid transport function to combat pathogens is unlikely to be an agronomically useful strategy due to the loss of biomass and seed yield, these characterized UMAMITs provide tools to study the link between amino acid levels and plant immune responses. For example, an inducible expression system of UMAMITs may be useful in identifying the early events triggered by enhanced amino acid export through RNAseq studies. Amino acids serve as the main N form acquired from the host in biotrophic pathogens, many of which induce accumulation of a specific set of amino acids at the infected site (Mckee et al., 1972; Kumar and Prasad, 1992; Horst et al., 2010a,b; Ward et al., 2010). Therefore, the pathway triggered by the overexpression of UMAMITs could represent the endogenous monitoring system for pathogen-induced alteration of amino acid metabolism. Positive regulation of SA pathway via amino acid export could interact with other SA-dependent defense mechanism activated in parallel, such as PAMP- and effector-triggered immunity (Pieterse et al., 2012). Indeed, a recent study revealed that amino acid transporter expression profiles in Arabidopsis leaves are different between compatible (i.e., the pathogen can establish an infection) and incompatible (i.e., the pathogen is incapable of infection) interactions, suggesting that amino acid transporter reprogramming is required to establish the infection (Sonawala et al., 2018). The significant question is whether the amino acid transporters are induced by the pathogens to support their growth, similar to the case of sugar exporters SWEET11 and 12 (Gebauer et al., 2017), or whether the plant actively regulates amino acid transporter activity to counter infection, as suggested by differential regulation of local amino acid transporters upon perception of pathogen-associated molecular patterns (PAMP) (Anderson et al., 2014) and systemic alteration of amino acid transporter activities in distal leaves (Schwachtje et al., 2018). Careful examination using genetics, physiology and molecular biology will be necessary to parse out such differences.

DATA AVAILABILITY STATEMENT

The raw data supporting the conclusions of this article will be made available by the authors, without undue reservation, to any qualified researcher.

AUTHOR CONTRIBUTIONS

JB, SO, JM, and GP designed the experiments. JB, US, BM, SF, and EC conducted experiments. JB, SO, SF, EC, and GP contributed in writing the manuscript. SO and GP supervised the project. All authors contributed to the article and approved the submitted version.

FUNDING

This work was supported by the National Science Foundation MCB 1052048 (SO), IOS 135336 (GP, JM, and SO), Virginia Agricultural Experiment Station and the Hatch Program of the National Institute of Food and Agriculture, U.S. Department of Agriculture, projects VA-135908, VA-160087 (GP), VA-160106 (JM), and VA-160050 (EC).

SUPPLEMENTARY MATERIAL

The Supplementary Material for this article can be found online at: https://www.frontiersin.org/articles/10.3389/fpls.2020.606386/full#supplementary-material

REFERENCES

Ahmed, M., and Kim, D. R. (2018). pcr: an R package for quality assessment, analysis and testing of qPCR data. *PeerJ* 6:e4473. doi: 10.7717/peerj.4473

Alvarez, C., Bermudez, M. A., Romero, L. C., Gotor, C., and Garcia, I. (2012). Cysteine homeostasis plays an essential role in plant immunity. *N. Phytol.* 193, 165–177. doi: 10.1111/j.1469-8137.2011.03889.x

Anderson, J. C., Wan, Y., Kim, Y. M., Pasa-Tolic, L., Metz, T. O., and Peck, S. C. (2014). Decreased abundance of type III secretion system-inducing signals in Arabidopsis mkp1 enhances resistance against *Pseudomonas* syringae. *Proc. Natl. Acad. Sci. U S A.* 111, 6846–6851. doi: 10.1073/pnas.1403248111

Bernsdorff, F., Doring, A. C., Gruner, K., Schuck, S., Brautigam, A., and Zeier, J. (2016). Pipecolic Acid Orchestrates Plant Systemic Acquired Resistance and Defense Priming via Salicylic Acid-Dependent and -Independent Pathways. *Plant Cell* 28, 102–129. doi: 10.1105/tpc.15.00496

Besnard, J., Pratelli, R., Zhao, C., Sonawala, U., Collakova, E., Pilot, G., et al. (2016). UMAMIT14 is an amino acid exporter involved in phloem unloading in Arabidopsis roots. *J. Exp. Bot.* 67, 6385–6397. doi: 10.1093/jxb/erw412

Besnard, J., Zhao, C., Avice, J. C., Vitha, S., Hyodo, A., Pilot, G., et al. (2018). Arabidopsis UMAMIT24 and 25 are amino acid exporters involved in seed loading. *J. Exp. Bot.* 69, 5221–5232. doi: 10.1093/jxb/ery302

Cao, P., Kim, S. J., Xing, A., Schenck, C. A., Liu, L., Jiang, N., et al. (2019). Homeostasis of branched-chain amino acids is critical for the activity of TOR signaling in Arabidopsis. *Elife* 8:e50747.

Chantranupong, L., Wolfson, R. L., and Sabatini, D. M. (2015). Nutrient-sensing mechanisms across evolution. *Cell* 161, 67–83. doi: 10.1016/j.cell.2015.02.041

Chen, Y. C., Holmes, E. C., Rajniak, J., Kim, J. G., Tang, S., Fischer, C. R., et al. (2018). N-hydroxy-pipecolic acid is a mobile metabolite that induces systemic disease resistance in Arabidopsis. *Proc. Natl. Acad. Sci. U S A.* 115, E4920–E4929.

Clough, S. J., and Bent, A. F. (1998). Floral dip: a simplified method for Agrobacterium-mediated transformation of Arabidopsis thaliana. *Plant J.* 16, 735–743. doi: 10.1046/j.1365-313x.1998.00343.x

Collakova, E., Aghamirzaie, D., Fang, Y., Klumas, C., Tabataba, F., Kakumanu, A., et al. (2013). Metabolic and Transcriptional Reprogramming in Developing Soybean (Glycine max) Embryos. *Metabolites* 3, 347–372. doi: 10.3390/metabo3020347

Forde, B. G., and Roberts, M. R. (2014). Glutamate receptor-like channels in plants: a role as amino acid sensors in plant defence? *F1000Prime Rep.* 6:37.

Fumarola, C., Monica, S. L., and Guidotti, G. G. (2005). Amino acid signaling through the mammalian target of rapamycin (mTOR) pathway: role of glutamine and of cell shrinkage. *J. Cell. Physiol.* 204, 155–165. doi: 10.1002/jcp.20272

Gebauer, P., Korn, M., Engelsdorf, T., Sonnewald, U., Koch, C., and Voll, L. M. (2017). Sugar accumulation in leaves of Arabidopsis *sweet11/sweet12* double mutants enhances priming of the salicylic acid-mediated defense response. *Front. Plant Sci.* 8:1378. doi: 10.3389/fpls.2017.01378

Goto, Y., Maki, N., Ichihashi, Y., Kitazawa, D., Igarashi, D., Kadota, Y., et al. (2020). Exogenous Treatment with Glutamate Induces Immune Responses in Arabidopsis. *Mol. Plant Microbe Interact.* 33, 474–487. doi: 10.1094/mpmi-09-19-0262-r

Hirner, A., Ladwig, F., Stransky, H., Okumoto, S., Keinath, M., Harms, A., et al. (2006). Arabidopsis LHT1 is a high-affinity transporter for cellular amino acid uptake in both root epidermis and leaf mesophyll. *Plant Cell* 18, 1931–1946. doi: 10.1105/tpc.106.041012

Horst, R. J., Doehlemann, G., Wahl, R., Hofmann, J., Schmiedl, A., Kahmann, R., et al. (2010b). Ustilago maydis infection strongly alters organic nitrogen allocation in maize and stimulates productivity of systemic source leaves. *Plant Physiol.* 152, 293–308. doi: 10.1104/pp.109.147702

Horst, R. J., Doehlemann, G., Wahl, R., Hofmann, J., Schmiedl, A., Kahmann, R., et al. (2010a). A model of Ustilago maydis leaf tumor metabolism. *Plant Signal Behav.* 5, 1446–1449.

Huang, W., Wang, Y., Li, X., and Zhang, Y. (2020). Biosynthesis and Regulation of Salicylic Acid and N-Hydroxypipecolic Acid in Plant Immunity. *Mol. Plant* 13, 31–41. doi: 10.1016/j.molp.2019.12.008

Hwang, I. S., An, S. H., and Hwang, B. K. (2011). Pepper asparagine synthetase 1 (CaAS1) is required for plant nitrogen assimilation and defense responses to microbial pathogens. *Plant J.* 67, 749–762. doi: 10.1111/j.1365-313x.2011.04622.x

Ikemura, T., Wada, K., and Aota, S. (1990). Giant G+C% mosaic structures of the human genome found by arrangement of GenBank human DNA sequences according to genetic positions. *Genomics* 8, 207–216. doi: 10.1016/0888-7543(90)90273-w

Kingsbury, J. M., Sen, N. D., and Cardenas, M. E. (2015). Branched-chain aminotransferases control TORC1 signaling in Saccharomyces cerevisiae. *PLoS Genet.* 11:e1005714. doi: 10.1371/journal.pgen.1005714

Kong, D., Hu, H. C., Okuma, E., Lee, Y., Lee, H. S., Munemasa, S., et al. (2016). L-Met Activates Arabidopsis GLR Ca(2+) Channels Upstream of ROS Production and Regulates Stomatal Movement. *Cell Rep.* 17, 2553–2561. doi: 10.1016/j.celrep.2016.11.015

Kumar, M., and Prasad, M. (1992). Organic Nitrogen-Metabolism of Crucifer Seedlings in Relation to Their Responses Towards Xanthomonas-Campestris Pv Campestris. *Zentralblatt Fur Mikrobiologie* 147, 92–102. doi: 10.1016/s0232-4393(11)80369-0

Ladwig, F., Stahl, M., Ludewig, U., Hirner, A. A., Hammes, U. Z., Stadler, R., et al. (2012). Siliques Are Red1 from Arabidopsis Acts as a Bidirectional Amino Acid Transporter That Is Crucial for the Amino Acid Homeostasis of Siliques. *Plant Physiol.* 158, 1643–1655. doi: 10.1104/pp.111.192583

Lageix, S., Lanet, E., Pouch-Pelissier, M. N., Espagnol, M. C., Robaglia, C., Deragon, J. M., et al. (2008). Arabidopsis eIF2alpha kinase GCN2 is essential for growth in stress conditions and is activated by wounding. *BMC Plant Biol.* 8:134. doi: 10.1186/1471-2229-8-134

Li, M. W., Auyeung, W. K., and Lam, H. M. (2013). The GCN2 homologue in Arabidopsis thaliana interacts with uncharged tRNA and uses Arabidopsis eIF2 alpha molecules as direct substrates. *Plant Biol.* 15, 13–18. doi: 10.1111/j.1438-8677.2012.00606.x

Liu, G., Ji, Y., Bhuiyan, N. H., Pilot, G., Selvaraj, G., Zou, J., et al. (2010). Amino acid homeostasis modulates salicylic acid-associated redox status and defense responses in Arabidopsis. *Plant Cell* 22, 3845–3863. doi: 10.1105/tpc.110.079392

Liu, R. X., and Finlayson, S. A. (2019). Sorghum tiller bud growth is repressed by contact with the overlying leaf. *Plant Cell Environ.* 42, 2120–2132. doi: 10.1111/pce.13548

Liu, Y., Chen, L., Zhang, N., Li, Z., Zhang, G., Xu, Y., et al. (2016). Plant-Microbe Communication Enhances Auxin Biosynthesis by a Root-Associated Bacterium, Bacillus amyloliquefaciens SQR9. *Mol. Plant Microbe Interact.* 29, 324–330. doi: 10.1094/mpmi-10-15-0239-r

Luna, E., Van Hulten, M., Zhang, Y., Berkowitz, O., López, A., Pétriacq, P., et al. (2014). Plant perception of β-aminobutyric acid is mediated by an aspartyl-tRNA synthetase. *Nat. Chem. Biol.* 10, 450–456. doi: 10.1038/nchembio.1520

Malamy, J., Carr, J. P., Klessig, D. F., and Raskin, I. (1990). Salicylic-Acid - a Likely Endogenous Signal in the Resistance Response of Tobacco to Viral-Infection. *Science* 250, 1002–1004. doi: 10.1126/science.250.4983.1002

Manzoor, H., Kelloniemi, J., Chiltz, A., Wendehenne, D., Pugin, A., Poinssot, B., et al. (2013). Involvement of the glutamate receptor AtGLR3.3 in plant defense signaling and resistance to Hyaloperonospora arabidopsidis. *Plant J.* 76, 466–480. doi: 10.1111/tpj.12311

Mcdowell, J. M., Hoff, T., Anderson, R. G., and Deegan, D. (2011). Propagation, storage, and assays with Hyaloperonospora arabidopsidis: a model oomycete pathogen of Arabidopsis. *Plant Immun. Methods Protoc.* 712, 137–151. doi: 10.1007/978-1-61737-998-7_12

Mckee, M. W., Fridrich, J. H., and Forshey, C. G. (1972). Some effects of Eastern X-disease on the nitrogen metabolism of peach leaves. *HortScience* 7, 393–394.

Müller, B., Fastner, A., Karmann, J., Mansch, V., Hoffmann, T., Schwab, W., et al. (2015). Amino Acid Export in Developing Arabidopsis Seeds Depends on UmamiT Facilitators. *Curr. Biol.* 25, 3126–3131. doi: 10.1016/j.cub.2015.10.038

Müller, T., Koch, W., and Wipf, D. (2006). 11 Amino Acid Transport in Plants and Transport of Neurotransmitters in Animals. *Communicat. Plants* 2006:153. doi: 10.1007/3-540-28516-4_11

Nakajo, T., Yamatsuji, T., Ban, H., Shigemitsu, K., Haisa, M., Motoki, T., et al. (2004). Glutamine is a key regulator for amino acid-controlled cell growth through the mTOR signaling pathway in rat intestinal epithelial cells. *Biochem. Biophys. Res. Communicat.* 326, 174–180. doi: 10.1016/j.bbrc.2004.11.015

Navarova, H., Bernsdorff, F., Doring, A. C., and Zeier, J. (2012). Pipecolic acid, an endogenous mediator of defense amplification and priming, is a critical regulator of inducible plant immunity. *Plant Cell* 24, 5123–5141. doi: 10.1105/tpc.112.103564

Pan, Q., Cui, B., Deng, F., Quan, J., Loake, G. J., and Shan, W. (2016). RTP1 encodes a novel endoplasmic reticulum (ER)-localized protein in Arabidopsis and negatively regulates resistance against biotrophic pathogens. *N. Phytol.* 209, 1641–1654. doi: 10.1111/nph.13707

Pieterse, C. M., Van Der Does, D., Zamioudis, C., Leon-Reyes, A., and Van Wees, S. C. (2012). Hormonal modulation of plant immunity. *Annu. Rev. Cell Dev. Biol.* 28, 489–521.

Pilot, G., Stransky, H., Bushey, D. F., Pratelli, R., Ludewig, U., Wingate, V. P. M., et al. (2004). Overexpression of glutamine dumper1 leads to hypersecretion of glutamine from hydathodes of Arabidopsis leaves. *Plant Cell* 16, 1827–1840. doi: 10.1105/tpc.021642

Pratelli, R., Guerra, D. D., Yu, S., Wogulis, M., Kraft, E., Frommer, W. B., et al. (2012). The ubiquitin E3 ligase LOSS OF GDU2 is required for GLUTAMINE

DUMPER1-induced amino acid secretion in Arabidopsis. *Plant physiol.* 158, 1628–1642. doi: 10.1104/pp.111.191965

Pratelli, R., Voll, L. M., Horst, R. J., Frommer, W. B., and Pilot, G. (2010). Stimulation of Nonselective Amino Acid Export by Glutamine Dumper Proteins. *Plant Physiol.* 152, 762–773. doi: 10.1104/pp.109.151746

Qi, Z., Stephens, N. R., and Spalding, E. P. (2006). Calcium entry mediated by GLR3. 3, an Arabidopsis glutamate receptor with a broad agonist profile. *Plant Physiol.* 142, 963–971. doi: 10.1104/pp.106.088989

Schaufelberger, M., Galbier, F., Herger, A., De Brito Francisco, R., Roffler, S., Clement, G., et al. (2019). Mutations in the Arabidopsis ROL17/isopropylmalate synthase 1 locus alter amino acid content, modify the TOR network, and suppress the root hair cell development mutant lrx1. *J. Exp. Bot.* 70, 2313–2323. doi: 10.1093/jxb/ery463

Schneider, A., Aghamirzaie, D., Elmarakeby, H., Poudel, A. N., Koo, A. J., Heath, L. S., et al. (2016). Potential targets of VIVIPAROUS1/ABI3-LIKE1 (VAL1) repression in developing Arabidopsis thaliana embryos. *Plant J.* 85, 305–319. doi: 10.1111/tpj.13106

Schwachtje, J., Fischer, A., Erban, A., and Kopka, J. (2018). Primed primary metabolism in systemic leaves: a functional systems analysis. *Sci. Rep.* 8:216.

Seo, P. J., and Park, C. M. (2010). MYB96-mediated abscisic acid signals induce pathogen resistance response by promoting salicylic acid biosynthesis in Arabidopsis. *N. Phytol.* 186, 471–483. doi: 10.1111/j.1469-8137.2010.03183.x

Shimobayashi, M., and Hall, M. N. (2016). Multiple amino acid sensing inputs to mTORC1. *Cell Res.* 26, 7–20. doi: 10.1038/cr.2015.146

Sonawala, U., Dinkeloo, K., Danna, C. H., Mcdowell, J. M., and Pilot, G. (2018). Review: Functional linkages between amino acid transporters and plant responses to pathogens. *Plant Sci.* 277, 79–88.

Stephens, N. R., Qi, Z., and Spalding, E. P. (2008). Glutamate receptor subtypes evidenced by differences in desensitization and dependence on the GLR3. 3 and GLR3. 4 genes. *Plant Physiol.* 146, 529–538. doi: 10.1104/pp.107.108134

Stuttmann, J., Hubberten, H. M., Rietz, S., Kaur, J., Muskett, P., Guerois, R., et al. (2011). Perturbation of Arabidopsis amino acid metabolism causes incompatibility with the adapted biotrophic pathogen Hyaloperonospora arabidopsidis. *Plant Cell* 23, 2788–2803. doi: 10.1105/tpc.111.087684

Tapken, D., Anschütz, U., Liu, L.-H., Huelsken, T., Seebohm, G., Becker, D., et al. (2013). A plant homolog of animal glutamate receptors is an ion channel gated by multiple hydrophobic amino acids. *Sci. Signal.* 6, ra47–ra47.

Tegeder, M., and Hammes, U. Z. (2018). The way out and in: phloem loading and unloading of amino acids. *Curr. Opin. Plant Biol.* 43, 16–21. doi: 10.1016/j.pbi.2017.12.002

Van Damme, M., Zeilmaker, T., Elberse, J., Andel, A., De Sain-Van Der, Velden, M., et al. (2009). Downy mildew resistance in Arabidopsis by mutation of HOMOSERINE KINASE. *Plant Cell* 21, 2179–2189. doi: 10.1105/tpc.109.066811

Van Loon, L. C., Rep, M., and Pieterse, C. M. (2006). Significance of inducible defense-related proteins in infected plants. *Annu. Rev. Phytopathol.* 44, 135–162. doi: 10.1146/annurev.phyto.44.070505.143425

Van Loon, L., and Van Strien, E. (1999). The families of pathogenesis-related proteins, their activities, and comparative analysis of PR-1 type proteins. *Physiol. Mol. Plant Pathol.* 55, 85–97. doi: 10.1006/pmpp.1999.0213

Vincill, E. D., Bieck, A. M., and Spalding, E. P. (2012). Ca2+ conduction by an amino acid-gated ion channel related to glutamate receptors. *Plant Physiol.* 159, 40–46. doi: 10.1104/pp.112.197509

Wang, D., Pajerowska-Mukhtar, K., Culler, A. H., and Dong, X. (2007). Salicylic acid inhibits pathogen growth in plants through repression of the auxin signaling pathway. *Curr. Biol.* 17, 1784–1790. doi: 10.1016/j.cub.2007.09.025

Ward, J. L., Forcat, S., Beckmann, M., Bennett, M., Miller, S. J., Baker, J. M., et al. (2010). The metabolic transition during disease following infection of Arabidopsis thaliana by *Pseudomonas* syringae pv. tomato. *Plant J.* 63, 443–457. doi: 10.1111/j.1365-313x.2010.04254.x

Wei, Z., Yang, T., Friman, V.-P., Xu, Y., Shen, Q., and Jousset, A. (2015). Trophic network architecture of root-associated bacterial communities determines pathogen invasion and plant health. *Nat. Communicat.* 6:8413.

Yang, H., Postel, S., Kemmerling, B., and Ludewig, U. (2014). Altered growth and improved resistance of Arabidopsis against *Pseudomonas* syringae by overexpression of the basic amino acid transporter AtCAT1. *Plant Cell Environ.* 37, 1404–1414. doi: 10.1111/pce.12244

Conflict of Interest: The authors declare that the research was conducted in the absence of any commercial or financial relationships that could be construed as a potential conflict of interest.

Copyright © 2021 Besnard, Sonawala, Maharjan, Collakova, Finlayson, Pilot, McDowell and Okumoto. This is an open-access article distributed under the terms of the Creative Commons Attribution License (CC BY). The use, distribution or reproduction in other forums is permitted, provided the original author(s) and the copyright owner(s) are credited and that the original publication in this journal is cited, in accordance with accepted academic practice. No use, distribution or reproduction is permitted which does not comply with these terms.

frontiers in Plant Science

ORIGINAL RESEARCH
published: 25 February 2021
doi: 10.3389/fpls.2021.633448

A Wild Allele of *Pyrroline-5-Carboxylate Synthase1* Leads to Proline Accumulation in Spikes and Leaves of Barley Contributing to Improved Performance Under Reduced Water Availability

*Felix Frimpong[1,2], Carel W. Windt[1], Dagmar van Dusschoten[1], Ali A. Naz[3], Michael Frei[4] and Fabio Fiorani[1]**

[1] Institute of Bio- and Geosciences, IBG-2: Plant Sciences, Forschungszentrum Jülich GmbH, Jülich, Germany, [2] CSIR-Crops Research Institute, Kumasi, Ghana, [3] Department of Plant Breeding, Institute of Crop Science and Resource Conservation, University of Bonn, Bonn, Germany, [4] Institute of Agronomy and Plant Breeding, Justus-Liebig-Universität Gießen, Gießen, Germany

OPEN ACCESS

Edited by:
Maurizio Trovato,
Sapienza University of Rome, Italy

Reviewed by:
Ahmed Sallam,
Assiut University, Egypt
Glen Fox,
The University of Queensland, Australia

***Correspondence:**
Fabio Fiorani
f.fiorani@fz-juelich.de

Specialty section:
This article was submitted to Plant Abiotic Stress, a section of the journal Frontiers in Plant Science

Received: 25 November 2020
Accepted: 25 January 2021
Published: 25 February 2021

Citation:
Frimpong F, Windt CW, van Dusschoten D, Naz AA, Frei M and Fiorani F (2021) A Wild Allele of Pyrroline-5-Carboxylate Synthase1 Leads to Proline Accumulation in Spikes and Leaves of Barley Contributing to Improved Performance Under Reduced Water Availability. Front. Plant Sci. 12:633448. doi: 10.3389/fpls.2021.633448

Water stress (WS) during spike development strongly affects final grain yield and grain quality in cereals. Proline, an osmoprotectant amino-acid, may contribute to alleviating the effects of cell and tissue dehydration. We studied five spring barley genotypes contrasting in their drought response, including two introgression lines, *S42IL-143* and *S42IL-141*, harboring a *Pyrroline-5-carboxylate synthase1- P5cs1* allele originating from the wild barley accession *ISR42-8*. We tested the hypothesis that barley genotypes harboring a wild allele at *P5cs1* locus are comparatively more drought-tolerant at the reproductive stage by inducing proline accumulation in their immature spikes. At the booting stage, we subjected plants to well-watered and WS treatments until physiological maturity. Several morpho-physiological traits had significant genotype by treatment interaction and reduction under WS. Varying levels of genotypic proline accumulation and differences in WS tolerance were observed. Spike proline accumulation was higher than leaf proline accumulation for all genotypes under WS. Also, introgression lines carrying a wild allele at *P5cs1* locus had a markedly higher spike and leaf proline content compared with the other genotypes. These introgression lines showed milder drought symptoms compared with elite genotypes, remained photosynthetically active under WS, and maintained their intrinsic water use efficiency. These combined responses contributed to the achievement of higher final seed productivity. Magnetic resonance imaging (MRI) of whole spikes at the soft dough stage showed an increase in seed abortion among the elite genotypes compared with the introgression lines 15 days after WS treatment. Our results suggest that proline accumulation at the reproductive stage contributes to the maintenance of grain formation under water shortage.

Keywords: barley, introgression lines, seed yield, proline accumulation, *pyrroline-5-carboxylate synthase1*, water stress

INTRODUCTION

The ability of crops to withstand WS is a critical aspect of the potential impact of climate change on crop productivity in agricultural systems (Ferguson, 2019; Gupta et al., 2020). Plants use different strategies to cope with water shortage: avoidance, escape, or tolerance. The escape strategy is an adaptive mechanism that involves rapid plant development to enable the completion of the full life-cycle before a drought event can occur (Shavrukov et al., 2017). In cereals, drought escape is associated with a short vegetative stage and early flowering time. The avoidance strategy involves minimization of water loss and optimization of water uptake, which comprises physiological responses that improve photosynthetic water use efficiency, such as stomatal closure (Blum, 2005; Basu et al., 2016; Fahad et al., 2017; Rodrigues et al., 2019), stay green (Tardieu et al., 2018; Wasaya et al., 2018; Sallam et al., 2019), deeper rooting (Arai-Sanoh et al., 2014; Lynch and Wojciechowski, 2015; Kebede et al., 2019), or the accumulation of osmolytes and osmoprotectants (Bandurska et al., 2017).

Drought is known to profoundly affect plant metabolism (Templer et al., 2017). The accumulation of compatible solutes such as sugars, proline, fructans, glycine betaine, and polyamines is associated with increased drought tolerance in plants (Bhaskara et al., 2015; Templer et al., 2017; Trovato et al., 2019). Drought stress increased proline concentration about 10-fold in the leaves of monocotyledons such as rice (*Oryza sativa*) and dicotyledons species such as *Brassica oleracea* seedlings (Dien et al., 2019; Podda et al., 2019).

Proline is synthesized from glutamate by the action of three enzyme coding genes, pyrroline-5 carboxylate synthase (*P5CS*), pyrroline-5-carboxylate synthase-2 (*P5CS2*), and pyrroline-5-carboxylate reductase (*P5CR*) (Bhaskara et al., 2015; Trovato et al., 2019). Several reports investigated the proline biosynthetic pathway and the corresponding key enzymes *P5CS* and *P5CR* have been well characterized (Forlani et al., 2015; Choudhury et al., 2017; Abdel-Ghani et al., 2019; Kamal et al., 2019). In higher plants, the most rate-limiting enzyme for proline synthesis is pyrroline-5-carboxylate synthase (Trovato et al., 2019). Proline biosynthesis occurs under both non-limiting and limiting growth conditions (Cattivelli et al., 2011; Nieves-Cordones et al., 2019). Under non-limiting growth conditions, proline is used in protein biosynthesis to maintain the housekeeping function of the cell (Hoffmann et al., 2017). Proline accumulation under WS is accompanied by the increased expression of *P5cs1* (Muzammil et al., 2018). The expression of both *P5cs1* and *P5CR* is increased in leaves when barley is exposed to drought, resulting in enhanced proline synthesis in the chloroplast, whereas *P5CS2* is primarily linked to proline synthesis in the cytosol (Sayed et al., 2012).

In barley, introgression lines carrying naturally occurring alleles (cross between *Scarlett* and wild type *ISR42-8*) associated with proline accumulation and leaf wilting under drought stress conditions were reported previously (Sayed et al., 2012; Honsdorf et al., 2014, 2017; Naz et al., 2014). To test the hypothesis that the allelic variant of *P5cs1* controls the drought-inducible QTL (*QPro.S42-1H*) in the donor parental line and progenies, Muzammil et al. (2018) performed a series of phenotypic evaluations. They demonstrated that the progeny introgression lines maintained leaf water content and photosynthetic activity longer compared with those of the cultivated parents under drought conditions. Nonetheless, to understand the integrative networks of plant metabolites and signaling molecules, the sites of their biosynthesis and action must be clarified (Kuromori et al., 2018). Understanding the specific target sites regulating seed filling events in leaves and seeds and how they are affected by abiotic stresses is imperative to enhance seed quality (Sehgal et al., 2018). Knowledge of the physiological, biochemical, and genetic mechanisms which govern seed filling under stressful environments helps to devise strategies to improve stress tolerance (Sehgal et al., 2018; Abdelrahman et al., 2020). Little attention has been paid to the role of proline in the reproductive organs (Heuer, 2016), especially spikes or seeds, and the changes in its concentration in different plant organs under WS. In this study, we addressed this knowledge gap by measuring spike and leaf proline content, changes in photosynthetic performance, and assessing barley seed abortion and GF under WS using MRI at the reproductive stages.

We tested the hypothesis that drought-induced proline accumulation in spikes of barley genotypes harboring the wild variant of *P5cs1* improves drought tolerance as measured by seed number and final yield in greenhouse experiments. To this end, we characterized a panel of contrasting elite genotypes and *P5cs1*-introgression lines and monitored morpho-physiological responses after water withdrawal during reproductive development.

MATERIALS AND METHODS

Plant Material

Four two-row and one six-row spring barley genotypes *S42IL-141*, *S42IL-143*, *Scarlett*, *Barke*, and *HOR10151* were chosen for this study based on the initial screening, their genetic background, breeding history, agronomical importance, and previously reported yield under drought stress conditions. *S42IL-141*, *S42IL-143* carried chromosomal introgressions at *P5cs1* locus from wild barley accession *ISR42-8* (Muzammil et al., 2018). *Barke* and Scarlett are elite German cultivars. *HOR10151* is a six-row traditional landrace known to escape drought when grown at high elevations of the Libyan region where it originated.

Growth Conditions and Water Stress Treatment

Two experiments were conducted in a greenhouse (Forschungszentrum Jülich, Germany, IBG2: Plant Sciences; 50°55′17.36″N, 6°21′45.61″E) in two consecutive years,

Abbreviations: *A*, net CO_2 assimilation; B, booting; DAWS, days after water stress; DLI, daily light integral; DSI, drought susceptibility index; *E*, transpiration rate; ETR, electron transport rate; FW, fresh weight; GF, grain filling; GSW, stomatal conductance; HD, heading; MRI, magnetic resonance imaging; PPFD, photosynthetic photon flux density; *P5cs1*, *pyrroline-5-carboxylate synthase1*; *P5CS2*, *pyrroline-5-carboxylate synthase2*; *P5CR*, *pyrroline-5-carboxylate reductase*; *P5C*, *pyrroline-5-carboxylate*; *ProDH1*, *proline dehydrogenase1*; WS, water stress; WW, well-watered.

June – October of 2018 and 2019 under long-day conditions (16 h/8 h day/night). Extra illumination (SON-T AGRO 400, Philips, Amsterdam, Netherlands) was automatically supplied when the ambient light intensity inside the greenhouse was <400 μmol m^{-2} s^{-1}, between 06:00 and 22:00 h. The average minimum and maximum greenhouse daily light integral (DLI, mol m^{-2} day^{-1}) were 6 and 13 in 2018 and 3 and 12 in 2019 (**Supplementary Figure 1**). Day/night minimum and maximum temperature of the greenhouse was ∼ 20 ± 4°C and 30 ± 4°C during the day and ∼ 16 ± 2°C and 20 ± 2°C during the night, respectively. Cumulative growing degree days were calculated assuming a base temperature of 0°C (Miller et al., 2001; Hecht et al., 2019) from the time of emergence until the ripening stage. These were 2,155 and 2,059 degree days in 2018 and 2019, respectively. Pre-germinated seeds of five genotypes were transplanted into 1.5 L pots upon reaching the three leaves stage. Peat soil (Einheitserde, "null type") was used for both experiments arranged in a 5 × 2 factorial randomized complete block design with six and fifteen replicates per genotype and treatment in 2018 and 2019, respectively. Three tablets of the 5 g Osmocote Exact slow-release fertilizer (14-8-11; N – P_2O_5 – K_2O + 2 MgO + trace elements) were applied per plant in three aliquots starting 2 weeks after transplanting. Pests and diseases were controlled chemically according to established greenhouse practices.

Water was administered with the help of an automated drip irrigation setup at the greenhouse (Netafilm, Adelaide, SA, Australia), watering the pots twice daily. Starting from the booting stage (BBCH-scale 41, Meier, 2001), all genotypes were subjected to two irrigation regimes. The treatments were WW and WS. We applied WS by first withholding water for the selected plants for 48 h, and then adjusted the irrigation volume three times per week to maintain target soil moisture per treatment. WW plants were irrigated daily (400 mL per plant) approximately to 50% g/g gravimetric soil water content in two aliquots per day; WS plants were irrigated daily (120 mL per plant) approximately to 20% g/g gravimetric soil water content in two aliquots per day (**Supplementary Figure 2**). Soil water content was monitored with the aid of a three-pin time-domain-reflectometry soil moisture Theta ML2 probe (Delta-T Devices Ltd., United Kingdom), after calibration (R^2 = 0.94) from volumetric to gravimetric soil water content. The corresponding soil water potential (Ψ soil) values of WW and WS were −0.001 and −1.5 MPa, respectively. These soil water potential values were estimated using eight-point water retention curves that were fitted with van Genuchten model (van Genuchten, 1980).

Morphometric and Physiological Measurements

Twice a week, two plants of each genotype were dissected under a stereomicroscope to observe spike developmental stages and characterize treatment effects. The stereomicroscope (Leica MZ12 stereo microscope, Germany) was equipped with a 1.0 × planochromatic objective and with 10 × eyepieces, a numerical aperture of 0.125, and a resolution of 375 line pairs/mm. The number of days to reach each stage of development was counted for both WW, and WS treated plants. Plant height and tiller number were determined at harvest. At harvest (20 days after WS) yield traits such as spike number, spike length (cm), spike weight (g), total grain weight (g), grain number, shoot fresh weight (g), and shoot dry weight (g) were determined on a per plant basis. A DSI for dry grain yield (g) per plant was calculated using the following formula (Haddadin, 2015):

$$DSI = \frac{1 - \frac{YD}{YP}}{1 - \frac{WD}{WP}}$$

where:

YD, mean yield of individual genotype under the WS condition.

YP, mean yield of individual genotype under the WW condition.

WD, mean of all genotypes under the WS condition.

WP, mean of all genotypes under the WW condition.

At harvest, fresh, and dry weight per plant (g) were determined for shoot and root (after washing) biomass. Percentage relative leaf water content of fully expanded leaves was calculated:

% *relative leaf water content* (*RWC*) = $\frac{(\text{fresh leaf weight} - \text{dry leaf weight})}{(\text{turgid leaf weight} - \text{dry leaf weight})} \times 100$, according to Barrs and Weatherley (1962), fifteen days after the WS application.

WS treated leaves were scored for wilting one time forenoon, fifteen days after the onset of treatment using a scale from 0 to 9. A score of 0 indicated no wilting and 9 is fully wilted (De Datta et al., 1988; Sallam et al., 2019). Gas exchange parameters (net CO_2 assimilation – *A*, μmol CO_2 m^{-2} s^{-1}, stomatal conductance – *gsw*, mmol H_2O m^{-2} s^{-1}, transpiration rate – *E*, mol H_2O m^{-2} s^{-1}, and intrinsic water use efficiency (*A/gsw)* –iWUE, μmol CO_2 $mmol^{-1}$ H_2O) were measured on the youngest leaf directly below the flag leaf on the main stem at one-time point during the experiment of 2018 (15 days after WS). The flag leaf of the main stem was used for the gas exchange measurements in 2019 at 3, 9, and 15 days after WS application. Fifteen and six plants per genotype per treatment in 2019 and 2018, respectively, were used for the gas exchange measurements. Leaves were clamped in the MultiPhase Flash ™ fluorometer chamber (551065), 10% blue light, 6 cm^2 LiCOR cuvette, and exposed to PPFD of 1,500 μmol $m^{-2}s^{-1}$, Airflow (500 mmol s^{-1}), block temperature of 25°C, 400 ppm of CO_2, humidity (RH) ranging between 50 and 65% using a LiCor 6,800 (LiCOR Inc., Lincoln, NE, United States). Instantaneous photosynthesis and GSW were measured after steady-state gas exchange conditions inside the cuvette were reached. Measurements were completed between 10:00 am and 3:00 pm during the day for all barley plants by following the randomization order of the experimental layout to account for the possible effects of time of day on the measurements, which could spuriously bias genotypic values and variability estimation as well.

Magnetic Resonance Imaging

The magnetic resonance imaging scans were carried out using a custom-built, vertical bore 4.7 T MRI scanner, driven by a Varian console VNMRS, vertical wide-bore MRI system (Varian Inc)[1].

[1]http://www.varianinc.com

The system was equipped with a quadrature to transmit/receive coil with an inner diameter of 100 mm and a 300 mT/m gradient system. The main spikes at the dough stage (BBCH-scale, 83) were collected together with a section of the stalk (>20 mm). The cut spikes were placed in a vial with tap water directly after excision. A robotic system (MiniLiner 3.0, Geiger Handling GmbH and Co. Kg, Jülich, Germany) was used to carefully lower and center the specimen into the MRI scanner. 2D images of developing spikes were acquired with an in-plane spatial resolution of 0.3750 and 0.1875 mm, using multi-spin-echo sequence based on the following set routines; 32 echoes, 1.5 s repetition time, echo time of $n \times 8$ ms, two averages, 512 × 256 image matrix, a field of view of 100 (read direction) by 50 mm (phase direction), at a slice thickness of 50 mm. The acquired datasets show amplitude images of water content per pixel (Edzes et al., 1998). Each spike was imaged for 12 min. An additional 10 min of preparation and setting the sample to the center of the magnet were required. For all spikes, the MRI images presented are amplitude parameter maps of a single echo image in gray values in their sagittal orientation after analyzing using image reconstruction set scripts from Spyder, scientific programming in Python 3.6.

Proline Determination in Barley Leaves and Spikes

Proline concentrations were determined based on the protocol of Bates et al. (1973), with few modifications. Six replicates of each of the flag leaf and immature spike samples were collected from both treatments and genotypes and immediately submerged in liquid nitrogen. Samples were stored at −80 °C. Samples were pulverized using pestle and mortar on ice. One hundred mg of the pulverized samples were weighed and extracted with 1.5 ml of 3% salicylic acid in chilled 2 mL tubes, vortexed, and centrifuged at 12,000 rpm for 10 min. Five hundred μL of the supernatant was directly transferred into cylindrical glass tubes (fitted with lids) on ice and 500 μL of glacial acetic acid and 2.5% ninhydrin reagent added. The mixture was then vigorously vortexed and incubated for 1 h in a water bath at 95 °C. The reaction was quickly terminated on ice. 1.5 mL of toluene was added, and the mixture was kept at room temperature for 30 min after vortexing. One hundred μL of the upper phase was then pipetted into 96 well plates, and the absorbance at 520 nm measured using a microplate reader (Synergy™ 2 Multi-Mode, BioTek, Winooski, Vermont, United States). An empirical calibration curve based on eight points of proline standard concentrations (0, 10, 20, 30, 50, 70, 90, and 100 μg/g) yielded a linear regression between proline concentration and the measured absorbance at 520 nm (R^2 = 0.998). This linear model was subsequently used for proline concentration calculation in the samples.

Statistical Analysis

All data were subjected to normality (Shapiro Wilk test) and variance homogeneity tests (Levene's test). Power transformation (Box and Cox, 1964) was performed for the gas exchange and proline measurements because normality or homogeneity conditions were not met. The main effects of genotypes and WS treatments, along with their corresponding interactions, were tested first using a three-way analysis of variance. We found treatment × genotype × year interaction effect for all data (except for spike length, **Supplementary Data Sheet 2**). Therefore, we proceeded to analyze the data using a year-specific two-way analysis of variance. We used the generalized linear model;

$\mu_{ijk} = \mu + \alpha_i + \beta_j + (\alpha\beta_{ij}) + \varepsilon_{ijk}$, where;

μ , grand mean.

α_i *and* β_j, main effects of WS treatment and genotypes of the *ith* and ($\alpha\beta_{ij}$) levels.

jth, interaction effect.

ε_{ijk} , error term.

built-in the "Agricolae" package of "R" statistical software, version 3.6.1 (R Core Team, 2019). Tukey's HSD (Honest Significant Difference test) was used to determine significant differences between treatment and genotypic means within plant traits. Spearman correlation coefficients for pair-wise comparisons for selected traits were computed.

RESULTS

Effects of Water Stress on Barley Morphology and Physiology

Pronounced leaf wilting was observed under WS for all the genotypes and treatments (**Figure 1**). However, the two introgression lines *S42IL-143* and *S42IL-141* showed milder wilting symptoms (−40%) than the elite barley types *Barke, Scarlett,* and *HOR10151* (**Tables 1**, **2**). The six-row barley type, *HOR10151* showed higher susceptibility to wilting than the introgression lines with more than 50% of its leaves drying 15 days after stress application (**Table 2** and **Figure 1**). Averagely, WS *S42IL-143* and *S42IL-141* had a wilting score of 2 or less while the elite lines were 3 and above (**Table 2**). None of the WW plants showed any wilting symptoms (**Table 1**). Results from both 2018 and 2019 experiments showed that introgression lines *S42IL-143* and *S42IL-141* maintained their RWC (>70%) both under WS and WW conditions **Table 2**. Differently from the WW conditions, elite cultivars showed smaller variations in RWC under WS (**Tables 1**, **2**). In 2019, *Barke* and *HOR10151* had the lowest RWC (∼35%, **Tables 1**, **2**) under WS.

The spike developmental stages from booting, heading, and anthesis up to the onset of GF were delayed by at least one day under WS treatment for all genotypes (**Supplementary Figure 3**). Barley genotype *HOR10151* had the most considerable delay (three days difference between WS and WW plants, **Supplementary Figure 3**). Plant performance for all genotypes was significantly reduced for both experimental years (**Table 1** and **Supplementary Table 2**). Relative to WW conditions, we observed a percentage reduction (%) of average plant height (18, 27), tiller number (19, 47), spike number (45, 38), grain number (30, 58), spike length (18, 22), grain weight (76, 76), RWC (15, 35), net CO_2 assimilation (56, 72), GSW (74, 77), transpiration rate (63,76), and ETR (31, 28) (**Supplementary Table 2**) in 2018 and 2019, respectively.

Prolonged WS of fifteen days led to several leaves drying and reduced net CO_2 assimilation by at least 50% (**Figure 2A**

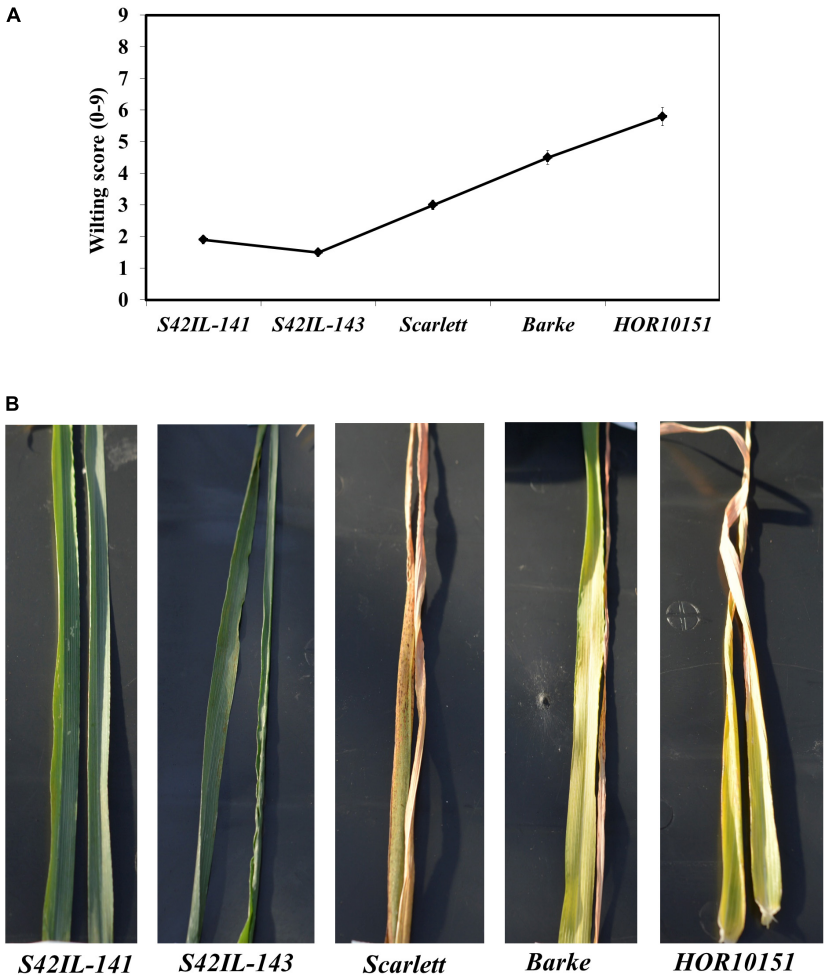

FIGURE 1 | Wilting severity by the different genotypes recorded forenoon, 15 days after onset of water stress adapted from De Datta et al., 1988. **(A)** Is a line graph depicting wilting scores for each genotype. **(B)** An illustration of the wilting score/drought symptoms as shown by representative leaves (leaf 5 and 6 fully expanded) of the different genotypes.

and **Figure 1**). Net CO_2 assimilation, GSW, transpiration rate, and ETR were significantly reduced due to WS (**Table 1**). Significant genotypic variations were observed in the gas exchange parameters under WW conditions (**Figures 2A–D**). For instance, net CO_2 assimilation in fully turgid leaves was between 22 and 24 μmol m^{-2} s^{-1} throughout the experiment period (**Figure 2A**). *Scarlett* had the lowest and *HOR10151* the highest net CO_2 assimilation under WW (**Figure 2A**). On the other hand, the WS plants had a net CO_2 assimilation rate between 2.5 and 10.7 μmol m^{-2} s^{-1} throughout the stress period (**Figure 2A**). *Barke* had the lowest value for net CO_2 assimilation (2.5 μmol m^{-2} s^{-1}), while the highest net CO_2 assimilation rate was by *S42IL-141*and *S42IL-143* (10.7 and 12.5 μmol m^{-2} s^{-1}) under WS, respectively (**Figure 2A**).

Transpiration rate was between 0.43 × 10^{-2} and 0.66 × 10^{-2} mol $m^{-2}s^{-1}$ under WW conditions, compared with 0.52 × 10^{-3} and 0.27 × 10^{-2} mol $m^{-2}s^{-1}$ under WS throughout the stress period (**Figure 2B**). *HOR10151* had the lowest transpiration rate, 0.52 × 10^{-3} mol $m^{-2}s^{-1}$ while *S42IL-143* transpired the most, 0.27 × 10^{-2} mol $m^{-2}s^{-1}$, 15 days after WS (**Figure 2B**). Stomatal conductance of fully turgid leaves was between 0.2 and 0.4 mol m^{-2} s^{-1} compared with WS leaves of 0.03 and 0.1 mol m^{-2} s^{-1} from booting to the onset of GF stages (**Figure 2C**). Introgression lines *S42IL-143* and *S42IL-141* maintained their photosynthetic activities by not only photosynthesizing at a higher rate several days after imposing WS but were also able to keep transpiring with low to moderate stomatal opening, ranging from 0.130 and 0.097 mol m^{-2} s^{-1} when the grain started filling (**Figure 2C**). These values were higher than those measured for *Barke, Scarlett,* and *HOR10151,* which were between 0.025 – 0.055 mol m^{-2} s^{-1} under WS (**Figure 2C**). Under WW conditions, intrinsic water use efficiency (iWUE) ranged between 59 and 105 μmol^{-1} CO_2 H_2O^{-1} (**Figure 2D**). iWUE of fully turgid flag leaves of *S42IL-141* was the lowest while *S42IL-143* was the highest across developmental stages. iWUE of the flag leaves of WS plants ranged between 65 and 122 $\mu mol^{-1} CO_2$ H_2O^{-1}. On average

TABLE 1 | Two-way analysis of variance of the plant traits in 2018 and 2019 under control, drought, genotypes, and genotype × treatment interaction, at the end of water stress application.

Traits	2018					2019				
	Control	Drought	Treatment	Genotype	G × T	Control	Drought	Treatment	Genotype	G × T
Plant height (cm)	92.9	75.9	***	NS	NS	93.3	67.8	***	***	NS
Tiller number	17.50	13.97	***	NS	NS	21.40	11.39	***	*	NS
Wilting/drought score	0.00	2.85	***	***	NA	0.07	3.36	***	***	NA
Relative leaf water content (%)	87.5	74.4	***	***	***	85.9	55.7	***	***	***
Spike number	18.35	10.00	***	***	*	26.40	16.39	***	***	***
Grain weight/plant (g)	12.57	2.91	***	***	***	14.22	4.37	***	***	***
Grain number per the main tiller	25.27	18	***	***	NS	28.84	11.05	***	***	***
Length of the main spike (cm)	10.61	8.68	***	***	NS	10.01	7.82	***	***	***
Shoot fresh weight (g)	59.01	46.13	***	***	**	35.8	19.9	***	***	NS
Shoot dry weight (g)	27.63	23.56	***	***	**	18.22	12.15	***	***	*
Root dry weight (g)	4.99	3.91	***	***	NS	3.99	2.91	***	***	NS
Root/shoot ratio (g)	0.18	0.17	NS	NS	NS	0.22	0.24	NS	NS	NS
A (μmol m^{-2} s^{-1})	28.83	13.13	***	***	***	21.51	6.08	***	***	***
E (mol m^{-2} s^{-1})	9.9E^{-3}	3.6E^{-3}	***	***	***	9E^{-3}	2E^{-3}	***	***	***
Ci (μmol mol^{-1})	260.86	176.54	***	***	***	239	216	*	NS	NS
VPDleaf	2.34	3.19	***	***	***	2.22	2.32	***	NS	NS
gsw (mol m^{-2} s^{-1})	0.43	0.11	***	***	***	0.28	0.063	***	***	***
iWUE (μmol CO_2 mmol^{-1} H_2O)	68	118	***	NS	*	81	95	***	***	***
ETR (μmol m^{-2} s^{-1})	163	99	***	***	***	139	100	***	***	***
Leaf proline (μg/g FW)	63	325	***	***	***	43	299	***	***	***
Spike proline (μg/g FW)	–	–	–	–	–	120	580	***	***	***

", **, and ***" – Follows the standard probability values (P ≤ 0.05, P ≤ 0.01, or P ≤ 0.001). Means of A, E, Ci, VPDleaf, gsw, iWUE, ETR, and proline were back-transformed to original values after transformation. A, net CO_2 assimilation; E, transpiration; gsw, stomatal conductance; VPDleaf, vapor pressure deficit of the leaf; iWUE, intrinsic water use; efficiency, A/gsw; ETR, electron transport rate; FW, fresh weight; NA, not analyzed; NS, not significant.*

TABLE 2 | Differential biochemical and yield traits in response to water stress among the genotypes and drought treatments.

Year	Genotype	Well-watered				Water stress				
		% Relative leaf water content	Grain weight/plant (g)	Grain number per main tiller	Length of the main spike (cm)	% Relative leaf water content	Wilting score	Grain weight/plant (g)	Grain number per main tiller	Length of the main spike (cm)
2018	*Barke*	89.4 ± 1.07ab	13.7 ± 0.33ab	20.5 ± 1.77a	10.6 ± 0.11bc	56.5 ± 1.07c	3.3 ± 0.18b	1.4 ± 0.33f	6.3 ± 1.77b	8.3 ± 0.11d
	HOR10151	86.4 ± 0.88ab	9.8 ± 1.39c	27.33 ± 3.50a	6.2 ± 0.26e	57.2 ± 0.88c	4.9 ± 0.14a	2.8 ± 1.39ef	17.33 ± 3.50ab	4.9 ± 0.26e
	Scarlett	90.9 ± 1.64a	14.0 ± 0.90a	25.7 ± 2.02a	11.7 ± 2.06ab	86.1 ± 1.64ab	2.9 ± 0.15bc	2.3 ± 0.90ef	18.2 ± 2.02a	9.2 ± 2.06cd
	IL141	87.4 ± 0.69ab	11.3 ± 0.72bc	26.5 ± 1.65a	12.7 ± 1.65a	85.3 ± 0.69ab	1.9 ± 0.15cd	5.3 ± 0.72de	23.7 ± 1.65a	10.7 ± 1.65bc
	IL143	85.6 ± 0.95ab	14 ± 0.52a	26.3 ± 1.41a	11.8 ± 1.40ab	84.6 ± 0.95b	1.2 ± 0.16de	6.7 ± 2.54d	24.2 ± 0.52a	10.4 ± 1.40bc
2019	*Barke*	87.5 ± 2.04a	14.0 ± 0.38a	23.6 ± 0.75b	10.0 ± 0.21bc	27.1 ± 1.99d	4.5 ± 0.11b	0.5 ± 0.24e	2.3 ± 0.63e	7.27 ± 0.29e
	HOR10151	84.6 ± 1.77a	10.6 ± 0.36b	43.2 ± 1.85a	6.5 ± 0.19e	28.6 ± 1.85d	5.8 ± 0.15a	1.1 ± 0.20de	4.0 ± 0.70de	4.5 ± 0.16f
	Scarlett	82.4 ± 1.42a	13.5 ± 0.51a	27.1 ± 1.05b	11.1 ± 0.22ab	56.9 ± 1.22c	3.0 ± 0.12c	2.7 ± 0.43d	9.5 ± 1.66d	8.47 ± 0.20d
	IL141	84.2 ± 1.19a	13.6 ± 0.58a	24.4 ± 1.22b	11.1 ± 0.32ab	73.6 ± 0.73b	1.9 ± 0.10d	4.9 ± 0.30c	22.1 ± 1.32bc	10.1 ± 0.26bc
	IL143	86.2 ± 2.11a	13.3 ± 0.38a	25.9 ± 1.12b	11.27 ± 0.23a	84.7 ± 1.01a	1.5 ± 0.12d	6.7 ± 0.24c	17.3 ± 1.23c	9.23 ± 0.23cd

Different letters indicate significant differences among treatments and genotypes based on Tukey's HSD test (P ≤ 0.05) within a trait. Values are least-square means ± standard errors of six replicates for 2018 and 15 replicates for 2019. Control plants showed no wilting and therefore scored zero and were not analyzed.

Barke and Scarlett had the lowest values at heading and onset of GF, respectively. *S42IL-141*had the highest iWUE under WS at booting and heading (**Figure 2D**). Interestingly, the iWUE of WS leaves of *S42IL-141*and *S42IL-143* increased by more than 20% compared with *Barke, Scarlett,* and *HOR10151* relative to their WW conditions (**Figure 2D**). iWUE of *Barke*, *Scarlet,* and *HOR10151* also increased marginally by 7% under WS on average. On average, elite genotypes *Barke, Scarlett,* and *HOR10151* had a lower increment of iWUE (7%) under WS than under WW conditions (**Figure 2D**).

Generally, barley plants exposed to WS reduced their photosynthetic capacity, transpired less by closing their stomata

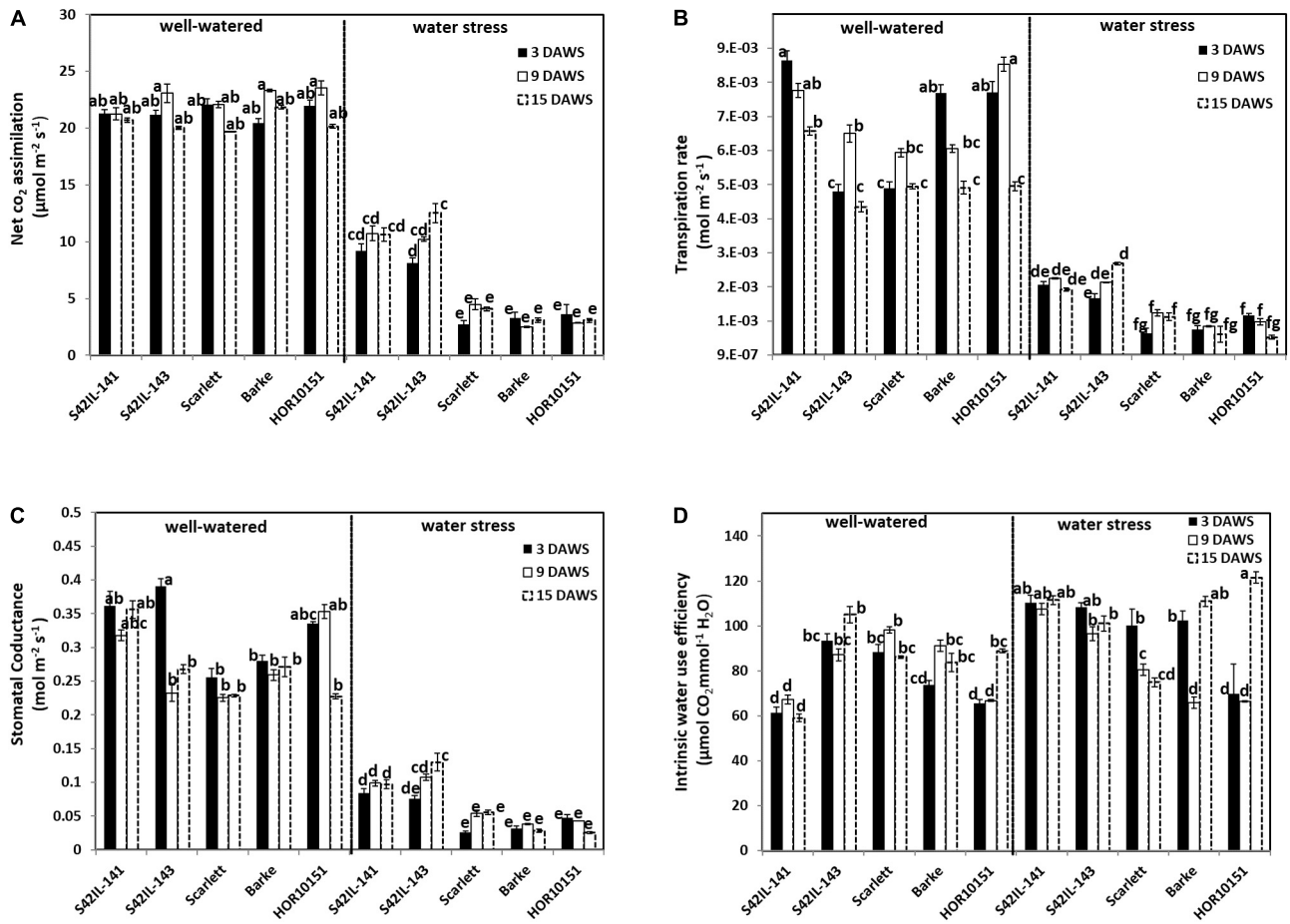

FIGURE 2 | Gas exchange measurements of the different barley genotypes under well-watered and water stress treatment. Measurements were taken at 3, 9, and 15 days after water stress (DAWS), at booting, heading, and the onset of grain filling stages of spike development, respectively. Means and standard error bars are shown. The different letters indicate significant differences in treatment means based on Tukey's (HSD) test (n = 15). **(A)** The net CO_2 assimilation. **(B)** Transpiration rate. **(C)** Stomatal conductance. **(D)** Intrinsic water use efficiency.

with an overall leaves dehydration compared with their counterparts under sufficient water supply. Under WS we observed two groups of genotypes for net CO_2 assimilation, GSW, and transpiration rate, with the two introgression lines as one, and the three elite materials as the other group (**Figures 2A–C**). Electron transport rate ranged from 74.49 to 179.51 µmol m^{-2} s^{-1} under WW conditions (**Supplementary Figure 4**). *Barke* had the lowest ETR while *S42IL-141* had the highest ETR under WW conditions. ETR was between 51.59 and 160.09 µmol m^{-2} s^{-1} under WS conditions (**Supplementary Figure 4**). Again, *Barke* had the least ETR, while *S42IL-143* had the highest ETR under WS (**Supplementary Figure 4**).

In terms of trait relationships (**Supplementary Figure 5**), percentage relative leaf water content was significantly ($P \leq 0.05$) and negatively correlated with wilting score ($r = -0.74$), iWUE ($r = -0.29$), and leaf proline ($r = -0.26$). The percentage relative leaf water content significantly ($P \leq 0.05$) and positively correlated with net CO_2 assimilation ($r = 0.73$), GSW ($r = 0.718$), transpiration rate ($r = 0.71$), electron transport rate ($r = 0.62$), grain weight ($r = 0.61$), grain number ($r = 0.66$), plant height ($r = 0.61$), and shoot biomass ($r = 0.36$). The leaves' susceptibility to drying, i.e., the wilting score was significant ($P \leq 0.05$) under WS and correlated negatively with reductions in net CO_2 assimilation rate ($r = -0.88$), GSW ($r = -0.87$), and transpiration rate ($r = -0.88$). However, leaf wilting correlated positively with leaf proline content ($r = 0.48$). The reduction in net CO_2 assimilation rate under WS was significant ($P \leq 0.05$) and correlated positively with reductions in GSW ($r = 0.96$), transpiration rate ($r = 0.97$), and grain weight ($r = 0.85$).

Barley Yield Traits Under Water Stress

Grain number per main tiller had a significant genotypic, treatment, and genotype × treatment interaction effect in the 2019 experiment (**Table 1**). In 2018, we observed a significant ($P \leq 0.001$) treatment effect and a genotypic effect, but no genotype × treatment interaction (**Table 1**). Grain number per main tiller ranged from 20 to 43 and from 2 to 24 for WW and WS treated plants, respectively (**Table 2**). The six-row barley, *HOR10151* had the highest number of grains per main tiller (27, 43) under WW conditions in 2018 and 2019, respectively.

*S42IL-141*and *S42IL-143* had the highest grain number per main tiller (24, 24, and 22, 17) under WS conditions in 2018 and 2019, respectively (**Table 2**). *Barke* had the lowest grain number per main tiller (20, 6, and 24, 2) in 2018 and 2019 under WW and WS conditions, respectively (**Table 2**). For all genotypes, we observed at least a 30% reduction in the grain number per the main tiller under WS for the 2018 and 2019 experimental years (**Supplementary Table 2**).

Water stress plants showed significant variations in total grain weight per plant in both 2018 and 2019 experimental years (**Table 1**). We observed at least a 76% reduction in grain weight for all the genotypes investigated (**Supplementary Table 2**). Grain weight ranged from 9.8 to 14.0 g under WW and from 0.5 to 7 g under WS conditions (**Table 2**). WW *Barke* had the highest grain weight of 14 g in 2018 and 2019 (**Table 2**). *S42IL-141*and *S42IL-143* had the highest grain weight of 5 and 7 g under WS conditions in 2018 and 2019 (**Table 2**). *S42IL-141*and *S42IL-143* had more than 40% in grain weight compared with *Barke, Scarlet,* and *HOR10151* under WS (**Table 2**). Grain weight correlated positively with grain number per main tiller ($r = 0.7$), shoot fresh weight ($r = 0.55$), plant height ($r = 0.76$), transpiration ($r = 0.83$), GSW ($r = 0.84$), and ETR ($r = 0.42$). These correlations were significant ($P \leq 0.05$; **Supplementary Figure 5**). Grain weight correlated negatively with proline ($r = -0.49$) and iWUE ($r = -0.41$). These correlations were significant ($P \leq 0.05$; **Supplementary Figure 5**). WS plants had reductions of at least 38, 30, 18, and 16% in spike number, grain number, shoot fresh weight, and shoot dry weight, respectively (**Table 1** and **Supplementary Table 2**).

Average DSI values based on the grain weight per plant ranged from 0.2 to 1.2 in 2018, and from 0.4 to 0.7 in 2019 in response to prolonged WS of 15 days, respectively (**Supplementary Table 3**). *Barke* had the highest DSI in both 2018 and 2019, which meant it was the most WS susceptible genotype (**Supplementary Table 3**). *P5cs1*-introgression line *S42IL-143*, on the other hand, had the least DSI in both 2018 and 2019 (**Supplementary Table 3**). Spike length had a significant genotype and genotype × treatment interaction effect in 2019 (**Table 1**). However, in 2018, a significant ($P \leq 0.01$) treatment effect and a genotypic effect, were observed, with no interaction effect for spike length (**Table 1**). Spike length ranged from 4.5 to 10.7 cm and 6.2 to 12.7 cm under WS and WW conditions, respectively, across genotypes for both experimental years (**Table 2**). The spikes of the introgression lines *S42IL-143* and *S42IL-141*were the longest, both under WW and WS (**Table 2**). The six-row barley, *HOR10151* had the shortest spike length, both under WW conditions and WS (**Table 2**). Generally, WS plants had spikes that were shorter by at least 18% (**Supplementary Table 2**). Spearman correlation coefficient resulted in significant ($P \leq 0.001$) and positive correlations between spike length and grain weight ($r = 0.69$), grain number ($r = 0.54$), and plant height ($r = 0.36$; **Supplementary Figure 5**). These data indicate that these reductions in spike length are associated with significant reductions in grain number and grain weight. Root dry weight had a significant ($P \leq 0.01$) treatment effect and a genotypic effect, with no interaction effect for both experimental years (**Table 1**). The average WW root dry weight (g) was 3.9 in 2019 compared with 4.9 in 2018. The average WS root dry weight (g) was 2.9 in 2019 compared with 3.9 in 2018 (**Table 1**). In 2019, *Barke* had the highest root dry weight (g) of 5.75 and 5.1 under WW and WS conditions, respectively. *Scarlett* and *S42IL-141* had the lowest root dry weight (g) of 2.9 and 4.1 under WW and WS, respectively. We found no significant differences in treatment effect, genotypic, and interaction effect in root/shoot ratio (dry weight) under WW and WS in 2018 and 2019 experiments (**Table 1**).

Proline Accumulation in Barley Leaves and Immature Spikes

Well-watered spike proline content ranged from 48 to 198 μg/g FW (**Figure 3A**). WW *Barke* and *HOR10151* had the lowest and highest spike proline, respectively. WS spike proline ranged from 319 to 884 μg/g FW (**Figure 3A**). Again, *Barke* had the lowest while *S42IL-141* had the highest spike proline under WS (**Figure 3A**). WW leaf proline ranged from 42 to 117 μg/g FW and 23 to 60 μg/g FW in 2018 and 2019, respectively (**Figure 3A** and **Supplementary Figure 6**). *S42IL-143, HOR10151,* and *Scarlett* had the lowest leaf proline under WW (**Figure 3A** and **Supplementary Figure 6**). *S42IL-141*and *Barke* had the and highest leaf proline under WW (**Figure 3A** and **Supplementary Figure 6**). Proline accumulated markedly both in the immature spikes and the leaves of barley, fifteen days after WS onset, particularly among the introgression lines (**Figure 3A** and **Supplementary Figure 6**). WS leaf proline ranged from 79 to 680 μg/g FW and 99 to 696 μg/g FW in 2018 and 2019, respectively (**Figure 3A** and **Supplementary Figure 6**). *Scarlett*, *Barke*, *and HOR10151* had the lowest leaf proline under WS (**Figure 3A** and **Supplementary Figure 6**). *S42IL-143* and *S42IL-143* had the highest leaf proline under WS (**Figure 3A** and **Supplementary Figure 6**). In detail, the immature spikes of WS introgression lines *S42IL-141*and *S42IL-143* had the highest mean proline concentrations (884 and 803 μg/g FW, respectively; **Figure 3A**). In contrast, immature spikes of the elite genotypes *Barke, Scarlett,* and *HOR10151* had the lowest mean proline concentrations (319, 341, and 552 μg/g FW, respectively) under WS (**Figure 3A**). *HOR10151* and *Scarlett,* compared with the other three genotypes, exhibited an increase of about 198 μg/g FW of spike proline under WW (**Figure 3A**). Leaf proline concentrations in the genotypes expressed per unit dry weight (DW) showed significant ($P \leq 0.001$) differences as well (**Supplementary Table 1**), which followed a similar trend to the proline concentrations measured per unit FW (**Figure 3A** and **Supplementary Table 1**). Leaf proline per dry biomass ranged from 5 to 14 μmol/g under WW and 5 – 55 μmol/g under WS (**Supplementary Table 1**). The introgression line *S42IL-143* had the highest proline concentration on a dry biomass basis, and the elite genotype, *Scarlett,* the lowest (**Supplementary Table 1**).

In the experiment of 2019, proline from the basal, central, and apical sections of the immature spikes showed significant differences among the genotypes and treatments (**Figure 3B**). WW spike proline from the apical, central, and basal sections ranged from 34, 72, and 37 to 192, 211, and 202 μg/g FW, respectively (**Figure 3B**). WW spike proline of *Barke* (34, 72, and 37 μg/g FW) from the apical, central, and basal sections,

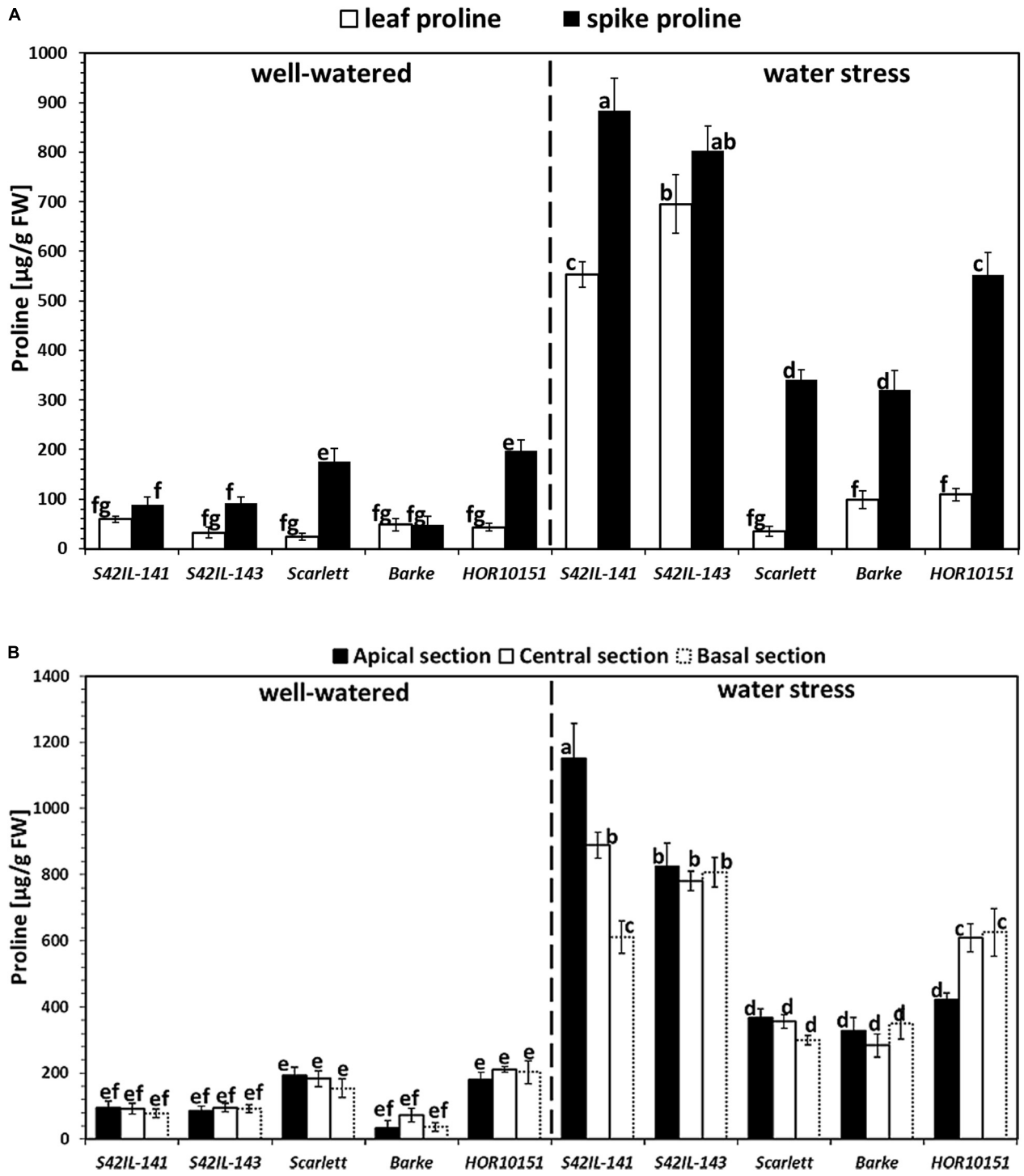

FIGURE 3 | Proline accumulation to the spikes and leaves among the five barley genotypes 15 days after water stress. Different letters on the bars denote significant differences ($P \leq 0.05$) according to Tukey's HSD test ($n = 6$). **(A)** Proline concentration to the spike and leaf measurements for 2019 under well-watered and water stress conditions. **(B)** Spike proline concentrations along the axis of the different spike sections for the 2019 experiment under well-watered and water stress conditions.

respectively, was the lowest (**Figure 3B**). The spike proline of the apical section of *Scarlett* (192 µg/g FW), was the highest among all the five genotypes under WW conditions. Spike proline from the central and basal sections of *HOR10151* (211 and 202 µg/g FW) was the highest under WW conditions (**Figure 3B**). WS spike proline from the apical, central, and basal sections ranged

from 327, 283, and 299 to 1151, 889, and 806 μg/g FW, respectively (**Figure 3B**). WS spike proline of *Barke* (327 and 283 μg/g FW) from the apical and central sections, respectively, were the lowest while *Scarlett* the lowest for the basal section (**Figure 3B**). Spike proline from the apical and central sections of *S42IL-141* (1151 and 889 μg/g FW) was the highest under WS conditions (**Figure 3B**). WS spike proline from the basal section of *S42IL-143* (809 μg/g FW) was highest among all five genotypes (**Figure 3B**).

The distribution of proline along the spike was not uniform for any of our barley genotypes under WS (**Figure 3B**). For instance, we found an increase of at least 40% in proline among the apical and central spike sections of *S42IL-141* (1152 and 889 μg/g FW) compared with *HOR10151* (422 and 609 μg/g FW), respectively (**Figure 3B**). This increase under WS did not follow a clear position-dependent gradient along the spike, although the introgression lines generally had at least a 10% higher spike proline (**Figure 3B**). There were no differences in proline content in the basal spike section of *S42IL-141* (612 μg/g FW) to the basal and central section of *HOR10151* (626 and 609 μg/g FW) under WS (**Figure 3B**). In summary, section-specific differences existed considering the apical, central, and basal spike proline of *S42IL-141* and *HOR10151* individually under WS.

Analysis of spike and leaf revealed a higher increase in proline concentration in the spikes than in the leaves for all genotypes under WS (**Figures 3A,B**). *P5cs1*-introgression lines had a significantly higher proline concentration in their developing spikes than the leaves under WS conditions, exhibiting an average difference of 30% (**Figure 3A**). Similarly, elite genotypes *Barke, Scarlett,* and *HOR10151* also had markedly more proline in their immature spikes than in the leaves under WS conditions (average difference of 134%, **Figure 3A**). However, in absolute terms, the introgression lines had higher spike proline content than the elite lines under WS (**Figures 3A,B**).

Imaging of Water-Stressed Spikes With MRI

To examine the effect of WS on seed abortion and filling early in the reproductive development phase (before grain maturation) of barley, we used MRI to scan immature spikes at the BBCH-scale, 83, i.e., at the soft milky dough stage (**Figures 4A,B** and **Supplementary Figure 7**). We acquired amplitude images of 2D projections of barley spikes and evaluated them for the presence of initiated, developing, fully developed, sterile, or aborted seeds (**Figures 4A,B** and **Supplementary Figure 7**). We did MRI scans of intact spikes at the early dough stage. Seed abortion was more prevalent among the elite genotypes (*Barke*, *Scarlett*, and *HOR10151*) than in the introgression lines (*S42IL-143* and *S42IL-141*) after prolonged 15 days of WS treatment (**Figures 4A,B**). Poor seed yield performance among the elite lines compared with the introgression lines under WS (**Tables 1**, **2**), were additionally revealed by several of our phenotypic traits (spike length, grain number, grain weight) similar to the MRI observations (**Figures 4A,B**). MRI scans (**Figure 4A**) of WW spikes of all genotypes showed a lower seed abortion rate, or no abortion at all, for all our barley types (**Figure 4A**). MRI scans of whole spikes grown under prolonged WS treatment, however, showed increased seed abortion (and in some cases complete spike abortion) among the elite genotypes, *Scarlett*, *Barke,* and *HOR10151*, much more so than the introgression lines, *S42IL-143*, and *S42IL-141* (**Figure 4B**). For all genotypes, WS-treated main spikes were found to contain shriveled or small developing grains (**Figure 4B**). Conversely, none of the spikes from WW plants showed shrunken seeds (**Figure 4A**).

Grain filling under WS thus was reduced more among the elite genotypes than in the introgression lines (**Figure 4B** and **Table 2**). Also, under WS grain number in *Scarlett*, *Barke,* and *HOR10151* was reduced more than in *S42IL-143* and *S42IL-141* (**Figure 4B**). These results were confirmed by the 2019 seed count (**Table 2**). At harvest, under WS the grain numbers of the main spike of *S42IL-143* and *S42IL-141* were 17 and 22, respectively; significantly higher than for the elite genotypes of *Scarlett*, *Barke,* and *HOR10151* (9.5, 2, and 4, respectively) (**Table 2**). Again, similar to what we observed in the MRI projections (**Figures 4A,B**), phenotypic spike length of *S42IL-143* and *S42IL-141* were significantly longer than *Scarlett*, *Barke,* and *HOR10151* under WS (**Tables 1**, **2**). In summary, both MRI and phenotypic data confirmed that the introgression lines performed better in terms of seed yield than the elite lines under WS.

DISCUSSION

We characterized barley *P5cs1*-introgression lines and their physiological responses to reduced water availability. To consolidate our findings, we conducted two experiments in a greenhouse with a genotype panel including the same introgression lines and elite cultivars and with the same type of WS treatment applied at pre-flowering stages and kept as constant as possible throughout spike and seed development. Calculation of thermal sums for the whole duration of the two experiments shows that there was a difference of only about 5% in cumulated degree-days between the experiments of 2018 and 2019 (see section "Materials and Methods"). However, average daily temperatures were generally lower (i.e., below 25°C) during and after flowering time in 2019 compared with 2018. DLI maximum values were very similar in both experimental years whereas the minimum values were generally lower in 2018 compared with 2019 (**Supplementary Figure 1**). Overall, under WW conditions we obtained very similar results in the two subsequent experimental years (**Supplementary Table 2**). We note that average grain weight per plant at harvest under WW conditions was somewhat higher in 2019 compared with 2018, which might be linked to the lower daily temperatures during GF. Imposing WS conditions at booting stages resulted in overall more severe effects in 2019 compared with 2018, in particular leading to a more pronounced decrease in tiller numbers and shoot weight at harvest on average, considering all genotypes (**Supplementary Table 2**). In addition, relative water content and net assimilation rates measured three days after the onset of the drought treatment were also lower in 2019 compared with 2018. Because these effects cannot be simply explained by temperature and DLI differences between the two years, we conclude that the

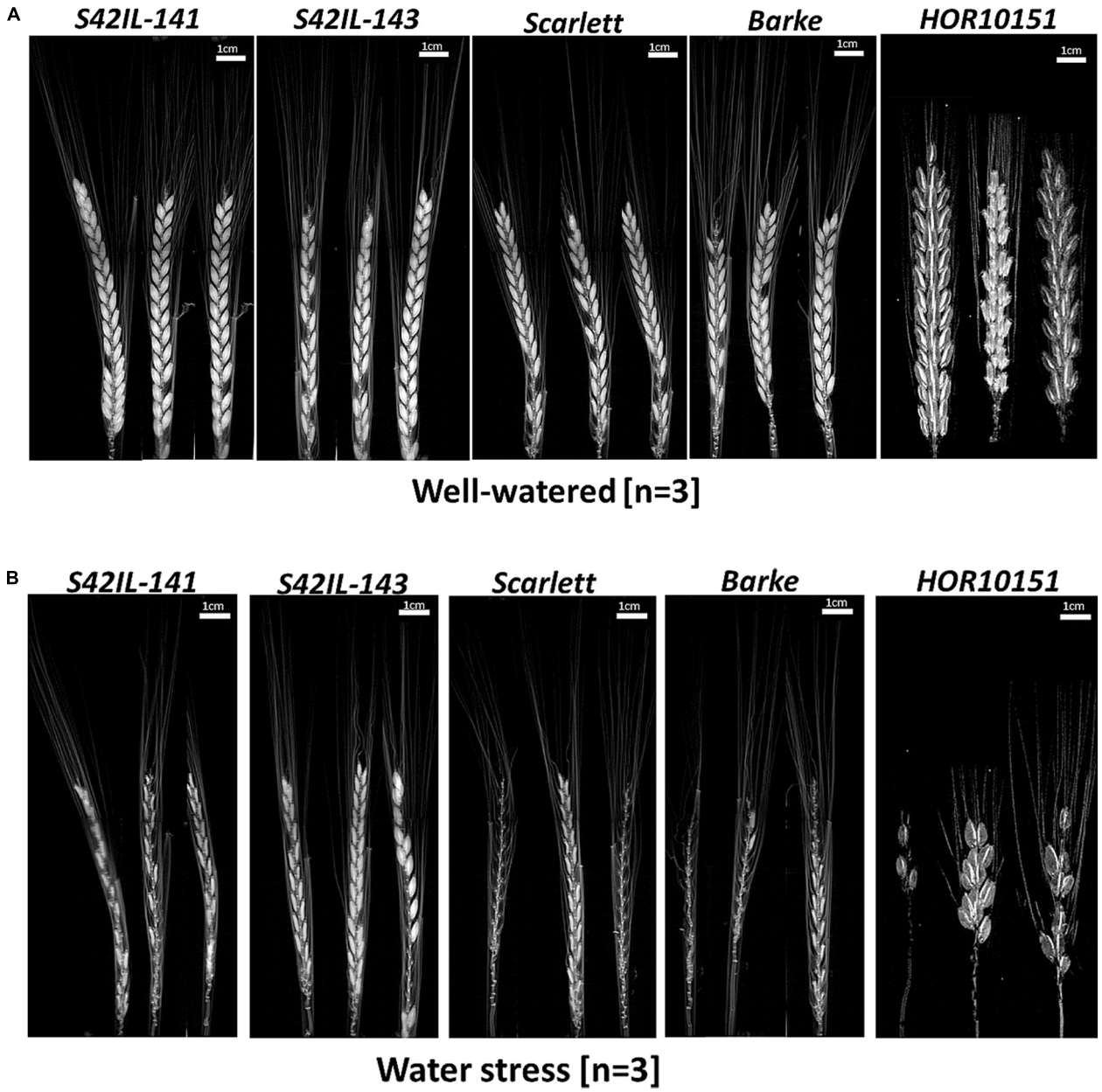

FIGURE 4 | MRI amplitude images of barley main spikes at BBCH-scale 83, 15 days after stress application. **(A)** Main spikes of *S42IL-141, S42IL-143, Scarlett, Barke,* and *HOR10151* grown under well-watered conditions. **(B)** Spikes from plants grown under water stress (n = 3, scale = 1 cm).

first few days after the onset of WS led to a more pronounced decrease in soil water content values in 2019, as we can observe by comparing the time profile of pot soil moisture measured by time-domain-reflectance sensors (**Supplementary Figure 2**).

Drought is a complex trait and may lead to several morpho-physiological alterations within a plant. As an adaptation to drought stress, plants adjust their transpiration, photosynthesis, and thus WUE, to prevent water loss and tissue damage while preserving the capacity for CO_2 assimilation (Belko et al., 2012; Li et al., 2017). Naz et al. (2014) and Muzammil et al. (2018) reported earlier on the same introgression lines, *S42IL-143*, and *S42IL-141* that they maintained 70% percentage relative leaf water content and displayed less severe wilting under WS. These findings were confirmed in our study. *S42IL-143* and *S42IL-141* maintained relative leaf water content of more than 70% even under WS (**Table 2**). On average, iWUE of the introgression and elite lines under WS increased by 20 and 7%, respectively. The two introgression lines often had very similar responses in terms of net CO_2 assimilation, GSW, and transpiration rate under WS (**Figures 2A–C**). Yang et al. (2019) reported similar increases in iWUE (39 and 37%) for their contrasting rice hybrid cultivars under drought. WS caused an increase in the

duration of spike development of all our barley genotypes. Earlier studies (Matin et al., 1989; Rani et al., 2018), reported a prolonged duration in spike development due to WS at GF. The impact of WS on plant floral development generally might either cause a shortened or prolonged life cycle taking into account genotype specificity leading to an overall reduction in productivity (Dolferus, 2014; Boussora et al., 2019). Similarly, Li et al. (2017) reported wide variations in gas exchange parameters of drought-treated flag leaves compared with control conditions at the heading stages of drought-susceptible wheat cultivars compared with tolerant genotypes.

Water shortage during the post-anthesis period has been shown to significantly reduce harvest index and grain yield (Vadez et al., 2014). Due to the dehydrating effect of the WS treatment, 15 days after stress the seeds of all genotypes became smaller (**Figure 4B**). All spikes showed strong reductions in spike length, seed size and number under WS conditions (**Figure 4B**). Consequently, there was a significant loss of 76% in total grain weight (all genotypes averaged; **Table 1**). The elite genotypes *HOR10151* or *Scarlett* and *Barke* showed pronounced leaf wilting symptoms, leaf dehydration, and significant seed abortion overtime under WS (**Table 2** and **Figures 1**, **4A,B**). *IL143* and *IL141* on the other hand showed less wilting symptoms and less leaf dehydration (**Figure 1**). These effects were also reflected in the spikes values. Grain number and size of the introgression lines were also severely affected by WS but performed better than the elite genotypes (**Figures 4A,B**). These results are similar to studies obtained with computed tomography of wheat grains under WS or heat treatment, which showed shriveled seeds in 3D projections (Tracy et al., 2017; Schmidt et al., 2020). These findings confirm that low water use during the post-anthesis period significantly reduces both harvest index and grain yield (Vadez et al., 2014) and further highlight the critical importance of maintenance of plant water status before and during the grain-filling period.

Prior studies have noted the importance of proline accumulation in many plant species, as one of the most prominent changes in plant metabolism during drought and low soil water potential (Shinde et al., 2016). Contrary to proline accumulation in reproductive organs, proline accumulation in leaves and roots has been extensively researched in earlier work (Verbruggen and Hermans, 2008). Proline accumulation in different plant organs is time-dependent and different concentrations have been reported for different plant species even under apparently similar stress scenarios. Proline accumulates rapidly and is degraded as the plant recovers (Dar et al., 2016; Heuer, 2016). Mickky et al. (2019) reported an increase in leaf proline content in ten wheat cultivars under drought conditions. They observed that proline accumulation was more pronounced in the drought-tolerant cultivars than in the sensitive ones. Similarly, in our investigation, we identified a more than fivefold increase in leaf proline under WS in the tolerant introgression lines *S42IL-143* and *S42IL-141,* much higher than in the susceptible elite genotypes *Barke*, *Scarlett*, and *HOR10151* (**Figures 3A,B**). In a similar study, Templer et al. (2017) found a more than fivefold increase for leaf proline content under drought and heat stress in their tolerant barley genotypes, as compared with control.

In the current study, we report higher proline contents in the reproductive structures of the WS immature spikes than in the leaves, for all our barley genotypes. Accumulation of proline in undeveloped seeds of *Vicia faba* indicated that proline might play an essential role in the development of generative organs (Venekamp and Koot, 1984). Numerous studies reported high-proline contents in Arabidopsis seeds developing under WS (Chiang and Dandekar, 1995; Schmidt et al., 2007), although data on proline accumulation in seeds of other species are more scarce (Dar et al., 2016). In our study, *P5cs1*-introgression lines accumulated the highest proline amounts (+30%) in their developing spike compared with leaves of elite genotypes (**Figure 3A**). These elite genotypes under WS had more than double the proline content in their immature spikes than in their leaves (**Figure 3B**).

Proline accumulation is a common physiological response to various stresses but is also part of the developmental program in generative tissues (Heuer, 2016). Proline may act as an osmoprotectant to protect the actively growing cellular and subcellular structures of the spike from dehydration under WS (Chiang and Dandekar, 1995). Further evidence suggests that proline is also involved in flowering and development both as a metabolite and possibly as a signal molecule (Dar et al., 2016). In our introgression lines, higher proline content was associated with higher relative leaf water content and a reduced wilting score (**Table 1**). As a protective mechanism to WS, barley, and wheat are known to allocate proline to actively growing vegetative tissues in shoots and roots. This is associated with reduced dehydration and wilting under WS (Delauney and Verma, 1993; Lee et al., 2009; Bandurska et al., 2017; Koenigshofer and Loeppert, 2019). In barley, Cai et al. (2020) reported that genotypes that show less leaf wilting under stress were able to osmotically adjust and better tolerate water shortage. In our study *P5cs1*-introgression lines showed less severe leaf wilting (−40%) under WS compared with elite counterparts, which indicates reduced susceptibility to soil drying conditions.

We found a higher ETR in the drought-tolerant introgression *S42IL-143* under WS than in the elite lines. As Shinde et al. (2016) emphasized, proline metabolism regenerates $NADP^+$ to provide a continued supply of electron acceptors for chloroplast electron transport. However, most drought susceptible genotypes like *Scarlett* fail to accumulate and use proline because of early leaf wilting and leaf death, resulting in proline reduction under drought conditions (Sayed et al., 2012). We found a higher net CO_2 assimilation rate, reduced transpiration, stomatal opening, intrinsic water use efficiency, and an active ETR several days after WS in *P5cs1-S42IL-143* and *S42IL-141*compared with *Barke*, *Scarlett*, and *HOR10151* under WS (**Figures 2A–D** and **Supplementary Figure 4**). The net CO_2 assimilation rate of *S42IL-143* and *S42IL-141*was more than double the rate of *Barke*, *Scarlett*, and *HOR10151* under WS. *S42IL-143* and *S42IL-141*had a marginally (5%) higher GSW compared with the elite

lines *Barke*, *Scarlett*, and *HOR10151* under WS. A contributing factor to the higher GSW and overall photosynthetic rate of the introgression lines under WS is their wild allele *P5cs1*. It has been shown to enhance the drought protective mechanism of proline biosynthesis (Szabados and Savouré, 2010; Sucre and Suárez, 2011; Allahverdiyev, 2015; Qamar et al., 2015). Several reports have already established that drought-tolerant barley genotypes accumulate proline to maintain GSW and active photosynthesis, even under dehydrating conditions, while drought-sensitive genotypes immediately reduce the stomatal aperture (Deng et al., 2013; Marok et al., 2013; Naz et al., 2014; Haddadin, 2015).

In the current study, our introgression lines achieved approximately double the grain weight of the elite lines under WS. Similar results were reported by Templer et al. (2017), who under drought conditions found a decrease of 65% in the harvest index in drought susceptible German cultivars, whereas drought-tolerant Mediterranean cultivars decreased not more than 14%. Based on a DSI which we calculated from the grain weight per plant, the most tolerant genotype was *S42IL-143* with the least DSI of 0.2, 0.4 in 2018, and 2019, respectively after fifteen days of WS (**Supplementary Table 3**). Haddadin (2015), reported a DSI of >1 for susceptible spring barley and <0.5 for tolerant types. A possible explanation for the higher grain yield under WS by *S42IL-143* and *S42IL-141*is the enhanced proline accumulation (Sayed et al., 2012). The observed proline increases due to WS also had significant correlations with reduced grain number, grain yield, plant height, and shoot biomass (**Supplementary Figure 5**). Sallam et al. (2018) previously reported an increase in grain proline and reduction in starch content due to heat stress, with significant reductions in yield per plot, grain yield per spike, and 1,000-kernel weight. Several studies reported a negative correlation between shoot proline concentration, growth and yield traits (Bandurska et al., 2017; Boussora et al., 2019). However, this negative correlation might be interpreted as an indication that the plants experienced WS, and not necessarily reflect a causal relation between proline accumulation and reduced plant growth and yield. On the contrary, in our study, we found drought-induced proline accumulation in the spikes of barley genotypes harboring the wild variant of *P5cs1* to be associated with improved drought tolerance, as expressed in their photosynthetic capacity, seed number, and final yield under WS.

Proline is a highly inter-convertible organic molecule. It is transiently up regulated to tackle the effect of drought stress, but can also be catabolized to energy rich metabolites as soon as water availability improves. It thus has multiple roles in drought stress adaptation and stress recovery (Szabados and Savouré, 2010; Forlani et al., 2019). Proline is likely associated with the energy demand of young dividing cells during resumed growth following stress relief (Verslues and Sharma, 2010). This possibility is also corroborated by findings at the transcriptional level in which *P5CS2*, *P5CR* (encoding *P5C* reductase), and *ProDH1* are upregulated in meristematic tissues such as root tips, shoot apices, lateral buds, and the inflorescence (Sharma et al., 2011). Young spike tissues of all our genotypes at their early grain development of the soft milky dough stages had accumulated more proline. Most root and leaf cells that are actively dividing, elongating, and developing also tend to accumulate proline under drought (Dar et al., 2016), which contributes to coping with drought stress during reproductive development and to increasing proline sink strength in those tissues (Kishor and Sreenivasulu, 2014). The question of where proline synthesis primarily occurs in plants upon imposition of stress still remains to be clarified. Proline metabolism varies among organs and tissues, and transport of proline within the plant is likely to occur (Koenigshofer and Loeppert, 2019). Aside from the relevance of proline in stress adaptation, the effect of higher proline content on grain quality need to be investigated comprehensively before utilizing these genetic resources in plant breeding. Therefore, in future work we will investigate the effect of proline mediated stress adaptation on grain quality, total protein content as well as on brewing quality traits.

CONCLUSION

Prolonged WS at the booting stage caused a significant reduction of 76% of barley grain weight per plant. We found drought-inducible proline accumulation to be not exclusive to the leaves, rather proline significantly accumulates in barley spikes and it may contribute to the maintenance of seed initiation and GF processes by preventing excessive water loss. Spike proline content under WS increased by more than 30% compared with leaf proline content in all our barley genotypes. *P5cs1*-introgression lines harboring a wild barley allele involved in the proline biosynthetic pathway had higher leaf and spike proline contents as well as a higher grain yield under WS conditions. Generally, the elite lines were much more affected by WS than the introgression lines on several morpho-physiological traits. *S42IL-143* and *S42IL-141* carrying the *P5cs1* allele from wild barley showed an increased WS tolerance associated with a reduced seed abortion rate and a higher spike proline concentration compared with Scarlett, *Barke,* and *HOR10151*. Our results suggest that proline accumulation in spikes of barley under WS plays a major role in the maintenance of final seed yield. Future studies will focus on the validation of presented physiological variation in field conditions as well as to evaluate the effect of elevated proline on grain quality traits.

DATA AVAILABILITY STATEMENT

The original contributions presented in the study are included in the article/**Supplementary Material**, further inquiries can be directed to the corresponding author.

AUTHOR CONTRIBUTIONS

FFr, CW, DD, AN, MF, and FFi conceptualized and designed the research. FFr conducted the experiments, analyzed the data, and wrote the manuscript. CW, DD, AN, MF, and FFi contributed to writing the manuscript. CW, DD, and FFi supervised the research. All authors approved the submitted version.

FUNDING

This work was institutionally funded through the Program Oriented Funding of the Helmholtz Association to IBG-2: Plant Sciences, Institute of Bio- and Geosciences, Forschungszentrum Jülich GmbH, Jülich, Germany.

ACKNOWLEDGMENTS

Special appreciation goes to Dr. Daniel Pflugfelder, Prof. Ingar Janzik, Dr. Robert Koeller, Prof. Uwe Rascher, Birgit Bleise, Silvia Braun, Esther Breuer, Andrea Neuwohner, Beate Uhlig, Katharina Wolter-Heinen, Kelvin Acebron, and Johannes Kochs for their technical support. We are also grateful to Dr. Asis Shrestha of the University of Bonn for his advisory role.

SUPPLEMENTARY MATERIAL

The Supplementary Material for this article can be found online at: https://www.frontiersin.org/articles/10.3389/fpls.2021.633448/full#supplementary-material

REFERENCES

Abdel-Ghani, A. H., Sharma, R., Wabila, C., Dhanagond, S., Owais, S. J., Duwayri, M. A., et al. (2019). Genome-wide association mapping in a diverse spring barley collection reveals the presence of QTL hotspots and candidate genes for root and shoot architecture traits at seedling stage. *BMC Plant Biol.* 19:216.

Abdelrahman, M., Burritt, D., Gupta, A., and Tsujimoto, H. (2020). Heat stress effects on source-sink relationships and metabolome dynamics in wheat. *J. Exp. Bot.* 71, 543–554. doi: 10.1093/jxb/erz296

Allahverdiyev, T. (2015). Effect of drought stress on some physiological traits of durum (*Triticum durum* Desf.) and bread (*Triticum aestivum* L.) wheat genotypes. *J. Stress Physiol. Biochem.* 11, 29–38.

Arai-Sanoh, Y., Takai, T., Yoshinaga, S., Nakano, H., Kojima, M., Sakakibara, et al. (2014). Deep rooting conferred by DEEPER ROOTING 1 enhances rice yield in paddy fields. *Sci. Rep.* 4:5563.

Bandurska, H., Niedziela, J., Pietrowska-Borek, M., Nuc, K., Chadzinikolau, T., and Radzikowska, D. (2017). Regulation of proline biosynthesis and resistance to drought stress in two barley (*Hordeum vulgare* L.) genotypes of different origin. *Plant Physiol. Biochem.* 118, 427–437. doi: 10.1016/j.plaphy.2017.07.006

Barrs, H., and Weatherley, P. (1962). A re-examination of the relative turgidity technique for estimating water deficits in leaves. *Aust. J. Biol. Sci.* 15, 413–428. doi: 10.1071/bi9620413

Basu, S., Ramegowda, V., Kumar, A., and Pereira, A. (2016). Plant adaptation to drought stress [version 1; peer review: 3 approved]. *F1000Research* 5, 1–10. doi: 10.12688/F1000RESEARCH.7678.1

Bates, L., Waldren, R., and Teare, I. (1973). Rapid determination of free proline for water-stress studies. *Plant Soil* 207, 205–207. doi: 10.1007/bf00018060

Belko, N., Zaman-Allah, M., Cisse, N., Diop, N. N., Zombre, G., Ehlers, J. D., et al. (2012). Lower soil moisture threshold for transpiration decline under water deficit correlates with lower canopy conductance and higher transpiration efficiency in drought-tolerant cowpea. *Funct. Plant Biol.* 39, 306–322. doi: 10.1071/fp11282

Bhaskara, G. B., Yang, T.-H., and Verslues, P. E. (2015). Dynamic proline metabolism: importance and regulation in water-limited environments. *Front. Plant Sci.* 6:484.

Blum, A. (2005). Drought resistance, water-use efficiency, and yield potential - are they compatible, dissonant, or mutually exclusive? *Aust. J. Agricult. Res.* 56, 1159–1168. doi: 10.1071/ar05069

Boussora, F., Allam, M., Guasmi, F., Ferchichi, A., Rutten, T., Hansson, M., et al. (2019). Spike developmental stages and ABA role in spikelet primordia abortion contribute to the final yield in barley (*Hordeum vulgare* L.). *Bot. Stud.* 60:13.

Box, G. E. P., and Cox, D. R. (1964). An analysis of transformations. *J. R. Soc. Ser. B* 26, 211–243.

Cai, K., Chen, X., Han, Z., Wu, X., Zhang, S., Li, Q., et al. (2020). Screening of worldwide barley collection for drought tolerance: the assessment of various physiological measures as the selection criteria. *Front. Plant Sci.* 11:1159.

Cattivelli, L., Ceccarelli, S., Romagosa, I., and Stanca, M. (2011). "Abiotic stresses in barley: problems and solutions," in *Barley: Production, Improvement, and Uses*, ed. S. E. Ullrich (Hoboken, NJ: John Wiley).

Chiang, H.-H., and Dandekar, A. M. (1995). Regulation of proline accumulation in *Arabidopsis thaliana* (L) Heynh. during development and in response to desiccation. *Plant Cell Environ.* 18, 1280–1290. doi: 10.1111/j.1365-3040.1995.tb00187.x

Choudhury, F. K., Rivero, R. M., Blumwald, E., and Mittler, R. (2017). Reactive oxygen species, abiotic stress and stress combination. *Plant J.* 90, 856–867. doi: 10.1111/tpj.13299

Dar, M. I., Naikoo, M. I., Rehman, F., Naushin, F., and Khan, F. A. (2016). "Proline accumulation in plants: roles in stress tolerance and plant development," in *Osmolytes and Plants Acclimation to Changing Environment: Emerging Omics Technologies*, eds N. Iqbal, R. Nazar, and A. Khan (Berlin: Springer).

De Datta, S. K., Malabuyoc, J. A., and Aragon, E. L. (1988). A field screening technique for evaluating rice germplasm for drought tolerance during the vegetative stage. *Field Crops Res.* 19, 123–134. doi: 10.1016/0378-4290(88)90050-0

Delauney, A. J., and Verma, D. P. S. (1993). Proline biosynthesis and osmoregulation in plants. *Plant J.* 4, 215–223. doi: 10.1046/j.1365-313x.1993.04020215.x

Deng, G., Liang, J., Xu, D., Long, H., Pan, Z., and Yu, M. (2013). The relationship between proline content, the expression level of P5CS (Δ1-pyrroline-5-carboxylate synthetase), and drought tolerance in Tibetan hulless barley (*Hordeum vulgare* var. nudum). *Russ. J. Plant Physiol.* 60, 693–700. doi: 10.1134/s1021443713050038

Dien, D. C., Mochizuki, T., and Yamakawa, T. (2019). Effect of various drought stresses and subsequent recovery on proline, total soluble sugar and starch metabolisms in rice (*Oryza sativa* L.) varieties. *Plant Prod. Sci.* 22, 530–545. doi: 10.1080/1343943x.2019.1647787

Dolferus, R. (2014). To grow or not to grow: a stressful decision for plants. *Plant Sci.* 229, 247–261. doi: 10.1016/j.plantsci.2014.10.002

Edzes, H. T., van Dusschoten, D., and Van As, H. (1998). Quantitative T2 Imaging of plant tissues by means Of multi-echo MRI microscopy. *Magn. Reson. Imaging* 16, 185–196. doi: 10.1016/s0730-725x(97)00274-9

Fahad, S., Bajwa, A. A., Nazir, U., Anjum, S. A., Farooq, A., Zohaib, A., et al. (2017). Crop production under drought and heat stress: plant responses and management options. *Front. Plant Sci.* 8:1147.

Ferguson, J. N. (2019). Climate change and abiotic stress mechanisms in plants. *Emerg. Top. Life Sci.* 3, 165–181. doi: 10.1042/etls20180105

Forlani, G., Bertazzini, M., Zarattini, M., Funck, D., Ruszkowski, M., and Nocek, B. (2015). Functional properties and structural characterization of rice δ1-pyrroline-5-carboxylate reductase. *Front. Plant Sci.* 6:565.

Forlani, G., Trovato, M., Funck, D., and Signorelli, S. (2019). "Regulation of proline accumulation and its molecular and physiological functions in stress defence," in *Osmoprotectant-Mediated Abiotic Stress Tolerance in Plants: Recent Advances and Future Perspectives*, eds M. A. Hossain, V. Kumar, D. J. Burritt, and M. Fujita (Cham: Springer International Publishing).

Gupta, A., Rico-Medina, A., and Cano-Delgado, A. I. (2020). The physiology of plant responses to drought. *Science* 368, 266–269.

Haddadin, M. F. (2015). Assessment of drought-tolerant barley varieties under water stress. *Intl. J. Agricult. Forestry* 5, 131–137.

Hecht, V. L., Temperton, V. M., Nagel, K. A., et al. (2019). Plant density modifies root system architecture in spring barley (*Hordeum vulgare* L.) through a change in nodal root number. *Plant Soil* 439, 179–200. doi: 10.1007/s11104-018-3764-9

Heuer, B. (2016). "Role of proline in plant response to drought and salinity," in *Pessarakli Handbook of Plant and Crop Stress*, Third Edn (Baco Raton, FL: CRC Press), 213–238. doi: 10.1201/b10329-12

Hoffmann, T., Bleisteiner, M., Kumar, S. P., Steil, L., Mäder, U., Völker, U., et al. (2017). Synthesis of the compatible solute proline by Bacillus subtilis: point mutations rendering the osmotically controlled proHJ promoter hyperactive. *Environ. Microbiol.* 19, 3700–3720. doi: 10.1111/1462-2920.13870

Honsdorf, N., March, T. J., and Pillen, K. (2017). QTL controlling grain filling under terminal drought stress in a set of wild barley introgression lines. *PLoS One* 12:e0185983. doi: 10.1371/journal.pone.0185983

Honsdorf, N., March, T. J., Berger, B., Tester, M., and Pillen, K. (2014). High-throughput phenotyping to detect drought tolerance QTL in wild barley introgression lines. *PLoS One* 9:e97047. doi: 10.1371/journal.pone.0097047

Kamal, N. M., Gorafi, Y. S. A., Abdelrahman, M., Abdellatef, E., and Tsujimoto, H. (2019). Stay-green trait: a prospective approach for yield potential, and drought and heat stress adaptation in globally important cereals. *Int. J. Mol. Sci.* 20. doi: 10.3390/ijms20235837

Kebede, A., Kang, M. S., and Bekele, E. (2019). Advances in mechanisms of drought tolerance in crops, with emphasis on barley. *Adv. Agron.* 156, 265–314. doi: 10.1016/bs.agron.2019.01.008

Kishor, K. P. B., and Sreenivasulu, N. (2014). Is proline accumulation per se correlated with stress tolerance, or is proline homeostasis a more critical issue? *Plant Cell Environ.* 37, 300–311. doi: 10.1111/pce.12157

Koenigshofer, H., and Loeppert, H. G. (2019). The up-regulation of proline synthesis in the meristematic tissues of wheat seedlings upon short-term exposure to osmotic stress. *J. Plant Physiol.* 237, 21–29. doi: 10.1016/j.jplph.2019.03.010

Kuromori, T., Seo, M., and Shinozaki, K. (2018). ABA transport and plant water stress responses. *Trends Plant Sci.* 23, 513–522. doi: 10.1016/j.tplants.2018.04.001

Lee, B. R., Jin, Y. L., Avice, J. C., Cliquet, J. B., Ourry, A., and Kim, T. H. (2009). Increased proline loading to phloem and its effects on nitrogen uptake and assimilation in water-stressed white clover (*Trifolium repens*). *New Phytol.* 182, 654–663. doi: 10.1111/j.1469-8137.2009.02795.x

Li, Y., Li, H., Li, Y., and Zhang, S. (2017). Improving water-use efficiency by decreasing stomatal conductance and transpiration rate to maintain higher ear photosynthetic rate in drought-resistant wheat. *Crop J.* 5, 231–239. doi: 10.1016/j.cj.2017.01.001

Lynch, J. P., and Wojciechowski, T. (2015). Opportunities and challenges in the subsoil: pathways to deeper rooted crops. *J. Exp. Bot.* 66, 2199–2210. doi: 10.1093/jxb/eru508

Marok, M. A., Tarrago, L., Ksas, B., Henri, P., Abrous-Belbachir, O., Havaux, M., et al. (2013). A drought-sensitive barley variety displays oxidative stress and strongly increased contents in low-molecular weight antioxidant compounds during water deficit compared to a tolerant variety. *J. Plant Physiol.* 170, 633–645. doi: 10.1016/j.jplph.2012.12.008

Matin, M. A., Brown, J. H., and Ferguson, H. (1989). Leaf water potential, relative water content, and diffusive resistance as screening techniques for drought resistance in barley. *Agron. J.* 81, 100–105. doi: 10.2134/agronj1989.00021962008100010018x

Meier, U. (2001). *Growth Stages of Mono- and Dicotyledonous Plants: German Federal Biological Research Centre for Agriculture and Forestry, BBCH-Monograph*. Berlin: BlackwellScience.

Mickky, B., Aldesuquy, H., and Elnajar, M. (2019). Drought-induced change in yield capacity of ten wheat cultivars in relation to their vegetative characteristics at heading stage. *Physiol. Mol. Biol. Plants* 25, 1137–1148. doi: 10.1007/s12298-019-00705-0

Miller, P., Lanier, W., and Brandt, S. (2001). *Using Growing Degree Days to Predict Plant Stages*. Bozeman: Mont State Univ USA Ext Serv.

Muzammil, S., Shrestha, A., Dadshani, S., Pillen, K., Siddique, S., Leon, J., et al. (2018). An ancestral allele of Pyrroline-5-carboxylate synthase1 promotes proline accumulation and drought adaptation in cultivated barley. *Plant Physiol.* 178, 771–782. doi: 10.1104/pp.18.00169

Naz, A. A., Arifuzzaman, M., Muzammil, S., Pillen, K., and Leon, J. (2014). Wild barley introgression lines revealed novel QTL alleles for root and related shoot traits in the cultivated barley (*Hordeum vulgare* L.). *BMC Genet.* 15, 1–12.

Nieves-Cordones, M., García-sánchez, F., Pérez-pérez, J. G., Colmenero-Flores, M. J., Rubio, F., and Rosales, A. M. (2019). Coping with water shortage : an update on the role of K +, Cl -, and water membrane transport mechanisms on drought resistance. *Front. Plant Sci.* 10:1619.

Podda, A., Pollastri, S., Bartolini, P., Pisuttu, C., Pellegrini, E., Nali, C., et al. (2019). Drought stress modulates secondary metabolites in *Brassica oleracea* L. convar. acephala (DC) Alef, var. sabellica L. *J. Sci. Food Agricul.* 99, 5533–5540. doi: 10.1002/jsfa.9816

Qamar, A., Mysore, K. S., and Senthil-Kumar, M. (2015). Role of proline and pyrroline-5-carboxylate metabolism in plant defense against invading pathogens. *Front. Plant Sci.* 6:503.

R Core Team (2019). *R: a Language and Environment for Statistical Computing*. Vienna: R Foundation for Statistical Computing.

Rani, S., Chaudhary, A., and Rani, K. (2018). Management strategies for abiotic stresses in barley. wheat and barley research. *J. Cereal Res.* 10, 151–165.

Rodrigues, J., Inzé, D., Nelissen, H., and Saibo, N. J. M. (2019). Source–sink regulation in crops under water deficit. *Trends Plant Sci.* 24, 652–663. doi: 10.1016/j.tplants.2019.04.005

Sallam, A., Alqudah, A., Börner, A., Dawood, M., and Baenziger, P. (2019). Drought stress tolerance in wheat and barley: advances in physiology, breeding and genetics research. *Intl. J. Mol. Sci.* 20:3137. doi: 10.3390/ijms20133137

Sallam, A., Amro, A., El-Akhdar, A., et al. (2018). Genetic diversity and genetic variation in morpho-physiological traits to improve heat tolerance in spring barley. *Mol. Biol. Rep.* 45, 2441–2453. doi: 10.1007/s11033-018-4410-6

Sayed, M. A., Schumann, H., Pillen, K., Naz, A. A., and Leon, J. (2012). AB-QTL analysis reveals new alleles associated to proline accumulation and leaf wilting under drought stress conditions in barley (*Hordeum vulgare* L.). *BMC Genet.* 13:61. doi: 10.1186/1471-2156-13-61

Schmidt, J., Claussen, J., Wörlein, N., Eggert, A., Fleury, D., Garnett, T., et al. (2020). Drought and heat stress tolerance screening in wheat using computed tomography. *Plant Methods* 16, 1–12.

Schmidt, R., Stransky, H., and Koch, W. (2007). The amino acid permease AAP8 is important for early seed development in *Arabidopsis thaliana*. *Planta* 226, 805–813. doi: 10.1007/s00425-007-0527-x

Sehgal, A., Sita, K., Siddique, K. H. M., Kumar, R., Varshney, R. K., et al. (2018). Drought or/and heat-stress effects on seed filling in food crops: impacts on functional biochemistry, seed yields, and nutritional quality. *Front. Plant Sci.* 9:1705.

Sharma, S., Villamor, J. G., and Verslues, P. E. (2011). Essential role of tissue-specific proline synthesis and catabolism in growth and redox balance at low water potential. *Plant Physiol.* 157, 292–304. doi: 10.1104/pp.111.183210

Shavrukov, Y., Kurishbayev, A., Jatayev, S., Shvidchenko, V., Zotova, L., Koekemoer, F., et al. (2017). Early flowering as a drought escape mechanism in plants: how can it aid wheat production? *Front. Plant Sci.* 8:1950.

Shinde, S., Villamor, J. G., Lin, W., Sharma, S., and Verslues, P. E. (2016). Proline coordination with fatty acid synthesis and redox metabolism of chloroplast and mitochondria. *Plant Physiol.* 172, 1074–1088.

Sucre, B., and Suárez, N. (2011). Effect of salinity and PEG-induced water stress on water status, gas exchange, solute accumulation, and leaf growth in Ipomoea pes-caprae. *Environ. Exp. Bot.* 70, 192–203. doi: 10.1016/j.envexpbot.2010.09.004

Szabados, L., and Savouré, A. (2010). Proline: a multifunctional amino acid. *Trends Plant Sci.* 15, 89–97. doi: 10.1016/j.tplants.2009.11.009

Tardieu, F., Simonneau, T., and Muller, B. (2018). The physiological basis of drought tolerance in crop plants: a scenario-dependent probabilistic approach. *Annu. Rev. Plant Biol.* 69, 733–759. doi: 10.1146/annurev-arplant-042817-040218

Templer, S. E., Ammon, A., Pscheidt, D., Ciobotea, O., Schuy, C., McCollum, C., et al. (2017). Metabolite profiling of barley flag leaves under drought and combined heat and drought stress reveals metabolic QTLs for metabolites associated with antioxidant defense. *J. Exp. Bot.* 68, 1697–1713. doi: 10.1093/jxb/erx038

Tracy, S. R., Gómez, J. F., Sturrock, C. J., Wilson, Z. A., and Ferguson, A. C. (2017). Non-destructive determination of floral staging in cereals using X-ray micro computed tomography (μCT). *Plant Methods* 13:37.

Trovato, M., Forlani, G., Signorelli, S., and Funck, D. (2019). "Proline metabolism and its functions in development and stress tolerance," in *Osmoprotectant-Mediated Abiotic Stress Tolerance in Plants: Recent Advances and Future*

Perspectives, eds M. A. Hossain, V. Kumar, D. J. Burritt, and M. Fujita (Berlin: Springer), 41–72. doi: 10.1007/978-3-030-27423-8_2

Vadez, V., Kholova, J., Medina, S., Kakkera, A., and Anderberg, H. (2014). Transpiration efficiency: new insights into an old story. *J. Exp. Bot.* 65, 6141–6153. doi: 10.1093/jxb/eru040

van Genuchten, M. (1980). A closed-form equation for predicting the hydraulic conductivity of unsaturated soils. *Soil Sci. Soc. Am. J.* 44, 892–898. doi: 10.2136/sssaj1980.03615995004400050002x

Venekamp, J. H., and Koot, J. M. (1984). The distribution of free amino acids, especially of proline, in the organs of field bean plants. *Vicia faba* L., during development in the field. *J. Plant Physiol.* 116, 343–349. doi: 10.1016/s0176-1617(84)80113-3

Verbruggen, N., and Hermans, C. (2008). Proline accumulation in plants: a review. *Amino Acids* 35, 753–759. doi: 10.1007/s00726-008-0061-6

Verslues, P. E., and Sharma, S. (2010). Proline metabolism and its implications for plant-environment interaction. *Arabidopsis Book* 8:e0140. doi: 10.1199/tab.0140

Wasaya, A., Zhang, X., Fang, Q., and Yan, Z. (2018). Root phenotyping for drought tolerance: a review. *Agronomy* 8:241. doi: 10.3390/agronomy8110241

Yang, X., Wang, B., Chen, L., Li, P., and Cao, C. (2019). The different influences of drought stress at the flowering stage on rice physiological traits, grain yield, and quality. *Sci. Rep.* 9:3742.

Conflict of Interest: The authors declare that the research was conducted in the absence of any commercial or financial relationships that could be construed as a potential conflict of interest.

Copyright © 2021 Frimpong, Windt, van Dusschoten, Naz, Frei and Fiorani. This is an open-access article distributed under the terms of the Creative Commons Attribution License (CC BY). The use, distribution or reproduction in other forums is permitted, provided the original author(s) and the copyright owner(s) are credited and that the original publication in this journal is cited, in accordance with accepted academic practice. No use, distribution or reproduction is permitted which does not comply with these terms.

frontiers in Plant Science

REVIEW
published: 07 May 2021
doi: 10.3389/fpls.2021.643403

Metabolism and Regulatory Functions of *O*-Acetylserine, *S*-Adenosylmethionine, Homocysteine, and Serine in Plant Development and Environmental Responses

Mutsumi Watanabe[1], Yukako Chiba[2] and Masami Yokota Hirai[3,4]*

[1] Graduate School of Biological Science, Nara Institute of Science and Technology, Ikoma, Japan, [2] Graduate School of Life Sciences, Faculty of Science, Hokkaido University, Sapporo, Japan, [3] RIKEN Center for Sustainable Resource Science, Yokohama, Japan, [4] Graduate School of Bioagricultural Sciences, Nagoya University, Nagoya, Japan

OPEN ACCESS

Edited by:
Rachel Amir, Migal - Galilee Research Institute, Israel

Reviewed by:
Markus Wirtz, Universität Heidelberg, Germany
Irene García, Institute of Plant Biochemistry and Photosynthesis (IBVF), Spain

***Correspondence:**
Masami Yokota Hirai
masami.hirai@riken.jp

Specialty section:
This article was submitted to Plant Metabolism and Chemodiversity, a section of the journal Frontiers in Plant Science

Received: *18 December 2020*
Accepted: *17 March 2021*
Published: *07 May 2021*

Citation:
Watanabe M, Chiba Y and Hirai MY (2021) Metabolism and Regulatory Functions of O-Acetylserine, S-Adenosylmethionine, Homocysteine, and Serine in Plant Development and Environmental Responses. Front. Plant Sci. 12:643403. doi: 10.3389/fpls.2021.643403

The metabolism of an organism is closely related to both its internal and external environments. Metabolites can act as signal molecules that regulate the functions of genes and proteins, reflecting the status of these environments. This review discusses the metabolism and regulatory functions of *O*-acetylserine (OAS), *S*-adenosylmethionine (AdoMet), homocysteine (Hcy), and serine (Ser), which are key metabolites related to sulfur (S)-containing amino acids in plant metabolic networks, in comparison to microbial and animal metabolism. Plants are photosynthetic auxotrophs that have evolved a specific metabolic network different from those in other living organisms. Although amino acids are the building blocks of proteins and common metabolites in all living organisms, their metabolism and regulation in plants have specific features that differ from those in animals and bacteria. In plants, cysteine (Cys), an S-containing amino acid, is synthesized from sulfide and OAS derived from Ser. Methionine (Met), another S-containing amino acid, is also closely related to Ser metabolism because of its thiomethyl moiety. Its S atom is derived from Cys and its methyl group from folates, which are involved in one-carbon metabolism with Ser. One-carbon metabolism is also involved in the biosynthesis of AdoMet, which serves as a methyl donor in the methylation reactions of various biomolecules. Ser is synthesized in three pathways: the phosphorylated pathway found in all organisms and the glycolate and the glycerate pathways, which are specific to plants. Ser metabolism is not only important in Ser supply but also involved in many other functions. Among the metabolites in this network, OAS is known to function as a signal molecule to regulate the expression of OAS gene clusters in response to environmental factors. AdoMet regulates amino acid metabolism at enzymatic and translational levels and regulates gene expression as methyl donor in

the DNA and histone methylation or after conversion into bioactive molecules such as polyamine and ethylene. Hcy is involved in Met–AdoMet metabolism and can regulate Ser biosynthesis at an enzymatic level. Ser metabolism is involved in development and stress responses. This review aims to summarize the metabolism and regulatory functions of OAS, AdoMet, Hcy, and Ser and compare the available knowledge for plants with that for animals and bacteria and propose a future perspective on plant research.

Keywords: aspartate-family amino acid, homocysteine, *O*-acetylserine, one-carbon metabolism, serine, *S*-adenosylmethionine, sulfur assimilation

INTRODUCTION

Plants (land plants) are photosynthetic auxotrophs that assimilate carbon dioxide and inorganic ions absorbed from the soil into organic compounds. They share common biosynthetic pathways for proteinogenic amino acids with prokaryotic microbes such as *Escherichia coli*. However, plant metabolism is compartmentalized into several organelles that have specific functions. It also differs from the metabolism of animals, as they consume nutrients through their diet.

Land plants have evolved complex body plans, which require developmental regulation of metabolism. They have also evolved adaptive mechanisms that regulate metabolism to cope with terrestrial environments that are harsher than aquatic environments. To understand why plants have evolved extant metabolic systems, a comparison of these systems with those in other organisms will be helpful. In this review, we aim to summarize commonalities and differences in metabolism related to sulfur (S)-containing amino acids and one-carbon (C_1) metabolism among plants, bacteria, and animals. The changes in metabolite content are due to metabolic regulation, and the metabolites in turn regulate metabolism. We also elucidate the regulatory functions of metabolites closely related to each other, focusing on four amino acids: *O*-acetylserine (OAS), *S*-adenosylmethionine (AdoMet), homocysteine (Hcy), and serine (Ser) (**Table 1**).

In the first part of this review, we introduce the metabolism of OAS (section "OAS Is a Key Metabolite in Cys Synthesis"), Hcy (section "Hcy Is Essential for *de novo* Met Synthesis and AdoMet Recycling"), and AdoMet (section "AdoMet Provides Methyl and Aminopropyl Moieties and Is Recycled in the Three Cycles") in the context of S assimilation and S-containing amino acid biosynthesis. We also introduce C_1 metabolism (section "One-Carbon Metabolism Involves Tetrahydrofolate and AdoMet Metabolism") and Ser metabolism (section "Ser Metabolism Interconnects Metabolic Network"), which are closely related to the metabolism of OAS, Hcy, and AdoMet. The metabolic pathways described in these chapters are overviewed in **Figure 1**. In the second part, we describe the regulatory control functions of OAS (section "OAS"), AdoMet (section "AdoMet"), Hcy (section "Hcy"), and Ser (section "Ser") in plants in comparison to those of bacteria and animals.

METABOLISM INVOLVING OAS, ADOMET, HCY, AND SER

OAS Is a Key Metabolite in Cys Synthesis

S assimilation of inorganic S into organic S in plants, bacteria, and yeast is especially important in nature because animals do not have these assimilatory mechanisms. Animals require methionine (Met) as an essential amino acid because it is a source of nutrient S (Brosnan and Brosnan, 2006). Sulfate is the principal source of S for plants and many bacteria (Leustek et al., 2000; Takahashi et al., 2011). To incorporate the S atom of sulfate into cysteine (Cys), which is the first organic compound with reduced S, the reduction of sulfate to sulfide is required. Plants universally use the adenosine-5′-phosphate (APS) reductase pathway (**Figure 2**), whereas bacteria use either the APS reductase (APR) pathway or the 3′-phospho-APS (PAPS) reductase pathway. In plants and sulfate-assimilating bacteria, inorganic sulfate is reduced to APS by ATP sulfurylase (ATPS) and then converted to sulfite by APR, which is reduced to sulfide by sulfite reductase (SiR; Bick et al., 2000). In other bacteria including *E. coli* or in yeast, sulfate is incorporated into APS by ATPS and then converted to PAPS by APS kinase (APK), which is reduced to sulfite by PAPS reductase and subsequently to sulfide by SiR (Masselot and De Robichon-Szulmajste, 1975; Sekowska et al., 2000). The biosynthesis of Cys represents the final step of sulfate assimilation. In bacteria and plants, Cys is synthesized from OAS, which is an activated Ser, by incorporating sulfide into the direct sulfhydrylation pathway (**Figure 2** for plants). Ser acetyltransferase (SERAT also called SAT) catalyzes the OAS synthesis from acetyl-CoA and Ser. Synthesized OAS is condensed with sulfide by OAS(thiol)lyase/OAS sulfhydrylase (OAS-TL also called OASS) to form Cys. In yeast, sulfide can be condensed with OAS to produce Cys or with *O*-acetylhomoserine to produce Hcy, which can be converted to cystathionine (CysT) and then to Cys. The budding yeast *Saccharomyces cerevisiae* has only *O*-acetylhomoserine pathway, while the fission yeast *Schizosaccharomyces pombe* has both pathways (Cherest and Surdin-Kerjan, 1992; Marzluf, 1997). Bacteria can also integrate thiosulfate into OAS to produce *S*-sulfocysteine catalyzed by OAS-TL and then Cys (Hulanicka et al., 1979; Nakamura et al., 1984). In bacteria, there are more than 20 genes required for the transport and assimilatory reduction of sulfate and

TABLE 1 | Abbreviations and synonyms used in this article.

	Abbreviations	Synonyms
Compounds		
5,10-Methenyl-THF	5,10=CH-THF	
5,10-Methylene-THF	5,10-CH_2-THF	
5-Methyl-THF	5-CH_3-THF	
10-Formyl-THF	10-HCO-THF	
1-Aminocyclopropane 1-carboxylate	ACC	
S-adenosylhomocysteine	AdoHcy	SAH
S-adenosylmethionine	AdoMet	SAM
Adenosine-5′-phosphate	APS	
Cystathionine	CysT	
Decarboxylated AdoMet	dAdoMet	dcSAM
1,2-Dihydro-3-keto-5-methylthiopentene	DHKMP	
Homocysteine	Hcy	Hcys
5′-Methylthioadenosine	MTA	
2-Keto-4-methylthiobutyrate	KMTB	KMBA
5-Methylthioribose	MTR	
5-Methylthioribose-1-phosphate	MTR-P	MTR-1-P
5-Methylthioribulose-1-phosphate	MTRu-P	MTRu-1-P
Nicotianamine	NA	
N-acetylserine	NAS	
O-acetylserine	OAS	
O-phosphohomoserine	OPH	
3′-Phospho-APS	PAPS	
3-Phosphoglycerate	PGA	
S-Methylmethionine	SMM	
Tetrahydrofolate	THF	
Enzymes		
ACC oxidase	ACO	
Arg decarboxylase	ADC	
Adenosine kinase	ADK	
AdoMet decarboxylase	AdoMetDC	SAMDC
Alanine:hydroxypyruvate (Ser:pyruvate) aminotransferase	AH-AT	
Aspartate kinase	AK	
APS kinase	APK	
APS reductase	APR	
Acidoreductone oxygenase	ARD	
ATP sulfurylase	ATPS	
Cystathionine β-lyase	CBL	
Cdystathionine γ-synthase	CGS	
Cysteine synthase complex	CSC	
Dehydratase-enolase-phosphatase-complex 1	DEP1	
Glycine decarboxylase complex	GDC	
10-Formyl-THF synthetase	FTHFS	
Glycerate dehydrogenase	GDH	
Glycerate kinase	GLYK	
Homocysteine *S*-methyltransferase	HcySMT	
Histone methyltransferase	HMT	
Hydroxypyruvate reductase	HPR	
Homoserine dehydrogenase	HSDH	
S-adenosylmethionine synthetase/methionine adenosyltransferase	MAT	SAM synthase, SAMS
Methionyl-tRNA synthetase	MetRS	
Methionine *S*-methyltransferase	MetSMT	
Methionine synthase	MS	
5,10-Methenyl-THF cyclohydrolase	MTHFC	
5,10-Methylene-THF dehydrogenase	MTHFD	
Bifunctional MTHFD/MTHFC	MTHFD/C	
5,10-Methylene-THF reductase	MTHFR	
5-Methylthioribose-1-phosphate isomerase	MTI	
5-Methylthioribose kinase	MTK	
5-Methylthioadenosine nucleosidase	MTN	
O-acetylserine-(thiol)-lyase	OAS-TL	OASS
3-Phosphoglycerate phosphatase	PGAP	
3-Phosphoglycerate dehydrogenase	PGDH	
3-Phosphoserine aminotransferase	PSAT	
3-Phosphoserine phosphatase	PSP	
S-Adenosylhomocysteine hydrolase	SAHH	
Serine acetyltransferase	SERAT	SAT
Serine hydroxymethyltransferase	SHM	SHMT
Sulfite reductase	SiR	
Spermidine synthase	SPDS	
Spermine synthase	SPMS	
Threonine synthase	TS	
Thermospermine synthase	TSPMS	

Cys biosynthesis from several operons belonging to a cys regulon regulated by a transcriptional regulator CysB (see section "OAS and *N*-Acetylserine Regulate Transcription in Bacteria and Plants"). Generally, the cytosol is the major site for the assimilation and synthesis of Cys in bacteria. In plants, the sulfate reduction pathway, which produces sulfide, is mainly localized to plastids, whereas the syntheses of OAS and Cys are localized to multiple compartments, including the cytosol, plastids, and mitochondria (Saito, 2004; Takahashi et al., 2011) (**Figure 1**). The activity distributions of the dominant SERAT and OAS-TL differed between the subcellular compartments, tissues, and species. For *Arabidopsis thaliana* (hereafter *Arabidopsis*), there are five SERAT isoforms and three OAS-TL isoforms, which are distributed over the three compartments (Noji et al., 1998; Wirtz et al., 2001; Kawashima et al., 2005; Haas et al., 2008; Heeg et al., 2008; Watanabe et al., 2008a,b). In *Arabidopsis* leaf, mitochondrial SERAT and cytosolic OAS-TL predominantly contribute to the production of OAS and Cys, respectively, but the dominant contributions seem to differ in other tissues, such as the roots, flower, silique, and seeds, and in different growth conditions (Heeg et al., 2008; Watanabe et al., 2008a,b; Birke et al., 2013). In other species, dominant SERAT activity was detected in the cytosol of *Citrullus vulgaris* seedlings (Saito et al., 1995), in plastids of *Spinacea oleracea* leaf (Brunold and Suter, 1982), and

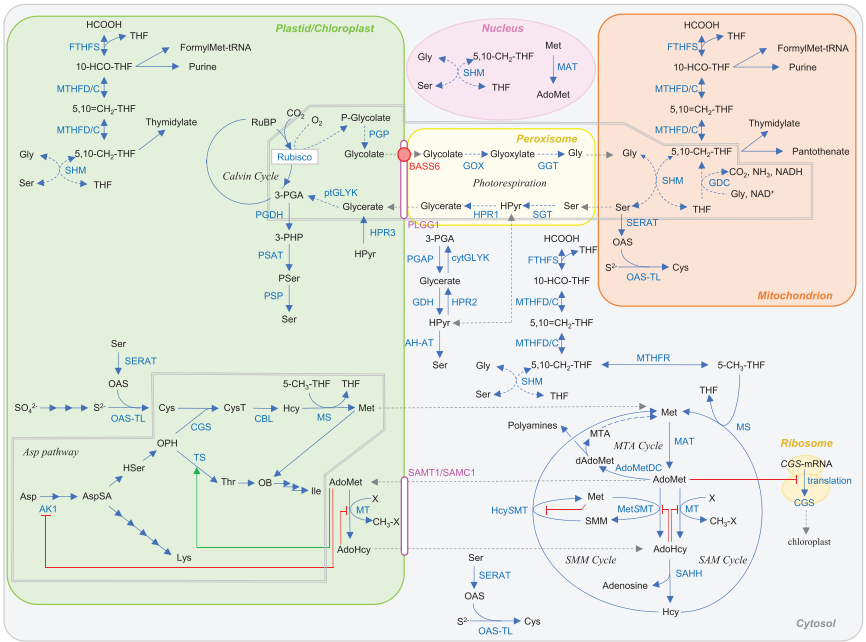

FIGURE 1 | Plant metabolic pathways targeted in this article. Red and green lines indicate repression and activation of the reaction by metabolites. Abbreviations: BASS6, bile acid sodium symporter 6; PLGG1, plastidal glycolate glycerate translocator 1; SAMT1/SAMC1, *S*-adenosylmethionine transporter 1/*S*-adenosylmethionine carrier 1. Other abbreviations are listed in **Table 1**.

in the mitochondria of *Phaseolus vulgaris* seedlings (Smith, 1972) and *Pisum sativum* leaves (Ruffet et al., 1995; Droux, 2003).

Hcy Is Essential for *de novo* Met Synthesis and AdoMet Recycling

Cys is further converted to another S-containing proteinogenic amino acid Met in plants and bacteria (**Figure 1** for plants). This metabolic pathway comprised three reactions catalyzed by CysT γ-synthase (CGS), CysT β-lyase (CBL), and Met synthase (MS). CGS catalyzes the formation of CysT from Cys and *O*-phosphohomoserine (OPH), whereas CBL generates Hcy from CysT. In the last step of Met synthesis, the methyl group is transferred to an S atom of Hcy by MS using 5-methyltetrahydrofolate (5-CH_3-THF) as a methyl donor. OPH provides a carbon skeleton of Met and works as the common biosynthetic precursor for threonine (Thr) and isoleucine (Ile). In plants, CGS and CBL are localized in the chloroplast, whereas MS is considered to exist in both the chloroplast and cytosol. Ravanel et al. (2004) reported that a chloroplastic MS isoform of *Arabidopsis* (AtMS3) was responsible for the methylation of Hcy that is synthesized *de novo* in this organelle, whereas two cytosolic MS isoforms (AtMS1 and AtMS2) are involved in the regeneration of Met from Hcy, which is derived from *S*-adenosylhomosysteine (AdoHcy), a product of methylation reactions that use AdoMet. The 5-CH_3-THF is synthesized by 5,10-CH_2-THF reductase (MTHFR) from methylene-THF (5,10-CH_2-THF) and serves as a methyl donor in the reactions catalyzed by MS. However, as the plastids lack MTHFR and cannot generate 5-CH_3-THF, it is not clear how they might make Met from Hcy (Christensen and MacKenzie, 2006). As AdoHcy inhibits methyltransferase activity (Tehlivets et al., 2013), degradation of AdoHcy by *S*-adenosylhomocysteine hydrolase (SAHH) into Hcy is important to maintain the activity of the methyltransferases involved in various important reactions. SAHH is localized only to the cytosol.

While bacteria have the same biosynthetic pathways for Met, animals cannot produce this amino acid and must acquire it from their diets. In animals, Cys is synthesized from Met via a pathway in which Met is sequentially converted to AdoMet, AdoHcy, Hcy, CysT, and finally Cys (Poloni et al., 2015).

In plant, Met is a member of the aspartate (Asp) family of amino acids because its carbon skeleton is derived from Asp. Among the nine essential amino acids for humans, lysine (Lys), Thr, Ile, and Met are synthesized from Asp in plants and bacteria. The biosynthetic pathway of these Asp-family amino acids (Asp pathway, surrounded by gray double line in **Figure 1**) in plants is finely regulated via feedback inhibition and stimulation of enzymatic activities by Lys, Thr, Ile, and AdoMet (Jander and Joshi, 2009; Galili et al., 2016). The pathway is also regulated at a translational level by AdoMet (see section "AdoMet Is a Critical Biomolecule Controlling Enzymatic Activity and Gene Expression at the Level of Transcription and Translation").

AdoMet Provides Methyl and Aminopropyl Moieties and Is Recycled in the Three Cycles

AdoMet is an important molecule that serves as a methyl donor in numerous methylation reactions in all living organisms. The

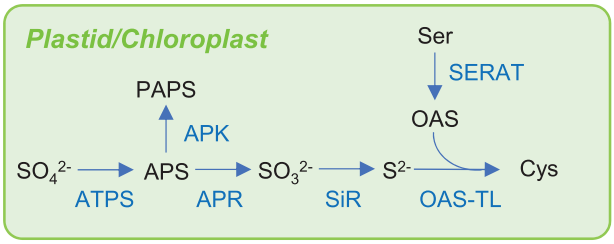

FIGURE 2 | Sulfur assimilation pathway in plant. Abbreviations are summarized in **Table 1**.

methylation of DNA and histones regulates gene expression and thus various biological phenomena. Decarboxylated AdoMet (dAdoMet) serves as an aminopropyl donor for the synthesis of polyamines, which regulate growth and development in all living organisms (see section "AdoMet-Derived Polyamines and Ethylene Are Regulatory Metabolites in Stress Responses"). In plants, AdoMet is a precursor of the phytohormone ethylene and the iron chelator nicotianamine (NA) (**Figure 3**).

AdoMet is synthesized from Met and ATP by AdoMet synthetase (also known as Met adenosyltransferase and thus abbreviated as MAT). In mammals, MAT isoenzymes were classically considered to be cytosolic proteins (Pajares et al., 2013). However, they were also found in the nucleus, suggesting that they may function to provide AdoMet for the methylation of DNA and histones (Pajares et al., 2013). Similarly, AdoMet was previously considered to be synthesized only in the cytosol of plants (Ravanel et al., 2004). However, recent studies have shown that MAT isoenzymes are localized both in the nucleus and cytosol in *Arabidopsis* (Mao et al., 2015; Chen et al., 2016). Methylation reactions using AdoMet also occur in chloroplasts. AdoMet is imported from the cytosol to chloroplasts via SAM transporter 1 (SAMT1)/SAM career 1 (SAMC1), which is localized to the chloroplast envelope membranes and functions as an AdoMet–AdoHcy antiporter (Bouvier et al., 2006; Palmieri et al., 2006). As mentioned above, AdoHcy, a product of methylation reactions, needs to be transported to the cytosol and degraded by SAHH to form Hcy.

Hcy derived from AdoHcy degradation is regenerated into Met by MS in the cytosol of yeast, mammals, and plants (**Figure 3**). Consequently, the conversion of Met–AdoMet–AdoHcy–Hcy–Met forms the SAM cycle in cytosol. In addition, plants have another Met recycling system from Hcy called the *S*-methylmethionine (SMM) cycle, which involves Met *S*-methyltransferase (MetSMT) and Hcy *S*-methyltransferase (HcySMT) in the cytosol. MetSMT and HcySMT catalyze the conversion of AdoMet to AdoHcy and Hcy to Met, respectively, coupled with the conversion between Met and SMM (Sauter et al., 2013). SMM is a storage form of S and methyl groups in the leaves and a transport form of reduced S in the phloem (Bourgis et al., 1999). The SMM cycle plays a role in the maintenance of the AdoMet/AdoHcy ratio (Kocsis et al., 2003), which is thought to be a metabolic indicator of the methylation potential (Hoffman et al., 1979; Moffatt and Weretilnyk, 2001).

In plants, AdoMet is utilized for the biosynthesis of polyamines, NA, and ethylene. In these biosynthetic reactions, 5′-methylthioadenosine (MTA) is generated as a common by-product. MTA is a product inhibitor of spermidine synthase (SPDS), spermine synthase (SPMS), thermospermine synthase (TSPMS), NA synthase, and ACC synthase (ACS) involved in ethylene biosynthesis, and its accumulation is toxic. Then, MTA is detoxified and recycled via the Met salvage cycle (also known as the Yang cycle or MTA cycle) in the cytosol to generate Met (Sauter et al., 2013) (**Figure 3**). This cycle is common in plants, mammals, and bacteria, but involved enzymes seem to have been recruited from different metabolic pathways, depending on organisms during evolution (Sekowska et al., 2019). Unexpectedly, transcriptome analyses suggested that the MTA cycle genes in plant are specifically expressed in phloem. This hypothesis on phloem-specific expression was confirmed experimentally and further resulted in identification of 5-methylthioribose-1-phosphate isomerase 1 (MTI1) and dehydratase-enolase-phosphatase complex 1 (DEP1), which had been missing enzymes in plant (Pommerrenig et al., 2011). DEP1 is responsible for the conversion of 5-methylthioribulose-1-phosphate (MTRu-P) to 1,2-dihydro-3-keto-5-methylthiopentene (DHKMP) in plant, whereas in *Bacillus*, the conversion is catalyzed by three enzymes. Interestingly, one of three enzymes, 2,3-diketo-5-methylthiopentyl-1-phosphate enolase in a non-photosynthetic bacterium *Bacillus*, is an analog of ribulose bisphosphate carboxylase/oxygenase (RuBisCO) (Ashida et al., 2003).

One-Carbon Metabolism Involves Tetrahydrofolate and AdoMet Metabolism

One-carbon (C_1)-substituted folates are required for the biosynthesis of various important molecules. The methyl moiety of AdoMet is also derived from C_1-substituted folates, and thus, C_1 metabolism is essential in all living organisms. C_1 derivatives of tetrahydrofolate (THF) are interconverted between different oxidation states, ranging from the most oxidized 10-formyl- (10-HCO-) THF through to 5,10-methenyl- (5,10=CH_2-) THF and 5,10-methylene- (5,10-CH_2-) THF to the most reduced 5-methyl- (5-CH_3-) THF (Hanson et al., 2000) (**Figure 4**). The 5,10-CH_2-THF is generated from the conversion of 5,10=CH_2-THF catalyzed by 5,10-CH_2-THF dehydrogenase (MTHFD). The 5,10-CH_2-THF is also synthesized via the reversible reaction of Ser and THF to form Gly and 5,10-CH_2-THF, which is catalyzed by Ser hydroxymethyltransferase (SHM). The conversion of 5,10=CH_2-THF to 10-HCO-THF is catalyzed by 5,10=CH-THF cyclohydrolase (MTHFC). The 10-HCO-THF is used for the synthesis of purines and formylmethionyl-tRNA, which is used for translation initiation in plastids and mitochondria (**Figure 1**). The 5,10-CH_2-THF is used for the synthesis of thymidylate and pantothenate. In eukaryotes, C_1 folate metabolism is found in multiple organelles, including the mitochondria and cytosol of mammals, whereas in plants, it is also found in plastids (Hanson et al., 2000; Christensen and MacKenzie, 2006).

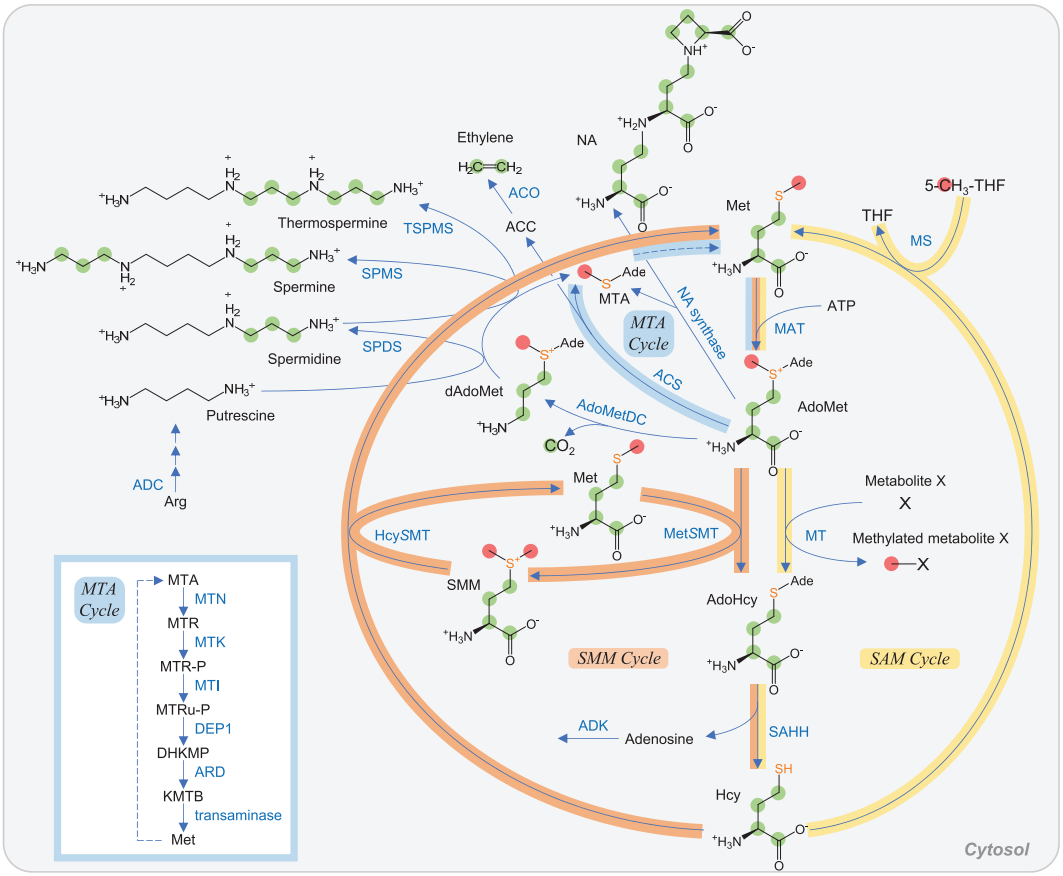

FIGURE 3 | AdoMet metabolism in plant. Carbon atoms of C_1 unit and those derived from Asp are shown as red and green circles, respectively. Sulfur atoms derived from Cys are highlighted in orange. SAM cycle, SMM cycle, and MTA cycle (also known as the Yang cycle or Met salvage cycle) are indicated in yellow, orange, and pale blue, respectively. Among the reactions of the MTA cycle, six steps from MTA to Met are shown in the lower left box. Abbreviations: Ade, adenosyl group. Other abbreviations are listed in **Table 1**.

However, MTHFR, which converts 5,10-CH_2-THF to 5-methyl-(5-CH_3-)THF, is found only in the cytosol (Hanson et al., 2000; Christensen and MacKenzie, 2006) (**Figure 4**). In the cytosol, Met is regenerated from Hcy via MS using 5-CH_3-THF as a methyl donor in yeast, mammals, and plants (Christensen and MacKenzie, 2006). In *Arabidopsis*, a point mutation in the cytosolic bifunctional MTHFD/MTHFC (MTHFD1) resulted in the increase of THF + 5,10-CH_2-THF (these two compounds were not distinguished by the analysis) and the decrease of 5,10=CH_2-THF + 10-HCO-THF (these two compounds were also not distinguished) (Groth et al., 2016). Moreover, the mutation caused the accumulation of AdoHcy and Hcy, DNA hypomethylation, and loss of histone H3 lysine 9 methylation, indicating the interconnection of THF metabolism, AdoMet recycling, and DNA methylation. One of the major differences among the organisms is that C_1 metabolism in mitochondria is related to photorespiration in plants (**Figure 1**). In the mitochondria of both photosynthetic and non-photosynthetic plant tissues, the major C_1 donor is Gly via mitochondrion-specific Gly decarboxylase complex (GDC). To satisfy the demands of photorespiration, the flux through GDC and SHM reactions is in the direction to make Ser from Gly. In contrast, in yeast, Ser is the major C_1 donor in the mitochondria, and the SHM reaction is reversible (Christensen and MacKenzie, 2006).

SHM is a conserved enzyme in living organisms from bacteria to higher plants and mammals and plays an important role in C_1 metabolism (McClung et al., 2000; Hanson and Roje, 2001; Bauwe and Kolukisaoglu, 2003). In plant, the SHM isoenzymes are localized in the cytosol, mitochondria, plastids, and nucleus (Ruszkowski et al., 2018). The *SHM* gene family consists of seven genes in *Arabidopsis*. The mitochondrial SHM1 and SHM2 are involved in the photorespiratory Gly-into-Ser conversion (Voll et al., 2006; Engel et al., 2007), and the plastidic SHM3 catalyzes a reversible hydroxymethyl group transfer from Ser to THF, yielding Gly and 5,10-CH_2-THF (Zhang et al., 2010). SHM7 in the nucleus lacks conventional SHM activity and is required for AdoMet production (see section "OAS Cluster Genes: OAS Functions as a Signal in Plants").

Fluxes through the C_1 pathways are particularly high in plants, because they are rich in methylated compounds such as lignin, alkaloids, and betaines (Hanson et al., 2000).

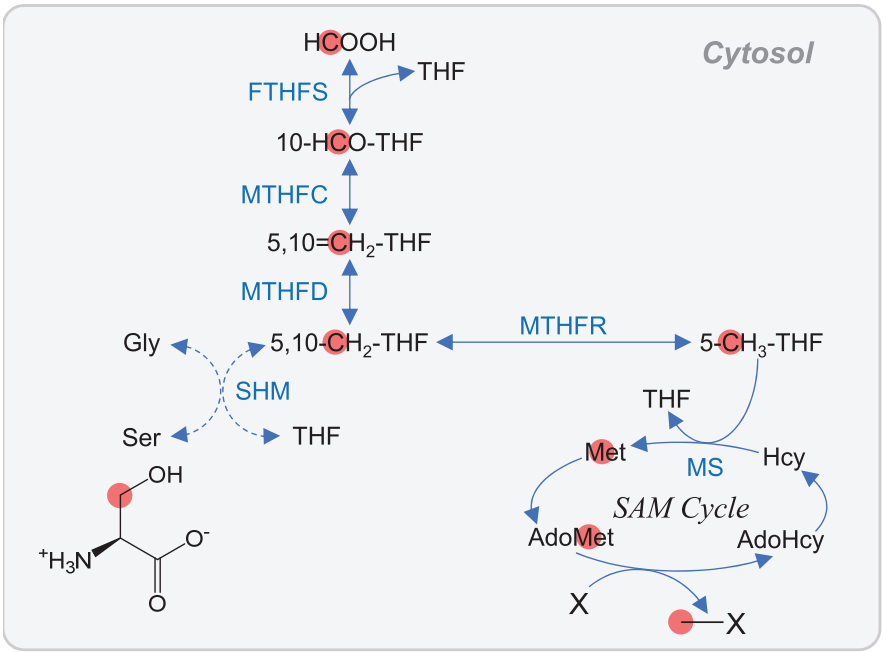

FIGURE 4 | C_1 metabolism in cytosol of plant. Carbon atoms of C_1 unit are shown as red circles. Abbreviations are listed in **Table 1**. In *Arabidopsis*, the cytosolic bifunctional MTHFD/MTHFC is encoded by *MTHFD1*.

Ser Metabolism Interconnects Metabolic Network

The proteinogenic amino acid Ser has a function as a precursor for various essential biomolecules such as nucleic acid bases, phospholipids, sphingolipids, and other amino acids in all organisms. In mammal, Ser metabolism plays crucial roles in, for example, brain development and function, as well as endothelial cell proliferation (Hirabayashi and Furuya, 2008; Vandekeere et al., 2018; Le Douce et al., 2020). In plants, Ser plays important roles not only in development (see below) but also in the response to environmental stresses, such as high salinity, flooding, and low temperature (Ho and Saito, 2001).

In contrast to the Asp-family amino acids that human must acquire from their diet, Ser can be synthesized in all living organisms including humans. Plants have three Ser biosynthetic pathways in different organelles: the glycolate pathway in mitochondria, the phosphorylated pathway in chloroplasts, and the glycerate (non-phosphorylated) pathway in cytosol (**Figure 5**).

The glycolate pathway forms a part of photorespiration processes (**Figures 1**, **5**) and is a major source of Ser in photosynthetic organs. In photorespiration, a toxic metabolite phosphoglycolate is formed via the oxygenase activity of RuBisCO in chloroplast. This metabolite is recycled to 3-phosphoglycerate (PGA) in the sequential reactions occurring across chromoplast, peroxisome, and mitochondrion and turned back to the Calvin–Benson cycle. In the glycolate pathway, two Gly molecules are converted to one Ser molecule catalyzed by GDC and SHM in the mitochondria. Two transporters are involved in photorespiration processes: the plastidal glycolate glycerate translocator 1 (PLGG1) responsible for the simultaneous export of glycolate from and import of glycerate into the chloroplast (Pick et al., 2013) and the bile acid sodium symporter (BASS6) for export of glycolate from chloroplast (South et al., 2017).

The phosphorylated pathway of Ser biosynthesis, recently called PPSB, is common in plants, bacteria, and animals. In this pathway, PGA is converted to Ser via three-step reactions catalyzed by 3-PGA dehydrogenase (PGDH), 3-phosphoserine aminotransferase (PSAT), and 3-phosphoserine phosphatase (PSP) (**Figure 5**). In plants, these enzymes are localized in the plastid (Ho et al., 1998, 1999; Benstein et al., 2013; Cascales-Miñana et al., 2013; Toujani et al., 2013a; Wulfert and Krueger, 2018). In *Arabidopsis*, PGDH, PSAT, and PSP are encoded by three genes, two genes, and one gene, respectively. Most of the genes are dominantly expressed in heterotrophic tissues, except AtPGDH3 and AtPSP1 (Benstein et al., 2013), suggesting that PPSB supplies Ser to the heterotrophic tissues. However, PPSB also plays a role in the photosynthetic organs when photorespiration is inhibited at night or under high CO_2 conditions (Ros et al., 2014). In *E. coli* and *Mycobacterium tuberculosis*, PGDH is feedback-inhibited by Ser (Pizer, 1963: Dey et al., 2005), whereas PGDH of human and rat is not (Achouri et al., 1997; Dey et al., 2008). In *Arabidopsis*, AtPGDH1 and AtPGDH3, but not AtPGDH2, are inhibited by Ser (Benstein et al., 2013; Okamura and Hirai, 2017). In a basal land plant *Marchantia polymorpha*, a single gene-encoded MpPGDH is inhibited by Ser (Akashi et al., 2018). In addition, AtPGDH1, AtPGDH3, and MpPGDH are activated by alanine, valine, Met, homoserine, and Hcy, suggesting interaction between PPSB and

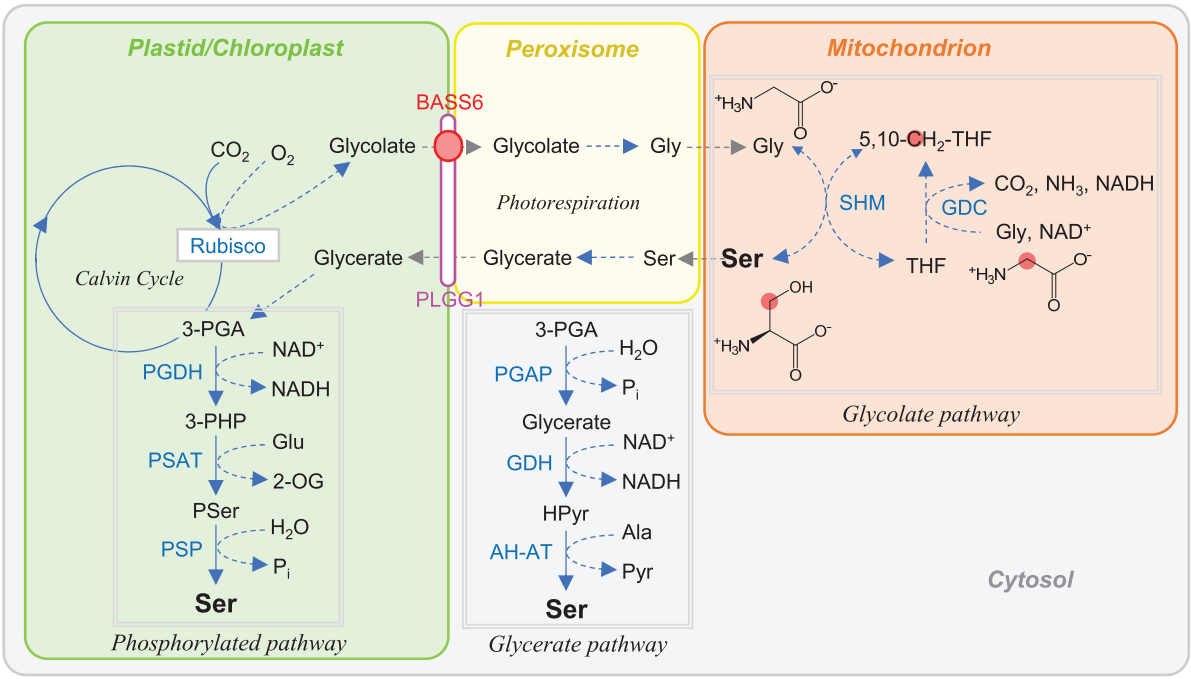

FIGURE 5 | Ser biosynthesis in plant. Carbon atoms of C_1 unit are shown as red circles. Abbreviations are listed in **Table 1**.

other amino acid metabolism (Okamura and Hirai, 2017; Akashi et al., 2018). AtPGDH1 and AtPSP1 are essential in pollen and embryo development (Benstein et al., 2013; Cascales-Miñana et al., 2013; Toujani et al., 2013b).

In the glycerate (non-phosphorylated) pathway, PGA is first dephosphorylated by PGA phosphatase and then subjected to the reactions catalyzed by glycerate dehydrogenase (GDH) and glycine:hydroxypyruvate (Ser:glyoxylate) and alanine:hydroxypyruvate (Ser:pyruvate) aminotransferases finally to form Ser (Igamberdiev and Kleczkowski, 2018). This pathway exists in the cytosol and is a major Ser source in the photosynthetic tissues of C_4 plants, in darkness in C_3 plants, and in non-photosynthetic tissues (Igamberdiev and Kleczkowski, 2018).

As mentioned in Section "OAS Is a Key Metabolite in Cys Synthesis," Ser is converted to OAS by SERAT and reacts with sulfide to form Cys. On the other hand, Ser reacts with indole and directly forms tryptophan (Trp) being catalyzed by Trp synthase. Thus, Ser provides a carbon skeleton to both Cys and Trp. Ser is also involved in C_1 metabolism via SHM (see section "One-Carbon Metabolism Involves Tetrahydrofolate and AdoMet Metabolism"). In this way, Ser metabolism interconnects S, Trp, and C_1 metabolism.

REGULATORY FUNCTION OF OAS, ADOMET, HCY, AND SER

The aforementioned pathways are mutually regulated by fine mechanisms that utilize key metabolites as signaling molecules. In the following chapters, we introduce the regulatory mechanisms involving four amino acids, OAS, AdoMet, Hcy, and Ser.

OAS

Briefly, OAS has a signal function to regulate S-responsive gene expression. OAS also regulates Cys biosynthesis at enzymatic level.

OAS and *N*-Acetylserine Regulate Transcription in Bacteria and Plants

OAS is considered a signal molecule in plants because it is highly accumulated in S-deficient conditions, and OAS and/or its isomer *N*-acetylserine (NAS) acts as a positive regulator for the biosynthesis of Cys and S utilization in bacteria (Ostrowski and Kredich, 1991; Lynch et al., 1994). In bacteria, the Cys regulon, consisting of more than 20 genes, is coordinately controlled by a LysR-type regulator CysB (Kredich, 1996; Van Der Ploeg et al., 2001; Parry and Clark, 2002). OAS and/or NAS bind to CysB, activating its binding to the promoter of genes in the Cys regulon and preventing autorepression (Kredich, 1996). Although several results from previous studies have suggested that OAS is spontaneously converted to NAS in a pH-dependent manner (Flavin and Slaughter, 1967) and that NAS is the true signal for the Cys regulon (Ostrowski and Kredich, 1989; Hryniewicz and Kredich, 1994; Lynch et al., 1994), recent research of ligand recognition by CysB in *Salmonella typhimurium* has proposed that CysB has two distinct ligand-binding sites: site-1 for sulfate and NAS and site-2 for NAS and OAS. The OAS remodels site-1 by binding to site-2 to enhance the NAS-mediated

activation through allosteric coupling between sites (Mittal et al., 2017). Furthermore, *N*,*O*-diacetylserine produced from OAS in *Salmonella enterica* may be the true signal for the Cys regulon (Vandrisse and Escalante-Semerena, 2018). More studies are required to fully confirm the activation mechanisms of CysB.

In plants, some studies have demonstrated that OAS and not NAS induced the expression of enzymes for the sulfate assimilation pathway (Neuenschwander et al., 1991; Hawkesford et al., 1995), which is the reason why OAS is considered a signal molecule in plants. However, the mechanisms for the transcriptional activation of S metabolism by OAS remain unclear in plants. Transcription regulators such as CysB or a receptor, which could be directory bound by OAS, have not yet been discovered.

OAS Cluster Genes: OAS Functions as a Signal in Plants

The role of OAS as a signal molecule in plants has been supported by the transcriptome analyses of sulfate starvation experiments (Hirai et al., 2003; Maruyama-Nakashita et al., 2003; Nikiforova et al., 2003), where OAS was accumulated in plants, and in OAS addition experiments (Koprivova et al., 2000; Kopriva et al., 2002; Hesse et al., 2003; Hopkins et al., 2005). The OAS concentration in *Arabidopsis* grown on full nutrient condition was approximately 1–10 nmol/g fresh weight in leaves and roots, whereas the concentration was increased by 10–100 times in S-starved plants (Maruyama-Nakashita et al., 2006; Hubberten et al., 2012a; Forieri et al., 2017). Hubberten et al. (2012b) succeeded in identifying OAS cluster genes (**Table 2**), which are specifically coexpressed with OAS accumulation, using metabolite–gene correlation analyses with time-series transcriptome and metabolome data in non-S-related experiments of *Arabidopsis*; the studies of natural diurnal oscillations (Espinoza et al., 2010) and responses to light and temperature (Caldana et al., 2011), where the OAS concentration was changed in the range from two to four times the baseline. Furthermore, they evaluated the OAS-correlated genes using inducible overexpression lines of SERAT (Hubberten et al., 2012b). The six OAS cluster genes were highly coexpressed in various experimental conditions in *Arabidopsis* (Obayashi et al., 2007, 2009; Mutwil et al., 2010) and in other plant species such as *Oryza sativa* and *Populus trichocarpa* (Mutwil et al., 2008; Mutwil et al., 2011). The promoter regions of the OAS cluster genes contained a conserved *cis*-element, UPE box (UP9 binding element; UPregulated by S deficit 9, see below), or UPE-like motif (Wawrzynska et al., 2010). Transcription factors in the ethylene-insensitive 3-like (EIL) family including S limitation 1 (SLIM1), which is a central transcriptional regulator of S responses in *Arabidopsis* (Maruyama-Nakashita et al., 2006), were reported to bind the UPE box (Wawrzynska et al., 2010).

Recent studies have shown that the OAS cluster genes are involved in S metabolism, although the function of APR3 has already been defined as a key-limiting enzyme in the assimilatory reduction of sulfate (Vauclare et al., 2002). The ChaC protein is considered to be a cation transporter because *ChaC* was identified as a gene of the Cha operon (Ca^{2+}/H^{+} antiporter) in *E. coli* (Ivey et al., 1993; Osborne et al., 2004). However, Kumar et al. (2012) found that mammalian ChaC has γ-glutamyl cyclotransferase (GGCT) activity degrading glutathione (GSH) to yield 5-oxoproline and cysteinyl-glycine for the recycling of GSH (Kumar et al., 2012). In the *Arabidopsis* genome, there are three ChaC genes, which all have GGCT activity (Kumar et al., 2015). Studies with knockout mutants or overexpression lines of the *GGCT2;1*, an OAS cluster gene, revealed that the GSH recycling by GGCT2;1 is important for heavy metal toxicity such as arsenite and cadmium (Paulose et al., 2013) and root system architecture during S starvation (Joshi et al., 2019).

The *low sulfur-induced* (*LSU*) gene was originally identified in *Nicotiana tabacum* as an S-responsive gene, named *UP9* (Wawrzynska et al., 2005). *UP9C*, which is one of six *UP9* genes, is highly upregulated under S starvation (Lewandowska et al., 2005) and has been suggested to be involved in the synthesis and signaling of ethylene (Moniuszko et al., 2013) and autophagy (Zientara-Rytter et al., 2011) through protein–protein interactions. In the *Arabidopsis* genome, there are four *LSU* genes, of which three (*LSU1*, *2LSU*, and *LSU3*) are induced by S deficiency (Nikiforova et al., 2003, 2005a; Sirko et al., 2015), but only *LSU1* was identified as an OAS cluster gene. In the large-scale interactome studies of proteins, LSU proteins have been identified as network hubs coordinating abiotic stress responses (Garcia-Molina et al., 2017; Vandereyken et al., 2018). Garcia-Molina et al. (2017) experimentally confirmed that LSU1 plays an important role in disease resistance to several abiotic stresses including nutrient deficiency, high salinity, or heavy metals via interactions with the chloroplastic Fe superoxide dismutase FSD2 (Garcia-Molina et al., 2017).

The *sulfur deficiency-induced* (*SDI*) gene was originally identified in wheat (*Triticum aestivum* var. Hereward) grown in S-deficient fields as an indicator of S status by cDNA-amplified fragment length polymorphism analysis (Howarth et al., 2005). In the *Arabidopsis* genome, there are five *SDI*

TABLE 2 | OAS cluster genes in *Arabidopsis*.

Gene name	AGI code	Annotation	Function	References
APR3	At4g21990	Adenosine-5′-phosphosulfate reductase 3	Sulfur assimilation	Vauclare et al., 2002
ChaC/GGCT2;1	At5g26220	ChaC-like protein/γ-glutamyl cyclotransferase	GSH degradation	Paulose et al., 2013; Joshi et al., 2019
LSU1	At3g49580	Low sulfur-induced 1		Garcia-Molina et al., 2017
SDI1	At5g48850	Sulfur deficiency-induced 1	glucosinolate biosynthesis repressor	Aarabi et al., 2016
SDI2	At1g04770	Sulfur deficiency-induced 2	glucosinolate biosynthesis repressor	Aarabi et al., 2016
SHM7/MSA1	At1g36370	Serine hydroxymethyltransferase 7/more sulfur accumulation1	*S*-adenosylmethionine production	Huang et al., 2016

genes categorized in the *Male-sterile 5* (*MS5*) gene family, of which two *SDI* genes (*SDI1* and *SDI2*) belong to the OAS cluster genes. Studies with knockout mutants or overexpression lines of the *SDI* genes revealed that SDI1 and SDI2 proteins acted as major repressors controlling glucosinolate biosynthesis in *Arabidopsis* (Aarabi et al., 2016). Further experiments using protein–protein interaction assays demonstrated that SDI1 physically interacts with MYB28, which is a positive regulator of aliphatic glucosinolates (Gigolashvili et al., 2007; Hirai et al., 2007; Sønderby et al., 2007; Malitsky et al., 2008), to repress the glucosinolate biosynthesis and use the sulfate preferentially for primary metabolites under S deficiency conditions (Aarabi et al., 2016, 2020).

The *SHM7* gene was identified as the causal gene of the ethyl methanesulfonate-mutagenized *more sulfur accumulation1-1* (*msa1-1*) mutant (Huang et al., 2016). Characterization of SHM7 and the *msa1-1* mutant revealed that SHM7 lacks conventional SHM activity, is localized in the nucleus, and is required for AdoMet production and maintaining S homeostasis epigenetically via DNA methylation of, for example, the sulfate transporter genes *SULTR1;1* and *SULTR1;2* (Huang et al., 2016).

OAS Regulates the Cys Synthase Complex

SERAT (a dimer of homotrimers) and OAS-TL (a dimer) in the final steps of Cys biosynthesis form a hetero-oligomeric Cys synthase complex (CSC) (Kredich et al., 1969; Wang and Leyh, 2012). The CSC plays an important role in plant and bacterial S metabolism to strictly regulate the Cys concentrations in cells. The function for this CSC formation is not metabolic channeling. In the CSC, SERATs are activated or stabilized, whereas OAS-TLs are inactivated. OAS-TLs are fully active in the free form (Kredich et al., 1969; Droux et al., 1998; Mino et al., 2001). The balance of the complex and free forms of SERAT and OAS-TL is regulated by precursors of Cys synthesis, OAS and sulfide (Kredich et al., 1969; Droux et al., 1998; Mino et al., 2001). OAS dissociates the CSC, whereas sulfide is associated with CSC formation; hence, the association stimulates OAS formation, whereas the dissociation stimulates both OAS consumption and Cys formation. In addition to the regulation of CSC, SERAT activity is feedback inhibited by Cys (Kredich et al., 1969; Hindson, 2003; Olsen et al., 2004). The quaternary structures of the CSC from the bacteria and plants are highly similar, but the affinity of the CSC formation and the regulation of Cys sensitivity of SERAT within the CSC are different (Wirtz et al., 2010). For example, the affinity of CSC in *Arabidopsis* is 10 times weaker than that of bacterial CSCs in *S. typhimurium*, *Haemophilus influenzae*, and *E. coli*. The CSC formation decreases the sensitivity of SERAT to feedback inhibition by Cys in plants, whereas that of bacterial SERAT is not affected by the CSC formation. SERATs in bacteria such as *E. coli* (Kredich, 1996; Hindson, 2003; Olsen et al., 2004) and *S. typhimurium* (Kredich, 1996) are sensitive to feedback inhibition by Cys. The importance of CSC formation was well studied in *Arabidopsis* and soybean. Cytosolic and mitochondrial SERATs in *Arabidopsis* and cytosolic SERAT in soybean, which are feedback-sensitive by Cys, are less sensitive to the inhibition in CSC *in vitro* assay (Wirtz et al., 2010). Furthermore, the importance of CSC formation *in vivo* to regulate SERAT activity, and consequently, Cys production was proven by analyzing *Arabidopsis* T-DNA mutants of mitochondrial SERAT and OAS-TL (Wirtz et al., 2012). In plants, generally there are multiple SERAT isoforms localized in several subcellular compartments. The presence of Cys feedback regulation differs both between plant species and between subcellular compartments. For example, cytosolic SERAT isoforms in *C. vulgaris* (Saito et al., 1995) and *Allium tuberosum* (Urano et al., 2000) and plastidial isoforms in *S. oleracea* (Noji et al., 2001) and *P. sativum* (Droux, 2003) are sensitive to the feedback inhibition.

Transporters of OAS Are Necessary for Signaling Function

In bacteria, to act as signal molecules binding to a regulator CysB in the nucleus, OAS and/or NAS, which are biosynthesized in the cytosol, need to be transported into the nucleus. Ions and small metabolites are expected to diffuse through water-filled channels in the nuclear pore complex (Beck and Hurt, 2017). In contrast to the bacteria, OAS, which is presumed to be a true signal in plants, is synthesized in multiple compartments, including the cytosol, plastids, and mitochondria (Saito, 2004; Takahashi et al., 2011). Several previous investigations using *Arabidopsis* knockout mutants of SERATs and OAS-TLs have implied that OAS and Cys are transported between cellular compartments (Heeg et al., 2008; Lopez-Martin et al., 2008; Watanabe et al., 2008a,b; Krueger et al., 2009). However, the transport system is currently unclear in plants, although several transporters of OAS and Cys such as YdeD, YfiK, Bcr, and TolC, which export both compounds from the cytosol to the outside of the cells, have been identified in bacteria (Dassler et al., 2000; Franke et al., 2003; Koronakis et al., 2004; Yamada et al., 2006). The subcellular distribution of OAS is a key issue. It is not yet clear in which compartment OAS acts as a signal molecule, how OAS induces the OAS cluster genes, or whether the distribution of OAS between the compartments is limited or not. The identification of the transport system will be helpful to elucidate the mechanisms of gene induction by OAS and to understand why OAS and Cys synthesis takes place in multiple compartments in plants.

OAS-Related Metabolites Also Function as Signals in S Assimilation Pathway

In addition to OAS, other OAS-related metabolites such as sulfide, Cys, and GSH, which are interconnected in S assimilation pathway, are also considered to be possible signal molecules (Kopriva, 2006; Rouached et al., 2008). Sulfide, Cys, and GSH, which are reduced forms of S, significantly decrease sulfate uptake and sulfate assimilation via changing the activity of enzymes and the transcript levels of genes (Brunold and Schmidt, 1976; Lappartient et al., 1999; Westerman et al., 2001; Vauclare et al., 2002). In S starvation conditions and feeding of each compound, the concentrations of these possible signal molecules were changed all together in plants, leading to disagreement regarding which metabolites were the true signals. Recent studies progressively revealed the specific function of each metabolite as a signal molecule. Sulfide has been proven to be involved in protein persulfidation causing changes in the protein functions (Aroca et al., 2018). Cys has been reported to stimulate the synthesis of

hormone abscisic acid (ABA) via inducing the transcript level of 9-*cis*-epoxycarotenoid dioxygenase 3 (NCED3), which is the key rate-limiting enzyme for ABA production (Batool et al., 2018). Dong et al. (2017) showed that *Arabidopsis* senses the availability of OAS as the carbon/nitrogen precursor for Cys synthesis with the general control non-derepressible 2 (GCN2) kinase and the availability of sulfide as the S precursor for Cys synthesis with the target of rapamycin by downregulation of glucose metabolism. The identification of distinct signal function of each metabolite could help to understand the whole framework of S starvation responses of plants.

AdoMet

The most important feature of regulatory function of AdoMet is that it could control epigenomic code via DNA/histone methylation in development and stress responses.

AdoMet Is a Critical Biomolecule Controlling Enzymatic Activity and Gene Expression at the Level of Transcription and Translation

AdoMet is recognized as an active form of Met and is one of the most important S-containing metabolites in plants. AdoMet is a key regulator of the Asp pathway, a major methyl donor for various methylation reactions, and a precursor of the polyamine, ethylene, and NA biosynthesis.

AdoMet is directly synthesized from Met and thus a critical biomolecule for regulation of the biosynthesis of Met and other amino acids in the Asp family. AdoMet acts as an allosteric effector for inhibition of Asp kinase and activation of Thr synthase (Azevedo et al., 1997; Mas-Droux et al., 2006) (**Figure 1**). While most of the key steps in the Asp pathway are regulated by allosteric enzymes, CGS, which catalyzes the first committed step of Met biosynthesis, is not one of them. CGS is functional in chloroplasts; however, AdoMet biosynthesis occurs in the cytosol. CGS is a chloroplast protein encoded by the nuclear *CGS1* gene in *Arabidopsis*. Its expression is regulated via negative feedback by temporal translation elongation arrest, followed by mRNA degradation in response to AdoMet (Chiba et al., 1999, 2003; Onouchi et al., 2005) (at the bottom right of **Figure 1**). *Arabidopsis mto1* mutants, which overaccumulate soluble Met, are defects in this posttranscriptional regulation. The *mto1* mutations are found as single amino acid changes in the short stretch of the CGS1 nascent peptide, called the MTO1 region. The MTO1 region acting as a *cis* element is necessary and sufficient for the feedback regulation of CGS1. The temporal translation arrest occurs at the Ser-94 codon immediately downstream of the MTO1 region. During the translation arrest, the CGS1 nascent peptide including the MTO1 region forms a compact conformation inside the ribosomal exit tunnel. Furthermore, the compaction is associated with the conformation changes of the rRNA in the ribosomal exit tunnel, which might be involved in the translational arrest of the *CGS1* gene in response to the AdoMet (Onoue et al., 2011). To maintain the homeostasis of the AdoMet produced in the cytosol, the translational feedback regulation of CGS1 in the cytosol is thought to be an appropriate system by which to achieve a prompt response to AdoMet.

AdoMet is a universal methyl group donor for various methylated metabolites. After the methyl group is transferred by methyltransferases to the accepted substrate, AdoHcy is produced and then rapidly hydrolyzed to Hcy and adenosine by SAHH, because AdoHcy is a strong inhibitor of all AdoMet-dependent methyltransferases. The AdoMet/AdoHcy ratio is thought to be a metabolic indicator of the methylation potential (Hoffman et al., 1979; Moffatt and Weretilnyk, 2001). DNA and histone proteins can be target for methylation. Their methylation status acts as an epigenetic code, which then influence the regulation of gene expression. In *Arabidopsis*, the steady-state levels of AdoMet and AdoHcy are reported to be ∼15 and ∼0.5 pmol/mg fresh weight, respectively, in rosette leaves (Groth et al., 2016), and 3.34 and 0.14 pmol/mg, respectively, in leaves (Rocha et al., 2005). The AdoMet/AdoHcy ratio varies according to conditions. For example, under S deficiency, AdoMet significantly decreased in seedlings, whereas AdoHcy remained unchanged, resulting in the decrease of the AdoMet/AdoHcy ratio (Nikiforova et al., 2005b). In another study, AdoMet in root significantly decreased, and DNA methylation pathway genes were downregulated under S deficiency, whereas AdoHcy also decreased to a greater extent than AdoMet, thus resulting in the increase of the AdoMet/AdoHcy ratio (Forieri et al., 2017). The study suggested that AdoMet amount itself is also important for methylation status. The AdoMet/AdoHcy ratio was also changed under iron (Fe) deficiency: the values were approximately 60 (control), 130 (S deficiency), and 180 (Fe deficiency) (calculated using the data from Forieri et al., 2017).

AdoMet/AdoHcy ratio is also important in mammals. Histone methyltransferases (HMTs) are enzymes that catalyze the transfer of methyl groups to histone proteins. Alterations to AdoMet-related metabolism affect the histone methylation status, suggesting a possible link between the AdoMet/AdoHcy ratio and HMT activity. These metabolic changes also lead to widespread secondary effects on stress responses and developmental pathways, which make it difficult to determine whether these changes on histone methylation are caused by the direct sensing of the AdoMet/AdoHcy ratio in the cells (Shyh-Chang et al., 2013; Ulanovskaya et al., 2013; Shiraki et al., 2014). However, recent studies have shown the direct effects of the AdoMet/AdoHcy ratio on histone methylation levels by demonstrating the kinetics of histone methylation turnover in response to AdoMet and AdoHcy availability (Mentch et al., 2015). As most of the HMTs are involved in the methylation of specific target genes, the metabolic status of AdoMet is critical for these gene-specific regulations.

In bacteria, AdoMet is an important metabolite, not only as a methyl group donor but also as an effector of riboswitches for regulating intracellular Met and AdoMet concentrations. Three evolutionarily distinct classes of AdoMet-binding riboswitches, the SAM-I, SAM-II, and SAM-III superfamilies, have been identified, of which the SAM-I riboswitch is widespread and the best studied in bacteria (Batey, 2011). The SAM-I riboswitches have been identified in many transcripts encoding enzymes involved in sulfate assimilation and Cys/Met biosynthesis, which include AdoMet biosynthesis itself (Grundy and Henkin, 1998). AdoMet is synthesized from Met and ATP by MAT and

is converted to AdoHcy after the methyltransferase reaction. AdoHcy is hydrolyzed to Hcy and adenosine by SAHH, and then, Hcy is recycled back to Met by MS. SAM-I, SAM-II, and SAM-III riboswitches were identified in the MAT, and SAM-I and SAM-III were in MS (Batey, 2011). The negative-feedback regulation of these enzyme genes by the AdoMet-binding riboswitch could be required for the proper maintenance of the intracellular AdoMet level.

AdoMet Metabolism and DNA/Histone Methylation Are Involved in Development and Stress Responses

As described in Section "AdoMet Is a Critical Biomolecule Controlling Enzymatic Activity and Gene Expression at the Level of Transcription and Translation," the AdoMet concentration and the AdoMet/AdHcy ratio in cells are related to the proper methylation potential of DNA and histone to maintain normal development. The studies using *Arabidopsis* mutants indicated that the AdoMet and folate metabolism affects the genome-wide DNA methylation level. The leaky mutants of SAMS3/MAT4 and SAHH1 (responsible for AdoMet synthesis and AdoHcy hydrolysis, respectively) and MTHFD1 (involving interconversion of folates) exhibited the genome-wide DNA demethylation and the reduced AdoMet/AdoHcy ratio, although the causal relationship between DNA demethylation and the reduced AdoMet/AdoHcy ratio remained to be further examined (Goto et al., 2002; Rocha et al., 2005; Groth et al., 2016; Meng et al., 2018). The knockout mutants of SAMS3/MAT4, SAHH1, and MTHFD1 genes were lethal, indicating that these genes are essential (Rocha et al., 2005; Groth et al., 2016). Adenosine kinase (ADK) catabolizes adenosine and thus enhances AdoHcy hydrolysis via SAHH (**Figure 3**; see section "Metabolism and a Putative Regulatory Role of Hcy"). In the ADK-deficient lines, AdoHcy increased by 12–43-fold, and the AdoMet/AdoHcy ratio was greatly reduced (AdoMet 17.39 μM and AdoHcy 0.34 μM in wild-type leaves) (Moffatt et al., 2002). The content of methyl-esterified pectin in seed mucilage was decreased with the reduced ADK activity. Considering morphological abnormality of the ADK-deficient lines, ADK plays an important function to AdoMet recycling and various methyltransferase reactions (Moffatt et al., 2002).

DNA methylation is involved in the various biotic and abiotic responses in plants. For instance, genome-wide DNA hypermethylation was observed in *Arabidopsis* roots in response to cyst nematode infection (Hewezi et al., 2017). Infection of bacterial pathogen also induced widespread differential DNA methylation in *Arabidopsis* leaves, which is negatively correlated with the expression of nearby transcripts (Dowen et al., 2012). In the case of abiotic stresses, early studies demonstrated abiotic stress-induced changes in DNA methylation patterns on genome-wide or specific regions, which are associated with transcriptional regulation of stress-responsive genes in some cases (Xu et al., 2015; Yong-Villalobos et al., 2015; Zhang et al., 2016). Afterward, research interest shifted to the epigenetic memory for abiotic stress responses in plants (Kinoshita and Seki, 2014; Chang et al., 2020). These studies suggest the interplays between the AdoMet and folate metabolism and epigenetic regulation that are important for plant stress adaptation. Recently, Gonzalez and Vera (2019) demonstrated that folate metabolism is key in the epigenetic regulation for plant immune system by elegant approach combining chemical and reverse genetic strategies.

Nutritional stresses alter metabolism and gene expression. Among them, Fe deficiency greatly affects S metabolism because Fe forms Fe-S clusters involved in electron transfer chains in mitochondria and chloroplasts (Balk and Schaedler, 2014). NA is a chelator of metal cations including Fe ions and synthesized by trimerization of three molecules of AdoMet (**Figure 3**). NA plays an important role in the internal transport of Fe, which is critical for proper reproductive development of plants (Takahashi et al., 2003). Fe deficiency resulted in increase of reduced S-containing metabolites including AdoMet, which might further result in higher accumulation of NA (Forieri et al., 2017). Also, a significant increase of the AdoMet/AdoHcy ratio under Fe deficiency might contribute to the large perturbation of transcription (Forieri et al., 2017).

AdoMet-Derived Polyamines and Ethylene Are Regulatory Metabolites in Stress Responses

AdoMet is also involved in stress responses through AdoMet-derived metabolites, such as polyamines and ethylene.

Polyamines are polycationic compounds with strong binding abilities for negatively charged biomacromolecules, such as acidic proteins, membrane phospholipids, and nucleic acids. Predominant forms of the polyamines in plants are diamine putrescine, triamine spermidine, and tetraamine spermine (**Figure 3**). Biosynthetic pathways for polyamines have been extensively studied in *Arabidopsis* (Hanfrey et al., 2001). The initial step of polyamine biosynthesis is decarboxylation of arginine (Arg) by Arg decarboxylase (ADC), and then two additional successive steps produce putrescine. Spermidine and spermine are synthesized by sequential additions of aminopropyl groups to putrescine and spermidine by SPDS and SPMS, respectively. These aminopropyl moieties are derived from dAdoMet produced by AdoMet decarboxylase (AdoMetDC) (**Figure 3**). Thermospermine, a structural isomer of spermine, is also produced from spermidine and dAdoMet by TSPMS. Interestingly, polyamine levels are increased in response to various abiotic stresses, such as salinity, drought, low and high temperatures, and nutrient deficiencies, suggesting a protective role for polyamines against environmental stresses (Groppa and Benavides, 2007; Alcázar et al., 2010). These responses are mostly due to the induction of gene expressions of polyamine biosynthesis genes under stress conditions (Alcázar et al., 2006, 2010; Cuevas et al., 2008). Especially, spermidine and spermine levels rely on the supply of dAdoMet. Elevated levels of spermine produced by the overexpression of *AdoMetDC* or *SPMS* genes in *Arabidopsis* enhanced the tolerance to drought and salt stresses (Gonzalez et al., 2011), whereas the *tspms*/*spms* double mutant showed opposite phenotypes due to reduced levels of spermine (Yamaguchi et al., 2006, 2007). Furthermore, transcriptome analyses using *AdoMetDC* or *SPMS* overexpressing plants demonstrated the inductions of several genes encoding key components in the stress signaling cascades, as well as a key enzyme of ABA biosynthesis, NCDE3, with spermine overaccumulation (Marco et al., 2011). The involvement of

AdoMet-dependent polyamine biosynthesis in stress responses has been revealed in many plant species other than *Arabidopsis* via genetic engineering. There are many examples showing that transgenic plants, such as rice, tobacco, and tomato, with the *AdoMetDC* gene from different species have acquired greater tolerances to various environmental stresses (Roy and Wu, 2002; Waie and Rajam, 2003; Cheng et al., 2009).

Ethylene is an important phytohormone involved in multiple physiological and morphological responses, such as inhibition of cell growth, induction of fruit ripening and abscission, and adaptation to environmental stresses. Its biosynthesis pathway consists of a simple two-step reaction: AdoMet is converted to 1-aminocyclopropane-1-carboxylic acid (ACC) by ACS, and then ACC is converted to ethylene by ACC oxidase (**Figure 3**). Ethylene biosynthesis is accelerated in response to various biotic and abiotic stresses, such as pathogen infection, osmotic, salt, and drought stresses. Under salt stress, plants must control reactive oxygen species (ROS) level to survive. ROS act as a signal molecule to acquire the salt stress tolerance, whereas excess ROS accumulation damages cellular structure (Qi et al., 2018). Ethylene has a dual role to modulate salt stress response: one is promoting ROS production and signaling to activate Na^+/K^+ transport (Jiang et al., 2013), and the other is inducing the expression of ROS scavengers through ethylene signaling pathway (Peng et al., 2014). Supply of AdoMet is crucial for ethylene biosynthesis. Induction of MAT genes in response to abiotic stresses has been reported in several species, such as barley, sugar beet, cucumber, and tomato (Sánchez-Aguayo et al., 2004; Ma et al., 2017; He et al., 2019). In the case of barley, HvSAMS3 protein accumulation in leaves was enhanced under combined drought and salt stresses. The *hvsams3* knockdown mutants reduced tolerance to the combined stress, which was associated with decreased level of ethylene and polyamines. Moreover, exogenous application of ethylene to the mutants improved the tolerance, suggesting that ethylene level relying on HvSAMS3 is important for acquisition of the tolerance to combined stresses at least in part (Ahmed et al., 2020).

Overall, these studies indicate that AdoMet is an important precursor of polyamine and ethylene and leads to stress tolerance in plants.

Hcy

Hcy metabolism seems to be influenced by environmental stresses, although there are few reports on its steady-state level owing to technical difficulty of measurement. Hcy regulates PGDH activity *in vitro* and thus may control Ser biosynthesis *in vivo*.

Metabolism and a Putative Regulatory Role of Hcy

As mentioned in Section "Ser Metabolism Interconnects Metabolic Network," the enzymatic activity of AtPGDH1, AtPGDH3, and MpPGDH is activated by Hcy *in vitro* with the lowest EC_{50} values among the other activator amino acids (23 μM for AtPGDH1; 69 μM for AtPGDH3; ∼20 μM for MpPGDH) (Okamura and Hirai, 2017; Akashi et al., 2018). In *Arabidopsis*, the steady-state levels of Hcy are < 1 pmol/mg fresh weight in rosette leaves (Groth et al., 2016). In the hypocotyls of yellow lupine (*Lupinus luteus*) seedlings, the concentration of total Hcy (including disulfide-bound forms) was 4.3 μM (Jakubowski and Guranowski, 2003). Under S deficiency, the relative abundance of Hcy in *Arabidopsis* seedling was not significantly changed (Nikiforova et al., 2005b). On the other hand, perturbation of folate metabolism affected Hcy level: a point mutation in MTHFD1 resulted in the increase of Hcy to ∼7 pmol/mg fresh weight in *Arabidopsis* rosette leaves (Groth et al., 2016).

In mammals, Hcy is generated by hydrolysis of AdoHcy. Hcy is then converted to Cys via the transsulfuration pathway catalyzed by CysT β-synthase and CysT γ-lyase, which is the reverse reaction of the *de novo* Hcy biosynthesis (catalyzed by CGS and CBL) in plants. Otherwise, Hcy is remethylated to form Met via MS (using 5-CH_3-THF as the methyl donor) or betaine–HcySMT (using betaine as the methyl donor). Hcy is considered toxic because its reduction power is stronger than that of Cys. Hcy is metabolized to Hcy-thiolactone by methionyl-tRNA synthetase (MetRS) in an error-editing reaction that prevents the translational incorporation of Hcy into proteins (Jakubowski, 2000; Jakubowski and Guranowski, 2003). Hcy-thiolactone synthesis is also found in bacteria and plants (see below). It is chemically reactive as its carbonyl group reacts with epsilon-amino group of Lys residues in proteins to form an amide bond (Hcy-*N*-protein), which leads to protein damage (Jakubowski, 2000; Jakubowski and Guranowski, 2003).

Overall, there is relatively little information available for Hcy in plants, and this is probably because it has been considered an intermediate of Met biosynthesis and a by-product of AdoMet metabolism. In contrast to its metabolism in animals, Hcy is the direct precursor of Met in plants and is synthesized in the chloroplast from Cys through the transsulfuration reactions catalyzed by CGS and CBL (see Asp pathway in **Figure 1**). Hcy is also generated from AdoHcy via SAHH reactions in the cytosolic AdoMet and SMM cycles (**Figure 3**). Because AdoHcy is generated as a by-product of various AdoMet-dependent methylation reactions and inhibits methyltransferase activities, it must be efficiently removed by SAHH. *Arabidopsis* possesses two SAHH isoforms, SAHH1 and SAHH2, and the null mutation of SAHH1 resulted in embryonic lethality (Rocha et al., 2005), indicating the importance of removal of AdoHcy. Biochemical analysis suggested that SAHH forms oligomeric protein complexes in phylogenetically divergent land plants and that light stress regulates protein complex formation and phosphorylation of SAHH, although the responses differed between *Arabidopsis* and *Physcomitrium patens* (Alegre et al., 2020).

SAHH also catalyzes the reverse reaction (i.e., AdoHcy synthesis), and the equilibrium is driven toward AdoHcy hydrolysis by the removal of the hydrolysis products, Hcy and adenosine (Guranowski and Pawełkiewicz, 1977; Pereira et al., 2007). Hcy is recycled in the SAM and SMM cycles (**Figure 3**), whereas adenosine is recycled predominantly by ADK; thus, SAHH and ADK are coordinately regulated developmentally and responding to environmental stresses (Pereira et al., 2007). For example, SAHH activity was increased by elicitation of the phytoalexin response in alfalfa cell culture (Edwards, 1996). The transcript levels of SAHH and ADK increased with increased NaCl concentration in spinach, probably to meet

increased demand of AdoMet for the synthesis of Gly betaine, a compatible osmolyte (Weretilnyk et al., 2001). The SAHH transcripts increased in response to a UV stimulus in parsley (Logemann et al., 2000).

Jakubowski and Guranowski (2003) reported that Hcy-thiolactone is synthesized in plants. In the hypocotyls of yellow lupine (*L. luteus*) seedlings, Hcy-thiolactone was detected at a concentration of < 0.6 μM. Treatment with the antifolate drug aminopterin, which inhibits the methylation of Hcy to Met, enhanced the accumulation of Hcy (245 μM) and the synthesis of Hcy-thiolactone. The level of Hcy-*N*-protein was also increased after the aminopterin treatment. The Met supplement inhibited Hcy-thiolactone synthesis in yellow lupine seedlings, suggesting the involvement of MetRS. The *E. coli* cells expressing rice (*O. sativa*) MetRS were found to catalyze the conversion of Hcy to Hcy-thiolactone. The Hcy-thiolactone-hydrolyzing enzyme was purified from yellow lupine seed meal, suggesting Hcy-thiolactone metabolism in plant.

Ser

Ser metabolism has important functions in development, although it remains to be clarified whether a regulatory molecule is Ser itself or Ser-related metabolites. Ser metabolism is also involved in stress responses such as salt tolerance and photosynthetic performance.

Ser Metabolism Affects S Metabolism

As mentioned in Section "Ser Metabolism Interconnects Metabolic Network," Ser metabolism interconnects S, Trp, and C_1 metabolism. In this section, we focus on the relationship between Ser biosynthesis and S metabolism, because Ser is the direct precursor of OAS production.

The OAS formation by SERAT is an interface between Ser as a nitrogen/carbon source and Cys metabolism as an S source. Therefore, the production of Ser affects that of OAS and then S metabolism. Although a variety of mutants in Ser biosynthesis have been reported and showed a complexity of metabolite changes independently of the Ser levels with growth phenotypes (Collakova et al., 2008; Benstein et al., 2013; Cascales-Miñana et al., 2013; Kuhn et al., 2013; Toujani et al., 2013a), a recent study by Anoman et al. (2019) revealed that deficient lines of the two genes in the phosphorylated pathway (*AtPGDH1* and *AtPSP1*) perturbed S homeostasis by regulating not only its biosynthesis, but also the transport and allocation of the thiols between photosynthetic and non-photosynthetic tissues. Specifically, the OAS level increased in both aerial parts and roots of *AtPSP1*- and *AtPGDH1*-deficient lines compared to controls (up to 2.7- and 4.2-fold the wild-type level, in the aerial parts and roots of *AtPSP1*-deficent line). Interestingly, in the presence of Ser in the growing medium, the OAS levels reverted to normal values (Anoman et al., 2019). On the other hand, in the *Arabidopsis* photorespiratory "*a bout de soufflé*" (*bou-2*) mutant, with reduced activity of the mitochondrial GDC multienzyme due to knockdown of mitochondrial BOU transporter protein, Ser was increased by fourfold (day) and 10-fold (night), whereas Cys was increased by fivefold (day) and threefold (night), compared to wild type (Samuilov et al., 2018).

The three Ser biosynthetic pathways are strictly regulated in terms of timing, tissue specificity, and transport of Ser between compartments, which results in some limitations to compensate for the loss of Ser in either compartment (Voll et al., 2006; Engel et al., 2011; Ros et al., 2014). In the case of *Arabidopsis*, the Ser concentration in the plants seems not to be affected by changes in the downstream products of S metabolism, such as OAS, Cys, GSH, or others (Watanabe et al., 2018). This might be caused by the bigger pool sizes of Ser compared to those of S metabolites or the tight regulation of Ser production by homeostatic mechanisms, including a feedback inhibition of, for example, AtPGDH1 activity by Ser and an activation by S-containing amino acids such as Cys, Hcy, and Met (Okamura and Hirai, 2017; Akashi et al., 2018). The EC_{50} values of AtPGDH1, AtPGDH3, and MpPGDH against Ser are 6.6, 1.3, and 1.5 mM, respectively. These values are likely within the biological range of Ser concentration in plastid, because Ser was present at 1.32 mM in chloroplasts from pea leaves (Mills and Joy, 1980).

The expression of *AtPGDH1* is positively regulated by MYB34 and MYB51, the transcription factors regulating the biosynthetic genes of Trp and Trp-derived indole glucosinolates (Benstein et al., 2013). In addition, Trp-derived metabolites such as indole acetic acid and indole glucosinolates were decreased in *AtPGDH1*-silenced plants, indicating that AtPGDH1 is involved in supplying the Ser used as the precursor of Trp biosynthesis (Benstein et al., 2013). The activation of AtPGDH1 activity by the S-containing amino acids may have a role to balance S and Trp metabolism.

Ser Metabolism Is Involved in Development and Environmental Adaptation

Ser metabolism is involved in adaptive responses to various environmental stresses. Plants subjected to low temperature and elevated salinity accumulate Ser (Ho and Saito, 2001). In certain halophytes, Ser is a precursor of ethanolamine, which is further converted to a compatible solute Gly betaine. A recent study showed that Ser was increased by threefold in aerial part and by eightfold in root of *Arabidopsis* under salt stress (Rosa-Tellez et al., 2020). In this case, the expression of *AtPGDH1* and *AtPGDH2* was induced, whereas that of *AtPGDH3* was repressed (Rosa-Tellez et al., 2020). This result indicated the isoform-specific functions of PGDH, although their roles in Ser accumulation remain to be clarified. Similarly, in *Beta vulgaris*, *BvPGDHa* was induced, whereas *BvPGDHb* was repressed under salt stress (Kito et al., 2017).

In *Arabidopsis*, each isoform of the phosphorylated pathway enzymes seems to have its specific function in development and stress responses. Among AtPGDHs, only the knockout of *AtPGDH1*, which was previously identified as the *embryo sac development arrest 9* (*EDA9*) gene, results in embryonic lethality (Benstein et al., 2013; Toujani et al., 2013a). *AtPGDH1* and *AtPGDH2* are regulated by MYB51, whereas *AtPGDH3* is not (Benstein et al., 2013). Similarly, *AtPSAT1*, but not *AtPSAT2*, is regulated by MYB51 (Benstein et al., 2013). Also, the expressions of *AtPGDH1*, *AtPGDH2*, and *AtPSAT1* are induced by infection of *Botrytis* (Benstein et al., 2013).

Because Ser biosynthesis involves NADH production (**Figure 5**), it is likely to affect $NAD(P)^+$/NAD(P)H homeostasis

and redox status of cell. In chloroplast, the reducing power is generated by photochemical reactions in the thylakoid membrane upon illumination. The redox cascade involving ferredoxin and thioredoxin ensures light-responsive coordination of chloroplast functions (Yoshida et al., 2020). AtPGDH1 is the target of redox regulation of chloroplast proteins, and this regulation is associated with the redox-active Cys pair uniquely found in land plant PGDH (Yoshida et al., 2020). Recently, Höhner et al. (2021) reported that AtPGDH3 plays a crucial role in NADH supply in plastid stroma and eventually in photosynthetic performance under natural fluctuating light environment.

The phosphorylated pathway plays a role in Ser supply in the photosynthetic organs when photorespiration is inhibited at night or under high CO_2 conditions (Ros et al., 2014). Among three AtPGDHs, only *AtPGDH1* expression was induced under high CO_2 conditions (Benstein et al., 2013).

In all above cases, the regulation of PGDH at the transcriptional or enzymatic levels is in an isoform-specific manner. Because the basal land plant *M. polymorpha* has a single PGDH, land plants may have evolved various types of PGDH after gene duplication during evolution to cope with various environmental stresses.

SUMMARY AND FUTURE PERSPECTIVES

In this review, we summarized the metabolism of S-containing amino acids and related compounds and the C_1 metabolism in plants, focusing on regulatory function of AdoMet, OAS, Hcy, and Ser, in comparison with those in bacteria and animals. The following are some aspects that should be addressed in the future, although some of them have been topics of discussion for a long time.

- It remains unclear why some enzymes exist redundantly in several compartments (e.g., SERAT and OAS-TL in the plastids, mitochondria, and cytosol). On the contrary, some enzymes are localized exclusively to specific compartments. For example, SAHH, which hydrolyzes AdoHcy, exists only in the cytosol, although AdoHcy is generated as a by-product by methyltransferase reactions in the cytosol, plastids, and nuclei, and inhibits methyltransferase activities.

- The above issue might be related to our insufficient understanding of enzyme localizations. Alternative splicing or alternative promoter usage may regulate subcellular localization of enzymes. For example, glycerate kinase, which is an essential enzyme for photorespiration and targeted to the chloroplast, is localized to the cytosol under shaded condition by phytochrome-mediated alternative promoter selection. It is a part of cytosolic photorespiratory bypass that alleviates fluctuating light-induced photoinhibition (Ushijima et al., 2017). The regulation of protein subcellular localization, which might be realized by translational regulation, is the issue we should tackle.

- Although several metabolic pathways function across organelles, not many transporters involved in the intercompartmental transport of metabolites have been identified. Considering previous efforts to find transporters, novel strategies for their identification are necessary. Bioinformatics and deep learning approaches may enable us to predict candidate genes. Transport mechanism of metabolites could be clarified by uptake experiments using isolated organelle, as is the case with Lee et al. (2014), where careful inspection of Cys uptake kinetics indicated the existence of multiple specific Cys transporters in the mitochondrial membranes. Such an approach is useful to identify transporters.

- The concentration of metabolites in each compartment is key for the regulation of metabolism. However, their measurements are difficult, because metabolites are rapidly converted to other metabolites by enzymatic and non-enzymatic reactions during the isolation of organelles for metabolite analyses. Metabolomics technology for subcellular-level analysis is required. Non-aqueous fractionation is a powerful technique to study the subcellular compartmentation of metabolites in three main cellular compartments, cytosol, plastids, and vacuoles. Krueger et al. (2009) clarified the distribution of S containing metabolites including sulfate, sulfide, OAS, Cys, γ-glutamyl Cys, and GSH in *Arabidopsis* using this method. Immunogold labeling method is also useful to study the metabolite distribution. Koffler et al. (2011) clarified the distribution of GSH precursors including Cys, γ-glutamyl Cys, glutamate, Gly in cytosol, plastids, mitochondria, nuclei, peroxisomes, and vacuoles in *Arabidopsis*.

- Furthermore, it must be considered that the metabolites may be non-uniformly present in the cell due to the generation of so-called membraneless organelles by phase separation. This is related to the concept of metabolon, in which metabolites are directly transferred from an enzyme to others in the sequential enzymatic reactions. In addition to the research to investigate protein condensates, live imaging of metabolites may help understand this issue.

It has long been known that amino acids regulate the activities of their biosynthetic enzymes in a feedback manner. As shown in this review, amino acids also regulate metabolism at translational and transcriptional levels, reflecting the status of internal and external environments. A recent study demonstrated that perturbation in Arg level results in stunted gametophore morphology in *P. patens* (Kawade et al., 2020). Arg itself or a related metabolite might be the metabolite, which directly regulates development.

In conclusion, with rapid advances in experimental technology, new regulatory mechanisms of metabolism and development will be discovered in which metabolites involved in amino acid metabolism act as signal molecules.

AUTHOR CONTRIBUTIONS

MW, YC, and MYH wrote the manuscript. All authors contributed to the article and approved the submitted version.

FUNDING

This study was supported by JSPS KAKENHI grant Nos. 19K06723 to MW and 20H04852 to MYH.

REFERENCES

Aarabi, F., Kusajima, M., Tohge, T., Konishi, T., Gigolashvili, T., Takamune, M., et al. (2016). Sulfur deficiency-induced repressor proteins optimize glucosinolate biosynthesis in plants. *Sci. Adv.* 2:e1601087. doi: 10.1126/sciadv.1601087

Aarabi, F., Naake, T., Fernie, A. R., and Hoefgen, R. (2020). Coordinating sulfur pools under sulfate deprivation. *Trends Plant Sci.* 25, 1227–1239. doi: 10.1016/j.tplants.2020.07.007

Achouri, Y., Rider, M. H., Schaftingen, E. V., and Robbi, M. (1997). Cloning, sequencing and expression of rat liver 3-phosphoglycerate dehydrogenase. *Biochem. J.* 323(Pt 2), 365–370. doi: 10.1042/bj3230365

Ahmed, I. M., Nadira, U. A., Qiu, C. W., Cao, F., Chen, Z. H., Vincze, E., et al. (2020). The barley *S*-adenosylmethionine synthetase 3 gene HvSAMS3 positively regulates the tolerance to combined drought and salinity stress in Tibetan wild barley. *Cells* 9:1530. doi: 10.3390/cells9061530

Akashi, H., Okamura, E., Nishihama, R., Kohchi, T., and Hirai, M. Y. (2018). Identification and biochemical characterization of the serine biosynthetic enzyme 3-phosphoglycerate dehydrogenase in *Marchantia polymorpha*. *Front. Plant Sci.* 9:956. doi: 10.3389/fpls.2018.00956

Alcázar, R., Altabella, T., Marco, F., Bortolotti, C., Reymond, M., Koncz, C., et al. (2010). Polyamines: molecules with regulatory functions in plant abiotic stress tolerance. *Planta* 231, 1237–1249. doi: 10.1007/s00425-010-1130-0

Alcázar, R., Marco, F., Cuevas, J. C., Patron, M., Ferrando, A., Carrasco, P., et al. (2006). Involvement of polyamines in plant response to abiotic stress. *Biotech. Lett* 23, 1867–1876. doi: 10.1007/s10529-006-9179-3

Alegre, S., Pascual, J., Trotta, A., Angeleri, M., Rahikainen, M., Brosche, M., et al. (2020). Evolutionary conservation and post-translational control of S-adenosyl-L-homocysteine hydrolase in land plants. *PLoS One* 15:e0227466. doi: 10.1371/journal.pone.0227466

Anoman, A. D., Flores-Tornero, M., Benstein, R. M., Blau, S., Rosa-Téllez, S., Bräutigam, A., et al. (2019). Deficiency in the phosphorylated pathway of serine biosynthesis perturbs sulfur assimilation. *Plant Physiol.* 180, 153–170. doi: 10.1104/pp.18.01549

Aroca, A., Gotor, C., and Romero, L. C. (2018). Hydrogen sulfide signaling in plants: emerging roles of protein persulfidation. *Front. Plant Sci.* 9:1369.

Ashida, H., Saito, Y., Kojima, C., Kobayashi, K., Ogasawara, N., and Yokota, A. (2003). A functional link between RuBisCO-like protein of *Bacillus* and photosynthetic RuBisCO. *Science* 10, 286–290. doi: 10.1126/science.1086997

Azevedo, R. A., Arruda, P., Turner, W. L., and Lea, P. J. (1997). The biosynthesis and metabolism of the aspartate derived amino acids in higher plants. *Phytochemistry* 46, 395–419. doi: 10.1016/s0031-9422(97)00319-1

Balk, J., and Schaedler, T. A. (2014). Iron cofactor assembly in plants. *Annu. Rev. Plant Biol.* 65, 125–153. doi: 10.1146/annurev-arplant-050213-035759

Batey, R. T. (2011). Recognition of S-adenosylmethionine by riboswitches. *Wiley Interdiscip. Rev. RNA* 2, 299–311. doi: 10.1002/wrna.63

Batool, S., Uslu, V. V., Rajab, H., Ahmad, N., Waadt, R., Geiger, D., et al. (2018). Sulfate is incorporated into cysteine to trigger ABA production and stomatal closure. *Plant Cell.* 30, 2973–2987. doi: 10.1105/tpc.18.00612

Bauwe, H., and Kolukisaoglu, U. (2003). Genetic manipulation of glycine decarboxylation. *J. Exper. Bot.* 54, 1523–1535. doi: 10.1093/jxb/erg171

Beck, M., and Hurt, E. (2017). The nuclear pore complex: understanding its function through structural insight. *Nat. Rev. Mol. Cell Biol.* 18, 73–89. doi: 10.1038/nrm.2016.147

Benstein, R. B., Ludewig, K., Wulfert, S., Wittek, S., Gigolashvili, T., Frerigmann, H., et al. (2013). *Arabidopsis* phosphoglycerate dehydrogenase1 of the phosphoserine pathway is essential for development and required for ammonium assimilation and tryptophan biosynthesis. *Plant Cell.* 25, 5011–5029. doi: 10.1105/tpc.113.118992

Bick, J. A., Dennis, J. J., Zylstra, G. J., Nowack, J., and Leustek, T. (2000). Identification of a new class of 5′-adenylylsulfate (APS) reductases from sulfate-assimilating bacteria. *J. Bacteriol.* 182, 135–142. doi: 10.1128/jb.182.1.135-142.2000

Birke, H., Heeg, C., Wirtz, M., and Hell, R. (2013). Successful fertilization requires the presence of at least one major O-acetylserine(thiol)lyase for cysteine synthesis in pollen of *Arabidopsis*. *Plant Physiol.* 163, 959–972. doi: 10.1104/pp.113.221200

Bourgis, F., Roje, S., Nuccio, M. L., Fisher, D. B., Tarczynski, M. C., Li, C., et al. (1999). S-methylmethionine plays a major role in phloem sulfur transport and is synthesized by a novel type of methyltransferase. *Plant Cell* 11, 1485–1498. doi: 10.2307/3870977

Bouvier, F., Linka, N., Isner, J.-C., Mutterer, J., Weber, A. P., and Camara, B. (2006). *Arabidopsis* SAMT1 defines a plastid transporter regulating plastid biogenesis and plant development. *Plant Cell* 18, 3088–3105. doi: 10.1105/tpc.105.040741

Brosnan, J. T., and Brosnan, M. E. (2006). The sulfur-containing amino acids: an overview. *J. Nutri.* 136, 1636S–1640S.

Brunold, C., and Schmidt, A. (1976). Regulation of adenosine-5′-phosphosulfate sulfotransferase activity by H2S in Lemna minor L. *Planta.* 133, 85–88. doi: 10.1007/bf00386010

Brunold, C., and Suter, M. (1982). Intracellular localization of serine acetyltransferase in spinach leaves. *Planta* 155, 321–327. doi: 10.1007/bf00429459

Caldana, C., Degenkolbe, T., Cuadros-Inostroza, A., Klie, S., Sulpice, R., Leisse, A., et al. (2011). High-density kinetic analysis of the metabolomic and transcriptomic response of *Arabidopsis* to eight environmental conditions. *Plant J.* 67, 869–884. doi: 10.1111/j.1365-313x.2011.04640.x

Cascales-Miñana, B., Munoz-Bertomeu, J., Flores-Tornero, M., Anoman, A. D., Pertusa, J., Alaiz, M., et al. (2013). The phosphorylated pathway of serine biosynthesis is essential both for male gametophyte and embryo development and for root growth in *Arabidopsis*. *Plant Cell* 25, 2084–2101. doi: 10.1105/tpc.113.112359

Chang, Y. N., Zhu, C., Jiang, J., Zhang, H., Zhu, J. K., and Duan, C. G. (2020). Epigenetic regulation in plant abiotic stress responses. *J. Integr. Plant Biol.* 62, 563–580. doi: 10.1111/jipb.12901

Chen, Y., Zou, T., and McCormick, S. (2016). S-adenosylmethionine synthetase 3 is important for pollen tube growth. *Plant Phys.* 172, 244–253. doi: 10.1104/pp.16.00774

Cheng, L., Zou, Y., Ding, S., Zhang, J., Yu, X., Cao, J., et al. (2009). Polyamine accumulation in transgenic tomato enhances the tolerance to high temperature stress. *J. Integr. Plant Biol.* 51, 489–499. doi: 10.1111/j.1744-7909.2009.00816.x

Cherest, H., and Surdin-Kerjan, Y. (1992). Genetic analysis of a new mutation conferring cysteine auxotrophy in *Saccharomyces cerevisiae*: updating of the sulfur metabolism pathway. *Genetics* 130, 51–58. doi: 10.1093/genetics/130.1.51

Chiba, Y., Ishikawa, M., Kijima, F., Tyson, R. H., Kim, J., Yamamoto, A., et al. (1999). Evidence for autoregulation of cystathionine γ-synthase mRNA stability in *Arabidopsis*. *Science* 286, 1371–1374. doi: 10.1126/science.286.5443.1371

Chiba, Y., Sakurai, R., Yoshino, M., Ominato, K., Ishikawa, M., Onouchi, H., et al. (2003). S-adenosyl-L-methionine is an effector in the posttranscriptional autoregulation of the cystathionine γ-synthase gene in *Arabidopsis*. *Proc. Natl. Acad. Sci. U.S.A.* 100, 10225–10230. doi: 10.1073/pnas.1831512100

Christensen, K. E., and MacKenzie, R. E. (2006). Mitochondrial one-carbon metabolism is adapted to the specific needs of yeast, plants and mammals. *Bioessays* 28, 595–605. doi: 10.1002/bies.20420

Collakova, E., Goyer, A., Naponelli, V., Krassovskaya, I., Gregory, J. F., Hanson, A. D., et al. (2008). *Arabidopsis* 10-formyl tetrahydrofolate deformylases are essential for photorespiration. *Plant Cell* 20, 1818–1832. doi: 10.1105/tpc.108.058701

Cuevas, J. C., López-Cobollo, R., Alcázar, R., Zarza, X., Koncz, C., Altabella, T., et al. (2008). Putrescine is involved in *Arabidopsis* freezing tolerance and cold acclimation by regulating abscisic acid levels in response to low temperature. *Plant Physiol.* 148, 1094–1105. doi: 10.1104/pp.108.122945

Dassler, T., Maier, T., Winterhalter, C., and Bock, A. (2000). Identification of a major facilitator protein from *Escherichia coli* involved in efflux of metabolites of the cysteine pathway. *Mol. Microbiol.* 36, 1101–1112. doi: 10.1046/j.1365-2958.2000.01924.x

Dey, S., Burton, R. L., Grant, G. A., and Sacchettini, J. C. (2008). Structural analysis of substrate and effector binding in *Mycobacterium tuberculosis* D-3-phosphoglycerate dehydrogenase. *Biochemistry* 47, 8271–8282. doi: 10.1021/bi800212b

Dey, S., Hu, Z., Xu, X. L., Sacchettini, J. C., and Grant, G. A. (2005). D-3-Phosphoglycerate dehydrogenase from Mycobacterium tuberculosis is a link between the *Escherichia coli* and mammalian enzymes. *J. Biol. Chem.* 280, 14884–14891. doi: 10.1074/jbc.m414488200

Dong, Y., Silbermann, M., Speiser, A., Forieri, I., Linster, E., Poschet, G., et al. (2017). Sulfur availability regulates plant growth via glucose-TOR signaling. *Nat. Commun.* 8:1174.

Dowen, R. H., Pelizzola, M., Schmitz, R. J., Lister, R., Dowen, J. M., Nery, J. R., et al. (2012). Widespread dynamic DNA methylation in response to biotic stress. *Proc. Natl. Acad. Sci. U.S.A.* 109, E2183–E2191.

Droux, M. (2003). Plant serine acetyltransferase: new insights for regulation of sulphur metabolism in plant cells. *Plant Physiol. Biochem.* 41, 619–627. doi: 10.1016/s0981-9428(03)00083-4

Droux, M., Ruffet, M. L., Douce, R., and Job, D. (1998). Interactions between serine acetyltransferase and O-acetylserine (thiol) lyase in higher plants – Structural and kinetic properties of the free and bound enzymes. *Eur. J. Biochem.* 255, 235–245. doi: 10.1046/j.1432-1327.1998.2550235.x

Edwards, R. (1996). S-adenosyl-l-methionine metabolism in alfalfa cell cultures following treatment with fungal elicitors. *Phytochemistry* 43, 1163–1169. doi: 10.1016/S0031-9422(96)00434-7

Engel, N., Ewald, R., Gupta, K. J., Zrenner, R., Hagemann, M., and Bauwe, H. (2011). The presequence of *Arabidopsis* serine hydroxymethyltransferase SHM2 selectively prevents import into mesophyll mitochondria. *Plant Physiol.* 157, 1711–1720. doi: 10.1104/pp.111.184564

Engel, N., Van Den Daele, K., Kolukisaoglu, U., Morgenthal, K., Weckwerth, W., Parnik, T., et al. (2007). Deletion of glycine decarboxylase in *Arabidopsis* is lethal under nonphotorespiratory conditions. *Plant Physiol.* 144, 1328–1335. doi: 10.1104/pp.107.099317

Espinoza, C., Degenkolbe, T., Caldana, C., Zuther, E., Leisse, A., Willmitzer, L., et al. (2010). Interaction with diurnal and circadian regulation results in dynamic metabolic and transcriptional changes during cold acclimation in *Arabidopsis*. *Plos One* 5:e14101. doi: 10.1371/journal.pone.0014101

Flavin, M., and Slaughter, C. (1967). Enzymatic synthesis of homocysteine or methionine directly from O-succinyl-homoserine. *Biochim. Biophys. Acta* 132, 400–405. doi: 10.1016/0005-2744(67)90158-1

Forieri, I., Sticht, C., Reichelt, M., Gretz, N., Hawkesford, M. J., Malagoli, M., et al. (2017). System analysis of metabolism and the transcriptome in *Arabidopsis thaliana* roots reveals differential co-regulation upon iron, sulfur and potassium deficiency. *Plant, Cell & Environment* 40, 95–107. doi: 10.1111/pce.12842

Franke, I., Resch, A., Dassler, T., Maier, T., and Bock, A. (2003). YfiK from *Escherichia coli* promotes export of O-acetylserine and cysteine. *J. Bacteriol.* 185, 1161–1166. doi: 10.1128/jb.185.4.1161-1166.2003

Galili, G., Amir, R., and Fernie, A. R. (2016). The regulation of essential amino acid synthesis and accumulation in plants. *Ann. Rev. Plant Biol* 67, 153–178. doi: 10.1146/annurev-arplant-043015-112213

Garcia-Molina, A., Altmann, M., Alkofer, A., Epple, P. M., Dangl, J. L., and Falter-Braun, P. (2017). LSU network hubs integrate abiotic and biotic stress responses via interaction with the superoxide dismutase FSD2. *J. Exper. Bot.* 68, 1185–1197. doi: 10.1093/jxb/erw498

Gigolashvili, T., Yatusevich, R., Berger, B., Mulle, R. C., and Flugge, U. (2007). The R2R3-MYB transcription factor HAG1/MYB28 is a regulator of methionine-derived glucosinolate biosynthesis in *Arabidopsis thaliana*. *Plant J.* 51, 247–261. doi: 10.1111/j.1365-313x.2007.03133.x

Gonzalez, B., and Vera, P. (2019). Folate metabolism interferes with plant immunity through 1C methionine synthase-directed genome-wide DNA methylation enhancement. *Mol. Plant.* 12, 1227–1242. doi: 10.1016/j.molp.2019.04.013

Gonzalez, M. E., Marco, F., Minguet, E. G., Carrasco-Sorli, P., Blazquez, M. A., Carbonell, J., et al. (2011). Perturbation of spermine synthase gene expression and transcript profiling provide new insights on the role of the tetraamine spermine in *Arabidopsis* defense against *Pseudomonas viridiflava*. *Plant Physiol.* 156, 2266–2277. doi: 10.1104/pp.110.171413

Goto, D. B., Ogi, M., Kijima, F., Kumagai, T., van Werven, F., Onouchi, H., et al. (2002). A single-nucleotide mutation in a gene encoding *S*-adenosylmethionine synthetase is associated with methionine over-accumulation phenotype in *Arabidopsis thaliana*. *Genes Genet. Syst.* 77, 89–95. doi: 10.1266/ggs.77.89

Groppa, M. D., and Benavides, M. P. J. A. A. (2007). Polyamines and abiotic stress: recent advances. *Amino Acids* 34:35. doi: 10.1007/s00726-007-0501-8

Groth, M., Moissiard, G., Wirtz, M., Wang, H., Garcia-Salinas, C., Ramos-Parra, P. A., et al. (2016). MTHFD1 controls DNA methylation in *Arabidopsis*. *Nat. Commun.* 7:11640.

Grundy, F. J., and Henkin, T. M. (1998). The S box regulon: a new global transcription termination control system for methionine and cysteine biosynthesis genes in gram-positive bacteria. *Mol. Microbiol.* 30, 737–749. doi: 10.1046/j.1365-2958.1998.01105.x

Guranowski, A., and Pawełkiewicz, J. (1977). Adenosylhomocysteinase from yellow lupin seeds. Purification and properties. *Eur. J. Biochem.* 80, 517–523. doi: 10.1111/j.1432-1033.1977.tb11907.x

Haas, F. H., Heeg, C., Queiroz, R., Bauer, A., Wirtz, M., and Hell, R. (2008). Mitochondrial serine acetyltransferase functions as a pacemaker of cysteine synthesis in plant cells. *Plant Physiol.* 148, 1055–1067. doi: 10.1104/pp.108.125237

Hanfrey, C., Sommer, S., Mayer, M. J., Burtin, D., and Michael, A. J. (2001). *Arabidopsis* polyamine biosynthesis: absence of ornithine decarboxylase and the mechanism of arginine decarboxylase activity. *Plant J.* 27, 551–560. doi: 10.1046/j.1365-313x.2001.01100.x

Hanson, A. D., and Roje, S. (2001). One-carbon metabolism in higher plants. *Ann. Rev. Plant Physiol. Plant Mol. Biol.* 52, 119–137.

Hanson, A. D., Gage, D. A., and Shachar-Hill, Y. (2000). Plant one-carbon metabolism and its engineering. *Trends Plant Sci.* 5, 206–213. doi: 10.1016/s1360-1385(00)01599-5

Hawkesford, M. J., Schneider, A., Belcher, A. R., and Clarkson, D. T. (1995). Regulation of enzymes involved in the sulphur-assimilatory pathway. *Zeitschr. Pflanzenernah. Bodenk.* 158, 55–57. doi: 10.1002/jpln.19951580110

He, M. W., Wang, Y., Wu, J. Q., Shu, S., Sun, J., and Guo, S. R. (2019). Isolation and characterization of *S*-adenosylmethionine synthase gene from cucumber and responsive to abiotic stress. *Plant Physiol. Biochem.* 141, 431–445. doi: 10.1016/j.plaphy.2019.06.006

Heeg, C., Kruse, C., Jost, R., Gutensohn, M., Ruppert, T., Wirtz, M., et al. (2008). Analysis of the *Arabidopsis* O-acetylserine(thiol)lyase gene family demonstrates compartment-specific differences in the regulation of cysteine synthesis. *Plant Cell* 20, 168–185. doi: 10.1105/tpc.107.056747

Hesse, H., Trachsel, N., Suter, M., Kopriva, S., Von Ballmoos, P., Rennenberg, H., et al. (2003). Effect of glucose on assimilatory sulphate reduction in *Arabidopsis thaliana* roots. *J. Exper. Bot.* 54, 1701–1709. doi: 10.1093/jxb/erg177

Hewezi, T., Lane, T., Piya, S., Rambani, A., Rice, J. H., and Staton, M. (2017). Cyst nematode parasitism induces dynamic changes in the root epigenome. *Plant Physiol.* 174, 405–420. doi: 10.1104/pp.16.01948

Hindson, V. J. (2003). Serine acetyltransferase of *Escherichia coli*: substrate specificity and feedback control by cysteine. *Biochem. J.* 375, 745–752. doi: 10.1042/bj20030429

Hirabayashi, Y., and Furuya, S. (2008). Roles of L-serine and sphingolipid synthesis in brain development and neuronal survival. *Prog. Lipid Res.* 47, 188–203. doi: 10.1016/j.plipres.2008.01.003

Hirai, M. Y., Fujiwara, T., Awazuhara, M., Kimura, T., Noji, M., and Saito, K. (2003). Global expression profiling of sulfur-starved *Arabidopsis* by DNA macroarray reveals the role of O-acetyl-L-serine as a general regulator of gene expression in response to sulfur nutrition. *Plant J.* 33, 651–663. doi: 10.1046/j.1365-313x.2003.01658.x

Hirai, M. Y., Sugiyama, K., Sawada, Y., Tohge, T., Obayashi, T., Suzuki, A., et al. (2007). Omics-based identification of *Arabidopsis* Myb transcription factors regulating aliphatic glucosinolate biosynthesis. *Proc. Natl Acad. Sci. U.S.A.* 104, 6478–6483. doi: 10.1073/pnas.0611629104

Ho, C. L., and Saito, K. (2001). Molecular biology of the plastidic phosphorylated serine biosynthetic pathway in *Arabidopsis thaliana*. *Amino Acids.* 20, 243–259. doi: 10.1007/s007260170042

Ho, C. L., Noji, M., and Saito, K. (1999). Plastidic pathway of serine biosynthesis. Molecular cloning and expression of 3-phosphoserine phosphatase from *Arabidopsis thaliana*. *J. Biol. Chem.* 274, 11007–11012. doi: 10.1074/jbc.274.16.11007

Ho, C. L., Noji, M., Saito, M., Yamazaki, M., and Saito, K. (1998). Molecular characterization of plastidic phosphoserine aminotransferase in serine biosynthesis from *Arabidopsis*. *Plant J.* 16, 443–452. doi: 10.1046/j.1365-313x.1998.00313.x

Hoffman, D. R., Cornatzer, W. E., and Duerre, J. A. (1979). Relationship between tissue levels of S-adenosylmethionine, S-adenylhomocysteine, and transmethylation reactions. *Can. J. Biochem.* 57, 56–65. doi: 10.1139/o79-007

Höhner, R., Day, P. M., Zimmermann, S. E., Lopez, L. S., Krämer, M., Giavalisco, P., et al. (2021). Stromal NADH supplied by PHOSPHOGLYCERATE DEHYDROGENASE3 is crucial for photosynthetic performance. *Plant Physiol.* 13:kiaa117.

Hopkins, L., Parmar, S., Baszczyk, A., Hesse, H., Hoefgen, R., and Hawkesford, M. J. (2005). O-acetylserine and the regulation of expression of genes encoding components for sulfate uptake and assimilation in potato. *Plant Physiol.* 138, 433–440. doi: 10.1104/pp.104.057521

Howarth, J. R., Barraclough, P. B., and Hawkesford, M. J. (2005). *A Highly Specific Sulfate-Deficiency Induced Gene (sdi1) From Wheat. Sulfur Transport and Assimilation in Plants in the Postgenomic Era*. Leiden: Backhuys Publishers, 161–164.

Hryniewicz, M. M., and Kredich, N. M. (1994). Stoichiometry of binding of CysB to the cysJIH, cysK, and cysP promoter regions of *Salmonella typhimurium*. *J. Bacteriol.* 176, 3673–3682. doi: 10.1128/jb.176.12.3673-3682.1994

Huang, X. Y., Chao, D. Y., Koprivova, A., Danku, J., Wirtz, M., Muller, S., et al. (2016). Nuclear localised MORE SULPHUR ACCUMULATION1 epigenetically regulates sulphur homeostasis in *Arabidopsis thaliana*. *PLoS Genet.* 12:e1006298. doi: 10.1371/journal.pgen.1006298

Hubberten, H. M., Drozd, A., Tran, B. V., Hesse, H., and Hoefgen, R. (2012a). Local and systemic regulation of sulfur homeostasis in roots of *Arabidopsis thaliana*. *Plant J.* 72, 625–635. doi: 10.1111/j.1365-313x.2012.05105.x

Hubberten, H. M., Klie, S., Caldana, C., Degenkolbe, T., Willmitzer, L., and Hoefgen, R. (2012b). Additional role of O-acetylserine as a sulfur status-independent regulator during plant growth. *Plant J.* 70, 666–677. doi: 10.1111/j.1365-313x.2012.04905.x

Hulanicka, M. D., Hallquist, S. G., Kredich, N. M., and Mojica, T. (1979). Regulation of O-acetylserine sulfhydrylase B by L-cysteine in *Salmonella typhimurium*. *J. Bacteriol.* 140, 141–146. doi: 10.1128/jb.140.1.141-146.1979

Igamberdiev, A. U., and Kleczkowski, L. A. (2018). The glycerate and phosphorylated pathways of serine synthesis in plants: the branches of plant glycolysis linking carbon and nitrogen metabolism. *Front. Plant Sci.* 14:318. doi: 10.3389/fpls.2018.00318

Ivey, D. M., Guffanti, A. A., Zemsky, J., Pinner, E., Karpel, R., Padan, E., et al. (1993). Cloning and characterization of a putative Ca2+/H+ antiporter gene from *Escherichia coli* upon functional complementation of Na+/H+ antiporter-deficient strains by the overexpressed gene. *J. Biolog. Chem.* 268, 11296–11303. doi: 10.1016/s0021-9258(18)82124-x

Jakubowski, H. (2000). Homocysteine thiolactone: metabolic origin and protein homocysteinylation in humans. *J. Nutr.* 130, 377S–381S. doi: 10.1093/jn/130.2.377S

Jakubowski, H., and Guranowski, A. (2003). Metabolism of homocysteine-thiolactone in plants. *J. Biol. Chem.* 278, 6765–6770. doi: 10.1074/jbc.m211819200

Jander, G., and Joshi, V. (2009). Aspartate-derived amino acid biosynthesis in *Arabidopsis thaliana*. *Arabidop. Book* 7:e0121. doi: 10.1199/tab.0121

Jiang, C., Belfield, E. J., Cao, Y., Smith, J. A., and Harberd, N. P. (2013). An *Arabidopsis* soil-salinity-tolerance mutation confers ethylene-mediated enhancement of sodium/potassium homeostasis. *Plant Cell* 25, 3535–3552. doi: 10.1105/tpc.113.115659

Joshi, N. C., Meyer, A. J., Bangash, S. A. K., Zheng, Z. L., and Leustek, T. (2019). *Arabidopsis* γ-glutamylcyclotransferase affects glutathione content and root system architecture during sulfur starvation. *New Phytol.* 221, 1387–1397. doi: 10.1111/nph.15466

Kawade, K., Horiguchi, G., Oikawa, A., Hirai, M. Y., Saito, K., Fujita, T., et al. (2020). Metabolic control of gametophore shoot formation through arginine in the moss *Physcomitrium patens*. *Cell Rep.* 25:5300.

Kawashima, C. G., Berkowitz, O., Hell, R., Noji, M., and Saito, K. (2005). Characterization and expression analysis of a serine acetyltransferase gene family involved in a key step of the sulfur assimilation pathway in *Arabidopsis*. *Plant Physiol.* 137, 220–230. doi: 10.1104/pp.104.045377

Kinoshita, T., and Seki, M. (2014). Epigenetic memory for stress response and adaptation in plants. *Plant Cell Physiol.* 55, 1859–1863. doi: 10.1093/pcp/pcu125

Kito, K., Tsutsumi, K., Rai, V., Theerawitaya, C., Cha-Um, S., Yamada-Kato, N., et al. (2017). Isolation and functional characterization of 3-phosphoglycerate dehydrogenase involved in salt responses in sugar beet. *Protoplasma* 254, 2305–2313. doi: 10.1007/s00709-017-1127-7

Kocsis, M. G., Ranocha, P., Gage, D. A., Simon, E. S., Rhodes, D., Peel, G. J., et al. (2003). Insertional inactivation of the methionine S-methyltransferase gene eliminates the S-methylmethionine cycle and increases the methylation ratio. *Plant Physiol.* 131, 1808–1815. doi: 10.1104/pp.102.018846

Koffler, B. E., Maier, R., and Zechmann, B. (2011). Subcellular distribution of glutathione precursors in *Arabidopsis thaliana*. Compartment-specific importance of glutathione during abiotic and biotic stress. J. Integr. *Plant Biol.* 53, 930–941. doi: 10.1111/j.1744-7909.2011.01085.x

Kopriva, S. (2006). Regulation of sulfate assimilation in *Arabidopsis* and beyond. *Ann. Bot.* 97, 479–495. doi: 10.1093/aob/mcl006

Kopriva, S., Suter, M., Von Ballmoos, P., Hesse, H., Krahenbuhl, U., Rennenberg, H., et al. (2002). Interaction of sulfate assimilation with carbon and nitrogen metabolism in *Lemna minor*. *Plant Physiol.* 130, 1406–1413. doi: 10.1104/pp.007773

Koprivova, A., Suter, M., Op Den, Camp, R., Brunold, C., and Kopriva, S. (2000). Regulation of sulfate assimilation by nitrogen in *Arabidopsis*. *Plant Physiol.* 122, 737–746. doi: 10.1104/pp.122.3.737

Koronakis, V., Eswaran, J., and Hughes, C. (2004). Structure andfunction of tolC: the bacterial exit duct for proteins and drugs. *Ann. Rev. Biochem.* 73, 467–489. doi: 10.1146/annurev.biochem.73.011303.074104

Kredich, N. M. (1996). "Biosynthesis of cysteine," in *Escherichia coli and Salmonella Typhimurium. Cellular and Molecular Biology*, Vol. 1, eds F. C. Neidhardt, R. Curtiss, J. L. Ingraham, E. C. C. Lin, K. B. Low, B. Magasanik, et al. (Washington, DC: American Society for Microbiology), 514–527.

Kredich, N. M., Becker, M. A., and Tomkins, G. M. (1969). Purification and characterization of cysteine synthetase, a bifunctional protein complex, from *Salmonella typhimurium*. *J. Biol. Chem.* 244, 2428–2439. doi: 10.1016/s0021-9258(19)78241-6

Krueger, S., Niehl, A., Lopez Martin, M. C., Steinhauser, D., Donath, A., Hildebrandt, T., et al. (2009). Analysis of cytosolic and plastidic serine acetyltransferase mutants and subcellular metabolite distributions suggests interplay of the cellular compartments for cysteine biosynthesis in *Arabidopsis*. *Plant Cell Environ.* 32, 349–367. doi: 10.1111/j.1365-3040.2009.01928.x

Kuhn, A., Engqvist, M. K., Jansen, E. E., Weber, A. P., Jakobs, C., and Maurino, V. G. (2013). D-2-hydroxyglutarate metabolism is linked to photorespiration in the shm1-1 mutant. *Plant Biol.* 15, 776–784. doi: 10.1111/plb.12020

Kumar, A., Tikoo, S., Maity, S., Sengupta, S., Sengupta, S., Kaur, A., et al. (2012). Mammalian proapoptotic factor ChaC1 and its homologues function as γ-glutamyl cyclotransferases acting specifically on glutathione. *Embo Rep.* 13, 1095–1101. doi: 10.1038/embor.2012.156

Kumar, S., Kaur, A., Chattopadhyay, B., and Bachhawat, A. K. (2015). Defining the cytosolic pathway of glutathione degradation in *Arabidopsis thaliana*: role of the ChaC/GCG family of γ-glutamyl cyclotransferases as glutathione-degrading enzymes and AtLAP1 as the Cys-Gly peptidase. *Biochem. J.* 468, 73–85. doi: 10.1042/bj20141154

Lappartient, A. G., Vidmar, J. J., Leustek, T., Glass, A. D. M., and Touraine, B. (1999). Inter-organ signaling in plants: regulation of ATP sulfurylase and sulfate transporter genes expression in roots mediated by phloem-translocated compound. *Plant J.* 18, 89–95. doi: 10.1046/j.1365-313x.1999.00416.x

Lee, C. P., Wirtz, M., and Hell, R. (2014). Evidence for several cysteine transport mechanisms in the mitochondrial membranes of *Arabidopsis thaliana*. *Plant Cell Physiol.* 55, 64–73. doi: 10.1093/pcp/pct155

Le Douce, J., Maugard, M., Veran, J., Matos, M., Jego, P., Vigneron, P. A., et al. (2020). Impairment of glycolysis-derived L-serine production in astrocytes contributes to cognitive deficits in Alzheimer's disease. *Cell Metab.* 31, 503–517. doi: 10.1016/j.cmet.2020.02.004

Leustek, T., Martin, M. N., Bick, J. A., and Davies, J. P. (2000). Pathways and regulation of sulfur metabolism revealed through molecular and genetic studies. *Ann. Rev. Plant Physiol. Plant Mol. Biol.* 51, 141–165.

Lewandowska, M., Wawrzynska, A., Kaminska, J., Liszewska, F., and Sirko, A. (2005). Identification of novel genes of *Nicotiana tabacum* regulated by short-term sulfur starvation. Sulfur transport and assimilation in plants in the post genomic era. *Paper of the 6th International Workshop on Plant Sulfur Metabolism, Chiba, Japan*, Chiba, 153.

Logemann, E., Tavernaro, A., Schulz, W., Somssich, I. E., and Hahlbrock, K. (2000). UV light selectively coinduces supply pathways from primary metabolism and flavonoid secondary product formation in parsley. *Proc. Natl. Acad. Sci. USA* 97, 1903–1907. doi: 10.1073/pnas.97.4.1903

Lopez-Martin, M. C., Becana, M., Romero, L. C., and Gotor, C. (2008). Knocking out cytosolic cysteine synthesis compromises the antioxidant capacity of the cytosol to maintain discrete concentrations of hydrogen peroxide in *Arabidopsis*. *Plant Physiol.* 147, 562–572. doi: 10.1104/pp.108.117408

Lynch, A. S., Tyrrell, R., Smerdon, S. J., Briggs, G. S., and Wilkinson, A. J. (1994). Characterization of the CysB protein of *Klebsiella aerogenes*: direct evidence that N-acetylserine rather than O-acetylserine serves as the inducer of the cysteine regulon. *Biochem. J.* 299, 129–136. doi: 10.1042/bj2990129

Ma, C., Wang, Y., Gu, D., Nan, J., Chen, S., and Li, H. (2017). Overexpression of *S*-adenosyl-L-methionine synthetase 2 from sugar beet M14 increased *Arabidopsis* tolerance to salt and oxidative stress. *Int. J. Mol. Sci.* 18:847. doi: 10.3390/ijms18040847

Malitsky, S., Blum, E., Less, H., Venger, I., Elbaz, M., Morin, S., et al. (2008). The transcript and metabolite networks affected by the two clades of *Arabidopsis glucosinolate* biosynthesis regulators. *Plant Physiol.* 148, 2021–2049. doi: 10.1104/pp.108.124784

Mao, D., Yu, F., Li, J., Van de Poel, B., Tan, D., Li, J., et al. (2015). FERONIA receptor kinase interacts with S-adenosylmethionine synthetase and suppresses S-adenosylmethionine production and ethylene biosynthesis in *Arabidopsis*. *Plant Cell Environ.* 38, 2566–2574. doi: 10.1111/pce.12570

Marco, F., Alcazar, R., Tiburcio, A. F., and Carrasco, P. (2011). Interactions between polyamines and abiotic stress pathway responses unraveled by transcriptome analysis of polyamine overproducers. *OMICS* 15, 775–781. doi: 10.1089/omi.2011.0084

Maruyama-Nakashita, A., Inoue, E., Watanabe-Takahashi, A., Yarnaya, T., and Takahashi, H. (2003). Transcriptome profiling of sulfur-responsive genes in *Arabidopsis* reveals global effects of sulfur nutrition on multiple metabolic pathways. *Plant Physiol.* 132, 597–605. doi: 10.1104/pp.102.019802

Maruyama-Nakashita, A., Nakamura, Y., Tohge, T., Saito, K., and Takahashi, H. (2006). *Arabidopsis* SLIM1 is a central transcriptional regulator of plant sulfur response and metabolism. *Plant Cell* 18, 3235–3251. doi: 10.1105/tpc.106.046458

Marzluf, G. A. (1997). Molecular genetics of sulfur assimilation in filamentous fungi and yeast. *Annu. Rev. Microbiol.* 51, 73–96. doi: 10.1146/annurev.micro.51.1.73

Mas-Droux, C., Biou, V., and Dumas, R. (2006). Allosteric threonine synthase. Reorganization of the pyridoxal phosphate site upon asym.metric activation through *S*-adenosylmethionine binding to a novel site. *J. Biol. Chem.* 281, 5188–5196.

Masselot, M., and De Robichon-Szulmajste, H. (1975). Methionine biosynthesis in *Saccharomyces cerevisiae*. I. Genetical analysis of auxotrophic mutants. *Mol. Gen. Genet.* 139, 121–132. doi: 10.1007/bf00264692

McClung, C. R., Hsu, M., Painter, J. E., Gagne, J. M., Karlsberg, S. D., and Salome, P. A. (2000). Integrated temporal regulation of the photorespiratory pathway. Circadian regulation of two *Arabidopsis* genes encoding serine hydroxymethyltransferase. *Plant Physiol.* 123, 381–391. doi: 10.1104/pp.123.1.381

Meng, J., Wang, L., Wang, J., Zhao, X., Cheng, J., Yu, W., et al. (2018). METHIONINE ADENOSYLTRANSFERASE4 mediates DNA and histone methylation. *Plant Physiol.* 177, 652–670. doi: 10.1104/pp.18.00183

Mentch, S. J., Mehrmohamadi, M., Huang, L., Liu, X., Gupta, D., Mattocks, D., et al. (2015). Histone methylation dynamics and gene regulation occur through the sensing of one-carbon metabolism. *Cell Metab.* 22, 861–873. doi: 10.1016/j.cmet.2015.08.024

Mills, W. R., and Joy, K. W. (1980). A rapid method for isolation of purified, physiologically active chloroplasts, used to study the intracellular distribution of amino acids in pea leaves. *Planta* 148, 75–83. doi: 10.1007/bf00385445

Mino, K., Imamura, K., Sakiyama, T., Eisaki, N., Matsuyama, A., and Nakanishi, K. (2001). Increase in the stability of serine acetyltransferase from *Escherichia coli* against cold inactivation and proteolysis by forming a bienzyme complex. *Biosci. Biotech. Biochem.* 65, 865–874. doi: 10.1271/bbb.65.865

Mittal, M., Singh, A. K., and Kumaran, S. (2017). Structural and biochemical characterization of ligand recognition by CysB, the master regulator of sulfate metabolism. *Biochimie* 142, 112–124. doi: 10.1016/j.biochi.2017.08.011

Moffatt, B. A., and Weretilnyk, E. A. (2001). Sustaining *S*-adenosyl-L-methionine-dependent methyltransferase activity in plant cells. *Physiol. Plant.* 113, 435–442. doi: 10.1034/j.1399-3054.2001.1130401.x

Moffatt, B. A., Stevens, Y., Allen, M., Snider, J., Pereira, L., Todorova, M., et al. (2002). Adenosine kinase deficiency is associated with developmental abnormalities and reduced transmethylation. *Plant Physiol.* 128, 812–821. doi: 10.1104/pp.010880

Moniuszko, G., Skoneczny, M., Zientara-Rytter, K., Wawrzynska, A., Glow, D., Cristescu, S. M., et al. (2013). Tobacco LSU-like protein couples sulphur-deficiency response with ethylene signalling pathway. *J. Experim. Bot.* 64, 5173–5182. doi: 10.1093/jxb/ert309

Mutwil, M., Klie, S., Tohge, T., Giorgi, F. M., Wilkins, O., Campbell, M. M., et al. (2011). PlaNet: combined sequence and expression comparisons across plant networks derived from seven species. *Plant Cell* 23, 895–910. doi: 10.1105/tpc.111.083667

Mutwil, M., Obro, J., Willats, W. G. T., and Persson, S. (2008). GeneCAT – novel webtools that combine BLAST and co-expression analyses. *Nucleic Acids Res.* 36, W320–W326.

Mutwil, M., Usadel, B., Schutte, M., Loraine, A., Ebenhoh, O., and Persson, S. (2010). Assembly of an interactive correlation network for the *Arabidopsis* genome using a novel heuristic clustering algorithm. *Plant Physiol.* 152, 29–43. doi: 10.1104/pp.109.145318

Nakamura, T., Iwahashi, H., and Eguchi, Y. (1984). Enzymatic proof for the identity of the S-sulfocysteine synthase and cysteine synthase B of *Salmonella typhimurium*. *J. Bacteriol.* 158, 1122–1127. doi: 10.1128/jb.158.3.1122-1127.1984

Neuenschwander, U., Suter, M., and Brunold, C. (1991). Regulation of sulfate assimilation by light and O-acetyl-l-serine in *Lemna minor* L. *Plant Physiol.* 97, 253–258. doi: 10.1104/pp.97.1.253

Nikiforova, V. J., Daub, C. O., Hesse, H., Willmitzer, L., and Hoefgen, R. (2005a). Integrative gene-metabolite network with implemented causality deciphers informational fluxes of sulphur stress response. *J. Experim. Bot.* 56, 1887–1896. doi: 10.1093/jxb/eri179

Nikiforova, V. J., Kopka, J., Tolstikov, V., Fiehn, O., Hopkins, L., Hawkesford, M. J., et al. (2005b). Systems rebalancing of metabolism in response to sulfur deprivation, as revealed by metabolome analysis of *Arabidopsis* plants. *Plant Physiol.* 138, 304–318. doi: 10.1104/pp.104.053793

Nikiforova, V., Freitag, J., Kempa, S., Adamik, M., Hesse, H., and Hoefgen, R. (2003). Transcriptome analysis of sulfur depletion in *Arabidopsis thaliana*: interlacing of biosynthetic pathways provides response specificity. *Plant J.* 33, 633–650. doi: 10.1046/j.1365-313x.2003.01657.x

Noji, M., Inoue, K., Kimura, N., Gouda, A., and Saito, K. (1998). Isoform-dependent differences in feedback regulation and subcellular localization of serine acetyltransferase involved in cysteine biosynthesis from *Arabidopsis thaliana*. *J. Biolog. Chem.* 273, 32739–32745. doi: 10.1074/jbc.273.49.32739

Noji, M., Takagi, Y., Kimura, N., Inoue, K., Saito, M., Horikoshi, M., et al. (2001). Serine acetyltransferase involved in cysteine biosynthesis from spinach: molecular cloning, characterization and expression analysis of cDNA encoding a plastidic isoform. *Plant Cell Physiol.* 42, 627–634. doi: 10.1093/pcp/pce078

Obayashi, T., Hayashi, S., Saeki, M., Ohta, H., and Kinoshita, K. (2009). ATTED-II provides coexpressed gene networks for *Arabidopsis*. *Nucleic Acids Res.* 37, D987–D991.

Obayashi, T., Kinoshita, K., Nakai, K., Shibaoka, M., Hayashi, S., Saeki, M., et al. (2007). ATTED-II: a database of co-expressed genes and cis elements for identifying co-regulated gene groups in *Arabidopsis*. *Nucleic Acids Res.* 35, D863–D869.

Okamura, E., and Hirai, M. Y. (2017). Novel regulatory mechanism of serine biosynthesis associated with 3-phosphoglycerate dehydrogenase in *Arabidopsis thaliana*. *Sci. Rep.* 7:3533. doi: 10.1038/s41598-017-03807-5

Olsen, L. R., Huang, B., Vetting, M. W., and Roderick, S. L. (2004). Structure of serine acetyltransferase in complexes with CoA and its cysteine feedback inhibitor. *Biochemistry* 43, 6013–6019. doi: 10.1021/bi0358521

Onouchi, H., Nagami, Y., Haraguchi, Y., Nakamoto, M., Nishimura, Y., Sakurai, R., et al. (2005). Nascent peptide-mediated translation elongation arrest coupled

with mRNA degradation in the CGS1 gene of *Arabidopsis*. *Genes Dev.* 19, 1799–1810. doi: 10.1101/gad.1317105

Onoue, N., Yamashita, Y., Nagao, N., Goto, D. B., Onouchi, H., and Naito, S. (2011). S-adenosyl-L-methionine induces compaction of nascent peptide chain inside the ribosomal exit tunnel upon translation arrest in the *Arabidopsis* CGS1 gene. *J. Biol. Chem.* 286, 14903–14912. doi: 10.1074/jbc.M110.211656

Osborne, M. J., Siddiqui, N., Iannuzzi, P., and Gehring, K. (2004). The solution structure of ChaB, a putative membrane ion antiporter regulator from *Escherichia coli*. *BMC Struct. Biol.* 4:9.

Ostrowski, J., and Kredich, N. M. (1989). Molecular characterization of the cysJIH promoters of *Salmonella typhimurium* and *Escherichia coli*: regulation by cysB protein and N-acetyl-L-serine. *J. Bacteriol.* 171, 130–140. doi: 10.1128/jb.171.1.130-140.1989

Ostrowski, J., and Kredich, N. M. (1991). Negative autoregulation of cysB in *Salmonella typhimurium*: in vitro interactions of CysB protein with the cysB promoter. *J. Bacteriol.* 173, 2212–2218. doi: 10.1128/jb.173.7.2212-2218.1991

Pajares, M. A., Álvarez, L., and Pérez-Sala, D. (2013). How are mammalian methionine adenosyltransferases regulated in the liver? A focus on redox stress. *FEBS Lett.* 587, 1711–1716. doi: 10.1016/j.febslet.2013.04.034

Palmieri, L., Arrigoni, R., Blanco, E., Carrari, F., Zanor, M. I., Studart-Guimaraes, C., et al. (2006). Molecular identification of an *Arabidopsis* S-adenosylmethionine transporter. Analysis of organ distribution, bacterial expression, reconstitution into liposomes, and functional characterization. *Plant Physiol.* 142, 855–865. doi: 10.1104/pp.106.086975

Parry, J., and Clark, D. P. (2002). Identification of a CysB-regulated gene involved in glutathione transport in *Escherichia coli*. *Fems Microbiol. Lett.* 209, 81–85. doi: 10.1111/j.1574-6968.2002.tb11113.x

Paulose, B., Chhikara, S., Coomey, J., Jung, H. I., Vatamaniuk, O., and Dhankher, O. P. (2013). A γ-glutamyl cyclotransferase protects *Arabidopsis* plants from heavy metal toxicity by recycling glutamate to maintain glutathione homeostasis. *Plant Cell* 25, 4580–4595. doi: 10.1105/tpc.113.111815

Peng, J., Li, Z., Wen, X., Li, W., Shi, H., Yang, L., et al. (2014). Salt-induced stabilization of EIN3/EIL1 confers salinity tolerance by deterring ROS accumulation in *Arabidopsis*. *PLoS Genet.* 10:e1004664. doi: 10.1371/journal.pgen.1004664

Pereira, L. A. R., Todorova, M., Cai, X., Makaroff, C. A., Emery, R. J. N., and Moffatt, B. A. (2007). Methyl recycling activities are co-ordinately regulated during plant development. *J. Exp. Bot.* 58, 1083–1098. doi: 10.1093/jxb/erl275

Pick, T. R., Bräutigam, A., Schulz, M. A., Obata, T., Fernie, A. R., and Weber, A. P. (2013). PLGG1, a plastidic glycolate glycerate transporter, is required for photorespiration and defines a unique class of metabolite transporters. *Proc. Natl. Acad. Sci. U.S.A.* 110, 3185–3190. doi: 10.1073/pnas.1215142110

Pizer, L. I. (1963). The pathway and control of serine biosynthesis in *Escherichia Coli*. *J. Biol. Chem.* 238, 3934–3944. doi: 10.1016/s0021-9258(18)51809-3

Poloni, S., Blom, H. J., and Schwartz, I. V. D. (2015). Stearoyl-CoA desaturase-1: is it the link between sulfur amino acids and lipid metabolism? *Biology (Basel)* 4, 383–396. doi: 10.3390/biology4020383

Pommerrenig, B., Feussner, K., Zierer, W., Rabinovych, V., Klebl, F., Feussner, I., et al. (2011). Phloem-specific expression of Yang cycle genes and identification of novel Yang cycle enzymes in *Plantago* and *Arabidopsis*. *Plant Cell* 23, 1904–1919. doi: 10.1105/tpc.110.079657

Qi, J., Song, C. P., Wang, B., Zhou, J., Kangasjarvi, J., Zhu, J. K., et al. (2018). Reactive oxygen species signaling and stomatal movement in plant responses to drought stress and pathogen attack. *J. Integr. Plant Biol.* 60, 805–826. doi: 10.1111/jipb.12654

Ravanel, S., Block, M. A., Rippert, P., Jabrin, S., Curien, G., Rébeillé, F., et al. (2004). Methionine metabolism in plants. *J. Biol. Chem.* 279, 22548–22557. doi: 10.1074/jbc.m313250200

Rocha, P. S. C. F., Sheikh, M., Melchiorre, R., Fagard, M., Boutet, S., Loach, R., et al. (2005). The *Arabidopsis* HOMOLOGY-DEPENDENT GENE SILENCING1 gene codes for an S-adenosyl-L-homocysteine hydrolase required for DNA methylation-dependent gene silencing. *Plant Cell.* 17, 404–417. doi: 10.1105/tpc.104.028332

Ros, R., Munoz-Bertomeu, J., and Krueger, S. (2014). Serine in plants: biosynthesis, metabolism, and functions. *Trends Plant Sci.* 19, 564–569. doi: 10.1016/j.tplants.2014.06.003

Rosa-Tellez, S., Anoman, A. D., Alcantara-Enguidanos, A., Garza-Aguirre, R. A., Alseekh, S., and Ros, R. (2020). PGDH family genes differentially affect *Arabidopsis* tolerance to salt stress. *Plant Sci.* 290:110284. doi: 10.1016/j.plantsci.2019.110284

Rouached, H., Wirtz, M., Alary, R., Hell, R., Arpat, A. B., Davidian, J. C., et al. (2008). Differential regulation of the expression of two high-affinity sulfate transporters, SULTR1.1 and SULTR1.2, in *Arabidopsis*. *Plant Physiol.* 147, 897–911. doi: 10.1104/pp.108.118612

Roy, M., and Wu, R. (2002). Overexpression of S-adenosylmethionine decarboxylase gene in rice increases polyamine level and enhances sodium chloride-stress tolerance. *Plant Sci.* 163, 987–992. doi: 10.1016/S0168-9452(02)00272-8

Ruffet, M. L., Lebrun, M., Droux, M., and Douce, R. (1995). Subcellular distribution of serine acetyltransferase from *Pisum sativum* and characterization of an *Arabidopsis thaliana* putative cytosolic isoform. *Eur. J. Biochem.* 227, 500–509. doi: 10.1111/j.1432-1033.1995.tb20416.x

Ruszkowski, M., Sekula, B., Ruszkowska, A., and Dauter, Z. (2018). Chloroplastic serine hydroxymethyltransferase from *Medicago truncatula*: a structural characterization. *Front. Plant Sci.* 9:584. doi: 10.3389/fpls.2018.00584

Saito, K. (2004). Sulfur assimilatory metabolism. The long and smelling road. *Plant Physiol.* 136, 2443–2450. doi: 10.1104/pp.104.046755

Saito, K., Yokoyama, H., Noji, M., and Murakoshi, I. (1995). Molecular cloning and characterization of a plant serine acetyltransferase playing a regulatory role in cysteine biosynthesis from watermelon. *J. Biolog. Chem.* 270, 16321–16326. doi: 10.1074/jbc.270.27.16321

Samuilov, S., Brilhaus, D., Rademacher, N., Flachbart, S., Arab, L., Alfarraj, S., et al. (2018). The photorespiratory BOU gene mutation alters sulfur assimilation and its crosstalk with carbon and nitrogen metabolism in *Arabidopsis thaliana*. *Front Plant Sci.* 9:1709.

Sánchez-Aguayo, I., Rodríguez-Galán, J. M., García, R., Torreblanca, J., and Pardo, J. M. (2004). Salt stress enhances xylem development and expression of S-adenosyl-L-methionine synthase in lignifying tissues of tomato plants. *Planta* 220, 278–285. doi: 10.1007/s00425-004-1350-2

Sauter, M., Moffatt, B., Saechao, M. C., Hell, R., and Wirtz, M. (2013). Methionine salvage and S-adenosylmethionine: essential links between sulfur, ethylene and polyamine biosynthesis. *Biochem. J.* 451, 145–154. doi: 10.1042/bj20121744

Sekowska, A., Ashida, H., and Danchin, A. (2019). Revisiting the methionine salvage pathway and its paralogues. *Microb. Biotechnol.* 12, 77–97. doi: 10.1111/1751-7915.13324

Sekowska, A., Kung, H. F., and Danchin, A. (2000). Sulfur metabolism in *Escherichia coli* and related bacteria: facts and fiction. *J. Mol. Microbiol. Biotech.* 2, 145–177.

Shiraki, N., Shiraki, Y., Tsuyama, T., Obata, F., Miura, M., Nagae, G., et al. (2014). Methionine metabolism regulates maintenance and differentiation of human pluripotent stem cells. *Cell Metab.* 19, 780–794. doi: 10.1016/j.cmet.2014.03.017

Shyh-Chang, N., Locasale, J. W., Lyssiotis, C. A., Zheng, Y., Teo, R. Y., Ratanasirintrawoot, S., et al. (2013). Influence of threonine metabolism on S-adenosylmethionine and histone methylation. *Science* 339, 222–226. doi: 10.1126/science.1226603

Sirko, A., Wawrzynska, A., Rodriguez, M. C., and Sektas, P. (2015). The family of LSU-like proteins. *Front. Plant Sci.* 5:774.

Smith, I. K. (1972). Studies of l-cysteine biosynthetic enzymes in *Phaseolus vulgaris* L. *Plant Physiol.* 50, 477–479. doi: 10.1104/pp.50.4.477

Sønderby, I. E., Hansen, B. G., Bjarnholt, N., Halkier, B. A., and Kliebenstein, D. J. (2007). A systems biology approach identifies a R2R3 MYB gene subfamily with distinct and overlapping functions in regulation of aliphatic glucosinolates. *PLoS One* 2:e1322. doi: 10.1371/journal.pone.0001322

South, P. F., Walker, B. J., Cavanagh, A. P., Rolland, V., Badger, M., and Ort, D. R. (2017). Bile acid sodium symporter BASS6 can transport glycolate and is involved in photorespiratory metabolism in *Arabidopsis thaliana*. *Plant Cell* 29, 808–823. doi: 10.1105/tpc.16.00775

Takahashi, H., Kopriva, S., Giordano, M., Saito, K., and Hell, R. (2011). Sulfur assimilation in photosynthetic organisms: molecular functions and regulations of transporters and assimilatory enzymes. *Ann. Rev. Plant Biol.* 62, 157–184. doi: 10.1146/annurev-arplant-042110-103921

Takahashi, M., Terada, Y., Nakai, I., Nakanishi, H., Yoshimura, E., Mori, S., et al. (2003). Role of nicotianamine in the intracellular delivery of metals and plant reproductive development. *Plant Cell.* 15, 1263–1280. doi: 10.1105/tpc.010256

Tehlivets, O., Malanovic, N., Visram, M., Pavkov-Keller, T., and Keller, M. (2013). S-adenosyl-L-homocysteine hydrolase and methylation disorders: yeast as a

model system. *Biochim. Biophys. Acta.* 1832, 204–215. doi: 10.1016/j.bbadis.2012.09.007

Toujani, W., Munoz-Bertomeu, J., Flores-Tornero, M., Rosa-Tellez, S., Anoman, A. D., Alseekh, S., et al. (2013a). Functional characterization of the plastidial 3-phosphoglycerate dehydrogenase family in *Arabidopsis*. *Plant Physiol.* 163, 1164–1178. doi: 10.1104/pp.113.226720

Toujani, W., Munoz-Bertomeu, J., Flores-Tornero, M., Rosa-Tellez, S., Anoman, A., and Ros, R. (2013b). Identification of the phosphoglycerate dehydrogenase isoform EDA9 as the essential gene for embryo and male gametophyte development in *Arabidopsis*. *Plant Signal Behav.* 8:e27207. doi: 10.4161/psb.27207

Ulanovskaya, O. A., Zuhl, A. M., and Cravatt, B. F. (2013). NNMT promotes epigenetic remodeling in cancer by creating a metabolic methylation sink. *Nat. Chem. Biol.* 9, 300–306. doi: 10.1038/nchembio.1204

Urano, Y., Manabe, T., Noji, M., and Saito, K. (2000). Molecular cloning and functional characterization of cDNAs encoding cysteine synthase and serine acetyltransferase that may be responsible for high cellular cysteine content in *Allium tuberosum*. *Gene* 257, 269–277. doi: 10.1016/s0378-1119(00)00399-1

Ushijima, T., Hanada, K., Gotoh, E., Yamori, W., Kodama, Y., Tanaka, H., et al. (2017). Light controls protein localization through phytochrome-mediated alternative promoter selection. *Cell* 171, 1316–1325.e12..

Van Der Ploeg, J. R., Eichhorn, E., and Leisinger, T. (2001). Sulfonate-sulfur metabolism and its regulation in *Escherichia coli*. *Arch. Microbiol.* 176, 1–8. doi: 10.1007/s002030100298

Vandekeere, S., Dubois, C., Kalucka, J., Sullivan, M. R., García-Caballero, M., Goveia, J., et al. (2018). Serine synthesis via PHGDH is essential for heme production in endothelial cells. *Cell Metab.* 28, 573–587. doi: 10.1016/j.cmet.2018.06.009

Vandereyken, K., Van Leene, J., De Coninck, B., and Cammue, B. P. A. (2018). Hub protein controversy: taking a closer look at plant stress response hubs. *Front. Plant Sci.* 9:694.

Vandrisse, C. M., and Escalante-Semerena, J. C. (2018). In *Salmonella enterica*, OatA (formerly YjgM) uses O-acetyl-serine and acetyl-CoA to synthesize N,O-Diacetylserine, which upregulates cysteine biosynthesis. *Front. Microbiol.* 9:2838.

Vauclare, P., Kopriva, S., Fell, D., Suter, M., Sticher, L., Von Ballmoos, P., et al. (2002). Flux control of sulphate assimilation in *Arabidopsis thaliana*: adenosine 5′-phosphosulphate reductase is more susceptible than ATP sulphurylase to negative control by thiols. *Plant J.* 31, 729–740. doi: 10.1046/j.1365-313x.2002.01391.x

Voll, L. M., Jamai, A., Renne, P., Voll, H., Mcclung, C. R., and Weber, A. P. M. (2006). The photorespiratory *Arabidopsis* shm1 mutant is deficient in SHM1. *Plant Physiol.* 140, 59–66. doi: 10.1104/pp.105.071399

Waie, B., and Rajam, M. V. (2003). Effect of increased polyamine biosynthesis on stress responses in transgenic tobacco by introduction of human S-adenosylmethionine gene. *Plant Sci.* 164, 727–734. doi: 10.1016/S0168-9452(03)00030-X

Wang, T., and Leyh, T. S. (2012). Three-stage assembly of the cysteine synthase complex from *Escherichia coli*. *J. Biolog. Chem.* 287, 4360–4367. doi: 10.1074/jbc.m111.288423

Watanabe, M., Kusano, M., Oikawa, A., Fukushima, A., Noji, M., and Saito, K. (2008a). Physiological roles of the β-substituted alanine synthase gene family in *Arabidopsis*. *Plant Physiol.* 146, 310–320. doi: 10.1104/pp.107.106831

Watanabe, M., Mochida, K., Kato, T., Tabata, S., Yoshimoto, N., Noji, M., et al. (2008b). Comparative genomics and reverse genetics analysis reveal indispensable functions of the serine acetyltransferase gene family in *Arabidopsis*. *Plant Cell* 20, 2484–2496. doi: 10.1105/tpc.108.060335

Watanabe, M., Tohge, T., Fernie, A. R., and Hoefgen, R. (2018). The effect of single and multiple SERAT mutants on serine and sulfur metabolism. *Front. Plant Sci.* 9:702.

Wawrzynska, A., Lewandowska, M., and Sirko, A. (2010). Nicotiana tabacum EIL2 directly regulates expression of at least one tobacco gene induced by sulphur starvation. *J. Experim. Bot.* 61, 889–900. doi: 10.1093/jxb/erp356

Wawrzynska, A., Lewandowska, M., Hawkesford, M. J., and Sirko, A. (2005). Using a suppression subtractive library-based approach to identify tobacco genes regulated in response to short-term sulphur deficit. *J. Experim. Bot.* 56, 1575–1590. doi: 10.1093/jxb/eri152

Weretilnyk, E. A., Alexander, K. J., Drebenstedt, M., Snider, J. D., Summers, P. S., and Moffatt, B. (2001). Maintaining methylation activities during salt stress: the involvement of adenosine kinase. *Plant Physiol.* 125, 856–865. doi: 10.1104/pp.125.2.856

Westerman, S., Stulen, I., Suter, M., Brunold, C., and De Kok, L. J. (2001). Atmospheric H_2S as sulphur source for *Brassica oleracea*: consequences for the activity of the enzymes of the assimilatory sulphate reduction pathway. *Plant Physiol. Biochem.* 39, 425–432. doi: 10.1016/s0981-9428(01)01258-x

Wirtz, M., Beard, K. F., Lee, C. P., Boltz, A., Schwarzländer, M., Fuchs, C., et al. (2012). Mitochondrial cysteine synthase complex regulates O-acetylserine biosynthesis in plants. *J. Biol. Chem.* 287, 27941–27947. doi: 10.1074/jbc.m112.372656

Wirtz, M., Berkowitz, O., Droux, M., and Hell, R. (2001). The cysteine synthase complex from plants – Mitochondrial serine acetyltransferase from *Arabidopsis thaliana* carries a bifunctional domain for catalysis and protein-protein interaction. *Eur. J. Biochem.* 268, 686–693. doi: 10.1046/j.1432-1327.2001.01920.x

Wirtz, M., Birke, H., Heeg, C., Muller, C., Hosp, F., Throm, C., et al. (2010). Structure and function of the hetero-oligomeric cysteine synthase complex in plants. *J. Biolog. Chem.* 285, 32810–32817. doi: 10.1074/jbc.m110.157446

Wulfert, S., and Krueger, S. (2018). Phosphoserine aminotransferase1 is part of the phosphorylated pathways for serine biosynthesis and essential for light and sugar-dependent growth promotion. *Front. Plant Sci.* 9:1712.

Xu, R., Wang, Y., Zheng, H., Lu, W., Wu, C., Huang, J., et al. (2015). Salt-induced transcription factor MYB74 is regulated by the RNA-directed DNA methylation pathway in *Arabidopsis*. *J. Exp. Bot.* 66, 5997–6008. doi: 10.1093/jxb/erv312

Yamada, S., Awano, N., Inubushi, K., Maeda, E., Nakamori, S., Nishino, K., et al. (2006). Effect of drug transporter genes on cysteine export and overproduction in *Escherichia coli*. *App. Environ. Microbiol.* 72, 4735–4742. doi: 10.1128/aem.02507-05

Yamaguchi, K., Takahashi, Y., Berberich, T., Imai, A., Miyazaki, A., Takahashi, T., et al. (2006). The polyamine spermine protects against high salt stress in *Arabidopsis thaliana*. *FEBS Lett.* 580, 6783–6788. doi: 10.1016/j.febslet.2006.10.078

Yamaguchi, K., Takahashi, Y., Berberich, T., Imai, A., Takahashi, T., Michael, A. J., et al. (2007). A protective role for the polyamine spermine against drought stress in *Arabidopsis*. *Biochem. Biophys. Res. Commun.* 352, 486–490. doi: 10.1016/j.bbrc.2006.11.041

Yong-Villalobos, L., González-Morales, S. I., Wrobel, K., Gutiérrez-Alanis, D., Cervantes-Peréz, S. A., Hayano-Kanashiro, C., et al. (2015). Methylome analysis reveals an important role for epigenetic changes in the regulation of the *Arabidopsis* response to phosphate starvation. *Proc. Natl. Acad. Sci. U.S.A.* 112, E7293–E7302.

Yoshida, K., Ohtaka, K., Hirai, M. Y., and Hisabori, T. (2020). Biochemical insight into redox regulation of plastidial 3-phosphoglycerate dehydrogenase from *Arabidopsis thaliana*. *J. Biol. Chem.* 295, 14906–14915. doi: 10.1074/jbc.ra120.014263

Zhang, B., Tieman, D. M., Jiao, C., Xu, Y., Chen, K., Fe, Z., et al. (2016). Chilling-induced tomato flavor loss is associated with altered volatile synthesis and transient changes in DNA methylation. *Proc. Natl. Acad. Sci. U.S.A.* 113, 15580–12585.

Zhang, Y., Sun, K. H., Sandoval, F. J., Santiago, K., and Roje, S. (2010). One-carbon metabolism in plants: characterization of a plastid serine hydroxymethyltransferase. *Biochem. J.* 430, 97–105. doi: 10.1042/bj20100566

Zientara-Rytter, K., Lukomska, J., Moniuszko, G., Gwozdecki, R., Surowiecki, P., Lewandowska, M., et al. (2011). Identification and functional analysis of Joka2, a tobacco member of the family of selective autophagy cargo receptors. *Autophagy* 7, 1145–1158. doi: 10.4161/auto.7.10.16617

Conflict of Interest: The authors declare that the research was conducted in the absence of any commercial or financial relationships that could be construed as a potential conflict of interest.

Copyright © 2021 Watanabe, Chiba and Hirai. This is an open-access article distributed under the terms of the Creative Commons Attribution License (CC BY). The use, distribution or reproduction in other forums is permitted, provided the original author(s) and the copyright owner(s) are credited and that the original publication in this journal is cited, in accordance with accepted academic practice. No use, distribution or reproduction is permitted which does not comply with these terms.

frontiers in Plant Science

ORIGINAL RESEARCH
published: 17 June 2021
doi: 10.3389/fpls.2021.665883

BZR1 Regulates Brassinosteroid-Mediated Activation of *AMT1;2* in Rice

Shuo Yang†, Depeng Yuan†, Yang Zhang†, Qian Sun and Yuan Hu Xuan**

College of Plant Protection, Shenyang Agricultural University, Shenyang, China

Although it is known that brassinosteroids (BRs) play pleiotropic roles in plant growth and development, their roles in plant nutrient uptake remain unknown. Here, we hypothesized that BRs directly regulate ammonium uptake by activating the expression of rice *AMT1*-type genes. Exogenous BR treatment upregulated both *AMT1;1* and *AMT1;2* expression, while this induction was impaired in the BR-receptor gene *BRI1* mutant *d61-1*. We then focused on brassinazole-resistant 1 (*BZR1*), a central hub of the BR signaling pathway, demonstrating the important role of this signaling pathway in regulating *AMT1* expression and rice roots NH_4^+ uptake. The results showed that BR-induced expression of *AMT1;2* was suppressed in *BZR1 RNAi* plants but was increased in *bzr1-D,* a gain-of-function *BZR1* mutant. Further EMSA and ChIP analyses showed that BZR1 bound directly to the BRRE motif located in the promoter region of *AMT1;2*. Moreover, cellular ammonium contents, $^{15}NH_4^+$ uptake, and the regulatory effect of methyl-ammonium on root growth are strongly dependent on the levels of *BZR1*. Overexpression lines of *BRI1* and *BZR1* and Genetic combination of them mutants showed that BZR1 activates *AMT1;2* expression downstream of BRI1. In conclusion, the findings suggest that BRs regulation of NH4$^+$ uptake in rice involves transcription regulation of ammonium transporters.

Keywords: brassinosteroids, ammonium uptake, BZR1, *AMT1;2*, rice

OPEN ACCESS

Edited by:
Sakiko Okumoto,
Texas A&M University, United States

Reviewed by:
Timothy O. Jobe,
University of Cologne, Germany
Trevor M. Nolan,
Duke University, United States

****Correspondence:***
Qian Sun
sunqian5328@syau.edu.cn
Yuan Hu Xuan
xuanyuanhu115@syau.edu.cn

† These authors have contributed equally to this work

Specialty section:
This article was submitted to Plant Physiology, a section of the journal Frontiers in Plant Science

Received: *09 February 2021*
Accepted: *10 May 2021*
Published: *17 June 2021*

Citation:
Yang S, Yuan DP, Zhang Y, Sun Q and Xuan YH (2021) BZR1 Regulates Brassinosteroid-Mediated Activation of AMT1;2 in Rice. Front. Plant Sci. 12:665883. doi: 10.3389/fpls.2021.665883

INTRODUCTION

Inorganic nitrogen (N) is an important plant nutrient and is absorbed from the rhizosphere in two forms, nitrate and ammonium. In the paddy field, high levels of NH_4^+ are of particular importance to the rice yield. Further understanding of the molecular basis and regulation of ammonium transport and its translocation to buds is needed to promote efficient nitrogen absorption and to improve crop yields. Ammonium transporter (AMT) proteins can induce high-affinity NH4+ uptake from the rhizosphere to root cells, and the transporter AMT2;1 has also been shown to play a crucial role in ammonium root-to-stem translocation (Giehl et al., 2017). Sequence analysis has identified 10 AMT members in the rice genome (Suenaga et al., 2003; Loque and von Wiren, 2004). Of these, AMT1;1, AMT1;2, and AMT1;3 are the main three AMTs. The expression patterns of these three proteins differ between different tissues with *AMT1;2* and *AMT1;3* mainly expressed in plant roots, while *AMT1;1* is constitutively expressed in different tissues (Sonoda et al., 2003a). In rice, overexpression of *AMT1;1* increases NH_4^+ uptake, improves plant growth and promotes yield production in limited N-fertilization conditions (Ranathunge et al., 2014).

However, the overexpression of *AMT1;3* has an opposite effect in regulating rice growth and NH_4^+ uptake to *AMT1;1* (Bao et al., 2015). Studies have shown that transcriptional regulation of *AMT* genes strongly influences the plant's N content and uptake of different forms of externally applied N. NH_4^+ can upregulate the expression of both *AMT1;1* and *AMT1;2*, and inhibit the expression of *AMT1;3*. Under N starvation conditions, *AMT1;3* is upregulated in response to NH_4^+ (Kumar et al., 2003; Sonoda et al., 2003a). Similar regulation at the posttranscriptional and posttranslational levels have also been observed in *Arabidopsis*. For example, AMT1;1 has been shown to be phosphorylated in C-terminal threonine residue to inhibit transporter activity in an $NH4^+$-dependent manner (Yuan et al., 2007; Lanquar et al., 2009), and further, CBL-interacting serine/threonine protein kinase 23 (CIPK23) was reported to phosphorylate AMT1 to inhibit ammonium uptake (Straub et al., 2017). Indeterminate domain 10 (IDD10), a transcription factor, has recently been shown to directly activate *AMT1;2* in rice (Xuan et al., 2013), furthermore, the ABI3/VP1 transcription factor RAVL1 activates *AMT1;2* to directly modulate NH_4^+ uptake in rice (Xuan et al., 2016).

Transcriptome studies using gain-of-function mutants of the BES1 transcription factor and wild-type plants have identified the *Arabidopsis* genes regulated by brassinosteroids (BRs). These genes included *AtAMT1;1* which was found to be upregulated by BR signaling activation (Goda et al., 2004; Yu et al., 2011). BRs are important phytohormones that bind to the cell surface receptor Brassinosteroid Insensitive 1 (BRI1), initiating a signaling cascade in which BRI1 binds to BRI1-Associated Receptor Kinase 1 (BAK1) leading to the downstream inactivation of the kinase Brassinosteroid Insensitive 2 (BIN2). The protein phosphatase PP2A dephosphorylates two master transcription factors Brassinozole-Resistant 1 (BZR1) and BRI1-EMS-Supperssor 1 (BES1), and the non-phosphorylated BZR1 and BES1 translocate to the nucleus to regulate the expression of BR responsive genes (Li and Chory, 1997; Li et al., 2002; Nam and Li, 2002; Kim and Wang, 2010; Yang et al., 2011; Guo et al., 2013; Tong and Chu, 2018). In addition, the stunting and BR-insensitive phenotype of *bri1* BR receptor mutants can be rescued by the enhanced stability of BES1 and BZR1 in *bes1-D* and *bzr1-D* gain-of-function mutants (Wang et al., 2002; Yin et al., 2002). In rice, RAVL1, an upstream component of BR signaling, regulates BR homeostasis through binding to an E-box motif in the promoter regions of the BR receptor and biosynthesis genes (Je et al., 2010). BRs treatment enhances the expression of *AMT1;1* and *AMT1;2* in rice (Xuan et al., 2016); however, the detailed mechanism remains obscure.

These findings raise the questions of whether BRs play a role in nutrient uptake, and whether there is a direct regulatory link between BZR1 and *AMT*s in rice. In this study, we first analyzed the expression of *AMT1* genes affected by BRs in the key BR signal transcription factor *BZR1* and the BR receptor gene *BRI1* mutants. We then investigated the expression patterns of *AMT1* family members in the roots of the *BRI1* mutant *d61-1*, *bzr1-D* siblings, as well as the *BZR1* knockdown *BZR1 RNAi*. Genetic combinations between *BRI1* and *BZR1* were generated to examine activation of BRI1 and BZR1 in BR-mediated induction of *AMT1;2*. In addition, the cellular ammonium contents and ^{15}N abundance were tested to investigate BZR1 function in ammonium uptake. Taken together, our results showed that BR-dependent ammonium uptake is partially controlled by BZR1.

MATERIALS AND METHODS

Plant Materials and Growth Conditions

The coding sequence of *BZR1* was cloned into the pCambia1302 vector to construct the BZR1-GFP-expressing plasmid. The pCambia1302-*BZR1* vector was subsequently transformed into Nipponbare rice calli to generate *BZR1-GFP* transgenic lines. The *bri1-D* in the Dongjin background as well as *d61-1*, *bzr1-D*, and *BZR1 RNAi* in the Nipponbare background were described previously (Yamamuro et al., 2000; Jeong et al., 2002; Bai et al., 2007; Qiao et al., 2017). *BZR1 RNAi*, *d61-1*, *bzr1-D*, *bri1-D*, *bri1-D*/*BZR1 RNAi*, *BZR1-GFP*, and *d61-1*/*bzr1-D* plants were grown in the greenhouse. Plants were first grown in distilled water (dH_2O) for 1 week and subsequently transferred to brassinolide (BL) solution for analyzing BR effects on *AMT1* expressions. Whole roots were harvested after 3 h of BL treatment. To examine the effects of NH_4^+ on the expression of *BZR1*, plants were grown in dH_2O for 2 weeks before transfer to N-free nutrient solution for a further 3 days of growth (Abiko et al., 2005). The plants were then grown in the nutrient solution containing 0.5 mM $(NH_4)_2SO_4$ at pH 5.5. The roots were sampled at 0 and 3 h after the transfer. To test the effects of methyl-ammonium (MeA) on root growth, we added 1 mM KNO_3 as the only source of N and different concentrations of MeA to 0.5 × MS medium, and cultivated wild-type, *BZR1 RNAi*, and *bzr1-D* plants in the modified medium. The primary root length was measured and recorded on the sixth day.

RNA Extraction and Quantitative RT-PCR Analysis

Cellular total RNA was isolated by using the TRIzol reagent (Takara, Dalian, LN, China), and the RNA was treated with RQ-RNase-free DNase (Promega, Madison, WI, United States) to eliminate genomic DNA contamination. The GoScript Reverse Transcription kit (Promega, Madison, WI, United States) was used to synthesize cDNA. Quantitative RT-PCR was performed using the Illumina Research Quantity software Illumina Eco 3.0 (Illumina, San Diego, CA, United States), and each gene expression was normalized against that of the *Ubiquitin* level. The primers used for qRT-PCR are listed in **Table 1**.

ChIP Assay

Rice calli (8 g) expressing *35S: BZR1:GFP*, and *35S:GFP* were used for the ChIP assay. A pre-immune serum was used for pre-absorption before immunoprecipitation, and an anti-GFP monoclonal antibody (Clontech, Takara Bio, Japan) was used for immunoprecipitation. The immunoprecipitated DNAs were analyzed by ChIP-PCR for identification of the BZR1 binding region. The immunoprecipitated DNA was normalized by each input DNA in ChIP-PCR (Je et al., 2010). The primers used for the ChIP-PCR are shown in **Table 1**.

TABLE 1 | Primer sequences used in this study.

Primer	Sequence
Ubiquitin F	CACGGTTCAACAACATCCAG
Ubiquitin R	TGAAGACCCTGACTGGGAAG
AMT1;1 F	AGTACGTCGAGGAGATCTAC
AMT1;1 R	ACGTCGTTCGTTCTGGATTG
AMT1;2 F	TAGACATGGCCTCCCATCTC
AMT1;2 R	TAAGCATGATGTTCATGGTG
AMT1;3 F	AGGAGTACGTCGAGCTGATC
AMT1;3 R	CTTGCTCCGGCGACTTTCTG
AMT1;2 P-F	GCTCGCGGGATGGCGATGCGCGCTC
AMT1;2 P-R	GACGCGCGTCAACACAGACTGTA
BZR1 RT-F	GGAGTTCGAGTTCGACAA
BZR1 RT-R	CTCGGCGTCGGCGCGAAATGA
BZR1 F	AAGCTTATGACGTCCGGGGCGGCGGCG
BZR1 R	GGATCCTTTCGCGCCGACGCCGAGCGTGAG
P1 F	AATTTCGCTGCCATTTCC
P1 R	AAGAAGGAAGCTAAAGGC
P2 F	GAGTTTAGTTCTTTTGAC
P2 R	AAACCTAGGAAATTGATG
P3 F	TTGGAAAAATAGACATAC
P3 R	CGTTTAGTGTTTGAATCG
P4 F	CATATTTGTTTGATTAAC
P4 R	TGTGATATAGGGGGCAAG
A F	GTCTCACCGGGCTGCGTGCGTACGCCGATA
A R	TATCGGCGTACGCACGCAGCCCGGTGAGAC
mA F	GTCTCACCGGGCTGTTTTTTTACGCCGATA
mA R	TATCGGCGTAAAAAAACAGCCCGGTGAGAC
B F	TGGTCGCATCGTCGTGCGTGAGCTGCCTATCG
B R	CGATAGGCAGCTCACGCACGACGATGCGACCA
mB F	TGGTCGCATCGTTTTTTTGAGCTGCCTATCG
mB R	CGATAGGCAGCTCAAAAAAACGATGCGACCA
D2-F	ATG TGA TAA CAG AGA CGC TGC GGT
D2-R	TGG TGA CCA AGT GGT GAA GGA AGA

Electrophoretic Mobility Shift Assay (EMSA)

BZR1 ORF sequences were sub-cloned into the pET28a (+) expression vector to produce His:BZR1 recombinant protein in *Escherichia coli* strain BL21 DE3 after 4 h of 0.5 mM IPTG treatment at 28°C. To perform EMSA, 1 μg of His:BZR1 protein and 40k cpm of the ^{32}P-labeled DNA probes were used. The protocol was followed as previously described (Je et al., 2010). Primers used in the EMSA are listed in **Table 1**.

Transcriptional Activity Analysis

The effector (*35S:BZR1*), reporters [*pAMT1;2* and BRRE (BR Responsive Element)-mutated promoter *mpAMT1;1*-GUS fusions] and an internal control (*35S:LUC*) were co-transformed into protoplasts from *Arabidopsis* for testing transcriptional activation (Yamaguchi et al., 2010). *35S:BZR1* was cloned into the *GAL4BD* region of the *p35S:GAL4BD* vector and 2.5 kb of normal and BRRE-mutated (in which CGTG$^{T}/_{C}$G was replaced by TTTTTT) *AMT1;2* promoters were cloned into the TATA region of the *p35S:TATA:GUS* vector (Xuan et al., 2013). PEG-mediated transformation and subsequent activity measurement were performed as previously described (Yoo et al., 2007).

Determination of Intracellular Ammonium Contents

Cellular ammonium contents in rice roots were calculated by using an F-kit (Roche, Basel, Switzerland) following the manufacturer's instructions (Oliveira et al., 2002).

^{15}N Uptake Analysis

Wild-type, *BZR1 RNAi*, *d61-1*, *bzr1-D*, *bri1-D*, *bri1-D/BZR1 RNAi*, and *d61-1/bzr1-D* plants were cultivated for a 2-week nursery period in deionized water, following which the seedlings were transferred to N-free nutrient solution to continue culturing (Sonoda et al., 2003b). After culturing for 3 days, the protoplasmic absorption of $^{15}NH_4^+$ was analyzed. The detailed method for the calculation of $^{15}NH_4^+$ influx and the ratio of ^{15}N to ^{14}N in the total N pool was as previously described (Xuan et al., 2016).

Statistical Analysis

Statistical analysis was performed with Prism 5 software (GraphPad, San Diego, CA, United States). All data were expressed as mean ± SE. Comparison between multiple groups was performed by using one-way ANOVA with values of $P < 0.05$ considered as significant, followed by Bonferroni' s multiple comparison tests.

RESULTS

BR Treatment Induces BRI1-Dependent AMT1 Transcription

Brassinolide is the most active form of BR. To investigate whether BR affects the expression of rice *AMT1*, we used a series of BL concentration gradients of 0, 10, 100, and 200 nm to treat the wild-type, a weak allele of rice *BRI1* mutant, *d61-1*, and the *BRI1* overexpression line *bri1-D* (Jeong et al., 2002), and compared the changes in the *AMT1* expression level under the different treatment conditions. Quantitative RT-PCR analysis showed different patterns in the response of the *AMT* gene to BR at the transcriptional level: *AMT1;1* and *AMT1;2* showed dose-dependent upregulation in response to BR treatment, while no obvious change was observed in *AMT1;3*. Without BR treatment, the transcription levels of *AMT1;2* and *AMT1;3* in the *d61-1* mutant were slightly lower than those of the control group, while in *bri1-D*, the transcription levels of these genes were higher than those of wild-type plants. Among the various genotypes treated with BR, the expression levels of *AMT1;1* and *AMT1;2* in wild-type plants were higher than the level of *d61-1*. The expression level of *AMT1;1* and *AMT1;2* in *bri1-D* was significantly higher than that of the wild-type plants. Also, expression of a BR biosynthetic gene *D2* was analyzed. The result indicated that

D2 expression was suppressed by BR treatment in a dose-dependent manner, and *D2* expression level was higher in *d61-1* while lower in *bri1-D* compared to wild-type plants (**Figure 1**). These results suggest that BR mediates the regulation of *AMT1;1* and *AMT1;2* transcription levels via the cell surface receptor BRI1.

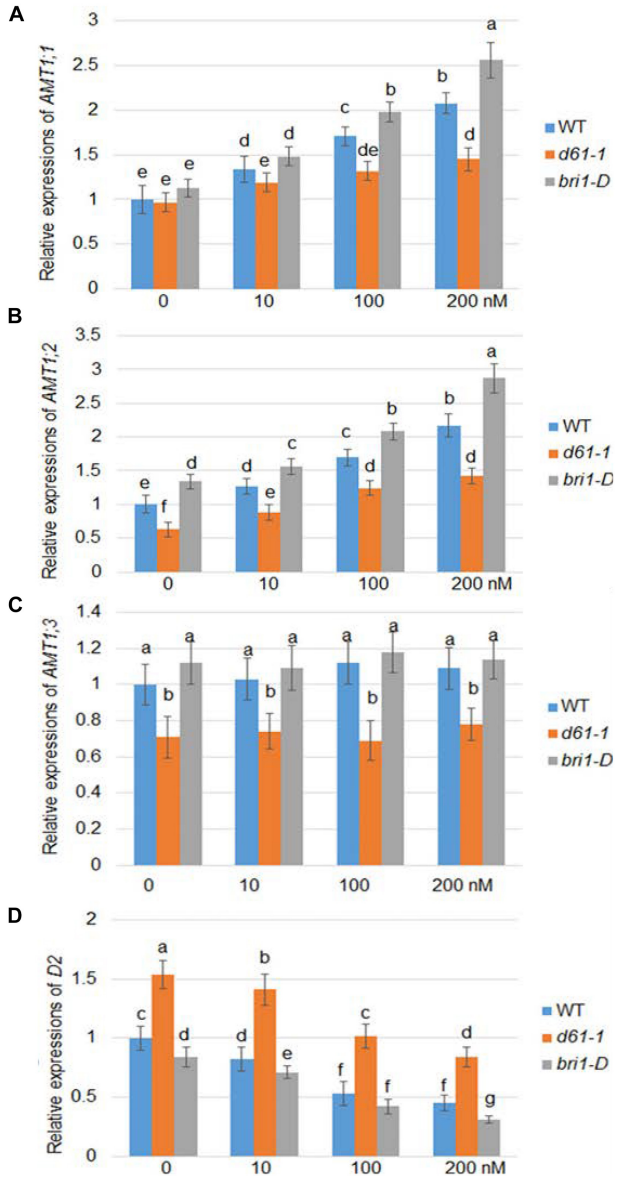

FIGURE 1 | BR-dependent *AMT1* expression in wild-type, *BRI1* mutant *d61-1*, and *BRI1* overexpression line *bri1-D* plant roots. Rice plants were grown for 7 days in distilled water, followed by 3 h with 0, 10, 100, or 200 nM brassinolide (BL). The expression levels of *AMT1 1* **(A)**, *AMT1 2* **(B)**, *AMT1 3* **(C)**, and *D2* **(D)** in plants treated with BL was measured by qRT-PCR using *Ubiquitin* to normalize the expression of each gene. Error bars indicate means ± SE (n = 3). The experiments were repeated at least three times. Different letters represent statistically significant differences ($P < 0.05$).

BR-Mediated Induction of AMT1;2 Depends on BZR1

As in *Arabidopsis*, rice BZR1 has been reported to be a key BR signaling transcription factor controlling the expression of downstream genes (Bai et al., 2007). To investigate the role of BZR1 in BR-mediated *AMT1* induction, *BZR1 RNAi* (*#1*), the knockdown transgenic line, and *bzr1-D* dominant mutant line were constructed (Bai et al., 2007; Ren et al., 2020). The changes in *AMT1;1* and *AMT1;2* transcription levels in these lines after BL treatment were monitored. The transcriptional abundance of *AMT1;1* was not affected by changes in BZR1 levels but could be increased in response to BL treatment in all plants (**Figure 2A**). Although the changes in the *AMT1;2* transcription level in the *BZR1 RNAi* mutants and *bzr1-D* were not significantly associated with BL treatment, they showed a significant decrease and increase, respectively. Only the *AMT1;2* expression levels correlated with the BZR1 level in a BR-dependent manner (**Figure 2B**). To verify *BZR1* levels in the *BZR1 RNAi* plants, qRT-PCR was performed. The results indicated that *BZR1* levels were reduced by about 60–70% in *BZR1 RNAi* lines (*#1-#4*). Also, *AMT1;2* expression levels were significantly lower in the *BZR1 RNAi* lines (*#1-#4*) than in the wild-type plants (**Figure 2C**).

BZR1 Directly Binds to the Promoter to Activate AMT1;2 Expression

Since the changes in the transcription level of *AMT1;2* are highly consistent with the changes in the expression level of BZR1, which indicated that BZR1 acts as a transcriptional activator upstream of *AMT1;2*. To verify whether the binding site of BZR1 includes the promoter of *AMT1;2*, we constructed transgenic plants of *35S:GFP* and *35S:BZR1:GFP* and performed ChIP assays. Promoter-sequence analysis showed that two BRRE (BR Responsive Element) motifs were located within a 2.5 kb stretch in front of the *AMT1;2* start codon (**Figure 3A**). We designed four primer pairs to amplify the four fragments (P1−P4) of the *AMT1;2* promoter and performed qPCR experiments to check the GFP-immunoprecipitates in *35S:GFP* and *35S:BZR1:GFP* transgenic siblings (**Figure 3B**). The ChIP results showed that BZR1 could bind directly to the *AMT1;2* promoter, especially in the P4 region. Since the P4 fragment harbors two putative BRRE motifs (**Figure 3A**), we further performed EMSA experiments to determine which of the BRRE motifs was responsible for the BZR1 binding. We designed two specific probes each containing a BRRE motif. The B probe showed stronger binding to BZR1 (**Figure 3A**) while the binding of the A probe was slightly weaker. When the probes were mutated, their binding to BZR1 was lost. These results suggest that BZR1 can bind both BRRE motifs in the P4 region but the binding strength is different (**Figure 3C**).

In the current study, we identified two *cis*-elements targeted by the promoter of BZR1 which are closely related to transcriptional activation of *AMT1;2*. To further verify whether these *cis*-elements have similar functions *in vivo*, we used the *Arabidopsis* protoplast system to perform transient expression assays (**Figure 3D**). We also used the *35S:BZR1* plasmid and a vector expressing GUS, which is strictly controlled by one

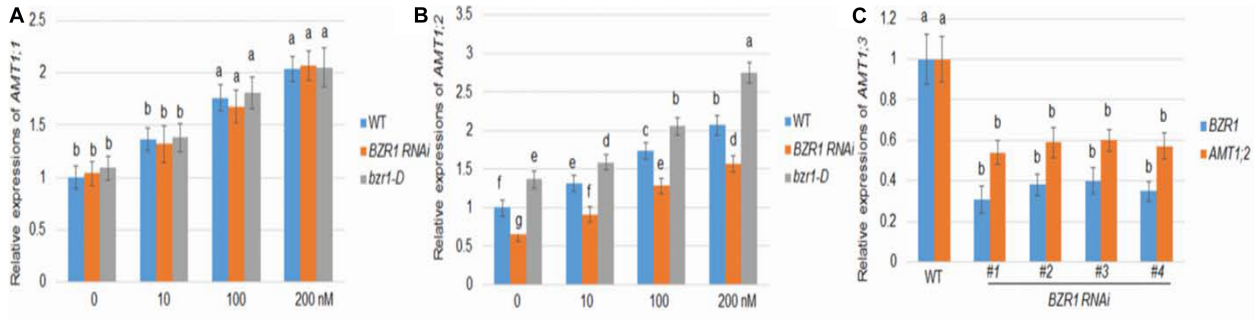

FIGURE 2 | BR-mediated *AMT1* expression in *BZR1 RNAi* and BZR1 constitutively active *bzr1-D* plant roots. Rice plants were grown in distilled water for 7 days and then treated with 0, 10, 100, or 200 nM BL for 3 h. **(A)** The expression levels of *AMT1;1* was measured by qRT-PCR. **(B)** The expression levels of *AMT1;2* was measured by qRT-PCR. *Ubiquitin* was used to normalize the expression of each gene. Data represent means ± SE (n = 3). **(C)** *BZR1* and *AMT1;2* expression levels in wild-type and *BZR1 RNAi* lines (*#1-#4*). Data indicate means ± SE (n = 3). The experiments were repeated at least three times. Different letters represent statistically significant differences ($P < 0.05$).

of four different types of 2.5 kb *AMT1;2* promoters namely, the native (pWT) and three mutated (pmP4) promoters. In *Arabidopsis* protoplasts, the *35S:BZR1* plasmid and the GUS vector are co-transformed into a vector expressing GUS. In these mutated promoters, BRRE motif sequences (CGTG$^T/_C$G) were observed to be replaced by the sequence TTTTTT. To eliminate the error caused by conversion efficiency, *35S:LUC* was used as an internal reference in each assay. By comparing the activity of the GUS genes under different promoter-driven conditions, we found that the GUS activity in *Arabidopsis* protoplasts was approximately twice that driven by the reporter gene promoter alone under the promoter pWT-driven conditions. Conversely, no detectable GUS activity was observed in the *Arabidopsis* protoplasts which were controlled by the mutant promoters (pmP4) (**Figure 3D**). These results indicated that direct combination with BZR1 is necessary for *AMT1;2* promoter activation.

BZR1 Affects the Absorption of NH_4^+ by Plant Roots

Root absorption of NH_4^+ is one of the main ways for plants to obtain N nutrients. To demonstrate whether BZR1 plays a role in this process, ^{15}N-labeled ammonium was used to determine the efficiency of N absorption. The NH_4^+ concentrations in the root tissues of the wild-type, *BZR1 RNAi*, and *bzr1-D* lines were also determined. Seventeen day-old hydroponic seedlings were soaked in 200 μM of $^{15}NH_4^+$ solution for 6 min, after which the short-term import rate of the ^{15}N-labeled ammonium in the plant roots was determined. Expressing the ^{15}N influx in μmoles g^{-1} root dry weight h^{-1} (Yuan et al., 2007, 2013), the $^{15}NH_4^+$ influx in the *BZR1 RNAi* plants was only 68% of that of the wild-type, while the influx of $^{15}NH_4^+$ in the *bzr1-D* plants was greater than that of the wild-type plants (**Figure 4A**). We introduced the concept of "^{15}N abundance," representing the proportion of ^{15}N to ^{14}N in the total N pool, to further explore the role of BZR1 in the short-range transport of NH_4^+. Compared with the ^{15}N internal flow results, the ^{15}N abundance in the total ^{15}N was lower in the *BZR1 RNAi* and higher in the *bzr1-D* plants compared to the wild-type (**Figure 4B**). The results of these short-term ^{15}N absorption experiments indicate that BZR1 plays an important role in mediating NH_4^+ influx.

BZR1 can regulate the expression of *AMT1;2* genes in plant roots. We suspect that this regulation may be related to the long-term transport process of NH_4^+ in the roots. Therefore, the NH_4^+ content in the rice roots of 3-day-old wild-type, *BZR1 RNAi*, and *bzr1-D* seedlings grown on 0.5 × MS medium was determined. As expected, the content of NH_4^+ in the roots of *BZR1 RNAi* was lower than in the wild-type seedlings, while the roots of *bzr1-D* plants contained more NH_4^+ than the wild-type plants (**Figure 4C**). Furthermore, a toxic ammonium analog, MeA, was used as a replacement addition to the NH_4^+-free medium using a concentration gradient. Wild-type, *BZR1 RNAi*, and *bzr1-D* plants were grown in this medium and the length of the plant's initial rooting was measured after 6 days of growth. In the absence of MeA, the primary roots of *BZR1 RNAi* were shorter than those of the wild-type and *bzr1-D*. With MeA treatment, the *BZR1 RNAi* root length was similar to that of the wild-type, while the *bzr1-D* roots were significantly shorter, the shortest in length among the three genetic lines (**Figures 4D,E**). These observations illustrated that the *BZR1 RNAi* response to MeA treatment is weaker than that of wild-type, while *bzr1-D* sensitivity to MeA treatment is relatively higher. Therefore, it can be inferred that BZR1 can participate in the process of rice root absorption of NH_4^+ in a long-term manner by regulating the expression of *AMT1;2* genes.

BZR1 Regulates *AMT1;2* at the Downstream of BRI1

As the expression of *AMT1;2* genes mediated by BR is inhibited in both the *d61-1* and *BZR1 RNAi* mutants, it is reasonable to speculate that *BZR1* and *BRI1* may affect the expression of *AMT1;2* genes. To investigate this, a series

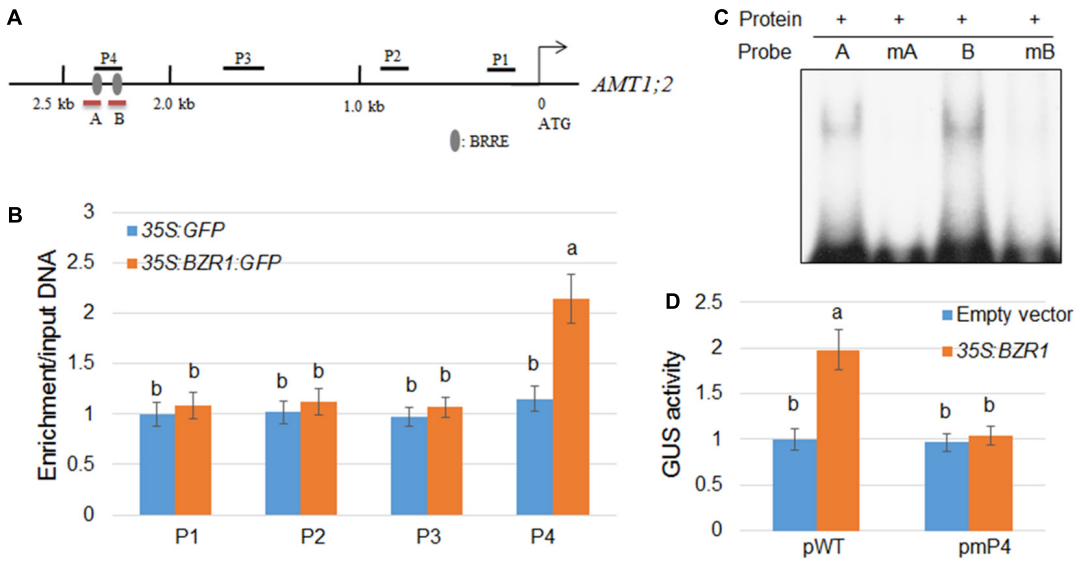

FIGURE 3 | Activation of *AMT1;2* by BZR1 via binding to BRRE elements in its promoter region. **(A)** Schematic diagram showing the position of BRRE in the *AMT1;2* promoter and probes used for ChIP detection. The gray oval represents BRRE, the letters P (1, 2, 3, 4) indicate the positions of the probe. Red lines under the BRRE elements indicate the probe used in the EMSA analysis. **(B)** An anti-GFP antibody was used to amplify immunoprecipitated DNA in the 2.5 kb *AMT1;2* promoter (P1–P4) for CHIP detection. The qPCR method was used to determine the relative ratios of immunoprecipitated DNA to input DNA. Input DNA was used for data normalization. Data represent means ± SE (n = 3). Transgenic plants expressing GFP and BZR1-GFP under control of 35S promoter were used. Different letters represent statistically significant differences (P < 0.05). **(C)** The affinity of BZR1 to each BRRE elements (A and B) located in P4 region was evaluated by EMSA. The BRRE motif sequence (CGTG$^{T}/_{C}$G) was replaced with the sequence TTTTTT in the mA and mB probes, and the mutant BRRE probes (mA and mB) were used as the negative controls. **(D)** 35S:BZR1 and each GUS-expressing vector were subjected to transient co-expression experiments under the control of the natural and BRRE-mutated *AMT1;2* promoters. The activation of the native promoter (pWT) and BRRE element mutated promoter (pmP4) was measured in protoplasts that were co-transformed with *35S:BZR1*. The GUS expression data was normalized by the luciferase gene driven by the 35S promoter. Error bars are ± SE of the means (n = 3). The experiments were repeated at least three times. Different letters represent statistically significant differences (P < 0.05).

of genetic analyses were employed: *d61-1* and *bzr1-D*, *BZR1 RNAi,* and *bri1-D* lines were individually hybridized and two genetic combinations were constructed. We then measured the effects of BR-dependent *AMT1;2* genes expression in the *d61-1*, *bzr1-D*, *d61-1/bzr1-D,* and wild-type lines without or without BL treatment. High levels of *AMT1;2* mRNA were observed in both the *bzr1-D* and *d61-1/bzr1-D* lines after 3 h of root treatment with BL. In *d61-1*, the mRNA level was somewhat lower than in *d61-1/bzr1-D* but higher than the wild-type in both lines (**Figure 5A**). The mRNA levels of *AMT1;2* in three other genotypes, including *bri1-D*, *BZR1 RNAi*, and *bri1-D/BZR1 RNAi* plants, were subsequently determined. We observed a similar low-level expression of *AMT1;2* mRNA in *BZR1 RNAi* and a high-level expression in *bri1-D* plants with or without BR treatment. However, the *BZR1 RNAi* blocked *AMT1;2* induction in the *bri1-D* background (**Figure 5B**). These results demonstrated that BZR1 positively regulates *AMT1;2* expression downstream of *BRI1* irrespective of exogenous BR stimulation.

Influence of BRI1 and BZR1 on NH_4^+-Dependent Expression of *AMT1;2* and NH_4^+ Uptake Activity

Since *AMT1;2* is significantly regulated by NH_4^+, we assessed the effects of *BRI1* and *BZR1* on NH_4^+-induced *AMT1;2* expression. To determine the NH_4^+-dependent *AMT1;2* gene expression, we treated 17-day-old seedlings originally grown in dH_2O and N-free nutrient medium with a 0.5 mM $(NH_4)_2SO_4$ solution. The whole roots of the plant were then collected at 0 and 3 h after treatment. To examine whether *BZR1* and *BRI1* play the same role in NH_4^+-dependent expression of *AMT1;2* as in BR-dependent induction, *BZR1* and *BRI1* mutants were used to examine the *AMT1;2* expression levels. When compared with wild type, both *bzr1-D* and *d61-1/bzr1-D* contained higher mRNA levels of *AMT1;2*, while those in *d61-1* were lower (**Figure 6A**). Furthermore, the *bri1-D* lines showed high levels of *AMT1;2* mRNA, with reduced *AMT1;2* mRNA expression in *BZR1 RNAi*, regardless of NH_4^+ treatment. Nevertheless, similar patterns of mRNA expression of *AMT1;2* were observed in *BZR1 RNAi* and *bri1-D/BZR1 RNAi* (**Figure 6B**). Taken together, these results indicated that *AMT1;2* expression was sensitive to the BZR1 level and that BZR1 acts downstream of BRI1 in this signaling pathway.

To determine the effects of BRI1 and BZR1 on the absorption of NH_4^+ in plant roots, we examined the import of ^{15}N-labeled ammonium in *BZR1* and *BRI1* genetic combinations. $^{15}NH_4^+$ influx was significantly lower in *d61-1*, while higher in *bzr1-D* or *d61-1/bzr1-D* than in the wild-type (**Figure 7A**). Also, the $^{15}NH_4^+$ influx was clearly lower in both *BZR1 RNAi* and *BZR1 RNAi/bri1-D*, while higher in *bri1-D* compared to wild-type plants (**Figure 7B**).

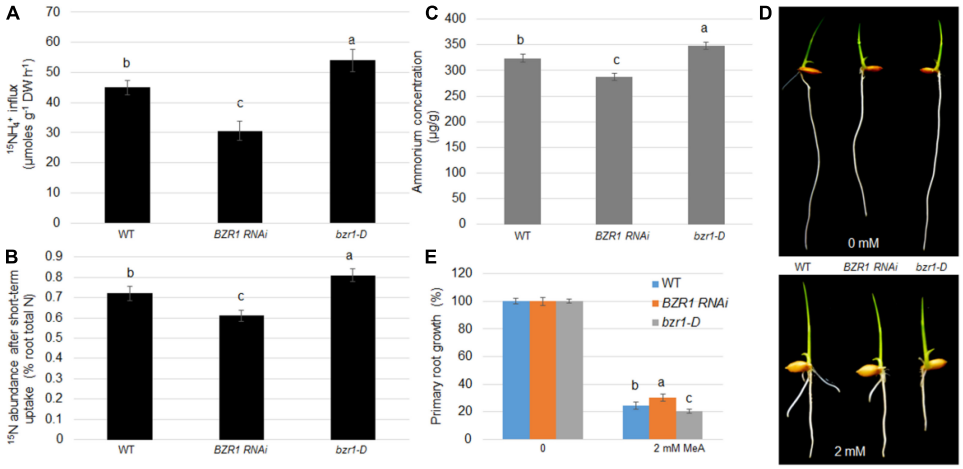

FIGURE 4 | BZR1 effects on NH_4^+ uptake in plants. **(A)** The wild-type, *BZR1 RNAi* and BZR1 constitutively active *bzr1-D* plants were hydro-cultured in deionized water for 2 weeks, and then grown in a nitrogen-free nutrient solution for 3 days. After exposure to 200 μM ^{15}N-labeled NH_4^+, the absorption of ammonium by rice roots was measured. Bars represent means ± SD (n = 6). **(B)** The wild-type, *BZR1 RNAi,* and *bzr1-D* plants were hydro-cultured in deionized water for 2 weeks, and then grown in a nitrogen-free nutrient solution for 3 days. After exposure to nutrient solution containing 200 μM ^{15}N-labeled NH_4^+ for 6 min, the absorption of ammonium by rice roots and the $^{15}NH_4^+$ abundance in relation to the total ^{15}N in roots was measured. Bars represent means ± SD (n = 6). **(C)** Intracellular NH_4 levels of wild-type, *BZR1,* and *bzr1-D* grown for 3 days in 0.5 × MS were detected in plant roots. Data represent means ± SE (n = 3). **(D)** Under different conditions with 0 or 2 mM MeA, wild-type, *BZR1 RNAi*, and *bzr1-D* were grown in a modified 0.5 × MS medium containing 1 mM KNO_3 for 6 days. MeA treatment significantly inhibited the growth of the primary root. In the absence of MeA treatment, the *BZR1 RNAi* primary root was shorter than that of the wild-type and *bzr1-D*. After 2 mM MeA treatment, bzr1-D showed a shorter primary root than *BZR1 RNAi* and wild-type. **(E)** The primary root growth was measured from wild-type, *BZR1 RNAi*, and *bzr1-D* with or without MeA supplementation as shown in **(D)**. Data represent means ± SE (n > 15 plants). The experiments were repeated at least three times. Different letters represent statistically significant differences (P < 0.05).

DISCUSSION

Although BRs are known for their pleiotropic roles in the regulation of plant growth and development, their effect on nutrient uptake is unclear. The activation of BR signaling has been shown by transcriptome analysis of BR treated wild-type or *bes1-D Arabidopsis* plants to positively regulate the expression of the AMT gene *AtAMT1;1* (Goda et al., 2004; Yu et al., 2011). Also, the BR signaling transcription factor RAVL1 activates *AMT1;2* to enhance NH_4^+ uptake in rice (Xuan et al., 2016). The possibility of a link between BRs and *AMT1* expression suggests that the process of root ammonium absorption may be coordinated with the physiological function of BRs in growth stimulation. In this study, we verified this issue by assessing the transcriptional levels of the AMT genes and the role they playing in ammonium uptake by the roots of rice lines, which genes involved in the regulation of BR homeostasis were modulated. We found high levels of BR susceptibility in all these genes which showed upregulated expression in response to BR treatment, especially the NH_4^+ transporter gene *AMT1;2*. Combining this result with the phenotype of higher NH_4^+ uptake, it can be inferred that this BR-dependent regulation is mediated by the direct binding between the transcription factor BZR1 and *AMT1;2* promoters. This regulation occurs after sensing BR signals. Thus, *AMT1;2*-mediated uptake of NH_4^+ can be seen as a physiological response mediated by BR.

BZR1 plays an important role in the coordination of ammonium uptake and BR signaling pathways. There are three lines of evidence that support this point. First, determination of the transcription level of *AMT1* genes in plants treated with exogenous BL showed that the *AMT1;2* in roots can respond to BL processing, increasing the level of transcription. BZR1 regulation plays a vital role in this process. Since the *AMT1;2* transcription level in *BZR1 RNAi* seedlings was also lower than that of the wild-type while the transcription level in the *bzr1-D* plants was higher; this expression pattern was also observed without BL treatment. Second, there was also a correlation between higher *AMT1;2* transcription levels and higher NH_4^+ uptake. We measured the rate of uptake of ^{15}N-labeled NH_4^+ by rice roots expressing different BZR1 levels. NH_4^+ uptake rates were compared at ^{15}N abundance and ^{15}N influx levels, and it was found that the NH_4^+ uptake of *BZR1 RNAi* was significantly lower than that of the wild-type, which may be explained by down-regulation of *AMT1;2*. This concept is further supported by the findings in *bzr1-D* roots, where the enrichment of $^{15}NH_4^+$ was higher than that in the wild-type. Therefore, in the presence of ammonium, a non-significant increase in NH_4^+ influx may be related to the down regulation of *AMT* mRNA levels (Yuan et al., 2007) or AMT protein activity (Lanquar et al., 2009; Yuan et al., 2013) at posttranscriptional or posttranslational levels. Furthermore, increased *BZR1* expression levels were also associated with increased ammonium abundance in roots. We observed that all these NH_4^+ uptake-related traits were affected in these lines with or without additional BR treatment. This observation suggests that BZR1 is a positive regulator of NH_4^+ uptake under any condition conducive to plant growth. To sum up, BZR1 is the coordination center between NH_4^+ absorption and general

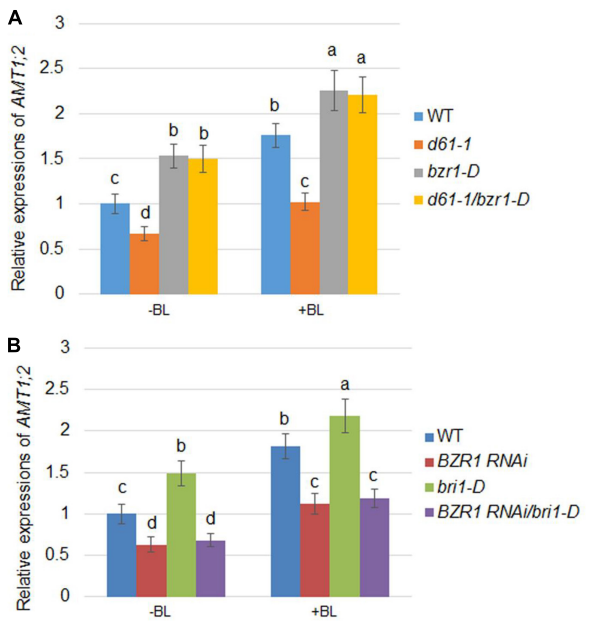

FIGURE 5 | BR-induced *AMT1;2* expression in the genetic combinations between *BZR1* and *BRI1*. **(A)** The expression levels of *AMT1;2* genes in wild-type, *BRI1* mutant *d61-1*, gain-of-function mutant *bzr1-D*, and their cross offspring *d61-1/bzr1-D* before and 3 h after BL treatment. **(B)** The expression levels of *AMT1;2* genes in the wild-type, *BZR1 RNAi*, *BRI1* overexpression line *bri1-D*, and their cross offspring *BZR1 RNAi/bri1-D* before and 3 h after BL treatment. The above plants were grown in distilled water for 7 days with or without treatment of 100 nM BL for 3 h. The expression levels of *AMT1;2* genes were measured by qRT-PCR. Sample mRNA levels were normalized to those of *Ubiquitin*. Data represent means ± SE (n = 3). The experiments were repeated at least three times. Different letters represent statistically significant differences ($P < 0.05$).

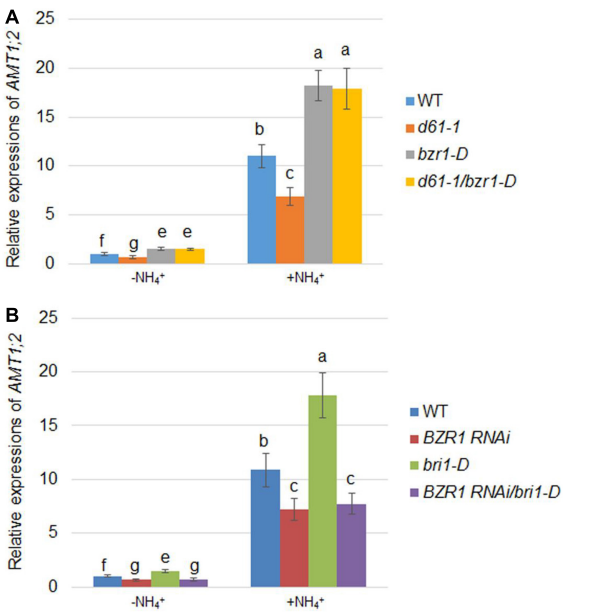

FIGURE 6 | NH_4^+-induced *AMT1;2* expression in *BZR1*, *BRI1*, and their genetic combinations. **(A)** NH_4^+-induced *AMT1;2* expression was detected in the wild-type, *BRI1* mutant *d61-1*, gain-of-function mutant *bzr1-D*, and their cross offspring *d61-1/bzr1-D*. **(B)** NH_4^+-induced *AMT1;2* expression was detected in *BZR1 RNAi*, *BRI1* overexpression line *bri1-D*, and their cross offspring *BZR1 RNAi/bri1-D*. Full root sampling was carried out on 17-day-old seedlings that were transferred to nutrient solution containing 0.5 mM $(NH_4)_2SO_4$ for 0 and 3 h. Measurement of *AMT1;2* expression levels using qRT-PCR. Sample mRNA levels were normalized with respect to those of *Ubiquitin*. Data represent means ± SE (n = 3). The experiments were repeated at least three times. Different letters represent statistically significant differences ($P < 0.05$).

growth promotion mediated by BRs. *AMT1;2* transcriptional level changes are significantly affected by BZR1 levels, suggesting a BZR1-dependent ammonium uptake pathway in roots. We have done further research on whether BZR1 directly regulates *AMT1;2* expression. Nine motifs were identified in the 2.5 kb promoter region of *AMT1;2* by promoter sequence analysis. EMSA, CHIP, and transient gene expression tests were used to further study the interaction between *AMT1;2* and BZR1. The two BRRE motifs in the promoter have been shown to be sites that bind BZR1 and directly activate *AMT1;2* transcription. In addition, although BZR1 can bind both BRRE motifs, the binding strength is different. It is likely that the positions of BRRE motifs in the promoter plays an important role in the regulation of *AMT1;2*. The comparison of BR- and NH_4^+-mediated expression of *AMT1;2* in *BZR1 RNAi*, *bzr1-D*, and wild-type plants indicates that constitutive activation of *AMT1;2* expression via BZR1 is independent of external signal stimulation. BRI1 performs a receptor function in BR signaling pathways and actively regulates BR-dependent *AMT1;2* expression through its signal reception. In addition, the roots of *d61-1*, the BRI1 mutant, accumulate less NH_4^+ than the corresponding wild-type, suggesting a positive role of BRI1 in regulating AMT-mediated NH_4^+ uptake in roots. The key BR signaling regulators BZR1, the BR receptor BRI1 play the putative role in the regulation of *AMT1;2* gene expression. Therefore, clarifying their inter-relationships enhances our understanding of the relationship between BR signaling and the mechanism of *AMT* regulation. We measured BR- or NH_4^+-mediated *AMT1;2* gene expression levels and $^{15}NH_4^+$ absorption in three rice lines with different combinations of *BZR1* and *BRI1* gene expression levels, including the line *bzr1-D* in the *d61-1* background and the line *bri1-D* in the *BZR1 RNAi* background. The activation of BRI1-induced *AMT1;2* requires BZR1 involvement, while the process of activation by BZR1 does not require BRI1 activity. Therefore, BZR1 plays a key role in coordinating root uptake of ammonium and BR-dependent plant growth gene expression regulation. Our study further elucidated a relationship between the two key factors BZR1 and BRI1 in the BR signaling pathway associated with regulation of *AMT1;2* gene expression and demonstrated that BZR1 was localized downstream of the *BRI1* during regulation of *AMT1;2* expression. It has been reported that BZR1 act as an integrator or master regulator to regulate plant growth, development, and immunity by directly interacting with key proteins from hormone signaling, stress signaling, cell elongation, flowering,

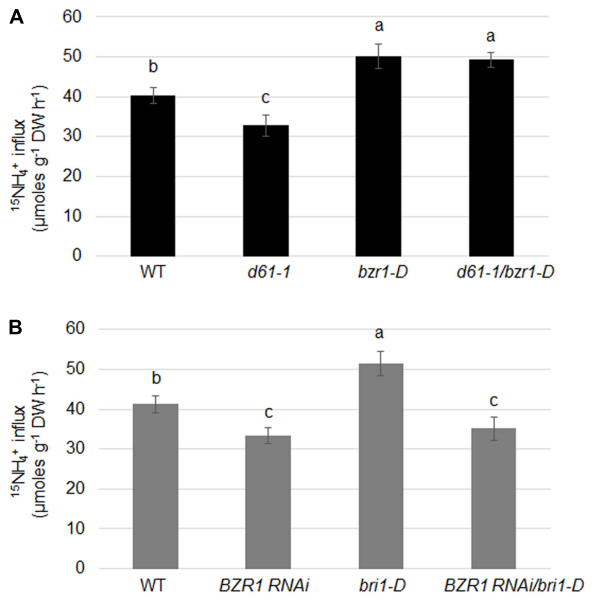

FIGURE 7 | BRI1 and BZR1 effects on NH_4^+ uptake in plants. **(A)** $^{15}NH_4^+$ abundance in total ^{15}N in roots of wild-type, *BRI1* mutant *d61-1*, gain-of-function mutant *bzr1-D*, and their cross offspring *d61-1/bzr1-D* plants. **(B)** $^{15}NH_4^+$ abundance in total ^{15}N in roots of wild-type, *BZR1 RNAi*, *BRI1* overexpression line *bri1-D*, and their cross offspring *BZR1 RNAi/bri1-D* plants. The 2-week-old hydroponic seedlings were further transferred and cultured in nitrogen-free nutrient solution. Three days later, plant roots were immersed in 200 μM ^{15}N-labeled NH_4^+ nutrient solution for 6 min. The rate of ammonium uptake by the roots was then determined. $^{15}NH_4^+$ abundance in total ^{15}N in roots was measured after 6 min of $^{15}NH_4^+$ uptake. Bars represent means ± SD (n = 6). The experiments were repeated at least three times. Different letters represent statistically significant differences ($P < 0.05$).

immune signaling and so on (Eunkyoo et al., 2012; Lozano-Duran et al., 2013; Eunkyoo et al., 2014; Li and He, 2015; Nolan et al., 2017; Tian et al., 2018). However, whether BZR1 functions as heterodimer to regulate *AMT1;2* needs to be further analyzed.

Ammonium strongly induces expression of *AMT1;1* and *AMT1;2,* the two major AMTs in rice roots. However, the molecular mechanism of ammonium-mediated *AMT1* gene expression is not clear. The present results on the effect of BRI1 on NH_4^+-induction of these genes suggest a complex mechanism for the regulation of *AMT1* expression. Nonetheless, our results further support the existence of a common genetic component between plant nutrient uptake and the hormonal regulatory mechanisms involved in plant growth and development. In the current study, we found that although *AMT1;1* responded to BR treatment and its expression was induced in roots, BZR1 does not appear to have the ability to regulate *AMT1;1* expression. Different expression patterns were observed during the response of each member of the *AMT1* gene family to BR processing. These findings suggest that different BR-mediated regulatory circuits may have different effects on the same *AMT1* gene.

In addition, a recent study has shown that NH_4^+-induced miR444 positively regulates BR biosynthesis to regulate rice root growth. This microRNA targets five MADS-box transcription repressors directly upstream of *BR-deficient dwarf 1* (*OsBRD1*), a key BR biosynthetic gene (Jiao et al., 2020), suggesting NH_4^+ signaling also activates BR biosynthesis. Together with our results, we propose that there is a complicated feedback regulatory mechanism between NH_4^+ and BR signaling. It would be useful to investigate the effects of NH_4^+ on BZR1 protein levels or modifications in the future. Our study also found a highly complex interaction between plant hormone signaling and nutrient absorption pathways. These complex regulatory networks involved in ammonium uptake in plants require further genetic and molecular studies to elucidate their detailed mechanisms.

CONCLUSION

Brassinosteroids play diverse functions in plant growth and development. In this study, we examined the role of BRs in ammonium uptake in rice. The data indicate that BR signaling activates *AMT1;1* and *AMT1;2* expression in the presence of the BR receptor BRI1, and the BR signaling transcription factor BZR1 directly activates *AMT1;2*. The further genetic study revealed that BZR1 activates *AMT1;2* expression downstream of *BRI1* to improve ammonium uptake in rice. These results indicate that BR signaling positively controls ammonium uptake partially via BZR1-mediated activation of *AMT1;2*, one of the key AMTs. Our analyses extend the knowledge of the BR-regulating module and its role in the regulation of nitrogen uptake in rice plants.

DATA AVAILABILITY STATEMENT

The original contributions presented in the study are included in the article/supplementary material, further inquiries can be directed to the corresponding author/s.

AUTHOR CONTRIBUTIONS

SY, YZ, and DY conceived this project. QS and YX provided the experimental design ideas and plant materials. YZ, SY, and DY carried out the experiments and generated the data. QS, YX, and DY contributed to the summary and analysis of the data. QS, YX, YZ, and SY wrote the manuscript. All authors contributed to the article and approved the submitted version.

FUNDING

This work was supported by the Support Plan for Innovative Talents in Colleges and Universities of Liaoning Province (LR2017037) and Natural Science Foundation of Liaoning Province (2020-YQ-05).

REFERENCES

Abiko, T., Obara, M., Ushioda, A., Hayakawa, T., Hodges, M., and Yamaya, T. (2005). Localization of NAD-isocitrate dehydrogenase and glutamate dehydrogenase in rice roots: candidates for providing carbon skeletons to NADH-glutamate synthase. *Plant Cell Physiol.* 46, 1724–1734. doi: 10.1093/pcp/pci188

Bai, M. Y., Zhang, L. Y., Gampala, S. S., Zhu, S. W., Song, W. Y., Chong, K., et al. (2007). Functions of OsBZR1 and 14-3-3 proteins in brassinosteroid signaling in rice. *Proc. Natl. Acad. Sci. U.S.A.* 104, 13839–13844. doi: 10.1073/pnas.0706386104

Bao, A., Liang, Z., Zhao, Z., and Cai, H. (2015). Overexpressing of OsAMT1-3, a high affinity ammonium transporter gene, modifies rice growth and carbon-nitrogen metabolic status. *Int. J. Mol. Sci.* 16, 9037–9063. doi: 10.3390/ijms16059037

Eunkyoo, O., Zhu, J. Y., Bai, M. Y., Augusto, A. R., Yu, S., and Wang, Z. Y. (2014). Cell elongation is regulated through a central circuit of interacting transcription factors in the *Arabidopsis hypocotyl*. *eLife* 3:e03031. doi: 10.7554/eLife.03031

Eunkyoo, O., Zhu, J. Y., and Wang, Z. Y. (2012). Interaction between BZR1 and PIF4 integrates brassinosteroid and environmental responses. *Nat. Cell Biol.* 14, 802–809. doi: 10.1038/ncb2545

Giehl, R. F. H., Laginha, A. M., Duan, F., Rentsch, D., Yuan, L., and von Wiren, N. (2017). A critical role of AMT2;1 in root-to-shoot translocation of ammonium in *Arabidopsis*. *Mol. Plant* 10, 1449–1460. doi: 10.1016/j.molp.2017.10.001

Goda, H., Sawa, S., Asami, T., Fujioka, S., Shimada, Y., and Yoshida, S. (2004). Comprehensive comparison of auxin-regulated and brassinosteroid-regulated genes in *Arabidopsis*. *Plant Physiol.* 134, 1555–1573. doi: 10.1104/pp.103.034736

Guo, H., Li, L., Aluru, M., Aluru, S., and Yin, Y. (2013). Mechanisms and networks for brassinosteroid regulated gene expression. *Curr. Opin. Plant Biol.* 16, 545–553. doi: 10.1016/j.pbi.2013.08.002

Je, B. I., Piao, H. L., Park, S. J., Park, S. H., Kim, C. M., Xuan, Y. H., et al. (2010). RAV-Like1 maintains brassinosteroid homeostasis via the coordinated activation of BRI1 and biosynthetic genes in rice. *Plant Cell* 22, 1777–1791. doi: 10.1105/tpc.109.069575

Jeong, D. H., An, S., Kang, H. G., Moon, S., Han, J. J., Park, S., et al. (2002). T-DNA insertional mutagenesis for activation tagging in rice. *Plant Physiol.* 130, 1636–1644. doi: 10.1104/pp.014357

Jiao, X., Wang, H., Yan, J., Kong, X., Liu, Y., Chu, J., et al. (2020). Promotion of BR biosynthesis by miR444 is required for ammonium-triggered inhibition of root growth. *Plant Physiol.* 182, 1454–1466. doi: 10.1104/pp.19.00190

Kim, T. W., and Wang, Z. Y. (2010). Brassinosteroid signal transduction from receptor kinases to transcription factors. *Annu. Rev. Plant Biol.* 61, 681–704. doi: 10.1146/annurev.arplant.043008.092057

Kumar, A., Silim, S. N., Okamoto, M., Siddiqi, M. Y., and Glass, A. D. (2003). Differential expression of three members of the AMT1 gene family encoding putative high-affinity NH4+ transporters in roots of *Oryza sativa* subspecies indica. *Plant Cell Environ.* 26, 907–914. doi: 10.1046/j.1365-3040.2003.01023.x

Lanquar, V., Loque, D., Hormann, F., Yuan, L., Bohner, A., Engelsberger, W. R., et al. (2009). Feedback inhibition of ammonium uptake by a phospho-dependent allosteric mechanism in *Arabidopsis*. *Plant Cell* 21, 3610–3622. doi: 10.1105/tpc.109.068593

Li, J., and Chory, J. (1997). A putative leucine-rich repeat receptor kinase involved in brassinosteroid signal transduction. *Cell* 90, 929–938. doi: 10.1016/S0092-8674(00)80357-8

Li, J., Wen, J., Lease, K. A., Doke, J. T., Tax, F. E., and Walker, J. C. (2002). BAK1, an *Arabidopsis* LRR receptor-like protein kinase, interacts with BRI1 and modulates brassinosteroid signaling. *Cell* 110, 213–222. doi: 10.1016/S0092-8674(02)00812-7

Li, Q. F., and He, J. X. (2015). BZR1 interacts with HY5 to mediate brassinosteroid- and lightregulated cotyledon opening in *Arabidopsis* in darkness. *Mol. Plant* 9, 113–125.

Loque, D., and von Wiren, N. (2004). Regulatory levels for the transport of ammonium in plant roots. *J. Exp. Bot.* 55, 1293–1305. doi: 10.1093/jxb/erh147

Lozano-Duran, R., Macho, A. P., Boutrot, F., Segonzac, C., Somssich, I. E., and Zipfel, C. (2013). The transcriptional regulator BZR1 mediates trade-off between plant innate immunity and growth. *elife* 2:e00983. doi: 10.7554/eLife.00983

Nam, K. H., and Li, J. (2002). BRI1/BAK1, a receptor kinase pair mediating brassinosteroid signaling. *Cell* 110, 203–212. doi: 10.1016/S0092-8674(02)00814-0

Nolan, T. M., Brennan, B., Yang, M., Chen, J., Zhang, M., Li, Z., et al. (2017). Selective autophagy of BES1 mediated by DSK2 balances plant growth and survival. *Dev. Cell* 41, 33–46. doi: 10.1016/j.devcel.2017.03.013

Oliveira, I. C., Brears, T., Knight, T. J., Clark, A., and Coruzzi, G. M. (2002). Overexpression of cytosolic glutamine synthetase. Relation to nitrogen, light, and photorespiration. *Plant Physiol.* 129, 1170–1180. doi: 10.1104/pp.020013

Qiao, S., Sun, S., Wang, L., Wu, Z., Li, C., Li, X., et al. (2017). The RLA1/SMOS1 Transcription factor functions with OsBZR1 to regulate brassinosteroid signaling and rice architecture. *Plant Cell* 29, 292–309. doi: 10.1105/tpc.16.00611

Ranathunge, K., El-Kereamy, A., Gidda, S., Bi, Y. M., and Rothstein, S. J. (2014). AMT1;1 transgenic rice plants with enhanced NH4(+) permeability show superior growth and higher yield under optimal and suboptimal NH4(+) conditions. *J. Exp. Bot.* 65, 965–979. doi: 10.1093/jxb/ert458

Ren, Y., Tian, X., Li, S., Mei, E., He, M., Tang, J., et al. (2020). *Oryza sativa* mediator subunit OsMED25 interacts with OsBZR1 to regulate brassinosteroid signaling and plant architecture in rice. *J. Integr. Plant Biol.* 62, 793–811. doi: 10.1111/jipb.12914

Sonoda, Y., Ikeda, A., Saiki, S., von Wiren, N., Yamaya, T., and Yamaguchi, J. (2003a). Distinct expression and function of three ammonium transporter genes (OsAMT1;1-1;3) in rice. *Plant Cell Physiol.* 44, 726–734. doi: 10.1093/pcp/pcg083

Sonoda, Y., Ikeda, A., Saiki, S., Yamaya, T., and Yamaguchi, J. (2003b). Feedback regulation of the ammonium transporter gene family AMT1 by glutamine in rice. *Plant Cell Physiol.* 44, 1396–1402. doi: 10.1093/pcp/pcg169

Straub, T., Ludewig, U., and Neuhauser, B. (2017). The Kinase CIPK23 inhibits ammonium transport in *Arabidopsis thaliana*. *Plant Cell* 29, 409–422. doi: 10.1105/tpc.16.00806

Suenaga, A., Moriya, K., Sonoda, Y., Ikeda, A., Von Wiren, N., Hayakawa, T., et al. (2003). Constitutive expression of a novel-type ammonium transporter OsAMT2 in rice plants. *Plant Cell Physiol.* 44, 206–211. doi: 10.1093/pcp/pcg017

Tian, Y., Min, F., Qin, Z., Lv, H., and Bai, M. Y. (2018). Hydrogen peroxide positively regulates brassinosteroid signaling through oxidation of the BRASSINAZOLE-RESISTANT1 transcription factor. *Nat. Commun.* 9:1063. doi: 10.1038/s41467-018-03463-x

Tong, H., and Chu, C. (2018). Functional specificities of brassinosteroid and potential utilization for crop improvement. *Trends Plant Sci.* 23, 1016–1028. doi: 10.1016/j.tplants.2018.08.007

Wang, Z. Y., Nakano, T., Gendron, J., He, J., Chen, M., Vafeados, D., et al. (2002). Nuclear-localized BZR1 mediates brassinosteroid-induced growth and feedback suppression of brassinosteroid biosynthesis. *Dev. Cell* 2, 505–513. doi: 10.1016/S1534-5807(02)00153-3

Xuan, Y. H., Duan, F. Y., Je, B. I., Kim, C. M., Li, T. Y., Liu, J. M., et al. (2016). Related to ABI3/VP1-Like 1(RAVL1) regulates brassinosteroid-mediated activation of AMT1;2 in rice (*Oryza sativa*). *J. Exp. Bot.* 68, 727–737. doi: 10.1093/jxb/erw442

Xuan, Y. H., Priatama, R. A., Huang, J., Je, B. I., Liu, J. M., Park, S. J., et al. (2013). Indeterminate domain 10 regulates ammonium-mediated gene expression in rice roots. *New Phytol.* 197, 791–804. doi: 10.1111/nph.12075

Yamaguchi, M., Ohtani, M., Mitsuda, N., Kubo, M., Ohme-Takagi, M., Fukuda, H., et al. (2010). VND-INTERACTING2, a NAC domain transcription factor, negatively regulates xylem vessel formation in *Arabidopsis*. *Plant Cell* 22, 1249–1263. doi: 10.1105/tpc.108.064048

Yamamuro, C., Ihara, Y., Wu, X., Noguchi, T., Fujioka, S., Takatsuto, S., et al. (2000). Loss of function of a rice brassinosteroid insensitive1 homolog prevents internode elongation and bending of the lamina joint. *Plant Cell* 12, 1591–1605. doi: 10.2307/3871176

Yang, C. J., Zhang, C., Lu, Y. N., Jin, J. Q., and Wang, X. L. (2011). The mechanisms of brassinosteroids' action: from signal transduction to plant development. *Mol. Plant* 4, 588–600. doi: 10.1093/mp/ssr020

Yin, Y., Wang, Z. Y., Mora-Garcia, S., Li, J., Yoshida, S., Asami, T., et al. (2002). BES1 accumulates in the nucleus in response to brassinosteroids to regulate

gene expression and promote stem elongation. *Cell* 109, 181–191. doi: 10.1016/S0092-8674(02)00721-3

Yoo, S.-D., Cho, Y.-H., and Sheen, J. (2007). *Arabidopsis mesophyll* protoplasts: a versatile cell system for transient gene expression analysis. *Nat. Protoc.* 2, 1565–1572. doi: 10.1038/nprot.2007.199

Yu, X., Li, L., Zola, J., Aluru, M., Ye, H., Foudree, A., et al. (2011). A brassinosteroid transcriptional network revealed by genome-wide identification of BESI target genes in *Arabidopsis thaliana*. *Plant J.* 65, 634–646. doi: 10.1111/j.1365-313X.2010.04449.x

Yuan, L., Gu, R., Xuan, Y., Smith-Valle, E., Loque, D., Frommer, W. B., et al. (2013). Allosteric regulation of transport activity by heterotrimerization of *Arabidopsis ammonium* transporter complexes in vivo. *Plant Cell* 25, 974–984. doi: 10.1105/tpc.112.108027

Yuan, L., Loque, D., Ye, F., Frommer, W. B., and von Wiren, N. (2007). Nitrogen-dependent posttranscriptional regulation of the ammonium transporter AtAMT1;1. *Plant Physiol.* 143, 732–744. doi: 10.1104/pp.106.093237

Conflict of Interest: The authors declare that the research was conducted in the absence of any commercial or financial relationships that could be construed as a potential conflict of interest.

Copyright © 2021 Yang, Yuan, Zhang, Sun and Xuan. This is an open-access article distributed under the terms of the Creative Commons Attribution License (CC BY). The use, distribution or reproduction in other forums is permitted, provided the original author(s) and the copyright owner(s) are credited and that the original publication in this journal is cited, in accordance with accepted academic practice. No use, distribution or reproduction is permitted which does not comply with these terms.

frontiers in Plant Science

ORIGINAL RESEARCH
published: 14 September 2021
doi: 10.3389/fpls.2021.672702

Enzymology and Regulation of δ^1-Pyrroline-5-Carboxylate Synthetase 2 From Rice

*Giuseppe Sabbioni[1], Dietmar Funck[2] and Giuseppe Forlani[1]**

[1]Department of Life Science and Biotechnology, University of Ferrara, Ferrara, Italy, [2]Plant Physiology and Biochemistry Laboratory, Department of Biology, University of Konstanz, Konstanz, Germany

Under several stress conditions, such as excess salt and drought, many plants accumulate proline inside the cell, which is believed to help counteracting the adverse effects of low water potential. This increase mainly relies upon transcriptional induction of δ^1-pyrroline-5-carboxylate synthetase (P5CS), the enzyme that catalyzes the first two steps in proline biosynthesis from glutamate. P5CS mediates both the phosphorylation of glutamate and the reduction of γ-glutamylphosphate to glutamate-5-semialdehyde, which spontaneously cyclizes to δ^1-pyrroline-5-carboxylate (P5C). In most higher plants, two isoforms of P5CS have been found, one constitutively expressed to satisfy proline demand for protein synthesis, the other stress-induced. Despite the number of papers to investigate the regulation of P5CS at the transcriptional level, to date, the properties of the enzyme have been only poorly studied. As a consequence, the descriptions of post-translational regulatory mechanisms have largely been limited to feedback-inhibition by proline. Here, we report cloning and heterologous expression of P5CS2 from *Oryza sativa*. The protein has been fully characterized from a functional point of view, using an assay method that allows following the physiological reaction of the enzyme. Kinetic analyses show that the activity is subjected to a wide array of regulatory mechanisms, ranging from product inhibition to feedback inhibition by proline and other amino acids. These findings confirm long-hypothesized influences of both, the redox status of the cell and nitrogen availability, on proline biosynthesis.

Keywords: proline biosynthesis, substrate affinity, product inhibition, enzyme regulation, redox status, NADPH/NADP$^+$ ratio

OPEN ACCESS

Edited by:
Omar Borsani,
Universidad de la República, Uruguay

Reviewed by:
Donald Becker,
University of Nebraska-Lincoln,
United States
Ernesto Cuevasanta,
Universidad de la República, Uruguay

***Correspondence:**
Giuseppe Forlani
flg@unife.it

Specialty section:
This article was submitted to Plant Abiotic Stress, a section of the journal Frontiers in Plant Science

Received: *26 February 2021*
Accepted: *10 August 2021*
Published: *14 September 2021*

Citation:
Sabbioni G, Funck D and Forlani G (2021) Enzymology and Regulation of δ^1-Pyrroline-5-Carboxylate Synthetase 2 From Rice. Front. Plant Sci. 12:672702. doi: 10.3389/fpls.2021.672702

INTRODUCTION

Water stress tolerance is a major goal for plant genetic improvement, and most likely a need to secure crop productivity threatened by ongoing climate changes (Ahanger et al., 2017). As soon as a lowering in soil water potential hinders water absorption at the root level, plants react by closing stomata and activate a series of mechanisms for osmotic compensation, among which a pivotal role is played by the accumulation of the so-called compatible osmolytes (Sharma et al., 2019). These osmoprotectants include sugars (Iordachescu and Imai, 2008), tertiary amines (Annunziata et al., 2019), and amino acids (Hildebrandt, 2018). Among amino acids, accumulation of the cyclic amino acid proline is the most widespread in plants and

other organisms (Verbruggen and Hermans, 2008; Meena et al., 2019). However, there are a number of reports indicating that the concentrations of accumulated proline are not high enough to contribute significantly to osmotic adjustment (e.g., Forlani et al., 2019a). Free proline is rapidly accumulated not only in response to drought and salinity, but also to cold, heavy metals, or pathogen attack (Hayat et al., 2012). Because of this variety of inducing stimuli, several other beneficial effects of proline have been hypothesized, ranging from stabilization of membranes and enzymes to reactive oxygen species scavenging, regulation of redox balance, or induction of antioxidant defenses (Liang et al., 2013; Kishor and Sreenivasulu, 2014; Govrin et al., 2019; Forlani et al., 2019b).

Whatever the exact, multifaceted role in the plant response to adverse conditions, stress-induced accumulation of proline has been shown to depend mainly upon an increase of its biosynthetic rate (Trovato et al., 2019). Several pathways have been described for the biosynthesis of this amino acid, being those from glutamate or ornithine as the major routes (Fichman et al., 2015). In bacteria, proline synthesis from glutamate is accomplished by three enzymes: γ-glutamyl kinase (EC 2.7.2.11) that catalyzes glutamate phosphorylation, NADPH-dependent γ-glutamyl phosphate reductase (EC1.2.1.41) that reduces the product to glutamate semialdehyde, which in solution spontaneously cyclizes to δ^1-pyrroline-5-carboxylate (P5C), and P5C reductase (EC1.5.1.2) that produces proline, using either NADH or NADPH as the electron donor (Chen et al., 2006; Csonka and Leisinger, 2007; Forlani et al., 2017). In higher plants, the first two steps were found to be catalyzed by a single bifunctional enzyme bearing both catalytic domains of glutamyl kinase and glutamyl-phosphate reductase, P5C synthetase (P5CS; Hu et al., 1992; Rai and Penna, 2013). Another plant enzyme able to synthesize glutamate semialdehyde was similarly isolated by trans-complementation of *proBA* mutants (Delauney et al., 1993). Because of the occurrence of such an ornithine-δ-aminotransferase (EC 2.6.1.13) and of the finding that mammalian P5CS is feedback-inhibited by ornithine (Hu et al., 1999), it was hypothesized that under conditions of osmotic stress and nitrogen limitation proline synthesis in plants proceeds through the glutamate pathway, while the ornithine pathway assumes prominence under high nitrogen input (Delauney and Verma, 1993; Anwar et al., 2018). Although some confirmatory results have been reported (Da Rocha et al., 2012), other findings have shown that ornithine-derived P5C is oxidized to glutamate in the mitochondrion (Funck et al., 2008; Winter et al., 2015), and – at least in *Arabidopsis* – proline biosynthesis is now believed to proceed exclusively *via* the glutamate pathway. Consistently, induction of *P5CS* was found in virtually all cases in which proline accumulation occurred in response to the exposure to stress conditions (Trovato et al., 2019).

Isolation and sequencing of *P5CS* led to the identification of two isogenes in several plant species and phylogenetic analyses demonstrated that *P5CS* duplication occurred independently in several taxonomic groups (Turchetto-Zolet et al., 2008; Rai and Penna, 2013, Fichman et al., 2015). These paralogs (named P5CS1 and P5CS2) showed non-overlapping roles, with varying temporal and spatial expression patterns. In *Arabidopsis thaliana*, *AtP5CS1* is expressed in most plant organs, whereas *AtP5CS2* is predominantly expressed in areas of active cell division (Strizhov et al., 1997; Székely et al., 2008). The analysis of GFP-fused proteins suggested partial chloroplastic localization of PCS1, whereas P5CS2:GFP was predominantly found in the cytosol (Székely et al., 2008). However, more recent data conclusively demonstrated a cytosolic localization of both isoenzymes (Funck et al., 2020). Transcription of the *P5CS* genes was differentially induced by drought, salinity, and abscisic acid and, consistently, the occurrence of a wide but different array of putative transcription factor binding sites was shown in the promoters of the two paralogs (Fichman et al., 2015; Zarattini and Forlani, 2017).

Knockout *p5cs1* mutants showed reduced proline synthesis under stress, hypersensitivity to salt stress, and accumulation of reactive oxygen species, whereas *p5cs2* mutations caused embryo abortion during late stages of seed development (Székely et al., 2008). Germination and establishment under ambient conditions, but not susceptibility to infection with *Pseudomonas syringae*, were impaired in *p5cs2* mutants, whereas stress-induced proline accumulation was much less affected than in *p5cs1* mutants (Funck et al., 2020). Overall, AtP5CS1 has therefore been identified as the major contributor to stress-induced proline accumulation, whereas AtP5CS2 plays a pivotal role in embryo development and growth. The rice (*Oryza sativa*) genome also contains two *P5CS* isogenes, which seem to have a somehow less defined role. *P5CS1*, located on chromosome 1, was induced by stress conditions, such as the exposure to salt, dehydration, and cold. *P5CS2*, mapping on chrosomome 5, was expressed in mature plant parts, yet it was also induced by salt and mannitol treatments (Rai and Penna, 2013; Forlani et al., 2015a).

Contrary to the large amount of information available on the regulation of *P5CS* gene expression in different plant tissues, during development and in response to environmental signals, very little is known about the biochemical features of P5CS isoenzymes and the occurrence of post-translational regulatory mechanisms. The activity of a single enzyme cloned from *Vigna aconitifolia* showed 50%-inhibition at 6 mM proline (Hu et al., 1992). The activity of the same enzyme and of a proline-insensitive form obtained by site-directed mutagenesis was characterized in more detail afterward, showing K_m values for glutamate and ATP of 3.6 and 2.7 mM, respectively (Zhang et al., 1995). However, these data were obtained using an assay method that measures only the partial glutamyl kinase activity, and not the full forward reaction catalyzed by the enzyme. Another study on the effect of osmotic stress on P5CS activity in *Arabidopsis* leaves used quantification of the inorganic phosphate released after glutamyl-phosphate reduction (Parre et al., 2010). An assay that follows the glutamate- and ATP-dependent oxidation of NADPH was used to analyze the activity of a recombinantly expressed putative P5CS from tomato, which has later been identified as a bacterial contamination in the cDNA library used (García-Ríos et al., 1997). A similar

assay has also been used to demonstrate the activity of P5CS overexpressed in switchgrass (*Panicum virgatum*; Guan et al., 2019). However, proper controls were not performed in any of these studies to test if the detected activity was influenced by the presence in the crude extracts of glutamine synthetase (EC 6.3.1.2), which also catalyzes the phosphorylation of glutamate and releases phosphate in the presence of even low concentrations of ammonia (Forlani et al., 2006). To the best of our knowledge, neither kinetic analysis of plant P5CS activity has been reported, nor the functional features of P5CS isozyme pairs have been investigated and compared so far. As a consequence, some long lasting hypotheses linking modulation of proline biosynthesis with either the nitrogen status (Delauney et al., 1993; Delauney and Verma, 1993) or the redox status (Sharma et al., 2011; Shinde et al., 2016) of the cell still await substantiation. Here, we report cloning, recombinant expression, purification, and functional characterization of P5CS2 from rice, providing a first body of evidence toward this goal.

MATERIALS AND METHODS

Cloning, Heterologous Expression, and Purification of Rice P5CS2

The coding sequence of *O. sativa* P5C synthetase 2 (locus Os05g38150; protein ID BAG95649) was amplified by PCR from cDNA clone J033099M14 (RGRC-NIAS) with the primers P5CS2-fw (caccATGGCGAGCGTCGACCCGT) and P5CS2-rev (agcatttgaccTCATTGCAAAG), and inserted by directional TOPO cloning into the expression vector pET151 that provides an N-terminal His_6-tag (Life Technologies, Carlsbad, CA, United States). For heterologous expression, *Escherichia coli* BL21(DE3) pLysS cells (Invitrogen, Carlsbad, CA, United States), made competent by the calcium chloride method, were transformed with the resulting vector pET151-*Os*P5CS2. Transformants were selected on LB plates containing 100 mg L^{-1} ampicillin and 50 mg L^{-1} chloramphenicol. After inducing the expression of the plant protein at 24°C by the addition of 1 mM IPTG to liquid LB medium, the cells were harvested by centrifugation and extracted by either sonication or grinding with 2 g g^{-1} alumina in a mortar at 4°C in extraction buffer (50 mM Na phosphate buffer, pH 7.5, containing 200 mM NaCl, 5 mM DTT, and 20 mM imidazole). The clarified extract was loaded at a constant flow of 10 ml h^{-1} onto a His-SpinTrap™ Nickel Sepharose Gel column (GE Healthcare, Little Chalfont, United Kingdom; 0.1 ml bed volume) for purification of the His-tagged protein. Stepwise washing and elution was achieved by increasing concentrations of imidazole in extraction buffer, while collecting 1-ml fractions. For activity assays, the purified enzyme was diluted into assay buffer (see below).

Alternatively, cells were extracted in 20 mM Tris-HCl buffer, pH 7.5, containing 5 mM DTT. Following centrifugation for 5 min at 10.000 *g*, the soluble extract was desalted by passage through a BioGel P6DG (BioRad) column, and loaded onto a DEAE-Sephacel (Pharmacia) column (1.5 cm diameter, 10 ml bed volume) equilibrated with the same buffer at a constant flow of 30 ml h^{-1}. The column was then eluted with a linear gradient from 0 to 250 mM NaCl (200 ml), for the collection of 4-ml fractions.

The His_6-tag was cleaved by treatment with His-tagged TEV protease (final concentration 0.1 mg ml^{-1}) for 20 min at pH 7.5. To remove TEV protease and the cleaved fragment, a negative chromatography on the same His-SpinTrap™ Nickel Sepharose Gel column was carried out after diluting the sample to lower imidazole concentration. Protein concentration was determined by the method of Bradford (1976), using bovine serum albumin as the standard. Enzyme preparations were stored at 4°C in the dark.

P5C Synthetase Assay

Glutamyl Kinase Assay

Glutamyl kinase assay was performed as described previously (Campanile et al., 1993), with minor modifications. Enzyme preparations (about 2 µg protein) were incubated up to 30 min at 30°C with 20 mM glutamate, 4 mM ATP, and 100 mM hydroxylamine hydrochloride in 50 mM Tris-HCl buffer, pH 7.5, in a final volume of 75 µl. The reaction was terminated by the addition of 150 µl of a colorimetric mixture consisting of 10% (w/v) $FeNO_3 \times 9\ H_2O$, 6.67% (v/v) HCl, and 5% (w/v) trichloroacetic acid. Following centrifugation for 3 min at 12,000 *g*, samples were read at 535 nm against non-incubated blanks. The γ-glutamyl-hydroxamate formed was quantified on the basis of a calibration curve obtained with an authentic standard.

Glutamyl Phosphate Reductase Assay

To determine glutamyl phosphate reductase activity (Campanile et al., 1993), enzyme preparations (about 2 µg protein) were incubated up to 20 min at 30°C with 2 mM DL-P5C, 5 mM $NADP^+$, and 10 mM K_2HPO_4 in 50 mM Tris-HCl buffer, pH 7.5, in a final volume of 200 µl. The P5C-dependent formation of NADPH was followed by reading the samples at 1 min intervals at 340 nm against blanks in which P5C had been omitted. The amount of NADPH formed was quantified on the basis of a calibration curve obtained with an authentic standard. DL-P5C was synthesized by the periodate oxidation of δ-*allo*-hydroxylysine and purified by cation exchange chromatography on a 200–400 mesh Dowex AG50W-X4 column, as previously described (Forlani and Funck, 2020).

NADPH Oxidation Assay

The physiological, forward reaction of P5C synthetase was measured by following the glutamate-dependent oxidation of NADPH in the presence of ATP. Aliquots of the purified enzyme preparations (0.5–1 µg protein) were incubated in a final volume of 200 µl with 20 mM L-glutamate, 4 mM ATP, and 0.4 mM NADPH in 50 mM Tris-HCl buffer, pH 7.5. When aiming at the evaluation of the effect of chlorides on enzyme activity, Tris-HCl buffer concentration was lowered to 10 mM, or replaced with 10 mM potassium phosphate buffer, pH 7.5. Incubation proceeded at 30°C for up to 20 min. The decrease of absorbance at 340 nm was determined at 0.5 min intervals

against exact blanks in which glutamate had been omitted. Assays were either performed in cuvettes with 0.2 or 1 cm pathlength (UVette; Eppendorf, Milan, Italy), or in 96-microwell plates. In the former case, OD_{340} was determined with a Novaspec plus spectrophotometer (Amersham Biosciences, Milan, Italy) equipped with an UVette adaptor. In the latter case, the plate was equilibrated at 30°C prior to enzyme addition, and absorbance was measured using a Ledetect plate reader (Labexim, Lengau, Austria) equipped with a LED plugin at 340 nm. Each sample was carried out in triplicate (technical replications). Each determination was repeated with at least three different enzyme preparations (biological replications). Presented data refer to a single enzyme preparation, and are means ± SE over technical replicates. Linear and non-linear regressions of data, as well as kinetic constant values, were computed using Prism 6 for Windows, version 6.03 (GraphPad Software, San Diego, CA, United States).

Analytical Methods

For SDS-PAGE analysis, samples were denatured by boiling for 5 min in a treatment buffer consisting of 2% (w/v) SDS, 10% (v/v) glycerol, and 5% (v/v) β-mercaptoethanol in 62.5 mM Tris–HCl buffer, pH 6.8. Sample aliquots (10–40 μl) were subjected to discontinuous sodium dodecyl sulfate (SDS)-polyacrylamide gel electrophoresis (PAGE) at 8 mA with a 5% stacking and a 10% separating gel. For total protein analysis, *E. coli* cells were harvested by centrifugation and directly resuspended in treatment buffer at 10 optical units (600 nm) ml^{-1}. For soluble protein analysis, *E. coli* cells were harvested by centrifugation, resuspended in 20 mM Tris-HCl buffer (pH 7.5) at 20 optical units (600 nm) ml^{-1}, and sonicated with five 1-min pulses at 70% amplitude with a UP50H ultrasonic processor (Hielsher Ultrasonic, Teltow, Germany). Samples were centrifuged again, and the supernatant was treated with the same volume of 2X treatment buffer. Gels were stained for proteins with Quick Coomassie Stain (Neo Biotech, Nanterre, France).

Inclusion bodies were isolated by differential centrifugation according to Upadhyay et al. (2012). Solubilization of proteins from inclusion bodies was performed with the methods reported by Singh et al. (2015).

To obtain peptide mapping, the purified protein was subjected to SDS-PAGE and then excised, destained, digested with both trypsin and pepsin, and analyzed by reversed phase liquid chromatography-tandem mass spectrometry using an Esquire 3000 spectrometer (Bruker Daltonics), connected to an Agilent 1100 HPLC. After sample injection, the column was washed for 5 min with 90% mobile phase A (0.1% formic acid) and 10% mobile phase B (0.1% formic acid in acetonitrile), and peptides were eluted using a linear gradient from 10 to 80% mobile phase B in 20 min at 50 μl min^{-1}. The Esquire mass spectrometer was operated in a data-dependent mode in which each full MS scan was followed by three MS/MS scans where the three most abundant molecular ions were dynamically selected and fragmented by collision-induced dissociation. Dynamic exclusion was allowed.

RESULTS

Heterologous Expression of *Oryza sativa* P5C Synthetase 2 in *E. coli* and Affinity Purification of the Catalytically Active Protein

The gene coding in rice for the stress-induced P5CS isoenzyme 2 (protein ID O04226) was cloned into the expression vector pET151 and used to transform *E. coli* BL21(DE3) pLysS cells. Following the treatment with IPTG, glutamate and ATP-dependent NADPH oxidation activity was detectable in crude extracts, which was not present in extracts from either non-induced cells or induced cells transformed with the empty vector. Simultaneously, a pronounced band of the predicted molecular mass (81.5 kDa) became evident upon SDS-PAGE analysis of total protein samples prepared at increasing time after IPTG addition (**Figure 1A**). Preliminary attempts to purify the plant protein from induced cells harvested 10–24 h after induction failed, since negligible protein amounts were found in the eluate from Nickel Affinity Gel columns. To understand the reason for such a failure, the presence of the protein was investigated by gel electrophoresis of samples obtained by either directly resuspending bacterial cells with denaturing treatment buffer (total protein), or using supernatants obtained after cell sonication (soluble protein). Results showed that in total protein samples the band of interest reached a maximal amount about 4 h after induction, and remained constant thereafter. On the contrary, after reaching maximal amounts in a similar timeframe, its presence among soluble proteins declined at increasing time to lowest levels. Consistent patterns were obtained when specific activity levels of glutamate and ATP-dependent NADPH oxidation were measured in cell free extracts from parallel samples (**Figure 1B**). Because results were suggestive of a fast and complete sequestering of the heterologous protein in inclusion bodies, induction was performed at lower temperatures, down to 15°C, but this did not lead to substantial improvements. As an alternative approach, protein solubilization from inclusion bodies was performed. Several treatments were tried with this aim, such as 5% (v/v) DMSO or *n*-propanol or 0.5–2% (w/v) n-dodecyl-β-D-maltoside, but the best results were obtained with urea: extraction with 5–6 M urea allowed a quantitative recovery of the protein in the supernatant, and the inclusion of 6 M urea into column buffers afforded satisfactory yields from the subsequent affinity chromatography step (**Figure 1C**). However, despite the many attempts by means of dilution, dialysis, or column desalting protocols, renaturation of purified samples did not provide an active protein. Active P5CS2 protein was obtained only when non-denaturing extracts were prepared from cells harvested 3–5 h after IPTG treatment, when bacterial cultures were still in the mid-exponential phase of growth. Even in this case, the attainment of homogeneous preparations required a careful setup of elution conditions from the affinity column, and extensive washing with buffers containing 50 and 100 mM imidazole was necessary to resolve the plant enzyme from contaminant *E. coli* proteins that were also retained by the resin (**Figure 1D**).

The identity of the purified protein was confirmed by peptide mapping, from which a 55%-coverage was obtained

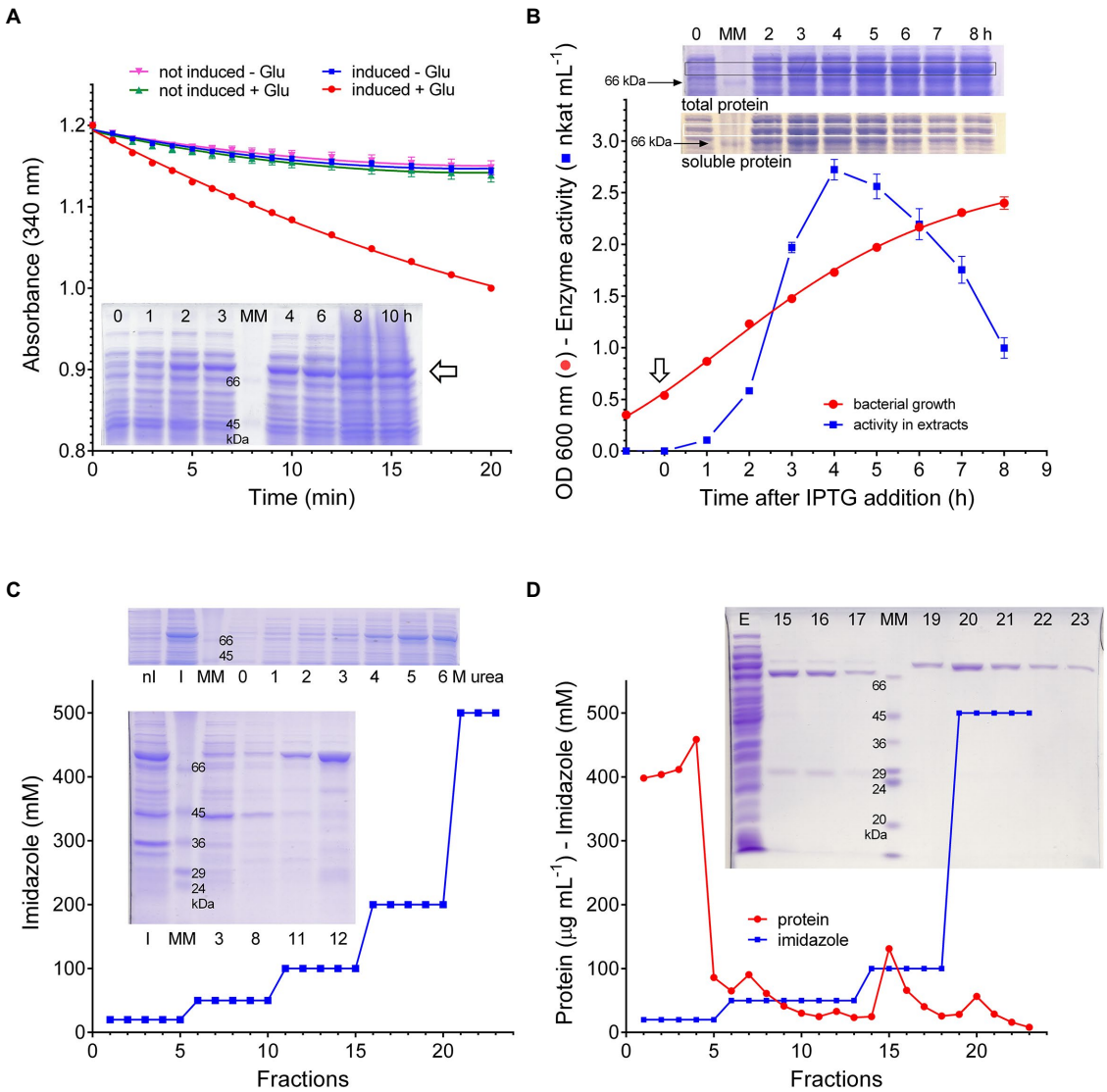

FIGURE 1 | Expression of rice *P5CS2* in *Escherichia coli*. Following the treatment with IPTG, extracts were prepared from bacterial cells transformed with the vector pET151-*Os*P5CS2. The measurement of NADPH oxidation in extracts prepared 4 h after induction showed the presence of a significant rate that was not evident neither in the absence of glutamate nor in extracts from non-induced cells. SDS-PAGE analysis of total protein from the same cultures, harvested at increasing time as indicated, disclosed the appearance of a new band (⇦) with a relative molecular mass (80 kDa) that was compatible with that expected for the recombinant protein **(A)**. When the time-course of the glutamate-dependent NADPH oxidation was measured, the attainment of maximal specific activity values was found 4–5 h after induction (⇩); thereafter, activity levels decreased progressively with time. Data are mean ± SE over triplicates. SDS-PAGE analysis of parallel samples, shown as insets, revealed a similar pattern for the 80 kDa band among soluble proteins; on the contrary, once the maximal levels was reached, it remains subsequently constant among total proteins **(B)**. Inclusion bodies were isolated by differential centrifugation from extracts from induced *E. coli* cells, and treated with increasing concentration of urea. SDS-PAGE analysis of the supernatant of the samples in this way obtained showed quantitative solubilization of the 80 kDa band at urea levels exceeding 4 M. Affinity chromatography in the presence of 6 M urea allowed the recovery of substantial levels of this protein, which eluted from the Ni^{++}-agarose column at 100 mM imidazole. The number of the lanes in the lower gel refers to the fraction of the eluate that was analyzed; nI, inclusion bodies from non-induced cells; I, induced cells; and MM, molecular weight markers **(C)**. Cell-free extracts were prepared from bacterial cells harvested 4 h after IPTG treatment, and extracts were loaded onto a Ni^{++}-agarose column. Proteins were then eluted by a stepwise imidazole gradient, and fractions were analyzed by SDS-PAGE. The samples eluted with 500 mM imidazole contained a single, homogeneous band with a relative molecular mass of about 80 kDa. Also in this case, numbers of the lanes in the gel refer to the fractions of the eluate that were analyzed; E, extract; MM, molecular weight markers **(D)**. All experiments were repeated three times on independent samples (biological replications), and very similar results were obtained.

(**Supplementary Figure S1**). The His_6-tail was removed by treatment with TEV protease and subsequent negative chromatography on the Nickel Affinity Gel column to get rid of the detached fragment and the protease. No differences were found in the enzymological features of the protein before and after the cleavage. Therefore, the removal was not carried out subsequently, also to avoid a consequent, partial loss of specific activity. The purified enzyme was in fact extremely

unstable, with a half-time of less than 24 h at 4°C (data not shown). Every attempt to identify stabilizing conditions failed. The only treatment that slightly increased the stability of recombinant P5CS2 was the addition of high concentrations of a reducing agent (dithiothreitol 5–10 mM) to extraction and column buffers, although in the latter case levels higher than 5 mM could not be used in order to avoid interference with the affinity gel. In the absence of dithiothreitol, activity was completely lost within 24 h. To overcome such drawback, small amounts of the protein were purified each day, and used for the characterization of the functional properties of the enzyme within 4–5 h after the isolation.

Activity Assays and Substrate Affinities

Rice P5CS2 was at first assayed with two colorimetric methods that had been previously described in the literature, i.e., the phosphorylation of glutamate in the presence of product-trapping hydroxylamine (glutamyl kinase assay), and the reverse, P5C-dependent reduction of $NADP^+$ in the presence of inorganic phosphate (glutamyl phosphate reductase assay). In both cases, activity was detectable when 1–2 μg of purified protein was incubated at 30°C up to 30 min. However, due to the low molar extinction coefficient of the glutamyl-hydroxamate assay (760 A_{535} M^{-1} cm^{-1}), very low absorbance values were obtained in the former case. In the latter, though the change in absorbance was much greater ($\varepsilon = 6{,}220$ A_{340} M^{-1} cm^{-1}), the activity rapidly lost linearity and was not proportional to the amount of enzyme, most likely because of the reversibility of the reaction. On the contrary, when all the three substrates (glutamate, ATP, and NADPH) were incubated with the purified protein (NADPH oxidation assay), a nearly linear rate of NADPH oxidation was detected at 340 nm (**Figure 2A**), which was significantly higher than both rates of the partial activities when data were expressed on a molar basis (**Figure 2B**). The simultaneous production of P5C was also verified (**Supplementary Figure S2**). Because this method measures in addition the full, physiological reaction, it was used thereafter throughout the characterization of the enzymological features of the enzyme. The presence of non-limiting ATP and glutamate concentrations was required to maintain a linear reaction rate over time. However, an initial burst of NADPH oxidation was evident even in the absence of one or both of the other substrates (**Figure 2C**). If equimolar amounts of NADPH were oxidized, similar results could imply the occurrence of a biphasic mechanism in which a rapid reaction of NADPH with the enzyme is followed by a slower steady-state process, in which glutamyl phosphate is produced and subsequently reduced to P5C. On the contrary, the amount of NADPH oxidized largely exceeded that of the enzyme in the reaction mixture, and the transfer of electrons to an enzyme-bound cofactor was not supported by the UV-vis spectrum of the purified protein (**Supplementary Figure S3**). The possibility therefore exists that such an initial burst may depend on a trace compound introduced with the enzyme or the buffer, which is rapidly reduced by NADPH. In any case, following a pre-incubation with the dinucleotide before the addition of glutamate and ATP, the resulting rate of NADPH oxidation was linear, and the rates in the stationary state with or without pre-incubation were comparable (**Supplementary Figure S4**). No detectable utilization of NADH was found, even at the highest concentration tested (0.5 mM). For the subsequent estimation of the steady state rate and the assessment of biochemical parameters and functional features, each sample was therefore read at 30 s intervals for 20 min against an exact blank in which glutamate had been omitted. The resulting difference in absorbance decreased almost linearly with time, and was strictly proportional to the amount of enzyme (**Figure 2D**). Under such standard assay conditions, a mean specific activity of 15.92 ± 0.43 nkat mg^{-1} protein ($n = 20$) was found.

Substrate affinities were evaluated by varying the concentration of a single substrate while maintaining the other substrates at saturating concentrations (20 mM glutamate, 4 mM ATP, and 0.4 mM NADPH, **Figures 3A–C**). Lineweaver-Burk plots of the results obtained in this way allowed estimation of apparent K_M values (**Table 1**). Consistent results were calculated in all cases for the maximal catalytic rate, with a V_{max} value of about 18 nkat (mg protein)$^{-1}$, which corresponds to only 1.5 catalytic events s^{-1}. Significant enzyme activity required the presence of 1–10 mM glutamate, 0.1–1 mM ATP, and 10–100 μM NADPH, but ATP concentrations exceeding 4 mM were found inhibitory (**Figure 3B**). Fitting the data to a substrate inhibition model ($Y = V_{max}{*}X/(K_{M(app)} + X{*}[1 + X/K_I])$, where V_{max} is the maximum enzyme velocity, if the substrate did not also inhibit enzyme activity, and K_I is the dissociation constant for substrate binding in such a way that two substrates can bind to an enzyme; equation 5.44 in Copeland, 2000) allowed calculation of a K_I value for ATP of 11.6 ± 5.1 mM. Multisubstrate enzymatic reactions may proceed through two different mechanisms, a sequential process in which the binding of all substrates must take place before the release of products, and a non-sequential or "ping-pong" mechanism in which one substrate binds, and one product is released before a second substrate binds, and a second product is released. Converging lines in a global Lineweaver-Burk plot (**Figure 3D**) are considered supportive of the former possibility. However, additional experiments to study the variation of apparent V_{max} and K_M while varying other substrates are needed to confirm the nature of the mechanism.

Product and Feed-Back Inhibition by Proline, Proline Analogues, and Metabolically Related Amino Acids

To evaluate the possible occurrence of post-translational regulative mechanisms, rice P5CS2 was assayed in the presence of increasing concentrations of products, analogues, and intermediates in proline synthesis, as well as other amino acids that are metabolically related, or represent an index of the nitrogen status of the cell. As expected, millimolar levels of proline were found inhibitory (**Figure 4A**), with a concentration inhibiting activity by 50% (IC_{50}) of less than 3 mM (**Table 2**). The four-atom ring analogue of proline, azetidine-2-carboxylate (A2CA), similarly inhibited P5CS2 activity, although with a 3.8-fold higher IC_{50}. Pipecolate, which

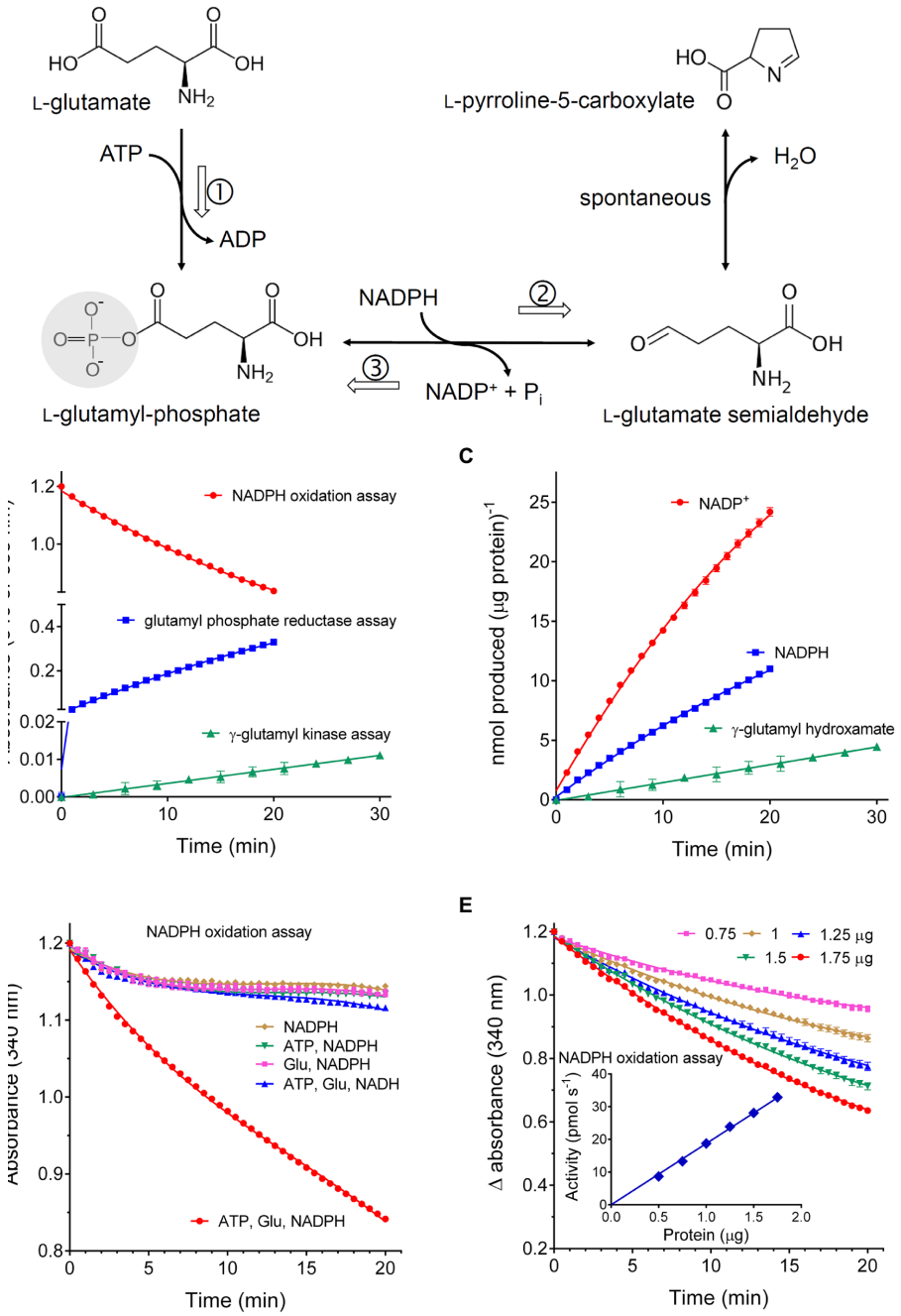

FIGURE 2 | Activity of recombinant rice P5C synthetase 2. **(A)** shows the reaction catalyzed by the enzyme: following glutamate phosphorylation and ADP release, glutamyl-phosphate is reduced using NADPH as the electron donor, yielding glutamate semialdehyde that spontaneously cyclizes to P5C. Three assay methods have been described: the glutamate kinase assay, which measures the formation of γ-glutamyl-hydroxamate in the absence of NADPH (①); the glutamyl-phosphate reductase assay, which follows the reverse, P5C- and Pi-dependent reduction of $NADP^+$ in the absence of glutamate (③); the NADPH oxidation assay in the presence of all three substrate, thereby following the full forward, physiological reaction of the enzyme (①+②). The purified protein was assayed with these three methods using aliquots corresponding to 2, 2, and 1 µg protein, respectively **(B)**. To obtain a quantitative comparison of the three methods, data in **(A)** were used to calculate the absolute amounts of the product formed in each case *per* µg of protein **(C)**. The NADPH oxidation assay was performed by incubating 1 µg of the purified protein with 0.4 mM NADPH in the presence of an array of all possible combinations of the other substrates. A mixture containing ATP and NADH instead of NADPH was also included. Non-limiting levels of all three substrates were required to maintain the rate of NADPH oxidation over time **(D)**. Because an initial burst of NADPH consumption was evident also in the absence of ATP and glutamate, the activity of increasing amounts of protein was measured against exact blanks in which glutamate had been omitted **(E)**. The inset shows that in this case activity values, calculated by interpolation of the linear rate of NADPH oxidation, were strictly proportional to the amount of the enzyme. In all cases, results are means ± SE over three technical replications. Each experiment was repeated three times with different enzyme preparations, obtaining very similar patterns.

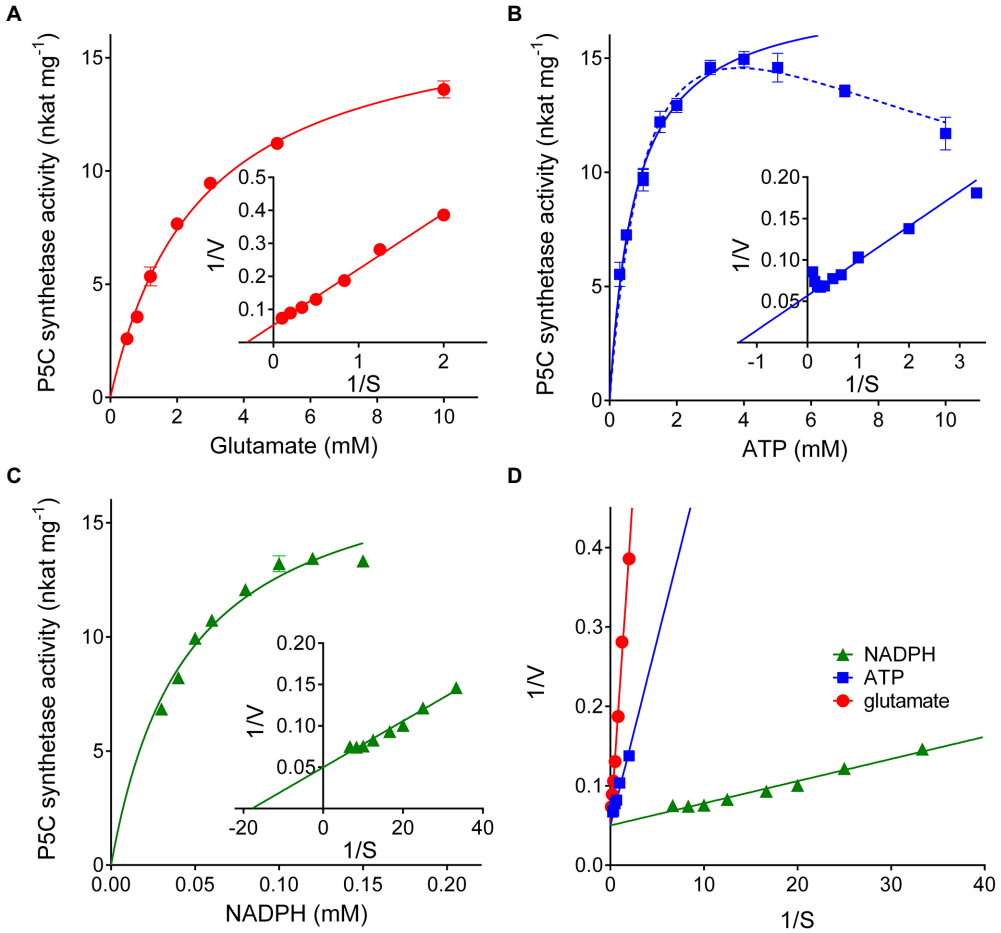

FIGURE 3 | Substrate affinity and catalytic properties of rice P5C synthetase 2. Enzyme activity was measured by the NADPH oxidation assay at varying the concentration of glutamate **(A)**, ATP **(B)**, or NADPH **(C)** while maintaining the fixed concentrations of the other substrates (20 mM glutamate, 4 mM ATP, and 0.4 mM NADPH). Lineweaver-Burk plots of data (the inset in each panel) allowed calculation of apparent affinities and V_{max} values (**Table 1**). Presented results are means ± SE over three technical replicates. The experiments were repeated three times with different enzyme preparations, obtaining very similar values. In panel **(B)**, the solid line refers to non-linear interpolation obtained by considering ATP concentrations up to 4 mM, whereas the dashed line is that obtained by considering all the experimental values using a substrate inhibition model. To gain information on the reaction mechanism of this multisubstrate enzyme, a combined Lineweaver-Burk graph was plotted **(D)**.

TABLE 1 | Kinetic properties of P5C synthetase 2 from rice.

Vmax (Glu)	17.38 ± 0.52	nkat (mg protein)$^{-1}$
Vmax (ATP)	17.96 ± 0.46	nkat (mg protein)$^{-1}$
Vmax (NADPH) steady-state rate	18.36 ± 0.64	nkat (mg protein)$^{-1}$
KM(app) for L-Glu	2.69 ± 0.19	mM
KM(app) for ATP*	0.764 ± 0.067	mM
KM(app) for NADPH steady-state rate	0.045 ± 0.004	mM

Value calculated from the Lineweaver-Burk plot of results obtained by considering ATP concentrations ≤ 4 mM. When all the results shown in* **Figure 3B *were considered using the inhibition model, a value of 1.29 ± 0.20 was instead found.*

differs from proline by an additional C-atom in the ring, was found completely ineffective in the range tested (**Figure 4A**). Up to 100 mM, D-proline was unable to interfere with the activity of P5CS2, whereas hydroxyproline and phosphonoproline showed partial inhibition (**Figure 4B**). On the whole, these results suggest that similarly-sized structural analogues of L-proline are able to bind to P5CS2 and mimic the feed-back inhibition of the enzyme.

Concerning the possibility that the P5CS2 may be subjected to product inhibition, the addition of micro to millimolar levels of P5C or inorganic phosphate to the assay mixture did not exert any significant effect. On the contrary, a remarkable inhibition was found in the case of both $NADP^+$ and ADP (**Figure 4C**). The latter was inhibitory only at concentrations exceeding that of ATP in the reaction mixture (4 mM), and 9 mM ADP was required to reduce activity by 50%. More interestingly, $NADP^+$ exerted a significant inhibition already at levels 5-fold lower than those of NADPH in the assay, and 50% inhibition was achieved when $NADP^+$ and NADPH were present at the same concentration (0.4 mM). NAD^+ was completely ineffective (not shown). The results therefore strengthen the possibility that P5CS activity may be regulated *in vivo* by both the adenylate charge and, mainly, by the redox status of the cell.

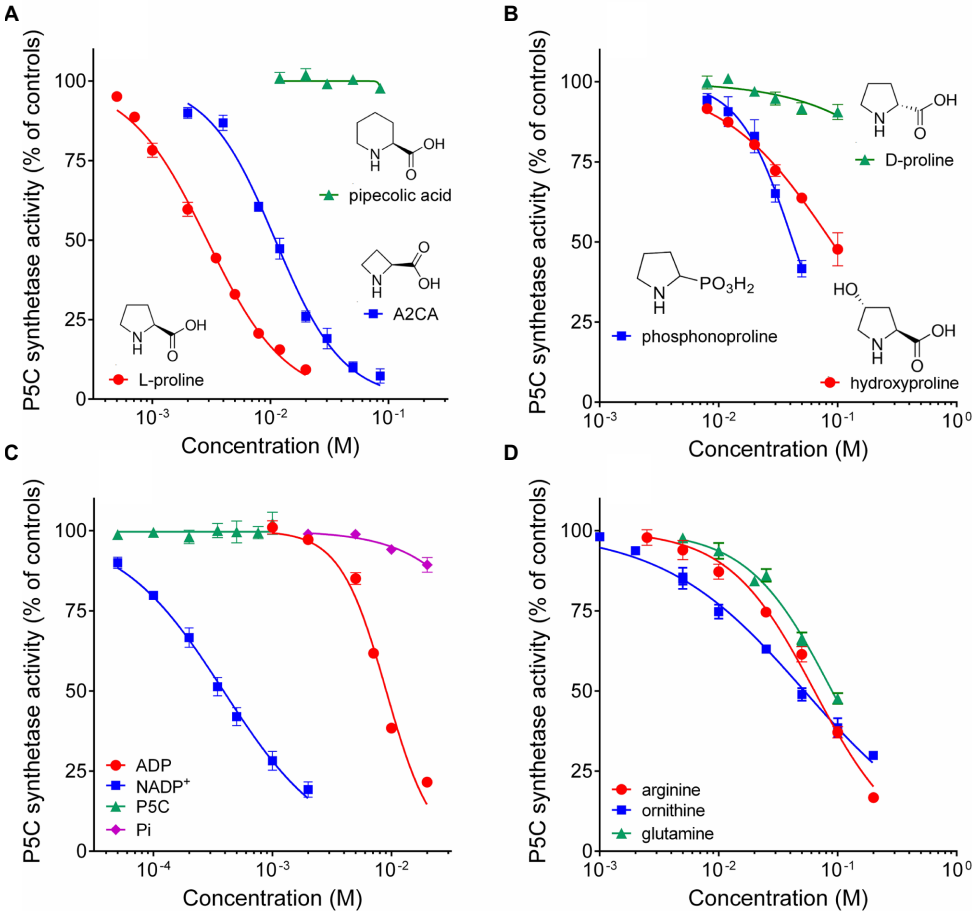

FIGURE 4 | Effect of reaction products and related amino acids on the activity of rice P5C synthetase 2. The activity of the purified protein was assayed in the presence of increasing concentrations of the final product of the pathway, L-proline, and its 4C (A2CA) and 6C (pipecolic acid) analogues **(A)**; of the D-isomer and other natural and synthetic analogues of proline **(B)**; of the four enzyme products **(C)**; of some amino acids that are metabolically interconnected with proline, or represent a cellular index of nitrogen availability **(D)**. Results were expressed as per cent of mean values in untreated controls. Presented data are means ± SE over three technical replicates. Each experiment was repeated three times with different enzyme preparations, and virtually identical patterns were obtained. Ornithine and arginine were added as hydrochlorides. To rule out the possibility that effects may depend on a consequent change in pH and not to the added substances, the actual pH in each sample was measured with a microelectrode at the end of the incubation. Non-linear regression of data (log[inhibitor] *vs.* normalized response – variable slope) was performed using GraphPad Prism; IC_{50} values and their confidence intervals are reported in **Table 2**.

TABLE 2 | Concentrations of selected substances able to inhibit by 50% the activity of *Oryza sativa* P5C synthetase 2.

	IC_{50} (mM)	Lower limit (mM)	Upper limit (mM)
L-proline	2.91	2.76	3.08
azetidine-2-carboxylic acid	11.0	10.2	11.9
phosphonoproline	42.2	37.8	47.3
L-4-hydroxyproline	89.5	76.4	105
$NADP^+$	0.389	0.365	0.414
ADP	9.06	8.40	9.77
ornithine	52.6	48.4	57.2
arginine	63.9	58.0	70.3
glutamine	89.7	83.7	96.2
Mg^{++}	34.8	27.6	46.4
Ca^{++}	4.09	3.60	4.63

Confidence intervals (p = 0.05) are also reported.

The effect of the presence of other amino acids was also analyzed. The addition of concentrations of ornithine exceeding 2 mM was found inhibitory (**Figure 4D**), and 50%-inhibition of P5CS activity was obtained at about 50 mM (**Table 2**). A similar pattern was evident also with arginine, though the effect was slightly lower. Enzyme activity was affected also by glutamine at concentrations exceeding 10 mM, with an IC_{50} value of about 100 mM. Asparagine and α-ketoglutarate were on the contrary ineffective up to 100 mM (data not presented).

Effect of Anions and Cations on Enzyme Activity

Finally, because the synthesis of proline is often induced by the exposure to hyperosmotic conditions, the effect of the main anions and cations present in plant cells on the activity of P5CS was investigated (**Figure 5**). When considered overall, data suggested

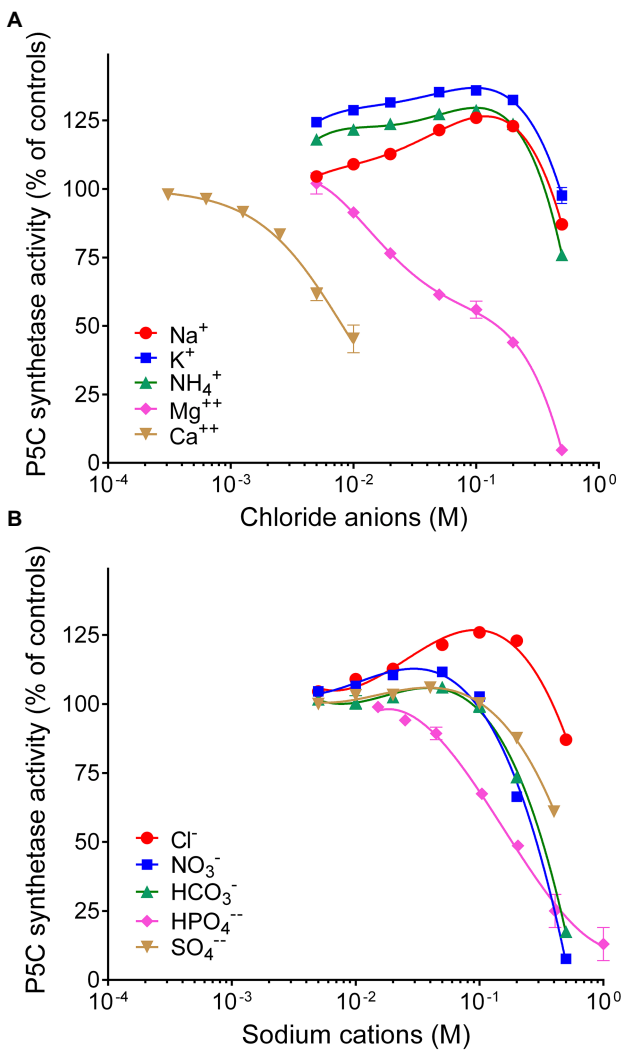

FIGURE 5 | Effect of anions and cations on the activity of rice P5C synthetase 2. The steady state rate of the enzyme was measured in the presence or in the absence of increasing concentrations of chlorides of various cations **(A)** or the sodium salts of various anions **(B)**, ranging from 0.3 mM to 1 M. To minimize ion presence in the assay mixture, in the former case, Tris-HCl buffer was replaced with 10 mM potassium phosphate buffer, pH 7.5, whereas in the latter case, its concentration was lowered to 10 mM. The actual pH in each sample was measured with a microelectrode at the end of the incubation, to ensure that the addition of salts did not cause a pH change in the reaction mixture. Activity was expressed as per cent of mean value in untreated controls. Data are means ± SE over three technical replicates. The experiments were repeated three times with different enzyme preparations, and almost identical patterns were obtained. To calculate the concentration of Mg^{++} ions able to inhibit activity by 50%, data were expressed with respect to parallel samples containing equimolar amounts of NaCl, to compensate the stimulatory effect of chlorides in the range 10–200 mM.

a stimulatory effect of chloride anions in the range 10–100 mM. On the contrary, sodium cations seem inhibitory, but only at concentrations exceeding 100 mM. Among the other anions, HPO_4^{--} reduced P5CS activity when added to the reaction mixture at levels higher than 20 mM. Unexpectedly, a strong inhibitory effect was evident with divalent Ca^{++} and Mg^{++}. Ca^{++} was more effective, although it had only a negligible effect at concentrations typically present in the cytosol. Mg^{++} ions at 20 mM, a level that had been routinely added to the γ-glutamyl kinase assay (Zhang et al., 1995), exerted 25% inhibition (**Figure 4A**), and 50%-inhibition was found at about 35 mM (**Table 2**).

DISCUSSION

Recombinant expression of rice P5CS isoenzyme 2 in *E. coli* and subsequent affinity purification to electrophoretic homogeneity yielded an active protein, but the activity was highly unstable. In the absence of reducing agents, the half-life of P5CS2 activity was less than 24 h. This feature is in striking contrast to the remarkable stability of the enzyme that catalyzes the second and last step in proline biosynthesis, P5C reductase, which retained more than 90% activity after 3-month storage at 4°C (Giberti et al., 2014; Ruszkowski et al., 2015; Forlani et al., 2015b). Another remarkable difference between the two enzymes concerns their catalytic constants, with P5CS2 catalyzing only 1.5 reactions s^{-1} per monomer, whereas rice P5C reductase showed the capability of reducing 350 to almost 5,000 P5C molecules s^{-1} under non-limiting conditions, depending on whether NADPH or NADH was the electron donor (Forlani et al., 2015b). Such a huge difference may be functional *in vivo* to avoid any accumulation of P5C, which has been hypothesized to exert (or trigger) cytotoxic effects (Deuschle et al., 2004; Qamar et al., 2015; Giberti et al., 2017), and could explain the lack of correlation between the expression level of P5C reductase and the intracellular concentration of proline (Hua et al., 1997). Moreover, a high lability of the enzyme that catalyzes the limiting step in a biosynthetic route may facilitate a rapid activation or deactivation of the pathway as a function of the cellular need for the final product. However, more evidence is required to confirm that P5CS2 may have a similar lability also inside the plant cell, where microenvironmental conditions or posttranslational modifications could improve its half-life. Both *A. thaliana* P5CS isoenzymes were found to be phosphorylated *in vivo* (PhosPhAt database; Durek et al., 2010) but no information is available about the influence of these modifications on the stability or activity of P5CS.

Proline biosynthesis from glutamate is competitively feedback-inhibited by proline binding near the glutamate binding site of the γ-glutamylkinase domain of P5CS, and Hill coefficients of 1.7–2 indicated cooperativity between proline binding to individual γ-glutamylkinase active sites (Zhang et al., 1995; Pérez-Arellano et al., 2010; Fichman et al., 2015). The activity of purified rice P5CS2 was inhibited by 50% at about 3 mM proline, and less than 20% catalytic rate was retained at 10 mM proline. These values are similar to the reported proline inhibition of the γ-glutamyl kinase activity of P5CS from *V. aconitifolia*, and roughly 20 times higher than the IC_{50} of *E. coli* γ-glutamyl kinase (Zhang et al., 1995; Pérez-Arellano et al., 2010). Moderate sensitivity to proline inhibition seems consistent with the role hypothesized for class 2 P5CS isozymes, i.e., to provide the

steady-state intracellular levels of proline required for protein synthesis (Rai and Penna, 2013). A phenylalanine residue (F133 in OsP5CS2) that was found critical for feedback inhibition of plant P5CS (Zhang et al., 1995) is conserved in both P5CS isoenzymes in rice, as well as in *Arabidopsis*. It remains to be analyzed, if differences at other positions render the stress-inducible isoforms less sensitive to inhibition by proline in order to allow proline accumulation. Interestingly, the 4C-ring analogue A2CA was also found to interact with rice P5CS2, thereby exerting a *false* feedback that was early hypothesized to explain part of the phytotoxic effects of this naturally-occurring compound (Nielsen et al., 1986).

The activity of rice P5CS was measured with three methods that had been described in the literature: by following the ATP-dependent phosphorylation of glutamate in the absence of NADPH (glutamyl kinase assay), the P5C-dependent reverse reduction of $NADP^+$ (glutamyl phosphate reductase assay), and the complete forward reaction in the presence of all three substrates (NADPH oxidation assay). The rate of glutamyl phosphate production was much lower than that of the whole reaction. This could depend on the lability of γ-glutamyl phosphate (Hayzer and Leisinger, 1980) even in the presence of product-trapping hydroxylamine. The alternative possibility that a slow kinase reaction is favored by a faster release of ADP in the presence of NADPH would imply a "ping-pong" mechanism for this multisubstrate enzyme. On the contrary, the occurrence of an initial burst of NADPH oxidation even in the absence of glutamate and ATP strengthens a biphasic mechanism in which a rapid reaction of NADPH with the enzyme is followed by a slower process in which glutamyl phosphate is produced and reduced. Considering that the glutamyl phosphate reductase assay is not sensitive to feedback inhibition by proline (Zhang et al., 1995; **Supplementary Figure S4**), these data emphasize the need of adopting the NADPH oxidation assay to obtain a reliable estimate of the biochemical features of P5CSs. However, the presence of several unrelated activities able to hydrolyze NADPH, coupled with the low specific activity of P5CS2, makes this assay poorly feasible if used with crude extracts. Accordingly, knockout of one P5CS isoform had only a small effect on total ATP- and glutamate-dependent NADPH oxidation in total protein extracts of *Medicago truncatula* (Nguyen et al., 2013). With the NADPH oxidation assay, the purified rice P5CS2 showed a K_m value for glutamate similar to those described previously, whereas the K_m value calculated for ATP (0.76 mM) was significantly lower than those reported for the half-reactions (glutamyl kinase assay) of the enzymes from *V. aconitifolia* (2.7 mM; Zhang et al., 1995) or *A. thaliana* (1.5 mM; Parre et al., 2010). Substrate inhibition was also found at ATP concentrations exceeding 4 mM. If we convert literature data (25–35 nmol g^{-1} fw; e.g., Yu et al., 2020) into molar levels on the assumption of an intracellular volume (excluding vacuoles) equal to about 2–4% of the total water content in rice leaves, the concentration of ATP in the cell should range from 0.6 to 1.5 mM. It is therefore likely that such inhibition does not have a physiological role. Our kinetic analysis of purified rice P5CS2 also enabled determination of the apparent K_m for NADPH as 45 μM, which had not been determined before for any plant P5CS.

The actual concentration of NADPH in the plant cell is not easy to be estimated, as literature data are expressed in nmol (g FW)$^{-1}$ (Queval and Noctor, 2007; Takahashi et al., 2009; Sharma et al., 2011). However, these values should correspond to cytosolic concentrations of NADPH ranging from 50 to 100 μM. This would imply that every fluctuation of the NADPH level could influence the rate of P5C synthesis. Taking into account that the exposure to stress conditions is well-known to induce cytosolic NADPH production through the oxidative pentose phosphate pathway (OPPP; Baxter et al., 2007), this would also explain the significant increase of proline homeostatic levels that rapidly occurred in rice cell cultures after the exposure to hyperosmotic stress even in the absence of any variation in P5CS expression levels (Forlani et al., 2015a). Indeed, following a treatment with PEG at −1.2 MPa, NADPH levels in 7-day-old seedlings of *A. thaliana* increased from 0.3 to 2 nmol (g FW)$^{-1}$ (i.e., from about 15 to 100 μM; Sharma et al., 2011). A higher rate of proline synthesis would in turn regenerate $NADP^+$, allowing sustained OPPP activity (Hare and Cress, 1997; Verslues and Sharma, 2010). Interestingly, we found that the activity of rice P5CS2 is also sensitive to product inhibition, with 50% reduction of the catalytic rate in the presence of equimolar levels (0.4 mM) of $NADP^+$ and NADPH. An even higher sensitivity to $NADP^+$ has been found for plant P5C reductases, but only if NADH was the electron donor, whereas the NADPH-dependent activity was unaffected (Giberti et al., 2014; Ruszkowski et al., 2015; Forlani et al., 2015b). The almost complete inability of rice P5CS2 to use NADH as cofactor indicates a strong interaction with the phosphate group of NADPH, which may explain why also $NADP^+$ may be bound strongly and thus inhibit NADPH binding. Structures of human P5CS (2H5G) and glutamyl phosphate reductase from yeast (1VLU) are available, but they do not include NADPH. $NADP^+$ levels in *Arabidopsis* usually range from 2 to 25 nmol (g FW)$^{-1}$, approximatively corresponding to 0.1–1.25 mM; Queval and Noctor, 2007; Takahashi et al., 2009; Sharma et al., 2011). If similar values were present also in rice, this would imply that under nonstressful conditions P5CS2 activity is significantly inhibited by $NADP^+$, but promptly activated under stress as a consequence of the above-mentioned reduction of the pyridine dinucleotide pool. Mechanisms linking the modulation of proline biosynthesis with the redox status of the cell have long been hypothesized (Hare and Cress, 1997; Sharma et al., 2011; Shinde et al., 2016). Characterization of rice P5CS2 provides for the first time useful elements to substantiate this hypothesis.

Also noteworthy is the finding that rice P5CS2 is inhibited not only by proline, but also by ornithine, arginine, and glutamine. In mammals, P5CS is not feedback-inhibited by proline, but its activity is regulated by ornithine, with a K_I value (0.4 mM) very near the predicted intracellular concentration of the intermediate (Hu et al., 1999). However, in mammals, the P5CS reaction serves both proline and arginine biosynthesis, whereas in plants, the first committed step of arginine production is the acetylation of glutamate, yielding a product that is then subjected to phosphorylation and reduction steps analogous

to those catalyzed by P5CS (Winter et al., 2015). This notwithstanding, it has been hypothesized that the glutamate pathway is the main route for proline synthesis in plants only under nitrogen limitation, whereas under high nitrogen input the ornithine pathway assumes prominence (Delauney and Verma, 1993; Anwar et al., 2018). Although the occurrence of the ornithine pathway has been questioned in *Arabidopsis* (Funck et al., 2008), the sensitivity of P5CS not only to ornithine, but also to amino acids that are abundant under high nitrogen input might provide the molecular basis of such regulative mechanism. P5CS2 was inhibited *in vitro* by ornithine and arginine concentrations higher than those found in rice cultured cells [4–15 nmol (g FW)$^{-1}$ and 15–76 nmol (g FW)$^{-1}$ for ornithine and arginine, which should correspond to about 0.1–0.4 and 0.4–4 mM, respectively; Forlani et al., 2014]. However, higher concentrations of ornithine, arginine, and glutamine are found in certain plant tissues as nitrogen storage forms [e.g., 0.4, 5, and 35 μmol (g FW)$^{-1}$, respectively, in 12 day-old *Arabidopsis* seedlings Majumdar et al., 2016; or 14, 53, and 9 μmol (g DW)$^{-1}$, respectively, in shoots of fertilized plants of *Vaccinium vitis-idaea* Ann-Brittedfast et al., 1994], and inside the cell cumulative effects also are likely to occur. Therefore, inhibition of P5CS activity by other amino acids than proline may have a physiological role under certain conditions.

On the other hand, the addition to the reaction mixture of chlorides in the 10–100 mM range was found to apparently stimulate P5CS2 activity up to 40%. This effect might be functional to proline accumulation under hyperosmotic stress. A similar effect has been shown to a much higher extent (up to 4-fold) also for P5C reductase, but only when NADPH was the electron donor (Forlani et al., 2015b). In *E. coli*, glutamate binding to the active site of γ-glutamylkinase is stabilized by an inter-subunit hydrogen bond network and it is perceivable that such a network may be sensitive to subtle changes in the quaternary structure brought about by altered ion concentrations in the cytosol (Pérez-Arellano et al., 2010). Crystallographic or mutational studies will be required to determine the effects of ion binding to P5CS. Contrary to *A. thaliana*, where mostly the P5CS1 isoform mediates stress-induced proline accumulation, both P5CS isoforms are important for proline accumulation and stress tolerance in rice (Hien et al., 2003; Hur et al., 2004; Forlani et al., 2015a). Indeed, to obtain a comprehensive picture of the post-translational regulation of the glutamate pathway for proline synthesis, the elucidation of functional properties of a P5CS family-1 member is also required. Work is currently in progress in our laboratory to fill this gap through cloning, heterologous expression, purification, and characterization of rice P5CS1.

DATA AVAILABILITY STATEMENT

The raw data supporting the conclusions of this article will be made available by the authors, without undue reservation.

AUTHOR CONTRIBUTIONS

GF designed the study, performed part of the experiments, elaborated the results, and drafted the paper. GS purified the P5CS2 protein and performed part of the experiments. DF cloned the *P5CS2* gene and performed peptide mapping. All authors contributed to the article and approved the submitted version.

FUNDING

This work was supported by grants from the University of Ferrara (FAR 2019 and 2020).

ACKNOWLEDGMENTS

The authors thank Michele Bertazzini for technical assistance during gene cloning and the Proteomics Center of the University of Konstanz for peptide mass fingerprinting.

SUPPLEMENTARY MATERIAL

The Supplementary Material for this article can be found online at: https://www.frontiersin.org/articles/10.3389/fpls.2021.672702/full#supplementary-material

REFERENCES

Ahanger, M. A., Akram, N. A., Ashraf, M., Alyemeni, M. N., Wijaya, L., and Ahmad, P. (2017). Plant responses to environmental stresses-from gene to biotechnology. *AoB Plants* 9:plx025. doi: 10.1093/aobpla/plx025

Ann-Brittedfast, T. N., Ericsson, A., and Nordén, L.-G. (1994). Accumulation of amino acids in some boreal forest plants in response to increased nitrogen availability. *New Phytol.* 126, 137–143. doi: 10.1111/j.1469-8137.1994.tb07539.x

Annunziata, M. G., Ciarmiello, L. F., Woodrow, P., Dell'Aversana, E., and Carillo, P. (2019). Spatial and temporal profile of glycine betaine accumulation in plants under abiotic stresses. *Front. Plant Sci.* 10:230. doi: 10.3389/fpls.2019.00230

Anwar, A., She, M., Wang, K., Riaz, B., and Ye, X. (2018). Biological roles of ornithine aminotransferase (OAT) in plant stress tolerance: present progress and future perspectives. *Int. J. Mol. Sci.* 19:3681. doi: 10.3390/ijms19113681

Baxter, C. J., Redestig, H., Schauer, N., Repsilber, D., Patil, K. R., Nielsen, J., et al. (2007). The metabolic response of heterotrophic *Arabidopsis* cells to oxidative stress. *Plant Physiol.* 143, 312–325. doi: 10.1104/pp.106.090431

Bradford, M. M. (1976). A rapid and sensitive method for the quantitation of microgram quantities of protein utilizing the principle of protein-dye binding. *Anal. Biochem.* 72, 248–254. doi: 10.1016/0003-2697(76)90527-3

Campanile, C., Forlani, G., Basso, A. L., Marasco, R., Ricca, E., Sacco, M., et al. (1993). Identification and characterization of the *proBA* operon of *Streptococcus bovis*. *Appl. Environ. Microbiol.* 59, 519–522. doi: 10.1128/aem.59.2.519-522.1993

Chen, M., Cao, J., Zheng, C., and Liu, Q. (2006). Directed evolution of an artificial bifunctional enzyme, γ-glutamyl kinase/γ-glutamyl phosphate reductase, for improved osmotic tolerance of *Escherichia coli* transformants. *FEMS Microbiol. Lett.* 263, 41–47. doi: 10.1111/j.1574-6968.2006.00397.x

Copeland, R.A. (2000). *Enzymes: A Practical Introduction to Structure, Mechanism, and Data Analysis*. *2nd Edn*. Bridgewater, NJ, USA: John Wiley & Sons.

Csonka, L. N., and Leisinger, T. (2007). "Biosynthesis of proline," in *EcoSal-Escherichia coli and Salmonella: Cellular and Molecular Biology*. eds. A. Block, R Curtis. III, J. B. Kaper, R. D. Karp, F. C. Neidhardt and T. Nystrom et al. (Washington, D.C: ASM Press).

Da Rocha, I. M. A., Vitorello, V. A., Silva, J. S., Ferreira-Silva, S. L., Viégas, R. A., Silva, E. N., et al. (2012). Exogenous ornithine is an effective precursor and the δ-ornithine amino transferase pathway contributes to proline accumulation under high N recycling in salt-stressed cashew leaves. *J. Plant Physiol.* 169, 41–49. doi: 10.1016/j.jplph.2011.08.001

Delauney, A. J., Hu, C. A., Kishor, P. B., and Verma, D. P. (1993). Cloning of ornithine δ-aminotransferase cDNA from *Vigna aconitifolia* by trans-complementation in *Escherichia coli* and regulation of proline biosynthesis. *J. Biol. Chem.* 268, 18673–18678. doi: 10.1016/S0021-9258(17)46682-8

Delauney, A. J., and Verma, D. P. S. (1993). Proline biosynthesis and osmoregulation in plants. *Plant J.* 4, 215–223. doi: 10.1046/j.1365-313X.1993.04020215.x

Deuschle, K., Funck, D., Forlani, G., Stransky, H., Biehl, A., Leister, D., et al. (2004). The role of δ1-pyrroline-5-carboxylate dehydrogenase in proline degradation. An update. *Plant Cell.* 16, 3413–3425. doi: 10.1105/tpc.104.023622

Durek, P., Schmidt, R., Heazlewood, J. L., Jones, A., MacLean, D., Nagel, A., et al. (2010). PhosPhAt: the *Arabidopsis thaliana* phosphorylation site database. An update. *Nucleic Acids Res.* 38, D828–D834. doi: 10.1093/nar/gkp810

Fichman, Y., Gerdes, S. Y., Kovács, H., Szabados, L., Zilberstein, A., and Csonka, L. (2015). Evolution of proline biosynthesis: enzymology, bioinformatics, genetics, and transcriptional regulation. *Biol. Rev. Camb. Philos. Soc.* 90, 1065–1099. doi: 10.1111/brv.12146

Forlani, G., Bertazzini, M., and Cagnano, G. (2019a). Stress-driven increase in proline levels, and not proline level itself, correlates with the ability to withstand excess salt in a group of 17 Italian rice genotypes. *Plant Biol.* 21, 336–342. doi: 10.1111/plb.12916

Forlani, G., Bertazzini, M., and Giberti, S. (2014). Differential accumulation of γ-aminobutyric acid in elicited cells of two rice cultivars showing contrasting sensitivity to the blast pathogen. *Plant Biol.* 16, 1127–1132. doi: 10.1111/plb.12165

Forlani, G., Bertazzini, M., Zarattini, M., and Funck, D. (2015a). Functional characterization and expression analysis of rice δ^1-pyrroline-5-carboxylate dehydrogenase provide new insight into the regulation of proline and arginine catabolism. *Front. Plant Sci.* 6:591. doi: 10.3389/fpls.2015.00591

Forlani, G., Bertazzini, M., Zarattini, M., Funck, D., Ruszkowski, M., and Nocek, B. (2015b). Functional properties and structural characterization of rice δ^1-pyrroline-5-carboxylate reductase. *Front. Plant Sci.* 6:565. doi: 10.3389/fpls.2015.00565

Forlani, G., and Funck, D. (2020). A specific and sensitive enzymatic assay for the quantitation of L-proline. *Front. Plant Sci.* 11:582026. doi: 10.3389/fpls.2020.582026

Forlani, G., Nocek, B., Chakravarthy, S., and Joachimiak, A. (2017). Functional characterization of four putative δ^1-pyrroline-5-carboxylate reductases from *Bacillus subtilis*. *Front. Microbiol.* 8:1442. doi: 10.3389/fmicb.2017.01442

Forlani, G., Obojska, A., Berlicki, Ł., and Kafarski, P. (2006). Phosphinothricin analogues as inhibitors of plant glutamine synthetases. *J. Agric. Food Chem.* 54, 796–802. doi: 10.1021/jf0526285

Forlani, G., Trovato, M., Funck, D., and Signorelli, S. (2019b). "Regulation of proline accumulation and its molecular and physiological functions in stress defense," in *Osmoprotectant-Mediated Abiotic Stress Tolerance in Plants: Recent Advances and Future Perspectives*. eds. M. A. Hossain, V. Kumar, D. J. Burritt, M. Fujita and P. Mäkelä (Switzerland: Springer Nature).

Funck, D., Baumgarten, L., Stift, M., von Wirén, N., and Schönemann, L. (2020). Differential contribution of P5CS isoforms to stress tolerance in *Arabidopsis*. *Front. Plant Sci.* 11:565134. doi: 10.3389/fpls.2020.565134

Funck, D., Stadelhofer, B., and Koch, W. (2008). Ornithine-δ-aminotransferase is essential for arginine catabolism but not for proline biosynthesis. *BMC Plant Biol.* 8:40. doi: 10.1186/1471-2229-8-40

García-Ríos, M., Fujita, T., LaRosa, P. C., Locy, R. D., Clithero, J. M., Bressan, R. A., et al. (1997). Cloning of a polycistronic cDNA from tomato encoding γ-glutamyl kinase and γ-glutamyl phosphate reductase. *Proc. Natl. Acad. Sci. U. S. A.* 94, 8249–8254. doi: 10.1073/pnas.94.15.8249

Giberti, S., Bertazzini, M., Liboni, M., Berlicki, Ł., Kafarski, P., and Forlani, G. (2017). Phytotoxicity of aminobisphosphonates targeting both δ^1-pyrroline-5-carboxylate reductase and glutamine synthetase. *Pest Manag. Sci.* 73, 435–443. doi: 10.1002/ps.4299

Giberti, S., Funck, D., and Forlani, G. (2014). Δ^1-pyrroline-5-carboxylate reductase from *Arabidopsis thaliana*: stimulation or inhibition by chloride ions and feedback regulation by proline depend on whether NADPH or NADH acts as co-substrate. *New Phytol.* 202, 911–919. doi: 10.1111/nph.12701

Govrin, R., Obstbaum, T., and Sivan, U. (2019). Common source of cryoprotection and osmoprotection by osmolytes. *J. Am. Chem. Soc.* 141, 13311–13314. doi: 10.1021/jacs.9b06727

Guan, C., Cen, H. F., Cui, X., Tian, D. Y., Tadesse, D., and Zhang, Y. W. (2019). Proline improves switchgrass growth and development by reduced lignin biosynthesis. *Sci. Rep.* 9:20117. doi: 10.1038/s41598-019-56575-9

Hare, P. D., and Cress, W. A. (1997). Metabolic implications of stress-induced proline accumulation in plants. *Plant Growth Regul.* 21, 79–102. doi: 10.1023/A:1005703923347

Hayat, S., Hayat, Q., Alyemeni, M. N., Wani, A. S., Pichtel, J., and Ahmad, A. (2012). Role of proline under changing environments: a review. *Plant Signal. Behav.* 7, 1456–1466. doi: 10.4161/psb.21949

Hayzer, D. J., and Leisinger, T. (1980). The gene-enzyme relationships of proline biosynthesis in *Escherichia coli*. *J. Gen. Microbiol.* 118, 287–293. doi: 10.1099/00221287-118-2-287

Hien, D. T., Jacobs, M., Angenon, G., Hermans, C., Thu, T. T., Van Son, L., et al. (2003). Proline accumulation and Δ^1-pyrroline-5-carboxylate synthetase gene properties in three rice cultivars differing in salinity and drought tolerance. *Plant Sci.* 65, 1059–1068. doi: 10.1016/S0168-9452(03)00301-7

Hildebrandt, T. M. (2018). Synthesis versus degradation: directions of amino acid metabolism during *Arabidopsis* abiotic stress response. *Plant Mol. Biol.* 98, 121–135. doi: 10.1007/s11103-018-0767-0

Hu, C. A., Delauney, A. J., and Verma, D. P. (1992). A bifunctional enzyme (δ^1-pyrroline-5-carboxylate synthetase) catalyzes the first two steps in proline biosynthesis in plants. *Proc. Natl. Acad. Sci. U. S. A.* 89, 9354–9358. doi: 10.1073/pnas.89.19.9354

Hu, C. A., Lin, W. W., Obie, C., and Valle, D. (1999). Molecular enzymology of mammalian δ^1-pyrroline-5-carboxylate synthase. Alternative splice donor utilization generates isoforms with different sensitivity to ornithine inhibition. *J. Biol. Chem.* 274, 6754–6762. doi: 10.1074/jbc.274.10.6754

Hua, X. J., van de Cotte, B., Van Montagu, M., and Verbruggen, N. (1997). Developmental regulation of pyrroline-5-carboxylate reductase gene expression in *Arabidopsis*. *Plant Physiol.* 114, 1215–1224. doi: 10.1104/pp.114.4.1215

Hur, J., Jung, K.-H., Lee, C.-H., and An, G. (2004). Stress-inducible *OsP5CS2* gene is essential for salt and cold tolerance in rice. *Plant Sci.* 167, 417–426. doi: 10.1016/j.plantsci.2004.04.009

Iordachescu, M., and Imai, R. (2008). Trehalose biosynthesis in response to abiotic stresses. *J. Integr. Plant Biol.* 50, 1223–1229. doi: 10.1111/j.1744-7909.2008.00736.x

Kishor, P. B. K., and Sreenivasulu, N. (2014). Is proline accumulation per se correlated with stress tolerance or is proline homeostasis a more critical issue? *Plant Cell Environ.* 37, 300–311. doi: 10.1111/pce.12157

Liang, X., Zhang, L., Natarajan, S. K., and Becker, D. F. (2013). Proline mechanisms of stress survival. *Antioxid. Redox Signal.* 19, 998–1011. doi: 10.1089/ars.2012.5074

Majumdar, R., Barchi, B., Turlapati, S. A., Gagne, M., Minocha, R., Long, S., et al. (2016). Glutamate, ornithine, arginine, proline, and polyamine metabolic interactions: the pathway is regulated at the post-transcriptional level. *Front. Plant Sci.* 7:78. doi: 10.3389/fpls.2016.00078

Meena, M., Divyanshu, K., Kumar, S., Swapnil, P., Zehra, A., Shukla, V., et al. (2019). Regulation of L-proline biosynthesis, signal transduction, transport, accumulation and its vital role in plants during variable environmental conditions. *Heliyon* 5:e02952. doi: 10.1016/j.heliyon.2019.e02952

Nguyen, M. L., Kim, G. B., Hyun, S. H., Lee, S.-Y., Lee, C.-Y., Choi, H.-K., et al. (2013). Physiological and metabolomic analysis of a knockout mutant suggests a critical role of *MtP5CS3* gene in osmotic stress tolerance of *Medicago truncatula*. *Euphytica* 193, 101–120. doi: 10.1007/s10681-013-0957-4

Nielsen, E., Forlani, G., Cella, R., and Parisi, B. (1986). Biochemical characterization of the natural resistance of rice to the proline analogue azetidin-2-carboxylic acid. *Plant Sci.* 44, 147–154. doi: 10.1016/0168-9452(86)90085-3

Parre, E., de Virville, J., Cochet, F., Leprince, A. S., Richard, L., Lefebvre-De Vos, D., et al. (2010). A new method for accurately measuring δ^1-pyrroline-5-carboxylate synthetase activity. *Methods Mol. Biol.* 639, 333–340. doi: 10.1007/978-1-60761-702-0_21

Pérez-Arellano, I., Carmona-Álvarez, F., Gallego, J., and Cervera, J. (2010). Molecular mechanisms modulating glutamate kinase activity. Identification of the proline feedback inhibitor binding site. *J. Mol. Biol.* 404, 890–901. doi: 10.1016/j.jmb.2010.10.019

Qamar, A., Mysore, K. S., and Senthil-Kumar, M. (2015). Role of proline and pyrroline-5-carboxylate metabolism in plant defense against invading pathogens. *Front. Plant Sci.* 6:503. doi: 10.3389/fpls.2015.00503

Queval, G., and Noctor, G. (2007). A plate reader method for the measurement of NAD, NADP, glutathione, and ascorbate in tissue extracts: application to redox profiling during *Arabidopsis* rosette development. *Anal. Biochem.* 363, 58–69. doi: 10.1016/j.ab.2007.01.005

Rai, A. N., and Penna, S. (2013). Molecular evolution of plant *P5CS* gene involved in proline biosynthesis. *Mol. Biol. Rep.* 40, 6429–6435. doi: 10.1007/s11033-013-2757-2

Ruszkowski, M., Nocek, B., Forlani, G., and Dauter, Z. (2015). The structure of *Medicago truncatula* δ^1-pyrroline-5-carboxylate reductase provides new insights into regulation of proline biosynthesis in plants. *Front. Plant Sci.* 6:869. doi: 10.3389/fpls.2015.00869

Sharma, A., Shahzad, B., Kumar, V., Kohli, S. K., Sidhu, G., Bali, A. S., et al. (2019). Phytohormones regulate accumulation of osmolytes under abiotic stress. *Biomol. Ther.* 9:285. doi: 10.3390/biom9070285

Sharma, S., Villamor, J. G., and Verslues, P. E. (2011). Essential role of tissue-specific proline synthesis and catabolism in growth and redox balance at low water potential. *Plant Physiol.* 157, 292–304. doi: 10.1104/pp.111.183210

Shinde, S., Villamor, J. G., Lin, W.-D., Sharma, S., and Verslues, P. E. (2016). Proline coordination with fatty acid synthesis and redox metabolism of chloroplast and mitochondria. *Plant Physiol.* 172, 1074–1088. doi: 10.1104/pp.16.01097

Singh, A., Upadhyay, V., Upadhyay, A. K., Singh, S. M., and Panda, A. K. (2015). Protein recovery from inclusion bodies of *Escherichia coli* using mild solubilization process. *Microb. Cell Factories* 14:41. doi: 10.1186/s12934-015-0222-8

Strizhov, N., Abrahám, E., Okrész, L., Blickling, S., Zilberstein, A., Schell, J., et al. (1997). Differential expression of two *P5CS* genes controlling proline accumulation during salt-stress requires ABA and is regulated by ABA1, ABI1 and AXR2 in *Arabidopsis*. *Plant J.* 12, 557–569. doi: 10.1046/j.1365-313x.1997.00557.x

Székely, G., Abrahám, E., Cséplo, A., Rigó, G., Zsigmond, L., Csiszár, J., et al. (2008). Duplicated *P5CS* genes of *Arabidopsis* play distinct roles in stress regulation and developmental control of proline biosynthesis. *Plant J.* 53, 11–28. doi: 10.1111/j.1365-313X.2007.03318.x

Takahashi, H., Takahara, K., Hashida, S. N., Hirabayashi, T., Fujimori, T., Kawai-Yamada, M., et al. (2009). Pleiotropic modulation of carbon and nitrogen metabolism in Arabidopsis plants overexpressing the *NAD kinase2* gene. *Plant Physiol.* 151, 100–113. doi: 10.1104/pp.109.140665

Trovato, M., Forlani, G., Signorelli, S., and Funck, D. (2019). "Proline metabolism and its functions in development and stress tolerance," in *Osmoprotectant-Mediated Abiotic Stress Tolerance in Plants: Recent Advances and Future Perspectives*. eds. M. A. Hossain, V. Kumar, D. J. Burritt, M. Fujita and P. Mäkelä (Switzerland: Springer Nature).

Turchetto-Zolet, A. C., Margis-Pinheiro, M., and Margis, R. (2009). The evolution of pyrroline-5-carboxylate synthase in plants: a key enzyme in proline synthesis. *Mol. Genet. Genomics* 281, 87–97. doi: 10.1007/s00438-008-0396-4

Upadhyay, A. K., Murmu, A., Singh, A., and Panda, A. K. (2012). Kinetics of inclusion body formation and its correlation with the characteristics of protein aggregates in *Escherichia coli*. *PLoS One* 7:33951. doi: 10.1371/journal.pone.0033951

Verbruggen, N., and Hermans, C. (2008). Proline accumulation in plants: a review. *Amino Acids* 35, 753–759. doi: 10.1007/s00726-008-0061-6

Verslues, P. E., and Sharma, S. (2010). Proline metabolism and its implications for plant-environment interaction. *Arabidopsis Book* 8:e0140. doi: 10.1199/tab. 0140

Williams, I., and Frank, L. (1975). Improved chemical synthesis and enzymatic assay of δ^1-pyrroline-5-carboxylic acid. *Anal. Biochem.* 64, 85–97. doi: 10.1016/0003-2697(75)90408-X

Winter, G., Todd, C., Trovato, M., Forlani, G., and Funck, D. (2015). Physiological implications of arginine metabolism in plants. *Front. Plant Sci.* 6:534. doi: 10.3389/fpls.2015.00534

Yu, P., Jiang, N., Fu, W., Zheng, G., Li, G., Feng, B., et al. (2020). ATP hydrolysis determines cold tolerance by regulating available energy for glutathione synthesis in rice seedling plants. *Rice* 13:23. doi: 10.1186/s12284-020-00383-7

Zarattini, M., and Forlani, G. (2017). Toward unveiling the mechanisms for transcriptional regulation of proline biosynthesis in the plant cell response to biotic and abiotic stress conditions. *Front. Plant Sci.* 8:927. doi: 10.3389/fpls.2017.00927

Zhang, C. S., Lu, Q., and Verma, D. P. (1995). Removal of feedback inhibition of δ^1-pyrroline-5-carboxylate synthetase, a bifunctional enzyme catalyzing the first two steps of proline biosynthesis in plants. *J. Biol. Chem.* 270, 20491–20496. doi: 10.1074/jbc.270.35.20491

Conflict of Interest: The authors declare that the research was conducted in the absence of any commercial or financial relationships that could be construed as a potential conflict of interest.

Publisher's Note: All claims expressed in this article are solely those of the authors and do not necessarily represent those of their affiliated organizations, or those of the publisher, the editors and the reviewers. Any product that may be evaluated in this article, or claim that may be made by its manufacturer, is not guaranteed or endorsed by the publisher.

Copyright © 2021 Sabbioni, Funck and Forlani. This is an open-access article distributed under the terms of the Creative Commons Attribution License (CC BY). The use, distribution or reproduction in other forums is permitted, provided the original author(s) and the copyright owner(s) are credited and that the original publication in this journal is cited, in accordance with accepted academic practice. No use, distribution or reproduction is permitted which does not comply with these terms.

Advantages of publishing in Frontiers

OPEN ACCESS
Articles are free to read for greatest visibility and readership

FAST PUBLICATION
Around 90 days from submission to decision

HIGH QUALITY PEER-REVIEW
Rigorous, collaborative, and constructive peer-review

TRANSPARENT PEER-REVIEW
Editors and reviewers acknowledged by name on published articles

Frontiers
Avenue du Tribunal-Fédéral 34
1005 Lausanne | Switzerland

Visit us: www.frontiersin.org
Contact us: frontiersin.org/about/contact

REPRODUCIBILITY OF RESEARCH
Support open data and methods to enhance research reproducibility

DIGITAL PUBLISHING
Articles designed for optimal readership across devices

FOLLOW US
@frontiersin

IMPACT METRICS
Advanced article metrics track visibility across digital media

EXTENSIVE PROMOTION
Marketing and promotion of impactful research

LOOP RESEARCH NETWORK
Our network increases your article's readership